Handbook of Cardiac Anatomy, Physiology, and Devices

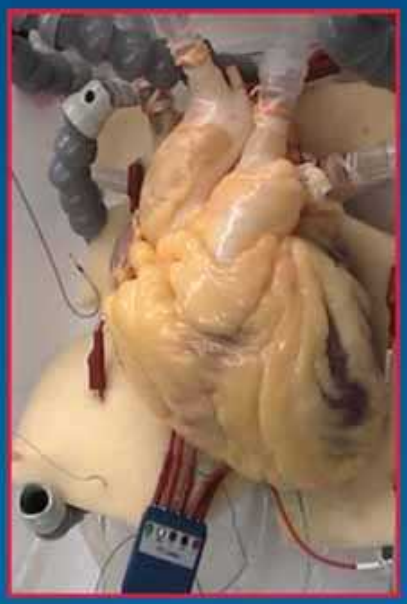

Edited by Paul A. Iaizzo, PhD

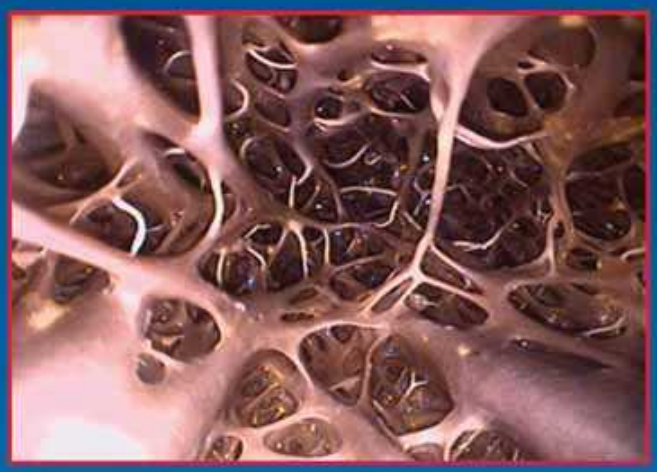

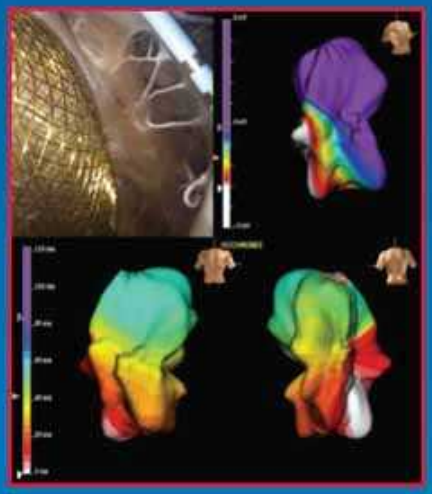

Includes Companion CD and The Visible Heart® CD

Humana Press

Handbook of Cardiac Anatomy, Physiology, and Devices

HANDBOOK OF CARDIAC ANATOMY, PHYSIOLOGY, AND DEVICES

Edited by

PAUL A. IAIZZO, PhD

Department of Surgery
University of Minnesota
Minneapolis, MN

HUMANA PRESS
TOTOWA, NEW JERSEY

999 Riverview Drive, Suite 208
Totowa, New Jersey 07512

humanapress.com

For additional copies, pricing for bulk purchases, and/or information about other Humana titles, contact Humana at the above address or at any of the following numbers: Tel: 973-256-1699; Fax: 973-256-8341; E-mail: humana@humanapr.com or visit our website at http://humanapr.com

This publication is printed on acid-free paper. ∞

ANSI Z39.48-1984 (American National Standards Institute) Permanence of Paper for Printed Library Materials.

Cover design by Patricia F. Cleary.

Cover illustrations: Images were created in the Visible Heart® Laboratory of Professor Iaizzo. *(Upper left)* An external view of an isolated human heart reanimated in vitro. (The heart was obtained via LifeSource as a r esearch gift from an organ donor whose heart was deemed not viable for transplantation.) *(Upper right)* An internal view of the apex of the left ventricle of a human heart; note the high degree of trabeculations. *(Lower right)* Serial endoscopic images showing movements, top-to-bottom, of a tricuspid valve, a pulmonary valve, a mitral valve, and an implanted mechanical aortic valve (left to right, respectively) from within functioning human hearts. *(Lower left)* Images obtained from an in vitro electrical mapping study of an isolated human heart: an EnSite® 3000 catheter is deployed in the left ventricle and a mapping catheter touches the endocardium. To the right is shown an anatomical isopotential map of excitation (voltage changes) and below it two views of constructed isochronal maps (time sequences of depolarization, anterior and posterior views).

Printed in China. 10 9 8 7 6 5 4 3 2 1

E-ISBN 1-59259-835-8

Library of Congress Cataloging-in-Publication Data

Handbook of cardiac anatomy, physiology, and devices / edited by
Paul A. Iaizzo.
p. cm. -- (Current clinical oncology)
Includes bibliographical references and index.
ISBN 1-58829-443-9 (alk. paper)
1. Heart--Anatomy--Handbooks, manuals, etc. 2.
Heart--Physiology--Handbooks, manuals, etc. 3.
Heart--Diseases--Treatment--Handbooks, manuals, etc. I. Iaizzo,
Paul A. II. Series: Current clinical oncology (Totowa, N.J.)
QM181.H36 2005
616.1'2--dc22
2004010861

PREFACE

The medical device industry in the US is growing at an incredibly rapid pace; in fact, today it is as large as the automobile industry in terms of revenues. Not only has our overall understanding of the molecular basis of disease dramatically increased, but so has the number of available devices to treat specific health problems. This is particularly true in the field of cardiac care. Advances in our understanding of disease processes are being made daily, and novel means to treat cardiac diseases are concomitantly being developed. With this rapid growth rate, the biomedical engineer has been challenged to either retool or continue to seek out sources of concise information.

The major impetus for developing the *Handbook of Cardiac Anatomy, Physiology, and Devices* was the need for a major resource textbook for students, residents, and practicing biomedical engineers. Another motivation was to promote the expertise, past and present, in the area of cardiovascular science at the University of Minnesota. As Director of Education for The Lillehei Heart Institute at the University of Minnesota, I believe that this book also represents an outreach opportunity to carry on the Lillehei legacy through the 21st century.

It may be of interest to note that there are several direct and indirect historical connections with C. Walton Lillehei. First, several of the individuals who contributed chapters had the privilege to work with him. Second, there is the connection with Medtronic, Inc.; founder Earl Bakken was one of the first true biomedical engineers, and he worked directly with Lillehei to develop implantable pacemakers at the University of Minnesota. In accordance with this latter collaboration, it turns out that there are numerous individuals currently working at Medtronic Inc. who strongly encouraged the University of Minnesota to develop outreach materials such as the *Handbook of Cardiac Anatomy, Physiology, and Devices*, as well as other educational programs.

More specifically, it was through my collaborations with Tim Laske, Mark Hjelle (my brother-in-law), and Dale Wahlstrom, all from the Cardiac Rhythm Management Division at Medtronic, Inc., who influenced the inception of this book in numerous ways including: (1) the development of the *Visible Heart*® media project in 1997, which is an ongoing effort to visualize functional cardiac anatomy and to make such images available for instruction; (2) the creation of the Physiology Industrial Advisory Board, which evaluated and subsequently created outreach programs to serve the greater local biomedical industry; and (3) the creation of the week-long short course, Advanced Cardiac Physiology and Anatomy, which was designed specifically for the biomedical engineer working in industry. Importantly, this course has been taught at the University of Minnesota for the past four years and is the basis of this textbook (the senior authors of most chapters present lectures in the course). Over the years, I have fielded numerous requests by engineers who have taken this course to develop more formal reference materials. In addition, many of the numerous Medtronic employees who have visited the *Visible Heart*® laboratory (over 500 individuals, with many repeat visits, in the past seven years) have routinely emphasized the need for advanced training opportunities in systems physiology, specifically for the seasoned biomedical employee. One last historical note of interest: my current laboratory (*Visible Heart*® laboratory), where isolated heart studies are performed weekly, is the same laboratory where C. Walton Lillehei and his many esteemed colleagues conducted a majority of their cardiovascular research studies in the late 1950s and early 1960s.

An added feature of this book that I hope will enhance its utility is a CD containing the *Visible Heart*® Viewer, which was developed as a joint venture between my laboratory at the University of Minnesota and the Cardiac Rhythm Management Division at Medtronic, Inc. An second *Companion CD* also contains various additional color images and movies that were provided by the authors to supplement their chapters.

Importantly, the accompanying media includes functional images of human hearts. These images were obtained from hearts made available via LifeSource, and more specifically through the generosity of families and individuals who made the final gift of organ donation (their hearts were not deemed viable for transplantation).

Acknowledgments

I would like to thank Medtronic, Inc. for their continued support of this collaborative project over the past seven years, and I especially acknowledge the commitment, partnership, and friendship of Tim Laske and Dale Wahlstrom, which has made our research possible. In addition, I would like to thank Jilean Dagenais and Mike Leners for their creative efforts in producing many of the movie and animation clips found on the *Companion CD*.

It is also my pleasure to thank the past and present graduate students who have worked in my laboratory and have also been contributors to this text, including: Edward Chinchoy, James Coles, Anthony Dupre, Kevin Fitzgerald, Alexander Hill, Ryan Lahm, Timothy Laske, Anna Legreid, Michael Loushin, Daniel Sigg, Nicholas Skadsberg, and Sarah Vincent. I feel extremely fortunate to have had the opportunity to work with such talented scientists and engineers. I have learned a great deal from each of them.

I would like to acknowledge the exceptional efforts of our Lab Coordinator, Monica Mahre, who: (1) assisted me in coordinating the efforts of the contributing authors; (2) skillfully incorporated my editorial changes; (3) verified the readability and formatting of each chapter; (4) pursued requested additions or missing materials for each chapter; (5) contributed as a coauthor; and (6) kept a positive outlook throughout. I would also like to thank Dee McManus for coordinating the support of

the Lillehei Heart Institute in their funding of illustrator Martin Finch, who prepared several of the original figures; Gary Williams for his computer expertise and assistance with numerous figures; William Gallagher and Charles Soule, who made sure the laboratory kept running smoothly while many of us were busy writing or editing; Dick Bianco for his support of our lab and this book project; the Chairman of the Department of Surgery, Dr. David Dunn, for his support and encouragement; and the Biomedical Engineering Institute at the University of Minnesota, headed by Dr. Jeffrey McCullough, who supported this project by funding the Cardiovascular Physiology Interest Group (most of whose members contributed chapters).

Finally, I would like to thank my family and friends for their support of my career and their assistance over the years. Without such encouragement, I would not have even dreamed of taking on such an ambitious project. Specifically, I would like to thank my wife Marge, my three daughters, Maria, Jenna, and Hanna, my mom Irene, and siblings, Mike, Chris, Mark, and Susan, for always being there for me. On a personal note, some of my motivation for working on this project comes from the memory of my father Anthony, who succumbed to sudden cardiac death at too early an age, and from the positive encouragement of my uncle Tom Halicki, who is doing well seven years after a heart transplant.

Paul A. Iaizzo, PhD

CONTENTS

CONTRIBUTORS

ATSUSHI ASAKURA, PhD • *Cardiovascular Division, Department of Medicine, University of Minnesota, Minneapolis, MN*

ROBERT J. BACHE, MD • *Cardiovascular Division, Department of Medicine, and Center for Magnetic Resonance Research, University of Minnesota, Minneapolis, MN*

VINCENT A. BARNETT, PhD • *Department of Physiology, University of Minnesota, Minneapolis, MN*

JOHN L. BASS, MD • *Department of Pediatrics, Division of Cardiology, University of Minnesota, Minneapolis, MN*

DAVID G. BENDITT, MD • *Cardiovascular Division, Department of Medicine, University of Minnesota, Minneapolis, MN*

RICHARD W. BIANCO • *Experimental Surgical Services, Department of Surgery, University of Minnesota, Minneapolis, MN*

GEORGE BOJANOV, MD • *Department of Anesthesiology, University of Minnesota, Minneapolis, MN*

R. MORTON BOLMAN III, MD • *Division of Cardiovascular and Thoracic Surgery, Department of Surgery, University of Minnesota, Minneapolis, MN*

EDWARD CHINCHOY, PhD • *Medtronic, Inc., Minneapolis, MN*

JAMES A. COLES, JR., PhD • *Medtronic, Inc., Minneapolis, MN*

ANTHONY DUPRE, MS • *Department of Surgery, University of Minnesota, Minneapolis, MN*

KEVIN FITZGERALD, MS • *Department of Surgery, University of Minnesota, Minneapolis, MN*

ARTHUR H. L. FROM, MD • *Cardiovascular Division, Department of Medicine, and Center for Magnetic Resonance Research, University of Minnesota, Minneapolis, MN*

ROBERT P. GALLEGOS, MD • *Division of Cardiac and Thoracic Surgery, Department of Surgery, University of Minnesota, Minneapolis, MN*

JENNIFER L. HALL, PhD • *Cardiovascular Division, Department of Medicine, University of Minnesota, Minneapolis, MN*

ALEXANDER J. HILL, PhD • *Medtronic, Inc., Minneapolis, MN*

PAUL A. IAIZZO, PhD • *Departments of Surgery, Physiology, and Anesthesiology, Director of Education for the Lillehei Heart Institute, University of Minnesota, Minneapolis MN*

MICHAEL JEROSCH-HEROLD, PhD • *Cardiac MRI Section, University of Minnesota, Minneapolis, MN*

RYAN LAHM, MS • *Medtronic, Inc., Minneapolis, MN*

TIMOTHY G. LASKE, PhD • *Medtronic, Inc., Minneapolis, MN*

JOSEPH LEE, BS • *Department of Biomedical Engineering, University of Minnesota, Minneapolis, MN*

ANNA M. LEGREID, PharmD • *Medtronic, Inc., Minneapolis, MN*

KENNETH K. LIAO, MD • *Division of Thoracic and Cardiovascular Surgery, Department of Surgery, University of Minnesota, Minneapolis, MN*

JAMIE L. LOHR, MD • *Division of Cardiology, Department of Pediatrics, University of Minnesota, Minneapolis, MN*

MICHAEL K. LOUSHIN, MD • *Department of Anesthesiology, University of Minnesota, Minneapolis, MN*

FEI LÜ, MD, PhD • *Cardiovascular Division, Department of Medicine, University of Minnesota, Minneapolis, MN*

MONICA A. MAHRE, BS • *Department of Surgery, University of Minnesota, Minneapolis, MN*

BRAD J. MARTINSEN, PhD • *Division of Cardiology, Department of Pediatrics, University of Minnesota, Minneapolis, MN*

DEE M. MCMANUS, BS • *Lillehei Heart Institute, University of Minnesota, Minneapolis, MN*

LESLIE W. MILLER, MD • *Cardiovascular Division, Department of Medicine, University of Minnesota, Minneapolis, MN*

J. ERNESTO MOLINA, MD, PhD • *Division of Cardiovascular and Thoracic Surgery, Department of Surgery, University of Minnesota, Minneapolis, MN*

SOON J. PARK, MD • *Department of Cardiovascular and Thoracic Surgery, California Pacific Medical Center, San Francisco, CA*

CARSTEN RICKERS, MD • *Department of Pediatric Cardiology, University Hospital Hamburg-Eppendorf, Hamburg, Germany*

ANDREW L. RIVARD, MD • *Department of Physiology, University of Minnesota, MN*

KENNETH P. ROBERTS, PhD • *Department of Urologic Surgery, University of Minnesota, Minneapolis, MN*

SCOTT SAKAGUCHI, MD • *Department of Medicine, University of Minnesota, Minneapolis, MN*

RAVI TEJA SEETHAMRAJU, PhD • *Siemens Medical Solutions USA, Inc.; Visiting Assistant Professor, Radiology, Harvard Medical School, Charlestown, MA*

DANIEL C. SIGG, MD, PhD • *Medtronic, Inc., Minneapolis, MN*

NICHOLAS D. SKADSBERG, PhD • *Departments of Biomedical Engineering and Surgery, University of Minnesota, Minneapolis, MN*

MICHAEL R. UJHELYI, PharmD, FCCP • *Medtronic, Inc., Minneapolis, MN*

SARAH VINCENT, MS • *Department of Surgery, University of Minnesota, Minneapolis, MN*

ANTHONY J. WEINHAUS, PhD • *Departments of Physiology and Genetics, Cell Biology, and Development, University of Minnesota, Minneapolis, MN*

ROBERT F. WILSON, MD • *Division of Cardiology, University of Minnesota, Minneapolis, MN*

JIANYI ZHANG, MD, PhD • *Division of Cardiology, Department of Medicine, University of Minnesota, Minneapolis, MN*

COMPANION CD

for *Handbook of Cardiac Anatomy, Physiology, and Devices*

The Companion CD serves to complement the text by including additional figures and/or short video clips to support the various chapters. The opening screen provides access to this material. Throughout the text, a cross reference to the Companion CD alerts the reader to the availability of this additional material.

The Companion CD is compatible with any XP Windows or Apple Macintosh operating system.

CONTENTS

CHAPTER 16 MECHANICAL ASPECTS OF CARDIAC PERFORMANCE

jpeg 1 Monitor display of electrocardiogram, blood pressures, and S_vO_2.

jpeg 2 Cannulation of a peripheral artery.

jpeg 3 Cannulation of a peripheral artery.

jpeg 4 Pressure transducer for monitoring blood pressures.

jpeg 5 Central venous access kit.

jpeg 6 Cannulation of right internal jugular vein.

jpeg 7 Pulmonary artery catheter.

jpeg 8 Inflated balloon at the distal tip of pulmonary artery catheter.

jpeg 9. Pulmonary artery catheter for continuous monitoring of cardiac output and mixed venous saturation.

jpeg 10 Millar catheter.

jpeg 11 Sensors on a Millar catheter.

CHAPTER 23 PACING AND DEFIBRILLATION

SECTION 2.2.

normal.mpg

SECTION 2.4.

AT.mpg

AF.mpg

VT.mpg

VF.mpg

SECTION 3.

styletNew.mpg

xray1.jpg

xray2.jpg

xray3.jpg

xray4.jpg

xray5.jpg

xray6.jpg

SECTION 4.8.

resync1.mpg

SECTION 5.10.

fluoro.avi

styletNew.mpg

5076huma.mpg

AApendFL.mpg

rva4074.mpg

5076humv.mpg

RV Apex.mpg

6944DEF1.mpg

6932humf.mpg

FIG. 11 connectorPlugIn.mpg

FIG. 33 energyVectorDual.mpg

CHAPTER 28 LESS-INVASIVE CARDIAC SURGERY

Fig. 1 Fig. 3 Fig. 5

Fig. 2 Fig. 4 Fig. 6

THE VISIBLE HEART®

CONTENTS

The Visible Heart®, a CD accompanying *Handbook of Cardiac Anatomy, Physiology, and Devices,* is designed to be a self-contained electronic textbook, developed via a collaboration between the University of Minnesota Medical School and Medtronic, Inc. It utilizes Visible Heart® technologies, a significant advancement in the modeling of the isolated heart that allows display of full-motion images captured from inside the endocardium of the functioning large mammalian heart.

With the support of LifeSource, The Visible Heart® presents images obtained from human hearts donated by generous individuals, whose final acts continue to enhance our understanding of the inner workings of the human heart and to contribute to lifesaving advances in cardiac medicine.

All images and videos on The Visible Heart® were captured in the laboratory of Dr. Iaizzo, utilizing the Visible Heart® technologies that are subject to pending US Patent Application No. 09/419,271 filed October 15, 1999 and PCT Application No. US99/24791, filed October 22, 1999 by the University of Minnesota and Medtronic, Inc.

INTRODUCTION 1

1 General Features of the Cardiovascular System

PAUL A. IAIZZO, PhD

CONTENTS

1. INTRODUCTION

Currently, approx 60 million individuals in the United States alone have some form of cardiovascular disease. More specifically, heart attacks continue to be an increasing problem in our society. Coronary bypass surgery, angioplasty, stenting, the implantation of pacemakers/defibrillators, and valve replacement are currently routine treatment procedures, with growing numbers of such procedures performed each year. However, such treatments often provide only temporary relief of the progressive symptoms of cardiac disease. Optimization of therapies and the development of new ones (e.g., coated vascular or coronary stents, left ventricular assist devices, and biventricular pacing) continue to dominate the cardiovascular biomedical industry.

The purpose of this chapter is to provide a general overview of the cardiovascular system as a quick reference as to the underlying physiological composition of this system. More details concerning the pathophysiology of the cardiovascular system and state-of-the-art treatments can be found in subsequent chapters. In addition, note that a list of sources and references is provided at the end of this chapter.

2. COMPONENTS OF THE CARDIOVASCULAR SYSTEM

The principal components considered to make up the cardiovascular system include the blood, blood vessels, heart, and lymphatic system.

From: *Handbook of Cardiac Anatomy, Physiology, and Devices*
Edited by: P. A. Iaizzo © Humana Press Inc., Totowa, NJ

2.1. Blood

Blood is composed of formed elements (cells and cell fragments) suspended in the liquid (plasma) fraction. Blood, considered the only liquid connective tissue in the body, has three general functions: (1) transportation (e.g., O_2, CO_2, nutrients, wastes, hormones); (2) regulation (e.g., pH, temperature, osmotic pressures); and (3) protection (e.g., against foreign molecules and diseases, as well as for clotting to prevent excessive loss of blood). Dissolved within the plasma are many proteins, nutrients, metabolic waste products, and various other molecules traveling between the organ systems.

The formed elements in blood include red blood cells (erythrocytes), white blood cells (leukocytes), and the cell fragments known as platelets. All are formed in bone marrow from a common stem cell. In a healthy individual, the majority (~99%) of blood cells are red cells, which have a primary role in O_2 exchange. Hemoglobin, the iron-containing heme protein that binds oxygen, is concentrated within the red cells; hemoglobin allows blood to transport 40 to 50 times the amount of oxygen that plasma alone could carry.

The white cells are required for the immune process to protect against infections and cancers. The platelets play a primary role in blood clotting. In a healthy cardiovascular system, the constant movement of blood helps keep these cells well dispersed throughout the plasma of the larger diameter vessels.

The *hematocrit* is defined as the percentage of blood volume occupied by the red cells (erythrocytes). It can be easily measured by centrifuging (spinning at high speed) a sample of blood, which forces these cells to the bottom of the centrifuge tube. The leukocytes remain on the top, and the platelets form a very

thin layer between the cell fractions (other, more sophisticated methods are also available to do such analyses). Normal hematocrit is approx 45% in men and 42% in women.

The total volume of blood in an average-size individual (70 kg) is approx 5.5 L; hence, the average red cell volume would be roughly 2.5 L. Because the fraction containing both leukocytes and platelets is normally relatively small or negligible, in such an individual the plasma volume can be estimated as 3.0 L. Approximately 90% of plasma is water, which acts: (1) as a solvent, (2) to suspend the components of blood, (3) in absorption of molecules and their transport, and (4) in the transport of thermal energy. Proteins make up 7% of the plasma (by weight) and exert a colloid osmotic pressure.

Protein types include albumins, globulins (antibodies and immunoglobulins), and fibrinogen. To date, more than 100 distinct plasma proteins have been identified, and each presumably serves a specific function. The other main solutes in plasma include electrolytes, nutrients, gases (some O_2, large amounts of CO_2 and N_2), regulatory substances (enzymes and hormones), and waste products (urea, uric acid, creatine, creatinine, bilirubin, and ammonia).

2.2. Blood Vessels

Blood flows throughout the body tissues in blood vessels via bulk flow (i.e., all constituents together and in one direction). An extraordinary degree of branching of blood vessels exists within the human body, which ensures that nearly every cell in the body lies within a short distance from at least one of the smallest branches of this system—a capillary. Nutrients and metabolic end products move between the capillary vessels and the surroundings of the cell through the interstitial fluid by diffusion. Subsequent movement of these molecules into a cell is accomplished by both diffusion and mediated transport. Nevertheless, blood flow through all organs can be considered as passive and occurs only because arterial pressure is kept higher than venous pressure via the pumping action of the heart.

In an individual at rest at a given moment, approx 5% of the total circulating blood is actually in capillaries. Yet, this volume of blood can be considered to perform the primary functions of the entire cardiovascular system, specifically the supply of nutrients and removal of metabolic end products. The cardiovascular system, as reported by the British physiologist William Harvey in 1628, is a closed-loop system, such that blood is pumped out of the heart through one set of vessels (arteries) and then returns to the heart in another (veins).

More specifically, it can be considered that there are two closed-loop systems that both originate and return to the heart—the pulmonary and systemic circulations (Fig. 1). The pulmonary circulation is composed of the right heart pump and the lungs, whereas the systemic circulation includes the left heart pump, which supplies blood to the systemic organs (i.e., all tissues and organs except the gas exchange portion of the lungs). Because the right and left heart pumps function in a series arrangement, both will circulate an identical volume of blood in a given minute (cardiac output, normally expressed in liters per minute).

In the systemic circuit, blood is ejected out of the left ventricle via a single large artery—the aorta. All arteries of the systemic circulation branch from the aorta (this is the largest artery of the body, with a diameter of 2–3 cm) and divide into progressively smaller vessels. The aorta's four principal divisions are: the ascending aorta (begins at the aortic valve, where, close by, the two coronary artery branches have their origin), the arch of the aorta, the thoracic aorta, and the abdominal aorta.

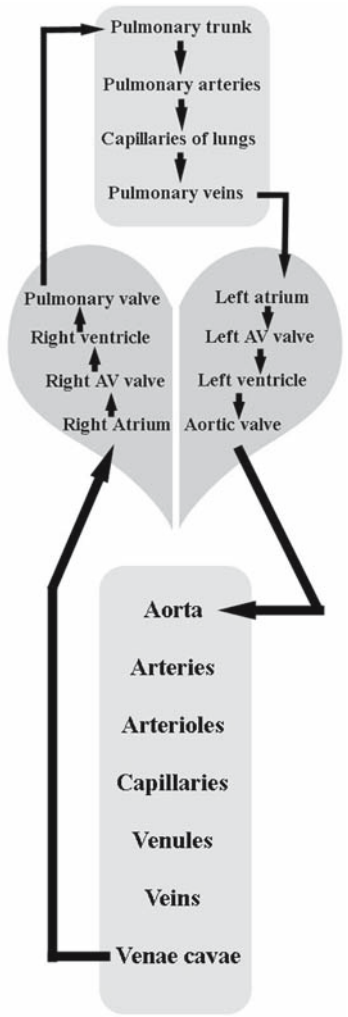

Fig. 1. The major paths of blood flow through pulmonary and systemic circulatory systems. AV, atrioventricular.

The smallest of the arteries eventually branch into arterioles. They, in turn, branch into an extremely large number (estimated at 10 billion in the average human body) of vessels with the smallest diameter, the capillaries. Next, blood exits the capillaries and begins its return to the heart via the venules. *Microcirculation* is a term coined to describe collectively the flow of blood through arterioles, capillaries, and venules (Fig. 2).

Importantly, blood flow through an individual vascular bed is profoundly regulated by changes in activity of the sympathetic nerves innervating the arterioles. In addition, arteriolar smooth muscle is very responsive to changes in local chemical conditions (i.e., those changes associated with increases or decreases in the metabolic rate of that given organ) within an organ.

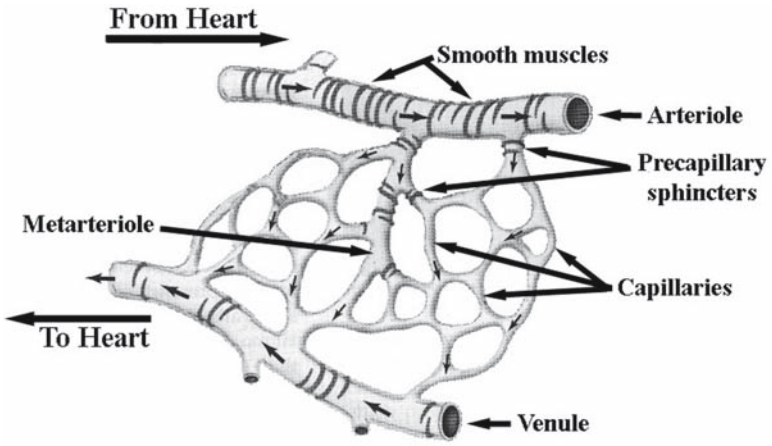

Fig. 2. The microcirculation, including arterioles, capillaries, and venules. The capillaries lie between, or connect, the arterioles and venules. They are found in almost every tissue layer of the body, but their distribution varies. Capillaries form extensive branching networks that dramatically increase the surface areas available for the rapid exchange of molecules. A metarteriole is a vessel that emerges from an arteriole and supplies a group of 10 to 100 capillaries. Both the arteriole and the proximal portion of the metarterioles are surrounded by smooth muscle fibers, which elicit contractions and relaxations so as to regulate blood flow through the capillary bed. Typically, blood flows intermittently through a capillary bed as a result of the periodic contractions of the smooth muscles (5–10 times per min; *vasomotion*), which are regulated both locally (metabolically) and by sympathetic control. (Figure modified from Tortora and Grabowski, 2000.)

Capillaries, which are the smallest and most numerous blood vessels in the human body (ranging from 5–10 μm in diameter and numbering around 10 billion), are also the vessels with the thinnest walls; an inner diameter of 5 μm is just wide enough for an erythrocyte to squeeze through. Further, it is estimated that there are 25,000 miles of capillaries in an adult; each capillary has an individual length of about 1 mm.

Most capillaries are little more than a single-cell-layer thick, consisting of a layer of endothelial cells and a basement membrane. This minimal wall thickness facilitates the capillary's primary function: to permit the exchange of materials between cells in tissues and the blood. As mentioned, small molecules (e.g., O_2, CO_2, sugars, amino acids, and water) are relatively free to enter and leave capillaries readily, promoting efficient material exchange. Nevertheless, the relative permeability of capillaries varies from region to region in the body with regard to the physical properties of their formed walls.

Based on such differences, capillaries are commonly grouped into two major classes: continuous and fenestrated. In the continuous capillaries, which are more common, the endothelial cells are joined such that the spaces between them are relatively narrow (i.e., narrow intercellular gaps). These capillaries are permeable to substances having small molecular sizes and/or high lipid solubilities (e.g., O_2, CO_2, and steroid hormones) and are somewhat less permeable to small water-soluble substances (e.g., Na^+, K^+, glucose, and amino acids). In fenestrated capillaries, the endothelial cells possess relatively large pores that are wide enough to allow proteins and other large molecules to pass through. In some such capillaries, the gaps between the endothelial cells are even wider than usual, enabling quite large proteins (or even small cells) to pass through. Fenestrated capillaries are primarily located in organs whose functions depend on the rapid movement of materials across capillary walls, e.g., kidneys, liver, intestines, and bone marrow.

If a molecule cannot pass between capillary endothelial cells, then it must be transported across the cell membrane. The mechanisms available for transport across a capillary wall differ for various substances depending on their molecular sizes and degree of lipid solubility. For example, certain proteins are selectively transported across endothelial cells by a slow, energy-requiring process known as *transcytosis*. In this process, the endothelial cells initially engulf the proteins in the plasma within capillaries by endocytosis. The molecules are then ferried across the cells by vesicular transport and released by exocytosis into the interstitial fluid on the other side. Endothelial cells generally contain large numbers of endocytotic and exocytotic vesicles, and sometimes these fuse to form continuous vesicular channels across the cell.

The capillaries within the heart normally prevent excessive movement of fluids and molecules across their walls, but clinical situations have been noted in which they may become "leaky." For example, "capillary leak syndrome," possibly induced following cardiopulmonary bypass, may last from hours to days. More specifically, in such cases, the inflammatory response in the vascular endothelium can disrupt the "gatekeeper" function of capillaries; their increased permeability will result in myocardial edema.

From capillaries, blood throughout the body then flows into the venous system. It first enters the venules, which then coalesce to form larger vessels, the veins (Fig. 2). Then veins from the various systemic tissues and organs (minus the gas exchange portion of the lungs) unite to produce two major veins: the inferior vena cava (lower body) and superior vena cava (above the heart). By way of these two great vessels, blood is returned to the right heart pump, specifically into the right atrium.

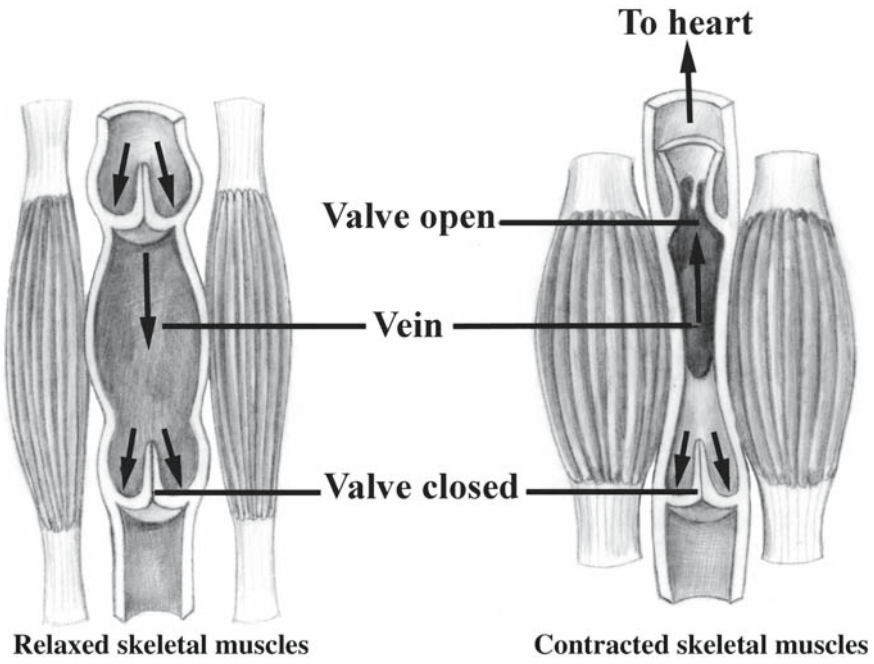

Fig. 3. Contractions of the skeletal muscles aid in returning blood to the heart; this is termed the *skeletal muscle pump*. While standing at rest, the relaxed vein acts as a reservoir for blood; contractions of limb muscles not only decrease this reservoir size (venous diameter), but also actively force the return of more blood to the heart. Note that the resulting increase in blood flow caused by the contractions is only toward the heart because of the valves in the veins.

Like capillaries, the walls of the smallest venules are very porous and are the sites from which many phagocytic white blood cells emigrate from the blood into inflamed or infected tissues. Venules and veins are also richly innervated by sympathetic nerves and smooth muscles that constrict when these nerves are activated. Thus, increased sympathetic nerve activity is associated with decreased venous volume, which results in increased cardiac filling and therefore increased cardiac output (via Starling's law of the heart).

Many veins, especially those in the limbs, also feature abundant valves (which are notably also found in the cardiac venous system), thin folds of the intervessel lining that form flaplike cusps. The valves project into the vessel lumen and are directed toward the heart (promoting unidirectional flow of blood). Because blood pressure is normally low in veins, these valves are important in aiding venous return by preventing the backflow of blood (which is especially true in the upright individual). In addition, contractions of skeletal muscles (e.g., in the legs) also play a role in decreasing the size of the venous reservoir and thus the return of blood volume to the heart (Fig. 3).

The pulmonary circulation is composed of a similar circuit. Blood leaves the right ventricle in a single great vessel, the pulmonary artery (trunk), which within a short distance (centimeters) divides into the two main pulmonary arteries, one supplying the right lung and another the left. Once within the lung proper, the arteries continue to branch down to arterioles and then ultimately form capillaries. From there, the blood flows into venules, eventually forming four main pulmonary veins that empty into the left atrium. As blood flows through the lung capillaries, it picks up oxygen supplied to the lungs by breathing air; hemoglobin within the red blood cells becomes loaded with oxygen (oxygenated blood).

2.3. Blood Flow

The task of maintaining an adequate interstitial homeostasis (the nutritional environment surrounding cells) requires that blood flows almost continuously through each of the millions of capillaries in the body. The following is a brief description of the parameters that govern flow through a given vessel. All bloods vessels have certain lengths L and internal radii r through which blood flows when the pressure in the inlet and outlet (P_i and P_o, respectively) are unequal; in other words, there is a pressure difference (ΔP) between the vessel ends that supplies the driving force for flow. Because friction develops between moving blood and the stationary vessel walls, this fluid movement has a given resistance (vascular) that is the measure of how difficult it is to create blood flow through a vessel. Then, a relative relationship among vascular flow, the pressure difference, and resistance (i.e., the basic flow equation) can be described:

$$\text{Flow} = \frac{\text{pressure difference}}{\text{resistance}} \quad \text{or} \quad Q = \frac{\Delta P}{R}$$

where Q is the flow rate (volume/time), ΔP is the pressure difference (mmHg), and R is the resistance to flow (mmHg $\times$ time/volume).

This equation may be applied not only to a single vessel, but also to describe flow through a network of vessels (i.e., the vascular bed of an organ or the entire systemic circulatory system). It is known that the resistance to flow through a cylindrical tube or vessel depends on several factors (described by Poiseuille), including (1) radius, (2) length, (3) viscosity of the fluid (blood), and (4) inherent resistance to flow, as follows:

$$R = \frac{8L\eta}{\pi r^4}$$

where r is the inside radius of the vessel, L is the vessel length, and η is the blood viscosity.

It is important to note that a small change in vessel radius will have a very large influence (fourth power) on its resistance to flow; for instance, decreasing the vessel diameter by 50% will increase its resistance to flow approx 16-fold.

If the preceding two equations are combined into one expression, which is commonly known as the Poiseuille equation, it can be used to approximate better the factors that influence flow though a cylindrical vessel:

$$Q = \Delta P \frac{\pi r^4}{8L\eta}$$

Nevertheless, flow will only occur when a pressure difference exists. Hence, it is not surprising that arterial blood pressure is perhaps the most regulated cardiovascular variable in the human body; this is principally accomplished by regulating the radii of vessels (e.g., arterioles and metarterioles) within a given tissue or organ system. Whereas vessel length and blood viscosity are factors that influence vascular resistance, they are not considered variables that can be easily regulated for the purpose of the moment-to-moment control of blood flow. Regardless, the primary function of the heart is to keep pressure within arteries higher than those in veins, hence creating a pressure gradient to induce flow. Normally, the average pressure in systemic arteries is approx 100 mmHg, and it decreases to nearly 0 mmHg in the great caval veins.

The volume of blood that flows through any tissue in a given period of time (normally expressed in milliliters/minute) is called the *local blood flow*. The velocity (speed) of blood flow (expressed in centimeters/second) can generally be considered inversely related to the vascular cross-sectional area such that velocity is slowest when the total cross-sectional area is largest.

2.4. Heart

The heart lies in the center of the thoracic cavity and is suspended by its attachment to the great vessels within a fibrous sac known as the pericardium; note that humans have relatively thick-walled pericardia compared to those of the commonly studied large mammalian cardiovascular models (i.e., canine, porcine, or ovine; *see also* Chapter 7). A small amount of fluid is present within the sac (pericardial fluid); it lubricates the surface of the heart and allows it to move freely during function (contraction and relaxation). The pericardial sac extends upward, enclosing the great vessels (*see also* Chapters 3 and 4).

The pathway of blood flow through the chambers of the heart is indicated in Fig. 4. Recall that venous blood returns from the systemic organs to the right atrium via the superior and inferior

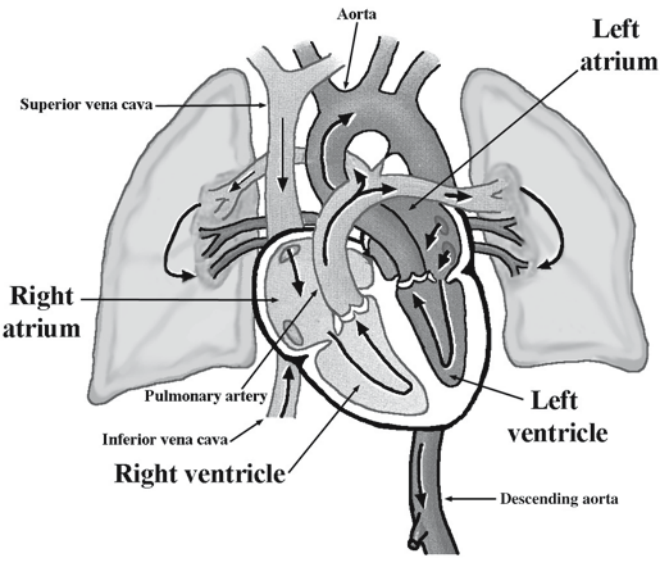

Fig. 4. Pathway of blood flow through the heart and lungs. Note that the pulmonary artery (trunk) branches into left and right pulmonary arteries. There are commonly four main pulmonary veins that return blood from the lungs to the left atrium. (Modified from Tortora and Grabowski, 2000.)

venae cavae. It next passes through the tricuspid valve into the right ventricles, and from there is pumped through the pulmonary valve into the pulmonary artery. After passing through the pulmonary capillary beds, the oxygenated pulmonary venous blood returns to the left atrium through the pulmonary veins. The flow of blood then passes through the mitral valve into the left ventricle and is pumped through the aortic valve into the aorta.

In general, the gross anatomy of the right heart pump is considerably different from that of the left heart pump; yet, the pumping principles of each are primarily the same. The ventricles are closed chambers surrounded by muscular walls, and the valves are structurally designed to allow flow in only one direction. The cardiac valves passively open and close in response to the direction of the pressure gradient across them.

The myocytes of the ventricles are organized primarily in a circumferential orientation; hence, when they contract, the tension generated within the ventricular walls causes the pressure within the chamber to increase. As soon as the ventricular pressure exceeds the pressure in the pulmonary artery (right) and/or aorta (left), blood is forced out of the given ventricular chamber. This active contractile phase of the cardiac cycle is known as *systole*. The pressures are higher in the ventricles than the atria during systole; hence, the tricuspid and mitral (atrioventricular) valves are closed. When the ventricular myocytes relax, the pressures in the ventricles fall below those in the atria, and the atrioventricular valves open; the ventricles refill, and this phase is known as *diastole*. The aortic and pulmonary (semilunar or outlet) valves are closed during diastole because the arterial pressures (in the aorta and pulmonary artery) are greater than the intraventricular pressures. For more details on the cardiac cycle, *see* Chapter 16.

The effective pumping action of the heart requires that there be a precise coordination of the myocardial contractions (millions of cells); this is accomplished via the conduction system of the heart. Contractions of each cell are normally initiated when electrical excitatory impulses (action potentials) propagate along their surface membranes. The myocardium can be viewed as a functional syncytium; action potentials from one cell conduct to the next cell via the gap junctions. In the healthy heart, the normal site for initiation of a heartbeat is within the sinoatrial node, located in the right atrium. For more details on this internal electrical system, refer to Chapter 9.

The heart normally functions in a very efficient fashion; the following properties are needed to maintain this effectiveness: (1) the contractions of the individual myocytes must occur at regular intervals and be synchronized (not arrhythmic); (2) the valves must fully open (not be stenotic); (3) the valves must not leak (not be insufficient or regurgitant); (4) the ventricular contractions must be forceful (not failing or lost because of an ischemic event); and (5) the ventricles must fill adequately during diastole (no arrhythmias or delayed relaxation). The subsequent chapters in this book cover normal and abnormal performance of the heart and various clinical treatments to enhance function.

2.5. Regulation of Cardiovascular Function

Cardiac output in a normal individual at rest ranges between 4 and 6 L/min, but during severe exercise the heart may be required to pump four to seven times this amount. There are two primary modes by which the blood volume pumped by the heart at any given moment is regulated: (1) intrinsic cardiac regulation in response to changes in the volume of blood flowing into the heart and (2) control of heart rate and cardiac contractility by the autonomic nervous system. The intrinsic ability of the heart to adapt to changing volumes of inflowing blood is known as the Frank–Starling mechanism (law) of the heart, named after the two great pioneering physiologists of a century ago.

In general, the Frank–Starling response can be described simply: The more the heart is stretched (increased blood volume), the greater will be the subsequent force of ventricular contraction and thus the amount of blood ejected through the semilunar valves (aortic and pulmonary). In other words, within its physiological limits, the heart will pump out all the blood that enters it without allowing excessive damming of blood in veins. The underlying basis for this phenomenon is related to the optimization of the lengths of sarcomeres (the functional subunits of striate muscle); there is optimization in the potential for the contractile proteins (actin and myosin) to form crossbridges. It should also be noted that "stretch" of the right atrial wall (e.g., because of increased venous return) can directly increase the rate of the sinoatrial node by 10–20%; this also aids in the amount of blood that will ultimately be pumped per minute by the heart. For more details on the contractile function of heart, refer to Chapter 8.

The pumping effectiveness of the heart is also effectively controlled by both the sympathetic and parasympathetic components of the autonomic nervous system. There is extensive innervation of the myocardium by such nerves (for more details of this innervation, *see* Chapter 10). To get a feel for how effective the modulation of the heart by this innervation is, it has been reported that the cardiac output often can be increased by more than 100% by sympathetic stimulation; in contrast, output can be nearly terminated by parasympathetic (vagal) stimulation.

Cardiovascular function is also modulated through reflex mechanisms that involve baroreceptors, the chemical composition of the blood, and/or via the release of various hormones. More specifically, baroreceptors, which are located in the walls of some arteries and veins, exist to monitor their relative blood pressure. Those specifically located in the carotid sinus help to maintain normal blood pressure reflexively in the brain, whereas those located in the area of the ascending arch of the aorta help to govern general systemic blood pressure (for more details, *see* Chapter 10).

Chemoreceptors that monitor the chemical composition of blood are located close to the baroreceptors of the carotid sinus and arch of the aorta in small structures known as the carotid and aortic bodies. The chemoreceptors within these bodies detect changes in blood levels of O_2, CO_2, and H^+. Hypoxia (a low availability of O_2), acidosis (increased blood concentrations of H^+), and/or hypercapnia (high concentrations of CO_2) stimulate the chemoreceptors to increase their action potential firing frequencies to the brain cardiovascular control centers. In response to this increased signaling, the central nervous system control centers (hypothalamus) in turn cause an increased sympathetic stimulation to arterioles and veins, producing vasoconstriction and a subsequent increase in blood pressure. In addition, the chemoreceptors simultaneously send neural input to the respiratory control centers in the brain to induce the appropriate control of respiratory function (e.g., increased O_2 supply and reduced CO_2 levels). It is beyond the scope of this book to discuss the details of the hormonal regulatory system, which include: (1) the renin–angiotensin–aldosterone system, (2) the release of epinephrine and norepinephrine, (3) antidiuretic hormones, and (4) atrial natriuretic peptides (released from the atrial heart cells).

The overall functional arrangement of the blood circulatory system is shown in Fig. 5. The role of the heart needs to be considered in three different ways: as the right pump, as the left pump, and as the heart muscle tissue with its own metabolic and flow requirements. As described here, the pulmonary (right heart) and systemic (left heart) circulations are arranged in a series. Thus, cardiac output increases in each at the same rate; hence, an increased systemic need for a greater cardiac output will automatically lead to a greater flow of blood through the lungs (inducing a greater potential for O_2 delivery).

In contrast, the systemic organs are functionally in a parallel arrangement; hence, (1) nearly all systemic organs receive blood with an identical composition (arterial blood), and (2) the flow through each organ can be and is controlled independently. For example, during exercise the circulatory response is an increase in blood flow through some organs (e.g., heart, skeletal muscle, and brain), but not others (e.g., kidney and gastrointestinal system). The brain, heart, and skeletal muscles typify organs in which blood flows solely to supply the metabolic needs of the tissue; they do not recondition the blood.

The blood flow to the heart and brain is normally only slightly greater than that required for their metabolism; hence, small

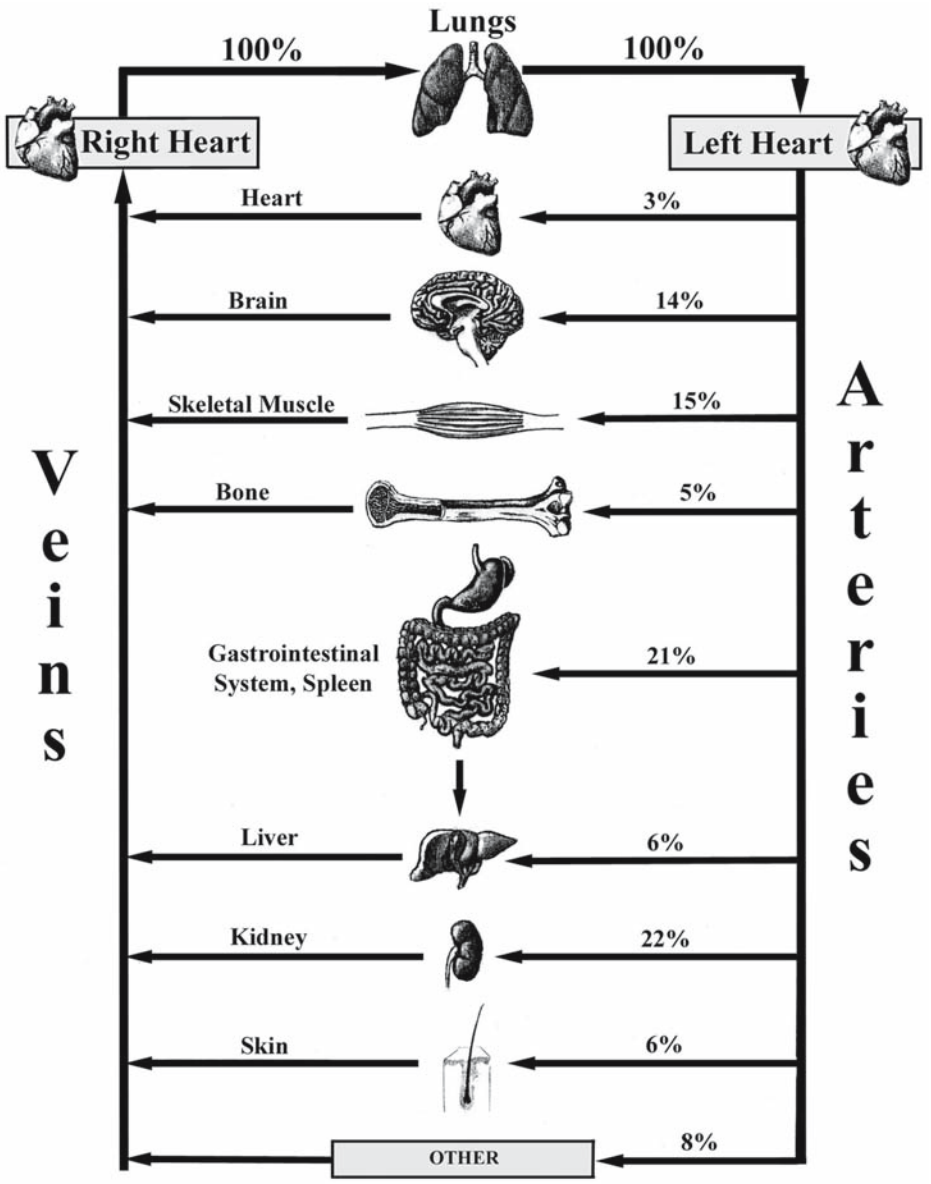

Fig. 5. A functional representation of the blood circulatory system at a given moment in time. The percentages indicate the approximate relative percentages of the cardiac output that is delivered to the major organ systems within the body of a healthy subject at rest.

interruptions in flow are not well tolerated. For example, if coronary flow to the heart is interrupted, electrical and/or functional (pumping ability) activities will be altered noticeably within a few beats. Likewise, stoppage of flow to the brain will lead to unconsciousness within a few seconds, and permanent brain damage can occur in as little as 4 min without flow. The flow to skeletal muscles can dramatically change (flow can increase from 20–70% of total cardiac output) depending on use, and thus their metabolic demand.

Many organs in the body perform the task of continually reconditioning the circulating blood. Primary organs performing such tasks include (1) the lungs (O_2 and CO_2 exchange); (2) the kidneys (blood volume and electrolyte composition, Na^+, K^+, Ca^{2+}, Cl^-, and phosphate ions); and (3) the skin (temperature). Blood-conditioning organs can often withstand, for short periods of time, significant reductions of blood flow without subsequent compromise.

2.6. Coronary Circulation

To sustain viability, it is not possible for nutrients to diffuse from the chambers of the heart through all the layers of cells that make up the heart tissue. Thus, the coronary circulation is responsible for delivering blood to the heart tissue itself (the myocardium). The normal heart functions almost exclusively as an aerobic organ with little capacity for anaerobic metabolism to produce energy. Even during resting conditions, 70–80% of the oxygen available in the blood circulating through the coronary vessels is extracted by the myocardium.

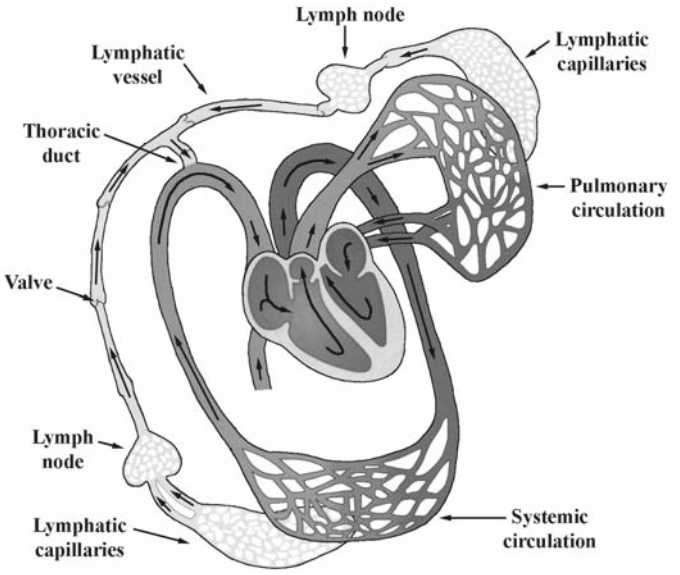

Fig. 6. Schematic diagram showing the relationship between the lymphatic system and the cardiopulmonary system. The lymphatic system is unidirectional, with fluid flowing from interstitial space back to the general circulatory system. The sequence of flow is from blood capillaries (systemic and pulmonary) to the interstitial space, to the lymphatic capillaries (lymph), to the lymphatic vessels, to the thoracic duct, into the subclavian veins (back to the right atrium). (Modified from Tortora and Grabowski, 2000.)

It then follows that, because of the limited ability of the heart to increase oxygen availability by further increasing oxygen extraction, increases in myocardial demand for oxygen (e.g., during exercise or stress) must be met by equivalent increases in coronary blood flow. Myocardial ischemia results when the arterial blood supply fails to meet the needs of the heart muscle for oxygen and/or metabolic substrates. Even mild cardiac ischemia can result in anginal pain, electrical changes (detected on an electrocardiogram), and the cessation of regional cardiac contractile function. Sustained ischemia within a given myocardial region will most likely result in an infarction.

As noted, as in any microcirculatory bed, the greatest resistance to coronary blood flow occurs in the arterioles. Blood flow through such vessels varies approximately with the fourth power of the radii of these vessels; hence, the key regulated variable for the control of coronary blood flow is the degree of constriction or dilatation of coronary arteriolar vascular smooth muscle. As with all systemic vascular beds, the degree of coronary arteriolar smooth muscle tone is normally controlled by multiple independent negative-feedback loops. These mechanisms include various neural, hormonal, and local nonmetabolic and local metabolic regulators.

It should be noted that the local metabolic regulators of arteriolar tone are usually the most important for coronary flow regulation; these feedback systems involve oxygen demands of the local cardiac myocytes. In general, at any point in time, coronary blood flow is determined by integrating all the different controlling feedback loops into a single response (i.e., inducing either arteriolar smooth muscle constriction or dilation). It is also common to consider that some of these feedback loops are in opposition. Interestingly, coronary arteriolar vasodilation from a resting state to one of intense exercise can result in an increase of mean coronary blood flow of approx 0.5–4.0 mL/min/g.

As with all systemic circulatory vascular beds, the aortic or arterial pressure (perfusion pressure) is vital for driving blood through the coronaries and thus needs to be considered another important determinant of coronary flow. More specifically, coronary blood flow varies directly with the pressure across the coronary microcirculation, which can be considered essentially as the aortic pressure because coronary venous pressure is typically near zero. However, because the coronary circulation perfuses the heart, some very unique determinants for flow through these capillary beds may also occur; e.g., during systole, myocardial extravascular compression causes coronary flow to be near zero, yet it is relatively high during diastole (note that this is the opposite of all other vascular beds in the body).

2.7. Lymphatic System

The lymphatic system represents an accessory pathway by which large molecules (e.g., proteins and long-chain fatty acids) can reenter the general circulation and thus not accumulate in the interstitial space. If such particles accumulate in the interstitial space, then filtration forces exceed reabsorptive forces, and edema occurs. Almost all tissues in the body have lymph channels that drain excessive fluids from the interstitial space (exceptions include portions of skin, the central nervous system, the endomysium of muscles, and bones with prelymphatic channels).

The lymphatic system begins in various tissues with blind-end specialized lymphatic capillaries that are roughly the size of regular circulatory capillaries, but they are less numerous (Fig. 6). However, the lymphatic capillaries are very porous and thus can easily collect the large particles within the interstitial fluid known as lymph. This fluid moves through the converging lymphatic vessels and is filtered through lymph nodes, in which bacteria and particulate matter are removed. Foreign particles that are trapped in the lymph nodes are destroyed (phagocytized) by tissue macrophages lining an inner meshwork of sinuses. Lymph nodes also contain T and B lymphocytes, which can destroy foreign substances by a variety of immune responses. There are approx 600 lymph nodes located along the lymphatic vessels; they are 1–25 mm long (bean shaped) and covered by a capsule of dense connective tissue. Lymph flow is unidirectional through the nodes (Fig. 6).

The lymphatic system is also one of the major routes for absorption of nutrients from the gastrointestinal tract (particularly for the absorption of fat and lipid-soluble vitamins A, D, E, and K). For example, after a fatty meal, lymph in the thoracic duct may contain as much as 1–2% fat.

The majority of lymph then reenters the circulatory system in the thoracic duct, which empties into the venous system at the juncture of the internal jugular and subclavian veins (which then enters into the right atrium; *see* Chapters 3 and 4). The flow of lymph from tissues toward the entry point into the circulatory system is induced by two main factors: (1) higher tissue inter-

stitial pressures and (2) the activity of the lymphatic pumps (contractions within the lymphatic vessels themselves, contractions of surrounding muscles, movement of parts of the body, and/or pulsations of adjacent arteries). In the largest lymphatic vessels (e.g., thoracic duct), the pumping action can generate pressures as high as 50–100 mm Hg. Valves located in the lymphatic vessel, like in veins, aid in the prevention of the backflow of lymph.

Approximately 2.5 L of lymphatic fluid enter the general blood circulation (cardiopulmonary system) each day. In the steady state, this indicates a total body net transcapillary fluid filtration rate of 2.5 L per day. When compared with the total amount of blood that circulates each day (approx 7000 L per day), this seems almost insignificant; however, blockage of such flow will quickly cause serious edema. Therefore, the lymphatic circulation plays a critical role in keeping the interstitial protein concentration low and in removing excess capillary filtrate from tissues throughout the body.

SOURCES

Alexander, R.W., Schlant, R.C., and Fuster, V. (eds.) (1998) *Hurst's the Heart, Arteries and Veins,* 9th Ed. McGraw-Hill, New York, NY.

Germann, W.J. and Stanfield, C.L. (eds.) (2002) *Principles of Human Physiology*. Pearson Education/Benjamin Cummings, San Francisco, CA.

Guyton, A.C. and Hall, J.E. (eds.) (2000) *Textbook of Medical Physiology,* 10th Ed. Saunders, Philadelphia, PA.

Mohrman, D.E. and Heller, L.J. (eds.) (2003) *Cardiovascular Physiology,* 5th Ed. McGraw-Hill, New York, NY.

Tortora, G.J. and Grabowski, S.R. (eds.) (2000) *Principles of Anatomy and Physiology,* 9th Ed. Wiley, New York, NY.

ANATOMY II

2 Cardiac Development

BRAD J. MARTINSEN, PhD AND JAMIE L. LOHR, MD

CONTENTS

1. INTRODUCTION TO HUMAN HEART EMBRYOLOGY AND DEVELOPMENT

The primary heart field, secondary heart field, cardiac neural crest, and proepicardium are the four major embryonic regions involved in the process of vertebrate heart development (Fig. 1). They each make an important contribution to overall cardiac development, which occurs with complex developmental timing and regulation. This chapter describes how these regions interact to form the final structure of the heart in relationship to the generalized developmental timeline of human embryology (Table 1).

The heart is the first organ to fully form and function during vertebrate development, and many of the underlying mechanisms are considered molecularly and developmentally conserved *(1)*. The description presented here is based on heart development research from the chick, mouse, frog, and human model systems. Importantly, numerous research findings have redefined the understanding of the primary heart field, which gives rise to the main structure of the heart (atria and ventricles) and have led to exciting discoveries of the secondary heart field, which gives rise to the outflow tracts of the mature heart *(2–4)*. These discoveries were a critical step in advancing our understanding of how the outflow tracts of the heart form, an area in which many congenital heart defects arise, and thus have had important implications for the understanding and prevention of human congenital heart disease *(5)*. In addition, great strides have also been made in our knowledge of the contribution of the cardiac neural crest and the epicardium to overall heart development.

From: *Handbook of Cardiac Anatomy, Physiology, and Devices*
Edited by: P. A. Iaizzo © Humana Press Inc., Totowa, NJ

2. PRIMARY HEART FIELD AND LINEAR HEART TUBE FORMATION

The cells that will become the heart are among the first cell lineages formed in the vertebrate embryo *(6,7)*. By day 15 of human development, the primitive streak has formed *(8)*, and the first mesodermal cells to migrate (gastrulate) through the primitive streak are cells fated to become the heart *(9,10)* (Fig. 2). These mesodermal cells migrate to an anterior and lateral position where they form bilateral primary heart fields (Fig. 1A) *(11)*. Studies of chick development have not supported the previously held notion of a medial cardiac crescent that bridges the two bilateral primary heart fields *(12)*. Complete comparative molecular and developmental studies between the chick and mouse are required to confirm these results. The posterior border of the bilateral primary heart field reaches to the first somite in the lateral mesoderm on both sides of the midline (Fig. 1A) *(3,12)*.

At day 18 of human development, the lateral plate mesoderm is split into two layers: somatopleuric and splanchnopleuric *(8)*. It is the splanchnopleuric mesoderm layer that contains the myocardial and endocardial cardiogenic precursors in the region of the primary heart fields as defined above.

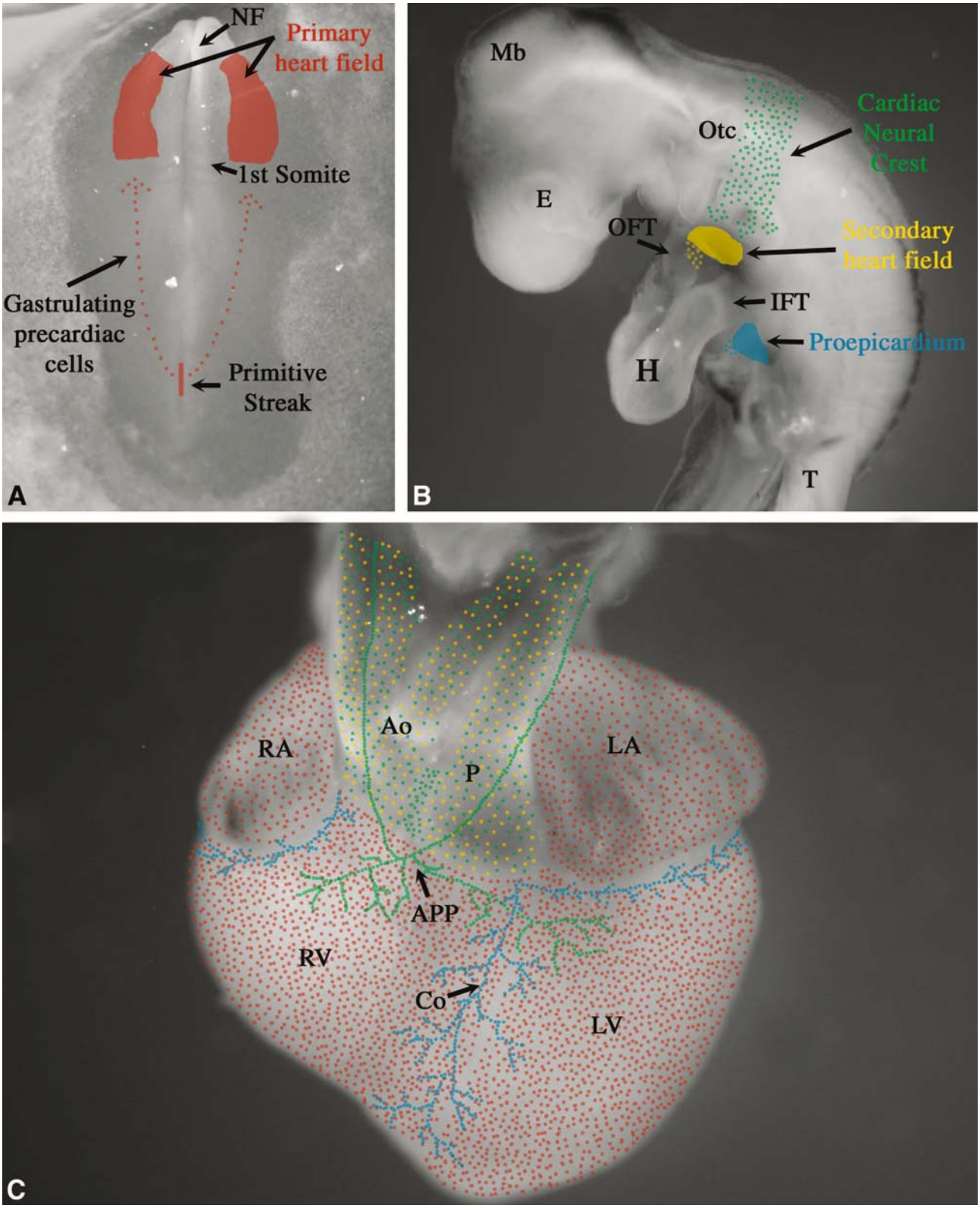

Fig. 1. The four major contributors to heart development illustrated in the chick model system: primary heart field, secondary heart field, cardiac neural crest, and proepicardium. **(A)** Day 1 chick embryo (equivalent to day 20 of human development). Red denotes primary heart field cells. **(B)** Day 2.5 chick embryo (equivalent to ~5 wk of human development). Green denotes cardiac neural crest cells; yellow denotes secondary heart field cells; blue denotes proepicardial cells. **(C)** Day 8 chick heart (equivalent to ~9 wk of human development). Green dots represent derivatives of the cardiac neural crest; yellow dots represent derivatives of the secondary heart field; red dots represent derivatives of the primary heart fields; blue dots represent the derivatives of the proepicardium. Ao, aorta; APP, anterior parasympathetic plexis; Co, coronary vessels; E, eye; H, heart; IFT, inflow tract; LA, left atrium; LV, left ventricle; Mb, midbrain; NF, neural folds; OFT, outflow tract; Otc, otic placode; P, pulmonary artery; RA, right atrium; RV, right ventricle; T, trunk.

Table 1
Developmental Timeline of Human Heart Embryology

Days of human development	*Developmental process*
0	Fertilization.
1–4	Cleavage and movement down the oviduct to the uterus.
5–12	Implantation of the embryo into the uterus.
13–14	Primitive streak formation (midstreak level contains precardiac cells).
15–17	Formation of the three primary germ layers (gastrulation): ectoderm, mesoderm, and endoderm. Midlevel primitive streak cells that migrate to an anterior and lateral position form the bilateral *primary heart field*.
17–18	Lateral plate mesoderm splits into the somatopleuric mesoderm and splanchnopleuric mesoderm. Splanchnopleuric mesoderm contains the myocardial and endocardial cardiogenic precursors in the region of the primary heart field.
18–26	Neurulation (formation of the neural tube)
20	Cephalocaudal and lateral folding brings the bilateral endocardial tubes into the ventral midline of the embryo.
21–22	Heart tube fusion.
22	Heart tube begins to beat.
22–28 (3–4 wk)	Heart looping and the accretion of cells from the *primary* and *secondary heart fields*.
22–28 (3–4 wk)	*Proepicardial cells* invest the outer layer of the heart tube and eventually form the epicardium and coronary vasculature.
22–28 (3–4 wk)	Neural crest migration starts.
32–37 (5–6 wk)	*Cardiac neural crest* migrates through the aortic arches and enters the outflow tract of the heart.
57+ (9 wk)	Outflow tract and ventricular septation complete.
Birth	Functional septation of the atrial chambers as well as the pulmonary and systemic circulatory systems.

Most of the human developmental timing information is from ref. *8*, except for the human staging of the secondary heart field and proepicardium, which was correlated from other model systems *(2–4,14)*.

Presumptive endocardial cells delaminate from the splanchnopleuric mesoderm and coalesce via vasculogenesis to form two lateral endocardial tubes (Fig. 2A) *(13)*.

During the third week of human development, two bilateral layers of myocardium surrounding the endocardial tubes are brought into the ventral midline during closure of the ventral foregut via cephalic and lateral folding of the embryo (Fig. 2A) *(8)*. The lateral borders of the myocardial mesoderm layers are the first heart structures to fuse, followed by the fusion of the two endocardial tubes to form one endocardial tube surrounded by splanchnopleuric-derived myocardium (Fig. 2B,C). The medial borders of the myocardial mesoderm layers are the last to fuse *(14)*. Thus, the early heart is continuous with noncardiac splanchnopleuric mesoderm across the dorsal mesocardium (Fig. 2C). This will eventually partially break down to form the ventral aspect of the linear heart tube with a posterior inflow (venous pole) and anterior outflow (arterial pole), as well as the dorsal wall of the pericardial cavity *(5,14)*. During the fusion of the endocardial tubes, the myocardium secretes an acellular matrix, forming the cardiac jelly layer that separates the myocardium and endocardium.

By day 22 of human development, the linear heart tube begins to beat. As the human heart begins to fold and loop from days 22–28 (described in the next section), epicardial cells will invest the outer layer of the heart tube (Fig. 1B and Fig. 3A), resulting in a heart tube with four primary layers: endocardium, cardiac jelly, myocardium, and epicardium (Fig. 3B) *(8)*.

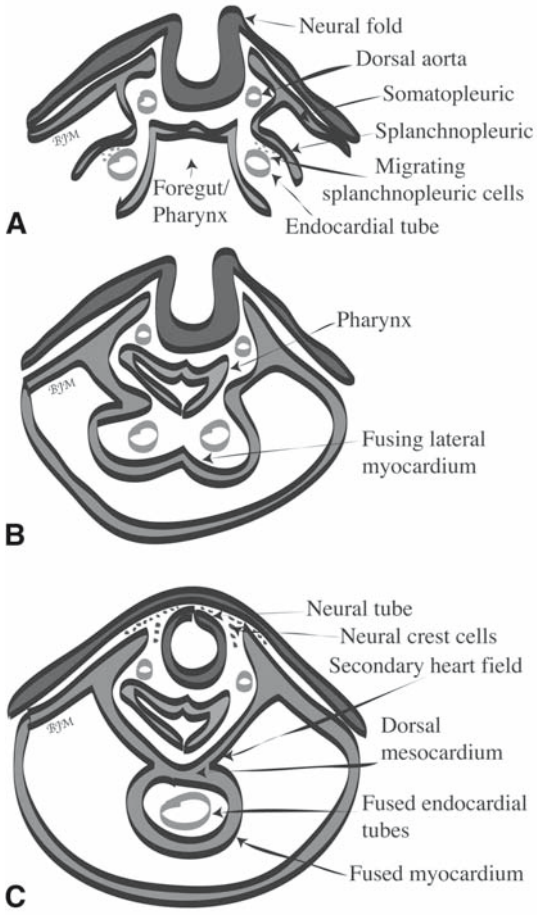

Fig. 2. Cross-sectional view of human heart tube fusion. **(A)** Day 20, cephalocaudal and lateral folding brings bilateral endocardial tubes into the ventral midline of the embryo. **(B)** Day 21, start of heart tube fusion. **(C)** Day 22, complete fusion, resulting in the beating primitive heart tube. Ectoderm, dark gray; mesoderm, gray; endoderm, white.

3. SECONDARY HEART FIELD, OUTFLOW TRACT FORMATION, AND CARDIAC LOOPING

A cascade of signals identifying the left and right sides of the embryo are thought to initiate the process of primary linear

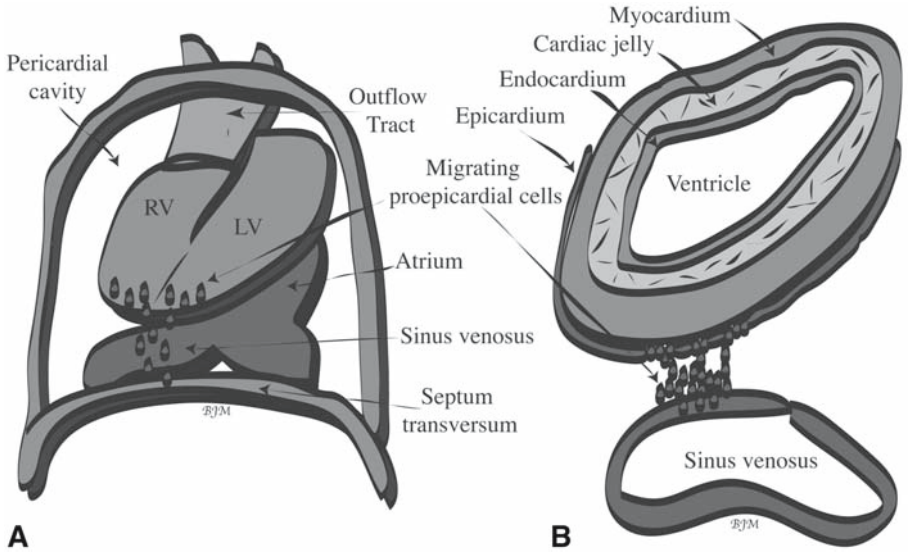

Fig. 3. Origin and migration of proepicardial cells. **(A)** Whole mount view of the looping human heart within the pericardial cavity at day 28. Proepicardial cells (dark gray dots, mesoderm origin) emigrate from the sinus venosus and possibly the septum transversum and then migrate out over the outer surface of the ventricles, eventually surrounding the entire heart. **(B)** Cross-sectional view of the looping heart showing the four layers of the heart: epicardium, myocardium, cardiac jelly, and endocardium. LV, left ventricle; RV, right ventricle.

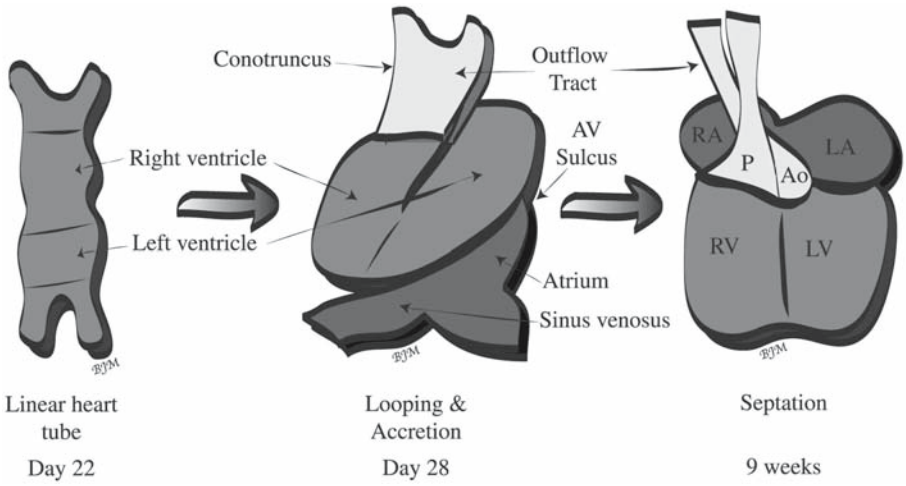

Fig. 4. Looping and septation of the human primary linear heart tube. Dark gray and white regions represent tissue added during the looping process from the primary and secondary heart field, respectively. Ao, aorta; AV, atrioventricular region; LA, left atrium; LV, left ventricle; P, pulmonary artery; RA, right atrium; RV, right ventricle.

heart tube looping *(15)*. The primary heart tube loops to the right of the embryo and bends, to allow convergence of the inflow (venous) and outflow (arterial) ends, from days 22–28 of human development (Fig. 4). This process occurs prior to the division of the heart tube into four chambers and is required for proper alignment and septation of the mature cardiac chambers.

During the looping process, the primary heart tube increases dramatically in length (four- to fivefold), and this process displaces atrial myocardium posteriorly and superiorly dorsal to the forming ventricular chambers *(5,8,15)*. During the looping process, the inflow (venous) pole, atria, and atrioventricular region are added to, or accreted from, the posterior region of the paired primary heart fields; the myocardium of proximal outflow tract (conus) and distal outflow tract (truncus) are added to the arterial pole from the secondary heart field *(2–4)*.

The secondary heart field (Fig. 1B and Fig. 2C) is located along the splanchnopleuric mesoderm (beneath the floor of the foregut) at the attachment site of the dorsal mesocardium *(2–4,14)*. During looping, the secondary heart field cells undergo epithelial-to-myocardial transformation at the outflow (arterial) pole and add additional myocardial cells onto the developing outflow tract. This lengthening of the primary heart tube appears to be an important process for the proper alignment of the inflow and outflow tracts prior to septation. If this process does not occur normally, ventricular septal defects and malpositioning of the aorta may occur *(14)*.

Thus, by day 28 of human development, the chambers of the heart are in position and are demarcated by visible constrictions and expansions that denote the sinus venosus, common atrial chamber, atrioventricular sulcus, ventricular chamber, and conotruncus (proximal and distal outflow tract) (Fig. 4) *(8,14)*.

4. CARDIAC NEURAL CREST AND OUTFLOW TRACT AND ATRIAL AND VENTRICULAR SEPTATION

Once the chambers are in their correct positions after looping, extensive remodeling of the primitive vasculature and septation of the heart can occur. The cardiac neural crest is an extracardiac (from outside the primary or secondary heart fields) population of cells that arises from the neural tube in the region of the first three somites up to the midotic placode level (rhombomeres 6–8) (Fig. 5). Cardiac neural crest cells leave the neural tube during weeks 3–4 of human development and migrate through aortic arches 3, 4, and 6 (Fig. 1B) and then eventually move into the developing outflow tract of the heart during weeks 5 and 6. These cells are necessary for complete septation of the outflow tract and ventricles (which is completed by week 9 of human development), as well as for the formation of the anterior parasympathetic plexis, which contributes to cardiac innervation and the regulation of heart rate *(8,16–18)*.

The primitive vasculature of the heart is bilaterally symmetrical, but during weeks 4 to 8 of human development, there is remodeling of the inflow end of the heart so that all systemic blood will flow into the future right atrium *(8)*. In addition, there is extensive remodeling of the initially bilaterally symmetrical aortic arch arteries into the great arteries (septation of the aortic and pulmonary vessels) that is dependent on the presence of the cardiac neural crest *(14,19)*. The distal outflow tract (truncus) *septates* into the aorta and pulmonary trunk via the fusion of two streams or prongs of cardiac neural crest that migrate into the distal outflow tract. In contrast, the proximal outflow tract septates by fusion of the endocardial cushions and eventually joins proximally with the atrioventricular endocardial cushion tissue and the ventricular septum *(20,21)*. The endocardial cushions are formed by both atrioventricular canal and outflow tract endocardial cells that migrate into the cardiac jelly, forming bulges or cushions.

Despite its clinical importance, to date almost nothing is known about the molecular pathways that determine cell lineages in the cardiac neural crest or that regulate outflow tract septation *(14)*. However, it is known that if the cardiac neural crest is removed before it begins to migrate, the conotruncal septa completely fails to develop, and blood leaves both the ventricles through what is termed a *persistent truncus arteriosus*, a rare congenital heart anomaly in humans. Failure of outflow tract septation may also be responsible for other forms of congenital heart disease, including transposition of the great vessels, high ventricular septal defects, and tetralogy of Fallot *(8,16,18)*.

The septation of the outflow tract (conotruncus) is tightly coordinated with the septation of both the ventricles and atria to produce a functional heart. All of these septa eventually fuse with the atrioventricular cushions, which also divide the left and right atrioventricular canals and serve as the source of cells for the atrioventricular valves. Prior to septation, the right atrioventricular canal and right ventricle expand to the right, causing a realignment of the atria and ventricles so that they are directly over each other. This allows venous blood entering from the sinus venosus to flow directly from the right atrium to the presumptive right ventricle without flowing through the presumptive left atrium and ventricle *(8,14)*. The new alignment also simultaneously provides the left ventricle with a direct outflow path to the truncus arteriosus and subsequently to the aorta.

Between weeks 4 and 7 of human development, the left and right atria undergo extensive remodeling and are eventually septated. However, during the septation process, a right-to-left shunting of oxygenated blood (oxygenated by the placenta) is created via shunts, ducts, and foramens (Fig. 6). Prior to birth,

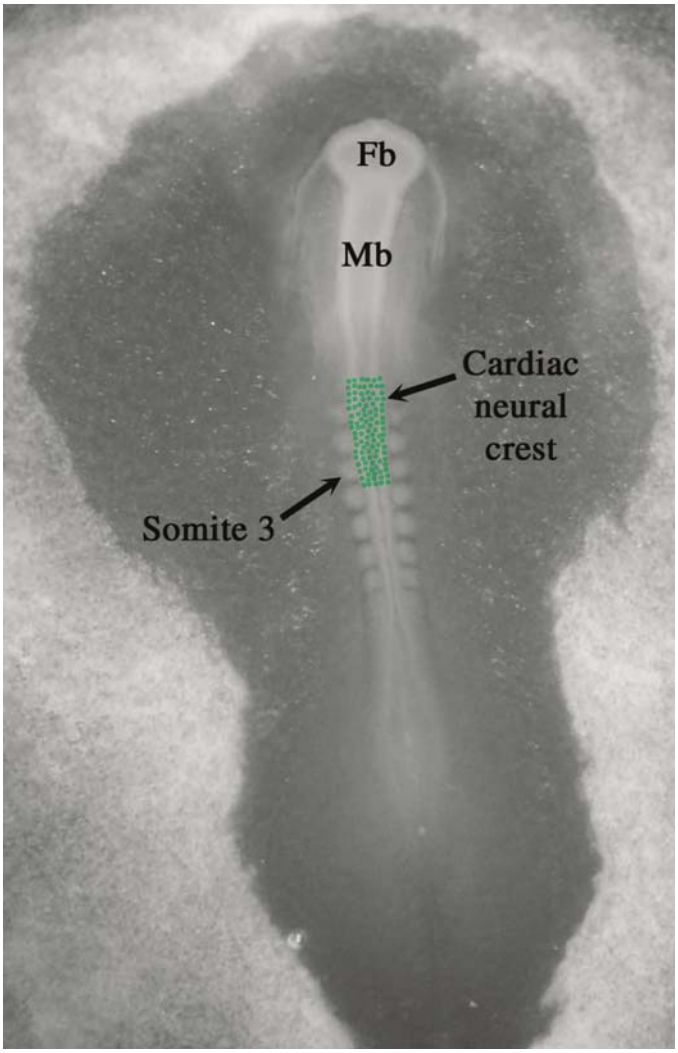

Fig. 5. Origin of the cardiac neural crest within a 34-h chick embryo. Green dots represent cardiac neural crest cells in the neural folds of hindbrain rhombomeres 6–8 (the region of the first three somites up to the midotic placode level). Fb, forebrain; Mb, midbrain.

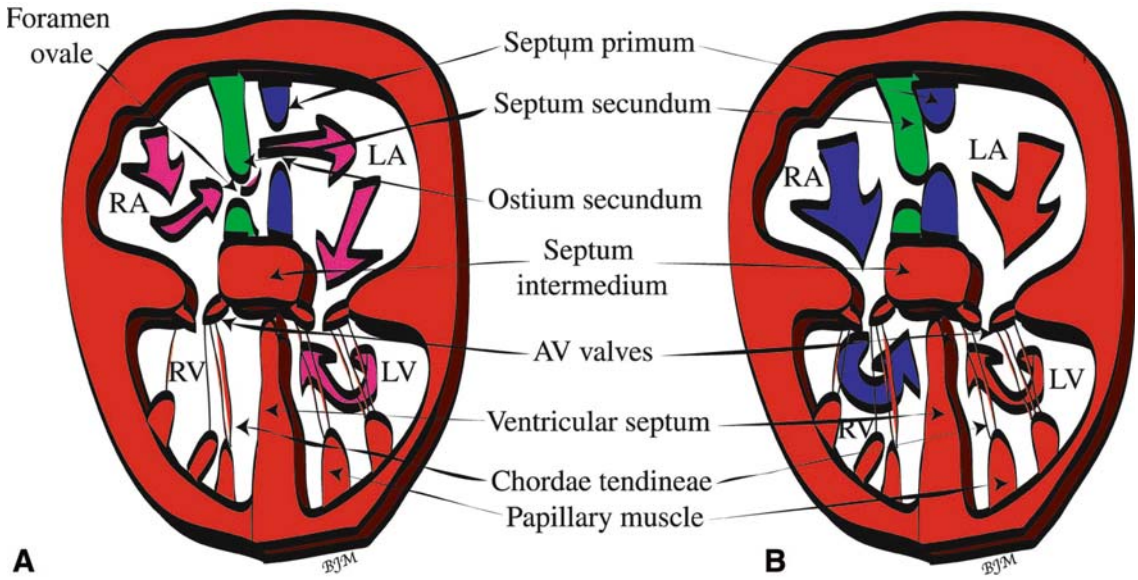

Fig. 6. Transition from fetal dependence on the placenta for oxygenated blood to self-oxygenation via the lungs. **(A)** Circulation in the fetal heart before birth. Pink arrows show right-to-left shunting of placentally oxygenated blood through the foramen ovale and ostium secundum. **(B)** Circulation in the infant heart after birth. The first breath of the infant and cessation of blood flow from the placenta cause final septation of the heart chambers (closure of the foramen ovale and ostium secundum) and thus separation of the pulmonary and systemic circulatory systems. Blue arrows show the pulmonary circulation, and the red arrows show the systemic circulation within the heart. AV, atrioventricular; LA, left atrium; LV, left ventricle; RA, right atrium; RV, right ventricle.

the use of the pulmonary system is not necessary, but eventually a complete separation of the systemic and pulmonary circulatory systems will be necessary for normal cardiac and systemic function *(8)*. Initially, the right sinus horn is incorporated into the right posterior wall of the primitive atrium, and the trunk of the pulmonary venous system is incorporated into the posterior wall of the left atrium via a process called *intussusception*.

At day 26 of human development, a crescent-shaped wedge of tissue, called the *septum primum*, begins to extend into the atrium from the mesenchyme of the dorsal mesocardium. As it grows, it diminishes the ostium primum, a foramen that allows shunting of blood from the right to the left atrium. However, programmed cell death near the superior edge of the septum primum creates a new foramen, the ostium secundum, which continues the right-to-left shunting of oxygenated blood. An incomplete, ridged septum secundum with a foramen ovale near the floor of the right atrium forms next to the septum primum; both fuse with the septum intermedium of the atrioventricular cushions *(8)*.

At the same time as atrial septation is beginning, at about the end of the fourth week of human development, the muscular ventricular septum begins to grow toward the septum intermedium (created by the fusion of the atrioventricular cushions), creating a partial ventricular septum. By the end of the ninth week of human development, the outflow tract septum has grown down onto the upper ridge of this muscular ventricular septum and onto the inferior endocardial cushion, which completely separates the right and left ventricular chambers.

Not until after birth, however, does the heart become functionally septated in the atrial region. At birth, dramatic changes in the circulatory system occur because of the transition from fetal dependence on the placenta for oxygenated blood to self-oxygenation via the lungs. During fetal life, only small amounts of blood are flowing through the pulmonary system because the fluid-filled lungs create high resistance, resulting in low-pressure and low-volume flow into the left atrium from the pulmonary veins. This allows the high-volume blood flow coming from the placenta to pass through the inferior vena cava into the right atrium, where it is then directed across the foramen ovale into the left atrium. The oxygenated blood then flows into the left ventricle and directly out to the body via the aorta. At birth, the umbilical blood flow is interrupted, stopping the high-volume flow from the placenta. In addition, the alveoli and pulmonary vessels open when the infant takes its first breath, dropping the resistance in the lungs and allowing more flow into the left atrium from the lungs. This reverse in pressure difference between the atria pushes the flexible septum primum against the ridged septum secundum and closes the foramen ovale and ostium secundum, resulting in the complete septation of the heart chambers (Fig. 6) *(8)*.

5. PROEPICARDIUM AND CORONARY ARTERY DEVELOPMENT

The last major contributor to vertebrate heart development discussed in this chapter is the proepicardium. Prior to heart looping, the primary heart tube consists of endocardium, cardiac jelly, and myocardium. It is not until the start of heart looping that the epicardium surrounds the myocardium, forming the fourth layer of the primary heart tube (Fig. 3) *(22)*. This population of cells will eventually give rise to the coronary

vasculature. A neural crest origin of the coronary vessels was originally hypothesized, but lineage tracing studies have shown that the neural crest gives rise to cells of the tunica media of the aortic and pulmonary trunks, but not to the coronary arteries *(13,23)*. These investigators also concluded that the coronary vasculature is derived from the proepicardial organ, a nest of cells in the dorsal mesocardium of the sinus venosus or septum transversum. These cells, which are derived from an independent population of splanchnopleuric mesoderm cells, migrate onto the primary heart tube between day 22 and day 28 of human development (Fig. 3), just as the heart begins its looping *(8,14)*. Prior to migration, these cells are collectively called the proepicardium or the proepicardial organ.

Interestingly, three lineages of the coronary vessel cells (smooth muscle, endothelial, and connective tissue cells) are segregated in the proepicardium prior to migration into the heart tube *(13,24)*. These cells will coalesce to form coronary vessels *de novo* via the process of vasculogenesis *(25)*. It has also been shown that the epicardium provides an intrinsic factor needed for normal myocardial development and is a source of cells needed for forming the interstitial myocardium and cushion mesenchyme *(14,26)*. It should be noted that an understanding of the embryological origin of the vascular system and its molecular regulation is thought to be important in helping to explain the varying susceptibility of different components of the vascular system to atherosclerosis *(13,27)*.

6. CARDIAC MATURATION

Although the embryonic heart is fully formed and functional by the 11th week of pregnancy, the fetal and neonatal heart continue to grow and mature rapidly, with many clinically relevant changes taking place after birth. During fetal development, or from the time after the embryo is completely formed in the first trimester of pregnancy until birth, the heart grows primarily by the process of cell division *(28–31)*. Within a few weeks after birth, the predominant mechanism of cardiac growth is cell hypertrophy; in other words, existing cardiac cells become larger rather than increasing significantly in number *(28–30)*.

The exact timing of this process and the mechanisms regulating these changes are not yet completely elucidated. In the classic explanation, mature cardiac cells lose the ability to divide; however, more recent work suggests that a limited amount of cell division can occur in adult human hearts damaged by ischemia *(32)*. This finding has led to a renewed interest in understanding the regulation of cell division during cardiac maturation. Additional maturational changes in both the fetal and neonatal heart include alterations in the composition of cardiac muscle, differences in energy production, and maturation of the contractile function. These changes, along with associated physiological changes in the transitional circulation, as discussed in Section 4, affect the treatments of newborns with congenital heart disease, particularly those requiring interventional procedures or cardiac surgery.

The hemodynamic changes associated with birth include a significant increase in left ventricular cardiac output to meet the increased metabolic needs of the newborn infant. This improvement in cardiac output occurs despite the fact that the neonatal myocardium has less muscle mass and less cellular organization than the mature myocardium. The newborn myocardium consists of 30% contractile proteins and 70% noncontractile mass (membranes, connective tissues, and organelles), in contrast to the adult myocardium, which is 60% contractile mass *(30)*. The myocardial cells of the fetus are rounded, and both the myocardial cells and myofibrils within them are oriented randomly. As the fetal heart matures, these myofibrils increase in size and number and orient to the long axis of the cell, which further contributes to improved myocardial function *(28)*. The fetal myocardial cell contains higher amounts of glycogen than the mature myocardium, suggesting a higher dependence on glucose for energy production; in experiments in nonprimate model systems, the fetal myocardium is able to meet its metabolic needs with lactate and glucose as the only fuels *(33)*. In contrast, the preferred substrate for energy metabolism in the adult heart is long-chain fatty acids, although the adult heart is able to utilize carbohydrates as well *(33,34)*. This change is considered to be triggered in the first few days or weeks of life by an increase in serum long-chain fatty acids with feeding, but the timing and clinical impact of this transition relative to an ill or nonfeeding neonate with cardiovascular disease is currently unknown.

In addition, the maturing myocardial cells undergo changes in the expression of their contractile proteins, which may be responsible for some of the maturational differences in cardiovascular function. Changes in expression of contractile proteins that may be important in humans include a gradual increase in the expression of myosin light chain 2 (MLC 2) in the ventricle from the neonatal period through adolescence. In the fetal ventricle, two forms of myosin light chain, MLC 1 and MLC 2, are expressed in equal amounts *(30,35)*. Increased MLC 1 expression is associated with increased contractility; for example, it has been documented in isolated muscle from patients with tetralogy of Fallot that both MLC 1 expression and contractility are increased *(36)*. After birth, there is a gradual increase in the amount of MLC 2, or the "regulatory" myosin light chain, which has a slower rate of force development but can be phosphorylated to increase calcium-dependent force development in mature cardiac muscle *(30,37)*.

There is also variability in actin isoform expression during cardiac development. The human fetal heart predominantly expresses cardiac α-actin; the more mature human heart expresses skeletal α-actin *(28,38)*. Actin is responsible for interacting with myosin cross bridges and regulating adenosine triphosphatase (ATPase) activity, and work done in the mouse model system suggests that the change to skeletal actin may be an additional mechanism of enhanced contractility in the mature heart *(28,39,40)*.

There are also developmental changes of potential functional significance within the regulatory proteins of the sarcomere. More specifically, the fetal heart expresses both α- and β-tropomyosin, a regulatory filament, in nearly equal amounts; after birth, the proportion of β-tropomyosin decreases, and α-tropomyosin increases, potentially to optimize diastolic relaxation *(28,41,42)*. Interestingly, an expression of high levels of β-tropomyosin in the neonatal heart has been linked to early death caused by myocardial dysfunction *(43)*.

Last, the isoform of the inhibitory troponin, troponin I, also changes after birth. The fetal myocardium contains mostly the skeletal isoform of troponin I *(28,44)*; after birth, the myocardium begins to express cardiac troponin I, and by approx 9 mo of age, only cardiac troponin I is present *(28,45,46)*. It should also be noted that cardiac troponin I can be phosphorylated to improve calcium responsivity and contractility, which may improve function in the more mature heart; it is thought that the skeletal form of troponin I may serve to protect the fetal and neonatal myocardium from acidosis *(30,39,47)*.

In summary, the full impact of these developmental changes in contractile proteins and their effect on cardiac function or perioperative treatment of the newborn with heart disease remains unclear at the present time. However, such insights may provide future modes for optimizing therapy in children.

Two of the most clinically relevant features of the immature myocardium are its requirement for high levels of extracellular calcium and a decreased sensitivity to β-adrenergic inotropic agents. The neonatal heart has a decrease in both volume and functional maturity of the sarcoplasmic reticulum, which stores intracellular calcium *(28)*. The paucity of intracellular calcium storage and subsequent release via the sarcoplasmic reticulum in the fetal and neonatal myocardium increases the requirements of these myocardia for extracellular calcium, so that exogenous administration of calcium can be used to augment cardiac contractility in the appropriate clinical setting. In addition, neonates and infants are significantly more sensitive to calcium channel blocking drugs than older children and adults and thus are at a higher risk for severe depression of myocardial contractility with the administration of these agents *(28,30,48)*.

Last, although data in humans are limited, there appears to be significantly decreased sensitivity to β-agonist agents in the immature myocardium and in older children with congenital heart disease *(30,49–51)*. This may be attributable to a paucity of receptors, sensitization to endogenous catecholamines at birth or with heart failure, or a combination of these and/or additional factors. Because of this decreased responsiveness to β-agonists, there is a common requirement clinically for administrating higher doses of β-agonist inotropic agents in newborns and infants. Importantly, alternative medications, including phosphodiesterase inhibitors, are often useful adjuncts to improve contractility in newborns with myocardial dysfunction *(30)*.

Although the structure of the heart is complete in the first trimester of pregnancy, cardiac growth and maturation occur in the fetus, newborn, and child. Many of these developmental changes, particularly decreased intracellular calcium stores in the immature sarcoplasmic reticulum and a decreased responsiveness to β-agonist inotropic agents, have a significant impact on the care of newborns, infants, and children with congenital heart disease, particularly those requiring surgical intervention early in life.

7. SUMMARY OF EMBRYONIC CONTRIBUTION TO HEART DEVELOPMENT

The contribution of the four major embryonic regions (primary heart field, secondary heart field, cardiac neural crest, and proepicardium; Fig. 1) to heart development illustrates the complexity of human heart development. Each of these regions makes a unique contribution to the heart, but they ultimately depend on each other for the creation of a fully functional organ.

An understanding of the mechanisms of human heart development provides clues to the etiology of congenital heart disease. Nevertheless, to date, the genetic regulatory mechanisms of these developmental processes are just starting to be characterized. A molecular review of heart development is outside the scope of this chapter, but several interesting molecular heart reviews have been published *(14,52,53)*. A better understanding of the embryological origins of the heart combined with the characterization of the genes that control heart development *(54)* may lead to many new clinical applications to treat congenital and adult heart disease.

REFERENCES

1. Srivastava, D. and Olson, E.N. (2000) A genetic blueprint for cardiac development. *Nature*. 407, 221–226.
2. Kelly, R.G., Brown, N.A., and Buckingham, M.E. (2001) The arterial pole of the mouse heart forms from Fgf10-expressing cells in pharyngeal mesoderm. *Dev Cell*. 1, 435–440.
3. Mjaatvedt, C.H., Nakaoka, T., Moreno-Rodriguez, R., et al. (2001) The outflow tract of the heart is recruited from a novel heart-forming field. *Dev Biol*. 238, 97–109.
4. Waldo, K.L., Kumiski, D.H., Wallis, K.T., et al. (2001) Conotruncal myocardium arises from a secondary heart field. *Development*. 128, 3179–3188.
5. Kelly, R.G. and Buckingham, M.E. (2002) The anterior heart-forming field: voyage to the arterial pole of the heart. *Trends Genet*. 18, 210–216.
6. Hatada, Y. and Stern, C.D. (1994) A fate map of the epiblast of the early chick embryo. *Development*. 120, 2879–2889.
7. Yutzey, K.E. and Kirby, M.L. (2002) Wherefore heart thou? Embryonic origins of cardiogenic mesoderm. *Dev Dyn*. 223, 307–320.
8. Sherman, L.S., Potter, S.S., and Scott, W.J. (eds.) (2001) *Human Embryology*, 3rd Ed. Churchill Livingstone, New York, NY.
9. Garcia-Martinez, V. and Schoenwolf, G.C. (1993) Primitive-streak origin of the cardiovascular system in avian embryos. *Dev Biol*. 159, 706–719.
10. Psychoyos, D. and Stern, C.D. (1996) Fates and migratory routes of primitive streak cells in the chick embryo. *Development*. 122, 1523–1534.
11. DeHaan, R.L. (1963) Organization of the cardiogenic plate in the early chick embryo. *Acta Embryol Morphol Exp*. 6, 26–38.
12. Ehrman, L.A. and Yutzey, K.E. (1999) Lack of regulation in the heart forming region of avian embryos. *Dev Biol*. 207, 163–175.
13. Harvey, R.P. and Rosenthal, N. (eds.) (1998) *Heart Development*. Academic Press, New York, NY.
14. Kirby, M.L. (2002) Molecular embryogenesis of the heart. *Pediatr Dev Pathol*. 5, 516–543.
15. Lohr, J.L. and Yost, J.H. (2000) Vertebrate model systems in the study of early heart development: xenopus and zebrafish. *Am J Med Genet*. 97, 248–257.
16. Kirby, M.L., Gale, T.F., and Stewart, D.E. (1983) Neural crest cells contribute to normal aorticopulmonary septation. *Science*. 220, 1059–1061.
17. Kirby, M.L. and Stewart, D.E. (1983) Neural crest origin of cardiac ganglion cells in the chick embryo: identification and extirpation. *Dev Biol*. 97, 433–443.
18. Kirby, M.L., Turnage, K.L., 3rd, and Hays, B.M. (1985) Characterization of conotruncal malformations following ablation of "cardiac" neural crest. *Anat Rec*. 213, 87–93.
19. Bockman, D.E., Redmond, M.E., and Kirby, M.L. (1989) Alteration of early vascular development after ablation of cranial neural crest. *Anat Rec*. 225, 209–217.

20. Waldo, K., Miyagawa-Tomita, S., Kumiski, D., and Kirby, M.L. (1998) Cardiac neural crest cells provide new insight into septation of the cardiac outflow tract: aortic sac to ventricular septal closure. *Dev Biol.* 196, 129–144.
21. Waldo, K.L., Lo, C.W., and Kirby, M.L. (1999) Connexin 43 expression reflects neural crest patterns during cardiovascular development. *Dev Biol.* 208, 307–323.
22. Komiyama, M., Ito, K., and Shimada, Y. (1987) Origin and development of the epicardium in the mouse embryo. *Anat Embryol.* 176, 183–189.
23. Noden, D.M., Poelmann, R.E., and Gittenberger-de Groot, A.C. (1995) Cell origins and tissue boundaries during outflow tract development. *Trends Cardiovasc Med.* 5, 69–75.
24. Mikawa, T. and Gourdie, R.G. (1996) Pericardial mesoderm generates a population of coronary smooth muscle cells migrating into the heart along with ingrowth of the epicardial organ. *Dev Biol.* 174, 221–232.
25. Noden, D.M. (1990) Origins and assembly of avian embryonic blood vessels. *Ann NY Acad Sci.* 588, 236–249.
26. Gittenberger-de Groot, A.C., Vrancken Peeters, M.P., Bergwerff, M., Mentink, M.M., and Poelmann, R.E. (2000) Epicardial outgrowth inhibition leads to compensatory mesothelial outflow tract collar and abnormal cardiac septation and coronary formation. *Circ Res.* 87, 969–971.
27. Hood, L.C. and Rosenquist, T.H. (1992) Coronary artery development in the chick: origin and development of smooth muscle cells, and effects of neural crest ablation. *Anat Rec.* 234, 291–300.
28. Anderson, P.A.W. (2000) Developmental cardiac physiology and myocardial function, In *Pediatric Cardiovascular Medicine* (Moller, J.H. and Hoffman, J.I.E., eds.), Churchill Livingstone, New York, NY, pp. 35–57.
29. Huttenbach, Y., Ostrowski, M.L., Thaller, D., and Kim, H.S. (2001) Cell proliferation in the growing human heart: MIB-1 immunostaining in preterm and term infants at autopsy. *Cardiovasc Pathol.* 10, 119–123.
30. Kern, F.H., Bengur, A.R., and Bello, E.A. (1996) Developmental cardiac physiology, In *Textbook of Pediatric Intensive Care*, 3rd Ed. (Rogers, M.C., ed.), Lippincott, Williams, and Wilkins, Baltimore, MD, pp. 397–423.
31. Kim, H.D., Kim, D.J., Lee, I.J., Rah, B.J., Sawa, Y., and Schaper, J. (1992) Human fetal heart development after mid-term: morphometry and ultrastructural study. *J Mol Cell Cardiol.* 24, 949–965.
32. Beltrami, A.P., Urbanek, K., Kajstura, J., et al. (2001) Evidence that human cardiac myocytes divide after myocardial infarction. *N Engl J Med.* 344, 1750–1757.
33. Vick, G.W. and Fisher, D.A. (1998) Cardiac metabolism, in *The Science and Practice of Pediatric Cardiology*, 2nd ed. (Garson, A.J., Bricker, T.J., Timothy, J., Fisher, D.J., and Neish, S.R., eds.), Williams and Wilkens, Baltimore, MD, pp. 155–169.
34. Opie, L.H. (1991) Carbohydrates and lipids, In *The Heart: Physiology and Metabolism*, 2nd Ed. (Opie, L.H., ed.), Raven Press, New York, NY, pp. 208–246.
35. Price, K.M., Littler, W.A., and Cummins, P. (1980) Human atrial and ventricular myosin light-chains subunits in the adult and during development. *Biochem J.* 191, 571–580.
36. Morano, M., Zacharzowski, U., Maier, M., et al. (1996) Regulation of human heart contractility by essential myosin light chain isoforms. *J Clin Invest.* 98, 467–473.
37. Morano, I. (1999) Tuning the human heart molecular motors by myosin light chains. *J Mol Med.* 77, 544–555.
38. Boheler, K.R., Carrier, L., de la Bastie, D., et al. (1991) Skeletal actin mRNA increases in the human heart during ontogenic development and is the major isoform of control and failing adult hearts. *J Clin Invest.* 88, 323–330.
39. Anderson, P.A.W., Kleinman, C.S., Lister, G., and Talner, N. (1998) Cardiovascular function during normal fetal and neonatal development and with hypoxic stress, in *Fetal and Neonatal Physiology,* 2nd Ed. (Polin, R.A. and Fox, W.W., eds.), Saunders, Philadelphia, PA, pp. 837–890.
40. Hewett, T.E., Grupp, I.L., Grupp, G., and Robbins, J. (1994) Alpha-skeletal actin is associated with increased contractility in the mouse heart. *Circ Res.* 74, 740–746.
41. Muthuchamy, M., Grupp, I.L., Grupp, G., et al. (1995) Molecular and physiological effects of overexpressing striated muscle beta-tropomyosin in the adult murine heart. *J Biol Chem.* 270, 30,593–30,603.
42. Palmiter, K.A., Kitada, Y., Muthuchamy, M., Wieczorek, D.F., and Solaro, R.J. (1996) Exchange of beta- for alpha-tropomyosin in hearts of transgenic mice induces changes in thin filament response to Ca^{2+}, strong cross-bridge binding, and protein phosphorylation. *J Biol Chem.* 271, 11,611–11,614.
43. Muthuchamy, M., Boivin, G.P., Grupp, I.L., and Wieczorek, D.F. (1998) Beta-tropomyosin overexpression induces severe cardiac abnormalities. *J Mol Cell Cardiol.* 30, 1545–1557.
44. Kim, S.H., Kim, H.S., and Lee, M.M. (2002) Re-expression of fetal troponin isoforms in the postinfarction failing heart of the rat. *Circ J.* 66, 959–964.
45. Hunkeler, N.M., Kullman, J., and Murphy, A.M. (1991) Troponin I isoform expression in human heart. *Circ Res.* 69, 1409–1414.
46. Purcell, I.F., Bing, W., and Marston, S.B. (1999) Functional analysis of human cardiac troponin by the in vitro motility assay: comparison of adult, foetal and failing hearts. *Cardiovasc Res.* 43, 884–891.
47. Morimoto, S. and Goto, T. (2000) Role of troponin I isoform switching in determining the pH sensitivity of Ca(2+) regulation in developing rabbit cardiac muscle. *Biochem Biophys Res Commun.* 267, 912–917.
48. Tanaka, H., Sekine, T., Nishimaru, K., and Shigenobu, K. (1998) Role of sarcoplasmic reticulum in myocardial contraction of neonatal and adult mice. *Comp Biochem Physiol A Mol Integr Physiol.* 120, 431–438.
49. Buchorn, R., Hulpke-Wette, M., Ruschewski, W., et al. (2002) Beta-receptor downregulation in congenital heart disease: a risk factor for complications after surgical repair? *Ann Thorac Surg.* 73, 610–613.
50. Schiffmann, H., Flesch, M., Hauseler, C., Pfahlberg, A., Bohm, M., and Hellige, G. (2002) Effects of different inotropic interventions on myocardial function in the developing rabbit heart. *Basic Res Cardiol.* 97, 76–87.
51. Sun, L.S. (1999) Regulation of myocardial beta-adrenergic receptor function in adult and neonatal rabbits. *Biol Neonate.* 76, 181–192.
52. Dees, E. and Baldwin, H.S. (2002) New frontiers in molecular pediatric cardiology. *Curr Opin Pediatr.* 14, 627–633.
53. McFadden, D.G. and Olson, E.N. (2002) Heart development: learning from mistakes. *Curr Opin Genet Dev.* 12, 328–335.
54. Martinsen, B.J., Groebner, N.J., Frasier, A.J., and Lohr, J.L. (2003) Expression of cardiac neural crest and heart genes isolated by modified differential display. *Gene Expr Patterns.* 3, 407–411.

3 Anatomy of the Thoracic Wall, Pulmonary Cavities, and Mediastinum

KENNETH P. ROBERTS, PhD
AND ANTHONY J. WEINHAUS, PhD

CONTENTS

1. INTRODUCTION

The thorax is the body cavity, surrounded by the bony rib cage, that contains the heart and lungs, the great vessels, the esophagus and trachea, the thoracic duct, and the autonomic innervation for these structures. The inferior boundary of the thoracic cavity is the respiratory diaphragm, which separates the thoracic and abdominal cavities. Superiorly, the thorax communicates with the root of the neck and the upper extremity. The wall of the thorax contains the muscles involved with respiration and those connecting the upper extremity to the axial skeleton. The wall of the thorax is responsible for protecting the contents of the thoracic cavity and for generating the negative pressure required for respiration. The thorax is covered by skin and superficial fascia, which contains the mammary tissue.

This chapter reviews the mediastinum and pulmonary cavities within the thorax and discusses their contents. The wall of the thorax and its associated muscles, nerves, and vessels are covered in relationship to respiration. The surface anatomical landmarks that designate deeper anatomical structures and sites of access and auscultation are reviewed. The goal of this chapter is to provide a complete picture of the thorax and its contents, with detailed anatomy of thoracic structures excluding the heart. A detailed description of cardiac anatomy is the subject of Chapter 4.

From: *Handbook of Cardiac Anatomy, Physiology, and Devices*
Edited by: P. A. Iaizzo © Humana Press Inc., Totowa, NJ

2. OVERVIEW OF THE THORAX

Anatomically, the thorax is typically divided into compartments; there are two bilateral pulmonary cavities; each contains a lung with its pleural covering (Fig. 1). The space between the pleural cavities is the mediastinum, which contains all the other structures found in the thorax. The mediastinum is divided into the superior and inferior compartments by a plane referred to as the "transverse thoracic plane"; it passes through the mediastinum at the level of the sternal angle and the junction of the T4 and T5 vertebrae (Fig. 1).

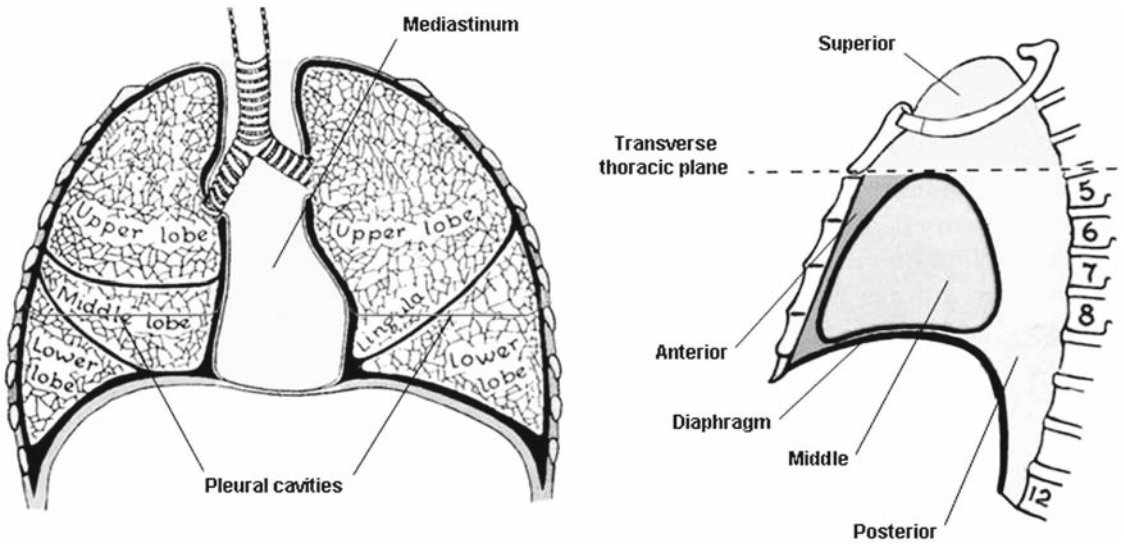

Fig. 1. The left panel is a diagrammatic representation of the pulmonary cavities, one on each side of the thorax with the mediastinum between. The right panel illustrates the divisions of the mediastinum. Adapted from Figs. 1.14 (left) and 1.24 of *Grant's Dissector,* 12th Ed., E. K. Sauerland (ed.). © 1999 Lippincott, Williams, and Wilkins, Philadelphia, PA.

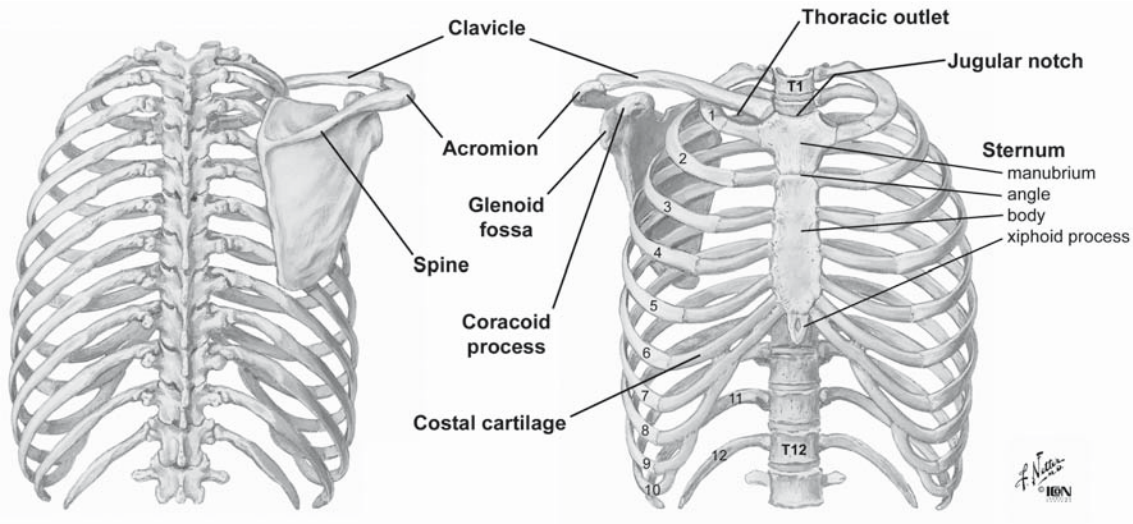

Fig. 2. The left panel illustrates the bones of the thorax from a posterior view. The right panel is an anterior view of the bony thorax.

The superior mediastinum contains the major vessels supplying the upper extremity, the neck, and the head. The inferior mediastinum, the space between the transverse thoracic plane and the diaphragm, is further divided into the anterior, middle, and posterior mediastinum. The middle mediastinum is the space containing the heart and pericardium. The anterior mediastinum is the space between the pericardium and the sternum. The posterior mediastinum extends from the pericardium to the posterior wall of the thorax.

The inferior aperture of the thorax is formed by the lower margin of the ribs and costal cartilages and is closed off from the abdomen by the respiratory diaphragm (Fig. 1). The superior aperture of the thorax leads to the neck and the upper extremity. It is formed by the first ribs and their articulation with the manubrium and first thoracic vertebra. The root of the neck is open to the superior aperture of the thorax, and numerous structures pass from the neck to the thoracic cavity. The clavicle crosses the first rib at its anterior edge close to its articulation with the manubrium. Structures exiting the superior thoracic aperture and communicating with the upper extremity pass between the first rib and clavicle.

3. BONES OF THE THORACIC WALL

3.1. The Thoracic Cage

The skeleton of the thoracic wall is composed of the 12 ribs, the thoracic vertebra and intervertebral discs, and the sternum. Attached to the thorax are the bones of the pectoral girdle, the clavicle and the scapula (Fig. 2). Of these, the clavicle is particularly important because it forms, with the first rib, the thoracic outlet to the upper extremity.

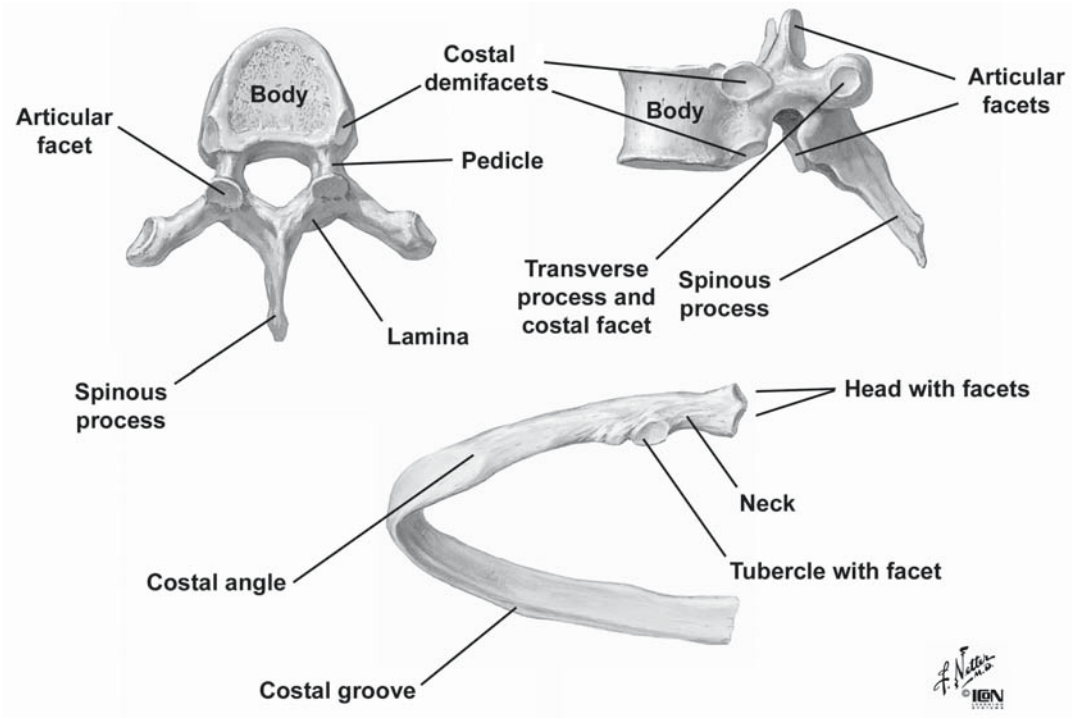

Fig. 3. The T6 vertebra as viewed from above (upper left) and laterally (upper right) and a typical rib (bottom).

The thoracic vertebrae comprise the middle portion of the posterior wall of the thorax. Each thoracic vertebra has a body anteriorly, two pedicles and two lamina that together form an arch creating the vertebral foramen; a relatively long spinous process projecting posteriorly and inferiorly; and two transverse processes projecting laterally and somewhat posteriorly (Fig. 3). Each thoracic vertebra articulates with at least one rib.

The first through 9th thoracic vertebrae have a set of costal facets on their bodies for articulation with the head of the rib. These costal facets are also called *demifacets*. The superior demifacet articulates with the head of the rib of the same number as the vertebra. The inferior demifacet articulates with the head of the rib below. The head of rib 1 articulates only with the T1 vertebra. Thus, this vertebra has a single facet for articulation with rib 1 and a demifacet for articulation with rib 2. The heads of ribs 10–12 articulate only with the vertebra of the same number. The articular facet on vertebrae T10–T12 is located at the junction of the body and pedicle (T10) or fully on the pedicle (T11 and T12). The first 10 thoracic vertebrae also have costal facets on their transverse processes for articulation with the tubercles of the ribs of the same number. The transverse processes of the thoracic vertebrae get progressively shorter, and the transverse processes of T11 and T12 do not articulate with the tubercles of their respective ribs.

The ribs form the largest part of the bony wall of the thorax (Fig. 2). Each rib articulates with one or two thoracic vertebrae, and the upper 10 ribs articulate directly or indirectly with the sternum anteriorly. The upper 7 ribs are referred to as "true" ribs because each connects to the sternum via its own costal cartilage. Ribs 8–10 are referred to as "false" ribs because they connect indirectly to the sternum. Each of these ribs is connected to the rib immediately above via their costal cartilage and ultimately to the sternum via the costal cartilage of the 7th rib. Ribs 11 and 12 are referred to as "floating" ribs because they do not connect to the sternum, but end in the musculature of the abdominal wall.

Each rib has a head that articulates with the thoracic vertebra and a thin flat shaft that is curved (Fig. 3). The costal angle, the sharpest part of the curved shaft, is located where the rib turns anteriorly. At the inferior margin of the shaft, the internal surface of the rib is recessed to form the costal groove. This depression provides some protection to the intercostal neurovascular bundle, something that must be considered when designing devices for intercostal access to the thorax. The heads of ribs 2–9 have two articular facets for articulation with the vertebra of the same level and the vertebra above. The heads of ribs 1, 10, 11, and 12 only articulate with the vertebra of the same number and consequently have only one articular facet. In ribs 1–10, the head is connected to the shaft by a narrowing called the "neck." At the junction of the head and the neck is a tubercle that has an articular surface for articulation with the costal facet of the transverse process. Ribs 11 and 12 do not articulate with the transverse process of their respective vertebra and do not have a tubercle or a neck portion.

The sternum is the flat bone that makes up the median anterior part of the thoracic cage (Fig. 2). It is composed of three parts: the manubrium, body, and xiphoid process. The manubrium (from the Latin word for *handle*, like the handle of a sword) is the superior part of the sternum; it is the widest and thickest part. The manubrium alone articulates with the clavicle

and the first rib. The sternal heads of the clavicle can be readily seen and palpated at their junction with the manubrium. The depression between the sternal heads of the clavicle above the manubrium is the suprasternal, or jugular, notch.

The manubrium and the body of the sternum lie in slightly different planes and thus form a noticeable and easily palpated angle, the sternal angle (of Louis), at the point where they articulate. The second rib articulates with both the body of the sternum and the manubrium and can easily be identified just lateral to the sternal angle. The body of the sternum is formed from the fusion of segmental bones (the sternebrae). The remnants of this fusion can be seen in the transverse ridges of the sternal body, especially in young people. The third through sixth ribs articulate with the body of the sternum, and the seventh rib articulates at the junction of the sternum and xiphoid process.

The xiphoid process is the most inferior part of the sternum and is easily palpated. It lies at the level of thoracic vertebra 10 and marks the inferior boundary of the thoracic cavity anteriorly. It also lies at the level even with the central tendon of the diaphragm and the inferior border of the heart.

3.2. The Pectoral Girdle

Many of the muscles encountered on the wall of the anterior thorax are attached to the bones of the pectoral girdle and the upper extremity. Because movement of these bones can have an impact on the anatomy of vascular structures communicating between the thorax and upper extremity, it is important to include these structures in a discussion of the thorax.

The clavicle is a somewhat S-shaped bone that articulates at its medial end with the manubrium of the sternum and at its lateral end with the acromion of the scapula (Fig. 2). It is convex medially and concave laterally. The scapula is a flat triangular bone, concave anteriorly, that rests upon the posterior thoracic wall. It has a posterior raised ridge called the "spine" that ends in a projection of bone called the "acromion," which articulates with the clavicle. The coracoid process is an anterior projection of bone from the superior border of the clavicle that serves as an attachment point for muscles that act on the scapula and upper extremity. The head of the humerus articulates with the glenoid fossa of the scapula, forming the glenohumeral joint. The clavicle serves as a strut to hold the scapula in position away from the lateral aspect of the thorax. It is a highly mobile bone, with a high degree of freedom at the sternoclavicular joint that facilitates movement of the shoulder girdle against the thorax. The anterior extrinsic muscles of the shoulder pass from the wall of the thorax to the bones of the shoulder girdle.

4. MUSCLES OF THE THORACIC WALL

4.1. The Pectoral Muscles

Several muscles of the thoracic wall, including the most superficial ones that create some of the contours of the thoracic wall, are muscles that act on the upper extremity. Some of these muscles form important surface landmarks on the thorax, and others have relationships to vessels that communicate with the thorax. In addition to moving the upper extremity, some of these muscles also can play a role in movement of the thoracic wall and participate in respiration. The pectoralis major muscle forms the surface contour of the upper lateral part of the thoracic wall (Fig. 4). It originates on the clavicle (clavicular head) and the sternum and ribs (sternocostal head) and inserts on the greater tubercle of the humerus. The lower margin of this muscle, passing from the thorax to the humerus, forms the major part of the anterior axillary fold. The pectoralis major muscle is a powerful adductor and medial rotator of the arm.

The pectoralis minor muscle is a much smaller muscle and lies directly beneath the pectoralis major muscle (Fig. 4). It originates on ribs 3–5 and inserts on the coracoid process of the scapula. This muscle forms part of the anterior axillary fold medially. It acts to depress the scapula and stabilizes it when upward force is exerted on the shoulder.

The anterior part of the deltoid muscle also forms a small aspect of the anterior thoracic wall. This muscle has its origin on the lateral part of the clavicle and the acromion and spine of the scapula (Fig. 4). It inserts on the deltoid tubercle of the humerus and is the most powerful abductor of the arm. The deltoid muscle borders the pectoralis major muscle. The depression found at the junction of these two muscles is called the *deltopectoral groove*. Importantly, within this groove the cephalic vein can consistently be found. The muscles diverge at their origins on the clavicle, creating an opening bordered by these two muscles and the clavicle known as the *deltopectoral triangle*. Through this space the cephalic vein passes to join the axillary vein.

The subclavius is a small muscle originating on the lateral inferior aspect of the clavicle and inserting on the sternal end of the first rib (Fig. 4). This muscle depresses the clavicle and exerts a medial traction on the clavicle that stabilizes the sternoclavicular joint. In addition to these actions, the subclavius muscle provides a soft surface on the inferior aspect of the clavicle that serves to cushion the contact of this bone with structures passing under the clavicle (i.e., nerves of the brachial plexus and the subclavian artery) when the clavicle is depressed during movement of the shoulder girdle, especially when the clavicle is fractured.

The serratus anterior muscle originates on the lateral aspect of the first eight ribs and passes laterally to insert on the medial aspect of the scapula (Fig. 5). This muscle forms the "serrated" contour of the lateral thoracic wall in individuals with good muscle definition. The serratus anterior forms the medial border of the axilla and acts to pull the scapula forward (protraction) and to stabilize the scapula against a posterior force on the shoulder.

4.2. The Intercostal Muscles

Each rib is connected to the ones above and below by a series of three intercostal muscles. The external intercostal muscles are the most superficial (Fig. 5). These muscles course in an obliquely medial direction as they pass from superior to inferior between the ribs. Toward the midline anteriorly, the external intercostal muscle fibers are replaced by the external intercostal membrane. Deep to the external intercostals are the internal intercostals (Fig. 5). The direction of the internal intercostal muscle fibers is perpendicular to the external intercostals. On the posterior end of the ribs, the internal intercostal muscle fibers are replaced by the internal intercostal membrane.

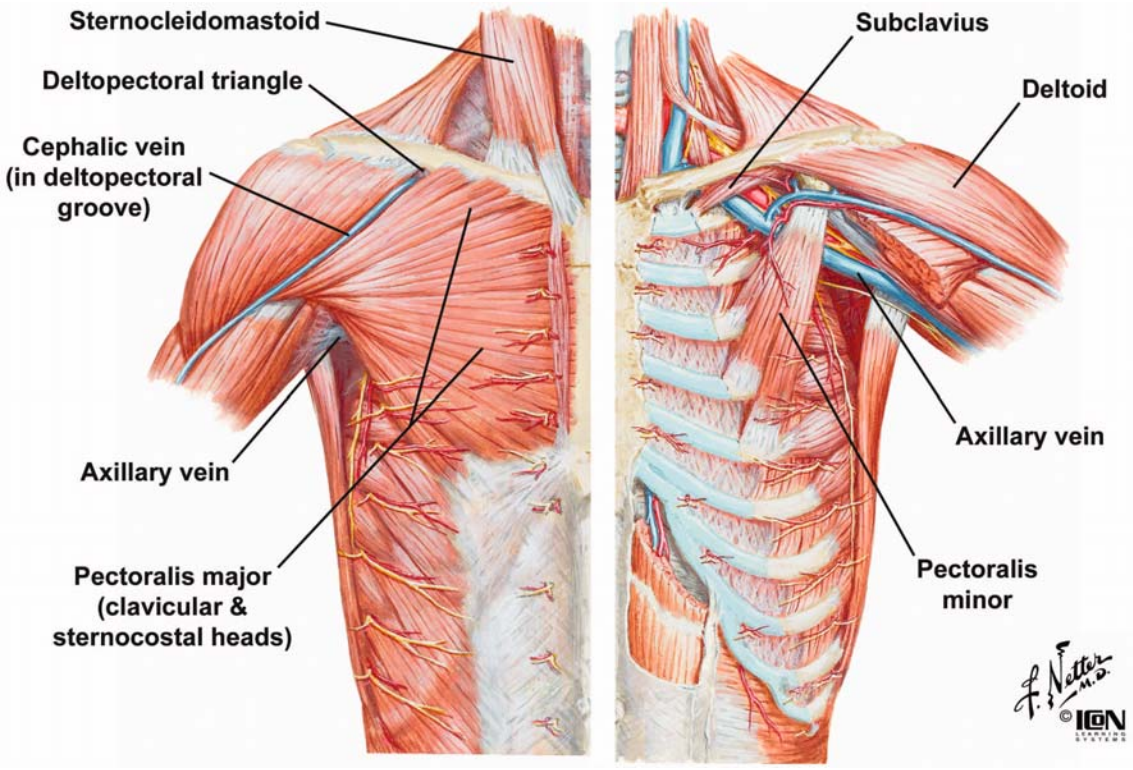

Fig. 4. The musculature of the anterior thoracic wall. The left panel shows the superficial muscles intact. The right panel shows structures deep to the pectoralis major muscle.

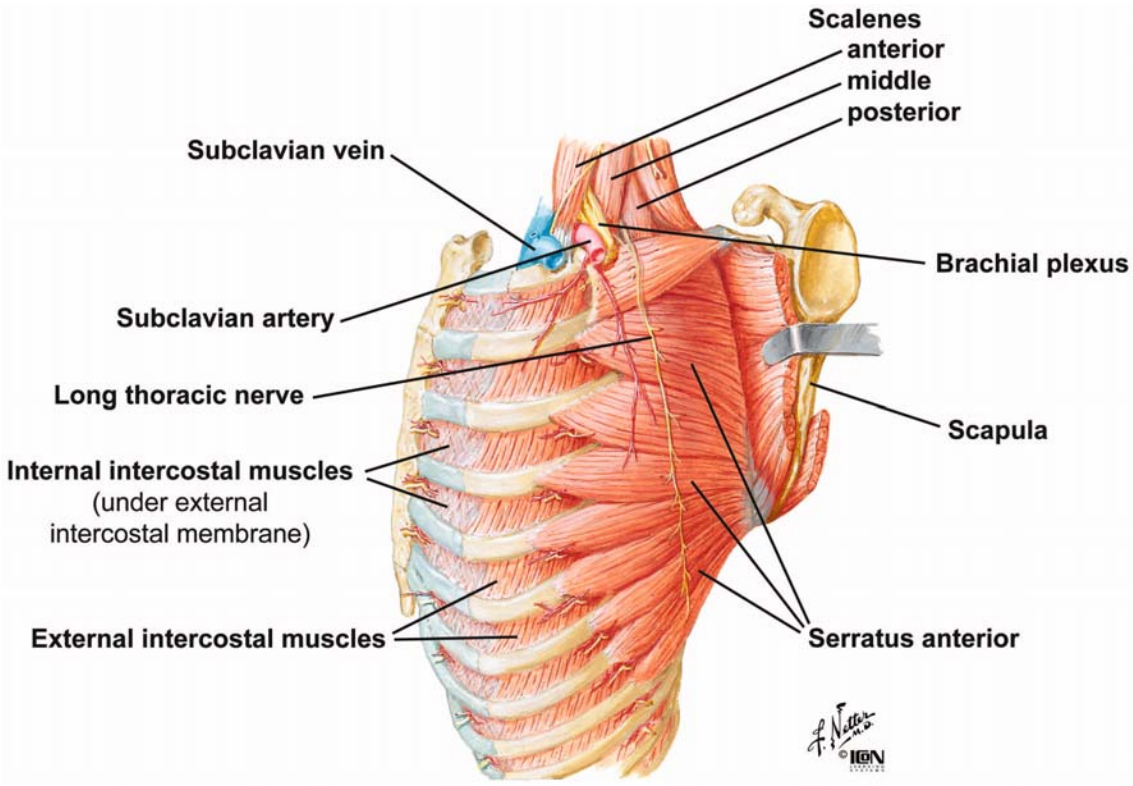

Fig. 5. A lateral view of the musculature of the thoracic wall.

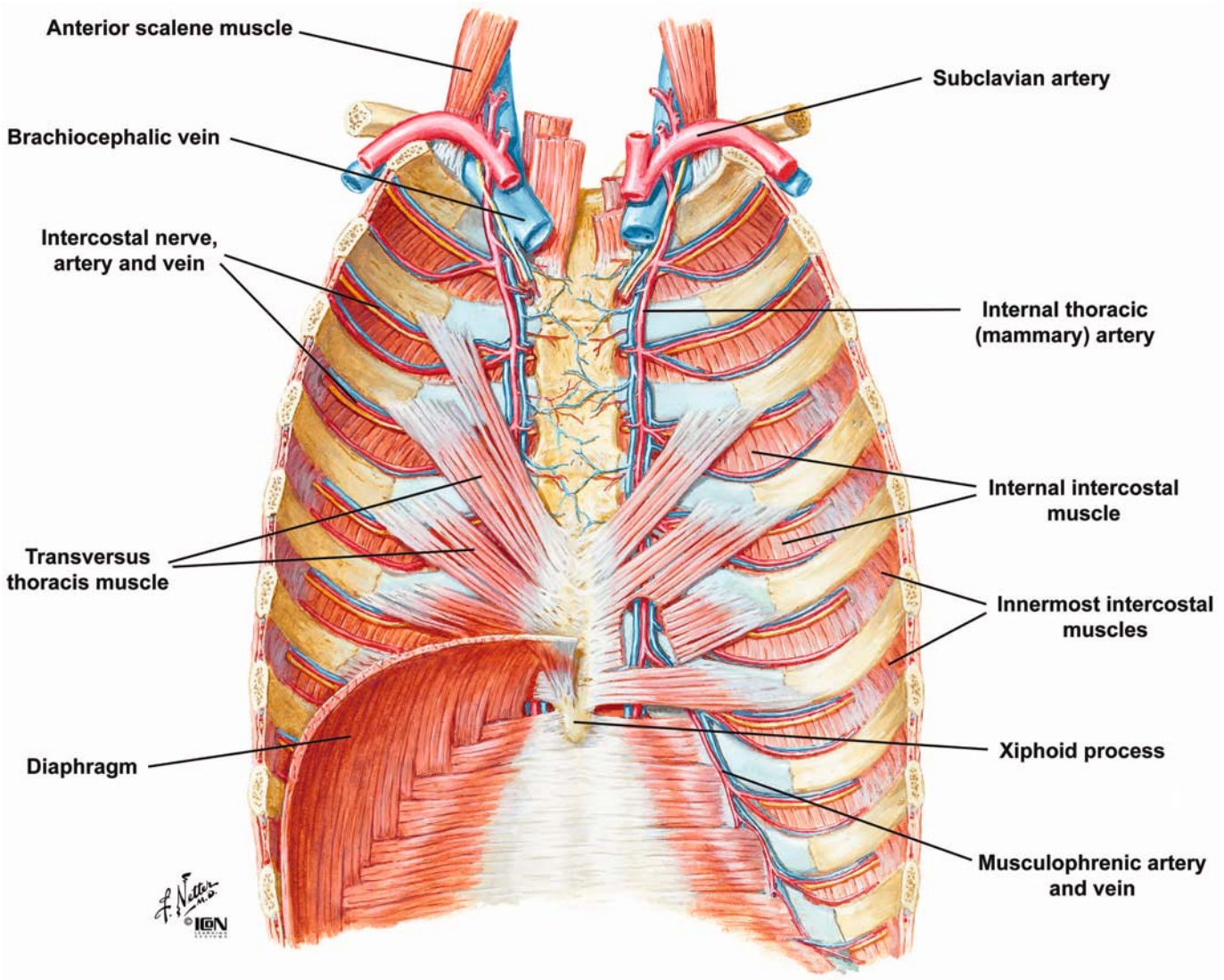

Fig. 6. The deep musculature of the anterior thoracic wall viewed from the posterior side.

The deepest layer of intercostal muscles is the innermost intercostal muscles (Fig. 6). These muscles have a fiber direction similar to that of the internal intercostals, but form a separate plane. The intercostal nerves and vessels pass between the internal and innermost intercostal muscles.

There are two additional sets of muscles in the same layer as the innermost intercostals: the subcostals and the transversus thoracis muscles. The subcostal muscles are located posteriorly and span more than one rib. The transversus thoracic muscles are found anteriorly and are continuous with the innermost muscle layer of the abdomen, the transversus abdominus, inferiorly. The transversus thoracis muscles pass from the internal surface of the sternum to ribs 2–6.

The intercostal muscles, especially the external and internal intercostals, are involved with respiration by elevating or depressing the ribs. The external intercostal muscles and the anterior interchondral part of the internal intercostals act to elevate the ribs. The lateral parts of the internal intercostal muscles depress the ribs. The innermost intercostals most likely have an action similar to that of the internal intercostals. The subcostal muscles probably help to elevate the ribs. The transversus thoracis muscles have little, if any, effect on respiration.

4.3. Respiratory Diaphragm

The respiratory diaphragm is the musculotendinous sheet separating the abdominal and thoracic cavities (Fig. 7). It is also considered the primary muscle of respiration. The diaphragm originates along the inferior border of the rib cage, the xiphoid process of the sternum, the posterior abdominal wall musculature, and the upper lumbar vertebra. The medial and lateral arcuate ligaments are thickenings of the investing fascia over the quadratus lumborum (lateral) and the psoas major (medial) muscles of the posterior abdominal wall that serve as attachments for the diaphragm (Fig. 7). The vertebral origins of the diaphragm are the right and left crura. The crura originate on the bodies of lumbar vertebrae 1–3, their intervertebral discs, and the anterior longitudinal ligament spanning these vertebrae.

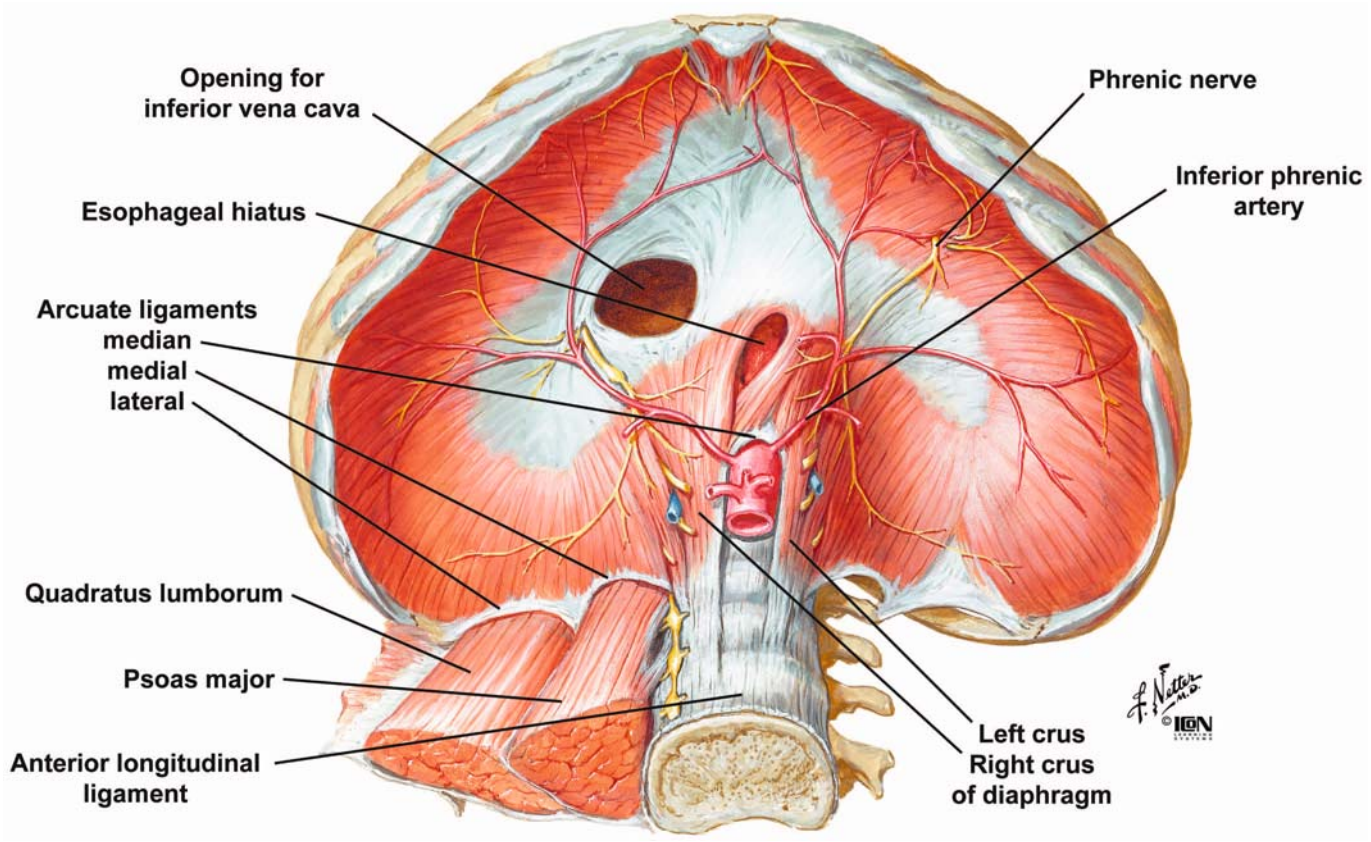

Fig. 7. The abdominal side of the respiratory diaphragm illustrating the origins of the muscle.

The diaphragm ascends from its origin to form a right and left dome; the right dome is typically higher than the left. The muscular part of the diaphragm contracts during respiration, causing the dome of the diaphragm to descend, increasing the volume of the thoracic cavity. The aponeurotic central part of the diaphragm, called the *central tendon*, contains the opening for the vena cava. The esophagus also passes through the diaphragm, and the hiatus for the esophagus is created by a muscular slip originating from the right crus of the diaphragm. The aorta passes from the thorax to the abdomen behind the diaphragm, under the median arcuate ligament created by the intermingling of fibers from the right and left crura of the diaphragm. The vena cava, esophagus, and aorta pass from the thorax to the abdomen at thoracic vertebral levels 8, 10, and 12, respectively.

4.4. Other Muscles of Respiration

The scalene muscles and the sternocleidomastoid muscle in the neck also contribute to respiration, especially during deep respiration (Figs. 4 and 5). The scalene muscles have their origin on the transverse processes of cervical vertebrae 4 to 6. The anterior and middle scalenes insert on the first rib and the posterior scalene on the second rib. As its name suggests, the sternocleidomastoid has its origin on the mastoid process of the skull and inserts on the medial aspect of the clavicle and the manubrium of the sternum. When contracting with the head and neck fixed, these muscles exert an upward pull on the thorax and assist in respiration.

The muscles of the anterior abdominal wall are also involved with respiration. These muscles, the rectus abdominus, external and internal abdominal obliques, and transversus abdominus, act together during forced expiration to pull down on the rib cage and to increase intra-abdominal pressure, forcing the diaphragm to expand upward. The mechanics of respiration are explained in detail in Section 11.3.

5. NERVES OF THE THORACIC WALL

The wall of the thorax receives its innervation from intercostal nerves (Fig. 8). These nerves are the ventral rami of segmental nerves leaving the spinal cord at the thoracic vertebral levels. Intercostal nerves are mixed nerves that carry both somatic motor and sensory nerves and autonomics to the skin. The intercostal nerves pass out of the intervertebral foramina and run inferior to the rib. As they reach the costal angle, the nerves pass between the innermost and the internal intercostal muscles.

The motor innervation to all the intercostal muscles comes from the intercostal nerves. These nerves give off lateral and anterior cutaneous branches that provide cutaneous sensory innervation to the skin of the thorax. The intercostal nerves also carry sympathetic nerve fibers to the sweat glands, smooth muscle, and blood vessels. However, the first two intercostal nerves are considered atypical. The first intercostal nerve divides shortly after it emerges from the intervertebral foramen. The larger superior part of this nerve joins the brachial plexus to provide innervation to the upper extremity. The lateral cuta-

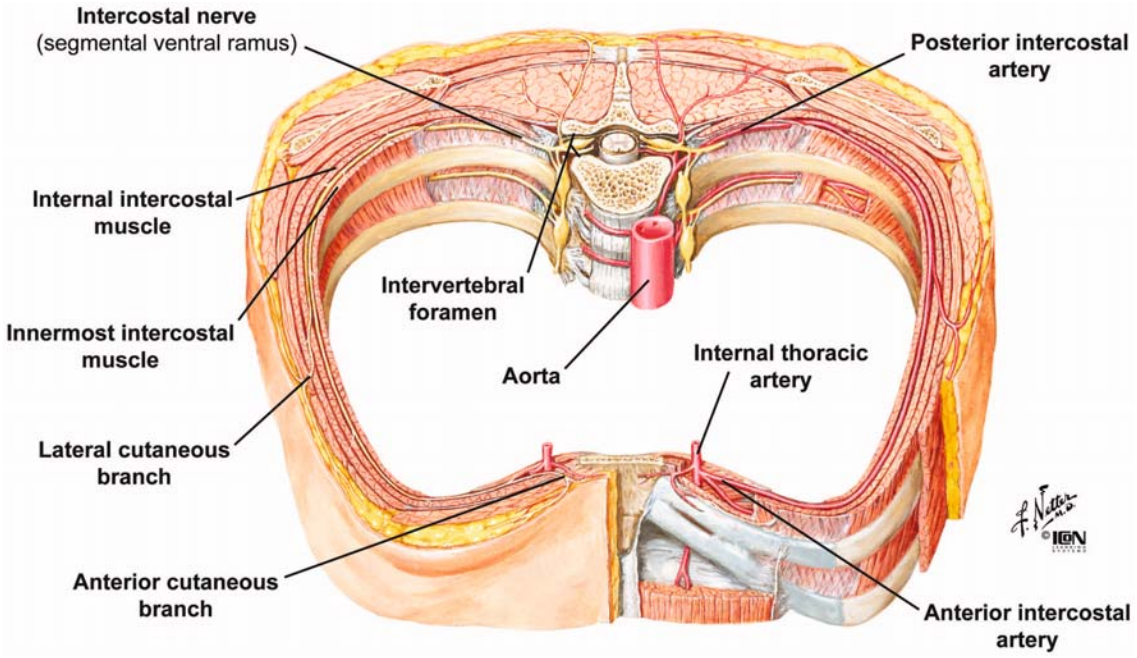

Fig. 8. A typical set of intercostal arteries and nerves.

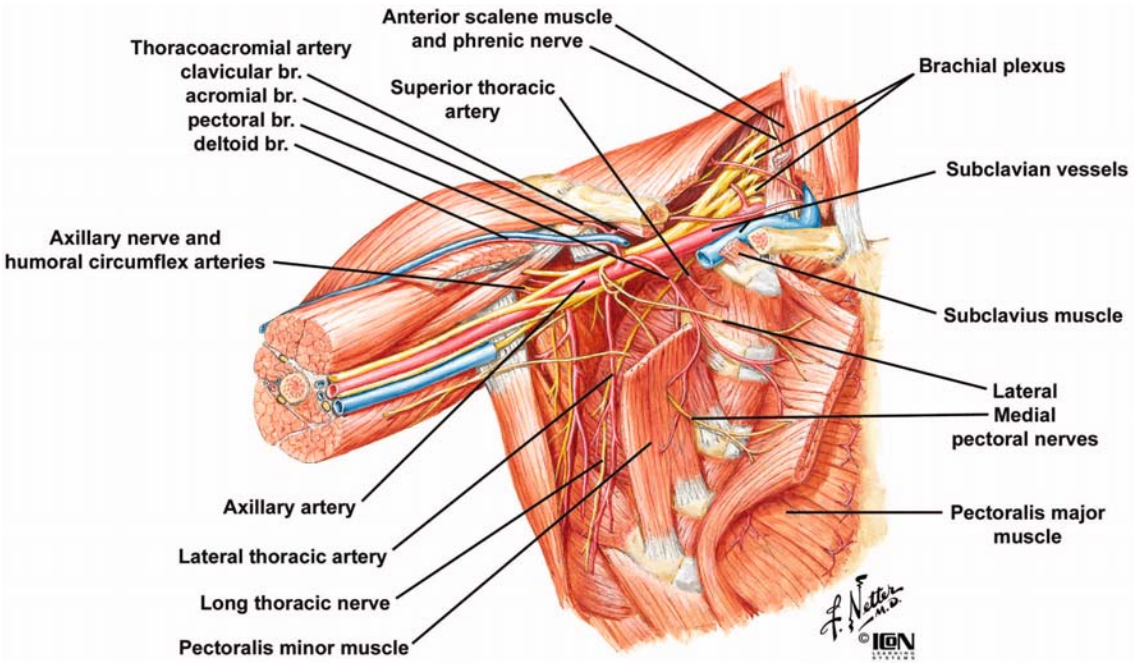

Fig. 9. The nerves and arteries of the axilla viewed with the pectoralis major and minor muscles reflected.

neous branch of the second intercostal nerve is large and typically pierces the serratus anterior muscle, passes through the axilla and into the arm as the intercostobrachial nerve, and provides sensory innervation to the floor of the axilla and medial aspect of the arm (Fig. 9). The nerve associated with the 12th rib is the subcostal nerve, because there is no rib below this level. It is a nerve of the abdominal wall.

The pectoral muscles receive motor innervation from branches of the brachial plexus of nerves (derived from cervical levels 5–8 and thoracic level 1) that supply the muscles of the shoulder and upper extremity. The lateral and medial pectoral nerves, branches of the lateral and medial cords of the brachial plexus, supply the pectoralis major and minor muscles (Fig. 9). The pectoralis major muscle is innervated by both nerves and the pectoralis minor muscle by only the medial pectoral nerve, which pierces this muscle before entering the pectoralis major muscle. The serratus anterior muscle is innervated by the long thoracic nerve, which originates from ventral rami of C5, C6, and C7 (Figs. 5 and 9). The deltoid muscle is innervated by the axillary nerve, a terminal branch of the pos-

terior cord of the brachial plexus. Finally, the subclavius muscle is innervated by its own nerve from the superior trunk of the brachial plexus.

6. VESSELS OF THE THORACIC WALL

The intercostal muscles and the skin of the thorax receive their blood supply from both the intercostal arteries and the internal thoracic artery (Fig. 8). Intercostal arteries 3–11 (and the subcostal artery) are branches directly from the thoracic descending aorta. The first two intercostal arteries are branches of the supreme intercostal artery, which is a branch of the costocervical trunk from the subclavian artery. The posterior intercostals run with the intercostal nerve and pass with the nerve between the innermost and internal intercostal muscles. The intercostals then anastomose with anterior intercostal branches arising from the internal thoracic artery descending immediately lateral to the sternum. The internal thoracic arteries are anterior branches from the subclavian arteries bilaterally. The anterior and posterior intercostal anastomoses create an anastomotic network around the thoracic wall. The intercostal arteries are accompanied by intercostal veins (Fig. 6). These veins drain to the azygos system of veins in the posterior mediastinum. The anatomy of the azygos venous system is described in detail in Section 10.2. Anteriorly, the intercostal veins drain to the internal thoracic veins, which in turn drain to the subclavian veins in the superior mediastinum.

The intercostal nerves, arteries, and veins run together in each intercostal space close to the rib above. They are characteristically found in this order (vein, artery, nerve), with the vein closest to the rib.

The diaphragm receives blood from the musculophrenic artery, a terminal branch of the internal thoracic artery, which runs along the anterior superior surface of the diaphragm (Fig. 6). There is also a substantial blood supply to the inferior aspect of the diaphragm from the inferior phrenic arteries, the most superior branches from the abdominal aorta that branch along the inferior surface of the diaphragm (Fig. 7).

The muscles of the pectoral region get their blood supply from branches of the axillary artery. This artery is the continuation of the subclavian artery emerging from the thorax and passing under the clavicle (Fig. 9). The first branch of the axillary artery, the superior (supreme) thoracic artery, gives blood supply to the first two intercostal spaces. The second branch forms the thoracoacromial artery or trunk. Subsequently, this artery gives off four sets of branches (pectoral, deltoid, clavicular, and acromial) that supply blood to the pectoral muscles, the deltoid muscle, the clavicle, and the subclavius muscle, respectively. The lateral thoracic artery, the third branch from the subclavian artery, participates along with the intercostal arteries in supplying the serratus anterior muscle. Additional distal branches from the axillary artery, the humeral circumflex arteries, also participate in blood supply to the deltoid muscle. Venous blood returns through veins of the same names to the axillary vein.

7. THE SUPERIOR MEDIASTINUM

The superior mediastinum is the space behind the manubrium of the sternum (Fig. 1). It is bounded by parietal (mediastinal) pleura on each side and the first four thoracic vertebrae behind. It is continuous with the root of the neck at the top of the first ribs and with the inferior mediastinum below the transverse thoracic plane, a horizontal plane that passes from the sternal angle through the space between the T4 and T5 vertebrae. Because of the inferior sloping of the first ribs, the superior mediastinum is wedge shaped as it is longer posteriorly. The superior mediastinum contains several important structures, including the branches of the aortic arch, the veins that coalesce to form the superior vena cava, the trachea, the esophagus, the vagus and phrenic nerves, the cardiac plexus of autonomic nerves, the thoracic duct, and the thymus (Fig. 10).

7.1. Arteries in the Superior Mediastinum

As the aorta emerges from the pericardial sac, it begins to arch posteriorly (Fig. 11). At the level of the T4 vertebra, the aorta has become vertical again, descending through the posterior mediastinum. The intervening segment is the arch of the aorta, and it courses from right to left as it arches posteriorly. It passes over the right pulmonary artery and ends by passing posterior to the left pulmonary artery. The trachea and esophagus pass posterior and to the right of the aortic arch.

The arch of the aorta gives off the major arteries that supply blood to the head and to the upper extremity. This branching is asymmetrical. The first and most anterior branch from the aorta is the brachiocephalic trunk. This arterial trunk bends toward the right as it ascends, and as it reaches the upper limit of the superior mediastinum, it bifurcates into the right common carotid and right subclavian arteries. The next two branches from the aortic arch, from anterior to posterior, are the left common carotid and the left subclavian arteries. These two arteries ascend almost vertically to the left of the trachea. The common carotid arteries will supply the majority of the blood to the head and neck. The subclavian arteries continue as the axillary and brachial arteries and supply the upper extremity.

The arch of the aorta and its branches make contact with the upper lobe of the right lung, and their impressions are normally seen on the fixed lung after removal. The brachiocephalic trunk, left common carotid, and the left subclavian do not give off consistent branches in the superior mediastinum. However, the subclavian arteries at the root of the neck give off the internal thoracic arteries, which reenter the superior mediastinum and descend along each side of the sternum.

On occasion, there will be an artery that branches from the aortic arch, the right common carotid, or one of the subclavian arteries and supplies the thyroid gland in the midline. This variant artery is called a *thyroid ima*. Because this artery is often found crossing the region where a tracheostomy is performed, it is important to remember that this artery is present in about 10% of individuals.

7.2. Brachiocephalic Veins

The bilateral brachiocephalic veins are formed by the merging of the internal jugular vein and the subclavian vein on both sides at the base of the neck (Fig. 11). The right brachiocephalic vein descends nearly vertically; the left crosses obliquely behind the manubrium to join the right and then form the superior vena cava. The superior vena cava continues inferiorly into the middle mediastinum, entering the pericardial sac. The brachiocephalic veins run anterior in the superior mediastinum.

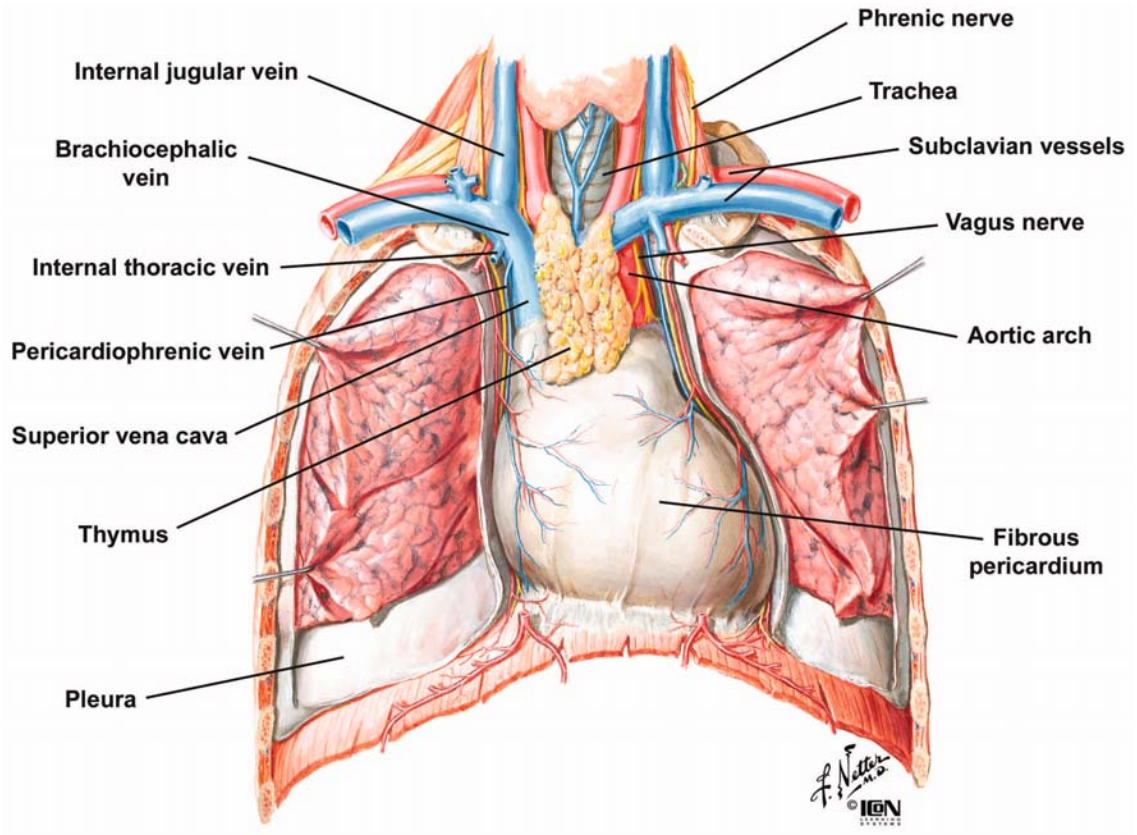

Fig. 10. Contents of the superior and middle mediastinum.

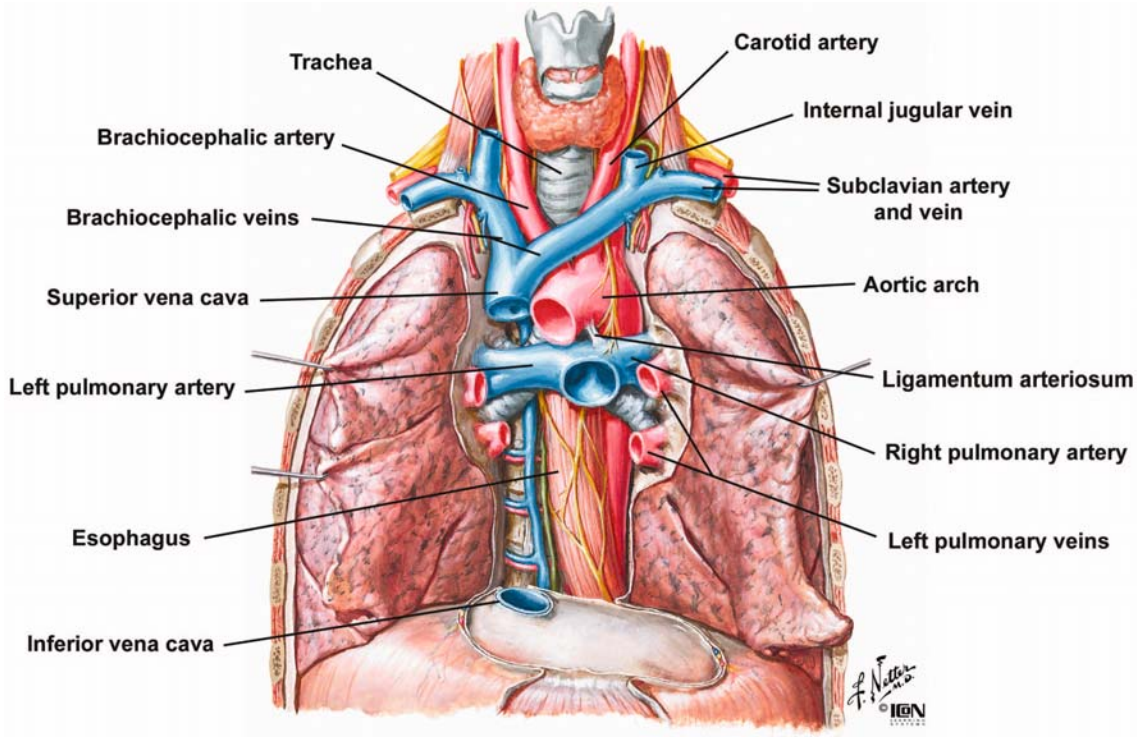

Fig. 11. Vessels of the superior and middle mediastinum.

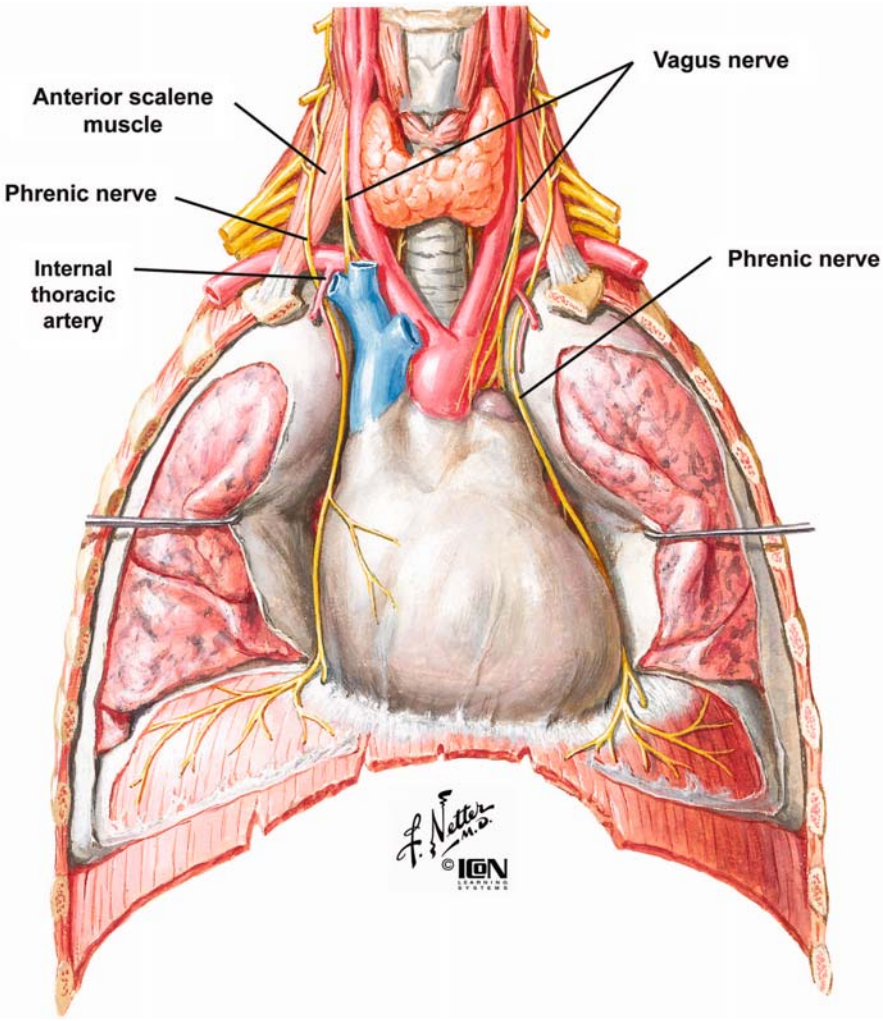

Fig. 12. Course of the phrenic nerve and vagus nerve in the superior and middle mediastinum.

The left brachiocephalic vein passes anterior to the three branches of the aortic arch and is separated from the manubrium only by the thymus (Fig. 10). The brachiocephalic veins receive the internal thoracic veins, the inferior thyroid veins, and the small pericardiophrenic veins. They also receive the superior intercostal veins from behind.

7.3. The Trachea and Esophagus

The trachea is a largely cartilaginous tube that runs from the larynx inferiorly through the superior mediastinum and ends by branching into the main bronchi (Fig. 11). It serves as a conduit for air to the lungs. The trachea can be palpated at the root of the neck, superior to the manubrium in the midline. The esophagus is a muscular tube that connects the pharynx with the stomach. The upper part of the esophagus descends behind the trachea, and in contact with it, through the superior mediastinum (Fig. 11). The esophagus continues through the posterior mediastinum behind the heart, pierces the diaphragm at the T10 level, and enters the stomach at the cardia. Both the trachea and esophagus are crossed on the left by the arch of the aorta. The impression of the aorta on the esophagus can usually be seen on a posterior-to-anterior radiograph of the esophagus coated with barium contrast. The trachea and esophagus are crossed on the right side by the azygos vein at the lower border of the superior mediastinum. Both the trachea and esophagus come into contact with the upper lobe of the right lung. The esophagus also contacts the upper lobe of the left lung. The arch of the aorta and its branches shield the trachea from the left lung.

7.4. Nerves of the Superior Mediastinum

Both the vagus nerve (cranial nerve 10) and the phrenic nerve pass through the superior mediastinum. The phrenic nerve originates from the ventral rami from cervical levels 3–5. This nerve travels inferiorly in the neck on the surface of the anterior scalene muscle, entering the superior mediastinum behind the subclavian vein and passing under the internal thoracic artery (Fig. 12). On the right, the phrenic nerve passes through the superior mediastinum lateral to the subclavian artery and the arch of the aorta. On the left, the phrenic nerve passes lateral to the brachiocephalic vein and the superior vena cava. The phrenic nerves then enter the middle mediastinum, where they pass anterior to the root of the lung, across the pericardium, finally piercing the diaphragm lateral to the base of the pericardium. Throughout their course, the phrenic nerves pass under the mediastinal pleura.

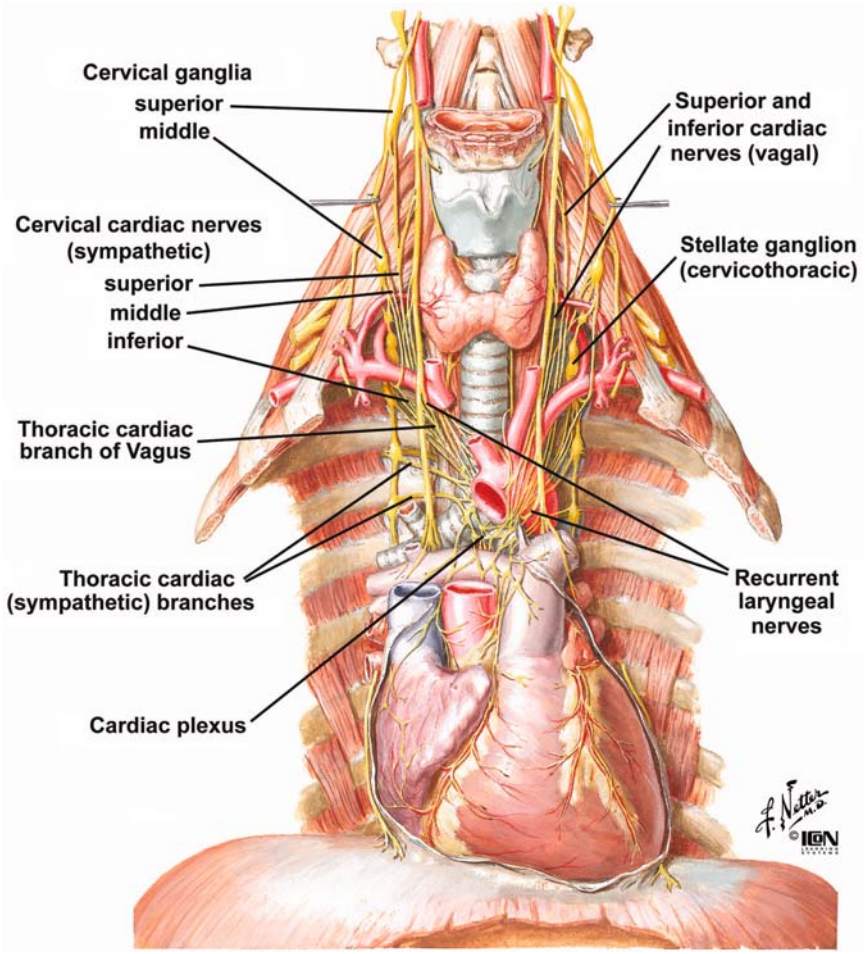

Fig. 13. Pattern of innervation in the superior mediastinum.

The phrenic nerves provide the motor innervation to the diaphragm ("C-3-4-5 keeps your diaphragm alive"); they provide sensory innervation to the pericardium, mediastinal and diaphragmatic pleura, and diaphragmatic peritoneum on the inferior surface of the diaphragm. The course of the right phrenic nerve behind the subclavian vein makes it susceptible to stimulation if current leaks from a pacing lead within the vessel.

The bilateral vagus nerves pass out of the skull via the jugular foramen and descend through the neck in the carotid sheath, just lateral to the common carotid arteries. These nerves are the parasympathetic supply to the thorax and most of the abdomen. On the right, the vagus crosses anterior to the subclavian artery, then turns posterior to pass behind the root of the lung and onto the esophagus. Before the right vagus enters the superior mediastinum, it gives off a recurrent laryngeal branch that passes behind the subclavian artery and ascends into the neck. On the left, the vagus passes lateral to the arch of the aorta, then turns posterior to pass behind the root of the lung and onto the esophagus (Fig. 12). At the level of the aortic arch, it gives off the left recurrent laryngeal nerve, which passes under the aorta just posterior to the ligamentum arteriosum and ascends into the neck.

The recurrent laryngeal nerves are the motor to most of the muscles of the larynx. It should be noted that an aneurysm in the arch of the aorta can injure the left recurrent laryngeal nerve and manifest as hoarseness of the voice caused by unilateral paralysis of the laryngeal musculature.

The right and left vagi contribute to the esophageal plexus of nerves in the middle mediastinum. The right and left vagi give off cardiac branches in the neck (superior and inferior cardiac nerves) and a variable number of small cardiac nerves in the superior mediastinum (thoracic cardiac branches) that provide parasympathetic innervation to the heart via the cardiac nerve plexus.

Sympathetic innervation to the heart is also found in the superior mediastinum. The heart receives postganglionic branches from the superior, middle, and inferior cardiac nerves, each branching from their respective sympathetic ganglia in the neck (Fig. 13). There are also thoracic cardiac nerves emanating from the upper four or five thoracic sympathetic ganglia. The uppermost thoracic ganglion and the inferior cervical ganglion are often fused to form an elongated ganglion called the *stellate ganglion*, which will give off the inferior cardiac nerve.

The cardiac plexus is located between the trachea, the arch of the aorta, and the pulmonary trunk (Fig. 13). It is a network of sympathetic and parasympathetic nerves derived from the branches described in this section and provides the overall-

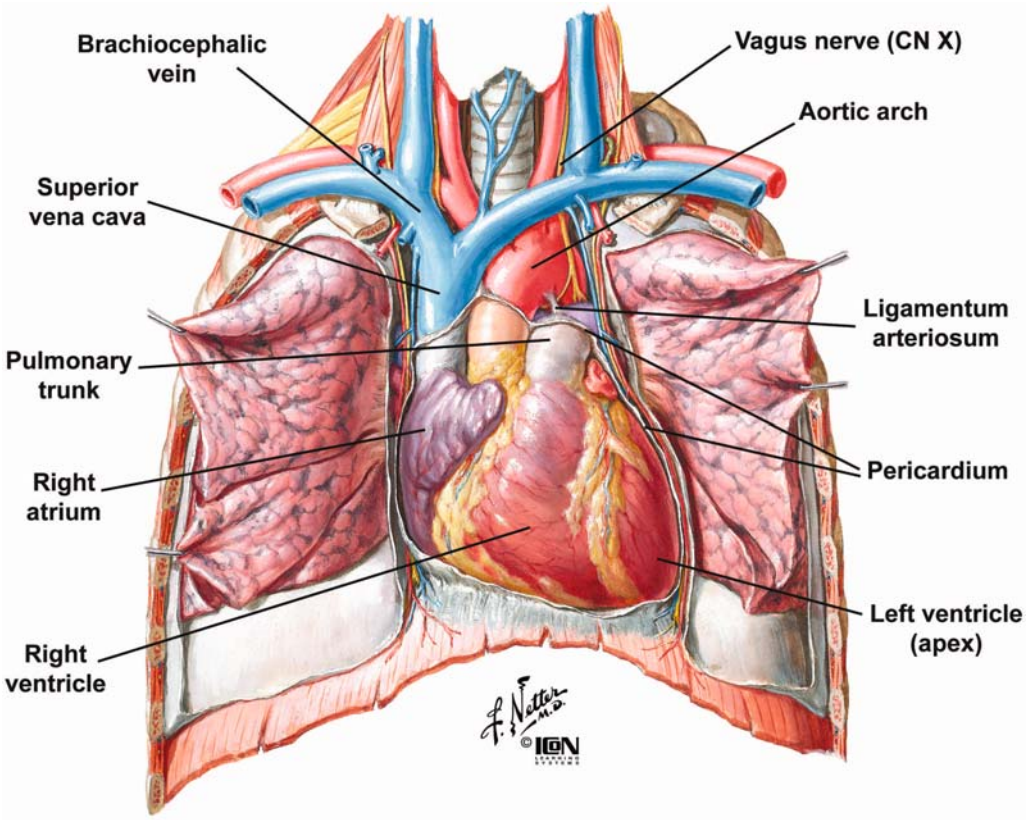

Fig. 14. The position of the heart in the middle mediastinum and the relationship of the pericardium to the heart and great vessels.

autonomic innervation to the heart. Nerves from the plexus reach the heart by traveling along the vasculature and primarily innervate the conduction system and the atria. The sympathetic components cause the strength and pace of the heartbeats to increase. The parasympathetics counter this effect. Pain afferents from the heart travel with the sympathetic nerves to the upper thoracic and lower cervical levels. This distribution accounts for the pattern of referred heart pain to the upper thorax, shoulder, and arm. (For more details on this autonomic innervation, *see* Chapter 10)

7.5. The Thymus

The thymus is found in the most anterior part of the superior mediastinum (Fig. 10). It is considered an endocrine gland, but is actually more important as a lymphoid organ. The thymus produces lymphocytes that populate the lymphatic system and bloodstream. It is particularly active in young individuals and becomes much less prominent with aging. The thymus is located directly behind the manubrium and may extend into the neck and inferiorly into the anterior mediastinum. It lies in contact with the aorta, left brachiocephalic vein, and trachea.

8. THE MIDDLE MEDIASTINUM

8.1. The Pericardium

The middle mediastinum is the central area of the inferior mediastinum occupied by the great vessels, pericardium, and heart (Fig. 14). Within this space, the heart is situated with the right atrium on the right, the right ventricle anterior, the left ventricle to the left and posterior, and the left atrium entirely posterior. The apex, a part of the left ventricle, is projected inferiorly and to the left.

The pericardium is the closed sac that contains the heart and the proximal portion of the great vessels. It is attached to the diaphragm inferiorly. The pericardium is a serous membrane, with a visceral and a parietal layer, into which the heart projects such that there is a potential space within the pericardial sac called the *pericardial cavity*. The visceral pericardium, also called the *epicardium*, covers the entire surface of the heart and base of the great vessels, reflecting to become parietal pericardium on the great vessels. The parietal pericardium is characterized by a thickened, strong outer layer called the *fibrous pericardium*. The fibrous pericardium is fused to the layer of parietal serous pericardium, creating a single layer with two surfaces. The fibrous pericardium has little elasticity and, by its fusion with the base of the great vessels, effectively creates a closed space in which the heart beats. The pericardial cavity can accumulate fluids under pathological conditions and create pressure within the pericardium, a condition known as *cardiac tamponade*. For a complete description of the pericardium and its features, *see* Chapter 7.

8.2. The Great Vessels

Great vessels is a composite term used for describing the large arteries and veins directly entering and exiting the heart

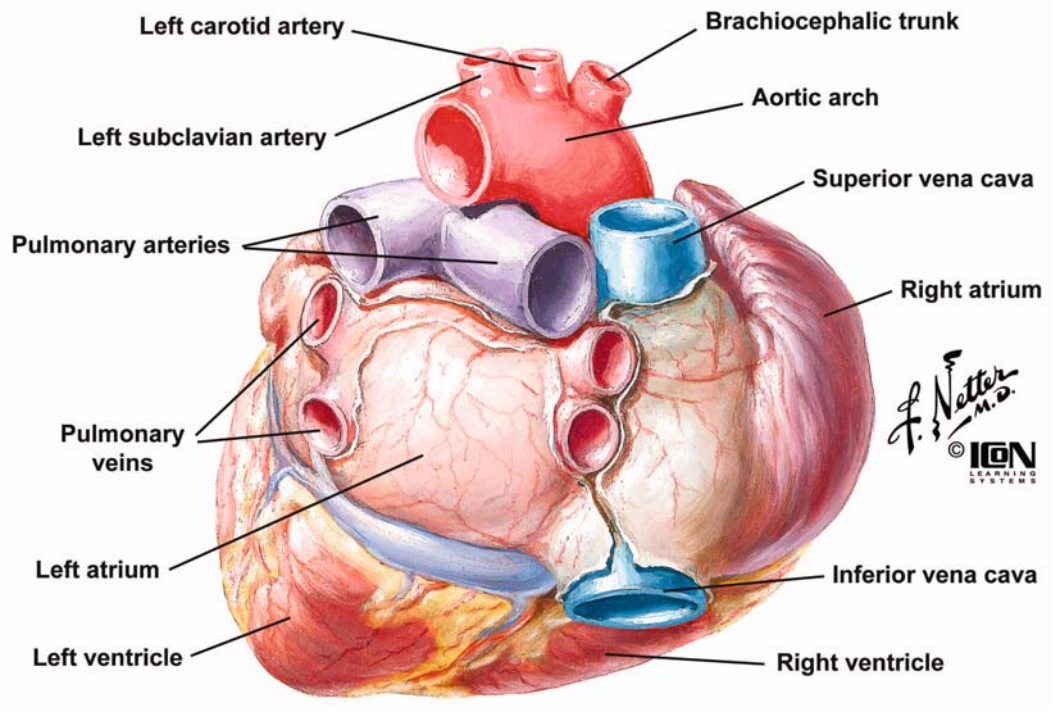

Fig. 15. The great vessels as viewed from the posterior side of the heart.

(Figs. 11 and 15). They include the superior and inferior vena cava, aorta, pulmonary trunk, and pulmonary veins. All of these vessels are found within the middle mediastinum. The inferior vena cava and the pulmonary veins are the shortest of the great vessels. The inferior vena cava enters the right atrium from below almost immediately after passing through the diaphragm. The pulmonary veins (normally two emerging from each lung) enter the left atrium with a very short intrapericardial portion. The superior vena cava is formed from the confluence of the right and left brachiocephalic veins. It also receives the azygos vein from behind and empties into the superior aspect of the right atrium. The pulmonary trunk ascends from the right ventricle on the anterior surface of the heart at an oblique angle to the left and posterior, passing anterior to the base of the aorta in its course.

As the pulmonary trunk emerges from the pericardium, it bifurcates into left and right pulmonary arteries, which enter the hilum of each lung (Fig. 11). The right pulmonary artery passes under the arch of the aorta to reach the right lung. The left pulmonary artery is connected to the arch of the aorta by the ligamentum arteriosum, the remnant of the ductus arteriosus, the connection between the aorta and pulmonary trunk present in the fetus. The aorta ascends from the left atrium at an angle to the right and curves back to the left and posterior as it becomes the aortic arch. As the aorta exits the pericardium, it arches over the right pulmonary trunk, passing to the left of the trachea and esophagus and entering the posterior mediastinum as the descending aorta (Fig. 15). Backflow of blood into either the aorta or the pulmonary trunk is prevented by the semilunar valves. The semilunar valves, each with a set of three leaflets, are found at the base of each of these great vessels. Immediately above these valves are the "aortic and pulmonary sinuses," which are regions where the arteries are dilated. The coronary arteries branch from the right and left aortic sinuses (*see* Chapter 4).

Also passing through the middle mediastinum are the phrenic nerves and the pericardiophrenic vessels (Fig. 10). The phrenic nerves pass out of the neck and through the superior mediastinum. They travel through the middle mediastinum on the lateral surfaces of the fibrous pericardium and under the mediastinal pleura to reach the diaphragm. The phrenic nerve on each side is accompanied by a pericardiophrenic artery, a branch from the proximal internal thoracic artery, and a pericardiophrenic vein, which empties into the subclavian vein. These vessels, as their names imply, supply the pericardium and the diaphragm as well as the mediastinal pleura.

9. THE ANTERIOR MEDIASTINUM

The anterior mediastinum is the subdivision of the inferior mediastinum bounded by the sternum anteriorly and the pericardium posteriorly (Fig. 1). It contains sternopericardial ligaments, made up of loose connective tissue, the internal thoracic vessels and their branches, lymphatic vessels and nodes, and fat. In children, the thymus often extends from the superior mediastinum into the anterior mediastinum.

10. THE POSTERIOR MEDIASTINUM

The posterior mediastinum is the division of the inferior mediastinum bounded by the pericardium anteriorly and the posterior thoracic wall posteriorly (Fig. 1). Structures found in the posterior mediastinum include the descending aorta, azygos system of veins, thoracic duct, esophagus, esophageal

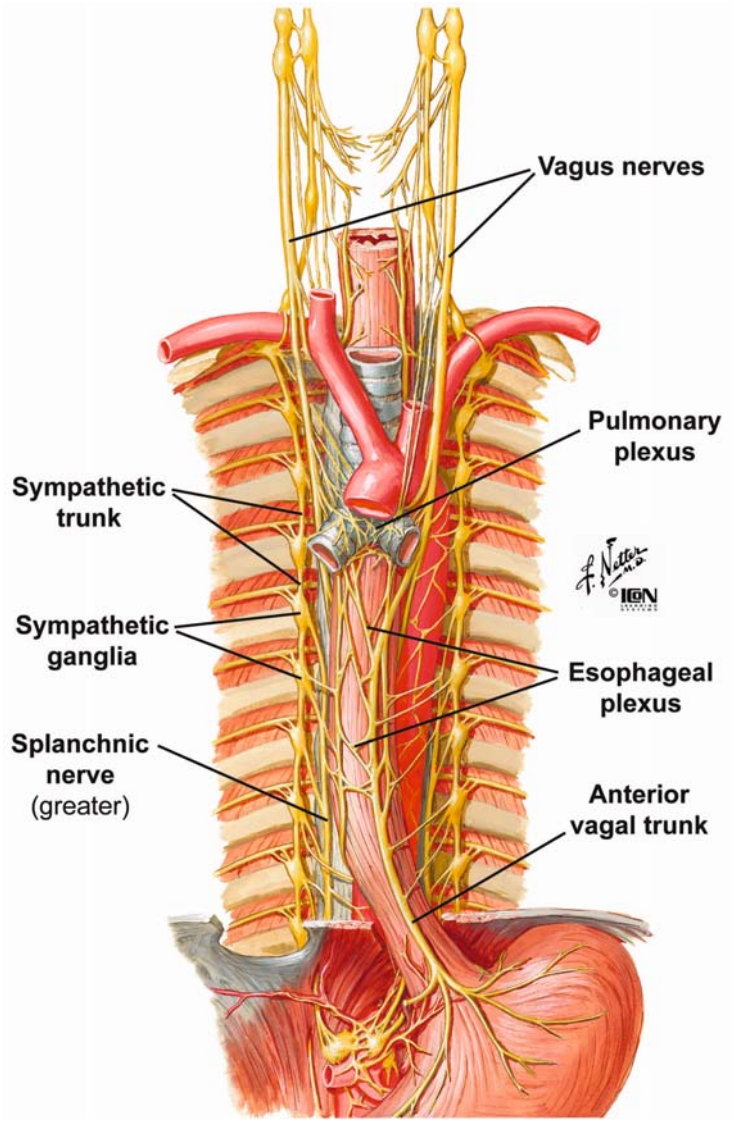

Fig. 16. Course of the esophagus in the posterior mediastinum and the esophageal plexus of nerves.

plexus, thoracic sympathetic trunk, and thoracic splanchnic nerves.

10.1. The Esophagus and Esophageal Plexus

The esophagus descends into the posterior mediastinum, passing along the right side of the descending aorta (Fig. 11). It passes directly behind the left atrium and veers to the left before passing through the esophageal hiatus of the diaphragm at the level of T10. Because of the juxtaposition of the esophagus to the heart, high-resolution ultrasound images of the heart can be obtained via the esophagus. As the bilateral vagus nerves approach the esophagus, they divide into several commingling branches, forming the esophageal plexus (Fig. 16). Toward the distal end of the esophagus, the plexus begins to coalesce into anterior and posterior vagal trunks that pass with the esophagus into the abdomen. The left side of the esophageal plexus from the left vagus nerve contributes preferentially to the anterior vagal trunk and likewise for the right vagus and the posterior vagal trunk, reflecting the normal rotation of the gut. The parasympathetic branches of the anterior and posterior vagal trunks comprise the innervation to the abdominal viscera as far as the splenic flexure.

10.2. The Azygos System of Veins

The azygos venous system in the thorax is responsible primarily for draining venous blood from the thoracic wall to the superior vena cava (Fig. 17). The azygos veins also receive venous blood from the viscera of the thorax, such as the esophagus, bronchi, and pericardium. The term *azygos* means unpaired and describes the asymmetry in this venous system. The system consists of the azygos vein on the right and the hemiazygos and accessory hemiazygos veins on the left.

Both the azygos vein and the hemiazygos vein are formed from the lumbar veins ascending from the abdomen and unit-

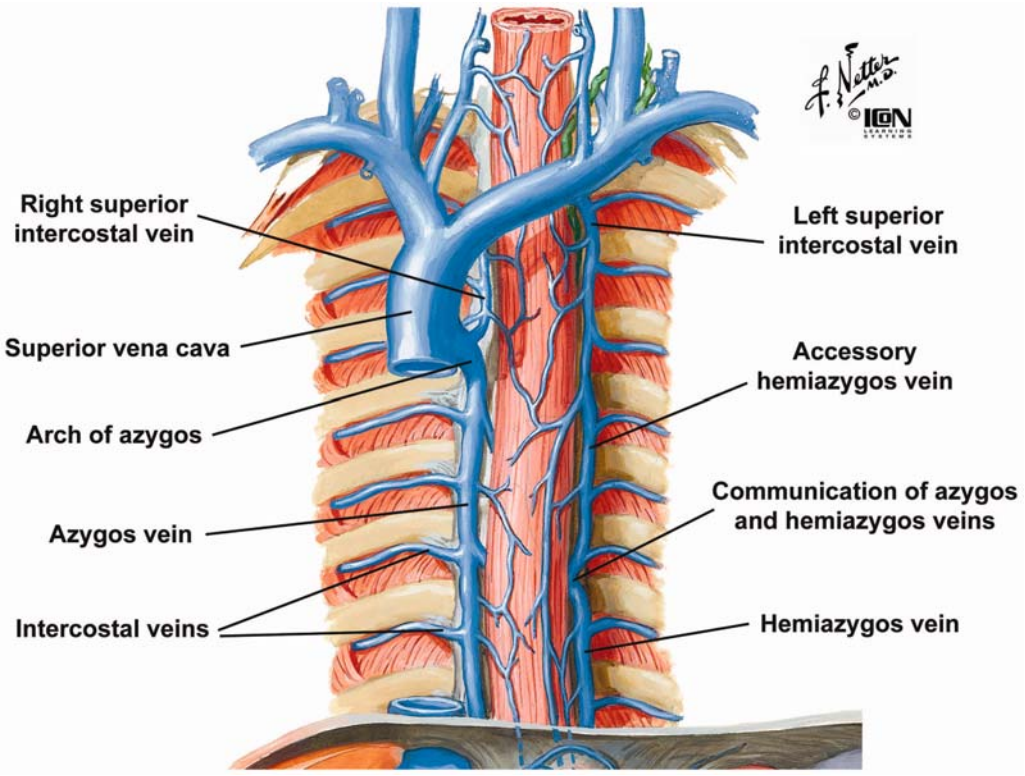

Fig. 17. The azygos venous system in the posterior mediastinum. This figure illustrates a "typical" pattern of the azygos and hemiazygos veins.

ing with the subcostal vein. On the right, the azygos vein is continuous, collecting blood from the right intercostal veins before arching over the root of the lung to join the superior vena cava. On the left, the hemiazygos vein ends typically at the level of T8 by crossing over to communicate with the azygos vein on the right. Above the hemiazygos vein, the accessory hemiazygos vein collects blood from the posterior intercostal veins. It typically communicates with the hemiazygos vein and crosses over to communicate with the azygos vein. On both sides, the second and third intercostal spaces are drained to a superior intercostal vein that not only drains directly to the subclavian vein, but also communicates with the azygos and accessory hemiazygos veins on their respective sides. The first intercostal vein drains directly to the subclavian vein. There is a tremendous amount of variation in the azygos system of veins, all of which is generally functionally inconsequential. However, it should be noted that the azygos system can be quite different in some of the large animal models used to study cardiac function (*see* Chapter 5).

10.3. The Thoracic Duct and Lymphatics

The thoracic duct is the largest lymphatic vessel in the body (Fig. 18). It conveys lymph from the cisterna chyli, which is the collection site for all lymph from the abdomen, pelvis, and lower extremities, back to the venous system. The thoracic duct enters the posterior mediastinum through the aortic hiatus and travels between the thoracic aorta and the azygos vein behind the esophagus. It ascends through the superior mediastinum to the left and empties into the venous system at or close to the junction of the internal jugular and subclavian veins. The thoracic duct often appears white because of the presence of chyle in the lymph and beaded because of the many valves within the duct. The thoracic duct also receives lymphatic drainage from posterior mediastinal lymph nodes, which collect lymph from the esophagus, posterior intercostal spaces, and posterior parts of the pericardium and diaphragm.

10.4. The Descending Thoracic Aorta

The descending thoracic aorta is the continuation of the aortic arch through the posterior mediastinum (Fig. 19). It begins to the left of the T5 vertebra and gradually moves to the middle of the vertebral column as it descends. It passes behind the diaphragm, under the median arcuate ligament (the aortic hiatus), and into the abdomen at the level of T12. The thoracic aorta gives off the 3rd–11th posterior intercostal arteries and the subcostal artery. It also supplies blood to the proximal bronchi and the esophagus via bronchial and esophageal branches. The superior phrenic arteries supply the posterior aspect of the diaphragm and anastomose with the musculophrenic and pericardiacophrenic branches of the internal thoracic artery.

10.5. The Thoracic Sympathetic Nerves

The sympathetic chain of ganglia, or "sympathetic trunk," extends from the sacral region to the cervical spine. It is also called the thoracolumbar division of the autonomic nervous system because preganglionic neurons of this system have their cell bodies in the thoracic and lumbar segments of the spinal cord, from T1 to L2. The thoracic portion of the sympathetic

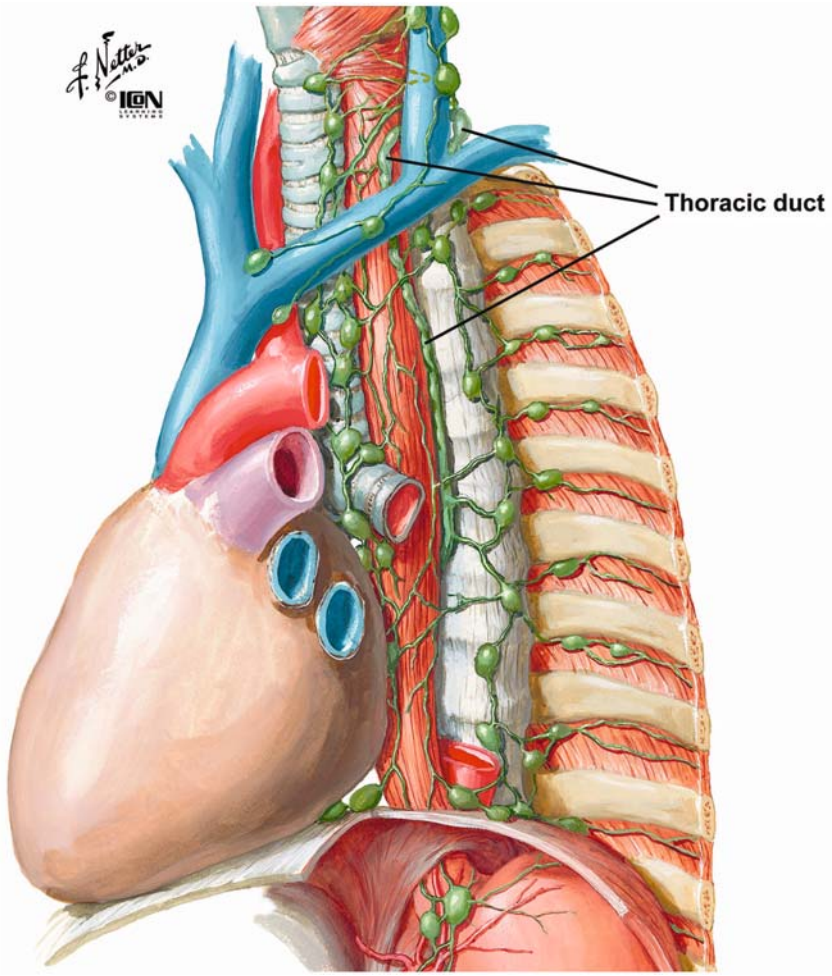

Fig. 18. The course of the thoracic duct in the posterior mediastinum through the superior mediastinum and ending at the junction of the internal jugular and subclavian veins.

trunk is found in the posterior mediastinum (Fig. 16). It is composed of sympathetic ganglia, located along the spine at the junction of the vertebrae and the heads of the ribs, and the intervening nerve segments that connect the ganglia. These sympathetic ganglia are also called *paravertebral sympathetic ganglia* because of their position along side the vertebral column.

There is approximately one sympathetic chain ganglion for each spinal nerve. There are fewer ganglia than nerves because some adjacent ganglia fuse during embryological development. Such fusion is most evident in the cervical region, where there are eight spinal nerves but only three sympathetic ganglia: the superior, middle, and inferior cervical ganglia (Fig. 13). The inferior cervical ganglion and the first thoracic (T1) ganglion are often fused, forming the cervicothoracic or stellate ("star-shaped") ganglion.

An axon of the sympathetic nervous system that emerges from the spinal cord in the thorax travels with the ventral nerve root to a ventral ramus (in the thorax, this would be an intercostal nerve) (Fig. 20). After traveling a short distance on this nerve, this presynaptic (preganglionic) neuron enters the chain ganglion at its level (Fig. 21). Within the ganglion, it either synapses or travels superiorly or inferiorly to synapse at another spinal cord level (C1 to S4). After synapsing, the postsynaptic (postganglionic) neuron travels out of the ganglion and on to the ventral ramus to its target structure or organ.

Presynaptic sympathetic nerves travel from the ventral ramus to the chain ganglion, and postsynaptic nerves travel back to the ventral ramus via small nerve fibers called *rami communicantes* (so named because they communicate between the ventral ramus and the sympathetic ganglion). The presynaptic neurons have myelin protective coatings, and the postsynaptic neurons do not. This pattern of myelination is true of all nerves in the autonomic system. The myelin coating appears white, and thus the presynaptic (myelinated) rami communicantes are called white rami communicantes, and the postsynaptic (unmyelinated) neurons are called the gray rami communicantes. The gray and white rami communicantes can be seen spanning the short distance between the intercostal nerves and the sympathetic ganglia in the posterior mediastinum (Fig. 8).

Also present in the posterior mediastinum are the thoracic splanchnic nerves, which leave the sympathetic trunk and run

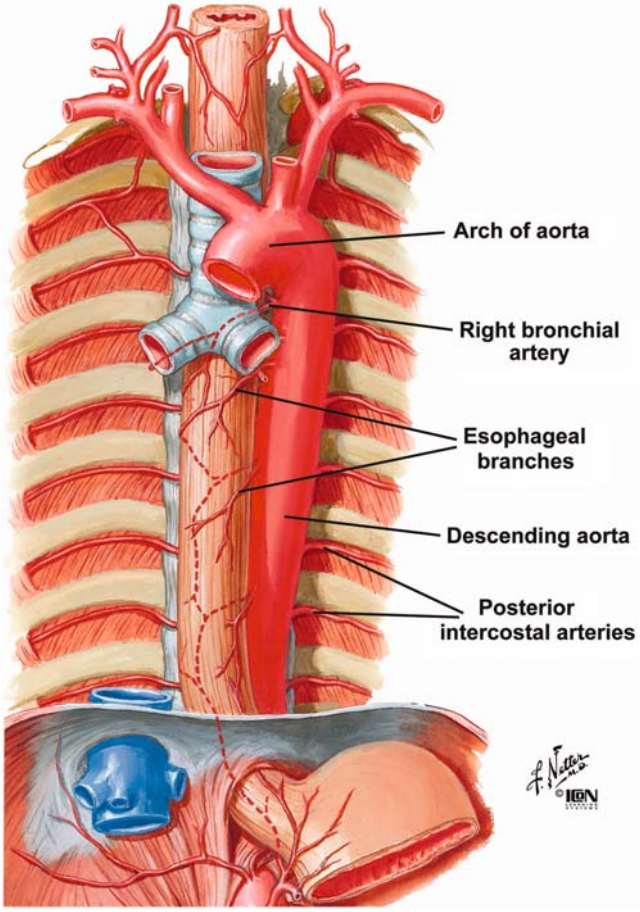

Fig. 19. Course of the descending aorta in the posterior mediastinum with posterior intercostal branches and branches to the esophagus and bronchi.

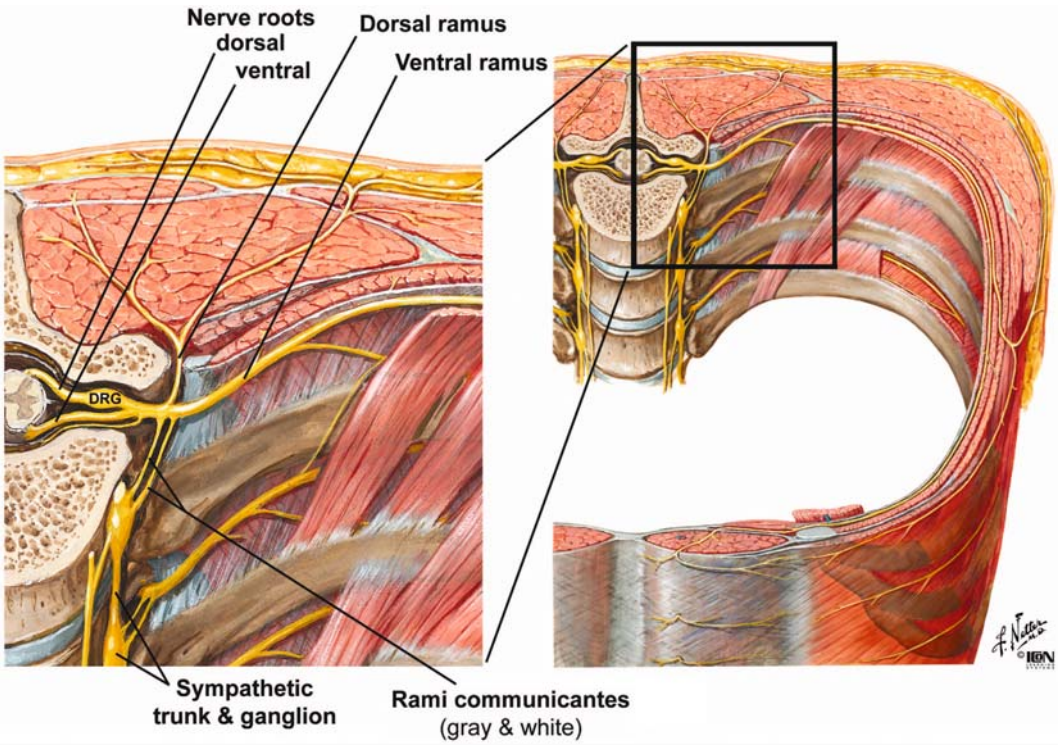

Fig. 20. A typical spinal nerve showing the communication of sympathetic nerves with the chain ganglia via white and gray rami communicantes.

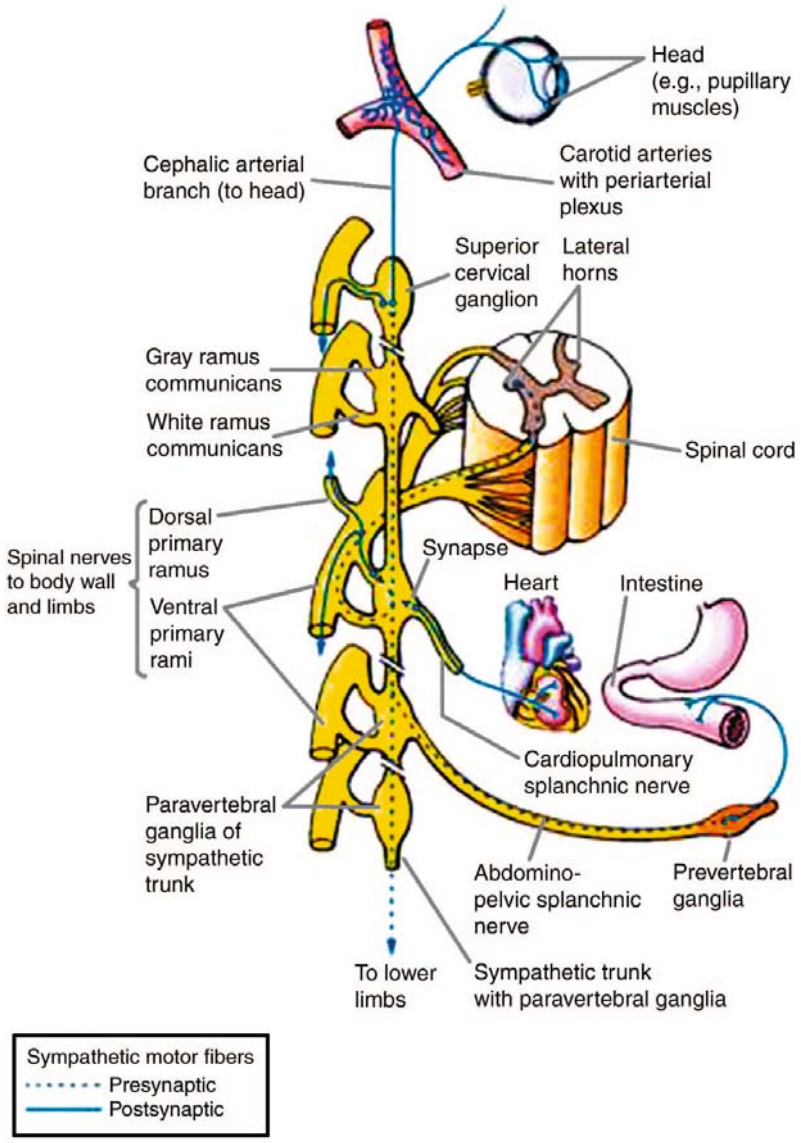

Fig. 21. The three options taken by presynaptic sympathetic fibers are illustrated. All presynaptic nerves enter the sympathetic trunk via white rami communicantes. They can synapse at their level and exit via gray rami communicantes and travel up or down the chain before synapsing, or they can exit before synapsing in the splanchnic nerves. Figure adapted from Figure 1.32 from *Clinically Oriented Anatomy,* 4th Ed., by Keith L. Moore and Arthur F. Dalley. © 1999 Lippincott, Williams, and Wilkins, Philadelphia, PA.

inferiorly toward the midline (Fig. 20). Splanchnic nerves are preganglionic sympathetic neurons that emerge from the spine and pass through the chain ganglion, but do not synapse (Fig. 21). In the thorax these preganglionic splanchnic nerves emerge from spinal cord segments T5–T12 and travel into the abdomen, where they synapse in collateral ganglia, called *prevertebral ganglia*, located along the aorta. The postganglionic fibers then innervate the abdominal organs. There are three splanchnic nerves that emerge in the thorax. The greater splanchnic nerves emerge from spinal cord segments T5–T9, although a few studies reported that they can emerge from T2–T10. The axons of the lesser and splanchnic nerves emerge from segments T10 and T11 and of the least splanchnic nerves emerge from T12.

11. PLEURA AND LUNGS

11.1. The Pleura

The bilateral pulmonary cavities contain the lungs and the pleural membranes (Fig. 1). The pleural membranes are continuous serous membranes that form a closed pleural cavity within each cavity (Fig. 10). The relationship of the lung to this membrane is the same as that of a fist (representing the lung) pushed into an underinflated balloon (representing the pleural membrane). The fist becomes covered by the membrane of the balloon, but it is not "inside" the balloon. In the case of the lung, the pleura in contact with the lung is the visceral pleura, and the outer layer, which is in contact with the inner wall of the thorax and the mediastinum, is the parietal pleura (Fig. 22). The space within the pleural sac is the pleural cavity. Under

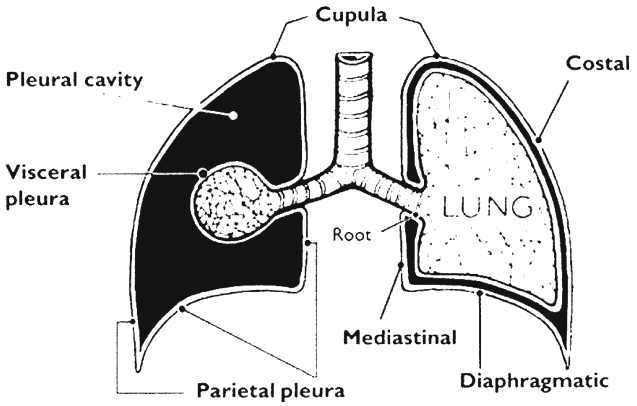

Fig. 22. Relationship of the lungs and walls of the thoracic cavity to the pleural membrane. Adapted from Fig. 1.15 of *Grant's Dissector,* 12th Ed., E. K. Sauerland (ed.). © 1999 Lippincott, Williams, and Wilkins, Philadelphia, PA.

normal conditions, the pleural cavity contains only a small amount of serous fluid and has no functional open space. It is referred to as a "potential space" because a real space can be created if outside material, such as blood, pathologic fluids, or air, is introduced into this space.

The parietal pleura is subdivided into specific parts based on the part of the thorax it contacts (Figs. 10 and 22). Costal pleura overlies the ribs and intercostal spaces. In this region, the pleura is in contact with the endothoracic fascia, the fascial lining of the thoracic cavity. The mediastinal and diaphragmatic pleura are named for their contact with these structures. The cervical pleura extends over the cupola of the lung; above the first rib into the root of the neck, it is strengthened by the suprapleural membrane, an extension of the endothoracic fascia over the cupola of lung.

The lines of pleural reflection are the locations along which the parietal pleura transitions from one region to the next (Fig. 23). The sternal line of reflection is the point at which costal pleura transitions to mediastinal pleura on the anterior side of the thorax. The costal line of pleural reflection lies along the origin of the diaphragm at which the costal pleura transitions to diaphragmatic pleura. Both the costal and sternal lines of reflection are very abrupt. The vertebral line of pleural reflection lies along the line at which costal pleura becomes mediastinal pleura posteriorly. This angle of reflection is shallower than the other two. The surface projections of the parietal pleura are discussed in Section 12.2.

The parietal pleura reflects onto the lung to become the visceral pleura at the root of the lung. A line of reflection descends from the root of the lung, much like the sleeve of a loose robe hangs from the forearm, forming the pulmonary ligament (Fig. 24). The visceral pleura covers the entire surface of each lung, including the surfaces in the fissures, where the visceral pleura on one lobe is in direct contact with the visceral pleura of the other lobe. On the surface of the lung, the visceral pleura is in contact with the parietal pleura.

The pleural cavity is the space inside the pleural membrane (Fig. 22). It is a potential space that under normal conditions contains only a small amount of serous fluid, which lubricates the movement of the visceral pleura against the parietal pleura during respiration. During expiration, the lungs do not entirely fill the most inferior aspect of the pulmonary cavity. This creates a region, along the costal line of reflection, in which the diaphragmatic and costal pleura come into contact with each other with no intervening lung tissue. This space is the costodiaphragmatic recess.

11.2. The Lungs

The primary function of the lungs is to acquire O_2, required for metabolism in tissues, and to release CO_2, a metabolic waste product from tissues. The lungs fill the pulmonary cavities and are separated from each other by structures in the mediastinum. In the living, the lung tissue is soft, light, and elastic, filling the pulmonary cavity and accommodating surrounding structures that impinge on the lungs. In the fixed cadaveric lung, the imprint of structures adjacent to the lungs is easily seen. Blood and air enter and exit the lung at the hilum or root of the lung via the pulmonary vessels and the bronchi.

Each lung is divided into a superior and inferior lobe by an oblique (major) fissure (Fig. 24). The right lung has a second, horizontal (minor) fissure that creates a third lobe called the *middle lobe*. Each lung has three surfaces—costal, mediastinal, and diaphragmatic—and an apex that extends into the cupula at the root of the neck. The costal surface is smooth and convex, and diaphragmatic surfaces are smooth and concave. The mediastinal surface is concave and is the site of the root of the lung, where the primary bronchi and pulmonary vessels enter and exit the lungs.

The mediastinal surface has several impressions created by structures in the mediastinum. The left lung has a deep impression (the *cardiac impression*) that accommodates the apex of the heart. There is also a deep impression of the aortic arch and the descending thoracic aorta behind the root of the lung. At the superior end of the mediastinal surface, there are impressions from the brachiocephalic vein and the subclavian artery and a shallow impression from the esophagus and trachea. On the right side, there are prominent impressions of the esophagus behind the root of the lung and the arch of the azygos vein, extending over the root of the lung. An impression of the superior vena cava and the brachiocephalic vein appears anterior and above the root of the lung. An impression of both the trachea and esophagus is seen close to the apex of the lung. Descending from the root of both lungs, the pulmonary ligament can be seen.

The lungs also have three borders where the three surfaces meet. The posterior border is where the costal and mediastinal surfaces meet posteriorly. The inferior border is where the diaphragmatic and costal surfaces meet. The inferior border of the lung does not extend to the costal pleural reflection. The anterior border is where the costal and mediastinal surfaces meet anteriorly. On the left lung, the cardiac impression creates a visible curvature on the anterior border called the *cardiac notch*. Below the cardiac notch, a segment of lung called the lingula protrudes around the apex of the heart.

The main bronchi are the initial right and left branches from the bifurcation of the trachea and enter the lung at the hilum (Fig. 25). Like the trachea, they are held open by C-shaped

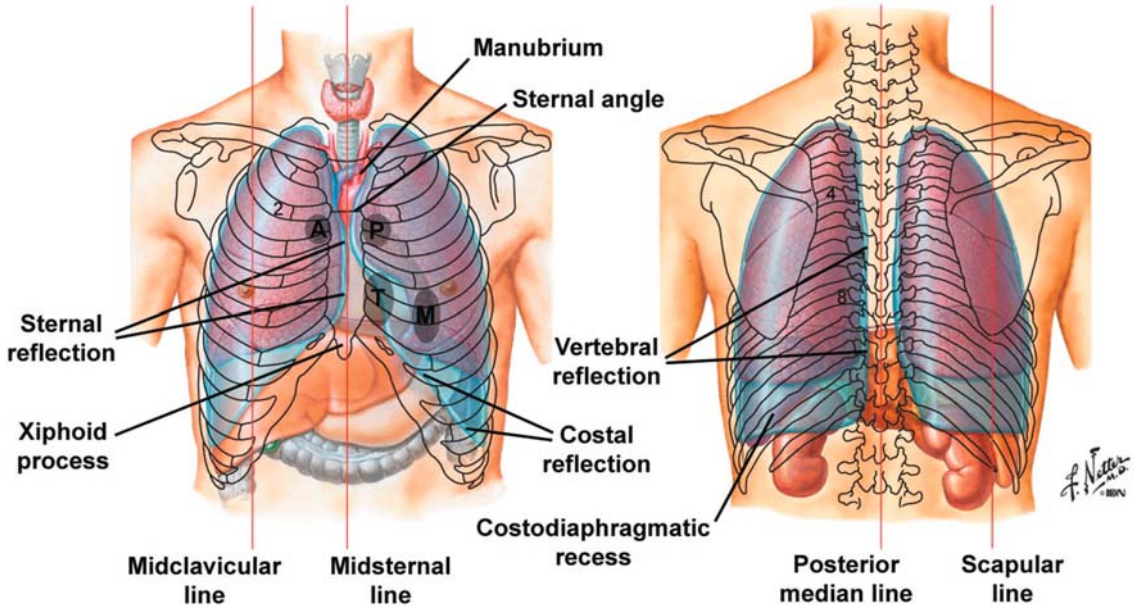

Fig. 23. Surface anatomy and important surface landmarks on the anterior and posterior thorax. The labeled gray areas mark the placement of a stethoscope for listening to heart sounds (auscultation), especially the sounds of the valves. A, aortic valve; P, pulmonary valve; T, tricuspid valve; M, mitral valve.

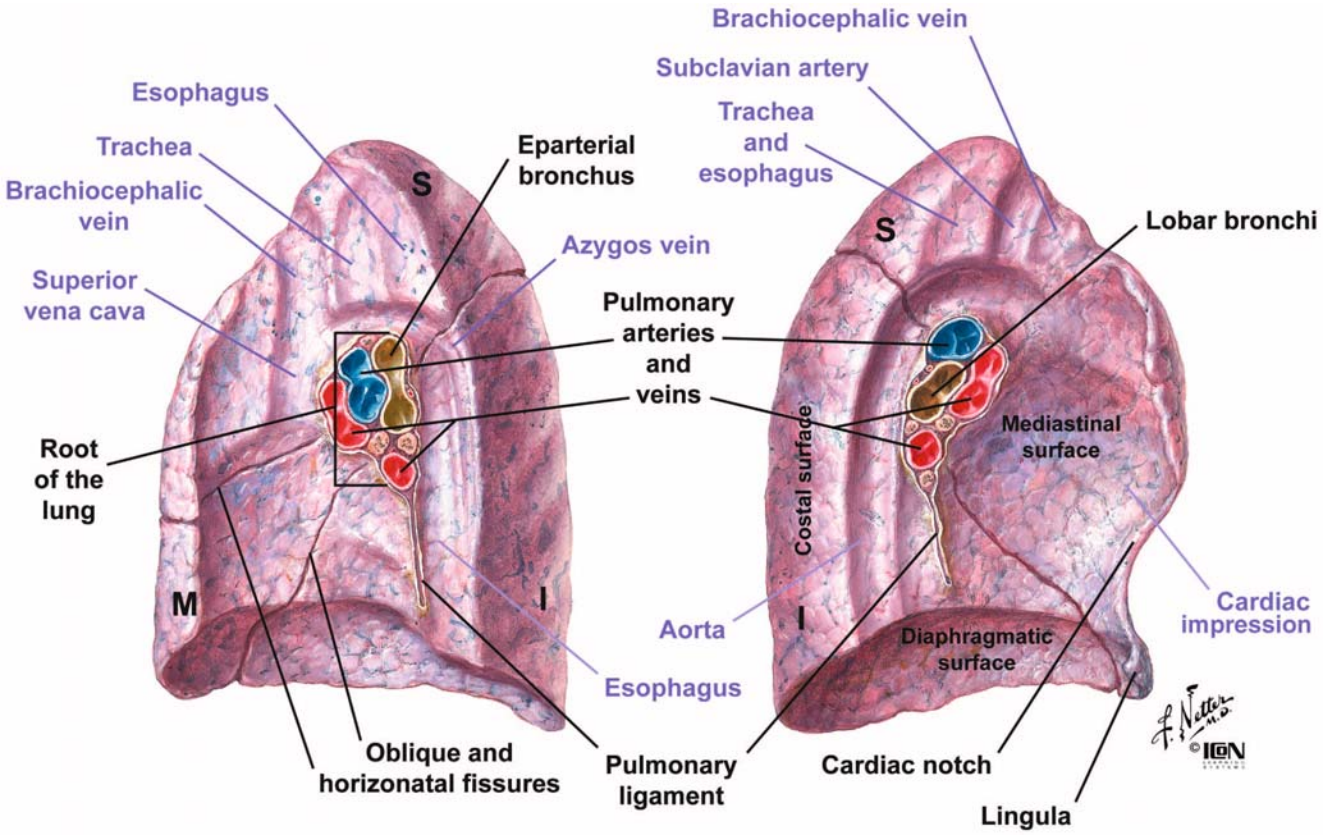

Fig. 24. Surface anatomy of the right (left) and left (right) lungs. S, superior lobe; I, inferior lobe; M, middle lobe.

segments of hyaline cartilage. The right main bronchus is wider and shorter and enters the lung more vertically than the left main bronchus. This is the reason aspirated foreign objects more often enter the right lung than the left. The left main bronchus passes anterior to the esophagus and under the aortic arch to enter the lung.

Once in the lung, the main bronchi branch multiple times to form the bronchial tree (Fig. 25). The first branching supplies

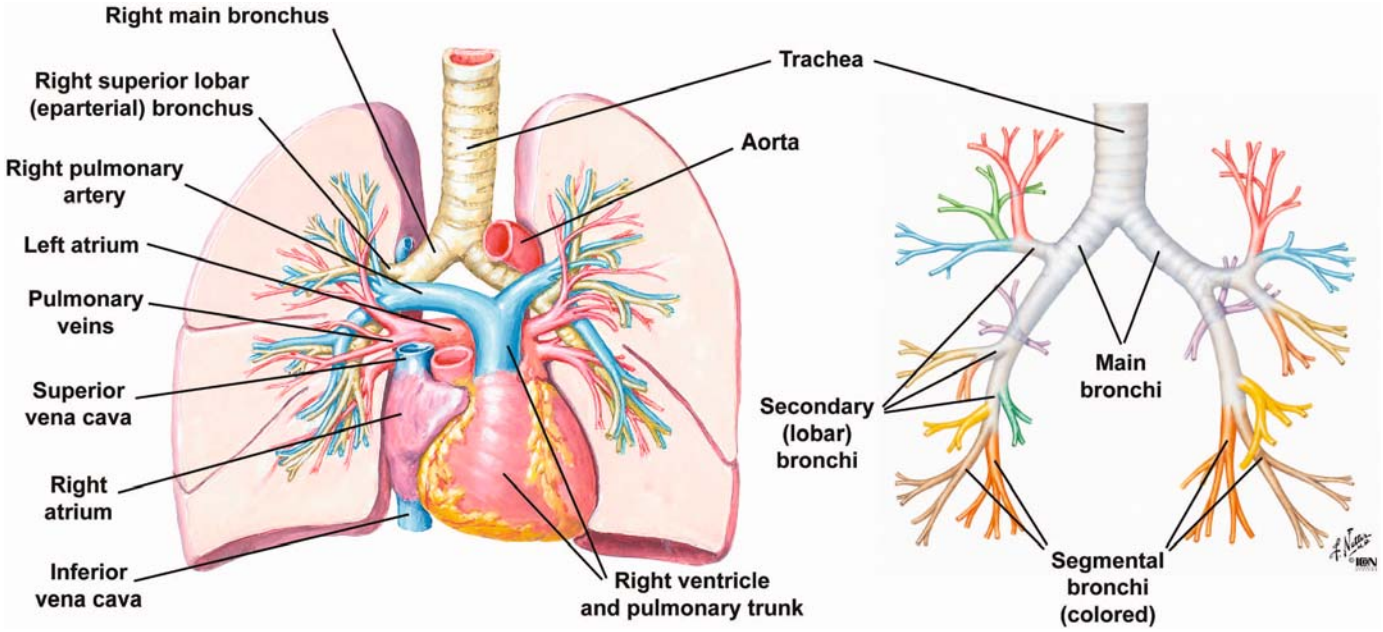

Fig. 25. Pattern of structure entering and leaving the root of the lung (left) and the branching pattern of the bronchi (right).

each lobe of the lung. These are the secondary or lobar bronchi. There are three lobar bronchi on the right and two on the left; these supply their respective lobes. The lobar bronchi branch into several segmental bronchi; each supplies air to a subpart of the lobe called a bronchopulmonary segment. Each bronchopulmonary segment has an independent blood supply and can be resected without impacting the remaining lung. The segmental bronchi then further divide into a series of intersegmental bronchi. The smallest intersegmental bronchi branch to become bronchioles, which can be distinguished from bronchi in that they contain no cartilage in their walls. The terminal bronchioles branch into a series of respiratory bronchioles, each of which contains alveoli. The respiratory bronchioles terminate by branching into alveolar ducts that lead into alveolar sacs, which are clusters of alveoli. It is in the alveoli that gases in the air are exchanged with the blood.

Each lung is supplied by a pulmonary artery that carries deoxygenated blood (thus they are colored blue in anatomical atlases) from the right ventricle of the heart (Fig. 25). Each pulmonary artery enters the hilum of the lung and branches with the bronchial tree to supply blood to the capillary bed surrounding the alveoli. The arterial branches have the same names as the bronchial branches. Oxygenated blood is returned to the left atrium of the heart via the paired pulmonary veins emerging from the hilum of both lungs. The pulmonary veins do not run the same course as the pulmonary arteries within the lung. At the hilum of the lung, the pulmonary artery is typically the most superior structure, with the main bronchus immediately below. On the right, the main bronchus is somewhat higher, and the superior lobar bronchus crosses superior to the pulmonary artery; it is referred to as the *eparterial bronchus*. The pulmonary veins exit the hilum of the lung inferior to both the main bronchus and the pulmonary artery.

Lymphatic drainage of the lungs is to tracheobronchial lymph nodes located at the bifurcation of the trachea (Fig. 26). A subpleural lymphatic plexus lies under the visceral pleura and drains directly to the tracheobronchial nodes. A deep lymphatic plexus drains along the vasculature of the lungs to pulmonary nodes along the bronchi, which communicate with bronchopulmonary nodes at the hilum, and from there to the tracheobronchial nodes. The lymphatic drainage from the lungs may either drain directly to the subclavian veins via the bronchomediastinal trunks, or into the thoracic duct.

The lungs receive innervation from the pulmonary plexus (Fig. 16). The parasympathetic nerves are from the vagus (cranial nerve 10), and they are responsible for constriction of the bronchi and vasodilatation of the pulmonary vessels; they are secretomotor to the glands in the bronchial tree. The sympathetics act opposite the parasympathetics. Pain afferents from the costal pleura and the outer parts of the diaphragmatic pleura are derived from the intercostal nerves. The phrenic nerves contain sensory afferents for the mediastinal pleura and the central part of the diaphragmatic pleura.

11.3. Mechanics of Respiration

Respiration is controlled by the muscles of the thoracic wall, the respiratory diaphragm, the muscles of the abdominal wall, and the natural elasticity of the lungs (Fig. 27). The diaphragm contracts during inspiration, causing the dome of the diaphragm to descend and the vertical dimension of the thoracic cavity to increase. Simultaneously, the ribs are elevated by contractions of external intercostal muscles and the interchondral parts of the internal intercostals. During deep inspiration, the ribs are further elevated by contractions of muscles in the neck. Elevation of the ribs increases the diameter of the thoracic cavity. The net result is the expansion of the pulmonary cavities.

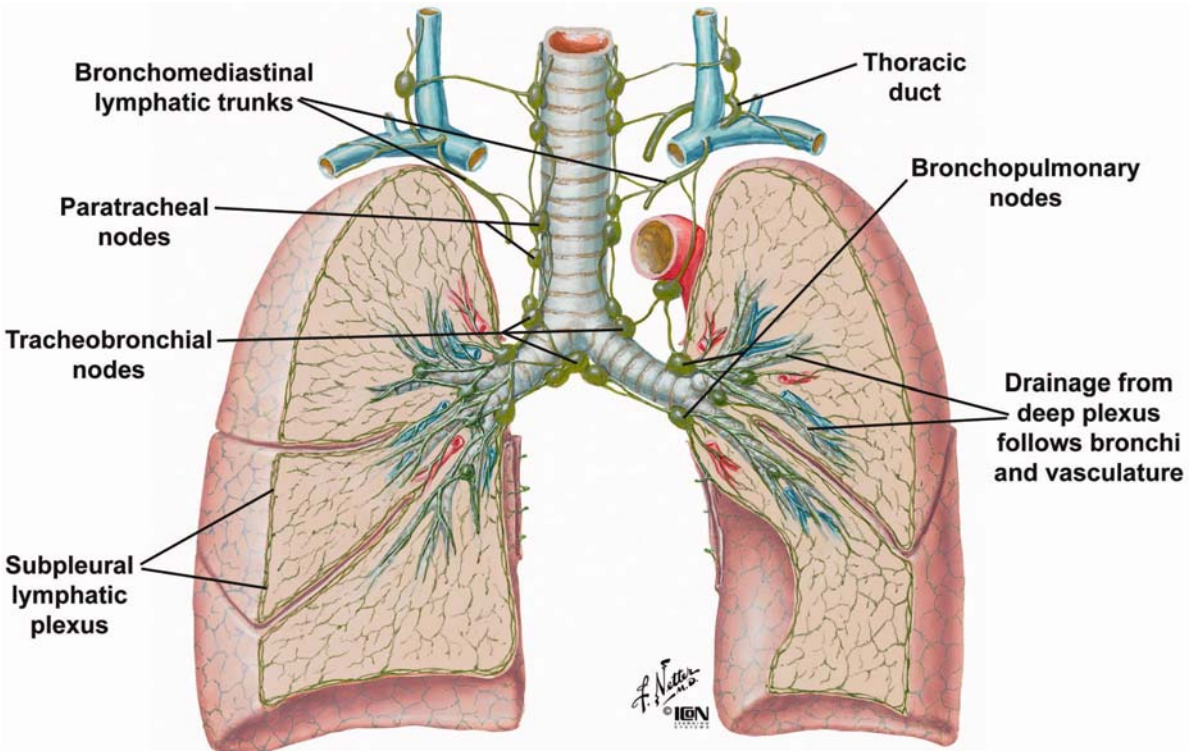

Fig. 26. Pattern of lymphatic drainage from the lungs.

When the walls of the thorax expand, the lungs expand with them because of the negative pressure created in the pleural cavity and the propensity of the visceral pleura to maintain contact with the parietal pleura because of the high surface tension of the liquid between these surfaces (somewhat like two plates of glass sticking together with water in between them). The resultant negative pressure in the lungs forces the subsequent intake of air.

Quiet expiration of air is primarily caused by the elastic recoil of the lungs when the muscles of inspiration are relaxed. Further expiration is achieved by contraction of the lateral internal intercostal muscles, depressing the ribs, and the contraction of abdominal muscles, causing increased abdominal pressure, which pushes up on the diaphragm. At rest, the inward pull of the lungs (in an attempt to deflate further) is at equilibrium with the springlike outward pull of the thoracic wall.

12. SURFACE ANATOMY

12.1. Landmarks of the Thoracic Wall

There are several defined vertical lines that demark regions of the anterior and posterior thoracic wall (Fig. 23). These lines are used to describe the location of surface landmarks and the locations of injuries or lesions on or within the thorax. The anterior median line runs vertically in the midline. It is also referred to as the *midsternal line*. The midclavicular line bisects the clavicle at its midpoint and typically runs through or close to the nipple. Three lines demarcate the axilla. The anterior axillary line runs vertically along the anterior axillary fold, and the posterior axillary line runs parallel to it along the posterior axillary fold. The midaxillary line runs in the midline of the axilla, at its deepest part. The scapular line runs vertically on the posterior thorax, through the inferior angle of the scapula. The posterior median line, also called the *midvertebral* or *midspinal line*, runs vertically in the midline on the posterior thorax.

The sternum lies subcutaneously in the anterior median line and can be palpated throughout its length. The jugular notch is found at the upper margin of the sternum, between the medial ends of the clavicle. The jugular notch is easily palpated and can usually be seen as a depression on the surface. The jugular notch represents the anterior junction of the superior mediastinum and the root of the neck. It lies at the level of the T2 vertebra posteriorly. The manubrium intersects with the body of the sternum about 4 cm inferior to the jugular notch, at the manubriosternal joint; this joint creates the sternal angle, which is normally visible on the surface of the thorax.

The sternal angle demarcates the inferior border of the superior mediastinum and lies at the level of the intervertebral disc between T4 and T5. The second rib articulates with the sternum at the sternal angle, making this site an excellent landmark for determining rib number. Immediately adjacent to the sternal angle is rib 2; the other ribs can be found by counting up or down from rib 2. Intercostal spaces are numbered for the rib above. On the posterior thorax, the fourth rib can be found at the level of the medial end of the spine of the scapula and the eighth rib at the inferior angle.

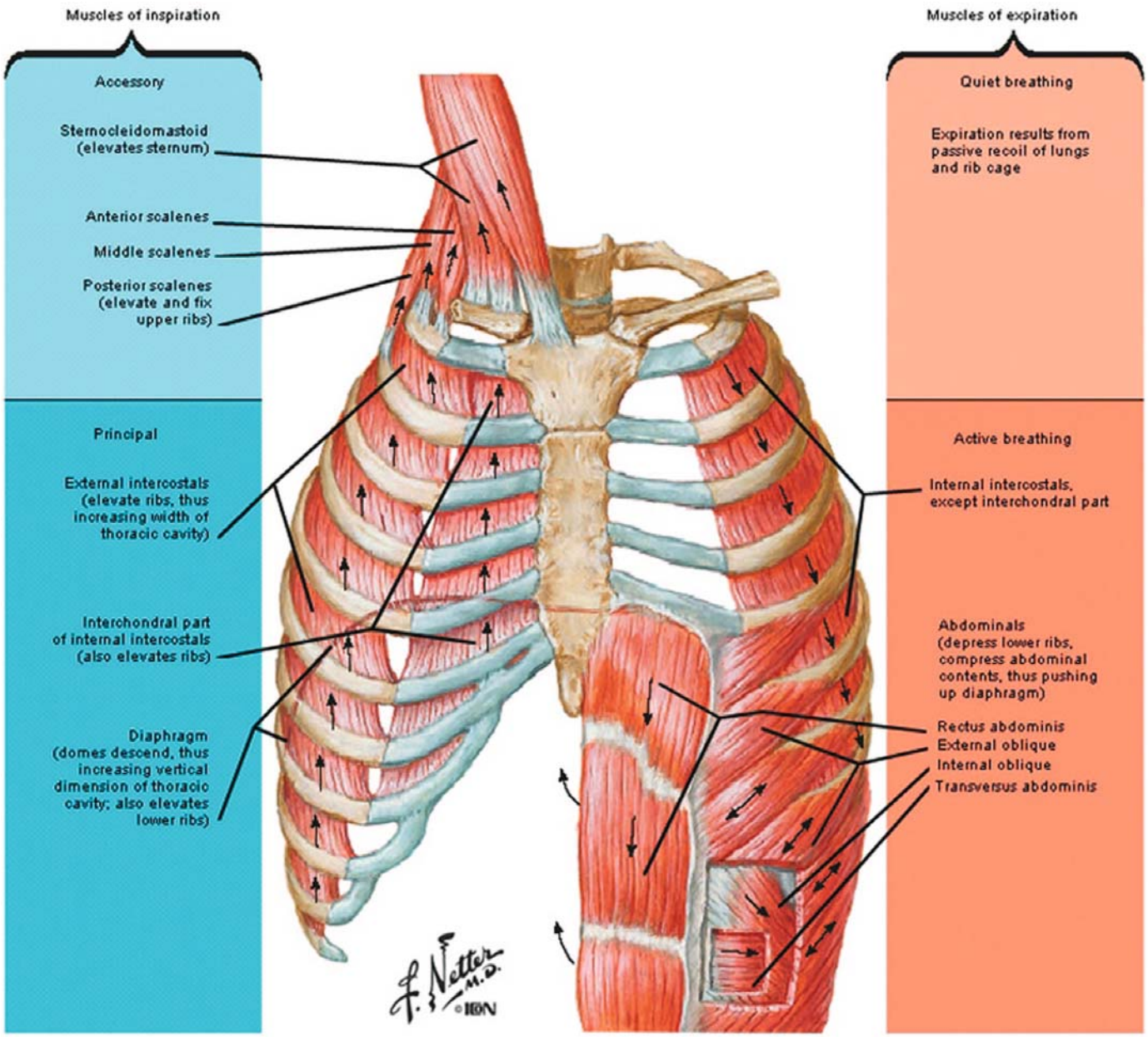

Fig. 27. The participation of muscles in respiration.

The manubrium overlies the junction of the brachiocephalic veins to form the superior vena cava (Fig. 23). The superior vena cava passes at the level of the sternal angle and at, or slightly to the right of, the border of the manubrium. The superior vena cava typically enters the right atrium behind the costal cartilage of the third rib on the right; it is sometimes accessed for various procedures, and knowledge of this surface anatomy is critical for such a procedure.

The xiphoid process is the inferior part of the sternum and lies in a depression, called the *epigastric fossa*, at the apex of the infrasternal angle formed by the convergence of the costal margins at the inferior border of the thorax (Fig. 23). The location of the xiphisternal joint is used as a landmark to determine hand position for cardiopulmonary resuscitation.

The breasts are also surface features of the thoracic wall. In women, the breasts vary greatly in size and conformation, but the base of the breast usually occupies the space between ribs 2 and 6, from the lateral edge of the sternum to the midaxillary line. The nipples, surrounded by an area of darker pigmented skin called the *areola*, are the prominent features of the breast. In men, the nipple is located anterior to the fourth intercostal space in the midclavicular line. Because of the variation in breast anatomy in the female, the location of the nipple is impossible to predict.

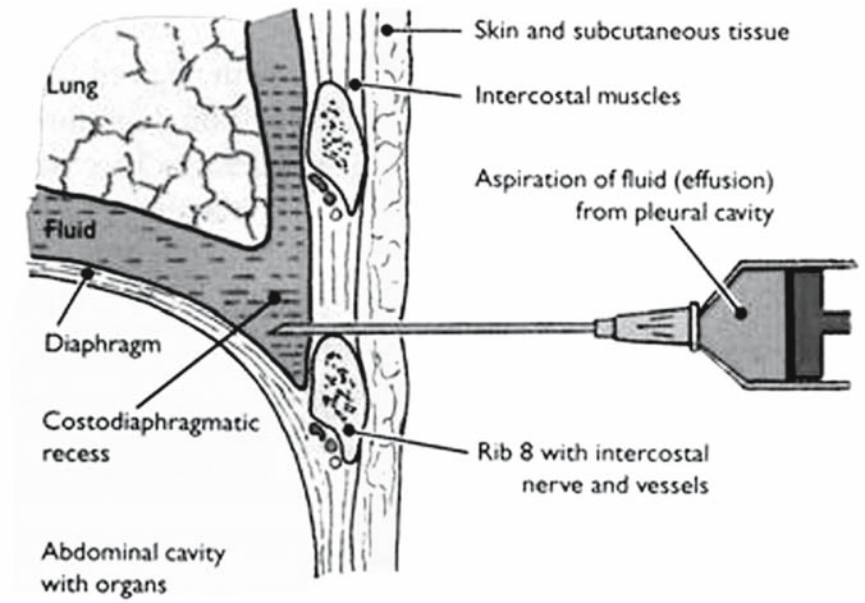

Fig. 28. Illustration of thoracocentesis. Figure adapted from Figure 1.16 from *Grant's Dissector,* 12th Ed., E. K. Sauerland (ed.). © 1999 Lippincott, Williams, and Wilkins, Philadelphia, PA.

12.2. The Lungs and Pleura

The pleural sac is outlined by the parietal pleura as it projects onto the surface of the lungs (Fig. 23). From the root of the neck, these projections follow the lateral edge of the sternum inferiorly. On the left, the border of the parietal pleura moves laterally at the level of fourth costal cartilage to accommodate the cardiac notch within the mediastinum. The pleura follows a line just superior to the costal margin, reaching the level of the tenth rib at the midaxillary line. Posteriorly, the inferior margin of the plural cavity lies at the level of T12, and the medial margin follows the lateral border of the vertebral column to the root of the neck.

In the superior parts of the pleural cavity, the visceral pleura of the lungs is in close contact with the parietal pleura, with the lungs consequently filling the plural cavity. Both lungs and parietal pleura (cervical part) extend above the clavicles into the supraclavicular fossae, at the root of the neck. At the inferior reaches of the pleural cavities, the lungs stop short of filling the plural cavity, reaching only to the level of the 6th rib in the midclavicular line, the eighth rib in the midaxillary line, and the tenth rib posteriorly, creating the costodiaphragmatic recesses. The major (oblique) fissures of the lungs extend along a line from the spinous process of T2 to the costal cartilage of the sixth rib. The minor (horizontal) fissure of the right lung lies under the fourth rib.

Under pathological conditions, fluid can accumulate in the pleural cavity. This fluid normally drains inferiorly and accumulates in the costodiaphragmatic recess. Thoracocentesis refers to the procedure used to drain such fluid (Fig. 28). A needle is inserted into the costodiaphragmatic recess by passing it through the middle of the intercostal space, taking care to avoid the primary intercostal neurovascular bundle immediately below the rib above and collaterals above the rib below.

12.3. The Heart

The heart and great vessels are covered by the sternum and central part of the thoracic cage (Fig. 23). The apex of the heart usually lies in the fifth intercostal space just medial of the midclavicular line. The upper border of the heart follows a line from the inferior border of the left second costal cartilage to the superior border of the right costal cartilage. The inferior border of the heart lies along a line from the right sixth costal cartilage to the fifth intercostal space, at the midclavicular line where the apex of the heart is located. The right and left borders follow lines connecting the right and left ends of the superior and inferior borders.

All four heart valves, the closing of which account for the heart sounds, lie well protected behind the sternum. The sounds of the individual valves closing are best heard at auscultatory sites to which their sounds are transmitted. The bicuspid (mitral) valve is heard at the apex of the heart in the region of the fourth or fifth intercostal space on the left near the midclavicular line. The tricuspid valve can be heard along the left margin of the sternum at the level of the fourth or fifth intercostal space. The pulmonary valve is heard along the left border of the sternum in the second intercostal space. The aortic valve is heard at the second intercostal space on the right sternal border. (For more details on heart sounds, *see* Chapter 14.)

12.4. Vascular Access

An understanding of the surface landmarks relative to the axilla and subclavian region is critical for successful access of the venous system via the subclavian vein. The subclavian vein passes over the first rib and under the clavicle at the junction of its middle and medial thirds; it courses through the base of the neck, where it passes anterior to the apex of the lung and the pleural cavity (Fig. 29). The subclavian vein is immediately

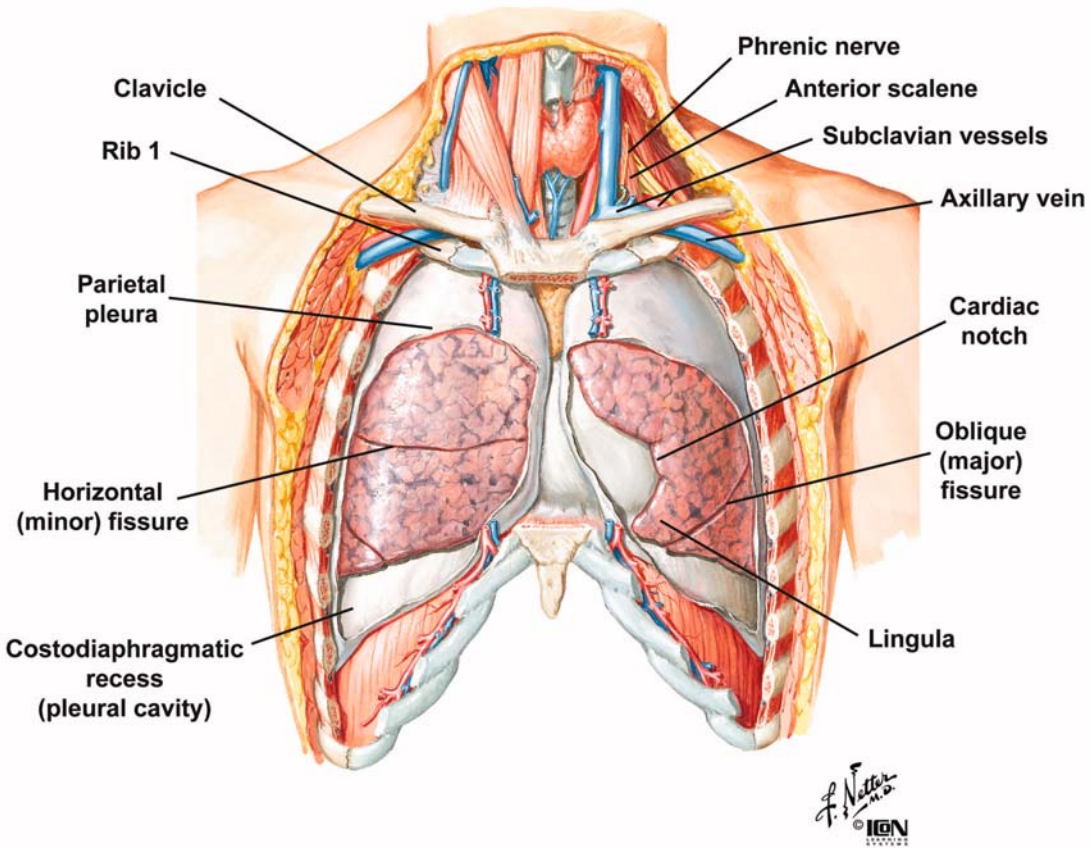

Fig. 29. Anatomy of the subclavian veins and surrounding structures.

anterior to the subclavian artery and is separated from the artery medially by the anterior scalene muscle. To access the subclavian vein, a needle is inserted approx 1 cm inferior to the clavicle at the junction of its medial and middle thirds, and the needle is aimed toward the jugular notch, parallel with the vein to minimize risk of injury to adjacent structures.

The most common complication of subclavian venous access is puncture of the apical pleura, with resulting pneumothorax or hemopneumothorax. In addition, the subclavian artery, lying behind the vein, also has the potential to be injured by this procedure. If subclavian access is attempted on the left, one must also be aware of the junction of the thoracic duct with the subclavian vein. Injury to the thoracic duct can result in chylothorax, the accumulation of lymph in the plural cavity. This is difficult to treat and has an associated high morbidity. When access of the subclavian is attempted for cardiac lead placement, care must be taken to avoid piercing the subclavius muscle or costoclavicular ligament. Passing the lead through these structures tethers it to the highly mobile clavicle, which may cause premature breakage of the lead.

12.5. Summary

Options for accessing, in a minimally invasive fashion, the heart are limited by the vascular anatomy of the superior mediastinum and the axilla. Percutaneous access strategies are limited by the bony anatomy of the thoracic cage. How a device interacts with the thorax and accommodates basic thoracic movements, and movements of the upper extremity and neck, must be understood for design of devices that will endure in the body. Thus, a thorough understanding of the thoracic anatomy surrounding the heart is important to those seeking to design and deploy devices for placement and use in the heart. With an understanding of the important thoracic anatomical relationships presented in this chapter, the engineer should be able to design devices with an intuition for the anatomical challenges that will be faced for proper use and deployment of the device.

SOURCES

Hollinshead, W.H. and Rosse, C. (1985) Part IV: Thorax, In *Textbook of Anatomy*, 4th Ed. Harper and Row, Philadelphia, PA, pp. 463–575.

Magney, L.E., Flynn, D.M., Parsons, J.A., et al. (1993) Anatomical mechanisms explaining damage to pacemaker leads, defibrillator leads, and failure of central venous catheters adjacent to the sternoclavicular joint. *Pacing Clin Electrophysiol.* 16, 445–457.

Moore, K.L. and Dalley, A.F. (1999) Thorax, In *Clinically Oriented Anatomy*, 4th Ed. Lippincott, Williams, and Wilkins, Philadelphia, PA, pp. 62–173.

Netter, F.H. (2003) *Atlas of Human Anatomy*, 3rd Ed. Icon Learning Systems, Teterboro, NJ.

Sauerland, E.K. (1999) The Thorax, in *Grant's Dissector*, 12th Ed. Lippincott, Williams, and Wilkins, Philadelphia, PA, pp. 1–39

Weinberger, S.E. (1998) Pulmonary anatomy and physiology—the basics, in *Principles of Pulmonary Medicine*, 3rd Ed. Saunders, Philadelphia, PA, pp. 1–20.

4 Anatomy of the Human Heart

ANTHONY J. WEINHAUS, PhD AND KENNETH P. ROBERTS, PhD

CONTENTS

1. INTRODUCTION

The heart is a muscular pump that serves two functions: (1) to collect blood from the tissues of the body and pump it to the lungs and (2) to collect blood from the lungs and pump it to all tissues of the body. The human heart lies in the protective thorax, posterior to the sternum and costal cartilages, and rests on the superior surface of the diaphragm. The heart assumes an oblique position in the thorax, with two-thirds to the left of midline. It occupies a space between the pleural cavities called the *middle mediastinum*, defined as the space inside the pericardium, the covering around the heart. This serous membrane has inner and outer layers, with a lubricating fluid in between. The fluid allows the inner visceral pericardium to "glide" against the outer parietal pericardium.

The internal anatomy of the heart reveals four chambers composed of cardiac muscle or myocardium. The two upper chambers (or atria) function mainly as collecting chambers; the two lower chambers (ventricles) are much stronger and function to pump blood. The role of the right atrium and ventricle is to collect blood from the body and pump it to the lungs. The role of the left atrium and ventricle is to collect blood from the lungs and pump it throughout the body. There is a one-way flow of blood through the heart; this flow is maintained by a set of four valves. The atrioventricular valves (tricuspid and bicuspid) allow blood to flow only from atria to ventricles. The semilunar valves (pulmonary and semilunar) allow blood to flow only from the ventricles out of the heart and through the great arteries.

A number of structures that can be observed in the adult heart are remnants of fetal circulation. In the fetus, the lungs do not function as a site for the exchange of oxygen and carbon dioxide, and the fetus receives all of its oxygen from the mother. In the fetal heart, blood arriving to the right side of the heart is passed through specialized structures to the left side. Shortly after birth, these specialized fetal structures normally collapse, and the heart takes on the "adult" pattern of circulation. However, in rare cases, some fetal remnants and defects can occur.

Although the heart is filled with blood, it provides very little nourishment and oxygen to the tissues of the heart. Instead, the tissues of the heart are supplied by a separate vascular supply committed only to the heart. The arterial supply to the heart arises from the base of the aorta as the right and left coronary arteries (running in the coronary sulcus). The venous drainage is via cardiac veins that return deoxygenated blood to the right atrium.

From: *Handbook of Cardiac Anatomy, Physiology, and Devices*
Edited by: P. A. Iaizzo © Humana Press Inc., Totowa, NJ

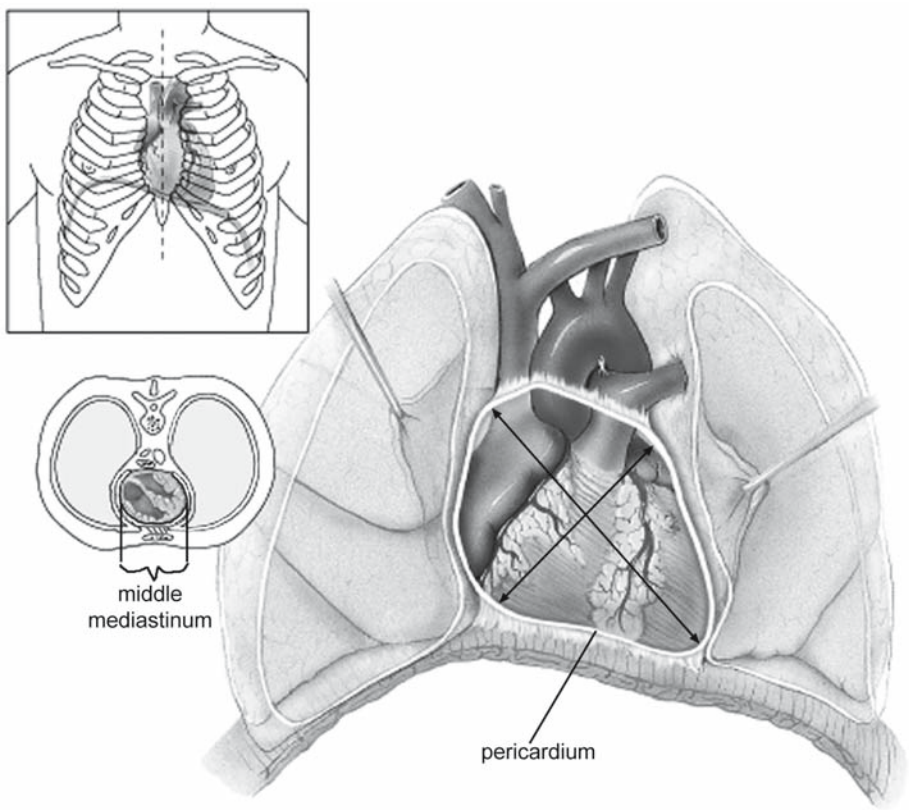

Fig. 1. Position of the heart in the thorax. The heart lies in the protective thorax, posterior to the sternum and costal cartilages, and rests on the superior surface of the diaphragm. The heart assumes an oblique position in the thorax, with two-thirds to the left of midline. It is located between the two lungs, which occupy the lateral spaces called the *pleural cavities*. The space between these two cavities is referred to as the *mediastinum*. The heart lies obliquely in a division of this space, the middle mediastinum, surrounded by the pericardium. (Figs. 18.2 a, b, c, p. 523 from *Human Anatomy*, 3rd Ed. by Elaine N. Marieb and Jon Mallatt. © 2001 by Benjamin Cummings. Reprinted by permission of Pearson Education, Inc.)

The heart is a muscular pump that serves two functions: (1) to collect oxygen-poor blood from the tissues of the body and pump this blood to the lungs to pick up oxygen and release carbon dioxide and (2) to collect oxygen-rich blood from the lungs and pump this blood to all of the tissues of the body.

It is important to note that, besides pumping oxygen-rich blood to the tissues of the body for exchange of oxygen for carbon dioxide, the blood also circulates many other important substances. Nutrients from digestion are collected from the small intestine and pumped through the circulatory system to be delivered to all cells of the body. Hormones are produced from one type of tissues and distributed to all cells of the body. The circulatory system carries waste materials (salts, nitrogenous wastes, and excess water) from cells to the kidneys, where they are extracted and passed to the bladder. The pumping of interstitial fluid from the blood into the extracellular space is an important function of the heart. Excess interstitial fluid is then returned to the circulatory system via the lymphatic system.

2. POSITION OF THE HEART IN THE THORAX

The heart lies in the protective thorax, posterior to the sternum and costal cartilages, and rests on the superior surface of the diaphragm. The thorax is often referred to as the thoracic cage because of its protective function of the delicate structures within. The heart is located between the two lungs, which occupy the lateral spaces, called the *pleural cavities*. The space between these two cavities is referred to as the *mediastinum* ("that which stands in the middle"; Fig. 1).

The mediastinum is divided first into the superior and inferior mediastinum by a midsagittal imaginary line called the *transverse thoracic plane*. This plane passes through the sternal angle (junction of the manubrium and body of the sternum) and the space between thoracic vertebrae T4 and T5. This plane acts as a convenient landmark because it also passes through the following structures: the bifurcation of the trachea, the superior border of the pericardium, the base of the aorta, and the bifurcation of the pulmonary trunk.

The human heart assumes an oblique position in the thorax, with two-thirds to the left of midline (Figs. 2 and 3). The heart is roughly in a plane that runs from the right shoulder to the left nipple. The base is located below the third rib as it approaches the sternum (note that the sternal angle occurs at the level of the second rib). The base is directed superiorly to the right of midline and posterior. The pointed apex projects to the left of midline and anterior. Thus, the heartbeat can be most easily palpated between the fifth and sixth ribs (just inferior to the left nipple)

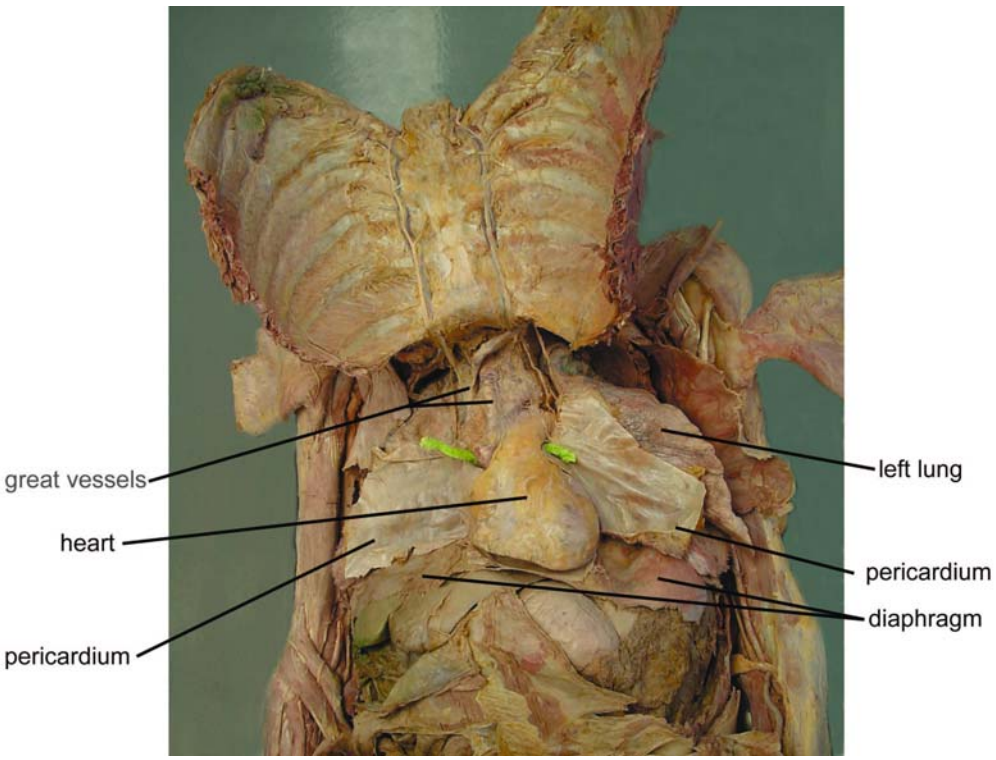

Fig. 2. Cadaveric dissection. Human cadaver dissection in which the ribs were cut laterally, and the sternum and ribs were reflected superiorly. This dissection exposes the contents of the thorax (heart, great vessels, lungs, and diaphragm).

from the apex of the heart where it comes into contact with the thoracic wall. Importantly, the heart lies in such an oblique plane that it is often referred to as horizontal. Thus, the anterior side is often referred to as superior and the posterior side as inferior.

Again, the heart is composed of four distinct chambers. There are two atria (left and right) responsible for collecting blood and two ventricles (left and right) responsible for pumping blood. The atria are positioned superior to (posterior to) and to the right of their respective ventricles (Fig. 3). From superior to inferior, down the anterior (superior) surface of the heart runs the anterior interventricular sulcus ("a groove"). This sulcus separates the left and right ventricles. The groove continues around the apex as the posterior interventricular sulcus on the posterior (inferior) surface. Between these sulci, located within the heart, is the interventricular septum ("wall between the ventricles"). The base of the heart is defined by a plane that separates the atria from the ventricles, called the *atrioventricular groove* or *sulcus*. This groove appears like a belt cinched around the heart. Because this groove appears as though it might also be formed by placing a crown atop the heart, the groove is also called the coronary (*corona* = "crown") sulcus. The plane of this sulcus also contains the atrioventricular valves (and the semilunar valves) and a structure that surrounds the valves called the *cardiac skeleton*. The interatrial ("between the atria") septum is represented on the posterior surface of the heart as the atrial sulcus. Also on the posterior (inferior) side of the heart, the crux cordis ("cross of the heart") is formed from the interatrial sulcus, posterior interventricular sulcus, and the relatively perpendicular coronary sulcus.

Note that the great arteries, aorta and pulmonary trunk, arise from the base of the heart. The right and left atrial appendages (or auricles, so named because they look like dog ears; *auricle* = "little ear") appear as extensions hanging off each atria.

The anterior (superior) surface of the heart is formed primarily by the right ventricle. The right lateral border is formed by the right atrium and the left lateral border by the left ventricle. The posterior surface is formed by the left ventricle and the left atrium, which is centered equally on the midline.

The acute angle found on the right anterior side of the heart is referred to as the *acute* margin of the heart and continues toward the diaphragmatic surface. The rounded left anterior side is referred to as the *obtuse* margin of the heart and continues posteriorly and anteriorly. Both right and left ventricles contribute equally to the diaphragmatic surface, lying in the plane of the diaphragm.

3. THE PERICARDIUM

The pericardium (*peri* = "around" + *cardia* = "heart") is the covering around the heart. It is composed of two distinct but continuous layers separated from each other by a potential space containing a lubricating substance called *serous fluid*. During embryological development, the heart moves from a peripheral location into a space called the *celomic cavity*. The cavity has

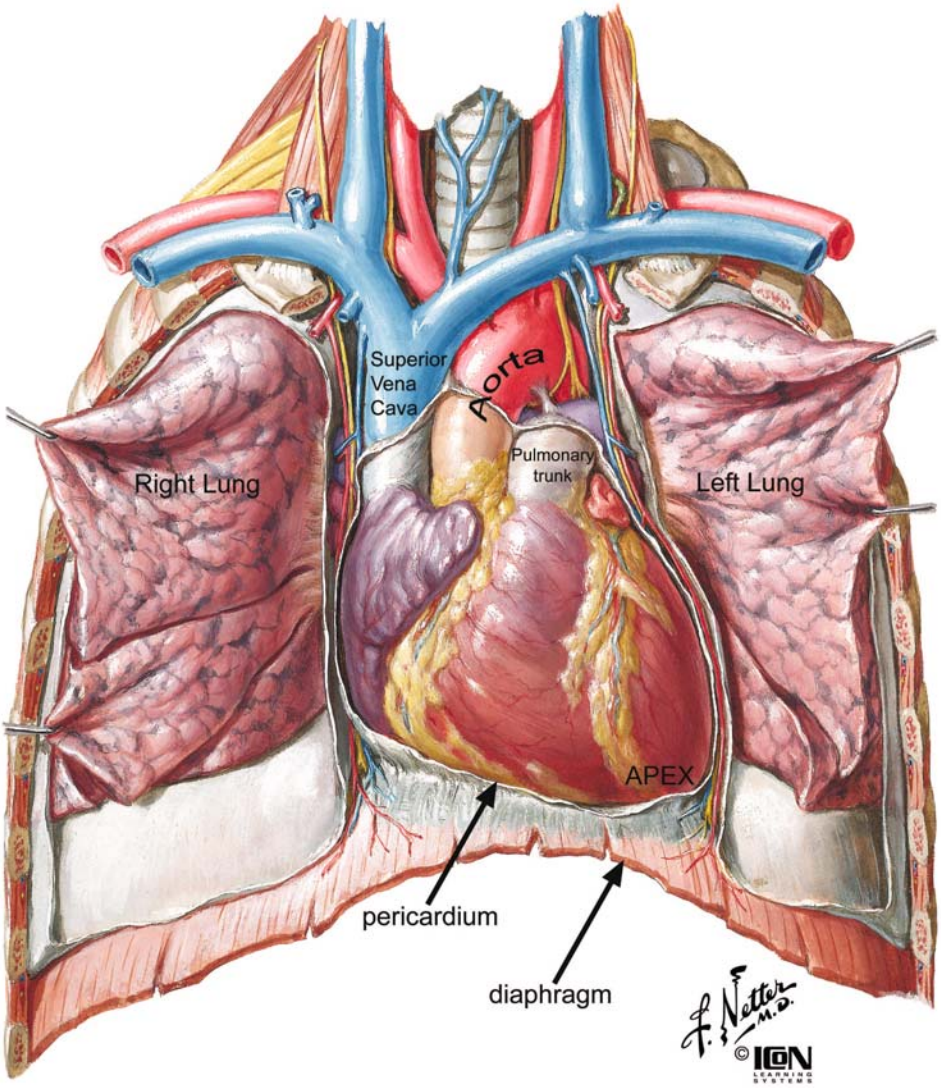

Fig. 3. The anterior surface of the heart. The atria are positioned superior to (posterior to) and to the right of their respective ventricles. From superior to inferior, down the anterior surface of the heart, runs the anterior interventricular sulcus ("a groove"). This sulcus separates the left and right ventricles. The base of the heart is defined by a plane, called the atrioventricular groove or sulcus, that separates the atria from the ventricles. Note that the great arteries, aorta, and pulmonary trunk arise from the base of the heart. The right and left atrial appendages appear as extensions hanging off each atria. The anterior (superior) surface of the heart is formed primarily by the right ventricle. The right lateral border is formed by the right atrium, and the left lateral border by the left ventricle. The posterior surface is formed by the left ventricle and the left atrium, which is centered equally on the midline.

a serous fluid-secreting lining. As the heart migrates into the cavity, the serous lining wraps around the heart. This process can be described as similar to a fist pushed into a balloon (Fig. 4). Note that the fist is surrounded by balloon; however, the fist does not enter the balloon, and the balloon is still one continuous layer of material. These same properties are true for the pericardium.

Furthermore, although it is one continuous layer, the pericardium is divided into two components. The part of the pericardium that is in contact with the heart is called the *visceral pericardium* (*viscus* = "internal organ") or *epicardium* (*epi* = "upon" + "heart"). The free surface of the epicardium is covered by a single layer of flat-shaped epithelial cells called *mesothelium*. The mesothelial cells secrete a small amount of serous fluid to lubricate the movement of the epicardium on the parietal pericardium. The epicardium also includes a thin layer of fibroelastic connective tissue, which supports the mesothelium, and a broad layer of adipose tissue, which serves to connect the fibroelastic layer to the myocardium. The part of the pericardium forming the outer border is called the *parietal pericardium* (*parietes* = "walls"). The parietal pericardium, in addition to a serous layer, also contains a fibrous or epipericardial layer, referred to as the *fibrous pericardium*. These layers contain collagen and elastin fibers to provide strength and some degree of elasticity to the parietal pericardium.

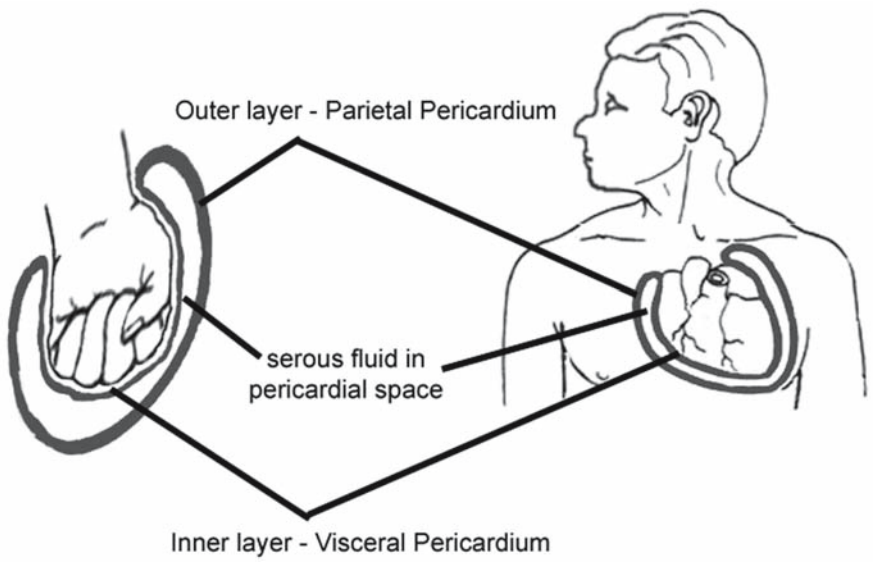

Fig. 4. The pericardium. The pericardium is the covering around the heart. It is composed of two distinct but continuous layers separated from each other by a potential space containing a lubricating serous fluid. During embryological development, the heart migrates into the celomic cavity, and a serous lining wraps around it, a process similar to a fist pushed into a balloon. Note that the balloon and the pericardium are one continuous layer of material. The pericardium can be divided into the visceral pericardium (epicardium) and the parietal pericardium. A small amount of serous fluid is secreted into the pericardial space to lubricate the movement of the epicardium on the parietal pericardium. The parietal pericardium contains an epipericardial layer called the *fibrous pericardium*.

Inferiorly, the parietal pericardium is attached to the diaphragm. Anteriorly, the superior and inferior pericardiosternal ligaments secure the parietal pericardium to the manubrium and the xiphoid process, respectively. Laterally, the parietal pericardium is attached to the parietal pleura (the covering of the lungs). In the space between these layers, the phrenic nerve (motor innervation to the diaphragm) and the pericardiacophrenic artery and vein (supplying the pericardium and diaphragm) are found running together.

Under normal circumstances, only serous fluid exists between the visceral and parietal layers in the pericardial space or cavity. However, the accumulation of fluid (blood from trauma, inflammatory exudate following infection) in the pericardial space leads to compression of the heart. This condition, called cardiac *tamponade* ("heart" + *tampon* = "plug"), occurs when the excess fluid limits the expansion of the heart (the fibrous pericardium resists stretching) between beats and reduces the ability to pump blood, leading to hypoxia (*hypo* = "low" + oxygen") (Fig. 5).

Superiorly, the parietal pericardium surrounds the aorta and pulmonary trunk (about 3 cm above their departure from the heart) and is referred to as the *arterial reflections* or *arterial mesocardium*; the superior vena cava, inferior vena cava, and pulmonary veins are referred to as the *venous reflections* or *venous mesocardium*. The outer fibrous/epipericardial layer merges with the outer adventitial layer of the great vessels. The inner serous layer becomes continuous with the visceral pericardium. The result of this reflection is that the heart hangs "suspended" within the pericardial cavity.

Within the parietal pericardium, a blind-ended saclike recess called the *oblique pericardial sinus* is formed from the venous reflections of the inferior vena cava and pulmonary veins (Fig. 6). A space called the *transverse pericardial sinus* is formed between the arterial reflections above and the venous reflections of the superior vena cava and pulmonary veins below. This sinus is important to cardiac surgeons in procedures such as coronary artery bypass grafting, for which it is important to stop or divert the circulation of blood from the aorta and pulmonary trunk. By passing a surgical clamp or ligature through the transverse sinus and around the great vessels, the tubes of a circulatory bypass machine can be inserted. Cardiac surgery is then performed while the patient is on cardiopulmonary bypass. (For more details on the pericardium, *see* Chapters 5 and 7.)

4. INTERNAL ANATOMY OF THE HEART

A cross section cut through the heart reveals three layers (Fig. 7): (1) a superficial visceral pericardium or epicardium (*epi* = "upon" + "heart"); (2) a middle myocardium (*myo* = "muscle" + "heart"); and (3) a deep lining called the "endocardium" (endo = "within," derived from the endoderm layer of the embryonic trilamina). The endocardium is a sheet of epithelium called *endothelium* that rests on a thin layer of connective tissue basement membrane. It lines the heart chambers and makes up the valves of the heart.

The myocardium is the tissue of the heart wall and the layer that actually contracts. The myocardium consists of cardiac muscles in a spiral arrangement of myocardium that squeeze blood through the heart in the proper directions (inferiorly through the atria and superiorly through the ventricles). Unlike all other types of muscle cells, cardiac muscle cells: (1) branch, (2) join at complex junctions called *intercalated discs* so that

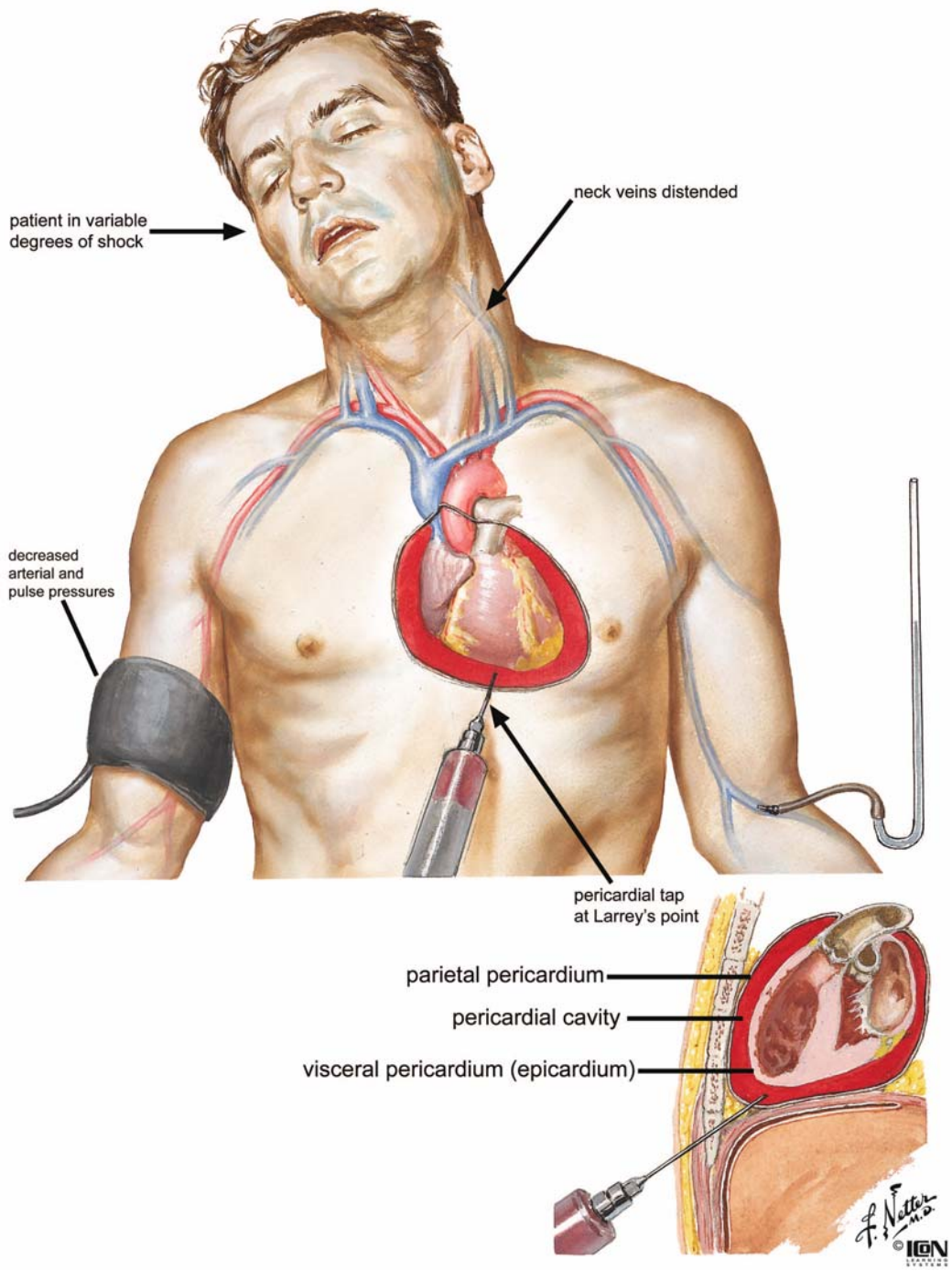

Fig. 5. Cardiac tamponade. Under normal circumstances, only serous fluid exists between the visceral and parietal layers of the pericardium. A condition called cardiac tamponade occurs when there is an accumulation of fluid in the pericardial space that leads to compression of the heart.

they form cellular networks, and (3) each contain single, centrally located nuclei. A cardiac muscle cell is not called a fiber. The term *cardiac muscle fiber*, when used, refers to a long row of joined cardiac muscle cells.

Like skeletal muscle, cardiac muscle cells are triggered to contract by the flow of Ca^{2+} ions into the cell. Cardiac muscle cells are joined by complex junctions called intercalated discs. The discs contain adherans to hold the cells together, and there are gap junctions to allow ions to pass easily between the cells. The free movement of ions between cells allows for the direct transmission of an electrical impulse through an entire network of cardiac muscle cells. This impulse in turn signals all the muscle cells to contract at the same time. For more details on the electrical properties of the heart, refer to Chapter 9.

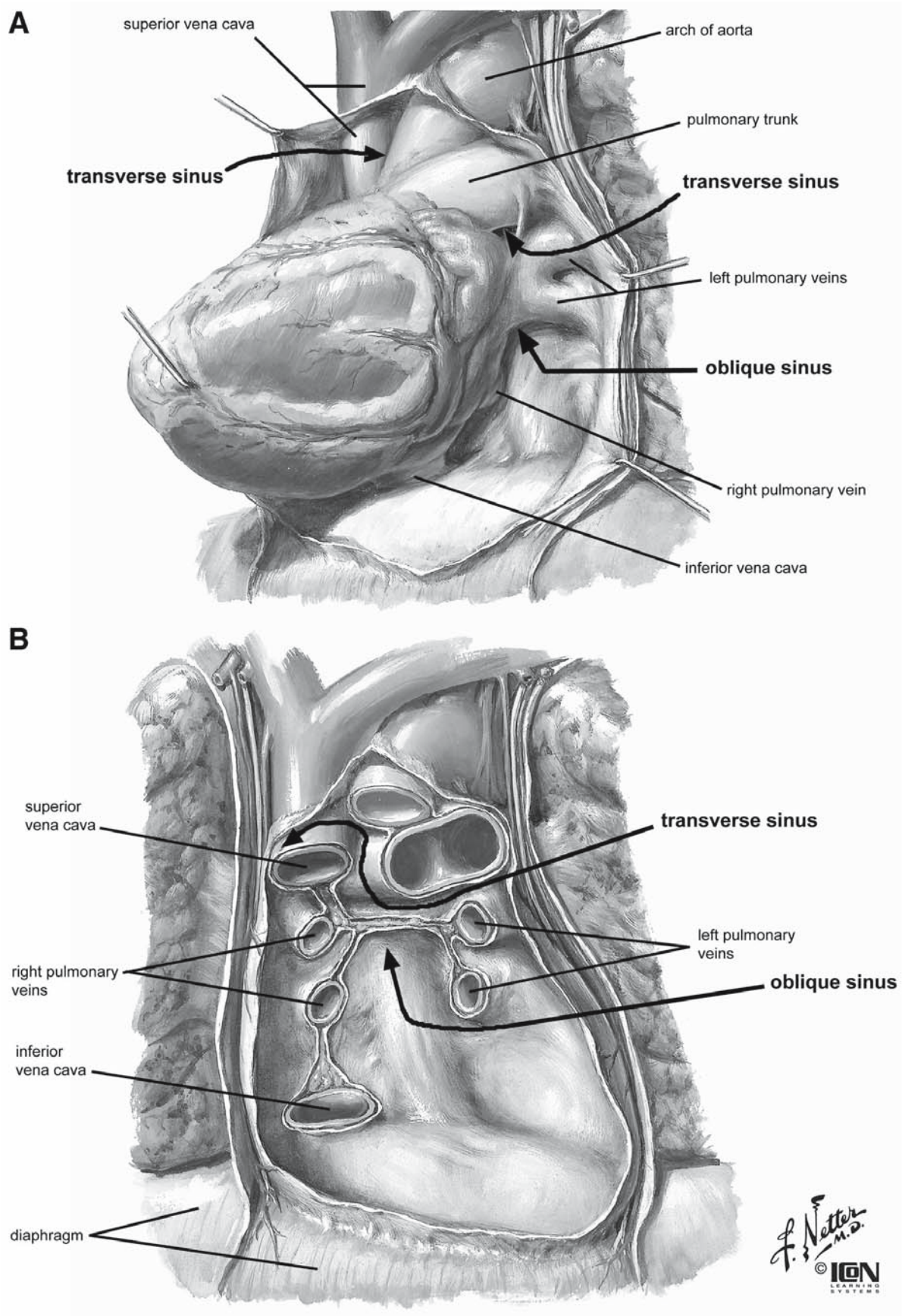

Fig. 6. Pericardial sinuses. A blind-ended sac called the oblique pericardial sinus is formed from the venous reflections of the inferior vena cava and pulmonary veins. Another sac, the transverse pericardial sinus, is formed between the arterial reflections above and the venous reflections of the superior vena cava and pulmonary veins below.

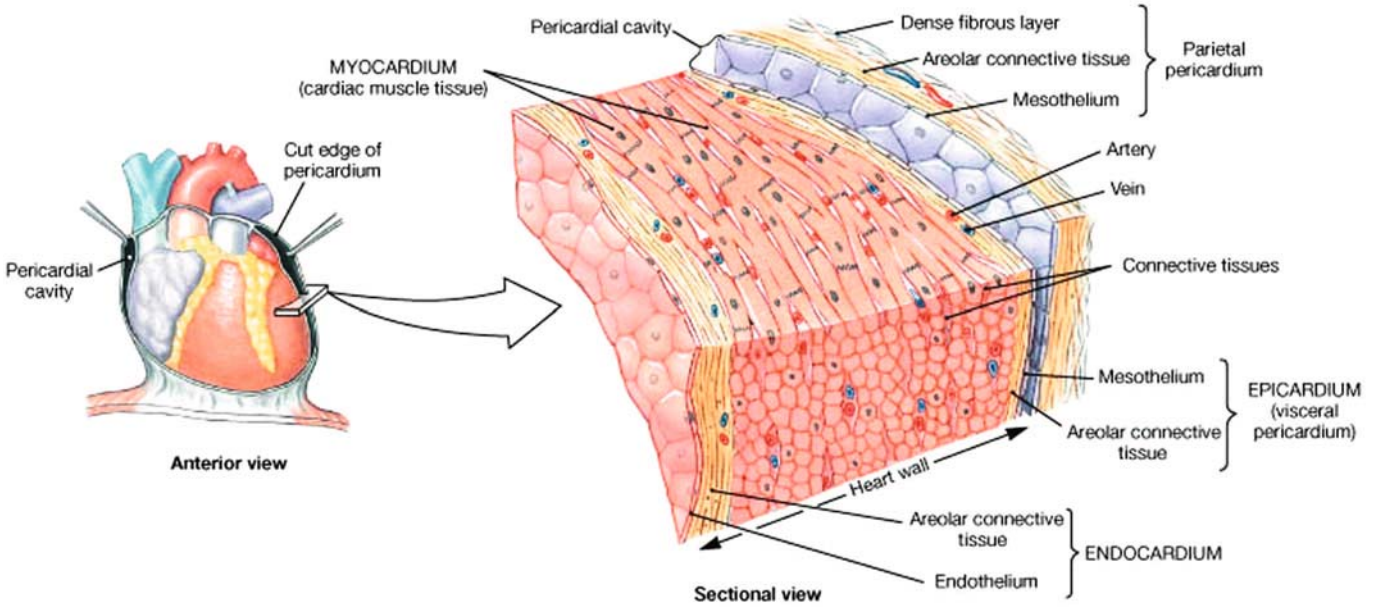

Fig. 7. Internal anatomy of the heart. The walls of the heart contain three layers: the superficial epicardium; the middle myocardium, which is composed of cardiac muscle; and the inner endocardium. Note that cardiac muscle cells contain intercalated disks that enable the cells to communicate and allow direct transmission of electrical impulses from one cell to another. (Fig. 21.3, p. 553 from *Human Anatomy*, 4th Ed. by Frederic H. Martini, Michael J. Timmons, and Robert B. Tallitsch. © 2003 by Frederic H. Martini, Inc. and Michael J. Timmons.)

4.1. Cardiopulmonary Circulation

To understand the internal anatomy of the heart, its function must be understood. The heart has two primary functions: (1) to collect oxygen-poor blood and pump it to the lungs for release of carbon dioxide in exchange for oxygen, and (2) to collect oxygen-rich blood from the lungs and pump it to all tissues in the body to provide oxygen in exchange for carbon dioxide.

The four chambers in the heart can be segregated into the left and the right side, each containing an atrium and a ventricle. The right side is responsible for collecting oxygen-poor blood and pumping it to the lungs. The left side is responsible for collecting oxygen-rich blood from the lungs and pumping it to all tissues in the body. Within each side, the atrium is a site for the collection of blood before pumping it to the ventricle. The ventricle is much stronger, and it is a site for the pumping of blood out and away from the heart (Fig. 8).

The right ventricle is the site for the collection of all oxygen-poor blood. The large superior and inferior venae cavae, among other veins, carry oxygen-poor blood from the upper and lower parts of the body to the right atrium. The right ventricle pumps the blood out of the heart and through the pulmonary trunk. The term *trunk* is a term that indicates an artery that bifurcates. The pulmonary trunk bifurcates into the left and right pulmonary arteries that enter the lungs. It is important to note that the term *artery* is always used for a vessel that carries blood away from the heart. This is irrespective of the oxygen content of the blood that flows through the vessel.

Once oxygenated, the oxygen-rich blood returns to the heart from the right and left lung through the right and left pulmonary veins, respectively (*vein*, a vessel carrying blood toward the heart). Each pulmonary vein bifurcates before reaching the heart. Thus, there are four pulmonary veins that enter the left atrium. Oxygen-rich blood is pumped out the heart by the left ventricle and into the aortic artery. The right side of the heart, the pulmonary artery, and pulmonary veins are part of the pulmonary circuit. This is because of their role in collecting blood from the tissues of the body and pumping it to the lungs (*pulmo* = "lungs"). The left side of the heart, the aortic artery, and the venae cavae are part of the systemic circuit. This is because of their role in collecting blood from the lungs and pumping it to all of the tissues of the body

Observing the heart from a superior viewpoint, the pulmonary trunk assumes the left, most anterior location projecting upward from the base of the heart. The aorta assumes a central location, and the superior vena cava is in the right, most posterior location. The general pattern of blood flow through the heart is shown in Fig. 9. Note that the function of atria is generally to collect; the function of ventricles is to pump. The right side is involved in pulmonary circulation, and the left side is involved in the systemic circulation. There is a unidirectional flow of blood through the heart; this is accomplished by valves.

4.2. The Right Atrium

The interior of the right atrium has three anatomically distinct regions, each a remnant of embryological development (Fig. 10): (1) The posterior portion of the right atrium has a smooth wall and is referred to as the *sinus venarum* (embryologically derived from the right horn of the sinus venosus);

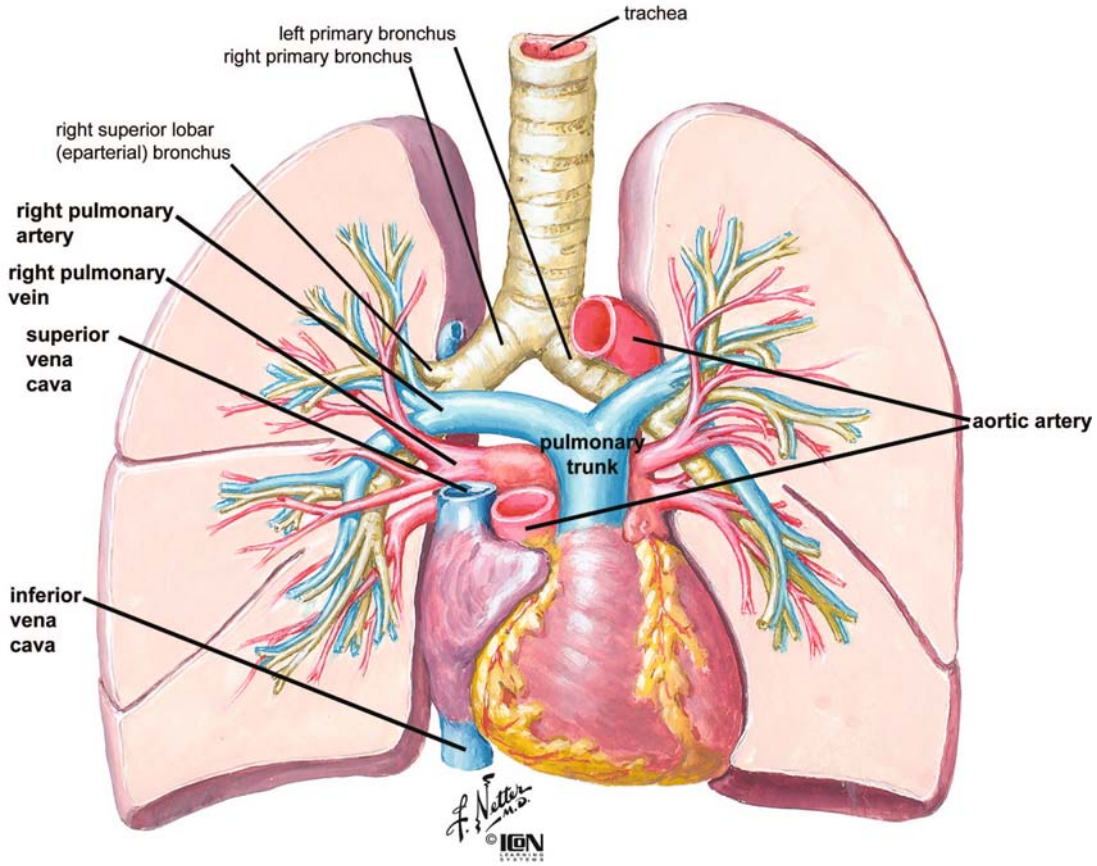

Fig. 8. Cardiopulmonary circulation. The four chambers in the heart can be segregated into the left and the right sides, each containing an atrium and a ventricle. The right side is responsible for collecting oxygen-poor blood and pumping it to the lungs. The left side is responsible for collecting oxygen-rich blood from the lungs and pumping it to the body. An artery is a vessel that carries blood away from the heart; a vein is a vessel that carries blood toward the heart. The pulmonary trunk and arteries carry blood to the lungs. Exchange of carbon dioxide for oxygen occurs in the lung through the smallest of vessels, the capillaries. Oxygenated blood is returned to the heart through the pulmonary veins and collected in the left atrium.

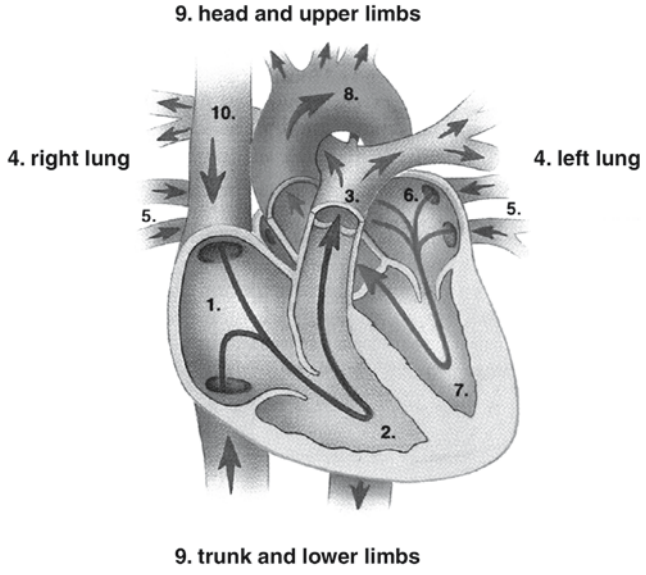

Fig. 9. Cardiac circulation. Blood collected in the right atrium is pumped into the right ventricle. On contraction of the right ventricle, blood passes through the pulmonary trunk and arteries to the lungs. The left atrium pumps the blood into the left ventricle. Contraction of the left ventricle sends the blood through the aortic artery to all tissues in the body. The release of oxygen in exchange for carbon dioxide occurs through capillaries in the tissues. Return of oxygen-poor blood is through the superior and inferior venae cavae, which empty into the right atrium. Note that a unidirectional flow of blood through the heart is accomplished by valves. Reprinted from *Principals of Human Anatomy*, by G.J. Tortora, © 1999 Biological Sciences Textbooks, Inc. This material is used by permission of John Wiley & Sons, Inc.

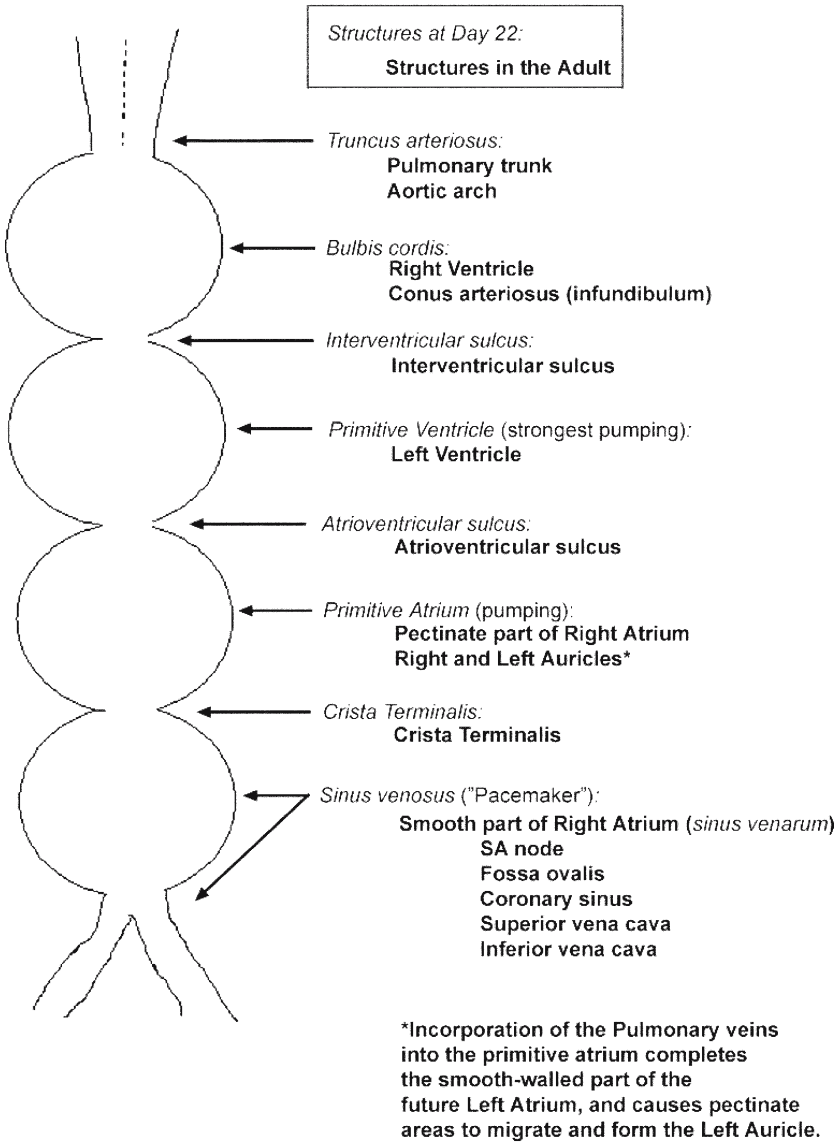

Fig. 10. Embryonic origin of the internal anatomy of the heart. The embryonic heart at day 22 is a linear heart tube. At this time, there are four divisions, and each contains structures that will remain associated with the division throughout development. During development, the linear tube folds to form two superior chambers (atria) and two inferior chambers (ventricles). SA, sinoatrial.

(2) the wall of the anterior portion of the right atrium is lined by horizontal, parallel ridges of muscle bundles that resemble the teeth of a comb, hence the name *pectinate muscle* (*pectin* = "a comb," embryologically derived from the primitive right atrium); and (3) the atrial septum (primarily derived from the embryonic septum primum and septum secundum). For more details on the embryology of the heart, refer to Chapter 2.

The purpose of Fig. 10 is to demonstrate that the smooth posterior wall of the right atrium holds most of the named structures of the right atrium. It receives both the superior and inferior venae cavae and the coronary sinus. It also contains the fossa ovalis, the sinoatrial node, and the atrioventricular node.

The inferior border of the right atrium contains the opening or ostium of the inferior vena cava and the os or ostium of the coronary sinus (Fig. 11). The coronary sinus is located on the posterior (inferior) side of the heart and receives almost all of the deoxygenated blood from the vasculature of the heart. The os of the coronary sinus opens into the right atrium anteriorly and inferiorly to the orifice of the inferior vena cava. A valve of the inferior vena cava (eustachian valve, a fetal remnant; Bartolommeo E. Eustachio, Italian Anatomist, 1520–1574) guards the orifice of the inferior vena cava. The valve of the coronary sinus (Thebesian valve; Adam C. Thebesius, German physician, 1686 to 1732) covers the opening of the coronary sinus to prevent backflow. Both of these valves vary in size and presence. For more details on the valves of the heart, refer to Chapter 27. These two venous valves insert into a prominent ridge, the sinus septum (eustachian ridge), which runs medial-lateral across the inferior border of the atrium and separates the os of the coronary sinus and inferior vena cava.

On the medial side of the right atrium, the interatrial septum (atrial septum) has interatrial and atrioventricular parts. The

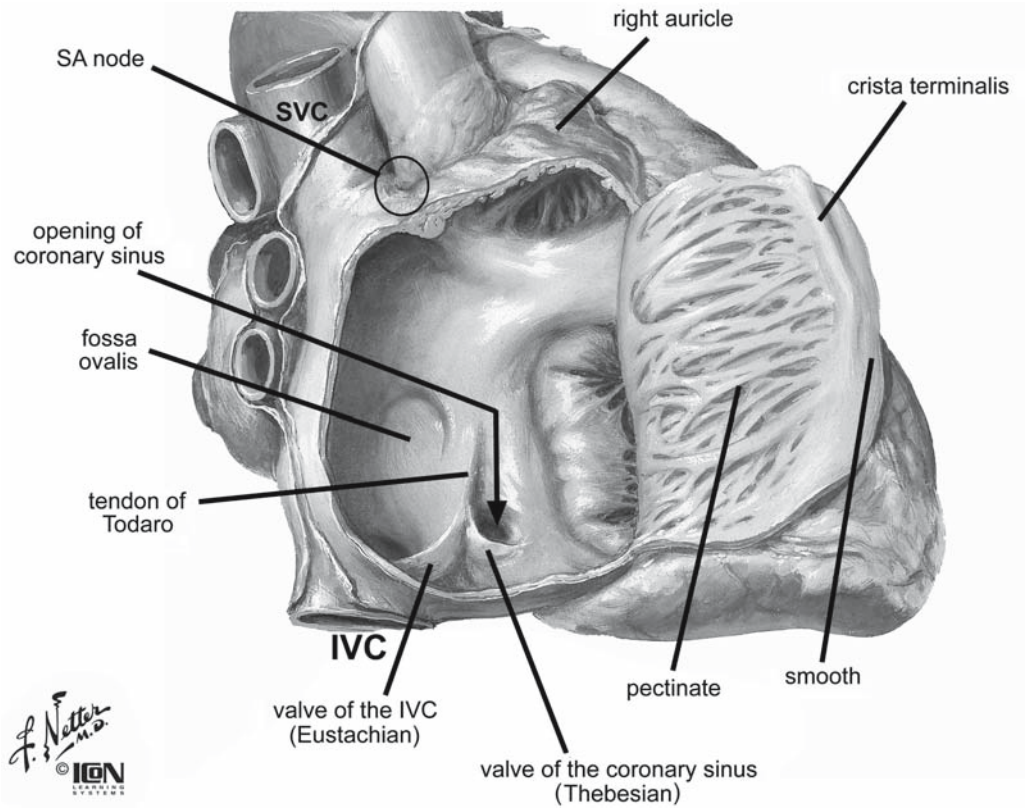

Fig. 11. Internal anatomy of the right atrium. The interior of the right atrium has three anatomically distinct regions: (1) the posterior portion, which has a smooth wall; (2) the wall of the anterior portion, which is lined by horizontal, parallel ridges of pectinate muscle; and (3) the atrial septum. IVC, inferior vena cava; SA, sinoatrial; SVC, superior vena cava.

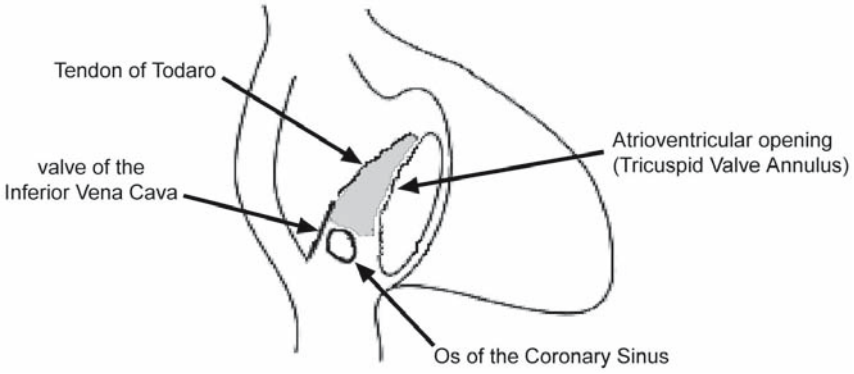

Fig. 12. Koch's triangle: three landmarks used to triangulate the location of the atrioventricular node (Koch's node) of the conduction system, including (1) coronary sinus, (2) atrioventricular opening, and (3) tendon of Todaro. Adapted from F. Anselme, B. Hook, K. Monahan, et al. (1966) Heterogeneity of retrograde fast-pathway conduction pattern in patients with atrioventricular nodal reentry tachycarda. *Circulation* 93, pp. 960–968.

fossa ovalis (a fetal remnant) is found in the interatrial part of the atrial septum. It appears as a central depression surrounded by a muscular ridge or limbus. The fossa ovalis is positioned anterior and superior to the ostia of both the inferior vena cava and the coronary sinus. A tendinous structure, the tendon of Todaro (Francesco Todaro, Italian anatomist, 1839–1918), connects the valve of the inferior vena cava to the central fibrous body (the right fibrous trigone ["triangle"]) as a fibrous extension of the membranous portion of the interventricular septum. It courses obliquely within the eustachian ridge and separates the fossa ovalis above from the coronary sinus below. This tendon is a useful landmark in approximating the location of the atrioventricular node (conduction system).

To approximate the location of the atrioventricular node, found in the floor of the right atrium and the atrial septum, it is necessary to form a triangle (triangle of Koch; Walter Koch, German Surgeon, unknown–1880) using lines that cross (1) the os of the coronary sinus posteriorly, (2) the right atrioventricular opening anteriorly, and (3) the tendon of Todaro superiorly (Fig. 12).

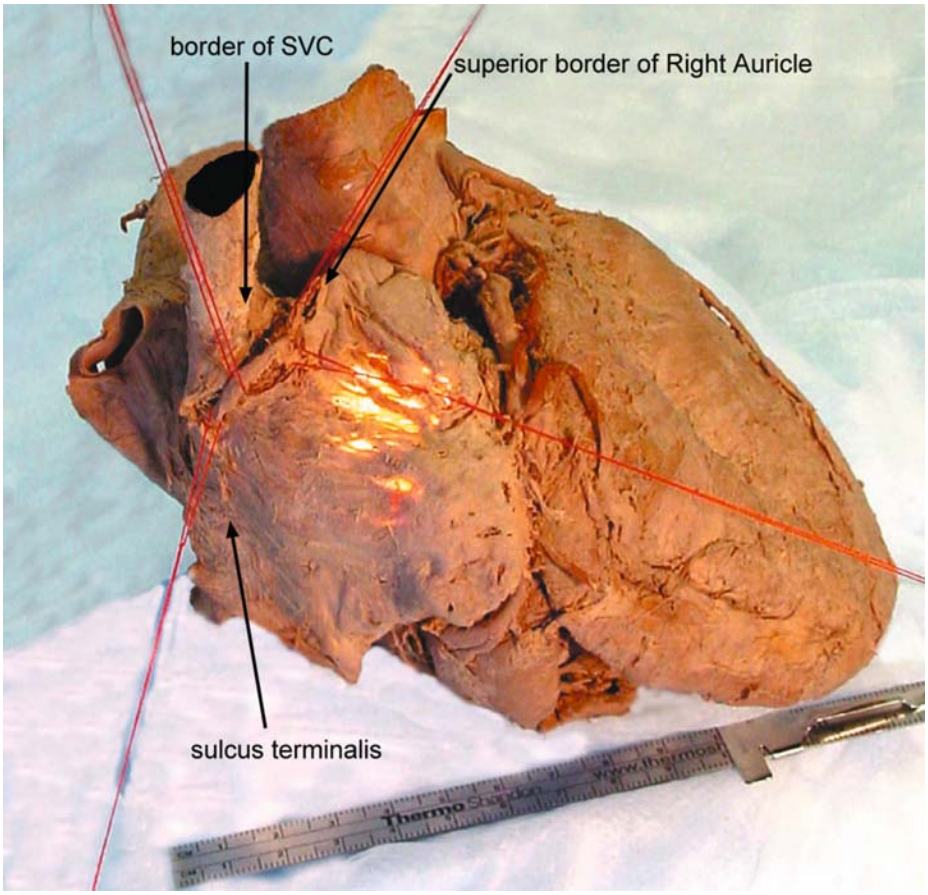

Fig. 13. The location of the sinoatrial node. Human cadaver heart demonstrating that the position of the sinoatrial node (pacemaker of the conduction system) in the smooth muscle portion of the right atrium is indicated by three lines: the sulcus terminalis, the lateral border of the superior vena cava, and the superior border of the right auricle. Note the muscle fiber bundles in the wall of the pectinate portion of the right atrium. SVC, superior vena cava.

In the lateral wall and the septum of the smooth portion of the right ventricle are numerous small openings in the endocardial surface. These openings are the ostia of the smallest cardiac (Thebesian) veins. These veins function to drain deoxygenated blood from the myocardium to empty into the right atrium, which is the collecting site for all deoxygenated blood.

In the anterior-superior portion of the right atrium, the smooth wall of the interior becomes pectinate. The smooth and pectinate regions are separated by a ridge, the *crista terminalis* (*crista* = "crest" + "terminal"). The ridge represents the end of the smooth wall and the beginning of the pectinate wall. It begins at the junction of the right auricle with the atrium and passes inferiorly over the "roof" of the atrium. The crista runs inferiorly and parallel to the openings of the superior and inferior vena cavae. Recall that the crista terminalis separates the sinus venosus and the primitive atrium in the embryo and remains to separate the smooth and the pectinate portions of the right atrium after development.

The crista terminalis on the internal side results in a groove on the external side, the *sulcus terminalis*. This is a useful landmark in approximating the location of the sinoatrial node (pacemaker of the conduction system). The intersection of three following lines indicates the position of the sinoatrial node: (1) the sulcus terminalis, (2) the lateral border of the superior vena cava, and (3) the superior border of the right auricle (Fig. 13).

On the "floor" of the right atrium is the atrioventricular portion of the atrial septum, which has muscular and membranous components. At the anterior and inferior aspect of the atrial septum, the tricuspid valve annulus (*annulus* = "ring") is attached to the membranous septum. As a result, a portion of the membranous septum lies superior to the annulus and therefore functions as a membranous atrial, and membranous ventricular, septum.

4.3. The Right Ventricle

The right ventricle receives blood from the right atrium and pumps it to the lungs through the pulmonary trunk and arteries. Most of the anterior surface of the heart is formed by the right ventricle (Fig. 14). Abundant, coarse trabeculae carneae ("beams of meat") characterize the walls of the right ventricle. Trabeculae carneae are analogous to pectinate muscle of the right atrium (as bundles of myocardium) and are found in both the right and left ventricles. The outflow tract, conus arteriosus ("arterial cone") or infundibulum ("funnel"), carries blood out

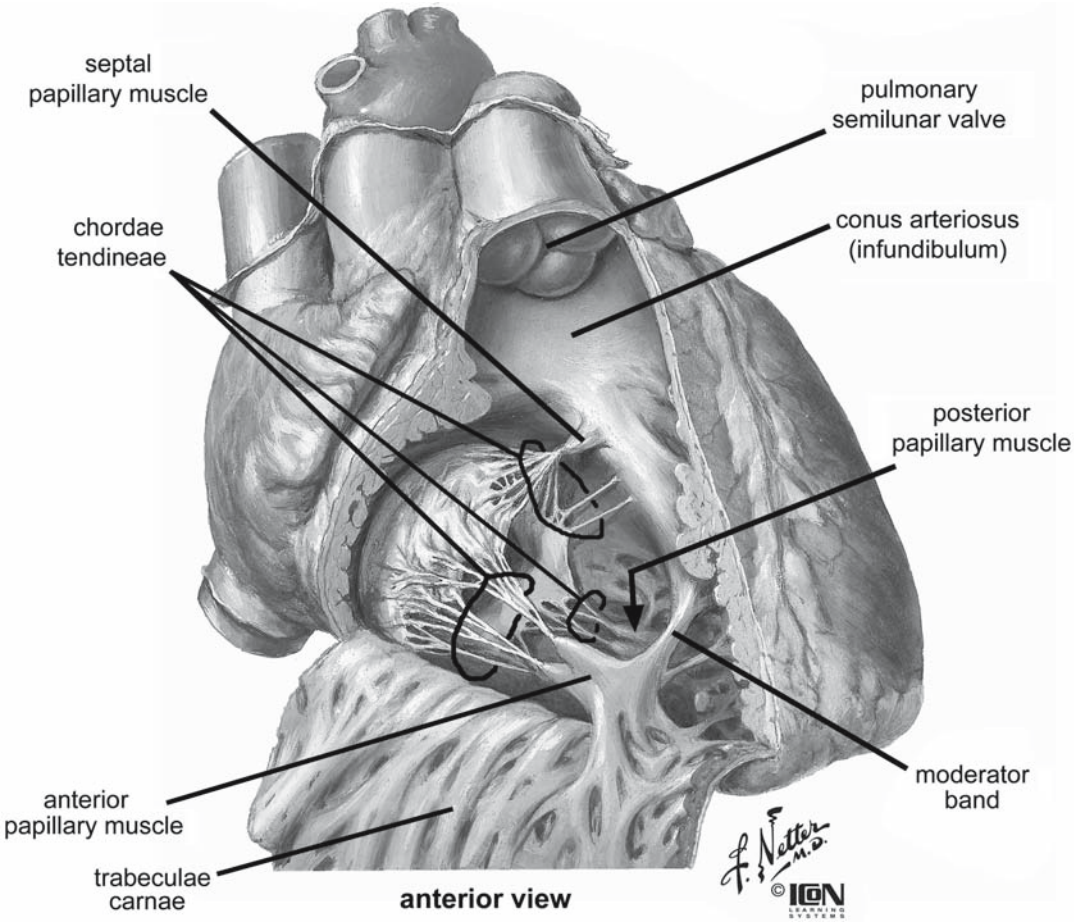

Fig. 14. Internal anatomy of the right ventricle. Coarse trabeculae carneae characterize the walls of the right ventricle. The conus arteriosus makes up most of the outflow tract. The right atrioventricular or tricuspid valve is made up of three sets of cusps, cordae tendineae and papillary muscles.

of the ventricle in an anterior-superior direction and is relatively smooth walled. A component of the conus arteriosus forms part of the interventricular septum. This small septum, the infundibular (conal) septum, separates the left and right ventricular outflow tracts and is located just inferior to both semilunar valves. Four distinct muscle bundles, collectively known as the *semicircular arch*, separate the outflow tract from the rest of the right atrium.

4.3.1. Tricuspid Valve

Blood is pumped from the right atrium through the atrioventricular orifice into the right ventricle. When the right ventricle contracts, blood is prevented from flowing back into the atrium by the right atrioventricular valve or tricuspid ("three cusps") valve. The valve consists of the annulus, three valvular leaflets, three papillary muscles, and three sets of chordae tendineae (Figs. 14 and 15). The atrioventricular orifice is reinforced by the annulus fibrosus of the cardiac skeleton (dense connective tissue). Medially, the annulus is attached to the membranous ventricular septum.

The tricuspid valve has three leaflets: anterior (superior), posterior (inferior), and septal. The anterior leaflet is the largest and extends from the medial border of the ventricular septum to the anterior free wall. This, in effect, forms a partial separation between the inflow and outflow tracts of the right ventricle. The posterior leaflet extends from the lateral free wall to the posterior portion of the ventricular septum. The septal leaflet tends to be somewhat oval in shape and extends from the annulus of the orifice to the medial side of the interventricular septum (on the inflow side), often including the membranous part of the septum.

Papillary ("nipple") muscles contract and "tug" down on chordae tendineae ("tendinous cords") attached to the leaflets to secure them in place in preparation for the contraction of the ventricle. This is done to prevent the prolapse of the leaflets into the atrium. This is somewhat analogous to the tightening of the sails on a yacht in preparation for a big wind. Note that the total surface area of the cusps of the atrioventricular valve is approximately twice that of the respective orifice, so that considerable overlap of the leaflets occurs when the valves are in the closed position. The leaflets remain relatively close together even during ventricular filling. The partial approximation of the valve surfaces is caused by eddy currents that prevail behind the leaflets and by tension exerted by the

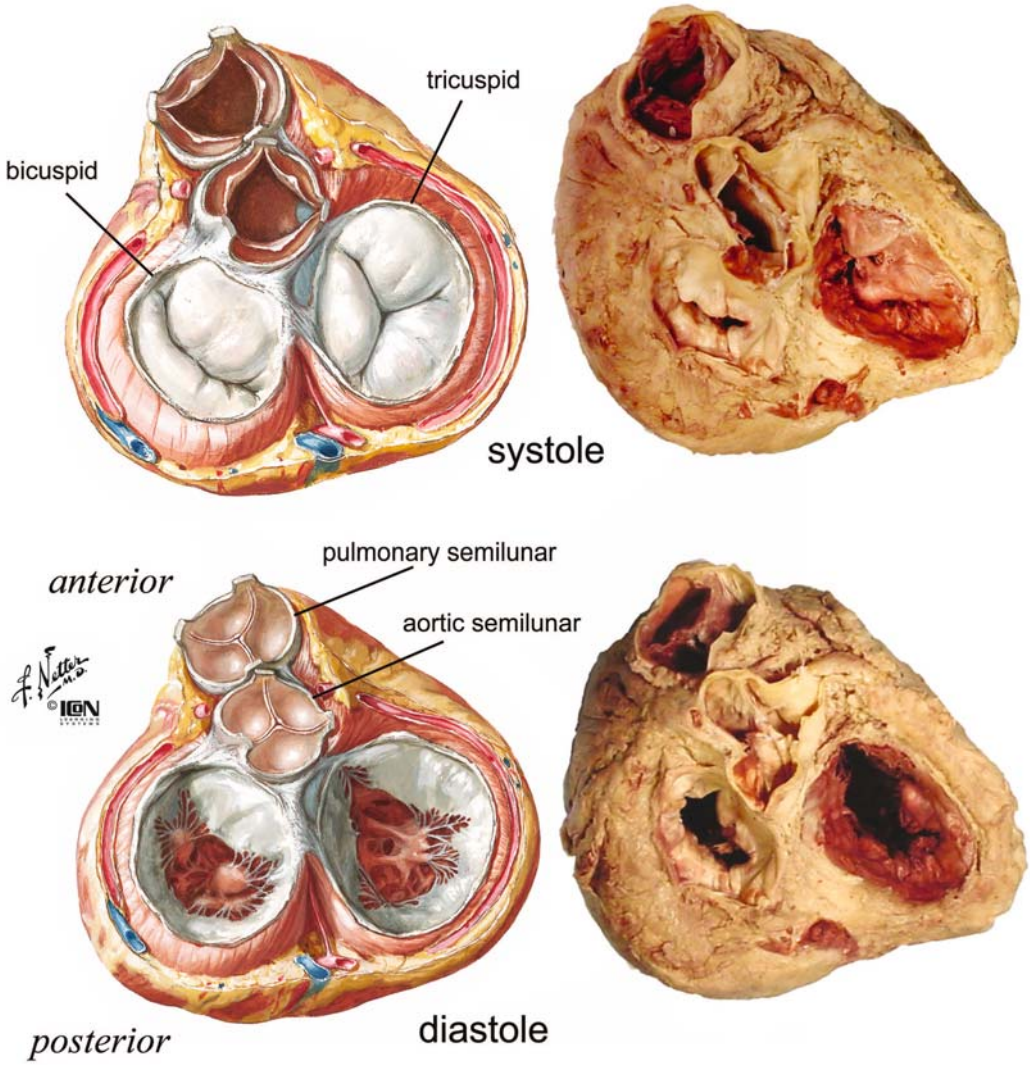

Fig. 15. Valves of the heart. During ventricular systole, atrioventricular valves close to prevent the regurgitation of blood from the ventricles into the atria. The right atrioventricular valve is the tricuspid valve; the left is the bicuspid valve. During ventricular diastole, the atrioventricular valves open as the ventricles relax, and the semilunar valves close. The semilunar valves prevent the backflow of blood from the great vessels into the resting ventricles. The valve of the pulmonary trunk is the pulmonary semilunar valve, and the aortic artery has the aortic semilunar valve. To the right of each figure are photographs of human cadaveric hearts.

chordae tendineae and papillary muscle. As the filling of the ventricle reduces, the valve leaflets float toward each other, but the valve does not close. The valve is closed by ventricular contractions, and the valve leaflets, which bulge toward the atrium but do not prolapse, stay pressed together throughout ventricular contraction (Fig. 15). The junction between two leaflets is called a *commissure* and is named by the two adjoining leaflets (anteroseptal, anteroposterior, and posteroseptal). Each commissure contains a relatively smooth arc of valvular tissue delineated by the insertion of the chordae tendineae.

There are three papillary muscles, just as there are three leaflets or cusps. The anterior papillary muscle is located in the apex of the right ventricle. This is the largest of the papillary muscles in the right ventricle, and it may have one or two heads. When this papillary muscle contracts, it pulls on chordae tendineae attached to the margins of the anterior and posterior leaflets. The posterior papillary muscle is small and located in the posterior lateral free wall. When this papillary contracts, it pulls on chordae tendineae attached to the posterior and septal leaflets. The septal papillary muscle (papillary of the conus) arises from the muscular interventricular septum near the outflow tract (conus arteriosus). This papillary muscle more often consists of a collection of small muscles in close proximity and has attachments to the anterior and septal valve leaflets. In addition, chordae tendineae in this region may extend simply from the myocardium and attach to the valve leaflets directly without a papillary muscle (Fig. 14). The most affected is the septal leaflet, which has restricted mobility because of extensive chordae tendineae attachment directly to the myocardium.

Near the anterior free wall of the right ventricle is a muscle bundle of variable size and the moderator band (occasionally absent). This muscle bundle extends from the interventricular

septum to the anterior papillary muscle and contains a component of the right bundle branch of the conduction system. It seems logical that the anterior papillary muscle, with its remote location away from the septum, would need special conduction fibers for it to contract with the other papillary muscles and convey control of the valve leaflets equal to the other valve leaflets. The moderator band is a continuation of another muscle bundle, the septal band (septal trabeculae) called *septomarginal trabecula*, and is a component of the semicircular arch (delineation of the outflow tract).

4.3.2. Pulmonary Semilunar Valve

During ventricular systole, blood is pumped from the right ventricle into the pulmonary trunk and arteries toward the lungs. When the right ventricle relaxes, in diastole, blood is prevented from flowing back into the ventricle by the pulmonary semilunar valve (Figs. 14 and 15). The semilunar valve is composed of three symmetric, semilunar-shaped cusps. Each cusp looks like a cup composed of a thin membrane. Each cusp acts like an upside-down parachute facing into the pulmonary trunk, opening as it fills with blood. This filled space or recess of each cusp is called the *sinus of Valsalva* (Antonio M. Valsalva, 1666–1723). On complete filling, the three cusps contact each other and block the retrograde flow of blood. Each of the three cusps is attached to an annulus such that the cusp opens into the lumen, forming a U shape. The annulus is anchored to both the right ventricular infundibulum and the pulmonary trunk. The cusps are named according to their orientation in the body: anterior, left (septal), and right.

The cusps collapse against the arterial wall as the right ventricle contracts, sending blood flowing past them. When the ventricle rests (diastole), the cusps meet in the luminal center. There is a small thickening on the center of the free edge of each cusp, at the point where the cusps meet. This nodule (of Arantius or Morgagni; Giulio C. [Aranzi] Arantius, Italian anatomist and physician, 1530–1589; Giovanni B. Morgagni, Italian anatomist and pathologist, 1682–771) ensures central valve closure. Radiating from this nodule around the free edge of the cusp is a ridge, the *linea alba* ("line" + "white").

4.4. The Left Atrium

The left atrium (Fig. 16) receives oxygenated blood from the lungs via the left and right pulmonary veins. The pulmonary veins enter the heart as two pairs of veins inserting posteriorly and laterally into the left atrium. In addition, the smallest (Thebesian) veins drain deoxygenated blood from the atrial myocardium directly into the atrium.

The left atrium is found midline, posterior to the right atrium and superior to the left ventricle. Anteriorly, a left atrial appendage (auricle) extends over the atrioventricular (coronary) sulcus. The walls of the atrial appendage are pectinate, and the walls of the left atrium are smooth; this reflects their embryological origin. The atrial appendage is derived from the primitive atrium (a strong pumping structure), and the atrium is derived from the fetal pulmonary vein as a connection with the embryonic pulmonary venous plexus. The venous structures are absorbed into the left atrium, resulting in the posteriolateral connections of the right and left pulmonary veins. The atrial septum of the left atrium is derived from the embryonic septum primum, resulting in the adult structure called the *valve of the foramen ovale* (a sealed valve flap).

4.5. The Left Ventricle

The left ventricle receives blood from the left atrium and pumps it through the aortic artery to all of the tissues of the body (Fig. 16). Most of the left lateral surface of the heart is formed by the left ventricle, also forming part of the inferior and posterior surface. As with the right ventricle, abundant trabeculae carneae characterize the walls of the left. However, in contrast to the right ventricle, the muscular ridges tend to be relatively fine. Also in contrast to the right ventricle, the myocardium in the wall of the left ventricle is much thicker. The interventricular septum appears from within the left ventricle to bulge into the right ventricle; this creates a barrel-shaped left ventricle.

4.5.1. Bicuspid (Mitral) Valve

Blood is pumped from the left atrium through the left atrioventricular orifice into the left ventricle. When the left ventricle contracts, blood is prevented from flowing back into the atrium by the left atrioventricular valve or bicuspid ("two cusps") valve (Figs. 15 and 16). The valve consists of the annulus, two leaflets, two papillary muscles, and two sets of chordae tendineae.

The atrioventricular orifice is partly reinforced by the annulus fibrosus of the cardiac skeleton. The annulus fibrosus supports the posterior and lateral two-thirds of the annulus. The remaining medial third is supported by attachment to the left atrium and fibrous support to the aortic semilunar valve.

The bicuspid valve has two leaflets: anterior (medial or aortic) and posterior (inferior or mural, "wall"). The two apposing leaflets of the valve resemble a bishop's hat or mitre. Thus, the bicuspid valve is often referred to as the *mitral valve* (Fig. 17).

The anterior leaflet is typically a trapezoidal shape. The distance from its attachment on the annulus to its free edge is longer than the length of attachment across the annulus. In contrast, the posterior leaflet is found to be relatively narrow, with a very long attachment distance across the annulus. The distance from annulus to free edge in the anterior cusp is twice as long as in the posterior cusp. The posterior cusp is so long and narrow that the free edge is often subdivided into the anterior, central, and posterior crescent shapes.

Papillary muscles, in conjunction with chordae tendineae, attach to the leaflets to secure them in place. This is done in preparation for the contraction of the ventricle to prevent the prolapse of the leaflets up into the atrium. As with the other atrioventricular valve (tricuspid), the total surface area of the two cusps of the valve is significantly greater than the area described by the orifice. There is considerable overlap of the leaflets when the valves are in the closed position (Fig. 15).

As with the tricuspid valve, the leaflets remain relatively close together, even when the atrium is contracting and the ventricle is filling. The partial approximation of the valve surfaces is caused by eddy currents that prevail behind the leaflets and by tension exerted by the chordae tendineae and papillary muscle. In the open position, the leaflets and commissures are in an oblique plane of orientation roughly parallel to the ventricular septum. The valve is closed by ventricular contractions.

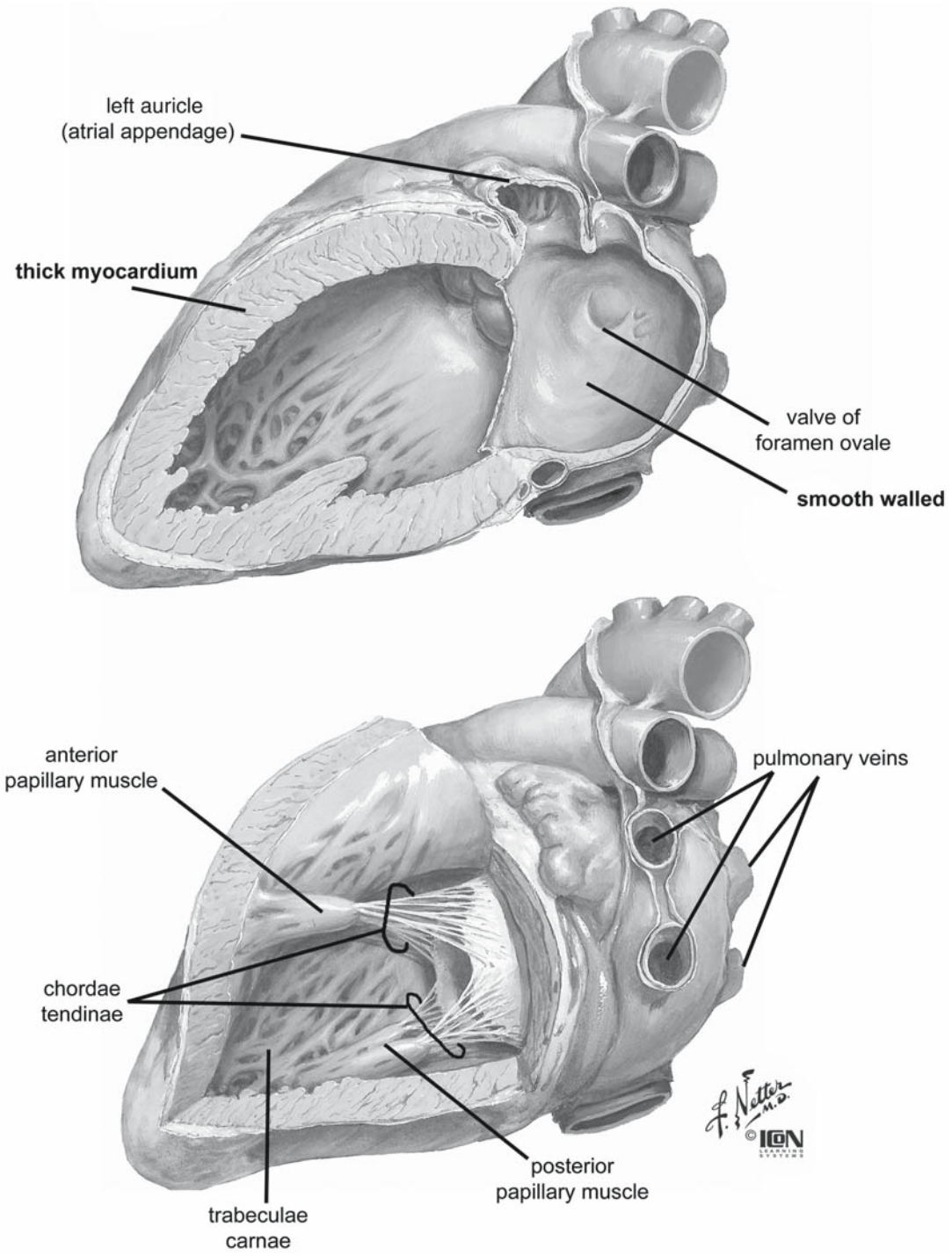

Fig. 16. Internal anatomy of the left atrium and ventricle. The left atrium receives oxygenated blood from the lungs via the left and right pulmonary veins. The pulmonary veins enter the heart as two pairs of veins inserting posteriorly and laterally. Anteriorly, the pectinate left auricle extends over the smooth-walled atrium. Most of the left lateral surface of the heart is formed by the left ventricle. Trabeculae carneae characterize the walls, and the myocardium is much thicker than the left ventricle. The interventricular septum bulges into the right ventricle, creating a barrel-shaped left ventricle.

The valve leaflets, which bulge toward the atrium, stay pressed together throughout the contraction and do not prolapse. The junctions of the two leaflets are called the "anterolateral" and the "posteromedial" commissures. The line of apposition of the leaflets during valvular closure is indicated by a fibrous ridge.

There are two distinct papillary muscles of the left ventricle that extend from the ventricular free wall toward and perpendicular to the atrioventricular orifice. The anterior papillary muscle is typically slightly larger than the posterior, and each papillary muscle consists of a major trunk that often has mul-

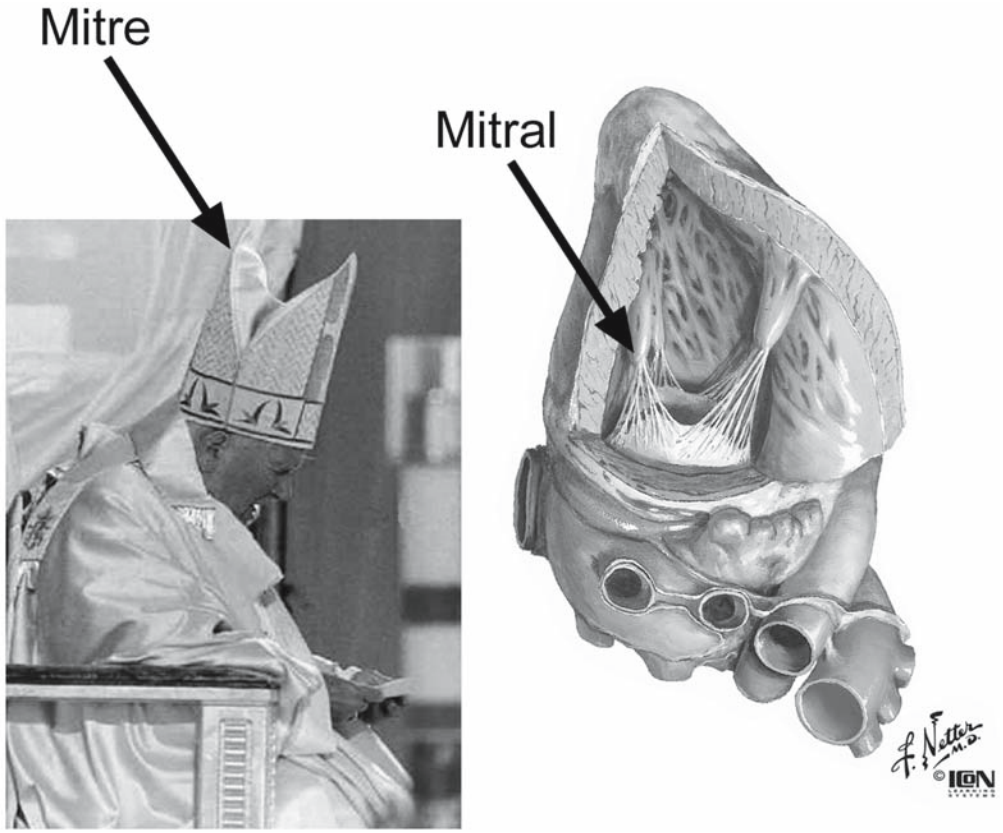

Fig. 17. The mitral valve. The mitral (left atrioventricular or bicuspid) valve is so named because of its resemblance to a cardinal's hat, known as a mitre. Left: Photo of the Pope that appears on the Vatican Web site.

tiple heads from which extend the chordae tendineae. The chordae tendineae of each papillary muscle extend to the two valvular commissures and to the multiple crescent shapes of the posterior cusp. Thus, each papillary muscle pulls on chordae from both leaflets. In addition, the posterior leaflet has occasional chordae that extend simply from the ventricular myocardium without a papillary muscle (similar to the septal papillary muscle of the right ventricle).

4.5.2. Aortic Semilunar Valve

During ventricular systole, blood is pumped from the left ventricle into the aortic artery to all of the tissues of the body. When the left ventricle relaxes in diastole, blood is prevented from flowing back into the ventricle by the aortic semilunar valve (Figs. 15 and 16). Like the pulmonary semilunar valve, the aortic valve is composed of three symmetric, semilunar-shaped cusps; each cusp acts like an upside-down parachute facing into the aortic artery, opening as it fills with blood. The filled space or recess of each cusp is called the sinus of Valsalva. On complete filling, the three cusps contact each other and block the flow of blood. Each of the three cusps is attached to an annulus ("ring") such that the cusp opens into the lumen, forming a U-shape. The cusps are firmly anchored to the fibrous skeleton within the root of the aorta. A circular ridge on the innermost aspect of the aortic wall, at the upper margin of each sinus, is the sinotubular ridge, the junction of the sinuses and the aorta.

At the sinotubular ridge, the wall of the aorta is thin, bulges slightly, and is the narrowest portion of the aortic artery. The cusps are named according to their orientation in the body: left and right (both facing the pulmonary valve) and posterior. Within the sinuses of Valsava, there are openings or ostia (*ostium* = "door or mouth") into the blood supply of the heart called *coronary arteries*. These ostia are positioned below the sinotubular junction near the center of the sinuses. Only the two sinuses facing the pulmonary valve (left and right) have ostia that open into the left and right coronary arteries, respectively. Coronary arteries carry oxygenated blood to the myocardium of the heart. During ventricular diastole, the aortic valve snaps shut as pressure in the aorta increases. Under such pressure, the walls of the great artery distend, the sinuses fill, and blood is sent under great pressure through the coronary ostia into the coronary arteries. The posterior (noncoronary) sinus is in a position that abuts the fibrous skeleton and the annuli of both atrioventricular valves (Fig. 15).

When the left ventricle contracts, the cusps collapse against the arterial wall as blood flows past them. When the ventricle rests (diastole), the cusps meet in the luminal center. As with the pulmonary valve, there is a small thickening on the center of the free edge of each cusp, at the point where the cusps meet. This nodule (of Arantius or Morgagni) ensures central valve closure. Radiating from this nodule around the free edge of the cusp is a ridge, the linea alba. This valve is exposed to

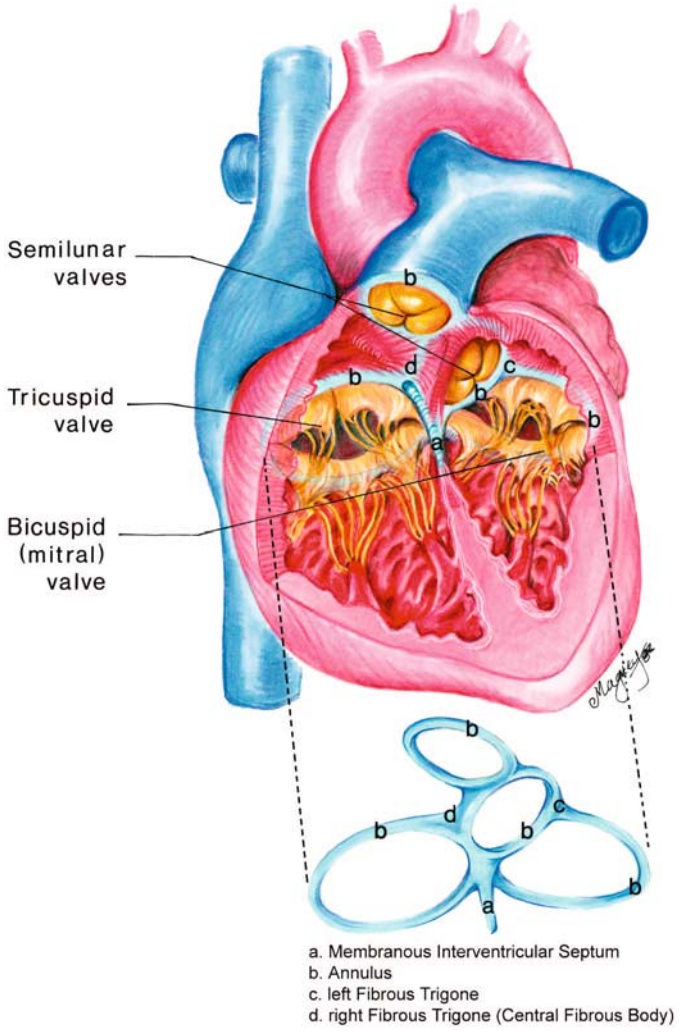

Fig. 18. The cardiac skeleton. A dense connective tissue that functions to attach the atrial and ventricular myocardium, support and reinforce the openings of the four valves of the heart, and electrically separate the ventricles from the atria. Courtesy of Jean Magney, University of Minnesota.

a greater degree of hemodynamic stress than the pulmonary valve. The aortic cusps can thicken, and the linea alba can become more pronounced. For this and other reasons, the aortic pulmonary valve is the most likely valve to be surgically repaired or replaced (*see* Chapter 27).

5. THE CARDIAC SKELETON

Passing transversely through the base of the heart is a fibrous framework or "skeleton" made of dense connective tissue, not bone as the name might suggest. The purpose of this tough, immobile scaffold is to: (1) provide an attachment for the atrial and ventricular myocardium, (2) anchor the four valves of the heart, and (3) electrically insulate the myocardium of the ventricles from the atria.

The supporting framework of the cardiac skeleton (Figs. 15 and 18) provides immobile support for the atrioventricular openings during atrial and ventricular contractions, as well as support for the semilunar valves against the high pressures generated during and after ventricular contractions. The skeleton is a formation of four attached rings, with the opening for the aortic semilunar valve in the central position and the other valve rings attached to it.

The triangular formation between the aortic semilunar valve and the medial parts of the tricuspid and bicuspid valve openings is the right fibrous trigone or the central fibrous body, the strongest portion of the cardiac skeleton. The smaller left fibrous trigone is formed between the aortic semilunar valve and the anterior cusp of the mitral valve. Continuations of fibroelastic tissue from the right and left fibrous trigones partially encircle the atrioventricular openings to form the tricuspid and bicuspid annulus or annulus fibrosus. The annuli serve as attachment sites for the atrioventricular valves as well as atrial and ventricular myocardium. Strong collagenous tissue passes anteriorly from the right and left fibrous trigones to encircle and support the aortic and pulmonary semilunar valve annuli.

The membranous interventricular septum is an inferior extension of the central fibrous body that attaches to the muscular interventricular septum. The membranous septum provides support for the medial (right and posterior) cusps of the aortic semilunar valve and continues superiorly to form part of the atrial septum. The tendon of Todaro is a fibrous extension of the membranous septum that is continuous with the valve (eustachian) of the inferior vena cava. The atrioventricular bundle of conduction fibers from the atrioventricular node penetrate the central fibrous body, pass through the membranous septum, and split into left and right bundle branches at the apex of the muscular septum (or the junction of the right and posterior cusps of the aortic semilunar valve).

6. THE FETAL HEART

By the third month of fetal development, the heart and all major blood vessels are basically formed, and the blood flow is generally the same direction as the adult. However, there are some major differences between fetal and postnatal circulation (Fig. 19). First, oxygenated blood flows toward the fetus and into the heart in umbilical veins, and deoxygenated blood flows away from the fetus in umbilical arteries. Second, the fetus obtains oxygen from the uterus through the placenta, and the fetal lungs are essentially nonfunctional. Therefore, fetal circulation has a number of features to direct most of the blood away from the lungs.

In fetal circulation, oxygenated blood from the placenta flows toward the heart. Most of it is diverted away from entering the liver (through the ductus venosus) and into the inferior vena cava. Thus, unlike the adult heart, oxygenated blood mixes with deoxygenated blood and collects in the right atrium. Because very little of this blood is required in the lungs, the fetus has three unique features to ensure that the blood is shunted from the right (pulmonary) side of the heart to the left (systemic) side. The first is an oval hole in the interatrial septum; this hole is called the *foramen ovale* ("oval hole"; the foramen ovale is not really a hole, but rather a valve covered by two flaps that prevent the regurgitation of blood). For more information on this topic, refer to Chapter 2.

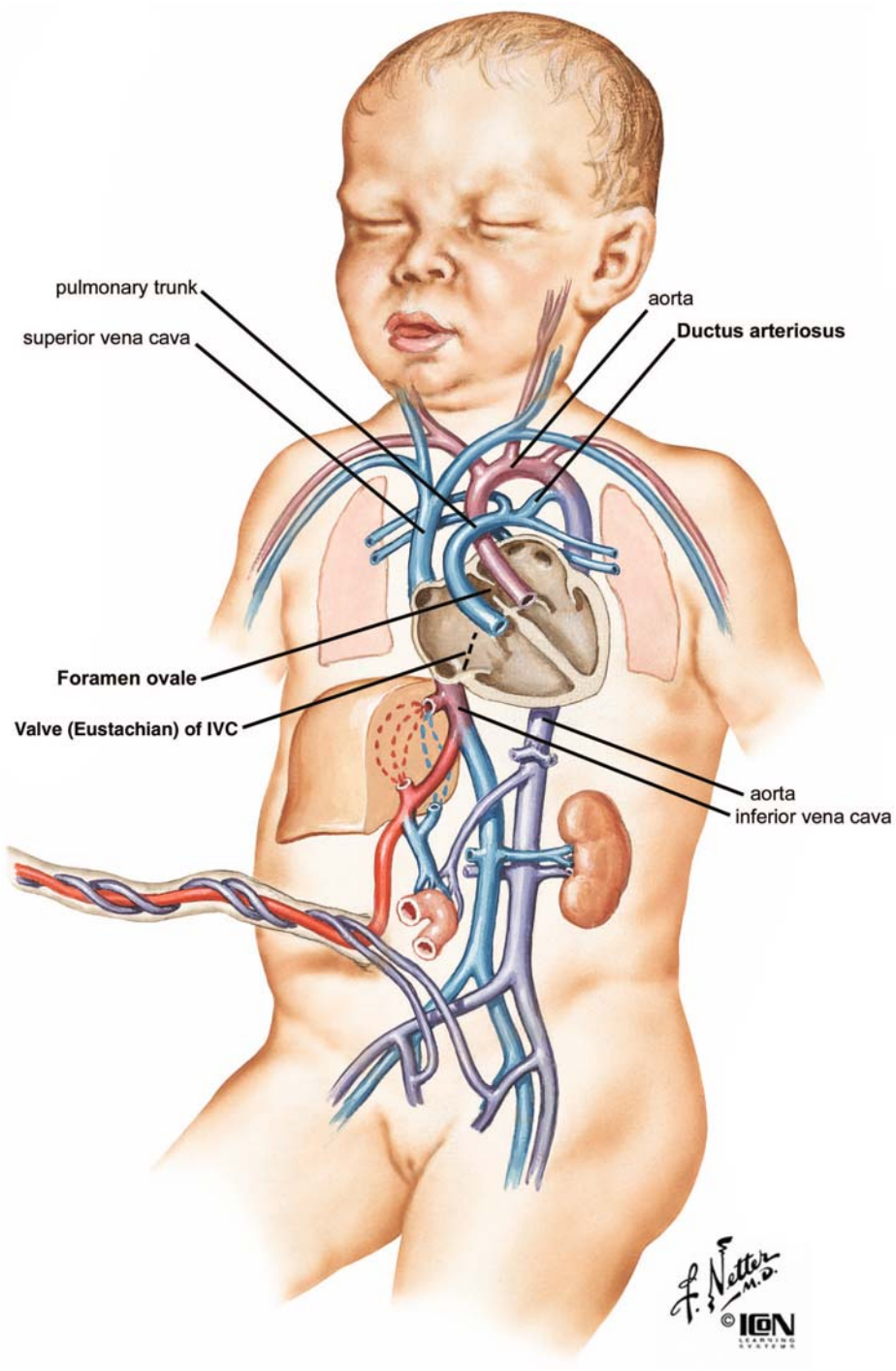

Fig. 19. Fetal circulation. The fetal heart has unique features to shunt blood away from the relatively nonfunctional lungs: foramen ovale, ductus arteriosus, and valve (eustachian) of the inferior vena cava (IVC).

Before birth, pressure is higher in the right atrium than in the left because of the large vasculature from the placenta. The foramen ovale is a passage for blood to flow from the right atrium into the left. A second feature of the fetal heart is the ligament of the inferior vena cava. This ligament is located inferior to the opening of the vena cava and extends medially to atrial septum passing inferior to the foramen ovale. It is much more prominent in the fetus than in the adult and functions in fetal circulation to direct, in a laminar flow, the blood coming into the right ventricle toward the foramen ovale, to pass into the left atrium.

The third feature of fetal circulation is a way for oxygenated blood that has been pumped from the right atrium to the right ventricle to be diverted from the pulmonary circulation into the

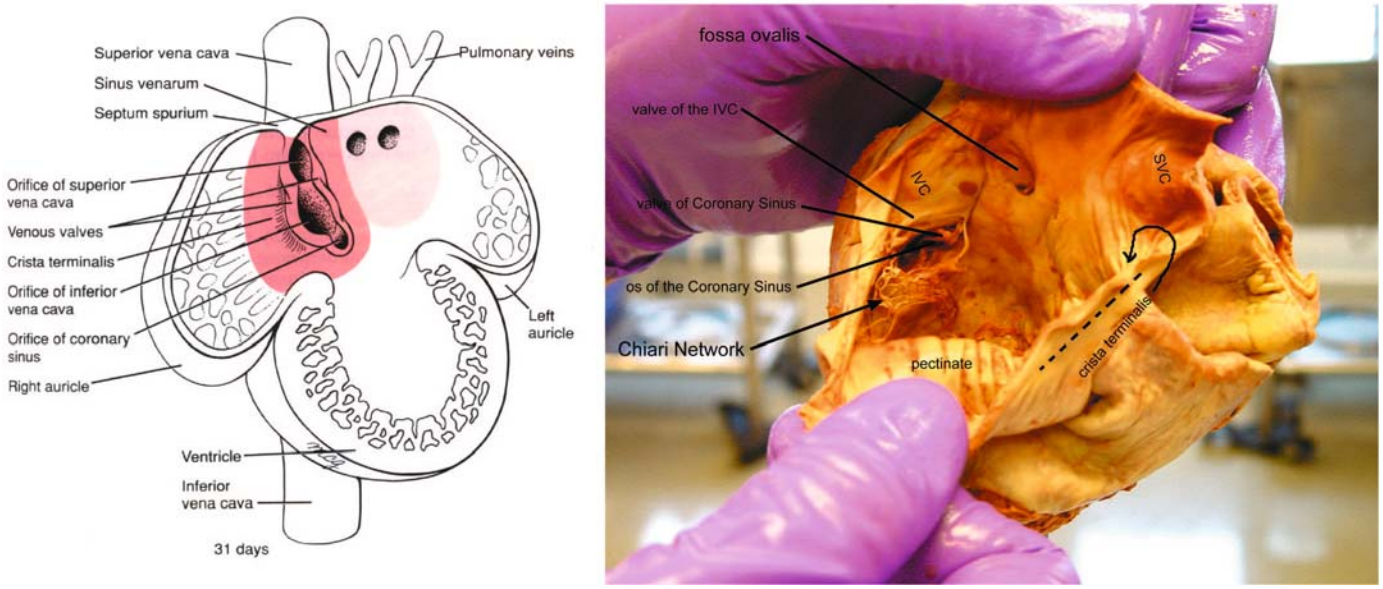

Fig. 20. Chiari network. The ostia of the superior and inferior venae cavae, as well as the coronary sinus, incorporate into the smooth wall of the definitive right atrium. Two tissue flaps develop on the sides of the ostia as the left and right venous valves. The left valve eventually gives rise to the septum secundum (definitive interatrial septum); the right valve gives rise to the valve of the inferior vena cava (eustachian), the valve of the coronary sinus (Thebesian), and the crista terminalis. Incomplete resorption of the right valve of the embryonic sinus venosus leads to the presence of a meshwork of fibrous strands attached to the edges of the eustachian valve or the Thebesian valve inferiorly and the crista terminalis superiorly. IVC, inferior vena cava; SVC, superior vena cava. Right: human cadaveric hearts. Left: from *Human Embryology*, 2nd Ed. (1997), W. J. Larsen (ed.), Churchill Livingstone, Inc., New York, NY, p. 163, Fig. 7-12. © 1997, with permission from Elsevier.

systemic circulation. Despite the shunt from the right atrium to the left, much of the oxygenated blood that enters the right atrium gets pumped into the right ventricle. The ductus arteriosus ("duct of the artery") is a connection between the left pulmonary artery and the aortic artery so that very little blood reaches the immature lungs. Because the pulmonary vascular resistance of the fetus is large, only one-tenth of right ventricular output passes through the lungs. The remainder passes from the pulmonary artery through the ductus arteriosus to the aorta. In the fetus, the diameter of the ductus arteriosus can be as large as that of the aorta.

Shortly after birth, the umbilical cord is cut, and the newborn takes a first breath. Rising concentrations of the hormone prostaglandin are believed to result in the closure of the ductus arteriosus (forming then the ligamentum arteriosum), and the lungs receive much more blood. The increase in pressure is translated to the left atrium; this pressure pushes together the two valve flaps of the foramen ovale (fossa ovalis), closing them and preventing the flow of blood from the right to the left atrium.

7. OTHER FETAL REMNANTS

7.1. Chiari Network

Between 3 and 4 weeks of fetal development, the openings of the superior and inferior venae cavae and future coronary sinus are incorporated into the posterior wall of the right atrium and become the sinus venarum (smooth) portion of the right atrium. A pair of tissue flaps, the left and right venous valves, develops on either side of the three ostia.

The left valve eventually becomes part of the septum secundum (which becomes the definitive interatrial septum). The right valve remains intact and forms the valve of the inferior vena cava (eustachian), the crista terminalis, and the valve of the coronary sinus (Thebesian) (Fig. 20).

Infrequently, incomplete resorption of the right valve of the sinus venosus may lead to the presence of a meshwork of fibrous strands attached to the edges of the eustachian valve or Thebesian valve inferiorly and the crista terminalis superiorly. This is called a *Chiari net* or *network* (Fig. 20). Remnants of the other valve, the left sinus venosus valve, may be found adherent to the superior portion of the atrial septum or the fossa ovalis. For more information on this topic, refer to Chapters 2 and 6.

7.2. Septal Defects

7.2.1. Atrial Septal Defect

The first step in the separation of the systemic and pulmonary circulation in the fetal heart is the separation of the definitive atrium. The adult interatrial septum is formed by the fusion of two embryonic septa. However, note that right-to-left shunting of oxygenated blood remains.

Between 3 and 4 weeks of development, the roof of the atrium becomes depressed and produces a wedge of tissue called the *septum primum* ("first partition") that extends inferiorly. During the fifth week, the crescent-shaped septum reaches the floor, thus separating the right and left atria and forming along its free edge a foramen, *ostium primum* ("first mouth/opening"). At the end of the sixth week, the growing

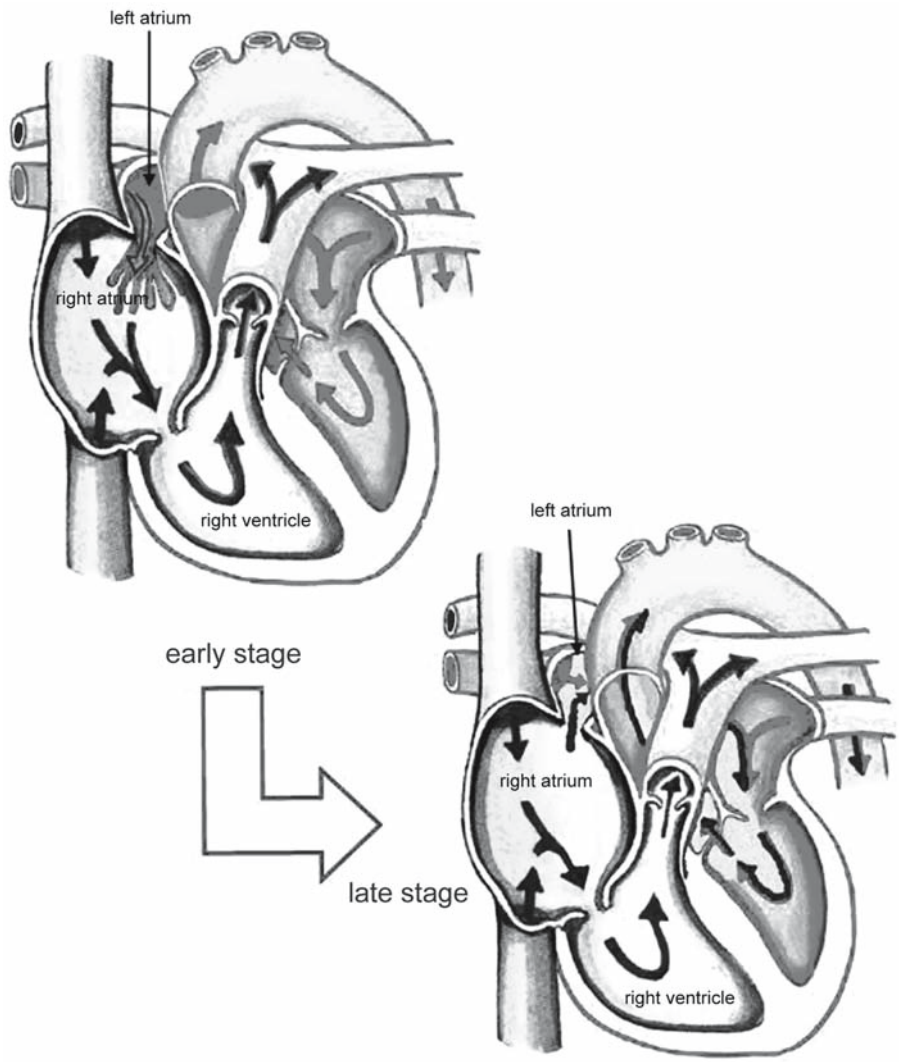

Fig. 21. Atrial septal defect. Incomplete formation of the septum secundum over the ostium secundum results in a persistent opening in the interatrial septum. After birth, the pressure in the left atrium is greater than in the right, and there is modest left-to-right shunting of blood. However, the right atrium responds to continuous increases in volume, and the pressure increases in the right side. The result is a reverse in the flow from the right to the left atrium, resulting in oxygen-poor blood in the aortic artery and symptoms of hypoxia. Modified from *Human Anatomy,* 4th Ed. (1995), K. M. Van De Graaff (ed.), Wm. C. Brown Communications, Inc., Dubuque, IA, p. 557. Reprinted by permission of The McGraw-Hill Companies.

edge of the septum primum reduces the ostium primum to nothing. At the same time, the septum primum grows perforations that coalesce to form a new foramen, the *ostium secundum* ("second opening"). Thus, a new channel for right-to-left blood flow opens before the old one closes.

At the same time, a second crescent-shaped wedge of tissue, the *septum secundum* ("second partition"), grows from the roof of the atrium. It is located adjacent to the septum primum on the side of the right atrium. Unlike the septum primum, the secundum is thick and muscular as it grows posteroinferiorly. It completely extends to the floor of the right atrium and leaves a hole in the inferior portion, the foramen ovale. Throughout the rest of fetal development, blood shunts from the right to the left atrium to pump out of the heart through the aortic artery. This shunt closes at birth because of the abrupt dilation of the pulmonary vasculature combined with the loss of flow through the umbilical vein. The increase in pressure in the left atrium and the loss of pressure in the right push the flexible septum primum against the septum secundum.

If the septum secundum is too short to cover the ostium secundum completely, an atrial septal defect allows left-to-right atrial flow after the septum primum and septum secundum are pressed together at birth (Fig. 21). This abnormality is generally asymptomatic during infancy. However, the persistent increase in flow of blood into the right atrium can lead to hypertrophy of the right atrium, right ventricle, and pulmonary trunk. In some cases, during adulthood (roughly 40 years of age) pulmonary hypertension develops, and the left-to-right shunt converts to a right-to-left shunt. Thus, increased pressure in the right atrium results in right-to-left blood flow across the atrial septum. This causes oxygen-poor blood to mix with the oxygen-rich blood returning to the left atrium from the lungs.

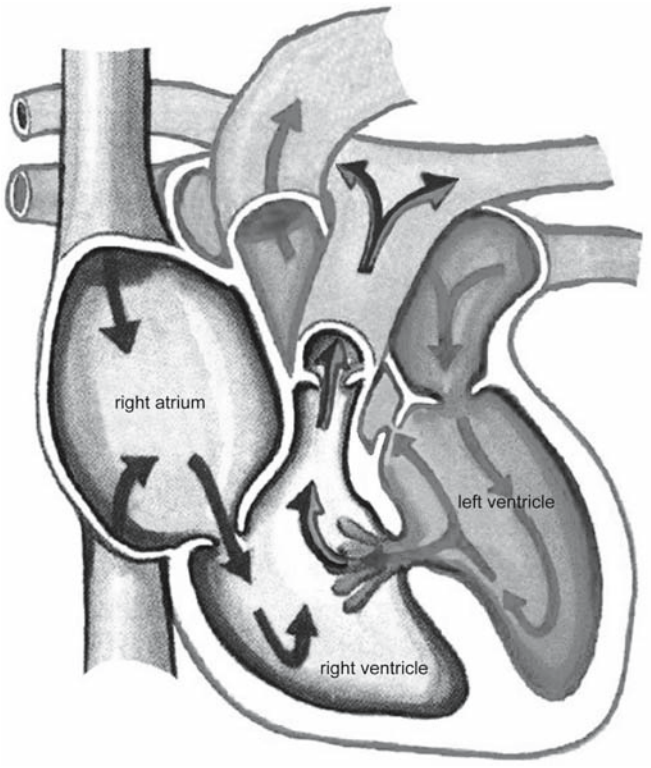

Fig. 22. Ventricular septal defect. Caused by abnormal development of the interventricular septum, a ventricular septal defect results in massive left-to-right shunting of blood. It is associated with pulmonary hypertension and deficient closure of atrioventricular valves after birth. Emergent surgical repair of this hole is indicated. Figure modified from *Human Anatomy,* 4th Ed. (1995), K. M. Van De Graaff (ed.), Wm. C. Brown Communications, Inc., Dubuque, IA, p. 557. Reprinted by permission of The McGraw-Hill Companies.

Oxygen-poor blood is then pumped out of the heart through the aortic artery, and the symptoms of hypoxia (low oxygen) result. Approximately 30% of normal hearts have a small patency with a valve-competent foramen ovale; this is not usually called an atrial septal defect (*See* also Chapter 29.)

7.2.2. Ventricular Septal Defect

The developmental formation of the interventricular septum is extremely complex. Simply, the septum forms as the growing walls of the right and left ventricles become more closely apposed to one another. The growth of the muscular septum commences at the inferior end and proceeds superiorly. Septation of the ventricles and formation of the ventricular outflow tracts (membranous interventricular septum) must occur in tight coordination. Ventricular septal defects can occur because of errors in this complex process. Failure of complete fusion of the membranous septum (from the aortic and pulmonary outflow tracts) and the muscular septum results in one type of ventricular septal defect, the most common congenital heart defect (Fig. 22).

Whatever the origin of a ventricular septal defect, the result is always a massive left-to-right shunting of blood. This is associated with pulmonary hypertension and deficient closure of atrioventricular valves after birth. This type of condition is often referred to in lay terms as a "baby born with a hole in the heart." Because of extreme hypoxia, there is usually immediate surgical repair of the defect. For additional information on such defects and the means for their repair, refer to Chapter 29.

8. VASCULATURE OF THE HEART

Although the heart chambers are filled with blood, it provides very little nourishment and oxygen to the tissues of the heart. The walls of the heart are too thick to be supplied by diffusion alone. Instead, the tissues of the heart are supplied by a separate vascular supply committed only to the heart. The arterial supply to the heart arises from the base of the aorta as the right and left coronary arteries (running in the coronary sulcus). The venous drainage is via cardiac veins that return deoxygenated blood to the right atrium.

The coronary arteries arise from the ostia in the left and right sinuses of the aortic semilunar valve, course within the epicardium, and encircle the heart in the atrioventricular (coronary) and interventricular sulci (Fig. 23).

8.1. Right Coronary Artery

The right coronary artery emerges from the aorta into the atrioventricular groove. It descends through the groove, then curves posteriorly, makes a bend at the crux of the heart, and continues downward in the posterior interventricular sulcus. Within millimeters after emerging from the aorta, the right coronary artery gives off two branches (Figs. 23 and 24). The conus (arteriosus) artery runs to the conus arteriosus (right ventricular outflow tract), and the atrial branch goes to the right atrium. This atrial branch gives off the sinoatrial nodal artery (in 50–73% of human hearts, according to various reports), which runs along the anterior right atrium to the superior vena cava, encircling it in a clockwise or counterclockwise direction before reaching the sinoatrial node. The sinoatrial nodal artery supplies the sinoatrial node, Bachman's bundle, crista terminalis, and the left and right atrial free walls.

The right coronary artery continues in the atrioventricular groove and gives off a variable number of branches to the right atrium and right ventricle. The most prominent of these is the right marginal branch, which runs down the right margin of the heart, supplying this part of the right ventricle. As the right coronary curves posteriorly and descends downward on the posterior surface of the heart, it gives off two to three branches. One is the posterior interventricular (posterior descending) artery, which runs in the posterior interventricular sulcus. It is directed toward the apex of the heart to supply the posterior free wall of the right ventricle. In 85–90% of human hearts, branches of this artery (posterior septal arteries) supply the posterior one-third of the interventricular septum (Fig. 25). The second artery is the atrioventricular nodal artery, which branches from the right coronary artery at the crux of the heart and passes anteriorly along the base of the atrial septum to supply the atrioventricular node (in 50–60 % of hearts), proximal parts of the bundles (branches) of His, and the parts of the posterior interventricular septum that surround the bundle branches. Another artery crosses the crux into the left atrioventricular groove to supply the diaphragmatic surface of the left ventricle and the posterior papillary muscle of the bicuspid valve.

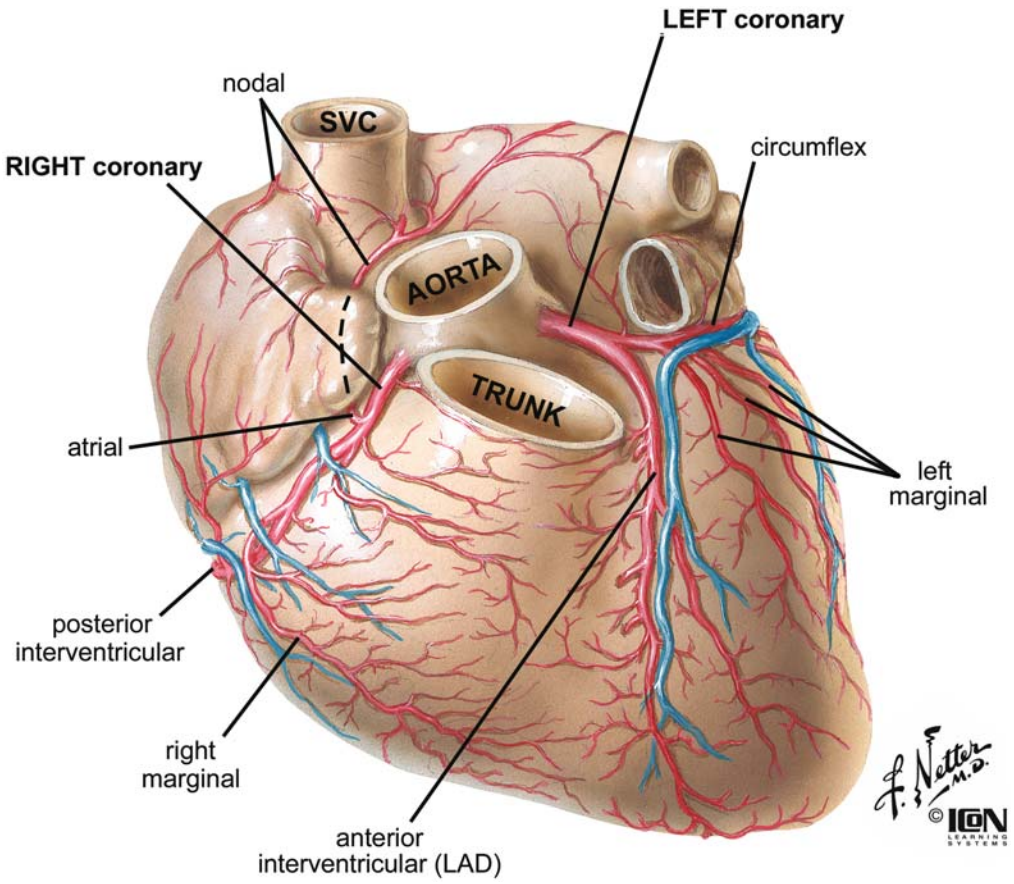

Fig. 23. Vascular supply to the heart. Arterial supply to the heart occurs via the right and left coronary arteries and their branches. Venous drainage occurs via cardiac veins. LAD, left anterior descending; SVA, superior vena cava.

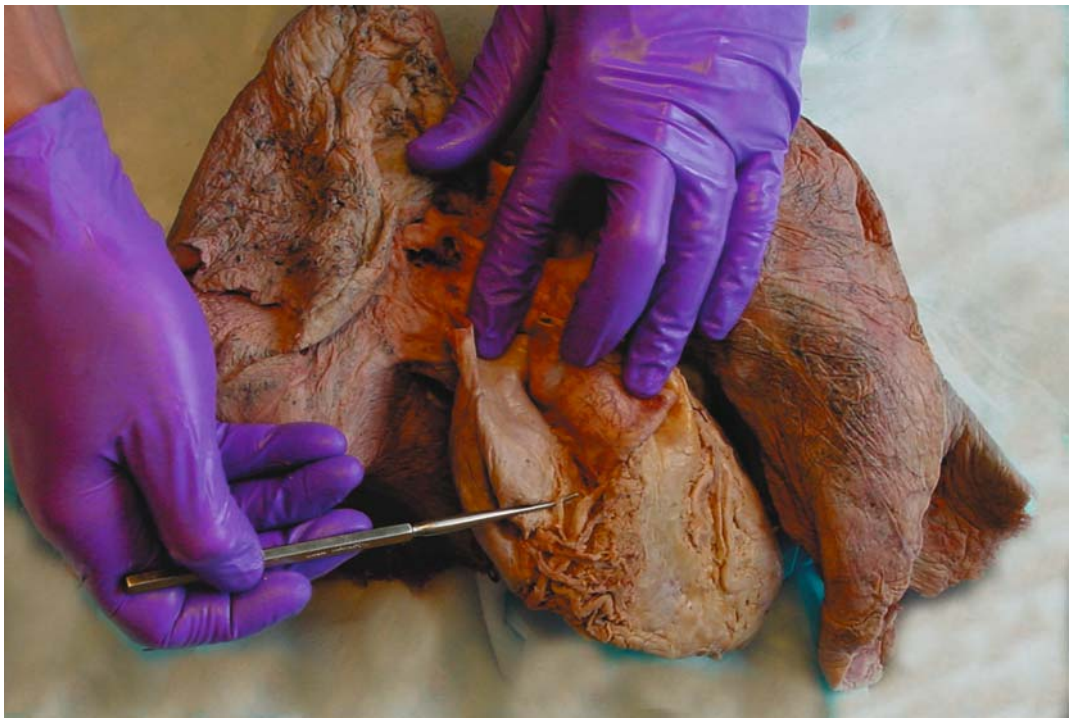

Fig. 24. Atrial branch of the right coronary artery. This atrial branch gives off the sinoatrial nodal artery, which runs along the anterior right atrium to the superior vena cava and encircles it in a clockwise, or sometimes counterclockwise, direction before reaching the sinoatrial node. The nodal artery can also pass intramurally through the right atrium to the sinoatrial node. The sinoatrial nodal artery supplies the sinoatrial node, Bachman's bundle, crista terminalis, and left and right atrial free walls.

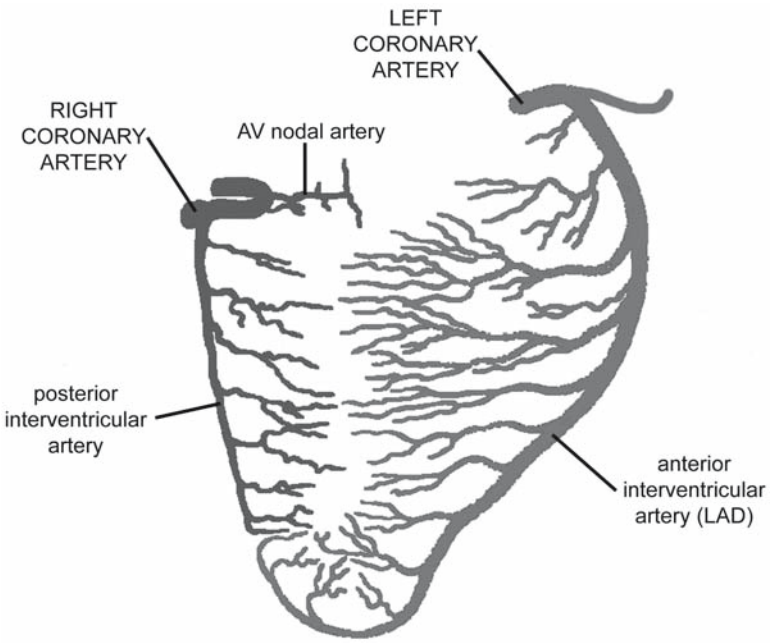

Fig. 25. Arterial supply to the interventricular septum. The right coronary artery supplies the posterior one-third of the interventricular septum, and the left coronary supplies the anterior two-thirds. The artery to the atrioventricular node commonly branches off the posterior interventricular artery. AV, atrioventricular; LAD, left anterior descending. Adapted from T.N. James and G.E. Burch (1958) Blood supply of the human interventricular septum. *Circulation* 17(3), pp. 391–396.

The right coronary artery also serves as an important collateral supply to the anterior side of the heart, left ventricle, and anterior two-thirds of the interventricular septum via the conus artery and communicating arteries in the interventricular septum (Fig. 25). Kugel's artery, which originates from either the right or left coronary artery, runs from anterior to posterior through the atrial septum. This artery serves as an important collateral connection from anterior arteries to the atrioventricular node and posterior arteries.

8.2. Left Coronary Artery

The left coronary artery (left main coronary artery) emerges from the aorta through the ostia of the left aortic cusp within the sinus of Valsalva (Fig. 23). The plane of the semilunar valve is tilted so that the ostium of the left coronary artery is superior and posterior to the right coronary ostium. The left coronary artery travels from the aorta, and passes between the pulmonary trunk and the left atrial appendage. Under the appendage, the artery divides (and is thus a very short vessel) into the anterior interventricular (left anterior descending) artery and the left circumflex artery. The left coronary artery may be completely absent; that is, the anterior interventricular and circumflex arteries arise independently from the left aortic sinus.

The anterior interventricular artery appears to be a direct continuation of the left coronary artery that descends into the anterior interventricular groove. Branches of this artery, anterior septal perforating arteries, enter the septal myocardium to supply the anterior two-thirds of the interventricular septum (in about 90% of hearts). The first branch, the *first septal perforator*, supplies a major portion of the atrioventricular conduction system. In about 80% of human hearts, the second or third perforator is the longest and strongest of the septal arteries and is often called the *main septal artery*. This artery supplies the middle portion of the interventricular septum. Oddly, this artery also sends a branch to the moderator band and the anterior papillary muscle of the tricuspid valve (right ventricle). This artery is often called the *moderator* artery.

Other branches of the anterior interventricular artery extend laterally through the epicardium to supply adjacent right and left ventricular free walls. The anterior interventricular artery also sends a branch to meet the conus artery from the right coronary to form an important collateral anastomosis called the *circle of Vieussens* (Raymond Vieussens, French anatomist, 1641–1715), as well as branches to the anterior free wall of the left ventricle called *diagonal arteries*. These are numbered according to their sequence of origin as first, second, and so on diagonal arteries. The most distal continuation of the anterior interventricular artery curves around the apex and travels superiorly in the posterior interventricular sulcus to anastomose with the posterior descending from the right coronary artery.

In summary, the anterior interventricular artery and its branches supply most of the interventricular septum: the anterior, lateral, and apical walls of the left ventricle; most of the right and left bundle branches; and the anterior papillary muscle of the bicuspid valve (left ventricle). It also provides collateral circulation to the anterior right ventricle, the posterior part of the interventricular septum, and the posterior descending artery.

The circumflex artery branches off the left coronary artery and supplies most of the left atrium, the posterior and lateral free walls of the left ventricle, and (with the anterior interventricular artery) the anterior papillary muscle of the bicuspid

valve. The circumflex artery may give off a variable number of left marginal branches to supply the left ventricle. The terminal branch is usually the largest of these branches. More likely, the circumflex artery may continue through the atrioventricular sulcus to supply the posterior wall of the left ventricle and (with the right coronary artery) the posterior papillary muscle of the bicuspid valve. In 40–50% of human hearts, the circumflex artery supplies the artery to the sinoatrial node.

In 30–60% of hearts, the left coronary artery may give off one or more intermediate branches that originate between the anterior interventricular and circumflex arteries. These extend diagonally over the left ventricle toward the apex of the heart and are thus named *diagonal* or *intermediate arteries*.

The anterior interventricular artery is the most commonly occluded of the coronary arteries. It is the major blood supply to the interventricular septum and the bundle branches of the conducting system. It is easy to see why coronary artery disease can lead to impairment or death (infarction) of the conducting system. The result is a "block" of impulse conduction between the atria and the ventricles; this block is known as *right/left bundle branch block*. Furthermore, branches of the right coronary artery supply both the sinoatrial and atrioventricular node in at least 50% of hearts. An occlusion in this artery could result in necrosis of the sinoatrial or atrioventricular nodes, thus preventing or interrupting the conduction of electrical activity across the heart. (For more information on coronary artery stenting, *see* Chapter 6.)

8.3. Cardiac Veins

The coronary arteries supply the heart with nutrients and oxygen. At the same time, waste products and carbon dioxide must be removed. An extensive network of intercommunicating veins provides venous drainage from the heart. The venous drainage of deoxygenated blood from all tissues is collected in the right atrium; this includes the venous drainage of the heart. Venous drainage of the heart is accomplished through three separate systems: (1) the cardiac venous tributaries, which converge to form the coronary sinus; (2) the anterior cardiac (anterior right ventricular) veins; and (3) the smallest cardiac (Thebesian) venous system (Fig. 26).

Most of the myocardium is drained by the cardiac veins that course parallel to the coronary arteries. These three large veins (the great, middle, and small cardiac veins) converge to form the coronary sinus.

On the anterior side of the heart, the great cardiac (anterior interventricular) vein lies within the anterior interventricular sulcus and runs from inferior to superior beside the anterior interventricular artery (Figs. 26 and 27). At the base of the heart, near the bifurcation of the left coronary artery, it turns and runs within the atrioventricular groove around the left side of the heart to the posterior. In the atrioventricular groove, on the posterior side of the heart, the great cardiac vein becomes the coronary sinus, which then empties into the right atrium. From the inside of the right atrium, it can be seen that the coronary sinus opens into the right atrium, forming an opening or *os* located anteriorly and inferiorly to the orifice of the inferior vena cava. There is a valve (Thebesian valve) that covers to varying degrees the opening of the coronary sinus to prevent backflow. The great cardiac vein is formed by the confluence of small venous tributaries from the left and right ventricles and anterior portion of the interventricular septum. As it ascends toward the coronary sinus, it receives small venous tributaries from the left atrium and left ventricle; it also receives a large left marginal vein, which runs parallel to the left marginal artery.

There are two structures that serve as the boundary between the termination of the great cardiac vein and the beginning of the coronary sinus. The first is the valve of Vieussens, which has the appearance of a typical venous valve and functions to prevent the backflow of blood from the coronary sinus into the great cardiac vein. The second is the space between the entry points of the oblique vein of the left atrium (of Marshall; John Marshall, English anatomist, 1818–1891) and the posterior vein of the left ventricle. The oblique vein of Marshall runs superior to inferior along the posterior side of the left atrium, providing venous drainage of the area. The posterior vein ascends to the coronary sinus from the inferior portion of the left ventricle and provides drainage of the area.

In addition to the great cardiac vein, the coronary sinus receives the middle cardiac vein (Figs. 26 and 28). Located on the posterior surface of the heart, it arises near the posterior aspect of the apex of the heart and runs from inferior to superior through the posterior interventricular sulcus. It then joins the coronary sinus within millimeters of the sinus entering into the right atrium. The middle cardiac vein is formed from venous confluence of tributaries that drain the posterior left and right ventricles and the interventricular septum.

The coronary sinus also receives the highly variable small cardiac vein. The small cardiac vein arises from the anterior/lateral/inferior portion of the right ventricle. It ascends and runs inferior to, and roughly parallel with, the marginal branch of the right coronary artery until it reaches the right atrioventricular sulcus. At this point, it turns and runs horizontally around to the posterior side of the heart and enters the coronary sinus with the middle cardiac vein. The small cardiac vein is extremely small or absent in 60% of humans. In about 50% of hearts, the small cardiac vein enters the right atrium directly.

Typically, about 85% of the heart's venous drainage occurs through the great, middle, and small cardiac veins through the coronary sinus to the right atrium. This elaborate system of veins drains the left ventricle, some of the right ventricle, both atria, and the anterior portion of the interventricular septum.

The second system of venous drainage of the heart is the anterior cardiac veins (Figs. 26 and 29). This system is distinguished from the other cardiac venous system because the anterior cardiac veins do not drain into the coronary sinus. Two to four anterior cardiac veins originate and drain the anterior right ventricular wall, travel superiorly to cross the right atrioventricular sulcus, and enter the right atrium directly. The sulcus is usually packed with adipose tissue. Through this adipose tissue run the anterior cardiac veins, the right coronary artery, and a branch of the coronary artery, the right atrial or nodal artery. The anterior cardiac veins pass over the right coronary artery in close proximity and in a perpendicular angle. A right marginal vein (when present) runs parallel with the right marginal artery before entering the right atrium directly

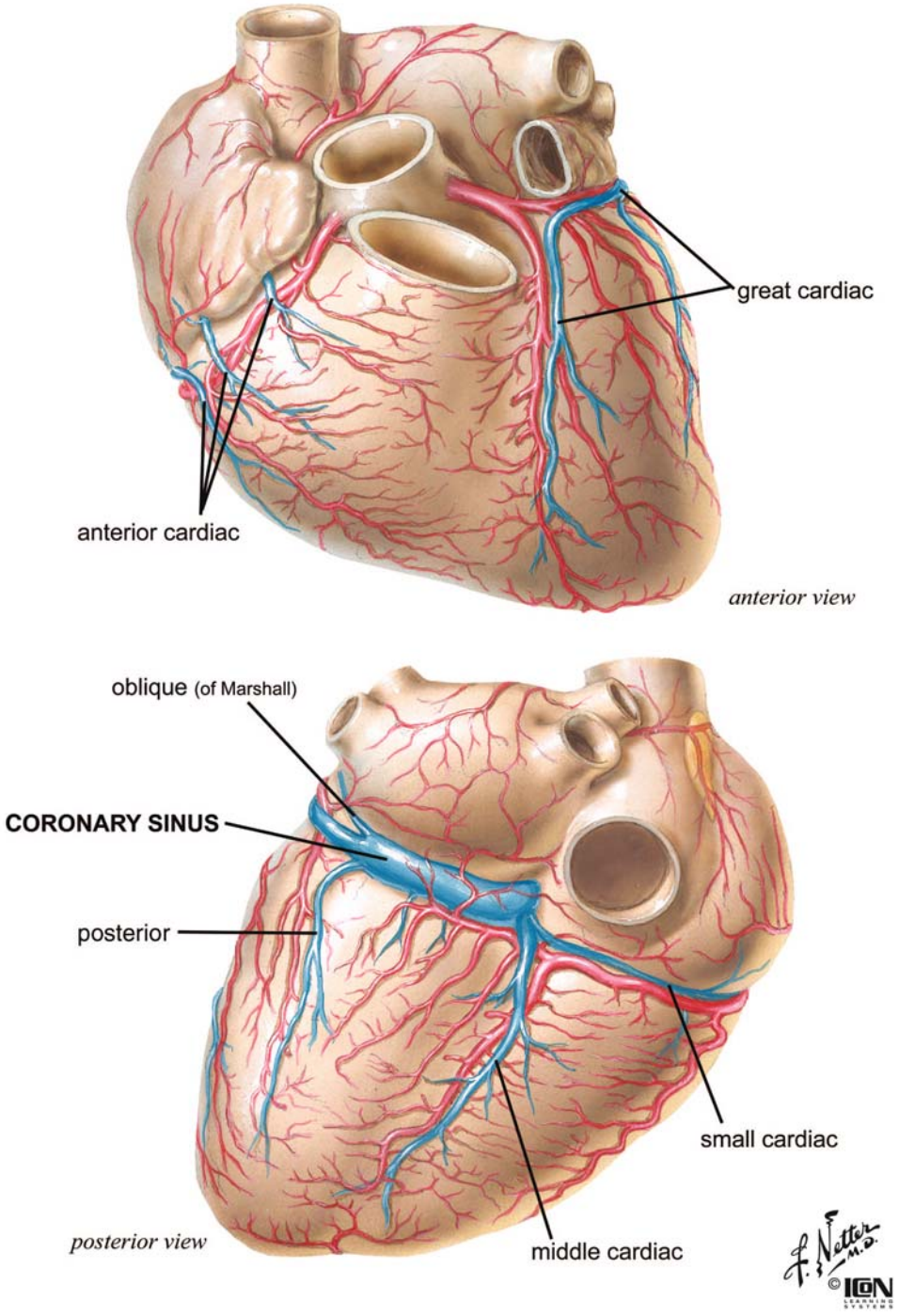

Fig. 26. Venous drainage of the heart. Three separate venous systems carry blood to the right atrium: the coronary sinus and its tributaries, the anterior cardiac veins, and the smallest (Thebesian) cardiac veins.

and is usually considered part of the anterior cardiac venous system.

The third system of venous drainage of the heart is the smallest cardiac venous system. This system is composed of a multitude of small intramural ("within the walls")/intramyocardial veins also called Thebesian veins. These are minute vessels that begin in the capillary beds of the myocardium and open directly into the chambers of the heart. Although called veins, they are valveless communications between myocardial capillaries and a chamber of the heart. These veins drain primarily into the right atrium, and to a lesser extent the right ventricle, near the septa. The openings of these veins can be seen macroscopically (Thebesian foramina) in the endocardium of the right atrium.

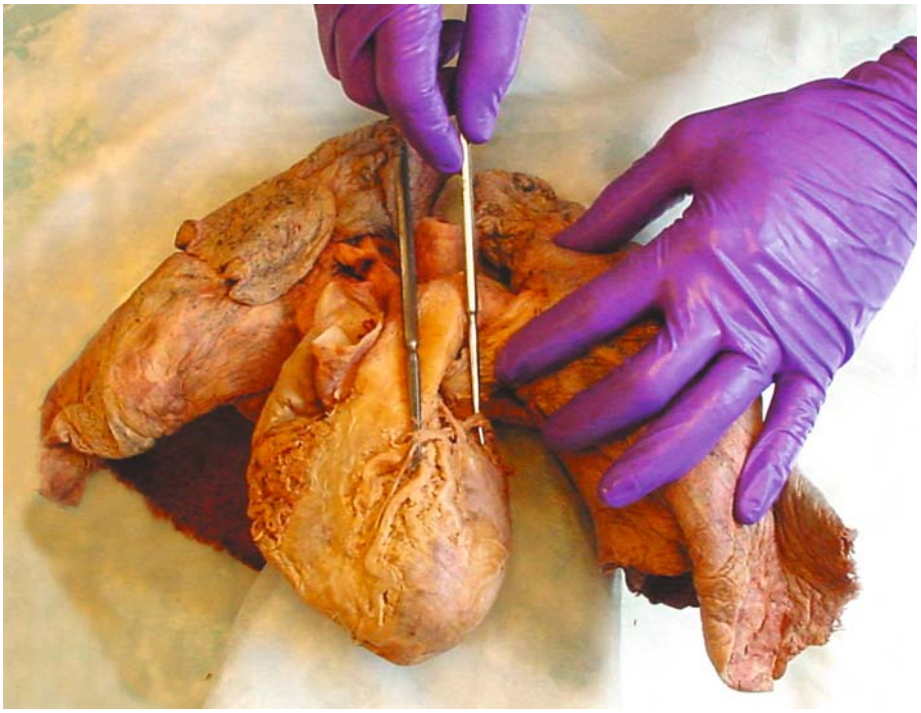

Fig. 27. The great cardiac vein. On the anterior side of the heart, the great cardiac vein lies within the anterior interventricular sulcus and runs from inferior to superior beside the anterior interventricular artery. At the base of the heart, it runs within the atrioventricular groove around the left side of the heart to the posterior. In the atrioventricular groove, on the posterior side of the heart, the great cardiac vein becomes the coronary sinus and empties into the right atrium.

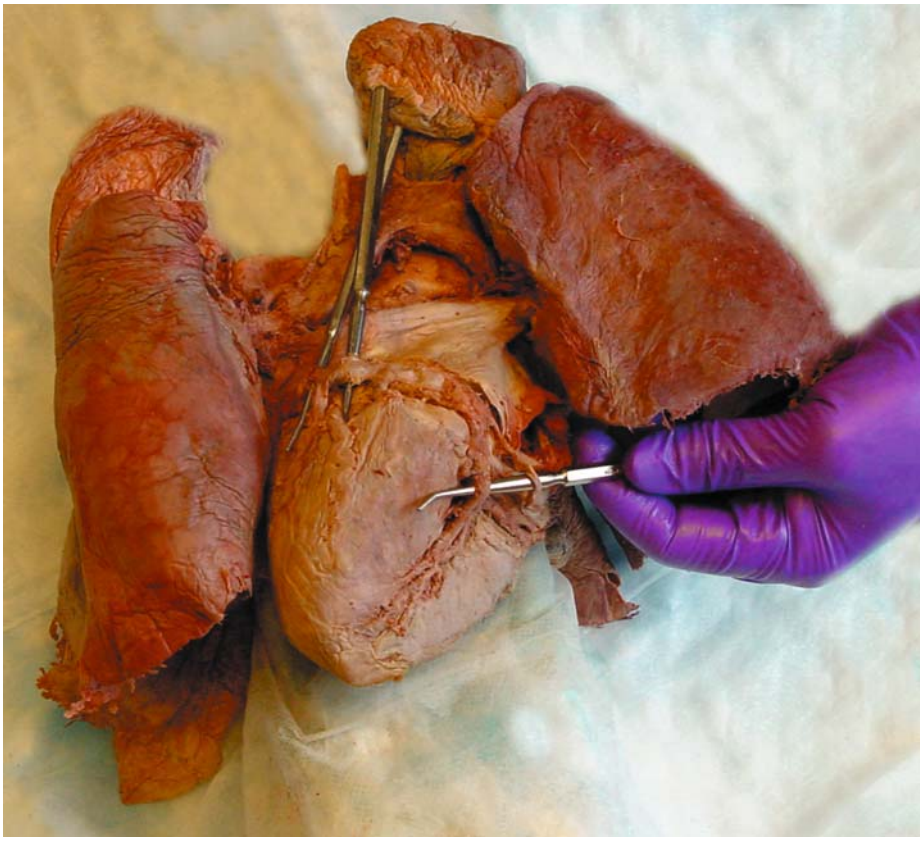

Fig. 28. The middle cardiac vein. The middle cardiac vein, located on the posterior surface of the heart, arises near the posterior aspect of the apex of the heart and runs from inferior to superior through the posterior interventricular sulcus before entering the coronary sinus. The middle cardiac vein is formed from venous confluence of tributaries that drain the posterior left and right ventricles and the interventricular septum.

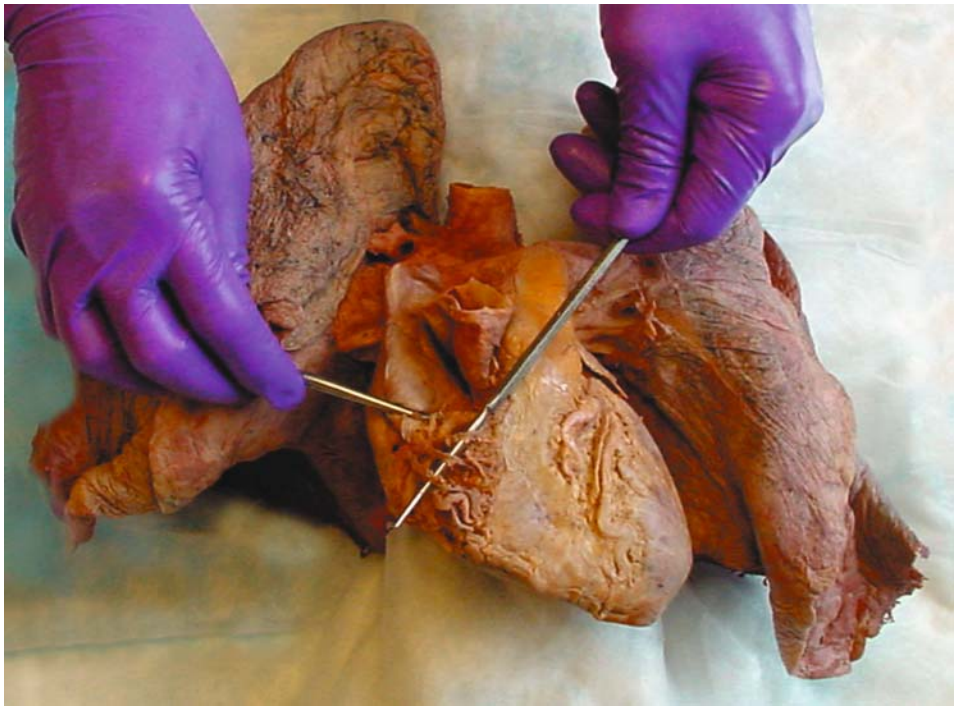

Fig. 29. Anterior cardiac veins. Two to four anterior cardiac veins originate and drain the anterior right ventricular wall. These veins travel superiorly to cross the right atrioventricular sulcus and enter into the right atrium. These veins are part of the smallest cardiac venous system that empties oxygen-poor blood directly into the right atrium without a communication with the coronary sinus.

8.4. Myocardial Bridges

The coronary arteries typically course on the myocardium or under/within the epicardium of the heart. Frequently, a portion of an artery deviates from its usual subepicardial position to follow an intramyocardial (intramural) course, either by traveling a significant length within the myocardium or beneath an arrangement of muscular slips ("myocardial bridges"). Myocardial bridging is most common in the middle segment of the anterior interventricular artery *(1)*. The myocardial fibers that cover or "bridge over" the anterior interventricular artery are direct extensions of the myocardium of the conus arteriosus of the right ventricle and cross the artery in a perpendicular direction. Myocardial bridges over the right coronary and the circumflex arteries are much less common. When present, these bridges are extensions of the respective atrial myocardium *(2)*. The prevalence of myocardial bridges from various sources is reported to occur in 5.4–85.7% of human hearts when measured from the cadaver *(3,4)* and 0.5–16% when measured from angiography in catheterization labs *(4–6)*.

Coronary arteries and their branches have a tortuous pattern as they run across the heart. Interestingly, studies employing angiography followed by detailed microdissection showed that a coronary artery with a typical tortuous shape takes on a perfectly straight pattern when it follows an intramyocardial course *(7)*.

Angiography has also shown that myocardial bridges are associated with narrowing of the lumen of the coronary artery. The narrowing appears during systole and disappears during diastole *(1)*. The appearance of straight running or systolic narrowing patterns seems to be an important diagnostic technique during angiography to discover intramyocardial segments of coronary arteries *(1)*. Myocardial bridging is usually a benign condition. Although there is contrasting evidence, atherosclerosis is uncommon within a myocardial bridge *(3)*; bridging might be providing some protection against plaque formation *(1)*.

9. AUTONOMIC INNERVATION OF THE HEART

The sinoatrial node produces a regular series of impulses and is called the "pacemaker" of the heart. The sinoatrial node spontaneously produces an impulse for contraction of the atrial myocardium, depolarizes the atrioventricular node, and sends an impulse through the bundle fibers to the ventricular myocardium. In addition to the pacemaker activity of the sinoatrial node, the heart is also under autonomic, or involuntary, control.

The autonomic nervous system is separated into the sympathetic and parasympathetic nervous systems. These two systems send neurons to the same target, but convey opposite effects. In emergency situations, sympathetic nerves travel to the heart and innervate the sinoatrial and atrioventricular nodes to increase the rate and force of contraction. In resting situations, parasympathetic nerves innervate the sinoatrial and atrioventricular nodes to slow the heart rate, reduce the force of contraction, and constrict the coronary arteries, thus saving energy.

Both the sympathetic and parasympathetic nerves are composed of a two-neuron pathway. These two neurons meet, or synapse, somewhere in the middle and form a structure called a *ganglion* ("swelling"). Neurons of the sympathetic nervous system emerge from the spinal cord. They emerge from all eight of the cervical segments and the first five of the thoracic spinal cord segments. These neurons travel laterally just centimeters from the spinal cord before they synapse. All of the neurons to the heart are believed to synapse in only two places: the middle cervical ganglion and the cervicothoracic (fused inferior cervical/first thoracic or stellate "star-shaped") ganglion. Multitudes of fibers then emanate from these ganglia and run to the heart as sympathetic cardiac nerves.

Parasympathetic neurons emerge directly from the brain as part of the vagus nerve or cranial nerve X. The vagus nerve and its branches form the parasympathetic part of the cardiac nerves running toward the heart.

Sympathetic and parasympathetic cardiac nerves interweave. In addition, nerves of the right and left side overlap; altogether, this huge group of common innervation forms the cardiac plexuses. The dorsal cardiac plexus is located posterior to the arch of the aorta near the bifurcation of the trachea. The ventral plexus is located anterior to the aorta. Nerves from the cardiac plexuses extend to the atria and ventricles, the sinoatrial node, the atrioventricular node, the coronary arteries, and the great vessels. It is generally believed that there is sympathetic and parasympathetic innervation of the myocardium that forms a network from the atria to the ventricles. For more details about the role of the autonomic nervous system in the physiological control of the heart, refer to Chapter 10.

COMPANION CD MATERIAL

Illustrations provided in color.

REFERENCES

1. Kalaria, V.G., Koradia, N., and Breall J.A. (2002) Myocardial bridge: a clinical review. *Catheter Cardiovasc Interv.* 57, 552–556.
2. Garg, S., Brodison, A., and Chauhan A. (2000) Occlusive systolic bridging of circumflex artery. *Catheter Cardiovasc Diagn.* 51, 477–478.
3. Polacek, P. (1961) Relation of myocardial bridge and loops on the coronary arteries to coronary occlusions. *Am Heart J.* 61, 44–52.
4. Irvin, R.G. (1982) The angiographic prevalence of myocardial bridging. *Chest.* 81, 198–202.
5. Noble, J., Bourassa, M.G., Petitclerc, R., and Dyrda, I. (1976) Myocardial bridging and milking effect of left anterior descending artery: normal variant or obstruction. *Am J Cardiol.* 37, 993–999.
6. Greenspan, M., Iskandrin, A.S., Catherwood, E., Kimbiris, D., Bemis, C.E., and Segal, B.L. (1980) Myocardial bridging of the left anterior descending artery valuation using exercise thallium-201 myocardial scintigraphy. *Catheter Cardiovasc Diagn.* 6, 173–180.
7. Lachman, N., Satyapal, K.S., and Vanker, E.A. (2002) Angiographic manifestation and anatomical presence of the intramural LAD: surgical significance. *Clin Anat.* 15, 426.

SOURCES

Berne, R.M., Levy, M. N., Koeppen, B.M., and Stanton, B.A. (eds.) (2004) *Physiology.* Mosby, St. Louis, MO.

Garson, A. (ed.) (1998) *The Science and Practice of Pediatric Cardiology.* Williams and Wilkins, Baltimore, MD.

Goss, C.M. (ed.) (1949) *Anatomy of the Human Body: Gray's Anatomy.* Lea and Febiger, Philadelphia, PA.

Hurst, J.W. (ed.) (1990) *The Heart.* McGraw-Hill, New York, NY.

Kumar, V. (ed.) (2003) *Robbins Basic Pathology.* Saunders, Philadelphia, PA.

Larson, W.J. (ed.) (1997) *Human Embryology.* Churchill Livingstone, New York, NY.

Moore, K.L. and Dalley, A.F. (eds.) (1999) *Clinically Oriented Anatomy.* Lippincott, Williams, and Wilkins, Philadelphia, PA.

Netter, F.H. (ed.) (2003) *Atlas of Human Anatomy.* ICON Learning Systems, Teterboro, NJ.

Stedman, T. (1972) *Stedman's Medical Dictionary.* Williams and Wilkins, Baltimore, MD.

5 Comparative Cardiac Anatomy

ALEXANDER J. HILL, PhD AND PAUL A. IAIZZO, PhD

CONTENTS

1. HISTORICAL PERSPECTIVE OF ANATOMY AND ANIMAL RESEARCH

Anatomy is one of the oldest branches of medicine, with historical records dating back at least as far as the 3rd century BC; animal research dates back equally as far. Aristotle (384–322 BC) studied comparative animal anatomy and physiology, and Erasistratus of Ceos (304–258 BC) studied live animal anatomy and physiology *(1)*. Galen of Pergamum (129–199 AD) is probably the most notable early anatomist who used animals in research to attempt to understand the normal structure and function of the body *(2)*. He continuously stressed the centrality of anatomy and made an attempt to dissect every day because he felt it was critical to learning *(3)*. His most notable work was *De Anatomicis Administrationibus* (On Anatomical Procedures), which when rediscovered in the 16th century, renewed interest in anatomy and scientific methods *(2)*.

The Renaissance was a period of great scientific discovery and included advances in our understanding of human and animal anatomy. Andreas Vesalius (1514–1564 AD) was arguably the greatest anatomist of the era *(4)*. He performed public nonhuman dissections at the University of Padua in Italy to teach anatomy and is credited with creating the field of modern anatomy *(2)*. His immediate successors at Padua were Matteo Realdo Colombo (1510–1559 AD), who described pulmonary circulation and the atrial and ventricular cavities, and Gabriele Falloppio (1523–1562 AD), who is credited with the discovery of the Fallopian tubes among other things *(4)*. Animal research flourished during this period because of a number of popular ideas launched by the Christian church and Rene Descartes. The church asserted that animals were under the dominion of man and, although worthy of respect, could be used to obtain information if it was for a "higher" purpose *(2)*. Descartes described humans and other animals as complex machines, with the human soul distinguishing humans from all other animals. This beast–machine concept was important for early animal researchers because, if animals had no souls, it was thought that they could not suffer pain. Furthermore, the reactions of animals were thought to be the response of automata and not reactions of pain *(2)*.

The concept of functional biomedical studies can probably be attributed to another great scientist and anatomist, William Harvey (1578–1657 AD). He is credited with one of the most outstanding achievements in science and medicine: a demonstration of the circulation of blood, which was documented in his publication *Exercitatio Anatomica De Motu Cordis et Sanguinis in Animalibus (De Motu Cordis)* in 1628. His work ushered in a new era in science, in which a hypothesis was formulated and then tested through experimentation *(4)*. Many great anatomists emerged during this period and made innumerable discoveries; many of these discoveries were named after the individuals who described them, including several researchers who studied cardiac anatomy such as the eustachian valve (Bartolomeo Eustachio), the Thebesian valve and Thebesian veins (Thebesius), and the sinus of Valsalva (Antonio Maria Valsalva).

It should be noted that, during this time period, in addition to animal dissection, dissections on deceased human bodies were performed, but not to the degree that they are today. In fact, it is written that, in general, during the post-Renaissance era there was a serious lack of human bodies available for approved dissection. Often, bodies were obtained in a clandestine manner, such as grave robbing, or the bodies of executed criminals were

From: *Handbook of Cardiac Anatomy, Physiology, and Devices*
Edited by: P. A. Iaizzo © Humana Press Inc., Totowa, NJ

provided for dissection. In spite of the lack of bodies for study, most structures in the human body, including microscopic ones, were described by various anatomists and surgeons between the 15th and early 19th centuries.

Early in the 19th century, the first organized opposition to animal research occurred. In 1876, the Cruelty to Animals Act was passed in Britain. It was followed in the United States by the Laboratory Animal Welfare Act of 1966, which was amended in 1970, 1976, and 1985. These two acts began a new era in how laboratory animals were treated and utilized in experimental medicine. Nevertheless, the necessity of animal research is still great; therefore, animals continue to be used for a variety of scientific purposes, including cardiovascular device research.

2. IMPORTANCE OF ANATOMY AND ANIMAL RESEARCH

Anatomy remains as quite possibly one of the most important branches of medicine. To diagnose and treat medical conditions, normal structure and function must be known because it is the basis for determining what is abnormal. Furthermore, structure typically has a great impact on the function of an organ, such as with the heart. For instance, a stenotic aortic valve will usually cause functional impairment of the left ventricle and lead to further pathological conditions (e.g., hypertrophy). Thus, knowledge of anatomy and pathology is fundamental in understanding not only how the body is organized, but also how the body works and how disease processes can affect it.

Likewise, animal research has been fundamental for much of the progress made in medicine. Most, if not all, of what we know about the human body and biology in general has been initially made possible through animal research. A1989 American Medical Association publication, cited in ref. *2*, listed medical advances that had emanated from animal research, including studies on acquired immunodeficiency syndrome (AIDS), anesthesia, cardiovascular disease, diabetes, hepatitis, and Parkinson's disease, to name only a few.

Currently, animal research is fundamental in developing new therapies aimed at improving the quality of life for patients with cardiovascular disease. Furthermore, early cardiac device prototype testing is commonly performed utilizing animal models, both with and without cardiovascular disease. More specifically, before an invasively used device (a class III medical device) can be tested in humans, the Food and Drug Administration requires sufficient data obtained from animal research indicating that the device functions in the desired and appropriate manner. Importantly, it is also critical to extrapolate subsequently that a given device will be safe when used in humans; that is, it will behave in humans in a manner similar to its determined function in the animal models. This extrapolation of animal data to the human condition requires that the animal model chosen for testing is similar in anatomy and physiology to that in humans. Unfortunately, detailed information relating human cardiac anatomy to that of the most common large mammalian animal models is still lacking.

The following historical example helps to illustrate how this lack of knowledge can have a dramatic effect on the outcomes of cardiovascular research. During the 1970s and 1980s, dogs were employed as the primary animal model in numerous studies aimed at identifying potential pharmacological therapies for reducing infarct size. However, a detailed understanding of the coronary arterial anatomy was either lacking or overlooked at the time; subsequently, it was shown that dogs have a much more extensive coronary collateral circulation relative to humans (Fig. 1). Thus, even when major coronary arteries were occluded, reliable and consistent myocardial infarcts were difficult to create. This led to false claims about the efficacy of many drugs in reducing infarct size; when tested in humans, these drugs usually did not produce the same results as those observed in the canine experiments *(5)*.

3. LARGE MAMMALIAN COMPARATIVE CARDIAC ANATOMY

In general, the hearts of large mammals share many similarities, and yet the sizes, shapes, and positions of the hearts in the thoracic cavities can vary considerably between species *(6)*. Typically, the heart is located in the lower ventral part of the mediastinum in large mammals *(7)*. Most quadruped mammals tend to have a less-pronounced left-sided orientation and a more ventrally tilted long axis of the heart compared to humans *(7)* (Fig. 2). In addition, hearts of most quadruped mammals tend to be elongated and have a pointed apex, with the exception of (1) dogs, which tend to have an ovoid heart with a blunt apex *(7)*; (2) sheep, which may have a somewhat blunt apex *(8)*; and (3) pigs, which have a blunt apex that is oriented medially *(8)*. Comparatively, human hearts typically have a trapezoidal shape *(9)* with a blunt apex. However, the apices of normal dog, pig, sheep, and human hearts are all formed entirely by the left ventricles *(8–11)* (Fig. 3).

Differences exist in the ratios of heart weight to body weight reported for large mammals. It is generally accepted that adult sheep and adult pigs have smaller ratios of heart weight to body weight than those of adult dogs. It has been reported that adult dogs have as much as twice the heart weight to body weight ratio (6.95:7 g/kg) as pigs (2.89:2.5 g/kg) and sheep (3.13:3 g/kg) *(12,13)*. The normal ratio of the adult human heart weight to body weight has been reported as 5 g/kg, which is similar to that of young pigs (animals 25–30 kg) *(14)*.

All large mammalian hearts are enclosed by the pericardium, which creates the pericardial cavity surrounding the heart. The pericardium is fixed to the great arteries at the base of the heart and is attached to the sternum and diaphragm in all mammals, although the degree of these attachments to the diaphragm varies between species *(6,7)*. Specifically, the attachment to the central tendinous aponeurosis of the diaphragm is firm and broad in humans and pigs, the phrenopericardial ligament is the only pericardial attachment in dogs, and the caudal portion of the pericardium is attached via the strong sternopericadial ligament in sheep *(6,7)*.

The pericardium consists of three layers: the serous visceral pericardium (epicardium), the serous parietal pericardium, and the fibrous pericardium. The serous parietal pericardium lines the inner surface of the fibrous pericardium, and the serous visceral pericardium lines the outer surface of the heart. The pericardial cavity is found between the outer two layers and contains the pericardial fluid.

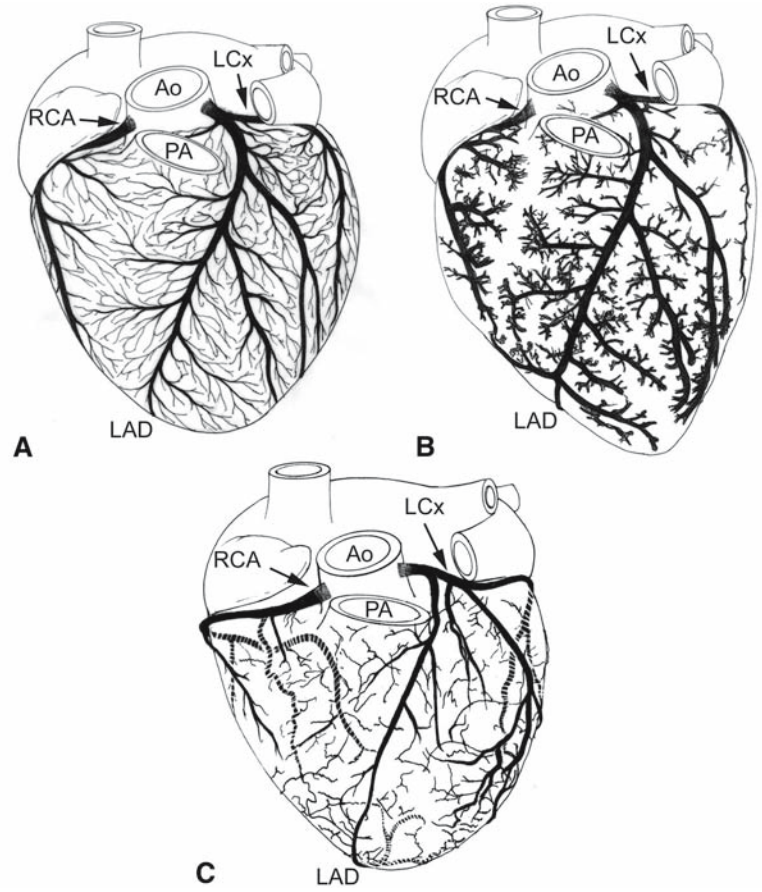

Fig. 1. The coronary arterial circulation in the dog **(A)**, pig **(B)**, and human **(C)**. Notice the extensive network of coronary collateralization in the dog heart, including many arterial anastomoses. The normal pig and human hearts have significantly less collateralization; each area of myocardium is usually supplied by a single coronary artery. Ao, aorta; LAD, left anterior descending artery; LCx, left circumflex artery; PA, pulmonary artery; RCA, right coronary artery.

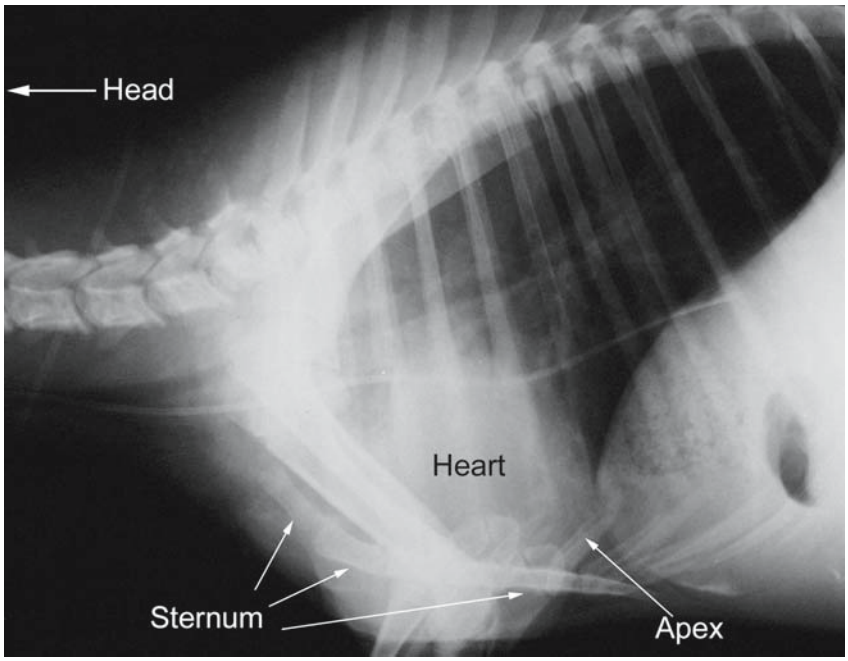

Fig. 2. Lateral radiograph of sheep thorax showing orientation of the heart while the animal is standing. The cranial direction is to the left and the ventral to the bottom. The apex of the heart is more ventrally tilted (down toward the sternum) than is seen in humans because of the posture of quadruped mammals. It should be noted, however, that this tilting is limited because of extensive attachments of the pericardium to the sternum and diaphragm.

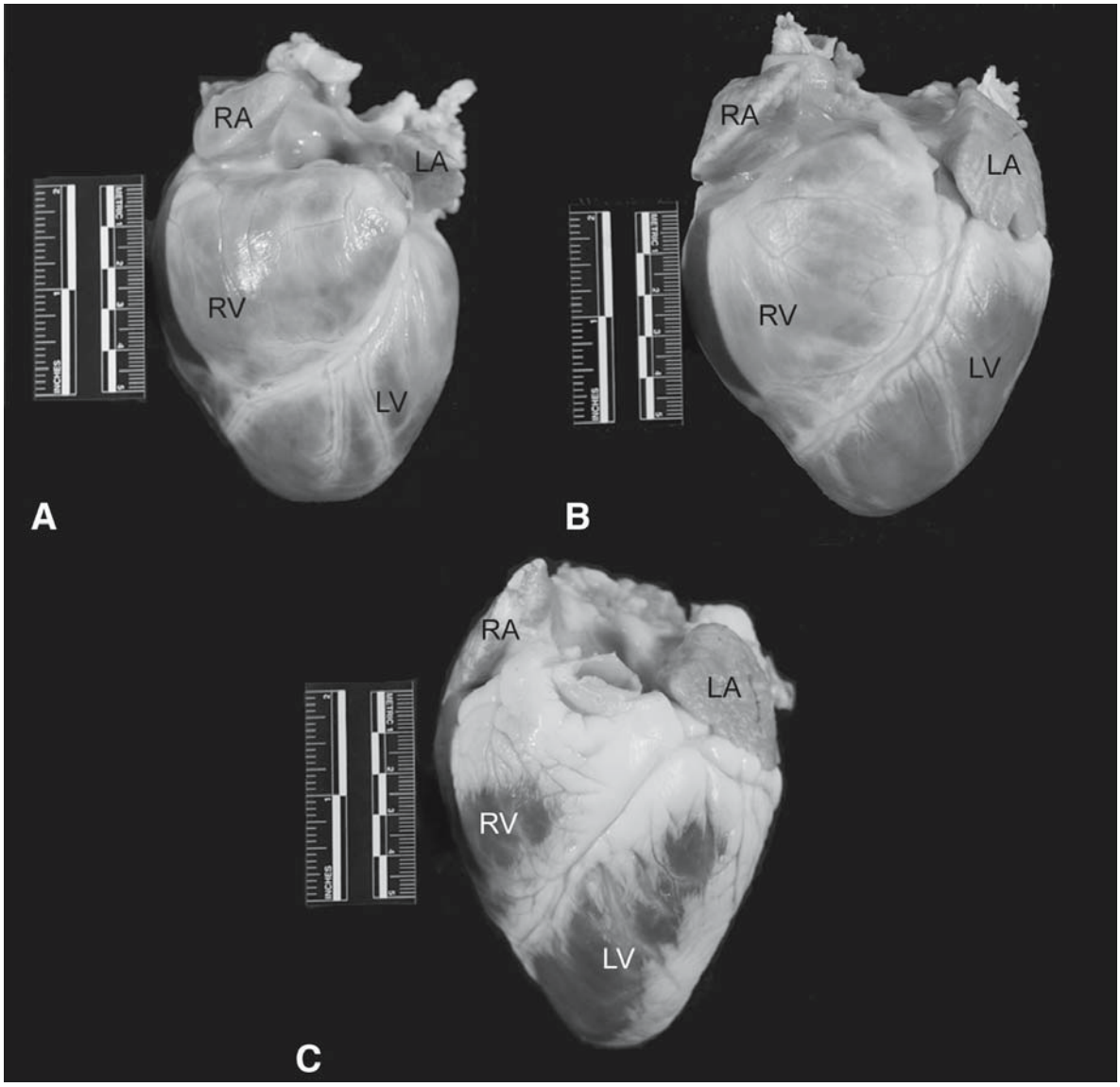

Fig. 3. The anterior aspect of the dog **(A),** pig **(B)**, and sheep **(C)** hearts. The apex is formed entirely by the left ventricle in these hearts. Also notice the differences in overall morphology of the hearts. The dog heart is much more round than the pig and sheep hearts and has a blunt apex. The pig heart has more of a "valentine" shape, with a somewhat blunt apex compared to the sheep heart. The sheep heart is much more conical and has a much more pronounced apex than dog or pig hearts. Also noteworthy is the presence of significant amounts of epicardial fat on the sheep heart compared with dog and pig hearts. LA, left atrium; LV, left ventricle; RA, right atrium; RV, right ventricle.

The pericardium is considered to serve many functions, including: (1) prevention of heart dilation; (2) protection of the heart from infection and adhesions to surrounding tissues; (3) maintenance of the heart in a fixed position in the thorax; and (4) regulation of the interrelations between the stroke volumes of the two ventricles *(15–17)*. However, it should be noted that the pericardium is not essential for survival because humans with congenital absence of the pericardium and pericardiectomized animals or humans can survive for many years *(15,18)*.

Although the basic structure of the pericardium is the same, there are important differences between species *(15,16,19)*. For instance, pericardial wall thickness increases with increasing heart size *(15)*. Nevertheless, humans are the notable exception to this rule, having a much thicker pericardium than animals with similar heart sizes *(15)*. Specifically, the pericardium of the human heart varies in thickness between 1 and 3.5 mm *(17)*; the average thicknesses of the pericardia of various animal species were found to be considerably thinner (sheep hearts 0.32 ± 0.01 mm; pig hearts 0.20 ± 0.01 mm; dog hearts 0.19 ± 0.01 mm) *(16)*. Differences in the amount of pericardial fluid are considered to exist as well. Holt reported that most dogs have 0.5–2.5 mL of pericardial fluid, with some dogs having up to 15 mL, compared to 20–60 mL in adult human cadaver hearts *(15)*.

Normal hearts of large mammals all consist of four chambers: two thin-walled atria and two ventricles with thicker walls. The heart is divided into separate right and left halves, with each half containing one atrium and one ventricle. In the fully devel-

oped heart with no associated pathologies, deoxygenated blood is contained in the right side of the heart and kept separate from oxygenated blood, which is on the left side of the heart.

The normal path of blood flow is similar among all large mammals. Specifically, systemic deoxygenated blood returns to the right atrium via the caudal (inferior in humans) vena cava and the cranial (superior in humans) vena cava. At the same time, oxygenated blood returns from the lungs via the pulmonary veins to the left atrium and fills the left ventricle. After atrial contraction forces the last of the blood into the ventricles, ventricular contraction ejects blood through the major arteries arising from each ventricle, specifically the pulmonary trunk from the right ventricle and the aorta from the left ventricle. Via the pulmonary arteries, blood travels to the lungs to be oxygenated, whereas aortic blood travels through both the coronary arterial system (to feed the heart) and the systemic circulation (to oxygenate bodily tissue).

3.1. The Atria

The right and left atria of adult mammalian hearts are separated by the interatrial septum. They are located at what is termed the *base* of the heart. The base receives all of the great vessels and is generally oriented superiorly, although there are reported differences in orientation among species; these differences are mostly dependent on the posture of the animal *(9,11,20)*. During development, blood is able to pass from the right to the left atrium, effectively bypassing the pulmonary circulation through a hole in the interatrial wall, termed the *foramen ovale*. The foramen ovale has a valvelike flap located on the left atrial side of the interatrial septum; this flap prevents backflow into the right atrium during left atrial contraction *(21)*. At the time of birth or soon thereafter, the foramen ovale closes and is marked in the adult heart by a slight depression on the right atrial side of the interatrial wall, termed the *fossa ovalis (11,21,22)*; it should be noted that it can remain patent in some individuals. Compared to humans, the fossa ovalis is more posteriorly (caudally) positioned in dogs and sheep *(7)*, but more deep set and superior in the pig heart *(9)*. The sinus venosus, a common separate structure in nonmammalian hearts, is incorporated into the right atrium and is marked by the sinoatrial node in large mammals *(21,22)*.

According to Michaëlsson and Ho (7), all the mammals studied (including dogs, pigs, and sheep) have principally the same atrial architecture, including the sinus venosus, crista terminalis, fossa ovalis, Eustachian valve (valve of the inferior vena cava), and Thebesian valve (valve of the coronary sinus). All large mammalian atria also have an earlike flap called the auricle or appendage *(9,11,22)*, although the size and shape of the auricle vary considerably between species *(7,9)*. In general, the junction between the right atrium and the right appendage is wide, whereas the junction on the left side is much more narrow *(7)*. Multiple pectinate muscles are found in both the right and left atrial appendages and on the lateral wall of the right atrium *(7,9,11)* (Fig. 4).

Commonly, there is one posterior (caudal or inferior) and one anterior (cranial or superior) vena cava, although in some mammals there are two anterior venae cavae *(21)*, and the location of the ostia of the venae cavae entering into the atrium varies *(7,9)*. Specifically, the ostia of the inferior and superior venae cavae enter at right, or nearly right, angles in the large mammalian animal models and enter the atrium nearly in line in humans *(9)*. Typically, the extent of the inferior vena cava between the heart and liver is long in domestic animals (>5 cm) and short in humans (1–3 cm) *(7)*.

The coronary sinus ostium is normally located in the posterior wall of the right atrium, but its location can differ slightly between species. Interestingly, the number of pulmonary veins entering the left atrium also varies considerably between species; human hearts typically have four *(9)* or occasionally five *(10)*, dog hearts have five or six *(11)*, and pig hearts have two primary pulmonary vein ostia within the left atrium *(9)*.

In all large mammalian hearts, the atria are separated from the ventricles by a layer of fibrous tissue called the *cardiac skeleton*, which serves as an important support for the valves and electrically isolates the atrial myocardium from the ventricular myocardium *(20)*.

3.2. The Ventricles

The left and right ventricles of the large mammals used for cardiovascular research contain essentially the same components that are structurally very similar to human hearts: an inlet region, an apical region, and an outlet region. The ventricles can be considered the major outflow pumping chambers of the heart, and as expected, their walls are significantly more muscular in nature than those of the atria. Importantly, the left ventricular walls are also notably more muscular than those of the right ventricle because the left ventricle must generate enough pressure to overcome the resistance of the systemic circulation, which is much greater than the resistance of the pulmonary circulation (normally more than four times greater). The walls of both ventricles near the apex have interanastomosing muscular ridges and columns termed the *trabeculae carneae* that serve to strengthen the walls and increase the force exerted during contraction *(7,11,21,22)*. However, large mammalian hearts reportedly do not have the same degree of trabeculations located in the ventricles compared to normal adult human hearts, and the trabeculations in animal hearts are commonly much coarser than those of human hearts *(7,9)* (Fig. 5).

Papillary muscles supporting the atrioventricular valves are found on the walls of the ventricles. Similar to human anatomy, in the majority of large mammalian animal hearts, the right ventricle has three papillary muscles, and the left ventricle has two, although interindividual and interspecies variations do occur *(7)*. Both ventricles typically have cross-chamber fibrous or muscular bands, which usually contain Purkinje fibers. Within the right ventricle of most dogs, pigs, and ruminants, a band termed the *moderator band* is typically present *(7)*. However, the origin and insertion of the band, as well as the composition of the band, differ notably between species. For example, in the pig heart, the band originates much higher on the septal wall compared to the structure in the human heart *(9)* (Figs. 5 and 6). In the dog heart, a branched or single muscular strand extends across the lumen from the septal wall near, or from the base of, the anterior papillary muscle *(11)* (Figs. 5 and 6).

However, Truex and Warshaw *(23)* did not find any moderator bands in the dog hearts (n = 12) they examined, but did

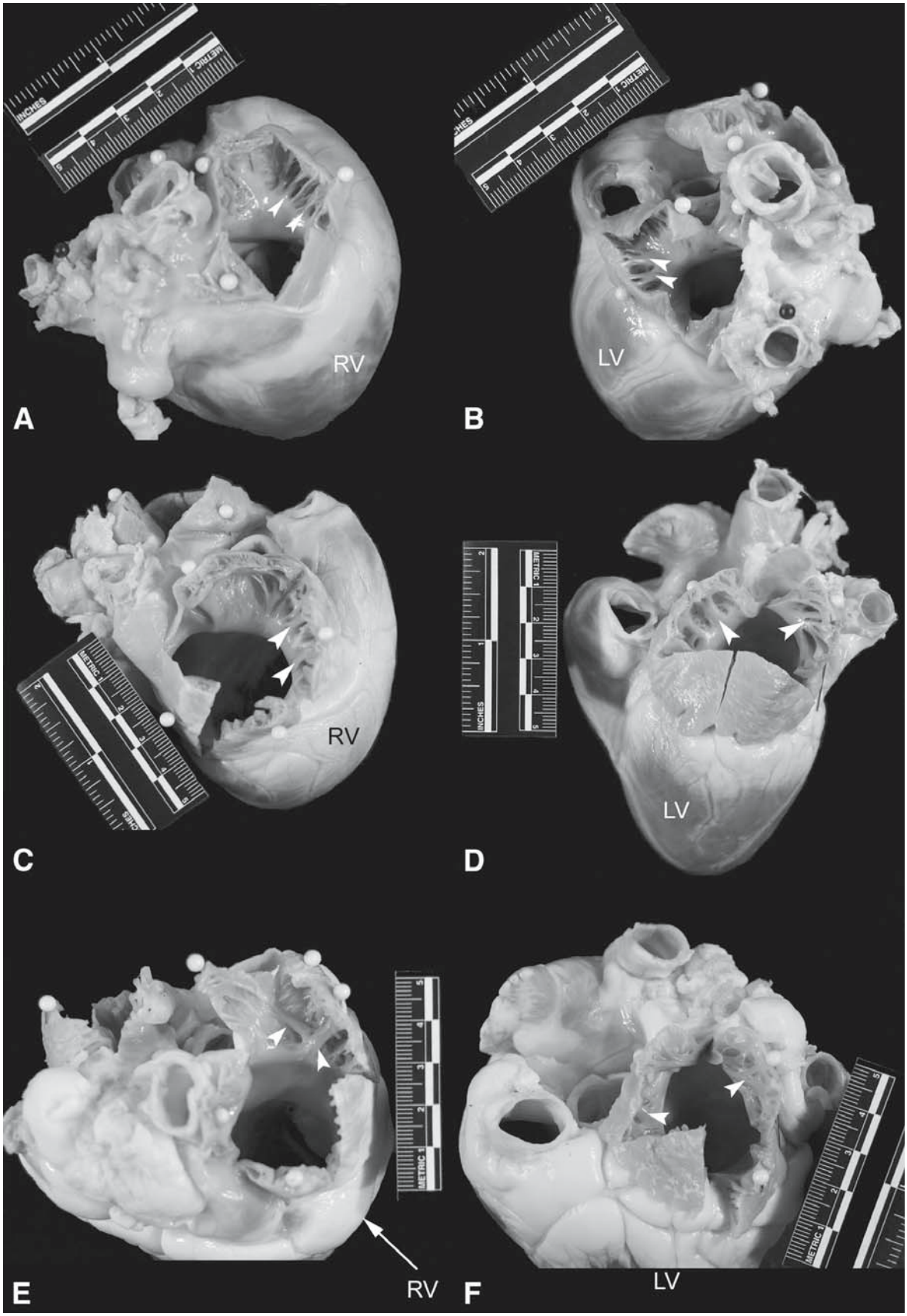

Fig. 4. The cranial (superior) aspect of dog **(A,B),** pig **(C,D)**, and sheep **(E,F)** hearts. Images on the left of the figure (A, C, and E) show opened right atrial appendages; images on the right (B, D, and F) show opened left atrial appendages. White arrows point to pectinate muscles that line the right and left atrial appendages. Notice that the right and left atrial appendages of the dog heart are tubular. In contrast, the right and left atrial appendages of the pig and sheep heart are more triangular in morphology. LV, left ventricle; RV, right ventricle.

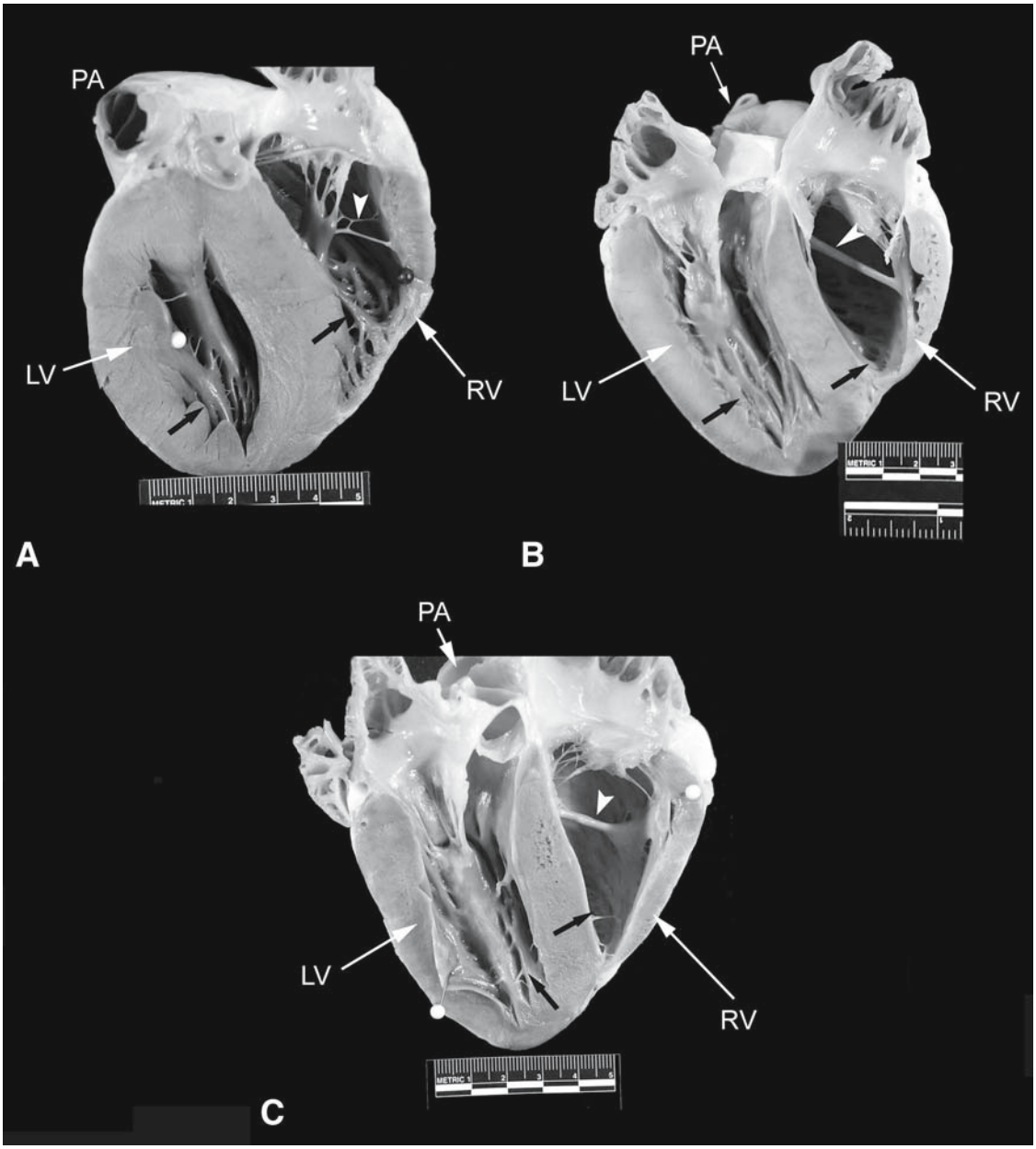

Fig. 5. Images showing dog **(A),** pig **(B),** and sheep **(C)** hearts that have been opened along the long axis to show both ventricular cavities. The anterior half of the heart is shown (left ventricle on the left and right ventricle on the right). Black arrows point to ventricular trabeculations, which are large and coarse. White arrows point to the moderator band. Notice that a fibrous, branched moderator band extends from the anterior papillary muscle to the free wall in the canine heart. In contrast, a muscular, nonbranched moderator band extends from the septal wall to the anterior papillary muscle in pig and sheep hearts. In addition, notice the presence of fibrous bands in the left ventricle. LV, left ventricle; PA, pulmonary artery; RV, right ventricle.

observe them in all sheep hearts ($n = 12$) and all pig hearts ($n = 12$), compared to 56.8% of the human hearts examined ($n = 500$). They described three types of moderator bands: a free arching band, a partially free arching band, and a completely adherent band. The potential for breed differences in animals and ethnic variability in humans must also be considered relative to variability.

It is interesting to note that, although general, anatomical textbooks state there is no specific structure named the moderator band in the left ventricle, left ventricular bands similar to the moderator band of the right ventricle have been described in the literature. For example, Gerlis et al. *(24)* found left ventricular bands in 48% of the hearts of children and in 52% of the adult human hearts studied. They also found that left ventricular bands were highly prevalent in sheep, dog, and pig hearts (Fig. 5).

3.3. The Valves

Large mammalian hearts have four valves with principally similar structures and locations. Two atrioventricular valves are located between each atrium and ventricle on both the right

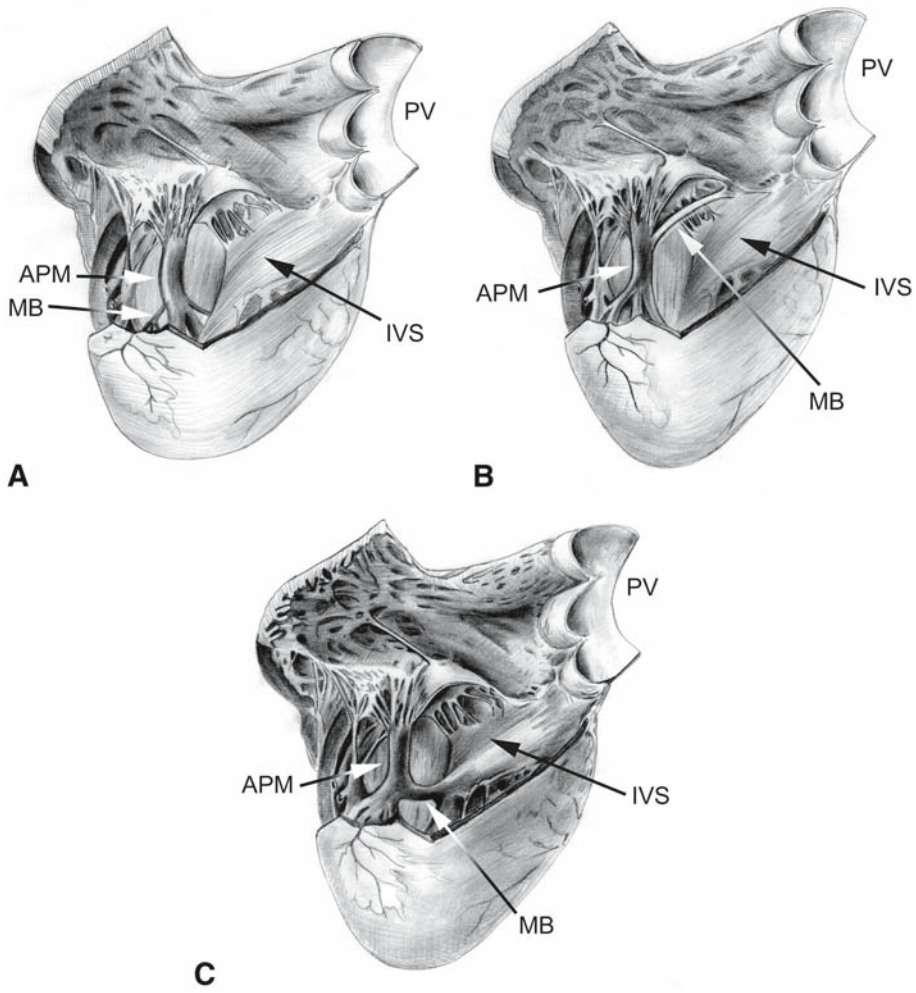

Fig. 6. An opened right ventricular cavity in dog **(A),** pig and sheep **(B),** and human **(C)** hearts. The structure of the moderator band differs greatly between these hearts. In the dog heart, there is a branching fibrous band that runs from the anterior papillary muscle to the free wall of the right ventricle. In the human heart, the moderator band is typically located near the apex and is thick and muscular. In the pig and sheep hearts, the moderator band originates much higher on the interventricular septum and travels to the anterior papillary muscle. It is not as thick as in the human heart, but is still muscular. Also, note that the anterior papillary muscle in the dog heart originates on the septal wall, as opposed to originating on the free wall of the human, pig, and sheep hearts. APM, anterior papillary muscle; IVS, interventricular septum; MB, moderator band; PV, pulmonary valve.

and left sides of the heart, and two semilunar valves lie between the ventricles and the major arteries arising from their outflow tracts. Chordae tendineae connect the fibrous leaflets of both atrioventricular valves to the papillary muscles in each ventricle and serve to keep the valves from prolapsing into the atria during ventricular contraction, thereby preventing backflow of blood into the atria. The semilunar valves, the aortic and pulmonic, do not have attached chordae tendineae and close because of pressure gradients developed across them.

The valve separating the right atrium and the right ventricle is termed the *tricuspid valve* because it has three major cusps: the anterosuperior, inferior, and septal. Typically, there are also three associated papillary muscles in the right ventricle. Interestingly, the commissures between the anterosuperior leaflet and the inferior leaflets are usually fused in dog hearts *(11)*, giving the appearance of only two leaflets. Interindividual and interspecies variations in the number of papillary muscles have also been reported *(7)*.

The valve separating the left atrium and the left ventricle is termed the *mitral* or *bicuspid valve* because it typically has two cusps, the anterior (aortic) and the posterior (mural). However, according to Netter *(10)*, the human mitral valve actually can be considered to have four cusps, including the two major cusps listed above and two small commissural cusps or scallops. In large mammalian hearts, two primary leaflets of the mitral valve are always present, but variations in the number of scallops exist and can be quite marked, giving the impression of extra leaflets *(7)*.

A fibrous continuity between the mitral valve and the aortic valve is present in humans and mammals, extending from the central fibrous body to the left fibrous trigone *(7)*. The length of this fibrous continuity, termed the *intervalvar septum* or

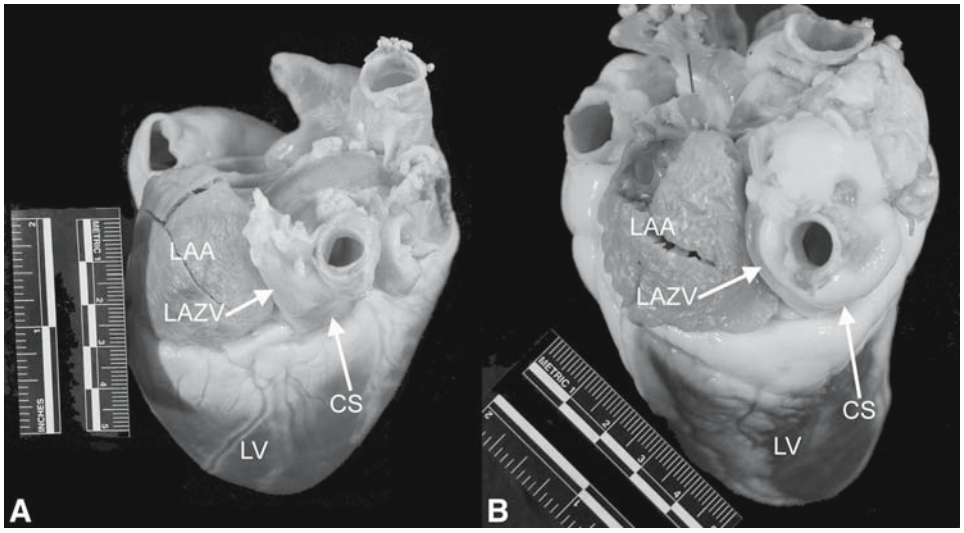

Fig. 7. Images showing the left azygous (hemiazygous) vein entering the coronary sinus in the pig **(A)** and sheep **(B)** hearts. The left azygous vein drains the thoracic cavity directly into the coronary sinus in these animals rather than emptying into the superior vena cava via the azygous as seen in dog and human hearts. Notice that it travels between the left atrial appendage and the pulmonary veins; the oblique vein of Marshall (oblique vein of the left atrium) travels this path in human and dog hearts. CS, coronary sinus; LAA, left atrial appendage; LAZV, left azygous vein; LV, left ventricle.

membranous septum, varies considerably in length in different animals, but notably is completely absent in sheep *(25)*. There are also differences in the fibrous ring supporting the mitral valve and in the composition of the leaflets of the mitral valve between species. For instance, according to Walmsley *(25)*, a segment of the ring at the base of the mural cusp is always present in the human heart, but is difficult to distinguish in certain breeds of dogs and inconspicuous in the sheep heart.

Differences in aortic valve anatomy have also been reported in the literature. Sands et al. *(26)* compared aortic valves of human, pig, calf, and sheep hearts. They found that interspecies differences in leaflet shape exist, but that all species examined had fairly evenly spaced commissures. In addition, they found that variations in leaflet thickness existed, particularly with sheep aortic valves, which were especially thin and fragile. They also found that there was a substantially greater amount of myocardial tissue supporting the right and left coronary leaflet bases in the animal hearts relative to humans.

3.4. The Coronary System

Mammalian hearts have an intrinsic circulatory system that originates with two main coronary arteries *(7)* with ostia that are located directly behind the aortic valve cusps. Coronary blood flow returns to the chambers of the heart at the coronary sinus via small coronary veins and by Thebesian veins, which drain deoxygenated cardiac blood into the right atrium, although these may enter into the right and left ventricles *(21,27)* and the left atrium *(28,29)*.

According to Michaëlsson and Ho (7), differences in perfusion areas exist between large mammalian species as well as within species; these differences have also been described in humans. Dogs and sheep typically have a left coronary type of supply, such that the majority of the myocardium is supplied via branches arising from the left coronary artery. In contrast, pigs typically have a balanced supply by which the myocardium is supplied equally from both right and left coronary arteries *(7)*. Yet, Crick et al. *(9)* found that most of the pig hearts they examined (80%) had right coronary dominance. Weaver et al. *(30)* found that the right coronary artery was dominant in 78% of the pigs they studied. Most human hearts (approx 90%) also display right coronary arterial dominance *(31)*.

Another important aspect of the coronary arterial circulation, one that is currently of great importance in myocardial ischemia research, is the presence or absence of significant coronary collateral circulation. Normal human hearts tend to have sparse coronary collateral development, which is very similar to that seen in pig hearts *(30)*. In contrast, it is now widely known that extensive coronary collateral networks can be seen in dog hearts *(5,32–35)*. Furthermore, Schaper et al. *(36)* found that the coronary collateral network of dogs was almost exclusively located at the epicardial surface; that of pig hearts, when present, was located subendocardially. They were unable to detect a significant collateral network in the hearts of sheep (Fig. 1).

There are three major venous pathways that drain the heart: the coronary sinus, anterior cardiac veins, and Thebesian veins *(29,37)*. Drainage from each of these venous systems is present in human hearts as well as in dog, pig, and sheep hearts *(9,11,21,29)*. Although the overall structure of the coronary venous system is similar across species, interindividual variations are common. Nevertheless, there is one notable difference in the coronary venous system between species that warrants mention: the presence of the left azygous vein draining the left thoracic cavity directly into the coronary sinus. Such a left azygous vein is typically present in both pig *(9)* and sheep hearts *(7)* (Fig. 7).

Table 1
Similarities and Differences in the Atrioventricular (AV) Conduction System of Dog, Pig, Sheep, and Human Hearts

	Location of the AV node	*AV node and His bundle junction*	*Length of the His bundle*	*Route of the His bundle*
Human	Located at the base of the atrial septum, anterior to the coronary sinus, and just above the tricuspid tricuspid valve.	End of the AV node and the beginning of the His bundle are nearly impossible to distinguish.	Total length of the unbranched portion is 2–3 mm. Penetrating bundle is 0.25–0.75 mm long. Bundle bifurcates just after emerging from the central fibrous body.	Bundle lies just beneath the membranous septum at the crest of the interventricular septum.
Pig	Lies on the right side of the crest of the ventricular septum and is lower on the septum than in humans.	No explicit information found.	Penetrating bundle is very short in comparison to humans.	Climbs to the right side of the summit of the ventricular septum, where it enters the central fibrous body. The bifurcation occurs more proximally than in humans.
Dog	Same as in humans.	Consists of internodal tracts of myocardial fibers.	Penetrating bundle is 1–1.5 mm long, significantly longer than the human penetrating bundle.	His bundle runs forward and downward through the fibrous base of the heart, just beneath the endocardium. There are at least three discrete His bundle branches of myocardium that join the atrial end of the AV node via a proximal His bundle branch.
Sheep	Located at the base of the atrial septum, anterior to the coronary sinus, just above the tricuspid valve, and at the junction of the middle and posterior one-third of the os cordis.	Junction is characterized by fingerlike projections, where the two types of tissue overlap; size and staining qualities of the initial Purkinje cells of the His bundle make it easy to distinguish between the end of the AV node and the beginning of the His bundle.	Portion of the bundle passing through the central fibrous body is ~1 mm. Bundle extends 4–6 mm beyond the central fibrous body before it bifurcates.	Unbranched bundle must pass beneath the os cordis to reach the right side of the ventricular septum. His bundle then remains relatively deep within the confines of the ventricular myocardium. Branching occurs more anteriorly in sheep than in humans.

Source: From refs. *41–44*.

3.5. The Lymphatic System

In addition to an intrinsic circulatory system, large mammalian hearts have an inherent and substantial lymphatic system that serves the same general function of the lymphatic system in the rest of the body. Patek *(38)* described the mammalian lymphatic system as follows: Hearts have subepicardial lymphatic capillaries that form continuous plexuses covering the whole of each ventricle. The lymphatic channels are divided into five orders, with the first order draining the capillaries and joining to become the second order and so on, until the lymph is drained from the heart via one large collecting duct of the fifth order. Johnson and Blake *(39)* reported that, in general, dogs, pigs, and humans have extensive subepicardial and subendocardial networks with collecting channels directed toward large ducts in the atrioventricular sulcus that are continuous with the main cardiac lymph duct. Furthermore, it was found that the lymphatic vessels of the normal heart are distributed in the same manner as the coronary arteries and follow them as two main trunks to the base of the heart *(40)*.

3.6. The Conduction System

All large mammalian hearts have a very similar conduction system with the following main components: sinoatrial node, atrioventricular node, bundle of His, right and left main bundle branches, and Purkinje fibers. Interspecies variations are well recognized, especially regarding the finer details of the arrangement of the transitional and compact components of the atrioventricular node *(7)*. In the mammalian heart, the sinoatrial node is the normal pacemaker *(7,21,22)* and is situated in roughly the same location—high on the right atrial wall near the junction of the superior vena cava and the right atrium.

Conduction spreads through the atria to the atrioventricular node (which is unique to both birds and mammals) *(22)* and then to the bundle of His, which is the normal conducting pathway from the atria to the ventricles, penetrating through the central fibrous body. Right and left main bundle branches emanate from the bundle of His and branch further to the Purkinje fibers, which spread conduction to the ventricles *(7)*. The atrioventricular node and bundle of His are located subendocardially in the right atrium within a region known as the *triangle of Koch*, which is delineated by the coronary sinus ostium, the membranous septum, and the septal/posterior commissure of the tricuspid valve. The presence of the os cordis is noted in sheep hearts, but not in dog, pig, or human hearts. It is a small, fully formed bone, lying deep in the atrial septum, that influences the location and course of the bundle of His in sheep hearts. Other known differences in the atrioventricular conduction system between human, pig, dog, and sheep hearts are documented in Table 1.

REFERENCES

1. Paul, E.F. and Paul, J. (eds.) (2001) *Why Animal Experimentation Matters: The Use of Animals in Medical Research*. Social Philosophy and Policy Foundation: Transaction, New Brunswick, NJ.
2. Monamy, V. (ed.) (2000) *Animal Experimentation: A Guide to the Issues*. Cambridge University Press, Cambridge, UK.
3. Nutton, V. (2002) Portraits of science. Logic, learning, and experimental medicine. *Science*. 295, 800–801.
4. Persaud, T.V.N. (ed.) (1997) *A History of Anatomy: The Post-Vesalian Era*. Charles C Thomas, Springfield, IL.
5. Hearse, D.J. (2000) Species variation in the coronary collateral circulating during regional myocardial ischaemia: a critical determinant of the rate of evolution and extent of myocardial infarction. *Cardiovasc Res*. 45, 215–219.
6. Getty, R. (1975) General heart and blood vessels, in *Sisson and Grossman's The Anatomy of the Domestic Animals,* 5th Ed. (Getty, R., ed.), Saunders, Philadelphia, pp. 164–175.
7. Michaëlsson, M. and Ho, S.Y. (eds.). (2000) *Congenital Heart Malformations in Mammals: An Illustrated Text*. Imperial College Press, London.
8. Ghoshal, N.G. (1975) Ruminant, porcine, carnivore: heart and arteries, in *Sisson and Grossman's The Anatomy of the Domestic Animals,* 5th Ed. (Getty, R., ed.), Saunders, Philadelphia, PA, pp. 960–1023, 1306–1342, 1594–1651.
9. Crick, S.J., Sheppard, M.N., Ho, S.Y., Gebstein, L., and Anderson, R.H. (1998) Anatomy of the pig heart: comparisons with normal human cardiac structure. *J Anat*. 193, 105–119.
10. Netter, F.H. (ed.) (1979), *Heart*. Ciba Pharmaceutical, Medical Education Division, West Caldwell, NJ.
11. Evans, H.E. (1993) The heart and arteries, in *Miller's Anatomy of the Dog,* 3rd Ed. (Miller, M.E. and Evans, H.E., eds.), Saunders, Philadelphia, PA, pp. 586–602.
12. Lee, J.C., Taylor, F.N., and Downing, S.E. (1975) A comparison of ventricular weights and geometry in newborn, young, and adult mammals. *J Appl Physiol*. 38, 147–150.
13. Holt, J.P., Rhode, E.A., and Kines, H. (1968) Ventricular volumes and body weight in mammals. *Am J Physiol*. 215, 704–715.
14. Hughes, H.C. (1986) Swine in cardiovascular research. *Lab Anim Sci*. 36, 348–350.
15. Holt, J.P. (1970) The normal pericardium. *Am J Cardiol*. 26, 455–465.
16. Naimark, W.A., Lee, J.M., Limeback, H., and Cheung, D.T. (1992) Correlation of structure and viscoelastic properties in the pericardia of four mammalian species. *Am J Physiol*. 263, H1095–H1106.
17. Spodick, D.H. (ed.) (1997) *The Pericardium: A Comprehensive Textbook*. Dekker, New York, NY.
18. Moore, T. and Shumacker, H.J. (1953) Congenital and experimentally produced pericardial defects. *Angiology*. 4, 1–11.
19. Elias, H. and Boyd, L. (1960) Notes on the anatomy, embryology and histology of the pericardium. *J New York Med Coll*. 2, 50–75.
20. Hurst, J.W., Anderson, R.H., Becker, A.E., and Wilcox, B.R. (eds.) (1988) *Atlas of the Heart*. McGraw-Hill, Gower Medical, New York, NY.
21. Montagna, W. (ed.) (1959) *Comparative Anatomy*. Wiley, New York, NY.
22. Kent, G.C. and Carr, R.K. (eds.) (2001) *Comparative Anatomy of the Vertebrates,* 9th Ed. McGraw Hill, Boston, MA.
23. Truex, R.C. and Warshaw, L.J. (1942) The incidence and size of the moderator band in man and mammals. *Anat Rec*. 82, 361–372.
24. Gerlis, L.M., Wright, H.M., Wilson, N., Erzengin, F., and Dickinson, D.F. (1984) Left ventricular bands. A normal anatomical feature. *Br Heart J*. 52, 641–647.
25. Walmsley, R. (1978) Anatomy of human mitral valve in adult cadaver and comparative anatomy of the valve. *Br Heart J*. 40, 351–366.
26. Sands, M.P., Rittenhouse, E.A., Mohri, H., and Merendino, K.A. (1969) An anatomical comparison of human pig, calf, and sheep aortic valves. *Ann Thorac Surg*. 8, 407–414.
27. Ansari A. (2001) Anatomy and clinical significance of ventricular Thebesian veins. *Clin Anat*. 14, 102–110.
28. Esperanca Pina, J.A., Correia, M., and O'Neill, J.G. (1975) Morphological study on the Thebesian veins of the right cavities of the heart in the dog. *Acta Anat*. 92, 310–320.
29. Ruengsakulrach, P. and Buxton, B.F. (2001) Anatomic and hemodynamic considerations influencing the efficiency of retrograde cardioplegia. *Ann Thorac Surg*. 71, 1389–1395.
30. Weaver, M.E., Pantely, G.A., Bristow, J.D., and Ladley, H.D. (1986) A quantitative study of the anatomy and distribution of coronary arteries in swine in comparison with other animals and man. *Cardiovasc Res*. 20, 907–917.
31. Anderson, R.H. and Becker, A.E. (eds.). (1992) *The Heart: Structure in Health and Disease*. Gower Medical, London, UK.
32. Weisse, A.B., Kearney, K., Narang, R.M., and Regan, T.J. (1976) Comparison of the coronary collateral circulation in dogs and baboons after coronary occlusion. *Am Heart J*. 92, 193–200.
33. Koke, J.R. and Bittar, N. (1978) Functional role of collateral flow in the ischaemic dog heart. *Cardiovasc Res*. 12, 309–315.
34. Redding, V.J. and Rees, J.R. (1968) Early changes in collateral flow following coronary artery ligation: the role of the sympathetic nervous system. *Cardiovasc Res*. 2, 219–225.
35. Kloner, R.A., Ganote, C.E., Reimer, K.A., and Jennings, R.B. (1975) Distribution of coronary arterial flow in acute myocardial ischemia. *Arch Pathol*. 99, 86–94.
36. Schaper, W., Flameng, W., and De Brabander, M. (1972) Comparative aspects of coronary collateral circulation. *Adv Exp Med Biol*. 22, 267–276.
37. Gregg, D. and Shipley, R. (1947) Studies of the venous drainage of the heart. *Am J Physiol*. 151, 13–25.
38. Patek, P.P. (1939) The morphology of the lymphatics of the mammalian heart. *Am J Anat*. 64, 203–249.
39. Johnson, R.A. and Blake, T.M. (1966) Lymphatics of the heart. *Circulation*. 33, 137–142.
40. Symbas, P.N., Cooper, T., Gantner, G.E.J., and Willman, V.L. (1963) Lymphatic drainage of the heart: effect of experimental interruption of lymphatics. *Surg Forum*. 14, 254–256.
41. Ho, S.Y., Kilpatrick, L., Kanai, T., Germroth, P.G., Thompson, R.P., and Anderson, R.H. (1995) The architecture of the atrioventricular conduction axis in dog compared to man: its significance to ablation of the atrioventricular nodal approaches. *J Cardiovasc Electrophysiol*. 6, 26–39.
42. Bharati, S., Levine, M., Huang, S.K., et al. (1991) The conduction system of the swine heart. *Chest*. 100, 207–212.
43. Anderson, R.H., Becker, A.E., Brechenmacher, C., Davies, M.J., and Rossi, L. (1975) The human atrioventricular junctional area. A morphological study of the A-V node and bundle. *Eur J Cardiol*. 3, 11–25.
44. Frink, R.J. and Merrick, B. (1974) The sheep heart: coronary and conduction system anatomy with special reference to the presence of an os cordis. *Anat Rec*. 179, 189–200.

6 The Coronary System and Associated Medical Devices

RYAN LAHM, MS AND PAUL A. IAIZZO, PhD

CONTENTS

1. INTRODUCTION

In general, there are three primary components of the coronary system. The first is the coronary arteries; this important group of vessels originates with the right and left main coronary arteries, which exit the ascending aorta just above the aortic valve. The smallest of the arteries eventually branch into arterioles. In turn, the arterioles branch into an extremely large number of capillaries, the smallest diameter vessels, which make up the second vessel system. Next, blood exits the capillaries and begins its return to the heart via the venules through the third component system of vessels, the venous drainage of the heart. Thus, the coronary veins drain the deoxygenated blood from the myocardium back to the right atrium, in which it joins with the systemic deoxygenated blood entering from the superior and inferior venae cavae.

Because coronary blood flow is so vital to the function of the heart, whenever disease states are present or an acute event occurs that obstructs this flow, consequences are commonly quite detrimental and/or often deadly. For example, changes in electrocardiograms can be recorded within beats when there is inadequate blood flow delivered to a region of the heart. More specifically, whenever coronary blood flow falls below that required to meet metabolic needs, the myocardium is considered ischemic; the pumping capability of the heart is impaired. and there are associated changes in electrical activity (e.g., increased risk of fibrillation). Prolonged ischemia can lead to myocardial infarction, commonly called a heart attack. This can cause permanent, irreversible myocardial cell death. Coronary artery disease remains the most common and lethal cardiovascular disease in the US population affecting both males and females *(1)*.

2. CORONARY ARTERIES

Oxygenated blood is pumped into the aorta from the left ventricle. This is where it enters the right and left main coronary arteries, and subsequent branching feeds the myocardial tissue of all four chambers of the heart. The ascending portion of the aorta is where the origins (ostia) of the right and left coronaries

From: *Handbook of Cardiac Anatomy, Physiology, and Devices*
Edited by: P. A. Iaizzo © Humana Press Inc., Totowa, NJ

reside; specifically, they exit the ascending aorta immediately superior to the aortic valve at the sinus of Valsalva. Blood flow into the coronary arteries is greatest during ventricular diastole *(2,3)*.

The right coronary artery courses along the right anterior atrioventricular groove just below the right atrial appendage and along the epicardial surface adjacent to the tricuspid valve annulus. It traverses along the tricuspid annulus until it reaches the posterior surface of the heart, where it then becomes the posterior descending artery and runs toward the apex of the left ventricle. Along its course, a number of branches emerge, most notably those that supply the sinus node and the atrioventricular node; hence, blockage of such vessels can lead to conduction abnormalities.

In addition, several marginal branches run to the right ventricular and right atrial epicardial surfaces. On exiting the ascending aorta, the left main coronary artery typically bifurcates quickly into the left circumflex and left anterior descending arteries. The left circumflex artery runs under the left atrial appendage on its way to the lateral wall of the left ventricle. Along the way, it spawns a number of branches that supply the left atrial and left ventricular walls. In some cases, a branch will course behind the aorta to the superior vena cava such that it can supply the sinus node. The left anterior descending artery supplies a major portion of the ventricular septum, including the right and left bundle branches of the myocardial conduction system and the anterior and apical portions of the left ventricle.

Coronary arteries are so vital to the function of the heart that whenever disease states are associated with flow restriction through the coronary arteries, and subsequently the remainder of the coronary circulation (capillaries and veins), the effects on cardiac performance are quite dramatic and often fatal. Coronary artery disease is generally defined as the gradual narrowing of the lumen of the coronary arteries because of coronary atherosclerosis. Atherosclerosis is a condition that involves thickening of the arterial walls from cholesterol and fat deposits that build up along the endoluminal surface of the arteries. With severe disease, these plaques may become calcified and so large that they produce stenoses within the vessels, thus permanently increasing the vascular resistance, which is normally low. When the walls of the coronary arteries thicken, the cross-sectional area of the arterial lumen decreases, resulting in higher resistance to blood flow through the coronary arteries (*see* Chapter 1 regarding the inverse fourth power relationship). This steady decrease in cross-sectional area can eventually lead to complete blockage of the artery. As a result, oxygen and nutrient supply to the myocardium drops below its demand. As the disease progresses, the myocardium downstream from the occluded artery becomes ischemic. Eventually, myocardial infarction may occur if the coronary artery disease is not detected and treated in a timely manner.

Myocardial ischemia not only impairs the electrical and mechanical function of the heart, but also will commonly result in intense, debilitating chest pain known as angina pectoris. However, anginal pain can often be absent in individuals with coronary artery disease when they are resting (or in individuals with early disease stages), but induced during physical exertion or with emotional excitement. Such situations are associated with an increase in sympathetic tone that increases myocardial oxygen consumption and subsequently ischemia when blood flow cannot keep up with myocardial metabolic needs. To date, typical treatment for angina resulting from coronary artery disease includes various pharmacological approaches, such as coronary vasodilator drugs (e.g., nitroglycerin); nitrates to reduce myocardial demand by dilating systemic veins and thus reducing preloads; or β-blockers (e.g., propranolol). However, in cases of intractable angina, the use of implantable spinal stimulators for pain management has been suggested.

3. CARDIAC CAPILLARIES

Capillaries represent an extraordinary degree of branching of very thin vessels, which ensures that nearly every myocyte lies within a short distance of at least one of these branches. Via diffusion, nutrients and metabolic end products move between the capillary vessels and the surroundings of the myocytes through the interstitial fluid. Subsequent movement of these molecules into a cell is accomplished by both diffusion and mediated transport. Nevertheless, as with all organs, blood flow through the capillaries within the heart can be considered passive and occurs only because coronary arterial pressure is kept higher than venous pressure, which is the case during diastole. Although capillaries are a very important part of the coronary system, the use of devices within them is relatively nonexistent because they are so small.

4. CORONARY VEINS

Conversely, in relation to the coronary arteries, the coronary veins make up a fine network of vessels beginning at the end of each capillary bed in the myocardium and ending at the right atrium. Usually, if a coronary artery is anatomically localized, a coronary vein will be close by because the coronary veins run alongside neighboring branches of coronary arteries.

The largest and most prominent vessel in the coronary venous system is the coronary sinus, which is located on the posterior surface of the heart just below the left atrium in the left atrioventricular groove. Fig. 1 (*see CoronaryVeins.mpg* on the Companion CD) illustrates the path location of the coronary sinus in an idealized heart model. It is typically found to run along the epicardial surface of the heart as it carries deoxygenated blood into the right atrium from the coronary venous network of primarily the left ventricle. It serves the same purpose as a conduit for the return of deoxygenated blood to the right atrium from the coronary circulation of the left ventricle as the venae cavae do for the systemic circulation. The coronary sinus ostium enters the right atrium between the inferior vena cava and the septal tricuspid valve leaflet. Often, a rudimentary flap of tissue called the Thebesian valve covers the ostium to varying degrees *(4–7)*. Figure 2 shows several examples of human coronary sinus ostia as viewed from the right atrium *(8)*.

The coronary sinus also has a number of veins flowing into it. These branches typically include: (1) the great cardiac vein; (2) the oblique vein of Marshall; (3) the lateral and posterior veins of the left ventricle; (4) the middle cardiac vein; and (5) the small cardiac vein *(9)*.

More specifically, the vein that drains the circulation of the ventricular septum and anterior ventricular walls is the anterior interventricular vein. This vein runs toward the basal surface of the heart and is more commonly referred to as the *great cardiac vein*. It empties into the coronary sinus near the lateral aspect of the left atrium at its intersection with the atrioventricular groove.

The point at which the great cardiac vein becomes the coronary sinus is also the location where the oblique vein of Marshall enters the coronary sinus after traveling along the posterior surface of the left atrium. The coronary sinus also accepts blood flow from the lateral and posterior veins of the left ventricle. These veins typically enter the coronary sinus on the lateral and posterior surface of the left ventricle, as their names would imply. The middle cardiac vein runs along the posterior surface of the left ventricle alongside the posterior descending artery. It then either spills its contents directly into the right atrium or will first enter the coronary sinus immediately before it enters the right atrium. The small cardiac vein drains the right ventricular and right atrial circulation before draining directly into the right atrium or into the coronary sinus near its ostium.

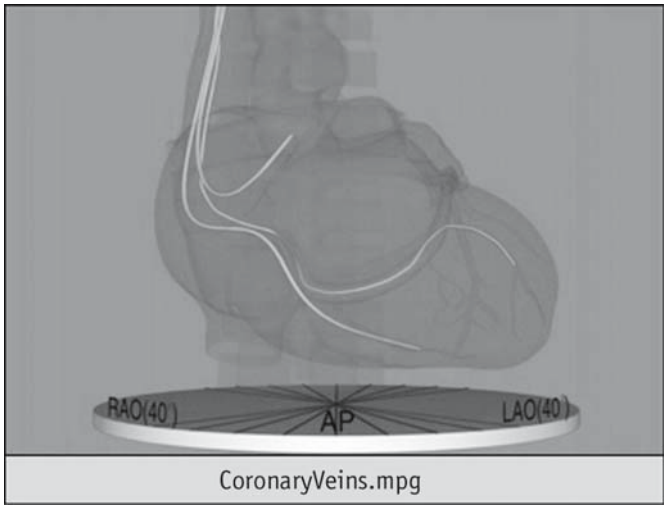

Fig. 1. Movie illustrating a semitransparent heart as it rotates about its vertical axis. The path of the coronary sinus is highlighted during the first portion of the movie. The three leads implanted during a biventricular implant procedure are shown and labeled. *See CoronaryVeins.mpg* on the Companion CD.

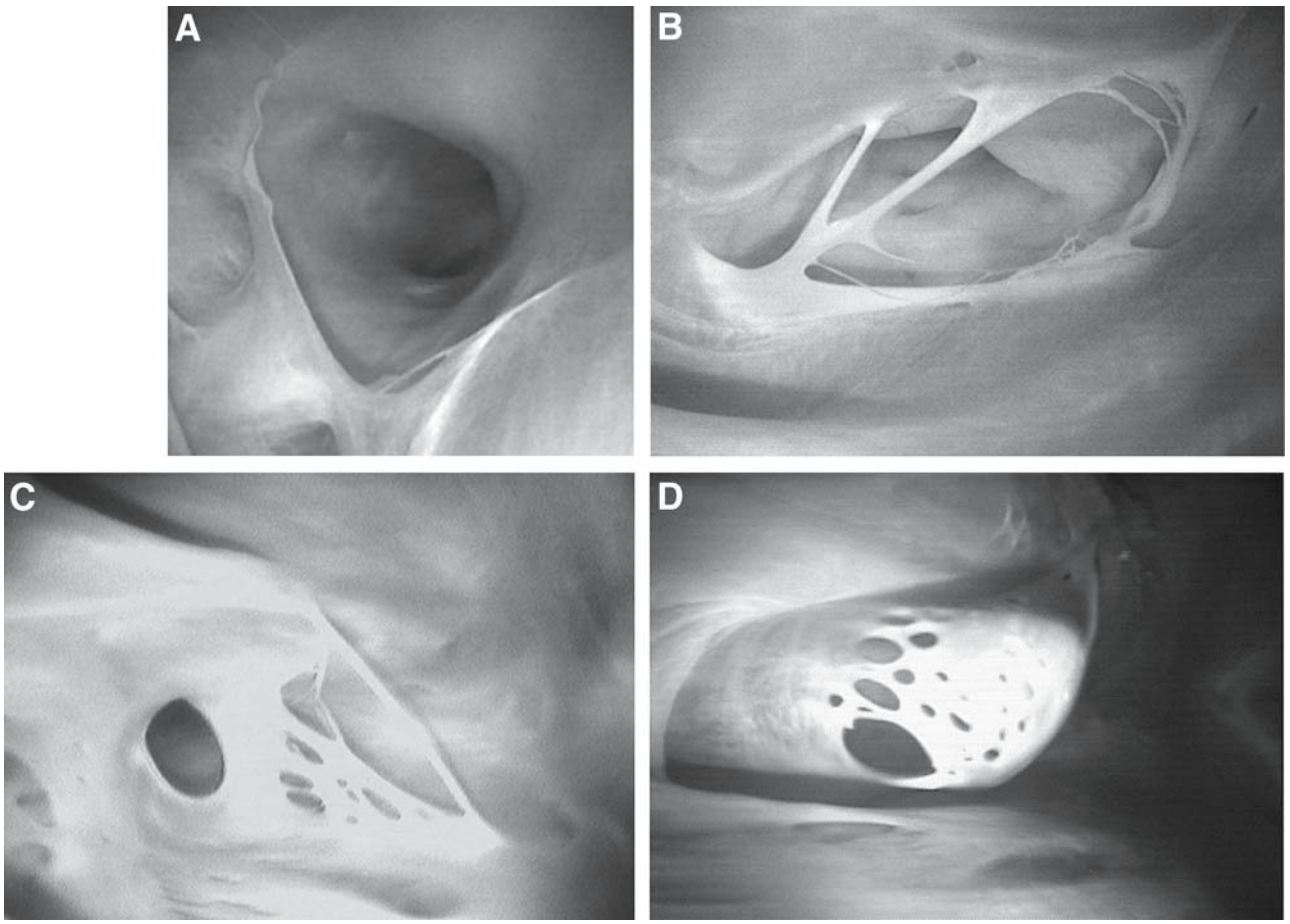

Fig. 2. Images of the coronary sinus ostium of four human hearts. Each image represents a single frame captured from images obtained from these isolated functioning human hearts *(8)*. In the human, portions of the coronary sinus ostium can be covered by the Thebesian valves, hence making access more difficult *(9)*. Reproduced with permission from ref. *8*. © 2003 Society of Thoracic Surgeons.

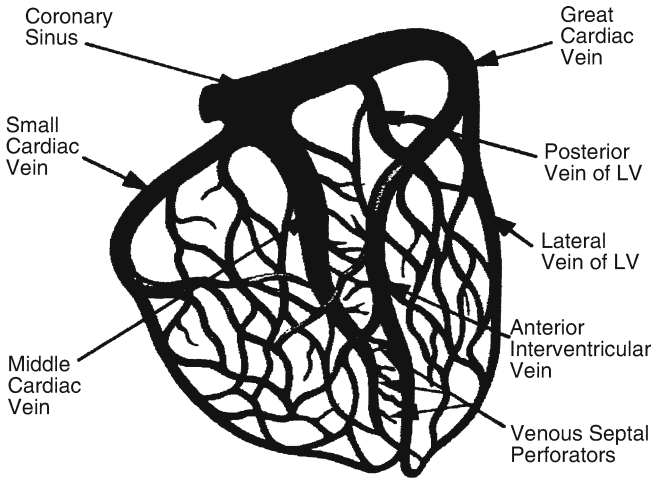

Fig. 3. Diagram of the cardiac venous tree. This image represents the structure expected in a normal human heart. This is a 2D projection representation of the 3D nature of the coronary venous anatomy. LV, left ventricle.

There are also a number of tiny veins called Thebesian veins that primarily drain the right atrial and right ventricular myocardium directly into these chambers without joining one of the principal coronary veins. Figure 3 illustrates a hypothetical coronary venous tree.

In certain types of disease states such as heart failure, the shape and orientation of this vascular tree may change because of remodeling of the myocardium, for instance, to compensate for decreased contractile function of portions of the ventricular myocardium.

5. ANASTOMOSES

Many tissues within the human body receive blood from branches of more than one artery, and if two or more arteries supply the same region, they are commonly connected. These connections, called *anastomoses*, provide alternate routes for blood to reach—particular group of cells. The myocardium may contain anastomoses that connect branches of a given coronary artery or extend between branches of different coronary arteries. They provide accessory pathways for arterial blood to reach a region of the myocardium if a main route becomes obstructed. It is then possible for the heart to receive sufficient oxygen even if one of its coronary arteries is partially blocked.

It should be noted that, in certain disease states, the degree of anatomoses increases. Nevertheless, in severe stages of coronary artery disease, even extensive anastomoses will not allow certain regions of the myocardium to be adequately perfused; complete obstruction of blood flow results in a myocardial infarction. To treat such a patient, either the vessel needs to be reopened by coronary angioplasty and stenting or a new pathway should be created via coronary artery bypass grafting.

6. ASSESSMENT AND VISUALIZATION OF THE CORONARY SYSTEM

Catheterization of the heart is an invasive procedure commonly employed for the subsequent visualization of the heart's coronary arteries, chambers, valves, and great vessels. It can also be used to: (1) measure pressures in the heart and blood vessels; (2) assess function, cardiac output, and diastolic properties of the left ventricle; (3) measure the flow of blood through the heart and coronary vessels; (4) determine the regional oxygen content of the blood (e.g., aortic and within the coronary sinus); (5) determine the status of the electrical conduction properties of the heart; and/or (6) assess septal or valvular defects.

Basic catheterization techniques involve inserting a long, flexible, radio-opaque catheter into a peripheral vein (for right heart catheterization) or a peripheral artery (for the left heart) and delivery of the system under fluoroscopy (continuous X-ray observation). Commonly, during this invasive procedure, a radio-opaque contrast medium is injected into a cardiac vessel or chamber. The procedure may specifically be used to visualize the coronary arteries, the aorta, pulmonary blood vessels, and the ventricles. It can provide pertinent clinical information such as structural abnormalities in blood vessels that restrict flow (such as those caused by an atherosclerotic plaque), ventricular blood volumes, myocardial wall thicknesses, and/or wall motion.

To date, the gold standard for visualizing the coronary system is coronary angiography. Yet, other methods for looking at the coronary system are under development. These methods include computed tomography angiograms and magnetic resonance angiograms. Through the use of injected contrast media and appropriate timing of image acquisition, these methods are providing researchers and clinicians with alternative ways to assess the presence of coronary plaques and stenoses.

7. MEDICAL DEVICES AND THE CORONARY SYSTEM

7.1. Devices and the Coronary Arteries

In recent years, several interventional medical devices have been developed to help treat coronary artery disease. These procedures involve complex medical instrumentation and delivery procedures that have evolved over time. Nevertheless, these devices have saved many lives over the years and are continually improved by scientists, engineers, and physicians.

Intricate medical devices are required for two main interventional procedures performed today on the coronary arteries. Percutaneous transluminal coronary angioplasty is a procedure during which a balloon catheter is introduced into the narrowed portion of the coronary artery lumen and inflated to reopen the artery to allow the return of a normal blood flow. During this procedure, it is common that a coronary stent is also placed such that restenosis of the artery is significantly delayed. A stent is a device made up of wire mesh that provides scaffolding to support the wall of the artery and keep its lumen open and free from the buildup of plaque. A picture of a balloon angioplasty catheter and a coronary stent are shown in Fig. 4.

Balloon angioplasty and coronary stents have prevented numerous patients from having to undergo coronary artery bypass graft surgery, which can be costly and painful. Both techniques and the devices required to make them successful have spawned a significant amount of literature defining a number of important parameters relating to the anatomy of the coro-

nary arteries. Such stents have been produced with a variety of drug coatings in further attempts to minimize the time for, or altogether eliminate, the possibility of restenosis. The most common drug used to coat stents is sirolimus (also known as rapamycin). Drugs like sirolimus work by stopping cell growth; they also stop scar tissue from forming within arteries that have been opened. For more details, refer to Chapter 33.

7.2. Devices and the Coronary Veins

Historically, the coronary veins have not been a focus of interventional procedure development. Recently, the coronary venous system, specifically the coronary sinus, has become a conduit for interventional devices used to treat heart failure as well as for myocardial protection during open heart surgery. These procedures involve the cannulation and catheterization of the coronary sinus, which allows access to the coronary venous network. More specifically, biventricular pacing procedures have become quite common *(10–18)* and have elicited greater interest in the coronary venous system.

Typically, during biventricular implant procedures, a catheter is introduced into the coronary sinus ostium with the aid of standard fluoroscopic imaging methods. Contrast dye is injected retrogradely into the coronary sinus such that the physician can understand its anatomy and that of the branches that feed it. A pacing lead is then delivered into a lateral branch of the coronary sinus, where it is positioned to pace the left ventricle. Although this procedure is relatively common, it can often be difficult and time intensive if the anatomy of the coronary system is not well understood. Figure 5 depicts such a procedure in fairly straightforward terms (*see PlaceLateral.mpg* on the Companion CD).

Myocardial protection is another procedure requiring device interaction with the coronary veins. During open heart surgery, the coronary sinus can be catheterized, and the coronary venous network is perfused retrograde with cardioplegia solution that helps to protect the heart from myocardial ischemia.

Both of the procedures mentioned in this section require intuition about the anatomical parameters of the coronary veins, especially the coronary sinus.

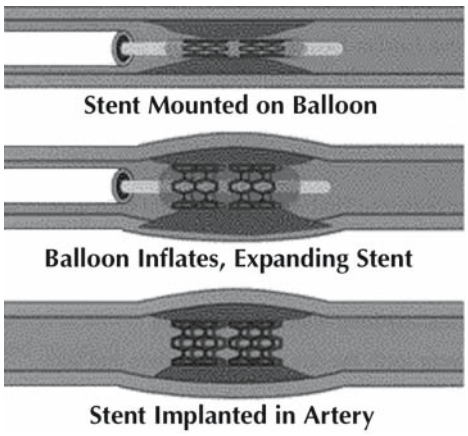

Fig. 4. An illustration of the stenting procedure. The balloon catheter with a collapsed stent mounted on it is placed in the artery at the location of narrowing. The balloon is inflated to open the artery and deploy the stent. Finally, the catheter is removed, and the stent is left behind.

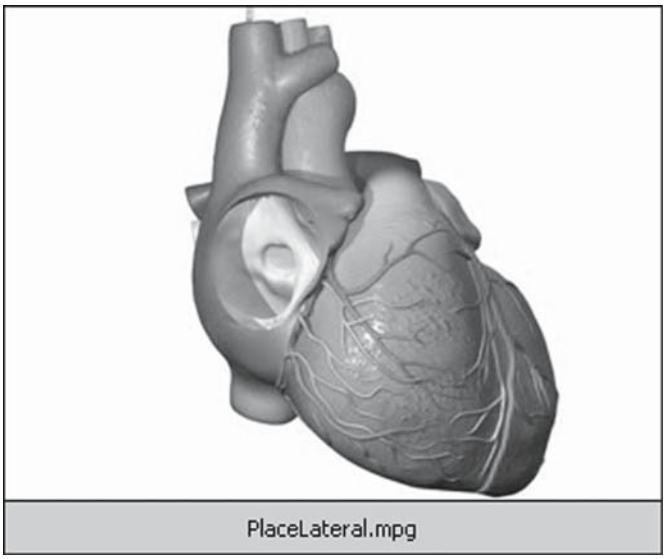

Fig. 5. Animated movie depicting coronary sinus cannulation and lead placement in basal, midventricular, and apical locations during a biventricular pacing implant procedure. *See PlaceLateral.mpg* on the Companion CD.

8. ENGINEERING PARAMETERS AND THE CORONARY SYSTEM

When faced with the task of designing and testing the devices used in these types of interventional procedures, a thorough understanding of the structural and geometric parameters of the coronary system is crucial for success. The main purpose of the following text is to summarize, at a basic level, the important anatomical parameters needed to design interventional devices and/or associated delivery procedures related to the coronary system.

From an engineering perspective, for the predesign of any medical device, there are a number of important parameters that should be familiar; this is especially true because of the complexity and variation found in the human coronary system. As with any device placed in the human body, an excellent understanding of the fundamental anatomical properties of the tissue with which the device interacts is vital to obtain acceptable results regarding: (1) delivery efficacy, (2) long-term device stability, and/or (3) overall performance. This is true not only chronically, but also maybe even more importantly for initial device delivery. Although biological reactions to materials placed inside the human body must be understood to guarantee long-term stability and performance of medical devices, the following discussion focuses on the macroscopic physical properties of the coronary vessels.

To simplify the coronary system down to its basic structure, each vessel branch in the vessel network can be defined in the simple terms of a flexible cylinder or tube. A tube is a hollow cylindrical structure of a known but variable length, radius, and wall thickness. This means the coronary arterial and venous networks can be defined in terms of a large number of interrelated tubes that feed and receive blood to and from one another. The parameters described here are those that must be defined to

understand fully the geometry and dynamic properties of this fine network of tubes so optimal devices may be designed to interact with them.

8.1. Diameter

The first and most basic parameter that must be known about the arteries and veins is their diameter. Yet, the diameters of both arteries and veins are not constant along their lengths *(19–21)*. Typically, coronary arteries taper and decrease in diameter as they move further away from their source *(20,21)*. This means that the left main and right coronary arteries have generally the largest diameters of the entire coronary arterial network; these diameters are typically around 4–5 mm and 3–4 mm, respectively *(20)*.

The more bifurcations an artery undergoes, the smaller its diameter will become. In the case of the coronary arteries, the vessels located at the very end of the network are the capillaries, which are typically on the order of 5–7 μm in diameter *(22)*. This is approx 600 times smaller than that of either the right or left main coronary arteries. Conversely, veins increase in diameter as they move from their source to their termination. Thus, the largest diameter vessel in the coronary venous network is the coronary sinus, which is located at the end of the network and has a diameter of approx 6–12 mm at its ostium *(7,19)*. The difference in diameter from one end of the venous system to the other is roughly a factor of 1200. However, in diseased states such as heart failure, the ostium tends to increase in diameter *(5)*. It is also important to recall that, because arteries and veins are made up of compliant tissue, their diameters change throughout the cardiac cycle because of pressure changes that occur during systole and diastole *(23)*.

The design of coronary stents and balloon angioplasty catheters relies heavily on the diameter of the vessels they are meant to enter. If a stent or balloon is designed with too large a diameter, when it is deployed within the artery it may cause a wall strain so high that it could be damaging to the artery. On the contrary, if the design has a diameter that is too small, the device will be ineffective. For example, in the case of an undersize stent, restenosis of the artery will occur much quicker than desired. In the case of the balloon catheter with a diameter that is too small, the lumen will not be opened up enough to cause any significant decrease in the degree of occlusion.

Another device that must be designed with vessel diameter in mind is the left ventricular pacing lead for heart failure. Because this lead is designed for placement in a lateral branch of the coronary sinus, it must have a small enough diameter to fit inside the vein, but also have a large enough diameter to stay in its intended location. It is considered that if such criteria are not met, the leads may not be useful or safe.

8.2. Cross-Sectional Profile

A parameter that is very closely related to vessel diameter is that of cross-sectional shape profile. Cross-sectional shape profile is determined by the shape of the vessel that results after slicing it perpendicular to its centerline. In a hypothetical cylinder, this profile would be a perfect circle. When arteries are diseased and contain significant amounts of atherosclerotic plaque, their cross-sectional profile can change from roughly circular to various different (and often quite complex) profiles, depending on the amount and orientation of the plaque. To date, coronary venous shape profiles have not been well documented, but they can be considered as noncircular in general because of the lower pressures within the vessel as well as the more easily deformable vessel walls in relation to the arteries.

The design of two devices in particular should be considered in relation to the cross-sectional shape of the coronary vessels—coronary stents and angioplasty catheter balloons. Because coronary arteries are typically circular in cross section, stents are designed also to be circular in their cross section. Interestingly, more often than not, the vessel to be stented has a pretreated cross section that is very far from circular. If a similar device were ever needed for placement in the relatively healthy coronary venous network, a different design would probably be initially considered because the cross-sectional profile of a coronary vein is generally noncircular. Angioplasty balloons have been designed with the consideration that coronary arteries are typically circular in cross section. When inflated, the balloon generates a shape that has a uniform diameter in cross section, which may be consistent with what a healthy coronary artery looks like in cross-section.

8.3. Ostial Anatomy

Understanding the anatomy of the ostia of each of the three most prominent vessels in the coronary system (the right coronary artery, left main coronary artery, and the coronary sinus) is especially important when interventional procedures require cannulation of the ostia to perform a specific procedure within the lumen of the vessel. This is true of nearly all procedures done on coronary vessels because they are typically aimed at the lumen of the vessel, but on occasion one may want to block off or place a flow-through catheter in the ostium.

The ostia of the coronary arteries are generally open with no obstructions except when coronary plaques form; in this case, they can become partially or even fully occluded. When occlusion is not present at the ostial origin of the coronary arteries, there are generally no naturally occurring anatomical structures to impede entrance into the vessels.

The coronary sinus ostium, as discussed in Section 4, often has a simple flap of tissue covering its opening into the right atrium; this flap is called the Thebesian valve. This valve can take many different forms and morphologies and can cover the coronary sinus ostium to varying degrees *(4,6–8,24,25)*. When the Thebesian valve is significantly prominent in the manner in which it covers the coronary sinus ostium, cannulation can be much more difficult than in other cases *(5,8)*.

This consideration is important as it specifically applies to the implantation of biventricular pacemaker leads. In the process of delivering a biventricular pacing lead, coronary sinus cannulation is of paramount importance because it is currently considered as the primary point of entry into the coronary venous network for pacemaker lead introduction for eventual pacing of the left ventricle. To design the optimal catheter or lead delivery procedure, the presence of the Thebesian valve should be fully considered in addition to other anatomical features.

8.4. Vessel Length

Each tube that makes up a section of the coronary arterial or venous network is also a branch that arises from a parent vessel. Each of these vessel branches has starting and ending points. Typically, vessel lengths can be measured directly on a specimen after the heart has been extracted. With the advent of 3D medical imaging techniques such as magnetic resonance imaging and computerized tomographic angiography, coronary vessel lengths can be measured in vivo by reconstructing them in space *(26–28)*.

One application for which vessel length is an important consideration is implantation of left ventricular leads in the lateral or posterior branches of the coronary sinus. Optimal lead designs should take into account the average length along the coronary sinus of the normal and/or diseased human heart where a candidate lateral branch enters. Foreknowledge of this parameter, either in a specific patient or across a population, might improve ease of implant. This information could also be useful in understanding the likelihood that a lead will not dislodge after initial fixation. Furthermore, when percutaneous transluminal coronary angioplasty procedures are performed, it is critical that the physician knows exactly where along the length of an artery the occlusion occurs and the relative distance needed from catheter entry to the site. These parameters are often measured using contrast angiography. When contrast is injected and fluoroscopic images are acquired, the location of the occluded arterial region can be quickly identified.

8.5. Tortuosity

Because the vessels in the coronary system course along a nonplanar epicardial surface, they are by nature tortuous. Thus, they have varying degrees of curvature along their lengths according to the topography of the epicardial surfaces on which they lie. If vessels were simply curvilinear entities such that they only lie in a single plane, their tortuosities would be much more easily defined. But, in reality, the vessels of the coronary system are not curvilinear. Rather, they are 3D curves that twist and turn in more than two dimensions. When the third dimension is added, the definition of tortuosity becomes much more complex. Not only must the curvature of each segment element be defined, but also the direction in which that curve is oriented.

The levels of tortuosity encountered in the coronary vessels may significantly influence device delivery and chronic performance. When a device such as a catheter or lead must be passed through a tortuous anatomy, such as that of the coronary vessels, the greater the curvature and change in curvature over the length of a vessel, the more difficult it will be to pass the device through it. For vessels that more closely resemble a straight line, these devices will pass through much more easily. It should also be noted that vessel tortuosity in humans is considered to increase with age. Therefore, patient age may be another important consideration when designing these types of devices and/or the mechanisms by which they are to be delivered.

8.6. Wall Thickness

All coronary vessel walls have a certain thickness. When a device is placed into the vessels of the coronary system, there is always a danger of perforation. In general, perforation takes place when a device is inadvertently introduced into the vessel lumen with a level of force and angle of incidence to the vessel wall that causes the device to perforate the wall and generate a hole through which blood can flow. This situation, although not very common, is not only very dangerous but can be lethal if not dealt with appropriately. Perforation is usually more often fatal when it happens in arteries as opposed to veins for two reasons: (1) more blood is lost under higher pressures in the arteries; and (2) loss of oxygenated blood to the body and the heart itself is more immediately detrimental than if deoxygenated blood were to exit the coronary veins.

Although it is clear that no device is meant to perforate the vessels of the coronary system, each should be developed with the worst-case scenario of perforation in mind, such that they will not be problematic for patients or physicians. It should be noted that the wall thickness of the larger coronary arteries (they are the thickest) is roughly 1 mm *(29,30)*. Interestingly, coronary venous wall thicknesses have not as yet been clearly defined in the literature.

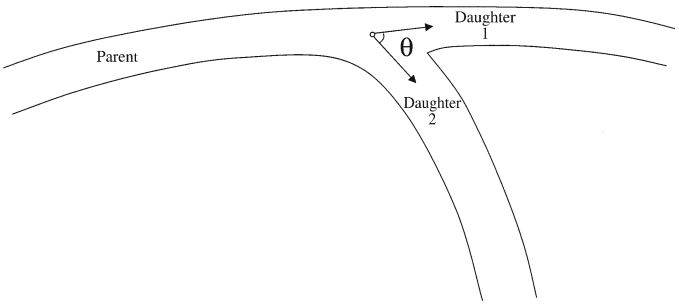

Fig. 6. Diagram of the branching angle between a parent vessel and its daughter. Angle θ represents the branching angle generated between the parent vessel and daughter 2.

8.7. Branch Angle

As a vessel bifurcates, at least those of the daughter branches, it is diverted in a different direction from the parent. This creates a situation in which the smaller vessel has a certain branching angle in relation to the direction of the parent vessel. Branching angles can be measured by calculating the angle between the trajectory of the parent vessel and its daughter. An example of this idea is illustrated in Fig. 6.

The branch angle of a daughter vessel is important to understand as it applies directly to when a biventricular pacing lead enters a posterior or lateral branch of the coronary sinus. Thus, the only way to optimize the design of this type of lead, such that it can easily make the turn into a branching vessel, is to know how gentle or severe that branching angle generally is. The more gradual the turn a lead has to take from a parent vessel to its daughter, the easier it is for an implanter to navigate in general.

8.8. Motion Characteristics

Because the vessels of the coronary system are attached directly to the epicardium, it follows that they are not stationary as the heart beats. Along with the simple 3D displacement that occurs over time because of motion, there are other mechanical parameters that are dynamic, such as curvature,

strain, and torsion. Each of these fundamental mechanical parameters can have significant effects on devices placed in the lumen of a deforming vessel. Devices such as stents and leads must be designed to withstand all types of strain, curvature, and torsion changes they are expected to experience over their lifetime within an arterial or venous vessel lumen. Additional necessary considerations include (1) the relative changes in both the 3D path of each vessel and changes in lumen diameter during a given cardiac cycle and (2) the relative influences associated with alterations in contractility states (e.g., the effects of exercise increasing cardiac output four- to sixfold).

9. SUMMARY

This chapter reviewed the anatomical and functional features of the coronary system. The effects of several disease processes on cardiac function relative to flow changes were discussed, as well as associated therapies. In addition, the use of the coronary system to gain access to various regions of the heart for specific clinical needs was described. Finally, pertinent issues that must be considered when designing devices for invasive placement within the coronary vessels were discussed.

ACKNOWLEDGMENT

The authors acknowledge the work of Mike Lerners in developing the animations used in this chapter.

COMPANION CD MATERIAL

CoronaryVeins.mpg (Fig. 1) and
PlaceLateral.mpg (Fig. 5)

REFERENCES

1. Alexander, R.W., Schlant, R.C., Fuster, V., O' Rourke, R.A., Roberts, R., and Sonnenblick, E. H. (eds.) (1999) *Hurst's: The Heart*. McGraw-Hill, New York, NY.
2. Kajiya, F., Matsuoka, S., Ogasawara, Y., et al. (1993) Velocity profiles and phasic flow patterns in the non-stenotic human left anterior descending coronary artery during cardiac surgery. *Cardiovasc Res*. 27, 845–850.
3. Kasprzak, J.D., Drozdz, J., Peruga, J.Z., Rafalska, K., and Krzeminska-Pakula, M. (2000) Definition of flow parameters in proximal nonstenotic coronary arteries using transesophageal Doppler echocardiography. *Echocardiography*. 17, 141–150.
4. Felle, P. and Bannigan, J.G. (1994) Anatomy of the valve of the coronary sinus (Thebesian valve). *Clin Anat*. 7, 10–12.
5. Hellerstein, H.K. and Orbison, J.L. (1951) Anatomical variations of the orifice of the human coronary sinus. *Circulation*. 3, 514–523.
6. Jatene, M., Jatene, F., Costa, R., Romero, S., Monteiro, R., and Jatene, A. (1991) Anatomical study of the coronary sinus valve—Thebesius valve. *Chest*. 100(Suppl.), 90S.
7. Ortale, J.R., Gabriel, E.A., Iost, C., and Marquez, C.Q. (2001) The anatomy of the coronary sinus and its tributaries. *Surg Radiol Anat*. 23, 15–21.
8. Hill, A., Coles, J.A., Jr., Sigg, D.C., Laske, T.G., and Iaizzo, P.A. (2003) Images of the human coronary sinus ostium obtained from isolated working hearts. *Annal Thorac Surg*. 26, 2108.
9. Hill, A.J., Laske, T.G., Coles, J.A., Jr., et al. In vitro studies of human hearts. Submitted to *Mayo Clinic Proceedings*, 2003.
10. Wong, K.L., Kocovic, D.Z., and Loh, E. (2001) Cardiac resynchronization: a novel therapy for heart failure. *Congest Heart Fail*. 7, 139–144.
11. Abraham, W.T. (2002) Cardiac resynchronization therapy for heart failure: biventricular pacing and beyond. *Curr Opin Cardiol*. 17, 346–352.
12. Aranda, J.M., Jr., Schofield, R.S., Leach, D., Conti, J.B., Hill, J.A., and Curtis, A.B. (2002) Ventricular dyssynchrony in dilated cardiomyopathy: the role of biventricular pacing in the treatment of congestive heart failure. *Clin Cardiol*. 25, 357–362.
13. Bakker, P.F., Meijburg, H.W., de Vries, J.W., et al. (2000) Biventricular pacing in end-stage heart failure improves functional capacity and left ventricular function. *J Interv Card Electrophysiol*. 4, 395–404.
14. Gerber, T.C., Nishimura, R.A., Holmes, D.R., Jr., et al. (2001) Left ventricular and biventricular pacing in congestive heart failure. *Mayo Clin Proc*. 76, 803–812.
15. Barold, S.S. (2001) What is cardiac resynchronization therapy? *Am J Med*. 111, 224–232.
16. Liu, D.M., Zhang, F.H., Chen, L., Zheng, H.P., and Zhong, S.Z. (2003) Anatomy of the coronary sinus and its clinical significance for retrograde cardioplegia. *Di Yi Jun Yi Da Xue Xue Bao*. 23, 358–360.
17. Tian, G., Dai, G., Xiang, B., Sun, J., Lindsay, W.G., and Deslauriers, R. (2001) Effect on myocardial perfusion of simultaneous delivery of cardioplegic solution through a single coronary artery and the coronary sinus. *J Thorac Cardiovasc Surg*. 122, 1004–1010.
18. Farge, A., Mousseaux, E., Acar, C., et al. (1996) Angiographic and electron-beam computed tomography studies of retrograde cardioplegia via the coronary sinus. *J Thorac Cardiovasc Surg*. 112, 1046–1053.
19. Doig, J.C., Saito, J., Harris, L., and Downar, E. (1995) Coronary sinus morphology in patients with atrioventricular junctional reentry tachycardia and other supraventricular tachyarrhythmias. *Circulation*. 92, 436–441.
20. Dodge, J.T., Jr., Brown, B.G., Bolson, E.L., and Dodge, H.T. (1992) Lumen diameter of normal human coronary arteries. Influence of age, sex, anatomic variation, and left ventricular hypertrophy or dilation. *Circulation*. 86, 232–246.
21. Zubaid, M., Buller, C., and Mancini, G.B. (2002) Normal angiographic tapering of the coronary arteries. *Can J Cardiol*. 18, 973–980.
22. Ono, T., Shimohara, Y., Okada, K., and Irino, S. (1986) Scanning electron microscopic studies on microvascular architecture of human coronary vessels by corrosion casts: normal and focal necrosis. *Scan Electron Microsc*. (Pt. 1), 263–270.
23. Ge, J., Erbel, R., Gerber, T., et al. (1994) Intravascular ultrasound imaging of angiographically normal coronary arteries: a prospective study in vivo. *Br Heart J*. 71, 572–578.
24. Silver, M.A. and Rowley, N.E. (1988) The functional anatomy of the human coronary sinus. *Am Heart J*. 115, 1080–1084.
25. Piffer, C.R., Piffer, M.I., and Zorzetto, N.L. (1990) Anatomic data of the human coronary sinus. *Anat Anz*. 170, 21–29.
26. Achenbach, S., Kessler, W., Moshage, W.E., et al. (1997) Visualization of the coronary arteries in 3D reconstructions using respiratory gated magnetic resonance imaging. *Coron Artery Dis*. 8, 441–448.
27. Achenbach, S., Ulzheimer, S., Baum, U., et al. (2000) Noninvasive coronary angiography by retrospectively ECG-gated multislice spiral CT. *Circulation*. 102, 2823–2828.
28. Li, D., Kaushikkar, S., Haacke, E.M., et al. (1996) Coronary arteries: 3D MR imaging with retrospective respiratory gating. *Radiology*. 201, 857–863.
29. Kim, W.Y., Stuber, M., Bornert, P., Kissinger, K.V., Manning, W.J., and Botnar, R.M. (2002) Three-dimensional black-blood cardiac magnetic resonance coronary vessel wall imaging detects positive arterial remodeling in patients with nonsignificant coronary artery disease. *Circulation*. 106, 296–299.
30. Gradus-Pizlo, I. and Feigenbaum, H. (2002) Imaging of the left anterior descending coronary artery by high-frequency transthoracic and epicardial echocardiography. *Am J Cardiol*. 21, 28L–31L.

SOURCES

Alexander, R.W., Schlant, R.C., and Fuster, V. (eds.). (1998) *Hurst's: The Heart, Arteries and Veins*, 9th Ed. McGraw-Hill, New York, NY.

Mohrman, D.E. and Heller, L.J. (eds.) (2003) *Cardiovascular Physiology*, 5th Ed. McGraw-Hill, New York, NY.

Tortora, G.J. and Grabowski, S.R. (eds.). (2000) *Principles of Anatomy and Physiology*, 9th Ed. Wiley, New York, NY.

7 The Pericardium

EDWARD CHINCHOY, PhD, MICHAEL R. UJHELYI, PharmD, FCCP, ALEXANDER J. HILL, PhD, NICHOLAS D. SKADSBERG, PhD, AND PAUL A. IAIZZO, PhD

CONTENTS

1. INTRODUCTION

The pericardium is a fibroserous conical sac structure encompassing the heart and roots of the great cardiac vessels. In humans, it is located within the mediastinal cavity posterior to the sternum and cartilages of the third, fourth, fifth, sixth, and seventh ribs of the left thorax and is separated from the anterior wall of the thorax. It is encompassed from the posterior resting against the bronchi, the esophagus, the descending thoracic aorta, and the posterior regions of the mediastinal surface of each lung. Laterally, the pericardium is covered by the pleurae and lies along the mediastinal surfaces of the lung. It can come in direct contact with the chest wall near the ventricular apical region, but varies with the dimensions of the long axes of the heart or with various disease states. Under normal circumstances, the pericardium separates and isolates the heart from contact of the surrounding tissues, allowing freedom of cardiac movement within the confines of the pericardial space (Fig. 1).

2. ANATOMY

In humans, the 1- to 3-mm thick fibrous pericardium forms a flask-shaped bag. The neck of the pericardium (superior aspect) is closed by its extensions surrounding the great cardiac vessels; the base is attached to the central tendon and to the muscular fibers of the left side of the diaphragm. Much of the diaphragmatic attachment of the pericardium consists of loose fibrous tissue that can be readily separated and/or isolated, but there is a small area over the central tendon where the diaphragm and the pericardium are completely fused.

Examination of the pericardium reveals that it is comprised of two interconnected different and separate structures. The outer sac is known as the *fibrous pericardium* and consists of fibrous tissue. The inner sac is known as the *serous pericardium* and is a delicate membrane composed of a single layer of flattened cells resting on loose connective tissue that lies within the fibrous pericardium, lining its inner walls. The heart enters the wall of the serous sac from above and behind, creating an infold encompassing nearly the entire pericardial cavity space. (*See also* Chapter 4, Fig. 4.)

The surrounding great vessels that receive fibrous prolongations from this serous pericardium include the aorta, the superior vena cava, the right and left pulmonary arteries, and the four pulmonary veins. The inferior vena cava enters the pericardium through the central tendon of the diaphragm, in which there exists a small area of fusion between the pericardium and the central tendon, but receives no covering from this fibrous layer.

From: *Handbook of Cardiac Anatomy, Physiology, and Devices*
Edited by: P. A. Iaizzo © Humana Press Inc., Totowa, NJ

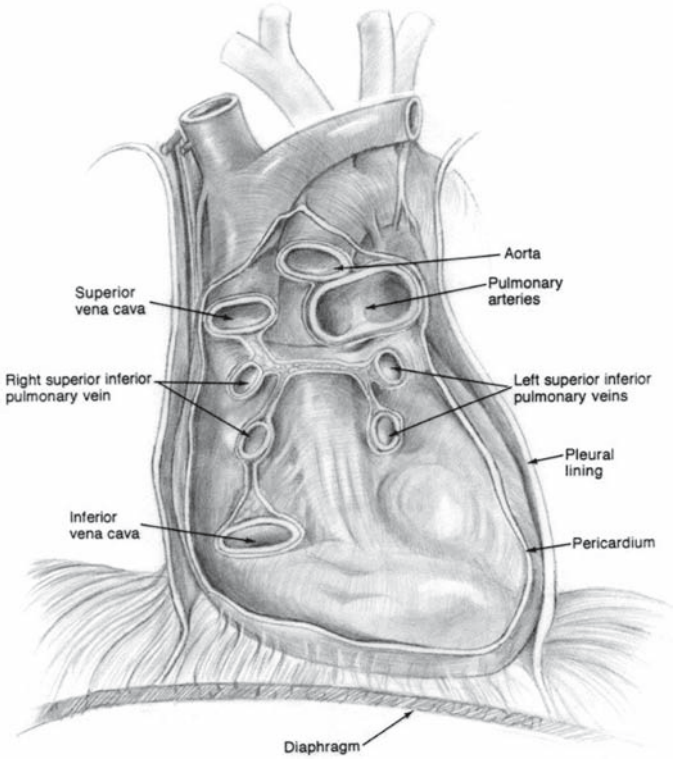

Fig. 1. A posterior view of the pericardial sac, with the anterior surface and heart cut away. It can be seen that the great vessels of the heart penetrate through the pericardium, which extends up these vessels for several centimeters.

Between the left pulmonary artery and subjacent pulmonary vein is a triangular fold of the serous pericardium known as the *ligament of the left vena cava* (vestigial fold of Marshall). It is formed by a serous layer over the remnant of the lower part of the left superior vena cava (duct of Cuvier), which regresses during fetal life, but remains as a fibrous band stretching from the highest left intercostal vein to the left atrium, where it aligns with a small vein known as the *vein of the left atrium* (oblique vein of Marshall), eventually opening into the coronary sinus. The pericardium is also attached to the posterior-sternal surface by superior and inferior sternopericardial ligaments, which securely anchor the pericardium and act to maintain the orientation of the heart inside the thorax.

As mentioned, the serous pericardium is a closed sac that lines the fibrous pericardium and consists of visceral and parietal portions. The visceral portion, which covers the heart and the great vessels, is commonly referred to as the *epicardium* and is continuous with the parietal layer that lines the fibrous pericardium. The parietal portion, which covers the remaining vessels, is arranged in the form of two tubes. The aorta and pulmonary artery are enclosed in one tube (the *arterial mesocardium*); the superior and inferior venae cavae and the four pulmonary veins are enclosed in the second tube (the *venous mesocardium*). There is an attachment to the parietal layer between the two branches, behind the left atrium, commonly referred to as the *oblique sinus*. There is also a passage between the venous and arterial mesocardia (i.e., between the aorta and pulmonary artery in front and the atria behind) that is termed the *transverse sinus*. The *superior sinus* or *superior aortic recess* extends upward along the right side of the ascending aorta to the origination point of the innominate artery. The superior sinus also joins the transverse sinus behind the aorta, and they are both continually fused until they reach the aortic root.

The arteries of the pericardium are derived from the internal mammary and its musculophrenic branch and from the descending thoracic aorta. The nerves innervating the pericardium are derived from the vagus and phrenic nerves and the sympathetic trunks.

3. MECHANICAL EFFECTS OF THE PERICARDIUM

The degree to which the pericardium alters wall movement varies depending on the ratio of cardiac to pericardial size, loading conditions, and the degree of active and passive filling. Closure of the pericardial sac following open heart surgery has been proposed to (1) avoid possible postoperative complications, (2) reduce the frequency of ventricular hypertrophy, and (3) facilitate future potential reoperations by reducing fibrosis *(1)*. Differences in ventricular performance dependent on the presence of the pericardium have been reported following cardiac surgery *(2,3)*.

The presence of the pericardium physically constrains the heart, often resulting in a depressive hemodynamic influence that limits cardiac output by restraining diastolic ventricular filling *(4,5)*. The physical constraint by the pericardium is translated into direct external mechanical forces that alter patterns in myocardial and systemic blood flow *(5,6)*. Direct primary and indirect secondary effects are observed as additional forces through the free wall. Because both the left- and right-side atria and ventricles are bound by a common septum, geometrical changes from chamber interactions are dynamic, depending on the different filling rates and ejection rates of each of the four chambers *(7,8)*. Thus, it is important to note that chamber-to-chamber interactions through the interventricular septum and by the pericardium further promote direct mechanical chamber interactions *(9–11)*.

The effects of the pericardium on mechanical measures of cardiac performance are generally not evident until ventricular and atrial filling limitations are reached, i.e., changing geometrical and mechanical properties through factors such as maximum chamber volumes and elasticity. These effects become more evident as these pericardial limitations become extended *(12,13)*. With the known force–length dependence of cardiac muscle, variation of chamber volumes through removal of the pericardium will influence isometric tension and therefore has a direct impact on systolic ejection. On the other hand, in specific cases when the restrictive role of the pericardium greatly increases, such as during cardiac tamponade, an increased intrapericardial fluid volume may result in critical restriction by the pericardium, which then clinically reduces cardiac performance *(14)*.

It should also be noted that intrathoracic pressure creates an additional interaction between the ventricles, as well as between the heart and lungs in a closed chest. Thus, studying cardiac function *in situ* (with an opened chest) or in vitro allows elimination of the influences of intrathoracic pressures

for identifying and quantifying pericardial influences on cardiac performance and ejection *(15)*. Such isolation of pericardial effects from diastolic filling is necessary because normal ventricular output is dependent on diastolic pressure independent of the presence of the pericardium *(16)*.

4. ISOLATED PERICARDIAL HEMODYNAMIC EFFECTS AND TRANSPLANTATION

Previous experiments have suggested that, in a normal intact heart at normal levels of right ventricular diastolic filling, the pericardium does not exert constraining effects on ventricular function *(3,8)*. However, with increasing levels of right ventricular preload pressure, pericardial constraint increases, significantly influencing right ventricular function *(17)*. By restricting atrial filling, the pericardium causes reductions in atrial systolic contributions to ventricular filling *(18)*, mediated by atrioventricular interaction in addition to the direct ventricular interaction *(8)*. In the left ventricle, at normal or only moderately elevated pressures, the pericardium has been reported to have a significant constraining effect on diastolic filling *(19)*, often occurring without detectable changes in pericardial pressure *(20,21)*. This suggests that, when normal cardiac limitations may be near maximum duress or capacity, such as during and following transplantation, the role of the pericardium may become more evident or prominent.

4.1. Four-Chamber Working In Vitro Model

With cardiac output physiologically dependent on diastolic pressure, in vitro, diastolic pressure and cardiac output can be controlled more without systemic influences. The sensitivity of the left ventricle to pericardial pressure is more evident given the differences in left ventricular performance with no significant difference in right ventricular performance associated with the effects of the pericardium. However, given the pericardial and chamber interactions, no attempt to separate or isolate the primary vs secondary pericardium effects on each chamber can be independently done.

In a study by our laboratory, we modeled pericardial effects during transplantation using swine hearts because of their anatomical and histological similarities to those of humans. The role of the pericardium hemodynamic function was investigated during and following simulated human orthotopic transplantation by use of an in vitro apparatus. This apparatus, capable of sustaining physiological cardiac function, was used to separate the pericardial influences from systemic effects and to simulate transplantation.

As detailed and documented in a previous study, the hemodynamic effects of explantation into the apparatus resulted in stability of ejecting parameters while working all four chambers *(22)*. This is consistent with previous reports in which considerations of metabolic and contractile differences were observed between nonejecting and ejecting models; further, the role of the pericardium was noted with consideration to recovery of both left and right ventricular performance following an ischemic period *(23,24)*.

Modified Krebs Henseleit buffer was used as perfusate with various additions to aid in maintenance of cardiac performance: ethylenediaminetetraacetic acid (EDTA) (0.32 mmol/L) to chelate toxic metal ions and free calcium concentration titration; insulin (10 U/L) to aid in glucose utilization; sodium pyruvate (2.27 mmol/L) as an additional energy substrate; and mannitol (16.0 mmol/L) to increase osmolarity and reduce cardiac edema. The in vitro approach was employed because, in vivo, ventricular output is coupled to the pulmonary system and flows through the coronary vessels, limiting chamber ejection rates (i.e., right ventricle output cannot be steadily greater than left atrial output). Decoupling these flows in vitro allowed intrinsic output of the left and right side to operate independently with controlled atrial preload.

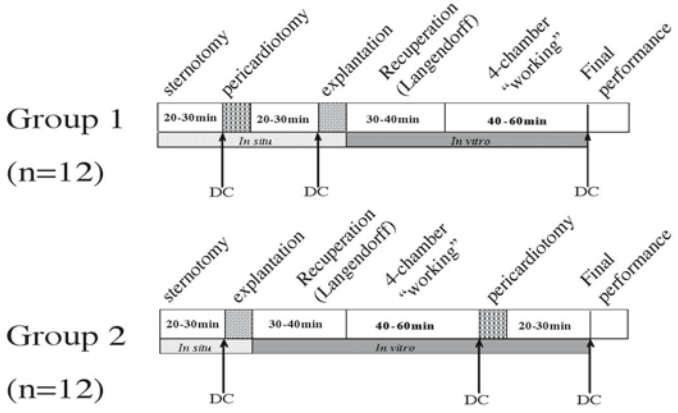

Fig. 2. Experimental protocols for groups 1 and 2. In group 1, a pericardiotomy was performed previous to explantation into the apparatus. In group 2, explantation preceded pericardiotomy. During all phases, the heart was allowed to stabilize until hemodynamic parameters were measured. DC, data collection.

In one group of animals (n = 12), cardiac hemodynamic parameters were measured *in situ* following pericardiotomy and explantation into an in vitro apparatus. In a second group (n = 12), cardiac hemodynamic parameters were measured *in situ* following explantation in vitro and pericardiotomy (Fig. 2; *see also MPEG 1* on the Companion CD.). Mean postmortem heart weights were statistically similar at 327 ± 3 g (group 1) and 346 ± 2 g (group 2). (*See JPEG 1* on the Companion CD.)

Comparison of baseline cardiac parameters following medial sternotomy revealed no statistical difference between the two groups ($p > 0.05$ for both right and left ±dP/dt). Performance was dependent on the order of pericardiotomy and explantation. Differences existed between the two groups with final in vitro left ventricular +dP/dt ($p < 0.001$); no difference was observed in final in vitro right ventricular +dP/dt ($p > 0.05$). With *in situ* pericardiotomy, left and right ventricular +dP/dt changes of 5.1 ± 16.5% and 27.7 ± 31.4%, respectively, were observed vs 21.1 ± 11.8% and 21.6 ± 28.9%, respectively, with in vitro pericardiotomy. Concordantly, changes of –2.7 ± 18.6% and 5.1 ± 20.1%, respectively, were observed in left ventricular +dP/dt associated with explantation following *in situ* pericardiotomy, compared to –2.0 ± 7.5% and 5.5 ± 24.5%, respectively, following in vitro pericardiotomy.

Several significant differences were associated with final in vitro cardiac performance with and without the pericardium in values of left ventricular +dP/dt (1126.1 ± 110.1 vs 925.3 ±

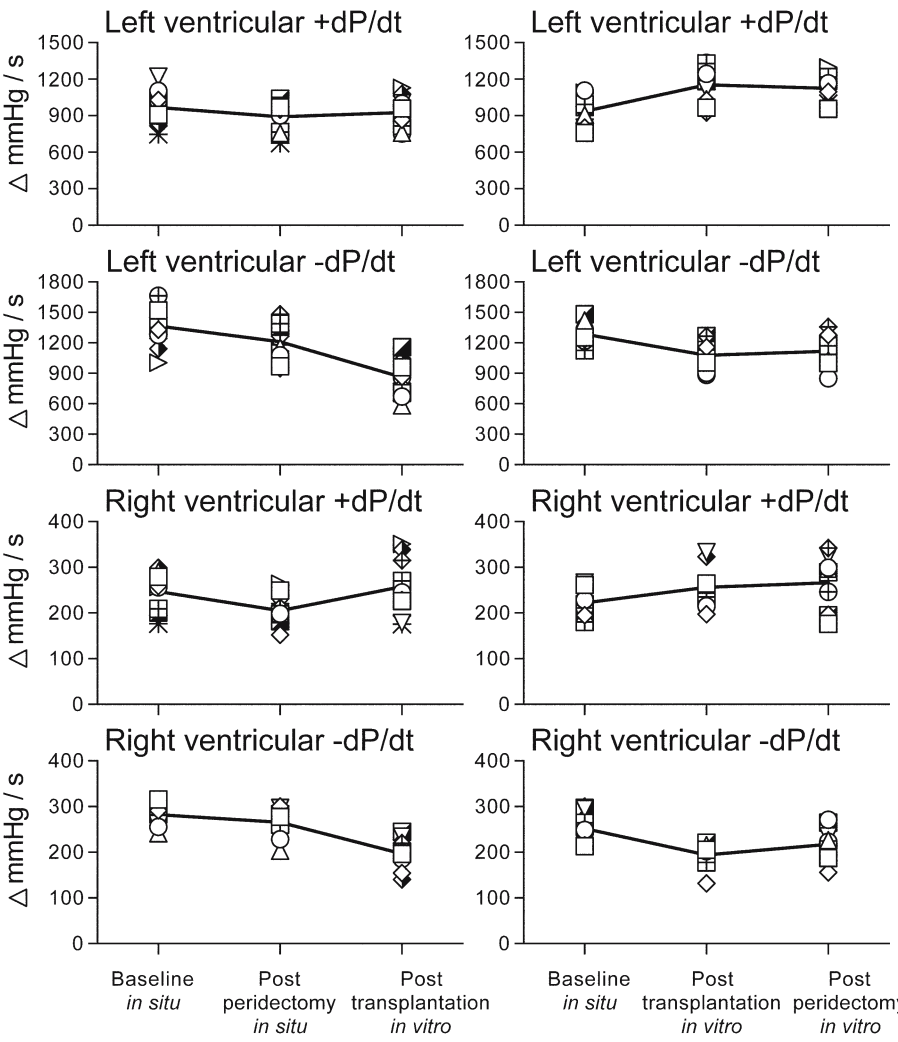

Fig. 3. Results detailing the effects of transplantation in vitro with and without the pericardium (n = 12 per set). *In situ* baseline control, pericardiotomy, and explantation in vitro maximum ±dP/dt performance characteristics as indicators of ventricular contractility and relaxation are shown.

117.7, respectively; $p < 0.05$) and –dP/dt (1116.4 ± 159.9 vs 859.2 ± 174.5, respectively) and in right ventricular –dP/dt (192.6 ± 33.6 vs 221 ± 39.8, respectively). No differences in right ventricular +dP/dt were observed between removing the pericardium *in situ* vs in vitro.

These findings indicated that an intact pericardium has a depressive influence on normal left ventricular performance and may help preserve left ventricular systolic function as measured by left ventricular +dP/dt following transplantation, but that these relative effects were not equivalent for both ventricles. The nonsymmetrical results between the left and right ventricles under constant filling preload and afterload resistance supported the notion that chamber reaction of one ventricle oppositely affects the other chamber because of interactions across the free wall. Yet, previous studies including both human and animal models have assumed similar *in situ* and in vitro function independent of the pericardium. Based on these findings, care should be taken when interpreting hemodynamic results with respect to the absence or presence of the pericardium, especially when the ratio of forces because of pericardial constraint affecting diastolic filling is unknown.

In group 1 (*in situ* pericardiotomy and explantation in vitro), a medial sternotomy was performed, and the rib cage was retracted, preserving the integrity of the pericardial sac, which was freed from the surrounding interthoracic tissues. *In situ* data were recorded to measure myocardial performance with rib cage pressure relieved. Following pericardiotomy, including all connective tissue and fat, hemodynamic measurements were then repeated as outlined above.

The hemodynamic effects were normalized with respect to the previous stage by calculating percentage of change associated with each procedure. In addition, the percentage change between initial *in situ* values and final in vitro values were determined. Group 1 *in situ* baseline data, the effects of *in situ* pericardiotomy, and the effects of explantation in vitro in the absence of the pericardium are shown in Fig. 3 and Table 1.

Table 1
Effects of Order of Pericardiotomy and In Vitro Transplantation

Mean ± SD (n = *12*)	*Baseline (in situ)*	*Postpericardiotomy (in situ)*	*Postexplantation (in vitro)*
Group 1			
Heart rate (beats/min)	97.6 ± 18.5	91.3 ± 13.4	87.9 ± 11.9
Cardiac output	3.4 ± 0.6	3.5 ± 0.7	2.2 ± 0.3
Left ventricular +dP/dt (mmHg/s)	967.7 ± 174.0	890.2 ± 181.4	925.3 ± 147.7 *
(% Δ from previous stage)	(−7.5 ± 9.6)	(5.1 ± 16.5)	
(% Δ from *in situ* baseline)	(−2.7 ± 18.6)		
Left ventricular −dP/dt (mmHg/s)	1364.7 ± 175.3	1210.6 ± 187.2	859.2 ± 174.5 *
(% Δ from previous stage)	(−10.7 ± 12.8)	(−27.3 ± 19.2)	
(% Δ from *in situ* baseline)	(−35.5 ± 19.1)		
Right ventricular +dp/dt (mmHg/s)	246.5 ± 38.7	204.9 ± 31.9	257.4 ± 55.7
(% Δ from previous stage)	(−15.2 ± 16.7)	(27.7 ± 31.4)	
(% Δ from *in situ* baseline)	(5.1 ± 20.1)		
Right ventricular −dp/dt (mmHg/s)	282.0 ± 21.9	265.0 ± 29.9	192.6 ± 33.6
(% Δ from previous stage)	(−6.0 ± 8.2)	(−25.1 ± 14.5)	
(% Δ from *in situ* baseline)	(−29.9 ± 13.5)		
Mean ± SD (n = *12*)	*Baseline (in situ)*	*Postexplantation (in vitro)*	*Postpericardiotomy (in vitro)*
Group 2			
Heart rate (beats/min)	93.8 ± 13.6	96.2 ± 21.1	93.2 ± 21.5
Cardiac output	3.5 ± 0.7	2.2 ± 0.3	2.4 ± 0.2
Left ventricular +dp/dt (mmHg/s)	935.3 ± 119.9	1152.5 ± 142.3	1126.1 ± 110.1 *
(% Δ from previous stage)	(23.7 ± 9.4)	(−2.0 ± 7.5)	
(% Δ from *in situ* baseline)	(21.1 ± 11.8)		
LV −dp/dt (mmHg/s)	1284 ± 115.7	1076.8 ± 143.5	1116.4 ± 159.9 *
(% Δ from previous stage)	(−18.6 ± 15.1)	(3.2 ± 6.5)	
(% Δ from *in situ* baseline)	(−12.5 ± 14.9)		
Right ventricular +dp/dt (mmHg/s)	221.8 ± 29.1	255.8 ± 43.6	266.1 ± 58.9
(% Δ from previous stage)	(16.2 ± 19.4)	(5.5 ± 24.5)	
(% Δ from *in situ* baseline)	(21.6 ± 28.9)		
Right ventricular −dp/dt (mmHg/s)	261.5 ± 33.4	198.8 ± 33.4	221.9 ± 39.8
(% Δ from previous stage)	(−19.8 ± 17.2)	(12.1 ± 12.8)	
(% Δ from *in situ* baseline)	(11.1 ± 16.0)		

*Statistical significance ($p < 0.05$).

Table 2
Normalized Changes in Cardiac Performance Associated With Pericardiotomy and Explantation In Vitro

Statistical significance of % Δ attributed with each stage	*Explantation*	*Pericardiotomy*
Left ventricular +dP/dt (group 1 vs group 2)	$p < 0.01$; significant	$p > 0.05$; not significant
Left ventricular −dP/dt (group 1 vs group 2)	$p > 0.05$; not significant	$p < 0.01$; significant
Right ventricular +dP/dt (group 1 vs group 2)	$p > 0.05$; not significant	$p < 0.05$; significant
Right ventricular −dP/dt (group 1 vs group 2)	$p > 0.05$; not significant	$p < 0.01$; significant

Similarly, for group 2, *in situ* baseline data, the effects of explantation in vitro in the presence of the pericardium, and in vitro pericardiotomy effects are shown.

The percentage change of cardiac performance associated with explantation and pericardiotomy was compared with statistical analysis; data are provided in Tables 2 and 3. With explantation, significant differences were observed with the intact pericardium only in left ventricular +dP/dt; no other parameters were affected. Conversely, pericardiotomy affected right ventricular +dP/dt and −dP/dt and left ventricular −dP/dt, depending on whether the pericardiotomy occurred prior to or following explantation. No significant difference in final in vitro cardiac output was observed, though it was observed during the experiment that, in all cases of in vitro pericardiotomy (group 2), cardiac output increased on removal of the pericardium.

The significantly smaller difference in percentage change of left ventricular +dP/dt associated with explantation with an intact pericardium vs without the pericardium suggests that, during orthotopic transplantation, the pericardium may help to preserve left contractile function (Table 2). Changes in right ventricular +dP/dt and −dP/dt were also noticed. During the same process, no difference was observed in right ventricular +dP/dt, suggesting that the left and right ventricles are affected differently by the pericardium.

Table 3
Effects of Pericardiotomy Preceding vs Following Explantation

Statistical difference with sequence of pericardiotomy and explantation in vitro	*Final in vitro performance*
Left ventricular +dP/dt (group 1 vs group 2)	$p < 0.01$; significant
Left ventricular -dP/dt (group 1 vs group 2)	$p < 0.01$; significant
Right ventricular +dP/dt (group 1 vs group 2)	$p > 0.05$; not significant
Right ventricular -dP/dt (group 1 vs group 2)	$p > 0.05$; not significant

5. ANATOMICAL ANIMAL COMPARISONS OF THE PERICARDIUM

The pericardium is fixed to the great arteries at the base of the heart and is attached to the sternum and diaphragm in all mammals, although the degree of these attachments to the diaphragm varies between and within species *(25,26)*. Specifically, the attachment to the central tendinous aponeurosis of the diaphragm is firm and broad in humans and pigs, the phrenopericardial ligament is the only attachment in dogs, and the caudal portion of the pericardium is attached via the strong sternopericardial ligament in sheep *(25,26)*.

Although the basic structure of the pericardium is the same, differences exist between various species with respect to both geometry and structure *(27–29)*. Generally, pericardial wall thickness usually increases with increasing heart and cavity size between the various species *(27)*. However, humans are a notable exception to this rule, having a much thicker pericardium than animals with similar heart sizes *(27)*. Specifically, the pericardium of human hearts varies in thickness between 1 and 3.5 mm *(30)*; the average pericardial thickness of various animal species was found to be considerably thinner (ovine hearts 0.32 ± 0.01 mm, porcine hearts 0.20 ± 0.01 mm, and canine hearts 0.19 ± 0.01 mm; *28*). Differences in the volume of pericardial fluid also exist. Holt *(27)* reported that most dogs have between 0.5 and 2.5 mL of pericardial fluid, with some dogs having up to 15 mL, compared to 20–60 mL in adult human cadaver hearts.

6. INTRAPERICARDIAL THERAPEUTICS AND DIAGNOSTICS

With recent advances in minimally invasive cardiac surgical procedures, it is likely that instances and abilities in preserving the integrity of the pericardium during cardiac surgery will increase. The diminished ability of cardiac cells to regenerate under adverse loading conditions impairs the ability to regenerate lost myocardial function, making procedures that reduce myocardial trauma of particular interest. In addition, access into the pericardial space provides a new route for numerous novel treatments and therapies that can be applied directly to the epicardial surface and/or the coronary arteries.

For quite some time, nonsurgical intrapericardial therapy has been employed in patients with sufficient fluid in the pericardial space, allowing a needle to be safely placed within the space *(31)*. This methodology has been used for patients with such clinical indications as, but not limited to, malignancies, recurrent effusions, uremic pericarditis, and/or connective tissue disease. Instrumenting the pericardium has been made possible by numerous techniques that allow for the study of intraperi-cardial therapeutics and diagnostics by clinicians and investigators alike. More specifically, the endoluminal delivery of various agents has been clinically limited because of short residence time, highly variable deposited agent concentration, inconsistency in delivery concentrations, and relatively rapid washout of agent from the target vessel *(32)*. A desired example of targeted application includes infusion of concentrated nitric oxide donors; which could present undesirable effects if systemically delivered. Further, one is allowed increased site specificity and the delivery of label-specific therapeutic agents to target cells, receptors, and channels.

A great deal of interest has been focused on delivery of angiogenic agents and various growth factors into the intraperi-cardial space *(33–35)*. In particular, research has concentrated on administration in patients with ischemic heart disease *(36,37)*. Early results indicated several benefits associated with the delivery of angiogenic agents, including increased collateral vessel development, regional myocardial blood flow, myocardial function in the ischemic region, and myocardial vascularity

6.1. Pericardial Pharmacokinetics

In the healthy human, the pericardium is generally believed to contain 20–25 mL of physiologic fluid (0.25 ± 15 mL/kg) situated within the cavity space *(38)*. Yet, dye studies suggested that pericardial fluid is not uniformly distributed over the myocardium, with the majority of pericardial fluid residing within the atriaventricular and interventricular grooves as well as the superior-transverse sinuses. Although the pericardial fluid is not uniformly distributed, pharmacokinetic studies suggested that there is complete mixing of the fluid so that pericardial fluid content is spatially uniform *(39–41)*. Hence, sampling pericardial fluid content should not vary by sampling location *(40)*.

Tissue distribution and drug clearance clearly affect all drug response. Because specific pericardial pharmacokinetic data remain unknown for the majority of compounds, pericardial drug disposition must be gleaned from physical chemical properties based on a few select studies. Pericardial fluid is cleared via lymphatics and epicardial vasculature, with the former being a very slow process *(42)*. In addition to these passive clearance mechanisms, the epicardial tissues contain metabolic enzymes that may clear compounds via a biotransformation process. This is likely to occur with certain labile peptides and small molecules such as nitric oxide.

Unfortunately, there is very little known today about pericardial drug metabolism. In general, it is considered that whether or not a compound residing in the pericardial space is cleared via lymphatic drainage, passive diffusion or biotransformation will depend on its molecular size, tissue affinity, water solubility, and enzymatic stability. Thus, compounds such as large proteins do not rapidly diffuse into the vascular space and are slowly cleared from the pericardial space, perhaps via lymphatics, unless of course they are biotransformed *(40,43)*. This yields a pericardial fluid clearance and residence time longer than the corresponding plasma half-life. For example, administering atrial natriuretic peptide into the pericardial fluid space had a fivefold longer clearance and residence time within the pericardial fluid space compared to plasma clearance of an intravenous dose *(43)*. Similarly, small water-insoluble compounds may also have very prolonged pericardial fluid residual times.

One case report documented that the pericardial fluid half-life of 5-fluorouracil was approx 10-fold longer than plasma half-life (16 vs 160 min); it should be noted that the patient in this investigation had metastatic breast carcinoma with pericardial involvement *(39)*. The patient had received a relatively large pericardial 5-fluorouracil dose (200 mg) to manage recurrent pericardial effusion. This large dose, however, was associated with nearly undetectable plasma levels, indicating minimal spillover from pericardial fluid into the systemic circulation. Although it was expected that 5-fluorouracil would have a longer pericardial residual time because it is water insoluble, it is unknown if these findings would occur in a healthy pericardial fluid space.

On the other hand, small water-soluble compounds have up to five- to eightfold shorter pericardial fluid clearance and residence times compared to plasma *(41)*. For example, procainamide is a water-soluble compound that has a pericardial fluid half-life ranging from 30 to 41 ± 2 min compared to the 180-min plasma half-life; it has been reported that the procainamide rapidly diffused out of the pericardial space with a terminal elimination half-life approximately five to seven times shorter than plasma *(44)*. However, procainamide spillover from pericardial fluid into plasma was not considered to produce measurable plasma concentrations because of the relatively low pericardial doses (0.5 to 2 mg/kg). Similarly, it is not surprising that the converse was also true, that intravenously administered procainamide rapidly diffused into the pericardial space, across a plasma-to-pericardial fluid concentration gradient, such that pericardial fluid procainamide concentrations were similar to plasma approx 20–30 min following an intravenous injection. The likely explanation for these findings is that the vast ventricular epicardial blood supply served as a clearing system (pericardial administration) or a delivery system (intravenous administration) according to drug concentration diffusion gradient. Importantly, the diffusion of pericardial-administered procainamide into the vascular space will likely prevent drug accumulation in ventricular tissue and a global pharmacological response.

In addition to pericardial drug residence and clearance times, the determination of distribution volume may be considerably important, particularly to achieve desired peak drug concentrations. There is a direct and inverse relationship between peak drug concentrations and drug distribution volumes, such that a low drug distribution volume achieves higher peak concentrations.

Perhaps of clinical importance, with the very small pericardial fluid volume, it is obvious that pericardial drug doses can be substantially reduced to achieve therapeutic concentrations. This was evident when sequential pericardial procainamide doses of 0.5, 1, and 2 mg/kg produced peak pericardial fluid concentrations that ranged from 250 to 900 μg/mL; these concentrations were nearly 1000-fold greater than peak plasma concentrations of procainamide following the administration of a 2-mg/kg intravenous dose. In a follow-up study, in which a single procainamide dose was employed, similar findings were documented; it was also reported that a pericardial fluid volume of distribution of 1.6 ± 0.2 mL/kg was observed, which is approx 1000-fold smaller than plasma procainamide volume of distribution of 2000 mL/kg. Although pericardial procainamide dosing produced very large pericardial fluid concentrations, procainamide could not be detected in the plasma given the very small doses.

With such a powerful diffusion gradient, it is likely that pericardial procainamide delivery can achieve very high atrial tissue concentrations. Indirect evidence of tissue distribution is a procainamide distribution volume that is larger (40–50 mL) than the estimated pericardial fluid volume of 20–30 mL. Because the procainamide pericardial volume of distribution exceeded the expected pericardial volume, there was some tissue distribution. These pharmacodynamic data suggest that tissue distribution mainly occurs in the atrium, likely because the atrium is a very thin structure with a low blood supply. Thus, this tissue architecture is ideal for specialized therapeutic drug diffusion and therefore differs from that of the ventricles.

Unfortunately, most pericardial procainamide pharmacokinetic studies performed to date have not directly measured tissue concentrations following infusion. However, in one study that evaluated the pharmacodynamic effects of pericardial amiodarone delivery, the amiodarone tissue distribution was quantified at several myocardial locations *(45)*. Not surprisingly, it was reported that atrial and epicardial ventricular tissue had the highest amiodarone tissue concentration; ventricular endocardial amiodarone tissue concentrations were approx 10-fold lower. However, importantly, the amiodarone levels were likely still within a therapeutic range. This was supported by the fact that pericardial amiodarone delivery prolonged endocardial ventricular refractory periods by up to 13%, which was equivalent to epicardial ventricular refractory period measurements and the magnitude of atrial refractory period prolongation. The similar refractory response between epicardial and endocardial measurements, with very large differences in amiodarone tissue concentrations, indicates that amiodarone effects are maximal at low tissue concentrations.

Unlike pericardial amiodarone administration, pericardial procainamide had no effect on endocardial ventricular refractory periods *(41)*. It is likely that such a beneficial ventricular tissue distribution does not occur with more water-soluble compounds such as procainamide. On the other hand, it is not surprising that amiodarone, when administered into the peri-

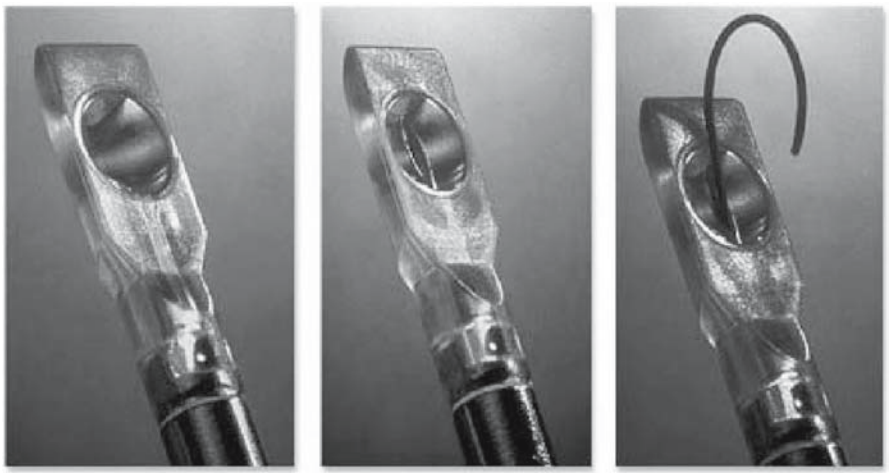

Fig. 4. The PerDUCER instrument uses a sheathed needle with a suction tip designed for grasping the pericardium to access the pericardial space using a transthoracic approach, thus minimizing the risk of myocardial puncture.

cardial space, could penetrate ventricular tissue and affect global ventricular electrophysiology because it is highly lipophilic and has a huge tissue distribution, including the intracellular space *(45)*.

Last, perhaps it is possible to modify molecules to achieve an optimal pericardial fluid residence time and thus their therapeutic outcomes (benefits). More specifically, for some agents, it may be desirable to have a short residence time. For example, pericardial drug delivery to cardiovert atrial fibrillation may require very high drug concentrations for only a brief duration, given the acute nature of the therapy. On the other hand, the ability to manage chronic conditions such as ischemic heart disease or heart failure may necessitate longer pericardial residual times. In this regard, Baek et al. *(46)* showed that a derivitized nitric oxide donor molecule, diazeniumdiolate, with bovine serum albumin resulted in a fivefold increase in pericardial fluid clearance and residence time vs a small molecule nitric oxide donor (diethylene-triamine/nitric oxide). This group went on to show that it may be possible that a single pericardial dose of the nitric oxide donor could inhibit in-stent restenosis. Unlike patients with any type of effusion, the normal pericardium is a very thin layer, bringing it closer to the heart and subsequently increasing the risk of harm to the patient.

6.2. Clinical Pericardial Access

Until recently, safely entering the normal pericardium or pericardial sac with minimal effusion was not realizable. Several unique biomedical devices or tools have been and continue to be developed to aid in accessing pericardial space using novel catheter designs, allowing controlled myocardial penetration during fluoroscopic visualization. Specifically, a technology has been developed that uses a sheathed needle with a suction tip designed for grasping the pericardium and accessing the pericardial space using a transthoracic approach and at the same time minimizing the risk of myocardial puncture; the PerDUCER® instrument (Comedicus, Inc., Columbia Heights, MN) is placed using subxiphoid access into the mediastinum under fluoroscopic guidance, and the apparatus is positioned onto the anterior surface of the pericardial sac (Fig. 4). Manual suction is applied to the side port resulting in a bleb of pericardium being captured. The needle is advanced to puncture the bleb and a guidewire is pushed through the needle into the pericardium. The PerDUCER® is removed and a standard delivery catheter is placed into position.

The ability to access the pericardial space as such has created new opportunities to understand further the role of the pericardium under normal cardiac function and following cardiac disease. Despite the growing literature establishing the feasibility of intrapericardial therapeutics and diagnostics, the results of clinical trials employing pericardially delivered agents directed toward angiogenesis, restenosis, and/or other coronary and myocardial indications are currently lacking.

7. SUMMARY

The pericardium is a unique structure that surrounds the heart and serves several important physiological functional roles. Removal of the pericardium or the buildup of fluids within this space will alter hemodynamic performance. Yet, often following open heart surgery, the pericardium is not repaired or closed; the rationale for this is under evaluation. Therapeutic approaches have been directed to exploit the access space that exists between the pericardium and the epicardial surface of the heart. Nevertheless, an important consideration when utilizing animal models to study such biomedical devices is that the pericardium in humans is much thicker than that of most commonly employed animal models.

COMPANION CD MATERIAL

JPEG 1. Posterior portion of the pericardial sac in a swine from which the heart was removed.

MPEG 1. The effect of removing the pericardium from an isolated swine heart.

REFERENCES

1. Angelini, G.D., Fraser, A.G., Koning, M.M., et al. (1990) Adverse hemodynamic effects and echocardiographic consequences of pericardial closure soon after sternotomy and pericardiotomy. *Circulation*. 82, IV397–IV406.
2. Reich, D.L., Konstadt, S.N., and Thys, D.M. (1990) The pericardium exerts constraint on the right ventricle during cardiac surgery. *Acta Anaesthesiol Scand*. 34, 530–533.
3. Daughters, G.T., Frist, W.H., Alderman, E.L., Derby, G.C., Ingels, N.B., Jr., and Miller, D.C. (1992) Effects of the pericardium on left ventricular diastolic filling and systolic performance early after cardiac operations. *J Thorac Cardiovasc Surg*. 104, 1084–1091.
4. Hammond, H.K., White, F.C., Bhargava, V., and Shabetai, R. (1992) Heart size and maximal cardiac output are limited by the pericardium. *Am J Physiol*. 263, H1675–H1681.
5. Abel, F.L., Mihailescu, L.S., Lader, A.S., and Starr, R.G. (1995) Effects of pericardial pressure on systemic and coronary hemodynamics in dogs. *Am J Physiol*. 268, H1593–H1605.
6. Allard, J.R., Gertz, E.W., Verrier, E.D., Bristow, J.D., and Hoffman, J.I. (1983) Role of the pericardium in the regulation of myocardial blood flow and its distribution in the normal and acutely failing left ventricle of the dog. *Cardiovasc Res*. 17, 595–603.
7. Beloucif, S., Takata, M., Shimada, M., and Robotham, J.L. (1992) Influence of pericardial constraint on atrioventricular interactions. *Am J Physiol*. 263, H125–H134.
8. Calvin, J.E. (1991) Optimal right ventricular filling pressures and the role of pericardial constraint in right ventricular infarction in dogs. *Circulation*. 84, 852–861.
9. Hess, O.M., Bhargava, V., Ross, J., Jr., and Shabetai, R. (1983) The role of the pericardium in interactions between the cardiac chambers. *Am Heart J*. 106, 1377–1383.
10. Janicki, J.S. and Weber, K.T. (1980) The pericardium and ventricular interaction, distensibility, and function. *Am J Physiol*. 238, H494–H503.
11. Shabetai, R., Mangiardi, L., Bhargava, V., Ross, J., Jr., and Higgins, C.B. (1979) The pericardium and cardiac function. *Prog Cardiovasc Dis*. 22, 107–134.
12. Belenkie, I., Dani, R., Smith, E.R., and Tyberg, J.V. (1992) The importance of pericardial constraint in experimental pulmonary embolism and volume loading. *Am Heart J*. 123, 733–742
13. Watkins, M.W. and LeWinter, M.M. (1993) Physiologic role of the normal pericardium. *Ann Rev Med*. 44, 171–180.
14. Janicki, J.S. (1990) Influence of the pericardium and ventricular interdependence on left ventricular diastolic and systolic function in patients with heart failure. *Circulation*. 81, III15–III20.
15. Weber, K.T., Janicki, J.S., Shroff, S., and Fishman, A.P. (1981) Contractile mechanics and interaction of the right and left ventricles. *Am J Cardiol*. 47, 686–695.
16. Kingma, I., Smiseth, O.A., Frais, M.A., Smith, E.R., and Tyberg, J.V. (1987) Left ventricular external constraint: relationship between pericardial, pleural and esophageal pressures during positive end-expiratory pressure and volume loading in dogs. *Ann Biomed Eng*. 15, 331–346.
17. Burkhoff, D., de Tombe, P.P., Hunter, W.C., and Kass, D.A. (1991) Contractile strength and mechanical efficiency of left ventricle are enhanced by physiological afterload. *Am J Physiol*. 260, H569–H578.
18. Burger, W., Straube, M., Behne, M., et al. (1995) Role of pericardial constraint for right ventricular function in humans. *Chest*. 107, 46–49.
19. Riddervold, F., Smiseth, O.A., and Myhre, E.S. (1992) Effect of the pericardium on atrial systolic function. *J Appl Physiol*. 73, 1360–1365.
20. Morris, A.L., Rabkin, S.W., Ayotte, B., and Sharma, G.P. (1981) Role of the pericardium and intact chest wall in the hemodynamic response to positive end-expiratory pressure ventilation. *Can J Physiol Pharmacol*. 59, 45–52.
21. Shabetai, R. (1988) Pericardial and cardiac pressure. *Circulation*. 77, 1–5.
22. Chinchoy, E., Soule, C.S., Houlton, A.J., et al. (2000) Isolated four-chamber working swine heart model. *Ann Thorac Surg*. 70, 1607–1614.
23. Mangano, D.T., Van Dyke, D.C., Hickey, R.F., and Ellis, R.J. (1985) Significance of the pericardium in human subjects: effects on left ventricular volume, pressure and ejection. *J Am Coll Cardiol*. 6, 290–295.
24. Mangano, D.T. (1980) The effect of the pericardium on ventricular systolic function in man. *Circulation*. 61, 352–357.
25. Getty, R. (1975) General heart and blood vessels, in *Sisson and Grossman's The Anatomy of the Domestic Animals,* 5th Ed. *(*Getty, R., ed.), Saunders, Philadelphia, PA, pp. 164–175.
26. Michaëlsson, M. and Ho, S.Y. (eds.). (2000) *Congenital Heart Malformations in Mammals: An Illustrated Text*. Imperial College Press, River Edge, NJ.
27. Holt, J.P. (1970) The normal pericardium. *Am J Cardiol*. 26, 455–465.
28. Naimark, W.A., Lee, J.M., Limeback, H., and Cheung, D.T. (1992) Correlation of structure and viscoelastic properties in the pericardia of four mammalian species. *Am J Physiol*. 263, H1095–H1106.
29. Elias, H. and Boyd, L. (1960) Notes on the anatomy, embryology and histology of the pericardium. *J New York Med Coll*. 2, 50–75.
30. Spodick, D.H. (ed.) (1997) *The Pericardium: A Comprehensive Textbook*. Dekker, New York, NY.
31. Spodick, D.H. (1997) Pericardial effusion and hydropericardium without tamponade, in *The Pericardium: A Comprehensive Textbook*. (Spodick, D.H., ed.), Dekker, New York, NY, pp. 126–132.
32. March, K.L. (1996) Methods of local gene delivery to vascular tissue. *Semin Interven Cardiol*. 1, 215–223.
33. Laham, R.J., Rezaee, M., Post, M., Xu, X., and Sellke, F.W. (2003) Intrapericardial administration of basic fibroblast growth factor: myocardial and tissue distribution and comparison with intracoronary and intravenous administration. *Catheter Cardiovasc Interv*. 58, 375–381.
34. Lazarous, D.F., Shou, M., Stiber, J.A., et al. (1997) Pharmacodynamics of basic fibroblast growth factor: route of administration determines myocardial and systemic distribution. *Cardiovasc Res*. 36, 78–85.
35. Tio, R.A., Grandjean, J.G., Suurmeijer, A.J., van Gilst, W.H., van Veldhuisen, D.J., and van Boven, A.J. (2002) Thoracoscopic monitoring for pericardial application of local drug or gene therapy. *Int J Cardiol*. 82, 117–121.
36. Laham, R.J. and Hung, D. (1999) Therapeutic myocardial angiogenesis using percutaneous intrapericardial drug delivery. *Clin Cardiol*. 22, I6–I9.
37. Landau, C., Jacobs, A.K., and Haudenschild, C.C. (1995) Intrapericardial basic fibroblast growth factor induces myocardial angiogenesis in a rabbit model of chronic ischemia. *Am Heart J*. 129, 924–931.
38. Choe, Y.H., Im, J.G., Park, J.H., Han, M.C., and Kim, C.W. (1987) The anatomy of the pericardial space: a study in cadavers and patients. *AJR Am J Roentgenol*. 149, 693–697.
39. Lerner-Tung, M.B., Chang, A.Y., Ong, L.S., and Kreiser, D. (1997) Pharmacokinetics of intrapericardial administration of 5-fluorouracil. *Cancer Chemother Pharmacol*. 40, 318–320.
40. Stoll, H.P., Carlson, K., Keefer, L.K., Hrabie, J.A., and March, K.L. (1999) Pharmacokinetics and consistency of pericardial delivery directed to coronary arteries: direct comparison with endoluminal delivery. *Clin Cardiol*. 22, I10–I16.
41. Ujhelyi, M., Hadsell, K., Euler, D., and Mehra, R. (2002) Intrapericardial therapeutics: a pharmacodynamic and pharmacokinetic comparison between pericardial and intravenous procainamide. *J Cardiovasc Electrophysiol*. 13, 605–611.
42. Hollenberg, M. and Dougherty, J. (1969) Lymph flow and131-I-albumin resorption from pericardial effusions in man. *Am J Cardiol*. 24, 514–522.
43. Szokodi, I., Horkay, F., Kiss, P., et al. (1997) Characterization and stimuli for production of pericardial fluid atrial natriuretic peptide in dogs. *Life Sci*. 61, 1349–1359.
44. Nolan, P.E. (1997) Pharmacokinetics and pharmacodynamics of intravenous agents for ventricular arrhythmias. *Pharmacotherapy*. 17, 65S–75S; discussion 89S–91S.

45. Ayers, G.M., Rho, T.H., Ben-David, J., Besch, H.R., Jr., and Zipes, D.P. (1996) Amiodarone instilled into the canine pericardial sac migrates transmurally to produce electrophysiologic effects and suppress atrial fibrillation. *J Cardiovasc Electrophysiol*. 7, 713–721.

46. Baek, S.H., Hrabie, J.A., Keefer, L.K., et al. (2002) Augmentation of intrapericardial nitric oxide level by a prolonged-release nitric oxide donor reduces luminal narrowing after porcine coronary angioplasty. *Circulation*. 105, 2779–2784.

III PHYSIOLOGY AND ASSESSMENT

8 Cardiac Myocytes

VINCENT A. BARNETT, PhD

CONTENTS

1. GENERAL CELLULAR MORPHOLOGY

All human cells can be considered biological machines surrounded by a membrane bilayer (plasma membrane). The average thickness or diameter of a nonmuscle cell is approx 10–20 μm. The encapsulating membrane is studded with various receptors for hormones or other circulating biochemicals (Fig. 1). The plasma membrane also contains a number of ion-specific pumps and channels. The interior of each cell contains enzymes and organelles specialized to support a wide array of biological functions. Key organelles include the nucleus (contains the genetic blueprint for cellular function), mitochondria (converts various energy sources to adenosine triphosphate, a general energy currency), and the endoplasmic reticulum and the Golgi apparatus (supports protein synthesis) (Fig. 1). Muscle cells are similar in that they use some of these common organelles, but different in that they are specialized to generate force.

2. CARDIAC MUSCLE CELLS

A comparison of an idealized cell to a cardiac muscle cell reveals several distinct specializations (Figs. 1 and 2). The shapes of mammalian cardiac fibers do not conform to a simple geometry, so measurement of their size is not straightforward, and a single measurement of length or width would be inadequate or often misleading. Yet, in general they tend to have a shorter width (10–40 μm) and a longer dimension (~50–200 μm) along the force generation axis. The individual cells sometimes possess branches (Fig. 2). Importantly, most of the internal volume of myocytes is devoted to a cytoskeletal lattice of contractile proteins with a liquid crystalline order that gives rise to a striated appearance under the microscope (Fig. 3). As with other cell types, the membrane bilayer contains a collection of ion channels and pumps and receptor proteins. In addition, the membranes of cardiac muscle cells contain unique proteins designed to connect cardiac myocytes to one another as both mechanical and electrical partners.

The arrangement of the contractile proteins in cardiac muscle cells is similar to that found in skeletal muscle. Yet, skeletal muscle cells tend to be much larger than cardiac cells; they can be centimeters long, with diameters ranging from 20 to 100 μm.

For comparison, the action of skeletal muscles can be voluntary or reflexively controlled (postural) and is thus under direct control of the nervous system. On the other hand, the action of cardiac muscle is involuntary and rhythmic (~80 contractions/min). This rate can be modulated by nervous system input, but it does not initiate cardiac contractions. Both muscle types are activated via a calcium-dependent process involving troponin (Tn), a protein that acts as a thin filament-based calcium sensor.

2.1. Myocyte Internal Structure

A closer examination of cardiac myocytes reveals several important structural features. First, similar to skeletal muscle, the contractile proteins are organized into *sarcomeres* (Fig. 4), which are the contractile functional units, bordered on each end by a protein matrix known as the Z line. The Z lines are primarily composed of the protein a-actinin. Within each sarcomere, there is an interdigitating lattice of thick and thin protein fila-

From: *Handbook of Cardiac Anatomy, Physiology, and Devices*
Edited by: P. A. Iaizzo © Humana Press Inc., Totowa, NJ

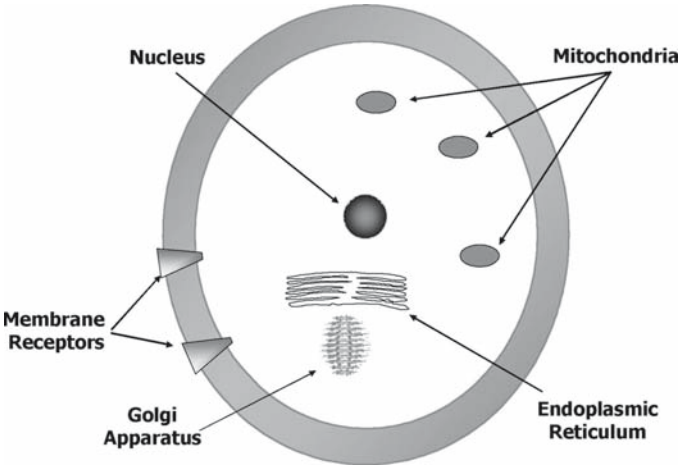

Fig. 1. General cellular morphology. This "typical cell" is a fluid-filled membrane vesicle. The membrane contains receptors and ion channels that act as "gatekeeper" molecules controlling the response of the cell to the external environment. The interior of the cell contains specialized organelles integral to the cell's function.

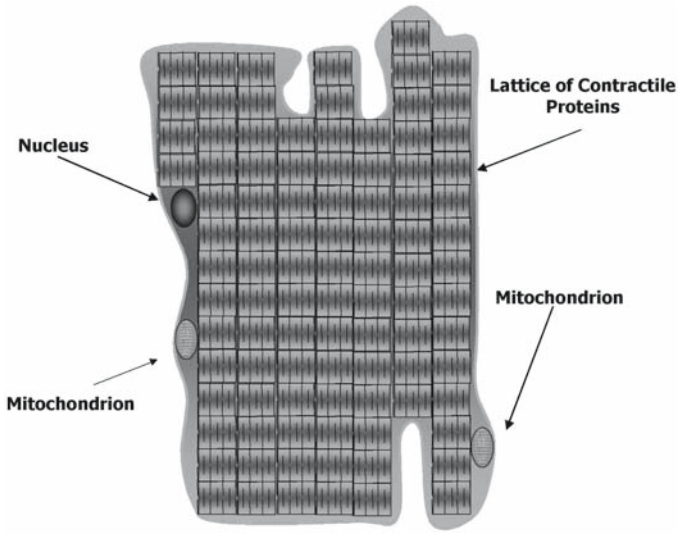

Fig. 2. Elements of cardiac cell morphology. The contractile proteins form a lattice that gives cardiac cells their distinctive appearance. The high concentration of contractile proteins relegates the nucleus, mitochondria, and other organelles to the periphery of the cell.

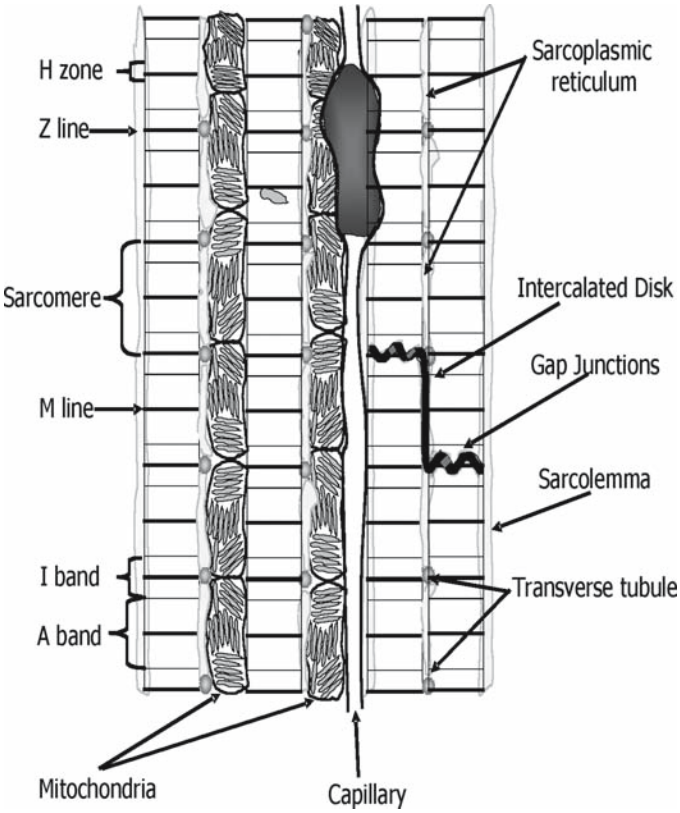

Fig. 3. Cardiac cell landmarks. This diagram points out key features of the sarcomeric structure within contractile myocardial cells. On the left side, key features of the sarcomeric organization of the contractile proteins are listed. The remaining labels highlight other key elements in cardiac cell structure. Note the intimate relationship between the contractile cells and the coronary blood vessel.

ments. The thin filaments extend from the Z line for about 1 μm toward the center of the sarcomere and are polymeric assemblies of globular subunits of the protein actin. The thick filaments are bipolar assemblies of the protein myosin.

Myosin molecules have long α-helical tails that form the backbone of the thick filaments, and each has two globular head domains. The bipolar nature of these filaments is such that the heads extend from each end of the filaments with a bare zone in the center (Fig. 4). Myosin heads possess the ability to form crossbridges with the actin thin filaments and, upon binding actin, act as the molecular motors responsible for muscle contraction. The region of the sarcomere in which the myosin filaments reside is known as the *A band* (Fig. 4). The area between A bands of adjacent sarcomeres is known as the *I band*; this area is bisected by the Z lines and is traversed by actin thin filaments that extend from the Z line toward the center of both sarcomeres (Fig. 4).

2.2. Tropomyosin and Troponin

As noted, the thin filaments are formed from the actin backbone, but they also carry the regulatory proteins tropomyosin (Tm) and Tn (Fig. 5). Tropomyosin is a double-stranded, α-helical, coiled-coil protein that spans seven actin monomers. In contrast, troponin is a globular protein complex with three subunits: (1) TnC, a calcium-binding subunit; (2) TnI, a subunit that inhibits muscle contraction; and (3) TnT, a subunit that connects the troponin complex to tropomyosin and actin. Tropomyosin molecules are aligned end to end around the helical coil of the thin filament with one Tn complex attached to each Tm molecule.

In relaxed muscle, tropomyosin binds to actin in such a way that it impedes the binding of the myosin heads to actin-binding sites. However, on muscle activation and the subsequent increase in myoplasmic calcium concentrations, free calcium binds to troponin, inducing a conformational change that is

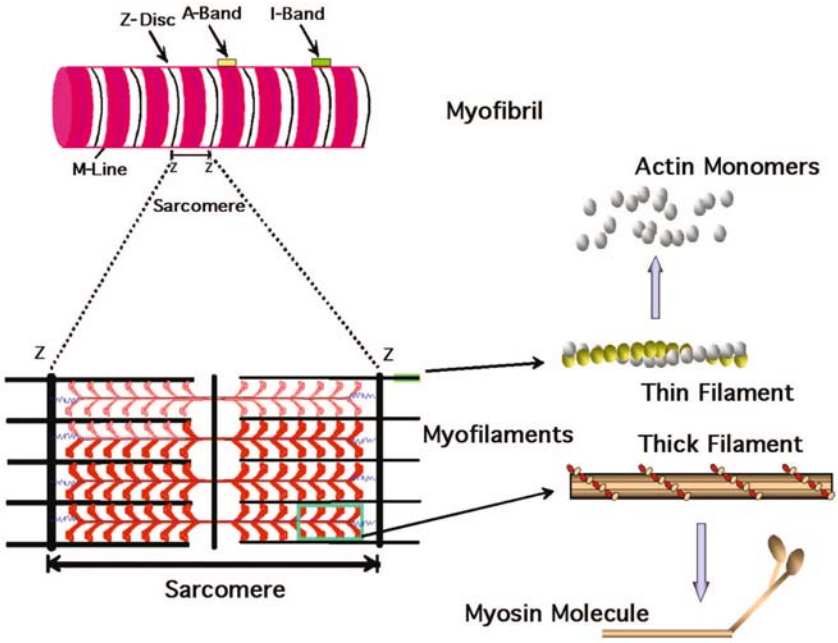

Fig. 4. Protein components of the contractile machinery. Each cardiac myocyte contains bundles of myofibrils that run the length of the cell. Myofibrils are a serial array of contractile units called sarcomeres. Within the sarcomeres, actin and myosin are arranged in filaments with interaction that is the molecular basis of muscle contraction.

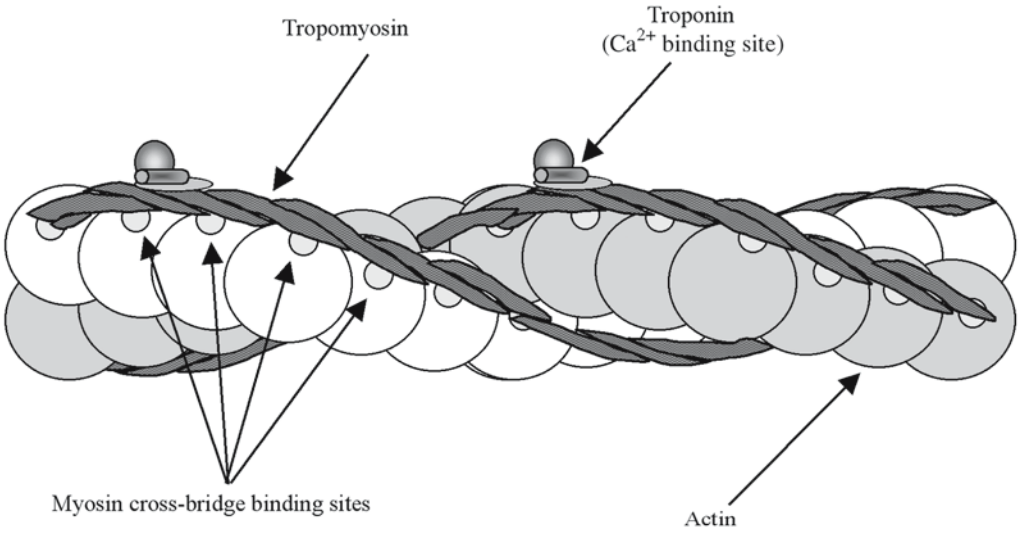

Fig. 5. Calcium regulation of contraction. The regulatory proteins troponin and tropomyosin regulate contraction by blocking the myosin-binding sites on actin in the absence of calcium. Calcium binding to troponin induces tropomyosin movement, allowing actomyosin force generation.

transmitted to tropomyosin; it shifts its position on the actin thin filament to reveal the site on actin required for strong myosin binding. Myosin can then bind to the thin filament in a manner conducive to force production. This association of tropomyosin with troponin over seven actin monomers represents the de facto regulatory unit along the thin filament.

3. FORCE PRODUCTION

In general, force production occurs as follows. First, during muscle relaxation, myosin can bind adenosine triphosphate (ATP) and hydrolyze it, but cannot use the energy released during hydrolysis to make force (Fig. 6) because of the inhibition of its binding to the thin filament by Tm and Tn. Next, after calcium binding to troponin has released the inhibition of the Tm–Tn complex on the thin filament, an energized myosin crossbridge can attach to the thin filament. This association with actin catalyzes the release of the products of hydrolysis (adenosine 5′-diphosphate [ADP] and inorganic phosphate [P_i]), and a concomitant conformational change of myosin head occurs while it is bound to actin (Fig. 6).

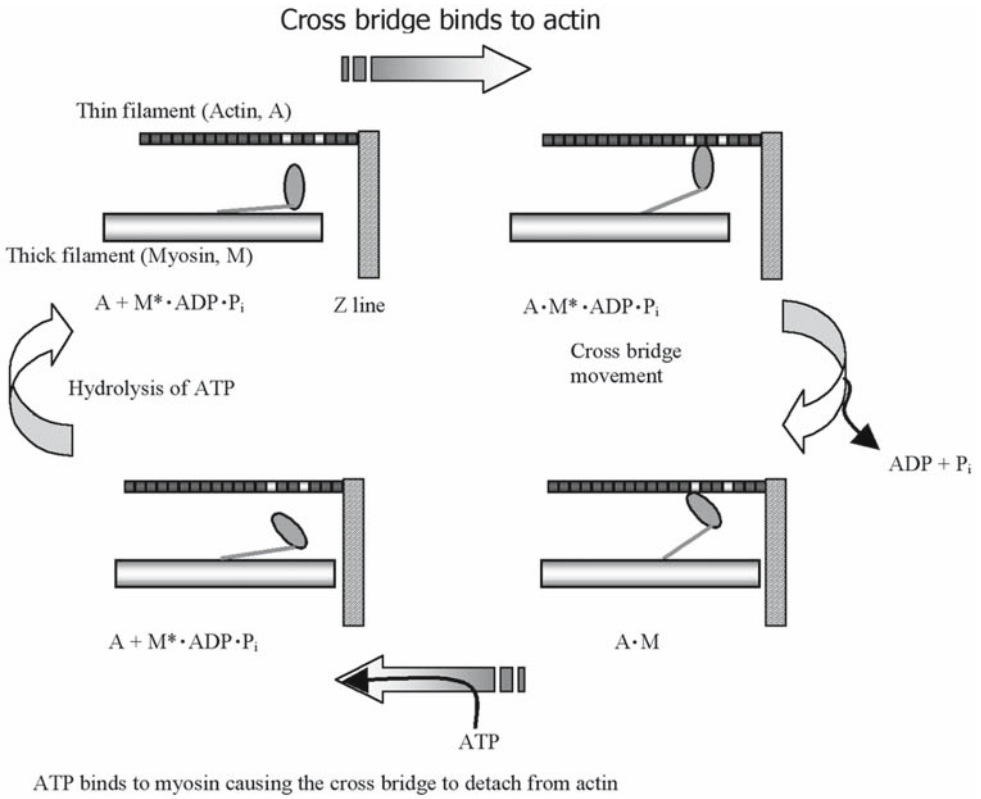

Fig. 6. Force generation cycle. *See* text for details. ADP, adenosine 5′-diphosphate; ATP, adenosine triphosphate; P_i, inorganic phosphate.

This conformational change pulls the actin thin filament past the thick filament. Once this is completed, myosin can rebind ATP, which reduces the affinity of myosin for actin and allows for crossbridge detachment. The subsequent hydrolysis of ATP in turn reenergizes the myosin crossbridge and prepares it for the next force-generating cycle. As long as the calcium concentration is high enough to keep the Tm–Tn complexes from blocking the myosin-binding sites on actin, the cycle continues.

It is important to remember that there is a direct connection between the overlap of the thick and thin filaments and the resultant force output developed by cardiac muscle cells. Sarcomere length is defined as the distance from Z line to Z line. In general, when this distance is approx 2.2 μm, maximal isometric force can be elicited (Fig. 7). If the myocyte is shortened from this length at rest, subsequent force generation decreases because of filament disorder that occurs in overly shortened sarcomeres. In contrast, if the myocyte is stretched, force decreases because of the decrease in overlap of the thick and thin filaments (i.e., a reduced potential for possible crossbridge formations) (Fig. 7). Rest length therefore tends to be slightly shorter than the length at which maximal force is produced. This association between myocyte length and the amount of force that can be generated is known as the *length–tension relationship*, which underlies the recruitable potential for times when increased contraction force is necessary.

The length of cardiac cells or myocytes is controlled in vivo through their shortening during systole and their stretching during diastole (Fig. 8). That the set point of the length–tension relationship can be tuned in this manner is, in part, the mechanical underpinning for Starling's law of the heart (e.g., stroke volume increases as cardiac filling increases).If cardiac filling adjusts the sarcomere length to a point closer to the plateau of the length–tension relationship (Fig. 7), this length change produces an alignment of the contractile proteins that can then result in greater force production during the next systole. It then also follows that the increased force that can occur during the isovolumic (isometric) phase of systole will result in a greater stroke volume.

4. CARDIAC MUSCLE ELECTRICAL ACTIVITY

Sarcomeres are linked end to end into assemblies known as myofibrils, which run the length of the long axis of the cardiac cell and are also placed side to side to fill most of the internal volume of the cell. The nucleus of a mature cardiac cell is found on the periphery of the cell along with the sarcoplasmic reticulum. The sarcoplasmic reticulum is a vesicular structure that acts as an internal calcium-store and is an analog of the endoplasmic reticulum of other cells.

Cardiac cells are connected and communicate with one another by junctions of two types. First, intercalated disks form strong mechanical bonds between myocytes that allow force to be transmitted across the myocardium. These structures are formed by the protein–protein associations at the membrane surface of the neighboring cells. Second, gap junctions form electrical connections between cardiac cells.

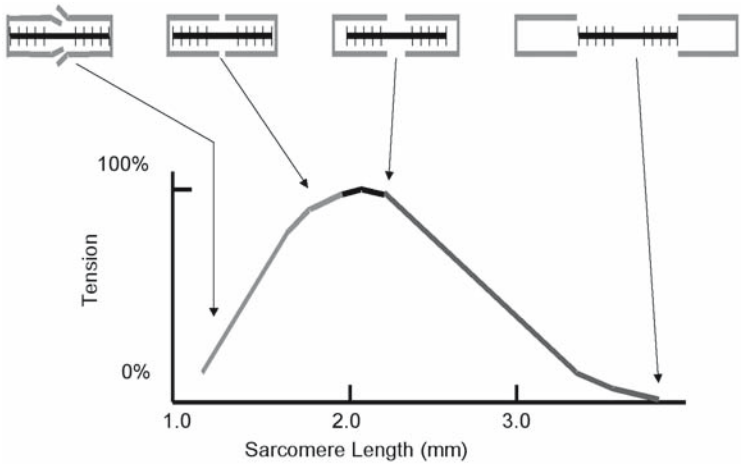

Fig. 7. Length–tension relationship. Isometric force is, in part, determined by the overlap of the thick and thin filaments. At short sarcomere lengths, the contractile proteins are too crowded to work optimally. At long sarcomere lengths, there is a progressive reduction in the overlap of the thick and thin filaments. Optimal overlap of the thick and thin filaments results in maximal isometric force output.

Proteins known as connexins form six-member hemi-channels called connexons on the surface of cardiac cells; connexons on the surface of adjacent cardiac cells dock with one another to form gap junctions. The opening of gap junctions provides for direct electrical and chemical communication between the cytoplasmic space of the adjoining cells. Most importantly, activation signals are passed through gap junctions from cell to cell in cardiac tissue. The electrical communication, provided by gap junctions, facilitates the seemingly simultaneous coordinated contractions of cardiac muscle (Fig. 10, p. 118). For more details, refer to Chapter 9. Note that intercalated discs connect ends of muscle cells to one another and enable frequent branching of myocardial cells at points of anastomosis; also note the separation of fiber paths by capillaries. With this arrangement of fibers, lateral shifting and interdigitation of cells is facilitated. However, longitudinal shifting of cells relative to one another is practically impossible (Fig. 11, p. 118).

The electrical activity of cardiac muscle cells is fundamental to normal function and takes advantage of the properties of the cell membrane to pass charged species selectively from inside to outside and vice versa. Most cells build a charge gradient through the action of ion pumps and ion-selective channels. The charge difference across a membrane is known as the resting membrane potential of a cell (Fig. 9). The energy related to discharging this potential is commonly coupled with cellular functions. In excitable cells, transient changes in the electrical potential (action potentials) are used to either communicate or do work. Importantly, in the myocyte, it is required to initiate the process known as *excitation–contraction–coupling*.

The extracellular fluid has an ionic composition similar to that of blood serum and has millimolar free calcium (Table 1). The intracellular concentration of calcium is higher, but at rest much of it is bound to proteins or sequestered in organelles (mitochondria, sarcoplasmic reticulum). Hence, free myoplasmic concentrations are very low (~10^{-7} m*M*) (Fig. 12).

ATP-dependent ion pumps, channel proteins, and ion exchange proteins are all required to maintain the difference in

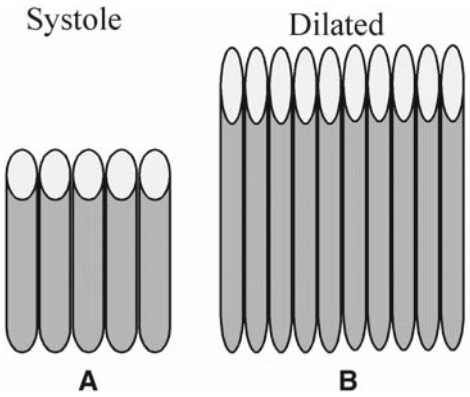

Fig. 8. A schematic illustration of the shape changes in ventricular fiber arrangement during the cardiac cycle is shown.

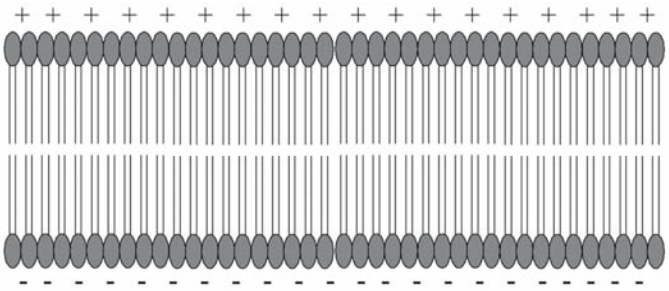

Fig. 9. Ion channels and pumps work to maintain a polarization of ions across the cell membrane. *See* text for details.

ion concentrations. This separation of charged species across a resistive barrier (in this case, the cell membrane) generates an electrical potential E_{ion}. For individual ions, the value of this potential can be calculated using the Nernst equation:

$$E_{ion} = -\frac{RT}{z\mathrm{F}} \ln \frac{[\text{Outside}]}{[\text{Inside}]}$$

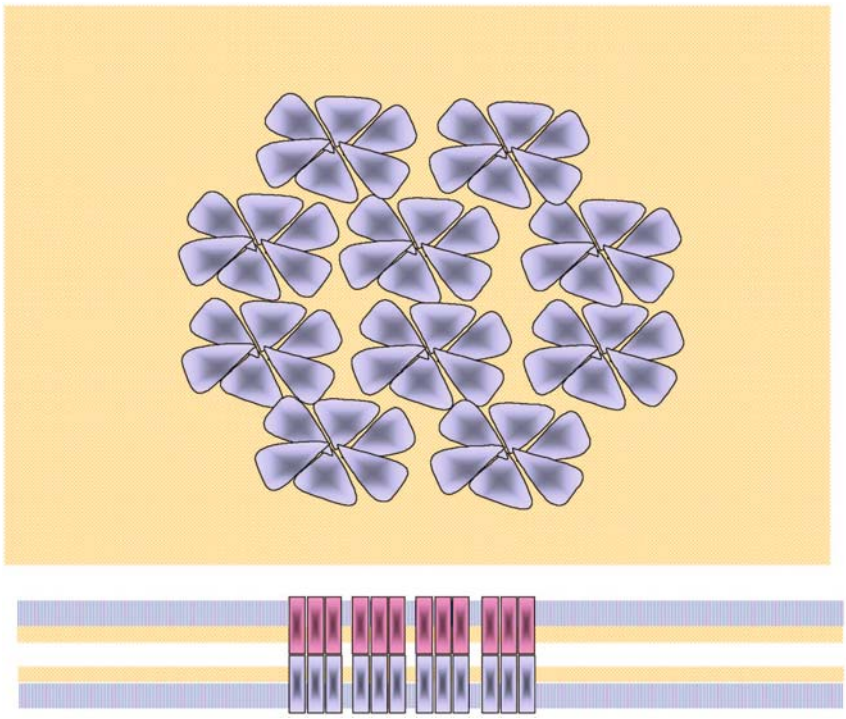

Fig. 10. Gap junctions. **(Above)** Surface of the cell membrane with a plaque of connexons. **(Below)** Gap junction formation by the docking of connexons on adjacent cell membranes.

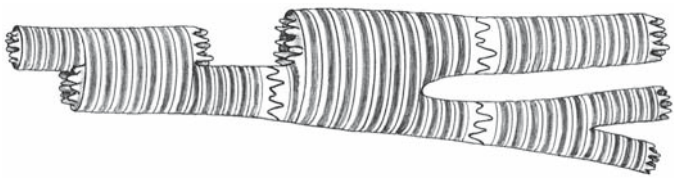

Fig. 11. Geometry of cardiac muscle cells. Cardiac cells often branch and connect to adjacent myocytes. At the intercalated disks between myocytes, gap junctions allow for cell–cell communication, and desmosomes provide mechanical support. *See* text for further details.

where R is the gas constant, T is the temperature (K), z is the valence of the ion (charge and magnitude), and F is the Faraday constant.

In Table 1, the concentrations of the ions (inside and outside) that play a role in the resting membrane potential of cardiac muscle cells are shown with their respective calculated equilibrium potentials. The measured membrane potential of a cardiac muscle cell is approx –90 mV, suggesting that it is primarily determined by either the chloride or potassium distribution. However, measurements of ion movements have shown that chloride is distributed passively across the cell membrane (following positive ion movement) and can therefore be ignored in such a calculation; this leaves potassium as the dominant ion species for control of the myocyte resting membrane potential.

More specifically, the membrane potentials of living cells depend on several other parameters, including the concentrations of ion species on both sides of the membrane as well as their relative permeabilities. To determine the overall membrane potential E_m, the Goldman–Hodgkin–Katz equation takes into account the equilibrium potentials for individual ions and the permeability (conductance) of the membrane for each species such that

$$E_m = \frac{g_{Na}}{g_{tot}} E_{Na} + \frac{g_K}{g_{tot}} E_K + \frac{g_{Ca}}{g_{tot}} E_{Ca}$$

where g_{Na} is the membrane conductance for sodium, g_K is the membrane conductance for potassium, g_{Ca} is the membrane conductance for calcium, g_{tot} is the total membrane conductance, E_{Na} is the equilibrium potential for sodium, E_K is the equilibrium potential for potassium, and E_{Ca} is the equilibrium potential for calcium.

Evaluation of the Goldman–Hodgkin–Katz equation using the values in Table 1 and the conductance values for sodium, potassium, and calcium results in a membrane potential of –90 mV.

As noted, cells can have a variety of ion-selective channels in their membranes. The term *gating* refers to the trigger required for opening such a channel. More specifically, voltage-gated ion channels respond to changes in the local membrane potential of the cell, ligand-gated ion channels respond to specific circulating biochemical factors, spontaneously active ion channels have a random frequency of opening and closing, whereas leak channels seem to be constitutively open, although at a low level. In addition to the aforementioned classification, based on their control mechanisms, channels can also be classified by their ion selectivity or the direction of ion passage that such a channel facilitates (Fig. 13).

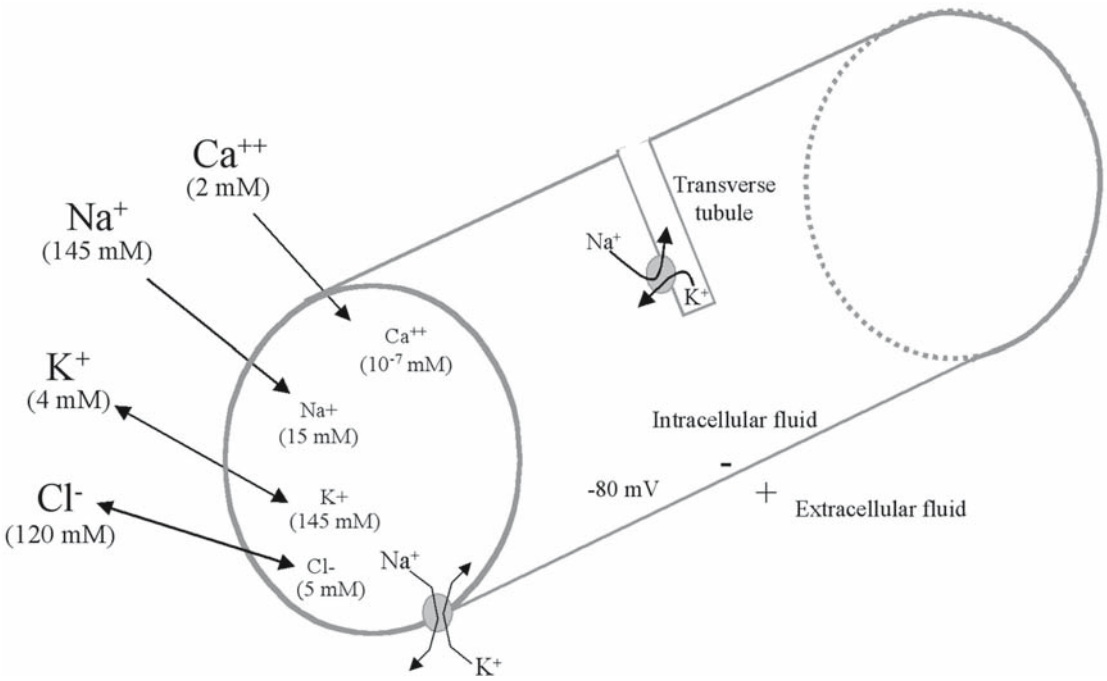

Fig. 12. "Typical" ionic distribution for cardiac cells. *See* text for further details.

Table 1
Internal and External Concentrations of Ion Species Involved in Determination of the Resting Potential of Cardiac Muscle Cells

Ion	[Inside]	[Outside]	Ratio of [Outside]/[Inside]	E_{ion}
Sodium	15 m*M*	145 m*M*	9.7	+60 mV
Potassium	150 m*M*	4 m*M*	0.027	–94 mV
Chloride	5 m*M*	120 m*M*	24 m	–83 mV
Calcium	10^{-7} *M*	2 m*M*	2×10^4	+129 mV

E_{ion}, the equilibrium potential calculated from the Nernst equation.

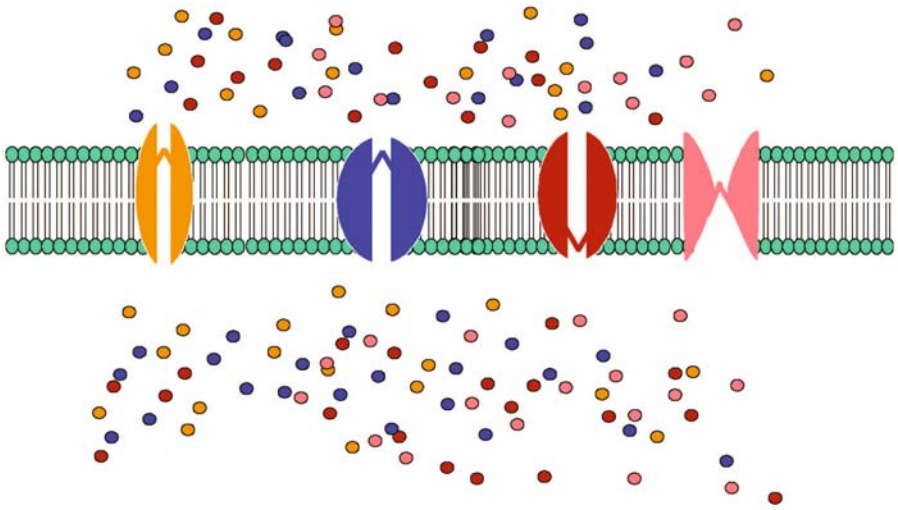

Fig. 13. Channels and the cell membrane. A wide range of channel proteins populates the membranes of cardiac muscle cells.

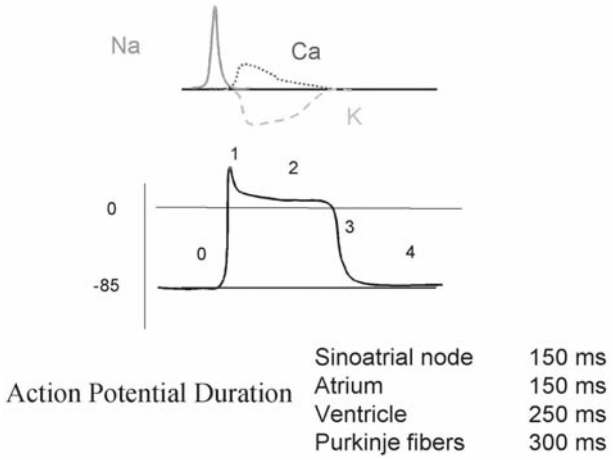

Fig. 14. Ionic conductance changes during the ventricular cardiac action potential. *See* text for details.

4.1 Cardiac Action Potentials

Cardiac action potentials occur because of transient changes in the cellular permeability to sodium, calcium, and potassium. A brief increase in sodium permeability depolarizes the cell and drives the membrane potential toward the sodium equilibrium potential (Fig. 14). This activates voltage-gated calcium and potassium channels. The subsequent opening of calcium channels allows calcium to enter the myocyte and sustains the depolarized state. The opening of the potassium channels allows potassium efflux from the cell and thus drives the membrane potential back toward the potassium equilibrium potential (more negative). The timing of these changes depends on the isoforms of the channel proteins present in each cell, with sinoatrial and atrial muscle action potentials lasting about 150 ms, ventricular muscle about 250 ms, and Purkinje fibers about 300 ms (*see also* Chapter 9). The primary difference between these cell types is often the duration of the plateau phase (phase 2), which is primarily a response to calcium channels (Fig. 15).

Fast-response cardiac cells, such as those of atrial and ventricular muscle and the Purkinje fibers, have an extremely rapid phase 0 or transition from the resting membrane potential to depolarization. As the sodium channels begin to close, an initial repolarization occurs that is labeled phase 1 . The opening of the L-type calcium channels and voltage-gated potassium channels results in a calcium influx that balances the potassium efflux. This results in the positive plateau (phase 2) of the fast-response action potential profile. As the calcium channels close, the potassium channels begin to dominate, and full repolarization of the cells occurs. From the initiation of the action potential through approximately half of the repolarization, the cell is refractory, meaning that it cannot respond to a new depolarization signal.

4.2. Pacemaker Cells

Slow-response cardiac cells, like sinoatrial and atrioventricular nodal cells, have what are considered unstable resting potentials; a gradual rise in their resting potentials crosses the threshold for opening of T-type calcium channels. The movement of calcium into the cells (phase 0) initiates depolarization. No initial repolarization or plateau occurs, so phases 1 and 2 are said to be absent. Repolarization (phase 3) is accomplished through the opening of voltage-gated potassium channels. Once the cell is repolarized (phase 4), leak channels (often attributed to slow sodium channels) contribute to instability of the resting potential and a gradual rise to the threshold value of the T-type calcium channels (Fig. 15).

The sinoatrial node is a specialized collection of cardiac myocytes in the right atrium that acts as the intrinsic cardiac pacemaker. The unstable resting potentials of the sinoatrial nodal cells lead to spontaneous depolarizations with a relatively rapid and regular repeat (i.e., more rapid than all other myocytes). The rapid pace of the depolarizations of the sinoatrial node contol cardiac activation through the principle of overdrive suppression. This principle states that the myocytes with the most rapid frequency of depolarization control the overall rhythm of the heart.The action potential of the sinoatrial node is sometimes referred to as a "slow response" because the upstroke of the depolarization is slower than that of the nonnodal cardiac cells that provide the contractile force during atrial or ventricular contraction. However, the rapid repeat of this depolarization gives the sinoatrial node overall control of the heart rate. The atrioventricular node works similarly but has a slower rate and is normally under the control of the sinoatrial node. In the event of damage to the sinoatrial node, the atrioventricular node assures ventricular contractions at its native (slower) rate. For additional details on cardiac action potential, *see* Chapter 9.

Excitation–contraction–coupling in cardiac muscle can be considered to begin with the depolarization of the sinoatrial node; this excitation quickly passes via gap junctions from cell to cell (Fig. 16). In contractile cardiac myocytes, this depolarization opens the voltage-gated sodium channels, which ultimately triggers the opening of the voltage-gated calcium channels. The opening of these channels results in increases of the myoplasmic calcium concentration, which in turn triggers calcium release from the sarcoplasmic reticulum; this last process is called *calcium-induced calcium release*. As noted in Section 2.2, the calcium binds to TnC on the thin filaments, causing conformational changes of this protein and then inducing the movement of Tm away from the myosin-binding site on actin. Myosin is then free to bind to actin and generate force.

Relaxation requires reduction of the internal calcium concentration. ATP-dependent calcium pumps in the sarcoplasmic reticulum resequester calcium into the lumen of this vesicular system. In myocytes, calcium pumps in the plasma membrane also help reduce cytosolic calcium by pumping calcium into the extracellular space. Furthermore, the sodium–calcium exchanger moves one calcium ion out of the cell at the expense of bringing in three sodium ions. The balance of sodium and potassium is restored through the action of the ATP-dependent Na/K-ATPase (adenosine triphosphatase). The use of these ion motive pumps reveals an important energetic consideration: For cardiac myocytes, both the contraction and relaxation of the cells require ATP.

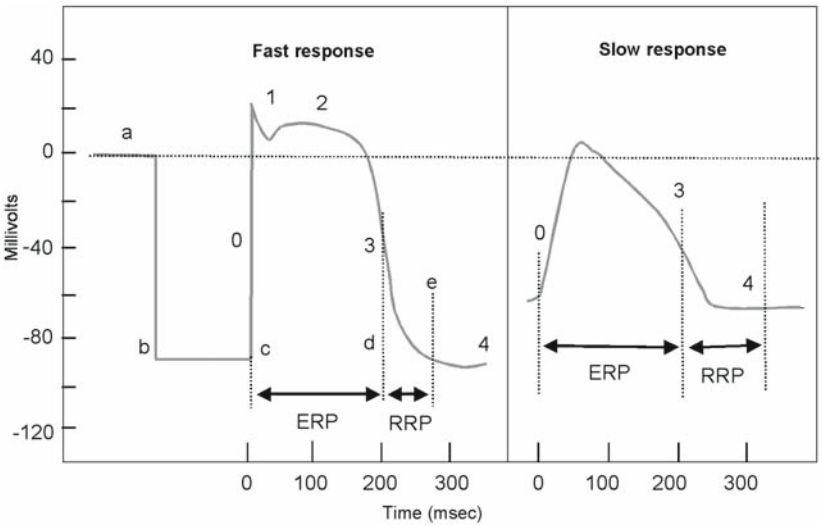

Fig. 15. Phases of the cardiac action potential. Phase 0, upstroke; phase 1, initial repolarization; phase 2, plateau; phase 3, repolarization; phase 4, resting membrane potential. ERP, effective refractory period; RRP, relative refractory period. *See* text for further details.

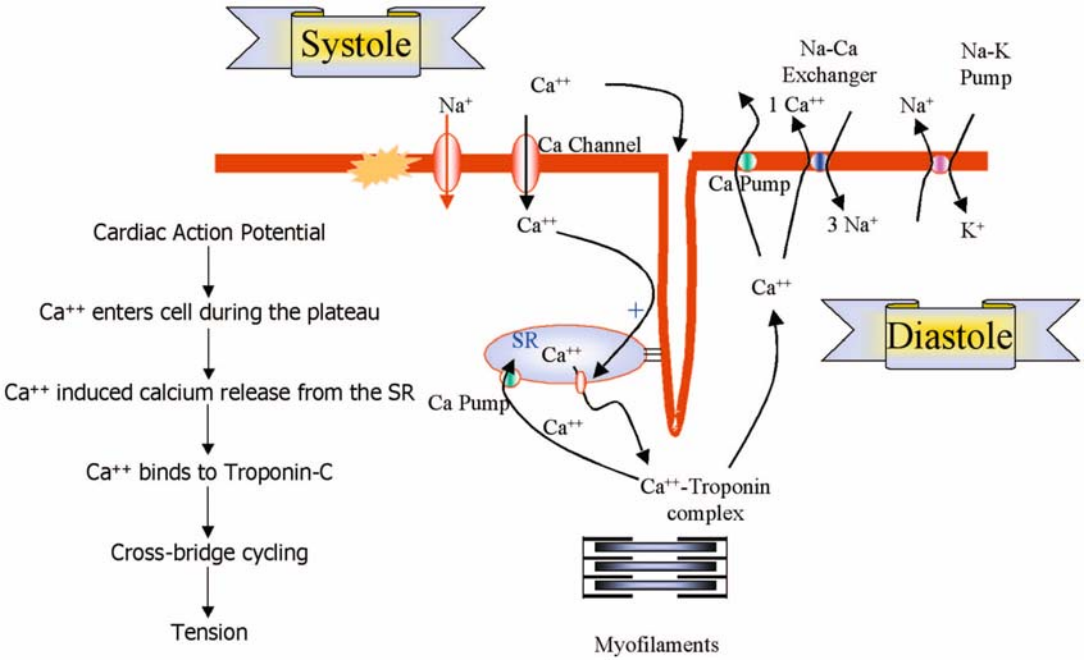

Fig. 16. Excitation–contraction–coupling in cardiac myocytes. The cascade of events that follow a cardiac action potential resulting in cellular contraction followed by relaxation. *See* text for details.

5. SUMMARY

In this chapter, the major cellular features and intracellular structures responsible for cell-to-cell cardiac communication and cardiac contractility were reviewed. In subsequent chapters, information is provided that builds on these details to gain a more complete understanding of cardiac physiology and pathophysiology.

SOURCES

Berne, R.M. and Levy, M.N. (eds.) (1997) *Cardiovascular Physiology,* 7th Ed. Mosby, St. Louis, MO (Chapter 2, Electrical Activity of the Heart, pp. 7–54; Chapter 3, The Cardiac Pump, pp. 55–82).

Berne, R.M. and Levy, M.N. (eds.) (1998) *Physiology,* 4th Ed. Mosby, St. Louis, MO (Chapter 23, The Cardiac Pump, pp. 360–378).

Costanzo, L.S. (1998) *Physiology*. Saunders, Philadelphia, PA (Chapter 4, Cardiovascular Physiology, pp. 99–162).

Germann, W. and Stanfield, C. (eds.) (2002) *Principles of Human Physiology*. Benjamin Cummings, San Francisco, CA (Chapter 12, The Cardiovascular System: Cardiac Function, pp. 369–402).

Mohrman, D.E. and Heller, L.J. (eds.) (2003) *Cardiovascular Physiology,* 5th Ed. Chapter 2, Characteristics of Cardiac Muscle Cells, McGraw-Hill, New York, NY, pp. 19–46.

Rhoades, R.A. and Tanner, G.A. (eds.) (1995) *Medical Physiology*. Little, Brown, Boston, MA (Chapter 10, Cardiac Muscle, pp. 193–206).

Vander,A., Sherman, J., and Luciano,D. (2001) *Human Physiology: The Mechanisms of Body Function,* 8th Ed. McGraw-Hill, Boston, MA (Chapter 14, Section C: The Heart,pp. 387–406).

9 The Cardiac Conduction System

TIMOTHY G. LASKE, PhD AND PAUL A. IAIZZO, PhD

CONTENTS

1. INTRODUCTION

Orderly contractions of the atria and ventricles are regulated by the transmission of electrical impulses that pass through modified cardiac muscle cells (the cardiac conduction system) interposed within the contractile myocardium. This intrinsic conduction system is composed of specialized subpopulations of cells that spontaneously generate electrical activity (pacemaker cells) or preferentially conduct this activity throughout the heart. Following an initiating activation (or depolarization) within the myocardium, this electrical excitation spreads throughout the heart in a rapid and highly coordinated fashion. This system of cells also functionally controls the timing of the transfer of activity between the atrial and ventricular chambers. Interestingly, a common global architecture is present in mammals, with significant interspecies differences existing at the histological level *(1,2)*.

Discoveries relating to the intrinsic conduction system within the heart are relatively recent. Gaskell, an electrophysiologist, coined the phrase *heart block* in 1882, and Johannes E. von Purkinje first described the ventricular conduction system in 1845. Importantly, Gaskell also related the presence of a slow ventricular rate to disassociation with the atria *(3)*. The discovery of the bundle of His is attributed to its namesake, Wilhelm His Jr. *(4)*. He described the presence in the heart of a conduction pathway from the atrioventricular node through the cardiac skeleton; the pathway eventually connected to the ventricles.

Tawara in 1906 verified the existence of the bundle of His *(5)*. Because of the difficulty in distinguishing the atrioventricular nodal tissue from the surrounding tissue, he defined the beginning of the bundle of His as the point at which these specialized atrioventricular nodal cells enter the central fibrous body (which delineates the atria from the ventricles). Tawara is also credited with being the first to identify clearly the specialized conduction tissues (modified myocytes) that span from the atrial septum to the ventricular apex, including the right and left bundle branches and Purkinje fibers.

A thorough understanding of the anatomy and function of the cardiac conduction system is important for those designing cardiovascular devices and procedures. Surgical interventions (heart valve replacements/repair, repair of septal defects, coronary bypass grafting, congenital heart repair, and so forth) are commonly associated with temporary or permanent heart block because of damage to the conduction system or disruption of its

From: *Handbook of Cardiac Anatomy, Physiology, and Devices*
Edited by: P. A. Iaizzo © Humana Press Inc., Totowa, NJ

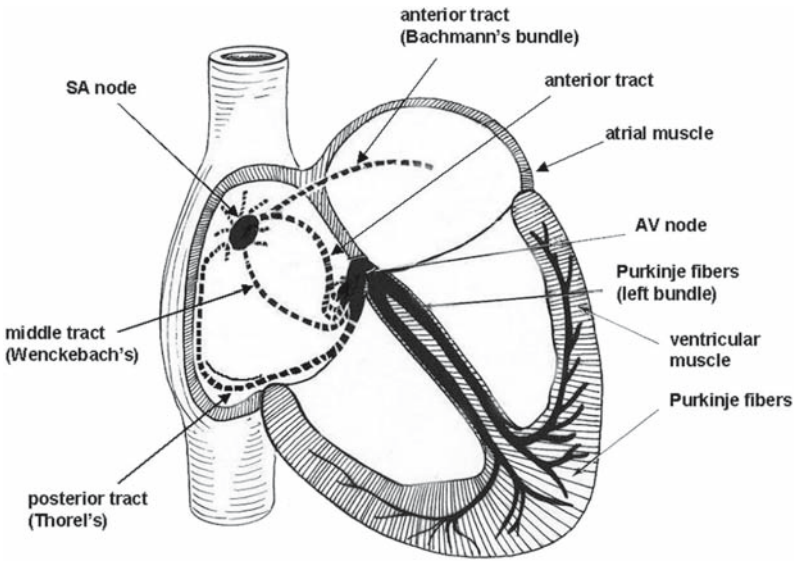

Fig. 1. The conduction system of the heart. Normal excitation originates in the sinoatrial (SA) node, then propagates through both atria (internodal tracts shown as dashed lines). The atrial depolarization spreads to the atrioventricular (AV) node, passes through the bundle of His (not labeled), and then to the Purkinje fibers, which make up the left and right bundle branches; subsequently, all ventricular muscle becomes activated

blood supply *(6–10)*. When designing corrective procedures or devices, the designer needs to consider means to avoid/correct damage to cellular structures of the conduction system. For example, advances in surgical techniques for the repair of ventricular septal defects have reduced the incidence of complete atrioventricular block from 16% in the 1950s to less than 1% currently *(11,12)*. In addition, for those patients with abnormal conduction systems, many rhythm control devices such as pacemakers and defibrillators aim to return the patient to a normal rhythm and contraction sequence *(13–21)*. Research is even investigating repair/replacement of the intrinsic conduction system using gene therapies *(22)*.

A final example illustrating why an understanding of the heart's conduction system is critical to the design of devices and procedures is cardiac ablation systems. These systems purposely modify the heart to: (1) destroy portions of the conduction system (e.g., atrioventricular nodal ablation in patients with permanent atrial fibrillation); (2) eliminate aberrant pathways (e.g., accessory pathway ablation in Wolff–Parkinson–White syndrome); or (3) destroy inappropriate substrate behavior (e.g., ablation of ectopic foci or reentrant pathways in ventricular tachycardias, Cox's Maze ablation for atrial fibrillation, etc.) *(23–26)*.

This chapter provides basic information on the cardiac conduction system to enhance one's foundation for future research and/or reading on this topic. The information in this chapter is not comprehensive and this should not be used to make decisions relating to patient care.

2. CARDIAC CONDUCTION OVERVIEW

The sinoatrial node in the right atrium normally serves as the natural pacemaker for the heart (Fig. 1). These pacemaker cells manifest spontaneous depolarizations and are responsible for generating the cardiac rhythm; such a rhythm would be classified as an intrinsic, automatic one. The frequency of this earliest depolarization is modulated by both sympathetic and parasympathetic efferent innervation. In addition, the nodal rate is modulated by the local perfusion and chemical environment (i.e., neurohormonal, nutritional, oxygenation, and so forth). Although the atrial rhythms normally emanate from the sino-atrial node, variations in the initiation site of atrial depolarization have been documented outside the histological nodal tissues, particularly at high atrial rates *(27–30)*.

The most conspicuous feature of the sinoatrial nodal cells is the poorly developed contractile apparatus (a feature common to all of the myocytes specialized for conduction), comprising only about 50% of the intracellular volume *(31)*. Although it cannot be seen grossly, the general location of the sinoatrial node is on the "roof" of the right atrium at the approximate junction of the superior vena cava, the right atrial appendage, and the sulcus terminalis. In the adult human, the node is approx 1 mm below the epicardium, 10–20 mm long, and up to 5 mm thick *(32)*. For more details on cardiac anatomy, refer to Chapter 4.

After the initial sinoatrial nodal excitation, the depolarization spreads throughout the atria. The exact mechanisms involved in the spread of impulses (excitation) from the sinoatrial node across the atria are controversial. However, it is generally accepted that: (1) the spread of depolarizations from nodal cells can go directly to adjacent myocardial cells, and (2) preferentially ordered myofibril pathways allow this excitation to transverse the right atrium rapidly to both the left atrium and the atrioventricular node.

Three preferential anatomical conduction pathways have been reported from the sinoatrial node to the atrioventricular node (Tawara's node) *(33)*. In general, these are the shortest

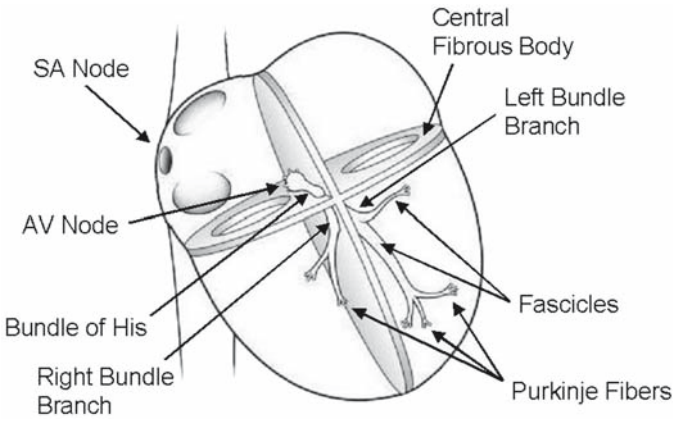

Fig. 2. The conduction system of the heart. Normal excitation originates in the sinoatrial (SA) node, then propagates through both atria. The atrial depolarization spreads to the atrioventricular (AV) node and passes through the bundle of His to the bundle branches/Purkinje fibers.

electrical routes between the nodes. They are microscopically identifiable structures, appearing to be preferentially oriented fibers, that provide a direct node-to-node pathway. In some hearts, pale-staining Purkinje-like fibers have also been reported in these regions (tracts are shown as dashed lines in Fig. 1**;** *see also internodaltracts.jpg* on the Companion CD). The anterior tract extends from the anterior part of the sinoatrial node, bifurcating into the so-called Bachmann's bundle (delivering impulses to the left atrium) and a tract that descends along the interatrial septum and connects to the anterior part of the atrioventricular node.

The middle (or Wenckebach pathway) extends from the superior part of the sinoatrial node, runs posterior to the superior vena cava, then descends within the atrial septum and may join the anterior bundle as it enters the atrioventricular node. The third pathway is the posterior (Thorel) pathway, which generally is considered to extend from the inferior part of the sinoatrial node, passing through the crista terminalis and the eustachian valve past the coronary sinus to enter the posterior portion of the atrioventricular node.

In addition to excitation along these preferential conduction pathways, general excitation is spread from cell to cell throughout the entire atrial myocardium via the specialized connections between cells, the gap junctions (which exist between all myocardial cell types, *see* Section 5).

Toward the end of atrial depolarization, the excitatory signal reaches the atrioventricular node. This excitation reaches these cells via the aforementioned atrial routes, with the final excitation of the atrioventricular node generally described as occurring via the slow or fast pathways. The slow and fast pathways are functionally, and usually anatomically, distinct routes to the atrioventricular node. The slow pathway generally crosses the isthmus between the coronary sinus and the tricuspid annulus and has a longer conduction time, but a shorter effective refractory period than the fast pathway. The fast pathway is commonly a superior route, emanating from the interatrial septum, and has a faster conduction rate, but a longer effective refractory period. Normal conduction during sinus rhythm occurs along the fast pathway, but high heart rates or premature beats often conduct through the slow pathway because the fast pathway may be refractory at these rates.

In general, the atrioventricular node is located in the so-called floor of the right atrium, over the muscular part of the interventricular septum, and inferior to the membranous septum. Following atrioventricular nodal excitation, the depolarization proceeds through to the bundle of His (also referred to as the *common bundle* or *His bundle*). The anatomical region in which the His bundle and the atrioventricular node both reside has been termed the *triangle of Koch*. The triangle is bordered by the coronary sinus, the tricuspid valve annulus along the septal leaflet, and the tendon of Todaro. After leaving the bundle of His, the depolarization spreads to both the left and the right bundle branches. These pathways carry depolarization to the left and right ventricles, respectively. Finally, the signal travels through the remainder of the Purkinje fibers and ventricular myocardial depolarization spreads (*see 7-1.mpg* [the conduction system] on the Companion CD).

In addition to the normal path of ventricular excitation, direct connections to the ventricular myocardium from the atrioventricular node and the penetrating portion of the bundle of His have been described in humans *(34)*. The function and prevalence of these connections, termed *Mahaim fibers*, is poorly understood. An additional aberrant pathway existing between the atria and ventricles has been termed *Kent's bundle* (the clinical manifestation of ventricular tachycardias caused by the presence of this pathway is termed *Wolff–Parkinson–White syndrome*). This accessory pathway is commonly ablated.

Alternate representations of the cardiac conduction system are shown in Figs. 2 and 3, with details of the ventricular portion of the conduction system shown in Fig. 4. More specifically, the left bundle branch splits into fascicles as it travels down the left side of the ventricular septum just below the endocardium (these can be visualized with proper staining). These fascicles extend for a distance of 5–15 mm, fanning out over the left ventricle; about midway to the apex of the left ventricle, the left bundle separates into two major divisions, the anterior and posterior branches (fascicles). These divisions extend to the base of the two papillary muscles and the adjacent myocardium.

In contrast, the right bundle branch continues inferiorly, as if it were a continuation of the bundle of His, traveling along the right side of the muscular interventricular septum. This bundle branch runs proximally just deep to the endocardium, and its course runs slightly inferior to the septal papillary muscle of the tricuspid valve before dividing into fibers that spread throughout the right ventricle. The complex network of conducting fibers that extends from either the right or the left bundle branches is composed of the rapid conduction cells known as *Purkinje fibers*. The Purkinje fibers in both the right and the left ventricles act as preferential conduction pathways to provide rapid activation and coordinate the excitation pattern within the various regions of the ventricular myocardium. As described by Tawara, these fibers travel within the trabeculations of the right and left ventricles and within the myocardium. Because of the tremendous variability in the degree and morphology of the trabeculations existing both within and between species, it is

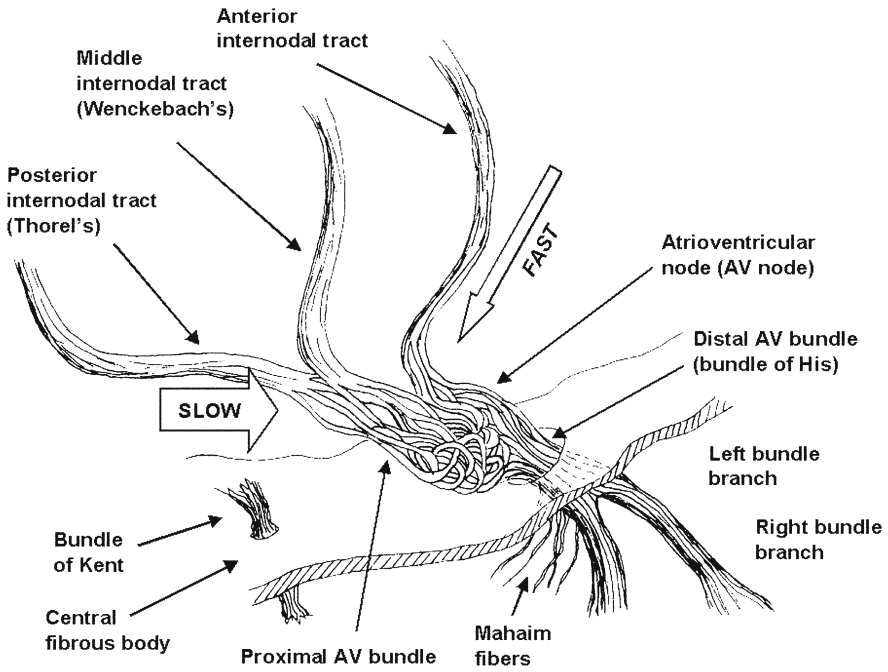

Fig. 3. Details of the atrioventricular nodal region. The so-called slow and fast conduction pathways are indicated by the arrows. To improve clarity in the visualization of the conduction anatomy, the fascicles of the atrioventricular (AV) node are not drawn to scale (their size was increased to allow visualization of the tortuosity of the conduction pathway), and the central fibrous body has been thinned. (T. Laske, 2004)

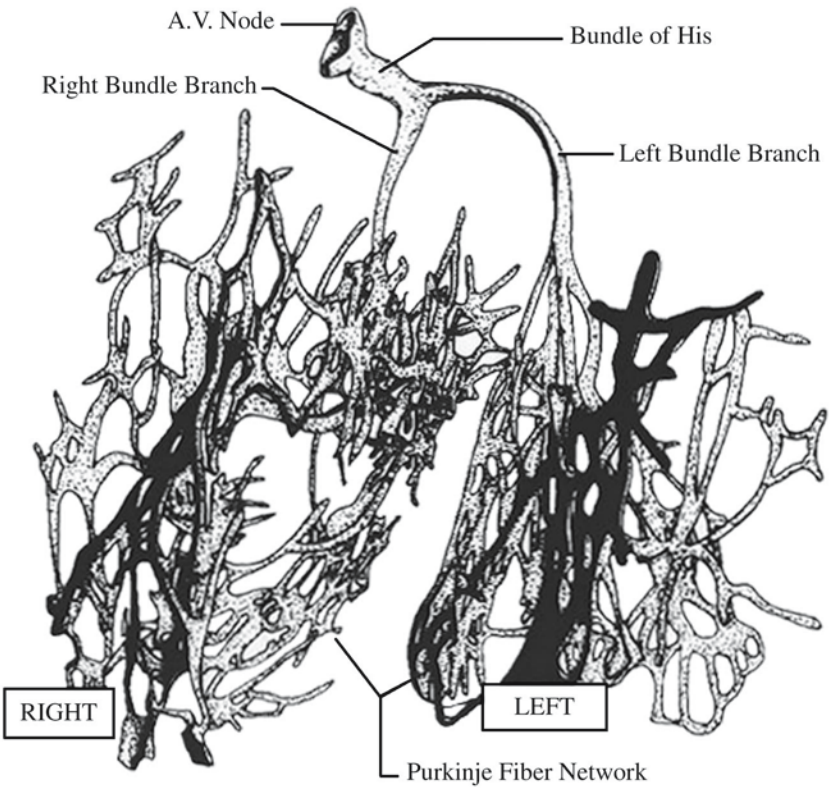

Fig. 4. The ventricular conduction system. The Purkinje network has a high interspecies and intraspecies variation, which likely results in variability in excitation and contractile patterns within the ventricles and may even lead to differences in cardiac fiber architecture. This variability is evident in the dramatic differences seen in the degree and morphology of the cardiac trabeculations (which typically contain these fibers). A.V., atrioventricular. Redrawn from D. L. DeHann, *Circulation*, 1961, 24, 458.

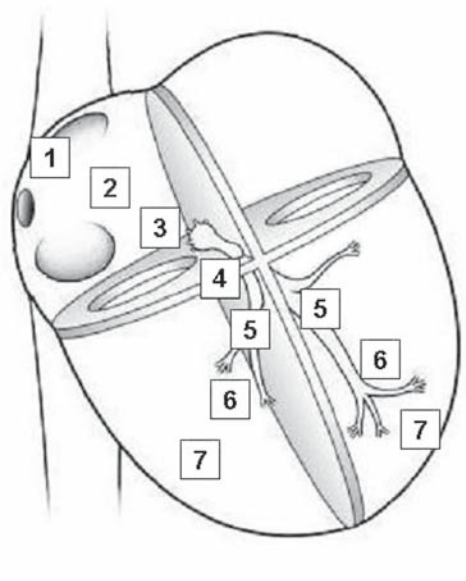

Normal Activation Sequence	Structure	Conduction velocity (m/sec)	Pacemaker rate (beats/min)
1	SA node	< 0.01	60 – 100
2	Atrial myocardium	1.0 – 1.2	None
3	AV node	0.02 – 0.05	40 – 55
4	Bundle of His	1.2 – 2.0	25 – 40
5	Bundle branches	2.0 – 4.0	25 – 40
6	Purkinje network	2.0 – 4.0	25 – 40
7	Ventricular myocardium	0.3 – 1.0	None

Fig. 5. Conduction velocities and intrinsic pacemaker rates of various structures within the cardiac conduction pathway. The structures are listed in the order of activation during a normal cardiac contraction, beginning with the sinoatrial (SA) node. Note that the intrinsic pacemaker rate is slower in structures further along the activation pathway. For example, the atrioventricular (AV) nodal rate is slower than the SA nodal rate. This prevents the AV node from generating a spontaneous rhythm under normal conditions because it remains refractory at rates above 55 beats/min. If the SA node becomes inactive, the AV nodal rate will then determine the ventricular rate. Tabulation adapted from A. M. Katz (ed.), *Physiology of the Heart,* 3rd Ed., 2001.

expected that variations in the left ventricular conduction patterns also exist. It should be noted that one of the most easily recognized conduction pathways commonly found in mammalian hearts is the moderator band, which contains Purkinje fibers from the right bundle branch (*see* Chapter 5).

Three criteria for considering a myocardial cell a "specialized conduction cell" were proposed by Aschoff *(35)* and Monckeberg *(36)* in 1910 and included: (1) histologically discrete features, (2) ability to track cells from section to section, and (3) insulation by fibrous sheaths from the nonspecialized contractile myocardium. It is noteworthy that only the cells within the bundle of His, the left and right bundle branches, and the Purkinje fibers satisfy all three criteria. No structure within the atria meets all three criteria, including Bachmann's bundle, the sinoatrial node, and the atrioventricular node (which are all uninsulated tissues).

3. CARDIAC RATE CONTROL

Under normal physiological conditions, the dominant pacemaker of the heart is the sinoatrial node, which in adults fires at a rate of 60–100 beats per minute, faster than any other region. In a person at rest, modulation by the parasympathetic nervous system is dominant and slows the sinoatrial nodal rate to about 75 action potentials per minute (or beats per minute when contractions are elicited). In addition to the cells of the sinoatrial node, other conduction system cells, specifically those found in the specialized fibers in the atrioventricular junction and His–Purkinje system, are capable of developing spontaneous diastolic depolarization. Rhythms generated by impulse formation within these cells (ectopic pacemakers) range from 25–55 beats per minute in the human heart (Fig. 5). These rhythms are commonly referred to as ventricular escape rhythms. These rhythms are important for patient survival because they maintain some degree of cardiac output when the sinoatrial or atrioventricular nodes are nonfunctional or are functioning inappropriately. These various populations of pacemaker myocytes (sinoatrial and atrioventricular nodal) elicit so-called slow-type action potentials (slow-response action potential; *see* Section 5).

In addition to the normal sources of cardiac rhythms, myocardial tissue can exhibit abnormal self-excitability. Such a site is also called an *ectopic pacemaker* or *ectopic focus*. This pacemaker may operate only occasionally, producing extra beats, or it may induce a new cardiac rhythm for some period of time. Potentiators of ectopic activity include caffeine, nicotine, electrolyte imbalances, hypoxia, or toxic reactions to drugs such as digitalis. For more detail on rate control of the heart, refer to Chapter 10.

4. CARDIAC ACTION POTENTIALS

Although cardiac myocytes branch and interconnect (mechanically via the intercalated disk and electrically via the gap junctions; *see* Section 5), under normal conditions they should be thought to form two separate functional networks: the atria and the ventricles. The atrial and ventricular tissues are separated by the fibrous skeleton of the heart (the central fibrous body). This skeleton is composed of dense connective tissue rings that surround the valves of the heart, fuse with one another, and merge

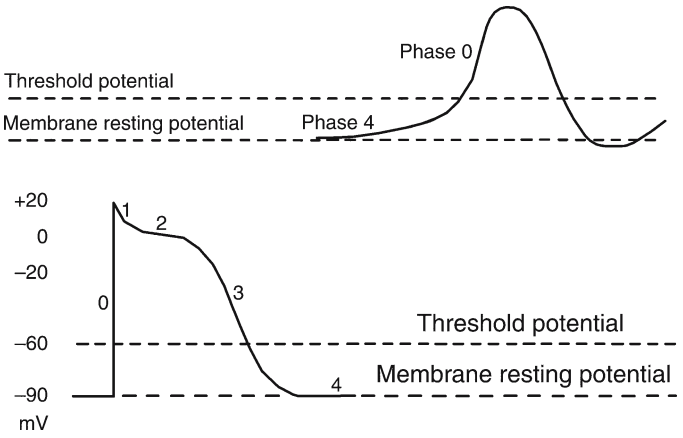

Fig. 6. Typical cardiac action potentials (slow on top and fast below). The resting membrane potential, threshold potential, and phases of depolarization (0–4) are shown.

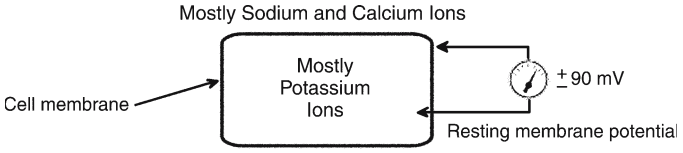

Fig. 7. A cardiac cell at rest. The intracellular space is dominated by potassium ions; the extracellular space has a higher concentration of sodium and calcium ions.

Table 1
Ion Concentrations for Mammalian Myocytes

Ion	*Intracellular concentration (millimolar)*	*Extracellular concentration (millimolar)*
Sodium (Na)	5–34	140
Potassium (K)	104–180	5.4
Chloride (Cl)	4.2	117
Calcium (Ca)		3

Source: Adapted from A.M. Katz (ed.), *Physiology of the Heart,* 3rd Ed., 2001.

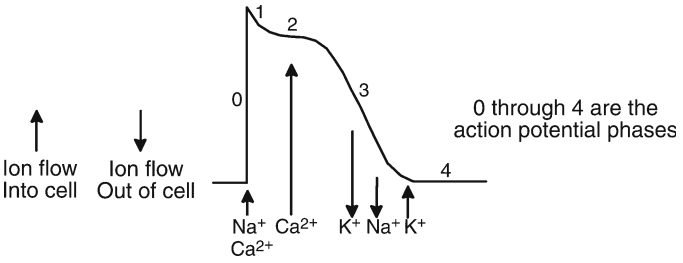

Fig. 8. Ion flow during the phases of a cardiac action potential.

with the interventricular septum. The skeleton can be thought to: (1) form the foundation to which the valves attach; (2) prevent overstretching of the valves; (3) serve as points of insertion for cardiac muscle bundles; and (4) act as an electrical insulator that prevents the direct spread of action potentials from the atria to the ventricles. Refer to Chapter 4 for further details on the cardiac skeleton.

A healthy myocardial cell has a resting membrane potential of approx –90 mV. The resting potential is described by the Goldman-Hodgkin-Katz equation, which takes into account the permeabilities *P*s as well as the intracellular and extracellular concentrations of ions [*X*], where *X* is the ion.

$$V_m = \left(2.3R * T/F\right) * \log_{10} \frac{P_K[K]_o + P_{Na}[Na]_o + P_{Cl}[Cl]_i + \ldots}{P_K[K]_i + P_{Na}[Na]_i + P_{Cl}[Cl]_o + \ldots}$$

In the cardiac myocyte, the membrane potential is dominated by the K^+ equilibrium potential. An action potential is initiated when this resting potential becomes shifted toward a more positive value of approx –60 to –70 mV (Fig. 6). At this threshold potential, the voltage-gated Na^+ channels of the cell open and begin a cascade of events involving other ion channels. In artificial electrical stimulation, this shift of the resting potential and subsequent depolarization is produced by the pacing system. The typical ion concentrations for a mammalian cardiac myocyte are summarized in Table 1 and graphically depicted in Fig. 7.

When a myocyte is brought to a threshold potential, normally via a neighboring cell, voltage-gated fast Na^+ channels actively open (activation gates); the permeability of the sarcolemma (plasma membrane) to sodium ions P_{Na^+} then increases. Because the cytosol is electrically more negative than extracellular fluid and the Na^+ concentration is higher in the extracellular fluid, Na^+ rapidly crosses the cell membrane. Importantly, within a few milliseconds, these fast Na^+ channels automatically inactivate (inactivation gates), and P_{Na^+} decreases.

The membrane depolarization caused by the activation of the Na^+ induces the opening of the voltage-gated slow Ca^{2+} channels located within both the sarcolemma and sarcoplasmic reticulum (internal storage site for Ca^{2+}) membranes. Thus, there is an increase in the Ca^{2+} permeability $P_{Ca^{2+}}$, which allows the concentration to dramatically increase intracellularly (Fig. 8). At the same time, the membrane permeability to K^+ ions decreases because of closing of K^+ channels. For approx 200–250 ms, the membrane potential stays close to 0 mV as a small outflow of K^+ just balances the inflow of Ca^{2+}. After this fairly long delay, voltage-gated K^+ channels open, and repolarization is initiated. The opening of these K^+ channels (increased membrane permeability) allows K^+ to diffuse out of the cell because of their concentration gradient. At this same time, Ca^{2+} channels begin to close, and net charge movement is dominated by the outward flux of the positively charged K^+, restoring the negative resting membrane potential (–90 mV; Figs. 8 and 9).

As mentioned, not all action potentials that are elicited in the cardiac myocardium have the same time-courses; slow- and fast-response cells have different shape action potentials with different electrical properties in each phase. Recall that

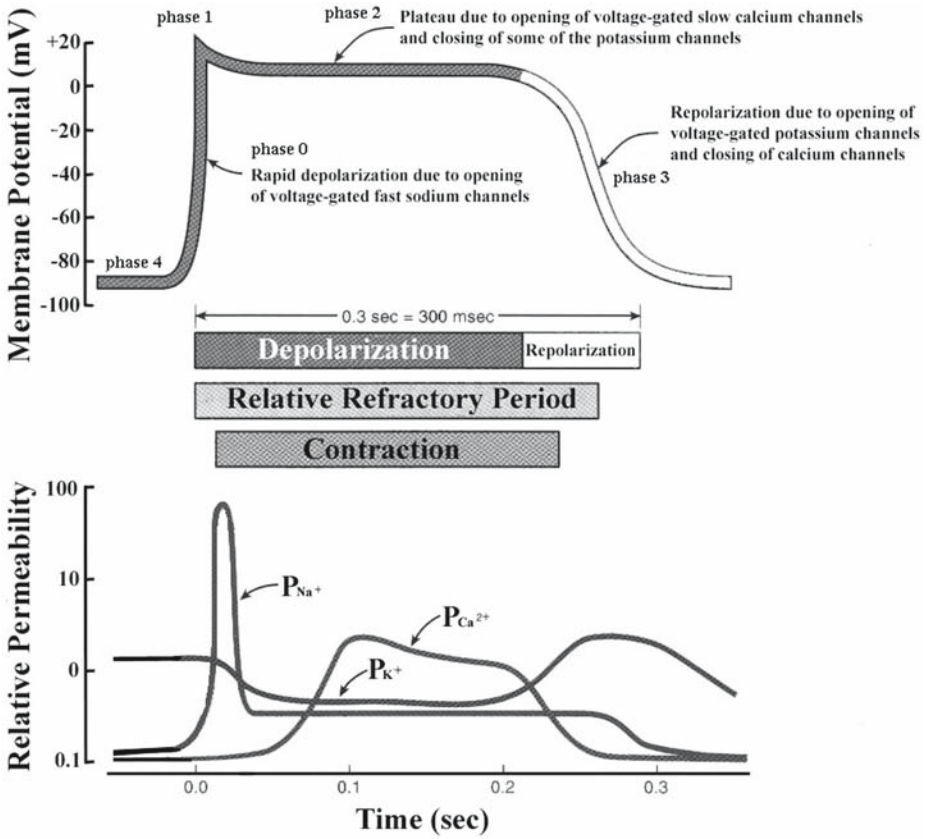

Fig. 9. A typical action potential of a ventricular myocyte and the underlying ion currents. The resting membrane potential is approx –90 mV (phase 4). The rapid depolarization is primarily because of the voltage-gated Na^+ current (phase 0), which results in a relatively sharp peak (phase 1) and transitions into the plateau (phase 2) until repolarization (phase 3). Also indicated are the refractory period and the timing of the ventricular contraction. Modified from G.J. Tortora and S.R. Grabowski (eds.), *Principles of Anatomy and Physiology,* 9th Ed., 2000.

the pacemaker cells (slow-response type) have the ability to depolarize spontaneously until they elicit action potentials.

Action potentials from such cells are also characterized by a slower initial depolarization phase, a lower amplitude overshoot, a shorter and less-stable plateau phase, and a repolarization to an unstable, slowly depolarizing resting potential (Fig. 10). In the pacemaker cells, at least three mechanisms are thought to underlie the slow depolarization that occurs during phase 4 (diastolic interval): (1) a progressive decrease in P_{K^+}; (2) a slight increase in P_{Na^+}; and (3) an increase in $P_{Ca^{2+}}$.

5. GAP JUNCTIONS (CELL-TO-CELL CONDUCTION)

In the heart, cardiac muscle cells (myocytes) are connected end to end by structures known as intercalated disks. These are irregular transverse thickenings of the sarcolemma, within which are desmosomes that hold the cells together and to which the myofibrils are attached. Adjacent to the intercalated disks are the gap junctions, which allow muscle action potentials to spread from one myocyte to the next. More specifically, the disks join the cells together by both mechanical attachment and protein channels. The firm mechanical connections are created between the adjacent cell membranes by

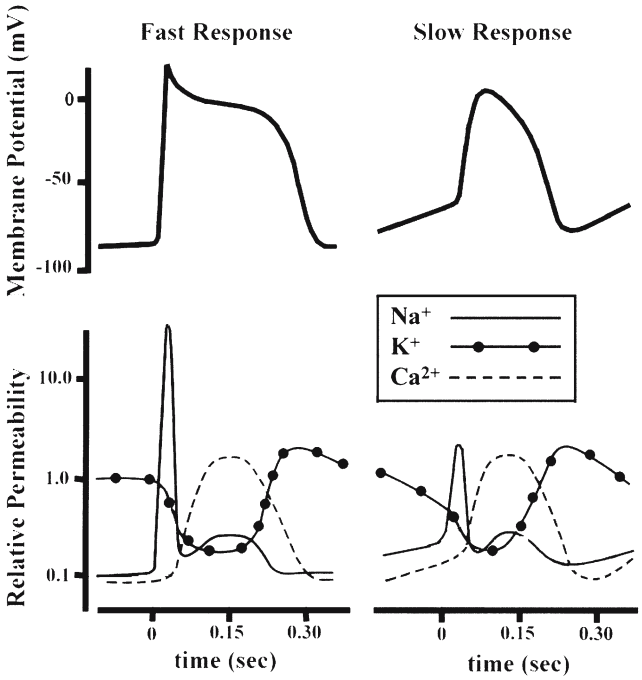

Fig. 10. The comparative time-courses of membrane potentials and ion permeabilities that would typically occur in a fast-response (left; e.g., ventricular myocyte) and a slow-response cell (right; e.g., a nodal myocyte). Modified from D.E. Mohrman and L.J. Heller (eds.), *Cardiovascular Physiology,* 5th Ed., 2003.

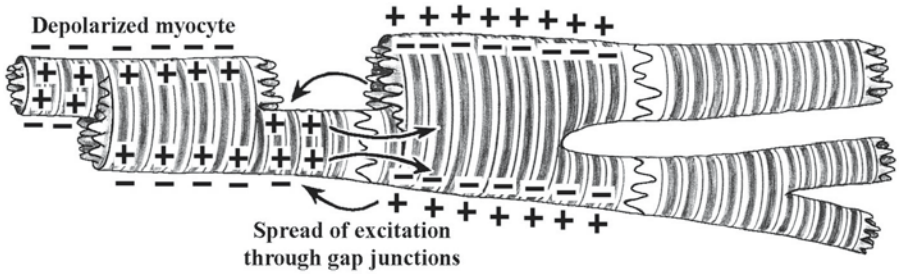

Fig. 11. Shown are several cardiac myocytes in different states of excitation. The depolarization that occurred in the cell on the left causes depolarization of the adjacent cell through cell-to-cell conduction via the gap junctions (nexus). Eventually, all adjoining cells will depolarize. An action potential initiated in any of these cells will be conducted from cell to cell in either direction.

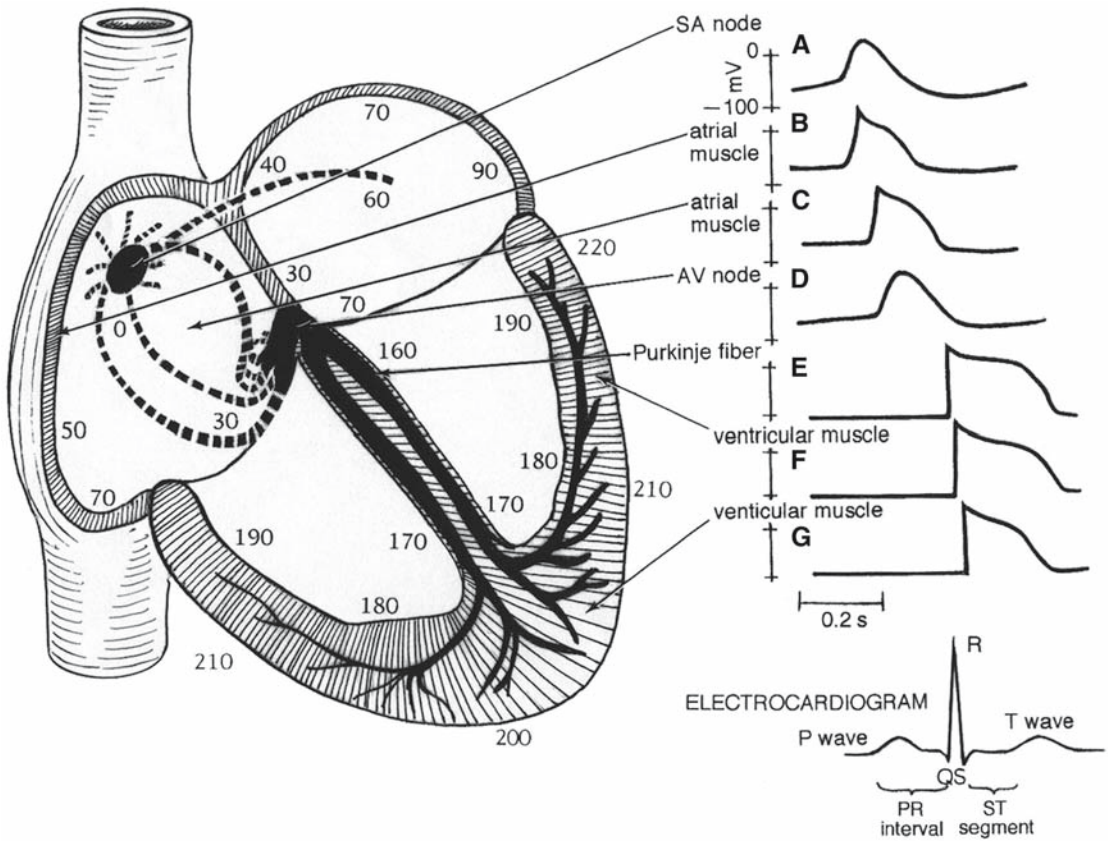

Fig. 12. Shown are the predominant conduction pathways in the heart and the relative time in milliseconds that cells in these various regions become activated following an initial depolarization within the sinoatrial (SA) node. To the right are typical action potential waveforms that would be recorded from myocytes in these specific locations. The SA and atrioventricular (AV) nodal cells have similar shaped action potentials. The nonpacemaker atrial cells elicit action potentials that have shapes somewhat between the slow-response (nodal) and fast-response cells (e.g., ventricular myocytes). The ventricular cells elicit fast-response-type action potentials; however, their durations vary in length. Because of the rapid excitation within the Purkinje fiber system, the initiation of depolarization of the ventricular myocytes occurs within 30 to 40 ms and is recorded as the QRS complex in the electrocardiogram.

proteins called adherins in the desmosome structures. The electrical connections (low-resistance pathways, gap junctions) between the myocytes are via the channels formed by the protein connexin. These channels allow ion movements between cells (Fig. 11).

As noted, not all cells elicit the same types of action potentials, even though excitation is propagated from cell to cell via their interconnections (gap junctions). The action potentials elicited in the sinoatrial nodal cells are of the slow-response type and those in the remainder of the atria have a more rapid depolarization rate (Fig. 12). Although there is a significant temporal displacement in the action potentials elicited by the myocytes of the two nodes (sinoatrial and atrioventricular), their action potential morphologies are similar.

It takes approx 30 ms for excitation to spread between the sinoatrial and atrioventricular nodes, and total atrial activation

occurs over a period of approx 70–90 ms (Fig.12). The speed at which an action potential propagates through a region of cardiac tissue is called the *conduction velocity* (Fig. 5). The conduction velocity varies considerably in the heart and is directly dependent on the diameter of the myocyte. For example, action potential conduction is greatly slowed as it passes through the atrioventricular node. This is because of the small diameter of these nodal cells, the tortuosity of the cellular pathway *(2)*, and the slow rate of rise of their elicited action potentials. This delay is important to allow adequate time for ventricular filling.

Action potentials in the Purkinje fibers are of the fast-response type (Fig. 12); that is, there are rapid depolarization rates that are partly caused by their large diameters. This feature allows the Purkinje system to transfer depolarization to the majority of cells in the ventricular myocardium nearly in unison. Because of the high conduction velocity in these cells that span the myocardium, there is a minimal delay in the time of onset of these cells. It is important to note that the ventricular cells that are last to depolarize have shorter duration action potentials (shorter Ca^{2+} current) and thus are the first to repolarize. The ventricular myocardium repolarizes within the time period represented by the T wave in the electrocardiogram.

6. THE ATRIOVENTRICULAR NODE AND BUNDLE OF HIS: SPECIFIC FEATURES

As mentioned in Section 3, the atrioventricular node and the bundle of His play critical roles in the maintenance and control of ventricular rhythms. In addition, both structures are frequently accessed during cardiac catheterization procedures: (1) as anatomical landmarks, (2) to allow insight into atrial–ventricular conduction behaviors, or (3) to ablate these structures or the surrounding tissues to terminate aberrant behaviors (e.g., reentrant tachycardias) or to prevent atrioventricular conduction in patients with chronic atrial fibrillation. Today, medical device designers have a strong interest to understand the details of the structural and functional properties of the atrioventricular node and the bundle of His for development of new therapies or to avoid inducing complications; hence, in the following section, such details are provided.

The myocytes located within the region of the atrioventricular node and the bundle of His have many unique characteristics. Specifically, both the atrioventricular node and His bundle are comprised primarily of "spiraled" myofibers that are then combined to form many collagen-encased fascicles. These fascicles are generally arranged in a parallel fashion in the proximal atrioventricular bundle (PAVB; the region of the atrioventricular node transitioning from the atrium into the body of the nodal tissues) and the distal atrioventricular bundle (DAVB; the penetrating portion of the bundle of His) and are interwoven within the atrioventricular node itself (the tortuosity of the cellular pathway within the atrioventricular node likely is a major contributor to the conduction delay in this region).

In general, the myocytes of the bundle of His are larger than those of the PAVB and the atrioventricular node, and the perinuclear regions of these myocytes are filled with glycogen. These cells uniquely utilize anaerobic metabolism instead of the normal aerobic metabolism used by the more abundant contractile myocardium. His myocytes have longer intercalated disks, and although all of the nodal tissues have thin end processes, they are less numerous in the His myocytes. His myocytes are innervated, but to a lesser extent than those in the atrioventricular node. Unlike the sinoatrial and atrioventricular nodes, the His bundle has no large blood vessels that supply it specifically. Table 2 is a summary of the histological characteristics of the bundle of His in comparison to the other nodal tissues.

It should be noted that the bundle of His can receive inputs from both the atrioventricular node and from transitional cells in the atrial septum In general, the His bundle is located adjacent to the annulus of the tricuspid valve, distal to the atrioventricular node, and slightly proximal to the right and left bundle branches. The functional origin may be ill defined, but as described above, it is typically considered to begin anatomically at the point the atrioventricular nodal tissue enters the central fibrous body.

The bundle of His is described as having three regions: the penetrating bundle, nonbranching bundle, and branching bundle. The penetrating bundle is the region that enters the central fibrous body. At this point, the His fascicles are insulated, but are surrounded by atrial tissue (superiorly and anteriorly), the ventricular septum (inferiorly), and the central fibrous body (posteriorly). Thus, the exact point at which the atrioventricular nodal tissues end and the bundle begins is difficult to define because it occurs over a transitional region. The penetrating bundle has been described as oval and was 1–1.5 mm long in young canines and 0.25–0.75 mm long in neonates *(1)*.

The nonbranching bundle passes through the central fibrous body and is surrounded on all sides by the central fibrous body. In this cardiac region, the His bundle still has atrial tissue superior and anterior to it, the ventricular septum inferior to it, and now the aortic and mitral valves posterior to it. The branching bundle is described to begin as the His exits the central fibrous body. At this point, it is inferior to the membranous septum and superior to the ventricular septum. The bundle is also at its closest to both the right and left ventricular chambers at this point. After leaving the central fibrous body, the bundle then bifurcates into the bundle branches; the right bundle branch passes into the myocardium of the interventricular septum, and the left bundle branch travels subendocardially along the septum in the left ventricle (as noted in Section 2). Figures 13 and 14 show canine histological sections of the bundle of His as they exit the central fibrous body (the branching bundle).

Electrophysiological studies of the bundle of His have most commonly been performed using catheters with polished electrodes and a short interelectrode spacing (i.e., those with 2-mm diameters). Because of the small amplitude of the His potential, special high-pass filtering must be used (>30 Hz). This high-pass setting must be used to separate the His signal from the low-frequency shift in the isopotential line between the atrial depolarization and the atrial repolarization/ventricular depolarization. His potentials can commonly be mapped by deploying an electrode in one of three ways: (1) endocardially in the right atrium at a point on the tricuspid annulus near the membranous septum; (2) epicardially at the base of the aorta near the right

Table 2
Summary of the Histological Characteristics of the Nodal and Perinodal Tissues in Canines

Feature	*Atrioventricular bundle (DAVB, His bundle)*	*Atrioventricular node (AVN)*	*Proximal atrioventricular bundle (PAVB)*
Nucleus	Clear perinuclear zone filled with glycogen	Clear perinuclear zone filled with glycogen	Clear perinuclear zone filled with glycogen
Metabolism	Anaerobic	Anaerobic	Anaerobic
Myofiber size	Largest	Mid	Smallest
Myofibers in fascicles?	Yes	Yes	Yes
Primary fascicles encased in collagen?	Yes	Yes	Yes
Secondary fascicles present?	Yes	Yes	Yes
Secondary fascicles encased in collagen?	Yes	Yes	Yes
Fascicular arrangement	Parallel	Interwoven ("massive whorl")	Parallel
Myofiber arrangement within fascicles	Least spiraling	Spiraled	Most spiraling
Cross-striations?	Delicate	Delicate	Delicate
End processes present on the myocytes?	Yes; short and delicate.	Yes; most numerous; extend from proximal parallel myofibers to central whorled fibers	Yes
Intercalated disks	Broad	Form short stacks	Broadest
Fat vacuoles?	Few or none	Few or none	Yes
Vascularization	No large vessels	No large vessels	Large vessels present
Innervation	Tendrils (sympathetic); no packets or fascicles of nerve endings present	Fascicles of boutons, tendrils (sympathetic), and varicosities (parasympathetic) present	Fascicles of boutons, tendrils (sympathetic), and varicosities (parasympathetic) present; sheaves of nerve endings extend along the length of the myofibers

Source: Compiled from ref. *2*.
DAVB, distal atrioventricular bundle.

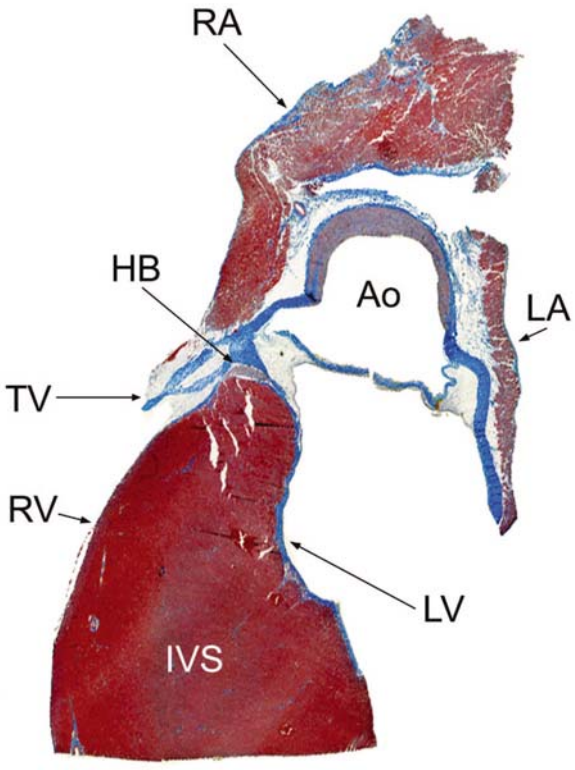

Fig. 13. Histological section through the bundle of His in a canine heart. The section was prepared using a modified Masson's trichrome stain (collagen/nuclei stain blue, muscle/keratin/cytoplasm stain red). Ao, aorta; HB, His bundle; IVS, interventricular septum; LA, left atrium; LV, left ventricular endocardium; RA, right atrium endocardium; RV, right ventricle endocardium; TV, tricuspid valve.

atrial appendage; or (3) radially within the noncoronary cusp of the aortic valve *(13–15,17,37)*.

Today, His potentials are commonly mapped to provide a landmark for ablation of the atrioventricular node and to assess atrial-to-ventricular conduction timing. In addition to direct electrical mapping, much can be learned about the general anatomical and functional properties of the cell lying within the bundle via attempts to stimulate it directly. For example, direct stimulation of the His bundle produces normal ventricular activation because of the initiation of depolarization into the intrinsic conduction pathway *(13,14,16)*. Thus, if attempts to stimulate the His bundle selectively frequently fail, pathological changes may be assumed *(17)*.

The His bundle has historically been thought to act only as a conduit for transferring depolarization. Ventricular escape rhythms have been known to emanate from the His bundle, but it was thought generally a relatively simple structure. To the contrary, evidence indicates that at least two general sources serve as inputs to the His bundle, and that it functions as at least two functionally distinct conduits. Using alternans (alternate beat variation in the direction, amplitude, and duration of any component of the electrocardiogram), the duality of its electrophysiology was demonstrated in isolated preparations from the region of the triangle of Koch in rabbit hearts *(37)*.

7. COMPARATIVE ANATOMY

All large mammalian hearts are considered to have a very similar conduction system with the following main components: the sinoatrial node, the atrioventricular node, the bundle

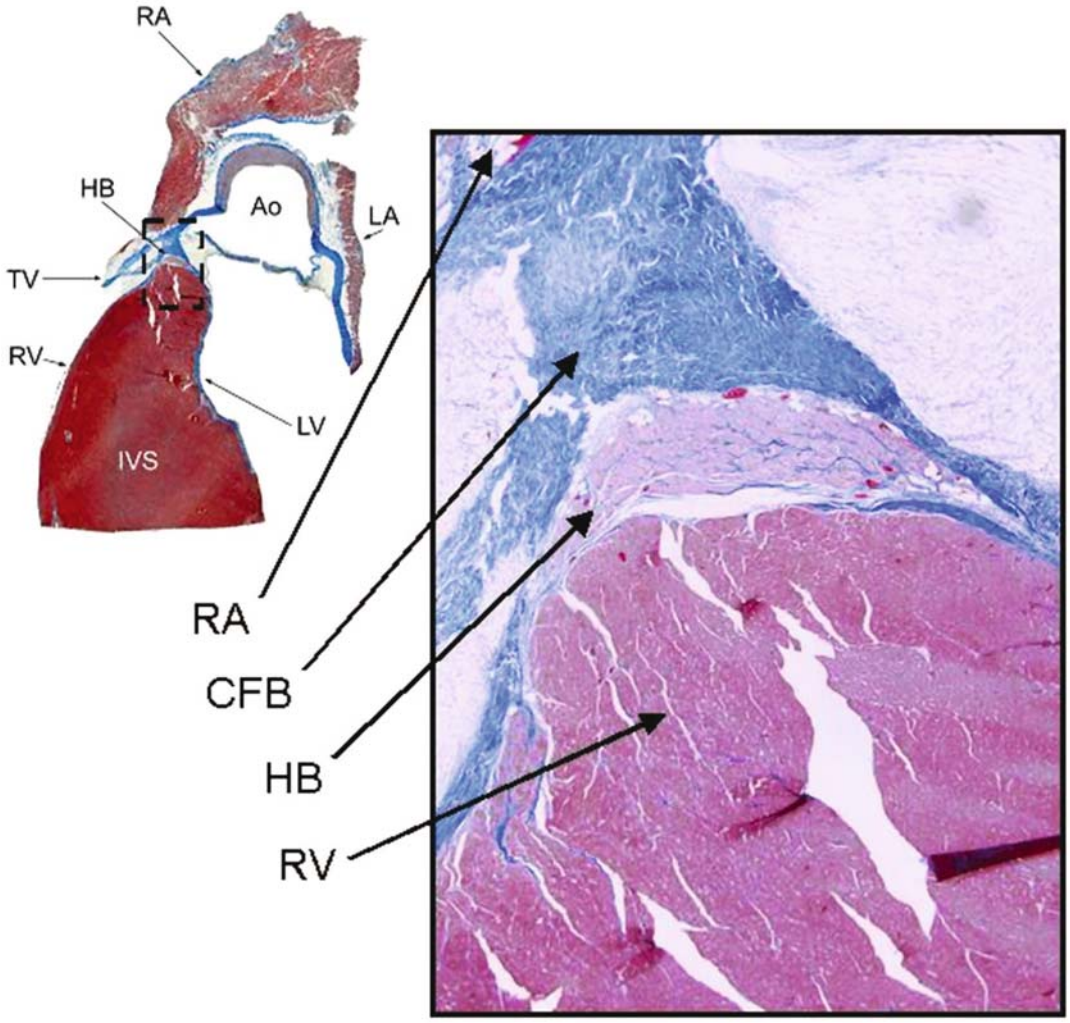

Fig. 14. Histological section through the bundle of His in a canine heart. The region enlarged is noted by the dashed lines in the original histological section. Both sections were prepared using a modified Masson's trichrome stain (collagen/nuclei stain blue, muscle/keratin/cytoplasm stain red). Ao, aorta; CFB, central fibrous body (provides structure and isolates the atrial from the ventricular tissues); HB, His bundle; IVS, interventricular septum; LA, left atrium; LV, left ventricular endocardium; RA, right atrium endocardium; RV, right ventricle endocardium; TV, tricuspid valve.

of His, the right and left main bundle branches, and the Purkinje fibers. Yet, interspecies variations are well recognized *(1,38–40)*. (For a summary of the major differences in the conduction systems between human, swine, canine, and ovine hearts, refer to Table 1, Chapter 5.)

More specifically, Bharati et al. *(38)* made a comparison of the electrophysiological properties of the swine and human heart (Table 3). In addition to significant differences in atrial (high right atrium–low right atrium) and atrial-ventricular conduction times (much shorter in the swine), the authors also found significantly more autonomic innervation within the atrioventricular node and penetrating bundle of the swine heart (thought to be both adrenergic and cholinergic). They concluded that this indicates a more important neurogenic component to the swine conduction system relative to the human heart. Because of this difference, they cautioned using swine as a model for assessing cardiac arrhythmias. Although the neurogenic differences between the human and swine are significant in vivo, isolation of such hearts results in denervation of the conduction systems and thus reduces or eliminates the relevance of this finding.

The canine is another commonly used model in biomedical device research. Information on atrial-to-ventricular timing in canines was published by Karpawich et al. *(15)*. They placed tripolar electrodes on the right atrial epicardium near the noncoronary cusp of the aorta of canines; the resulting timing recorded was extracted from the article and is tabulated in Table 4.

8. FUTURE RESEARCH

Although much is known, a great deal of supposition and controversy remain associated with the understanding of the cardiac conduction system. Specifically, characterization of the anatomy and electrophysiology of the atrioventricular nodal

Table 3
Comparison of Swine to Human Electrophysiology

Parameter	*Swine: Average ± SD (range)*	*Normal human*
Heart rate (beats/min)	132 ± 32 (91–167)	60–100
PR interval (ms)	94 ± 27 (50–120)	3- to 5-year-old: 110–150 5- to 9-year-old: 120–160
QT interval (ms)	256 ± 69 (150–340)	HR = 150: 210–280 HR = 100: 260–350
HRA–LRA (ms)	10 ± 0 (10)	2- to 5-year-old: 6–38 6- to 10-year-old: 0–41
LRA–H (ms)	63 ± 2 (60–65)	2- to 5-year-old: 45–101 6- to 10-year-old: 40–124
H–V (ms)	25 ± 7 (20–35)	2- to 5-year-old: 27–59 6- to 10-year-old: 28–52

Source: Adapted from ref. *38*.
H, His; HR, heart rate; HRA, high right atrium; LRA, low right atrium; V, ventricle.

Table 4
Tabulation of Activation Timing

	P-wave to R-wave interval (ms)	*Atrial activation to His bundle electrogram (ms)*	*His bundle electrogram to ventricular activation (ms)*
Mean	92.1	77.5	29
Standard deviation	18.4	11.5	8.9
Maximum	120	100	50
Minimum	70	60	20

Source: Data compiled from ref. *15*.

region and the bundle of His continues to be an area of great scientific interest and controversy *(41–43)*. For example, current clinical interest associated with the atrioventricular node and the His bundle has focused on their potential stimulation for ultimately improving hemodynamics in patients requiring pacing *(13–18)* and their use in atrioventricular nodal reentrant tachycardias *(1,2,37,44)*. In addition to these applied research investigations, there is a need for additional basic scientific investigations to improve the understanding of the fundamental physiology of the heart's conduction system and the mechanisms of cardiac activation in normal and diseased tissues; the findings from these studies will provide a foundation for future therapies.

9. SUMMARY

This chapter reviewed the basic architectures and functions of the cardiac conduction system to provide the reader with a working knowledge and vocabulary related to this topic. Although a great deal of literature exists regarding the cardiac conduction system, numerous questions remain relating to the detailed histologic anatomy and cellular physiology of these specialized conduction tissues and also how they become modified in disease states. Future findings associated with the overall function and anatomy of the cardiac conduction system will likely lead to improvements in therapeutic approaches and medical devices.

ACKNOWLEDGMENTS

We acknowledge the contributions of Medtronic Training and Education for graphical support; Rebecca Rose, Louanne Cheever, and Alex Hill of Medtronic for the histological sectioning and staining; and Anthony Weinhaus for additional details on atrial anatomy.

COMPANION CD MATERIAL

Section 2
internodaltracts.jpg
7-1.mpg The conduction system.

REFERENCES

1. Ho, S.Y., Kilpatrick, L., Kanai, T., Germroth, P.G., Thompson, R.P., and Anderson, R.H. (1995) The architecture of the atrioventricular conduction axis in dog compared to man—its significance to ablation of the atrioventricular nodal approaches. *Cardiovasc Electrophysiol*. 6, 26–39.
2. Racker, D.K. and Kadish, A.H. (2000) Proximal atrioventricular bundle, atrioventricular node, and distal atrioventricular bundle are distinct anatomic structures with unique histological characteristics and innervation. *Circulation*. 101, 1049–1059.
3. Furman, S. (1995) A brief history of cardiac stimulation and electrophysiology—the past 50 years and the next century. North American Society of Pacing and Electrophysiology (NASPE) Keynote Address, Toronto, Ontario, Canada.

4. His, W., Jr. (1893) Die Tatigkeit des embryonalen herzens und deren bedcutung fur die lehre von der herzbewegung beim erwachsenen. *Artbeit Med Klin Leipzig*. 1, 14–49.
5. Tawara, S. (1906) *Das Reizleitungssystem des Saugetierherzens: Eine anatomisch-histologische Studie uber das Atrioventrikular-bundel und die Purkinjeschen Faden*. Gustav Fischer, Jena, Germany, pp. 9–70, 114–156.
6. Sorensen, E.R., Manna, D., and McCourt, K. (1994) Use of epicardial pacing wires after coronary artery bypass surgery. *Heart Lung*. 23, 487–492.
7. Villain, E., Ouarda, F., Beyler, C., Sidi, D., and Abid, F. (2003) Predictive factors for late complete atrioventricular block after surgical treatment for congenital cardiopathy [in French]. *Arch Mal Coeur Vaiss*. 96, 495–498.
8. Bae, E.J., Lee, J.Y., Noh, C.I., Kim, W.H., and Kim, Y.J. (2003) Sinus node dysfunction after fontan modifications—influence of surgical method. *Int J Cardiol*. 88, 285–291.
9. Hussain, A., Malik, A., Jalal, A., and Rehman, M. (2002) Abnormalities of conduction after total correction of Fallot's tetralogy: a prospective study. *J Pak Med Assoc*. 52, 77–82.
10. Bruckheimer, E., Berul, C.I., Kopf, G.S., et al. (2002) Late recovery of surgically-induced atrioventricular block in patients with congenital heart disease. *J Interv Card Electrophysiol*. 6, 191–195.
11. Ghosh, P.K., Singh, H., and Bidwai, P.S. (1989) Complete A-V block and phrenic paralysis complicating surgical closure of ventricular septal defect—a case report. *Indian Heart J*. 41, 335–337.
12. Hill, S.L., Berul, C.I., Patel, H.T., et al. (2000) Early ECG abnormalities associated with transcatheter closure of atrial septal defects using the Amplatzer septal occluder. *J Interv Card Electrophysiol*. 4, 469–474.
13. Deshmukh, P., Casavant, D.A., Romanyshyn, M., and Anderson, K. (2000) Permanent direct His-bundle pacing: a novel approach to cardiac pacing in patients with normal His-Purkinje activation. *Circulation*. 101, 869–877.
14. Karpawich, P., Gates, J., and Stokes, K. (1992) Septal His-Purkinje ventricular pacing in canines: a new endocardial electrode approach. *Pacing Clin Electrophysiol*. 15, 2011–2015.
15. Karpawich, P.P., Gillette, P.C., Lewis, R.M., Zinner, A., and McNamera, D.G. (1983) Chronic epicardial His bundle recordings in awake nonsedated dogs: a new method. *Am Heart J*. 105, 16–21.
16. Scheinman, M.M. and Saxon, L.A. (2000) Long-term His-bundle pacing and cardiac function. *Circulation*. 101, 836–837.
17. Williams, D.O., Sherlag, B.J., Hope, R.R., El-Sherif, N., Lazzara, R., and Samet, P. (1976) Selective versus non-selective His bundle pacing. *Cardiovasc Res*. 10, 91–100.
18. Karpawich, P.P., Rabah, R., and Haas, J.E. (1999) Altered cardiac histology following apical right ventricular pacing in patients with congenital atrioventricular block. *Pacing Clin Electrophysiol*. 22, 1372–1377.
19. de Cock, C.C., Giudici, M.C., and Twisk, J.W. (2003) Comparison of the haemodynamic effects of right ventricular outflow-tract pacing with right ventricular apex pacing: a quantitative review. *Europace*. 5, 275–278.
20. Cleland, J.G., Daubert, J.C., Erdmann, E., et al. (2001) The CARE-HF study (CArdiac REsynchronisation in Heart Failure study): rationale, design and end-points. *Eur J Heart Fail*. 3, 481–489.
21. Leclercq, C. and Daubert, J.C. (2003) Cardiac resynchronization therapy is an important advance in the management of congestive heart failure. *J Cardiovasc Electrophysiol*. 14, S27–S29.
22. Miake, J., Marban, H., and Nuss, B. (2002). Biological pacemaker created by gene transfer. *Nature*. 419, 132–133.
23. Nattel, S., Khairy, P., Roy, D., et al. (2002) New approaches to atrial fibrillation management: a critical review of a rapidly evolving field. *Drugs*. 62, 2377–2397.
24. Takahashi, Y., Yoshito, I., Takahashi, A., et al. (2003) AV nodal ablation and pacemaker implantation improves hemodynamic function in atrial fibrillation. *Pacing Clin Electrophysiol*. 26, 1212–1217.
25. Bernat, R. and Pfeiffer, D. (2003) Long-term Rand learning curve for radio frequency ablation of accessory pathways. *Coll Antropol*. 27, 83–91.
26. Gaita, F., Riccardi, R., and Gallotti, R. (2002) Surgical approaches to atrial fibrillation. *Card Electrophysiol Rev*. 6, 401–405.
27. Betts, T.R., Roberts, P.R., Ho, S.Y., and Morgan, J.M. (2003) High density mapping of shifts in the site of earliest depolarization during sinus rhythm and sinus tachycardia. *Pacing Clin Electrophysiol*. 26, 874–882.
28. Boineau, J.B., Schuessler, R.B., Hackel, D.B., et al. (1980) Widespread distribution and rate differentiation of the atrial pacemaker complex. *Am J Physiol*. 239, H406–H415.
29. Boineau, J.B., Schuessler, R.B., and Mooney, C.R. (1978) Multicentric origin of the atrial depolarization wave: the pacemaker complex. Relation to the dynamics of atrial conduction, P-wave changes and heart rate control. *Circulation*. 58, 1036–1048.
30. Lee, R.J., Kalman, J.M., Fitzpatrick, A.P., et al. (1995) Radiofrequency catheter modification of the sinus node for 'inappropriate' sinus tachycardia. *Circulation*. 92, 2919–2928.
31. Tranum-Jensen, J. (1976) The fine structure of the atrial and atrioventricular (AV) junctional specialized tissues of the rabbit heart, in *The Conduction System of the Heart: Structure, Function, and Clinical Implications* (Wellens, H.J.J., Lie, K.I., and Janse, M.J., eds.), Lea and Febiger, Philadelphia, PA, pp. 55–81.
32. Waller, B.F., Gering, L.E., Branyas, N.A., and Slack, J.D. (1993) Anatomy, histology, and pathology of the cardiac conduction system: Part I. *Clin Cardiol*. 16, 249–252.
33. Garson, A.J., Bricker, J.T., Fisher, D.J., and Neish, S.R. (eds.). (1998) *The Science and Practice of Pediatric Cardiology. Volume I*. Williams and Wilkins, Baltimore, MD, pp. 141–143.
34. Becker, A.E. and Anderson, R.H. (1976) The morphology of the human atrioventricular junctional area, in *The Conduction System of the Heart: Structure, Function, and Clinical Implications* (Wellens, H.J.J., Lie, K.I., and Janse, M.J., eds.), Lea and Febiger, Philadelphia, PA, pp. 263–286.
35. Aschoff, L. (1910) Referat uber die herzstorungen in ihren bezeihungen zu den spezifischen muskelsystem des herzens. *Verh Dtsch Ges Pathol*. 14, 3–35.
36. Monckeberg, J.G. (1910) Beitrage zur normalen und pathologischen anatomie des herzens. *Verh Dtsch Ges Pathol*. 14, 64–71.
37. Zhang, Y., Bharati, S., Mowrey, K.A., Shaowei, Z., Tchou, P.J., and Mazgalev, T.N. (2001) His electrogram alternans reveal dual-wavefront inputs into and longitudinal dissociation within the bundle of His. *Circulation*. 104, 832–838.
38. Bharati, S., Levine, M., Huang, S.K., et al. (1991) The conduction system of the swine heart. *Chest*. 100, 207–212.
39. Anderson, R.H., Becker, A.E., Brechenmacher, C., Davies, M.J., and Rossi, L. (1975) The human atrioventricular junctional area. A morphological study of the A-V node and bundle. *Eur J Cardiol*. 3, 11–25.
40. Frink, R.J. and Merrick, B. (1974) The sheep heart: coronary and conduction system anatomy with special reference to the presence of an os cordis. *Anat Rec*. 179, 189–200.
41. Becker, A.E. and Anderson, R.H. (2001) Proximal atrioventricular bundle, atrioventricular node, and distal atrioventricular bundle are distinct anatomic structures with unique histological characteristics and innervation—response. *Circulation*. 103, e30–e31.
42. Bharati, S. (2001) Anatomy of the atrioventricular conduction system—response. *Circulation*. 103, e63–e64.
43. Magalev, T.N., Ho, S.Y., and Anderson, R.H. (2001) Special Report: Anatomic-electrophysiological correlations concerning the pathways for atrioventricular conduction. *Circulation*. 103, 2660–2667.
44. Kucera, J.P. and Rudy, Y. (2001) Mechanistic insights into very slow conduction in branching cardiac tissue—a model study. *Circulation Res*. 89, 799–806.

SOURCES

Alexander, R.W., Schlant, R.C., and Fuster, V. (eds.) (1998) *Hurst's: The Heart: Arteries and Veins,* 9th Ed. McGraw-Hill, New York, NY.
Katz, A.M. (ed.) (2001) *Physiology of the Heart,* 3rd Ed. Lippincott, Williams, and Wilkins, Philadelphia, PA.
Mohrman, D.E. and Heller, L.J. (eds.) (2003) *Cardiovascular Physiology,* 5th Ed. Langer Medical Books/McGraw-Hill, New York, NY.

Tortora, G.J. and Grabowski, S.R. (eds.) (2000) *Principles of Anatomy and Physiology,* 9th Ed. Wiley, New York, NY.
Wellens, H.J.J., Lie, K.I., and Janse, M.J. (eds.) (1976) *The Conduction System of the Heart: Structure, Function, and Clinical Implications*. Lea and Febiger, Philadelphia, PA.

10 Autonomic Nervous System

KEVIN FITZGERALD, MS, ROBERT F. WILSON, MD, AND PAUL A. IAIZZO, PhD

CONTENTS

1. INTRODUCTION

The autonomic nervous system coordinates involuntary control of viscera and other tissues throughout the body, with the exception of skeletal muscle. This branch of the central nervous system, organized into parasympathetic and sympathetic divisions, integrates efferent and afferent fibers that regulate the activities of the majority of organs, glands, and smooth musculature found in the body. The presynaptic cell bodies of neurons composing both categories originate in the gray matter of the spinal column, but are classified by fundamental differences. Anatomically, the origin of the sympathetic (thoracolumbar) division of the central nervous system lies between the first thoracic (T1) and the second or third lumbar section (L2 or L3). In contrast, the exiting fibers of the parasympathetic division (craniosacral) originate from both the medulla oblongata and the sacral portion of the spinal cord (S2 to S4).

The primary neurotransmitter released during depolarization can be used as another means of characterizing the two branches of the autonomic nervous system. In the sympathetic division, norepinephrine is the principal postsynaptic neurotransmitter, whereas acetylcholine is the chief transmitter found throughout the parasympathetic division. The primary physiological response induced by each respective neurotransmitter is also a useful way to categorize the divisions of the autonomic nervous system. Such classifications are important considerations when investigating the autonomic nervous system regulation and function of the heart.

From: *Handbook of Cardiac Anatomy, Physiology, and Devices*
Edited by: P. A. Iaizzo © Humana Press Inc., Totowa, NJ

2. SYMPATHETIC ANATOMY

Cell bodies of presynaptic sympathetic efferent neurons are found in the paired lateral horns of the spinal cord, an area identifiable between the T1 and L2 or L3 vertebrae. The axons, or nerve fibers of these cells, exit the interior of the spinal cord through ventral rootlets, which coalesce to form the larger ventral roots and eventually become the ventral rami. Sympathetic fibers almost immediately divert into white rami communicantes (Fig. 1), branching from these spinal nerves, which connect them to paired columns of parasympathetic ganglia called the *sympathetic trunks* located on either side of the spinal cord. Vertebrae from T1 to S5 have corresponding pairs of ganglia; all are interconnected with both ascending and descending nerve fibers, forming the complex columnlike structures *(1)*.

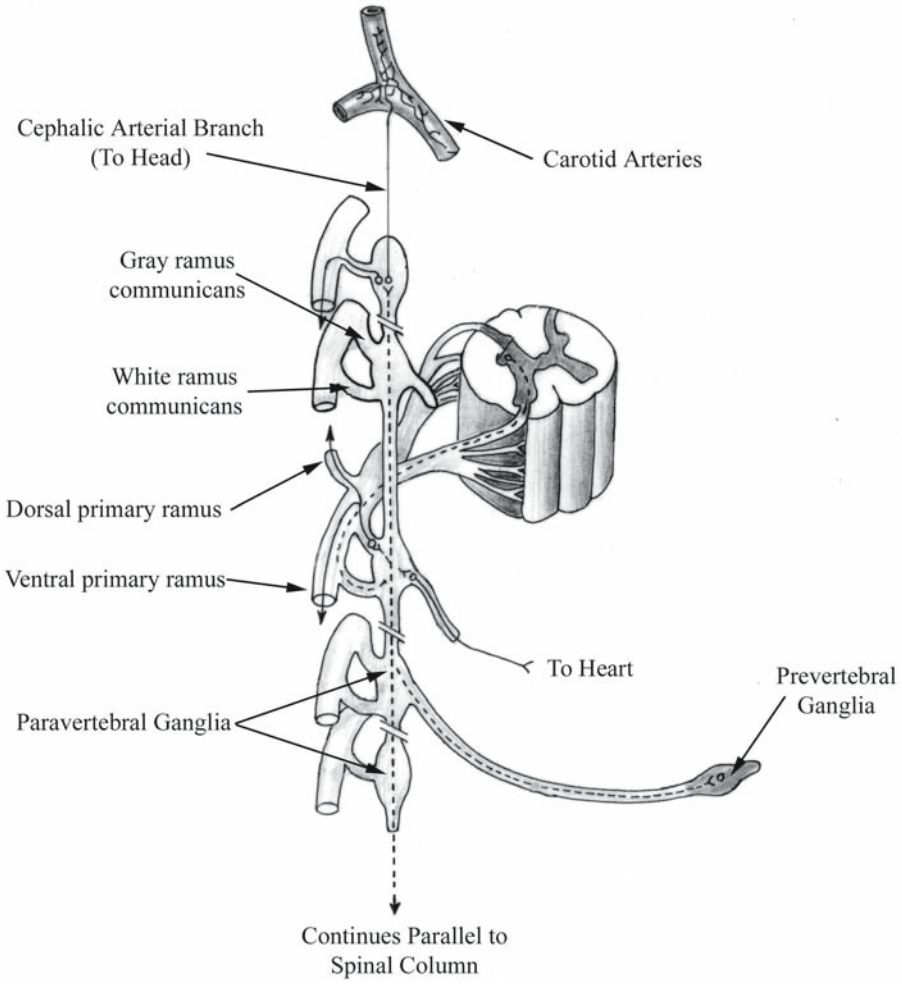

Fig. 1. Pathways of sympathetic motor fibers. The three potential paths of travel taken by presynaptic sympathetic motor fibers can be seen above. Preganglionic fibers traveling to the heart and other areas of the thoracic cavity synapse either immediately on reaching the sympathetic trunk or traverse to other levels to synapse. Complete passage through the paired trunks also occurs with prevertebral ganglia. Modified from ref. *1*.

Preganglionic sympathetic neurons synapse within the ganglia of the sympathetic trunk. The 10- to 20-nm separation distance *(2)* between presynaptic and postsynaptic cells is called the *synaptic cleft*, in which neurotransmitter is released from synaptic vesicles. Acetylcholine is the neurotransmitter released from preganglionic neurons in both the sympathetic and parasympathetic branches of the autonomic nervous system. This compound binds to receptors on postsynaptic cell membranes, causing localized depolarizations of these cells, which may subsequently initiate action potentials that propagate down their axons. Postganglionic neurotransmitters vary between the two branches. In the sympathetic nervous system, norepinephrine is the primary postsynaptic neurotransmitter released. Such junctions can also be activated by epinephrine, and both can often be associated with cotransmitters such as dopamine *(2)* and histamine *(3)*. Both norepinephrine and epinephrine play important roles during sympathetic stimulation of the heart, as is discussed in this chapter.

Three primary paths of travel are commonly identified for presynaptic (also referred to as *preganglionic*) nerve fibers on reaching the sympathetic trunk. A preganglionic fiber can immediately synapse on the cell body of a postganglionic fiber at the level of the trunk on which the fiber entered. Preganglionic fibers can also follow a route that traverses through the sympathetic trunk, then either ascends or descends to synapse within a higher or lower level ganglion. A third, but less common, path of travel for presynaptic neurons involves passing through the sympathetic trunk completely, then synapsing within a prevertebral ganglion in close proximity to the viscera to be innervated. In general, presynaptic fibers traveling to the head, neck, thoracic cavity, and limbs will follow one of the first two courses. Innervation of organs and glands located in the abdominopelvic cavity follow the third path through prevertebral ganglia (Fig. 1).

A variation of the second path occurs primarily with innervation of sweat glands, hair follicles, and peripheral arteries. Presynaptic nerves that arrive at the paired sympathetic ganglion traverse through the white rami communicantes. Instead of immediately continuing to peripheral regions of the body after synapsing, the postsynaptic neurons next travel through

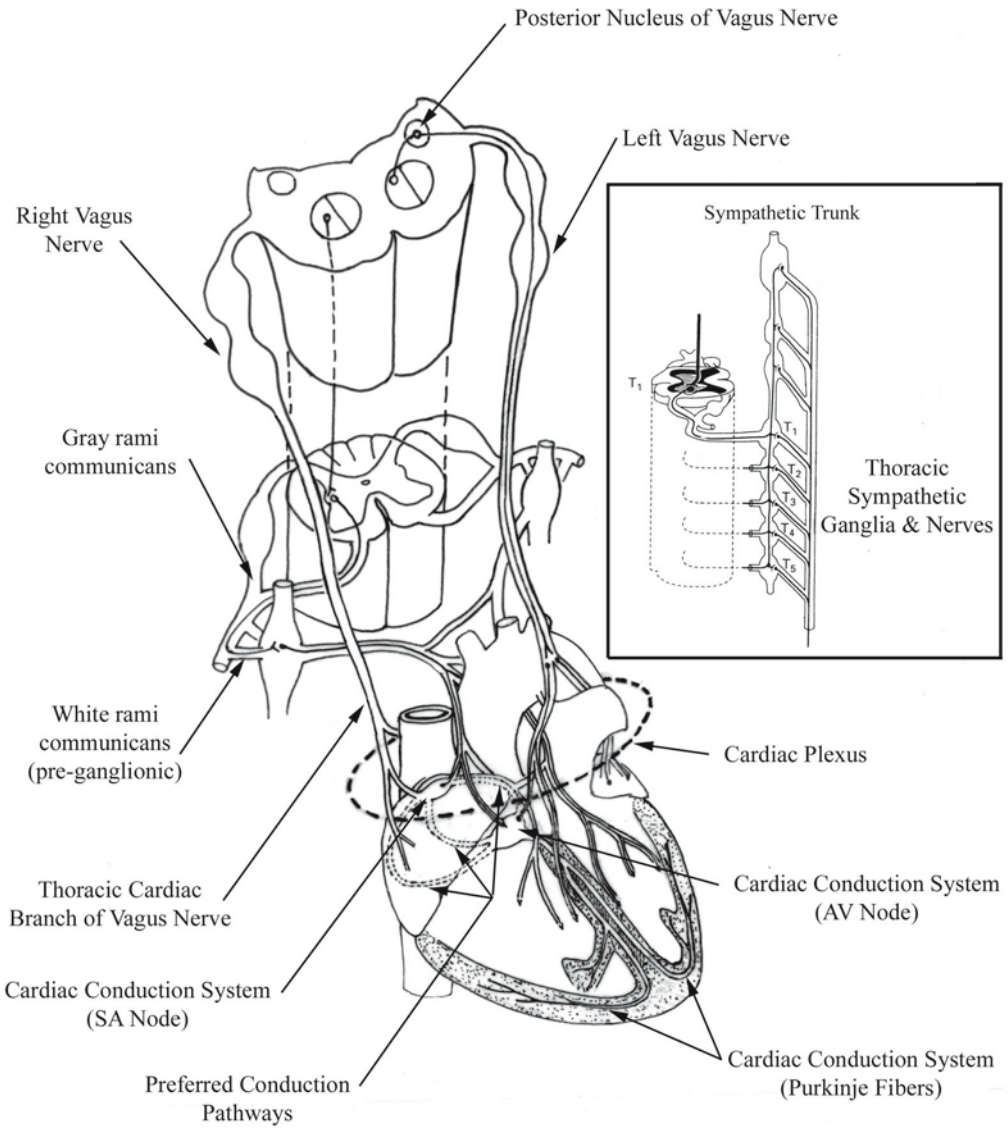

Fig. 2. Autonomic innervation of the heart. Vagal innervation of the right atrium can be observed. The area where many axons congregate just prior to innervation of the heart is depicted as the cardiac plexus. Sympathetic fibers branching from an arbitrary vertebral level of the paired sympathetic trunks is also illustrated. AV, atrioventricular; SA, sinoatrial. Modified from ref. *4*. © 2001 by Frederic H. Martini. Reprinted by permission of Pearson Education, Inc.

gray (unmyelinated) rami (Fig. 1) and exit along large bundles of nerve fibers called *primary rami*. From the primary rami, smaller nerve branches bifurcate and act to control the vasculature (vasodilation and vasoconstriction), hair follicle stimulation, and sweating. If the nerves are destined for the head, their cell bodies are located in the superior cervical ganglion, and their axons follow the path of the carotid arteries to their respective destinations. The muscles of the eye are also innervated by this collection of sympathetic neurons.

Nerve fibers traveling from the central nervous system to a destination elsewhere in the body are termed *efferent*. *Afferent nerves* carry information from various locations in the body to the central nervous system. Frequently, these respective paths of travel occur in parallel, with their fibers bunched closely together to form larger nerve branches. The main nerve branches controlling the sympathetic behavior of the heart and lungs are the cardiopulmonary splanchnic nerves, which consist of both efferent and afferent fibers. Efferent nerves navigate a route originating from the ganglia in the upper cervical region (superior, middle, and inferior cervical ganglia) and the upper thoracic (T1 to T5) levels of the sympathetic trunk. The inferior, middle, and superior cardiac nerves in turn originate from corresponding cervical ganglia and approach the base of the heart before branching into smaller nerves and distributing themselves throughout much of the myocardium and vasculature. The cardiac plexus can be considered an imaginary grouping of the nerve bundles traveling to and from the heart (Fig. 2).

Incoming postsynaptic sympathetic neurons that innervate the human heart are highly concentrated around and near the aortic arch. Some of this innervation occurs throughout the aortic arch itself, as well as at the base of the ascending portion of the vessel. Many branches from these nerves continue down the aorta or under the arch to the pulmonary trunk, where they again diverge and track with the pulmonary arteries. Still more neuronal bifurcations have been identified that then extend to reach other areas of the heart, including both atria and the right and left ventricles. Sympathetic innervation of the sinoatrial and atrioventricular nodes is important for control of heart rate, but has not been distinguished in greater concentration at these areas relative to elsewhere in the atria *(5,6)*. Many nerves have been identified epicardially, often following the path of the coronary arteries and veins *(5,7)*. In general, sympathetic innervation is more highly concentrated in the ventricles than in the atria *(8)*. Within the ventricles, a higher distribution is observed toward the base of the heart as opposed to the apex, with nerves in the epicardium at a slightly greater concentration than in the endocardium. This latter tendency is also evident in the atria *(8)*.

3. ADRENAL MEDULLA

The sympathetic nervous system also controls the hormonal secretions of the paired suprarenal (adrenal) glands in the abdomen, which are components of the endocrine system. Specifically, preganglionic fibers, with their cell bodies located in the lower thoracic (T10–T12) segments of the spinal cord, travel to the adrenal medulla by the abdominopelvic splanchnic nerves. It is in the medulla, or central portions of the suprarenal glands, that norepinephrine and epinephrine are released into the bloodstream *(1)*. The release of these catecholamines into the blood is considered a postsynaptic response initiated from this type of sympathetic activation. Specifically, the cortex surrounding the medulla portions of the adrenal glands are responsible for producing multiple steroid hormones. As blood drains from the highly vascularized cortex to the medulla, the aforementioned hormones can be used to convert norepinephrine to epinephrine. The respective mechanisms of action for these two similarly structured catecholamines are discussed in Section 9.

4. PARASYMPATHETIC ANATOMY

The parasympathetic (craniosacral) nervous system branches from four paired cranial nerves and the lower sacral segment of the spinal cord (S2–S4). The vagus nerve (cranial nerve X) is the main effector for cardiac functions controlled by input from the parasympathetic branch of the autonomic nervous system (Fig. 2). Efferent fibers of the vagus nerves originate in the medulla oblongata and weave through the neck alongside the carotid arteries to the thoracic and abdominopelvic cavities, bifurcating many times along the way to innervate an assortment of organs. Specifically, the efferent fibers of the cranial parasympathetic branch communicate with blood vessels of the head and other viscera; the sacral portion of the spinal cord innervates viscera of the lower abdominopelvic cavity, like the urinary bladder and colon, as well as their respective blood vessels.

Unlike the short sympathetic preganglionic fibers, the parasympathetic division of the autonomic nervous system generally has very long preganglionic fibers and short postsynaptic fibers. Hence, the parasympathetic ganglia are often located very proximal to, or actually within, the target organ. As discussed, acetylcholine is the primary neurotransmitter at both preganglionic and postganglionic junctions.

Within the heart, the majority of the parasympathetic ganglia are located near the sinoatrial node and within the conduction tissue surrounding the atrioventricular node *(5)*. Consequently, the right and left vagus nerves envelope a large and overlapping portion of the atria, in which short postsynaptic fibers from both branches act on the conduction centers of the heart (Fig. 2). However, the endings of the right vagus primarily innervate the sinoatrial nodal region, and many projections from the left are typically observed at the atrioventricular node *(5)*. In fact, high concentrations of vagal innervation situated within a localized region of epicardial fat near the atrioventricular node have been described for the human heart, and it is hypothesized that nerves located within this "pad" have little effect on behavior of the sinoatrial node *(9)*. Thus, it is likely that each region is controlled independent of the other. Parasympathetic junctions are also observed in the ventricles, but only at one-half to one-sixth as frequently as sympathetic innervation *(8)*. Nevertheless, nerves of the parasympathetic division of the autonomic nervous system outnumber those of the sympathetic division in the atria by 30–60% *(8)*. Interestingly, although sympathetic innervation has been described to occur at approximately an equal distribution between the endocardial and epicardial surfaces of the heart, vagal nerve endings are reportedly located at almost twice the density (1.7 to 1) within the myocardium when compared with their epicardial distribution *(8)*.

5. BARORECEPTORS

The autonomic nervous system plays a vital role in the regulation of blood pressure throughout the body. Specialized receptors sensitive to changes in arterial diameter are located at various strategic locations within the upper thoracic cavity and neck. These specialized nerve clusters are commonly known as *arterial baroreceptors*. Substantial groupings of such baroreceptors can be found at the arch of the aorta and in the internal carotid arteries (just distal to where the common carotid bifurcates). This focal density of carotid baroreceptors is also termed the *carotid sinus*. The majority of such receptors are located in areas within these arteries where the walls decrease in thickness, enabling pressure changes to be somewhat magnified at these locations (Fig. 3).

Under even minimal pressure increases, these large arteries will elicit detectable wall dilations. In contrast, under decreased pressure, the internal diameter will decline, also resulting in a change of firing frequency of these receptors. The axons of these afferent neurons travel from baroreceptors along parasympathetic corridors to the medullary cardiovascular center in the brain stem. Under increases in the mean pressure detected by these arterial baroreceptors, efferent sympathetic stimulation will decrease, which is accompanied by an increase in parasympathetic outflow to the heart. This neural activity is intended to return the mean pressure to a normal state. The opposite autonomic response would commence if the mean arterial pressure at the baroreceptor locations decreased. The

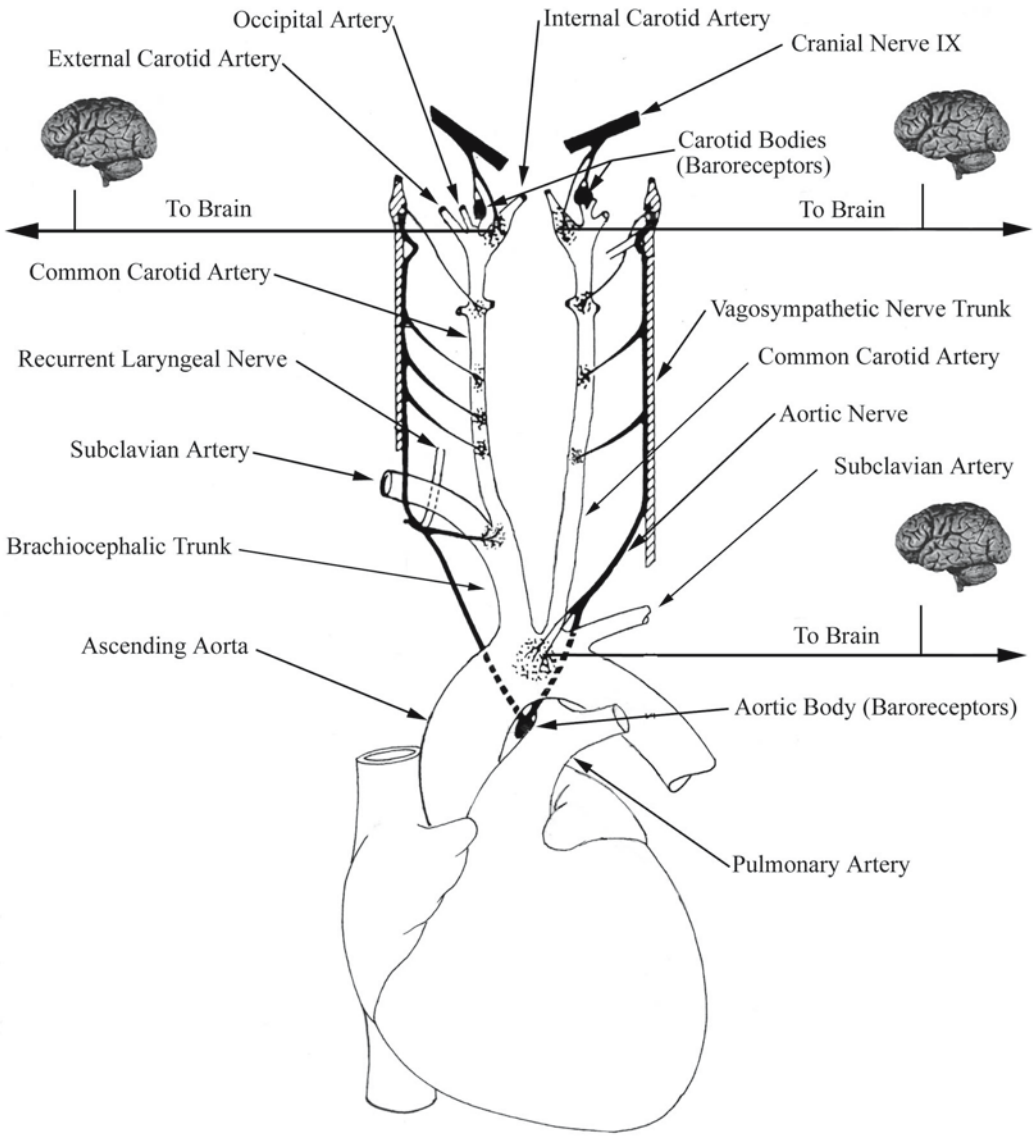

Fig. 3. Arterial baroreceptors. Receptors located at the bifurcations of the carotid arteries and aortic arch convey information to the brain and vasculature to help regulate pressure fluctuations. Modified from ref. *23*. © 1980, with permission from Elsevier.

synergistic functioning briefly noted here between both divisions of the autonomic nervous system is discussed in much greater detail in Sections 6 through 10.

6. HOMEOSTASIS

The tendency to maintain the internal environment of the body at a relatively constant level is known as *homeostasis*. The heart itself exerts perhaps the greatest control influences on countless parameters involving the circulation of blood throughout the body. The heart communicates with the central nervous system via both branches of the autonomic nervous system. Both the sympathetic and parasympathetic divisions work together in the synergistic control of antagonistic influences to prevent potentially harmful fluctuations in a variety of bodily functions. Although it is obvious that significant changes do occur, an array of physiological responses involving the heart (homeostatic control mechanisms) mediated by the autonomic nervous system quickly reverses these changes to return within the reasonable ranges required to maintain overall health. In general, homeostatic control functions are the underlying determinants of parasympathetic and sympathetic outflow.

7. HYPOTHALAMIC CONTROL

The autonomic control of the heart is highly modulated by activity within the portion of the brain known as the hypothalamus. Afferent fibers from the brain stem (medulla oblongata) and spinal cord convey information via the autonomic afferent system to the hypothalamic nuclei within the central nervous system *(10)*, whereas impulses that leave the hypothalamus travel along efferent fibers to the various sympathetic and parasympathetic ganglia as noted above. Most parasympathetic response signals have been determined to originate from the anterior portions of the hypothalamus, whereas sympathetic activity stems primarily from the posterior portions *(6,10)*.

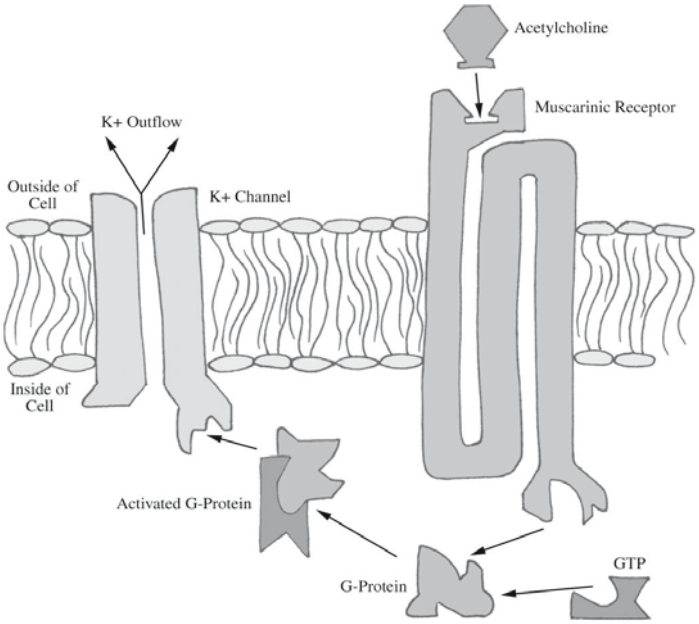

Fig. 4. The effect of acetylcholine on cardiac muscle cells. Potassium channels within a cellular membrane are opened as a result of binding an activated G protein. Acetylcholine released by parasympathetic neurons activates these G proteins by binding with muscarinic receptors within the membrane. The effect of norepinephrine on cardiac muscle cells is propagated in a similar manner, with differences as described in the text. GTP, guanosine triphosphate.

Direct electrical stimulation of specific sites within the hypothalamus can initiate preprogrammed patterned changes in heart rate, blood pressure, and peripheral resistance *(5)*.

As noted, afferent axons from the aortic and carotid baroreceptors principally travel to the medullary cardiovascular centers, with neural pathways continuing onward to the hypothalamus *(6)*. It should be noted that temperature regulation of the body is also centered within the hypothalamus. Thus, during exposure to cold, the hypothalamus initiates appropriate autonomic responses to maintain body temperature, like vasoconstriction and shivering. The contraction of the peripheral vasculature motivates a redistribution of blood flow to vital organs like the heart and brain to maintain their suitable function *(2)*. The shiver reflex induced by the hypothalamus increases heat production, which in turn causes additional adjustments in blood flow and cardiac activity. The opposite outcome occurs during exposure to high degrees of heat, such that sweating is initiated via postganglionic sympathetic neurons, and vasodilation of the vasculature supplying the skin is amplified.

The regulation of bodily processes is an important responsibility of the hypothalamus, and it performs such tasks via the autonomic pathways, hence regulating countless systems within the body simultaneously. Keeping this relative state of constancy throughout the body, regardless of extreme changes that may occur externally, is referred to as homeostasis; in nearly all cases, there are direct effects on cardiac performance.

In addition to the influence the hypothalamus has on autonomic pathways, emotional and hormonal changes are modulated in this region of the brain to promote homeostasis. Furthermore, pituitary gland function is mediated by the hypothalamus, inducing or suppressing hormonal release from this important part of the endocrine system to the rest of the body. Some of these hormones act as cotransmitters in the presence of acetylcholine or norepinephrine within synapses eliciting parasympathetic or sympathetic activity *(2)*; dopamine is one example.

8. EFFECTOR PATHWAYS TO THE HEART

Within the myocardium, parasympathetic nerve fibers release acetylcholine when stimulated. Cardiac cells contain muscarinic receptors embedded within their lipid bilayer, which can activate G proteins found in the cytoplasm upon binding with acetylcholine. Activation occurs when a bound GDP (guanosine diphosphate) molecule is replaced by a GTP (guanosine triphosphate) structure. Subsequently, this response allows the altered protein to bind with potassium channels in the membrane and causes them to open, thus increasing potassium permeability (Fig. 4). As a result, heart rate will generally decrease due to an efflux of potassium ions (K^+) from cardiac cells because the cellular membrane becomes more polarized as the potential moves closer to the K^+ equilibrium potential of –90 mV *(6)*. This hyperpolarization makes the generation of action potentials more difficult and thus slows the rate of firing of the sinoatrial node. Activated G proteins will remain in such a state until GTP is hydrolyzed to form inactive GDP *(2,11)*.

The type of regulatory control in the case described above involves the direct opening of K^+ channels by G proteins within a cardiac muscle cell. It should also be noted that indirect opening of potassium channels may also occur after acetylcholine binds to the muscarinic receptors. Furthermore, activated G proteins may also cause some increase in the production of arachidonic acid, which acts as a secondary messenger that can result in increased K^+ permeability caused by subsequent cleavage of membrane lipids *(11)*.

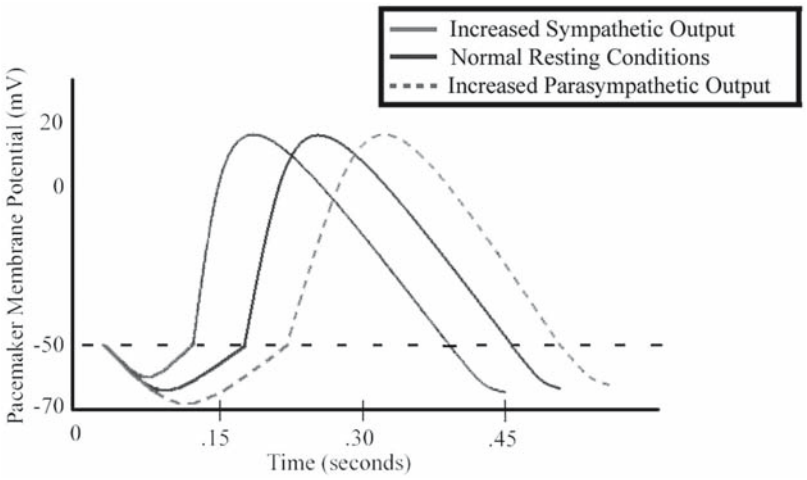

Fig. 5. The effects of changes in sympathetic and parasympathetic outflow to the heart. The heart will increase its rate of contraction during increased sympathetic neural stimulation. This time is required for the cardiac pacemaker cells to reach threshold decreases. In contrast, increased parasympathetic outflow will decrease the heart rate and increase the time to threshold.

The modulation of G proteins is also an important aspect of sympathetic effects on cardiac behavior. More specifically, sympathetic fibers release norepinephrine at postsynaptic terminals of cardiac muscle cells, and receptors located within the cellular membrane bind with the norepinephrine to stimulate α_1 adrenergic receptors. Next, G proteins replace GDP at their binding sites with GTP when activated by the excited α_1-receptors, causing an increase in the production of cyclic adenosine 5′-monophosphate (cAMP) within the cardiac myocytes. The increased cAMP levels cause molecules of protein kinase A to phosphorylate large numbers of calcium channels within the cellular membrane. This addition of a phosphate group not only causes Ca^{2+} channels to remain open longer, but also allows a greater number of channels to open, thus contributing to the influx of calcium ions into each cell on activation *(6)*. In other words, the threshold for depolarization will be more easily attained because of the greater number of available calcium channels, thus allowing greater calcium incursion during activation and resulting in higher contraction strength.

An advantage of the mechanisms of action involving G proteins is that autonomic modulation can be sustained without constant nerve fiber stimulation. That is, a burst of synaptic activity causing the release of either acetylcholine or norepinephrine can initiate these aforementioned processes.

9. SPECIFIC SYMPATHETIC AND PARASYMPATHETIC CARDIAC CONTROLS

9.1. Heart Rate

The rate at which a normal adult heart completes one cardiac cycle, during rest, is approx 70 beats per minute *(6)*. This heart rate is maintained at this relatively constant value via a continuous firing of the vagus nerve, called *basal* (or *vagal*) *tone*. The heart rate will increase when vagal tone is overcome by increased activity of sympathetic nerves to the heart, which release norepinephrine and cause a rise in the sinoatrial nodal depolarization rate (Fig. 5). An increase of this nature is referred to as a *positive chronotropic effect*.

As stated above, the fundamental cause of this increase in heart rate is an increase in activated calcium channels in myocardial cell membranes, increasing the speed at which depolarization occurs. This increased sympathetic outflow can be initiated by a large array of internal and external stimuli, including but not limited to exercise, an increase in body temperature, trauma, or stress. In addition, a concurrent release of epinephrine from the adrenal medulla can further amplify the same effects on myocardial ion channels, although to elicit a significant rise in heart rate the amount of the hormone liberated must be fairly substantial *(6)*.

Parasympathetic discharge increases potassium ion permeability in cardiac myocytes, thus increasing the threshold for depolarization to occur spontaneously in the sinoatrial node. As a result, the heart rate declines (Fig. 5). This autonomic neural input predominates during sleep and other sedentary states, eliciting an increase in cardiac cycle time and therefore enabling the heart to expend less energy *(2)*. In addition to decreasing the slope of the pacemaker potential, parasympathetic stimulation may also induce a so-called pacemaker shift *(5)*; true pacemaker cells can become more inhibited than the latent pacemakers, thus shifting the initiations of spontaneous depolarizations from the true pacemakers to the latent ones *(5)*.

Conduction velocity is the measure of the spread of action potentials through the heart. Parasympathetic stimulation above normal tonic activity slows this conduction velocity, and this response is termed *negative dromotropic effect*. It follows that an increase in conduction velocity commonly accompanying sympathetic stimulation has a *positive dromotropic effect*. The atrioventricular node is the location within the heart where conduction speed variation is most notable. Refer to Chapter 9 for more details on specific mechanisms of cardiac pacemaker mechanisms.

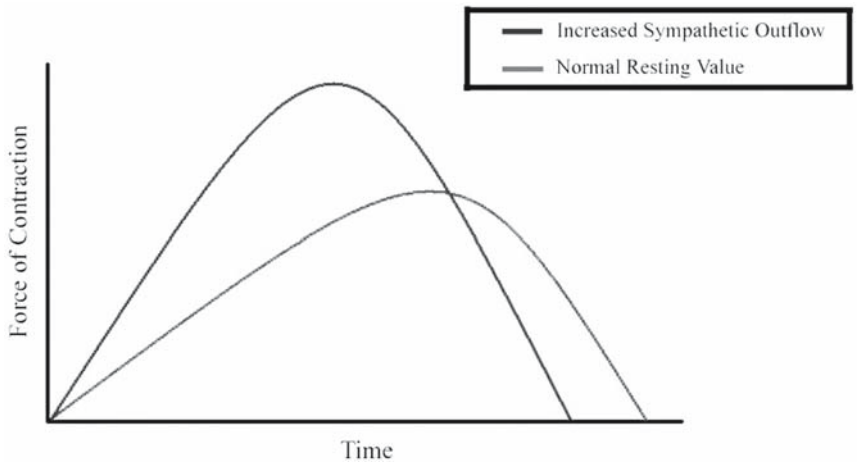

Fig. 6. Effect of increased sympathetic stimulation on contractility (*see* text for details).

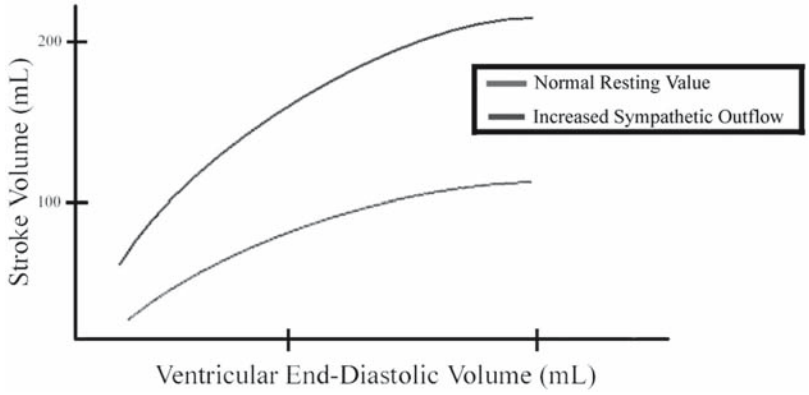

Fig. 7. Effect of increased sympathetic stimulation on stroke volume (*see* text for details).

The control mechanisms of heart rate may also be dependent on gender *(12)*. Women have been shown to exhibit higher resting frequencies of parasympathetic input than men of similar age, possibly indicating a more dominant control of heart rate via vagal stimulation than their male counterparts *(12)*.

9.2. Stroke Volume and Contractility

Like heart rate, the amount of blood ejected from the ventricles during systole is greater when the heart is modulated by an increased sympathetic input (Fig. 6). The underlying mechanism for this increased stroke volume is enhanced cardiac myocyte contractility, and the magnitude of this response is strongly affected by preload and afterload conditions, as predicted by the Frank-Starling law *(6)*. Such an increase in contractility is characterized as a *positive inotropic effect*. Myocytes usually increase in length in proportion to their preload, and because they become more elongated, they also have the capability to shorten over this greater distance. This increased amount of shortening leads to an enhanced strength of contraction of the heart. As described previously, sympathetic excitation facilitates a larger and more rapid Ca^{+2} influx into cardiac cells, which further augments the degree of overall contraction during systole *(11)*.

Combined with a larger preload, the increased contractility due to calcium ion influx will raise the stroke volume of the heart (Fig. 7). Such an increase in stroke volume results in a larger ejection fraction of blood from the chambers of the heart. *(2)*. However, stroke volume is also dependent on afterload created by the relative diameter of the peripheral arteries, and will not increase as significantly under sympathetic stimulation if the afterload is elevated.

As expected from the often-antagonistic nature of the autonomic nervous system, parasympathetic stimulation decreases contractility. However, the relative decrease in contractility is much less significant than the increase in this parameter that sympathetic input provides *(2)*.

An important concept to note involves simultaneous increases in heart rate and stroke volume: because cardiac output is the product of these two quantities, its overall value commonly increases with sympathetic stimulation. Conversely, cardiac output normally decreases with a higher rate of parasympathetic input. This is common when the body is in a sedentary state; hence, tissue oxygen and metabolite requirements are not as high.

The time necessary for the heart to contract and relax fully decreases under sympathetic stimulation, due primarily to the

larger proportion of the cardiac cycle that is made available for filling. Although an increase in heart rate makes the total duration of the cardiac cycle shorter *(2)*, the corresponding rise in contractility causes the muscular contractions to commence more rapidly and with greater force than under resting conditions. This translates to a decrease in the amount of time necessary for contraction of the heart during a complete cardiac cycle. Thus, the heart is relaxed for a greater portion of the cycle, enabling enhanced filling of the chambers to provide a greater volume of blood ejected for each contraction.

9.3. Baroreceptor Pressure Regulation

Arterial pressure, or afterload, is regulated in the short term by baroreceptors that are primarily located in the walls of the aorta and carotid arteries. In particular, baroreceptors sense both magnitude and rate of stretch of arterial walls because of pressure fluctuations within the vessels *(6)*. The afferent fibers projecting from the baroreceptors convey this information concerning pressure shifts to the autonomic nervous system, which in turn responds by either increasing or decreasing sympathetic or parasympathetic drive. A basal tonic activity can be identified from the receptors; this activity progresses to the higher cardiovascular centers. The frequency of impulses can increase or decrease in response to these pressure changes. Decreased arterial dilation causes sympathetic nerves to increase their discharge rate and escalate the release of norepinephrine, thus increasing heart rate, stroke volume, and peripheral resistance *(2)*.

The baroreceptor reflex functions as a negative-feedback system *(6)*, such that a decrease in arterial stretch will induce an increased sympathetic discharge, accordingly raising cardiac output. This in turn will increase blood delivered to the vessels containing baroreceptors, increase pressure, and decrease the tonic activity of these receptors. Homeostatic control of arterial pressure is thus administered because the decreased baroreceptor discharge rate will cause a lowered degree of sympathetic activity and revert the cardiac output back toward its basal value. In other words, the response of the baroreceptors ultimately removes the stimulus causing the initial response *(6)*.

Importantly, long-term pressure regulation is not accomplished via baroreceptor input because of their adaptive nature (accommodation). That is, if pressure in the aorta and carotid arteries remains elevated for sustained periods, the tonic firing rates will eventually return toward resting values regardless of whether the pressures remain elevated. Long-term regulation of pressure involves numerous complex hormonal mechanisms, which are extensively influenced by the hypothalamic and medullary cardiovascular centers.

9.4. Arteriolar Pressure Regulation

Because the heart is responsible for delivery of blood to every part of the body, homeostatic control often involves changing the amount of blood provided by the circulatory system to a given tissue, organ, or organ system. For example, the gastrointestinal system at rest normally receives approx 20% of the blood pumped by the heart during each cardiac cycle. However, during times of intense stress or exertion, the blood provided to this area may drastically decrease, while the proportion of blood provided to the heart and skeletal muscles may increase notably. Such changes in blood supply are commonly mediated by changes in resistance of the peripheral vasculature.

At rest, the smooth muscle cells in the walls of arterioles throughout the body remain slightly contracted because of a combination of influences from the central nervous system, hormonal distribution within the vasculature, or localized organ effects. The relative degree of contraction within the arterioles is referred to as their *basal tone*. The stretching of the arterioles due to pulsatile blood pressure is thought to be the cause of the constant state of stress within such vessels *(6)*. Arterioles innervated by sympathetic fibers possess an increased contractile tone, termed the *neurogenic tone*, because of the sustained activation of these fibers.

Control of the vascular peripheral resistance is achieved by varying the firing frequency within these sympathetic fibers. More specifically, postganglionic fibers release the neurotransmitter norepinephrine, which binds to α_1-adrenergic receptors within the smooth muscle cells in arteriolar walls. Thus, an increase in the firing activity of these neurons produces an increase in norepinephrine levels, which in turn binds with more α_1-receptors and causes an overall decrease in the diameters of arterioles. In contrast, a lowering of the basal tonic activity causes vasodilation since less neurotransmitter is available for binding, causing the smooth muscle cells to relax.

The relative firing rates of arteriolar sympathetic neurons innervating a given tissue are also modulated by the need for blood elsewhere in the body. For example, if a hemorrhage occurs in the abdomen and results in significant bleeding, sympathetic activity to that area will increase, causing less blood to flow to these damaged tissues in an attempt to preserve adequate levels of flow to the heart and brain. It should be noted that other regulators exist for the control of vasomotion and the tonic activity of the sympathetic system. Local increases in extracellular cation concentrations, acetylcholine levels, and even norepinephrine itself can act to prevent extreme vasoconstriction. Adrenergic receptors that are pharmacologically different from those in smooth muscle cells *(6)* have been identified on postganglionic sympathetic neurons themselves and are given an α_2 designation. These receptors bind with the neurotransmitter and inhibit its release if the amount previously liberated is excessive (negative feedback).

Blood flow through the coronary arterioles is primarily regulated by local metabolic controls that are highly coupled with myocardial oxygen consumption. That is, subtle increases in oxygen consumption by the heart will result in an increase in blood flow through the coronaries. Elevated sympathetic activity of the systemic vasculature typically induces a subsequent decrease in the diameter of the peripheral arteries. However, during sympathetic excitation, vasodilation predominates in the coronary arterioles instead of vasoconstriction; this is because oxygen consumption is raised significantly by concurrently inducing higher heart rates and levels of contractility. The factors motivating metabolic regulation therefore outweigh the vasoconstrictive effects of sympathetic innervation of the coronaries.

Blood flow to skeletal muscle is controlled in a manner similar to that for the coronary arteries in that local meta-

bolic factors play a vital role in regulating vessel resistance. Although increased sympathetic activity may decrease the blood flow to a resting skeletal muscle by a factor of four *(6)*, a muscle undergoing exercise (and thus in the presence of elevated sympathetic activity) can elicit an increase in blood flow almost 20 times that of normal resting values *(6)*. However, this muscle response must occur in conjunction with a drastic decrease in the blood flow within other tissues or organs, such as those of the abdominal cavity or nonexercising muscles. This course of action allows the total peripheral resistance to remain at a functional level. Homeostatic control during exercise also exists at the skin. To cool the body from the increased metabolic heat production, sweat glands become active, and blood flow increases significantly over the normal resting value to dissipate excess body heat. The active vasodilation is the result of metabolic activity overcoming the increased sympathetic outflow to skin arterioles.

During the digestion of food, increased blood flow occurs in the stomach and intestines. Parasympathetic discharge to the heart increases, and sympathetic stimulus declines, lowering the heart rate. This concentration of blood to the abdominal organs facilitates the movement of nutrients to areas of the body in need and is a good example of how both branches of the autonomic nervous system work together to sustain a level of balance throughout the entire body.

The suprarenal glands can also contribute to vasomotion. Because norepinephrine is released directly into the bloodstream from these endocrine glands, arteriolar constriction in the systemic organs can result. The human "fight-or-flight" response elicited under stressful or exciting circumstances originates within the hypothalamus and via hormones travels to the pituitary gland and later the adrenal cortex, where the agent cortisol is released into the bloodstream and adrenal medulla. It is in the medulla that cortisol activates the enzyme necessary to convert norepinephrine to epinephrine, which is released into the bloodstream to amplify increased sympathetic activity *(2,3)*. Blood flow to the skin and other internal organs (like the stomach and intestines) is greatly decreased by increasing sympathetic (and decreasing parasympathetic) tonic activity; flow to skeletal muscles and the heart increases considerably. This process can be thought of as simply delivering blood to the areas of the body most in need to deal with the demanding circumstances. The direct release of these agents into the bloodstream allows for their rapid circulation, which helps contract arterioles along with conventional sympathetic outflow. The so-called "adrenaline rush" experienced during periods of great tension or exhilaration comes from the adrenal glands.

Regulation of the veins and venules in the body is carried out by many of the same mechanisms as that for arterioles. Although veins have smooth muscle in their walls complete with α_1-receptors that respond to norepinephrine, their basal tonic activity is much lower than that observed in arterioles. Thus, venules at rest can be considered to be in a more dilated state. The wall thickness of veins is also significantly less than that found in arteries, which enables the consequences of physical effects to be more prominent in veins. That is, the overall blood volume associated with veins can be greatly affected by compressive forces. For example, in skeletal muscle, the degree of muscle contraction around the vessel can push large amounts of blood back toward the heart, which enables quicker filling within the right atrium and enables sustained physical activity. If skeletal muscles surrounding veins are relaxed, the venous system can act as a blood reservoir.

Vasculature of skeletal muscles and the liver can have a unique effect on homeostasis via noninnervated α_2-receptors located in arteriolar walls. Increased blood levels of epinephrine can activate these receptors, which along with G proteins *(6,11)* act to catalyze an intracellular chemical reaction, resulting in decreased cytoplasmic levels of Ca^{2+} and a hyperpolarization of the cellular membrane. This in turn decreases the contractile machinery sensitivity to Ca^{2+}, causing vasodilation *(6)*. Vasodilation in the presence of epinephrine is in contrast to the decrease in vessel diameter caused by the chemically similar compound norepinephrine. The α_2-receptors are more sensitive to epinephrine than α_1-receptors *(6)*. Thus, a small elevation in the concentration of epinephrine in the bloodstream (possibly provided by the adrenal medulla) can cause vasodilation. However, if the level of catecholamine increases, the more numerous α_1-receptors will be activated and cause vasoconstriction. It is important to note that there is no neural input to α_2-receptors, and norepinephrine therefore has no effect on their activation.

It can be seen that the parasympathetic and sympathetic effects of the heart and vasculature often elicit opposite physiological responses, yet work in conjunction to maintain homeostasis.

10. CARDIAC DENERVATION

Denervation can be divided into two categories: preganglionic and postganglionic. Preganglionic denervation is caused primarily by disease or injury of the vasomotor centers in the brain or spinal cord above T10; it leaves intact the postganglionic nerve fiber and many reflexes that occur at the ganglionic level. Preganglionic denervation not only results in loss of centrally mediated cardiac reflexes, but also leads to dysfunctions in the control of peripheral vascular tone and inability to control blood pressure with changes in position. Shy-Drager syndrome is a classic example of preganglionic denervation affecting the cardiovascular system *(13)*.

Postganglionic denervation can occur as the result of several neurodegenerative processes, after certain types of cardiac surgery, or after cardiac transplantation. Loss of the postganglionic nerve cell body results in Wallerian degeneration of the distal nerve, with loss of axonal integrity and neurotransmitter availability. Loss of neurotransmitters at the neural junction with the distal target (e.g., cardiac conduction tissue or cardiac myocytes) leads to an increase in neurotransmitter receptor numbers and densities. This, combined with a loss of neurotransmitter metabolism by the degenerated neuron, makes both the cardiac conduction system and muscle hypersensitive to circulating catecholamines (so-called denervation hypersensitivity).

Cardiac transplantation is the most complete form of cardiac denervation, resulting in loss of both sympathetic and parasympathetic innervation, with Wallerian degeneration of the intracardiac nerve fibers *(14)*. Yet, diabetes is the most common cause of partial cardiac denervation in humans *(15)*. Diabetic

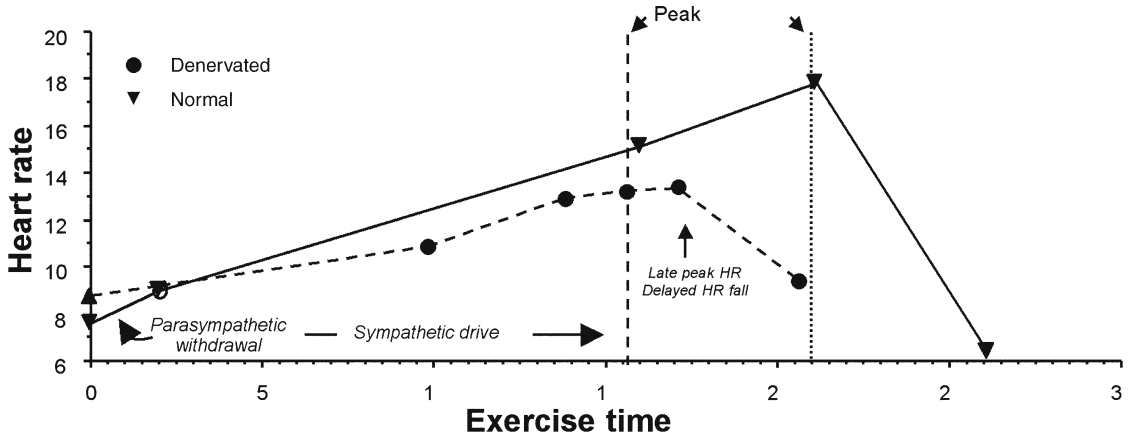

Fig. 8. The heart rate response to treadmill exercise is shown for normally innervated subjects (solid line) and patients with cardiac denervation after heart transplantation (dashed line). The denervated patients have higher resting heart rates, but heart rates rise more slowly with exercise because the increase in heart rates depends primarily on circulating catecholamines. After cessation of exercise, heart rates in the denervated patients continue to rise briefly and then fall slowly as circulating catecholamines are metabolized.

neuropathy can result in losses of both sympathetic and parasympathetic efferent and afferent pathways. As with other neurodegenerative diseases, neuronal loss is typically patchy and permanent. Other diseases leading to cardiac denervation include infiltrative diseases such as amyloidosis.

10.1. Effects of Denervation on Basal Cardiac Function

The loss of tonic parasympathetic vagal inhibition of sinus node depolarization causes a rise in basal heart rate and loss of heart rate fluctuation with respiration. The resting heart rates of patients with a heart transplant typically are in the range of 95–100 beats/min. A number of reflexes, mediated primarily through the vagal nerves, are absent, including carotid sinus slowing of heart rate, the pulmonary inflation reflex, and the Bezold-Jarisch reflex.

In contrast, the resting inotropic state of the cardiac muscle and myocardial blood flow are normal after denervation. Basal ventricular function is changed minimally by denervation. Measures of systolic contraction (such as dP/dt, ejection fraction, and cardiac output) are usually preserved. Preservation of pump function after denervation may be related in part to an upregulation of β-catecholamine receptors on myocytes and the conduction system, leading to an amplification of the response to blood-borne catecholamines *(16)*.

Coronary blood flow in the denervated heart is unchanged at rest and increases normally with exercise. Coronary flow reserve (a measure of maximal coronary blood flow) is typically normal; although in animals the response to ischemia is blunted *(17,18)*.

Afferent sensation to pain (e.g., from ischemia), chemoreceptor stimulation (e.g., from ischemia, hyperosmolar contrast media), and stretch receptor stimulation (e.g., from pressure overload) are absent in the recently transplanted heart. This aspect of denervation is important because coronary occlusion because of transplant-related coronary arteriopathy is common, and the absence of anginal pain removes an important warning symptom.

10.2. Effects of Denervation on Exercise Hemodynamics

Cardiac denervation results in a blunting of the chronotropic response to exercise. With exercise, heart rate increases because of an increase in plasma catecholamines (released primarily from the adrenal glands) rather than from direct sympathetic stimulation of the sinus node. Thus, heart rate increase is delayed; the heart rate peaks well after cessation of exertion and remains elevated until the circulating catecholamines can be metabolized (Fig. 8).

Exercise or stress also will both result in a delayed increase in inotropic status, similar to the changes in chronotropic response. Unlike status, resting ventricular function, peak inotropic states and ejection fractions are typically reduced.

10.3. Reinnervation

Sympathetic neural reinnervation of the heart occurs in nearly all animals undergoing auto-transplantation and in most patients undergoing orthotropic transplantation. Reinnervation typically occurs over both the aortic and atrial suture lines (left more than right), extending from the base of the heart to the apex. The rate of reinnervation is slow (years), and in humans, it is patchy and considered incomplete. The anterior wall typically reinnervates earlier and more densely than the rest of the left ventricle *(19)*. The sinus node reinnervates to some degree in over 75–80% of patients.

Reinnervation results in partial normalization of the chronotropic and inotropic responses to exercise *(20,21)*. Thus, the reinnervated patients can exercise longer and have higher maximal oxygen consumptions. In addition, cardiac pain sensation (i.e., angina) can return, although the regional nature of reinnervation results in reduced or patchy sensation to ischemia in most transplant recipients *(22)*. Parasympathetic reinnervation has been reported in a small number of transplant recipients; it is accompanied by return of respiratory-mediated fluctuation in heart rate and carotid sinus slowing of heart rate.

11. SUMMARY

The autonomic nervous system and the role it plays in governing the behavior of the cardiovascular system is dramatic in both its complexity and importance to life. The antagonistic nature of the parasympathetic and sympathetic branches of this system allows rapid and essential changes in parameters such as heart rate, contractility, and stroke volume to deliver metabolites and nutrients to tissues and organs that need them at any given time. Increased sympathetic outflow relative to normal resting conditions most often causes an excitatory response in physiological parameters (such as heart rate and/or smooth muscle contraction), whereas parasympathetic stimulation usually results in calming adjustments (decreased contractility and/or vasodilation). It is important to note that both branches exhibit influences that do not rigidly fit into these general guidelines.

REFERENCES

1. Moore, K.L. and Dalley, A.F., III (eds.). (1999) *Clinically Oriented Anatomy,* 4th Ed. Lippincott, Williams, and Wilkins, Philadelphia, PA.
2. Vander A., Sherman J., Luciano D. (eds.) (2001) *Human Physiology,* 8th Ed. McGraw-Hill, Boston, MA.
3. Hansen, J.T. and Koeppen, B.M. (eds.) (2002*) Netter's Atlas of Human Physiology.* Icon Learning Systems, Teterboro, NJ.
4. Martini, F.H. (ed.) (2001) *Fundamentals of Anatomy and Physiology,* 5th Ed. Cummings, New York, NY.
5. Berne, R.M. and Levy, M.N. (eds.). (1977) *Cardiovascular Physiology,* 3rd Ed. Mosby, St. Louis, MO.
6. Mohrman, D.E. and Heller, L.J. (eds.). (2003) *Cardiovascular Physiology,* 5th Ed. Lange Medical Books/McGraw-Hill, New York, NY.
7. Netter, F.H. (ed.) (1998) *Atlas of Human Anatomy,* 2nd Ed. Novartis, East Hanover, NJ.
8. Kawano H., Okada R., and Yano K. (2003) Histological study on the distribution of autonomic nerves in the human heart. *Heart Vessels.* 18, 32–39.
9. Quan, K., Lee, J.H., Van Hare, G., Biblo, L., Mackall, J., and Carlson, M. (2002) Identification and characterization of atrioventricular parasympathetic innervation in humans. *J Cardiovasc Electrophys.* 13, 735–739.
10. Nolte, J. (ed.) (2002) *The Human Brain: An Introduction to Its Functional Anatomy,* 5th Ed. Mosby, St. Louis, MO.
11. Matthews, G.G. (ed.) (1998) *Cellular Physiology of Nerve and Muscle,* 3rd Ed. Blackwell Science, Malden, MA.
12. Evans, J.M., Ziegler, M.G., Patwardhan, A.R., et al. (2001) Gender differences in autonomic cardiovascular regulation: spectral, hormonal and hemodynamic indexes. *J Appl Physiol.* 91, 2611–2618.
13. Ziegler, M.G., Lake, C.R., and Kopin, I.J. (1977) Sympathetic nervous system defect in primary orthostatic hypotension. *N Engl J Med.* 296, 293.
14. Williams, V.L., Cooper, T., and Hanlon, C.R. (1963) Neural responses following autotransplantation of the canine heart. *Circulation.* 27, 713.
15. Watkins, P.J. and MacKay, J.D. (1980) Cardiac denervation in diabetic neuropathy. *Ann Intern Med.* 92, 304–307.
16. Vatner, D.E., Lavallee, M., Amano, J., Finizola, A., Homcy, C.J., and Vatner, S.F. (1985) Mechanisms of supersensitivity to sympathomimetic amines in the chronically denervated heart of the conscious dog. *Circ Res.* 57, 55–64.
17. Lavallee, M., Amano, J., Vatner, S.F., Manders, W.T., Randall, W.C., and Thomas, J.X. (1985) Adverse effects of chronic denervation in conscious dogs with myocardial ischemia. *Circ Res.* 57, 383–392.
18. McGinn, A.L., Wilson, R.F., Olivari, M.T., Homans, D.C., and White, C.W. (1988) Coronary vasodilator reserve after human orthotopic cardiac transplantation. *Circulation.* 78, 1200–1209.
19. Schwaiger, M., Hutchins, G.D., Kalff, V., et al. (1991) Evidence for regional catecholamine uptake and storage sites in the transplanted human heart by positron emission tomography. *J Clin Invest.* 87, 1681–1690.
20. Wilson, R.F., Johnson, T.H., Haidet, G.C., Kubo, S.H., and Mianuelli, M. (2000) Sympathetic reinnervation of the sinus node and exercise hemodynamics after cardiac transplantation. *Circulation.* 101, 2727–2733.
21. Bengel, F.M., Ueberfuhr, P., Schlepel, N., Reichart, B., and Schwaiger, M. (2001) Effect of sympathetic reinnervation on cardiac performance after heart transplantation. *N Engl J Med.* 345, 731–738.
22. Stark, R.P., McGinn, A.L., and Wilson, R.F. (1991) Chest pain in cardiac transplant recipients: evidence for sensory reinnervation after cardiac transplantation. *N Engl J Med.* 324, 1791–1794.
23. Mountcastle, V.B. (ed.) (1980) *Medical Physiology,* 14th Ed. Mosby, St. Louis, MO.

11 Cardiac and Vascular Receptors and Signal Transduction

Physiological and Pathophysiological Roles of Important Cardiac and Vascular Receptors

DANIEL C. SIGG, MD, PhD

CONTENTS

1. INTRODUCTION

Cellular physiological functions are regulated via signaling mechanisms in essentially any cell type of any organ. Although myocardial cells are unique in that they are interconnected to each other with gap junctions and act as an electrical syncytium, there are nevertheless an enormous number of important cellular receptors that allow the cells to receive and respond to various signals. Many of these receptors are located on the cellular membrane.

It would be elusive and clearly beyond the scope of this review to discuss all the receptors of all the cell types in the cardiovascular system. The understanding of molecular cardiovascular biology is continuously growing. Therefore, it is the general aim of this chapter to focus on selected physiologically and pathophysiologically important cardiac and vascular receptors. Nevertheless, many of the principles and mechanisms discussed in the chapter, using certain receptor subtypes as examples, are applicable to related receptor systems and should make it easier to study and understand a "new" receptor signaling system.

Furthermore, a thorough review of the normal function of these receptors is important and very helpful in understanding the altered function of the same receptor systems and associated signaling mechanisms in disease states. For example, how a β-receptor antagonist (β-blocker, a drug that is known to depress cardiac contractility) may be beneficial in the treatment of heart failure, a state of depressed cardiac function, is reviewed.

This chapter also largely focuses on the large and important family of G protein-coupled receptors, with particular emphasis on the β-adrenergic receptor (β-AR) signaling system. The β-AR system has important functions in both normal cardiac physiology and cardiac disease. Other important G protein-

From: *Handbook of Cardiac Anatomy, Physiology, and Devices*
Edited by: P. A. Iaizzo © Humana Press Inc., Totowa, NJ

Table 1
Classification of Cardiovascular Receptors

By location	*By receptor types*
Cardiac receptors	G Protein-coupled receptors
• Myocardial	Tyrosine-kinase-linked receptors
• Conduction system	Guanylate-cyclase-linked receptors
• Other	
Vascular receptors	Other receptors (low-sensitivity lipoprotein receptor, nicotin acetylcholine receptor, peptidergic)
• Endothelial	
• Vascular smooth muscle	
• Other	

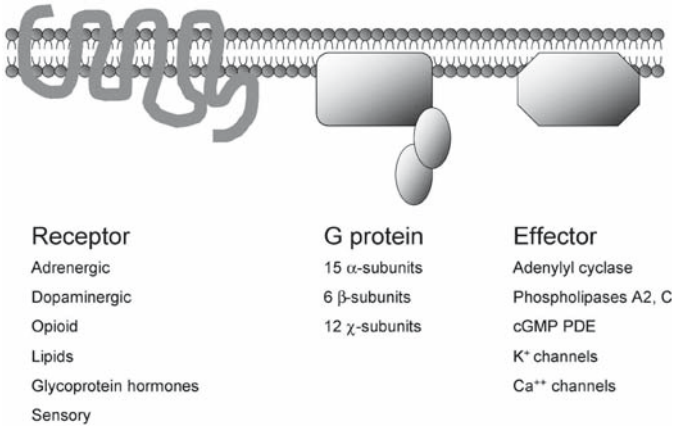

Fig. 1. G protein-receptor-coupled signaling. The ubiquitous seven-transmembrane receptor systems are composed of a receptor, a heterotrimeric G protein, and an effector system. The complexity of this system can be appreciated by the number of receptor types and subtypes, G protein subtypes, and different effector systems.

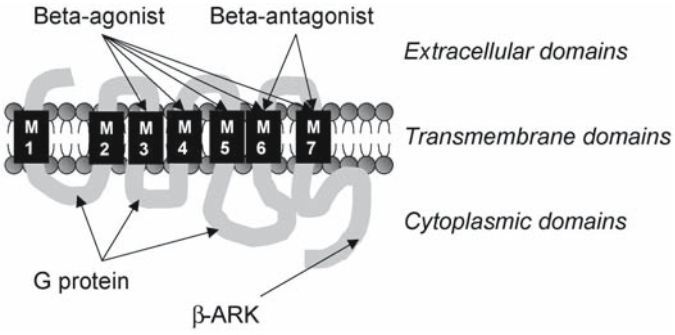

Fig. 2. The molecular schematic structure of a β-adrenergic receptor. Note the three main domains: extracellular, transmembrane, and cytoplasmic. The transmembrane domains are important for ligand binding. The transmembrane domain M3-7 is important in agonist binding, whereas the domains M6 and M7 are involved in antagonist binding (β-receptor blockers). The cytoplasmic domains contain important binding sites for interactions with G proteins as well as various kinases such as β-adrenergic receptor kinase (β-ARK).

coupled receptors are reviewed, such as α-adrenergic receptors (α-ARs) and muscarinic receptors. Finally, non-G protein receptor systems, such as tyrosine-kinase-linked receptors and guanylate-cyclase-related receptors, are briefly discussed.

2. DEFINITION

Cell receptors allow extracellular substances to bind for regulation of intracellular function or metabolism, typically without having to enter the cell. A number of types of cellular receptors can initiate a signal that ultimately modulates cellular function. Most of the "classic" receptors are cell surface receptors, spanning the whole cell membrane and thereby allowing mediation of signals from the extracellular site to the intracellular site. The largest, and possibly most important, group is the family of G protein-coupled receptors. An attempt to classify cardiovascular receptors either by location or by receptor type is shown in Table 1.

3. G PROTEIN-COUPLED RECEPTOR (SEVEN-TRANSMEMBRANE-SPANNING RECEPTORS) AND SIGNAL TRANSDUCTION

3.1. Overview

G protein-coupled receptors are functionally closely related to ion channels. The G protein-coupled receptors are part of a growing gene family identified as binding agonists such as adenosine, catecholamines, acetylcholine (ACh), light, odorants, angiotensin, histamine, opioids, and many others.

3.2. Receptor Structure

Interestingly, there are several structural similarities between ion channels and G protein-coupled receptors. Both are integral membrane proteins with seven-transmembrane domains, which form bundles with a central pocket. In G proteins, the pockets are the binding sites for the receptor ligands, and they are typically located on the extracellular site of the protein; the N-terminal tail is located extracellularly as are three extracellular loops. Three loops connecting the transmembrane domains and the C-terminal domain are located intracellularly (Figs. 1 and 2). The exact functions of the extracellular loops remain largely unknown. It is considered that the transmembrane domains are involved in receptor binding. The intracellular loops, particularly loop III and the C-terminal tail, are important for receptor coupling to the associated G protein. Finally, both loop III and C-terminal tail are important for regulation of receptor function and contain phosphorylation and other posttranslational modification sites.

3.3. Receptor Coupling

The G protein receptors interact intimately with G proteins. G proteins are complexes consisting of three subunits: α, β, and χ. There are different classes of G proteins, and attempts have

Table 2
β-Adrenergic Receptor Subtypes: G Proteins, Tissue Distributions, Effectors, and Signals

Receptor	β_1	β_2	β_3
Primary G protein	Gs Gs/Gi	Gs/Gi	
Tissue distribution	Heart	Vessels, heart, lung, kidney	Adipose, heart
Primary effector in heart tissue	Adenylyl cyclase, L-type calcium channel	Adenylyl cyclase, L-type calcium channel	Adenylyl cyclase
Signals	cAMP/PKA	cAMP/PKA, MAPK	cAMP/PKA

cAMP, cyclic adenosine 3′,5′-monophosphate; Gi, inhibitory G protein; Gs, stimulatory G protein; MAPK, mitogen-activated protein kinase; PKA, protein kinase A.

been made to classify them according to different subtypes. For example, common α-subunits include: (1) α_s (stimulatory), which activates adenyl cyclase (AC); (2) α_i (inhibitory), which inhibits AC; (3) α_0, which modulates calcium channels and phospholipase C; and (4) α_z, which activates phospholipase C. In general, each α-subunit contains a region that interacts with the receptor, a site that binds GTP (guanosine triphosphate), and a site that interacts with the effector system.

3.4. Receptor Function and Regulation

The traditional concepts of G protein-coupled receptor function are best illustrated in Fig. 1. First, an agonist binds to a receptor molecule, and then the seven-transmembrane-spanning receptor molecule interacts with a specific G protein; this in turn modulates a specific effector. Examples of typical agonists, receptors, G proteins, and effectors are provided in Fig. 1. Although this illustration provides a general summary of the individual components needed for proper G protein-coupled receptor function, a more thorough understanding of the G protein receptor-mediated signaling, as well as its regulation, is best accomplished by the more specific example of the well-characterized β-AR system. Therefore, the discussion starts with the physiologically, pathophysiologically, and clinically highly relevant seven-transmembrane-spanning β-AR.

4. β-ADRENERGIC RECEPTORS

4.1. Classification of β-Adrenergic Receptors

Table 2 summarizes the general features of β-AR subtypes identified to date *(1)*; note that there are three subtypes. Although all of the subtypes can be found in the heart, the predominant subtype in the vasculature is the β_2-AR. Importantly, norepinephrine and epinephrine are the endogenous agonists (catecholamines) that bind specifically to all three β-AR subtypes.

Pharmacologically, β_1- and β_2-receptors are characterized by an equal affinity for the exogenous full agonist isoproterenol and epinephrine; norepinephrine (the neurotransmitter of the sympathetic nervous system) has a 10- to 30-fold greater affinity for the β_1-AR subtype. Also, β_1-ARs are more closely located to synaptic nerve termini than β_2-ARs and are therefore exposed and activated by higher concentrations of released norepinephrine.

4.2. β-Adrenergic Activation and Cardiovascular Function

β-ARs are probably one of the most important (and most widely studied) types of cardiac receptor systems. Activation of β-ARs regulates important cardiovascular functions and is integral to the body's "flight-and-fight" response. For example, during exercise, heart rate and contractility both increase, cardiac conduction accelerates, and cardiac relaxation (which is an active process requiring adenosine triphosphate [ATP]) is enhanced. Moreover, vascular relaxation (vasodilation) of many vascular beds can be observed during exercise (e.g., in skeletal muscles).

All these effects are at least partially a direct consequence of β-AR activation and involve key elements of G protein receptor signaling: (1) receptor binding, (2) G protein activation, and (3) activation of an effector system. Importantly, most of these specific physiological cardiac effects are mediated via activation of β_1-AR; the vascular effects are mediated through the β_2-receptor subtype. However, heart muscle also contains β_2-receptors (as well as β_3-receptors). Nevertheless, the β_1-receptor subtype is the predominant cardiac isoform in healthy humans. More specifically, although there is a substantial population of β_2-receptors in the atria, only around 20–30% of the total β-AR population are β_2-ARs in the left ventricle *(2)*.

Not only is the activation of β-ARs and their associated signaling transduction key in understanding the physiology of the cardiovascular system, but also it has been recognized over the past decades that β-AR activations also play key roles in cardiac disease processes such as heart failure *(3)*. For example, an apparent paradox exists, namely, that β-adrenergic blockers (β-receptor antagonists) are beneficial in patients with heart failure; this is discussed in more detail next.

4.2.1. Effects of β-Receptor Activation on the Heart

β-Receptor activation on the heart regulates cardiac function on a beat-to-beat basis. Specifically, β-AR stimulation causes increases in heart rates (positive chronotropic effect), increases in contractility (positive inotropic effect), enhancements in cardiac relaxation (positive lusitropic effect), and/or increases in conduction velocities (positive dromotropic effect). The molecular mechanisms leading to each of these specific effects are discussed. For further details, refer to the textbook by Opie *(4)*. Other important effects on cardiac myocytes that should be noted include those caused by enhanced metabolism.

4.2.2. Positive Chronotropic Effect

When activated, β-ARs located on the cells that make up the sinoatrial node increase the firing rate of the sinoatrial node. Although the mechanisms of these effects are not fully understood, they are known to involve activation of G proteins and

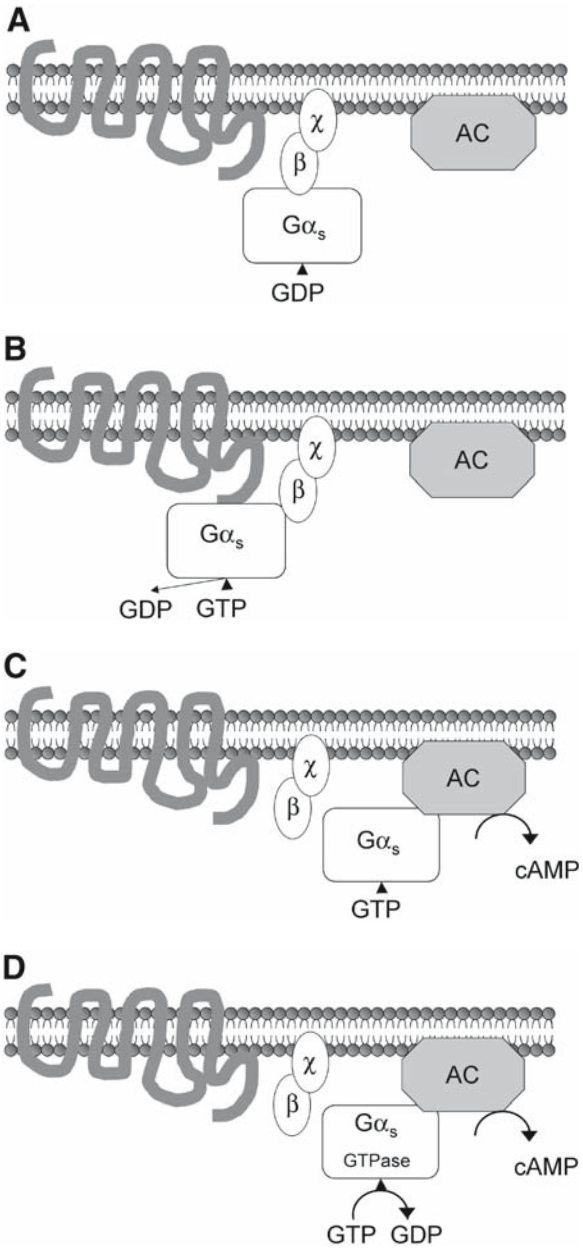

Fig. 3. G protein receptor activation and coupling with adenylyl cyclase (AC) during β-adrenergic receptor activation. **(A)** The receptor is inactive; GDP (guanosine diphosphate) is bound to the α-subunit of stimulatory G protein. **(B)** The agonist binds to receptor, which leads to receptor G protein interaction; GTP (guanosine triphosphate) binds to stimulatory G proteins (α-subunit, Gαs). **(C)** The G-subunits dissociate, and Gαs stimulates adenylate cyclase, with subsequent formation of cAMP (cyclic adenosine 3′,5′-monophosphate). **(D)** Gαs guanosine triphosphatase (GTPase) becomes active, GDP re-forms, and the activation cycle ends.

formation of cyclic adenosine 3′,5′-monophosphate (cAMP), called a "second messenger." Cyclic AMP can then bind to ion channels, which are partly responsible for the diastolic (phase 4) depolarization of sinoatrial nodal cells. These ion channels, referred to as hyperpolarization activated cyclic nucleotide-gated (HCN) channels, have some unique properties; they (1) activate during hyperpolarization (more negative membrane potentials); (2) are responsive to cAMP; (3) are conductive for both Na^+ and K^+ ions; and (4) can be blocked by cesium.

Cyclic AMP binding to the intracellular domain of these ion channels shifts their activation curves to more positive potentials, which increases the rates of "spontaneous" depolarization of sinoatrial nodal cells and ultimately their firing rates. The chronotropic effects can be mediated either via norepinephrine released from sympathetic nerve endings in the sinoatrial node or from circulating catecholamines (epinephrine and norepinephrine). From an integrative physiology standpoint, increasing heart rates is an adaptive response to an increased demand of oxygen and cardiac output in the periphery. Accelerating the heart rate will in turn increase cardiac output if stroke volume remains constant (Cardiac output = Heart rate × Stroke volume).

4.2.3. Positive Inotropic Effects

As mentioned, cardiac output needs to increase during exercise. One way to accomplish this is by increasing the heart rate; another is to increase stroke volume, such as by increasing cardiac filling (increasing preload). This can be accomplished by increasing the venous tone of the great veins, which will increase filling of the heart chambers. It should be noted that this is an effect that is also mediated by adrenergic receptors, but in this particular case, by α-ARs causing venoconstriction (secondary to increased calcium influx). Such an increased preload then induces increased filling (and stretching) of the myocardial chambers, and via the Frank-Starling mechanism, stroke volume becomes augmented. However, stroke volume can also be efficiently improved by increasing the contractile force of the heart muscle at a given constant muscle length (i.e., independent of fiber length); this is called a *positive inotropic effect* and is mediated by activation of β-ARs, both β_1-AR and/or β_2-AR. The detailed molecular mechanisms involve the following processes (Fig. 3):

1. β-Agonist binds to either β_1- or β_2-receptor.
2. GTP binds to the stimulatory α-subunit of the G protein (Gαs) and activates it.
3. The G-subunits dissociate (the α-subunit dissociates from the β-subunit and χ-subunit).
4. The α-subunit (containing GTP) stimulates the effector protein AC.
5. cAMP is formed, and GTP is hydrolyzed to GDP (guanosine diphosphate) plus Pi (the α-subunit/GTP is a GTPase [guanosine 5′-triphosphatase]).
6. The α-subunit/GDP binds to the β- and χ-subunits, and the initial (inactive) resting state reforms.

4.2.4. The Second Messenger Concept

cAMP is one of the key effector molecules in many of the signaling processes involving β-ARs (and in many other receptor systems). This molecule is commonly referred to as a second messenger and is one of many second messengers identified that are involved in cellular signal transduction. Another highly relevant second messenger is cyclic guanosine monophosphate (cGMP); cGMP is typically formed in vascular cells after binding nitric oxide, but is also formed in cardiac and other cells after binding natriuretic peptides (NPs). As the name

implies, these molecules trigger additional signaling mechanisms. Importantly, cAMP is present in all cardiac myocytes; it is rapidly turned over, and there is a constant dynamic balance between cAMP generation and breakdown via phosphodieasterases (enzymes that break down cAMP).

Although cAMP can increase in response to β-adrenergic activation, there are other pharmacologically active agents that can lead to increased cAMP levels via alternate mechanisms. For example, glucagon is known to stimulate AC via a non-β-AR mechanism; forsokolin stimulates AC directly; and phosphodieasterase inhibitors such as milrinone, amrinone, and others inhibit the breakdown of cAMP, resulting in increased cAMP levels. The exact mechanism of how formation of cAMP leads to increased cardiac contractility in cardiac myocytes is discussed in the following paragraphs.

It is known that cAMP enhances the activity of protein kinase A. Once activated, protein kinase A causes phosphorylation of numerous proteins, including voltage-dependent sarcolemmal calcium channels, phospholamban (located in the sarcoplasmic reticulum), troponin I, and troponin C. The primary effect of phosphorylating the calcium channels and phospholamban is that this increases calcium influx during a cardiac activation cycle and increases calcium uptake by the sacroplasmic reticulum.

Working in concert, these effects will ultimately result in increased calcium transients during cardiac excitation–contraction coupling. Further, these increased intracellular calcium transients will result in increased ATP splitting by the myosin ATPase (adenosine triphosphatase), which then increases the rate of development of contractile force (and increases deinhibition of actin and myosin by the interaction of calcium with troponin C), ultimately causing an increase in total cardiac force development. If this stimulation is maintained, this effect or response often becomes attenuated over time. Also, cAMP levels may decrease, for example, because of activation of calmodulin, which activates cAMP breakdown via phosphodieasterase activation and via activation of β-AR kinase (β-ARK activation and downregulation).

It is important to recognize that the response to β-AR stimulation cannot simply be explained by overall increased tissue levels of cAMP. It has been speculated that cAMP may be compartmentalized in the heart, with a specific compartment available to increase contractility *(5)*. In addition, it has been shown that both β_2-ARs and β_1-ARs mediate positive inotropic responses independent of cAMP generation. This last response may, in some cases, be one of the myopathic mechanisms in chronic heart failure by resulting in increased systolic and diastolic calcium levels *(6)*.

The complexity of the β-AR stimulatory G protein AC signaling system can be further illustrated by the fact that there are approx 20 identified Gαs, five β-subtypes, and 11 χ-subtypes, in addition to 9 isoforms of AC *(7)*. In cardiac tissue, isoforms V and VI of AC are considered to predominate. Specific anchoring proteins enable the juxtaposition of protein kinase A with its specific target proteins (A-kinase-anchoring proteins), which may account for the resulting compartmentalization (and complexity) of both physiological and pathophysiological responses.

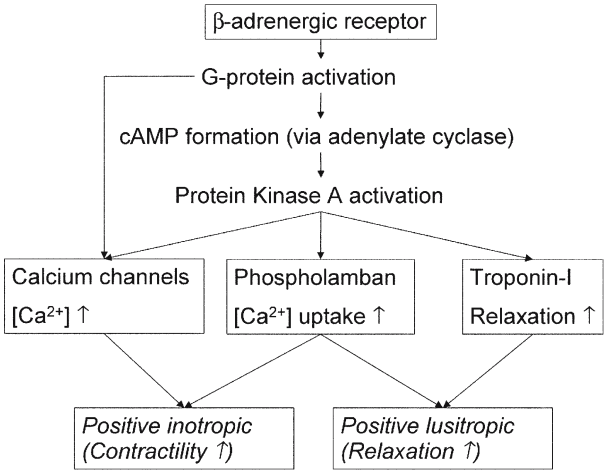

Fig. 4. The major intracellular signaling mechanisms involved in the regulation of cardiac contractility and relaxation following β-adrenergic receptor activation. It should be noted that there is also the possibility that L-type voltage-dependent calcium channels can be activated via a direct effect of a stimulatory G protein (Gαs) subsequent to β-adrenergic receptor (both β_1- and β_2-adrenergic receptors) activations. This overall signaling pathway is cAMP (cylic adenosine 3′,5′-monophosphate) independent. The resulting increased systolic and diastolic calcium fluxes are considered to become a potentially myopathic mechanism in chronic heart failure.

4.2.5. Positive Lusitropic Effects

Phospholamban can be activated by protein kinase A (via cAMP) or by increased calcium levels subsequent to voltage-gated calcium channel activation (secondary to protein kinase A phosphorylation). This typical phosphorylation of phospholamban leads to increased activity of this enzyme, which then results in enhanced calcium removal from the cytosol back into the sarcoplasmic reticulum. It is known that the activation of troponin I, via protein kinase A, increases the rate of crossbridge detachment and relaxation. Importantly, both of these responses will increase the rate of relaxation, an active process to remove calcium from the cytosol. A basic summary of the mechanisms of β-adrenergic increase in cardiac contractility and relaxation is provided in Fig. 4.

4.2.6. Dromotropic Effects

Activation of the voltage-gated (L-type) calcium channels in the atrioventricular node enhances conduction in these nodal cells as well as in the Purkinje fibers.

4.2.7. Metabolic Effects

In general, the metabolic effects mediated via the β-AR system include: (1) increases in glycogen formation (via increased glycogenolysis as well as decreased formation of glycogen); (2) the stimulation of lipolysis; or (3) increases in ATP production (via glycolysis/citrate cycle). Some of these metabolic effects may be mediated via the β_3-AR (e.g., control of lipolysis). The β_3-AR is also considered to have some regulatory function in cardiac (and vascular) contractility (e.g., negative inotropic effects) *(8)*.

4.2.8. Effects of β-Receptor Activation in the Vasculature

The main physiological function of β-AR activation is vascular relaxation (vasodilation), which is induced via a reduction of cytosolic calcium levels in the smooth muscle cells composing these vessels, with relaxation having the greatest importance in arterioles. These relaxation responses are mediated via the β_2-AR subtype and are antagonized by α-AR activation (α_1-receptor subtype). The effects of α-receptor signal transduction are discussed further below. The most significant effects on dilation in the coronary artery bed are mediated via metabolic waste products (CO_2 and so forth).

4.3. β-Adrenergic Regulation

To understand β-AR regulation best, it is useful to review the molecular structure of this receptor. Basically, the receptor is composed of three types of domains: (1) the extracellular domain; (2) the transmembrane domains, which are involved in the agonist and antagonist binding (ligand binding); and (3) the intracellular or cytoplasmic domains, which are important for G protein interactions and interactions with kinases such as β-ARK (Fig. 2).

4.3.1. β-Adrenergic Receptor Desensitization and Downregulation

Receptor *downregulation* can be defined as a reduced presence in functional numbers of receptors in the cell membrane. Downregulation could result from internalization (and destruction in lysosomes), decreased rates of receptor degradation (nonlysosomal), or decreased synthesis. *Desensitization* can be defined as receptor refractoriness, a state of decreased activity following continued stimulation.

Yet, it should be noted that one cannot always identify a clear distinction between these two definitions in the literature. For example, the β-receptor can become desensitized during isoproterenol stimulation (a classic pharmacological β-adrenergic agonist). In contrast, during continuous β-AR stimulation, the enzyme β-ARK increases its activity; β-ARK phosphorylates the cytoplasmic domain sites of the β-AR (Fig. 2) and is able to uncouple the receptor from the Gαs (stimulatory G protein). This response acts as a block of the signal, and activation of AC is decreased; in other words, AC is uncoupled from the β-AR. Resensitization can occur once the receptor has been dephosphorylated. This mechanism is called *agonist-specific desensitization*. *Non-agonist-specific* desensitization can occur via second messenger cAMP (and via diacylglycerol [DAG], which activates protein kinase A and C), which phosphorylates the G protein-coupled receptors.

Specific examples of "physical" downregulation include internalization of receptors during continuous prolonged β-AR stimulation, which can be induced either pharmacologically (such as in an intensive care unit setting) or is observed in heart failure (increased sympathetic tone and circulating catecholamines). This last response may be a protective mechanism to minimize calcium overload of the cardiac myocytes secondary to β-adrenergic stimulation. Additional clinical examples of receptor regulation include hypersensitivity to β-AR agonists after propranolol (a β-AR blocker) withdrawal following long-term use. This enhanced sensitivity is considered to be caused by receptor externalization. Another example is drug tolerance to dobutamine (or other β-AR agonists); the molecular mechanisms underlying this clinical phenomenon may be desensitization.

Although agonist-specific and unspecific desensitization can be viewed as one of the classical concepts of receptor regulation, G protein receptor kinases, such as β-ARK and associated proteins (β-arrestins), seem to function by other mechanisms. For example, β-arrestins are considered to interact with a G protein-coupled receptor and thus inhibit further G protein coupling after the receptor has been phosphorylated by β-ARK. Even though this more traditional role is now well established, β-arrestins have also been shown to be involved in receptor internalization as well as complex additional signaling mechanisms (e.g., mitogen-activated protein kinase [MAPK] pathways) *(9,10)*. Internalization (also known as *sequestration* or *endocytosis*) may serve various functions including: resensitization (dephosphorylation of receptor) and recycling; or altering signaling processes. Typically, the mechanisms of internalization involve the classically described clathrin-coated pit processes (caveolae) and also noncoated pit mechanisms. Another interesting role of β-arrestins is in ubiquitination; this is a means by which proteins are marked for subsequent degradation. For example, β-arrestin ubiquitination is important for β_1-AR internalization; receptor ubiquitination is necessary for lysosomal targeting and degradation of the receptors *(11)*. The gene regulation of the β-AR has been extensively reviewed elsewhere *(7)*.

4.4. The Association Between β-Adrenergic Receptors and Cardiac Disease

The function of the β-AR signaling pathway not only is of great importance in the normal regulation of physiological cardiac vascular function, but also has critical, although different, roles in chronic heart failure. Heart failure is a syndrome defined by an inability of the heart to pump adequate amounts of blood to the body organs. The normal physiological response to an inadequate blood (oxygen) supply is to increase the cardiac output (and thereby oxygen delivery) via activation of the adrenergic nervous system (sympathetic nervous system); this response is characterized by an increase in circulating catecholamines.

Although this sympathetic response would intuitively be seen as beneficial, and indeed is also initially adaptive, in reality the sustained β-AR activation and increased norepinephrine tissue levels *(12)* are associated with negative biological effects. Therefore, a sustained β-AR response in fact may be considered both maladaptive and inappropriate.

Consistent with this notion, adrenergic drive is increased in virtually all chronically failing human hearts with systolic dysfunction, as well as in all animal models of hemodynamic overload. Thus, adrenergic drive can also be considered as a "servo-control" mechanism to maintain cardiac performance at an acceptable level *(7)*. On the molecular level the proportion of β_1- to β_2-adrenergic subreceptor populations in normal human ventricles shifts from 75/25 in diseased human ventricles to about 50/50 in normal human ventricles *(13)*. Both receptor subtypes are typically desensitized because of uncou-

pling of the receptors from their signaling pathways associated with increased β-AR phosphorylation as well as upregulation of the inhibitory G protein, Gi.

To illustrate the maladaptive β-AR signaling response, it is important to consider that β-adrenergic agonists, given to patients with chronic heart failure, may actually increase mortality. In contrast, the administration of β-blockers has been shown to improve survival; β-AR blockers in 2003 were one of the cornerstones of medical/drug therapy for patients with chronic heart failure.

In certain patients with cardiac failure, there is a situation in which increased adrenergic drive is required to maintain the circulatory needs of their bodies. The more the heart is activated adrenergically, the more profound are the effects of desensitization, which in turn activates the adrenergic system even more, ultimately causing myocardial tissue damage. Based on the studies in which β-AR blocking agents were administered, it is generally believed that the β-AR system is central in this vicious (pathological) cycle, which is commonly characterized by progressive remodeling and myocardial dysfunction.

4.4.1. β-Adrenergic Signaling and Heart Failure

One of the hallmarks of chronic heart failure is adrenergic overdrive leading to β-AR downregulation and desensitization. In particular, β_1-ARs have been shown to be downregulated selectively; the β_2-ARs are relatively increased, so that as mentioned above, the population of β_1 to β_2 shifts from 75/25 to about 50/50. The marked uncoupling of the β-AR receptors from the G proteins is attributable to increased levels of β-ARK1, as well as increased inhibitory G protein (Gi) *(14)*. This in turn results not only in attenuated β-AR signaling, but also in activation of additional pathways involved in ventricular remodeling (*see* below).

The shift of the β_1/β_2-AR subpopulation to an increased number of β_2-receptors is only one of the phenomena associated with chronic heart failure. More specifically, β_2-ARs couple to a number of signaling pathways, including a potential coupling to an inhibitory G protein (Gαi). Also, β_2-ARs may modulate several G protein-independent pathways, including inhibition of sodium–hydrogen exchangers as well as a non-protein kinase A-dependent interactions with L-type calcium channels *(15,16)*. There is a variety of other G protein-independent pathways in which the β_2-ARs have been implicated, such as those associated with phosphatidylinositol kinase, phospholipase C/protein kinase C (PKC), or arachidonic acid signaling. And, although many details of these mechanisms remain poorly understood, it is becoming more clear that some of these pathways may also play important roles in the molecular pathobiology of heart failure.

One of the widely recognized mechanisms of β-AR desensitization is agonist-dependent β-ARK-mediated phosphorylation of the β-AR itself. Moreover, the β-γ-subunits of the G proteins can act as signaling molecules themselves, with the potential of activating many downstream targets of pathways, such as ACs, PLC, PLA2, PI3K, K^+ channels, or Src-Ras-Raf-MEK-MAPK *(7)*.

The potentially toxic effects of long-term β_1-AR receptor activation are also illustrated by the fact that selective β_1-AR agonist or receptor overexpression leads to increased cardiac apoptosis (programmed cell death) *(17–19)*. The mechanisms by which such apoptosis is activated has been attributed partly to initial activation of calcineurin via increased intracellular calcium through L-type calcium channels *(20)*. In addition, direct toxic effects of catecholamines on the myocytes have been described as a result of direct β-AR activation *(12)*.

Table 3
β-Adrenergic Receptor Signaling Pathways in Heart Failure

Molecule	*Change*
β_1-AR	↓, uncoupled
β_2-AR	No change, uncoupled
β-ARK1	↑
β-Arrestin 1 and 2	No change
Ga1	↑

Source: Modified from ref. *1*.
AR, adrenergic receptor; ARK, adrenergic receptor kinase.

Other effects of chronic β-AR signaling include production of cytotoxicity via calcium overload, increased free-radical formation, as well as stimulation of pathological hypertrophy *(7)*. For example, the marked uncoupling of β_1- and β_2-receptors from their physiological signaling pathways not only results in attenuation of the β-AR signaling, but also allows for the coupling of the receptors with other (possibly myopathic) signaling pathways involved in ventricular remodeling (MAPK and PI3K cascades). As alluded, β-receptor antagonists may be beneficial in chronic heart failure. Specifically, the β_1-specific β-AR blocking drug metoprolol produces reverse remodeling similar to a combined α-β-blocker carvedilol, suggesting that β_1-AR receptor signaling is an important determinant of pathological hypertrophy in human heart failure *(21)*.

Last, genetic heterogeneity in expression of the β-AR in the general population has been identified, which may affect disease susceptibility. For example, a substitution of threonine to isoleucine at amino acid 164 in the β_2-AR has been associated with reduced survival and exercise tolerance in patients with heart failure *(22,23)*.

A summary of the known changes in β-AR signaling is provided in Table 3. It should be mentioned that investigations using transgenic animal models have greatly helped elucidate some of the important disease mechanisms associated with adrenergic receptor reception pathways; they have also served as tools in identifying and testing novel or evolving therapeutic targets for the treatment of heart failure *(1)*.

5. α-ADRENERGIC RECEPTORS

5.1. Physiology

Two major α-AR subtypes have been identified: α_1 and α_2. The α_1-type receptors have been described as present in the heart, vessels, and smooth muscle. The primary response to their activation in cardiac cells is phospholipase C-β, which leads to an increase in DAG and inositol triphosphate ($InsP_3$)

and activation of both PKC and MAPKs. Physiological receptor agonists include norepinephrine and epinephrine, and a Gq protein is the primary associated G protein *(24)*. In general, the primary physiological importance of α_1-receptors is far greater in the vasculature, leading to calcium influx and vasoconstriction via the second messenger $InsP_3$. In cardiac muscle cells, α_1-receptors have been shown to induce a positive inotropic effect; this response is associated with formation of $InsP_3$ *(25)*. The α_2-receptors have been identified on coronary vessels and in the central nervous system (presynaptic); they reduce the activity of AC (and protein kinase A) via an inhibitory G protein.

In summary, the primary physiological role of α_1-receptors is within the vasculature for the regulation of vascular tone via vasoconstriction, which is secondary to calcium influx into the smooth muscle cells of the circulatory arterioles.

5.2. Role in Disease States

In general, in patients with heart failure, the α_1-AR system will elicit an increase in receptor density and is also characterized by changes in inotropic responses *(26)*. In addition, α_1-AR activation promotes cardiomyocyte hypertrophy via activation of hypertrophic MAPK pathways.

6. ROLE OF ADRENERGIC AND OTHER RECEPTORS IN MYOCARDIAL HYPERTROPHY

Repeated increased workloads on the heart lead to cardiac hypertrophy. Hypertrophy is characterized by increased contractile protein content (and muscle mass), myofilament reorganization, and reexpression of embryonic markers. As discussed, myocyte cell growth by G protein-coupled receptors may involve not only ras and MAPK pathways, but also other signaling pathways (e.g., calcineurin, P-I3-K and phosphotidylinositol-3-OH). Abnormal β-AR function with hypertrophy is also characteristic; in particular, elevated myocardial levels of β-ARK1 can be detected *(27)*. As mentioned, α_1-receptor signaling also may be very important in the development of cardiac hypertrophy. Specifically, Gq-coupled receptors, such as angiotensin, α-1-AR, and endothelin, can all activate hypertrophic MAPK pathways *(28,29)*.

To summarize, the cardiac hypertrophic response may not be compensatory to reduce wall stress, but rather maladaptive, thus increasing mortality. In particular, signaling pathways involving catecholamines (norepinephrine and epinephrine) and Gq-coupled receptors seem to activate hypertrophic responses. Targeting these specific signaling pathways may be a novel therapeutic approach for the potential treatment of "maladaptive" cardiac hypertrophy and ultimately heart failure. For further details on this topic, refer to the review by Rockman et al. *(1)*.

7. MUSCARINIC RECEPTORS

The muscarinic receptor system in the heart is also an associated G protein-coupled receptor system. The main cardiac receptor subtype (M2 receptor) is a cholinergic receptor, and thus it mediates primary parasympathetic (cholinergic) nervous system responses. Its general function is to balance and antagonize the sympathetic effects of β-AR activation simultaneously, with its most pronounced effects on the controls of the sinoatrial (heart rate, chronotropic effects) and atrioventricular nodes (conduction, dromotropic effects). There exist very few muscarinic M2 receptors in the ventricles, hence activated negative inotropic (contractility) effects subsequent to M2 receptor activation are very small.

A typical control signal mediated via the vagus nerve leads to a local release of ACh in the sinoatrial and atrioventricular nodes. ACh then binds to the M2 receptor, activates an inhibitory G protein (Gαi), and essentially decreases the activity of AC, which directly leads to opening of K^+ channels.

In the sinoatrial node, vagal stimulation tends to flatten the diastolic depolarization, which then induces a slowing of heart rate (bradycardia, negative chronotropic effect), possibly not only via the effects of reduced cAMP availability on I_f current (hyperpolarization activated cyclic nucleotide-gated channel), but also via activation of a potassium outward current, which in concert decreases the spontaneous firing rate of the sinoatrial node.

In the atrioventricular nodal tissue, vagal stimulation also activates an inhibitory G protein, which causes a slowing conduction velocity via a decreased calcium influx through L-type calcium channels. Clinically, the effects of vagal stimulation on the atrioventricular node are detected as increased atrioventricular nodal conduction times (e.g., prolonged PR interval).

The M3 muscarinic subtype is primarily found in vascular smooth muscle cells. Its activation leads to contraction of vascular smooth muscles via a Gq/11-PLC-InsP3-mediated calcium influx (as well as DAG/PKC, cAMP elevation).

8. OTHER G PROTEIN-COUPLED CARDIOVASCULAR RECEPTORS

There is a variety of other G protein-coupled cardiovascular receptor systems that have important roles in cardiac physiology and pathophysiology. It is beyond the scope of this chapter to review all these systems in detail, but for comprehensiveness, a representative list of nonadrenergic and nonmuscarinic G protein-coupled receptor systems and their respective functions considered important is provided in Table 4.

9. RECEPTOR CROSS TALK

Cross talk between receptors refers to a biological phenomenon by which interactive regulatory (or modulatory) messages are sent from one receptor to another. Many of the aforementioned receptor pathways are engaged in some degree of cross talk, which is commonly via second messengers and/or protein kinases, which in turn modulate G protein-mediated messages. Although the current understanding of receptor cross talk is far from complete, it is clear that receptor cross talk is integral for sustaining a coherent function of the cardiovascular system and has implications in both normal physiology and cardiac disease states.

The following is an example of cardiovascular cross talk with relevance to the pharmacological treatment of cardiac disease. As reviewed here, heart failure generally is characterized not only by dysfunction of the β-AR receptor system (downregulation of β_1-receptors, uncoupling of β-AR and AC), but also by the renin-angiotensin system (downregulation of angiotension II type 1 (AT1) receptors); distinct signaling path-

Table 4
Other Cardiovascular G-Protein-Coupled Receptor Systems

Family	*Type*	*Cardiovascular function*	*G-Protein*	*Signaling*
Adenosine	A1	Bradycardia	Gi/o	AC inhibition; [K^+] opening
	A2A	Vasodilation	Gs/G15	AC, PLC-β
	A2B	Vascular smooth muscle relaxation	Gq/11?	PLC/AC-mediated calcium activation
	A3	A1 modulation	Gi3	AC inhibition; PLC, InsP3-mediated calcium increase
Angiotensin	AT1	Vascular smooth muscle contraction; cell proliferation; cell hypertrophy; antinatriuresis	Gq/11	PLC/PKC-mediated calcium elevation
	AT2	Vasodilation; apoptosis; growth inhibition; natriuresis; nitric oxide production	Gia2/Gia3	MAPK activation; [K^+] opening; PTPase activation leading to T-type calcium channel closure
Endothelin	ETA	Vasoconstriction	Gq/11	PLC/InsP3; cAMP
	ETB	Vasodilation/vasoconstriction (ETB2)	Gi; Gq/11	cAMP inhibition; PLC/InsP3 calcium increase
Opioid	OP1 (delta), OP3 (mu)	Central cardiovascular regulation (OP1, 3); cardioprotection (OP1)	Gia1/3; Go	I_K conductance activation; reduction in neuronal I_{Ca}; AC inhibition; PKC and K_{ATP} channel activation (cardioprotection)

AC, adenyl cyclase; AT1, AT2, angiotensin receptor 1, 2; ETA, endothelin A; ETB, endothelin B; Gi, inhibitory G protein; Gs, stimulatory G protein; Gq/11, Go, G15, other G proteins; ICa, voltage-dependent calcium channel (current); IK, voltage dependent potassium channel (current); InsP3, inositol triphosphate; K_{ATP}, potassium ATP channel; MAPK, MAP Kinase; OP1, delta-opioid receptor; OP3, mu-opioid receptor; PKC, protein kinase C; PLC, phospholipase C.

ways characterize both β-AR (e.g., via Gs and AC) and AT1 receptor signaling (e.g., via Gq/11 and PLC-β).

It was shown that selective blockade of β-AR inhibited angiotensin-induced contractility; selective blockade of AT1 receptors reduced catecholamine-induced reduction in heart rate *(30)*. These unusual transinhibitory effects were considered caused by underlying G protein-receptor uncoupling. Furthermore, direct interactions of these receptor systems were demonstrated in vivo, and it is speculated that such interactions may have a profound role in determining the ultimate responses to drugs designed to block a given receptor (e.g., β-AR blockers, AT1 receptor blockers). Cardiovascular receptor cross talk has been extensively reviewed by Dzimiri *(31)*.

10. GUANYLATE-CYCLASE-LINKED RECEPTORS

10.1. Soluble Guanylyl Cyclase (Receptor for Nitric Oxide)

Although structurally different, the general principles of receptor signaling as discussed for β-AR apply also for nitric oxide/guanylyl cyclase (GC) signaling. Specifically, the agonist (nitric oxide) is a universal signaling molecule present in all tissues, and its role is important not only in normal physiology, but also in disease. Physiologically, nitric oxide is produced by several isoforms of the enzyme nitric oxide synthase (NOS). Three isoforms have been described to function within the cardiovascular system: eNOS, iNOS, and nNOS.

Nitric oxide is a small, lipid-soluble gas molecule that readily crosses cell membranes. Inside the cell, it typically binds to a receptor, the soluble (cytoplasmatic) GC (an enzyme that converts GTP to cyclic 3′,5′-GMP). cGMP is the second messenger and, in the cardiovascular system, can activate two major effector systems: cGMP-regulated phosphodiesterases and cGMP-dependent protein kinases (cGKs).

In the vascular smooth muscle cells, nitric oxide inhibits vascular smooth muscle constriction (causes vasodilation) via inhibition of cytoplasmic calcium release. However, the underlying mechanisms for the important vasodilatory effect of nitric oxide are complicated and involve a cGMP-dependent protein kinase (cGKI); these pathways have been reviewed in detail elsewhere *(32)*. Nitric oxide has also been shown to reduce vascular smooth muscle proliferation (clinically important in in-stent restenosis) and migration. It is well established that nitric oxide release may reduce platelet adhesion and activation, as well as vascular inflammation *(33)*. Importantly, nitric oxide insufficiency is considered an important factor in endothelial dysfunction, leading to the increased susceptibility for arterial thrombosis formation *(34)*.

The relevance of nitric oxide signaling is not limited to vascular biology or pathobiology; it has been demonstrated that nitric oxide has an important pathophysiological role in heart failure as well—in the modulation of cardiac function, cardiovascular protection, or in the regulation of apoptosis *(35–37)*.

10.2. Membrane Guanylyl Cyclase A (Receptors for Natriuretic Peptides)

To date, at least seven membrane-bound enzymes synthesizing cGMP have been identified. All seven of these membrane GCs have a common structure (Fig. 5). For the purpose of this discussion, guanylyl cyclase A (GC-A) has the greatest importance relative to the heart and thus is discussed in detail.

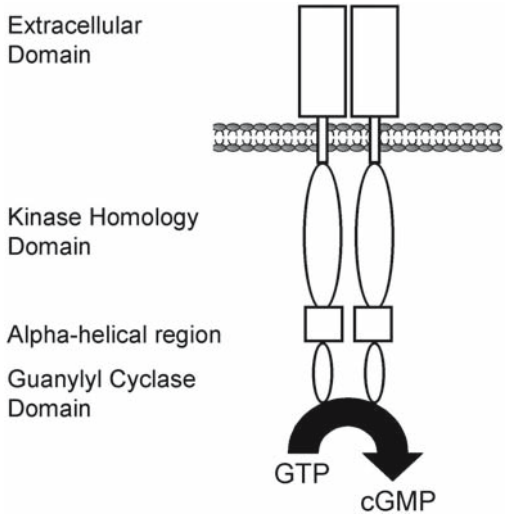

Fig. 5. Basic topology of membrane guanylyl cyclase A receptor. The membrane guanylyl cyclase forms homodimers or higher order structures. cGMP, cyclic guanosine monophosphate; GTP, guanosine triphosphate. Modified from ref. *38*. © 2003 Lippincott, Williams, and Wilkins.

10.3. Physiology

Currently, three NPs have been identified: ANP, BNP, and CNP. Both ANP and BNP bind to GC-A and are released in the heart; they are considered cardiac hormones. In general, CNP is mainly produced by the vascular endothelium and may be a regulator of vascular tone and cell growth through guanylyl cyclase B activation.

The receptor consists of an extracellular domain, a kinase homology domain, an α-helical amphipathic region (hinge region), and a C-terminal GC (catalytic) domain (Fig. 5). This receptor is considered to exist in dimers.

The major effects of GC-A are via the formation of and the activation by cGMP. In general, because the agonists are circulating hormones (peptides), a variety of organ systems can be affected simultaneously following ANP/BNP release. ANP is mainly produced in the atrium, and BNP is produced primarily in the ventricles. The primary triggering factors for ANP/BNP release are wall stretch or pressure increases, but they may also involve neurohumoral factors (glucocorticoids, catecholamines, angiotensin II, and so forth). The main effect of ANP/BNP release is modulation of blood pressure/volume. The half-lives of ANP/BNP are around 2–5 min.

Interestingly, although both ANP and BNP bind to the same receptors, it has been shown that targeted genetic disruption of ANP or BNP in mice induces a unique phenotype; ANP-deficient mice show arterial hypertension, hypertrophy, and cardiac death, and the BNP-deficient mice phenotype is characterized mostly by cardiac fibrosis. More specifically, BNP has a lower affinity to GC-A than ANP and may act mostly as a local paracrine (antifibrotic) factor. Also, under physiological conditions, the ANP levels are much higher than BNP levels in the circulating blood, and the potency for induced vasorelaxation is also less for BNP compared to ANP *(38)*.

The cardiovascular effects of ANP–GC-A are complex, but can be summarized as hypovolemic and hypotensive, effects that are induced via hormonal, renal, vascular, central nervous system, and other mechanisms. The mostimportant hypotensive effects also involve decreased sympathetic activity and complex renal responses, which subsequently lead to increased diuresis *(38)*.

10.4. Role in Cardiac Disease

During chronic hemodynamic overload, ANP and, to an even greater level, BNP expression in the cardiac ventricles is significantly increased. This response may not only maintain both arterial blood pressure and volume homeostasis, but also locally prevent hypertrophy (ANP) and fibrosis (BNP) factors. Although ANP/BNP levels are increased in patients with cardiac hypertrophy or heart failure, the GC-A-mediated effects of these peptides are diminished.

Mechanisms for these responses may be postreceptor defects such as dephosphorylation of GC-A, sequestration of NP by a clearance receptor, altered transcriptional regulation at the gene level, or others *(31)*. However, the processes regulating GC-A activity (and desensitization) are largely unknown. Yet, synthetic BNP (nesiritide) and ANP (anaritide) have been shown to be highly beneficial in the acute treatment of heart failure. Hence, it is conceivable that the thorough understanding of the mechanisms for chronic desensitization, as well as regulation of GC-A receptor signaling, might be important for the development of novel therapeutic approaches for various forms of cardiac disease.

11. SUMMARY

Cellular physiological functions are regulated via signaling mechanisms in essentially any cell type of any organ. Although myocardial cells are unique in that they are interconnected to each other with gap junctions and act as an electrical syncytium, there is nevertheless an enormous number of important cellular receptors that allow the cells to receive and respond to various signals. This chapter reviewed the role and signaling mechanisms of selected physiologically and pathophysiologically important cardiac and vascular receptors, with emphasis not only on G protein-coupled receptors (e.g., β-ARs), but also on non-G protein-coupled receptor systems, such as GC-related receptors (e.g., receptors for nitric oxide).

REFERENCES

1. Rockman, H.A., Koch, W.J., and Lefkowitz, R.J. (2002) Seven-transmembrane-spanning receptors and heart function. *Nature*. 415, 206–212.
2. del Monte, F., Kaufmann, A.J., Poole-Wilson, P.A., et al. (1993) Coexistence of functioning β-1 and β-2 adrenoreceptors in single myocytes from human ventricle. *Circulation*. 88, 854–863.
3. Bristow, M.R., Hershberger, R.E., Port, J.D., et al. (1990) B-adrenergic pathways in non-failing and failing human ventricular myocardium. *Circulation*. 82, 112–125.
4. Opie, L. (1998) Receptors and signal transduction, in *The Heart: Physiology, From Cell to Circulation,* 3rd Ed. (Opie, L., ed.), Lippincott, Williams, and Wilkins, Philadelphia, PA, pp. 173–207.
5. Hohl, C.M. and Li, Q. (1991) Compartmentation of camp in adult canine ventricular myocytes. Relation to single cell free calcium transients. *Circ Res*. 69, 1369–1379.

6. Lader, A.S., Xiao, Y.F., Ishikawa, Y., et al. (1998) Cardiac Gsα overexpression enhances L-type calcium channels through an adenylyl cyclase independent pathway. *Proc Natl Acad Sci USA*. 95, 9669–9674.
7. Port, J.D. and Bristow, M.R. (2001) Altered B-adrenergic receptor gene regulation and signaling in chronic heart failure. *J Mol Cell Cardiol*. 33, 887–905.
8. Gauthier, C., Langin, D., and Balligand, J.L. (2000) B3-adrenoceptors in the cardiovascular system. *Trends Pharmacol Sci*. 21, 426–431.
9. Laporte, S.A., Oakley, R.H., Holt, J.A., Barak, L.S., and Caron, M.G. (2000) The interaction of β-arrestin with the AP-2 adaptor is required for the clustering of β-2 adrenergic receptor into clathrin coated pits. *J Biol Chem*. 275, 23,120–126.
10. Luttrell, L.M., Ferguson, S.S., Daaka, Y., et al. (1999) B-arrestin-dependent formation of β-2 adrenergic receptor-Src protein kinase complexes. *Science*. 283, 655–661.
11. Shenoy, S.K., McDonald, P.H., Kohout, T.A., and Lefkowitz, R.J. (2001) Regulation of receptor fate by ubiquitination of activated β-2 adrenergic receptor and β-arrestin. *Science*. 294, 1574–1577.
12. Mann, D., Kent, R., Parsons, B., and Cooper, I.V.G. (1992) Adrenergic effects on the biology of the adult mammalian cardiocyte. *Circulation*. 85, 790–804.
13. Bristow, M.R., Ginsburg, R., Umans, V., et al. (1986) B 1 and b 2-adrenergic receptor subpopulations in nonfailing and failing human ventricular myocardium: coupling of both receptor subtypes to muscle contraction and selective b 1-receptor down-regulation in heart failure. *Circ Res*. 59, 297–309.
14. Ungerer, M., Parruti, G., Bohm, M., et al. (1994) Expression of β-arrestins and β-adrenergic receptor kinases in the failing human heart. *Circ Res*. 74, 206–213.
15. Steinberg, S.F. (1999) The molecular basis for distinct β-AR subtype action in cardiomyocytes. *Circ Res*. 85, 1101–1111.
16. Lader, A.S., Xiao, Y.F., Ishikawa, Y., et al. (1998) Cardiac Gsa overexpression enhances L-type calcium channels through an adenylyl cyclase independent pathway. *Proc Natl Acad Sci USA*. 95, 9669–9674.
17. Communal, C., Singh, K., Sawyer, D.B., and Colucci, W.S. (1999) Opposing effects of β-1 and β-2 adrenergic receptor on cardiac myocyte apoptosis: role of a pertussis toxin sensitive G protein. *Circulation*. 100, 2210–2212.
18. Zaugg, M., Xu, W., Lucchinetti, E., Shafiq, S.A., Jamali, N.Z., and Siddiqui, M.A. (2000) B-adrenergic receptor subtypes differentially affect apoptosis in adult rat ventricular myocytes. *Circulation*. 102, 344–350.
19. Bisognano, J.D., Weinberger, H.D., Bohlmeyer, T.J., et al. (2000) Myocardial-directed overexpression of the human β-1-adrenergic receptor in transgenic mice. *J Mol Cell Cardiol*. 32, 817–830.
20. Saito, S., Hiroi, Y., Zou, Y., et al. (2000) B-adrenergic pathway induces apoptosis through calcineurin activation in cardiac myocytes. *J Biol Chem*. 275, 34,528–34,533.
21. Lowes, B.D., Gill, E.A., Abraham, W.T., et al. (1999) Effects of carvedilol on left ventricular mass, chamber geometry, and mitral regurgitation in chronic heart failure. *Am J Cardiol*. 83, 1201–1205.
22. Liggett, S.B., et al. (1998) The Ile164 B-2 AR polymorphism adversely affects the outcome of congestive heart failure. *J Clin Invest*. 102, 1534-9.
23. Wagoner, L.E., Craft, L.L., Singh, B., et al. (2000) Polymorphisms of the β-2 AR determine exercise capacity in patients with heart failure. *Circ Res*. 86, 834–840.
24. Graham, R.M., Perez, D.M., Hwa, J., and Piascik, M.T. (1996) Alpha-AR subtypes. Molecular structure, function and signaling. *Circ Res*. 78, 737–749.
25. Otani, H., Otani, H., and Das, D.K. (1988) Alpha-1 adrenoreceptor mediated phosphoinisotidie breakdown and inotropic response in rate left ventricular papillary muscles. *Circ Res*. 62, 8–17.
26. Hwang, K.C., Grady, C.D., Sweet, W.E., and Moravec, C.S. (1996) Alpha-1 adrenergic receptor coupling with Gh in the failing human heart. *Circulation*. 94, 718–726.
27. Choi, D.J., Koch, W.J., Hunter, J.J., and Rockman, H.A. (1997) Mechanism of β-adrenergic receptor desensitization in cardiac hypertrophy is increased β-ARK. *J Biol Chem*. 272, 17,223–17,229.
28. Knowlton, K.U., Michel, M.C., Itani, M., et al. (1993) The a1A-adrenergic receptor subtype mediates biochemical, molecular, and morphologic features of cultured myocardial cell hypertrophy. *J Biol Chem*. 268, 15,374–15,380.
29. Sugden, P.H. (1999) Signaling in myocardial hypertrophy: life after calcineurin? *Circ Res*. 84, 633–646.
30. Barki-Harrington, L., Luttrell, L.M., and Rockman, H.A. (2003) Dual inhibition of β-adrenergic and angiotensin II receptors by a single antagonist. *Circulation*. 108, 1611–1618.
31. Dzimiri, N. (2002) Receptor crosstalk: Implications for cardiovascular function, disease and therapy. *Eur J Biochem*. 269, 4713–4730.
32. Münzel, T., Feil, R., Mülsch, A., Lohmann, S.M., Hofmann, F., and Walter, U. (2003) Physiology and pathophysiology of vascular signaling controlled by cyclic guanosine 3′,5′-cyclic monophosphate-dependent protein kinase. *Circulation*. 108, 2172–2183.
33. von der Leyen, H.E. and Dzau, V.J. (2001) Therapeutic potential of nitric oxide synthase gene manipulation. *Circulation*. 103, 2760–2765.
34. Loscalzo, J. (2001) Nitric oxide insufficiency, platelet activation, and arterial thrombosis. *Circ Res*. 88, 756–7562.
35. Champion, H.C., Skaf, M.W., and Hare, J.M. (2003) Role of nitric oxide in the pathophysiology of heart failure. *Heart Fail Rev*. 8, 35–46.
36. Jugdutt, B.I. (2003) Nitric oxide and cardiovascular protection. *Heart Fail Rev*. 8, 29–34.
37. Young-Myeong, K., Bombeck, C.A., and Billiar, T.R. (1999) Nitric oxide as a bifunctional regulator of apoptosis. *Circ Res*. 84, 253–256.
38. Kuhn, M. (2003) Structure, regulation, and function of mammalian membrane guanylyl cyclase receptors, with a focus on guanylyl cyclase A. *Circ Res*. 93, 700–709.

12 Reversible and Irreversible Damage of the Myocardium

New Ischemic Syndromes, Ischemia/Reperfusion Injury, and Cardioprotection

JAMES A. COLES JR., PhD, DANIEL C. SIGG, MD, PhD, AND PAUL A. IAIZZO, PhD

CONTENTS

1. INTRODUCTION

The goal of this chapter is to provide a review of the physiology and pathophysiology of myocardial ischemia. In the past, it was thought that a lack of blood flow to the heart resulted in irreversible myocardial damage and necrosis (infarction). However, more recent evidence has suggested that there are several clinical scenarios, in presentation falling between the basic definitions of ischemia and infarction, in which the heart may recover a variable degree of preischemic function even though some degree of necrosis has occurred. Furthermore, with technological advances that allow intentional cardiac arrest during cardiac surgery, as well as noninvasive cardiac angioplasty (opening) of occluded coronary arteries, the phenomenon of reperfusion injury has at the same time been added as a sometimes-debilitating clinical syndrome. This chapter explores these new ischemic syndromes and describes up-to-date means for protecting the heart from these conditions (cardioprotection).

From: *Handbook of Cardiac Anatomy, Physiology, and Devices*
Edited by: P. A. Iaizzo © Humana Press Inc., Totowa, NJ

2. BASIC CARDIAC METABOLISM

The average healthy human heart weighs about 300 g or approx 0.5% of the total body mass, yet the oxygen demand of the heart accounts for 7% of the resting body oxygen consumption and consequently 5% of the cardiac output. The normal myocardial oxygen consumption MVO_2 per minute is approx 8 mL O_2/100 g and varies widely between normal, diseased, and exercising states. The MVO_2 is primarily dependent on the coronary blood flow (CBF) and the removal of oxygen from the coronary blood as follows: Arterial (CaO_2) contents minus Venous (coronary sinus, CSO_2) contents, such that

$$MVO_2 = CBF \times (CaO_2 - CSO_2).$$

Secondary determinants that influence MVO_2 include heart rate, myocardial stroke work, afterload, and/or the inotropic state of the heart.

During cardiac surgery, MVO_2 can vary extensively, with the greatest MVO_2 occurring immediately after bypass; replenishing energy stores requires a high oxygen demand (repaying oxygen debt). In contrast, cardiac arrest combined with myocardial hypothermia dramatically reduce MVO_2 (Fig. 1). It should be noted that hypothermic and normothermic modes of

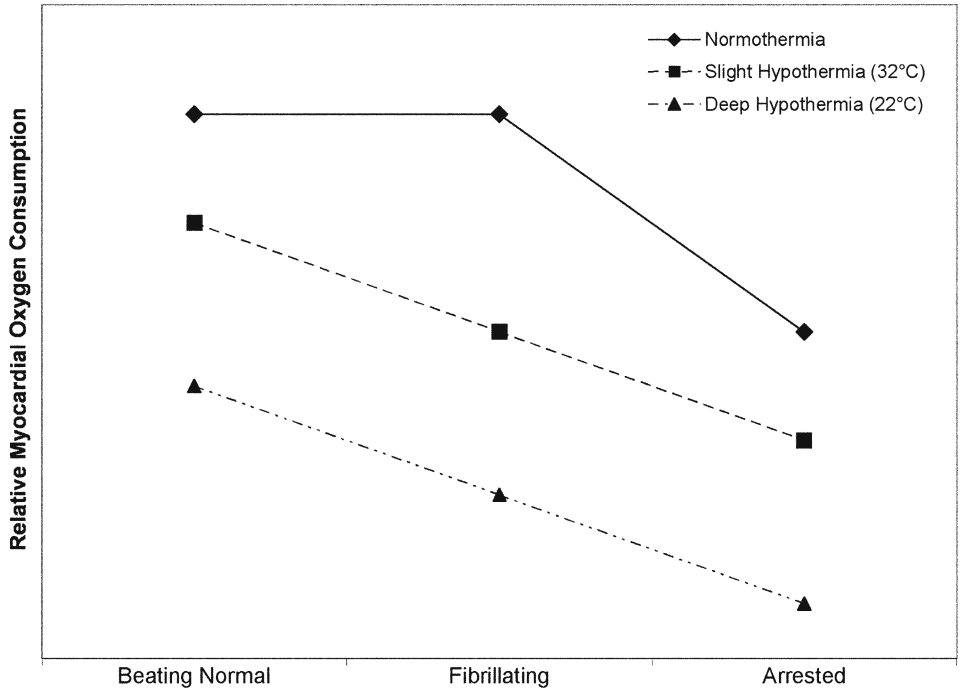

Fig. 1. Influence of temperature on myocardial metabolism. Although it is expected that hypothermia decreases myocardial oxygen consumption in the beating and fibrillating heart, there also exists a significant difference between the normothermic and hypothermic arrested heart. This indicates that the heart still has a measurable oxygen demand while arrested. Also notable is the difference in myocardial oxygen consumption between the fibrillating and arrested heart at either temperature.

cardiac arrest differ in their degrees of MVO_2 reduction. In all cases, the arrested heart still has an oxygen demand; hence, there will always be an imbalance of oxygen demand and delivery (i.e., some degree of ischemia).

3. MYOCARDIAL ISCHEMIA

The basic definition of myocardial ischemia is a greater myocardial tissue oxygen demand than oxygen supply. During short-term ischemic episodes, the heart's defense mechanism seeks to remedy this imbalance by downregulating myocardial contractile function and, concomitantly, increasing the rate of glycolysis (anaerobic energy production). Consequently, sarcolemmal glucose transport increases, and intracellular acidosis resulting from a buildup of the glycolytic breakdown products causes further inhibition of the contractile apparatus.

Even though energy production continues in the absence of oxygen, the glycolytic pathway is an inefficient means for producing adenosine triphosphate (ATP). As an ischemic episode becomes more severe or prolonged, the heart becomes unable to produce enough energy via glycolysis, and cellular necrosis ensues. For example, 10 min of ischemia result in about 50% depletion of ATP, and after approx 30 min of normothermic ischemia without significant collateral blood flow, irreversible damage or necrosis may occur *(1)*. Anatomically, the most vulnerable layer of the heart is the subendocardium; because of the higher systolic wall stress in this layer compared to the mid- and epicardial layers, there exists a relatively greater metabolic demand.

4. NEW ISCHEMIC SYNDROMES

In the past, it was generally believed that extended periods of myocardial ischemia led to irreversible damage of the myocardial or infarcted (necrotic) tissue. However, more recently, between the clinical conditions of transient ischemia (angina pectoris) and myocardial infarction, five additional ischemic syndromes have been described (Figs. 2 and 3) *(2,3)*. The *stunned* myocardium is characterized by postischemic impairment of myocardial function, but it is considered acute and completely reversible.

The *hibernating* myocardium is also characterized by depressed myocardial function of variable duration, primarily caused by impaired oxygen delivery through an occluded vessel, and recovery of function occurs on reflow to the ischemic region. The hibernating myocardium is similar to the stunned myocardium, with the main difference that reperfusion is not the cause of myocardial hibernation, as is the case with myocardial stunning. However, hibernation can be considered a state of chronic stunning; yet, the exact mechanism of hibernation remains largely unknown *(4)*.

The *maimed* myocardium is considered the most severe syndrome. It is characterized by irreversible myocardial damage that follows ischemia and reperfusion, and there is a delayed recovery to only partial preischemic function.

In *ischemic preconditioning*, multiple brief (<5 min) ischemic episodes followed by reperfusion subsequently enhance the myocardial tolerance to a longer (<45 min) ischemic event

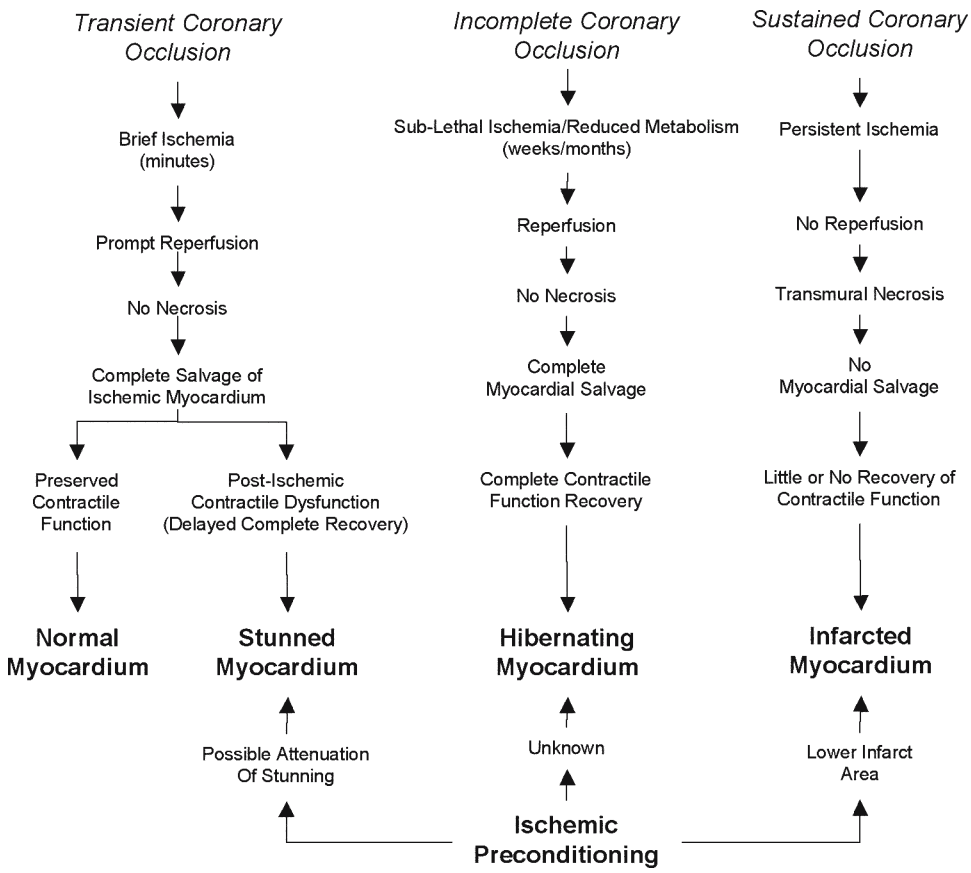

Fig. 2. Consequences of myocardial ischemia. The stunned myocardium usually results from a transient coronary occlusion followed by prompt reperfusion; however, it may also occur following prolonged ischemia in the preconditioned heart. Preconditioning may lessen the infarct area following a sustained coronary occlusion; however, the relationship between preconditioning and the maimed myocardium is unknown. Modified from ref. *15*. © 1995, with permission from Elsevier.

(Figs. 3 and 4). Patients with electrocardiogram changes of ischemia and contractile failure who lack chest pain may be experiencing *silent ischemia*. It has been proposed that these patients are either less sensitive to painful stimuli or their ischemia is somewhat milder *(3)*.

4.1. Myocardial Stunning

There are two general theories for explaining the pathomechanism underlying myocardial stunning, and they are not mutually exclusive. The formation of free-radical reactive species or alterations in intracellular calcium, both with a detrimental effect on the myocardium, have been speculated as the principal causes of postischemic stunning *(5)*. Intracellular acidosis during ischemia can potentially generate intracellular calcium oscillations and calcium overload on reperfusion via activation of the sarcolemmal Na^+/H^+ exchanger (Fig. 4) *(6)*.

Experimental studies have shown that the calcium sensitivity of the contractile apparatus is decreased in the stunned myocardium, thereby resulting in lower maximal force generation even at higher than normal transient calcium levels *(7,8)*. Furthermore, decreased myofilament sensitivity to calcium is considered primarily responsible for systolic dysfunction; for example, the stunned myocardium is still responsive to inotropic stimulation. Of additional interest are the findings that cardiac troponin I (cTnI) degradation products were discovered in the human myocardium during aortic cross-clamping with bypass, and that serum levels of cTnI increased during reperfusion, peaking approx 24 h following cross-clamp removal *(9)*. This preliminary evidence further suggests that cTnI degradation products may potentially be utilized as biomarkers for stunning.

During the early stage of stunning, it is considered beneficial to prevent calcium oscillations and thus attenuate significant injury caused by reperfusion. This has been accomplished experimentally by utilizing Ca^{2+} antagonists, inorganic blockers, ryanodine, low-calcium reperfusion buffers, or Na^+/H^+ exchange (NHE) blockers *(10)*. Conversely, when contractility is suppressed, as in the late stage of stunning, therapies should include those that increase the amplitudes of intracellular calcium transients, inducing inotropic responses. Included in this subset are high-calcium buffers, Ca^{2+} agonists, catecholamines, and phosphodiesterase inhibitors. Importantly, many of these therapies are specific to the stage or degree of stunning, and hence the timing of their use is critical so they do not become a detrimental therapy.

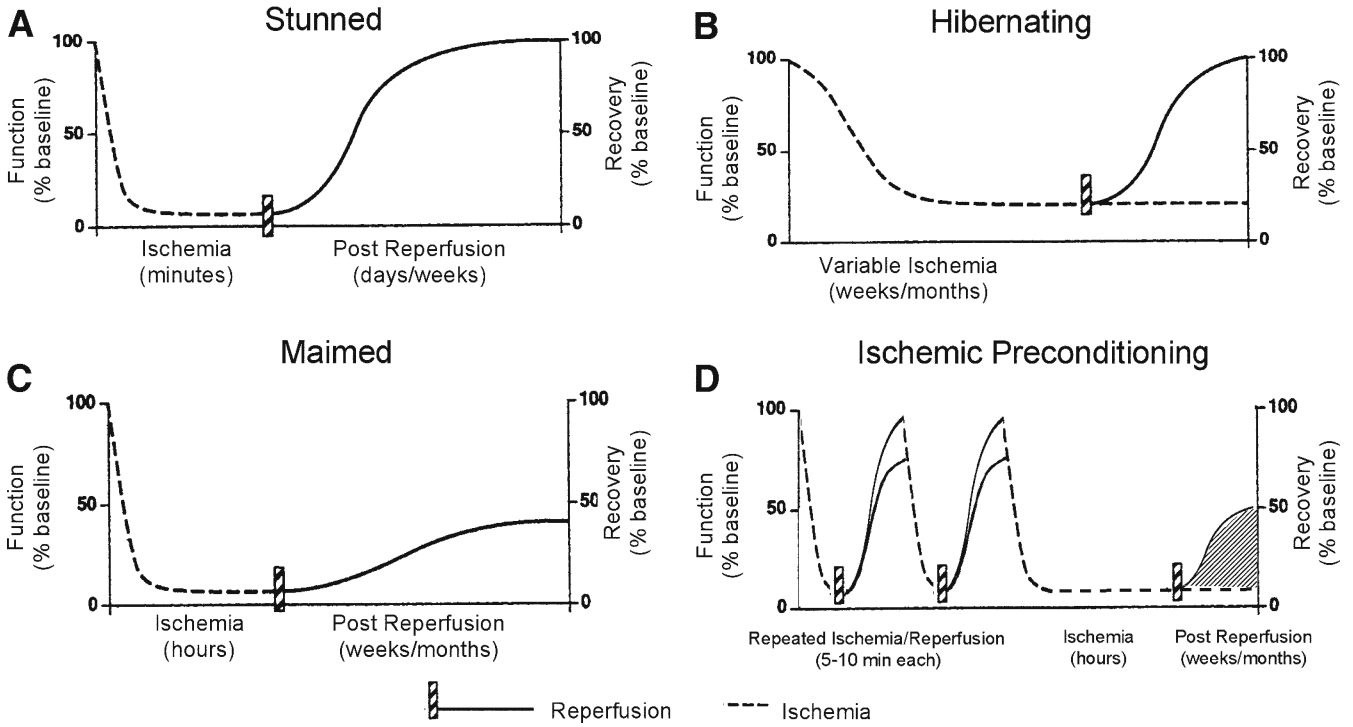

Fig. 3. New ischemic syndromes that do not fall within the realm of classic acute reversible and irreversible myocardial ischemia. **(A)** The stunned myocardium is characterized by a decrease in function following an ischemic event in which there is a complete absence of necrosis from ischemia or reperfusion and a complete functional recovery hours to days later. **(B)** The hibernating myocardium is characterized by chronic depressed myocardial function because of sublethal ischemia lasting for weeks to months, and revascularization may result in complete recovery of function. **(C)** The maimed myocardium has permanent damage resulting from a preceding prolonged ischemic episode and has some functional recovery that does not return to preischemic levels. **(D)** Ischemic preconditioning exists when short ischemic episodes followed by reperfusion confer myocardial protection during a subsequent prolonged ischemic event. However, two areas of uncertainty exist in the preconditioning phenomenon: (1) Functional recovery following the preceding short ischemic events may not return to preischemic levels; and (2) although it is known that ischemic preconditioning lessens infarct size, it is uncertain whether long-term functional recovery following the prolonged ischemic episode is significantly improved (via decreased myocardial stunning). Only delayed ischemic preconditioning has been shown to attenuate myocardial stunning. Modified from ref. *15*. © 1995, with permission from Elsevier.

For instance, hypocalcemia during and following cardiopulmonary bypass is a common occurrence mainly attributed to the utilization of priming fluids, citrated blood, and large doses of heparin during bypass *(11)*. Normally, hypocalcemia is successfully corrected with the administration of calcium chloride; however, calcium levels may return to preoperative levels prior to removal from cardiopulmonary bypass without supplemental calcium *(12)*. Therefore, the risk of stunning and myocardial damage may actually be increased with generalized calcium chloride administration; there exists a lack of specific therapeutic guidelines for calcium administration during and following bypass.

4.2. Hibernating Myocardium

As discussed in this section, myocardial stunning and hibernation are related in terms of a depressed state of contractility and in the potential for dysfunctional myocardium to return to normal. However, it must be restated that, although stunning can be attributed to the reperfusion following a brief bout of ischemia, the hibernating myocardium is in a chronic hypocontractile state because of a decreased oxygen supply and thus may only recover full function with revascularization. In addition, many of the underlying mechanisms of stunning are considered directly related to the detrimental effects of reperfusion injury (discussed in Section 5) *(13)*. Although there is an absence of necrosis with myocardial hibernation, morphological changes to the myocardial architecture, such as loss of myofibrils and increased interstitial fibrosis, may occur if this state persists *(14)*.

4.3. Maimed Myocardium

The maimed myocardium closely resembles a classic myocardial infarction in that ischemia-induced necrosis leads to loss of contractile performance. Unlike myocardial stunning, the duration of ischemia is long enough to result in necrosis; however, there can be partial recovery of function to this ischemic region following reperfusion *(15)*. An example of the maimed myocardium syndrome would be seen in patients who exhibit an incomplete recovery of myocardial function following drug-induced or mechanical (angioplasty) reperfusion of an occluded coronary artery and then demonstrate regions of viable myocardium in the ischemic area.

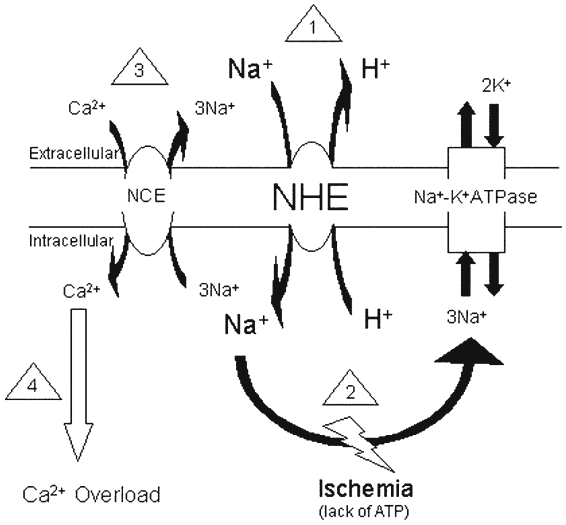

Fig. 4. Reperfusion injury via the Na^+-H^+ exchanger (NHE). Reperfusion injury-induced calcium overload can be explained in part by activation of the NHE. (1) Intracellular acidosis from a prior ischemic episode activates the NHE on reperfusion, thereby decreasing intracellular acidosis and increasing Na^+ influx. (2) Intracellular sodium is primarily removed from the cell via the Na^+-K^+ATPase (adenosine triphosphatase) during normal myocardial function. However, after ischemia (i.e., during the early stages of reperfusion), the lack of abundance of ATP (adenosine triphosphate) does not allow for normal operation of the pump and intracellular Na^+ increase. (3) Consequently, the Na^+-Ca^{2+} exchanger (NCE), which normally operates by extruding Ca^{2+} from the cytoplasm, is the primary mechanism for intracellular Na^+ removal operating in a reverse mode. (4) Intracellular Ca^{2+} overload results from NCE activation, possibly causing arrhythmias, stunning, and necrosis.

4.4. Ischemic Preconditioning

Ischemic preconditioning is a biological phenomenon by which brief ischemic episodes, followed by reperfusion, protect tissue from a subsequent prolonged ischemic event *(16)*. In the myocardium, ischemic preconditioning has been shown to be potentially infarct limiting *(16)* as well as antiarrhythmic *(17)*, although the latter of these effects has been disputed. It is also well established that endogenous opioid receptor activation participates in myocardial ischemic preconditioning *(18)*, and that preischemic administration of synthetic opioid agonists can mimic the benefits of ischemic preconditioning *(19)*. Although ischemic and opioid preconditioning have been convincingly shown to delay cell death in various experimental animal models, the clinical applicability of these aforementioned observations may be limited to situations in which the ischemic event can be anticipated (e.g., on- or off-bypass cardiac surgery, percutaneous transluminal coronary angioplasty, or stenting procedures) *(20)*. For a more comprehensive review of ischemic and opioid preconditioning, *see* ref. *21* (ischemic preconditioning) or *22* (opioid preconditioning).

4.5. Silent Ischemia

Silent ischemia refers to single or multiple asymptomatic episodes of transient ischemia. In some cases, silent ischemia can occur in the weeks following an acute myocardial infarction in patients with a history of coronary artery disease. In other scenarios a seemingly normal healthy individuals may experience episodes of silent ischemia that go relatively unnoticed. Detection of silent ischemia primarily relies on electrocardiographic monitoring, either in the form of 24-h Holter monitoring (ambulatory) or an exercise- or stress-induced assessment session. In both cases, ischemia is detected by asymptomatic ST elevations *(23)*. Silent ischemia is postulated to be related to a lack of oxygen supply rather than an increase in oxygen demand; however, controversy remains concerning the mechanism by which silent ischemia can proceed unnoticed.

4.6. How Can the Heart Be Protected From Ischemia?

As shown in Fig. 1, there are several means of decreasing myocardial oxygen demand when the oxygen supply is compromised. These include hypothermia, pharmacologically decreasing the heart rate, or controlled cardiac arrest. In addition, as mentioned in Section 4.4., ischemic or pharmacological preconditioning of the heart are other means of protecting the heart from an ischemic episode (cardioprotection). However, these aforementioned therapies require anticipation of the ischemic event, such that the therapies can be administered prior to or early during the ischemia. When anticipation of ischemia is not possible, for example, in acute myocardial infarction, interventions that reestablish blood flow and oxygen to the ischemic zone (reperfusion) are the primary therapies.

5. REPERFUSION INJURY

Although immediate restoration of blood flow and oxygen to ischemic tissue is ultimately a beneficial and important therapy, it should be noted that additional myocardial damage can occur on myocardial reperfusion. In what has been termed the *oxygen paradox*, the resupply of oxygen to a hypoxic cell simultaneously activates two intracellular processes of particular interest: the membrane-bound calcium pumps and the contractile apparatus. Resumption of contractile activity in the presence of oscillating and increasing intracellular Ca^{2+} levels can force the heart into a state of hypercontracture and cause intracellular edema. Collectively, these etiologies may ultimately result in membrane disruption and cell death.

Reperfusion injury can present or be associated with one or more of the following pathologies: (1) reperfusion arrhythmias, (2) microvascular damage and no reflow, (3) accelerated cell death, (4) myocardial stunning, or (5) postpump syndrome in procedures requiring cardiopulmonary bypass (Fig. 5). Reperfusion injury may cause immediate myocardial necrosis in severely damaged cells and delayed necrosis in cells adjacent to the ischemic region, or conversely, complete recovery of myocardial function may occur despite an ischemic episode. Of importance, necrosis occurring during the ischemic episode must be differentiated from that which may occur following reperfusion, especially when discussing therapies targeted at attenuating reperfusion injury.

Assessment of reperfusion injury following ischemia is often difficult to perform, especially in the postsurgical patient. Yet, the determination of the presence or extent of injury can be

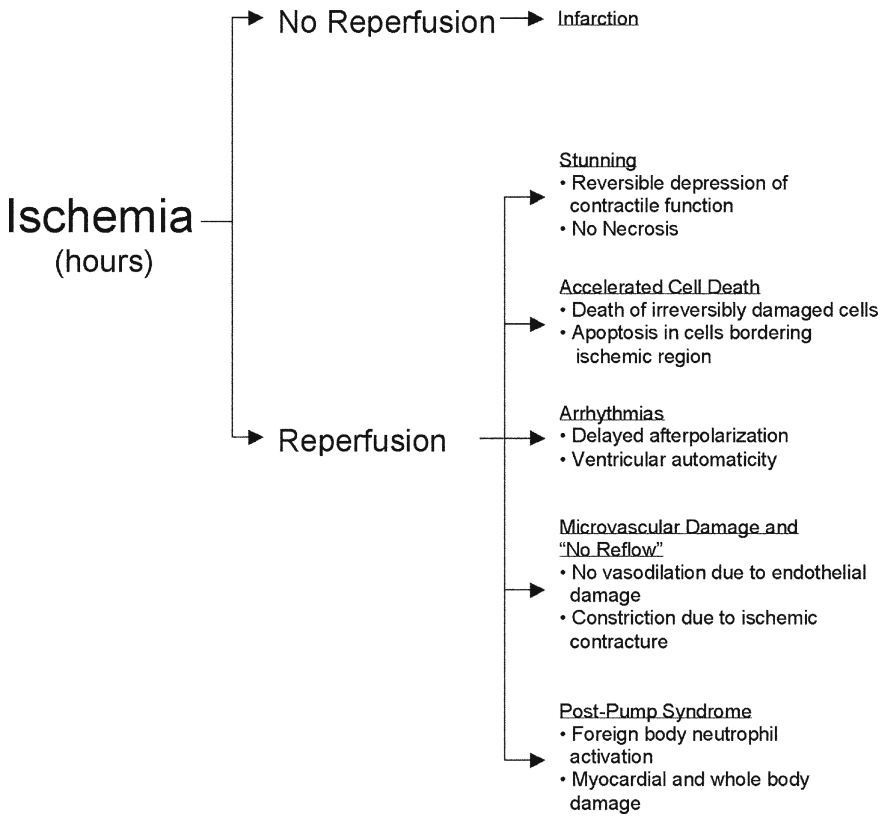

Fig. 5. Aspects of reperfusion injury. Although reperfusion is still the most beneficial therapy for ischemia, any combination of the stunning, accelerated cell death, arrhythmias, microvascular damage, or postpump syndrome could occur, thus leading to postischemic dysfunction or necrosis.

indirectly accomplished by hemodynamic monitoring (pressures, cardiac outputs, echocardiography) and examining blood levels of cardiac enzymes (creatine kinase–MB fraction [CK-MB], troponin I, lactate dehydrogenase [LDH], and/or aspartate transferase [AST]). Ideally, left ventricular end-diastolic pressure–volume measurements would provide functional and quantitative information relative to the degree of reperfusion injury; however, clinically such data are difficult and rarely feasible to obtain. On the other hand, myocardial viability can be assessed with inotropic stimulation as the postischemic stunned or the potentially reversibly injured myocardium will display an increased heart rate and contractility; the irreversibly injured (necrotic) myocardium exhibits little to no response to the inotrope (e.g., by dopamine stress echocardiography). Note that, by definition, myocardial stunning is reversible; therefore, within days, a depressed cardiac function caused by stunning should recover (Figs. 2 and 3). This phenomenon is observed clinically when patients following coronary artery bypass grafting require 24–48 h of inotropic support.

5.1. Aspects of Reperfusion Injury

5.1.1. Myocardial Stunning

As discussed in Section 4.1., the presence of intracellular oxygen free radicals and increased intracellular calcium during reperfusion leads to a reversible hypocontractile state of variable, yet normally brief duration.

5.1.2. Accelerated Cell Death

Accelerated cell death on reperfusion mostly refers to cells that have been irreversibly damaged during the prior ischemic episode and are destined to die despite reperfusion. However, irreversible damage is not a prerequisite for cell death; on reperfusion, detrimental ischemia-induced intracellular alterations may also occur in viable cells. During reperfusion, the development of increased sarcolemmal permeability caused by ischemia allows for the uncontrolled influx of calcium, resulting in hypercontracture, decreased energy production, or cell death. In addition, it should be noted that there is a paradoxical finding that apoptosis-related cell death in postischemic viable myocardium is lessened by early reperfusion and is accelerated in irreversibly ischemic-damaged cells *(24)*.

5.1.3. Arrhythmias

Similar to myocardial stunning, increased episodes of arrhythmias on reperfusion may be in part caused by the presence of free radicals during ischemia or intracellular calcium oscillations at reflow. The restoration of flow enables the cell to resynthesize ATP. This abundance of energy and increased intracellular calcium at reperfusion may lead to excess

cycling, which in turn may cause delayed after-depolarizations and ventricular automaticity *(25)*. Interestingly, a Gaussian (bell-shaped) relationship has been described between duration of ischemia and severity of reperfusion arrhythmias, with the peak occurring with reperfusion after 5–20 min of ischemia *(3)*. This is presumably because of the finding that, in severe ischemic episodes, the production of ATP during reperfusion is limited because of increased cellular necrosis, and consequently energy-dependent calcium oscillations are reduced *(26)*.

The timing and speed of reperfusion are also considered to influence the occurrences and severity of induced arrhythmias. It has been speculated that sudden reperfusion is associated with a higher incidence of arrhythmias than is a gradual reperfusion. Whether this phenomenon occurs in humans is controversial because a study comparing revascularization, with either thrombolysis (a relatively slow reperfusion) or percutaneous transluminal coronary angioplasty (rapid reperfusion), of patients diagnosed with acute myocardial infarction revealed no differences in the occurrence of arrhythmias upon reperfusion *(27)*.

5.1.4. Microvascular Damage and No Reflow

The "no-reflow" phenomenon is defined to occur when an attempt to reperfuse an ischemic area, by removing an occlusion regionally or reestablishing coronary flow globally, does not result in reflow to the area at risk. In fact, a study of patients diagnosed with acute myocardial infarction and treated with thrombolytic therapy revealed that approximately one-third of this study group showed impaired regional coronary flow 5 d after treatment *(28)*.

There are two proposed mechanisms to explain this immediate or delayed no reflow: (1) endothelial damage induced by free radicals causes edema development and inhibits the release of vasodilatory agents into the coronary circulation; or (2) ischemic contracture of the myocardium mechanically constricts flow through the coronary system *(3)*. In addition, activated neutrophils reintroduced at reperfusion can adhere to damaged endothelium and, in severe cases, cause platelet aggregation and restenosis *(29)*. Importantly, cardioplegia-induced global myocardial ischemia can cause regional no flow, and infarctions will develop as a consequence of this phenomenon.

5.1.5. Postpump Syndrome

When blood comes in contact with foreign nontissue surfaces, such as during cardiopulmonary bypass, a circulatory inflammatory response may be triggered. A host of cell types is typically activated during such a foreign body response, including monocytes, macrophages, endothelial cells, T cells, and eventually neutrophils. In a process collectively referred to as *neutrophil trafficking*, these cells accumulate and adhere to the damaged endothelial layer *(3)*. They then migrate into the vascular interstitial space, which results in liberation of free radicals and leukotrienes *(3)*. This in turn may promote not only postsurgical myocardial damage, but also widespread systemic damage or multiorgan dysfunction *(30)*. For example, it has been reported that cases of cerebral edema can develop after cardiopulmonary bypass; this is considered to be mediated by bypass-related inflammation and endothelial cell activation *(31)*.

6. EXAMPLES OF CURRENT PHARMACOLOGICAL CARDIOPROTECTIVE THERAPIES

Listed in this section are current examples of pharmacological therapies targeted at protecting the myocardium from damage caused by ischemia and reperfusion injury.

6.1. Na^+/H^+ Exchange Blockers

Although activation of the Na^+/H^+ exchanger (NHE) in response to acidosis is a feedback mechanism that enables the myocardial cell to maintain a fairly stable pH range, NHE activation may not always be beneficial. During ischemia, there is often a buildup of metabolic products that is caused by the anaerobic breakdown of ATP; the production of lactate and high CO_2 levels drive the intra-cellular pH below a tolerable level. However, a comparable decrease in the extracellular pH occurs during low-flow and no-flow ischemia, and importantly, NHE activity is inhibited. Then, when blood flow is reestablished to the ischemic region, this inhibition is removed, and both the NHE and the $Na–HCO_3^-$ symport are simultaneously activated in an attempt to restore the internal pH rapidly *(32)*. With the normalization of intracellular pH via the NHE, there is an increase in internal Na^+. Under normal conditions, cells primarily extrude Na^+ via Na^+-K^+ATPase; however, because of depleted energy reserves, the postischemic cell relies on the Na^+-Ca^{2+} exchanger for Na^+ normalization. Importantly, this results in increased intracellular Ca^{2+} levels, which, as mentioned in Section 5, significantly contribute to the pathology of reperfusion injury (Fig. 4).

In experimental animals, various NHE inhibitors have been observed to be beneficial when administered either prior to ischemia or prior to reperfusion. Specifically, cariporide (NHE-1 specific) has been reported to reduce postischemic edema, arrhythmias, apoptosis, infarct size, contracture, enzyme efflux, and hypertrophy and prevent free-radical damage, preserve ATP, and enhance myocardial preservation following prolonged storage *(33–40)*. In the GUARDIAN (Guard During Ischemia Against Necrosis) clinical trial, cariporide pretreatment prior to coronary artery bypass grafting resulted in a 25% reduction in mortality or myocardial infarction following surgery *(41)*. Further supporting its use during routine cardiac surgery, Myers and Karmazyn *(42)* found that hypothermia potentiated the benefits of cariporide, specifically when cariporide was administered during reperfusion.

However, in a clinical trial (the ESCAMI trial [Evaluation of the Safety and Cardioprotective Effects of Eniporide in Acute Myocardial Infarction]) in which eniporide (another NHE-1 inhibitor) was administered on reperfusion to patients undergoing percutaneous transluminal coronary angioplasty or thrombolysis for acute myocardial infarction, eniporide failed to show any significant reduction in either infarct size or occurrence of clinical events following treatment *(43)*. Furthermore, cariporide administration, during reperfusion following global hypothermic ischemia, failed to show any beneficial hemodynamic effects relative to control hearts (unpublished data from our laboratory).

Although the use of NHE blockers is still considered experimental, their future use in cardiac surgery and following ischemia/reperfusion remains promising. Interestingly, the

prospect of using them as a combined therapy with other cardioprotective therapies, such as ischemic preconditioning, is being addressed, and initial results have suggested that the combined therapies produce additive benefit *(44)*.

6.2. Antioxidants

Antioxidants are speculated to attenuate or prevent reperfusion injury by acting as: (1) free-radical scavengers; (2) inhibitors of free-radical generation; (3) metal chelators, thereby removing the free-radical-generating catalyst; (4) promoters of endogenous antioxidant production; or (5) inhibitors of apoptosis via the upregulation of *Bcl-2* (a gene involved in the apoptosis signaling pathway) *(45)*. However, experimental animal models and human clinical trials have together provided conflicting results concerning the therapeutic benefits of antioxidants to attenuate reperfusion injury. Interestingly, many typical thiol-containing drugs commonly used for treating both coronary artery disease and heart failure have also been shown to exhibit antioxidantlike effects within the myocardium; these include β-adrenergic antagonists propanolol *(46)*, metoprolol *(47)*, and carvedilol *(48)*, as well as angiotensin-converting enzyme inhibitors, iron-chelating agents, and Ca^{2+} channel blockers *(45)*.

6.3. Calcium Channel Antagonists

Experimentally, the administration of a calcium channel antagonist is believed to help preserve myocardial function and metabolism in case studies employing normothermic ischemia, crystalloid cardioplegia, or blood cardioplegia *(1)*. More specifically, their use was reported to prevent ATP hydrolysis and calcium influx during ischemia and improve cardioplegia delivery by coronary vasodilation. However, the potential use of calcium channel blockers for myocardial protection is considered limited because of their negative inotropic and dromotropic effects, which could be specifically problematic in patients with preoperative poor ventricular function. Hence, further studies are needed to determine the potential utility of newer calcium channel antagonists such as amlodipine and felodipine, agents that may elicit fewer side effects in very ill patients. The current applications of calcium channel antagonists are in patients with normal preoperative function who are at risk for postoperative hypertension, tachycardia, coronary spasm, and/or ischemia *(1)*.

6.4. Glucose–Insulin–Potassium Solution

Perioperative depletion of myocardial glycogen stores has been correlated with a higher incidence of arrhythmias, low output syndrome, and/or infarction *(49)*. Consequently, in one study, Iyengar et al. *(49)* preoperatively dosed patients with a glucose–insulin–potassium solution and a bolus of exogenous glucose and found zero incidences of perioperative ischemic complications (compared to a 44% occurrence in patients not receiving the solutions). This beneficial effect was attributed to increased preoperative glycogen stores, enhanced perioperative aerobic metabolism, and reduced free fatty acid circulation in the hypoxic hearts, all of which are mediated by glucose and insulin. Future studies are needed to validate such a therapy.

6.5. Growth Factors

The administration of growth factors for cardioprotective means is typically done in attempts to minimize or prevent apoptosis, which is known to occur in addition to necrosis during (prolonged) myocardial ischemia and reperfusion. In general, it is thought that reperfusion injury accelerates apoptosis in viable postischemic cells, adding to the overall necrosis *(50)*. A link was described between apoptosis and reperfusion in humans following acute myocardial infarctions in which apoptosis was significant in cells within and bordering the infarcted region *(51)*. Experimental animal studies have shown infarct-reducing benefits of several growth factor proteins when given during ischemia or during reperfusion, including transforming growth factor-β1 *(52)*, insulin *(53)*, insulin-like growth factor 1 *(54)*, fibroblast growth factor *(55)*, and cardiotrophin 1 *(56)*.

6.6. Glutamate/Aspartate

The amino acids glutamate and aspartate, when added to the cardiopulmonary bypass circuit, have been shown to reduce lipid peroxidation and preserve myocardial function following tissue reoxygenation *(57)*. Similarily, the addition of amino acids to cardioplegia has yielded similar positive results *(58)*. Although most of the benefits were attributed to the ability of the amino acids to produce ATP anaerobically via substrate phosphorylation, evidence has further linked their benefits to inhibition of free-radical production and better retention of endogenous antioxidants *(57)*.

6.7. Nitric Oxide

In addition to being a potent vasodilator, nitric oxide (NO) reduces platelet aggregation and neutrophil adherence and is considered to act as a free-radical scavenger. NO is synthesized from the amino acid L-arginine by nitric oxide synthase. It is thought that L-arginine levels decline during ischemia, leading to lower NO production and thus a greater injury potential *(1)*. Although the addition of NO donors to cardioplegia solutions has been shown to beneficially increase ischemic NO levels *(59)*, there are conflicting opinions regarding the benefits of NO because of its negative inotropic effects.

7. CONCLUSIONS

The intent of this chapter was to outline the principles of ischemia and reperfusion injury and introduce the concept of cardioprotection. Although the intent of many of the past cardioprotective therapies was to protect the myocardium from ischemic necrosis, it may be that reperfusion injury following ischemia in the forms of stunning, arrhythmias, or additional cellular necrosis may occur despite such cardioprotective efforts. Therefore, as a new era in the operating room and catheterization laboratories evolves and allows for surgery on patients in poorer health, it is imperative that current myocardial protective strategies again be rigorously enhanced to counter the potential increased risks of ischemia and reperfusion injuries in such populations.

REFERENCES

1. Rao, V. and Weisel R. D., (1997) Intraoperative protection of organs: Hhypothermia, cardioplegia, and cerebroplegia,Chapter 10, in *Car-*

diac Surgery in the Adult. Edmunds, L.H. (ed.), McGraw-Hill, New York, NY, pp. 295–318.
2. Yellon, D.M., Rahimtoola, S.H., Opie, L.H., et al. (eds.). (1997) Ischemic injury and myocardial protection: evolving concepts, Jennings, R. B., and Ischemic diastolic dysfunction and postischemic diastolic stunning, Apstein, C. S., Varma, N., and Eberli, F. R., in *New Ischemic Syndromes: Beyond Angina and Infarction*. Lippincott-Raven, New York, NY, pp. 10–20, 106–114.
3. Opie, L.H. (1998) The Heart: Physiology, from Cell to Circulation. Lippincott-Raven, New York, NY, 515–589
4. Shen, Y.T. and Vatner, S.F. (1995) Mechanism of impaired myocardial function during progressive coronary stenosis in conscious pigs. Hibernation versus stunning? *Circ Res*. 76, 479–88.
5. Bolli, R. and Marban, E. (1999) Molecular and cellular mechanisms of myocardial stunning. *Physiol Rev*. 79, 609–634.
6. Karmazyn, M. and Moffat, M.P. (1993) Role of Na^+/H^+ exchange in cardiac physiology and pathophysiology: mediation of myocardial reperfusion injury by the pH paradox. *Cardiovasc Res*. 27, 915–924.
7. Miller, W.P., McDonald, K.S., and Moss, R.L. (1996) Onset of reduced Ca^{2+} sensitivity of tension during stunning in porcine myocardium. *J Mol Cell Cardiol*. 28, 689–697.
8. Kusuoka, H., Koretsune, Y., Chacko, V.P., et al. (1990) Excitation-contraction coupling in postischemic myocardium. Does failure of activator Ca^{2+} transients underlie stunning? *Circ Res*. 66, 1268–1276.
9. McDonough, J.L., Labugger, R., Pickett, W., et al. (2001) Cardiac troponin I is modified in the myocardium of bypass patients. *Circulation*. 103, 58–64.
10. Opie, L.H. and du Toit, E.F. (1992) Postischemic stunning: the two-phase model for the role of calcium as pathogen. *J Cardiovasc Pharmacol*. 20, S1–S4.
11. Aguilera, I.M. and Vaughan, R.S. (2000) Calcium and the anaesthetist. *Anaesthesia*. 55, 779–790.
12. Robertie, P.G., Butterworth, J.F., Royster, R.L., et al. (1991) Normal parathyroid hormone responses to hypocalcemia during cardiopulmonary bypass. *Anesthesiology*. 75, 43–48.
13. Bolli, R., Patel, B.S., Jeroudi, M.O., et al. (1988) Demonstration of free radical generation in "stunned" myocardium of intact dogs with the use of the spin trap alpha-phenyl *N*-tert-butyl nitrone. *J Clin Invest*. 82, 476–485.
14. Heusch, G.,and Schulz, R. (2002) Myocardial hibernation. *Ital Heart J*. 3, 282–284.
15. Boden, W.E., Brooks, W.W., Conrad, C.H., et al. (1995) Incomplete, delayed functional recovery late after reperfusion following acute myocardial infarction: "maimed myocardium." *Am Heart J*. 130, 922–932.
16. Murry, C.E., Jennings, R.B., and Reimer, K.A. (1986) Preconditioning with ischemia: a delay of lethal cell injury in ischemic myocardium. *Circulation*. 74, 1124–1136.
17. Lawson, C.S., Coltart, D.J., and Hearse, D.J. (1993) "Dose"-dependency and temporal characteristics of protection by ischaemic preconditioning against ischaemia-induced arrhythmias in rat hearts. *J Mol Cell Cardiol*. 25, 1391–1402.
18. Schultz, J.E., Rose, E., Yao, Z., et al. (1995) Evidence for involvement of opioid receptors in ischemic preconditioning in rat hearts. *Am J Physiol*. 268, H2157–H2161.
19. Coles, J.A., Jr., Sigg, D.C., and Iaizzo, P.A. (2003) Role of kappa-opioid receptor activation in pharmacological preconditioning in swine. *Am Journal Physiol Heart Circ Physiol*. 284, 2091–2099.
20. Sigg, D.C., Coles, J.A., Jr., Gallagher, W.J., et al. (2001) Opioid cardioprotection: myocardial function and energy metabolism. *Ann Thorac Surg*. 72, 1576–1582.
21. Yellon, D.M. and Downey, J.M. (2003) Preconditioning the myocardium: from cellular physiology to clinical cardiology. *Physiol Rev*. 83, 1113–1151.
22. Gross, G.J. (2003) Role of opioids in acute and delayed preconditioning. *J Mol Cell Cardiol*. 35, 709–718.
23. Cohn, P.F., Fox, K.M., and Daly, C. (2003) Silent myocardial ischemia. *Circulation*. 108, 1263–1277.
24. Fliss, H. and Gattinger, D. (1996) Apoptosis in ischemic and reperfused rat myocardium. *Circ Res*. 79, 949–956.
25. Opie, L.H. and Coetzee, W.A. (1988) Role of calcium ions in reperfusion arrhythmias: relevance to pharmacologic intervention. *Cardiovasc Drugs Ther*. 2, 623–636.
26. Manning, A.S. and Hearse, D.J. (1984) Reperfusion-induced arrhythmias: mechanisms and prevention. *J Mol Cell Cardiol*. 16, 497–518.
27. Wehrens, X.H., Doevendans, P.A., Ophuis, T.J., et al. (2000) A comparison of electrocardiographic changes during reperfusion of acute myocardial infarction by thrombolysis or percutaneous transluminal coronary angioplasty. *Am Heart J*. 139, 430–436.
28. Maes, A., Van de Werf, F., Nuyts, J., et al. (1995) Impaired myocardial tissue perfusion early after successful thrombolysis. Impact on myocardial flow, metabolism, and function at late follow-up. *Circulation*. 92, 2072–2078.
29. Forde, R.C. and Fitzgerald, D.J. (1997) Reactive oxygen species and platelet activation in reperfusion injury. *Circulation*. 95, 787–789.
30. Menasche, P., Peynet, J., Haeffner-Cavaillon, N., et al. (1995) Influence of temperature on neutrophil trafficking during clinical cardiopulmonary bypass. *Circulation*. 92, II334–II340.
31. Anderson, R.E., Li, T.Q., Hindmarsh, T., et al. (1999) Increased extracellular brain water after coronary artery bypass grafting is avoided by off-pump surgery. *J Cardiothorac Vasc Anesth*. 13, 698–702.
32. Karmazyn, M. (1998) The myocardial sodium-hydrogen exchanger (NHE) and its role in mediating ischemic and reperfusion injury. *Keio J Med*. 47, 65–72.
33. Inserte, J., Garcia-Dorado, D., Ruiz-Meana, M., et al. (1997) The role of the Na^+-H^+ exchange occurring during hypoxia in the genesis of reoxygenation-induced myocardial oedema. *J Mol Cell Cardiol*. 29, 1167–1175.
34. Garcia-Dorado, D., Gonzalez, M.A., Barrabes, J.A., et al. (1997) Prevention of ischemic rigor contracture during coronary occlusion by inhibition of Na(+)-H(+) exchange. *Cardiovasc Res*. 35, 80–89.
35. Klein, H.H., Bohle, R.M., Pich, S., et al. (1997) Time delay of cell death by Na^+/H^+ exchange inhibition in regionally ischemic, reperfused porcine hearts. *J Cardiovasc Pharmacol*. 30, 235–240.
36. Shipolini, A.R., Yokoyama, H., Galinanes, M., et al. (1997) Na^+/H^+ exchanger activity does not contribute to protection by ischemic preconditioning in the isolated rat heart. *Circulation*. 96, 3617–3625.
37. Yoshida, H. and Karmazyn, M. (2000) Na(+)/H(+) exchange inhibition attenuates hypertrophy and heart failure in 1-week post-infarction rat myocardium. *Am J Physiol Heart Circ Physiol*. 278, H300–H304.
38. Myers, M.L., Farhangkhoee, P., and Karmazyn, M. (1998) Hydrogen peroxide induced impairment of post-ischemic ventricular function is prevented by the sodium-hydrogen exchange inhibitor HOE 642 (cariporide). *Cardiovasc Res*. 40, 290–296.
39. Mathur, S. and Karmazyn, M. (1997) Interaction between anesthetics and the sodium-hydrogen exchange inhibitor HOE 642 (cariporide) in ischemic and reperfused rat hearts. *Anesthesiology*. 87, 1460–1469.
40. Hartmann, M. and Decking, U.K. (1999) Blocking Na(+)-H(+) exchange by cariporide reduces Na(+)-overload in ischemia and is cardioprotective. *J Mol Cell Cardiol*. 31, 1985–1995.
41. Theroux, P., Chaitman, B.R., Danchin, N., et al.(2000) Inhibition of the sodium-hydrogen exchanger with cariporide to prevent myocardial infarction in high-risk ischemic situations. Main results of the GUARDIAN trial. Guard During Ischemia Against Necrosis (Guardian) Investigators. *Circulation*. 102, 3032–3038.
42. Myers, M.L. and Karmazyn, M. (1996) Improved cardiac function after prolonged hypothermic ischemia with the Na^+/H^+ exchange inhibitor HOE 694. *Ann Thorac Surg*. 61, 1400–1406.
43. Zeymer, U., Suryapranata, H., Monassier, J.P., et al. (2001) The Na^+/H^+ exchange inhibitor eniporide as an adjunct to early reperfusion therapy for acute myocardial infarction. *J Am Coll Cardiol*. 38, 1644–1650.

44. Bugge, E. and Yterhus, K. (1995) Inhibition of sodium-hydrogen exchange reduces infarct size in the isolated rat heart- a protective additive to ischaemic preconditioning. *Cardiovasc Res*. 29, 269–274.
45. Dhalla, N.S., Elmoselhi, A.B., Hata, T., et al. (2000) Status of myocardial antioxidants in ischemia-reperfusion injury. *Cardiovasc Res*. 47, 446–456.
46. Khaper, N., Rigatto, C., Seneviratne, C., et al. (1997) Chronic treatment with propranolol induces antioxidant changes and protects against ischemia-reperfusion injury. *J Mol Cell Cardiol*. 29, 3335–3344.
47. Kalaycioglu, S., Sinci, V., Imren, Y., et al. (1999) Metoprolol prevents ischemia-reperfusion injury by reducing lipid peroxidation. *Jpn Circ J*. 63, 718–721.
48. Feuerstein, G.Z., Yue, T.L., Cheng, H.Y., et al. (1993) Myocardial protection by the novel vasodilating beta-blocker, carvedilol: potential relevance of anti-oxidant activity. *J Hypertens*. 11, S41–S48.
49. Iyengar, S.R., Charrette, E.J., Iyengar, C.K., et al. (1976) Myocardial glycogen in prevention of perioperative ischemic injury of the heart: a preliminary report. *Can J Surg*. 19, 246–251.
50. Yellon, D.M. and Baxter, G.F. (1999) Reperfusion injury revisited: is there a role for growth factor signaling in limiting lethal reperfusion injury? *Trends Cardiovasc Med*. 9, 245–249.
51. Saraste, A., Pulkki, K., Kallajoki, M., et al. (1997) Apoptosis in human acute myocardial infarction. *Circulation*. 95, 320–323.
52. Baxter, G.F.M., Brar, B.K., Latchman, D.S., Yellon, D.M. (1998) Infarct-limiting action of transforming growth factor beta-1 in isolated rat heart is abolished. *Circulation*. 100, 1–9.
53. Baines, C.P., Wang, L., Cohen, M.V., et al. (1999) Myocardial protection by insulin is dependent on phospatidylinositol 3-kinase but not protein kinase C or KATP channels in the isolated rabbit heart. *Basic Res Cardiol*. 94, 188–198.
54. Buerke, M., Murohara, T., Skurk, C., et al. (1995) Cardioprotective effect of insulin-like growth factor I in myocardial ischemia followed by reperfusion. *Proc Natl Acad Sci USA*. 92, 8031–8035.
55. Cuevas, P., Carceller, F., Martinez-Coso, V., et al. (1999) Cardioprotection from ischemia by fibroblast growth factor: role of inducible nitric oxide synthase. *Eur J Med Res*. 4, 517–524.
56. Stephanou, A., Brar, B., Heads, R., et al. (1998) Cardiotrophin-1 induces heat shock protein accumulation in cultured cardiac cells and protects them from stressful stimuli. *J Mol Cell Cardiol*. 30, 849–855.
57. Morita, K., Ihnken, K., Buckberg, G.D., et al. (1995) Studies of hypoxemic/reoxygenation injury: without aortic clamping. VIII. Counteraction of oxidant damage by exogenous glutamate and aspartate. *J Thorac Cardiovasc Surg*. 110, 1228–1234.
58. Drinkwater, D.C., Jr., Cushen, C.K., Laks, H., et al. (1992) The use of combined antegrade-retrograde infusion of blood cardioplegic solution in pediatric patients undergoing heart operations. *J Thorac Cardiovasc Surg*. 104, 1349–1355.
59. Nakanishi, K., Zhao, Z.Q., Vinten-Johansen, J., et al. (1995) Blood cardioplegia enhanced with nitric oxide donor SPM-5185 counteracts postischemic endothelial and ventricular dysfunction. *J Thorac Cardiovasc Surg*. 109, 1146–1154.

13 The Effects of Anesthetic Agents on Cardiac Function

MICHAEL K. LOUSHIN, MD

CONTENTS

1. INTRODUCTION

Today, anesthesia is considered necessary for many types of surgeries and procedures. In general, anesthesia may provide analgesia, amnesia, hypnosis, and muscle relaxation. The depth of administered anesthesia can vary from minimal sedation to general anesthesia (Table 1). General anesthesia typically causes significant alterations in hemodynamics, especially during induction of anesthesia. Importantly, both inhalational and intravenous anesthetics can affect cardiovascular performance; this includes effects on cardiac output, heart rate, systemic vascular resistance, cardiac conduction system, myocardial contractility, coronary blood flow, or blood pressures. Yet, the choice of inhalational and intravenous anesthetics is typically associated with the patient's underlying cardiovascular status, such as the presence of heart failure and hypovolemia. The primary goal of this chapter is to make commonly employed methodologies and anesthetics more familiar to the reader, with particular attention to the potential influences on the cardiovascular system.

From: *Handbook of Cardiac Anatomy, Physiology, and Devices*
Edited by: P. A. Iaizzo © Humana Press Inc., Totowa, NJ

2. ANESTHESIA INDUCTION SEQUENCE

A typical general anesthesia induction sequence for an adult is as follows: after establishing intravenous access and placement of standard American Society of Anesthesiologists *(1)* monitors, a patient is preoxygenated with 100% oxygen. An induction dose of intravenous medications such as propofol, an opioid, and a muscle relaxant are administered (*see JPEG 1*, on the Companion CD and description at end of chapter). After the patient is rendered unconscious and anesthetized, direct laryngoscopy is performed, and the trachea intubated with an endotracheal tube. After confirmation of endotracheal intubation, the patient is placed on an anesthesia ventilator and next ventilated with a combination of anesthetic gases, air, and oxygen (*see JPEG 2*, on the Companion CD and description at end of chapter). Note, if a total intravenous anesthetic technique (such as propofol and opioid infusion) is chosen, anesthetic gases are not administered.

The cardiovascular depressant effects of most anesthetics typically become evident during and immediately following induction. Maintaining cardiovascular stability requires careful titration of medications, knowledge of clinical and basic

Table 1
Continuum of Depth of Sedation Definition of General Anesthesia and Levels of Sedation/Analgesia

	Minimal sedation (anxiolysis)	*Moderate sedation/analgesia ("conscious sedation")*	*Deep sedation/analgesia*	*General anesthesia*
Responsiveness	Normal response to verbal stimulation	Purposeful response to verbal or tactile stimulation	Purposeful response following repeated or painful stimulation	Unarousable even with painful stimulus
Airway	Unaffected	No intervention required	Intervention may be required	Intervention often required
Spontaneous ventilation	Unaffected	Adequate	May be inadequate	Frequently inadequate
Cardiovascular function	Unaffected	Usually maintained	Usually maintained	May be impaired

Excerpted from *ASA Standards, Guidelines and Statements*, 2003, of the American Society of Anesthesiologists. A copy of the full text can be obtained from ASA, 520 N. Northwest Highway, Park Ridgewood, IL 60068-2573.

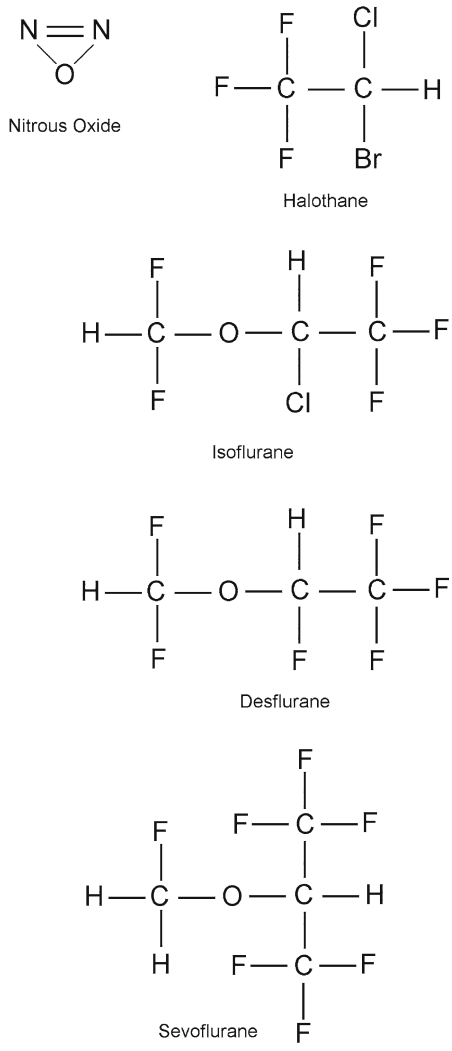

Fig. 1. Chemical structure of commonly administered inhalational anesthetics.

Table 2
Minimal Alveolar Concentration (MAC) of Inhalational Anesthetics

Agent	*MAC % (% of 1 atmosphere)*	*Vapor pressure (at 20°C)*
Desflurane	6.0	680
Halothane	0.75	243
Isoflurane	1.2	240
Sevoflurane	2.0	160
Nitrous oxide	105	
Xenon	70	

science in physiology and pharmacology, and diligent monitoring of vital signs (*JPEG 3*).

Typically, induction of general anesthesia in children by placement of an intravenous catheter for preinduction may be traumatic to the child or difficult because of noncooperation. Instead, initial mask induction with halothane, sevoflurane, or nitrous oxide is frequently utilized. After placement of American Society of Anesthesiologists monitors, a high concentration of halothane or sevoflurane along with oxygen is administered via a face mask. After the patient becomes unconscious, a peripheral intravenous catheter is placed, and a similar adult general anesthesia and airway management sequence follows.

Direct laryngoscopy and endotracheal intubation can often stimulate the upper and lower airways, which in turn may cause significant changes in blood pressures and heart rate if airway responses are not blunted. Commonly, titration of anesthetics and opioids administration is used to blunt these airway and associated sympathetic responses.

3. INHALATIONAL ANESTHETICS

Commonly used inhalational anesthetics include nitrous oxide, isoflurane, desflurane, halothane, and sevoflurane (Fig. 1). Each of these inhalational anesthetics has a specific minimum alveolar concentration (MAC) at which general anesthesia is considered induced (Table 2). MAC is defined as the minimum alveolar concentration of an inhaled anesthetic required to prevent movement in 50% of patients in response to a surgical incision. It is important to note that infants have a higher MAC than adults, and pregnant women and elderly patients have lower MAC requirements.

MAC is additive, that is, the 0.5 MAC of nitrous oxide and the 0.5 MAC of isoflurane result in 1 MAC total anesthesia. More specifically, the brain anesthetic partial pressure is dependent on factors such as inspired (F_I) and alveolar (F_A) concentration of anesthetic gas. The brain (F_B) concentration of anesthetic is dependent on F_A and F_I:

$$F_I \leftrightarrow F_A \leftrightarrow F_B$$

Table 3
Cardiovascular Effects of Inhalational Anesthetics

	Heart rate	*Blood pressure*	*Systemic vascular resistance*	*Cardiac output*	*Sensitize to epinephrine*	*Coronary dilation*
Desflurane	+	–	– –	0/–	0/+	+
Halothane	0	– –	0/–	–	+++	+
Isoflurane	+	– –	– –	–	0/+	++
Sevoflurane	0	– –	–	0/–	0/+	0
Nitrous oxide	+	0	0	0	0	0

0, no change; +, increased; ++, more increased; +++, most increased; –, decreased; – –, more decreased; – – –, most decreased.

Anesthetic uptake is determined by its blood solubility, cardiac output, and the difference between alveolar and venous partial pressure *(2)*. The greater the uptake of anesthetic gas, the slower is the rate of induction. Inhalational anesthetics with lower blood:gas solubility (i.e., desflurane and sevoflurane) will cause faster induction and emergence from general anesthesia.

3.1. Blood Pressure and Systemic Vascular Resistance

All volatile anesthetics (e.g., isoflurane, desflurane, sevoflurane, and halothane) cause dose-dependent effects on cardiovascular function. For example, these agents cause a dose-dependent decrease in mean arterial blood pressure *(3–6)*. The relative decrease in mean arterial blood pressure is considered to be caused by decreases in systemic vascular resistance, myocardial contractility, sympathetic output, or a combination of these. In particular, isoflurane, desflurane, and sevoflurane cause greater decreases in systemic vascular resistance compared to halothane (Table 3). Further, increasing doses of halothane result in small changes in system vascular resistance *(7)*, and decreases in mean arterial pressure. Yet, halothane administration is associated with decreases in cardiac output.

In general, volatile anesthetics decrease systemic vascular resistance by causing peripheral vasodilation, thus increasing blood flow to cutaneous and skeletal muscle tissues *(3)*. It should be noted that nitrous oxide causes a minimal alteration of systemic vascular resistance when administered alone.

3.2. Cardiac Conduction System and Heart Rate

Baroreceptors located near the aortic root, carotid arteries, and other sites detect changes in arterial blood pressures which then influences cardiovascular function. A typical baroreceptor reflex from the carotid artery includes the afferent (cranial nerve IX) and efferent (cranial nerve X) nerves. An increase in arterial blood pressure is detected by the baroreceptors, causing a reflex decrease in the heart rate. A decrease in arterial blood pressure causes a reflex tachycardia to maintain cardiac output and organ perfusion. Importantly, volatile anesthetics cause dose-dependent decreases in baroreceptor reflex activities *(8)*; hence, hemodynamic compensatory responses are attenuated by volatile anesthetics *(9,10)*. It is common that alterations in hemodynamics caused by volatile anesthetics may require administrations of other pressor medications to offset the attenuation of these normal physiological protective functions.

Volatile anesthetics may also cause specific cardiac dysrhythmias. Specifically, volatile anesthetics have been reported both to slow the rate of sinoatrial node discharge and to increase ventricular and His bundle conduction times *(11)*, which may increase the development of nodal rhythms. Further, volatile anesthetics may increase ventricular automaticity by altering potassium and calcium ion channels *(11)*.

It has been reported that halothane increases the incidence of ventricular dysrhythmias, especially when coadministered with epinephrine; in contrast, the coadministration of epinephrine with isoflurane, desflurane, or sevoflurane has minimal effects on increasing the incidence of ventricular dysrhythmias *(12–14)*. Furthermore, halothane may blunt the reflex increases in heart rates that typically accompany decreases in blood pressure; it may also slow conduction from the sinoatrial node, resulting in junctional ventricular rhythms.

Sevoflurane and desflurane are also known to blunt sympathetic baroreflex sensitivity partially. Importantly, isoflurane is well known to cause significant decreases in systemic vascular resistances and thus in blood pressure. Yet, the baroreceptor response remains partially intact, and cardiac output is maintained relatively stable with isoflurane via associated increases in heart rate.

3.3. Coronary Blood Flow

In general, volatile anesthetics cause a dose-dependent coronary vasodilation, with isoflurane having a greater effect than halothane *(15,16)*. Increasing the concentration of isoflurane increases coronary blood flow and this has the potential to cause "coronary steal" syndrome *(17,18)*. Coronary steal is caused by vasodilation of healthy coronary arteries and shunting of blood from myocardium at risk to areas not at risk; in coronary artery disease, areas at ischemic risk for myocardial ischemia have coronary arteries that are already maximally vasodilated. Desflurane and sevoflurane have not been associated with coronary steal syndrome *(19,20)*. Nevertheless, the exact clinical significance of coronary steal in humans is generally considered somewhat unresolved.

3.4. Contractility and Cardiac Output

Volatile anesthetics depress myocardial contractility by inducing alterations of calcium ion flux *(21)*. The mechanism of negative inotropic effects of volatile anesthetics include: decreased free Ca^{2+}, decreased Ca^{2+} release from sarcoplasmic reticulum, and/or altered contractile protein response to Ca^{2+} *(21,22)*. Halothane diminishes myocardial contractility more

than isoflurane, desflurane, and nitrous oxide. Isoflurane and sevoflurane cause minimal change in contractility and thus allow for better maintained systemic cardiac output *(22)*. Because of the better cardiovascular stability following either isoflurane or sevoflurane administration compared to halothane, the former agents are utilized frequently in patients with congenital heart defects or depressed myocardial function.

Because of the simultaneous stimulation of the sympathetic nervous system, the myocardial depressant effects of nitrous oxide are usually not evident in healthy individuals. Yet, in a compromised and failing myocardium, its depressant effects on contractility become much more evident. More specifically, nitrous oxide has been associated with sympathomimetic effects because it increases plasma catecholamines, mydriasis, and vasoconstriction of both systemic and pulmonary circulations *(23)*. When nitrous oxide is administered with opioids such as fentanyl, the sympathomimetic effects are abolished. Therefore, the combined administration of nitrous oxide and opioids may result in a significant overall decrease in mean arterial pressure and cardiac output.

The abrupt increase in a patient's desflurane concentration has been associated with a significant increase in sympathetic output, resulting in increased heart rate and mean arterial pressure. A proposed mechanism for this sympathetic stimulation is that it is caused by airway and lung irritation with a high concentration of desflurane *(24)*. A smaller increase in sympathetic output is commonly associated with isoflurane administration, whereas sevoflurane, because of lack of airway irritation with its administration, is not associated with any increase in sympathetic output, even with a very rapid increase in concentration. Because of the favorable airway properties of sevoflurane, it is used frequently for inhalation induction of anesthesia in children. Importantly, a high concentration of sevoflurane (4–8%) for rapid mask induction is well tolerated in children.

3.5. Pulmonary Blood Flow

Volatile anesthetics are potent bronchodilators; in some cases, they have been used for the treatment of status asthmaticus. In general, it is considered that volatile anesthetics may cause a mild decrease in pulmonary vascular resistance, whereas with nitrous oxide, they can cause a significant increase in pulmonary vascular resistance. In patients with congenital heart defects (i.e., intracardiac shunts, single ventricle, transposition of great arteries, tetralogy of Fallot), the properties of select volatile anesthetics may be critical in offering better cardiovascular stability. Administration of nitrous oxide in patients with preexisting pulmonary artery hypertension may exacerbate the strain on the right heart by increasing pulmonary vascular resistance. The elevated pulmonary vascular resistance may also result in right-to-left intracardiac shunting in susceptible patients (i.e., those with ventriculoseptal defect). Volatile anesthetics may also diminish the degree of hypoxic pulmonary vasoconstriction, which may result in hypoxia.

3.6. Cardioprotection/Preconditioning

The potential for myocardial preconditioning with volatile anesthetics has been extensively studied. Importantly, halogenated volatile anesthetics have been shown to provide cardioprotection against injury associated with ischemia and reperfusion *(25–28)*. The mechanism of cardioprotection seems to be similar to ischemic preconditioning first described by Murray et al. *(29)* and thus likely involves the mitochondrial potassium (K_{ATP}) channel *(30)*.

3.7. Future Inhalational Anesthetics

Xenon was first used as an anesthetic gas in humans by Cullen and Gross in 1951 *(31)*. Xenon, an inert gas, has many properties that make it an ideal anesthetic gas. It has very low toxicity and is nonexplosive and nonflammable. The MAC of xenon is approx 70%. Its very low blood-to-gas solubility partition coefficient (0.115) provides for fast onset and emergence from anesthesia *(32)*. Preliminary clinical studies with xenon have shown minimal adverse effects on the cardiovascular system and general hemodynamics parameters *(32–34)*. More specifically, xenon has been shown to induce minimal effects on alterations in heart rates, coronary blood flows, left ventricular pressures, and/or atrioventricular conduction times *(35)*. However, factors that may limit the use of xenon as an anesthetic gas are its cost and unique delivery system; xenon must be extracted from the atmosphere, and the process is expensive. Nevertheless, special breathing and delivery systems are in development.

All volatile anesthetics may trigger malignant hyperthermia in susceptible patients. Malignant hyperthermia is an inherited pharmacogenetic disorder that affects skeletal muscle and is characterized by a hypermetabolic response when exposed to a triggering agent such as volatile anesthetics and succinylcholine. Disregulation of the ryanodine receptor, the calcium release channel of sarcoplasmic reticulum, is involved in the unregulated release of calcium from this storage site. Signs and symptoms of malignant hyperthermia include sympathetic hyperactivity, elevated carbon dioxide production, muscle rigidity, hyperthermia, metabolic acidosis, dysrhythmias, and hyperkalemia. Treatment of malignant hyperther-mia requires removal of the triggering agent, intravenous administration of dantrolene, and management of the associated symptoms.

4. INTRAVENOUS ANESTHETICS

4.1. Barbiturates

In general, barbiturates cause central nervous system inhibition (depression) by enhancing the effects of γ–aminobutyric acid (GABA) *(36)*. Barbiturates bind to the GABA receptor complex, which increases chloride channel activity, causing subsequent inhibition of the central nervous system. The GABA receptor complex has binding affinities for GABA, barbiturates, benzodiazepines, propofol, and alcohol *(23)*.

Thiopental (3–5 mg/kg) and methohexital (1.5–2 mg/kg) are common barbiturates used for induction of general anesthesia (Fig. 2). After intravenous injection of thiopental or methohexital, anesthesia is induced rapidly, within seconds. The duration of induced anesthesia after a single bolus dose of intravenous barbiturate is short (approx 5 min) because of rapid redistribution from the brain to other tissues, such as muscle and adipose. Importantly, intraarterial injection of thiopental can result in severe vasospasm, which may lead to thrombosis, tissue injury, or gangrene. If intraarterial injections do occur, counteractive

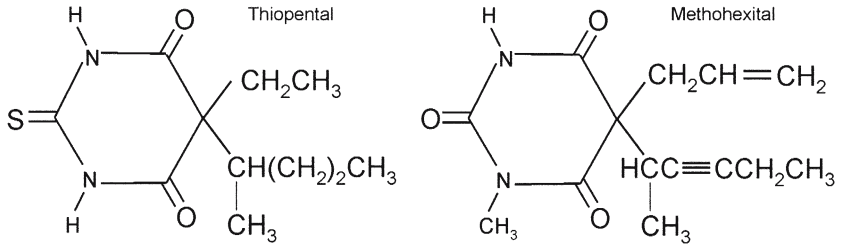

Fig. 2. Chemical structure of thiopental and methohexital.

measures such as sympathetic nerve blocks or administration of papaverine, phenoxybenzamine, or lidocaine may be initiated to decrease arterial vasospasm.

Administration of barbiturates is typically associated with decreases in mean arterial pressure, which result from both induced vasodilation and decreased myocardial contractility (Table 4). Barbiturates have been shown to cause dose-related myocardial depression, which is not as pronounced as that associated with volatile anesthetics. Barbiturates may cause a slight depression of carotid and aortic baroreceptors; therefore, a decrease in mean arterial pressure leads to reflex tachycardia. If intravenous barbiturates are administered slowly, relative hemodynamic stability can be maintained *(37)*. In contrast, a rapid infusion of barbiturates, especially in hypovolemic patients, may result in significant hypotension. Subsequently, typical increases in heart rates on barbiturate administration are not present if the baroreceptor reflexes are not intact, as in heart transplant patients or in isolated heart preparations. Importantly, barbiturates do not generally sensitize the myocardium to the potential arrhythmic effects of administered catecholamines.

Table 4
Cardiovascular Effects of Intravenous Anesthetics

	Heart rate	*Blood pressure*	*Systemic vascular resistance*	*Cardiac output*
Thiopental	+	–	–	+
Ketamine	++	++	+	++
Propofol	0/–	– –	– –	–
Etomidate	0	0/–	0	0
Fentanyl	0/–	0	0	0
Morphine	0/–	0/–	0/–	0
Midazolam	0	0	0	0
Methohexital	++	–	–	0/–
Meperidine	++	0/–	0/–	0/+

0, no change; +, increased; ++, more increased; +++, most increased; –, decreased; – –, more decreased; – – –, most decreased.

4.2. Benzodiazepines

Benzodiazepines are considered to produce central nervous system depression by binding to the GABA receptor complex and ultimately increasing chloride channel activity. Benzodiazepines, such as midazolam and diazepam, are often administered as adjuncts to anesthesia for sedation, amnesia, and anxiolysis. Benzodiazepines themselves do not have analgesic properties. However, they possess anticonvulsant properties and hence are utilized in acute management of seizures.

Interestingly, the acute administration of benzodiazepines is not associated with significant changes in hemodynamic parameters; blood pressure, heart rate, and systemic vascular resistance are fairly well maintained. However, systemic vascular resistance decreases in a dose-related fashion *(38)*, but a typical dose required for sedation and anxiolysis in adults (1–2 mg iv) usually is not associated with any significant hemodynamic alteration.

More specifically, induction of anesthesia with midazolam (0.2–0.3 mg/kg iv) is associated with a decrease in systemic vascular resistance, but with a minimal effect on cardiac output; the baroreceptor reflex remains intact, and a decrease in mean arterial pressure results in a responsive increase in heart rate. It has been reported that diazepam elicits even fewer cardiovascular effects than midazolam. At most, diazepam may cause a minimal change in blood pressure and systemic vascular resistance. Therefore, coadministration of diazepam and nitrous oxide is not associated with significant decreases in cardiovascular function *(39)*; thus, it is employed in patients for whom such concerns may be justified.

4.3. Opioids

Opioids are analgesics commonly administered as adjuncts to anesthesia. Opioids currently used in clinical practice include fentanyl, morphine, meperidine, sufentanil, and remifentanil (Table 5). All opioids exert their effect by interacting with opioid receptors (mu_1, mu_2, kappa, or delta) (Table 6); they are adjuncts to help blunt sympathetic responses to noxious stimuli. Overall, opioids cause minimal changes in cardiac output and blood pressure. Yet, opioids will generally cause bradycardia by increasing vagal tone.

Typically, at very high doses, opioids may have the following effects on hemodynamics: inhibition of the autonomic nervous system, direct myocardial depression, and/or induced histamine release. More specifically, one in vitro study of human atrial myocardium found that fentanyl, remifentanil, and sufentanil did not modify inotropic effects; alfentanil caused negative inotropy by affecting calcium regulation *(40)*. However, it has also been reported that opioids such as fentanyl may depress rat myocardial contractility by affecting calcium regulation *(41)*. Finally, it is considered that morphine may cause decreases in mean arterial pressures by causing histamine release and bradycardia.

Table 5
Opioid Agonists Commonly Used in Clinical Practice

	Heart rate	*Blood pressure*	*System vascular resistance*	*Contractility*	*Histamine*
Meperidine	++	–	–	+/–	++
Morphine	0/–	–	–	–	++
Fentanyl	0/–	0	0	0	0
Alfentanil	–	0/–	–	0/–	0
Sufentanil	–	0/–	0/–	0/–	0
Remifentanil	–	0	0	0	0

0, no change; +, increased; ++, more increased; +++, most increased; –, decreased; – –, more decreased; – – –, most decreased.

Table 6
Opioid and Opioid Receptors

Drug	*Mu receptor*	*Delta deceptor*	*Kappa receptor*
Morphine	+++	+?	+
Fentanyl	+++	?	
Sufentanil	+++	+	+
Buprenorphine	+	– –	
Naloxone	– – –	–	– –
Naltrexone	– – –	–	– – –
Nalbuphine	– –	++	
DPDPE	++		
DADLE	+	+++	+?
NorBNI	–	–	– – –
DSLET	+	++	
Naltrindole	–	– – –	–

Source: Modified from Goodman and Gilman's (2001) *The Pharmacological Basis of Therapeutics,* 10th Ed. (Hardman, J.G. and Limbird, L.E., eds.), McGraw-Hill, New York, NY.

DPDPE, [D-Pen^{2,5}]–enkephalin; DADLE, [D-Ala^{2}, D-Leu^{5}]–enkephalin; NorBNI, nor-binaltorphimine; DSLET, [D-Ser^{2}, Leu^{5}, Thr^{6}]–enkephalin

0, no change; +, increased; ++, more increased; +++, most increased; –, decreased; – –, more decreased; – – –, most decreased.

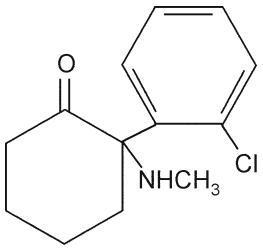

Fig. 3. Chemical structure of ketamine.

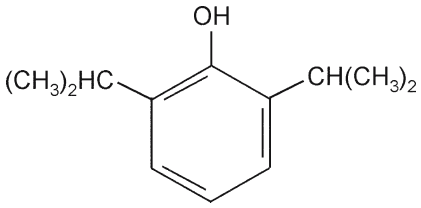

Fig. 4. Chemical structure of propofol.

4.4. Ketamine

Ketamine is a phencyclidine derivative (Fig. 3) that causes intense analgesia and dissociative anesthesia. Patients who receive ketamine can obtain a cataleptic state with open eyes or ocular nystagmus. The typical routes for ketamine administration include intravenous (1–2 mg/kg), intramuscular (3–6 mg/kg), or oral (5–6 mg/kg). In general, the effects of ketamine on the central nervous system are considered caused by interactions with multiple receptors, including *N*-methyl-D-asparate, monoaminergic, opioid, or muscarinic receptors.

Potential side effects of ketamine include the stimulation of the central sympathetic nervous system and thus an increase in circulating epinephrine and norepinephrine. In patients for whom maintenance of myocardial contractility and systemic vascular resistance is vital (i.e., because of hypovolemia, trauma, and shock), ketamine may better stimulate the cardiovascular system to maintain cardiac output and blood pressure; ketamine acts to cause an increase in heart rate, blood pressure, cardiac output, and myocardial oxygen consumption.

It should be noted that pulmonary artery pressure may also become increased after the administration of ketamine. Another important side effect attributed to ketamine administration is bronchodilation; thus, patients with, or at risk for, bronchospasm may benefit from ketamine induction. In contrast, in patients with depleted catecholamine stores, ketamine may cause a serious depression of myocardial function *(42)*; thus, its use may be contraindicated in patients with coronary artery disease, subaortic stenosis, or increased intracranial pressures.

4.5. Propofol

Propofol (1% solution) is a 2,6-diisopropylphenol (Fig. 4) that is typically administered intravenously for sedation or induction of anesthesia. Importantly, intravenous injections of propofol (1.5–2 mg/kg) are associated with rapid (30–60 s) loss of consciousness; hence, this has obvious clinical advantages. A maintenance infusion of propofol is typically achieved with 100–200 μg/kg/min iv. Additional advantages of propofol include clear awakening, small cumulative effects, and decreased incidence of nausea and vomiting.

Propofol is considered also to interact with GABA receptors and activate them in a similar fashion as barbiturates. Likewise, activation of GABA receptors by propofol increases the con-

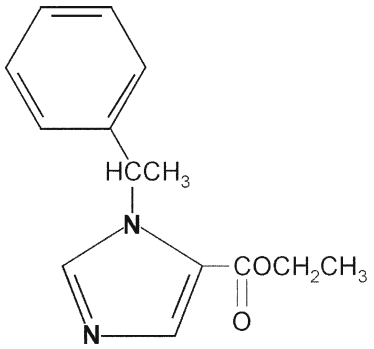

Fig. 5. Chemical structure of etomidate.

Table 7
Nondepolarizing Muscle Relaxants

	Histamine release	*Vagal blockade*
Atracurium	+	0
Cisatracurium	0	0
Mivacurium	+	0
Pancuronium	0	++
Rocuronium	0	0/+
Vecuronium	0	0
Tubocurarine	+++	0
Succinylcholine	0	–

0, no change; +, increased; ++, more increased; +++, most increased; –, decreased; – –, more decreased; – – –, most decreased.

ductance of chloride channels, resulting in inhibition of postsynaptic neurons.

Of clinical significance, the administration of propofol commonly causes a decrease in both systemic vascular resistance and cardiac contractility, hence resulting in decreased cardiac output. This reduction in systemic vascular resistance (and vasodilation) is considered caused by decreased sympathetic vasoconstrictor activation of vascular smooth muscle *(43)*. The inhibition of sympathetic tone by propofol is reported to be greater than inhibition of parasympathetic activity; this may result in significant bradycardia and even asystole *(44–46)*. The induced decrease in cardiac contractility is likely because of decreases in calcium uptake into the sarcoplasmic reticulum. Decreased reuptake of calcium results in less calcium available for the next activation sequence *(47)*.

Again it should be noted that, in patients with decreased left ventricular function (e.g., the elderly and patients with hypovolemia), the administration of propofol may result in severe hypotension. Therefore, the careful titration of propofol and adequate intravascular hydration are important for these types of patients.

4.6. Etomidate

Etomidate (Fig. 5) is an imidazole compound that is water soluble at lower pH and lipid soluble at physiologic pH. Rapid loss of consciousness is accomplished after intravenous injection of etomidate (0.2–0.4 mg/kg). It is important to recognize that etomidate lacks analgesic properties and does not blunt sympathetic responses to direct laryngoscopy and endotracheal intubation.

Generally, etomidate provides cardiovascular and pulmonary stability; typical induction doses of etomidate result in minimal changes in heart rate and cardiac output. Myocardial contractility is well maintained at doses needed to induce general anesthesia *(23)* and is considered to produce less myocardial depression compared to thiopental *(48)*. Etomidate does not induce significant histamine release, but it does depress adrenocortical function by inhibiting the conversion of cholesterol to cortisol *(49)*. Specifically, a single induction dose of etomidate can cause adrenal suppression for 5–8 h *(50)*, and a continuous infusion of etomidate will cause further adrenocortical suppression.

4.7. Nondepolarizing Muscle Relaxants

The majority of nondepolarizing muscle relaxants have minimal effects on cardiovascular and hemodynamic stability. When induced, nondepolarizing muscle relaxants are believed to elicit their cardiovascular effects by stimulating the release of histamine and affecting muscarinic and nicotinic receptors (Table 7). For example, pancuronium may cause vagal blockade (antimuscarinic effect) at the sinoatrial node, resulting in elevation of heart rate. The administration of pancuronium is also associated with activation of the sympathetic nervous system *(51,52)*. Likewise, large doses of atracurium and mivacurium are associated with histamine release, which may result in tachycardia and hypotension; such patients may display facial flushing as a result of histamine release. Interestingly, cisatracurium (a stereoisomer of atracurium) is not associated with histamine release. Finally, vecuronium and rocuronium are agents that are considered totally devoid of significant cardiovascular effects.

4.8. Depolarizing Muscle Relaxant

Succinylcholine is a depolarizing muscle relaxant; it has a structure similar to acetylcholine and mimics it by binding to nicotinic cholinergic receptors. The duration of action of succinylcholine is short (minutes) and is broken down by the abundant pseudocholinesterase enzyme. Importantly, the administration of succinylcholine may be associated with cardiac dysrhythmias (i.e., junctional rhythm and sinus bradycardia) by its muscarinic activity at the sinoatrial node. Administration of succinylcholine may also be associated with hyperkalemia in susceptible patients, such as those with malignant hyperthermia, muscular dystrophy, spinal cord injury, and burn injury. More specifically, in boys with Duchenne muscular dystrophy, the administration of succinylcholine has been linked to episodes of sudden cardiac death.

5. PHYSIOLOGIC EFFECTS OF ACUPUNCTURE

Acupuncture involves stimulation of specific anatomical locations on the skin to alter energy flow patterns throughout the body. The skin can be stimulated by manual or electrical stimulation or the more typical placement of small metallic needles. Acupuncture has been used in China for thousands of

years; there has been a surge of interest in these nontraditional methodologies in the United States.

Acupuncture has been utilized for treatment and prevention of multiple health conditions, such as chronic pain, nausea and vomiting, obesity, substance abuse, and asthma. Stress response and cardiovascular effects of pain have reportedly been attenuated by nonpharmacological techniques such as acupuncture; it modulates the body's pain system, increases the release of endogenous opioids *(53)*, and/or decreases postoperative pain *(54)*. In a feline cardiovascular model, the utilization of electroacupuncture induced improvements in regional cardiac wall motion activity during myocardial ischemia *(55)*. Furthermore, acupressure applied to females undergoing elective cesarean section with spinal anesthesia displayed a reduction in nausea and vomiting *(56)*.

The potential advantages of acupuncture for the treatment of medical conditions continue to be investigated. With initial studies indicating numerous promising benefits of acupuncture for treatment of multiple medical conditions, the National Institutes of Health Consensus Conference has recommended that acupuncture be included in comprehensive management and may be useful as an adjunct treatment or an acceptable alternative *(57)*. Finally, limitations in the validation of acupuncture may stem from difficulty creating randomized, blinded, placebo-controlled clinical studies.

6. ANESTHESIA AND TEMPERATURE REGULATION

General and regional anesthesia are often associated with disregulation of body temperature and thus decreases in core body temperature. Most of the body heat lost during anesthesia is via convection and radiation, with some losses caused by conduction and evaporation. Principally, anesthetics cause the core body heat to redistribute to the periphery, resulting in a drop in core body temperature *(58)*. Under anesthesia, patients become poikilotherms (have minimal ability to thermoregulate). Therefore, multiple modalities to maintain normothermia during surgery have been developed, including forced-air warming devices, fluid warmers, ventilator humidifiers, water mattresses and vests, radiant lamps, and warm blankets. Other modalities for warming patients include altering ambient room temperatures or the temperatures of irrigation solutions.

Importantly, postoperative hypothermia may be associated with (1) delayed awakening from general anesthesia, (2) slowed drug metabolism, (3) coagulopathy, (4) vasoconstriction and poor tissue perfusion, (5) increases in blood viscosity, and/or (6) induced shivering. Importantly, postoperative shiver may be detrimental in patients with coronary artery disease because shivering causes increases in oxygen consumption and tachycardia. Currently, meperidine is clinically approved for treatment of excessive shivering in postoperative situations.

7. MYOCARDIAL PRECONDITIONING WITH INHALATIONAL AND INTRAVENOUS ANESTHETICS

Since the initial report by Murray et al. *(29)* on ischemic preconditioning of dog myocardium, there has been great interest in myocardial preconditioning with pharmacological agents. This includes myocardial preconditioning with volatile anesthetics such as desflurane *(59)*, isoflurane *(60,61)*, and sevoflurane *(62)* and intravenous opioid agonists *(63,64)*. Pharmacological preconditioning is not limited to cardiac tissue only; other tissues, such as lungs, brain, and skeletal muscle *(65)*, may benefit from preconditioning. In summary, preconditioning with anesthetics may offer life-extending benefits in cardiac vascular and organ transplantation surgical patients. (For more details on this topic, *see* Chapter 12.)

8. HEART TRANSPLANT

With the increasing numbers of successful heart transplants, anesthetic management of the patient after a heart transplant procedure requires special considerations. A transplanted heart is totally denervated and usually has a higher basal heart rate (90–110 beats/min); direct autonomic nervous system effects are mostly absent. Thus, agents such as atropine and glycopyrrolate will not cause an increase in heart rate. Vagal stimulation maneuvers such as carotid massage and oculocardiac reflex are also minimized. However, acetylcholinesterase inhibitors such as neostigmine have been associated with severe bradycardia. If bradycardia develops, administration of direct-acting cardiac agents such as isoproterenol or epinephrine may be required. The transplanted heart continues to respond to circulating catecholamines, and thus maintenance of cardiac output is aided by increased stroke volume (Frank-Starling relationship); maintaining adequate preload is considered essential in patients post-heart transplant. (*See* Chapter 10 for additional information.)

9. SUMMARY

With the aging population and an increase in health problems such as obesity, diabetes, and coronary artery diseases, perioperative management and anesthetic technique and medications that promote cardiovascular stability continue to offer challenges and new developments in the field of anesthesiology. These include new anesthesia medications, medical equipment and surgical technology, and anesthetic and surgical techniques. With further understanding of inhalational and intravenous anesthetics, maintaining stable, physiological cardiovascular function may be possible.

COMPANION CD MATERIAL

JPEG 1.
An anesthesiologist administering intravenous medications to a patient for induction of general anesthesia.

JPEG 2.
An anesthesia machine and ventilator.

JPEG 3.
An anesthesiologist titrating the dose of an inhalational anesthetic to maintain anesthesia and cardiovascular stability.

REFERENCES

1. American Society of Anesthesiologists (October 2003) *ASA Standards, Guidelines and Statements*. American Society of Anesthesiologists, Park Ridge, IL.

2. Eger, E.I., II (1974) Uptake of inhaled anesthetics: the alveolar to impaired anesthetic difference, in *Anesthetic Uptake and Action* (Eger, E.I., II, ed.), Williams and Wilkins, Baltimore, MD, p. 77.
3. Stevens, W., Cromwell, T., Halsey, M., et al. (1971) The cardiovascular effects of a new inhalation anesthetic, Forane, in human volunteers at constant arterial carbon dioxide tension. *Anesthesiology*. 35, 8–16.
4. Eger, E.I. II, Smith, N., and Stoelting, R., et al. (1970) Cardiovascular effects of halothane in man. *Anesthesiology*. 32, 396–489.
5. Weiskopf, R., Cahalan, M., Eger, E.I., II, et al. (1991) Cardiovascular actions of desflurane in normocarbic volunteers. *Anesth Analg*. 73, 143–156.
6. Holaday, D. and Smith, F. (1981) Clinical characteristics and biotransformation of sevoflurane in healthy human volunteers. *Anesthesiology*. 54, 100–106.
7. Pavlin, E.G. and Su, J.Y. (1994) Cardiopulmonary pharmacology, in *Anesthesia* (Miller, R, ed.), Churchill Livingstone, Philadelphia, PA, p. 145.
8. Muzi, M. and Ebert, T.J. (1995) A comparison of baroreflex sensitivity during isoflurane and desflurane anesthesia in humans. *Anesthesiology*. 82, 919–925.
9. Duke, P.C., Townes, D., and Wade, J.G. (1977) Halothane depresses baroreflex control of heart rate in man. *Anesthesiology*. 46, 184–187.
10. Kotrly, K.J., Ebert, T.J., Vucins, E., et al. (1984) Baroreceptor reflex control of heart rate during isoflurane anesthesia in humans. *Anesthesiology*. 60, 173–179.
11. Atlee, J.L. and Bosnjak, Z.J. (1990) Mechanisms for cardiac dysrhythmias during anesthesia. *Anesthesiology*. 72, 347–374.
12. Navarro, R., Weiskopf, R.B., Moore, M.A., et al. (1994) Humans anesthetized with sevoflurane or isoflurane have similar arrhythmic response to epinephrine. *Anesthesiology*. 80, 545–549.
13. Moore, M.A., Weiskopf, R.B., Eger, E.I., et al. (1994) Arrhythmogenic doses of epinephrine are similar during desflurane or isoflurane anesthesia in humans. *Anesthesiology*. 79, 943–947.
14. Johnston, R.R., Eger, E.I., and Wilson, C. (1976) A comparative interaction of epinephrine with enflurane, isoflurane, and halothane in man. *Anesth Analg*. 55, 709–712.
15. Crystal, G.J., Khoury, E., Gurevicius, J., and Salem, M.R. (1995) Direct effects of halothane on coronary blood flow, myocardial oxygen consumption, and myocardial segmental shortening in *in situ* canine hearts. *Anesth Analg*. 80, 256–262.
16. Crystal, G.J. and Salem, M.R. (2003) Isoflurane causes vasodilation in the coronary circulation. *Anesthesiology*. 98, 1030.
17. Priebe, H. and Foex, P. (1987) Isoflurane causes regional myocardial dysfunction in dogs with critical coronary artery stenoses. *Anesthesiology*. 66, 293–300.
18. Cason, B.A., Verrier, E.D., London, M.J., et al. (1987) Effects of isoflurane and halothane on coronary vascular resistance and collateral myocardial blood flow: their capacity to induce coronary steal. *Anesthesiology*. 67, 665–675.
19. Kersten, J.R., Brayer, A.P., Pagel, P.S., et al. (1994) Perfusion of ischemic myocardium during anesthesia with sevoflurane. *Anesthesiology*. 81, 995–1004.
20. Eger, E. (1994) New inhaled anesthetics. *Anesthesiology*. 80, 906–922.
21. Pavlin, E.G. and Su, J.Y. (1994) Cardiopulmonary pharmacology, in *Anesthesia* (Miller R, ed.), Churchill Livingstone, Philadelphia, PA, p. 148.
22. Rivenes, S.M., Lewin, M.B., Stayer, S.A., et al. (2001) Cardiovascular effects of sevoflurane, isoflurane, halothane, and fentanyl-midazolam in children with congenital heart disease. *Anesthesiology*. 94, 223–229.
23. Stoelting, R.K. (1999) *Pharmacology and Physiology in Anesthetic Practice,* 3rd Ed. Lippincott, Williams, and Wilkins, Philadelphia, PA.
24. Muzi, M., Ebert, T.J., Hope, W.G., et al. (1996) Site(s) mediating sympathetic activation with desflurane. *Anesthesiology*. 85, 737–747.
25. Warltier, D.C., Al Wathiqui, M.H., Kampine, J.P., et al. (1988) Recovery of contractile function of stunned myocardium in chronically instrumented dogs is enhanced by halothane or isoflurane. *Anesthesiology*. 69, 552–565.
26. Marijic, J., Stowe, D.F., Turner, L.A., et al. (1990) Differential protective effects of halothane and isoflurane against hypoxic and reoxygenation injury in the isolated guinea pig heart. *Anesthesiology*. 73, 976–983.
27. Novalija, E., Fujita, S., Kampine, J.P., et al. (1999) Sevoflurane mimics ischemic preconditioning effects on coronary flow and nitric oxide release in isolated hearts. *Anesthesiology*. 91, 701–712.
28. Conzen, P.F., Fischer, S., Detter, C., et al. (2003) Sevoflurane provides greater protection of myocardium than propofol in patients undergoing off-pump coronary artery bypass surgery. *Anesthesiology*. 99, 826–833.
29. Murray, C.E., Jennings, R.B., and Reimer, K.A. (1986) Preconditioning with ischemia: a delay of lethal cell injury in ischemic myocardium. *Circulation*. 74, 1124–1136.
30. Zaugg, M., Lucchinetti, E., Spahn, D.R., et al. (2002) Volatile anesthetics mimic cardiac preconditioning by priming the activation of mitochondrial K_{ATP} channels via multiple signaling pathways. *Anesthesiology*. 97, 4–14.
31. Cullen, S.C. and Gross, E.G. (1951) The anesthetic properties of xenon in animals and human beings with additional observation on krypton. *Science*. 1113, 580–582.
32. Rossaint, R., Reyle-Hahn, R., Schulte, J., et al. (2003) Multicenter randomized comparison of the efficacy and safety of xenon and isoflurane in patients undergoing elective surgery. *Anesthesiology*. 98, 6–13.
33. Lachmann, B., Armbruster, S., Schairer, W., et al. (1990) Safety and efficacy of xenon in routine use as an inhalational anesthetic. *Lancet*. 335, 1413–1415.
34. Luttrop, H.H., Romner, B., Perhag, L., et al. (1993) Left ventricular performance and cerebral hemodynamics during xenon anesthesia: a transesophageal echocardiography and transcranial Doppler sonography study. *Anesthesia*. 48, 1045–1049.
35. Stowe, D.F., Rehmert, G.C., Wai-Meng, K., et al. (2000) Xenon does not alter cardiac function or major cation currents in isolated guinea pig hearts of myocytes. *Anesthesiology*. 92, 516–522.
36. Franks, N.P. and Lieb, W.R. (1994) Molecular and cellular mechanisms of general anaesthesia. *Nature*. 367, 607–614.
37. Seltzer, J.L., Gerson, J.I., and Allen, F.B. (1980) Comparison of the cardiovascular effects of bolus vs incremental administration of thiopentone. *Br J Anaesth*. 52, 527–529.
38. Sunzel, M., Paalzow, L., Berggren, L., et al. (1988) Respiratory and cardiovascular effects in relation to plasma levels of midazolam and diazepam. *Br J Clin Pharmacol*. 25, 561569.
39. McCammon, R.L., Hilgenberg, J.C., Stoelting, R.K. (1980) Hemodynamic effects of diazepam-nitrous oxide in patients with coronary artery disease. *Anesth Analg*. 59, 438–441.
40. Hanouz, J., Yvon, A., Guesne, G., et al. (2001) The in vitro effects of remifentanil, sufentanil, fentanyl, and alfentanil on isolated human right atria. *Anesth Analg*. 93, 543–549.
41. Kanaya, N., Kahary, D.R., Murray, P.A., and Damron, D.S. (1998) Differential effects of fentanyl and morphine on intracellular calcium transients and contraction in rate ventricular myocytes. *Anesthesiology*. 89, 1532–1542.
42. Waxman, K., Shoemaker, W.C., and Lippmann, M. (1980) Cardiovascular effects of anesthetic induction with ketamine. *Anesth Analg*. 58, 355–358.
43. Robinson, J.F., Ebert, T.J., O'Brien, T.J., et al. (1997) Mechanisms whereby propofol mediates peripheral vasodilation in humans. Sympathoinhibition or direct vascular relaxation? *Anesthesiology*. 86, 64–72.
44. Bray, R.J. (1995) Fatal myocardial failure associated with a propofol infusion in a child. *Anaesthesia*. 50, 94.
45. Tramer, M.R., Moore, R.A., and McQuay, H.J. (1997) Propofol and bradycardia: causation, frequency and severity. *Br J Anaesth*. 78, 642–651.
46. James, M.F.M., Reyneke, C.J., and Whiffler, K. (1989) Heart block following propofol: a case report. *Br J Anaesth*. 62, 213–215.
47. Sprun, J., Lgletree-Hughes, M.L., McConnell, B.K., et al. (2001) The effects of propofol on the contractility of failing and nonfailing human heart muscles. *Anesth Analg*. 93, 550–559.

48. Kissin, I., Motomura, S., Aultman, D.F., et al. (1983) Inotropic and anesthetic potencies of etomidate and thiopental in dogs. *Anesth Analg*. 62, 961–965.
49. Fragen, R.J., Shanks, C.A., Molteni, A., et al. (1984) Effects of etomidate on hormonal responses to surgical stress. *Anesthesiology*. 61, 652–656.
50. Wagner, R.L., White, P.F., Kan, P.B., et al. (1984) Inhibition of adrenal steroidogensis by anesthetic etomidate. *N Engl J Med*. 310, 1415–1421.
51. Ivankovich, A.D., Miletich, D.J., Albrecht, R.F., et al. (1975) The effect of pancuronium on myocardial contraction and catecholamine metabolism. *J Pharm Pharmacol*. 27, 837–841.
52. Domenech, J.S., Garcia, R.C., Sastain, J.M.R., et al. (1976) Pancuronium bromide: an indirect sympathomimetic agent. *Br J Anaesth*. 48, 1143–1148.
53. Han, J.S. (1986) Physiologic and neurochemical basis of acupuncture analgesia, in *The International Textbook of Cardiology* (Cheng, T.O., ed.), Pergamon, New York, NY, pp. 1124–1126.
54. Felhendler, D.P.T. and Lisander, B. (1996) Pressure on acupoints decreases postoperative pain. *Clin J Pain*. 12, 326–329.
55. Li, P., Pitsillides, K.F., Rendig, S.V., et al. (1998) Reversal of reflex-induced myocardial ischemia by median nerve stimulation: a feline model of electroacupuncture. *Circulation*. 97, 1186–1194.
56. Stein, D.J., Birnbach, D.J., Danzer, B.I., et al. (1997) Acupressure versus intravenous metoclopramide to prevent nausea and vomiting during spinal anesthesia for cesarean section. *Anesth Analg*. 84, 342–345.
57. Acupuncture. NIH Consensus Conference. *JAMA*. (1998) 280, 1518–1524.
58. Sessler, D.I. (1997) Mild perioperative hypothermia. *N Engl J Med*. 336, 1630–1637.
59. Hanouz, J., Yvon, A., Massetti, M., et al. (2002) Mechanisms of desflurane-induced preconditioning in isolated human right atria in vitro. *Anesthesiology*. 97, 33–41.
60. Kersten, J.R., Schmeling, T.J., Hettrick, D.A., et al. (1996) Mechanism of myocardial protection by isoflurane: role of adenosine triphosphate-regulated potassium (KATP) channels. *Anesthesiology*. 85, 794–807.
61. Belhomme, D., Peynet, J., Louzy, M., et al. (1999) Evidence for preconditioning by isoflurane in coronary artery bypass graft surgery. *Circulation*. 100, II340–II344.
62. De Hert, S., ten Broeck, P., Mertens, E., et al. (2002) Sevoflurane but not propofol preserves myocardial function in coronary surgery patients. *Anesthesiology*. 97, 42–49.
63. Sigg, D.C., Coles, J.A., Jr., Gallagher, W.J., Oeltgen, P.R., and Iaizzo, P.A. (2001) Opioid preconditioning: myocardial function and energy metabolism. *Ann Thorac Surg*. 72, 1576–1582.
64. Sigg, D.C., Coles, J.A., Jr., Oeltgen, P.R., and Iaizzo, P.A. (2002) Role of delta-opioid receptors in infarct size reduction in swine. *Am J Physiol Heart Circ Physiol*. 282, H1953–H1960.
65. Hong, J.B., Sigg, D.C., Upson, K., Oeltgen, P.R., Harlow, H.H., and Iaizzo, P.A. (2003) Role of delta-opioid receptors in preventing ischemic damage of isolated porcine skeletal muscle. (Currently not published; private manuscript.)

14 Blood Pressure, Heart Tones, and Diagnoses

GEORGE BOJANOV, MD

CONTENTS

1. BLOOD PRESSURE

Fundamental to providing comprehensive care to patients is the ability to obtain an accurate medical history and carefully perform and interpret a physical examination. The optimal selection of further tests, treatments, and use of subspecialists depends on well-developed skills for taking patient history and a physical diagnosis. An important part of a normal physical examination is obtaining a blood pressure reading and auscultation of the heart tones, which both represent critical cornerstones in evaluating a patient's hemodynamic status and diagnosing and understanding physiological and anatomical pathology.

Naive ideas about circulation and blood pressure date as far back as ancient Greece. It took until the 18th century for the first official report to describe an attempt to measure blood pressure, when Stephen Hales published a monograph on "haemastatics" in 1733. He conducted a series of experiments involving cannulation of arteries in horses and invasive direct blood pressure measurement; unfortunately, his method was not applicable for humans at that time. There were many subsequent contributions to the art of measuring and understanding blood pressure during the next two centuries. One of the greatest of these was described in a publication in *Gazetta medica di Torino* called "A New Sphygmomanometer" by Dr. Riva-Rocci in 1896; it is recognized as the single most important advancement in practical noninvasive methods for blood pressure estimation in humans.

From: *Handbook of Cardiac Anatomy, Physiology, and Devices*
Edited by: P. A. Iaizzo © Humana Press Inc., Totowa, NJ

In 1916, French physician Rene Laennec invented the first stethoscope, which was constructed from stacked paper rolled into a solid cylinder. Prior to his invention, physicians around the world would place one of their ears directly on the patient's chest to hear heart or lung sounds. After Dr. Laennec's initial success, several new models were produced, primarily of wood. His stethoscope was called a "monaural stethoscope." The "binaural stethoscope" was invented in 1829 by a physician named Camman in Dublin and later gained wide acceptance; in the 1960s, the Camman stethoscope was considered the standard for superior auscultation.

It is essential that health care professionals and bioengineers understand how these important diagnostic parameters are obtained, their sensitivities, and how best to interpret them.

1.1. Physiology of Blood Pressure

Blood pressure is the force applied on the arterial walls as the heart pumps blood through the circulatory system. The rhythmic contractions of the left ventricle result in cyclic changes in the blood pressure. During ventricular systole, the heart pumps blood into the circulatory system, and the pressure within the arteries reaches its highest level; this is called *systolic blood pressure*. During diastole, the pressure within the arterial system falls and is called *diastolic blood pressure*.

The mean of the systolic and diastolic blood pressures during the cardiac cycle represents the time-weighted average arterial pressure; this is called *mean arterial blood pressure*. Alternating systolic and diastolic pressures create outward and inward movements of the arterial walls, perceived as arterial pulsation or *arterial pulse*. *Pulse pressure* is the difference between systolic and diastolic blood pressures.

Blood pressure is measured in units called millimeters of mercury (mmHg). A "normal" systolic blood pressure is less than 140 mmHg; a "normal" diastolic blood pressure is less than 90 mmHg. Blood pressure higher than normal is called *hypertension*, and one lower than normal is called *hypotension*. Hence, normal mean arterial pressure is between 60 and 90 mmHg. Mean arterial pressure is normally considered a good indicator of tissue perfusion and can be measured directly using automated blood pressure cuffs or calculated using the following formulas:

$$MAP = DBP + PP/3 \text{ or } MAP = [SBP + (2 \times DBP)]/3$$

where PP = SBP – DBP; MAP is mean arterial pressure, DBP is diastolic blood pressure, PP is pulse pressure, and SBP is systolic blood pressure.

Blood flow throughout the circulatory system is directed by pressure gradients. By the time blood reaches the right atrium, which represents the end point of the venous system, pressure has decreased to approx 0 mmHg. The two major determinants of blood pressure are: (1) cardiac output, which is the volume of blood pumped by the heart per minute; and (2) systemic vascular resistance, which is the impediment offered by the vascular bed to flow. Systemic vascular resistance is controlled by many factors, including vasomotor tone in arterioles, terminal arterioles, or precapillary sphincters. Blood pressure can be calculated using the formula

$$BP = CO \times SVR$$

where BP is blood pressure, CO is cardiac output, and SVR is systemic vascular resistance.

Blood pressure decreases by 3–5 mmHg in arteries that are 3 mm in diameter. It is approx 85 mmHg in arterioles, which accounts for approx 50% of the resistance of the entire systemic circulation. Blood pressure is further reduced to around 30 mmHg at the point of entry into capillaries and then becomes approx 10 mmHg at the venous end of the capillaries.

The speed of the advancing pressure wave during each cardiac cycle far exceeds the actual blood flow velocity. In the aorta, the pressure wave speed may be 15 times faster than the flow of blood. In an end artery, the pressure wave velocity may be as much as 100 times the speed of the forward blood flow.

As the pressure wave moves peripherally through the arterial system, wave reflection distorts the pressure waveform, causing an exaggeration of systolic and pulse pressures. This enhancement of the pulse pressure in the periphery causes the systolic blood pressure in the radial artery to be 20–30% higher than the aortic systolic blood pressure and the diastolic blood pressure to be approx 10–15% lower than the aortic diastolic blood pressure. Nevertheless, the mean blood pressure in the radial artery will closely correspond to the aortic mean blood pressure.

1.2. Methods of Measuring Blood Pressure

Arterial blood pressure can be measured both noninvasively and invasively; these methods are described next.

1.2.1. Noninvasive Methods

1.2.1.1. Palpation

Palpation is a relatively simple and easy way to assess systolic blood pressure. A blood pressure cuff containing an inflatable bladder is applied to the arm and inflated until the arterial pulse felt distal to the cuff placement disappears. Then, the pressure in the cuff is released at a speed of approx 3 mmHg per heartbeat until the arterial pulse is felt again. The pressure at which the arterial pulsations start is the systolic blood pressure. Diastolic blood pressure and mean arterial pressure cannot be readily estimated using this method. Furthermore, the measured systolic blood pressure using the palpation method is often an underestimation of the true arterial systolic blood pressure because of the insensitivity of the sense of touch and the delay between blood flow below the cuff and the appearance of arterial pulsations distal to the cuff.

1.2.1.2. Doppler Method

The Doppler method is a modification of the palpation method and uses a sensor (Doppler probe) to determine blood flow distal to the blood pressure cuff. The Doppler effect is the shift of the frequency of a sound wave when a transmitted sound wave is reflected from a moving object. When a sound wave shifts (e.g., as caused by blood movement in an artery), it is detected by a monitor as a specific swishing sound. The pressure of the cuff, at which blood flow is detected by the Doppler probe, is the arterial systolic blood pressure.

This method is more accurate (less subjective) in estimating systolic blood pressure compared to the palpation method. It has also been quite a useful method in detecting systolic blood pressure in patients who are in shock, have low-flow states, are obese, or are pediatric patients. Disadvantages of the Doppler method include: (1) inability to detect diastolic blood pressure; (2) necessity for sound-conducting gel between the skin and the probe (because air is a poor conductor of ultrasound); (3) likelihood of a poor signal if the probe is not applied directly over an artery; and (4) potential for motion and electrocautery unit artifacts.

1.2.1.3. Auscultation (Riva–Rocci Method)

The auscultation method uses a blood pressure cuff placed around an extremity (usually an upper extremity) and a stethoscope placed above a major artery just distal to the blood pressure cuff (e.g., the brachial artery if using the cuff on the upper extremity). Inflation of the blood pressure cuff above the systolic blood pressure flattens the artery and stops blood flow distal to the cuff. As the pressure in the cuff is released, the artery becomes only partially compressed, which creates conditions for turbulent blood flow within the artery and produces the so-called Korotkoff sounds, named after the individual who first described them. Korotkoff sounds are caused by the vibrations created when blood flow in partially flattened arteries transforms from laminar into turbulent, and they persist as long as there is an increased turbulent flow within a vessel. Systolic blood pressures are determined as the pressures of the inflated cuffs at which Korotkoff sounds are first detected. Diastolic blood pressures are determined as the cuff pressure at which Korotkoff sounds become muffled or disappear.

Sometimes, in patients with chronic hypertension, there is an "auscultatory gap" that represents disappearance of the normal Korotkoff sounds in a wide pressure range between the systolic and the diastolic blood pressures. This condition will lead to inaccurately low blood pressure assessments. Korotkoff sounds

can also be difficult to detect in patients who are in low-flow states or in those with marked peripheral vasoconstriction. The use of microphones and electronic amplification of such signals can greatly increase the sensitivity of this method. Yet, considerations for systematic errors include motion artifact and electrocautery interference.

1.2.1.4. Oscillometry

Oscillometry is defined as the blood pressure measurement method that uses automated blood pressure cuffs. Arterial pulsations cause oscillations in the cuff pressure. These oscillations are at their maximum when the cuff pressure equals the mean arterial pressure and decrease significantly when the cuff pressures are above the systolic blood pressure or below the diastolic blood pressure. Advantages of this approach are the ease and reliability of use. Some of the potential technical problems include motion artifacts, electrocautery unit interference, and inability to measure accurate blood pressure when patients elicit arrhythmias.

1.2.1.5. Blood Pressure Cuff Pressure

When using blood pressure cuffs for such measurements, it is important to select them in accordance with the patient's size. Blood pressure cuffs for adult and pediatric patients come in variable sizes. An appropriate size means that the cuff's bladder length is at least 80% and the cuff width is at least 40% of the arm circumference. If the cuff is too small, it will take more pressure to occlude arterial blood flow completely, and the resultant measured pressures will be falsely elevated. If the cuff is too large, however, the pressure inside the cuff needed for complete occlusion of the arterial blood flow will be less, and the measured pressures will be falsely low.

Blood pressure is most commonly taken while the patient is seated with the arm resting on a table and slightly bent, which positions the arm at the same level as the patient's heart. This same principle should be applied if the patient is in a supine position; the blood pressure cuff should be level with the heart. If the location of the blood pressure cuff during blood pressure measurements is above or below the patient's heart level, registered blood pressure will be either lower or higher than the patient's actual blood pressure. This difference can be represented as the height of a column of water interposed between the blood pressure cuff and the heart levels. To convert centimeters of water (cmH_2O) to millimeters of mercury, the measured height of the water column should be multiplied by a conversion factor of 0.74 (1 cmH_2O = 0.74 mmHg).

All of the aforementioned methods for assessing blood pressure do so indirectly by registering blood flow below the blood pressure cuff. Other noninvasive methods include plethysmography and arterial tonometry.

1.2.1.6. Plethysmography

The plethysmographic method for blood pressure measurement uses the fact that arterial pulsations cause a transient increase in the blood volume of an extremity and thus in the volume of the whole extremity. A finger plethysmograph determines the minimum pressures needed by a finger cuff to maintain constant finger blood volume. A light-emitting diode and a photoelectric cell detect changes in the finger volume and rapidly adjust the cuff pressure, which can be displayed as a beat-to-beat tracing. Thus, in healthy patients, the blood pressure measured on the finger will correspond to the aortic blood pressure; this will not be true for patients with low peripheral perfusion, like those with peripheral artery disease, hypothermia or low-flow states.

1.2.1.7. Arterial Tonometry

Tonometry devices can determine beat-to-beat arterial blood pressures by adjusting the pressure required to partially flatten a superficial artery located between a tonometer and a bony surface (e.g., radial artery). These devices commonly consist of an electronic unit and a pressure-sensing head. The pressure-sensing head includes an air chamber with adjustable air pressure and an array of independent pressure sensors that, when placed directly over the artery, assess intraluminal arterial pressures. The resultant pressure record resembles an invasive arterial blood pressure waveform. Limitations to these methods include motion artifacts and the need for frequent calibrations.

1.2.2. Invasive Methods of Blood Pressure Measurement

1.2.2.1. Indications

Indications for the use of direct blood pressure monitoring (arterial cannulation) include hemodynamic instability, intraoperative monitoring in selected patients, and use of vasoactive drugs like dopamine, epinephrine, norepinephrine, and the like.

1.2.2.2. Cannulation Sites

The arteries most often selected for cannulation are the radial, ulnar, brachial, femoral, dorsalis pedis, or axillary. Cannulation of an artery should be avoided if there is: (1) documented lack of collateral circulation, (2) a skin infection on the site of cannulation, and/or (3) a preexisting vascular deficiency (e.g., Raynaud's disease). The radial artery is the most often selected artery for invasive blood pressure monitoring because of its easily accessed superficial location and good collateral flow to the region it supplies.

1.2.2.3. Techniques

The two frequently utilized techniques for arterial cannulation are: (1) a catheter over a needle or (2) Seldinger's technique. When using the first technique, the operator enters the blood vessel with a needle that has a catheter placed over it. After free blood flow is documented through the needle, the catheter is advanced over the needle into the artery, and the needle is withdrawn. The catheter is then connected to the pressure-transducing system. When using Seldinger's technique, the operator first enters the artery with a needle. After free blood flow is confirmed through the free end of the needle, the operator places a wire through the needle into the blood vessel and withdraws the needle. Then, a plastic catheter is advanced into the artery over the steel wire, the wire is removed, and the catheter is connected to a transducer system. Both methods require sterile techniques and skilled operators.

1.2.2.4. Considerations

Arterial cannulation provides beat-to-beat numerical information and tracing waveforms of arterial blood pressures and is considered a gold standard in blood pressure monitoring. Invasive arterial pressure monitoring systems or kits commonly

include a catheter (20-gauge catheter for adults), tubing, a transducer, and an electronic monitor for signal amplification, filtering, and analysis. Such pressure transducers are usually based on the strain gauge principle: Stretching a wire of silicone crystal changes its electrical resistance. The catheter, the connective tubing, and the transducer are filled with saline. A pressure bag provides a continuous saline flush of the system at a rate of 3–5 mL/h. The system should also allow for intermittent flush boluses as needed.

The quality of the information gathered depends on the dynamic characteristics of the whole system. The complex waveform obtained from the arterial pulse can be expressed as a summation of simple sine and cosine waves using a method called "Fourier analysis." Most invasive blood pressure monitoring systems have natural frequencies of approx 16–24 Hz, which must exceed the frequency of the arterial pulse waveform to reproduce it correctly. This natural frequency is described as the frequency at which the system oscillates when disturbed. Another property of the catheter-tubing-transducer system is the "dumping coefficient." The dumping coefficient characterizes how quickly oscillations in the system will decay.

Both the natural frequency and the dumping coefficient are primarily determined by the length, size, and compliance of the catheter and tubing and by presence of air bubbles or cloths trapped in the fluid column. This chapter does not go into details of how to determine and change the system characteristics. Briefly, "underdumping" the system will exaggerate artifacts like a "catheter whip" and can result in a significant overestimation of the systolic blood pressure. "Overdumping" will blunt the response of the system and lead to an underestimation of the systolic blood pressure. In addition, systems with low natural frequencies will show amplifications of the pressure curves, causing overestimation of the systolic blood pressures. Diastolic blood pressures will also be affected by altering the above factors, but to a lesser degree. Note that system response characteristics can be optimized by using short and low-compliance tubing and by avoiding air trapping when the system is flushed.

When an invasive blood pressure system is connected to a patient, it should be zero referenced and calibrated. Zero referencing is performed by placing the transducer at the level of the midaxillary line, which corresponds to the level of the patient's heart. The system is opened to air and closed to the patient, and then the transducing system is adjusted to a 0 mmHg baseline. For this, it is not necessary for the transducer to be at the level of the midaxillary line as long as the stopcock, which is opened to air during the zero reference, is at that level. The system is then opened to the patient and ready for use.

System calibrations are separate procedures and involve connecting the invasive blood pressure systems to mercury manometers, closing the systems to the patient, and pressurizing the systems to specified pressures. Then, the gains of the monitor amplifiers are adjusted until displayed pressures equal the pressures in the mercury manometers. Recommendations are to perform zero referencing at least every clinical shift and calibration at least once daily. It should be noted that some of the more contemporary transducer designs rarely require external calibration.

When connected to the patient, such monitoring systems provide digital readings of systolic, diastolic, and mean blood pressures and, commonly, pressure waveforms. Watching the trend of the waveform and its shape can provide other important information as well. More specifically, the top of the waveform represents the systolic pressure, and the bottom is the diastolic blood pressure. The dicrotic notch is caused by the closure of the aortic valve and the backsplash of blood against the closed valve. The rate of the upstroke of the arterial blood pressure wave depends on the myocardial contractility; the rate of the downstroke is affected by the systemic vascular resistance. Exaggerated variation in the size of the waves with respiration suggests hypovolemia. Integrating the areas under the waveforms can be used for calculations of the values of the mean arterial pressures. *See also* Chapter 16 for more details on pressure waveforms.

1.2.2.5. Complications

Potential complications associated with arterial cannulation include bleeding, hematoma, infection, thrombosis, ischemia distal to the cannulation site, vasospasm, embolization with air bubbles or thrombi, nerve damage, pseudoaneurysm, atheroma, and inadvertent intraarterial drug injection.

1.3. Diagnoses

1.3.1. Pulsus Paradoxus

Inspiration can decrease arterial pressure by more than 10 mmHg; the inspiratory venous pressure stays relatively unchanged. Normally, the arterial and venous blood pressures fluctuate throughout the respiratory cycle, decreasing with inspiration and rising with expiration. This fluctuation in the blood pressure under normal conditions is less than 10 mmHg. Inspiration increases venous return, therefore increasing the right heart output transiently, according to the Frank-Starling law. As the blood is sequestered in the pulmonary circulation during inspiration, the left heart output is reduced transiently, accounting for the normal lower systolic pressure during this phase. The right ventricle contracts more vigorously and mechanically bulges the interventricular septum toward the left ventricle, reducing its size and accounting for the lower systolic blood pressure.

Certain conditions drastically reduce the transmural or distending (filling) pressure of the heart and interfere with the diastolic filling of the two ventricles. In such cases, there is an exaggeration of the inspiratory fall in the systolic blood pressure, which results from reduced left ventricular stroke volume and the transmission of negative intrathoracic pressure to the aorta. Common causes for such reductions include pericardial effusion, adhesive pericarditis, cardiac tamponade, pulmonary emphysema, severe asthma, paramediastinal effusion, endocardial fibrosis, myocardial amyloidosis, scleroderma, mitral stenosis with right heart failure, tricuspid stenosis, hypovolemia, and/or pulmonary embolism. Associated clinical signs include a palpable decrease in pulse with inspiration and decrease in the inspiratory systolic blood pressure more than 10 mmHg compared to the expiratory pressure.

1.3.2. Pulsus Alternans

An alternating weak and strong peripheral pulse is usually caused by alternating weak and strong heart contractions. It

may be found in patients with severe heart failure, various degrees of heart block, or arrhythmias. Pulsus alternans is characterized by a regular rhythm and must be distinguished from pulsus bigeminus, which is usually irregular.

1.3.3. Bigeminal Pulse

A bigeminal pulse is caused by occurrences of premature contractions (usually ventricular) after every other beat, which results in alternation in the strength of the pulse. Bigeminal pulse can often be confused with pulsus alternans. However, in contrast to the latter, in which the rhythm is regular, in pulsus bigeminus the weak beat always follows a shorter pulse interval.

1.3.4. Pulse Deficit

Pulse deficit is the inability to detect arterial pulsations when the heart beats, as can be observed in patients with atrial fibrillation, in states of shock, or with premature ventricular complexes and the like. The easiest way to detect pulse deficit is to place a finger over the radial artery while monitoring the QRS complexes on an electrocardiogram monitor. A QRS complex without a detected corresponding pulse represents a pulse deficit. In the presence of atrioventricular dissociation, when atrial activity is irregularly transmitted to the ventricles, the strength of the peripheral arterial pulse depends on the timing of the atrial and ventricular contractions. In a patient with rapid heartbeats, the presence of such variations suggests ventricular tachycardia; with an equally rapid rate, an absence of variation of pulse strength suggests a supraventricular mechanism.

1.3.5. Wide Pulse Pressure

Wide pulse pressure, or as it is often called "water hammer pulse," is observed in cases of severe aortic regurgitation and consists of an abrupt upstroke (percussion wave) followed by rapid collapse later in systole with no dicrotic notch.

1.3.6. Pulsus Parvus et Tardus

The phenomenon of pulsus parvus et tardus is observed in cases of aortic stenosis and is caused by reductions in stroke volumes and prolonged ejection phases, which produce reductions and delays in the volume increments inside aortas. "Tardus" refers to delayed or prolonged early systolic accelerations; "parvus" refers to diminished amplitudes and rounding of the systolic peaks.

1.3.7. Bisferiens Pulse

A bisferiens pulse is characterized by two systolic peaks—the percussion and tidal waves—separated by a distinct midsystolic dip; the peaks are often equal, or one may be larger. It occurs in conditions in which a large stroke volume is ejected rapidly from the left ventricle and is observed most commonly in patients with pure aortic regurgitation or with a combination of aortic regurgitation and stenosis. A bisferiens pulse also occurs in patients with hypertrophic obstructive cardiomyopathy. In these patients, the initial prominent percussion wave is associated with rapid ejection of blood into the aorta during early systole, followed by a rapid decline as obstruction becomes prominent in midsystole and by a tidal wave. Very rarely does it occur in individuals with a normal heart.

1.3.8. Dicrotic Pulse

Not to be confused with a bisferiens pulse, in which both peaks occur in systole, the dicrotic pulse is characterized by a second peak that is in diastole immediately after the second heart sound. The normally small wave that follows aortic valve closure (dicrotic notch) is exaggerated and measures more than 50% of the pulse pressure on direct pressure recordings. It usually occurs in conditions such as cardiac tamponade, severe heart failure, and hypovolemic shock, in which a low stroke volume is ejected into a soft elastic aorta. Rarely, a dicrotic pulse is noted in healthy adolescents or young adults.

2. HEART TONES

2.1. Physiology and Normal Heart Sounds

Heart tones are caused primarily by vibrations created by pressure differentials during closure of the heart valves. Normal opening of the heart valves is a relatively slow process and makes no audible sounds. The heart tones are relatively brief and characterized by varying intensity (loudness), frequency (pitch), and quality (timbre). To understand heart tones better, it is necessary to review briefly the physiology of cardiac events. The electric impulse for cardiac contraction starts from the sinus node, located in the right atrium, thus causing the right atrium to contract first. Contraction of the ventricles—the left is slightly more rapid—results in mitral valve closure before closure of the tricuspid valve. Ejection, on the other hand, starts in the right ventricle because the right ventricular ejection normally occurs at a much lower pressure than the left ventricular ejection. Ejection ends first in the left ventricle, causing the aortic valve to close slightly before the pulmonic valve.

The *first heart sound* (S1) arises from closure of the mitral valve (M1), followed by closure of the tricuspid valve (T1). The initial component of the first heart sound (M1) is most prominent at the cardiac apex. The second component (T1), if present, normally presents at the left lower sternal border; it is less commonly heard at the apex and is seldom heard at the base. When the first heart sound is dramatically split, like in Ebstein's anomaly of the tricuspid valve (associated with delayed right ventricular activation), its first component is normally louder.

As mentioned, the intensity of the sound will increase with increases of the pressure gradients across a particular valve. With increases in the pressure gradients, the blood velocities and the resultant forces for valve closure will increase, causing loud and easily detectable sounds. Another factor that affects the intensity of the sound produced by an atrioventricular valve is the valvular position at the onset of systole. When ventricular contraction occurs against a wide-open valve, the leaflets will achieve higher velocity and thus a louder heart sound compared to a valve with partially closed leaflets at the beginning of systole.

The *second heart sound* (S2) is caused by closure of the aortic and the pulmonic valves, normally with a first component caused by the aortic valve closure (A2), followed by the pulmonic valve closure (P2).

The physiological *third heart sound* (S3) (Fig. 1) occurs shortly after A2, and is a low-pitched vibration caused by the rapid ventricular filling during diastole. S3 can commonly be heard in children, adolescents, and young adults. When detect-

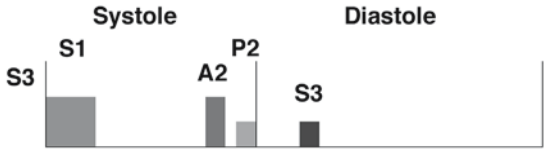

Fig. 1. Normal heart physiology introducing the third heart sound (*see* text for details). S1, first heart sound; S3, third heart sound; A2, aortic valve closure; P2, pulmonic valve closure.

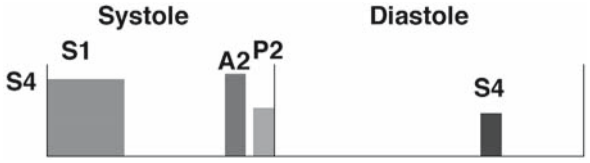

Fig. 2. Normal heart physiology introducing the fourth heart sound (*see* text for details). S1, first heart sound; S4, fourth heart sound; A2, aortic valve closure; P2, pulmonic valve closure.

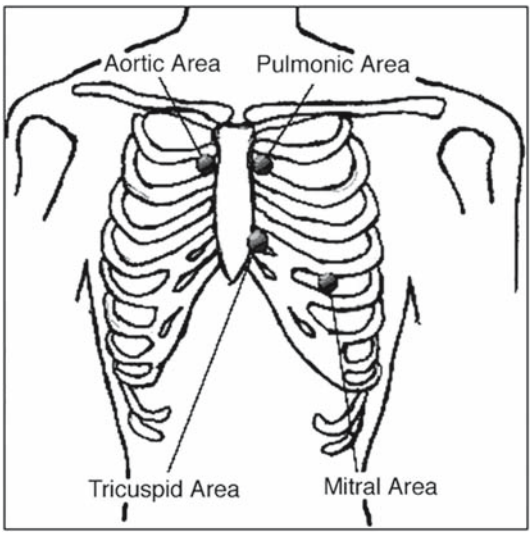

Fig. 3. Auscultatory areas, including the aortic, pulmonic, mitral, and tricuspid auscultation areas.

able after the age of 30 years, S3 is considered "ventricular gallop" and is a sign of possible pathology; in most such cases, there is diastolic dysfunction associated with ventricular failure. Yet the third heart sounds sometimes persist beyond age 40 years, especially in women.

The physiological *fourth heart sound* (S4) (Fig. 2) is a soft, low-pitched noise heard in late diastole, just before S1. S4 is generated by rapid ventricular filling during atrial systole, which causes vibrations of the left ventricular wall and the mitral apparatus. Normally, S4 is heard in infants, small children, and adults over 50 years of age. A loud S4, especially associated with shock, is a pathological sign and is referred to as an S4 gallop.

2.2. Auscultatory Areas

The heart sounds generated by the various valves are best heard over so-called auscultatory areas, which bear the valve names, but do not specifically correspond to the anatomical locations of the valves.

The *aortic auscultation area* is located in the second intercostal space at the right sternal border (Fig. 3). The *pulmonic auscultation area* is located in the second intercostal space at the left sternal border. The *mitral auscultation area* is found at the heart's apex, which is in the fifth intercostal space, left from the sternum. This area is also called a left ventricular or apical area. The *tricuspid auscultation area* is located at the left lower sternal border. For patients with a left thoracic heart position (normal situs), auscultation should begin at the cardiac apex and continue with the left lower sternal border (inflow), proceeding interspace after interspace up the left sternal border to the left base and then to the right base (outflow). This type of examination permits the clinician to think physiologically, following the inflow-outflow direction of the blood flow.

To distinguish between the first and the second heart sounds easily, it should be pointed out that there is a longer pause between S2 and S1 than between S1 and S2 because systole is shorter than diastole. S1 is also of longer duration and lower pitch, and S2 is of shorter duration and higher pitch. S1 is best heard at the heart apex, and S2 is best auscultated over the aortic and pulmonic areas.

Although the normal heart sounds represent normally occurring phenomena in a normal heart, cardiac pathology can change the intensity or the time occurrence of the sounds and even create new ones, often called murmurs (e.g., because of valvular or congenital anomalies).

2.3. Abnormal Heart Sounds

Conditions that can accentuate S1 include mitral stenosis (most often), left-to-right shunts, hyperkinetic circulatory states, accelerated atrioventricular conduction, and tricuspid stenosis. Diminished S1 can be caused by mitral and tricuspid stenosis, moderate or severe aortic regurgitation, slow atrioventricular conduction, or hypocontractility states. A diminished S1 can also be caused by thick chest walls, such as in individuals with excessively developed body musculature or in patients with emphysema.

A *variability in the S1* sound can be observed in states causing variation in the velocity of the atrioventricular valve closures, such as ventricular tachycardia, atrioventricular block, ventricular pacemakers, atrial fibrillation, and so on. An *accentuated S2* is present in: (1) diastolic or systolic hypertension, (2) aortic coarctation, (3) aortic dilation, (4) atherosclerosis of the aorta, and (5) pulmonary hypertension; it is characterized by a loud pulmonary component of the second heart sound. A *diminished S2* is detected most often with aortic valvular stenosis, pulmonic stenosis, and pulmonary emphysema.

Splitting of S2 can be normal during inspiration. When considered abnormal, it is associated with: (1) delayed activation of the right ventricle; (2) prolonged right ventricular ejection time relative to left ventricular ejection time (like in pulmonic stenosis, mitral regurgitation, ventricular septal defect); or

(3) increased impedance of the pulmonary vasculature (as in massive pulmonary embolism or pulmonary hypertension). *Persistent splitting of the S2* refers to cases in which the aortic and pulmonic components of the second heart sound remain audible during both inspiration and exhalation. Persistent splitting may be because of a delay in the pulmonary component, as occurs with complete right bundle branch block, or can be caused by early timing of the aortic component associated with mitral insufficiencies. Directional changes in the interval of the split (greater with inspiration, lesser with exhalation) in the presence of both components define the split as persistent, but not fixed.

Fixed splitting of S2 is commonly found in patients with atrial septal defects, severe pulmonic stenoses, or right ventricular failures. This term applies when the interval between the aortic and pulmonary components is not only wide and persistent, but also remains unchanged during the respiratory cycle.

Paradoxical splitting refers to a reversed sequence of semilunar valve closure, with the pulmonary component (P2) preceding the aortic component (A2). Paradoxical splitting of S2 is caused by a delay in the A2 varying with the inspiratory cycle and can be caused by: (1) a complete left bundle branch block; (2) premature right ventricle contractions; (3) ventricular tachycardia; (4) severe aortic stenosis; (5) left ventricular outflow obstruction; (6) hypertrophic cardiomyopathy; (7) coronary artery disease; (8) myocarditis; or (9) congestive cardiomyopathy.

Normally, blood flow in the heart is primarily laminar and does not produce murmurs. Murmurs can be detected whenever there is a pathology causing turbulent flow, such as with abnormal shunts, obstructions to flow, or induced reverse flow. Turbulent flow creates vibrations that can be heard as murmurs. Murmurs are described on the basis of appearance in relation to the cardiac cycle and on the basis of changes in intensity (loudness), frequency (pitch), configuration (shape), quality, duration, or direction of radiation. For example, intensity or loudness is graded from 1 to 6. Based on time of existence relative to the cardiac cycle, murmurs are classified as systolic, diastolic, or continuous. Depending on their life cycle during systole or diastole, they are further subclassified into early, mid-, and late systolic or diastolic murmurs:

- *Early systolic murmur* begins with S1 and ends before the midsystole.
- *Midsystolic murmur* starts after S1 and ends before S2.
- *Late systolic murmur* begins in the middle of systole and ends at S2.
- *Holosystolic murmur* starts with S1 and continues for the duration of the whole systole.
- *Early diastolic murmur* begins with S2.
- *Middiastolic murmur* begins after S2.
- *Late diastolic murmur* begins just before S1.
- *Continuous murmur* continues during both systole and diastole.

Based on changes in intensity, murmurs are described as: (1) *crescendo*, increasing in intensity; (2) *decrescendo*, decreasing in intensity; (3) *crescendo–decrescendo*, when the intensity of the murmur first increases and then decreases; and (4) *plateau*, for which the intensity of the murmur remains constant.

2.4. Dynamic Auscultation

The term *dynamic auscultation* refers to the technique of adjusting circulatory dynamics by means of respiration or various other physiological or pharmacological maneuvers to determine their effects on the dynamics of heart sounds and murmurs. Variables that can affect sound and murmurs include: (1) changes in venous return representing the cardiac preload; (2) changes in systemic vascular resistances; (3) changes in contractility; (4) changes in heart rate or rhythm; or (5) any maneuver that affects the pressure gradients within the heart. Diagnostic maneuvers often used for altering heart sounds include inspiration, expiration, a recumbent position, a left semilateral position, exercise, standing, sitting up, or leaning forward.

Inspiration causes decreased intrathoracic pressure, increased venous return, increased right ventricular preload, and decreased pulmonary vascular resistance. A voluntary inspiration can be used to increase the intensity of S3 and S4 gallops, tricuspid and pulmonic stenosis or regurgitation murmurs, or mitral and tricuspid clicks. Inspiration also causes splitting of S2, which is caused by prolonged right ventricular ejection. *Expiration* causes just the opposite—decreased venous return to the heart (preload) and decreased right-sided flow. Sounds and murmurs originating on the left side of the heart tend to be accentuated during expiration.

Change in the patient's position can affect the intensity of the heart sounds as well, mostly by increasing the ventricular preload and ventricular sizes and by bringing the heart closer to the chest wall. The *recumbent position* accentuates murmurs of mitral and tricuspid stenosis. The *left semilateral position* accentuates left-sided S3 and S4, mitral opening snap, and mitral regurgitation murmurs. *Standing* affects general hemodynamics by pooling blood in the lower extremities and decreasing heart filling pressures and ventricular sizes. Thus, standing is used to accentuate mitral and tricuspid clicks. *Sitting up* accentuates the tricuspid valve opening snap, and *sitting up* and *leaning forward* are the best maneuvers for enhancing murmurs of aortic and pulmonic regurgitation or aortic stenosis murmurs. *Exercise* commonly causes increases in heart rates, shortens diastole, elevates left atrial pressure, and shortens the time for closure of the heart valves. Hence, physiological changes during exercise increase amplitudes of S1, S2, S3, S4, mitral opening snaps, existing mitral regurgitations or stenoses, or patent ductus arteriosus murmurs.

Two other pathological sounds that might be heard when auscultating the heart are *clicks* and *opening snaps*. Clicks are caused by rapid movement of valvular structures. Systolic clicks are referred to as ejection or nonejection clicks, depending on their timing relative to the systole. Ejection clicks, which occur early in systole, indicate semilunar valve anomalies and, in rare conditions, great vessel lesions. Nonejection clicks are heard in mid-to-late systole and represent mitral (more often) or tricuspid valve prolapse. A *tricuspid valve opening snap* is usually heard when there is tricuspid valve stenosis and in conditions associated with increased blood flow across the tricuspid valve (e.g., presence of large atrial septal defect). The *mitral valve opening snap* when present is considered caused by elevated left atrial pressure forces causing rapid valve open-

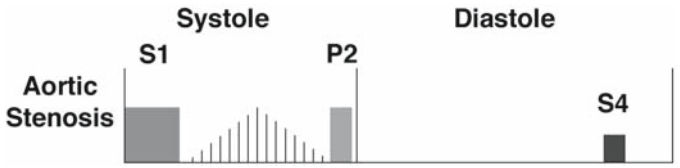

Fig. 4. Representation of aortic stenosis murmur caused by a stenotic aortic valve. This is normally a holosystolic crescendo–decrescendo murmur best heard at the aortic auscultatory area. S1, first heart sound; S4, fourth heart sound; P2, pulmonic valve closure.

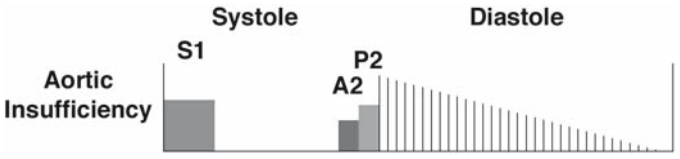

Fig. 5. Representation of aortic insufficiency, an early decrescendo diastolic murmur originating in the left side of the heart and best heard over the aortic and pulmonic auscultation areas. S1, first heart sound; A2, aortic valve closure; P2, pulmonic valve closure.

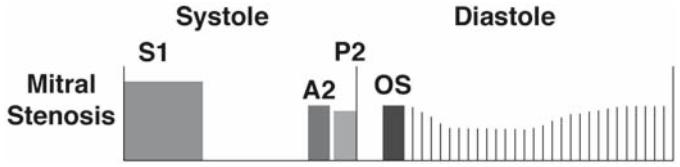

Fig. 6. The mitral stenosis murmur, a decrescendo–crescendo holodiastolic murmur, is caused by a stenotic mitral valve. Best heard at the mitral auscultation area, this murmur is accentuated by exercise and by assuming a recumbent position. S1, first heart sound; A2, aortic valve closure; P2, pulmonic valve closure; OS, opening snap.

ing to the point of maximum excursion. The mitral valve opening snap is detected most often in cases of mitral stenosis and less often in ventricular septal defects, second or third atrioventricular blocks, patent ductus arteriosus, hyperthyroidism, and the like. The mitral valve opening snap is similar in quality to a normal heart sound and is often confused with a splitting of S2. The differential diagnosis of mitral valve opening snap vs other heart sound has been described in detail elsewhere and is not a topic of this chapter.

2.5. Specific Murmurs

The *aortic stenosis murmur* (Fig. 4) is caused by a stenotic aortic valve and is commonly a holosystolic crescendo–decrescendo murmur best heard at the aortic auscultatory area. The high-velocity jet within the aortic root results in radiation of the murmur upward, to the right second intercostal space, and further into the neck. Although the murmur in the second right intercostal space is harsh, noisy, and impure, the murmur heard when auscultated over the left apical area is pure and often considered musical. The harsh basal murmur is believed to be caused by the vibrations created when the high-velocity jet of blood is ejected through the aortic root. The musical second component of the aortic stenosis murmur originates from periodic high-frequency vibrations of the fibrocalcific aortic cusps and can be quite loud and heard even from a distance. When present it can be accentuated by expiration, sitting up, and leaning forward. The high-frequency apical midsystolic murmur of aortic stenosis should be distinguished from the high-frequency apical murmur of mitral regurgitation, a distinction that may be difficult or impossible, especially if the aortic component of the second heart sound is soft or absent.

The murmur caused by *pulmonary valve stenosis* is a characteristic midsystolic murmur originating in the right side of the heart and best auscultated over the pulmonic auscultation area. This murmur begins after the first heart sound or with a pulmonary ejection sound, rises to a peak in crescendo, and then decreases in a slower decrescendo slightly before a delayed or soft pulmonary component of the second heart sound. The length and the profile of the murmur are dependent on the degree of pulmonic obstruction.

The murmur caused by *aortic insufficiency* (Fig. 5) is an early decrescendo diastolic murmur originating in the left side of the heart and best heard over the aortic and pulmonic auscultation areas. This murmur begins with the aortic component of the second heart sound. The intensity and the configuration of such a murmur tend to reflect the volumes and rates of regurgitant flows. Radiation of this murmur to the right sternal border commonly signifies aortic root dilation, as in Marfan syndrome. In chronic aortic regurgitation, the aortic diastolic pressure always significantly exceeds the left ventricular diastolic pressure, so the decrescendo is subtle, and the murmur is well heard throughout diastole. The diastolic murmur of acute severe aortic regurgitation differs from the chronic aortic regurgitation murmur primarily in that the diastolic murmur is relatively short because the aortic diastolic pressure rapidly equilibrates with the rapidly rising diastolic pressure in the nondilated left ventricle. The aortic insufficiency murmur is accentuated by expiration, sitting up, or leaning forward.

A *pulmonary regurgitation murmur* is an early diastolic murmur originating from the right side of the heart. Often, the second heart sound is split, and the murmur proceeds from its latter part. It is loud primarily because the elevated pressure exerted on the incompetent pulmonary valve begins at the moment that right ventricular pressure drops below the pulmonary arterial diastolic pressure. The high diastolic pressure generates high-velocity regurgitant flow and results in a high-frequency blowing murmur that may last throughout diastole. Because of the persistent and significant difference between the pulmonary arterial and right ventricular diastolic pressures, the amplitude of the murmur is usually relatively uniform throughout most of the diastole.

A *mitral stenosis murmur* (Fig. 6) is caused by a stenotic mitral valve and is considered a decrescendo–crescendo holodiastolic murmur. It is heard best at the mitral auscultation area and is accentuated by exercise and by assuming a recumbent position. A mitral stenosis murmur that lasts up to the first heart sound, even after long cardiac cycles, indicates that the stenosis is severe enough to generate a persistent gradient even at the end of long diastoles.

The murmur caused by *tricuspid stenosis* is middiastolic in origin and differs from the mitral stenosis middiastolic murmur in two important respects: (1) the loudness of the tricuspid murmur increases with inspiration, and (2) the tricuspid murmur is auscultated over a relatively localized area along the left lower sternal border. Detectable inspiratory increases in loudness occur because of augmentations of the right ventricular volumes, decreases in right ventricular diastolic pressures, and increases of the gradients and flows across the stenotic tricuspid valve. This murmur is best detected over the left lower sternal border because it originates within the inflow portion of the right ventricle and is then transmitted to the overlying chest wall.

A *mitral regurgitation murmur* (Fig. 7) is caused by an insufficiency of the mitral valve and is a systolic murmur best heard at the mitral auscultation area. It is accentuated by exercise and left semilateral positioning. Acute severe mitral regurgitation is often accompanied by an early systolic murmur or holosystolic murmur that has a decrescendo pattern, diminishing or ending before the second heart sound. The physiological mechanism responsible for this early systolic decrescendo murmur is primarily acute severe regurgitation into a relatively normal-size left atrium with limited distensibility. The regurgitant flow is maximal in early systole and minimal in late systole, and the murmur typically follows this pattern.

Another described early systolic murmur is the *tricuspid regurgitation murmur* (Fig. 8), often associated with infective endocarditis. The mechanisms responsible for the timing and configuration of this murmur are analogous to those described for mitral regurgitation. It is a systolic murmur best heard at the tricuspid area and is best accentuated by inspiration.

The murmurs associated with *atrial septal defects* (Fig. 9) are commonly systolic murmurs caused by increased blood flows through the pulmonic valves and are best heard over the pulmonic auscultation area. Most often, the atrial septal defect involves the fossa ovalis, is midseptal in location, and is of the ostium secundum type. This type of defect is a true deficiency of the atrial septum and should not be confused with a patent foramen ovale. The magnitude of the left-to-right shunt through an atrial septal defect depends on the size of the defect and the relative compliance of the ventricles as well as the relative resistances in both the pulmonary and the systemic circulations. The increased pulmonic valve flows cause a delay (splitting) in the pulmonic components of the second heart sound.

The murmur commonly associated with *patent ductus arteriosus* (Fig. 10) is caused by a turbulent continuous flow through the ductus connecting the aorta with the main pulmonary artery. It is a continuous "machinery" murmur, heard in both systole and diastole, because aortic pressures are higher than the pressures in the pulmonary artery throughout the cardiac cycle. Other associated clinical findings in such patients include bounding peripheral pulses, an infraclavicular and interscapular systolic murmur, precordial hyperactivity, hepatomegaly, and either multiple episodes of apnea and bradycardia or respiratory dependency.

The murmurs associated with *ventricular septal defects* (Fig. 11) are systolic murmurs, with intensity depending on the size of the defect; they are primarily caused by blood flow

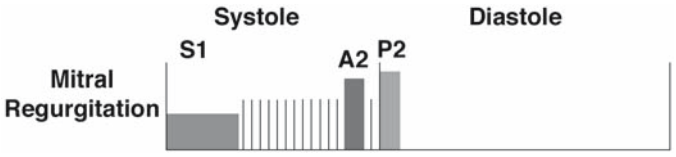

Fig. 7. Caused by an insufficiency of the mitral valve, the mitral regurgitation murmur is a systolic murmur best heard at the mitral auscultation area. S1, first heart sound; A2, aortic valve closure; P2, pulmonic valve closure.

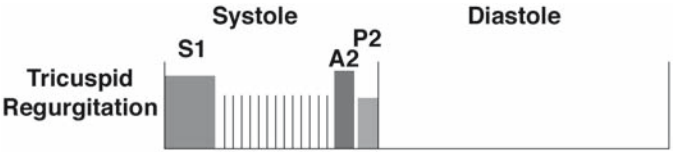

Fig. 8. The tricuspid regurgitation murmur is often associated with infective endocarditis. It is a systolic murmur best heard at the tricuspid area and is accentuated by inspiration. S1, first heart sound; A2, aortic valve closure; P2, pulmonic valve closure.

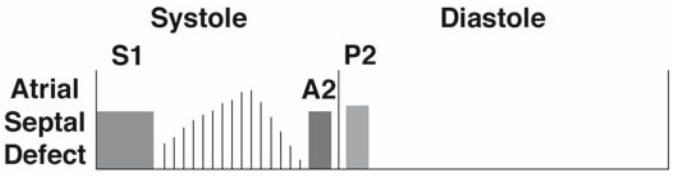

Fig. 9. Murmurs associated with atrial septal defects are normally systolic murmurs caused by increased blood flows through the pulmonic valves; such murmurs are best heard over the pulmonic auscultation area. S1, first heart sound; A2, aortic valve closure; P2, pulmonic valve closure.

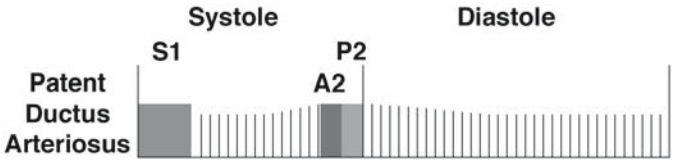

Fig. 10. Commonly associated with patent ductus arteriosus, this murmur is caused by a turbulent continuous flow through the ductus connecting the aorta with the main pulmonary artery. S1, first heart sound; A2, aortic valve closure; P2, pulmonic valve closure.

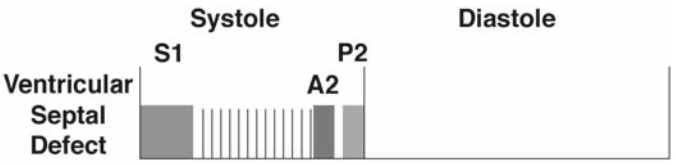

Fig. 11. Murmurs associated with ventricular septal defects are systolic murmurs primarily caused by blood flow from the left to the right ventricle (or the right to the left ventricle in Eisenmenger's syndrome). S1, first heart sound; A2, aortic valve closure; P2, pulmonic valve closure.

from the left to the right ventricle or the right to the left ventricle in Eisenmenger's syndrome. Eisenmenger's syndrome is the reversing of left-to-right shunt in patients with atrial septal defects, ventricular septal defects, or patent ductus arteriosus. Such murmurs are best heard at the mitral auscultation area or at the heart apex.

3. SUMMARY

In conclusion, I would like to reiterate the clinical importance of deeply understanding and using the basic physiological principles in interpreting "simple things" like blood pressure and heart tones should not be underestimated. It should also be noted that the descriptions of the general scientific and clinical principles used in this chapter have been simplified for clarity and can vary significantly in a clinical population. Even the most sophisticated electronic monitors cannot necessarily reduce the need for acquiring sound clinical skills such as inspection, palpation, percussion, auscultation, and so on. Even though "fancy" methods for monitoring can facilitate clinical decision making, to date there is almost no evidence that they reduce morbidity and mortality; yet, they can add significantly to the overall cost of care.

SOURCES

Barash, R.G., Cullen, B.F., and Stoelting, R.K. (eds.) (2001) *Clinical Anesthesia*, 4th Ed. Lippincott, Williams, and Wilkins, Philadelphia, PA.

Braunwald, E. (ed.) (1997) *Heart Disease: A Textbook of Cardiovascular Medicine*, 5th Ed. Saunders, Philadelphia, PA.

Faulconer, A. and Keys, T.E. (eds.) (1993) *Foundations of Anesthesiology*, Vols. 1 and 2. The Wood Library–Museum of Anesthesiology, Park Ridge, IL.

Kaplan, J.A., Reich, D.L., and Konstadt, S.N. (eds.) (1999) *Cardiac Anesthesia*, 4th Ed. Saunders, Philadelphia, PA.

McVicker, J.T. (2001) Blood pressure measurement—does anyone do it right? An assessment of the reliability of equipment in use and the measurement techniques of clinicians. *J Fam Plann Reprod Health Care*. 27, 163–164.

Miller, R.D. and Cucchiara, R.F. (eds.) (1994) *Anesthesia*, 4th Ed., Vols. 2 and 2. Churchill Livingstone, New York, NY.

Mohrman, D.E. and Heller, L.J. (eds.) (1997) *Cardiovascular Physiology*, 4th Ed. McGraw-Hill, New York, NY.

O'Brien, E., Pickering, T., Asmar, R., et al. (2002) Working Group on Blood Pressure Monitoring of the European Society of Hypertension, international protocol for validation of blood pressure measuring devices in adults. *Blood Press Monit*. 7, 3–17.

Stoelting, R.K. (1999) *Pharmacology and Physiology in Anesthetic Practice*, 3rd Ed. Lippincott-Raven, Philadelphia, PA.

15 Basic ECG Theory, Recordings, and Interpretation

ANTHONY DUPRE, MS, SARAH VINCENT, MS, AND PAUL A. IAIZZO, PhD

CONTENTS

1. THE ELECTROCARDIOGRAM

An electrocardiogram (ECG; in German, the electrokardiogram, EKG) is a measure of how the electrical activity of the heart changes over time as action potentials propagate throughout the heart during each cardiac cycle. However, this is not a direct measure of the cellular depolarization and repolarization with the heart, but rather the relative, cumulative magnitude of populations of cells eliciting changes in their membrane potentials at a given point in time; it shows electrical differences across the heart when depolarization and repolarization of these atrial and ventricular cells occur.

The human body can be considered, for the purposes of an ECG, a large-volume conductor. It is basically filled with tissues surrounded by a conductive ionic fluid. You can imagine that the heart is suspended inside of that conductive medium. During the cardiac cycle, the heart contracts in response to action potentials moving along the chambers of the heart. As it moves, there will be one part of the cardiac tissue that is depolarized and another part that is at rest or polarized. This results in a charge separation, or dipole, which is illustrated in Fig. 1.

From: *Handbook of Cardiac Anatomy, Physiology, and Devices*
Edited by: P. A. Iaizzo © Humana Press Inc., Totowa, NJ

The dipole causes current flow in the surrounding body fluids between the ends of the heart, resulting in a fluctuating electric field throughout the body. This is much like the electric field that would result, for example, if a common battery were suspended in a saltwater solution (an electrically conductive medium). The opposite poles of the battery would cause current flow in the surrounding fluid, creating an electric field that could be detected by electrodes placed in the solution. A similar electrical field around the heart can be detected using electrodes attached to the skin. The intensity of the voltage detected depends on the orientation of the electrodes with respect to that of the dipole ends. The amplitude of the signal is proportional to the mass of tissue involved in creating that dipole at any given time. Using electrodes on the surface of the skin to detect the voltage of this electrical field is what provides the electrocardiogram.

It is important to note, as might be expected, that because the ECG is measured on the skin, any potential differences within the body can have an effect on the electrical field detected. This is why it is considered important for diagnostic purposes that, while recording an ECG from an individual, the individual should remain as still as possible. Movements require the use of skeletal muscles, which then contribute to the changes in volt-

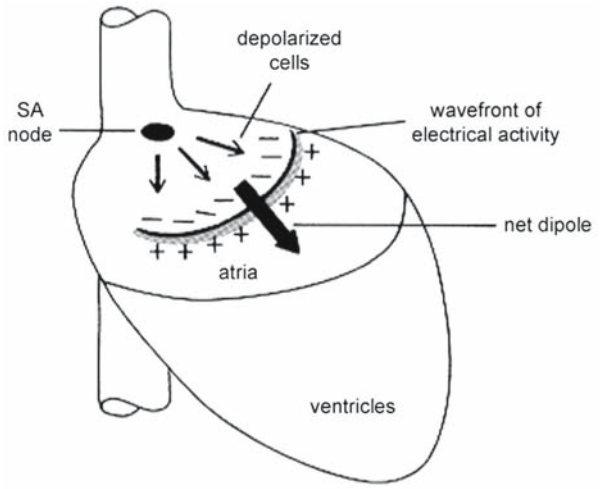

Fig. 1. After conduction begins at the sinoatrial (SA) node, cells in the atria begin to depolarize. This creates an electrical wavefront that moves down toward the ventricles, with polarized cells at the front, followed by depolarized cells behind. The separation of charge results in a dipole across the heart (the large black arrow shows its direction). Modified from D.E. Mohrman and L.J. Heller (eds.), *Cardiovascular Physiology*, 5th Ed., 2003. Reproduced with permission of the McGraw-Hill Companies.

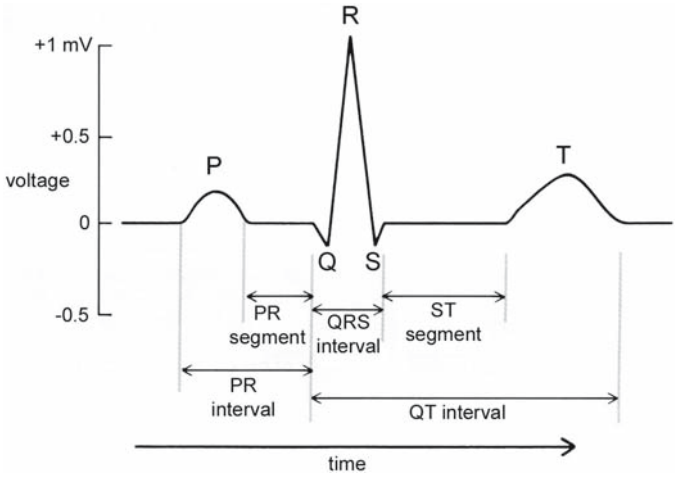

Fig. 2. A typical ECG waveform for one cardiac cycle measured from the lead II position. The P wave denotes atrial depolarization, the QRS indicates ventricular depolarization, and the T wave denotes ventricular repolarization. The events on the waveform occur on a scale of hundreds of milliseconds. Modified from D.E. Mohrman and L.J. Heller, (eds.), *Cardiovascular Physiology*, 5th Ed., 2003. Reproduced with permission of the McGraw-Hill Companies.

ages detected using electrodes on the surface of the body. When the monitored patient is essentially motionless, it is considered a "resting ECG," the type of ECG signals discussed in the majority of this chapter.

2. THE ECG WAVEFORM

When an ECG is recorded, a reading of voltage vs time is produced, which is normally displayed as millivolts (mV) and seconds. A typical lead II ECG waveform is shown in Fig. 2. For this recording, the negative electrode was placed on the right wrist, and the positive electrode was placed on the left ankle, giving the standard lead II ECG (explained in Section 3.1.). It shows a series of peaks and waves that corresponds to ventricular or atrial depolarization and repolarization, with each segment of the signal representing a different event associated with the cardiac cycle.

The cardiac cycle begins with the firing of the sinoatrial node in the right atrium. This firing is not detected by the surface ECG because the sinoatrial node is not composed of an adequately large quantity of cells to create an electrical potential with a high enough amplitude to be recorded with distal electrodes (signal amplitude is lost as it dissipates through the conductive medium). The atria then depolarize, giving rise to the P wave. This represents the coordinated depolarization of the right and left atria and the onset of atrial contraction. The P wave is normally around 80–100 ms in duration. As the P wave ends, the atria are completely depolarized and are beginning contraction.

The signal then returns to baseline, and action potentials (not large enough to be detected) spread to the atrioventricular node and bundle of His. Then, roughly 160 ms after the beginning of the P wave, the right and left ventricles begin to depolarize, resulting in what is called the QRS complex, representing the beginning of ventricular contraction, which is around 80 (60–100) ms in duration. Typically, the first negative deflection is the Q wave, the large positive deflection is the R wave, and if there is a negative deflection after the R wave, it is called the S wave. The exact shape of the QRS complex, as explained in Section 3.2., depends on the placement of electrodes from which the signals are recorded.

Simultaneous with the QRS complex, atrial contraction has ended, and the atria are repolarizing. However, the effect of this global atrial repolarization is sufficiently masked by the much larger amount of tissue involved in ventricular depolarization and is thus not normally detected in the ECG. During ventricular contraction, the ECG signal returns to baseline. The ventricles then repolarize after contraction, giving rise to the T wave. Note that the T wave is normally the last-detected potential in the cardiac cycle; thus, it is followed by the P wave of the next cycle, repeating the process.

Of clinical importance in the ECG waveform are several notable parameters (regions), which include the P–R interval, the S–T segment, and the Q–T interval**.** The P–R interval is measured from the beginning of the P wave to the beginning of the QRS complex and is normally 120–200 ms long. This is basically a measure of the time it takes for an impulse to travel from atrial excitation and through the atria, atrioventricular node, and remaining fibers of the conduction system. The S–T segment is the period of time when the ventricles are completely depolarized and contracting and is measured from the S wave to the beginning of the T wave. The Q–T interval is measured from the beginning of the QRS complex to the end of the T wave; this is the time segment from when the ventricles begin their depolarization to the time when they have repolarized to their resting potentials and is normally about 400 ms in duration.

An obvious observation made concerning the QRS complex is that it has a much higher peak and shorter duration than

either the P or T waves. This is because ventricular depolarization occurs over a greater mass of cardiac tissue (i.e., a greater number of myocytes are depolarizing at the same time); furthermore, the ventricular depolarization is much more synchronized than either atrial depolarization or ventricular repolarization. For additional details relative to the types of action potential that occur in various regions of the heart, refer to Chapter 9.

It is also very important to note that deflections in the ECG waveform represent the change in electrical activity caused by atrial or ventricular depolarization and repolarization and not necessarily generalized cardiac contractions or relaxations, which take place on a slightly longer time-scale (*see* Fig. 3). Shown in Fig. 3 are the certain points on the ECG waveform and how they relate to other events in the heart during the cardiac cycle.

One last thing that should be noted relative to the ECG waveform is the sometimes-detected potential referred to as the U wave. Its presence is not fully understood, but is considered by some to be caused by late repolarization of the Purkinje system. If detected, the U wave will be toward the end of the T wave and have the same polarity (positive deflection). However, it has a much shorter amplitude and usually ascends more rapidly than it descends (which is the opposite of the T wave).

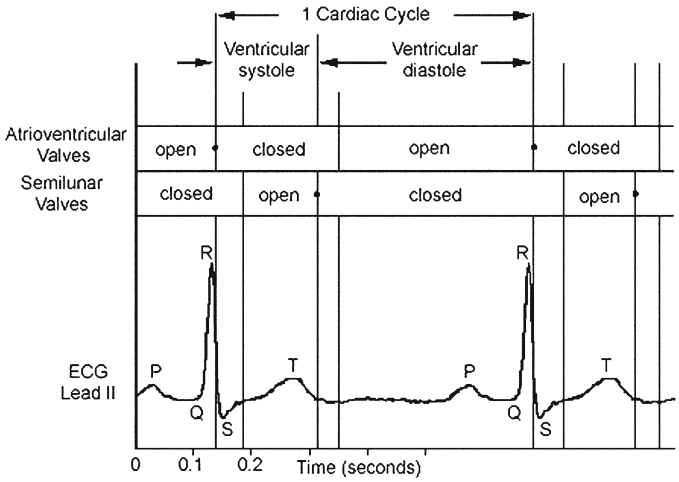

Fig. 3. A typical lead II electrocardiogram (ECG) waveform is compared to the timing of atrioventricular and semilunar valve activity, along with which segments of the cardiac cycle the ventricles are in systole/diastole.

3. MEASURING THE ECG

Typically, the ECG is measured from the surface of the skin, which can be done by placing two electrodes directly on the skin and reading the potential difference between them. This is possible because these signals are transmitted throughout the body. Again, as stated above, the detected waveform features depend not only on the amount of cardiac tissue involved, but also on the orientation of the electrodes with respect to the dipole in the heart. In other words, the ECG waveform will look slightly different when measured from different electrode positions, and typically an ECG is obtained using a number of different electrode locations (e.g., limb leads or precordial) or configurations (unipolar, bipolar, modified bipolar). which, fortunately, have been standardized by universal application of certain conventions.

3.1. Bipolar Limb Leads

The three most commonly employed lead positions used today are referred to as leads I, II, and III. For the purposes of explaining the position of these leads, imagine the torso of the body as an equilateral triangle as illustrated in Fig. 4. This forms what is known as Einthoven's triangle (named for the Dutch scientist who first described it). Electrodes are placed at each of the vertices of the triangle, and a single ECG trace (lead I, II, or III) is measured along the corresponding side of the triangle using the electrodes at each end (because each lead uses one electrode on either side of the heart, leads I, II, and III are also referred to as the bipolar leads). The plus and minus signs shown in Fig. 4 indicate the polarity of each lead measurement and are notably considered as the universal convention. (For reasons that become clear in this chapter, the vertices of the triangle can be considered to be at the wrists and left ankle for electrode placement, as well as the shoulders and lower torso.)

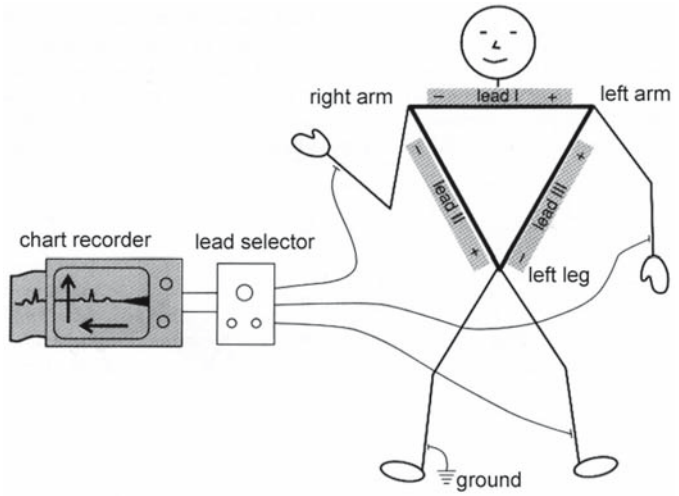

Fig. 4. The limb leads are attached to the corners of Einthoven's triangle on the body. Each lead uses two of these locations for a positive and a negative lead. The plus and minus signs indicate the orientation of the polarity conventions. Modified from D.E. Mohrman and L.J. Heller (eds.), *Cardiovascular Physiology*, 5th Ed,, 2003. Reproduced with permission of the McGraw-Hill Companies.

As an example, if the lead II ECG trace shows an upward deflection, it would mean that the voltage measured at the left leg (or bottom apex of the triangle) is more positive than the voltage measured at the right arm (or upper right apex of the triangle). One notable time-point at which this happens is during the P wave. Imagine the orientation of the heart as shown in Fig. 5, with the action potential propagation across the atria creating a dipole pointed downward and to the left side of the body. This can be represented as an arrow (shown in Fig. 5) showing the magnitude and direction of the dipole in the heart. This dipole would, overall, create a more positive voltage reading at the left ankle electrode than at the right wrist electrode, thus eliciting the positive deflection of the P wave on the lead II ECG.

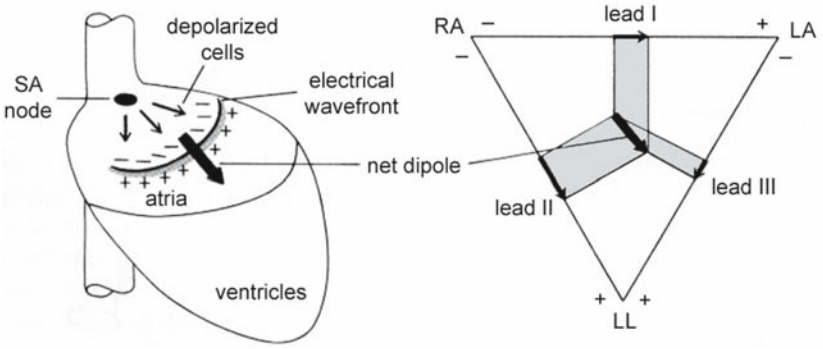

Fig. 5. The net dipole occurring in the heart at any one point in time is detected by each lead (I, II, and III) in a different way because of the different orientations of each lead set relative to the dipole in the heart. In this example, the projection of the dipole on all three leads is positive (the arrow is pointing toward the positive end of the lead), which gives a positive deflection on the electrocardiogram during the P wave. Furthermore, lead II detects a larger amplitude signal than lead III does from the same net dipole (i.e., the net dipole projects a larger arrow on the lead II side of the triangle than on the lead III side). LA, left arm; LL, left leg; RA, right arm; SA, sinoatrial. Figure from D.E. Mohrman and L.J. Heller (eds.), *Cardiovascular Physiology*, 5th Ed., 2003.

Now, imagine how that same action potential propagation would appear on the other lead placements, leads I and III, if placed at the center of Einthoven's triangle (Fig. 5, right side). Each of these lead placements can be thought of as viewing the electrical dipole from three different directions: lead I from the top, lead II from the lower right side of the body, and lead III from the lower left side, all looking at the heart in the frontal plane. In this example, the atrial depolarization creates a dipole that gives a positive deflection for all three leads because the arrow's projection onto each lead (or in other words, measuring the cardiac dipole from each lead) results in the positive end of the dipole pointed more toward the positive end of the lead than the negative end. This is why atrial depolarization (P wave) appears as a positive deflection for each lead (although wave magnitude is different in each). Ventricular depolarization, however, is a bit more complicated, as is discussed in detail in Section 3.2.; briefly, it results in various directions of the Q- and S-wave potentials depending on which lead trace is utilized for recording.

3.2. Electrical Axis of the Heart

The direction and magnitude of the overall dipole of the heart at any instant (represented by the arrow in Fig. 5, for example) is also known as the heart's "electrical axis," which is a vector originating in the center of Einthoven's triangle such that the direction of the dipole is typically assessed in degrees. The convention for this is to use a line horizontal across the top of Einthoven's triangle as 0° and move clockwise downward (pivoting on the negative end of lead I) as the positive direction. It should be noted that the electrical axis is actually changing direction throughout the cardiac cycle as different parts of the heart depolarize/repolarize in different directions. Fig. 6 shows the dipole spreading across the heart during a typical cardiac cycle, beginning with atrial depolarization. Each panel is accompanied by a diagram of the corresponding deflections on each ECG lead (I, II, and III). Keep in mind that, at certain points, the electrical axis of the heart may give opposite deflections on the various ECG leads.

As can be observed in Fig. 6, depolarization begins at the sinoatrial node in the right atrium, forming the P wave. The atria depolarize downward and to the left, toward the ventricles, followed by a slight delay at the atrioventricular node before the ventricles depolarize. The initial depolarization in the ventricles normally occurs on the left side of the septum, creating a dipole pointed slightly down and to the right. This gives a negative deflection of the Q wave for leads I and II; however, it is positive in lead III. Depolarization then continues to spread down the ventricles toward the apex, which is when the most tissue mass is depolarizing at the same time, with the same orientation. This gives the large positive deflection of the R wave for all three leads. Ventricular depolarization then continues to spread through the cardiac wall and finally finishes in the left ventricular lateral wall. This results in a positive deflection for leads I and II; however, lead III shows a lower R-wave amplitude along with a negative S-wave deflection.

After a sustained depolarized period (the S–T segment), the ventricles then repolarize. This occurs anatomically in the opposite direction of depolarization. However, one must keep in mind that the arrow in Fig. 6 represents the electrical axis of the heart (or the dipole) and does not necessarily show the direction that the repolarization wave is moving. Thus, even though the wave is moving from epicardium to endocardium (the direction of repolarization), the dipole (and therefore the electrical axis) remains in the same orientation as during depolarization. This explains why the T wave is also a positive deflection on leads I and II and negative (or nonexistent) on Lead III. The ventricles are then repolarized, returning the signal to its baseline potential (value).

During the cardiac cycle, the electrical axis of the heart (viewed from the plane of the limb leads) is always changing in both magnitude and direction. The average of all instantaneous electrical axis vectors gives rise to the "mean electrical axis" of the heart. Most commonly, it is taken as the average dipole (or electrical axis) direction during the QRS complex since this is the highest and most synchronized signal on the waveform. Typically, to find the mean electrical axis, area calculations

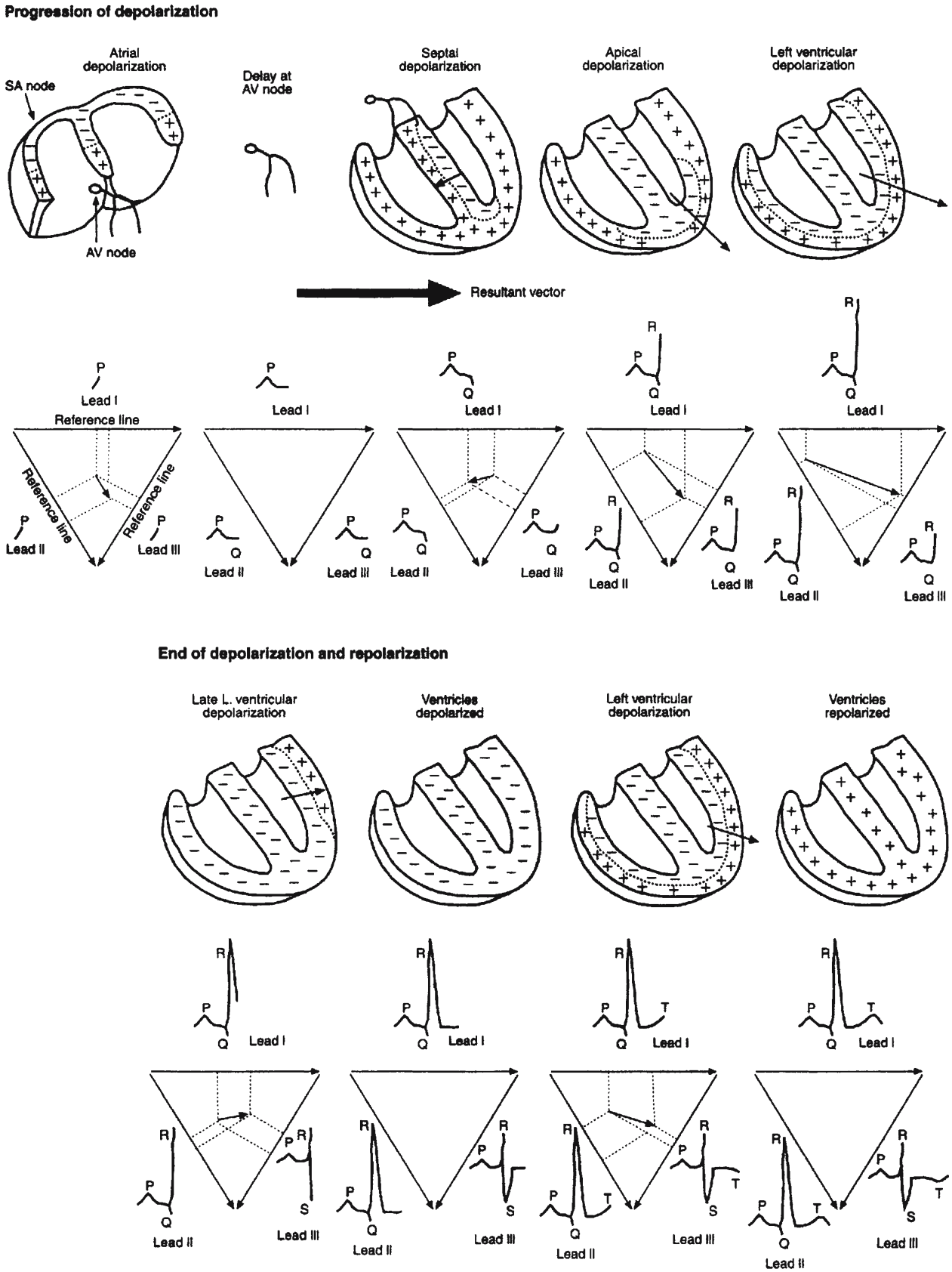

Fig. 6. The net dipole of the heart (indicated by the arrow) as it progresses through one cardiac cycle, beginning with firing of the sinoatrial (SA) node and finishing with the complete repolarization of the ventricular walls. Each heart shows the charge separation inside the myocardium, along with a corresponding Einthoven's triangle diagram below it, which displays how the net dipole is defected by each of the bipolar limb leads. Notice the change in direction and magnitude of the dipole during one complete cardiac cycle. AV, atrioventricular. Modified from L. R. Johnson (ed.), *Essential Medical Physiology*, 3rd Ed., 2003. With permission of Elsevier.

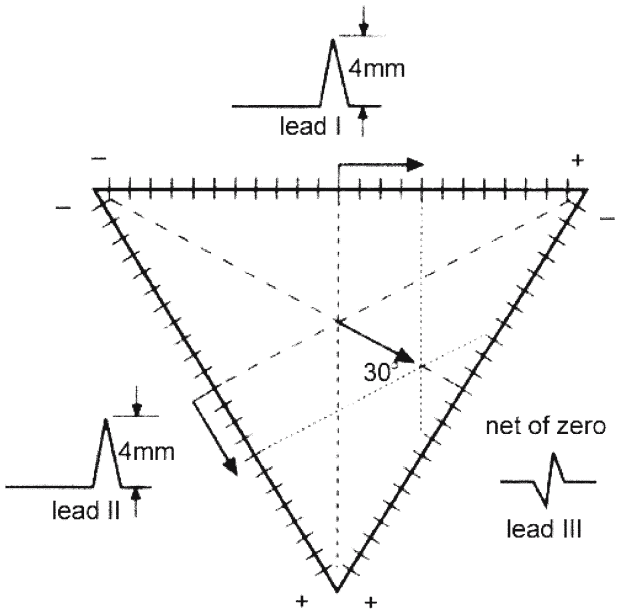

Fig. 7. The amplitudes of the lead I and II R waves are plotted along the corresponding leg of Einthoven's triangle starting at the midpoint and drawn with a length equal to the height of the R wave (units used to measure the amplitude can be arbitrary because the direction, not the magnitude, of the axis is important). The direction of the plot is toward the positive end of the lead if the R wave has a positive deflection and negative if it has a negative deflection. Perpendiculars from each point are then drawn into the triangle and meet at a point. A line drawn from the center of the triangle to this point gives the angle of the mean electrical axis. Because the normal activation sequence in the heart generally goes down and left, this is also the direction of the mean electrical axis in most people. The normal range is anywhere from 0° to +90°. Modified from L.R. Johnson (ed.), *Essential Medical Physiology*, 3rd Ed., 2003.

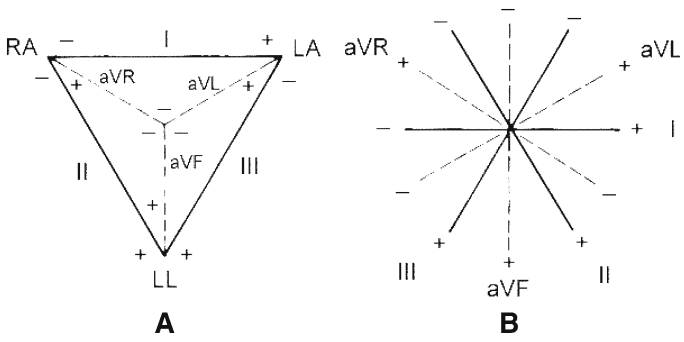

Fig. 8. **(A)** The augmented leads are shown on Einthoven's triangle along with the other three frontal plane leads (I, II, and III). **(B)** The hex axial reference system for all six limb leads is shown, with solid and dashed lines representing the bipolar and unipolar leads, respectively. aVL, voltage recorded between left arm limb lead and neutral reference lead; aVF, voltage recorded between left leg lead and neutral reference lead; aVR, voltage recorded between right arm limb lead and neutral reference lead; LA, left arm; LL, left leg; RA, right arm. Modified from D.E. Mohrman and L.J. Heller (eds.), *Cardiovascular Physiology*, 5th Ed., 2003. Reproduced with permission of the McGraw-Hill Companies.

from under the QRS complexes from at least two leads are needed. However, it is easier and more commonly determined by an estimate using the deflection (positive or negative) and height of the R wave. Figure 7 shows a simple example of using leads I and II to find the electrical axis of the heart. It should be noted that, in the normal human heart, the electrical axis of the heart roughly corresponds to the anatomical orientation of the heart (from base to apex).

3.3. The 12-Lead ECG

Leads I, II, and III are the bipolar limb leads discussed thus far. There are three other leads that use the limb electrodes; these are the unipolar limb leads. Each of these leads uses an electrode pair that consists of one limb electrode and a "neutral reference lead" created by hooking up the other two limb locations to the negative lead of the ECG amplifier. In other words, each lead has its positive end at the corresponding limb lead and runs toward the heart, the location of its "negative" end, directly between the other two limb leads. These are referred to as the *augmented unipolar limb leads*. The voltage recorded between the left arm limb lead and the neutral reference lead is called lead aVL; similarly, the right arm limb lead is aVR, and the left leg lead is aVF (Fig. 8).

The remaining 6 of the 12 lead recordings are the 6 chest leads. These leads are also unipolar; however, they measure electrical activity in the traverse plane instead of the frontal plane. Similar to the unipolar limb leads, a neutral reference lead is "created," this time using all 3 limb leads connected to the negative ECG lead, which basically puts it in the center of the chest. The 6 positive, or "exploring," electrodes are placed as shown in Fig. 9 (around the chest) and are labeled V1 through V6 (the V meaning voltage). These chest leads are also known as the *precordial leads*. Figure 9A shows a simple cross-section (looking superior to inferior) of the chest, depicting the relative position of each electrode in the traverse plane. Figure 9A also shows a typical waveform obtained from each of these leads. The 3 bipolar limb leads, 3 unipolar limb leads, and 6 precordial leads make up the 12-lead ECG.

4. SOME BASIC INTERPRETATION OF THE ECG TRACE

The ECG waveform and mean electrical axis are quite useful in the clinical setting. The ECG is considered one of the most important monitors of a patient's cardiovascular status and is commonly used for measurements as basic as the heart rate. Most ECG monitoring devices used today include automated systems that detect changes in durations between subsequent QRS complexes (i.e., the duration of one cycle).

Simply, determination of the PR intervals provides information regarding whether a patient may have heart block. Elongated PR intervals (longer than ~0.21 s) serve as a good indication that conduction through the atrioventricular node is slowed to some degree (first-degree heart block). Conduction in the atrioventricular node may even intermittently fail, which would elicit a P wave without a subsequent QRS complex before the next P wave (second-degree heart block). An ECG trace showing P waves and QRS complexes beating independently of each other indicates the atrioventricular node has ceased to transmit impulses (third-degree heart block).

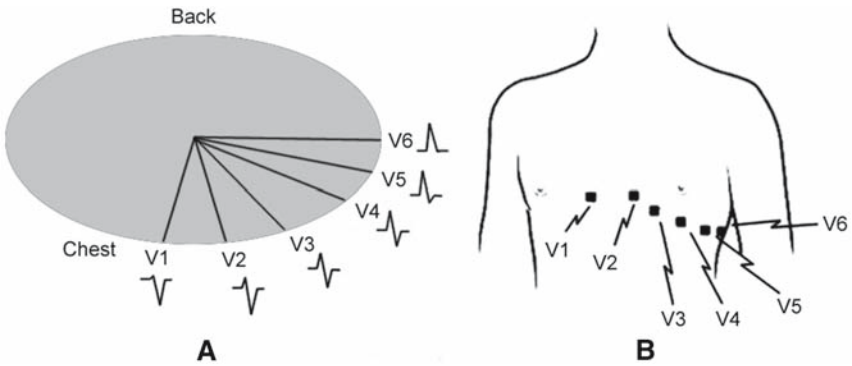

Fig. 9. **(A)** A cross-section of the chest shows the relative position of the six precordial leads in the traverse plane, along with a typical waveform detected for ventricular depolarization. **(B)** An anterior view of the chest shows common placement of each precordial lead, V1 through V6.

Prolonged Q–T intervals (which are normally no more than 40% of the cardiac cycle length) are normally an indication of delayed repolarization of the cardiomyocytes, possibly caused by irregular opening or closing of sodium or potassium channels. More important, though, is the elevation of the S–T segment, which typically indicates a regional ventricular ischemia. The S–T segment elevation (or depression) can also be used as an indication of many other abnormalities, including myocardial infarction, coronary artery disease, and pericarditis.

The electrical axis is also a helpful diagnostic tool. For example, in the case of left ventricular hypertrophy, the left side of the heart is enlarged with greater tissue mass. This could cause the dipole during ventricular contraction (and therefore the mean electrical axis) to point more towards the left.

Much more can be said about specific interpretations of the intervals and segments that make up the ECG waveform. For more details on changes in ECG patterns associated with various conditions or abnormalities, refer to Chapter 9.

5. LEAD PLACEMENT IN THE CLINICAL SETTING

In a clinical setting, not all 12 leads are displayed at the same time, and most often, not all leads are measured simultaneously. A common setup used is a five-wire system consisting of the two arm leads, which are actually placed on the shoulder areas, two leg leads placed where the legs join the torso, and one chest lead. This arrangement allows display of any of the limb leads (I, II, III, aVR, aVL, and aVF) and one of the precordial leads, depending on where the chest electrode is placed. Figure 10 shows the positioning of these five electrodes on the patient's body.

Nevertheless, the exact anatomical placement of the leads is very important for obtaining accurate ECG traces for clinical evaluations; moving an electrode even slightly away from its so-called correct position could cause dramatically different traces and possibly lead to misdiagnosis. A slight exception to this rule is the limb leads, which do not necessarily need to be placed at the proximal portion of the limb as described in the preceding paragraph. However, the limb leads for the most part need to be equidistant from each other relative to the heart (i.e., for determination of the electrical axis to be accurate).

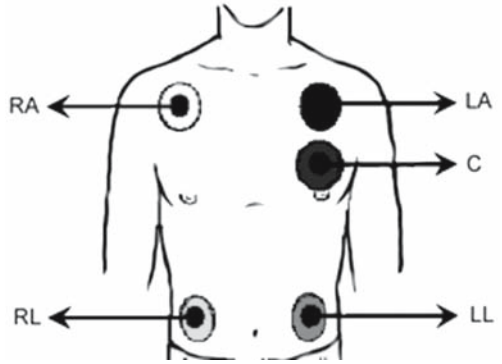

Fig. 10. Placement of the common five-wire electrocardiogram electrode system leads on the shoulders, chest, and torso. The chest electrode is placed according to the desired precordial lead position. C, chest; LA, left arm; LL, left leg; RA, right arm; RL, right leg.

6. ECG DEVICES

The invention of electrocardiography has had an immeasurable impact on the field of cardiology. It has provided insights into the structure and function of both healthy and diseased hearts. The ECG has evolved into a powerful diagnostic tool for heart disease, especially for the detection of arrhythmias and acute myocardial infarction. The use of the ECG has become a standard of care in cardiology, and new advances using this technology are continually introduced.

The discovery of intrinsic electrical activity of the heart can be traced to as early as the 1840s. Specifically, in 1842, the Italian physicist Carlo Matteucci first reported that an electrical current accompanies each heartbeat. Soon after, the German physiologist Emil DuBois-Reymond described the first action potential that accompanies muscle contraction. Additionally, Rudolph von Koelliker and Heinrich Miller recorded the first cardiac action potential using a galvanometer in 1856.

Subsequently, the invention of the capillary electrometer in the early 1870s by Gabriel Lippmann led to the first recording of a human electrocardiogram by Augustus D. Waller. The capillary electrometer is a thin glass tube containing a column of mercury that sits above sulfuric acid. With varying electrical potentials, the mercury meniscus moves, and this can be

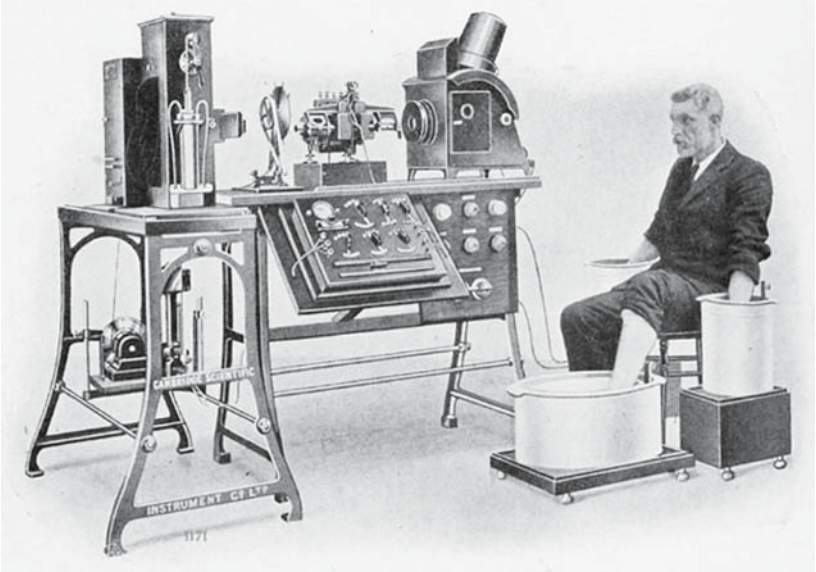

Fig. 11. Willem Einthoven's string galvanometer consisted of a massive electromagnet with a thin, silver-coated string stretched across it. Electric currents passing through the string caused it to move from side to side in the magnetic field generated by the electromagnet. The oscillations in the string provided information on the strength and direction of the electrical current. The deflections of the string were then magnified using a projecting microscope and recorded on a moving photographic plate. Courtesy of the NASPE-Heart Rhythm Society History Project.

observed through a microscope. Using this capillary electrometer, Waller was the first to show that the electrical activity precedes the mechanical contraction of the heart. He was also the first to show that the electrical activity of the heart can be seen by applying electrodes to both hands or to one hand and one foot; this was the first description of "limb leads." Interestingly, Waller would often publicly demonstrate this with his dog, Jimmy, who would stand in jars of saline during the recording of the ECG.

One of the next major breakthroughs in electrocardiography came with the invention of the string galvanometer by Willem Einthoven in 1901. The following year, he reported the first electrocardiogram, which used his string galvanometer. Einthoven's string galvanometer consisted of a massive electromagnet with a thin, silver-coated string stretched across it. Electric currents that passed through the string would cause it to move from side to side in the magnetic field generated by the electromagnet. The oscillations in the string would give information regarding the strength and direction of the electrical current. The deflections of the string were magnified using a projecting microscope and were recorded on a moving photographic plate (Fig. 11). Years earlier, utilizing recordings from a capillary electrometer, Einthoven was also the first to label the deflections of the heart's electrical activity as P, Q, R, S, and T.

In 1912, Einthoven made another major contribution to the field of electrophysiology by deriving a mathematical relationship between the direction and size of the deflections recorded by the three limb leads. This hypothesis is known as Einthoven's triangle (described in Section 3.1). The standard 3 limb leads were used for three decades before Frank Wilson described unipolar leads and the precordial lead configuration. The 12-lead ECG configuration used today consists of the standard limb leads from Einthoven and the precordial and unipolar limb leads based on Wilson's work.

Following Einthoven's invention of the string galvanometer, electrocardiography quickly became a research tool for both physiologists and cardiologists. Much of the current knowledge involving arrhythmias was developed using the ECG. In 1906, Einthoven published the first results of ECG tracings of atrial fibrillation, atrial flutter, ventricular premature contractions, ventricular bigeminy, atrial enlargement, and induced heart block in a dog. Einthoven was awarded the Nobel Prize for his work and inventions in 1924.

Thomas Lewis was one of the pioneering cardiologists who utilized the capabilities of the ECG to further scientific knowledge of arrhythmias. His findings were summarized in his books *The Mechanism of the Heart Beat* and *Clinical Disorders of the Heart Beat*, published in 1911 and 1912, respectively. He also published over 100 research papers describing his work. Interestingly, Lewis was also the first to use the terms sinoatrial node, pacemaker, premature contractions, paroxysmal tachycardia, and atrial fibrillation. For more information on arrhythmias, *see* Chapter 22.

Myocardial infarction and angina pectoris were also extensively studied with ECG using the string galvanometer device. More specifically, numerous clinical investigators studied the changes within the ECG signal that were associated with the onset of myocardial infarction in both animals and humans. By the 1930s, the characteristic features of the ECG for the diagnostic indications of myocardial infarction had been identified. Subsequently, the connection between angina pectoris and coronary occlusion was made. Specifically, while studying electrocardiographic changes accompanying angina pectoris, Francis Wood and Charles Wolferth performed the first

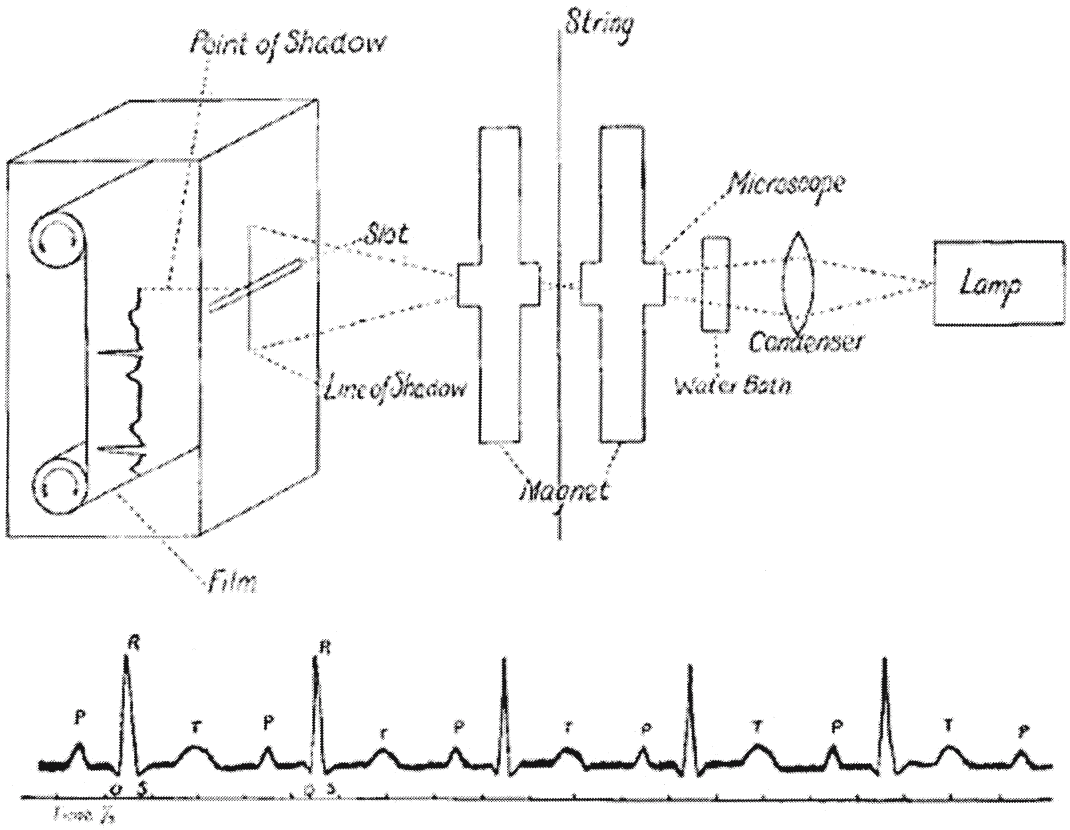

Fig. 12. A diagram of Cambridge Scientific Instrument Company's smaller version of the string galvanometer and electrocardiogram of a normal rhythm. Reprinted courtesy of the NASPE-Heart Rhythm Society History Project.

use of the exercise electrocardiographic stress test. Their use of exercise for ECG analyses stemmed from the observation that many of their patients experienced angina during physical exertion. This technique was not routinely used, however, because it was thought to be very dangerous. Nevertheless, with these advances in protocols and technologies, the ECG emerged as a common diagnostic tool for physicians.

ECG equipment has come a long way since Einthoven's string galvanometer. Yet, Cambridge Scientific Instrument Company (United Kingdom) was the first to manufacture this instrument back in 1905. It was massive, weighing in at 600 pounds. A telephone cable was used to transmit the electrical signals from a hospital over a mile away to Einthoven's laboratory. A few years later, Max Edelman of Cambridge Scientific Instrument Company manufactured a smaller version of the instrument (Fig. 12). However, it was not until the 1920s that bedside machines became available. A few years later, a "portable" version was manufactured in which the instrument was contained in two wooden cases, each weighing close to 50 pounds. In 1935, the Sanborn Company (Andover, MA) manufactured an even smaller version of the unit that only weighed about 25 pounds.

Use of the ECG in a nonclinical setting became possible in 1949 with Norman Jeff Holter's invention of the Holter monitor. The first version of this instrument was a 75-pound backpack that could continuously record the ECG and transmit these signals via radio. Subsequent versions of such systems were dramatically reduced in size, but the next version utilized tape or digital recording of the signal. Today, miniaturized systems (Fig. 13) allow patients to be monitored over longer periods of time (usually 24 h) to help diagnose any problems with rhythm or ischemic heart disease.

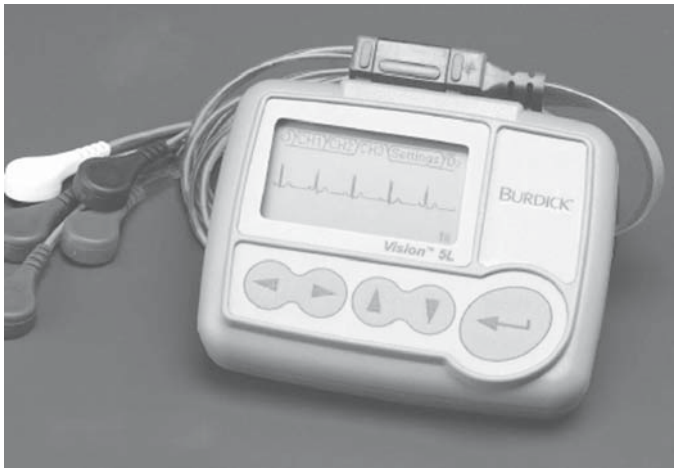

Fig. 13. A version of the Holter monitor that is used currently. The one here is manufactured by Burdick, Inc. (Dearfield, WI).

Fig. 14. A loop recorder with pacemaker and detection capabilities is shown. This model is manufactured by LifeWatch Inc. (Buffalo Grove, IL).

Fig. 15. A loop recorder. The one pictured here is manufactured by LifeWatch, Inc.

The use of computers for the analysis of ECGs began in the 1960s. In 1961, Hubert Pipberger described the first computer analysis of ECG signals, an analysis that recognized abnormal records. Computer-assisted ECG analyses were introduced into the clinical setting in the 1970s. The use of computers, microcomputers, and microelectronic circuits has had a huge impact on electrocardiography. The size of the equipment has been drastically reduced to pocket size or even smaller for some applications. Computer programs can also provide summaries of information recorded from the ECG, including heart rates, heart rate variability, multiple types of arrhythmias, and variations in QRS, ST, QT, or T patterns. This has allowed continuous monitoring of patients over much longer time periods, which can greatly help in the diagnosis of patients with infrequent symptoms. However, there are some concerns that have surfaced with the use of computers for ECG analyses, including decreased basic training in the interpretations of ECGs and a reduction in the detection of new pattern changes associated with different disease states.

Currently, there are three general types of instruments utilized in the collection of electrocardiograms. Continuous

Fig. 16. The Reveal, an implantable electrocardiogram loop recorder, manufactured by Medtronic, Inc., Minneapolis, MN.

recorders, like the Holter monitor described earlier, are attached to the surface of the body and continuously record signals for a predetermined duration. Most such systems record from at least three different ECG leads. When using this method, patients must record their daily activities and the time of the onset of symptoms. Event recorders are another type of instrument used for ECG collection. There are two basic types of event recorders: a postevent recorder (worn continuously and self-activating when cardiac symptoms appear) and a miniature solid-state recorder (placed on the precordium to record the rhythm when symptoms appear). Today, these devices can be as small as a credit card.

A second type of event recorder available is the preevent recorder. Such devices are similar to those used for postevent recorders, but a memory loop is used to enable the recording of information several minutes before and after the onset of symptoms. Some examples of loop recorders are shown in Figs. 14 and 15. The Reveal™, a miniature version of a preevent recorder that can be implanted subcutaneously, is currently available and is shown in Fig. 16 (Usinoatrial, Medtronic Inc., Minneapolis, MN). This device is used for patients who elicit infrequent symptoms (hence, they remain undiagnosed) and for those in whom external recorders are considered impractical.

The third type of ECG instrument that is used is a real-time monitoring system. With this type of instrument, the data are not recorded within the device, but are transmitted transtelephonically to a distal recording station. Such instruments are commonly used for monitoring patients who have a potentially dangerous condition so the technician can quickly identify the rhythm abnormality and make arrangements for proper management of the condition.

7. SUMMARY

As cardiomyocytes depolarize and propagate action potentials throughout the heart, a charge separation (or dipole) is created. By utilizing the resultant electrical field present in the body, electrodes can be placed around the heart to measure potential differences as the heart depolarizes and repolarizes. This measurement gives rise to the ECG, normally consisting of the P wave for atrial depolarization, the QRS complex for ventricular depolarization, and the T wave for ventricular repolarization.

There are up to 12 different standard positions, or leads, available to detect the ECG. Most commonly, a 5-wire system

is used clinically and can be used for the 3 bipolar limb leads (which make up Einthoven's triangle), the 3 unipolar limb leads, and 1 precordial (chest) lead at a time. At least two lead traces are needed to calculate the heart's electrical axis, which gives the general direction of the heart's dipole at any given instant. The heart's mean electrical axis is then the average dipole direction during the cardiac cycle (or more commonly, during ventricular depolarization).

The recorded ECG remains one of the most vital monitors of a patient's cardiovascular status and is used today in nearly every clinical setting. Electrocardiography has come a long way since it was first used in the early 1900s. New instruments and analysis techniques are continually being developed. The ECG has also been used in combination with other implantable devices, such as pacemakers and defibrillators. The trend has been toward developing smaller, easier-to-use devices that can gather a wealth of information for use in patient diagnosis and treatment.

SOURCES

Alexander, R.W., Schlant, R.C., and Fuster, V. (eds.). (1998) *Hurst's The Heart, Arteries and Veins,* 9th Ed. McGraw-Hill, New York, NY.

Burchell, H.B. (1987) A centennial note on Waller and the first human electrocardiogram. *Am J Cardiol.* 59, 979–983.

Drew, B.J. (1993) Bedside electrocardiogram monitoring. *AACN Clin Issues.* 4, 25–33.

Fye, B.W. (1994) A history of the origin, evolution, and impact of electrocardiography. *Am J Cardiol.* 73, 937–949.

Hurst, J.W. (1998) Naming of the waves in the ECG, with a brief account of their genesis. *Circulation.* 98, 1937–1942.

Jacobson, C. (2000) Optimum bedside cardiac monitoring. *Progr Cardiovasc Nurs.* 15, 134–137.

Johnson, L.R. (ed.). (2003) *Essential Medical Physiology,* 3rd Ed. Elsevier Academic Press, San Diego, CA.

Kossmann, C.E. (1985) Unipolar electrocardiography of Wilson: a half century later. *Am Heart J.* 110, 901–904.

Krikler, D.M. (1987) Historical aspects of electrocardiography. *Cardiol Clin.* 5, 349–355.

Mohrman, D.E. and Heller, L.J. (eds.) (2003) *Cardiovascular Physiology,* 5th Ed. McGraw-Hill, New York, NY.

Rautaharju, P.M. (1987) A hundred years of progress in electrocardiography1: early contributions from Waller to Wilson. *Can J Cardiol.* 3, 362–374.

Scher, A.M. (1995) Studies of the electrical activity of the ventricles and the origin of the QRS complex. *Acta Cardiol.* 50, 429–465.

Wellens, H.J.J. (1986) The electrocardiogram 80 years after Einthoven. *J Am Coll Cardiol.* 3, 484–491.

ON-LINE SOURCES

http://www.lifewatchinc.com/
http://www.medcatalog.com/
http://www.medicalsolutionsinc.com/
http://www.naspe.org/

16 Mechanical Aspects of Cardiac Performance

MICHAEL K. LOUSHIN, MD AND PAUL A. IAIZZO, PhD

CONTENTS

1. INTRODUCTION

This chapter is a review of commonly utilized monitoring techniques performed to assess the function of the general cardiovascular system. Specifically, means to assess arterial blood pressure, central venous pressure, pulmonary artery pressure, mixed venous oxygen saturation, cardiac output, pressure–volume loops, and Frank-Starling curves are described. Basic physiological principals underlying cardiac function are also briefly discussed.

Under normal physiological conditions, the human heart functions as two separate pumps: (1) the right heart pumps blood through the pulmonary circulation, and (2) the left heart pumps blood through the systemic circulation. Each contraction of the heart and subsequent ejection of blood creates pressures that are commonly monitored clinically to assess the function of the heart and its work against resistance. In general, the mechanical function of the heart is described by the changes in pressures, volumes, and flows that occur within a given cardiac cycle. A single cardiac cycle is one complete sequence of myocardial contraction and relaxation.

2. CARDIAC CYCLE

The normal electrical and mechanical events of a single cardiac cycle of the left heart are correlated in Fig. 1. The mechanical events of the left ventricular pressure–volume curve are displayed in Fig. 2. During a single cardiac cycle, the atria and ventricles do not beat simultaneously; the atrial contraction

From: *Handbook of Cardiac Anatomy, Physiology, and Devices*
Edited by: P. A. Iaizzo © Humana Press Inc., Totowa, NJ

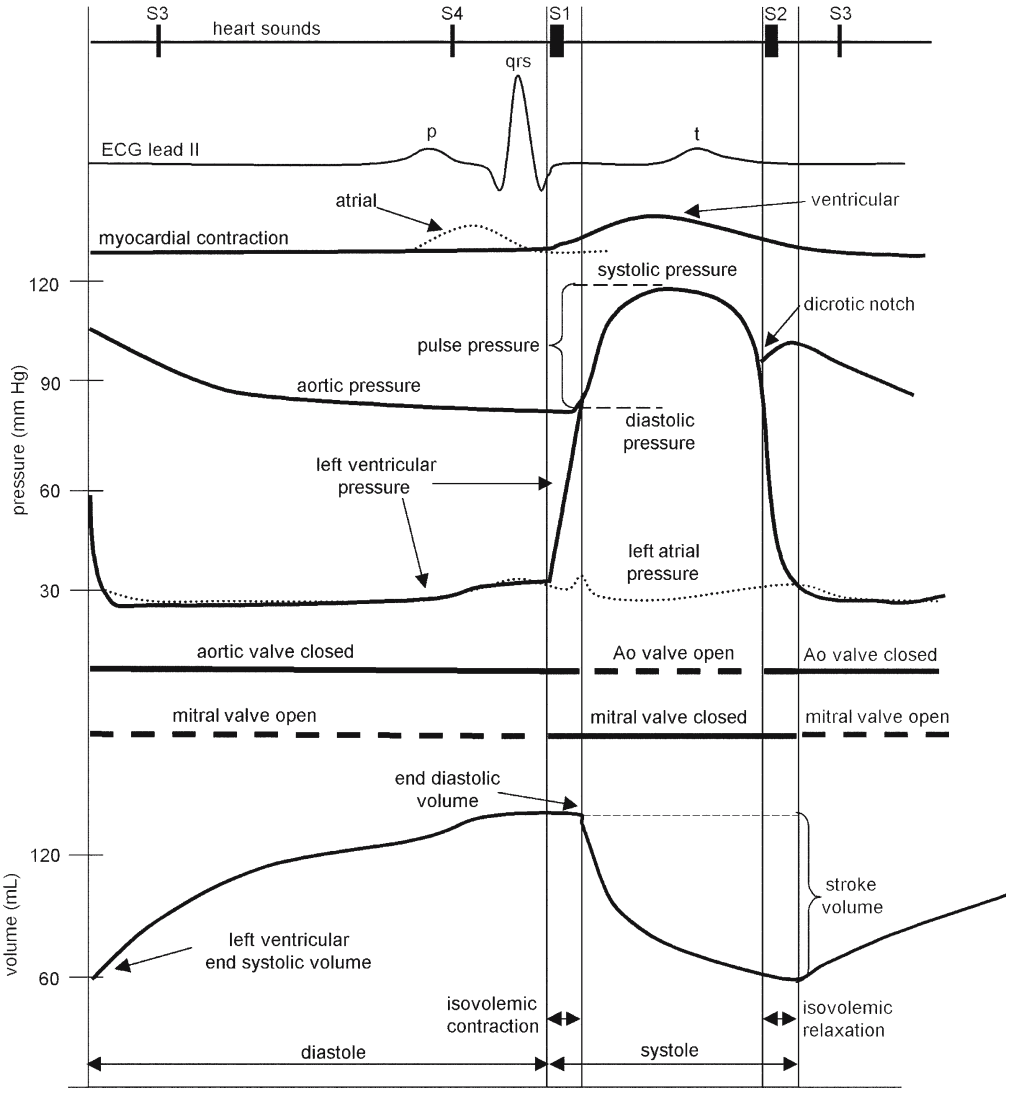

Fig. 1. Electrical and mechanical events of a single cardiac cycle of the left heart (*see* text for details). ECG, electrocardiogram.

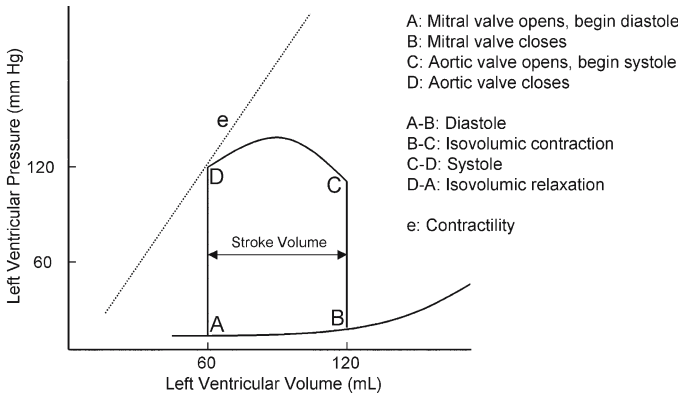

Fig. 2. Pressure–volume diagram of a single cardiac cycle (*see* text for details).

occurs prior to ventricular contraction. This timing delay allows for proper filling of all four chambers of the heart.

Recall that the left and right heart pumps function in parallel. The diastolic phase of the cardiac cycle begins with the nearly simultaneous opening of the tricuspid and mitral valves (atrioventricular valves). The atrioventricular valves open when the pressures in the ventricles fall below those in the atria. This can be observed in Fig. 1 for the left heart, in which the mitral valve opens when the left ventricular pressure falls below the left atrial pressure. At this moment, passive filling of the ventricle begins. In other words, blood that has accumulated in the atria behind the closed atrioventricular valves passes rapidly into the ventricles, and this causes an initial drop in the atrial pressures. Later, pressures in all four chambers rise together as the atria and ventricles continue to fill passively in unison with blood returning to the heart through the veins (pulmonary veins to the left atrium and the superior and inferior vena cava to the right atrium).

Contractions of the atria are initiated near the end of ventricular diastole, which is initiated by depolarization of the

atrial myocardial cells (sinoatrial node). Atrial depolarization is elicited as the P wave of the electrocardiogram (Fig. 1, ECG [electrocardiogram] lead II). The excitation and subsequent development of tension and shortening of atrial cells cause atrial pressures to rise. Active atrial contraction forces additional volumes of blood into the ventricles (often referred to as "atrial kick"). The atrial kick can contribute a significant volume of blood toward ventricular preload (~20%).

At normal heart rates, the atrial contractions are considered essential for adequate ventricular filling. As heart rates increase, atrial filling becomes increasingly important for ventricular filling because the time interval between contractions for passive filling becomes progressively shorter. Atrial fibrillation and/or asynchronized atrial-ventricular contractions can result in minimal contribution to preload via atrial contraction. Throughout diastole, atrial and ventricular pressures are nearly identical because of the open atrioventricular valves, which offer little or no resistance to blood flow. It should also be noted that contraction and movement of blood out of the atrial appendage (auricle) can be an additional source for increased blood volume (preload).

Ventricular systole begins when the excitation passes from the right atrium through the atrioventricular node and through the remainder of the conduction system (His bundle and left and right bundle branches) to cause ventricular myocardial activation. This depolarization of ventricular cells underlies the QRS complex within the ECG (Fig. 1). As the ventricular cells contract, intraventricular pressures increase above those in the atria, and the atrioventricular valves abruptly close. Closure of the atrioventricular valves results in the first heart sound, S1 (Fig. 1). As pressures in the ventricles continue to rise together in a normally functioning heart, they eventually reach a critical threshold pressure at which the semilunar valves (pulmonary valve and aortic valve) open.

The mechanical events of a single cardiac cycle and its pressure–volume relationship are displayed in Fig. 2. The normal time-period between semilunar valve closures and atrioventricular valve openings is referred to as the *isovolumic contraction phase*. During this interval, the ventricles can be considered closed chambers. Ventricular wall tension is greatest just prior to opening of the semilunar valves. Ventricular ejection begins only when the semilunar valves open. In early left heart ejection, blood enters the aorta rapidly and causes the pressure within it to rise. Importantly, pressure builds simultaneously in both the left ventricle and the aorta as the ventricular myocardium continues to contract. This period is often referred to as the *rapid ejection phase*. A similar phenomenon occurs for the right heart; however, the pressures developed and required to open the pulmonary valve are considerably lower.

Pressures in the ventricles and outflow vessels (the aorta and pulmonary arteries) ultimately reach maximum peak systolic pressures. Under normal physiological conditions, the contractile forces in the ventricles diminish after achieving peak systolic pressures. Throughout ejection, there are minimal pressure gradients across the semilunar valves because of the large annular diameters. Eventually, the ventricular myocardium elicits minimal contraction to a point at which intraventricular pressures fall below those in the outflow vessels.

This fall in pressures causes the semilunar valves to close rapidly. Closure of these valves is associated with the second heart sound, S2 (Fig. 1). A quick reversal in both aortic and pulmonary artery pressures is observed at this point because of backpressure filling the semilunar valve leaflets. The backpressure on the valves causes the incisura or dicrotic notch, which can be detected by local pressure recording (e.g., with a locally placed Millar catheter). After complete closure of these valves, the intraventricular pressure falls rapidly, and the ventricular myocardium relaxes. For a brief period, all four cardiac valves are closed, which is commonly referred to as the *isovolumetric relaxation phase*. Eventually, intraventricular pressure falls below the rising atrial pressures, the atrioventricular valve opens, and a new cardiac cycle is initiated.

3. CARDIAC PRESSURE–VOLUME CURVES

Ventricular function can be analyzed and graphically displayed with a pressure–volume diagram. Both systolic and diastolic pressure–volume relationships during a single cardiac cycle are displayed in Fig. 2. Pressure–volume assessment of myocardial function on intact myocardium involves multiple factors, such as preload, afterload, heart rate, and contractility. The area inside the pressure–volume loop is an estimate of the myocardial energy (work = pressure × volume) utilized for each stroke volume (stroke volume = end-diastolic volume – end-systolic volume). The shape of the normal pressure–volume loop changes with alterations in myocardial compliance, contractility, and/or valvular and myocardial disease.

Pressure–volume loops are displayed by plotting ventricular pressure (y axis) against ventricular volume (x axis) during a single cardiac cycle (Fig. 2). Points and segments along the pressure–volume loop correlate with specific mechanical events of the ventricle. The width of the pressure–volume loop is the stroke volume. Myocardial contractility is represented by the slope of the end-systolic pressure–volume relationship; this relationship defines the maximal pressure generated over time with a given myocardial contractility state. Contractility is proportional to change in pressure over time (dP/dt). The passive ventricular filling during diastole is defined by the end-diastolic pressure–volume relationship, and ventricular compliance is inversely proportional to the slope of the end-diastolic pressure–volume relationship.

The effect of heart rate on the pressure–volume relationship cannot be assessed with a single pressure–volume loop. Instead, multiple pressure–volume loops must be obtained to assess effects of heart rate on the pressure–volume loop. By altering variables such as afterload, contractility, and preload, the mechanical events and pressure–volume relationship are displayed.

The pressure–volume diagram shows events of a single cardiac cycle (Fig. 2):

A: Mitral valve opens, begin diastole
B: Mitral valve closes, end diastole
C: Aortic valve opens, begin systole
D: Aortic valve closes, end systole
A–B: Diastole, ventricular filling
B–C: Isovolumic contraction
C–D: Systole, ventricular ejection
D–A: Isovolumic relaxation
e: Contractility slope

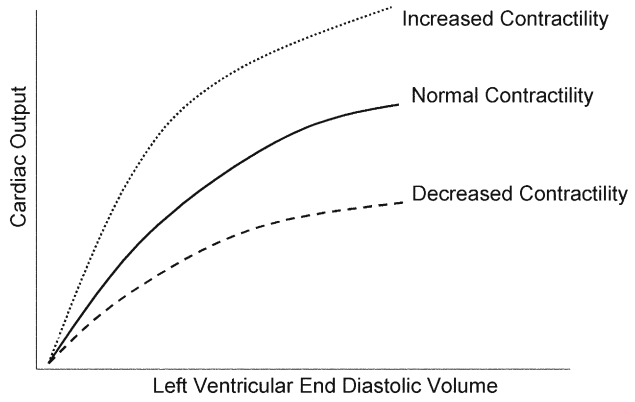

Fig. 3. Frank-Starling relationship. As the end-diastolic volume increases, the cardiac output also increases. Excessive preload may eventually result in decreased cardiac output.

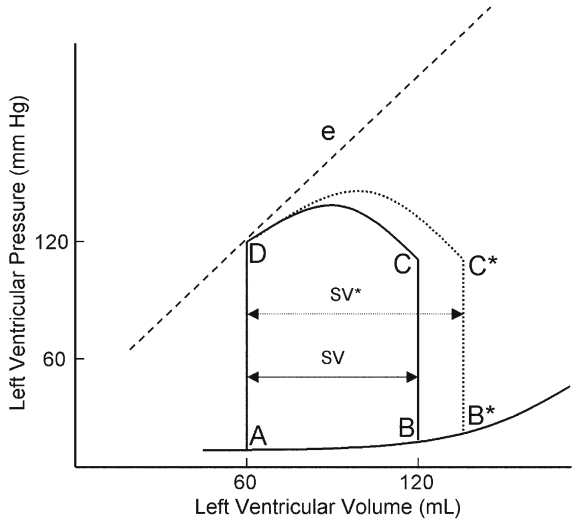

Fig. 4. Effect of acutely increasing preload on the pressure–volume loop. Increasing preload while maintaining normal afterload and contractility results in increased stroke volume (SV*). e, contractility line; SV, stroke volume.

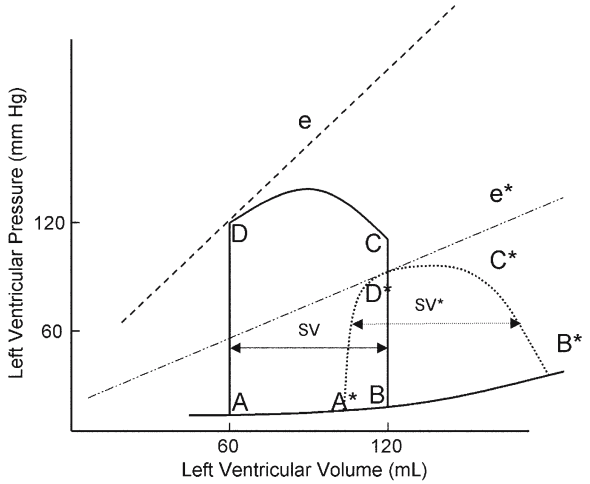

Fig. 5. Effect of ventricular failure on the pressure–volume loop. In heart failure, the myocardium compensates its inability to contract by increasing preload in an attempt to maintain stroke volume. Excessive preload eventually leads to worsening of heart failure. e and e*, contractility lines; SV, stroke volume.

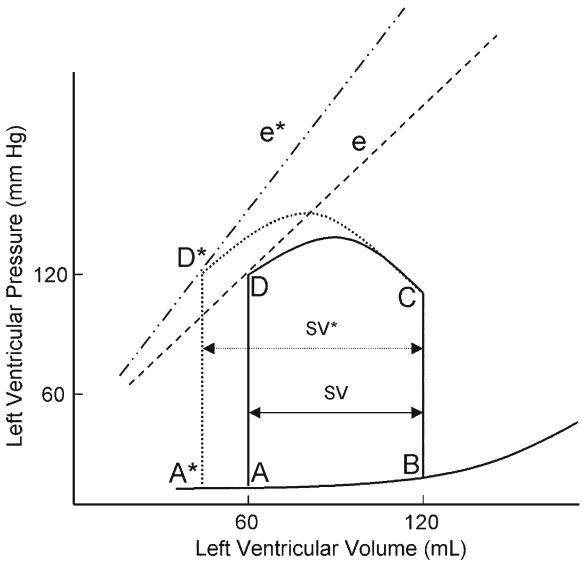

Fig. 6. Effect of acutely increasing contractility on the pressure–volume loop. Increasing contractility while maintaining normal preload and afterload results in increased stroke volume (SV*). Note the increased slope of the contractility line (e*). The area of loop D* is larger, indicating greater myocardial work per stroke volume. e and e*, contractility lines; SV, stroke volume.

4. PRELOAD

Preload is determined by the end-diastolic ventricular volume; it is determined by passive and active emptying of the atrium into the ventricle. Factors that affect this relationship, such as mitral stenosis and ventricular hypertrophy, will affect preload. The Frank-Starling curve displays the relationship between preload and stroke volume; as end-diastolic volume increases, the stroke volume increases until the end-diastolic volume becomes too excessive to allow proper ventricular contraction (Fig. 3).

A pressure–volume loop also displays the relationship between preload and stroke volume (Fig. 4). Preload is the volume of blood in the ventricle at the end of diastole (point B in Fig. 4). An increase in preload is displayed by a right shift of the end-diastolic volume curve (A–B* in Fig. 4). In a normally functioning ventricle, an increase in preload while maintaining normal contractility and afterload results in increased stroke volume (SV* in Fig. 4). Excessive preload will not continue to result in increased stroke volume. Excessive overdistention of the ventricle may result in heart failure (Fig. 5).

5. CONTRACTILITY

Contractility is the ability of the myocardium to pump blood without changes in preload or afterload; it is influenced by intracellular calcium concentrations, the autonomic nervous system, humoral changes, and/or pharmacological agents. A sudden increase in contractility with unchanged preload and afterload will result in increased stroke volume by ejecting more volume out of the ventricle (Fig. 6). The aortic valve opens at the same pressure, and the ventricle ejects blood for-

ward. Increased myocardial contractility forces more blood out of the ventricle during systole, which is displayed by a lower end-systolic volume.

Note the change in SV* (Fig. 6) with increased contractility; the end-systolic volume is lower because of increased contractility, resulting in increased stroke volume. With increased myocardial contractility and unchanged preload, the resulting pressure–volume loop shifts to the left, maintaining normal stroke volume**.** An increase in contractility is graphically displayed by the increase in the slope of line e* in Fig. 6. During ejection, the myocardium contracts from C to D* (Fig. 6). During conditions of lower end-diastolic volume, a normal stroke volume may be maintained by increasing contractility. Administration of inotropes such as dopamine and epinephrine will increase contractility, which assists in maintaining adequate stroke volume during low-contractility states such as heart failure and/or cardiogenic shock.

In heart failure, the myocardium has decreased capacity to pump blood and maintain normal cardiac output. Heart failure may be acute (e.g., acute myocardial infarction, acute cardiogenic shock, or fluid overload), or it may be chronic (e.g., chronic congestive heart failure). In progressive heart failure, the myocardium often compensates its inability to contract by increasing preload and decreasing afterload in an attempt to maintain stroke volume (Fig. 5)

The increase in preload moves the myocardium up the Frank-Starling curve. By increasing end-diastolic volume, normal stroke volume may be maintained. The increase in preload and worsening heart failure eventually lead to ventricular dilation and venous congestion. During heart failure, sympathetic tone increases as levels of circulating norepinephrine and epinephrine attempt to maintain normal cardiac output by increasing contractility and heart rate. The body's compensatory mechanism for heart failure may eventually become counterproductive and thus even worsen the situation.

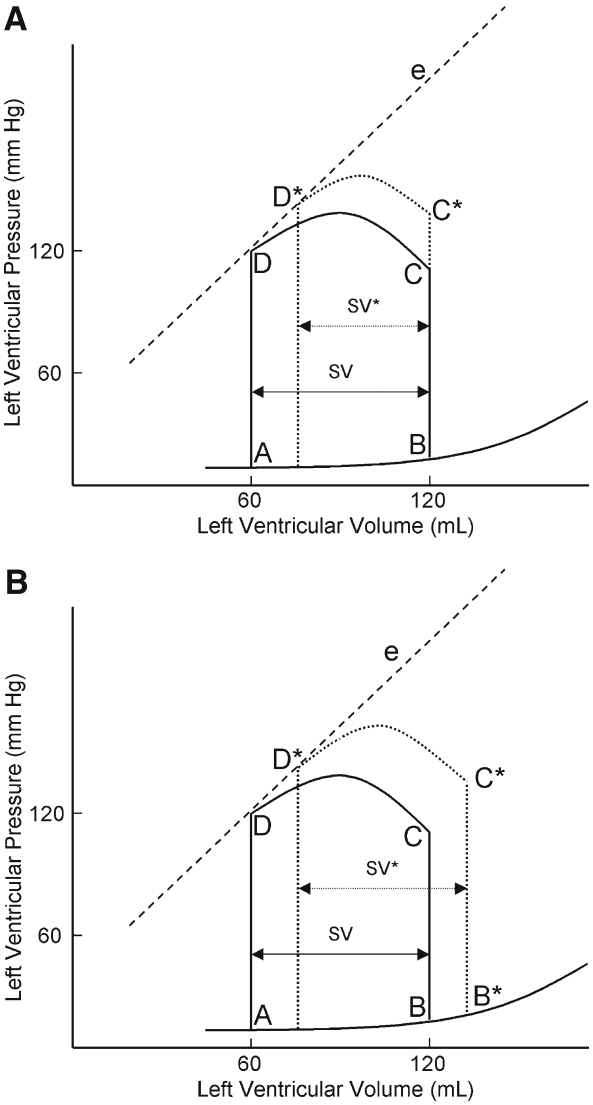

Fig. 7. **(A)** Effect of acutely increasing afterload on the pressure–volume loop. An increase in afterload while maintaining normal contractility and preload results in decreased stroke volume (SV*). A higher pressure is also required before the aortic valve opens (C*). **(B)** Restoration of stroke volume after increasing afterload. An increase in afterload while maintaining normal contractility and preload results in decreased stroke volume (SV*). A higher pressure is also required before the aortic valve opens (C*). e, contractility line; SV, stroke volume.

6. AFTERLOAD

Afterload is another vital component of stroke volume and therefore blood pressure. Afterload is most often equated with ventricular wall tension. Wall tension is also considered as the pressure the ventricle must overcome to eject a volume of blood past the aortic valve. In most normal clinical situations, afterload is assumed to be proportional to systemic vascular resistance. Wall tension is greatest at the moment just before opening of the aortic valve. Wall tension is described by LaPlace's law:

$$\text{Circumferential stress} = Pr/2H$$

where circumferential stress is the wall tension, P is the intraventricular pressure, r is the ventricular radius, and H is the wall thickness.

An increase in afterload requires ventricular pressure to increase during isovolumic contraction before the aortic valve opens (Fig. 7). Because of the increase in afterload, the ability of the ventricle to eject blood is decreased. This results in decreased stroke volume (SV* in Fig. 7A) and increased end-systolic volume (B* in Fig. 7B). If afterload remains increased, the myocardium establishes a new steady state that is shifted to the right, and stroke volume is restored. A patient with severe aortic stenosis will likely elicit a pressure–volume loop as in Fig. 7. The myocardium usually compensates by increasing contractility to maintain adequate stroke volume. Patients with hemodynamically significant aortic stenosis often develop left ventricular hypertrophy.

Afterload may be inversely related to cardiac output. In a dysfunctional myocardium, such as with congestive heart failure, stroke volume decreases with increases in afterload. Increases in afterload also requires the myocardium to expend more energy to eject blood during systole.

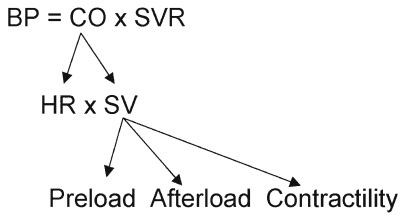

Fig. 8. Blood pressure monitoring. Blood pressure is proportional to the product of cardiac output and systemic vascular resistance. BP, blood pressure; CO, cardiac output ; HR, heart rate; SV, stroke volume; SVR, systemic vascular resistance.

7. BLOOD PRESSURE MONITORING

The cardiovascular system is most commonly assessed by monitoring arterial blood pressure. Blood pressure is proportional to the product of cardiac output and systemic vascular resistance:

$$BP = CO \times SVR$$
$$CO = HR \times SV$$
$$MAP = 1/3\ SBP + 2/3\ DBP$$

where BP is blood pressure, CO is cardiac output, SVR is systemic vascular resistance, HR is heart rate, SV is stroke volume, MAP is mean arterial pressure, SBP is systolic blood pressure, and DBP is diastolic blood pressure. Stroke volume is dependent on preload, afterload, and contractility (Fig. 8).

Blood pressure can be defined to consist of three components: systolic blood pressure, mean arterial pressure (MAP), and diastolic blood pressure. Systolic blood pressure is the peak pressure during ventricular systole, MAP is used clinically as a crucial determinant for adequate perfusion of the major organs, and diastolic blood pressure is the main determinant for myocardial perfusion. Recall that the majority of coronary blood flow occurs during diastole.

In general, arterial blood pressure monitoring involves two techniques: noninvasive (indirect) and invasive (direct) methods. The decision to utilize either blood pressure monitoring method depends on multiple factors such as cardiovascular stability or instability, need for frequent arterial blood samples, frequency of blood pressure recordings, or major surgery and trauma. One of the advantages of an invasive blood pressure monitor is that it provides continuous, beat-to-beat blood pressures (*see JPEG 1* on the Companion CD). Direct arterial blood pressure monitoring is considered a requirement during cardiopulmonary bypass surgery. Because there is no pulsatile flow during such surgery, the noninvasive methods to monitor blood pressure cannot be employed.

7.1. Noninvasive Arterial Blood Pressure Monitoring

Noninvasive blood pressure assessment is the most utilized and simplest technique to monitor arterial blood pressure. This technique utilizes a blood pressure cuff and the principle of pulsatile flow. A blood pressure cuff is applied to a limb such as forearm or leg and is inflated to a pressure greater than systolic blood pressure, which stops blood flow distal to the inflated cuff. As the pressure in the cuff is gradually decreased, blood flow through the artery is restored. The change in arterial pressure and flow creates oscillations that can be detected by auscultation of Korotkoff sounds and oscillometric methods.

For accurate blood pressure measurement, the width of the cuff should be approximately one-third the circumference of the limb. A small, improper size cuff will overestimate systolic blood pressure; a large cuff will underestimate the pressure. The rate of cuff deflation should be slow enough to hear Korotkoff sounds or detect oscillations. Noninvasive blood pressure monitors do not work if there is no pulsatile flow.

The automated method of noninvasive blood pressure monitoring is the oscillometric technique. Oscillometric blood pressure monitors are basically composed of oscillotonometers and a microprocessor. The blood pressure cuff is inflated until no oscillation is detected. As the cuff pressure is decreased, flow in the distal blood vessel is restored, and the amplitude of oscillations increases. A large increase in arterial wave oscillation amplitude is recorded as systolic blood pressure, the peak oscillation as MAP, and the sudden decrease in amplitude as diastolic blood pressure (Fig. 9). Because of the relative sensitivity of such a monitoring system, the MAP is usually the most accurate and reproducible measurement. For more details on such monitoring, refer to Chapter 14.

7.2. Invasive Arterial Blood Pressure Monitoring

Continuous blood pressure monitoring is best accomplished by direct intraarterial blood pressure monitoring. Direct pressure monitoring allows for continuous, beat-to-beat monitoring of arterial pressure, and the recorded arterial waveform provides information relative to cardiovascular function. Direct pressure monitoring is often obtained in clinical settings such as major trauma and vascular surgery, sepsis, and cardiopulmonary bypass, for which there is no pulsatile flow. Further, patients with significant cardiopulmonary disease may require invasive arterial blood pressure monitoring (Table 1).

As noted, besides providing blood pressure information, the arterial waveform also presents information about cardiovascular function. For example, the upstroke of an arterial waveform correlates with myocardial contractility (dP/dT), and the downstroke gives information relative to peripheral vascular resistance. The position of the dicrotic notch gives insights regarding the systemic vascular resistance; e.g., a low dicrotic notch position on the arterial waveform may infer low vascular resistance, and a high dicrotic notch usually relates to higher systemic vascular resistance. Furthermore, by integrating the area under the curve of the arterial waveform, the stroke volume may also be estimated.

Direct arterial blood pressure monitoring typically involves cannulation of a peripheral artery and transducing the pressure (*see JPEG 2*, *JPEG 3* on the Companion CD). An indwelling arterial catheter is connected to pressure tubing containing saline; this tubing is connected to a pressure transducer and monitoring system. Typical transducers contain strain gauges (strain wires or silicon crystals) that distort with changes in blood pressure. The strain gauges typically contain a variable-resistance transducer and a diaphragm that links the fluid wave to electrical signals. When the transducer diaphragm is distorted, there is a change in voltage across resis-

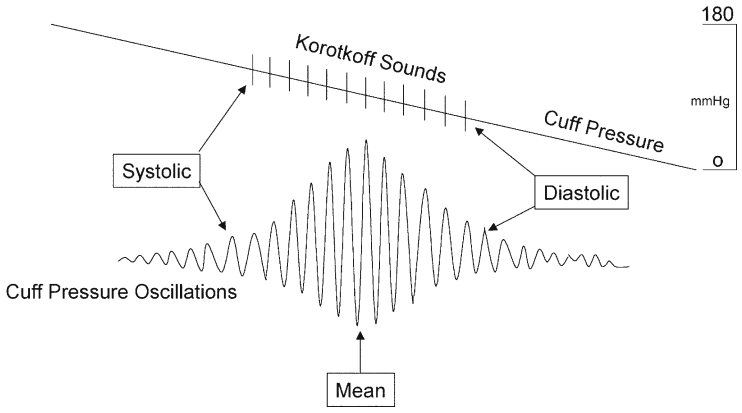

Fig. 9. Noninvasive blood pressure monitoring. As blood flow is restored with release of the blood pressure cuff, the arterial wave oscillations increase. The increase in oscillation amplitudes is associated with systolic blood pressure and presence of Korotkoff sounds. The peak of oscillations is associated with mean arterial pressure. Return of oscillations to baseline is diastolic blood pressure and end of Korotkoff sounds.

Table 1
Relative Indications for Direct Arterial Blood Pressure Monitor

- Major surgery
- Major trauma
- Major vascular (i.e., carotid endarterectomy, aortic aneurysm)
- Cardiopulmonary bypass surgery
- Myocardial dysfunction (i.e., myocardial ischemia/infarct, heart failure, dysrhythmias)
- Uncontrolled/labile blood pressure (i.e., hypertension, hypotension)
- Inaccurate noninvasive monitor (i.e., morbid obesity)
- Sepsis/shock
- Pulmonary dysfunction

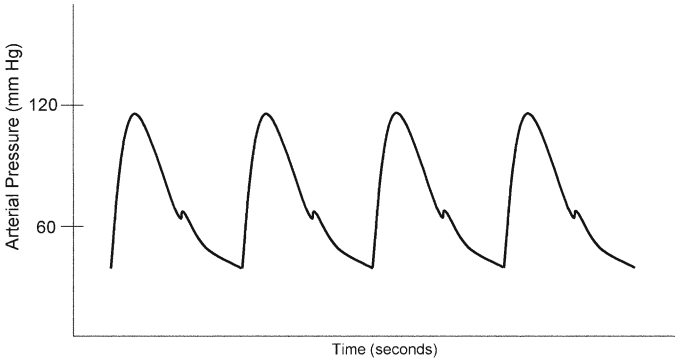

Fig. 10. Arterial blood pressure wave. A typical optimally damped arterial blood pressure waveform. The peak portion of the waveform corresponds to the systolic blood pressure and the trough corresponds with the diastolic blood pressure. The dicrotic notch is associated with closing of the aortic valve. Information about cardiovascular function can be estimated from the waveform. The upstroke correlates with myocardial contractility. The downstroke and position of the dicrotic notch give information about systemic vascular resistance. The stroke volume is estimated by integrating the area under the curve.

tors of a Wheatstone bridge circuit (*see JPEG 4* on the Companion CD).

The transducer is constructed using such a circuit so that voltage output can be calibrated proportional to the blood pressure. Standard pressure transducers are calibrated to 5 μV per volt excitation per millimeter of mercury *(1)*. Commonly, the electrical signals from such pressure-monitoring systems are filtered, amplified, and displayed on a monitor, thus providing a typical arterial pressure waveform. It is important that the arterial pressure transducer be positioned and calibrated accurately at the level of the heart; an improper transducer height will result in inaccurate blood pressures. If the pressure transducer is positioned too high, the blood pressure is underestimated; a lower positioned transducer will overestimate the actual blood pressure.

Typical clinical sites for intraarterial cannulation for arterial pressure monitoring are the radial, brachial, axillary, or femoral arteries. Although the ascending aorta is the ideal place to monitor arterial pressure waveforms, this is not practical in most clinical settings. However, it should be noted that pressure measurements in the more peripheral arteries become distorted when compared to central aortic pressure waveform (Fig. 10). Peripherally, the systolic blood pressure may be higher and diastolic blood pressure lower, and the MAP is usually similar to central aortic pressure.

The pressure waveform becomes more distorted as pressure is measured farther away from the aorta. This distortion is caused by a decrease in arterial compliance and reflection and oscillation of the blood pressure waves. For example, an arterial pressure wave monitored from the dorsalis pedis will be significantly different from a central aortic wave when it is graphically displayed (Fig. 11). There is also a loss in amplitude or absence of the dicrotic notch, an increase in systolic blood pressure, and a decrease in diastolic blood pressure. One should also be aware of the possible appearance of a reflection wave as the blood pressure is monitored from a peripheral site. Importantly, risks associated with an indwelling intraarterial pressure catheter include thrombosis, emboli, infection, nerve injury, and hematoma.

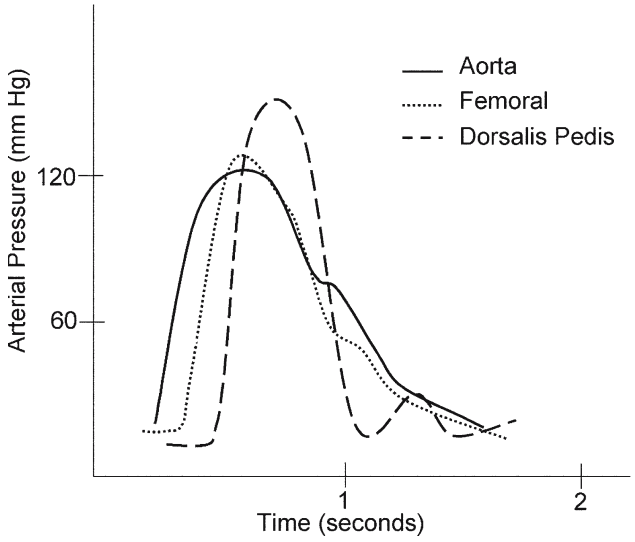

Fig. 11. Arterial pressure wave. The arterial waveform is recorded from the ascending aorta. As the pressure monitoring site is moved more peripherally, the morphology of the waveform changes because of changes in arterial wall compliance as well as oscillation and reflection of the arterial pressure wave. Notice in the dorsalis pedis arterial waveform the absence of the dicrotic notch, overestimation of systolic blood pressure, and underestimation of diastolic pressure. Also note the presence of a small reflection wave.

8. PRESSURE TRANSDUCER SYSTEM

In clinical settings, arterial and venous blood pressures and waveforms are displayed using a pressure transducer monitoring system. A typical pressure transducer monitoring system includes: (1) an indwelling intravascular catheter; (2) pressure tubing; (3) a pressure transducer; (4) a stopcock and flush valve; (5) a high-pressure fluid bag; and (6) a graphical display monitor and microprocessor (Fig. 12A,B).

The pressure wave derived from the transducer system is a summation of sine waves at different frequencies and amplitudes. The fundamental frequency (first harmonic) is equal to the heart rate. Therefore, at a heart rate of 120 beats/min, the fundamental frequency is 2 Hz. Because the first 10 harmonics of the fundamental frequency make significant contributions to the arterial waveform *(2)*, frequencies up to 20 Hz make major contributions to the pressure waveform. The maximum significant frequency in the arterial blood pressure signal is approx 20 Hz *(3)*.

All materials have a natural frequency, also known as the *resonant frequency*. The natural frequency of the monitoring system is the frequency at which the pressure-monitoring system resonates and amplifies the actual blood pressure signal *(3,4)*. If the natural frequency of the system is near the fundamental frequency, the blood pressure waveform will be amplified, giving an inaccurate pressure recording. The natural frequency is defined by the following equation *(5)*:

$$fn = (d/8) * (3/\pi L \rho Vd) \text{ ^1/2}$$

$$\varsigma = (16n/d \text{ ^3}) * (3LVd/\pi\rho) \text{ ^1/2 (damping coefficient)}$$

where fn is the natural frequency, d is the tubing diameter, n is the viscosity of fluid, L is the tubing length, ρ is the density of fluid, and Vd is the transducer fluid volume displacement.

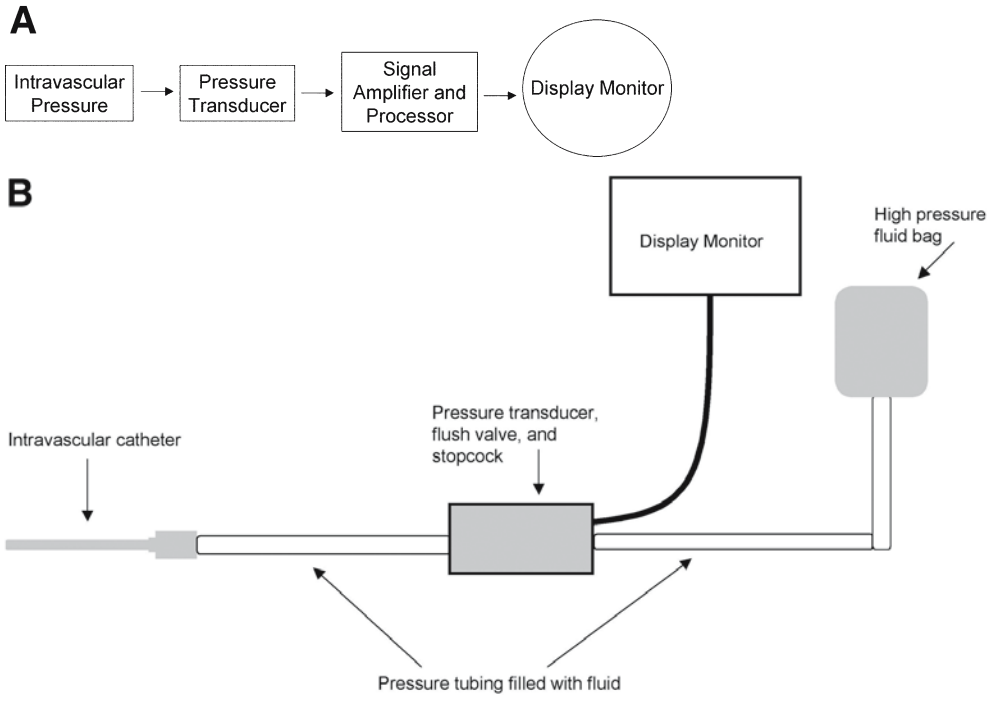

Fig 12. **(A)** and **(B)** Schematics of a pressure transducer monitoring system (*see* text for details).

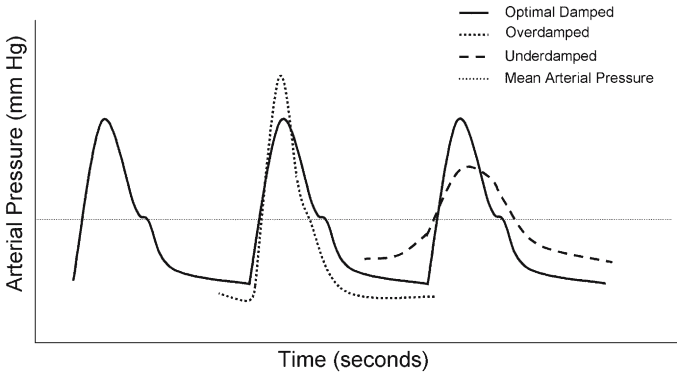

Fig. 13. Effect of damping on the arterial pressure wave. In an underdamped pressure-monitoring system, the pressure wave overestimates the systolic blood pressure and underestimates the diastolic blood pressure. In an overdamped system, the pressure wave underestimates the systolic blood pressure and overestimates the diastolic blood pressure. The mean arterial pressure remains essentially unchanged.

To increase accuracy of the blood pressure waveform assessment, the natural frequency needs to be increased as the amount of distortion is reduced. The optimal natural frequency should be at least 10 times the fundamental frequency, which is then greater than the 10th harmonic of the fundamental frequency *(2,3)*. Therefore, the natural frequency should be greater than 20 Hz. In clinical settings, the input frequency is usually close to the monitoring system's natural frequency, which ranges from 10 to 20 Hz. When the input frequency is close to the natural frequency, the system amplifies the actual pressure signal. Ideally, the natural frequency should exceed the maximum significant frequency in a blood pressure signal, which is about 20 Hz *(3)*. An amplified system typically requires damping to minimize distortion; yet, an underdamped system will result in amplification, and an overdamped system will result in reduced amplification.

The ability of the system to extinguish oscillations through viscous and frictional forces is the damping coefficient ς *(6)*. Some degree of damping may be required to prevent overamplifications of blood pressure waveform. More damping may be required, especially in patients with higher heart rates, such as neonates. At higher heart rates, the 10th harmonic of the fundamental frequency will approach the natural frequency, and the waveform is amplified. Overamplification, or ringing, can be adjusted by increasing the damping coefficient. Specifically, in an overamplified system, a connector with an air bubble can intentionally be placed in line with the pressure transducer; the air bubble serves to damp the system to diminish ringing.

The accuracy of pressure transducers is considered optimal in the following situations: low compliance of the pressure catheter and tubing, low density of fluid in the pressure tubing, and short tubing with a minimal number of connectors. Note that a suboptimal pressure system may produce an underdamped or overdamped pressure waveform; an underdamped waveform will overestimate systolic blood pressure, and an overdamped waveform will underestimate systolic blood pressure.

Damping occurs when factors such as compliance of tubing, air bubbles, and blood clots decrease the peaks and troughs of the pressure sine waves by absorbing energy and diminish the waveform. In an underdamped system, the pressure waves can generate additive harmonics, which may also lead to an overestimated blood pressure. In an overdamped system, a pressure wave may be impeded from adequately propagating forward. Overdamping may occur because of air bubbles in the pressure lines, kinks, blood clots, low-flush bag pressures, and multiple stopcocks or injection ports. This often results in underestimation of systolic blood pressure and overestimation of diastolic blood pressure. Fortunately, the MAP in all such situations is minimally affected by dampening (Fig. 13).

Optimal pressure waveforms can be obtained when there is balance between the degree of damping and distortion from the pressure tubing system. A simple way to assess damping is to observe the results from a high-pressure fluid flush. In such a flush test, the pressure transducer system is flushed, and the resulting oscillations (ringing) are observed. In an optimally damped system, baseline results after one oscillation (Fig. 14). In an overdamped system, the baseline is reached without oscillations, and the waveform is blunted. In an underdamped system, the flush test results in multiple oscillations, before the waveform returns to baseline.

9. CENTRAL VENOUS PRESSURE MONITORING

An estimate of intravascular volume status and right heart function can be assessed with a central venous pressure catheter. Central venous pressure is ideally considered as the mean venous blood pressure at the junction of the right atrium and the inferior and superior venae cavae. The central venous pressure (Tables 2 and 3) is an estimate of right heart filling pressures and may be used to assess both right heart function and the circulating blood volume.

The central venous pressure is dependent on multiple factors, such as intravascular volume, functional capacitance of veins, and status of the right heart. A limitation of central venous pressure monitoring is that it does not give direct information about the left heart. Indications for central venous catheter placement may include monitoring of cardiac filling pressures, administration of drugs, and/or rapid infusion of large amounts of fluids (Table 4).

A typical central venous pressure kit is shown in *JPEG 5* (*see JPEG 5* on the Companion CD). It is critical to calibrate and position the pressure transducer system properly at the level of the right atrium. Because the numeric value of central venous pressure is small (2–12 mmHg), minor changes in transducer height will cause significant inaccuracies in central venous pressure assessment.

There are multiple sites for placement of central venous catheters. Common sites used in clinical practice are the internal jugular and subclavian veins (*see JPEG 6* on the Companion CD). Central venous access is also accomplished by placement of a long catheter via the antecubital, external jugular, and femoral veins. Complications of central venous catheter placement may include inadvertent arterial puncture (i.e., carotid and subclavian arteries), venous air embolism, pneumothorax, chylothorax, loss of guide wire, nerve injury, cardiac dysrhythmias, and/or infections.

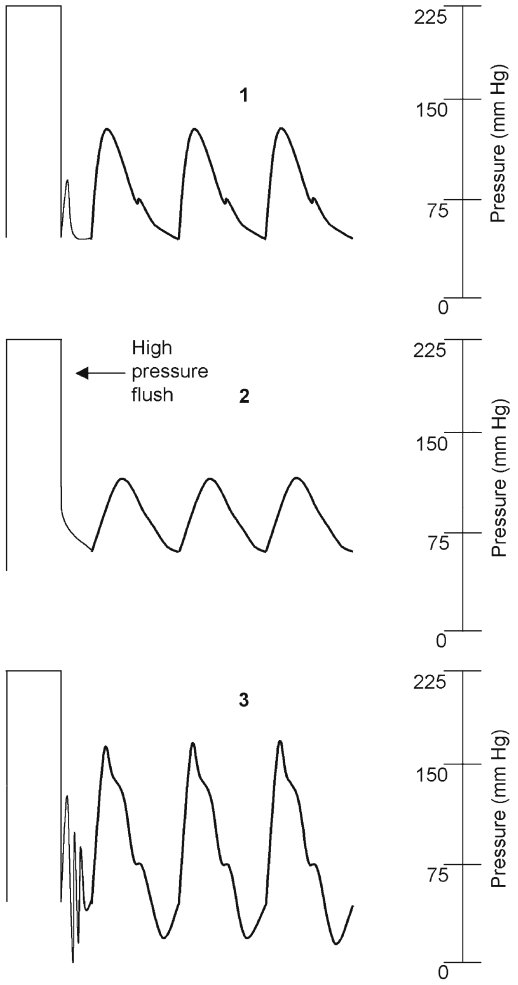

Fig. 14. High-pressure flush test**. 1**, In an optimally damped pressure-monitoring system, the pressure wave returns to baseline after one oscillation. **2**, In an overdamped system, the wave returns to baseline without any oscillations. The systolic blood pressure is underestimated and diastolic pressure overestimated. **3**, In an underdamped system, the wave oscillates multiple times before returning to baseline. The arterial wave is amplified. The systolic pressure is overestimated and diastolic pressure underestimated. The mean arterial pressure usually is not significantly affected by overdamping or underdamping.

Table 2
Intracardiac Pressures

Pressures	*Mean*	*Range*
Left atrium	8	4–12
Left ventricle systolic	125	90–140
Left ventricle end-diastolic	8	4–12
Right atrium	5	2–12
Right ventricle systolic	25	15–30
Right ventricle end-diastolic	5	0–10
Pulmonary artery systolic	23	15–30
Pulmonary artery diastolic	10	5–15
Pulmonary capillary wedge	10	5–15
Mean pulmonary artery	15	10–20

Table 3
Cardiac Hemodynamic Parameters

Parameter	*Derived formula*	*Range*
CO	HR × SV	4–6 L/min
CI	CO/BSA	2.6–4.3 L/min/m^2
SV	CO × 1000/HR	50–120 mL/beat
SI	SV/BSA	30–65 mL/beat/m^2
SVR	(MAP – CVP) × 80/CO	800–1400 dyne s cm^{-5}
SVRI	(MAP – CVP) × 80/CI	1500–2300 dyne s $cm^{-5}m^2$
PVR	(PAP – PCWP) 80/CO	140–250 dyne s cm^{-5}
PVRI	(PAP – PCWP) 80/CI	240–450 dyne s $cm^{-5}m^2$
LVSWI	1.36 (MAP – PCWP) SI/100	45–60 g m/m^2
RVSWI	1.36 (PAP – CVP) SI/100	5–10 g m/m^2

BSA, body surface area; CI, cardiac index; CO, cardiac output; CVP, central venous pressure; HR, heart rate; LVSWI, left ventricular stroke work index; MAP, mean arterial pressure; PAP, pulmonary artery pressure; PCWP, pulmonary capillary wedge pressure; PVR, pulmonary vascular resistance; PVRI, pulmonary vascular resistance index; RVSWI, right ventricular stroke work index; SI, stroke index; SV, stroke volume; SVR, systemic vascular resistance; SVRI, systemic vascular resistance index.

There are multiple types of central venous catheters, ranging from a single lumen to multiple lumen (double, triple, quad lumens) catheters. Typically, multilumen catheters have slower flow rates because of the smaller radii of incorporated lumens. Recall that resistance to flow is proportional to the fourth power of the radius.

After placement of a central venous pressure catheter, all ports must be aspirated and flushed to confirm proper intravascular placement. In clinical practice, a chest x-ray is often obtained to confirm proper positioning of such a catheter. If a pneumothorax develops after accidental puncture of a lung, it will also be evident on chest x-ray.

The central venous pressure waveform gives important information about the mechanical events occurring during a cardiac cycle (Fig. 15). An *a* wave is caused by atrial contraction that occurs after the P wave on the ECG. The *c* wave occurs during the start of ventricular systole as the tricuspid valve is pushed up toward the right atrium. The next portion of the waveform is the *x* descent, which represents the tricuspid valve being pulled down toward the right ventricle in late systole. The *v* wave correlates with passive filling of the right atrium while the tricuspid valve is closed. The *y* descent completes the waveform and represents the opening of the tricuspid valve, passive emptying of the right atrium, and filling of the right ventricle during diastole.

The central venous pressure waveform provides information primarily concerning the right heart. Yet, the same waveform can be observed for the left heart by recording the pulmonary capillary wedge pressure from a pulmonary artery catheter (discussed in Section 10). The central venous pressure waveform is affected by respirations; thus, it should be read at end expiration. The central venous pressure value is typically defined as the mean venous pressure at the end of exhalation during spontaneous or controlled ventilation. At end expiration, the intrathoracic pressure is closest to atmospheric pressure.

There are multiple clinical conditions that will affect the recorded central venous pressure waveform. For example, tricuspid stenosis may result in large ("cannon") *a* waves

Table 4
Relative Indications for Central Venous Pressure Catheter

- Large fluid shifts
- Vascular access
- Infusion of medication
- Venous blood sampling
- Major trauma and surgery
- Monitoring of intravascular volume status
- Aspiration of venous air embolus

Table 5
Relative Indications for Pulmonary Artery Catheter

- Major organ transplant (liver, heart, lung)
- Cardiopulmonary bypass surgery
- Pulmonary hypertension
- Sepsis/shock
- Aortic aneurysm surgery
- Heart failure (right and/or left heart)
- Pulmonary embolus

See ASA Guidelines for more detailed indications and contraindications *(35)*.

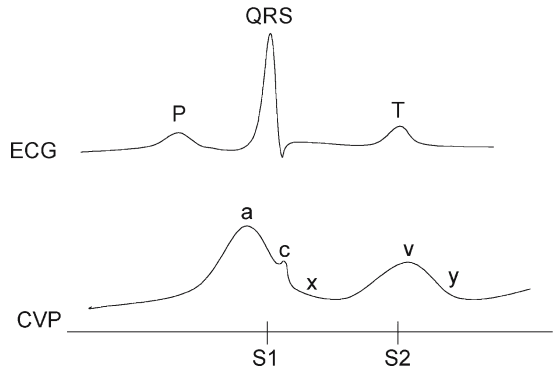

Fig. 15. Central venous pressure wave. The central venous pressure waveform consists of *a*, *c*, *v* waves and *x* and *y* descents. The *a* wave is associated with atrial contraction. The *c* wave occurs as the tricuspid valve bulges up toward the right atrium during early ventricular systole. The *v* wave is associated with passive filling of the right atrium with closed valve. The *x* descent corresponds to the tricuspid valve being pulled down toward the right ventricle during late systole. The *y* descent corresponds with opening of the tricuspid valve as the right atrium begins to empty. CVP, central venous pressure; ECG, electrocardiogram. S1, heart sound 1; S2, heart sound 2.

(Fig. 16) as the right atrium contracts and pushes blood past a stenotic valve. Abnormal cardiac nodal rhythms, ventricular arrhythmias, or heart block will result in cannon *a* waves because the atrium and ventricle are not synchronized and the atrium may be contracting against a closed tricuspid valve. Large *a* waves may also occur when the resistance to right atrium emptying is significantly increased, as in tricuspid and pulmonary valve stenosis, right ventricular hypertrophy, or pulmonary artery hypertension.

Regurgitant valve disorders such as tricuspid regurgitation will result in large *v* waves (Fig. 17), representing overfilling of the atrium. Specifically, the large *v* wave occurs as blood volume from the right ventricle, during systole, backflows into the right atrium past the incompetent tricuspid valve. A noncompliant right ventricle, as in ischemia and heart failure, may also result in large *v* waves. During atrial fibrillation, *a* waves are absent because of ineffective atrial contractions. Again, similar waveforms for the left heart are seen from a pulmonary capillary wedge pressure waveform. Diagrams of cannon *a* and *v* waves are displayed in Figs. 16 and 17.

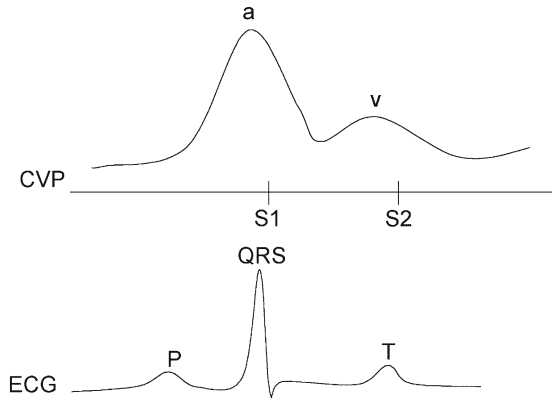

Fig. 16. Cannon *a* waves. A severely stenotic tricuspid valve or a junctional rhythm (atrium contracting against a closed tricuspid valve) causes a large a wave. The mechanical events of the waveform must be correlated with the electrical events of the electrocardiogram (ECG). CVP, central venous pressure. S1, heart sound 1; S2, heart sound 2.

10. PULMONARY ARTERY PRESSURE MONITORING

The pulmonary artery catheter was first introduced into clinical practice by Swan and Ganz *(7)*. Since its introduction, the pulmonary artery catheter is often used in the management of critically ill patients and in those undergoing major cardiac surgery (Table 5). Yet, the effectiveness of pulmonary artery catheter monitors and their effect on patient morbidity and mortality continues to be debated and researched *(8)*. Current modifications also allow for continuous monitoring of pulmonary artery pressures, cardiac outputs, central venous pressures, mixed venous oxygen saturations (S_VO_2), and pulmonary

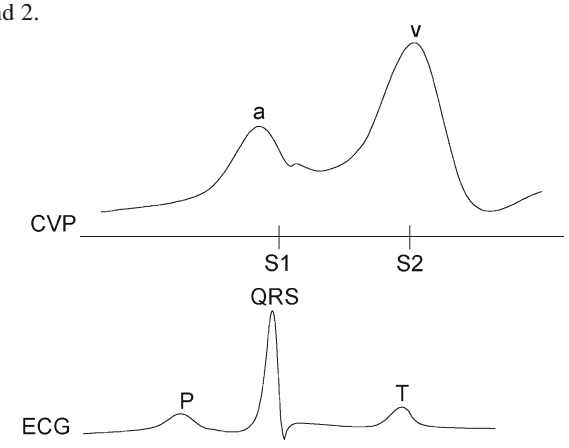

Fig. 17. Cannon *v* waves. An incompetent tricuspid valve (tricuspid regurgitation) abolishes the *x* descent and causes cannon *v* waves as volume from the right ventricle backflows into the right atrium during ventricular systole. CVP, central venous pressure; ECG, electrocardiogram. S1, heart sound 1; S2, heart sound 2.

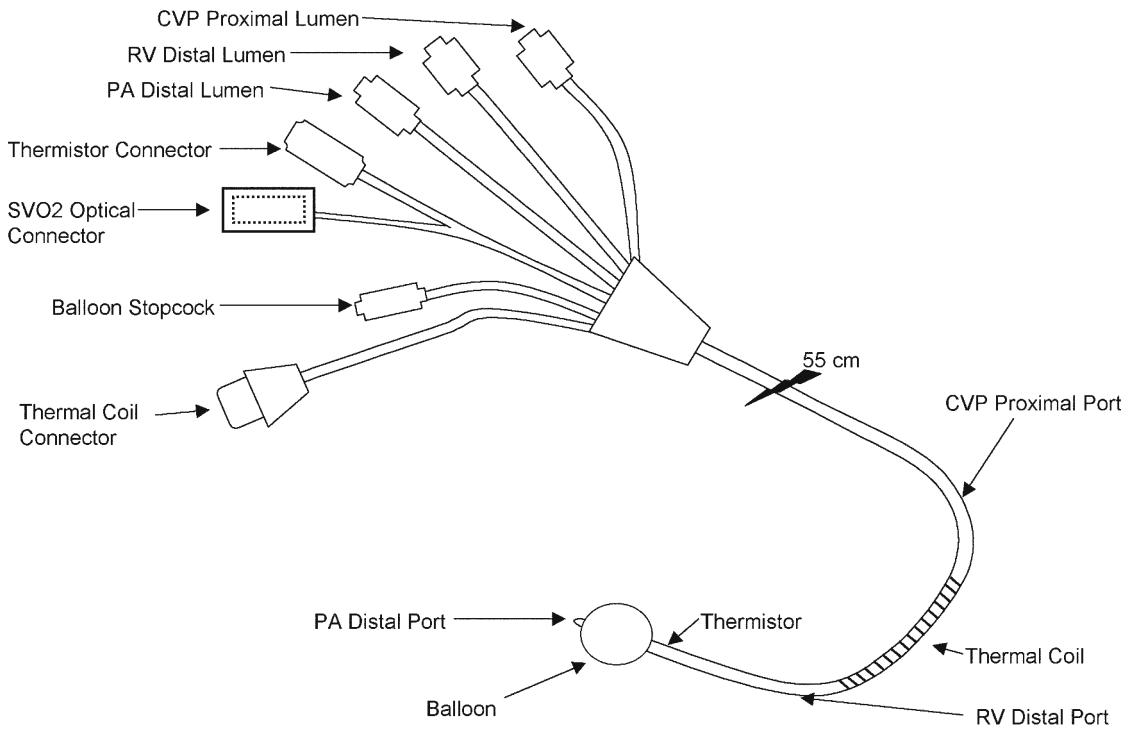

Fig. 18. Pulmonary artery catheter. A diagram of a typical pulmonary artery catheter with continuous cardiac output and mean venous oxygen saturation monitoring capabilities. Notice the addition of the thermal coils, thermistors, and optical components to the catheter. CVP, central venous pressure; PA, pulmonary artery; RV, right ventricle; S_VO2, venous oxygen saturation. Diagram courtesy of Sock Lake Group LLC, Roseville, MN.

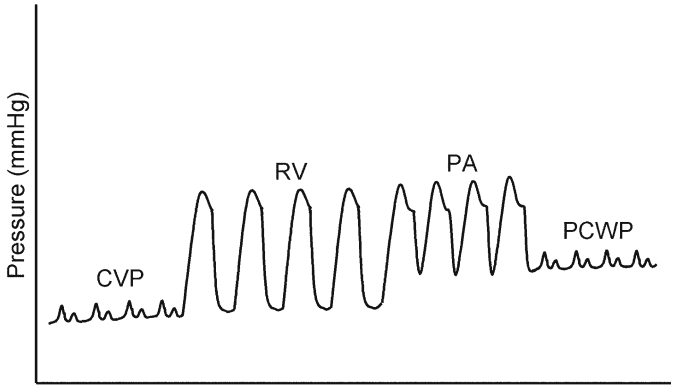

Fig. 19. Right heart blood pressure waveforms. As the pulmonary artery catheter is floated into the distal pulmonary artery, the morphology of the pressure waves changes as it goes through the chambers of the heart. CVP, central venous pressure; PA, pulmonary artery pressure; PCWP, pulmonary capillary wedge pressure; RV, right ventricle pressure.

capillary wedge pressures (Fig. 18 [*see JPEG 7* on the Companion CD]).

One of the advantages of the pulmonary artery catheter is that blood pressure information associated with the left heart may also be obtained via the pulmonary capillary wedge pressure. Under conditions of normal pulmonary physiology and left ventricular function and compliance, the pulmonary capillary wedge pressure is proportional to the left ventricular end-diastolic pressure, which is proportional to left ventricular end-diastolic volume. Left ventricular preload is best estimated by left ventricular end-diastolic volume:

$$CVP \sim PAD \sim PCWP \sim LAP \sim LVEDP \sim LVEDV$$

where CVP is the central venous pressure, PAD is the pulmonary artery diastolic pressure, PCWP is the pulmonary capillary wedge pressure, LAP is the left atrial pressure, LVEDP is the left ventricular end-diastolic pressure, and LVEDV is the left ventricular end-diastolic volume.

Typically, after establishing central venous access, a pulmonary artery catheter is "floated" into the pulmonary artery with the catheter balloon inflated (*see* MPEG of pulmonary artery catheter on the Visible Heart® CD). The location of the pulmonary artery catheter balloon is monitored by analysis of the waveform as the catheter is floated from the vena cava to the right atrium, to the right ventricle, and ultimately into the pulmonary artery (Fig. 19). Once the catheter is in the pulmonary artery, it is advanced further until the balloon wedges into a distal arterial branch of the pulmonary artery (Fig. 20). The mean pressure and waveform are the pulmonary capillary wedge pressure. Under normal physiological conditions, this pressure correlates well with the left atrial pressure. However, the pulmonary artery catheter balloon should not be kept inflated for long durations or kept in wedged position because of the possibility of this causing pulmonary artery rupture.

Whenever the catheter is advanced, the balloon (*see JPEG 8* on the Companion CD) should be inflated, and when it is pulled

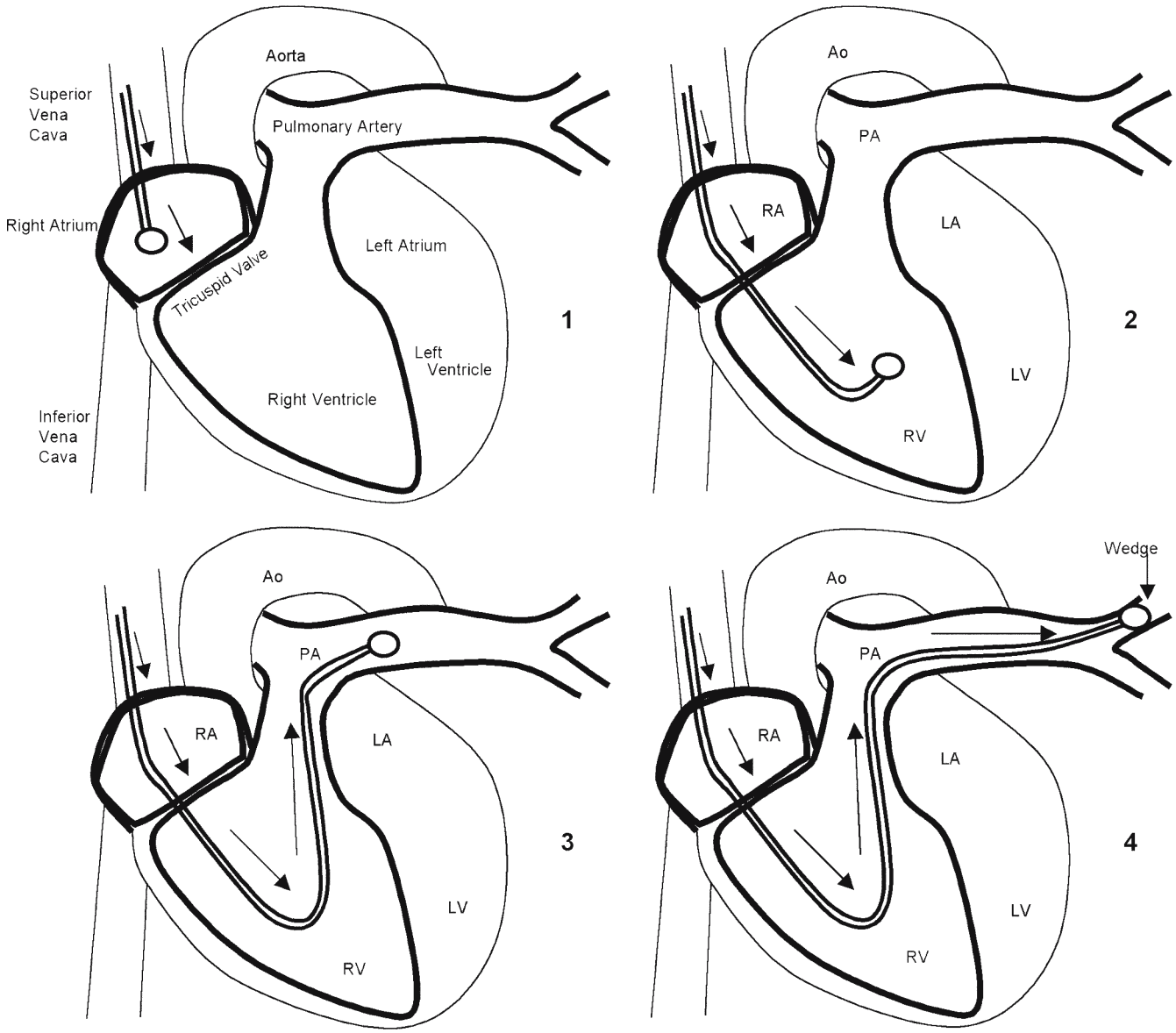

Fig. 20. Floating a pulmonary artery catheter through chambers of a heart until the balloon wedges in the distal pulmonary artery. 1, Tip (balloon) of PA catheter in the right atrium.; 2, tip of PA catheter in the right ventricle; 3, tip of PA catheter in pulmonary artery; 4, tip of PA catheter wedged in the distal pulmonary artery. Ao, aorta; LA, left atrium; LV, left ventricle; PA, pulmonary artery; RA, right atrium; RV, right ventricle. Diagram courtesy of Sock Lake Group LLC, Roseville, MN.

back (or removed), the balloon should be deflated. The balloon on most pulmonary artery catheters holds a specific volume of air (1.5 mL). Exceeding this volume may result in balloon rupture or catastrophic pulmonary artery rupture. Most currently available catheter systems come with a balloon inflation syringe that minimizes the risk of such an error.

As with all pressure transducers, the pulmonary artery catheter pressure transducer must be accurately calibrated and zeroed prior to obtaining pressure readings. The pressure transducer should be zeroed at the level midway between the anterior and posterior chest at the level of the sternum; this is usually near the level of the right atrium. The pulmonary artery pressure should be obtained at end expiration (either spontaneous or mechanical ventilations).

Proper positioning of the pulmonary artery catheter in the lung region is important in obtaining accurate pressure measurements. Because a greater portion of blood flow goes to the right lung (~55%), the balloon of the pulmonary artery catheter most often floats to the right pulmonary artery. West et al. *(9)* categorized three lung zones (I, II, III) based on the correlation among pulmonary arterial pressure, alveolar pressure, and venous pressure. Proper placement of the pulmonary artery catheter requires the catheter tip to be in zone III. This is the area in the lung where blood flow is uninterrupted and therefore

capable of transmitting the most accurate blood pressure; it is also the zone least affected by airway pressures.

For the pulmonary capillary wedge pressure to correlate best with left atrial pressures, the distal tip of the catheter should be in a patent vascular bed. If the catheter tip is in the area of lung where alveolar pressure is greater than perfusion pressure, the pulmonary capillary wedge pressure will reflect the alveolar pressure and not left atrial pressure. Controlled mechanical ventilation utilizing positive end-expiratory pressure decreases the size of West zone III and may affect correlation of pulmonary capillary wedge pressure and left atrial pressure *(4)*. Other clinical settings in which pulmonary capillary wedge pressure may not accurately reflect left atrial pressure include those for patients with pulmonary vascular disease, mitral valve disease, chronic obstructive pulmonary disease, and those administered positive end-expiratory pressure *(10)*.

It is possible to convert zone III into zone II, and even zone I, with major increases in pulmonary alveolar pressure, such as positive-pressure ventilation and positive end-expiratory pressure *(11)*. Again, conditions such as positive-pressure ventilation, obstructive and restrictive lung disease, and cardiac diseases (i.e., valvular and altered ventricular compliance, tachycardia, and pneumonectomy) are situations for which pulmonary capillary wedge pressures do not accurately correlate with left ventricular end-diastolic pressures *(12,13)* and hence left ventricular end-diastolic volumes.

The pulmonary capillary wedge pressure waveform is similar to the central venous pressure waveform and occurs at a similar time-point within the cardiac cycle. Myocardial changes (i.e., myocardial ischemia) that commonly occur in compliance and valvular disease will affect the waveform. Large *v* waves occur with mitral regurgitation, myocardial ischemia, papillary muscle dysfunction, and infarction (Fig. 17). Large *v* waves may look similar to the pulmonary artery waveform. To prevent errors in interpreting pulmonary capillary wedge pressure and pulmonary artery pressure, the waveform must be viewed and correlated with the ECG tracing. The *v* wave will always occur after the QRS complex and peak systemic arterial waveform and will not have a dicrotic notch. The pulmonary artery waveform has a dicrotic notch. A large *a* wave typically occurs in patients with mitral stenosis or left ventricular hypertrophy.

Pulmonary artery catheters may be contraindicated in patients with known abnormal anatomy of the right heart, such as tricuspid and pulmonic valve stenosis or masses in the right heart. Such catheters may also be contraindicated in patients with left bundle branch block of the myocardial conduction system; floating the pulmonary artery catheter through the right heart may cause right bundle branch block and increase the risk of developing complete heart block. The existence of cardiac pacer leads is not a contraindication, but may make placement of a pulmonary artery catheter more difficult (*see* MPEG of pulmonary artery catheter and pacer wires on the Visible Heart CD).

Care also must be taken when removing such a catheter. Reported complications associated with pulmonary artery catheters include cardiac arrhythmias, heart block, pulmonary artery rupture, infection, and/or pulmonary infarction *(14)*. During cardiac surgery such as lung and heart transplant, it is possible to have the pulmonary artery catheter inadvertently sutured in the surgical field. Note that any resistance to catheter removal must alert the clinician to the above possibility.

11. CARDIAC OUTPUT/CARDIAC INDEX MONITORING

Determining cardiac output is now considered vital when managing a critically ill patient, particularly those with severe cardiac disease, pulmonary disease, or multiorgan failure. Cardiac output is the total blood flow pumped by the heart, measured in liters per minute (L/min); in an average adult, cardiac output is approx 5–6 L/min. Cardiac output is often equated with global ventricular systolic function. Any increase in demand for oxygen delivery is usually accomplished with an increase in cardiac output. Furthermore, increasing cardiac output is an important factor in oxygen delivery. Cardiac output is dependent on heart rate and stroke volume. In a normal heart, stroke volume is dependent on preload, afterload, and contractility. Myocardial wall motion abnormalities and valvular dysfunction will also affect stroke volume.

Starling's law describes the relationship between cardiac output and left ventricular end-diastolic volume (Fig. 3). As preload is increased, the cardiac output increases in direct proportion to the left ventricular end-diastolic volume until an excessive preload is reached. At this point, increases in left ventricular end-diastolic volume do not result in increased cardiac output and may actually decrease it.

Because of variations in body size and weight, cardiac output is frequently expressed as a cardiac index. Cardiac index is equal to cardiac output divided by body surface area and has a normal range of 2.5–4.3 L/min/m^2:

$$CO = HR \times SV$$

$$CI = CO/BSA$$

where CO is cardiac output, HR is heart rate, SV is stroke volume, CI is cardiac index, and BSA is body surface area.

The equation for cardiac output can be derived by rearranging the oxygen extraction equation. Oxygen extraction is the product of cardiac output and the difference between arteriovenous oxygen content:

$$VO_2 = CO \times (C_aO_2 - C_vO_2)$$

where VO_2 is oxygen extraction, CO is cardiac output, C_aO_2 is arterial oxygen content, and C_vO_2 = venous oxygen content.

Rearranging the oxygen extraction equation allows calculation of cardiac output:

$$CO = VO_2/(C_aO_2 - C_vO_2)$$

A limitation of the Fick method is that frequent blood samples from the arterial and venous circulation are required. Expiratory gas must also be analyzed to measure oxygen consumption.

Cardiac output can also be measured by utilizing an indicator (dye) dilution technique or a thermodilution technique. In the indicator dilution technique, a nontoxic dye (e.g., methylene blue or indocyanine green) is injected into the right heart. The dye mixes with blood and goes out the pulmonary artery to the systemic circulation. A circulating arterial blood sample with diluted indicator dye is collected and measured using spectrophotometric analysis. Repeat cardiac output measure-

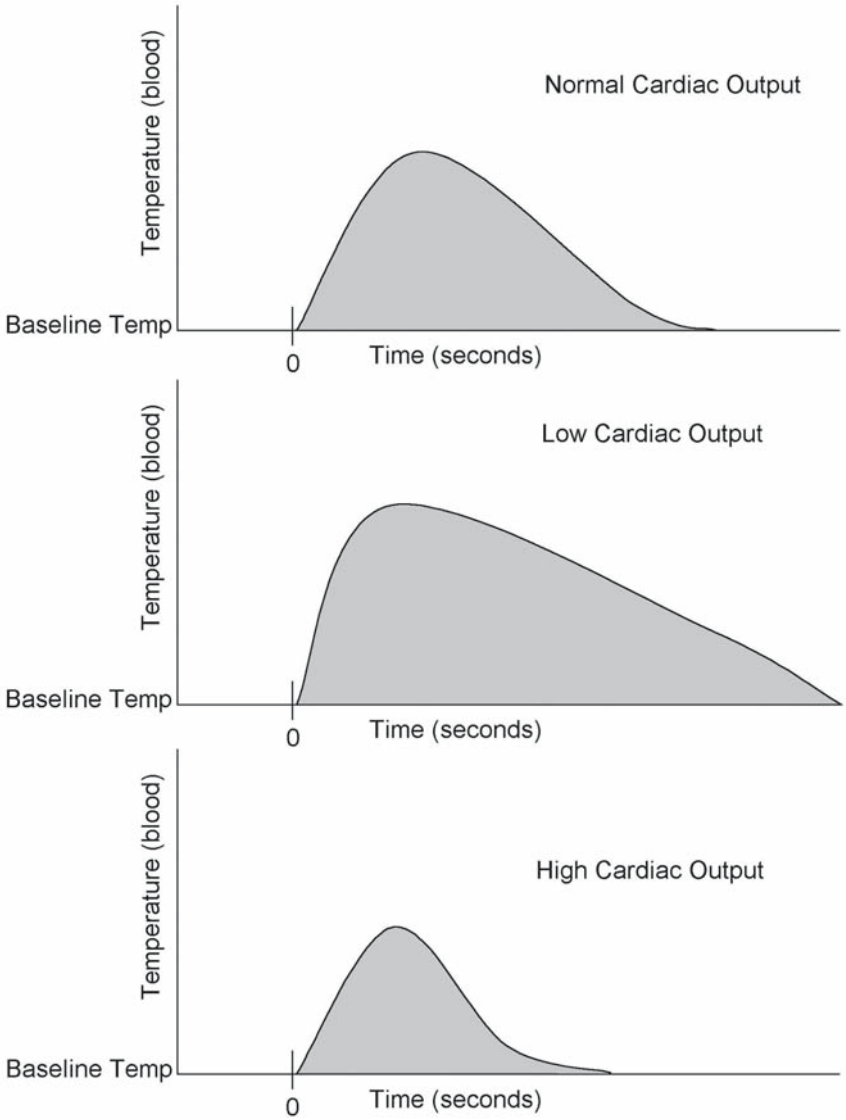

Fig 21. Cardiac output monitoring. Cardiac output is inversely proportional to the area under the thermodilution curve.

ments utilizing the indicator dilution technique are limited because of increasing concentrations of dye with each subsequent measurement.

The thermodilution method to measure cardiac output is a modification of the indicator dilution technique initially described by Fegler *(15)* in 1954. Thermodilution techniques are not affected by recirculation, as are the indicator dilution techniques. Typically, the distal tips of the pulmonary artery catheters contain thermistors that detect temperatures of the blood. The more proximal portion of the pulmonary artery catheter contains an opening that allows for injection of fluid such as normal saline or D_5W (dextrose 5% in water). The injected solution may be at an ambient temperature or iced. An iced solution increases the temperature differential and therefore the signal-to-noise ratio *(16)*; thus, it is considered better than an injectate at room temperature.

A computer program within the monitoring system commonly calculates the cardiac output utilizing the thermodilution cardiac output equation. The components of the equation include the following: specific heat of blood, specific gravity of blood and injectate, volume of injectate, and area of blood temperature curve. A modified Stewart-Hamilton equation *(17)* can also be used to calculate cardiac output:

$$CO = V(T_b - T_i) \times K_1 \times K_2 / \int \Delta T_b(t)dt$$

where CO is cardiac output in liters per minute, V is volume of injectate (mL), T_b is initial blood temperature (°C), T_i is initial injectate temperature, K_1 is density factor, K_2 is a computation constant, and $\int \Delta T_b(t)dt$ is the integral of blood temperature change over time.

Cardiac output is inversely proportional to the area under the curve (Fig. 21).

Nevertheless, an accurate calculation of cardiac output requires both proper position of the pulmonary artery catheter and a consistent volume of injectate. Situations such as tricuspid and pulmonic value regurgitation and intracardiac shunts will cause recirculation of blood and thus result in false elevation of cardiac output. The errors of intermittent bolus thermodilution techniques include volume and temperature of injectate, technique of injection, and timing of injection with the respiratory cycle *(18)*. Cardiac output measurements are also affected by clinical conditions such as tricuspid insufficiency, intracardiac shunts, or atrial fibrillation *(10)*.

The accuracy of the system depends on the measurement of temperature differences from the injection port to the distal measurement thermistor. In the thermodilution technique, the volume of injectate must be constant (10 mL). Smaller amounts of cold solution reaching the thermistor will result in a higher cardiac output. Such detected differences may be caused by actual increased cardiac output, small amounts of injectate, warm indicator or injectate, a clot on the thermistor, or a wedged catheter. A calculated small cardiac output will result when the blood reaching the thermistor is too cold; this may occur if there is too large an amount of injectate, if the solution is too cold, if there is an actual decrease in cardiac output, or if the patient has an intracardiac shunt.

Continuous cardiac output monitoring has been made possible with advanced pulmonary artery catheters (*see JPEG 9* on the Companion CD). Typically, continuous cardiac output monitors utilize a thermal coil positioned in the right ventricle; this coil intermittently heats the blood. Once the continuous cardiac output catheter and system reach a steady state with the surroundings, the thermal coil intermittently heats blood. The temperature change of the surrounding blood is detected by a thermistor located at the distal tip of the pulmonary artery catheter. The recorded blood temperature varies inversely with cardiac output.

A major limitation of the continuous cardiac output method is its slow response time to acute changes in cardiac output *(18,19)*. Although the response time may be slow, it is still faster in detecting cardiac output changes than the traditional intermittent thermodilution technique. In general, continuous cardiac output monitoring is considered more accurate than the intermittent thermodilution technique *(20,21)*.

Noninvasive methods to measure cardiac output include Doppler modalities, transpulmonary dilution technique *(22,23)*, gas rebreathing technology *(23,24)*, and bioimpedance *(23,25, 26)* technique. Briefly, the noninvasive Doppler method to measure cardiac output is an esophageal Doppler monitor. An esophageal Doppler probe is placed, and an ultrasound beam is directed at the descending aorta. By knowing the cross-sectional area of the aorta and blood velocity, the stroke volume is calculated *(23)*.

The transpulmonary dilution method for measuring cardiac output requires injections of an indicator (lithium or thermodilution) in the venous circulation (central or peripheral) and subsequent assessment of the indicator level of the systemic arterial circulation; a typical example is the lithium chloride solution technique *(27–29)*. Lithium chloride indicator is injected through a central or peripheral vein, and the plasma concentration of this indicator is measured via a lithium-specific electrode connected to the arterial line *(30)*. A concentration–time curve is generated, and cardiac output is calculated from the area under the curve associated with the lithium ion concentrations *(31)*.

The thoracic bioimpedance method measures cardiac output by detecting the change in flow of electricity with alteration in blood flow *(23)*. For thoracic bioimpedance, a low-amplitude and high-frequency current is transmitted and then sensed by sets of electrodes placed on both sides of the thorax and neck. The cardiac alterations in impedance (resistance to current flow) are analyzed and calculated as the blood volume changes for each heartbeat (stroke volume). The thoracic bioimpedance method of measuring cardiac output may be useful in clinical situations such as major trauma *(32,33)* and cardiac disease *(34)*.

Gas technology utilizing the measurement of carbon dioxide *(23,35)* applies the Fick principle of oxygen consumption and cardiac output, but substitutes carbon dioxide production for oxygen consumption. By determining the change in CO_2 production and end-tidal CO_2, modification of the Fick equation can be applied to calculate cardiac output *(36)*:

$$CO = \Delta VCO_2/\Delta EtCO_2$$

where CO is cardiac output, ΔVCO_2 is change in CO_2 production, and $\Delta EtCO_2$ is end-tidal CO_2.

It should be noted that the accuracy of the carbon dioxide rebreathing method to measure cardiac output is, at present, inconclusive *(36–39)*.

12. MIXED VENOUS SATURATION MONITORING

Mixed venous oxygen saturation monitoring (S_vO_2) typically utilizes reflective spectrophotometric technology to measure the amount of oxygen in mixed venous blood. Yet, a true mixed venous blood sample is measured in the pulmonary artery. Systemic venous blood with different oxygen extraction ratios returns to the right atrium via the superior and inferior venae cavae, mixes and equilibrates in the right ventricle, and flows out past the pulmonic valve to the pulmonary artery. As blood travels past the S_vO_2, catheter light emitted from the catheter tip is reflected off the red blood cells and is detected by a photodetector. The difference in wavelengths of emitted and reflected light is processed to estimate S_vO_2 (Fig. 22).

Continuous venous saturation (S_vO_2) monitoring has been made possible with the adaptation of a pulmonary artery catheter with fiberoptic technology (*see JPEG 9* on the Companion CD). Such monitoring utilizes the principle of reflectance spectrophotometry, which uses multiple wavelengths of transmitted light at specific intensities that is then reflected from red blood cells. For example, oxygenated hemoglobin absorbs most infrared light (940 nm) and reflects or transmits most red light (660 nm); this is the reason that oxyhemoglobin looks red, and deoxyhemoglobin appears blue. The tip of the S_vO_2 catheter emits light with specific wavelengths, which measures both oxyhemoglobin and deoxyhemoglobin as red blood cells flow past the tip of the catheter. The difference between absorption of light between saturated and desaturated hemoglobin results in the calculated S_vO_2 value.

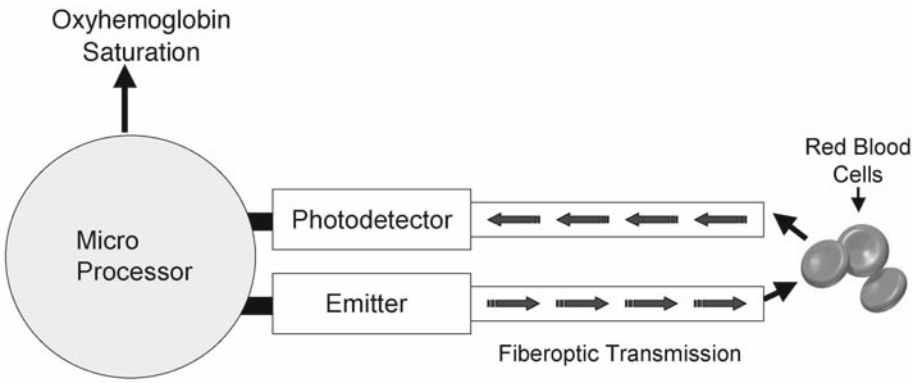

Fig 22. Mixed venous saturation monitoring (S_vO_2). Spectrophotometric technology such as pulse oximeter and mixed venous oxygen saturation monitors are utilized to measure the amount of oxygenated hemoglobin in circulating blood. A specific wavelength (infrared) is emitted, and the reflected wavelength off the red blood cells is detected and processed.

The S_vO_2 equation is a modification of the Fick equation; S_vO_2 is derived by rearranging the Fick equation as follows:

$$VO_2 = C_{(a\text{-}v)}O_2 \times CO \times 10$$

$$S_vO_2 = S_aO_2 - VO_2/DO_2$$

DO_2 = Volume of O_2 delivered per minute

$$= CO \times C_aO_2 \times 10$$

VO_2 = Oxygen consumption per minute

$$= C_{(a\text{-}v)}O_2 \times CO \times 10$$

S_aO_2 = Arterial O_2 saturation (1.0)

$$C_aO_2 = 1.39 \times Hgb \times S_pO_2 + 0.003 \times P_aO_2$$

where VO_2 is oxygen consumption, C_aO_2 is arterial oxygen content, C_vO_2 is venous oxygen content, CO is cardiac output, DO_2 is oxygen delivery, S_aO_2 is arterial oxygen saturation, Hgb is hemoglobin, S_pO_2 is oxygen saturation, and P_aO_2 is partial pressure of arterial oxygen.

Accurate measurement of S_vO_2 requires that vasoregulation be intact *(40)*, and there must be a continuous flow of blood past the tip of the catheter. S_vO_2 values may be incorrect if the tip of the pulmonary artery catheter migrates into the distal pulmonary artery or comes in contact with the arterial wall. Other causes of incorrect S_vO_2 values include miscalibration of the microprocessor or light intensity that is too low. Note that the tip of the catheter must be in the pulmonary artery to have true mixed venous oxygen.

Mixed venous oxygen saturation (S_vO_2) monitoring provides information about the balance between total body oxygen consumption and delivery. S_vO_2 (0.65–0.75) measures the amount of oxygen not taken up by organs and tissues. Therefore, the lower the S_vO_2 is, the higher the fraction extraction of oxygen by the tissues is, and a possible imbalance between oxygen consumption and oxygen delivery may exist. S_vO_2 is dependent on arterial oxygen saturation, oxygen consumption, concentration of hemoglobin, and cardiac output. A significant change in S_vO_2 may be caused by decreased oxygen delivery (decreased cardiac output and hemoglobin), increased oxygen consumption, or decreased arterial oxygen saturation.

Continuous S_vO_2 monitoring is useful in conditions for which there is significant oxygen transport imbalance, including severe cardiac and respiratory disease, sepsis, or dysfunctional oxygen transport *(41)*. During stable arterial oxygen content and consumption, S_vO_2 reflects cardiac output *(42,43)*. Furthermore, monitoring of S_vO_2 may provide vital information in the medical management of either critically ill *(44,45)* or cardiac surgery patients *(46)*. If S_vO_2 drops during a period of increased oxygen demand, it may indicate inadequate tissue perfusion and oxygen delivery; this information would not be available with the monitoring of cardiac output alone.

It is considered that S_vO_2 may be a better measurement of myocardial performance than cardiac output itself. Acute decrease in S_vO_2 below 0.65 indicates a disparity between oxygen delivery and oxygen consumption. A change in S_vO_2 greater than ±0.1 is considered significant. Medical management of critically ill patients by implementing measures to keep S_vO_2 normal may decrease morbidity and mortality *(30,47)*. Conditions for which S_vO_2 is greater than 0.75 include increased oxygen delivery and low oxygen consumption. S_vO_2 may be elevated during septic shock, hyperoxygenation, and cyanide toxicity and in patients with arterial venous shunts *(40,41)*. The increase in S_vO_2 during sepsis is caused by the loss of vasoregulation and does not mean that organ tissues are adequately oxygenated. Under general anesthesia, the S_vO_2 value is increased because of the decreased metabolic requirement for oxygen by tissues.

In clinical settings for which a pulmonary artery S_vO_2 catheter is not possible (i.e., for pediatric patients), a central venous oxygen saturation ($S_{cv}O_2$) monitor may be used. The advantage of $S_{cv}O_2$ is that a pulmonary artery catheter is not required; only central venous access is needed. The $S_{cv}O_2$ obtains venous oxygen saturation readings from the superior vena cava or right atrium. During normal physiological and hemodynamic conditions, $S_{cv}O_2$ correlates well with S_vO_2 *(48–50)*. However, in critical illness and shock, the $S_{cv}O_2$ does not accurately reflect the true S_vO_2 *(51–53)*; therefore, true S_vO_2 can only be measured in the pulmonary artery in such cases *(54)*. Resuscitation and medical management of critically ill patients with a

$S_{cv}O_2$ monitor may provide benefits over conventional monitors, such as provision of vital signs and central venous pressure *(51)*.

13. SONOMICROMETRY

Sonomicrometry is a basic laboratory tool that uses the transmission of ultrasound energy through tissue to measure distance. Ultrasound sonomicrometry is typically used to measure the distance between two fixed points in a soft tissue environment and to quantify the function and dynamics of cardiac, skeletal, or smooth muscles. The piezoelectric (sonomicrometry) crystals function omnidirectionally and act as both receiver and transmitter, with some systems allowing for as many as 32 peers. Complex, moving, 3D geometry can be modeled using techniques like sonomicrometry array localization.

Understanding the velocity of ultrasound through tissue is critical to acquiring accurate dimensions in a sonomicrometry system. The velocity of ultrasound is affected by a variety of factors, including muscle fiber direction and composition, as well as the contractile state. In most biological tissues, the velocity of sound is approx 1540 m/s.

Traditionally, sonomicrometry has been used to determine cardiac function on large research animals (dogs, pigs, sheep, and so forth). Both in vivo and in vitro studies can be performed to elucidate global cardiac function under a variety of conditions. A typical study parameter includes the assessment of ventricular volume, which when coupled with ventricular pressure, gives the experimenter access to a variety of cardiac parameters, including heart rate, cardiac output, and stroke volume.

Regional studies, which focus on specific areas of the heart, are also popular. The advent of 3D sonomicrometry, or "sonomicrometry array localization," has made possible the detailed study of discrete anatomical points throughout the cardiac cycle *(55,56)*. A volume of data exists describing the motion of valves, papillary muscles, ventricles, and atria. Another application involves tracking mobile components through the heart, such as cardiac catheters *(57)*.

A sonomicrometry system can use as few as 2 crystals, but typically between 6 and 32 are employed. Transducers are the piezoelectric crystals that are attached to electronics consisting of a pulse generator and a receiver. Distance is measured by energizing the transmitter with a train of high-voltage spikes or square waves (both less than a microsecond in duration) to produce ultrasound. This excites the piezoelectric crystal to begin oscillating at its resonant frequency. This vibratory energy propagates through the medium and eventually comes in contact with the piezoelectric crystal acting as the receiver. This crystal begins vibrating and generates a signal on the order of 1 mV. The piezoelectric signal is amplified, and the distance between the pair of crystals is calculated. By monitoring the difference in time from transmission to reception of the signal and knowing the speed of sound through the particular medium, the intercrystal distance can be calculated. These computations take less than 1 ms.

In sonomicrometry array localization, the 3D position of each crystal is calculated from multiple intertransducer distances. This is done using a statistical technique called *multidimensional scaling*; such scaling gives the experimenter the ability to take the scalar sonomicrometer measurements and to generate 3D geometry. Multidimensional scaling generates 3D coordinates for each crystal from a group of chord lengths in the array.

By starting with an initial coordinate estimate and applying the Pythagorean theorem, a matrix of estimated distances is generated that corresponds to the actual measured distances. Using an iterative approach, multidimensional scaling then optimizes the value for the distance calculation by minimizing what is called the *stress function*. If the distances measured between crystals are exact (no measurement error), then one solution with zero stress exists that represents the intercrystal distances exactly. As measurement error increases, a zero solution to the stress function becomes impossible, and the iterations begin seeking a minimum value. The globally minimum stress point defines the optimum 3D configuration. A similar style is used to generate an estimate of the error associated with each distance. The result of this analysis is a 3D moving model with an average error of approx 2 mm.

The advent and feasibility assessment of this technique was described in detail by Ratcliffe et al. *(55)* and Gormann et al. *(56)*. The first application of this technology described the 3D modeling of the ovine left ventricle and mitral valve. The study involved a 16-transducer array in which 3 transducers were sutured to the chest wall, and the remaining 13 were placed both epicardially and endocardially on the ventricular wall, the papillary muscles, and the mitral valve. The 3 crystals attached to the chest wall provided a fixed-coordinate system from which whole-body motion could be differentiated from cardiac motion. This study produced 3D depictions of the shape of the mitral annulus throughout the cardiac cycle, as well as quantitative images of ventricular torsion. This type of application opens up many possibilities relative to chronic studies focusing on ventricular remodeling following traumas like myocardial infarction.

Another interesting application of sonomicrometry, available because of the development of sonomicrometry array localization, is the cardiac catheter tracking described by Meyer et al. *(57)*. The system involved placing seven sonomicrometric crystals epicardially around an ovine heart and tracking the position of a catheter with anywhere from one to five attached crystals. In this system, average distance errors on the order of 1.0 mm were demonstrated. The clinically relevant end point for this tool would be to replace the epicardial transceivers with transceivers mounted in catheters and deployed endocardially in a minimally invasive manner.

14. TRANSDUCER CATHETERS

Common clinical methods to monitor arterial and venous pressures utilize a pressure transducer system that requires a fluid-filled system. Transducer catheters such as Millar catheters (*see JPEG 10* on the Companion CD) monitor pressures directly from the tip of the catheter. A sensor (*see JPEG 11* on the Companion CD) placed directly at the end of the catheter allows direct and constant measurement of pressures, thus eliminating the intrinsic inaccuracies of a fluid-filled system.

Transducer catheters are more accurate than conventional fluid-filled systems. Motion artifact is nearly eliminated, and the issues of overdamped and underdamped systems are not present. Accurate pressure readings can be obtained with the catheter at any height; readings are not affected by the height of the pressure transducer as in the conventional system. With transducer catheters, there is no time delay because pressure is monitored directly at the source. Compared to the conventional fluid system, transducer catheters have high fidelity (>10 MHz).

15. SUMMARY

Advanced methods and technology continue to be developed for the assessment of cardiac hemodynamics. Such monitoring can be used acutely; however, many new technologies are in development (miniaturized implantable sensors) for chronic monitoring of the cardiac patient. In this chapter, we provided a general overview of several devices and systems that can be used either clinically or experimentally to monitor cardiac performance. However, it should be reiterated that to understand best how the output of such devices can be used for the assessment of cardiac function, an in-depth understanding of underlying basic cardiac physiology must be possessed.

COMPANION CD MATERIAL

JPEG 1. Monitor display of electrocardiogram, blood pressures, and S_vO_2
JPEG 2. Cannulation of a peripheral artery.
JPEG 3. Cannulation of a peripheral artery.
JPEG 4. Pressure transducer for monitoring blood pressures.
JPEG 5. Central venous access kit.
JPEG 6. Cannulation of right internal jugular vein.
JPEG 7. Pulmonary artery catheter.
JPEG 8. Inflated balloon at the distal tip of pulmonary artery catheter.
JPEG 9. Pulmonary artery catheter for continuous monitoring of cardiac output and mixed venous saturation.
JPEG 10. Millar catheter.
JPEG 11. Sensors on a Millar catheter.

VISIBLE HEART® CD

MPEG of pulmonary artery catheter.
MPEG of pulmonary artery catheter and pacer wires.

REFERENCES

1. Gardner, R.M. (1996) Accuracy and reliability of disposable pressure transducers coupled with modern monitors. *Crit Care Med.* 24, 879–882.
2. Skeehan, T.M. and Thys, D.M. (1995) Monitoring of the cardiac surgical patient, in *A Practical Approach to Cardiac Anesthesia,* 2nd Ed. (Hensley, F.A. and Martin, D.E., eds.), Little, Brown, and Company, Boston, MA, p. 102.
3. Gorback, M.S. (1988) Considerations in the interpretation of systemic pressure monitoring, in *Complications in Critical Care Medicine* (Lumb, P.D. and Bryan-Brown, C.W., eds.), Year Book, Chicago, IL, p. 296.
4. Shasby, D.M., Dauber, I.M., Pfister, S., et al. (1980) Swan-Ganz catheter location and left atrial pressure determine the accuracy of wedge pressure when positive end expiratory pressure is used. *Chest.* 80, 666–670.
5. Snyder, J.V. and Carroll, G.C. (1982) Tissue oxygenation: a physiologic approach to a clinical problem. *Curr Probl Surg.* 19, 650.
6. Stanley, T.E. and Reves, J.G. (1994) Cardiovascular monitoring, in *Anesthesia,* 4th ed. (Miller, R.D., ed.), Churchill Livingstone, Boston, MA, p. 1167.
7. Swan, H.J.C., Ganz, W., Forrester, J., Marcus, H., Diamon, G., and Chonette, D. (1970) Catheterization of the heart in man with use of a flow-directed balloon-tipped catheter. *N Engl J Med.* 283, 447–451.
8. American Society of Anesthesiologists Task Force on Pulmonary Artery Catheterization (2003) Practice guidelines for pulmonary artery catheterization. *Anesthesiology.* 99, 989–1014.
9. West, J.B., Dollery, C.T., and Naimark, A. (1964) Distribution of blood flow in isolated lung; relation to vascular and alveolar pressures. *J Appl Physiol.* 19, 713–724.
10. Wesseling, K.H. (1996) Finger arterial pressure measurement with Finapres. *Z Kardiol.* 3, 38–44.
11. Brandstetter, R.D., Grant, G.R., Estilo, M., Rahim, R., Sing, K., and Gitler, B. (1998) Swan-Ganz catheter: misconceptions, pitfalls, and incomplete user knowledge-an identified trilogy in need of correction. *Heart Lung.* 27, 218–222.
12. Wittnich, C., Trudel, J., Zidulka, A., and Chiu, R.C. (1986) Misleading "pulmonary wedge pressure" after pneumonectomy: its importance in postoperative fluid therapy. *Ann Thorac Surg.* 42, 192–196.
13. Van Aken, H. and Vandermeersch, E. (1988) Reliability of PCWP as an index for left ventricular preload. *Br J Anaesth.* 60, 85–95.
14. Stanley, T.E. and Reves, J.G. (1994) Cardiovascular monitoring, in *Anesthesia,* 4th Ed. (Miller, R.D., ed.), Churchill Livingstone, Boston, MA, pp. 1184–1185.
15. Fegler, G. (1954) Measurement of cardiac output in anesthetized animals by thermodilution method. *Q J Exp Physiol.* 39, 153.
16. Pearl, R.G.B., Rosenthal, M.H., Mielson, L., et al. (1986) Effect of injectate volume and temperature on thermodilution cardiac output determination. *Anesthesiology.* 64, 798.
17. Reich, D.L., Moskowitz, D.M., and Kaplan, J.A. (1999) Hemodynamic monitoring, in *Cardiac Anesthesia,* 4th Ed. (Kaplan, J.A., Reich, D.L., and Konstaelt, S.N., eds.), Saunders, Philadelphia, PA.
18. Burchell, S.A., Yu, M., Takiguchi, S.A., Ohta, R.M., and Myers, S.A. (1997) Evaluation of a continuous cardiac output and mixed venous oxygen saturation catheter in critically ill surgical patients. *Crit Care Med.* 25, 388–391.
19. Poli d Figueiredo, L.F., Malbouisson, L.M.S., Varicoda, E.Y., et al. (1999) Thermal filament continuous thermodilution cardiac output delayed response limits its value during acute hemodynamic instability. *J Trauma.* 47, 288–293.
20. Mihaljevi, T., vonSegesser, L.K., Tonz, M., et al. (1995) Continuous versus bolus thermodilution cardiac output measurements: a comparative study. *Crit Care Med.* 23, 944–949.
21. Mihm, F.G., Gettinger, A., Hanson, C.W., et al. (1998) A multicenter evaluation of a new continuous cardiac output pulmonary artery catheter system. *Crit Care Med.* 26, 1346–1350.
22. Della, R.G., Costa, M.G., Pompei, L., et al. (2002) Continuous and intermittent cardiac output measurement: pulmonary artery catheter versus aortic transpulmonary technique. *Br J Anaesth.* 88, 350–356.
23. Pamley, C.L. and Pousman, R.M. (2002) Noninvasive cardiac output monitoring. *Curr Opin Anaesthesiol.* 15, 675–680.
24. Christensen, P., Clemensen, P., Andersen, P.K., et al. (2000) Thermodilution versus inert gas rebreathing for estimation of effective pulmonary blood flow. *Crit Care Med.* 28, 51–56.
25. Imhoff, M., Lehner, J.H., and Lohlein, D. (2000) Noninvasive whole-body electrical bioempedance cardiac output and invasive thermodilution cardiac output in high-risk surgical patients. *Crit Care Med.* 28, 2812–2818.
26. Shoemaker, W.C., Wo, C.C., Bishop, M.H., et al. (1994) Multicenter trial of a new thoracic electrical bioempedance device for cardiac output estimation. *Crit Care Med.* 22, 1907–1912.

27. Linton, R.A., Band, D.M., and Haire, K.M. (1994) A new method of measuring cardiac output in main using lithium dilution. *Br J Anaesth.* 71, 262–266.
28. Linton, R., Band, D., O'Brian, T., et al. (1997) Lithium dilution cardiac output measurement: a comparison with thermodilution. *Crit Care Med.* 25, 1767–1768.
29. Kurita, T., Morita, K., Kato, S., et al. (1997) Comparison of the accuracy of the lithium dilution technique with the thermodilution technique for measurement of cardiac output. *Br J Anaesth.* 79, 770–775.
30. Rivers, E., Nguyen, B., Havstad, S., et al. (2001) Early goal-directed therapy in the treatment of severe sepsis and septic shock. *N Engl J Med.* 345, 1368–1377.
31. Band, D.M., Linton, R.A., Jonas, M.M., et al. (1997) The shape of indicator dilution curves used for cardiac output measurement in man. *J Physiol.* 498, 225–229.
32. Shoemaker, W.C. (2002) New approaches to trauma management using severity of illness and outcome prediction based on noninvasive hemodynamic monitoring. *Surg Clin North Am.* 82, 245–255.
33. Shoemaker, W.C., Wo, C.C., Chan, L., et al. (2001) Outcome prediction of emergency patients by noninvasive hemodynamic monitoring. *Chest.* 120, 528–537.
34. Drazner, M.H., Thompson, B., Rosenberg, P.B., et al. (2002) Comparisons of impedance cardiography with invasive hemodynamic measurements in patients with heart failure secondary to ischemic or nonischemic cardiomyopathy. *Am J Cardiol.* 89, 993–995.
35. Binder, J.C. and Parkin, W.G. (2001) Non-invasive cardiac output determination: comparison of a new partial-rebreathing technique with themodilution. *Anaesth Intensive Care.* 28, 427–430.
36. Maxwell, R.A., Gibson, J.B., Slade, J.B., et al. (2001) Noninvasive cardiac output by partial CO_2 rebreathing after severe chest trauma. *J Trauma.* 51, 849–853.
37. Tachibana, K., Imanaka, H., Miyano, H., et al. (2002) Effect of ventilatory settings on accuracy of cardiac output measurement using partial CO2 rebreathing. *Anesthesiology.* 96, 96–102.
38. Botero, M. and Lobato, E.B. (2001) Advances in noninvasive cardiac output monitoring: an update. *J Cardiothorac Vasc Anesth.* 15, 631–640.
39. Kotake, Y., Moriyama, K., Innami, Y., et al. (2003) Performance of noninvasive partial CO_2 rebreathing cardiac output and continuous thermodilution cardiac output in patients undergoing aortic reconstruction surgery. *Anesthesiology.* 99, 283–288.
40. Snyder, J.V. and Carroll, G.C. (1982) Tissue oxygenation: a physiologic approach to a clinical problem. *Curr Probl Surg.* 19, 650.
41. Keech, J. and Reed, R.L., II. (2003) Reliability of mixed venous oxygen saturation as an indicator of the oxygen extraction ratio demonstrated by a large patient data set. *J Trauma.* 54, 236–241.
42. Jain, A., Shroff, S.G., Jnicki, J.S., et al. (1991) Relation between venous oxygen saturation and cardiac index. Nonlinearity and normalization for oxygen uptake and hemoglobin. *Chest.* 99, 1403–1409.
43. Inomata, S., Nishikawa, T., and Taguchi, M. (1994) Continuous monitoring of mixed venous oxygen saturation for detecting alterations in cardiac output after discontinuation of cardiopulmonary bypass. *Br J Anaesth.* 72, 11–16.
44. Rivers, E., Nguyen, B., Vastad, S., et al. (2001) Early goal-directed therapy in the treatment of severe sepsis and septic shock. *N Engl J Med.* 345, 1368–1377.
45. Kraft, P., Steltzer, H., Hiesmayr, M., et al. (1993) Mixed venous oxygen saturation in critically ill septic shock patients: the role of defined events. *Chest.* 103, 900–906.
46. Waller, J.L., Kaplan, J.A., Bauman, L.I., et al. (1982) Clinical evaluation of a new fiberoptic catheter oximeter during cardiac surgery. *Anesthe Analg.* 61, 676–679.
47. Vedrinne, C., Bastien, O., De Varax, R., et al. (1997) Predictive factors for usefulness of fiberoptic pulmonary artery catheter for continuous oxygen saturation in mixed venous blood monitoring in cardiac surgery. *Anesth Analg.* 85, 2–10.
48. Goldman, R.H., Klughaupt, M., Metcalf, T., et al. (1968) Measured central venous oxygen saturation in patients with myocardial infarction. *Circulation.* 38, 941–946.
49. Berridye, J.C. (1992) Influence of cardiac output on correlation between mixed venous and central venous oxygen saturation. *Br J Anaesth.* 89, 409–410.
50. Davies, G.G., Mendehall, J., and Symrey, T. (1988) Measurement of right atrial oxygen saturation by fiberoptic oximetry accurately reflects mixed venous oxygen saturation in swine. *J Clin Monit.* 4, 99–102.
51. Rivers, E.P., Ander, D.S., and Powell, D. (2001) Central venous oxygen saturation monitoring in the critically ill patient. *Curr Opin Crit Care.* 7, 204–211.
52. Lee, J., Wright, F., Barber, R., et al. (1972) Central venous oxygen saturation in shock: a study in man. *Anesthesiology.* 36, 472–478.
53. Scheinman, M.M., Brown, M.A., and Rapaport, E. (1969) Critical assessment of use of central venous oxygen saturation as a mirror of mixed venous oxygen in severely ill cardiac patients. *Circulation.* 40, 165–172.
54. Edwards, J.D. and Mayall, R.M. (1998) Importance of the sampling site for measurement of mixed venous oxygen saturation in shock. *Crit Care Med.* 26, 1356–1360.
55. Ratcliffe, M.B., Gupta, K.B., Streicher, T.J., et al. (1995) Use of sonomicrometry and multidimensional scaling to determine the three-dimensional coordinates of multiple cardiac locations: feasibility and initial implementation. *IEEE Trans Biomed Eng.* 42, 587–597.
56. Gorman, J.H., III, Gupta, K.B., Streicher, J.T., et al. (1996) Dynamic three-dimensional imaging of the mitral valve and left ventricle by rapid sonomicrometry array localization. *J Thorac Cardiovasc Surg.* 112, 712–725.
57. Meyer, S. and Wolf, P.D. (1997) Application of sonomicrometry and multidimensional scaling to cardiac catheter tracking. *IEEE Trans Biomed Eng.* 44, 1061–1067.

17 Energy Metabolism in the Normal and Diseased Heart

ARTHUR H. L. FROM, MD AND ROBERT J. BACHE, MD

CONTENTS

1. INTRODUCTION

Although this chapter is devoted to a discussion of myocardial metabolism, it should be understood that all energy-requiring processes in the biosphere are dependent on capture of solar energy and its entrapment in molecules that can be used to fuel biological processes such as cardiac contraction. The synthesis by plants of molecules such as glucose from CO_2 and H_2O is powered by the sun via the process of photosynthesis. Photons radiated by the sun are trapped by chlorophyll and used to drive the synthesis of adenosine triphosphate (ATP). ATP has two phosphate bonds with high levels of stored chemical energy (Fig. 1).

The energy released by breakdown of these high-energy phosphate bonds is captured and used to drive the synthesis of glucose. Hence, a portion of the energy derived from the sun is ultimately stored in the form of chemical bonds resident in the chemically stable glucose molecule. The chemical energy stored in glucose can be released in a controlled fashion by enzyme-catalyzed reactions to drive the synthesis of other species of molecules, including fatty acids (another convenient storage molecule for chemical energy), as well as for resynthesis of ATP.

Because animals are unable to convert solar energy to a storable form of chemical energy, all animal life is ultimately powered by the photosynthetic process in plants. The ingestion of plants supplies animals with usable forms of stored chemical energy. Even carnivores ultimately depend on energy storage compounds that have passed up the food chain from plants.

The general aim of this chapter is to discuss processes involved in the transfer of chemical bond energy contained in the ingested energy storage molecules that we call food into ATP, which is the common energy currency of the heart and all other biological tissues.

In the myocardium, as in other biological tissues, most energy-requiring processes use ATP as the immediate source of energy. Hydrolysis of the terminal phosphate bond of ATP releases energy that can be captured and used to drive energy-requiring processes, such as protein synthesis, muscle contraction, and ion transport. The ability of the heart to pump blood to the pulmonary and systemic circulations is dependent on the availability of ATP. Because tissue stores of ATP are very modest, continuous synthesis is required to maintain ATP levels sufficient to drive energy-requiring processes. The energy required for ATP synthesis is derived from the controlled breakdown of the chemical bonds in carbohydrates (glucose) and fatty acids.

The purposes of this chapter are to: (1) describe mechanisms for delivery of carbon substrate and oxygen to the heart; (2) describe the biochemical pathways that transfer chemical bond energy in carbon substrates to ATP in the normal heart; and (3) discuss some of the alterations in these processes that

From: *Handbook of Cardiac Anatomy, Physiology, and Devices*
Edited by: P. A. Iaizzo © Humana Press Inc., Totowa, NJ

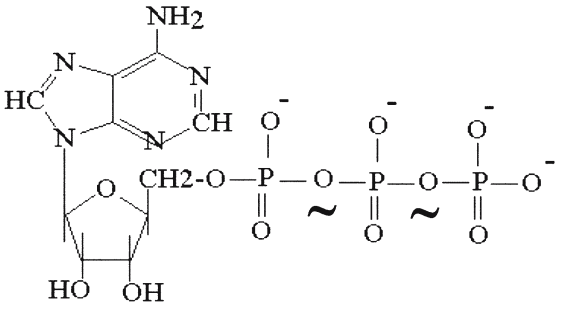

Fig. 1. Adenosine triphosphate (ATP) is the major source of chemical energy used to power the reactions that support contractile and other processes in myocardium and all other tissues. The ~ symbol is used to designate a phosphate bond with a very high level of stored chemical energy. Although ATP contains two ~ phosphate bonds, only hydrolysis of the terminal phosphate bond releases the energy that directly powers cellular processes.

occur in the diseased heart. It should be understood that this relatively brief summary of myocardial metabolism is of necessity a superficial overview of the individual topics discussed. A list of references (primarily current topical reviews and research reports, plus several standard texts) is provided at the end of the chapter for more detailed review of the major topics presented here.

2. MYOCARDIAL BLOOD FLOW

Blood containing carbon substrate and oxygen is delivered to the heart by two main coronary arteries that originate from the proximal aorta and course over the surface of the heart (epicardium). These arteries arborize into progressively smaller branches that turn inward to penetrate the epicardium and supply blood to the myocardium (Fig. 2). In the left ventricle, the heart muscle is typically subdivided into transmural layers; these are termed the subepicardium (outer layer), the midmyocardium, and the subendocardium (innermost layer).

The coronary arterial tree terminates in muscular vessels 60–150 μm in diameter termed *arterioles*. The arterioles are the major locus of resistance to blood flow (MBF), and contraction or relaxation of the smooth muscle in the walls of the arterioles (vasomotion) provides the mechanism for control of the rate of blood flow into the myocardium.

Each arteriole supplies an array of capillaries, thin-walled tubes comprised of a single layer of endothelial cells, across which most of the exchange of nutrients, oxygen, and metabolic waste products occurs. At their terminal end, the capillaries coalesce into venules, the initial component of the cardiac venous system that conducts blood back into the venous circulation primarily through the coronary sinus, which drains into the right atrium.

2.1. Regulation of Myocardial Blood Flow

Coronary blood flow is closely regulated in response to changes in energy requirements of the myocardium. The principal work of the heart is muscle contraction, which generates the pressure that drives blood through the arterial system of the body. Elevation of cardiac ATP expenditure during exercise or other stresses increases myocardial demand for oxygen and carbon substrate. Often, there is a need to assess the effects of changes of the rate of myocardial energy expenditure on cardiac performance (e.g., during exercise stress testing). Because routine measurement of myocardial oxygen consumption (MVO_2) is not practical, a rough estimate of the change in the energy demands of the heart can be obtained as the product of systolic blood pressure multiplied by the times per minute that pressure generation occurs (heart rate), termed the *rate–pressure product*. This measurement provides a simple estimate of changes in metabolic requirements of the heart in clinical situations.

The coronary circulation operates on the principle of "just-in-time" delivery of oxygen and carbon substrate. In other words, coronary blood flow is regulated to be only minimally greater than required to meet the ambient metabolic demands of the heart. As a result, the heart extracts 70–80% of the O_2 from the blood as it flows through the coronary capillaries. Because of this high level of basal oxygen extraction, there is little ability to increase oxygen uptake by increased extraction of oxygen from the blood. As a result, increases in myocardial energy requirements during exercise or other stress must be satisfied by parallel increases of coronary blood flow. Because ATP and oxygen stores in the myocardium are very low, the response time for the increase in coronary flow during an increase in cardiac work must be rapid, on the order of a few seconds. From these considerations, it is clear that highly responsive signaling systems must exist between myocardial metabolic processes and vasomotor activity in the resistance vessels that control coronary blood flow. To date, the nature of these signaling systems is not totally clear despite intense study over the last 75 years.

2.2. Biological Signals Regulating the Coronary Circulation

The regulatory signals can be classified as having feedback or feed-forward characteristics; the final common response to these signals is relaxation of the vascular smooth muscle cells that make up the resistance vessels that control coronary blood flow (Fig. 3). Several major feedback mechanisms resulting from increased cardiomyocyte metabolism (including adenosine, nitric oxide [NO], and other less-defined signals) cause opening of ATP-sensitive potassium channels (K_{ATP}) on the sarcolemma of smooth muscle cells of the coronary arterioles. Opening of these channels allows potassium to escape from the cytosol of the smooth muscle cells, resulting in hyperpolarization (increased negativity) of the cell membrane. The increased negativity of the membrane causes sarcolemmal voltage-dependent calcium channels to close; as a result, calcium entry is reduced, the muscle relaxes (vasodilation), and coronary blood flow increases. In addition to effects on the K_{ATP} channels, adenosine (a product of ATP utilization in the cardiomyocyte) has potent, direct dilator effects on arteriolar smooth muscle.

Another feedback signal is NO generated by the vascular endothelium. Mechanotransduction of flow-induced shear forces exerted on the endothelial cells augments NO synthesis. In addition to causing potassium channel opening, NO also

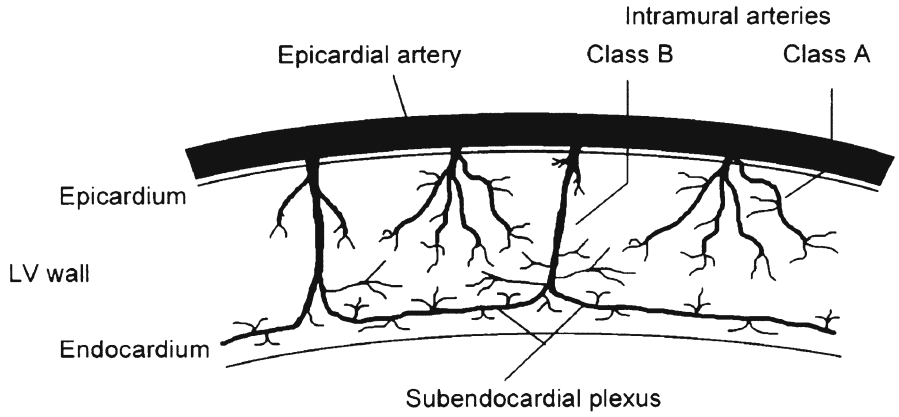

Fig. 2. The transmural distribution of the coronary arterial system is depicted. The large conductance arteries traversing the epicardial surface supply shallow and deep branches to the subepicardium (outer-most myocardial layers) and subendocardium (inner-most myocardial layers), respectively. These perforating vessels arborize to create the arteriolar network that supplies the myocardial capillary bed. LV, left ventricle. Reprinted from D.J. Duncker and R.J. Bache, Regulation of coronary vasomotor tone under normal conditions and during acute myocardial hypoperfusion, *Pharmacol Ther*., 86, 87–110, © 2000, with permission from Elsevier.

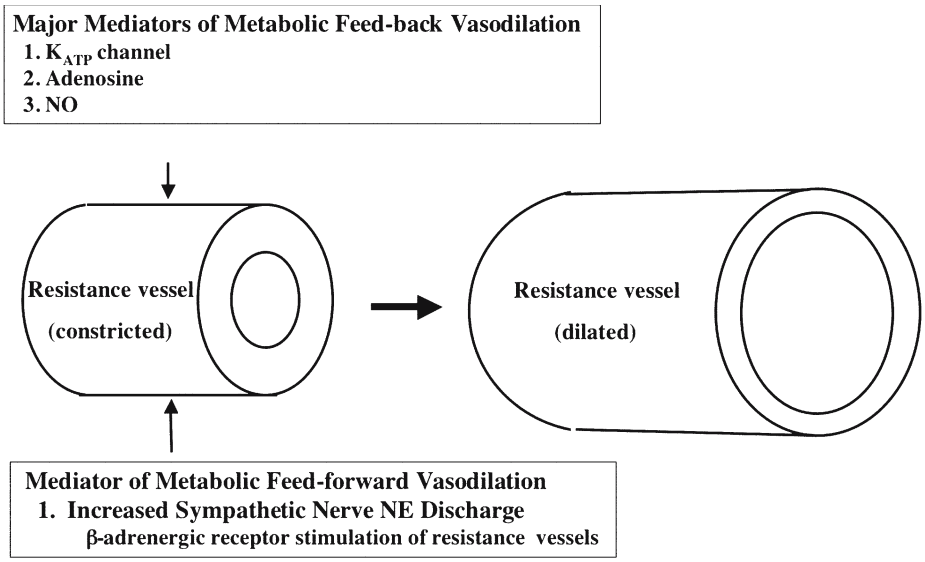

Fig. 3. Major feedback and feed-forward mechanisms underlying metabolic vasodilation of resistance vessels are depicted. *See* text for discussion. NO, nitric oxide; K_{ATP} channel, adenosine triphosphate-inhibited potassium channel; NE , norepinephrine.

directly relaxes vascular smooth muscle. Importantly, this brief discussion does not include all of the known feedback mechanisms involved in regulation of coronary blood flow.

Increases of cardiac sympathetic nerve activity, such as during exercise, activate a feed-forward mechanism for control of coronary blood flow that augments the local metabolic vasodilator influences. The sympathetic neurotransmitter norepinephrine activates α- and β-adrenergic receptors in vascular smooth muscle. Activation of α-adrenergic receptors causes modest constriction of the large coronary arteries; however, because these arteries function as conduit vessels that offer little resistance to blood flow, this has little effect on coronary flow. However, activation of β-adrenergic receptors on the coronary arterioles results in relaxation (vasodilation) of these resistance vessels; the resultant decrease of coronary resistance causes an increase in blood flow that is not dependent on local metabolic mechanisms for regulation of coronary vasomotor tone.

Pharmacological studies have shown that simultaneous blockade of the coronary K_{ATP} channels, adenosine, and NO pathways significantly decreases myocardial blood flow in the resting animal. Moreover, the increase of coronary flow that normally occurs during exercise is severely blunted, resulting in a perfusion–metabolism mismatch that is accompanied by evidence of ischemia in the normal heart. Hence, activation of these three pathways appears to be the primary means by which metabolic vasodilation is achieved in the heart. However, in the normal situation, blockade of any one of these

mechanisms for smooth muscle relaxation elicits compensatory activation of the other pathways to minimize changes in coronary blood flow.

2.3. Blood Flow in the Diseased Heart

Coronary blood flow in the diseased heart can be limited by: (1) partial or complete obstruction of the large coronary arteries (e.g., as in atherosclerotic disease); (2) decreased responsiveness of the signaling systems relating MBF to myocardial energy requirements; or (3) increases in extravascular forces acting to compress the small vessels in the wall of the left ventricle. In the case of obstructive coronary disease, a moderately narrowed vessel may functionally restrict blood flow only during periods of increased work (i.e., it reduces vasodilator reserve); a severely narrowed vessel may limit blood flow even when the subject is at rest. In the presence of a moderate coronary obstruction, the arteriolar bed can maintain adequate blood flow by metabolic signaling-based arteriolar vasodilation. That is, a decrease in small-vessel resistance can compensate for the resistance offered by the coronary artery stenosis. However, when the capacity for vasodilation of the arterioles has been exhausted, any further increase in cardiac work cannot result in an increase of blood flow, and the myocardium supplied by the narrowed vessel will become ischemic. There is also some evidence that malfunction of metabolic signaling pathways in the arteriolar resistance vessels can aggravate (e.g., in patients with nonobstructive atherosclerotic disease or with diabetes) or cause (syndrome X) myocardial ischemia.

In the normal heart, blood flow to the inner layers of the left ventricle occurs principally during diastole. This is because tissue pressures in the wall of the left ventricle during systole are so great that inner-layer arterioles are squeezed shut by the extravascular compressive forces. Diastolic left ventricular tissue pressures are also greatest in the subendocardium. As the heart fails and/or becomes hypertrophied, these extravascular compressive forces increase as left ventricular diastolic pressure (i.e., ventricular filling pressure) increases.

Slowing of myocyte relaxation also encroaches on the interval of diastole in the hypertrophied or failing heart. In the normal heart, autoregulatory (i.e., metabolic vasodilation) processes cause arteriolar vasodilation in the subendocardium to compensate for systolic underperfusion. However, increases of left ventricular diastolic pressure that occur in the failing heart may compress the arteriolar bed in the inner myocardial layers sufficiently to overwhelm autoregulatory mechanisms, particularly those that normally maintain adequate subendocardial blood flow. Because subendocardial blood flow occurs predominantly during diastole, tachycardia also acts to impede blood flow in the subendocardium by shortening the interval of diastole.

Thus, even in the absence of obstructive coronary artery disease, functional abnormalities can limit blood flow to the inner myocardial layers of the diseased heart. These abnormalities are often then associated with a reduction of the ATP synthetic capacity in the subendocardium. Thus, the extravascular forces that act on the small coronary vessels embedded in the myocardium cause the subendocardium to be the region of the ventricular wall that is most vulnerable to hypoperfusion and ischemia.

3. INTERMEDIARY METABOLISM AND BIOENERGETICS IN THE NORMAL HEART

3.1. Carbon Substrate Selection

The primary carbon substrates (Fig. 4) taken up and metabolized by the myocardium are free fatty acids and glucose. The heart readily takes up and metabolizes pyruvate, lactate and ketone bodies, but the generally low blood concentrations of these substrates limit their utilization. However, under certain conditions such as exercise, which can markedly elevate the blood lactate content, or during periods when blood levels of ketone bodies are elevated, utilization of these substrates may be dominant. A detailed discussion of the regulation of blood levels of these substrates exceeds the scope of this chapter, but a few orienting comments are appropriate regarding glucose and free fatty acid availability.

Blood glucose levels are maintained within a narrow range (~5 m*M*) in nondiabetic subjects. Its homeostasis is maintained by a balance among alimentary uptake of glucose, glucose release from the liver (which can synthesize glucose or release glucose from the glycogen storage pool), and the uptake and metabolism of glucose by the various organ systems. Glucose uptake is strongly influenced by the pancreatic secretion of insulin, a hormone that enhances glucose transport into the cells of many tissues.

The heart has often been labeled as an omnivore because of its capacity to consume virtually any available carbon substrate. Glucose is transported into the cardiomyocyte by a family of sarcolemmal glucose transport proteins, some of which are insulin dependent. Fatty acids enter myocytes via a sarcolemmal fatty acid transport protein, and pyruvate and lactate enter via a sarcolemmal monocarboxylic acid transporter. Utilization of glucose by the heart is largely regulated by the availability of fatty acids in the blood. Thus, in the fasted state, blood fatty acid levels are high, and fatty acids are the predominant cardiac substrate despite normal blood glucose levels.

In contrast, during vigorous exercise, blood lactate levels can rise markedly and compete strongly with fatty acids and glucose despite substantial blood levels of the latter substrates. After a carbohydrate meal, however, blood glucose levels rise and elicit insulin secretion. Insulin stimulates glucose uptake by the heart and other tissues and causes blood fatty acid levels to decrease. As a result, myocardial glucose consumption increases, and fatty acid consumption decreases. Nevertheless, fatty acids and lactate are the favored cardiac substrates when they are available in sufficient concentrations in the blood.

3.2. Glucose Metabolism

Figure 5 shows a flowchart for glucose metabolism. Glucose enters the cardiomyocyte via the sarcolemmal glucose transport proteins, GLUT1 (which is insulin independent) and GLUT4 (which is insulin dependent). Once in the cell, glucose is phosphorylated to glucose-6-phosphate by the enzyme hexokinase. Because glucose-6-phosphate is membrane impermeable, it is effectively trapped within the cell, where it can enter the glycogen synthesis pathway (glycogen is a macromolecular polymeric storage form of glucose) or undergo molecular rearrangement via the enzyme phosphohexose isomerase to

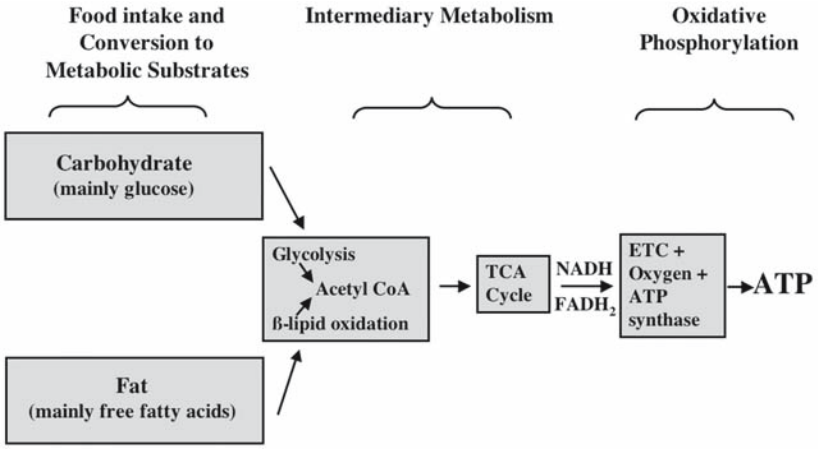

Fig. 4. A general overview of carbon substrate metabolism in the heart. Ingested food is broken down into usable carbon substrates, primarily glucose and fatty acids. The pathways that convert amino acids and other molecules to glucose are not shown. Glucose and fatty acids are processed (via intermediary metabolic processes) to yield the reducing equivalents nicotinamide adenine dinucleotide (NADH) and flavin adenine dinucleotide ($FADH_2$), which supply the electrons to the ETC that, in turn, powers oxidative phosphorylation. The last processes, which occur in mitochondria in the presence of oxygen, supply almost all of the adenosine triphosphate (ATP) synthesized in the heart. CoA, coenzyme A; ETC, electron transport chain; TCA, tricarboxylic acid.

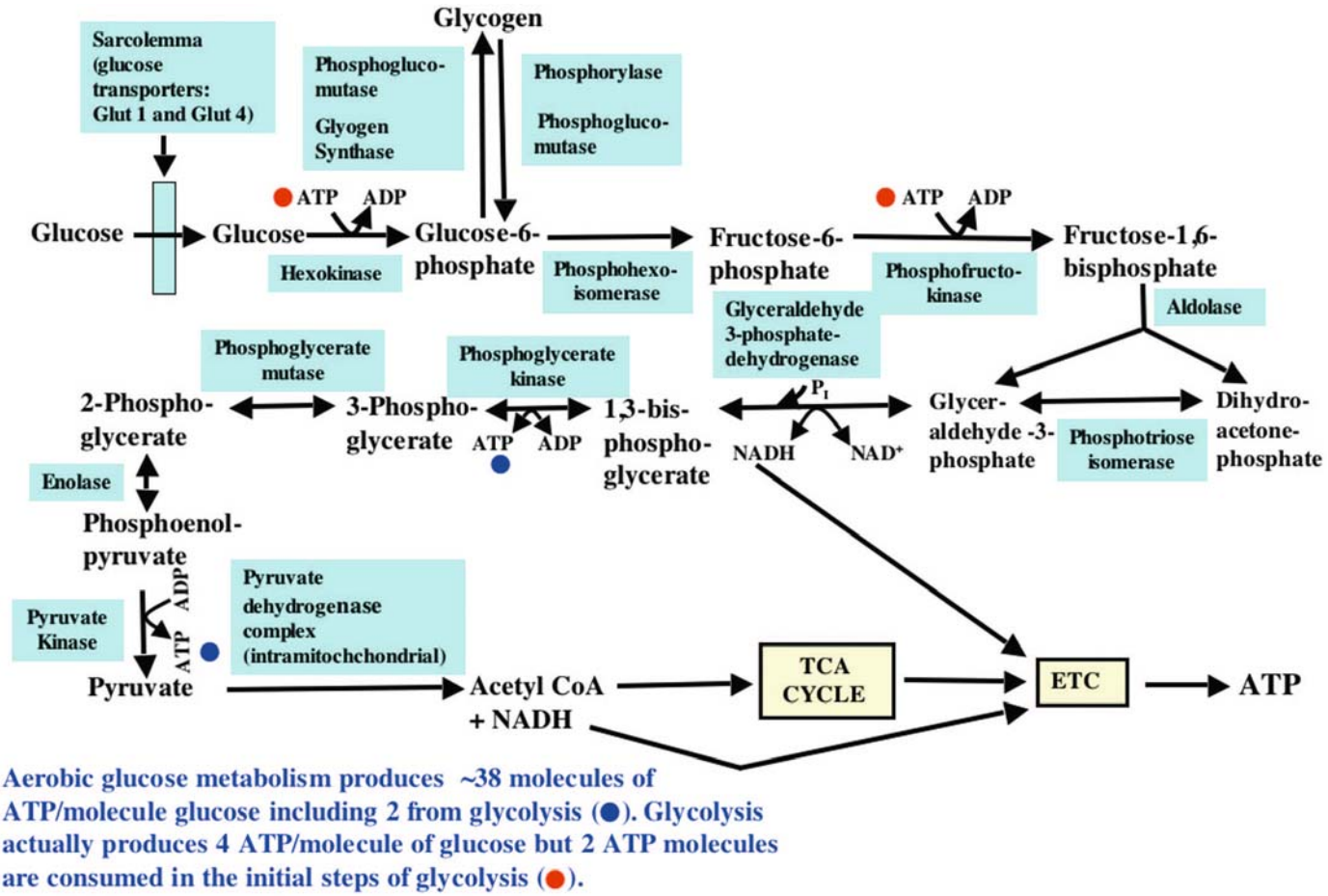

Fig. 5. A flowchart depicting the cellular uptake of glucose and the pathways through which glucose metabolism proceeds. The red dots indicate reactions which consume ATP and the blue dots designate reactions which produce ATP.*See* text for discussion. ADP, adenosine diphosphate; ATP, adenosine-triphosphate; ETC, electron transport chain; NAD, NADH, nicotinamide adenine dinucleotide; TCA, tricarboxylic acid.

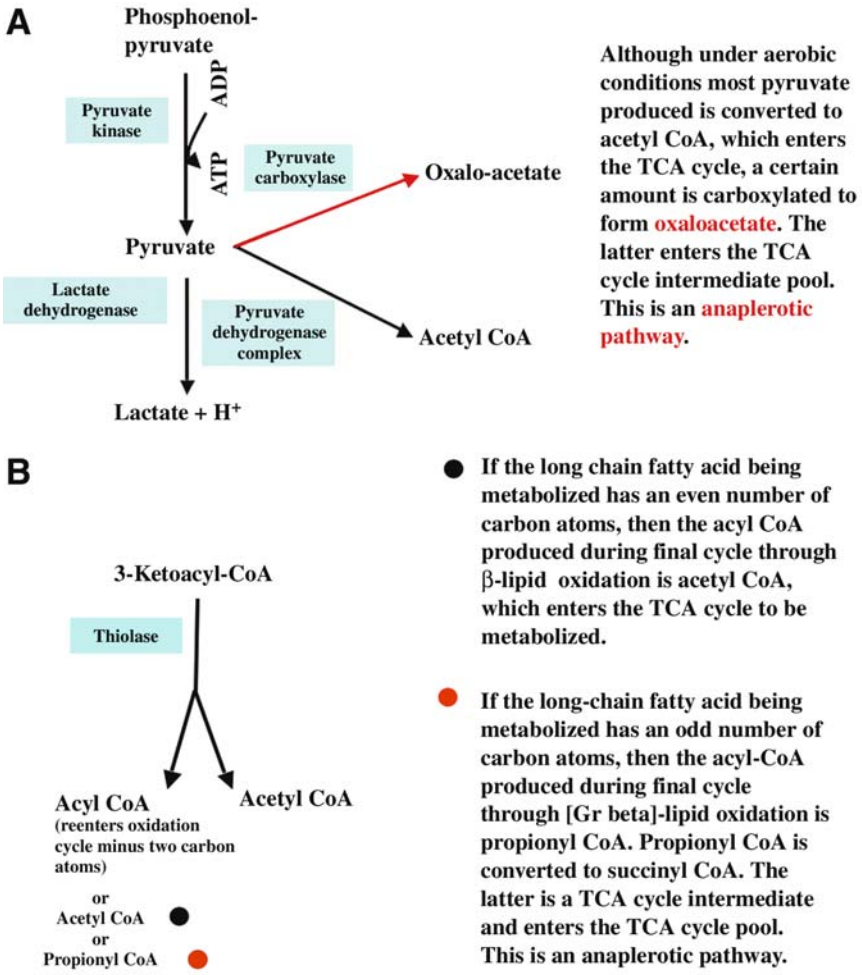

Fig. 6. Anaplerotic processes supply substrate used to maintain the tricarboxylic acid (TCA) cycle intermediate pool size. In contrast, cataplerotic processes remove substrates from the TCA cycle intermediate pool and decrease its size. The balance between these two processes determines the TCA cycle pool size. **(A)** Glucose (via its metabolic product pyruvate) contribution to anaplerosis. **(B)** The β-oxidation of odd-numbered carbon chain fatty acids contribution to anaplerosis. Figure 8, which is a flowchart for β-lipid oxidation, should be reviewed before examining Fig. 6B, which depicts the terminal reaction of β-lipid oxidation. ADP, adenosine diphosphate; ATP, adenosine-triphosphate; CoA, coenzyme A.

form fructose-6-phosphate. A second phosphorylation of fructose-6-phosphate via phosphofructo-kinase generates fructose-1,6-bisphosphate. Each of these phosphorylations consumes one molecule of ATP.

Fructose-1-6-bisphosphate is next split into glyceraldehyde-3-phosphate and dihydroacetone phosphate by the enzyme aldolase. These two products are in constant exchange with each other via the enzyme phosphotriose isomerase. Glyceraldehyde-3-phosphate is phosphorylated to form 1,3-bisdiphos-phoglycerate by the enzyme glyceraldehyde-3-phosphate dehydrogenase. The phosphate bond in the one position has a high-energy content (signified by the ~P symbol); this reaction also simultaneously reduces oxidized nicotinamide adenine dinucleotide (NAD^+) to its reduced form (NADH). Cytosolic oxidation of NADH and transport of the two removed electrons and H^+ into the mitochondrial matrix then occurs via the malate–aspartate shuttle (not shown in Fig. 5). In the mitochondrial matrix, NAD^+ is reduced to NADH which can be utilized by the mitochondria to generate ATP (*see* Section 3.8.).

In the next reaction, the high-energy phosphate bond in 1,3-bisdiphosphoglycerate is transferred to adenosine diphosphate (ADP) to form ATP and 3-phosphoglycerate via the enzyme phosphoglycerate kinase. The latter molecule is converted to 2-phosphoglycerate by the enzyme phosphoglycerate mutase**.** Enolase, another cytosolic enzyme, then converts 2-phosphoglycerate to the ~P-containing molecule phosphoenolpyruvate, which is converted to pyruvate by the enzyme pyruvate kinase. During this reaction, the ~P in phosphoenolpyruvate is transferred to ADP to form a second ATP molecule. Pyruvate can then enter the mitochondria to be metabolized further by the pyruvate dehydrogenase (PDH) complex of enzymes. Both the PDH complex, which converts pyruvate to acetyl CoA (coenzyme A) (and NAD^+ to NADH), and the tricarboxylic acid (TCA) cycle that metabolizes acetyl CoA are located within the mitochondria (Figs. 5, 6A, and 7). Within the mitochondria,

another metabolic pathway for pyruvate exists. The enzyme pyruvate carboxylase converts pyruvate to oxaloacetate, which is a TCA cycle intermediate (Figs 6A and 9). The significance of the latter reaction is discussed in the legend of Fig. 6.

Within the cytosol, pyruvate can be converted to lactic acid by lactic acid dehydrogenase (LDH). Lactate is then exported from the cell via the monocarboxylic acid transporter (Figs. 5 and 13). This reaction results in the oxidation of NADH to NAD^+, and as will be shown in Section 4.1.l., this reaction is critical when the availability of oxygen to the cardiomyocyte is limited. Conversely, under aerobic conditions, lactate can be transported into the cytosol by the monocarboxylic acid transporter to be converted to pyruvate by LDH. The LDH-catalyzed reaction also reduces NAD^+ to NADH, and the reducing equivalents from NADH can be transferred into the mitochondrial matrix by the malate–aspartate shuttle.

During glycolysis of one glucose molecule, two pyruvate molecules, four ATP molecules, and two NADH molecules are produced. However, because two ATP molecules are consumed early in the glycolytic pathway, the net production of ATP is two molecules/glucose molecule. As indicated, pyruvate and NADH are utilized in the mitochondria for oxidative generation of ATP. Therefore, complete metabolism of glucose, which includes oxidation of the products of glycolysis, results in formation of many more ATP molecules *(38)* than does glycolysis alone *(2)*. However, when mitochondrial function is severely oxygen limited, the oxidative contribution to ATP synthesis is lost, and there is a net production of two ATP molecules from each glucose molecule passing through the glycolytic pathway.

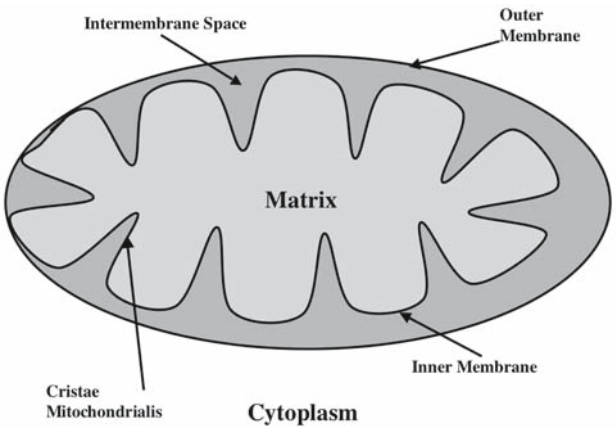

Fig. 7. The major features of mitochondrial morphology. *See* text for discussion.

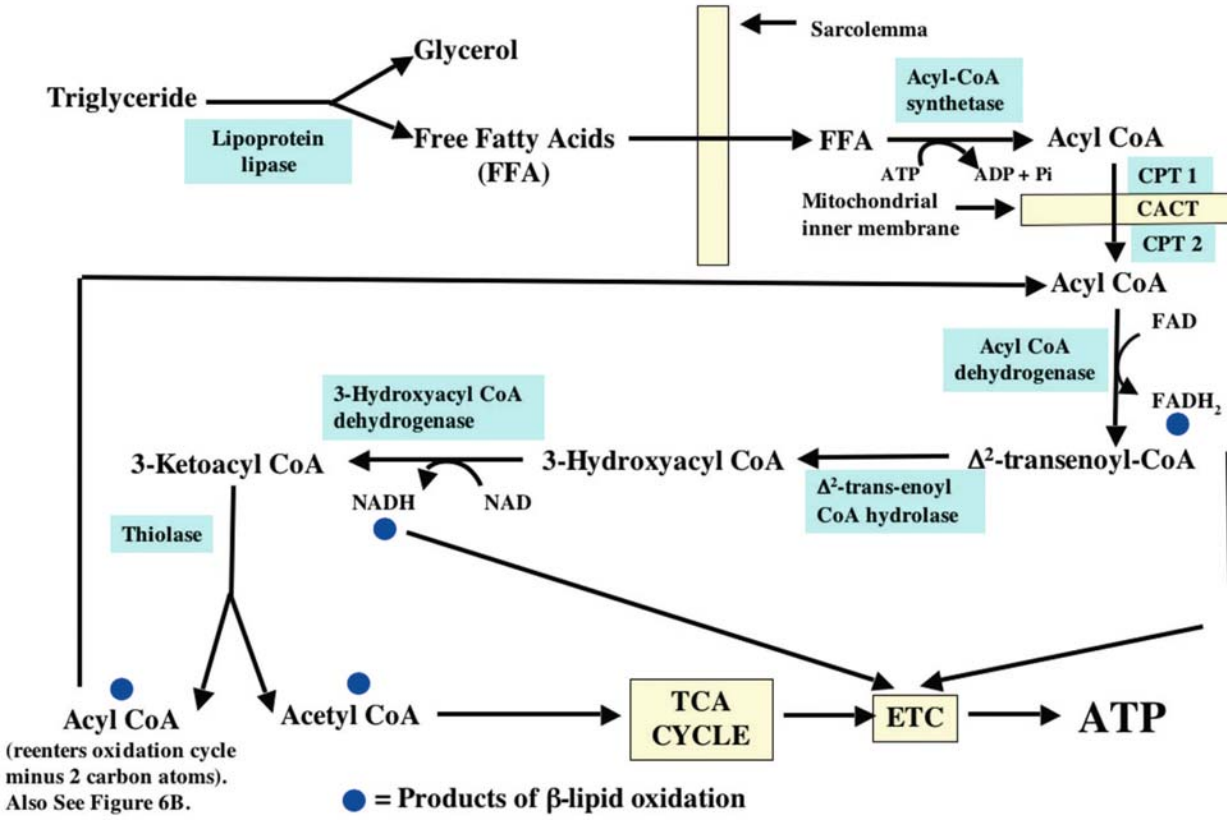

Fig. 8. Flowchart depicting the cellular uptake of free fatty acids and the pathways through which their metabolism proceeds. Blue dots indicate products of β-lipid oxidation. *See* text for discussion. ATP, adenosine triphosphate; CoA, coenzyme A; CPT, carnitine palmatoyl-transferase; CACT, carnitine-acylcarnitine transporter: ETC, electron transport chain; $FADH_2$, flavin adenine dinucleotide; FFA, free fatty acids; NADH, nicotinamide adenine dinucleotide; TCA, tricarboxylic acid.

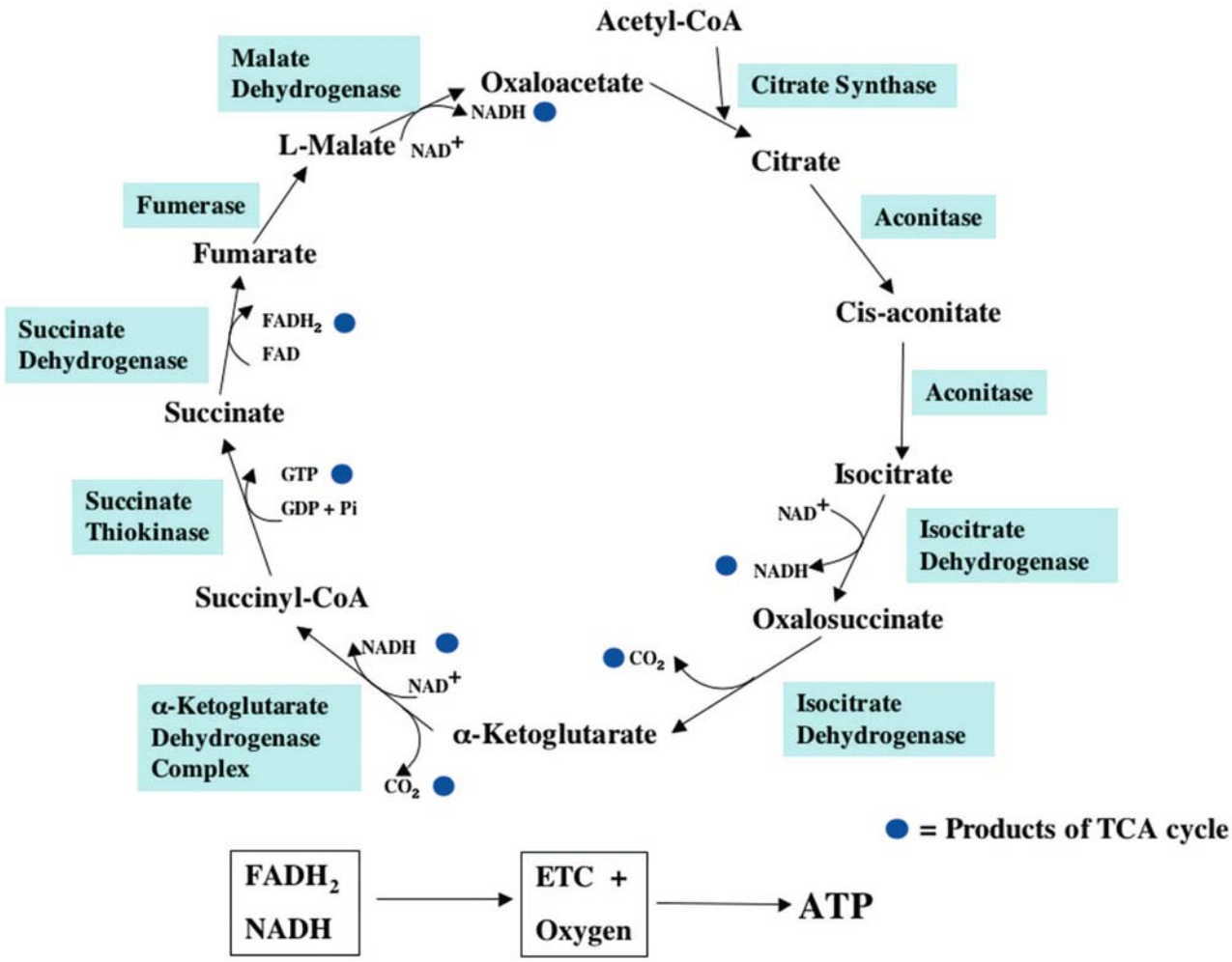

Fig. 9. The tricarboxylic acid (TCA) cycle is depicted. The filled blue circles are the products resulting from one turn of the TCA cycle. *See* text for discussion. ATP, adenosine triphosphate; CoA, coenzyme A; ETC, electron transport chain; FAD, oxidized flavin adenine dinucleotide; $FADH_2$, reduced flavin adenine dinucleotide; GDP, guanosine 5′-diphosphate; GTP, guanosine 5′-triphosphate; NAD^+, oxidized nicotinamide adenine dinucleotide; NADH, reduced nicotinamide adenine dinucleotide; Pi, inorganic phosphate.

3.3. The Mitochondrion

Mitochondria, which are the primary site of ATP synthesis in most mammalian cells, contain the β-lipid oxidation enzymes, the TCA cycle enzymes, the electron transport chain (ETC), and the F_1F_0-H^+-ATPase (also called F_1F_0-ATP synthase or ATP synthase). To understand better the location of these systems, mitochondrial structure is briefly reviewed (Figs. 7,10, and 11). The inner mitochondrial membrane contains the ETC, F_1F_0-H^+-ATPase, adenine nucleotide translocase, and other transporters. The matrix contains the TCA cycle enzymes, β-lipid oxidation enzymes, and other enzymes and reactants. The cristae are invaginations that markedly expand the surface area of the inner membrane and thereby the contents of enzymes associated with the inner membrane.

The membrane-bound components of the enzyme pathways are positioned to optimize the flow of substrates through their reaction sequences. The mitochondrial outer membrane forms a boundary between the cellular cytoplasm and the mitochondrial intermembrane space. The intermembrane space contains creatine kinase, which is important to high-energy phosphate transport out of mitochondria (Fig. 12) and cytochrome-*c*, a component of the ETC. The importance of the intermembrane space to oxidative ATP synthesis is discussed in Sections 3.6. and 3.7.

3.4. Fatty Acid Metabolism

Figure 8 presents a flowchart for the β-lipid oxidation pathway. Dietary long-chain, nonesterified, free fatty acids (NEFAs) are usually the predominant cardiac substrate. They are transported in the blood bound to plasma albumin or in the form of triacylglycerol, which is also bound to albumin. The latter can be broken down to release NEFA by an enzyme present in the plasma and at the surface of the capillary and cardiomyocyte.

After dissociating from albumin, NEFAs are transported into the cardiomyocyte by sarcolemmal fatty acid transport proteins. Within the cell, NEFAs are bound to fatty acid-binding proteins, which provide solubility. Once in the cell, NEFA mol-

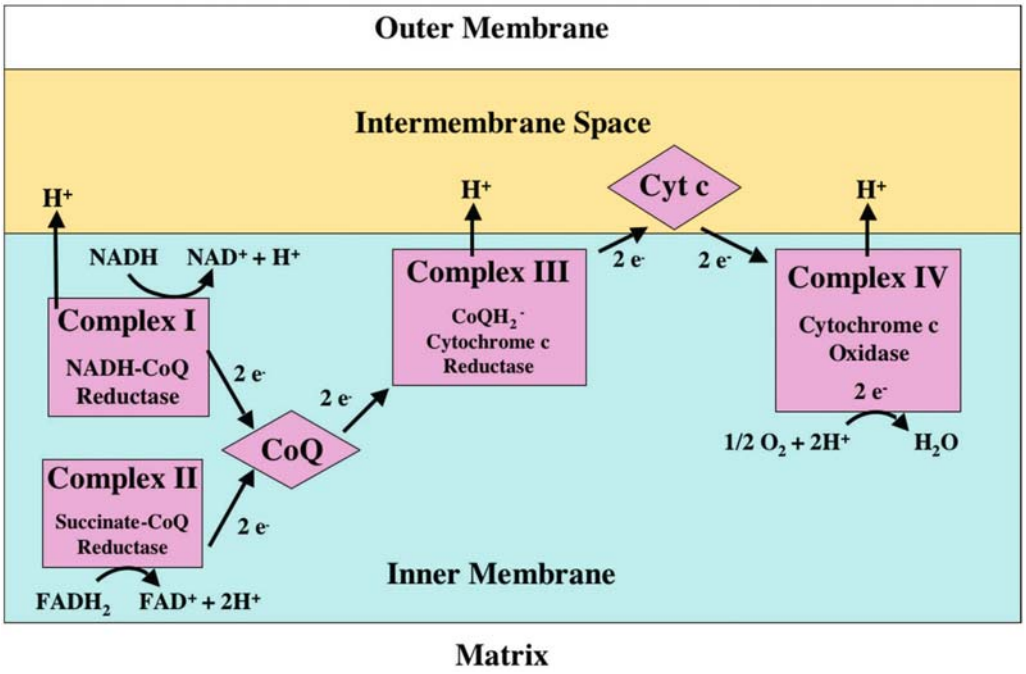

Fig. 10. The electron transport chain (ETC) is depicted. *See* text for discussion. $FADH_2$, flavin adenine dinucleotide; NAD, NADH, nicotinamide adenine dinucleotide, FAD, oxidized flavin adenine dinucleotide; CoQ, coenzyme Q; Cyt c, cytochrome c.

ecules are either reesterified and stored as triglycerides or activated by acyl CoA synthetase (in the presence of free CoA and ATP) to form a long-chain acyl CoA.

Because long-chain acyl CoA cannot readily diffuse through the mitochondrial inner membrane, the long-chain acyl CoA is converted to long-chain acyl carnitine by carnitine palmatoyltransferase 1 (CPT1) at the outer surface of the inner mitochondrial membrane and then transported across the inner membrane by carnitine-acylcarnitine translocase (which also transports free carnitine liberated by carnitine palmatoyl-transferase 2 [CPT2] back into the intermembrane space).

The long-chain acylcarnitine is next converted back to acyl CoA at the inner surface of the mitochondrial inner membrane by CPT2. Long-chain acyl CoA is then processed by a sequence of enzyme-catalyzed reactions that comprise the β-lipid oxidation pathway. If the long-chain acyl CoA has an even number of carbon atoms, then the final products of the last cycle of an acyl CoA molecule through the β-oxidation sequence are two acetyl CoA molecules (Fig. 6B). However, if the long-chain acyl CoA has an odd number of carbon atoms, then the products of the last cycle through β-oxidation are one acetyl CoA and one propionyl CoA. Unlike acetyl CoA, propionyl CoA cannot enter the TCA cycle.

Propionyl CoA can be converted to succinyl CoA, which is a TCA cycle intermediate (Fig. 6B). Hence, this pathway contributes to the maintenance of the TCA cycle intermediate pool size; both pyruvate molecules produced from glucose and odd-numbered fatty acid molecules that undergo complete β-oxidation contribute to maintenance of the TCA intermediate pool. Processes that add molecules to the TCA intermediate pool are termed *anaplerotic* (Fig. 6A,B), and those that remove intermediates from the pool are called *cataplerotic*. The importance of these processes to TCA cycle function is illustrated in a clinical example presented in Section 4.3.

The products of complete β-oxidation of a fatty acid are acetyl CoA (and propionyl CoA if the acyl chain has an odd number of carbons), NADH, and reduced flavin adenine dinucleotide ($FADH_2$). Yet, consumption of acetyl CoA by the TCA cycle and NADH and $FADH_2$ by the ETC cannot occur in the absence of oxygen. Thus, β-oxidation also cannot occur under anoxic or ischemic conditions. Therefore, markedly ischemic myocardium does not support fatty acid-derived ATP synthesis, and the only remaining source of ATP synthesis is anaerobic glycolysis.

3.5. The TCA Cycle

The carbon substrate consumed by the TCA cycle is acetyl CoA. Acetyl CoA is produced by glycolysis and β-lipid oxidation as described in Sections 3.2. and 3.4., respectively. Figure 9 shows the individual reactions of the TCA cycle. In the first step of the cycle, acetyl CoA contributes two carbon atoms to oxaloacetate to form citrate and free CoA. This reaction is catalyzed by the enzyme citrate synthase. Citrate then enters a sequence of reactions that ultimately generate two molecules of CO_2 and four reducing equivalents in the form of NADH (3) and $FADH_2$ (1). One high-energy phosphate molecule (guanosine 5′-triphosphate) is also produced, which can be converted to ATP. During this process, citrate (a six-carbon molecule) is stepwise decarboxylated and ultimately converted back to oxaloacetate, a four-carbon molecule that, when condensed with a new acetyl CoA, reinitiates the sequence of reactions.

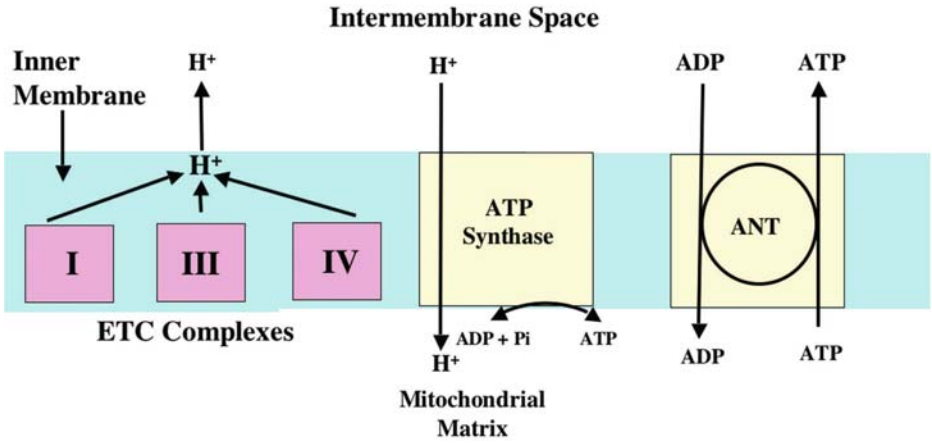

Fig. 11. The mechanism of oxidative phosphorylation and the transport of adenosine triphosphate (ATP) from the mitochondrial matrix to the intermembrane space are depicted. *See* text for discussion. ADP, adenosine diphosphate; Pi, inorganic phosphate; ANT, adenine nucleotide transporter; ETC, electron transport chain.

The reducing equivalents generated, NADH and $FADH_2$, deliver electrons to the ETC. Rate-limiting enzymes of the TCA cycle are the PDH complex (which precedes, but is not really a component of the TCA cycle), isocitrate dehydrogenase, and α-ketoglutarate dehdrogenase; these enzymes are highly regulated, as discussed in Section 3.7. Interestingly, for elucidating the TCA cycle (also known as the Krebs cycle), Sir Hans Krebs was awarded the Nobel Prize in Medicine or Physiology in 1953.

3.6. The Electron Transport Chain and Oxidative Phosphorylation

The substrates of the ETC are NADH and $FADH_2$. The ETC (Fig. 10) is composed of two freely diffusible compounds (ubiquinone, also known as coenzyme Q, which is confined to the mitochondrial inner membrane, and cytochrome-*c*, which is located in the intermembrane space) and four functional complexes (I, II, III, and IV), which are contained within the mitochondrial inner membrane. The complexes are composed of catalytic and non-catalytic proteins (and their cofactors).

NADH interacts with the ETC by transferring electrons to (and thereby reducing) complex I, which in turn then reduces ubiquinone. $FADH_2$ interacts with the ETC by transferring electrons to complex II, which, like complex I, also transfers its electrons to ubiquinone. Reduced coenzyme Q then diffuses to complex III and transfers its electrons. Next, complex III reduces cytochrome-*c*, which diffuses to complex IV and transfers electrons to this complex. The latter, when fully reduced by four electrons, reduces O_2 to two O^{-2} ions. Each O^{-2} combines with two H^+ to form H_2O in an irreversible reaction.

During the process of electron transport, electrons release energy as they pass through the sequence of complexes. The purpose of the ETC is to capture this free energy and use it to pump H^+ from the mitochondrial matrix across the inner membrane into the intermembrane space. In this regard, complexes I, III, and IV function as proton pumps (Figs. 10 and 11). These pumps create an electrochemical gradient ($\Delta\mu H^+$) composed of an electrical potential and a chemical potential (the latter reflected by ΔpH) across the inner mitochondrial membrane.

As a consequence of proton transport, the mitochondrial matrix is more negative than the intermembrane space. The F_1F_0-ATPase, which is also located in the inner mitochondrial membrane (Fig. 11), is the major pathway of H^+ return from the intermembrane space into the matrix. The energy released by the passage of H^+ down this electrochemical potential gradient is captured by the F_1F_0-ATPase and used to drive the reaction Pi + ADP → ATP (Pi is inorganic phosphate). In this way, much of the energy released by the metabolism of glucose and fatty acids is transferred to the terminal high-energy phosphate bond of ATP.

The concept of proton pumping into the intermembrane space, and the use of the electrochemical gradient thus formed to synthesize ATP, is known as the *chemiosmotic theory*. In recognition of this (initially quite controversial) insight, Sir Peter Mitchell was awarded the Nobel Prize in Chemistry in 1978. The production of ATP by mitochondria is termed *oxidative phosphorylation*; in virtually every human tissue (heart, brain, kidney, etc.), oxidative phosphorylation is the primary source of ATP generation.

To date, the precise mechanisms by which the F_1F_0-H^+-ATPase generates ATP from its substrates ADP and Pi remain under investigation. However, a number of characteristics of the process are well established. The F_1F_0-H^+-ATPase has been shown to be a near-equilibrium enzyme. In other words, the reaction can occur in both directions. However, both in isolated mitochondria that are generating ATP under conditions of excess carbon substrate, ADP, and oxygen and also in perfused and in vivo hearts, the F_1F_0-H^+-ATPase operates far out of equilibrium, so virtually all fluxes are in the ADP + Pi → ATP direction. In the presence of abundant oxygen, the F_1F_0-H^+-ATPase is kinetically controlled by the concentrations of its immediate substrates ADP and Pi, which are not usually limiting, and the magnitude of the proton electrochemical potential gradient across the mitochondrial inner membrane. Hence, ADP levels alone can regulate the rate of ATP synthesis so long as Pi, oxygen and carbon substrates are not limiting and the resulting proton gradient is very large. However, in

vivo regulatory mechanisms are far more complicated than those described by this simple scheme.

3.7. Regulation of Oxidative Phosphorylation

As pointed out, a simple kinetic regulatory scheme for oxidative phosphorylation with ADP and Pi availabilities controlling the ATP synthetic rate is valid when both oxygen and reducing equivalents are in excess. Under these conditions, the high proton electrochemical gradient will drive ATP synthesis until ADP falls to levels that are rate limiting. From this point, the rate of ADP *production* determines the steady-state rate of ATP synthesis. Because ADP is a product of ATP hydrolysis, the steady-state rate of ATP synthesis is determined by the steady-state rate of ATP hydrolysis (i.e., the rate of ATP utilization) and the steady-state ADP level required to support that rate of ATP synthesis.

This simple feedback regulation of ATP synthesis can be demonstrated in the perfused rat heart if the perfusate contains unphysiologically high concentrations of carbon substrates such as pyruvate or octanoate. Under these experimental conditions, myocardial ADP concentrations become low enough to regulate oxygen consumption kinetically; an increase in the rate of ATP utilization will cause ADP levels to rise, which in turn stimulates an increase in the rate of oxygen consumption. In this construct, the increased rate of delivery of ADP to the F_1F_0-ATPase increases the rate of ATP synthesis as long as ADP levels rise to values capable of supporting the new higher rate of ATP synthesis. In other words, ADP levels must increase concordant with the rate of ATP synthesis. This type of regulation is well described by the single-substrate Michalis-Menten model.

However, in large animal hearts (e.g., dog, swine, and human) in vivo ADP levels are higher than in the isolated perfused rat heart and are well above the usual kinetic regulatory range described in studies of isolated mitochondria or perfused rat hearts. Further, as MVO_2 increases, ADP levels actually remain fairly constant in the in vivo large animal heart. This does not mean that ADP availability is not crucial to the rate of ATP synthesis. When the rate of ATP expenditure is increased, there must always be an identical increase in the rate of ADP delivery to mitochondria (once a new steady state is reached). This increase in the rate of ADP delivery to the ATP synthase is obligatory, but a change in steady-state ADP levels is not.

The observation that ADP levels did not increase in the in vivo myocardium as the rate of ATP synthesis increased led to the recognition that additional regulatory systems were required to explain the data in in vivo models. Further, the overall regulatory processes must have very rapid response times regarding facilitation of ATP synthesis. The last is required because myocardial contents of ATP and creatine phosphate (PCr; another high-energy phosphate bond storage molecule that serves to buffer ATP levels) are only sufficient to support a few seconds of ATP expenditure in the absence of ATP synthesis. The reaction converting cytosolic ATP to PCr is rapid and near equilibrium via the enzyme creatine kinase. Figure 12 provides a brief overview of the ~P and ADP transport function of PCr.

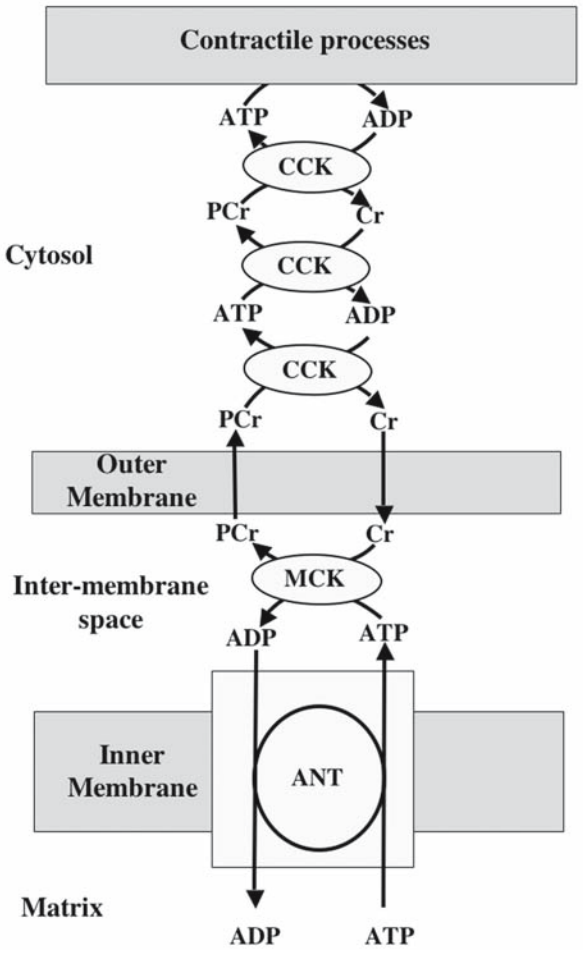

Fig. 12. The creatine kinase shuttle (CKS) hypothesis is depicted. The diffusion rate of adenosine diphosphate (ADP) across the outer mitochondrial membrane and through the cytosol is relatively slow. The CKS (and other shuttle systems not described; *see* source at end of this chapter) is thought to facilitate the transfer of ADP from sites of adenosine triphosphate (ATP) utilizing reactions to the mitochondrial intermembrane space and to facilitate the transfer of ATP to the sites of utilization. The way the shuttle is proposed to function is as follows: The adenine nucleotide transporter (ANT), which is not rate limiting, transports ADP from the mitochondrial intermembrane space to the mitochondrial matrix, where it is rephosphorylated back to ATP. The ANT simultaneously transports newly synthesized ATP from the matrix to the intermembrane space. Within the intermembrane space, the mitochondrial isozyme of creatine kinase (MCK) transfers the terminal high-energy phosphate of ATP to creatine (Cr) to form phosphocreatine (PCr). PCr then diffuses into the cytosol, and the ADP produced by this reaction in the intermembrane space is returned to the mitochondrial matrix by ANT, where it is rephosphorylated. The PCr that has diffused into the cytosol is then used as a high-energy phosphate donor for the rephosphorylation of cytosolic ADP by the cytosolic isozyme of creatine kinase (CCK). Because CCK has an extremely rapid turnover rate, it can facilitate transport of ATP from the mitochondria to the site of its hydrolysis and of ADP from the hydrolysis site back to the mitochondrial outer membrane. There, PCr leaving the mitochondria is used to rephosphorylate ADP, and the Cr liberated from PCr diffuses into the mitochondrial inner membrane space to be rephosphorylated. As a result, cytosolic ADP levels (including those in proximity to the points of ATP utilization) are kept at low levels even if the rate of ATP utilization increases. The stability of ADP levels in the face of increasing ATP utilization permits ATP to maintain a high level of free energy that can be transferred to energy requiring cellular processes.

A discussion of additional regulatory mechanisms for oxidative phosphorylation is presented next, and a review of the discussion of cardiomyocyte contraction mechanisms presented in Chapter 8 will refresh understanding of cardiomyocyte Ca^{2+} dynamics relevant to the following discussion.

During exercise, increased norepinephrine release by the sympathetic nervous system activates β-adrenergic receptors in cardiomyocytes. Their activation causes an increase of heart rate (by acting on the sinoatrial node) and an increase of Ca^{2+} entry into the cytosol of the cardiomyocytes via the sarcolemmal voltage-dependent Ca^{2+} channel. The increased Ca^{2+} entering the cytosol, together with β-adrenergic receptor-stimulated activation of sarcoplasmic reticulum Ca^{2+} pumping, increases sarcoplasmic reticulum Ca^{2+} stores. The more fully loaded sarcoplasmic reticulum can then release more Ca^{2+} per beat into the cytosol, resulting in a larger systolic cytosolic Ca^{2+} transient.

Both the increased frequency (heart rate) and the larger Ca^{2+} transient size serve to increase the "average" Ca^{2+} level in the cytosol. Mitochondria normally transport Ca^{2+} in and out of the matrix and maintain a "steady-state" matrix Ca^{2+} level that is related to average cytosolic Ca^{2+}. In response to higher average cytosolic Ca^{2+} levels, mitochondrial Ca^{2+} uptake increases, resulting in an increase in the steady-state level of matrix Ca^{2+}.

Increased mitochondrial matrix Ca^{2+} has at least two important effects on oxidative phosphorylation. First, as mentioned, the TCA cycle has three rate-limiting enzymes (PDH, isocitrate dehydrogenase, and α-ketoglutarate dehydrogenase), and the activities of these enzymes are partly regulated by mitochondrial matrix Ca^{2+} levels. When these enzymes interact with Ca^{2+}, their sensitivities to their respective substrates are increased. This accelerates their reaction rates and increases the rates of acetyl CoA entry into and flux through the TCA cycle without requiring pyruvate, acetyl CoA levels, or TCA cycle pool intermediate levels to rise, provided the rate of delivery of acetyl CoA to the TCA cycle is increased sufficiently to support the increased TCA cycle flux rate. Therefore, glucose uptake and glycolysis-mediated delivery of pyruvate to, and its rate of metabolism by, PDH must increase or the rates of fatty acid uptake by the cell and β-oxidative delivery of acetyl CoA to the TCA cycle must increase to support the increased rate of TCA cycle flux. In practice, the rates of cellular substrate uptake, glycolytic flux, and β-oxidation all respond to metabolic signaling, and the required increases in the rates of acetyl CoA production occur.

A major consequence of an increased TCA cycle flux is more rapid generation of mitochondrial NADH and $FADH_2$, which are the major substrates for the ETC. The subsequent stimulation of ETC flux results from an increased rate of NADH generation and a primary stimulation of ETC complex activities by other metabolic signals present during periods of increased ATP demand. Increased rates of ETC flux result in increased rates of H^+ pumping by the ETC, which serve to maintain the electrochemical gradient across the inner mitochondrial membrane at a level adequate to support the increased rate of ATP synthesis. In addition, the F_1F_0-ATPase is regulated such that the fraction of this enzyme that is in the active state is increased by elevation of mitochondrial matrix Ca^{2+}. An increased fraction of the enzyme in the active state is beneficial during periods of increased ATP synthesis because an increased amount of active enzyme increases the rate of ATP synthesis without requiring ADP levels to rise as long as the rate of ADP delivery to mitochondria increases appropriately (which it will when the rate of ATP utilization increases).

These observations support the concept that increased average cardiomyocyte cytosolic Ca^{2+} levels (e.g., that occur during exercise) act as a feed-forward signal for oxidative phosphorylation. This signal stimulates, in a parallel manner, ATP utilization by the contractile processes and ATP synthesis by the F_1F_0-ATPase. The net effect of these regulatory mechanisms (and additional feedback regulatory mechanisms not discussed) is to facilitate flux of basic food-derived carbon substrates through the metabolic sequences without requiring the cytosolic concentrations of the initial and intermediate substrates (including ADP) to increase.

The rapid response time of the entire system also allows ATP levels to remain relatively constant despite wide and rapid fluctuations in the rate of ATP utilization. Because these mechanisms allow both ADP and ATP levels and the ATP/ADP ratio to remain stable at increased ATP synthetic rates, the free energy that can be released by ATP hydrolysis and transferred to other reactions is maintained constant despite the increased rate of ATP expenditure. Control theory as applied to the regulation of oxidative phosphorylation, glycolysis, and β-lipid oxidation, and the TCA cycle has been the subject of detailed study. A more detailed discussion of this topic is presented in the sources listed at the end of this chapter.

4. METABOLISM IN ABNORMAL MYOCARDIUM

4.1. Metabolism in Ischemic Myocardium

The most common cause of inadequate myocardial ATP synthesis is ischemia, and the most frequent cause of myocardial ischemia is occlusive coronary artery disease. If narrowed coronary arteries can conduct adequate blood flow to sustain aerobic metabolism in the dependent myocardium during basal levels of activity but do not allow sufficient increases in flow to meet increased demands for ATP production during states of increased cardiac work (as would be caused by exercise), then it is classified as *demand ischemia*. This state can often be observed in patients with stable, inducible angina pectoris; the patient is asymptomatic at rest or during mild exertion, but when the work of the heart exceeds the ability of a narrowed coronary artery to meet the increased blood flow demand, then ischemia ensues, and the patient experiences chest pain. In response to the symptom of chest pain, the patient will commonly discontinue exercise. During the ensuing rest period, the cardiac work falls into the range at which the narrowed coronary artery can meet the blood flow demand, and the ischemia is relieved.

In contrast, in *supply ischemia* the coronary artery narrowings are so severe that they limit blood flow in the absence of increased ATP demand; that is, ischemia occurs when the patient is at rest. Supply ischemia is generally caused by an acute narrowing or abrupt complete closure of coronary vessels; the latter often causes myocardial infarction. Less com-

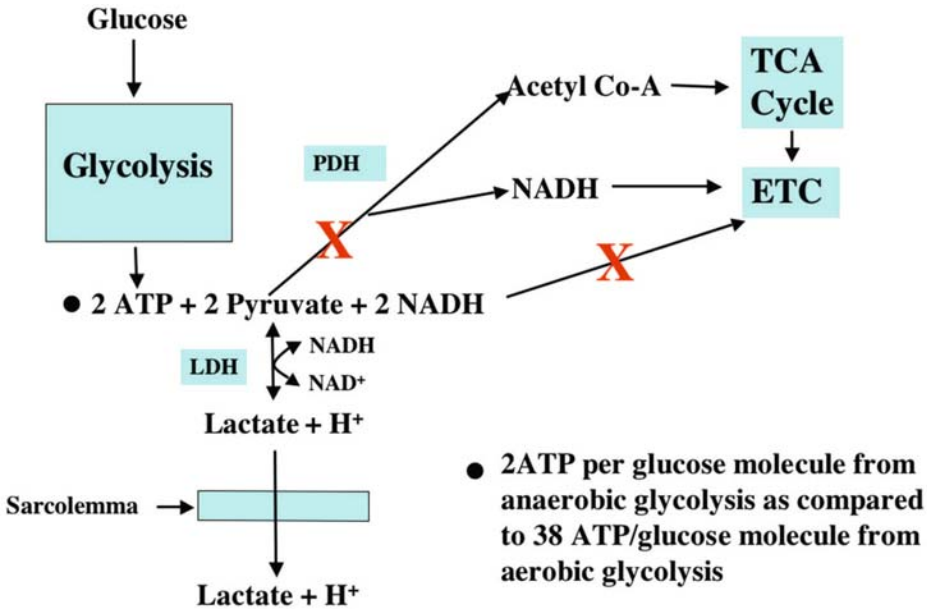

Fig. 13. A flowchart for anaerobic glucose metabolism is depicted. A large red X indicates metabolic pathways blocked during ischemia. *See* text for discussion. ATP, adenosine-triphosphate; CoA, coenzyme A; ETC, electron transport chain; LDH, lactic acid dehydrogenase; NAD, oxidized nicotinamide adenine dinucleotide ; NADH, reduced nicotinamide adenine dinucleotide; PDH, pyruvate dehydrogenase; TCA, tricarboxylic acid.

monly, supply ischemia can occur as the result of coronary spasm, in which inappropriate (pathological) vasoconstriction of an epicardial coronary artery causes transient total or near total reduction of flow.

Although the nature of the myocardial ischemic process is qualitatively similar in supply and demand ischemias, supply ischemia is generally considered more clinically threatening. Because of the greater vulnerability of the inner myocardial layers of the left ventricle to blood flow reduction, mild ischemia is usually confined to the subendocardium; as the coronary obstruction becomes more severe, ischemia proceeds as a wavefront from subendocardium to subepicardium until the full wall is involved.

When myocardial blood flow is limited, both oxygen and carbon substrate availabilities in turn can limit the ATP synthetic rate, but it is usually the oxygen deficit that is most critical. This is because the myocyte has substantial carbon substrate reserves (i.e., glycogen and triglyceride stores), but is unable to store a significant quantity of oxygen. Consequently, when coronary blood flow is insufficient to meet myocardial needs, the severity of the oxygen deficit determines the extent of limitation of oxidative phosphorylation. Nevertheless, the effect of oxygen limitation is confined to oxidative phosphorylation because glycolytic ATP synthesis does not require oxygen (Figs. 5 and 13).

During hypoxia (in which blood oxygen content is markedly reduced, but blood flow is not limited) or in ischemic conditions (in which blood flow is restricted, but blood oxygen content is normal), electron transport by the ETC slows or stops depending on the severity of the oxygen deficit because electrons cannot be transferred from cytochrome oxidase to molecular oxygen (the terminal electron acceptor). As a consequence, the pumping of H^+ from the mitochondrial matrix into the intermembrane space stops because it depends on energy liberated as electrons pass through the ETC. As a result, the protonmotive force across the inner mitochondrial membrane begins to dissipate, and mitochondrial ATP synthesis fails.

If the dissipation of the H^+ gradient is marked, then the F_1F_0-H^+-ATPase operates in the reverse direction; that is, it converts ATP to ADP and uses energy liberated by ATP hydrolysis to pump H^+ back into the intermembrane space. Hence, mitochondria can either synthesize ATP under physiological conditions or degrade ATP when oxygen is severely limited. Because the H^+ electrochemical potential is used to energize other mitochondrial transport functions in addition to supporting ATP synthesis, mitochondrial degradation of ATP during periods of oxygen limitation may serve to preserve nonoxidative mitochondrial function for a time at the expense of hastening the fall in cytoplasmic ATP levels.

Glycolysis, which in principle can proceed normally in the absence of oxygen, is also limited when blood flow is reduced during ischemia. Oxygen limitation causes cessation of ETC function and thereby stops the mitochondrial consumption of reducing equivalents transferred from cytosolic NADH. This occurs because mitochondrial NADH oxidation also stops, mitochondrial NAD^+ levels fall, and there is no recipient for reducing equivalents transported from the cytosolic NADH pool. Cytosolic NAD^+ is a substrate of glyceraldehyde phosphate dehydrogenase (GAPDH), and if the NADH generated by that reaction is not oxidized back to NAD^+ by the transfer of reducing equivalents into the mitochondria by the malate–aspartate shuttle or the conversion of glycolytically produced

pyruvate into lactate by LDH and the subsequent efflux of lactate and accompanying H^+ions from the myocyte, then the lack of NAD^+ inhibits GAPDH.

Therefore, factors that limit the rates of glycolytic ATP synthesis during ischemia are accumulations of cytosolic NADH, lactate and H^+ ions. Under conditions of unrestricted coronary flow, the myocardium can rapidly export both of these ions even when the glycolytic rate is markedly increased; that is, a low oxygen content of coronary arterial blood which limits oxygen delivery to the myocyte does not *per se* limit lactate and H^+ export. In contrast, when the myocardium is ischemic, the capacity to export lactate and protons decreases in proportion to the severity of the blood flow reduction. Because the conversion of pyruvate to lactate results in the oxidation of cytosolic NADH, the availability of NAD^+ to GAPDH is further reduced when rising levels of lactate slow this reaction and glycolysis ultimately stops for this reason or because glycogen stores are exhausted (Figs. 5 and 9). In contrast, during hypoxia, coronary flow is not restricted, and glycolysis proceeds at a rapid rate because metabolic signaling activates both the rate-limiting glycolytic reactions and the transport of glucose into the myocyte. During moderate ischemia, when both glucose and oxygen delivery are impaired, myocyte glycogen stores are the main source of glucose for glycolysis. When glycogen stores are exhausted, the rates of glucose delivery to, and lactate clearance from, the ischemic myocyte (which are limited) control the rate of glycolysis.

These concepts have specific importance in patients with coronary artery disease because they define the boundaries for viability of the ischemic myocardium. In the moderately ischemic myocardium, contractile function rapidly decreases in response to: (1) decreased ATP availability, (2) accumulation of H^+ ions, and (3) other less-well-defined factors. However, if residual coronary blood flow during ischemia is sufficient to permit some glycolysis (by allowing the export of some lactate and H^+ and the import of glucose), then modest ATP production and, consequently, viability may be preserved for some time. In contrast, during acute total coronary occlusion, glycolysis is rapidly inhibited, and myocardial death will occur. Hence, a level of coronary blood flow that is insufficient to maintain oxidative phosphorylation and contractile function may support sufficient glycolytic ATP production to sustain myocardial viability until appropriate medical or surgical treatment can restore blood flow to the ischemic myocardium.

4.2. Metabolism in Hypertrophied and Failing Hearts

During fetal life, the myocardium primarily metabolizes glucose rather than fatty acids. This pattern of metabolism is well suited to the lower oxygen levels found in fetal arterial blood; glucose metabolism requires less oxygen than fatty acid metabolism. In addition, the lower cardiac work levels (lower blood pressure) occurring in the fetus are adequately supported by ATP production through glycolysis and pyruvate oxidation. After birth, substrate preference of the heart (now in a higher oxygen environment and operating at a higher workload) rapidly shifts to the adult pattern of predominant fatty acid oxidation. This change of substrate preference is the result of upregulated expression of genes controlling the transport of fatty acids into the myocyte and their subsequent metabolism in the cytosol and mitochondria. This upregulation in the expression of genes involved in fatty acid metabolism, and oxidative phosphorylation is commonly referred to as the shift from a fetal to an adult gene expression pattern.

A chronic mechanical overload produced by hypertension, heart valve abnormalities, or destruction of a portion of the left ventricle by infarct initially results in some degree of left ventricular dilation. Left ventricular wall tension increases as a consequence of the La Place relationship between wall tension and chamber radius. The increased wall tension activates changes in the expression patterns of a number of genes involved in both myocyte growth (hypertrophy) and metabolism. The resultant increase of left ventricular wall thickness returns systolic wall stresses more toward normal, often resulting in a prolonged period of compensated myocardial hypertrophy.

However, myocardial hypertrophy is associated with important changes in energy metabolism. These include reductions of high-energy phosphate compounds (HEP; i.e., ATP and CP) levels and alterations in carbon substrate preference with decreased utilization of free fatty acids and increased dependence on glucose. This shift in the myocardial gene expression to increased glucose and decreased fatty acid utilization is referred to as a reversion to the fetal gene expression pattern. Subsequently, reductions in the levels of enzymes and transporters crucial to oxidative phosphorylation also occur. Although the increased glucose metabolism and decreased fatty acid metabolism associated with this reversion (to a fetal gene expression pattern) may have energetic benefits, the overall ATP synthetic capacity of severely hypertrophied and failing myocardium is significantly reduced. Whatever the cause, the period of compensated hypertrophy in an overloaded heart is often followed by contractile dysfunctions of the myocytes with ultimate progressive left ventricular dysfunction, then to be diagnosed as the clinical syndrome of heart failure.

It has been unclear whether decreased ATP synthetic capacity in hypertrophied or failing cardiomyocytes actually constrains contractile performance and contributes to the progression to a decompensated state. The issue has been whether contractile dysfunction in the failing heart is caused primarily by a limited ability of the contractile apparatus to consume ATP or whether the reduced ability to produce ATP is also contributory. Experimental data have shown that the upregulation of glucose metabolism that occurs in hypertrophied or failing myocardium may not adequately compensate (from the standpoint of ATP synthetic capacity) for the downregulation of fatty acid metabolism that occurs in these hearts.

Interestingly, transgenic mice that overexpressed a cardiomyocyte sarcolemmal glucose transporter (which caused an increase of glucose uptake and metabolism) were far less likely than nontransgenic mice to develop cardiac decompensation or die when subjected to chronic pressure overload of the left ventricle (induced by surgical narrowing of the ascending aorta). This finding implies that augmentation of glucose uptake is beneficial to the chronically overloaded heart, but that

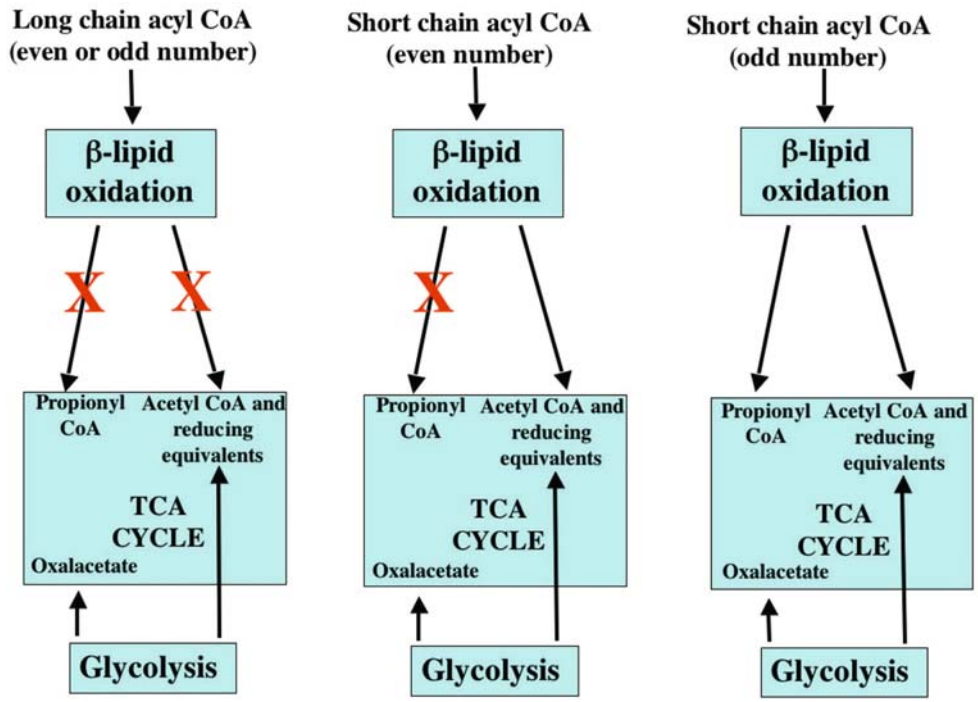

Fig. 14. The effects of very long-chain acyl-dehydrogenase deficiency on the metabolism of long-chain fatty acids (even and odd numbered), short-chain fatty acids (even numbered), and short-chain fatty acids (odd numbered). Only the last can also supply anaplerotic substrate to the tricarboxylic acid (TCA) cycle. A large red X indicates metabolic pathways that cannot be used by a specific type of free fatty acid. *See* discussion in text. CoA, coenzyme A.

the fetal shift in gene expression (substrate preference) that normally occurs in this condition is insufficient to compensate for the bioenergetic abnormalities present in the hypertrophying myocardium.

The discussion of cardiac dysfunction considers the possibility that acquired defects in the overloaded cardiomyocyte may limit ATP synthesis sufficiently to constrain mechanical function. Yet, abnormalities of left ventricular function can add an ischemic component to the metabolic abnormalities of hypertrophied and failing myocardium even in the absence of occlusive coronary artery disease. As discussed, increased ventricular filling pressures and tachycardia in the abnormal heart can limit the ability of myocardial blood flow (especially in the subendocardium) to increase normally in response to an increased metabolic rate. Hence, in the chronically overloaded heart, acquired intrinsic abnormalities of the cardiomyocytes and superimposed limitations of blood flow can act together to compromise cardiomyocyte ATP synthetic capacity and thus further impair cardiac function.

4.3. Primary (Genetic) Myocardial Metabolic Abnormalities

As described previously, changes in gene expression associated with cardiac hypertrophy or heart failure can cause various abnormalities of myocardial metabolism that in turn may act to constrain contractile function. However, "primary" (genetically determined) abnormalities of carbon substrate metabolism or oxidative phosphorylation can also cause myocyte hypertrophy and failure. Refer to the sources at the end of this chapter for more information on such defects. A dramatic example of this type of genetically induced metabolic abnormality and a successful therapeutic approach based on sound biochemical principles have been described and are discussed next.

An inherited deficiency of the enzyme very long-chain acyl-CoA dehydrogenase (VLCAD) is known to be associated with cardiomyopathy and skeletal muscle myopathy (Fig. 14). Because most dietary fatty acids are of the long-chain type, the deficiency of VLCAD results in a markedly increased cardiac dependence on glucose for ATP generation. The fact that even upregulated glucose metabolism cannot adequately support cardiac function is indicated by the development of progressive myopathy (although the cytosolic accumulation of long-chain fatty acids also contributes to the myopathy).

The classical treatment has been to replace the long-chain fatty acids in such an individual's diet with even-numbered short- or medium-chain length fatty acids such as octanoate or decanoate. The short-chain fatty acids bypass the metabolic roadblock, because the medium- and short-chain acyl-CoA dehydrogenases are normal in these patients. This strategy induces increased fatty acid utilization and causes clinical improvement; unfortunately, in many such patients, cardiac and skeletal muscle myopathies persist.

Why does feeding even-numbered short-chain length fatty acids not fully correct the muscle defects in these patients despite the augmentation of acetyl CoA delivery to the TCA cycle? It should be recalled that VLCAD deficiency causes

limitation of both acetyl CoA and propionyl CoA delivery to the TCA cycle. Thus, although even-numbered short-chain fatty acids supply acetyl CoA, they do not supply the anaplerotic substrate propionyl CoA and consequently cannot correct the lack of an anaplerotic contribution from β-lipid oxidation. Hence, an increase in consumption of even-numbered short-chain fatty acids would not be able to correct the decrease in TCA intermediate pool size resulting from a propionyl CoA deficiency (Fig. 6B).

Following this logic, dietary supplementation with an odd-numbered short-chain fatty acid would permit β-lipid oxidation to supply both acetyl CoA and propionyl CoA (the latter would increase TCA intermediate pool size). In fact, when patients were treated with the short-chain seven-carbon fatty acid heptanoate, they showed marked improvement in both skeletal muscle and cardiac abnormalities. Hence, this disorder was effectively managed by understanding the basic biochemical defect and prescribing a treatment strategy that compensated for this defect.

5. SUMMARY

This chapter reviewed the metabolic pathways involved in transferring the energy in dietary carbon substrates (primarily glucose and fatty acids) to ATP, the molecule that serves as the ultimate source of energy driving contractile and other processes in the heart. Normal cardiac function depends on both adequate delivery of carbon substrates and oxygen to the heart by the coronary circulation and the ability of the heart to extract and metabolize these substrates at rates sufficient to support a wide range of ATP demands. The effects of several disease processes on cardiac metabolism were discussed, and the concept that the diseased heart may be energy limited was presented. Last, an example of effective therapy based on an understanding of an abnormal metabolic pathway emphasized the need for a strong clinical knowledge of such energetic pathways.

ACKNOWLEDGMENT

This work was supported by NIH/Grants HL33600, HL58840, HL20598 and HL21872.

REFERENCES

Regulation of Myocardial Blood Flow

Duncker, D.J. and Bache, R.J. (2000) Regulation of coronary vasomotor tone under normal conditions and during acute myocardial hypoperfusion. *Pharmacol Ther*. 86, 87–110.

Gorman, M.W., Tune, J.D., Richmond, K.N., and Feigl, E.O. (2000) Feedforward sympathetic coronary vasodilation in exercising dogs. *J Appl Physiol*. 89, 1892–1902.

Ishibashi, Y., Duncker, D.J., Zhang, J., and Bache, R.J. (1998) ATP-sensitive K^+ channels, adenosine, and nitric oxide-mediated mechanisms account for coronary vasodilation during exercise. *Circ Res*. 82, 346–359.

Myocardial Substrate Selection

Drake, A.J., Haines, J.R., and Noble, M.I. (1980) Preferential uptake of lactate by the normal myocardium in dogs. *Cardiovasc Res*. 14, 65–72.

Drake-Holland, A.J., Van der Vusse, G.J., Roemen, T.H., et al. (2001) Chronic catecholamine depletion switches myocardium from carbohydrate to lipid utilisation. *Cardiovasc Drugs Ther*. 15, 111–117.

Lehman, J.J. and Kelly, D.P. (2002) Transcriptional activation of energy metabolic switches in the developing and hypertrophied heart. *Clin Exp Pharmacol Physiol*. 29, 339–345.

Glucose and Fatty Acid Metabolism, Tricarboxylic Acid Cycle Function, and Electron Transport Chain Function

Berg, J.M., Stryer, L., and Tymoczko, J.L. (eds.). (2002) *Biochemistry*, 5th Ed. Freeman, New York, NY.

Murray, R.K., Mayes, P.A., Rodwell, V.W., Granner, D.K.,Granner, D. (eds). (2003) *Harper's Illustrated Biochemistry*, 26th Ed. Lange Medical Books/McGraw-Hill, New York, NY.

Intermediary Metabolism and Oxidative Phosphorylation

Aimar-Beurton, M., Korzeniewski, B., Letellier, T., Ludinard, S., Mazat, J.P., and Nazaret, C. (2002) Virtual mitochondria: metabolic modelling and control. *Mol Biol Rep*. 29, 227–232.

Brand, M.D. and Curtis, R.K. (2002) Simplifying metabolic complexity. *Biochem Soc Trans*. 30, 25–30.

Cortassa, S., Aon, M.A., Marban, E., Winslow, R.L., and O'Rourke, B. (2003) An integrated model of cardiac mitochondrial energy metabolism and calcium dynamics. *Biophys J*. 84, 2734–2755.

From, A.H.L., Zimmer, S.D., Michurski, S.P., et al. (1990) Regulation of the oxidative phosphorylation rate in the intact cell. *Biochemistry*. 29, 3731–3743.

Hochachka, P.W. (2003) Intracellular convection, homeostasis and metabolic regulation. *J Exp Biol*. 206, 2001–2009.

Korzeniewski, B. (2001) Theoretical studies on the regulation of oxidative phosphorylation in intact tissues. *Biochem Biophys Acta*. 1504, 31–45.

Korzeniewski, B. (2002) Parallel activation in the ATP supply-demand system lessens the impact of inborn enzyme deficiencies, inhibitors, poisons or substrate shortage on oxidative phosphorylation in vivo. *Biophys Chem*. 96, 21–31.

Kushmerick, M.J. and Conley, K.E. (2002) Energetics of muscle contraction: the whole is less than the sum of its parts. *Biochem Soc Trans*. 30, 227–231.

Ludwig, B., Bender, E., Arnold, S., Huttemann, M., Lee, I., and Kadenbach, B. (2001) Cytochrome C oxidase and the regulation of oxidative phosphorylation. *Chembiochem*. 2, 392–403.

Territo, P.R., Mootha, V.K., French, S.A., and Balaban, R.S. (2000) Ca(2+) activation of heart mitochondrial oxidative phosphorylation: role of the F(0)/F(1)-ATPase. *Am J Physiol Cell Physiol*. 278, C423–C435.

Zhang, J., Murakami, Y., Zhang, Y., et al. (1999) Oxygen delivery does not limit cardiac performance during high work states. *Am J Physiol*. 277, H50–H57.

High-Energy Phosphate Shuttles

Dzeja, P.P. and Terzic, A. (2003) Phosphotransfer networks and cellular energetics. *J Exp Biol*. 206, 2039–2047.

Metabolism During Ischemia

Sambandam, N. and Lopaschuk, G.D. (2003) AMP-activated protein kinase (AMPK) control of fatty acid and glucose metabolism in the ischemic heart. *Prog Lipid Res*. 42, 238–256.

Stanley, W.C., Lopaschuk, G.D., Hall, J.L., and McCormack, J.G. (1997) Regulation of myocardial carbohydrate metabolism under normal and ischaemic conditions. Potential for pharmacological interventions. *Cardiovasc Res*. 33, 243–257.

Metabolism in Hypertrophied and Failing Myocardium

Lehman, J.J. and Kelly, D.P. (2002) Transcriptional activation of energy metabolic switches in the developing and hypertrophied heart. *Clin Exp Pharmacol Physiol*. 29, 339–345.

Liao, R., Jain, M., Cui, L., et al. (2002) Cardiac-specific overexpression of GLUT1 prevents the development of heart failure attributable to pressure overload in mice. *Circulation*. 106, 2125–2131.

Ning, X.H., Zhang, J., Liu, J., et al. (2000) Signaling and expression for mitochondrial membrane proteins during left ventricular remodeling and contractile failure after myocardial infarction. *J Am Coll Cardiol.* 36, 282–287.

Young, M.E., Laws, F.A., Goodwin, G.W., and Taegtmeyer, H. (2001) Reactivation of peroxisome proliferator-activated receptor alpha is associated with contractile dysfunction in hypertrophied rat heart. *J Biol Chem.* 276, 44,390–44,395.

Inherited Defects in Myocardial Metabolism

DiMauro, S. and Schon, E.A. (2003) Mitochondrial respiratory-chain diseases. *N Engl J Med.* 348, 2656–2668.

Roe, C.R., Sweetman, L., Roe, D.S., David, F., and Brunengraber, H. (2002) Treatment of cardiomyopathy and rhabdomyolysis in long-chain fat oxidation disorders using an anaplerotic odd-chain triglyceride. *J Clin Invest.* 110, 259–269.

18 Introduction to Echocardiography

JAMIE L. LOHR, MD

CONTENTS

1. INTRODUCTION

The use of ultrasound to provide noninvasive evaluation of cardiac structure and function was a revolutionary advancement in cardiac care in the late 20th century *(1)*. Development of the field of echocardiography has allowed detailed serial examinations of the development, structure, and function of the human heart in normal physiological states and in pathological conditions. Echocardiography has increased the diagnostic accuracy of noninvasive cardiac evaluation and provides a tool for the monitoring of diagnostic and therapeutic procedures. The goals of this chapter are to: (1) provide a brief overview of the types of echocardiography in clinical use today, (2) review the physical principles that underlie this clinical tool, and (3) demonstrate how echocardiography can be used to assess cardiac structure and function.

Prior to the 1970s, diagnosis of congenital and acquired heart disease was achieved by the combination of physical examination, electrocardiography (ECG), and invasive cardiac catheterization. Unfortunately, clinical examination and ECG are often not very specific diagnostic tools. Cardiac catheterization, although greatly augmenting noninvasive clinical information, can be a stressful and risky procedure, particularly in the young or very ill patient. Initial attempts at imaging the heart using reflected sound waves were made in the 1950s, with improvement in the experimental technology and its initial clinical application in the 1960s *(1)*. During the 1970s, simple motion-mode (M-mode) or linear images were available to define cardiac structures, but these were not adequate for providing great diagnostic detail in complex congenital heart disease. During the 1980s, the technology to provide 2D real-time imaging of the heart was developed, and this subsequently revolutionized noninvasive evaluation of cardiac structure and function. In the late 1980s, techniques of Doppler ultrasound, including color mapping, were developed to extend the analyses of cardiac function and hemodynamics *(1)*. By the late 1980s, many cardiac defects could be diagnosed accurately and repaired completely without invasive testing.

From: *Handbook of Cardiac Anatomy, Physiology, and Devices*
Edited by: P. A. Iaizzo © Humana Press Inc., Totowa, NJ

2. PHYSICAL PRINCIPLES OF ECHOCARDIOGRAPHY

2.1. Ultrasound Imaging of Tissues

Echocardiography uses the properties of sound waves to differentiate tissues of varied density in the human body. Sound travels in mechanical waves with a speed dependent on the density and elastic properties of the medium in which they are traveling *(2)*. This property of tissue is termed its *acoustic density*. Ultrasound waves, which are used in medical applications, have frequencies that are higher than those audible to the human ear. Ultrasound frequencies are generally over 20,000 cycles per second, or hertz, and most cardiac applications are performed using frequencies of 2 million to 10 million hertz, or 2–10 megahertz (MHz).

When a sound wave, which is generated by electrical stimulation of a piezoelectric crystal, travels through an interface between two tissues of varied acoustic density, such as myocardium and blood, a portion of the energy is reflected backward (the reflected wave), and the rest travels forward through the next tissue (the refracted wave). The reflected wave is received by the transducer, turned back into electrical energy, amplified, and displayed *(1)*. If there is too much variance between the acoustic density of the tissues imaged (as in air-filled lung and myocardium or bone and myocardium), the entire ultrasound wave is reflected, and the cardiac structures cannot be imaged *(1)*.

The amount of reflected wave detected during ultrasound imaging depends not only on the acoustic characteristics of the interface, but also on the angle of incidence or interrogation. An ultrasound beam that encounters a flat surface perpendicular to the beam will reflect a wave in the direction of the transmitted sound. In contrast, a beam parallel to a structure or that encounters an irregularly shaped structure, as is common in tissue imaging, will be reflected with a degree of scatter that is proportional to the angle of incidence *(2)*.

2.2. Resolution of Structures

The ability of cardiac ultrasound to provide anatomical resolution depends on the wavelength of the sound used. The speed of transmission, the frequency, and the wavelength are related by the equation

$$c = f \times \lambda \text{ or } \lambda = c/f$$

where c is the speed of sound in the medium, f is the frequency of the wave (in hertz or cycles per second), and λ is the wavelength. Thus, a higher frequency transducer will produce a smaller wavelength and improved resolution along the path of the beam, also termed *axial resolution (1)*.

According to Geva *(1)*, axial resolution is generally two times the wavelength used, so that a 3.5-MHz transducer has a wavelength of 0.43 mm and an axial resolution of 0.86 mm, and a 7.5-mHz transducer (commonly used in pediatric imaging) has a wavelength of 0.2 mm and axial resolution of approx 0.4 mm. Unfortunately, the use of high-frequency transducers is limited because the smaller wavelength cannot penetrate as deeply into tissue, and they are therefore less useful for cardiac imaging in adults. Lateral resolution in echocardiography is impacted by the diameter of the beam width, which is a function of the transducer size, shape, and focal plane as well as the frequency *(1)*.

3. IMAGING MODALITIES

3.1. M-Mode Echocardiography

M-mode, or motion-mode, echocardiography was the first type of ultrasound used for clinical cardiovascular imaging. Its use today is primarily limited to assessment of valve motion and reliable reproducible measurements of chamber sizes and function *(1,3)*. In M-mode echocardiography, a narrow ultrasound beam is pulsed rapidly in a single plane through the heart, and the movements of the structures in that single plane are plotted against time with very high temporal and axial resolutions.

M-mode echocardiography can be used to assess cardiac wall thickness, aortic root size, chamber sizes, or ventricular function. In general, left ventricular function is quantitated using M-mode by determining the percentage of fractional shortening of the left ventricle, which is calculated using the following equation:

$$\text{SF}(\%) = \frac{\text{LVEDD} - \text{LVESD}}{\text{LVEDD}} \times 100$$

where SF is the shortening fraction, LVEDD is the left ventricular end-diastolic dimension; and LVESD is the left ventricular end-systolic dimension.

Normal values vary with age and range from 35–45% in infants to 28–44% in adolescents and adults *(4,5)*.

3.2. 2D Imaging

Two-dimensional imaging provides an arc of imaging planes by employing multiple ultrasound beams to provide a cross-sectional view of the heart. Currently, 2D imaging provides the majority of information about cardiac structure and function in routine clinical studies. Two-dimensional imaging requires the presence of multiple beams of ultrasound interrogation in a single transducer, and several types of transducers are available to achieve this.

Transducers available for 2D imaging include mechanical (a sweeping or rotating ultrasound beam), phased array (multiple independently controlled sources), and linear array (a line of crystals simultaneously generating a beam of ultrasound). Today, phased-array transducers are most commonly used because of their: (1) small size, (2) ability to provide simultaneous 2D and M-mode or Doppler imaging, and (3) improved control of focal length for a more uniform image throughout the field of view *(6)*.

In addition to using 2D imaging for viewing anatomical detailing, left ventricular function can be quantitated by this mode using an estimated left ventricular ejection fraction. This method, which has been shown to correlate well with angiographic estimates of ventricular function, takes advantage of the conical shape of the left ventricle to estimate end-diastolic and end-systolic ventricular volumes from tracings of 2D images using Simpson's biplane rule *(3)*. The ejection fraction is calculated as follows:

$$\text{EF}(\%) = \frac{\text{LV EDV} - \text{LV ESV}}{\text{LV EDV}} \times 100$$

where EF is ejection fraction, LV EDV is left ventricular end-diastolic volume, and LV ESV is left ventricular end-systolic volume.

Normal values for ejection fraction are approx 55–65%, and cardiac output can be estimated by multiplying the volume ejected with each beat (stroke volume) by the heart rate using the equation

$$\text{CO} = \text{HR} \times \text{SV}$$

where CO is cardiac output, HR is heart rate, and SV is stroke volume.

3.3. Doppler Ultrasound

The Doppler principle, described by Christian Johann Doppler in 1843, states that the frequency of transmitted sound is altered when the source of the sound is moving *(2)*. The classic

example is the change in pitch of a train whistle as it moves, getting higher as it approaches the receiver and lower as it moves away from it. This change in frequency, or Doppler shift, also occurs when the source of sound is stationary, and the waves are reflected off a moving target, including red blood cells in the vasculature. The shift in frequency is related to the velocity of the moving target, as well as the angle of incidence, and is described by the equation

$$f_d = \frac{2(f_0)(V)\cos\varnothing}{c}$$

where f_d is the observed Doppler frequency shift, f_0 is the transmitted frequency, c is the velocity of sound in human tissue at 37°C (~1560 m/s), V is blood flow velocity, and $\varnothing$ is the intercept angle between the ultrasound beam and the blood flow.

Using this principle, Doppler ultrasound can be used to estimate the velocity of blood flow in the human heart and vasculature noninvasively. Using a modified Bernoulli equation in which pressure drop is equal to four times the velocity squared ($4V^2$), Doppler ultrasound can also be used to estimate chamber pressures and gradients and to provide significant noninvasive hemodynamic data.

3.4. Continuous Wave Doppler

Continuous wave Doppler is performed using a single transducer with two separate elements for transmission and reception of sound waves, so that there is continuous monitoring of the Doppler shift. This technique allows detection of very high velocity blood flow, but does not allow localization of the site of velocity shift along the line of interrogation *(1)*.

3.5. Pulsed Wave Doppler

Pulsed wave Doppler uses bursts of ultrasound alternating with pauses to detect Doppler shift in a localized region. The timing between the generation of the ultrasound wave and detection of the reflected wave determines the depth of interrogation. Pulsed wave Doppler is useful to measure velocity changes in a region defined by 2D echocardiography; however, the spatial resolution limits the velocity shifts detected. In general, the maximal velocity shift detectable is one-half of the Doppler sampling rate (pulse repetition frequency) and is designated the *Nyquist limit (1)*. The maximal sampling rate is determined by the distance of the sampling site from the transducer and the transducer frequency, so that sampling from a transducer position nearer to the region to be interrogated and using a lower frequency transducer will improve the detection and localization of higher velocity flow *(1)*.

3.6. Color Doppler Flow Mapping

Color Doppler flow mapping uses the principles of pulsed Doppler to examine multiple points along the scan lines. The mean velocity and direction of these signals are calculated and then displayed, superimposed on a 2D image. By convention, flow directed toward the transducer is red, and flow directed away from the transducer is blue. Accelerated or turbulent flow is given a different color, typically yellow and green. Color flow mapping is valuable because of the large amount of information that can be obtained in a single image. It can also aid in the localization of flow acceleration, quantitation of valvular regurgitation, visualization of intracardiac shunting, or assessment of arterial connections. Information obtained from color Doppler can also be refined by pulsed wave Doppler and continuous wave Doppler interrogation.

3.7. Quantification of Pressure Gradients Using Doppler Shift Measurements

Today, quantification of pressure gradients using Doppler echocardiography can provide hemodynamic information that could previously be obtained only by invasive cardiac catheterization. Specifically, the Bernoulli equation *(3,7)* defines the relationship between velocity shift across an obstruction and the pressure gradient caused by the obstruction. For practical purposes, the proximal velocity is neglected, and the simplified equation becomes:

$$\text{pressure difference} = \text{distal velocity squared} \times 4$$

This is a valuable way to estimate pressure drops across obstructive valves or pressure differences between chambers (i.e., based on the velocity of valvar regurgitation or intracardiac shunting).

4. CLINICAL APPLICATIONS OF CARDIAC ULTRASOUND

4.1. Transvaginal and Transabdominal Fetal Echocardiography

The human fetal heart is fully developed and functional by 11 wk after conception. Using transvaginal ultrasound, the structure and functional characteristics of the fetal heart can be observed as early as 9 wk of gestational age *(8)*. This technique remains the most useful type of fetal cardiac imaging until approx 16 wk of gestation. At that time, transabdominal imaging becomes the preferred method (Fig. 1). Fetal imaging is routinely performed at 16–20 wk of gestational age, and image quality improves until about 24–28 wk of gestational age *(8)*. The quality of fetal images can be reduced by loss of amniotic fluid, maternal body habitus, fetal bone density, or the fetal position.

M-mode, 2D, and Doppler ultrasound techniques are useful for an analysis of the anatomy and function of the fetal heart, as well as for the diagnoses and monitoring of fetal arrhythmias. In general, fetal echocardiography has contributed to: (1) improved understanding of the natural history of many forms of congenital heart disease; (2) improved monitoring and obstetric care of fetuses with structural heart diseases and arrhythmias; and (3) attempts at in utero correction of valvar abnormalities *(9,10)*.

4.2. Transesophageal Echocardiography

Transesophageal echocardiography allows imaging of the heart from the esophagus or stomach, which improves image resolution by eliminating much of the acoustic interference from the lungs and chest wall and at the same time allowing for a reduced distance of the ultrasound source from the heart. Transesophageal imaging is performed using either a biplane probe (two single-plane arrays set at perpendicular planes) or a rotating single-array probe that provides multiple planes of view (an omniplane probe).

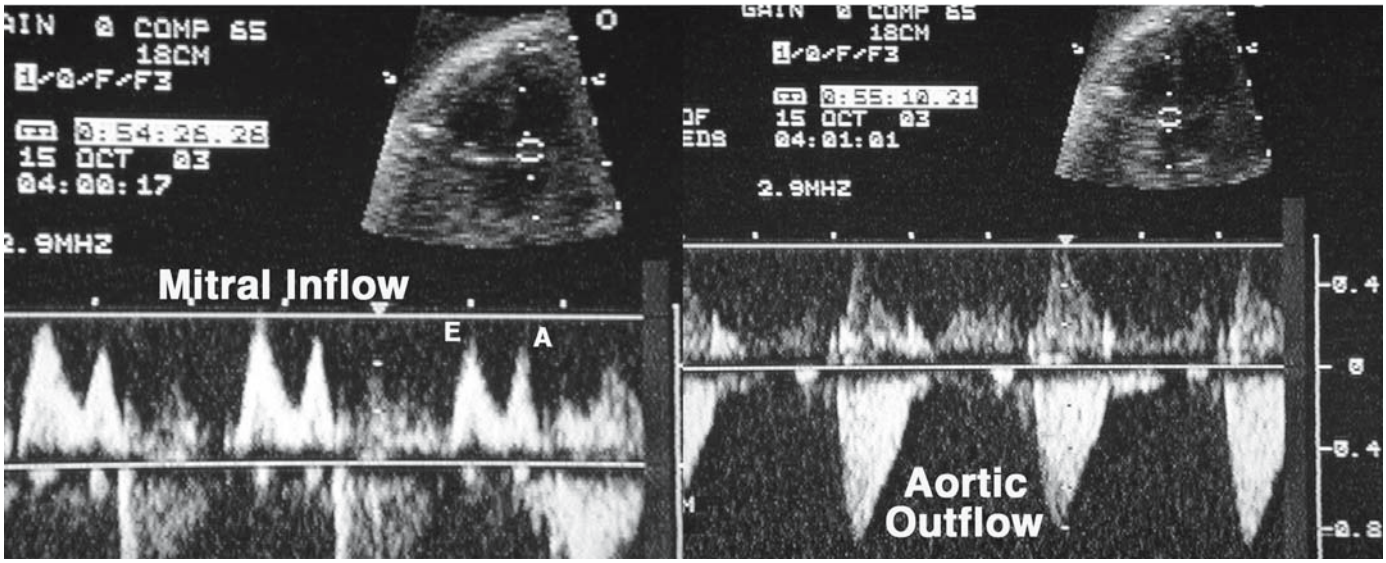

Fig. 1. Fetal echocardiogram at approx 24 wk of gestation. Four-chamber views are shown with pulse wave Doppler analysis of mitral inflow and aortic outflow. Mitral inflow is characterized by two waves, an E wave representing passive filling of the left ventricle in diastole and an A wave representing active filling of the ventricle with atrial systole. Doppler flows are less than 1 m/s, indicating unobstructed blood flow, and the interval between aortic outflow signals is approx 0.5 s, indicating a fetal heart rate of 120 beats/min.

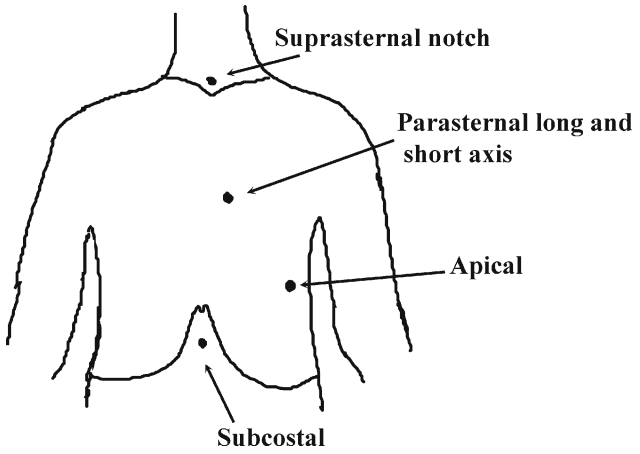

Fig. 2. Diagram of the chest showing transducer position for standard transthoracic echocardiographic windows. A typical examination in a cooperative patient is performed in a standard order: parasternal, apical, subcostal, and then suprasternal notch views. Perpendicular imaging planes can be obtained from each position by rotating the transducer 90°.

Today, transesophageal probes come in sizes appropriate for use in adults, children, and infants. Transesophageal echocardiography is used when improved resolution is required or when transthoracic windows are unavailable, as is typical in the operating room or cardiac catheterization laboratory *(3)*. It also has become a routine form of intraoperative monitoring for open heart surgery and is useful to detect incomplete repairs prior to separation from cardiopulmonary bypass *(11)*. Further, it is a useful adjunct to interventional cardiac catheterization procedures. Transesophageal echocardiography typically requires sedation or anesthesia and thus adequate patient monitoring . It is significantly more invasive than standard transthoracic echocardiography and can be complicated by airway compromise or dysphagia *(3,12,13)*.

4.3. Transthoracic Echocardiography

Transthoracic echocardiography is the most common method for cardiac imaging. It is noninvasive, can be performed in any cooperative patient, and only rarely requires sedation or anesthesia. Yet, images obtained are limited by patient size and can be complicated by interference from soft tissues, bone, or lung. The transthoracic echocardiogram is performed from standard windows on the chest (Fig. 2) and requires the use of multiple transducers at varied ultrasound frequencies to maximize the 2D image resolution and Doppler ultrasound information obtained. Most commonly, images are obtained by trained and licensed cardiac sonographers and then interpreted by a cardiologist.

4.4. Standard Transthoracic Examination

The standard transthoracic cardiac echo includes images from parasternal, apical, suprasternal notch, and subcostal imaging windows (Fig. 2). Two-dimensional sectors are imaged in each window to provide anatomical details and functional analyses. The highest frequency transducer set at the lowest depth possible is used to maximize image resolution while scanning for anatomical detail. Two-dimensional images are then used to guide Doppler ultrasound interrogations, often with a lower frequency transducer that will optimize Doppler information. Two-dimensional images are also used to guide M-mode measurements of chamber sizes and functions, and Doppler gradients are calculated across valves and shunts to maximize the hemodynamic information obtained.

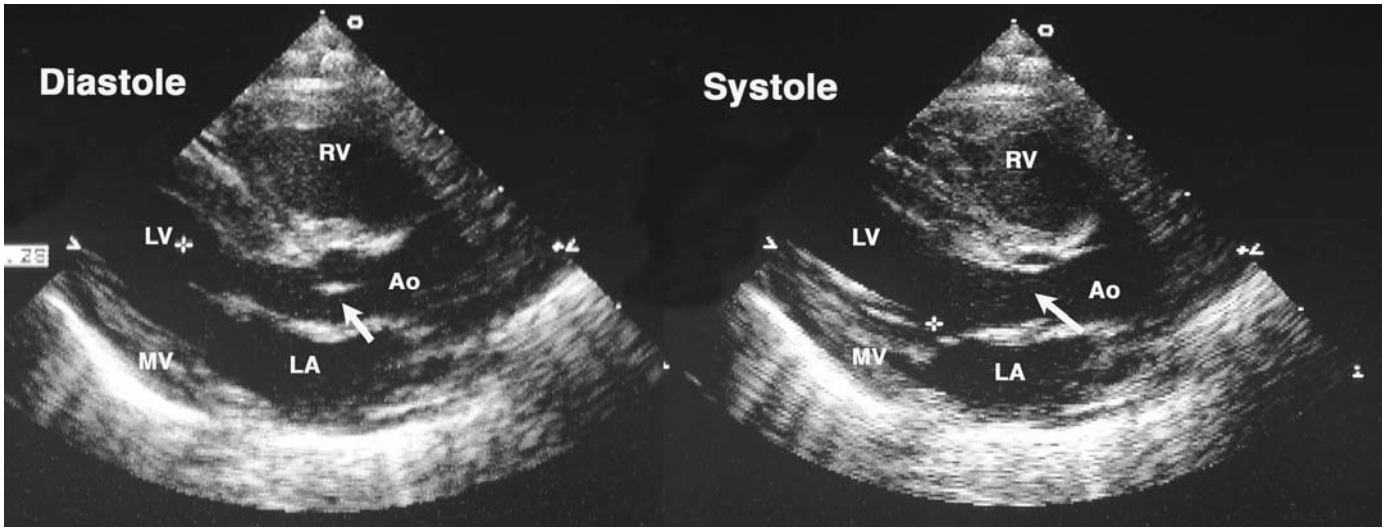

Fig. 3. Transthoracic parasternal long-axis views in a newborn infant. These views demonstrate the long axis of the left side of the heart. **Frame 1** is in diastole with an open mitral valve to accommodate left ventricular filling and a closed aortic valve (arrow). **Frame 2** is in systole with an open aortic valve (arrow) and closed mitral valve (*). White dots on the sector border represent centimeter marks. Ao, aorta; LA, left atrium; LV, left ventricle; MV, = mitral valve; RV, right ventricle.

The standardized transthoracic echocardiograms are obtained by scanning at four regions on the chest wall: the parasternal window, the apical window, the subcostal region, and the suprasternal notch (Fig. 2). Parasternal "long-axis" views are used to obtain long-axis images of the left side of the heart, including the left atrium, left ventricle, and aorta (Fig. 3). A subtle tilt of the transducer inferiorly from this position gives views of the right atrium, tricuspid valve, and right ventricle, and tilting leftward brings the pulmonary valve and main pulmonary artery into view.

Turning the transducer and scan plane by 90° results in short-axis views of the heart in planes from the base of the heart (region of the aorta and tricuspid and pulmonary valves) to the apex (Fig. 4A–D). M-mode measurements of the left-sided chambers are obtained from parasternal short-axis windows and can be used to assess chamber sizes and functions (Fig. 4E,F). Apical windows reveal standard four-chamber views of the left atrium, mitral valve, left ventricle, right atrium, tricuspid valve, and right ventricle (Fig. 5A,B). This view sends the ultrasound beam parallel to the septal structures, so it is not adequate to assess the integrity of the atrial or ventricular septa. Tilting the transducer anteriorly results in a five-chamber view that allows excellent visualization of the left ventricular outflow tract and aorta. Doppler gradients across the mitral, tricuspid, and aortic valves can be obtained from this view (Fig. 5C), and the velocity of tricuspid valve regurgitation can be used to estimate right ventricular and pulmonary artery systolic pressures.

Subcostal views are particularly useful in patients with lung disease or in those who have had recent open heart surgery. From subcostal images, the orientation of the heart in the chest and the major vascular connections can be established. Subcostal views also provide excellent visualization of the intraatrial septum (Fig. 6A) and four-chamber views in patients with poor apical windows. Suprasternal notch views are most useful for visualization of the aortic arch, its branching vessels, and the descending thoracic aorta (Fig. 6C), as well as for determining the Doppler shifts across the aortic valve. This view is also important to exclude vascular abnormalities, including coarctation of the aorta.

5. NEW TECHNIQUES IN CARDIAC ULTRASOUND

The use of ultrasound for cardiac imaging and investigation of hemodynamics has been revolutionary in the diagnosis and treatment of heart disease. Currently, ultrasound techniques available for use on a limited clinical or investigational basis include intravascular ultrasound, 3D and 4D imaging, and embryonic cardiac imaging. Intravascular ultrasound uses catheters with ultrasound transducers mounted on the tips. These transducers are capable of cross-sectional imaging or true sector imaging using phased-array ultrasound transducers mounted on their tips *(3,14)*.

As technology has improved, relatively small catheters and high-frequency transducers are available for imaging of the aorta and pulmonary arteries, aortic and pulmonary valves, and coronary arteries. Coronary artery imaging has been particularly useful in heart transplant patients as a means to detect intimal thickening associated with chronic rejection *(15)* and in patients with Kawasaki syndrome who develop coronary artery aneurysms *(3)*. Intravascular ultrasound has also been used for intracardiac monitoring of interventional procedures *(14)*.

Three-dimensional imaging technology has been improved so that cardiac images can be displayed in real time (called *4D imaging*). Three- and 4D images are useful for creation of a movable 3D image to assist with surgical planning *(1)*.

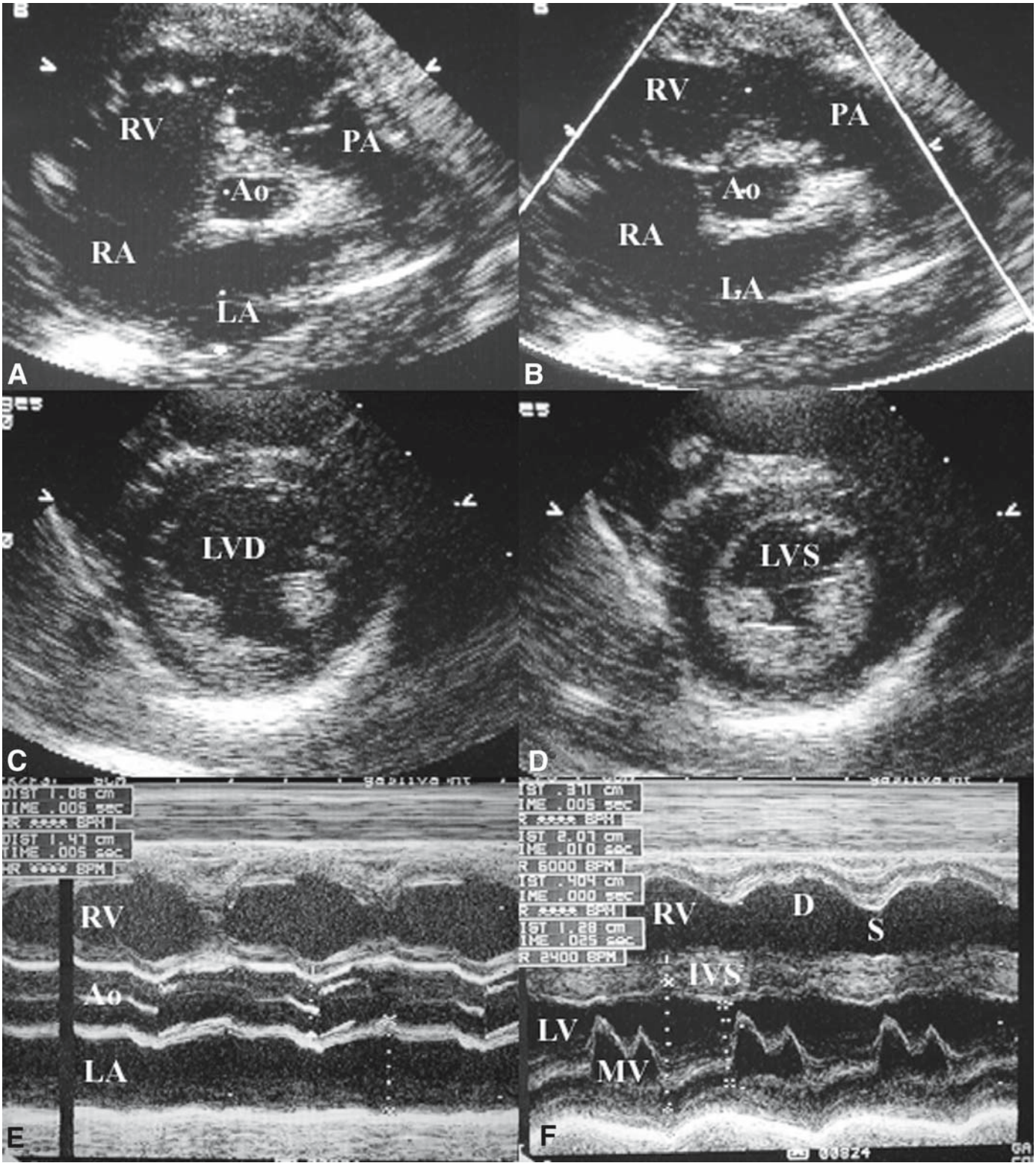

Fig. 4. Two-dimensional and motion-mode (M-mode) images obtained from parasternal short-axis views. **(A)** View through the base of the heart in diastole. **(B)** Same imaging plane in systole with the pulmonary valve open. M-mode measurements of the right ventricle, aorta, and left atrium **(E)** are obtained in this plane. **(C)** Cross-sectional or short-axis view of the left ventricle at the level of the papillary muscles in diastole. **(D)** Same plane in systole. This is the appropriate level for quantification of left ventricular function by shortening fraction. **(F)** M-mode recording at the level of the mitral valve, a plane just above that seen in C and D. Abnormalities of mitral valve motion can be demonstrated in this plane. Ao, aorta; D, diastole; IVS, = interventricular septum; LA, left atrium; LV, left ventricle; LV, left ventricle, diastole; LVS, left ventricle, systole; PA, main pulmonary artery; RA, right atrium; RV, right ventricle; S, systole.

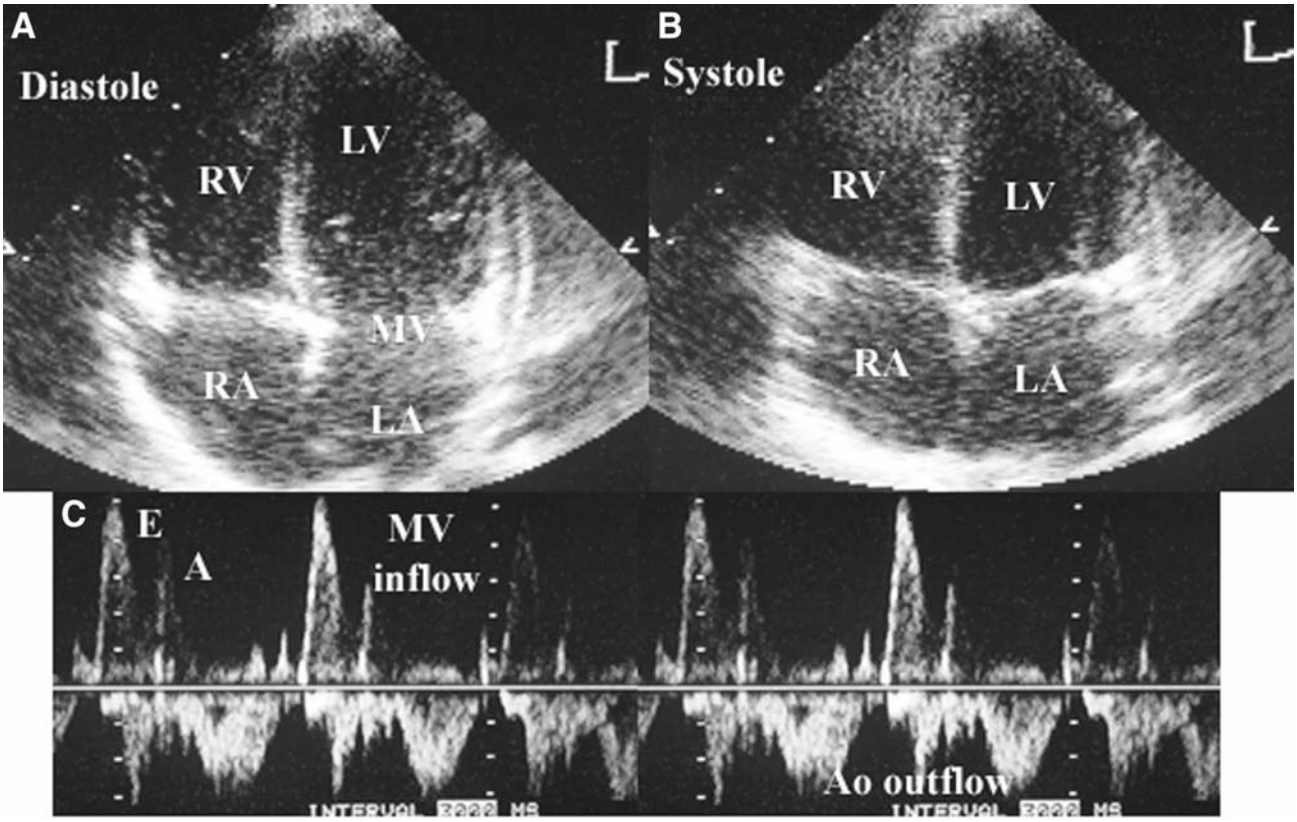

Fig. 5. **(A)** Two-dimensional apical four-chamber view of the heart in diastole (open mitral valve). (**B)** Same imaging plane in systole (closed atrioventricular valves). The pulsed wave Doppler tracing **(C)** demonstrates mitral inflow toward the transducer (above the baseline) and aortic outflow away from the transducer (below the baseline). The mitral valve inflow tracing shows passive filling of the left ventricle during early diastole **(E)** followed by active filling of the left ventricle in late diastole with the onset of atrial contraction (A). Aortic outflow occurs in systole. LA, left atrium; LV, left ventricle; MV, mitral valve; RA, right atrium; RV, right ventricle.

Unfortunately, to date available large transducer sizes and slow image processing capabilities make 3D and 4D imaging inappropriate for routine cardiac ultrasound examinations *(7)*.

Last, ultrasound imaging technology has been improved so that the heart can be studied during embryonic development. For example, pregnant mice can be anesthetized and undergo fetal cardiac imaging as early as 8–9 d after conception so that the anatomy and blood flow patterns can be observed during both normal and abnormal cardiac development *(16–18)*.

SUMMARY

The development and application of clinical echocardiography has allowed thorough, accurate, and noninvasive evaluation of cardiac structure and function. Transthoracic echocardiography is a mainstay of cardiac diagnosis and monitoring in both adult and pediatric patients. Advances in 2D imaging allow significant anatomical detail to be visualized, especially in smaller patients, and Doppler ultrasound allows direct visualization of altered flow patterns and noninvasive investigation of hemodynamics. The use of transesophageal echocardiography, although slightly more invasive, has become routine when improved resolution and intraprocedural monitoring are required. Future directions include increased utilization of intravascular ultrasound for diagnosis and monitoring of interventional procedures, improvement in 3D ultrasound techniques that will make them appropriate for routine imaging, and the use of embryonic imaging to study normal and abnormal heart development.

ACKNOWLEDGMENTS

I would like to thank Jim Berry and Kim Berry for providing the images shown in this chapter and Kim Berry for review of this manuscript.

REFERENCES

1. Geva, T. (1998) Echocardiography and Doppler ultrasound, in *The Science and Practice of Pediatric Cardiolog y,* 2nd Ed. (Garson, A., et al., eds.), Williams and Wilkins, Philadelphia, PA, pp. 789–843.
2. Vermilion, R.P. (1997) Basic physical principles, in *Echocardiography in Pediatric Heart Disease* (Snider, R., ed.), Mosby-Year Book, St. Louis, MO, pp. 1–10.
3. Snider, R., Serwer, G., and Ritter, S. (eds.). (1997) *Echocardiography in Pediatric Heart Disease*, Mosby-Year Book, St. Louis, MO.
4. Colan, S.D., Parness, I.A., and Spevak, P.J. (1992) Developmental modulation of myocardial mechanics: age and growth related alterations in afterload and contractility. *J Am Coll Cardiol*. 19, 619–629.
5. Gutgessel, H.P., Paquet, M., Duff, D.F., and McNamara, D.G. (1977) Evaluation of left ventricular size and function by echocardiography: results in normal children. *Circulation*. 56, 457–462.
6. Vermilion, R.P. (1997) Technology and instrumentation, in *Echocardiography in Pediatric Heart Disease,* 2nd Ed. Mosby, St Louis, MO.

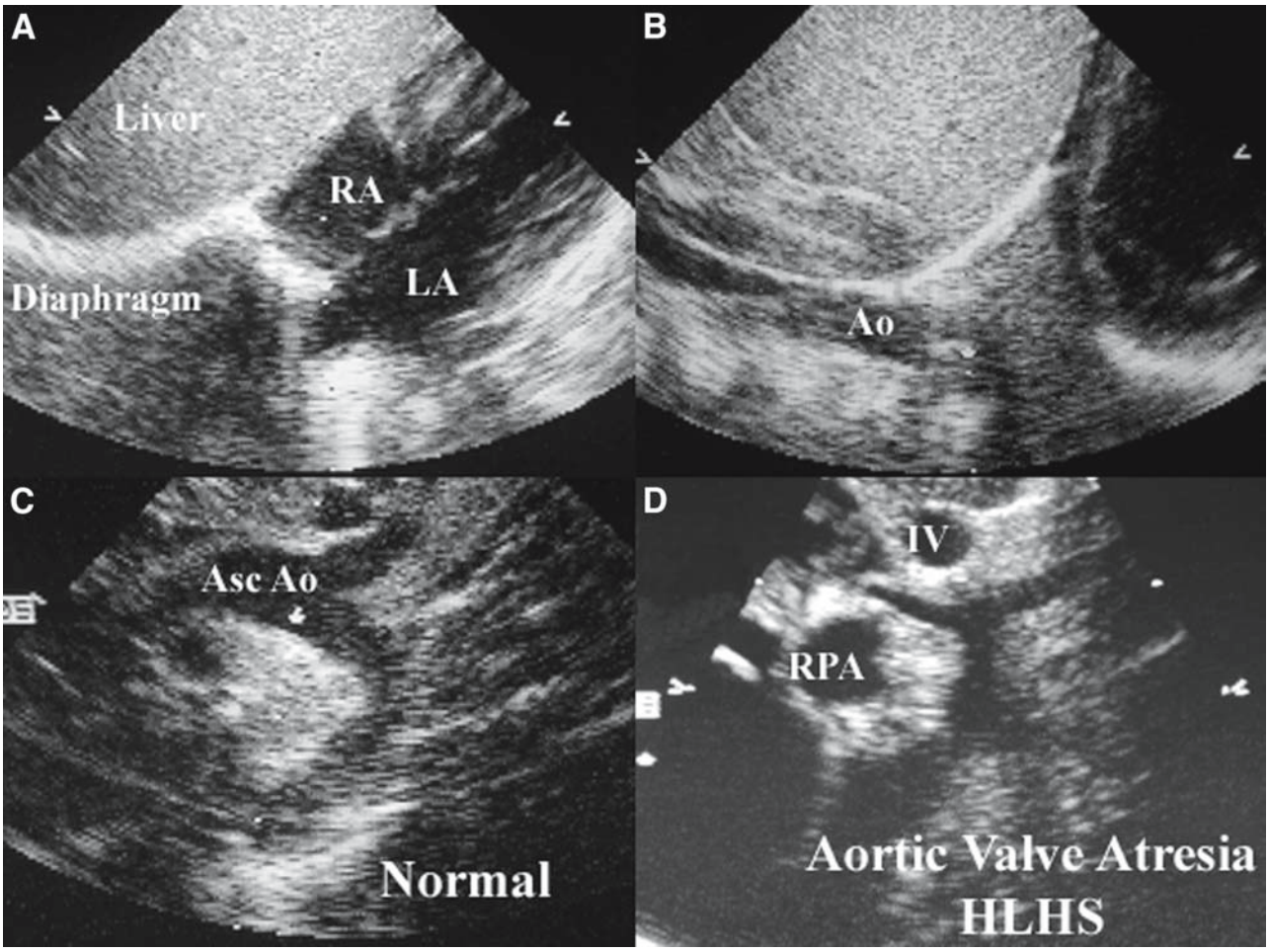

Fig. 6. **(A,B)** Two-dimensional images from subcostal windows and **(C,D)** suprasternal notch windows. Subcostal views provide orientation of the heart relative to the abdominal organs as in A, which shows a rightward liver and leftward cardiac apex. Subcostal windows also provide excellent four-chamber views, as well as short-axis views, of the interatrial septum in smaller individuals, as shown in A. B is a subcostal view showing the descending thoracic aorta at the level of the diaphragm. C is a suprasternal notch view of a normal aortic arch. D shows the severe hypoplasia of the ascending aorta seen in a patient with hypoplastic left heart syndrome (HLHS) caused by aortic atresia. LA, left atrium; Ao, aorta; AscAo, ascending aorta; IV, innominate vein; RA, right atrium; RPA, right pulmonary artery.

6a. Snider, A.R., Serwer, G.A., Ritter, S.B., and Gersony, R.A. (eds.) (1997) *Echocardiography in Pediatric Heart Disease*. Mosby-Year Book, St. Louis, MO, pp. 11–21
7. Danford, D.A. and Murphy, D.J., Jr. (1998) Basic foundations of echocardiography and Doppler ultrasound, in *The Science and Practice of Pediatric Cardiology* (Garson, A., et al., eds.), Williams and Wilkins, Philadelphia, PA, pp. 539–558.
8. Allan, L. (2000) The normal fetal heart, in *Textbook of Fetal Cardiology* (Allan, L., Hornberger, L., and Sharland, G., eds.), Greenwich Medical Media Limited, London, UK, pp. 55–91.
9. Tworetzky, W. and Marshall, A.C. (2003) Balloon valvuloplasty for congenital heart disease in the fetus. *Clin Perinatol*. 30, 541–550.
10. Tulzer, G., Artz, W., Franklin, R.C., Loughna, P.V., Mair, R., and Gardiner, H.M. (2002) Fetal pulmonary valvuloplasty for critical pulmonary stenosis or atresia with intact septum. *Lancet*. 360, 1567–1568.
11. Randolph, G.R., Hagler, D.J., Connolly, H.M., et al. (2002) Intraoperative transesophageal echocardiography during surgery for congenital heart defects. *J Thorac Cardiovasc Surg*. 124, 1176–1182.
12. Stevenson, J.G. (1999) Incidence of complications in pediatric transesophageal echocardiography: experience in 1650 cases. *J Am Soc Echocardiogr*. 12, 527–532.
13. Rousou, J.A., Tighe, D.A., Garb, J.L., et al. (2000) Risk of dysphagia after transesophageal echocardiography during cardiac operations. *Ann Thorac Surg*. 69, 486–489.
14. Ziada, K.M., Tuzcu, E.M., and Nissen, S.E. (1999) Application of intravascular ultrasound imaging in understanding and guiding percutaneous therapy for atherosclerotic coronary disease. *Cardiol Rev*. 7, 289–300.
15. Costello, J.M., Wax, D.F., Binns, H.J., Backer, C.L., Mavroudis, C., and Pahl, E. (2003) A comparison of intravascular ultrasound with coronary angiography for evaluation of transplant coronary artery disease in pediatric heart transplant recipients. *J Heart Lung Transplant*. 22, 44–49.
16. Srinivasan, S., Baldwin H.S., Aristizabal, O., Kwee, L., Labow, M., and Turnbull, D.H. (1998) Noninvasive, in utero imaging of mouse embryonic heart development with 40-MHz echocardiography. *Circulation*. 98, 912–918.
17. Zhou Y.Q., Foster, F.S., Qu D.W., Zhang M., Harasiewic, K.A., and Adamson, S.L. (2002) Applications for multifrequency ultrasound biomicroscopy in mice from implantation to adulthood. *Physiol Genomics*. 10, 113–126.
18. Visualsonics, *Insight Through In Vivo Imaging*, Vevo 660 System Product Information, Visualsonics, 3080 Yonge Street, Suite 6020, Box 89, Toronto, Canada. *See* website: (www.visualsonics.com).

19 Cardiac Magnetic Resonance Imaging

MICHAEL JEROSCH-HEROLD, PhD, RAVI TEJA SEETHAMRAJU, PhD, AND CARSTEN RICKERS, MD

CONTENTS

1. INTRODUCTION

Magnetic resonance imaging (MRI) has proven to be extremely versatile and useful for studying cardiac anatomy and function, both for providing a deeper understanding of cardiac physiology and as a means to diagnose cardiac diseases. The capabilities of MRI as a tomographic imaging modality to capture, with high spatial resolution, the anatomy of 3D structures was already well appreciated before the first attempts were made to apply MRI to the heart. Cardiac motion, compounded by respiratory motion and blood flow in the ventricular cavities and large vessels, initially imposed formidable barriers to the acquisition of artifact-free magnetic resonance (MR) images that could depict the cardiac anatomy with sufficient detail. It has taken well over 10 years for cardiac MRI to mature to the point at which it can be applied in a routine fashion in the clinic. In the future, other cardiac imaging modalities such as ultrasound imaging and nuclear imaging may be partially eclipsed by MRI for selected applications.

This chapter provides a condensed review of the basic principles of MRI and introduces some of the concepts and terminology necessary to understand the application of MRI to the heart. We then describe a wide range of cardiac applications of MRI, including those that should be of interest to the biomedical engineer. Our choice of topics is rather judicious because a complete exposition of the principles and applications of cardiac MRI could now fill an entire book.

From: *Handbook of Cardiac Anatomy, Physiology, and Devices*
Edited by: P. A. Iaizzo © Humana Press Inc., Totowa, NJ

2. PHYSICAL PRINCIPLES AND TECHNIQUES OF CARDIAC MRI

2.1. Magnetic Resonance

Felix Bloch and Edward Purcell discovered independently, in 1946 *(1,2)*, that nuclei with a magnetic dipole moment gave rise to a resonance phenomenon when immersed in a magnetic field and subjected to a pulsed or continuous radiofrequency excitation. MR is based on the interaction of nuclear magnetic moments with externally applied magnetic fields, both static fields and time-varying fields. For the sake of simplicity, we can think of atomic nuclei having an intrinsic angular momentum called *spin* because these are microscopic magnetic dipoles. Immersion of atoms with a nuclear magnetic dipole moment in a magnetic field, in the absence of other interactions or disturbances, would cause alignment of the magnetic dipoles along the direction of the applied magnetic field, similar to what happens to a compass needle placed in a magnetic field. The interaction of a nuclear magnetic dipole with an external magnetic field can be considered quite weak (e.g., in comparison to the

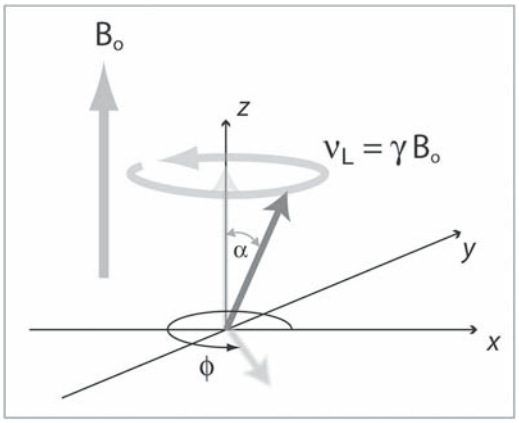

Fig. 1. A single magnetic dipole moment in a static magnetic field of strength B_0. It is customary to align the z-axis of a rectangular coordinate system with the direction of the externally applied static magnetic field B_0. In this example, the magnetic moment, initially aligned with the applied magnetic field, was tipped away from the z-direction by an angle α through application of an oscillating magnetic field (not shown). The oscillating magnetic field is kept on only for the time necessary to tip the magnetic dipole moment by a certain angle, α in this example. After turning the oscillating magnetic field off, the magnetic dipole moment precesses about the B_0 direction at a frequency $\nu_L = \gamma \cdot B_0$, where γ is a constant, the gyromagnetic ratio, and represents a property of the nucleus. For ^{1}H nuclei, γ equals 42.6 MHz/T. The angle φ denotes the phase angle of the magnetization component in the x–y plane, orthogonal to the direction of B_0.

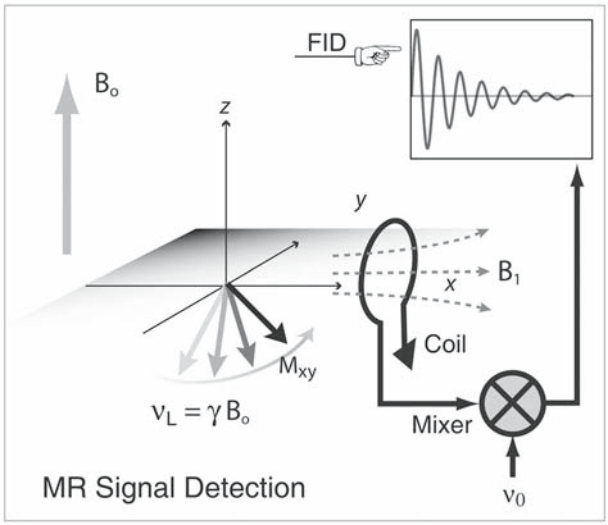

Fig. 2. The transverse magnetization component of a nuclear dipole precesses at the Larmor frequency and produces an oscillating magnetic flux density that can be detected with a wire loop that is part of a resonant circuit. The induced voltage is amplified and mixed with the signal of an oscillator. The low-frequency component from the mixer is a free induction decay with frequency $\nu_L - \nu_0$. Often, two coils, oriented perpendicular to each other, are used to detect the signal from the M_x and M_y components of the transverse magnetization, which are in quadrature; that is, they have a relative phase difference of 90°. By detection of the quadrature components, it is possible to determine the sign of the difference $\nu_L - \nu_0$, and by combination of the two signals, after phase shifting one by 90°, one improves the signal-to-noise ratio by a factor of $\sqrt{2}$. FID, free induction decay; MR, magnetic resonance.

thermal energy at room temperature of atoms or molecules that carry some nuclear magnetic moment). Therefore, the detection of the magnetic resonance signal benefits from the application of strong magnetic fields. For current MRI systems, magnetic field strengths ranging from 1 to 3 tesla (T) are typical.

2.2. Larmor Precession

A magnetic dipole subjected to a static magnetic field, if tipped away from the direction of the magnetic field, will precess about the direction of the static magnetic field (Fig. 1). This precession has a rotation frequency ν_L that is directly proportional to the magnetic field strength B_0. For hydrogen nuclei, the precession frequency varies with field strength as

$$\nu_L = 42.6[\text{MHz/Tesla}] \cdot B_0[\text{Tesla}]$$

The precession frequency is also known as the *Larmor frequency*.

Tipping a nuclear magnetic moment away from the direction of the z-axis (B_0 direction) can be accomplished by applying an oscillating magnetic field, denoted by B_1, in a direction perpendicular to B_0. The radiofrequency transmitter should be tuned to a frequency close to the Larmor frequency to elicit a resonant excitation. On MRI scanners, the oscillating magnetic fields can be switched on and off for very precise fixed durations, therefore controlling the angle by which the magnetic moment is tipped away from the B_0 direction.

It is customary to refer to the magnetic fields oscillating at radiofrequencies and turned on for brief durations as *radiofrequency pulses*. A pulse that tips the magnetic moment from the z-axis into the x–y plane is referred to as a *90° radiofrequency pulse*. A pulse that inverts the orientation of the magnetic moment is called a *180°* or *inversion pulse*.

2.3. Free Induction Decays

After a radiofrequency excitation pulse, the static magnetic field B_0 causes precession of the transverse magnetization component, which can be detected with an external coil as shown in Fig. 2. Immediately after a radiofrequency excitation, individual magnetic moments that were tipped into the transverse plane are in phase; that is, they have the same phase angle. If all magnetic moments were to precess at exactly the same Larmor frequency, this phase coherence would persist.

Residual magnetic field inhomogeneities, magnetic dipole interactions between neighboring nuclei, molecule-specific shifts of the precession frequency, and other factors produce a distribution of Larmor frequencies. The frequency shifts relative to a reference frequency can be tissue specific, as in the case of ^{1}H nuclei in fat. The spread of Larmor frequencies results in a slow loss of phase coherence of the transverse magnetization; that is, the sum of all transverse magnetization components decays with time.

The decay following a radiofrequency excitation is called *free induction decay* and often has the shape of an exponential function with an exponential time constant denoted as T_2, roughly on the order of approx 0.1–10^2 ms for ^{1}H nuclei in biological systems. In the laboratory frame of reference, the transverse magnetization can be expressed as a complex quantity M_{xy}:

$$\begin{aligned} M_{xy} &= M_x + i \cdot M_y = \left[M_0 \cos\omega_L t + iM_0 \cos\omega_L t\right] \cdot \exp(-t/T_2) \\ &= M_0 \exp(i\omega_L t) \cdot \exp(-t/T_2) \end{aligned}$$

where $\omega_L = 2\pi\nu_L$, and M_x and M_y denote the x and y components of the transverse magnetization.

In magnetic resonance research, the useful information extracted by spectroscopic or imaging studies is derived from analysis of the frequency modulation of the MR signal. To detect the frequency-modulated signal, heterodyne detection is used; that is, the received signal is mixed with an oscillating waveform of frequency $\omega_0 = 2\pi\nu_0$, close to the Larmor frequency, to obtain a low-frequency signal that can be digitized. If the $\Delta\omega$ denotes the difference between $\omega_L = 2\pi\nu_L$ and ω_0, then the mixed-down signal component can be described as

$$M_+ = M_0 \exp(i\Delta\omega \cdot t) \cdot \exp(-t/T_2)$$

This process of heterodyne detection can also be thought of in terms of using a rotating reference frame. Instead of observing the precession of the transverse magnetization in a laboratory reference frame, a reference frame that rotates with a frequency ω_0 about the B_0 direction can be used. Seen from this rotating reference frame, the transverse magnetization rotates at a frequency $\Delta\omega$. If the rotation frequency is exactly matched to the Larmor frequency (i.e., $\omega_0 = \omega_L$), then the (transverse) magnetization is stationary, and the static magnetic field B_0 is effectively zero in this rotating frame of reference.

The concept of a rotating reference frame is quite powerful to describe the application of an oscillating magnetic field B_1. In the rotating frame, a magnetic field rotating at a frequency ω_0 will appear stationary. The effect of a radiofrequency pulse can be described in the rotating frame as a precession of the magnetization vector about the magnetic field that B_t is stationary.

2.4. Transverse Magnetization Decay: T_2 and T_2^*

The loss of phase coherence of the transverse magnetization, characterized by the decay time T_2, is slowest if the magnetic moments are embedded in a homogeneous sample and subjected to a homogeneous magnetic field. In the presence of field inhomogeneities and other factors that cause a spread of Larmor frequencies, the transverse magnetization decay is further shortened. To distinguish this *latter* situation, a time constant T_2^* is introduced that is characteristic of the exponential decay of the transverse magnetization in "heterogeneous" environments. It follows that T_2^* is always shorter than T_2.

2.5. Longitudinal Magnetization Recovery: T_1

After any radiofrequency excitation that tips the magnetization vectors away from the direction of the applied static magnetic field B_0, the nuclear spins will over time realign themselves with the magnetic field to reach the same alignment as before the radiofrequency excitation. This process requires the exchange of energy between atomic nuclei and their environments. The recovery of the longitudinal magnetization component M_z in many cases follows an exponential function

$$M_z(t) = M_0 \cdot \left[1 - \eta \cdot \exp(-t/T_1)\right]$$

where M_0 denotes the equilibrium magnetization before any radiofrequency pulses are applied, and η gives the degree of inversion of the transverse magnetization, with $\eta = 1$ for a 90° pulse and $\eta = 2$ for a 180° pulse.

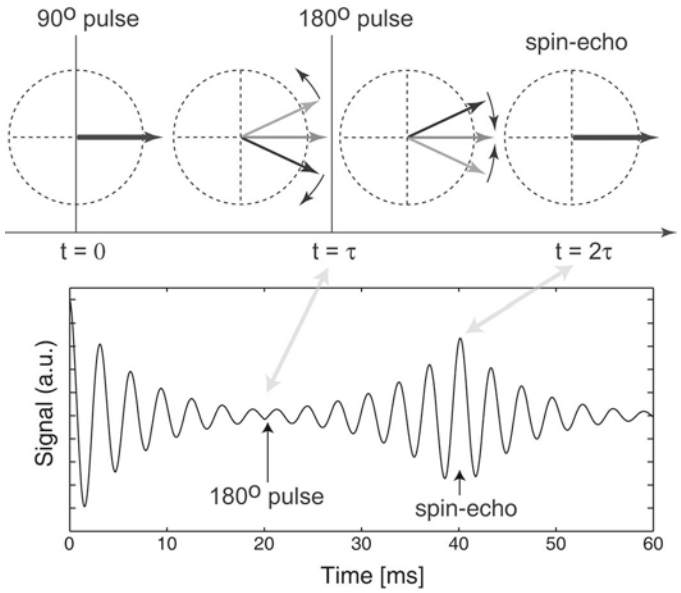

Fig. 3. After an initial 90° radiofrequency excitation pulse, all magnetic moments are in phase, but slowly drift out of phase because of a distribution of Larmor frequencies. The figure illustrates this situation in a rotating frame of reference in which the Larmor frequency of one magnetic moment exactly matches the rotation frequency of the reference frame. By applying a 180° pulse at $t = \tau$, the magnetic moment precessing more rapidly than the average (light gray arrow) has a negative phase after the 180° pulse and vice versa for the magnetic moment precessing more slowly (solid black arrow). The precession frequency of the magnetic moments remains unchanged, and they regain phase coherence at $t = 2\tau$. The initial free induction decay and the echo signal after the 180° pulse are shown in the graph. By applying another 180° pulse at $t = 3\tau$, a second spin-echo can be produced at $t = 2\tau$, and this can be repeated while t is not much larger than T_2. This example also illustrates the fact that decay of the echo amplitudes (with time constant T_2) is considerably slower than the free induction decay (with time constant T_2^*).

2.6. The Spin-Echo

A loss of phase coherence because of any spread in Larmor frequencies, such as that caused by magnetic field inhomogeneities, can be (at least partially) reversed by applying a 180° pulse that flips the magnetization in the x–y plane over such that the faster precessing spins now lag behind, and the more slowly precessing spins are ahead, compared to spins precessing at the mean Larmor frequency.

Figure 3 illustrates how the spin-echo is a very effective means of rephasing the spins, such that after the 180° pulse an attenuated mirror image of the free induction decay is observed. Once the echo amplitude peaks, the spread of Larmor frequencies again causes a loss of phase coherence. Multiple 180° pulses can be applied to reverse the loss of phase coherence repeatedly and thereby produce a train of spin-echoes. The decay of the spin-echo amplitudes is governed by the decay constant T_2; a free induction decays with a characteristic time constant T_2^*, with $T_2^* < T_2$.

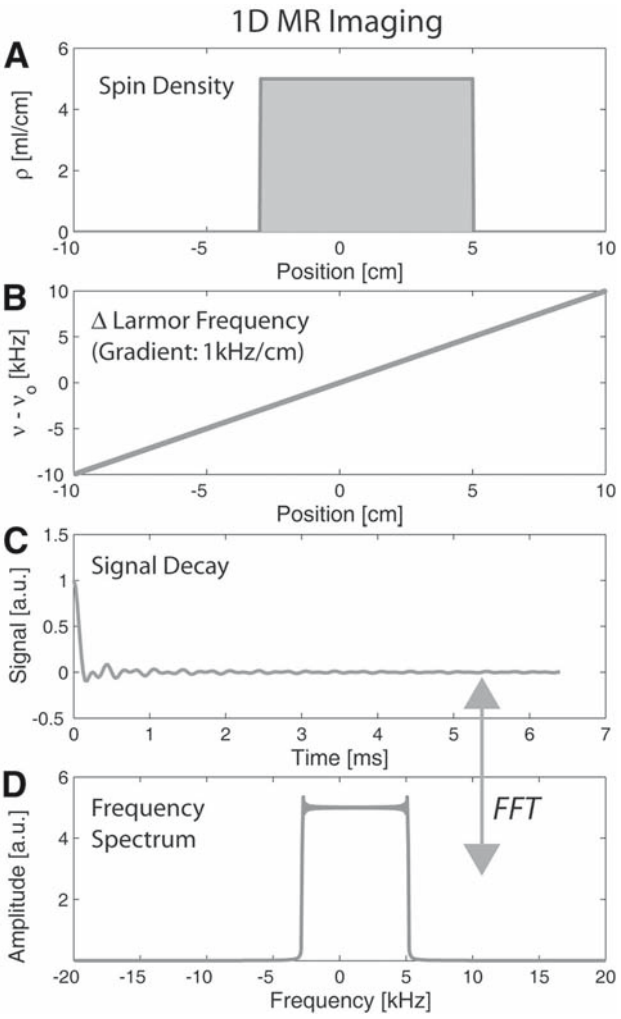

Fig. 4. **(A)** An illustration of the principle of magnetic resonance imaging (MRI) for a one-dimensional (1D) distribution of spins with a density distribution as a function of position. **(B)** The variation of the Larmor frequency in the presence of a linear magnetic field gradient. **(C)** The free induction decay recorded after application of a short radiofrequency pulse and in the presence of a magnetic field gradient. **(D)** The frequency spectrum of the signal in (C) is calculated by Fourier analysis with a fast Fourier transform (FFT). The frequency profile reproduces the shape of the spin density distribution shown in (A), and this is a result of the linear variation of the Larmor frequency as a function of the position during application of a magnetic field gradient. MR, magnetic resonance.

Importantly, for cardiac imaging applications, it is useful to note that the spin-echo and spin-echo trains in particular provide a method to attenuate the signal from flowing blood while obtaining "normal" spin-echoes from stationary or slow-moving tissue.

2.7. Magnetic Resonance Imaging

The basic concept of MRI consists of producing a spatial variation of the magnetic field, which gives rise to a distribution of Larmor frequencies. A linear variation of the magnetic field strength will cause a one-to-one correspondence between the Larmor frequency and a spatial position. A gradient that is applied during the recording of the MR signal is called a *readout gradient*. The readout gradient creates a distribution of frequencies of width proportional to the readout gradient strength G_r and to the extent in the readout direction of the object that is imaged. The decay of transverse magnetization is recorded while this magnetic field gradient is left on. The frequency contents of the free induction decay are analyzed by Fourier transformation. As shown in Fig. 4, the 1D frequency spectrum will be proportional to the density distribution of nuclear magnetic moments along the direction of the applied magnetic field gradient.

The MR signal needs to be sampled at a frequency that takes into account the extremes of this frequency distribution. If the desired field of view dimension in the direction of the readout gradient is L_x, then the sampling frequency needs to be equal to or greater than the Nyquist frequency f_{Nyq}; that is, the sampling frequency should at least be as large as the Nyquist frequency:

$$f_{Nyq} = 2 \cdot L_x \cdot \gamma \cdot G_r$$

2.8. Slice-Selective Excitation

As a tomographic imaging modality, MRI relies on the selective excitation of spins within a slice or slab of arbitrary, user-specified orientation, position, and thickness. The selective excitation of the nuclear spins requires the application of a radiofrequency pulse, which produces the desired response (e.g., the creation of a transverse magnetization component) only within a well-defined region, typically a slice of thickness Δx. For small tip angles, this creation of a transverse magnetization component can be described in terms of the frequency spectrum of the applied radiofrequency pulse.

For a slice-selective radiofrequency excitation, the desired slice orientation determines the direction of the magnetic field gradient. A radiofrequency excitation of limited bandwidth excites spins in a slice that is perpendicular to the direction of the applied magnetic field gradient, and the slice width is proportional to the bandwidth of the radiofrequency pulse (Fig. 5).

2.9. Spatial Phase Encoding

The basic idea of phase encoding consists of applying a gradient pulse that gives rise to a position-dependent phase angle change for the transverse magnetization. We denote the angle of the transverse component in the rotating frame by φ and refer to it as the phase of the transverse magnetization. Under ideal conditions, the phase angle φ is the same for all spins in the slice right after a radiofrequency excitation.

Application of a gradient pulse $G_x(t)$ in the x direction for a duration T causes the phase to vary as a function of the x-coordinate, and the phase angle at the end of the gradient pulse is given by

$$2\pi\varphi(x) = 2\pi\gamma \cdot x \cdot \int_0^T G_x(t) \cdot dt = k_x x$$

The quantity k_x is termed a *wave vector* and has units of inverse length. The transverse magnetization can be expressed in the rotating frame as a complex quantity with magnitude

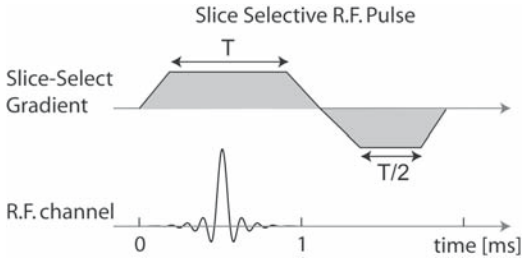

Fig. 5. Waveforms that are applied along the radiofrequency (R.F.) and one gradient channel during a slice-selective radiofrequency excitation. The gradient channels are typically given logical names, such as "slice-select" and "readout." The direction for the slice selection gradient can be arbitrary and is achieved by using three equivalent gradient coil sets for gradients in the x, y, and z directions and applying a combination of waveforms on all three gradient channels according to the desired slice orientation. To avoid this complexity in pulse sequence diagrams, the waveforms for the "logical" gradient channels, as shown here, are typical. Gradient waveforms usually have trapezoidal shapes; that is, they rapidly ramp up, maintain constant amplitude for a well-defined duration, and then ramp down. The radiofrequency pulse in this example has the shape of a sinc function to excite a rectangular profile. The tails of the radiofrequency waveform were attenuated with a Hanning windowing function to avoid "ringing" artifacts in the slice profile.

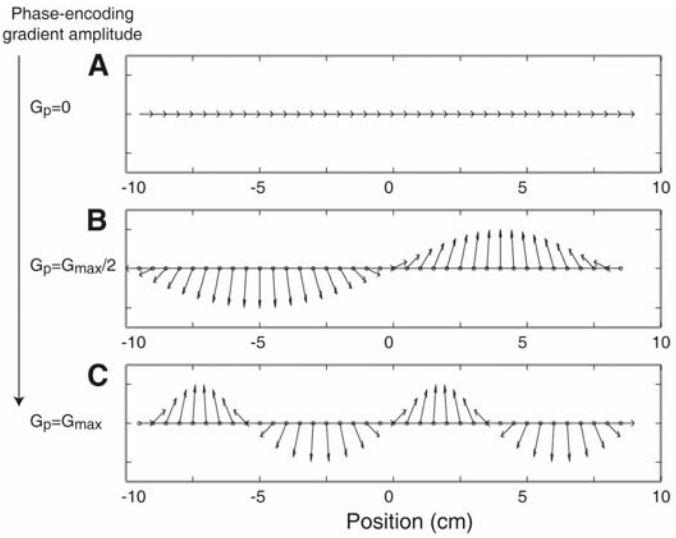

Fig. 6. An array of magnetic moments stacked up along the horizontal axis. In this example, only the transverse component of the magnetization is shown as vectors, aligned initially with the horizontal axis, after application of a radiofrequency pulse. The phase φ of the transverse magnetization is measured here with respect to the horizontal axis. **(A)** Without application of a phase-encoding pulse, all magnetization vectors point in the same direction (center graph for $G_p = 0$). **(B)** Applying a phase-encoding gradient pulse in the direction of the horizontal axis will result in a variation of the phase of the transverse magnetization in the direction of the phase-encoding gradient. **(C)** Increasing the amplitude of the phase-encoding gradient will increase the phase warp. The transverse magnetization components M_x and M_y vary sinusoidally, such as $M_x \propto \cos(k_x x)$ for a phase encoding pointing in the x direction.

proportional to the local spin density $\rho(x,y)$ in the slice plane, and sinusoidal dependence on the phase angle $\varphi(x)$:

$$M_{xy} = M_x + i \cdot M_y \sim \rho(x,y) \cdot \exp[-ik_x x]$$
$$= \rho\left[\cos(k_x x) + i \cdot \sin(k_x x)\right]$$

The quantity k_x is the spatial frequency at which the x and y components of the transverse magnetization (M_x and M_y) are modulated by application of the phase-encoding gradient in the x direction. We refer to the variation of the magnetization phase as *phase warp*.

For a 1D distribution of spins, as in the example of Fig. 6, the signal that is recorded after a phase encoding can be represented as a sum or integral, with each contribution weighted by a phase factor to account for the phase warp produced by a phase encoding gradient:

$$S_i = \int_{-L/2}^{+L/2} \rho(x) \cdot \exp(-i\,\gamma\, k_x^i x) \cdot dx$$

The index i is a label for the phase-encoding pulse. S_i is the ith Fourier component of the spin density distribution $\rho(x)$. L denotes the spatial extent of the object to be imaged; that is, $\rho(x) = 0$ when $|x| > L$. The spin density distribution $\rho(x)$ can be reconstructed if the phase encodings are repeated for a range of k_x values to sample the spin density distribution at different length scales or spatial frequencies. The phase encodings are repeated N times to achieve a spatial resolution in the direction of the phase-encoding gradient of $\Delta x = L/2N$.

2.10. 2D Imaging With Phase Encoding and Readout Gradients

The combined use of phase-encoding gradients and readout gradients allows progress beyond the determination of 1D density profiles and imaging of the density of spins in a thin slice, with x and y denoting the two orthogonal axes in the slice plane. T_1 and T_2 relaxation effects are neglected in the following discussion for simplicity. The (relative) variation of the phase along the x direction, which was produced by a previous phase-encoding gradient pulse, is preserved if we now switch on a (readout) gradient in the orthogonal y direction. The readout gradient G_y in the y direction is left on while the signal is detected.

A 2D data matrix is built up by repeating the signal readouts for different k_x values (i.e., phase-encodings). This means that the radiofrequency excitation, phase encoding pulse, and readout gradient pulses are repeated, and for each repetition, the phase-encoding gradient amplitude is incremented to cover a range of k_x values centered around $k_x = 0$. The time it takes to repeat this group of encoding steps is called the *repetition time*; it is one of the basic parameters that determines the total time for acquiring an image.

The final result of repeating the radiofrequency excitation, readouts, and phase encodings M times is a data matrix $S(k_x,k_y)$,

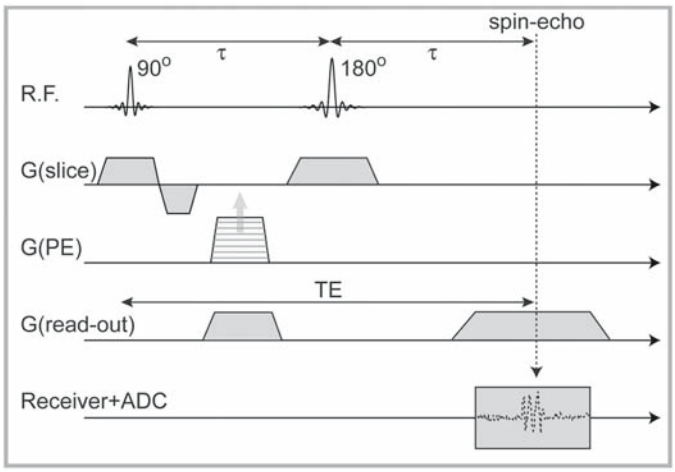

Fig. 7. A pulse sequence diagram for a spin-echo imaging sequence showing the waveforms applied on the radiofrequency, the three channels for the orthogonal magnetic field gradients, and the receiver channel of a magnetic resonance imaging (MRI) scanner. The activity along the gradient and radiofrequency "channels" of the scanner is shown in separate rows. The sequence starts with a slice-selective 90° excitation, followed by a phase encoding and a dephasing gradient on the readout channel. After a slice-selective 180° pulse, a readout gradient is applied, and the spin-echo appears at the center of the gradient readout pulse if the duration of the dephasing gradient is half the duration of the readout gradient. This sequence diagram block is repeated for each different phase encoding. The phase-encoding gradient amplitude is incremented with each repetition, and this is denoted in the diagram by the light gray arrow superposed on the phase-encoding waveform. Note that the two gradient pulses applied on the readout channel have the same polarity to produce a spin-echo with the 180° radiofrequency pulse interposed between the two gradient pulses. The gray-shaded box on the "receiver channel" indicates the time when the analog-to-digital converter (ADC) and receiver are "on" to record the spin-echo signal. PE, phase encoding; R.F., radiofrequency; TE, echo time.

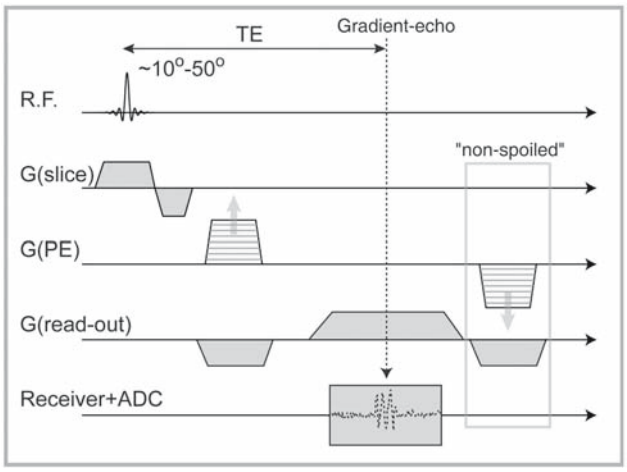

Fig. 8. Pulse sequence diagram for an imaging sequence that uses gradient echoes for readout of the signal. The initial radiofrequency pulse generally has a flip angle much smaller than 90° to maximize the signal when the repetition time is relatively short (~2–10 ms) compared to repetition times of spin-echo imaging sequences. The gradient echo results from two gradient pulses on the read channel with opposite polarity. The maximum amplitude of the gradient echo occurs when the integral of the gradient waveforms is zero, that is, when the areas under the negative and positive polarity lobes of the gradient waveforms cancel out. PE, phase encoding; R.F., radiofrequency; TE, echo time.

which can be Fourier transformed to obtain the spin density $\rho(x,y)$. The spatial resolution of the resulting image in the phase encoding Δx and readout directions Δy is determined by the number of readout samples N and the number of phase encodings that were applied: $\Delta x = L_x/2N$ and $\Delta y = L_y/2M$. The field of view dimensions L_x and L_y are determined by the magnitude of the sampling steps in data space (Δk_x, Δk_y): $L_{x,y} = 2\pi/\Delta k_{x,y}$.

2.11. Spin-Echo Imaging

In a spin-echo imaging sequence, the readout gradient is applied during the formation and decay of a spin-echo. A single encoding step starts with a slice-selective 90° pulse. The phase-encoding gradient can be applied immediately afterward; simultaneously, a "dephasing" gradient pulse can be applied along the readout axis. A (slice-selective) 180° pulse at time $t = 2\tau$ causes the appearance of a spin-echo at $t = \tau$. A readout gradient pulse is centered on the echo center. The basic building block of the spin-echo sequence, shown in Fig. 7, is repeated N times for N phase-encoding steps.

A train of echoes can be produced by a string of 180° pulses that are spaced 2τ apart and result in a considerable speedup of the image acquisition. This technique is therefore called *fast spin-echo imaging* to distinguish it from the single-echo variant described above.

2.12. Gradient Echo Imaging

Spin-echoes provide an effective means of refocusing the transverse magnetization. A similar, but nevertheless different, type of echolike effect can be achieved by applying two gradient pulses of opposite polarity instead of a 180° radiofrequency pulse. The first gradient pulse causes a rapid dephasing of the transverse magnetization. The second gradient pulse, of opposite polarity, can reverse this effect. An echo-type signal is observed and peaks at the point at which the phase warp produced by the first pulse is cancelled. This type of echo is called a *gradient echo*. A pulse sequence diagram for a gradient echo imaging sequence is shown in Fig. 8.

A train of gradient echoes can be created by consecutive pairs of dephasing and rephasing gradient waveforms. The acquisition of multiple phase-encoded gradient echoes after a single radiofrequency excitation is useful for very rapid image acquisition, but is limited by the T_2^* decay of the signal.

A variation of the gradient echo technique that reestablishes phase coherence to the best possible degree before application of the next radiofrequency excitation (i.e., the next phase-encoding step) can be used to produce a steady state. This allows the application of radiofrequency pulses with fairly large flip angles. Instead of relying on T_1 relaxation to return

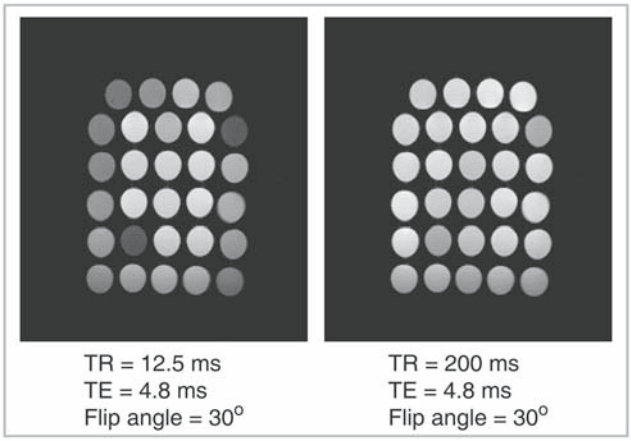

Fig. 9. Gradient echo images of phantom tubes filled with saline solution and different concentrations of a paramagnetic substance that reduces the T_1 of saline in proportion to its concentration in the saline solution. The saline samples with the shortest T_1 appear brightest because the saturation of a T_1-weighted signal with a gradient echo sequence is weakest for the short T_1s. The image to the left, acquired for a shorter repetition time (TR) than the image on the right, has the stronger T_1 weighting. The signal intensity contrast between different saline samples is more pronounced for the image on the left, acquired with a shorter repetition time, because of the stronger T_1 weighting. The images were acquired with a relatively short echo time (TE) of 4.8 ms to minimize contrast from differences in T_2. The paramagnetic substance in the saline samples was an aqueous solution of gadopentetate dimeglumine, a *N*-methylglucamine salt of the gadolinium complex of diethylenetriamine pentaacetic acid, which is a magnetic resonance contrast agent routinely used in clinical practice.

the magnetization from the transverse plane to the B_0 direction, the magnetization is toggled back and forth by the radiofrequency pulses between the *z*-axis and the transverse plane. The attainable signal-to-noise ratio with this approach is significantly higher than with "conventional" gradient echo imaging. This type of gradient echo imaging is referred to in the literature by various acronyms: "steady-state free precession imaging," "true FISP," or "balanced fast field echo imaging." In particular, for cardiac cine studies, this technique has led to a marked improvement of image quality. Steady-state free precession works best with very short repetition times, which in turn impose high demands on the gradient system of the MR scanner in terms of ramping gradients up and down.

2.13. Contrast Weighting

Biological tissues and blood have approximately the same density of ^{1}H nuclei, and spin density images show poor contrast to differentiate, for example, tissue from blood or fat from muscle. One of the most appealing aspects of MRI is the ability to manipulate the image contrast based on differences in the T_1 or T_2 relaxation times. For a gradient echo sequence, the T_1 weighting is determined by the combination of flip angle and repetition time. Reducing repetition time or increasing the flip angle increases the T_1 weighting in the image. The same applies to a spin-echo sequence (Fig. 9).

The T_2^* weighting of a gradient echo image is controlled by the time delay between the radiofrequency pulse and the center of the readout window, that is, the echo time TE. The T_2 weighting of the spin-echo signal is similarly determined by the echo time. In a fast spin-echo sequence, multiple echoes can be used to read out the signal with different phase encodings for each echo. The echo chosen for reading out the phase encodings with low k values will determine the effective T_2 contrast of the image. We note that the "coarse" features of an image and the image contrast are determined by the low spatial frequency components in the data matrix $S(k_x,k_y)$. If the first few echoes in an echo train are chosen for the low k value encodings, then the T_2 weighting is less than if these phase encodings are instead moved to the later echoes in the echo train.

Controlling the T_1 weighting through adjustment of repetition time and the flip angle imposes some limits that can be circumvented by applying an inversion pulse before the image acquisition and performing the image acquisition as rapidly as possible. The time between the inversion pulse and the start of the image acquisition controls the T_1 contrast in this case. The image acquisition after the magnetization inversion is typically performed with a gradient echo sequence that uses small flip angles; that is, the T_1 contrast is controlled by the prepulse and the delay after the prepulse, instead of the repetition time, and the flip angle α of the gradient echo image acquisition. Gradient echo imaging with a magnetization preparation in the form of a 180° or 90° radiofrequency pulse is often the method of choice for rapidly acquiring T_1-weighted images of the heart.

MR contrast agents provide a further means for controlling the image contrast by injecting a compound with paramagnetic ions that reduce the T_1 of blood and tissue permeated by the agent. The local T_1 reduction depends on: (1) delivery of contrast agent to the tissue region through the blood vessels, (2) the degree to which the contrast agent molecules can cross barriers such as the capillary barrier, and (3) the distribution volume of the contrast agent within the tissue. The contrast seen after injection of such an agent can be used to determine pathology, such as the breakdown of the cardiac cell membranes or an above-normal concentration of contrast agent in infarcted myocardium.

3. MRI OF CARDIAC ANATOMY, FUNCTION, PERFUSION, AND VIABILITY

3.1. Cardiac Morphology and Tissue Characterization

Spin-echo techniques are the method of choice for imaging cardiac anatomy and for tissue characterization. Figure 10 shows an example of a T_2-weighted fast spin-echo image of a canine thorax with an in-plane resolution of approx 1.2 mm and for a 4-mm thick slice.

3.2. Cardiac Function

MRI is now considered the gold standard for assessing the hemodynamics of the ventricles of the heart and measuring parameters such as ejection fraction, end-diastolic volume, end-systolic volume, stroke volume, and cardiac mass. Cine loops are acquired to follow the changes in ventricular dimensions

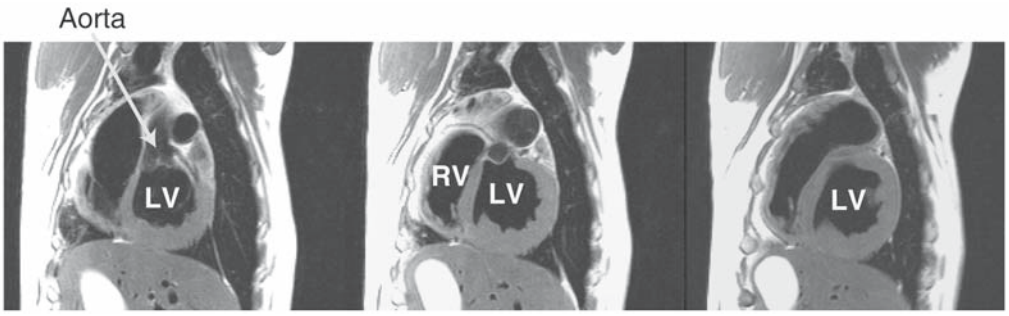

Fig. 10. Cardiac anatomy of a canine heart imaged with a T_2-weighted fast spin-echo sequence and in-plane resolution of 1.2 mm. Cardiac structures such as the left ventricle (LV), right ventricle (RV), and aorta are labeled. The signal from blood in the ventricular cavities was nulled by a magnetization preparation consisting of radiofrequency inversion pulses. Furthermore, the use of an echo train, with seven spin-echoes in this case, and a long effective echo time also causes attenuation of the signal from moving blood. These so-called black-blood imaging techniques are very useful for anatomical imaging to avoid image artifacts from flowing blood.

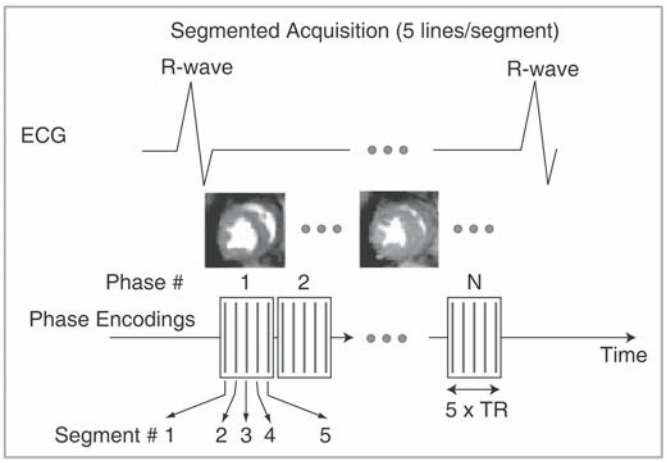

Fig. 11. Illustration of the principle of segmented acquisitions of data as used for imaging multiple phases of the cardiac cycle in ventricular function studies. The image acquisition is synchronized to the cardiac cycle by triggering of the pulse sequence with the R-wave on the electrocardiogram (ECG). The total number of phase encodings is split into five groups or segments in this example. The same five phase encodings are performed during each phase of one cardiac cycle. During the next R-to-R interval, five other phase encodings are performed for each cardiac phase. The R-wave-triggered acquisition of phase encodings is repeated k times to obtain a total of $k \cdot 5$ phase encodings. The temporal extent of each cardiac phase is shown in the diagram by the boxes that contain the symbolic representations of the phase-encoded lines as vertical lines. The temporal resolution of the resulting cine loop is determined by the number of lines per segment (five in this example) and the repetition time for each phase-encoding step. Typical resolutions are on the order of 40–50 ms for resting heart rates and higher during inotropic stimulation of the patient's heart. The image acquisition is performed while the patient holds his or her breath. In this example, the required duration of the breath hold would be k heartbeats, with k typically on the order of 10–20, depending on the heart rate. TR, repetition time.

over the entire cardiac cycle and assess cardiac function. The acquisition of each image in the cine loop is broken up into several "segments," and the image segments are acquired over consecutive heartbeats, as shown in Fig. 11.

The acquisition of such image segments for each cardiac phase is synchronized with the heart cycle by gating of the encoding steps with the patient's electrocardiogram. This technique works well as long as the subject has a regular heartbeat. The final result of the segmented acquisition is a series of images, one for each phase of the cardiac cycle. These images can be played as a cine loop (e.g., to assess ventricular function). The sharpest quality of images can be obtained by having the patient hold his or her breath during image acquisition.

The segmented data acquisition approach *(3)* always involves a tradeoff between temporal resolution (i.e., number of frames covering one R-to-R interval) and spatial resolution, because the image acquisition needs to be performed within a time short enough to allow for suspended breathing. With cardiac ultrasound, the image acquisition is rapid enough that it can be performed in "real-time" mode, something that only now is considered possible with MRI. To date, obtaining MRI real-time frame rates of 10 frames/s still involves significant compromises in terms of spatial resolution. In patients without a (regular) sinus rhythm, new real-time MRI techniques have started to offer a viable alternative.

3.3. Myocardial Tagging

Cine imaging of the heart can be combined with a series of magnetization preparation pulses that null the longitudinal magnetization along thin parallel stripes in the slice plane. The stripes appear as black lines on the MR images. This stripe pattern is created immediately after the R-wave and before acquisition of the segmented phase encodings (Fig. 11). The stripe lines visible in the resulting images are "embedded" in the tissue and are therefore distorted if any myocardial motion occurs. Thus, intramyocardial displacements can be tracked through monitoring visible motion of the tag lines.

Figure 12 shows an example of a myocardial stripe pattern laid down at end-diastole and, in a second frame, the same pattern at end-systole with evident distortion of the tag lines because of myocardial contraction. The tag lines, created right after the R-wave, tend to fade during the cardiac cycle because of T_1 relaxation, but for normal resting heart rates (e.g., 60–70

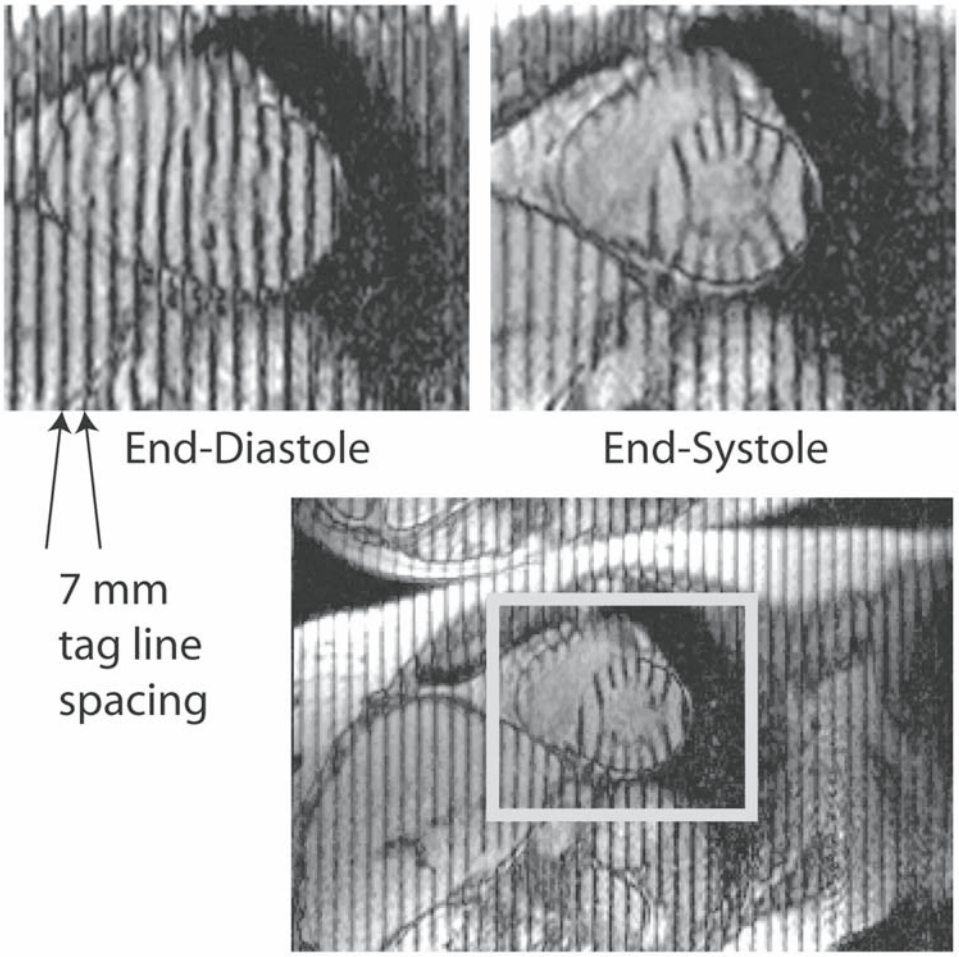

Fig. 12. Images with spatial modulation of magnetization in the form of vertical stripes in a human volunteer. The vertical tag lines were created right after the R-wave of the electrocardiogram. The upper left panel shows a magnified view of the heart during this initial phase. A second image is shown on the upper right for an end-systolic phase, with the distortion of the tag lines caused by cardiac contraction clearly apparent. The tagging technique is equivalent to the implantation of intramyocardial markers. Tracking of the tag lines over the cardiac cycle allows determination of myocardial strains and has been shown to provide a sensitive method for assessing regional wall motion abnormalities.

beats/min), the tag lines can persist long enough to allow visualization of cardiac motion over nearly the entire R-to-R interval. Tag lines in the ventricular blood pool disappear very quickly because of the rapid motion and mixing of blood in the ventricle; this effect is useful for recognizing the endocardial border.

It has been shown that tagging techniques and analysis of myocardial strain patterns yield higher sensitivity compared to "conventional" cine MRI for the detection of mild wall motion abnormalities. Initial studies leading to these observations were confined to research studies, mostly in animal models with well-characterized levels of myocardial ischemia *(4)*. The clinical application of MR tagging, particularly when it involves quantification of the myocardial strain patterns, is still hindered by the considerable efforts required for post-processing the images. Continuing research in this area has led to new approaches, such as the harmonic phase (HARP; *5,6*) and displacement encoding with stimulated echoes (DENSE) *(7)* techniques, that may circumvent such bottlenecks and result in a more widespread clinical application of MR tagging techniques.

3.4. MRI Cine of the Heart During Stress

The use of inotropic agents such as dobutamine in combination with echocardiography is a common practice for detecting wall motion abnormalities. Catecholamines such as dobutamine increase the myocardial contractility and the heart rate, thereby causing an increased oxygen demand that may lead to acute ischemia in myocardial regions with compromised blood supply, fibrosis, or other progressive pathologies. In regions in which dobutamine induces ischemia, the endocardial excursion does not increase to the same extent as in nonischemic myocardial wall segments.

MR imaging under dobutamine stress is typically performed at several levels of inotropic stimulation. The dobutamine dosage is incremented at intervals of 3–4 min, starting with a dosage of 10 μg/kg body weight per minute. The increase in dobutamine dosage is stopped at a maximum of 40 μg/kg/min

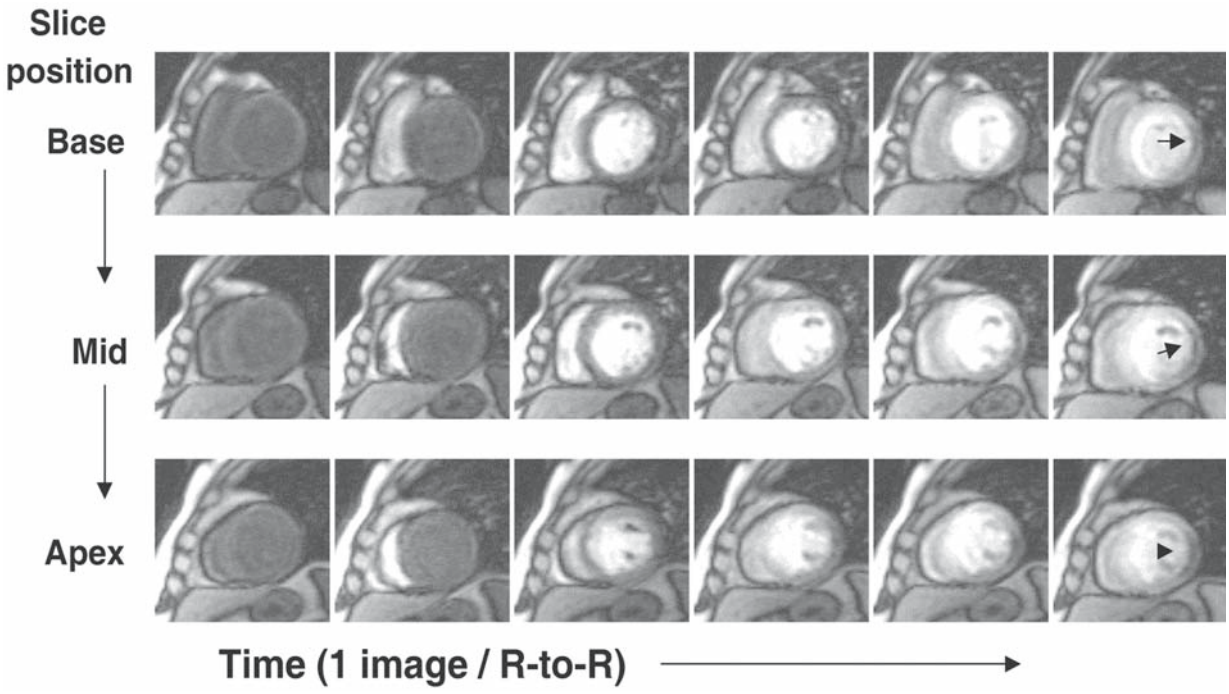

Fig. 13. Example images for three different slice locations during different phases of contrast agent transit. Images for each slice location are arranged in horizontal rows. These images were acquired with a rapid T_1-weighted gradient echo sequence (repetition time = 2.2 ms, echo time = 1.2 ms, flip angle 15°) in a patient with a perfusion defect in the lateral wall, highlighted by the arrow in the images. Cardiac motions appear frozen as the acquisition time for each image is short on the time-scale of a heart beat, and the image acquisition is synchronized to the heart rhythm by use of the R-wave on the electrocardiogram as a trigger signal for the scanner.

or at a lower dosage if a wall motion abnormality becomes visible. Dobutamine stress testing requires rapid feedback from the images to avoid excessive stress to the patient that could result in a cardiac arrest or an excessive ischemic insult. Ideally, monitoring of ventricular function at different levels of dobutamine-induced stress should be accomplished with (near) real-time feedback from the cine images *(8)*. Importantly, a recent comparison of wall motion studies performed in the same subjects with MRI and ultrasound by Nagel et al. *(9)* has demonstrated a significantly higher diagnostic accuracy of stress MRI in comparison to stress echocardiography.

3.5. Myocardial Perfusion

Rapid MR imaging of the heart during passage of an injected contrast agent bolus can be used to assess blood flow in the heart muscle *(10–12)*. The term *perfusion*, as used in this context, refers to blood flow in the tissue through the coronary arterial network from the epicardial artery, through arterioles with diameters of 5–100 μm, down to the capillaries, and through the venous network. The flow of blood is, under these circumstances, best described as the amount of a labeled substance that can traverse a unit volume of tissue per unit of time.

For MRI studies of tissue perfusion, a contrast agent is typically used as a tracer, thereby introducing a labeled substance with flow through myocardial tissue that is tracked by rapid serial imaging of the heart. The wash-in of contrast agent into the myocardium produces signal intensity changes in the images. Under normal conditions, the wash-in of an injected contrast agent takes only a couple of heartbeats. More specifically, following the time-course of contrast enhancement in the myocardium after injection of a contrast agent such as Gd-DTPA (gadolinium diethylenetriamine pentaacetic acid) provides a means to detect areas of ischemia in the heart.

To date, assessment of perfusion with MRI is generally accomplished by 2D T_1-weighted imaging of multiple slices during each heartbeat. An example of the resulting images is shown in Fig. 13. Typically, these imaging protocols use a non-slice-selective 180° or 90° radiofrequency pulse for T_1 weighting, followed by a rapid gradient echo readout of the image in less than 200 ms. The regional contrast enhancement should ideally be proportional to the contrast agent concentration. Such an approximately linear relationship between regional signal intensity and contrast agent concentration is only observed at lower contrast agent dosages, typically less than 0.05 mmol/kg of Gd-DTPA for fast, inversion recovery-prepared gradient echo sequences (repetition time less than 3 ms; echo time less than 2 ms) *(13)*. A more marked contrast enhancement can be obtained with higher contrast agent dosages, but then the kinetics of the contrast agent and the correlation of contrast enhancement with tissue blood flow cannot be well assessed in a quantitative manner.

Rapid contrast agent administration is crucial for assessing myocardial perfusion with such agents, as this improves the

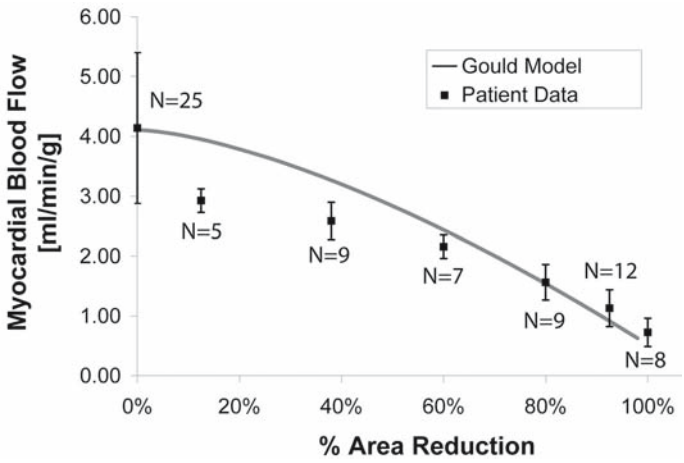

Fig. 14. Relation between myocardial blood flow measured during maximal vasodilation (e.g., with adenosine in a region downstream from an epicardial lesion) and the percentage lumen area reduction resulting from an epicardial lesion. Magnetic resonance perfusion studies were performed in patients who underwent coronary angiography after magnetic resonance imaging (MRI) exams. The myocardial blood flow was determined by quantitative analysis of the myocardial contrast enhancement *(13)*. The gray curve was calculated from the model equation of Gould and Lipscomb *(65)*, which related myocardial blood flow to the reduction of the maximal cross-sectional lumen area reduction.

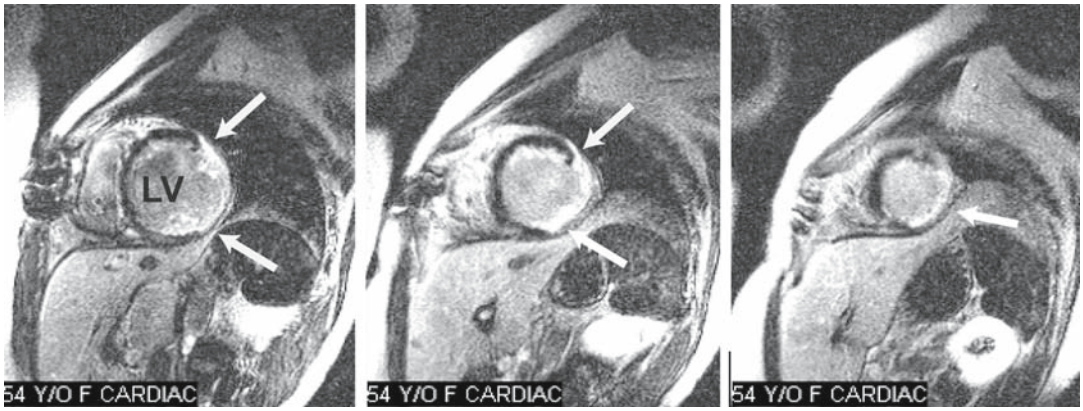

Fig. 15. T_1-weighted images acquired in a patient with a myocardial infarct; images were taken at 15 min after injection of 0.2 mmol/kg of Gd-DTPA (gadolinium diethylenetriamine pentaacetic acid) contrast agent. Infarcted myocardium appears brighter than noninfarcted myocardium. The T_1 contrast is adjusted to null the signal intensity in normal myocardium because this leads to the most pronounced contrast between infarcted and noninfarcted myocardium. Images were acquired for short-axis views and for different levels. LV, left ventricle.

sensitivity for detecting changes of myocardial blood flow *(14)*. Therefore, the goal is to ensure that the primary bottleneck to the rate of contrast enhancement is the rate of transport of contrast agent through myocardial tissue, and not the rate at which the contrast agent is injected. The presence of a narrowing in the coronary arteries is best detected when the resistance vessels downstream have been vasodilated. The relation between the degree of stenosis and blood flow reduction during maximal vasodilation is illustrated in Fig. 14.

3.6. Myocardial Viability

Extracellular contrast agents such as Gd-DTPA, commonly used for MRI perfusion studies, normally cross the cell membrane only after severe myocardial injury; thus, loss of myocardial viability has occurred *(15–19)*. The distribution volume of an extracellular contrast agent is larger in injured than in normal myocardial tissue. Given sufficient time, an extracellular contrast agent reaches an approximate equilibrium distribution at which the contrast enhancement of tissue relative to the contrast enhancement in the ventricular blood pool is proportional to the distribution volume *(20,21)*. Loss of viability and leakage of the contrast agent into the cell results in T_1-weighted signal hyperenhancement, as shown in Fig. 15.

The timing for imaging of hyperenhancement is important. The time to reach 90% of equilibrium concentration depends on the distribution volume, but generally does not exceed 15 min *(15)*. Larger infarcts can show a core zone that initially lacks enhancement even at 5 min or longer after contrast agent injection. This phenomenon, linked to microvascular obstruction, was shown to carry a graver prognosis for the patient than if the core no-enhancement zone was absent *(22,23)*.

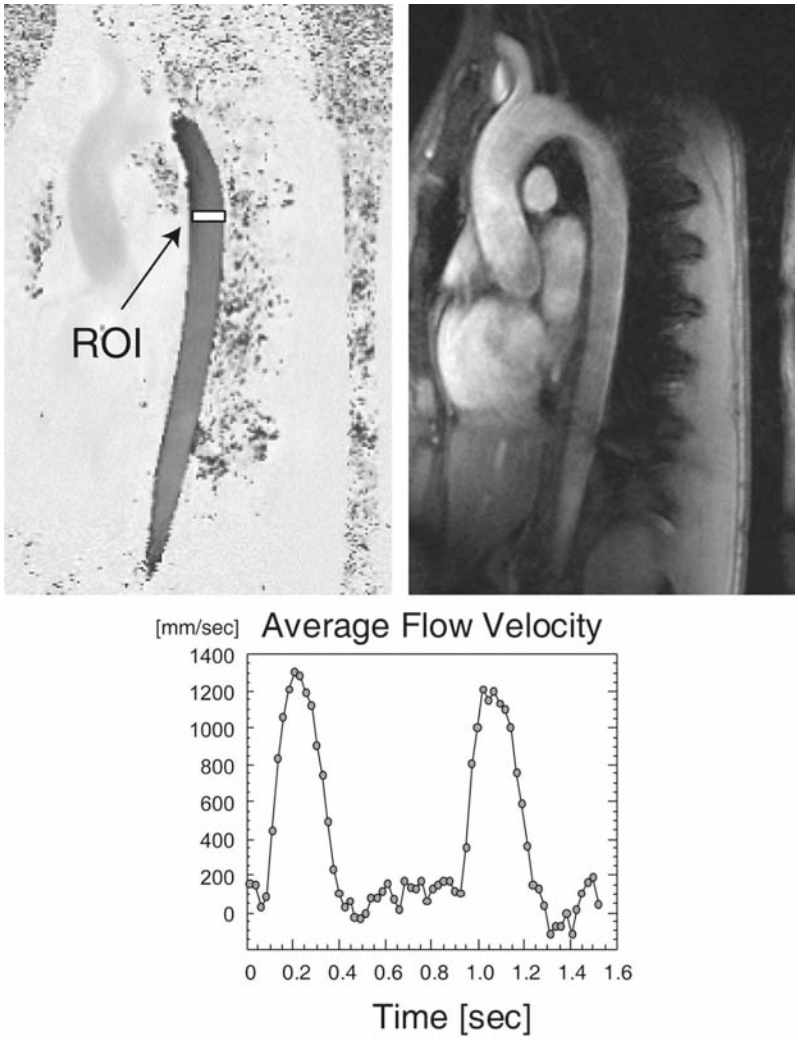

Fig. 16. Phase contrast imaging of the aorta in a human volunteer. Both the magnitude and phase images are shown. Images were acquired for 70 cardiac phases, covering approx 2.5 heartbeats. A region of interest (ROI; white box) was placed on the phase images in the thoracic aorta to determine the variation of the flow velocity in the vertical direction of the image plane. The variation of the velocity is shown in the graph.

3.7. MRI-Based Flow Velocity Measurements

A recorded MR signal can be represented in terms of a magnitude and a phase component. MRI images can elicit the spatial variations of the signal magnitudes, but it is also possible to create maps showing the spatial variations of the signal phases. It can be shown that the phase of the signal is sensitive to the velocity of tissue or blood. The so-called phase contrast MRI technique uses the phases of the signals to measure velocities. For an in-depth discussion, we refer the reader to the literature. An example of a phase contrast flow velocity measurement in an aorta is shown in Fig. 16.

3.8. Imaging of Fiber Structure

The analysis of myocardial microstructure is considered an important factor in understanding underlying pathologies because the structural fiber arrangement is modified over the time-course of various cardiac diseases. The tissue microstructure of the myocardium may be characterized by the resulting distribution of field inhomogeneities. Koehler et al. *(24)* showed that this structure can be observed on T_2^* maps of rat hearts at 11.75 T, a field strength much higher than used in current clinical MRI scanners. In this study, an in-plane resolution of 78 μm and a slice thickness of 250 μm were achieved, which compares quite favorably with photographs of postmortem histological sections. The field inhomogeneities revealed by T_2^* did provide structural information about biological tissue (both normal and scar tissue), as shown in Fig. 17. Two obvious advantages of this "NMR technique" compared to conventional histology are its noninvasive nature and speed.

4. INTERVENTIONAL MRI

To date, X-ray-based fluoroscopic techniques have been the gold standard for most invasive diagnostic and therapeutic applications for the heart. With the advent of ultrafast MRI and the development of MRI-compatible catheters and guidewires,

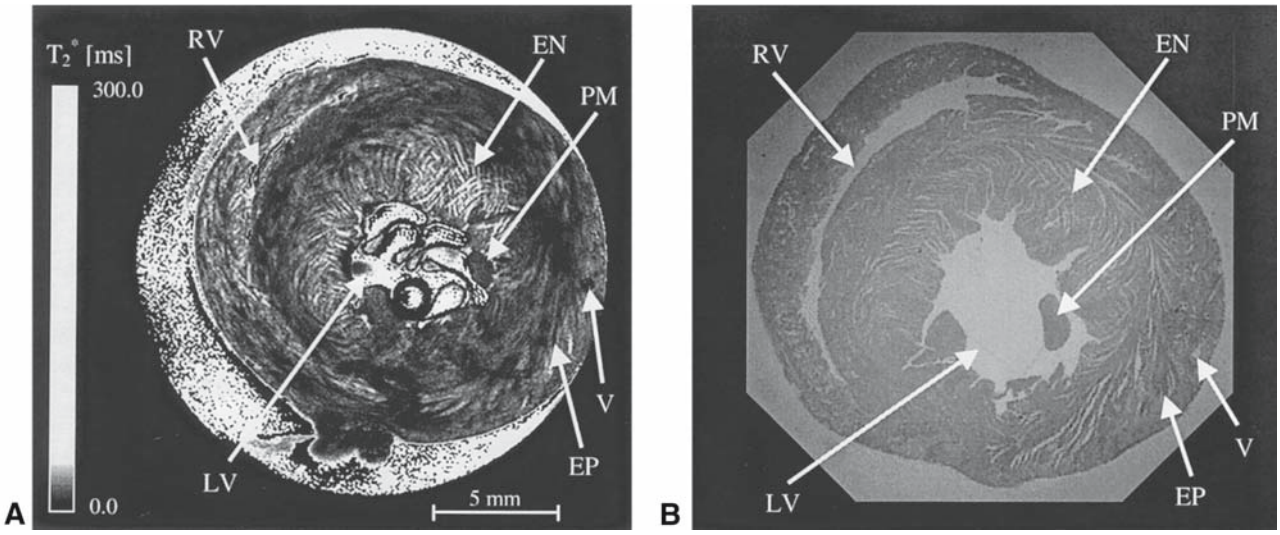

Fig. 17. **(A)** T_2^* map of an isolated beating rat heart in the short-axis view. Indicated is the epicardial myocardium (EP), the endocardial myocardium (EN), the left ventricle (LV) with a balloon inside, the collapsed right ventricle (RV), papillary muscle (PM), and vessel (V). Imaging parameters were as follows: field of view = 20 × 20 mm, matrix = 256 × 256, and spatial resolution = 78 μm in plane. The slice thickness was varied between 250 μm and 1 mm. **(B)** Corresponding histological section. To minimize motion artifacts from the beating heart, data were collected in middiastole. Image provided by Dr. Sascha Köhler and Dr. Peter M. Jakob, Physikalisches Institut, Universität Würzburg, Germany.

the goal of achieving real-time guidance by MRI for cardiovascular interventions is emerging as a new alternative *(25)*. The use of MRI for guided interventions would eliminate the reliance on ionizing radiation and iodinated contrast agents, an important advantage particularly for pediatric patients.

To date, continuous improvements of MRI techniques and MRI scanner hardware have rendered it feasible to achieve fluoroscopic image rates of 5–15 images/s *(26)*. Thus, it is possible to use MRI for guiding interventional cardiovascular procedures, such as coronary catherization *(27)* or gene therapy delivery *(28)*, with close to real-time image refresh rates. Initial interventional studies with MRI guidance have demonstrated the advantages of MRI, including the ability to image arbitrarily oriented cross-sections, interactive steering of the image plane, and excellent soft tissue contrast for the detection and visualization of lesions *(29)*.

Several other technical advances have also been crucial for performing interventional procedures under MRI guidance, including: (1) development of 1.5-T magnets with short bores that allow access to the groin area for catheter-based procedures; (2) liquid crystal image displays that can be exposed to high magnetic fields to allow the operator to perform an intervention and control MRI scan parameters from a position right next to the magnet; and (3) development of catheter-based MRI antennae *(30)* for localized intravascular signal reception and high-resolution imaging.

4.1. MR-Compatible Devices

MR-guided interventions, such as the pulmonary artery dilation shown in Fig. 18, can only be performed with devices free of ferromagnetic components because severe magnetic field and image distortions would be encountered, not to mention the physical forces exerted on the device itself by the static magnetic field *(31)*. Even without the use of ferromagnetic materials near the MRI-compatible devices, image artifacts are not entirely unavoidable. On the other hand, this can be used as an advantage to differentiate the device from surrounding tissue or blood, thereby providing a means to track the position of the device; this method of device monitoring is termed *passive tracking*.

For example, in our laboratory we have used a customized, MRI-compatible variation of the Amplatzer® Septal Occluder (AGA Medical, Golden Valley, MN), which consists of a nitinol wire mesh that produces minimal artifacts *(32)*. This device is visible on MR images by causing a relatively small signal void in its proximity. Experiments have been conducted in our laboratory for closure of an atrial septal defect with the Amplatz device under MRI guidance *(32)*. (For more information on such devices, *see* Chapter 29.)

In addition to passive tracking, we have taken advantage of active tracking devices in the form of miniature radiofrequency-receiving antennae mounted on a catheter tip (SurgiVision Inc., Gaithersburg, MD). With these miniature antennae, it is possible to acquire images from very small fields of view, that is, to achieve high spatial resolution if the external receiving antennae have been switched off. Such miniature antennas also enable imaging of vessel walls (plaque and aneurysm imaging), surrounding soft tissue (tumor, hematoma), or atrial septal anatomy, or obtaining a signal-to-noise ratio in the images not achievable with external antennae. Furthermore, the image generated by a coil on the tip of a device can be superimposed on other MR images, obtained simultaneously with external antennas, for device tracking during an interventional procedure.

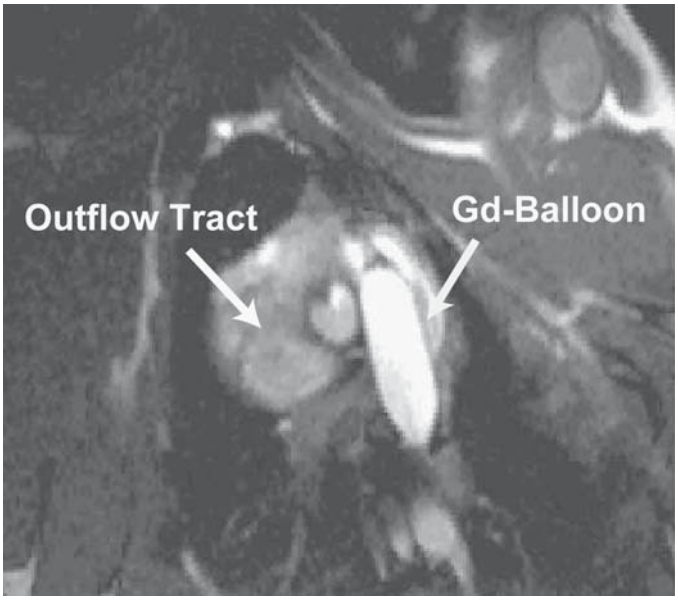

Fig. 18. Axial snapshot obtained with a gradient echo sequence with steady-state free precession and optimized for real-time imaging at frame rates up to 8 images/s. The image was acquired for a slice at the level of the aortic root and the main pulmonary artery in a porcine model of pulmonary stenosis. The balloon was filled with gadolinium contrast agent and saline (1:20) for optimal contrast. In the center of the image is the aorta with the left ventricle trigger catheter in place. The balloon is fully inflated (4–5 bar) in the main pulmonary artery. The operatively created stenosis was successfully dilated during the procedure guided by magnetic resonance imaging.

5. MRI AND BIOMEDICAL DEVICES

5.1. MRI Safety and Compatibility

Most currently used implantable devices contain metallic parts that would both seriously interfere with MR cardiac imaging, or pose a safety risk for the patient. Implanted devices with ferromagnetic parts are considered a strict contraindication for cardiac MRI because of the potential hazards caused by movement, dislodgement, or heating effects. Although cardiac pacemakers are implanted in large numbers of patients, little has been accomplished to date to make pacemakers MRI compatible or MRI safe.

A notable exception is a study that employed fiber-optic cardiac pacing leads; the study reported that the use of such leads resulted in an absence of heating effects and only minimal magnetic deflection forces *(33)*. Fiber-optic catheters attached to a wearable temporary external photonic pulse generator may therefore provide in the future a means for safely performing MRI studies on patients with implanted pacemakers.

MRI compatibility can be defined as the property of a device not to interfere with imaging, such as by causing distortions of the magnetic field that cause signal loss. A device may be MR compatible, but that does not necessarily mean it is MR safe. The latter requires that the exposure to a strong static magnetic field, pulsing of the magnetic field gradients, and applications of radiofrequency pulses do not cause adverse effects. For example, the pulsing of the magnetic field gradients produces a changing magnetic flux that can induce current flow in lead wires, which in turn may lead to tissue heating. The presence of metallic parts can also cause an inhomogeneous deposition of radiofrequency power in the vicinity of the device, which could lead to radiofrequency heating of tissue or blood. Implanted cardiac pacemakers are therefore not only a contraindication for cardiac exams, but for MRI exams in general. Investigators have reported that MRI imaging caused temperature elevations as high as 23°C at 0.5 T and 60°C at 1.5 T at pacing lead tips *(34,35)*.

It is foreseen that completely new safety concerns will be raised when MRI is performed using intravascular coils *(36,37)*. Such intravascular coils may, for example, be used to examine vulnerable plaque on vessel walls; therefore, localized heating in the vicinity of the coil could disrupt the plaque, with catastrophic consequences. Heating strongly depends on the wavelength (MRI frequency), geometry of the body and the device, and placement of the body and device with respect to each other and within the MR system.

Our group conducted temperature measurements on the potential heating effects within a gel phantom to study the interaction when employing a miniature, loopless intravascular antenna; a 1-m loopless, coaxial (dipole) antenna was connected to a decoupling, matching, and tuning (DMT) interface. The DMT contained a radiofrequency trap circuit and an active detuning circuit with a radiofrequency PIN diode. During the radiofrequency transmit phase, the PIN diode was activated and presented a short circuit for signals traveling on the inner conductor of the loopless antenna.

The effectiveness of the decoupling mechanism was tested in an 8-in diameter and 20-in long cylindrical gel phantom with a dielectric constant of 81 and conductivity of 0.7 Siemens/m. Temperature changes in the vicinity of the device were measured while a conventional spin-echo sequence was continuously running. We found that the exact temperature rise varied as a function of insertion depth and position of the coil in the phantom and the magnet bore. In the connected state, the temperature increase never exceeded 4°C and, in most cases, remained below 1°C. However, in the absence of a DMT or with malfunction of the DMT, a temperature rise in excess of 30°C could be produced for the identical scan parameters; this underlines the need for careful safety mechanisms in coils used for interventional MRI.

5.2. Testing of Biomedical Devices With MRI

Cardiac MRI also provides a unique opportunity to test, in vivo, the performance of implanted devices such as prosthetic heart valves and heart pacing devices (those that would be MRI compatible). In patients with artificial aortic valves, the flow downstream from the implanted valve may be severely altered. These changes have been associated with an increased risk of thrombus formation and mechanical hemolysis. MRI velocity mapping is considered very useful for the noninvasive evaluation of the flow profiles in patients with a mechanical valve prosthesis *(38,39)*. For example, Botnar et al. *(40)* found that peak flow velocity in the aorta was significantly higher in patients with a valvular prosthesis than in normal controls. In

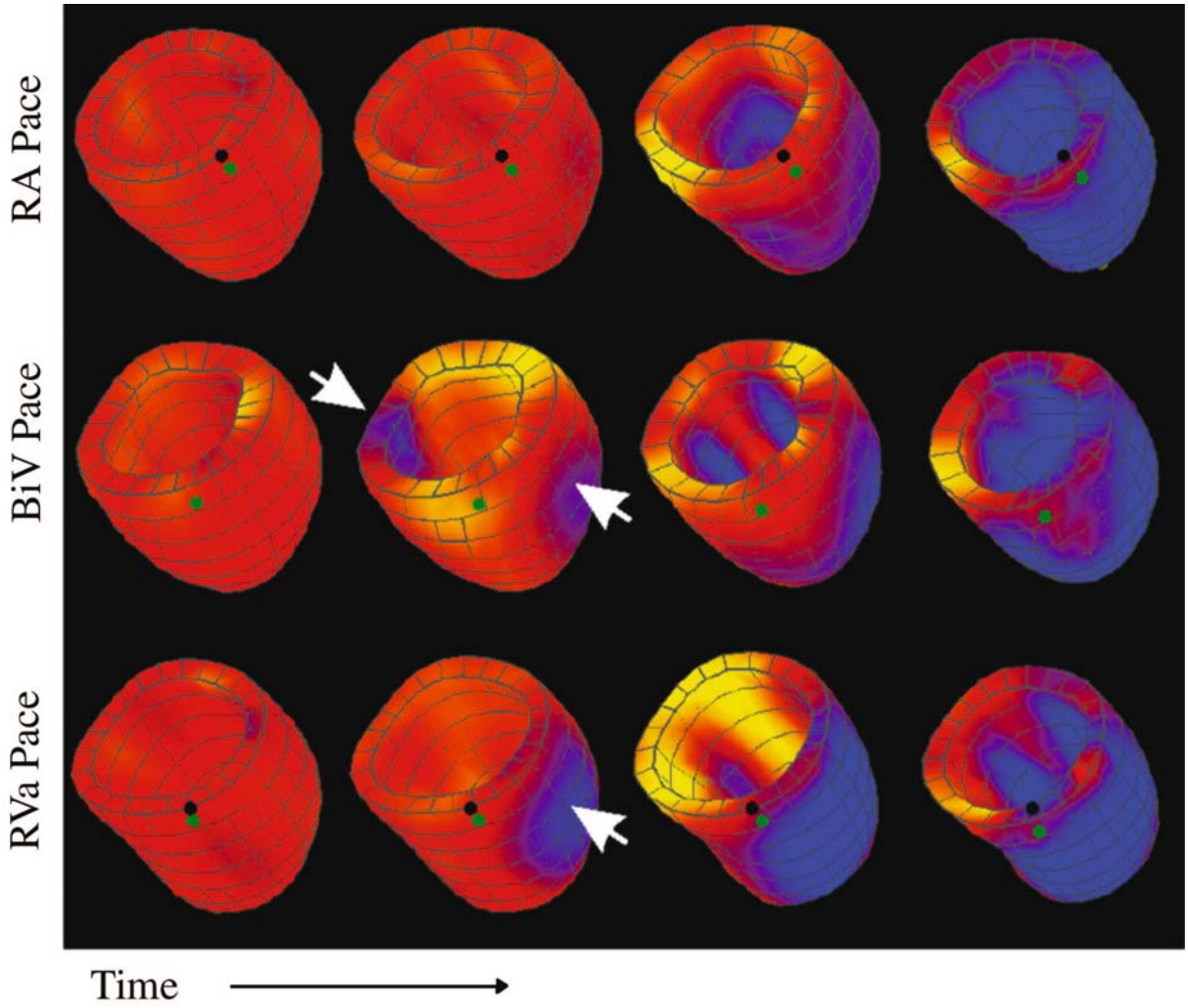

Fig. 19. The temporal evolution of left ventricular shortening measured by magnetic resonance imaging tagging under different pacing protocols: right atrial pacing (top row), biventricular pacing (middle row), and right ventricular apex pacing (bottom row). Blue, contraction; red, reference state; yellow, stretch. Data are shown for late diastole after tagging (first column), early systole (second column), midsystole (third column), and late systole (last column). These measurements give precise quantification of the regional mechanical consequences of different pacing protocols. BiV, biventricular; RA, right atrial; RVa, right ventricular apex. Image provided by Dr. Eliot McVeigh (National Institutes of Health and Johns Hopkins Medical School). Further details about this study can be found in B.T. Wyman, W.C. Hunter, F.W. Prinzen, O.P. Faris, and E.R. McVeigh (2002), Effects of single- and biventricular pacing on temporal and special dynamics of ventricular contraction. *Am J Physiol Heart Circ Physiol.* 282, H372–H379.

the same study, the investigators also found that diastolic mean flow was negative in patients after valve replacement, but not in controls.

Interestingly, the usefulness of MRI for assessing the function of cardiac pacing devices has already been proven in experimental animal studies, although currently there are still hurdles for performing cardiac MRI on patients with such devices. More specifically, Prinzen, Wyman, and coworkers *(41,42)* showed that MR tissue tagging can be used to evaluate mechanical activation in the left ventricle for different pacing sites, as shown in Fig. 19. These investigators were able to show with MRI that the propagation of mechanical activation for right ventricular apex pacing elicited regional variations, whereas left ventricular base pacing did not.

6. QUANTITATIVE ANALYSIS OF FUNCTION, PERFUSION, AND VIABILITY

Postprocessing of cardiac MRI studies represents the stage at which the full potential of the cardiac MRI examination may be best realized. Postprocessing is composed of two major steps: image postprocessing and data postprocessing. The first step largely involves segmentation algorithms to delineate and extract features and structures of interest from the collected images. The second step consists mainly of applying mathematical and statistical methods to aid in a given diagnosis. We focus here on the analysis of MR cine and perfusion studies.

For many cardiac protocols, the myocardium is the area of interest for analysis, so the myocardium must be segmented

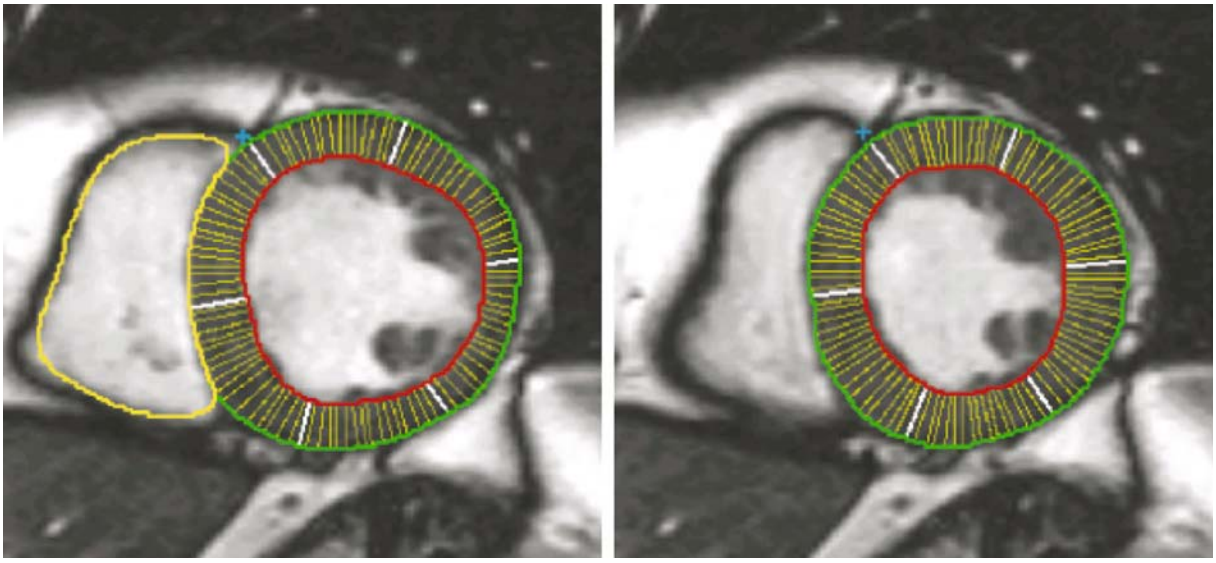

Fig. 20. Example of myocardial segmentation for two images corresponding to the end-diastolic **(left)** and end-systolic **(right)** phases in a patient with poor cardiac function. The red contours are drawn around the blood pool demarking the endocardium. The green contour is drawn around the epicardium. The yellow contour delineates the right ventricular blood pool. For this particular patient, the cross-section of ventricular cavity with the short-axis view changed significantly less than in a healthy normal. Also shown are chords connecting the endocardial and epicardial borders. The chords are orthogonal to a centerline between the two contours. The chords measure the true thickness of the myocardium as opposed to radial chords, which emanate from the center of the left ventricle.

from the rest of the image to extract further information, such as to utilize contrast enhancement in a perfusion study or monitor systolic thickening of the wall for a MR cine study.

6.1. Analysis of Ventricular Function by MRI

The quantitative analysis of ventricular function is based on the segmentation of the myocardium. In general, this is achieved by drawing contours on the endocardial and epicardial borders of the myocardium (Fig. 20).

The ventricular volumes of interest are the end-diastolic and end-systolic volumes, as well as derived parameters such as the stroke volume and ejection fraction. Although ventricular volumes have been computed from differently oriented views of the heart, analysis of the short-axis views is most widely used in cardiac MRI because of its proven accuracy *(43–46)*. In the simplest case, myocardial segmentation is performed only for the images corresponding to the end-diastolic and end-systolic phases. The *end-diastolic phase* is defined as the phase containing the largest blood pool area in the left ventricle. The *end-systolic phase* is identified as the image containing the smallest blood pool area (Fig. 21).

Once the end-diastolic and end-systolic phases are fixed, the contours are drawn in the images for the end-diastolic and end-systolic phases for all slices containing the left ventricle. In images for a basal slice of the left ventricle, part of the aorta and aortic valve may be visible. It should be noted that inclusion of contours above the mitral valve plane will significantly overestimate the values for myocardial mass and ventricular volume. Thus, the careful inclusion or exclusion of slices near the base of the heart for determination of the volumes at end-diastole and end-systole is of considerable importance for an accurate determination of the ventricular volumes. Once all contours are drawn and verified, the ventricular volume can be computed by simple slice summation using Simpson's rule with the slice thickness as an increment.

Young et al. *(46)* proposed a method of speeding up the process of contour drawing by placing guide points on the endocardial and epicardial borders instead of drawing continuous contours for both borders. The algorithm then automatically detects the myocardial borders by interpolation between the guide points. This user-friendly method reduces the burden of generating contours compared to the conventional tracing of the contours. Swingen et al. *(47)* modified the guide point technique by including feedback from continuously updated 3D models of the heart to evaluate both the placement of guide points and the accuracy of the computed volumes. They showed that the combined use of short- and long-axis views results in more accurate estimates of the ventricular volumes and the myocardial mass compared to exclusive reliance on short-axis views.

Parameters of interest for volumetric analyses are as follows:

- *Left ventricular mass:* the myocardial mass is obtained by multiplying the myocardial volume by the myocardial specific gravity (1.05). Myocardial volume is calculated as the difference between the epicardial and endocardial volumes. The normal mean for left ventricular mass is 92 ± 16 g/m^2 of body surface area.
- *Stroke volume:* the stroke volume is calculated as the difference between end-diastolic and end-systolic blood or chamber volumes, and it represents the volume of blood ejected by a ventricle per heartbeat (in the absence of aortic regurgitation).

Unless shunts and valvular regurgitation are present, the calculated stroke volumes of the two ventricles should be nearly equal. This is a rule of thumb for verification of the volume computation.

- *Ejection fraction:* this is the ratio of the ventricular stroke volume to the end-diastolic volume. The normal range is between 55 and 65%. An ejection fraction of less than 40% is considered to indicate impaired ventricular function.
- *Cardiac output:* this is the product of stroke volume and heart rate. It is a measure of the volume of blood ejected by the heart per beat. For an average adult, it is 4–8 L/min. Cardiac output is often corrected by normalization with respect to the body surface area.

6.2. Analysis of Wall Motion

Wall motion analysis is performed to measure the changes in thickness of the left ventricular wall from diastole to systole *(9,48–52)*. Wall motion abnormalities are commonly associated with many cardiac diseases, including dilated cardiomyopathy, end-stage valvular disease, and ischemic heart disease.

The assessment of myocardial wall thickness, thickening, and wall motion abnormalities proceeds from the segmentation along the endocardial and epicardial borders. A centerline is drawn between the myocardial contours *(53)*. Approximately 100 chords are then drawn orthogonal to the centerline at equal intervals to intersect the two myocardial contours (Fig. 5). With the centerline technique, the chords are optimally placed to measure the exact thickness of the transmural myocardium *(53)*.

Parameters of interest for wall motion analyses include the following:

- *Myocardial thickness:* the lengths of the orthogonal chords, from the endocardial to the epicardial borders, measure myocardial thicknesses.
- *Myocardial thickening:* differences in end-diastolic and end-systolic thicknesses, as a percentage of end-diastolic thickness, are a measure of thickening.

7. PERFUSION ANALYSIS

Myocardial perfusion is a measure of blood flow (e.g., mL/min) per unit mass of myocardial tissue. Myocardial perfusion should ideally match the demand for oxygen in the myocardium. Perfusion is commonly assessed at both rest and with induced stress to evaluate the capacity of the coronary circulation to increase blood flow above its baseline level and thus match increases in oxygen demand. A ratio of the perfusion parameters, measured at stress and divided by the value for rest, will give a so-called perfusion reserve. In healthy individuals, myocardial blood flow increases approximately three- to fourfold above its baseline level with maximal vasodilation; with disease, the perfusion reserve decreases, and a flow reserve on the order of 2.5:1 is often used as the cutoff for deciding whether disease is present.

The analysis of myocardial perfusion can be carried to different levels, depending on the diagnostic needs and resources available. One type of qualitative analysis associated with nuclear imaging is performed by visual comparison of the contrast enhancement in different myocardial sectors. The images are often viewed for this purpose in cine mode; delays in contrast enhancement or a reduced peak contrast enhancement relative to other myocardial sectors are interpreted as signatures of locally reduced myocardial blood flow. However, to do so, the absence of image artifacts is important if the analysis is purely qualitative and visual; no image postprocessing is necessary. Nevertheless, a qualitative analysis might have limited capability to detect global reductions of myocardial perfusion, especially in patients with multivessel coronary artery disease.

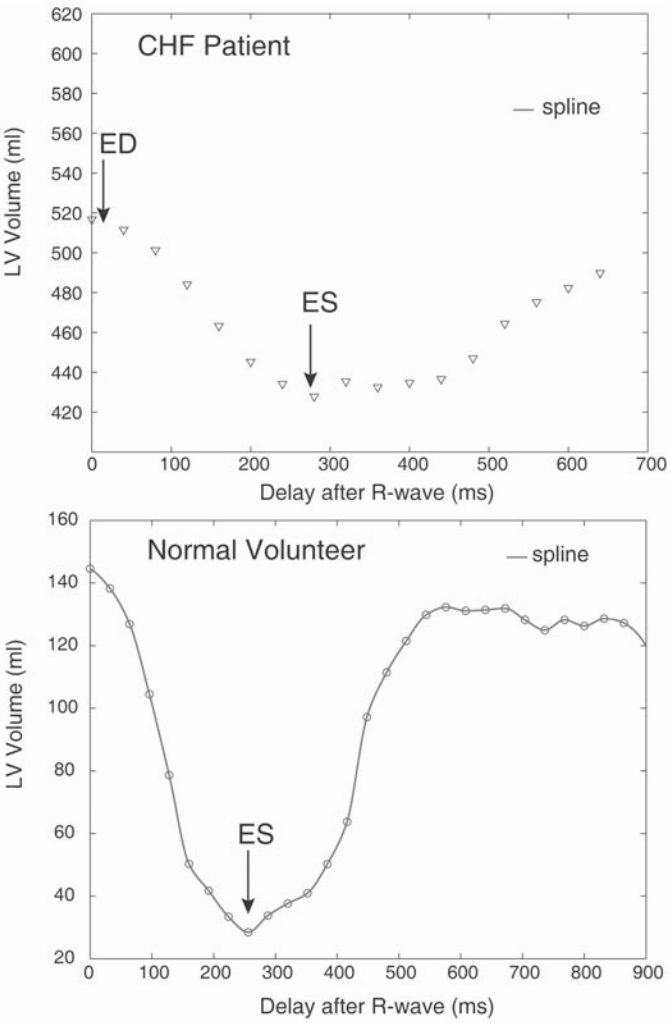

Fig. 21. Volume–time graph with the end-diastolic and end-systolic phases identified by ES and ED symbols, respectively. The upper graph shows the variation of left ventricular (LV) volume over the cardiac cycle for a patient with congestive heart failure (CHF), and the lower graph is the same type of graph for a healthy volunteer. The patient with CHF had an enlarged ventricle (i.e., large volume) and a very low ejection fraction. Because of the low ejection fraction, the curve in the upper graph is relatively flat. Ventricular volumes were calculated by Simpson's rule from a set of short-axis images. The endocardial border had been traced on each cine frame to obtain a complete curve of left ventricular volume vs time.

A quantitative analysis of MRI perfusion studies commonly starts with image segmentation, similar to the procedure for analysis of cine studies. A user segments one image with good contrast enhancement along the endocardial and epicardial

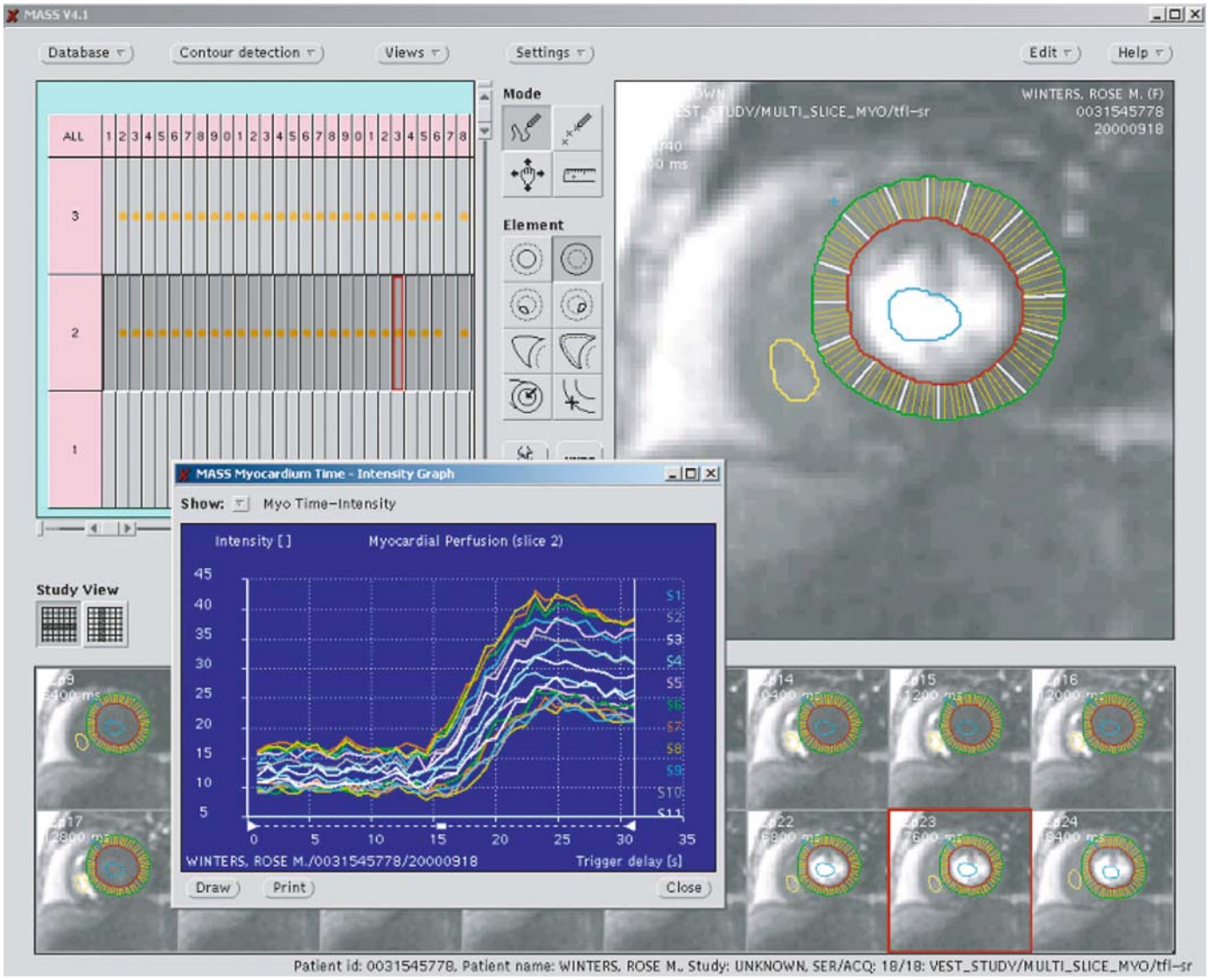

Fig. 22. Graphical user interface of software for analysis of perfusion studies. Segmentation contours are drawn by the user to define the endocardial and epicardial borders. Similar to the approach used for cine analysis, the analysis is carried out on a sector basis; in this case, 16 sectors have been defined. The drawn contours can be copied to other images for the same slice position in the perfusion study. After adjustment of the contours in each image, the software calculated the mean signal intensity in each myocardial sector. As a result, graphs are obtained depicting the change in signal intensity in each myocardial sector as a function of image number or time (*see* inset panel).

borders of the left ventricle. These contours are then either copied to the remaining images in the data set or an automatic algorithm is employed to identify the borders of the myocardium and adjust the contour positions.

The latter option is extremely useful because the number of images in a perfusion data set can be very large compared to a cine data set. The task of simply copying the contours to all other images would require extensive manual editing of the contour by the user. Unlike cine images, the myocardial boundaries can be slightly blurred in perfusion images because of the reduced spatial resolution and cardiac motion. Segmentation of myocardial perfusion images is therefore considered more challenging than for cine MR studies.

Once the myocardium is extracted by image segmentation, it is divided into smaller segments or sectors similar to those defined in cine wall motion analyses. Specifically, signal intensity averages are calculated in each myocardial segment. Typically, the myocardium is divided into four segments at the apex and up to eight sectors at the base; recently, the use of six sectors has been proposed for standardization of this task *(54)*. The signal intensity averages can be plotted vs the image number or vs the time from the beginning of the perfusion scan. Various parameters that characterize the contrast enhancement kinetics are computed from these curves for assessing perfusion. The interface of a software tool that is used for analysis of MR perfusion studies is shown in Fig. 22.

7.1. Curve Fitting

As the perfusion images are acquired quite rapidly (<250 ms per image), there is often significant noise in the images. Thus, to extract perfusion parameters, it is useful to perform some curve fitting to smooth the signal intensity curves. One widely used choice for this purpose is the gamma variate function *(55),* which approximates the first-pass portion of the measured curves quite well. A gamma variate curve fitted to a signal intensity curve obtained from an MR perfusion study in a patient study is shown in Fig. 23. Nevertheless, there are certain constraints for the gamma variate analyses; for instance, it is best optimized only when the first-pass portion of the curve is used (from the foot to the peak of the curve).

A number of parameters have been proposed for a semiquantitative assessment of perfusion. Commonly used parameters are the following:

- *Percentage peak enhancement:* the peak signal normalized by the derived average baseline signal (i.e., signal before arrival of contrast agent expressed as a percentage).
- *Upslope:* the slope of the first-pass segment primarily from the start of appearance of the contrast (foot) in the myocardium to the peak.
- *Time to peak:* the time from the foot to the peak of the curve.
- *Mean transit time:* the average time required for a unit volume of blood to transit through the region of interest. It can be determined as the ratio of blood volume in the region of interest to the blood flow through the region of interest. This value can be estimated from the gamma variate fit to the tissue curve.
- *Dynamic distribution volume:* the area under the signal intensity curve, often normalized by the area under the corresponding curve for the left ventricle.

The upslope parameter is increasingly becoming the most widely used parameter for a semiquantitative evaluation of myocardial perfusion. The upslopes of the tissue curves are generally normalized by the upslope of the signal intensity curves for a region of interest in the center of the left ventricle, with the latter considered as an arterial input in the analysis. A *ratio*, defined as the normalized upslopes of the tissue curve measured for maximal vasodilation, divided by the corresponding upslope value at rest has been proposed as a perfusion reserve index *(56–59)*. The perfusion reserve derived from the upslopes generally underestimates the actual ratio of blood flows for maximal vasodilation and rest by approx 40% *(60)*.

We have shown that accurate myocardial blood flow estimates can be obtained by MRI methodologies in comparison to invasive studies employing radio isotope-labeled microspheres *(61–65)*; the latter are acknowledged as gold standards for the measurement of blood flow in tissues. MRI perfusion imaging may therefore play a pivotal future role in assessing novel therapeutic approaches for treating coronary artery disease, and automated quantitative analyses of MR perfusion measurements would play an essential role in this task.

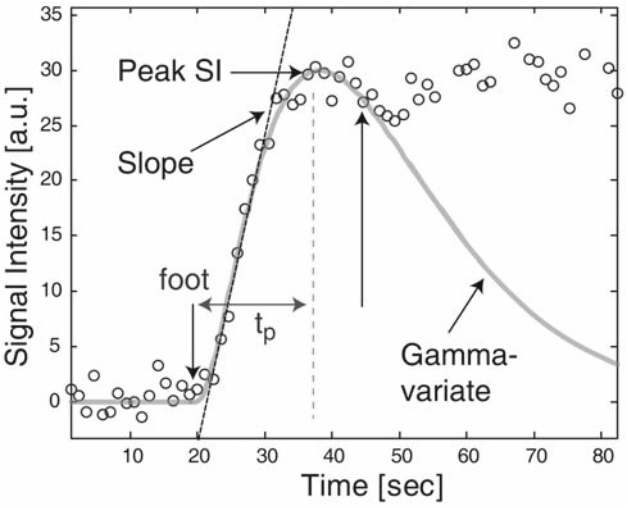

Fig. 23. Signal intensity (SI) curve for a myocardial sector in the lateral wall. Each of the data points (circles) represents the mean SI measured in the images for the user-defined myocardial sector. The images were acquired with a fast, T_1-weighted gradient echo sequence during injection of a 0.075 mmol/kg bolus of Gd-DTPA (gadolinium diethylenetriamine pentaacetic acid), an extracellular magnetic resonance contrast agent. The gamma variate function can only be used to fit the portion of the tissue curve corresponding to the first pass of the contrast agent. The gray curve represents the best fit of the gamma variate function to be part of the experimental data, covering the range indicated by the vertical arrows. The gamma variate fit was extrapolated to the end of the measurement range. In many cases, the end of the first pass and the appearance of the recirculation component can be best ascertained from the SI changes observed in the left ventricular blood pool. Also shown are semiquantitative perfusion parameters such as the slope, peak SI, and the time from the foot to the peak t_p.

8. CONCLUSIONS

For the biomedical engineer, cardiac MRI represents an opportunity to study the function of the heart and use this insight to design better biomedical devices. Because of the increasing relevance of cardiac MRI in the clinical arena, it will become important to address the challenges inherent in the use of cardiac MRI in patients with implanted devices.

ACKNOWLEDGMENTS

We gratefully acknowledge support of our cardiac MRI research with funding through R01 HL65394-01 and R01 HL65580-01 from the National Institutes of Health, and through a research fellowship grant from the Deutsche Forschungsgemeinschaft (DFG RI 1040/1-1).

REFERENCES

1. Purcell, E.M., Torrey, H.C., and Pound, R.V. (1946) Resonance absorption by nuclear magnetic moments in a solid. *Phys Rev*. 69, 37.
2. Bloch, F., Hansen, W.W., and Packard, M. (1946) Nuclear induction. *Phys Rev*. 69, 127.
3. Schulen, V., Schick, F., Loichat, J., et al. (1996) Evaluation of K-space segmented cine sequences for fast functional cardiac imaging. *Invest Radiol*. 31, 512–522.
4. Kraitchman, D.L., Wilke, N., Hexeberg, E., et al. (1996) Myocardial perfusion and function in dogs with moderate coronary stenosis. *Magn Reson Med*. 35, 771–780.
5. Osman, N.F., McVeigh, E.R., and Prince, J.L. (2000) Imaging heart motion using harmonic phase MRI. *IEEE Trans Med Imaging*. 19, 186–202.
6. Osman, N.F., Kerwin, W.S., McVeigh, E.R., and Prince, J.L. (1999) Cardiac motion tracking using CINE harmonic phase (HARP) magnetic resonance imaging. *Magn Reson Med*. 42, 1048–1060.

7. Aletras, A.H., Ding, S., Balaban, R.S., and Wen, H. (1999) DENSE: displacement encoding with stimulated echoes in cardiac functional MRI. *J Magn Reson.* 137, 247–252.
8. Hundley, W.G., Hamilton, C.A., Thomas, M.S., et al. (1999) Utility of fast cine magnetic resonance imaging and display for the detection of myocardial ischemia in patients not well suited for second harmonic stress echocardiography. *Circulation.* 100, 1697–1702.
9. Nagel, E., Lehmkuhl, H.B., Bocksch, W., et al. (1999) Noninvasive diagnosis of ischemia-induced wall motion abnormalities with the use of high-dose dobutamine stress MRI: comparison with dobutamine stress echocardiography. *Circulation.* 99, 763–770.
10. Manning, W.J., Atkinson, D.J., Grossman, W., Paulin, S., and Edelman, R.R. (1991) First-pass nuclear magnetic resonance imaging studies using gadolinium-DTPA in patients with coronary artery disease. *J Am Coll Cardiol.* 18, 959–965.
11. Rossum, A.C., Keijer, T., and Hofman, M. (1993) First-pass MRI of myocardial perfusion at rest and after pharmacologically induced vasodilatation in patients with coronary artery disease, in *Book of Abstracts: Society of Magnetic Resonance in Medicine,* New York, NY, p. 543.
12. Wilke, N., Jerosch-Herold, M., Stillman, A.E., et al. (1994) Concepts of myocardial perfusion imaging in magnetic resonance imaging. *Magn Reson Q.* 10, 249–286.
13. Jerosch-Herold, M., Wilke, N., Stillman, A.E., and Wilson, R.F. (1998) Magnetic resonance quantification of the myocardial perfusion reserve with a Fermi function model for constrained deconvolution. *Med Phys.* 25, 73–84.
14. Kroll, K., Wilke, N., Jerosch-Herold, M., et al. (1996) Modeling regional myocardial flows from residue functions of an intravascular indicator. *Am J Physiol.* 271, H1643–H1655.
15. Tong, C.Y., Prato, F.S., Wisenberg, F., et al. (1993) Techniques for the measurement of the local myocardial extraction efficiency for inert diffusible contrast agents such as gadopentate dimeglumine. *Magn Reson Med.* 30, 332–336.
16. Tong, C.Y., Prato, F.S., Wisenberg, F., et al. (1993) Measurement of the extraction efficiency and distribution volume for Gd-DTPA in normal and diseased canine myocardium. *Magn Reson Med.* 30, 337–346.
17. Lima, J.A., Judd, R.M., Bazille, A., Schulman, S.P., Atalar, E., and Zerhouni, E.A. (1995) Regional heterogeneity of human myocardial infarcts demonstrated by contrast-enhanced MRI. Potential mechanisms. *Circulation.* 92, 1117–1125.
18. Judd, R.M., Lugo-Olivieri, C.H., Arai, M., et al. (1995) Physiological basis of myocardial contrast enhancement in fast magnetic resonance images of 2-day-old reperfused canine infarcts. *Circulation.* 92, 1902–1910.
19. Kim, R.J., Chen, E.L., Lima, J.A., and Judd, R.M. (1996) Myocardial Gd-DTPA kinetics determine MRI contrast enhancement and reflect the extent and severity of myocardial injury after acute reperfused infarction. *Circulation.* 94, 3318–26.
20. Pereira, R.S., Prato, F.S., Wisenberg, G., and Sykes, J. (1996) The determination of myocardial viability using Gd-DTPA in a canine model of acute myocardial ischemia and reperfusion. *Magn Reson Med.* 36, 684–693.
21. Pereira, R.S., Prato, F.S., Sykes, J., and Wisenberg, G. (1999) Assessment of myocardial viability using MRI during a constant infusion of Gd-DTPA: further studies at early and late periods of reperfusion. *Magn Reson Med.* 42, 60–68.
22. Rochitte, C.E., Lima, J.A., Bluemke, D.A., et al. (1998) Magnitude and time course of microvascular obstruction and tissue injury after acute myocardial infarction. *Circulation.* 98, 1006–1014.
23. Wu, K.C., Zerhouni, E.A., Judd, R.M., et al. (1998) Prognostic significance of microvascular obstruction by magnetic resonance imaging in patients with acute myocardial infarction. *Circulation.* 97, 765–772.
24. Köhler, S., Hiller, K.H., Waller, C., Jakob, P.M., Bauer, W.R., and Haase, A. (2003) Visualization of myocardial microstructure using high-resolution T imaging at high magnetic field. *Magn Reson Med.* 49, 371–375.
25. Lardo, A.C. (2000) Real-time magnetic resonance imaging: diagnostic and interventional applications. *Pediatr Cardiol.* 21, 80–98.
26. Kerr, A.B., Pauly, J.M., Hu, B.S., et al. (1997) Real-time interactive MRI on a conventional scanner. *Magn Reson Med.* 38, 355–367.
27. Serfaty, J.M., Yang, X., Foo, T.K., Kumar, A., Derbyshire, A., and Atalar, E. (2003) MRI-guided coronary catheterization and PTCA: a feasibility study on a dog model. *Magn Reson Med.* 49, 258–263.
28. Yang, X., Atalar, E., Li, D., et al. (2001) Magnetic resonance imaging permits in vivo monitoring of catheter-based vascular gene delivery. *Circulation.* 104, 1588–1590.
29. Lardo, A.C., McVeigh, E.R., Jumrussirikul, P., et al. (2000) Visualization and temporal/spatial characterization of cardiac radiofrequency ablation lesions using magnetic resonance imaging. *Circulation.* 102, 698–705.
30. Atalar, E., Bottomley, P.A., Ocali, O., et al. (1996) High resolution intravascular MRI and MRS by using a catheter receiver coil. *Magn Reson Med.* 36, 596–605.
31. Strouse, P.J. and Beekman, R.H., 3rd. (1996) Magnetic deflection forces from atrial septal defect and patent ductus arteriosus-occluding devices, stents, and coils used in pediatric-aged patients. *Am J Cardiol.* 78, 490–491.
32. Rickers, C., Jerosch-Herold, M., Hu, X., et al. (2003) Magnetic resonance image-guided transcatheter closure of atrial septal defects. *Circulation.* 107, 132–138.
33. Greatbatch, W., Miller, V., and Shellock, F.G. (2002) Magnetic resonance safety testing of a newly-developed fiber-optic cardiac pacing lead. *J Magn Reson Imaging.* 16, 97–103.
34. Sommer, T., Vahlhaus, C., Lauck, G., et al. (2000) MR imaging and cardiac pacemakers: in-vitro evaluation and in-vivo studies in 51 patients at 0.5 T. *Radiology.* 215, 869–879.
35. Achenbach, S., Moshage, W., Diem, B., Bieberle, T., Schibgilla, V., and Bachmann, K. (1997) Effects of magnetic resonance imaging on cardiac pacemakers and electrodes. *Am Heart J.* 134, 467–473.
36. Nitz, W.R., Oppelt, A., Renz, W., Manke, C., Lenhart, M., and Link, J. (2001) On the heating of linear conductive structures as guide wires and catheters in interventional MRI. *J Magn Reson Imaging.* 13, 105–114.
37. Yeung, C.J., Susil, R.C., and Atalar, E. (2002) RF safety of wires in interventional MRI: using a safety index. *Magn Reson Med.* 47, 187–193.
38. Houlind, K., Eschen, O., Pedersen, E.M., Jensen, T., Hasenkam, J.M., and Paulsen, P.K. (1996) Magnetic resonance imaging of blood velocity distribution around St. Jude Medical aortic valves in patients. *J Heart Valve Dis.* 5, 511–517.
39. Walker, P.G., Pedersen, E.M., Oyre, S., et al. (1995) Magnetic resonance velocity imaging: a new method for prosthetic heart valve study. *J Heart Valve Dis.* 4, 296–307.
40. Botnar, R., Nagel, E., Scheidegger, M.B., Pedersen, E.M., Hess, O., and Boesiger, P. (2000) Assessment of prosthetic aortic valve performance by magnetic resonance velocity imaging. *MAGMA.* 10, 18–26.
41. Prinzen, F.W., Hunter, W.C., Wyman, B.T., and McVeigh, E.R. (1999) Mapping of regional myocardial strain and work during ventricular pacing: experimental study using magnetic resonance imaging tagging. *J Am Coll Cardiol.* 33, 1735–1742.
42. Wyman, B.T., Hunter, W.C., Prinzen, F.W., and McVeigh, E.R. (1999) Mapping propagation of mechanical activation in the paced heart with MRI tagging. *Am J Physiol.* 276, H881–H891.
43. van der Geest, R.J. and Reiber, J.H. (1999) Quantification in cardiac MRI. *J Magn Reson Imaging.* 10, 602–608.
44. van der Geest, R.J., Lelieveldt, B.P., and Reiber, J.H. (2000) Quantification of global and regional ventricular function in cardiac magnetic resonance imaging. *Top Magn Reson Imaging.* 11, 348–358.
45. van der Geest, R.J., de Roos, A., van der Wall, E.E., and Reiber, J.H. (1997) Quantitative analysis of cardiovascular MR images. *Int J Card Imaging.* 13, 247–258.
46. Young, A.A., Cowan, B.R., Thrupp, S.F., Hedley, W.J., and Dell'Italia, L.J. (2000) Left ventricular mass and volume: fast calcu-

lation with guide-point modeling on MR images. *Radiology.* 216, 597–602.
47. Swingen, C., Seethamraju, R.T., and Jerosch-Herold, M. (2003) An approach to the three-dimensional display of left ventricular function and viability using MRI. *Int J Cardiovasc Imaging.* 19:325–336.
48. Matheijssen, N.A., de Roos, A., Doornbos, J., Reiber, J.H., Waldman, G.J., and van der Wall, E.E. (1993) Left ventricular wall motion analysis in patients with acute myocardial infarction using magnetic resonance imaging. *Magn Reson Imaging.* 11, 485–492.
49. Holman, E.R., Vliegen, H.W., van der Geest, R.J., et al. (1995) Quantitative analysis of regional left ventricular function after myocardial infarction in the pig assessed with cine magnetic resonance imaging. *Magn Reson Med.* 34, 161–169.
50. Baer, F.M., Voth, E., LaRosee, K., et al. (1996) Comparison of dobutamine transesophageal echocardiography and dobutamine magnetic resonance imaging for detection of residual myocardial viability. *Am J Cardiol.* 78, 415–419.
51. Baer, F.M., Voth, E., Schneider, C.A., Theissen, P., Schicha, H., and Sechtem, U. (1995) Comparison of low-dose dobutamine-gradient-echo magnetic resonance imaging and positron emission tomography with [18F] fluorodeoxyglucose in patients with chronic coronary artery disease. A functional and morphological approach to the detection of residual myocardial viability. *Circulation.* 91, 1006–1015.
52. Nagel, E. and Fleck, E. (1999) Functional MRI in ischemic heart disease based on detection of contraction abnormalities. *J Magn Reson Imaging.* 10, 411–417.
53. Sheehan, F.H., Bolson, E.L., Dodge, H.T., Mathey, D.G., Schofer, J., and Woo, H.W. (1986) Advantages and applications of the centerline method for characterizing regional ventricular function. *Circulation.* 74, 293–305.
54. Cerqueira, M.D., Weissman, N.J., Dilsizian, V., et al. (2002) Standardized myocardial segmentation and nomenclature for tomographic imaging of the heart: a statement for healthcare professionals from the Cardiac Imaging Committee of the Council on Clinical Cardiology of the American Heart Association. *Circulation.* 105, 539–542.
55. Thompson, H.K., Starmer, C.F., Whalen, R.E., and McIntosh, H.D. (1964) Indicator transit time considered as a gamma variate. *Circ Res.* 14, 502–515.
56. Al-Saadi, N., Nagel, E., Gross, M., et al. (2000) Noninvasive detection of myocardial ischemia from perfusion reserve based on cardiovascular magnetic resonance. *Circulation.* 101, 1379–1383.
57. Al-Saadi, N., Nagel, E., Gross, M., et al. (2000) Improvement of myocardial perfusion reserve early after coronary intervention: assessment with cardiac magnetic resonance imaging. *J Am Coll Cardiol.* 36, 1557–1564.
58. Schwitter, J., Nanz, D., Kneifel, S., et al. (2001) Assessment of myocardial perfusion in coronary artery disease by magnetic resonance: a comparison with positron emission tomography and coronary angiography. *Circulation.* 103, 2230–2235.
59. Panting, J.R., Gatehouse, P.D., Yang, G.Z., et al. (2002) Abnormal subendocardial perfusion in cardiac syndrome X detected by cardiovascular magnetic resonance imaging. *N Engl J Med.* 346, 1948–1953.
60. Ibrahim, T., Nekolla, S.G., Schreiber, K., et al. (2002) Assessment of coronary flow reserve: comparison between contrast- enhanced magnetic resonance imaging and positron emission tomography. *J Am Coll Cardiol.* 39, 864–870.
61. Jerosch-Herold, M., Wilke, N., Wang, Y., et al. (1999) Direct comparison of an intravascular and an extracellular contrast agent for quantification of myocardial perfusion. *Int J Card Imaging.* 15, 453–464.
62. Jerosch-Herold, M., Swingen, C., and Seethamraju, R.T. (2002) Myocardial blood flow quantification with MRI by model-independent deconvolution. *Med Phys.* 29, 886–897.
63. Jerosch-Herold, M., Hu, X., Murthy, N.S., Rickers, C., and Stillman, A.E. (2003) MRI of myocardial contrast enhancement with MS-325 and its relation to myocardial blood flow and the perfusion reserve. *J Magn Reson Imaging.* 18, 544–554.
64. Mühling, O.M., Wang, Y., Panse, P., et al. (2003) Transmyocardial laser revascularization preserves regional myocardial perfusion: an MRI first pass perfusion study. *Cardiovasc Res.* 57, 63–70.
65. Gould, K.L. and Lipscomb, K. (1974) Effects of coronary stenosis on coronary flow reserve and resistance. *Am J Cardiol.* 34, 48–55.

IV DEVICES AND THERAPIES

20 Historical Perspective of Cardiovascular Devices and Techniques

DEE M. MCMANUS, BS, MONICA A. MAHRE, BS, AND PAUL A. IAIZZO, PhD

CONTENTS

1. INTRODUCTION

The era from 1950 to 1967 was an incredible time of innovation within the University of Minnesota's Department of Surgery in the newly emerging field of open heart surgery. There were many reasons for this, but most importantly it was attributable to the following: (1) the university had excellent facilities, including a unique privately funded 80-bed heart hospital for pediatric and adult patients, and (2) the Department of Surgery was led by a chair, Owen H. Wangensteen, MD, who "created the milieu and the opportunities for great achievements by many of his pupils," and was considered the "mentor of a thousand surgeons" (Fig. 1, Table 1) *(1)*.

More specifically, Dr. Wangensteen encouraged his medical students to "step out of the box," look at problems in different ways, and not assume that those who went before them had all the answers. He also believed strongly in collaborations with the basic science departments, specifically the Department of Physiology, with the department head, Maurice Visscher, who played an integral role in supporting both research and the clinical training of surgical residents. To that end, Wangensteen instituted a 2-year research program for all residents; this surgical PhD program was the only one in the country at its inception, and it still exists today.

An important part of the innovative surge was that many surgical residents were returning from World War II, which had recently provided them with life-and-death situations when managing MASH (mobile army surgical hospital) units—they had little or no fear of death. Their generation was not afraid of "pushing the envelope" to help patients. By today's standards, they would be viewed as "mavericks" or "cowboys," but in fact they had little to lose, as on the battlefields where they received their early exposure; their patients were dying or had little chance of survival without the novel techniques successfully implemented in Minnesota.

One of these young war-experienced surgeons was C. Walton Lillehei, who returned to the University of Minnesota in 1950 to complete his surgical residency after leading an Army MASH unit in both North Africa and Italy (Fig. 2). Walt, as he was

From: *Handbook of Cardiac Anatomy, Physiology, and Devices*
Edited by: P. A. Iaizzo © Humana Press Inc., Totowa, NJ

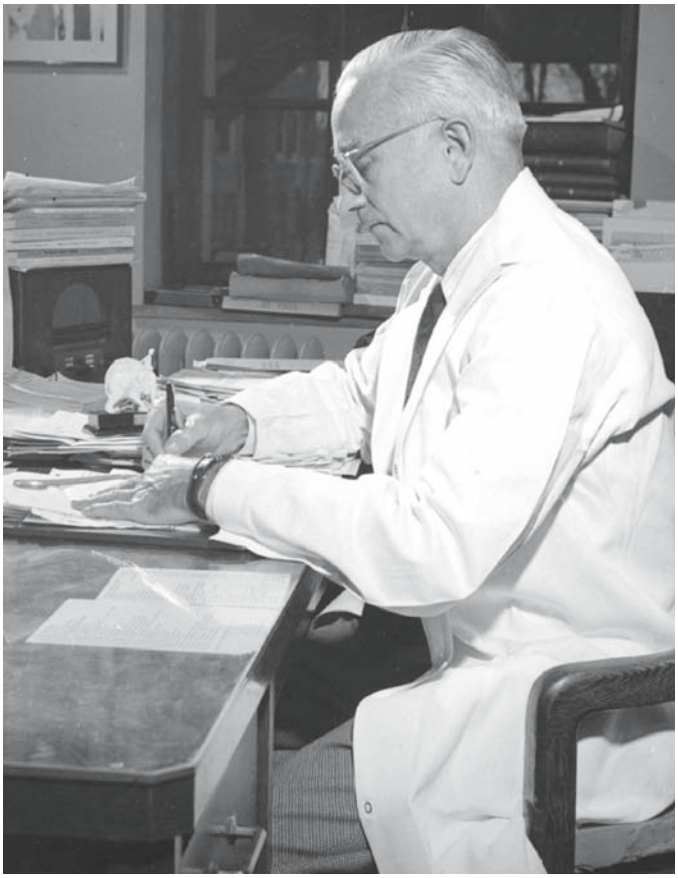

Fig. 1. "The Chief," Dr. Owen H. Wangensteen, the youngest Surgery Department chair at age 31 years (chair from 1930 to 1967).

Table 1
Department of Surgery at the University of Minnesota: Chairs/Interim Heads

Surgery department chair/interim head	*Position*	*Years served*
Arthur C. Strachauer	Department chair	–1925, 1927–1929
Owen H. Wangensteen	Department chair	1930–1967
John S. Najarian	Department chair	1967–1993
Edward W. Humphrey	Interim chair	1993–1994
Frank B. Cerra	Interim chair	1994–1995
David L. Dunn	Department chair	1995–Present

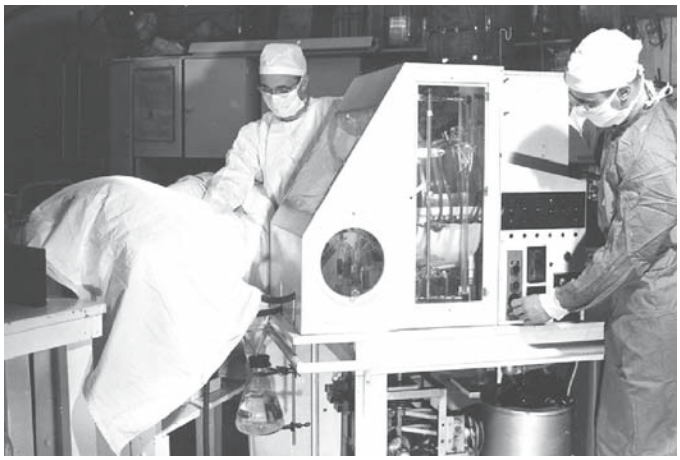

Fig. 3. Clarence Dennis with the first heart–lung machine at the University of Minnesota.

Fig. 2. Walt Lillehei in Army uniform.

called, was a bright (he completed his master's and doctoral degrees during this time also) and impulsive maverick, always pushing to the next level of care for his clinical patients, for whom he had great empathy. Lillehei and his team launched many surgical innovations during this period, primarily because of their hands-on research experiences in the experimental dog laboratories.

Interestingly, prior to 1950, the heart was considered the core of human emotion, with a role in human feelings toward others and even the soul itself. It was not until the medical profession began to view the heart more physiologically, as a pump or machine within the body, that researchers and clinicians began to develop new ways to repair and replace worn-out parts of the heart; innovations in the field of cardiac surgery then flourished (Table 2).

Such innovation became prominent at the University of Minnesota. Soon thereafter, Dr. Clarence Dennis designed the first heart–lung machine for total cardiopulmonary bypass, which was subsequently tested successfully on dogs (Fig. 3). However, when Dennis and his team used the heart–lung machine in the clinical area for the first time on April 5, 1951, the patient died because of complications. A second patient also died during surgery from massive air embolism. Not long after, Dr. Dennis moved his machine and most of his team to New York City *(1)*.

Table 2
University of Minnesota Milestones

1887	New standards requiring medical students to pass exams and gain medical examining board approval (led by Medical School Dean Perry Millard)
1911	Minnesota became the first state to mandate hospital internships for medical students
1930s	Discovery of link between cholesterol and heart disease (Ancel Keys)
1950	First adaptation of the mass spectrograph (Alfred Nier)
1951	First attempt to use a heart–lung machine (Clarence Dennis)
1952	First successful open heart surgery using hypothermia (F. John Lewis)
1953	First jejunoileal bypass (Richard L.Varco)
1954	First open heart procedure using cross-circulation (C. Walton Lillehei)
1954	First surgical correction of tetralogy of Fallot (C. Walton Lillehei)
1955	First successful use of the bubble oxygenator (Richard DeWall)
1958	First use of a small, portable, battery-powered pacemaker (Earl Bakken)
1963	First human partial ileal bypass (Henry Buckwald)
1966	First clinical pancreas transplant (William D. Kelly and Richard C. Lillehei)
1966–1968	First prosthetic heart valves (Lillehei-Nakib toroidal disk, 1966; Lillehei-Kaster pivoting disk, 1967; Kalke-Lillehei rigid bileaflet prosthesis, 1968)
1967	Bretylium, a drug developed by Marvin Bacaner, saved the life of Dwight Eisenhower
1967	World's first heart transplant (Dr. Christiaan Barnard, trained by C. Walton Lillehei)
1968	First successful bone marrow transplant (Robert A. Good)
1969	Invention of implantable drug pump (Henry Buckwald, Richard Varco, Frank Dorman, Perry L. Blackshear, Perry J. Blackshear)
1976	Medical Device Amendment to FDA Cosmetic Act
1977	First implant of St. Jude mechanical heart valve at University Hospital
1988	HDI/Pulse Wave® profiler founded (Hypertension Diagnostics Inc. [St. Paul, MN], Jay Cohn, Stanley Finkelstein).
1993	Angel Wings transcatheter closure device invented (Gladwin Das)
1994	First successful simultaneous pancreas–kidney transplant using a living donor (David Sutherland)
1995	Amplatzer Occlusion Devices founded (AGA Medical Corp., Kurt Amplatz)
1997	First kidney–bowel transplant (Rainer Gruessner)
1999	CardioPump Device evaluated (Keith Lurie et al.)
2000	By 2000, University alumni have founded 1500 technology companies in Minnesota, contributing at least $30 billion to the state's economy
2000	By 2000, University's medical school has produced more family doctors than any other institution in the United States

The next major University of Minnesota (worldwide) milestone in cardiac surgery was the first open heart surgery using hypothermia on September 2, 1952, by Dr. F. John Lewis (Fig. 4). This procedure, suggested by Dr. W.G. Bigelow of Toronto, lowered the body temperature of patients 12–15º to reduce their blood flow, thereby reducing the body's need for oxygen. Brain cells would die after 3–4 min at normal temperature without oxygen, but hypothermia allowed Dr. Lewis and his university research team (Drs. Mansur Taufic, C. Walton Lillehei, and Richard Varco) to successfully complete a 5.5-min repair of the atrial septum on a 5-year-old patient. This was recognized as a landmark in the history of cardiac surgery; until this time, no surgeon had succeeded in opening the heart to perform intracardiac repair under direct vision. Hypothermia with inflow stasis proved to be excellent for some of the simpler surgical repairs, but it was inadequate for more extensive cardiac procedures. "The basic problem was the lack of any means to rewarm a cold, nonbeating heart" *(2)*.

The next milestone, although not accomplished at the University of Minnesota, occurred on May 6, 1953, when Dr. J. Gibbon closed an atrial septal defect using a pump oxygenator for an intracardiac operation. Although this first success with the pump oxygenator was well received, it aroused surprisingly

Fig. 4. In this 1952 photo, Richard L. Varco (left) and F. John Lewis stand behind the hypothermia machine that they used during the world's first successful open heart surgery.

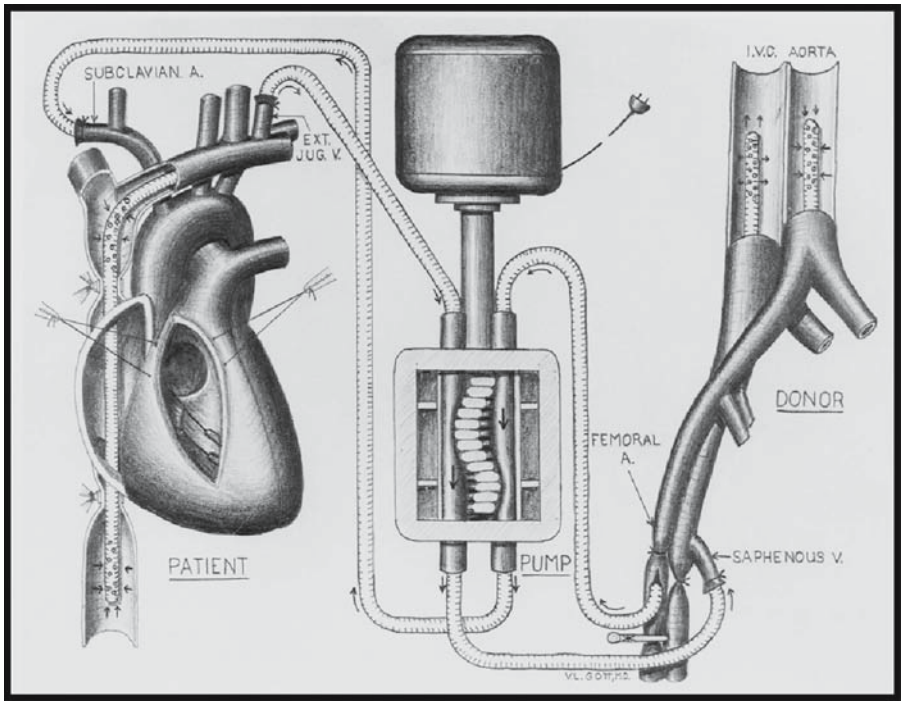

Fig. 5. Diagram of cross-circulation.

little excitement or enthusiasm among cardiologists and cardiac surgeons at that time, likely because other centers had launched their own experiments with bubble oxygenators. Interestingly, Gibbon was never able to repeat his one clinical success; he ultimately became discouraged and did not use the pump oxygenator again.

> *There was a common scenario, namely, good results with acceptable survival in the experimental animals but nearly universal failure when the same apparatus and techniques were applied to human beings. Thus, many of the most experienced investigators concluded with seemingly impeccable logic that the problems were not with the perfusion techniques or the heart lung machines. Rather, they came to believe that the "sick human heart" ravaged by failure, could not possibly be expected to tolerate the magnitude of the operation required and then recover with good output, as occurred when the same machines and techniques were applied to healthy dogs. Thus, discouragement and pessimism about the future of open heart surgery was widespread. (2)*

2. CROSS-CIRCULATION

Extracorporeal circulation by controlled cross-circulation was introduced clinically on March 26, 1954 (Fig. 5). The use of cross-circulation for intracardiac operations was an immense departure from established surgical practice at the time and was the major breakthrough that motivated innovations in the area of open heart surgery *(3)*. The thought of taking a normal healthy human being into the operating room to provide donor circulation was considered unacceptable and even immoral by some critics. The risks to the donors were: (1) blood incompatibility, (2) infection, (3) air embolism, and (4) blood volume imbalance. Regardless, Lillehei and his team completed 45 such operations between 1954 and 1955. In early 1955, three additional bypass methods were introduced and successfully employed, including: (1) perfusion from a reservoir of arterialized blood, (2) heterologous (dog) lungs as an oxygenator, and (3) the DeWall-Lillehei disposable bubble oxygenator *(2)*.

The likely single most important discovery that contributed to the success of clinical open heart operations was the realization of the vast discrepancy between the total body flow rate *thought* necessary and what was *actually* necessary. Lillehei and his team are credited with applying the findings of two British surgeons (A. T. Andreasen and F. Watson) who had identified the azygos factor—the ability of dogs to survive up to 40 min without brain damage when all blood flow was stopped except through the azygos vein.

Specifically, Morley Cohen and Lillehei hypothesized that when blood flow was low, the blood vessels dilated to receive a larger share of the blood; the tissues absorbed a much higher proportion of the oxygen compared to normal circulation. Previously, it was thought that basal or resting cardiac output at 100–160 mL/kg/min was the required safe maintenance during cardiopulmonary bypass. In contrast, the azygos flow studies showed that 8–14 mL/kg/min maintained the physiological integrity of the vital centers, but Lillehei added a margin of safety and set his basic perfusion rate at 25–30 mL/kg/min. This approach reduced excessive complications of blood loss, excessive hemolysis, abnormal bleeding, and renal shutdown *(2)*.

Altogether, 45 patients (aged 5 months to 10 years) underwent open heart surgery with cross-circulation at the Variety Club Children's Hospital (Minneapolis, MN). Prior to this surgery, these patients had lesions that were considered hopelessly unrepairable. Of this group, 49% of the patients lived to be long-term survivors (longer than 30 years) and to lead normal productive lives; 11 of the female long-term survivors subsequently became pregnant and gave birth to a total of 25 children, all free from any congenital heart defects. In addition, all 45 donors survived, with only 1 donor experiencing a significant complication.

It should be noted that, during this period of time, an intense competition/collaborative relationship existed with the Mayo Clinic (Rochester, MN), the only other site where open heart surgery was routinely being performed. Lillehei recalled in his interview with G. Wayne Miller (author of *King of Hearts* [Random House, New York, 2000]) that the Mayo Clinic operated 7 days a week, so on Saturdays when Lillehei's team did not perform surgery, they would travel to the Mayo Clinic and watch Dr. John Kirklin and his colleagues (Miller, G.W., Transcriptions of audio tapes for book, University of Minnesota Archives).

Dr. Kirklin was successfully using a modification of the Gibbon heart–lung machine and, after observing his achievements, Lillehei began a slow transition away from cross-circulation and toward using a heart–lung machine, but one of his own design (Fig. 6). In the beginning, Lillehei used the heart–lung machine for simpler, more straightforward cases and continued using cross-circulation for the more complicated cases. Although its clinical use was short-lived, cross-circulation is still considered today as an important stepping stone in the development of cardiac surgery.

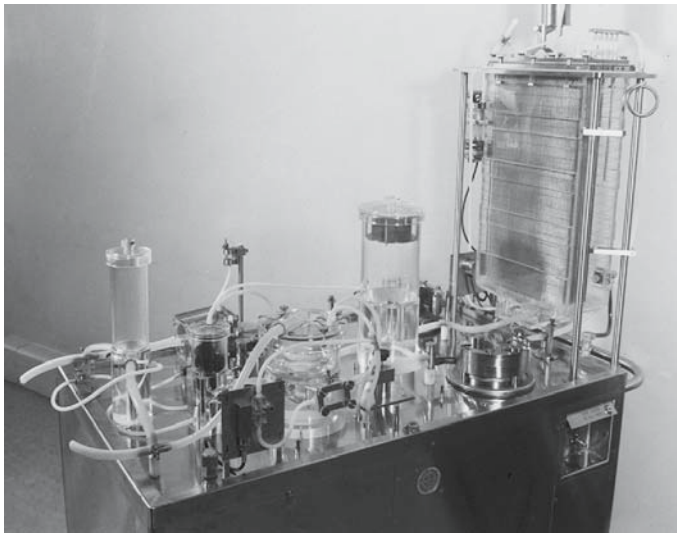

Fig. 6. Mayo Clinic's heart–lung machine was as big as a Wurlitzer organ; it cost thousands of dollars and required great skill to operate.

3. LILLEHEI-DEWALL BUBBLE OXYGENATOR

John Gibbon MD, from Boston, Massachusetts, invented the cardiopulmonary bypass procedure and performed the first intracardiac repair using extracorporeal perfusion in 1953. His bubble oxygenator, which looked surprisingly like a computer, was manufactured and financed by IBM; this achievement stimulated rapid development of the knowledge base and equipment necessary for accurate diagnoses of cardiac disease and successful intracardiac operations.

It was recognized that the main problems with film oxygenators were (1) poor efficiency, (2) excessive hemolysis, (3) large priming volumes, and (4) the development of bubbles and foam in the blood. All designs required blood flows of 2.2 L/m^2/min, usually three to four units of blood for priming, and another two units of blood for the rest of the circuit. Furthermore, after each use, the machine had to be broken down, washed, rinsed in hemolytic solutions, reassembled, resterilized, and reconfigured.

During this era, Richard DeWall came to work at the University of Minnesota, initially, as an animal attendant in Lillehei's research lab. DeWall would manage the pump while the anesthesiologists would take breaks, and soon he began to take an interest in the problems associated with oxygenating blood. Eventually, Lillehei challenged DeWall to find a way to eliminate bubbles in the procedure. Subsequently, DeWall produced a huge technological breakthrough in 1955 by developing a bubble oxygenator with a unique method for removing bubbles from the freshly oxygenated blood (Fig. 7). In DeWall's design, blood entered the bottom of a tall cylinder along with oxygen passed through sintered glass to create bubbles. As the bubbles and blood rose, gas exchange occurred at the surface of each bubble. At the top of the cylinder, arterialized bubble-rich blood passed over stainless steel wool coated with silicone antifoam; it then traveled through a long helical settling coil to allow bubbles to rise slowly and exit the blood.

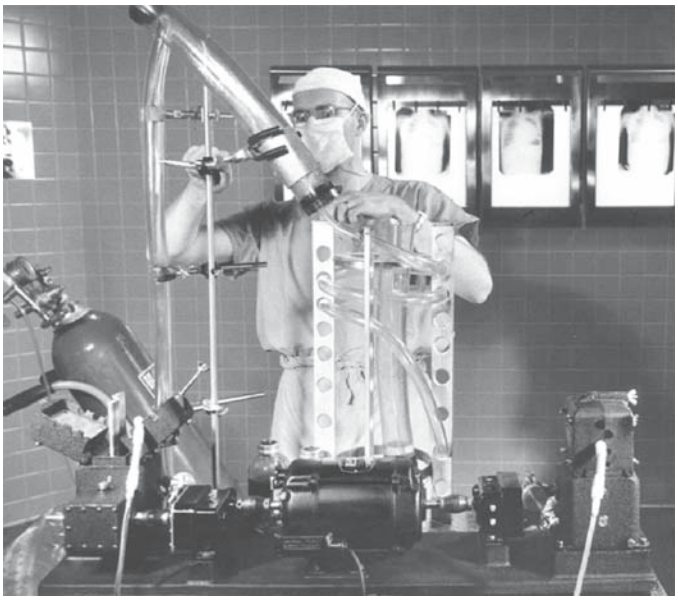

Fig. 7. University of Minnesota's bubble oxygenator cost $15 and was easy to use. Richard DeWall is shown here with his model in 1955.

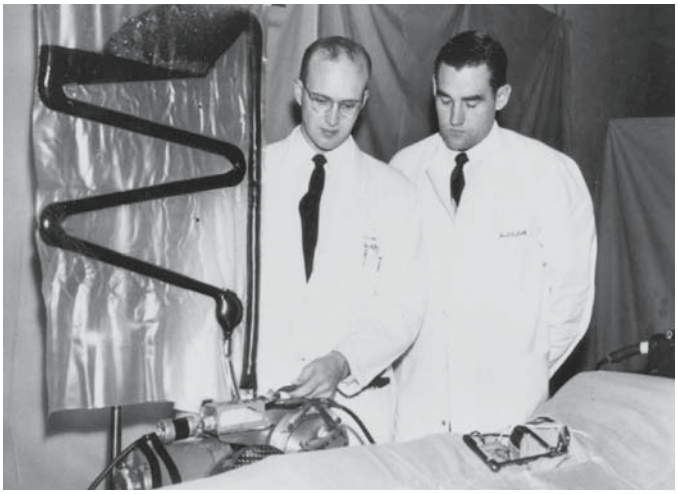

Fig. 8. Richard DeWall and Vince Gott look at the first commercially manufactured sterile bubble oxygenator in 1956.

Two important components in the Lillehei-DeWall bubble oxygenator were the tubing and the silicon antifoam solution. The tubing was Mayon polyethylene tubing (typically used in the dairy industry and in the production of mayonnaise), available from Mayon Plastics (Hopkins, MN), with a company chief executive officer who was a classmate of Lillehei's and a graduate of the university's chemical engineering program. The silicone antifoam solution, Antifoam A, was used to coat the tubing to prevent foaming of the liquids transported.

The oxygenator was wonderfully efficient; animals (and later patients) did not show detectable effects of residual gas emboli. More important, this design eventually led to the development of a plastic, prepackaged, disposable, sterile oxygenator that replaced the expensive stainless steel, labor-intensive screen, and film devices. An economic and reliable oxygenator had arrived, and the medical industry began to use disposable components for the heart–lung machine.

Two years after its introduction, the DeWall-Lillehei bubble oxygenator had been used in 350 open heart operations at the University of Minnesota. DeWall steadily improved the device through three generations of models, but it remained a very simple, disposable, and heat-sterilizable device that could be built to accommodate only the amount of blood required for each patient and then discarded.

In 1956, another one of Lillehei's residents, Vincent Gott, invented a bubble oxygenator in which DeWall's helix design was flattened and enclosed between two heat-sealed plastic sheets (Fig. 8). This sheet bubble oxygenator proved to be the key to subsequent widespread acceptance of the device for open heart surgery because it could be easily manufactured and distributed in a sterile package; it was inexpensive enough to be disposable. The University of Minnesota licensed rights to manufacture and sold the device to Travenol Inc. (Minneapolis, MN). With the bubble oxygenator and techniques developed by Lillehei and his colleagues, the University of Minnesota had become prominent for the making open heart surgery possible and relatively safe *(4)*.

4. HEART BLOCK AND THE DEVELOPMENT OF THE PACEMAKER

An unexpected clinical benefit from the development of open heart surgery was the discovery of a revolutionary new concept for treatment of complete heart block. Heart block is caused when the electrical impulse that begins high in the right atrium fails to reach the pumping chambers—the ventricles. Deprived of their normal signal, the ventricles may beat slowly on their own, but at a rate that limits activity and typically results in heart failure. In the early intracardiac procedures for more difficult surgeries, it was subsequently determined that complete heart block occurred because of injury of the heart's conduction system, induced by stitches in about 10% of the operations. With the existing treatment for complete block, the application of positive chronotropic drugs or electrodes to the surface of the chest, there were no 30-day survivors.

In 1952, Paul Zoll, a cardiologist in Boston, utilized the first human pacemaker unit on a patient—a large tabletop external unit with a chest electrode. It was successfully used to resuscitate patients in the hospital, but delivered 50–150 V, which was incredibly painful for children and typically left scarring and/or blisters. In addition, it used an alternating current electrical source, limiting the mobility of the patient to the length of the cord. Spurred by such adversity, Lillehei and his research team found, in 1956, that an electrode directly connected to the ventricular muscle from a pulse generator producing repetitive electrical stimuli of small magnitude (5-10 mA) provided very effective control of the heart rate and an 89% survival rate for patients with prior heart block.

On January 30, 1957, a pacemaker lead made of a multistrand, braided stainless steel wire in a Teflon sleeve was implanted into a patient's ventricle myocardium, with the other end brought through the surgical wound and attached to external stimulation. The utilized pacemaker (pulse generator) was a Grass physiological stimulator borrowed from the university's Physiology Department. This procedure was designed for short-term pacing, with removal of the wires 1–2 weeks after the patient's heart had regained a consistent rhythm.

Following near disaster for a pacemaker-dependent patient when the electrical service failed in the University hospital because of a storm, Lillehei asked his medical equipment repairman, Earl Bakken, to design a battery-powered, wearable pacemaker to improve the patient's mobility (Fig. 9). This Bakken did, using a circuit modified from a diagram for a transistorized metronome in *Popular Electronics* magazine as a model (Fig. 10); a few months later, such as device was used clinically on April 14, 1958.

Bakken's transistor pulse generator made a miraculous "overnight" transition from bench testing to clinical use; this invention then set the stage for creation of the cardiac pacing industry. For the next decade or so, it would become common practice to put new devices or prototypes (even fully implantable ones) into clinical use immediately and then iron out the imperfections based on the accumulation of clinical experiences. This humanitarian practice developed because most of the early patients were close to death, and no other treatments existed *(5)*. Eventually, Medtronic, Inc. (Minneapolis, MN),

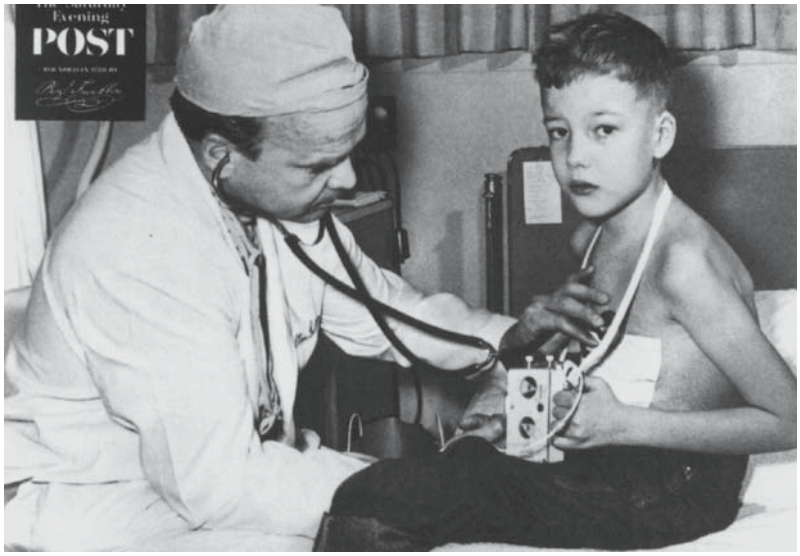

Fig. 9. C. Walton Lillehei and young patient with battery-powered, wearable pacemaker.

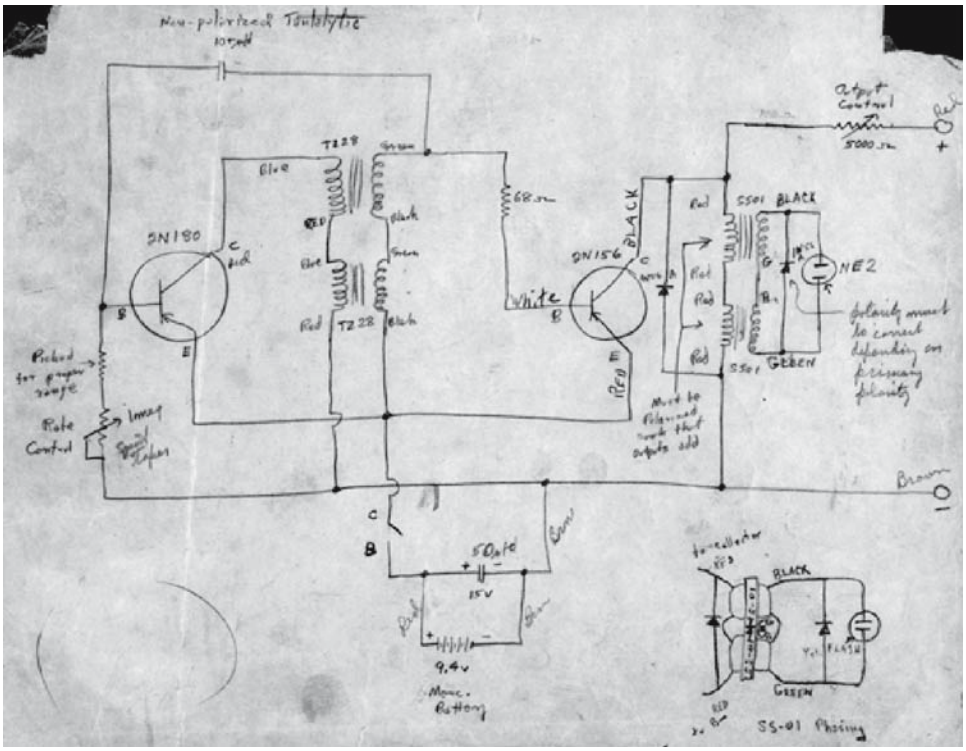

Fig. 10. Earl Bakken's original design for the battery-operated pacemaker.

under Bakken's leadership, became the world's leading manufacturer of cardiac pacemakers, beginning with the Model 5800.

The first generation of the 5800 pacemaker was black, but was quickly changed to white to look cleaner and more sanitary (Fig. 11). Between 1959 and 1964, only a few hundred pacemakers were sold because of the reusability of this system and the short-term postsurgery focus; orders soared once the pacemaker became implantable and redefined for long-term pacing use. Nevertheless, the 5800 pacemaker became the symbol for Medtronic's shared belief in medical progress through technology; this was celebrated during an unveiling, at his retirement celebration in 1994, of a bronze statue of Earl Bakken holding the 5800 pacemaker. Years later, the 5800 was viewed by Lillehei as a technological watershed: "It was the fruit of interdisciplinary collaboration, exemplifying the marriage of medicine and technology, long-lasting friendships, and mutual respect."

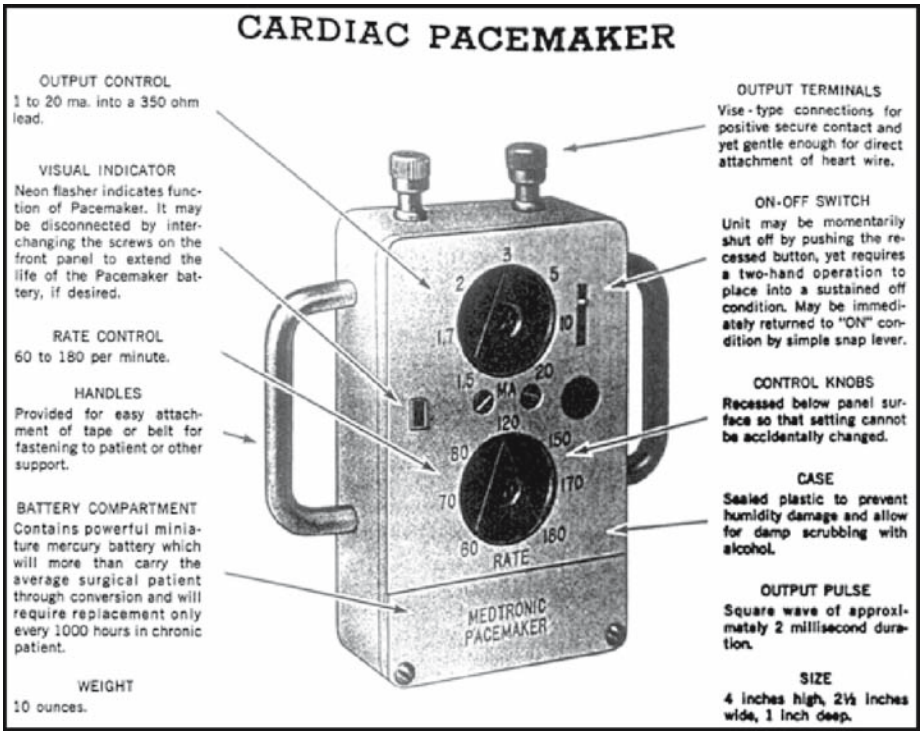

Fig. 11. A page from the Medtronic catalog advertising the 5800 pacemaker.

5. HEART VALVES

The initial development process in the field of prosthetic heart valves involved the search for biologically compatible materials and hemologically tolerant designs; success could not be achieved without the union of these two factors. At that time, there was no satisfactory mechanism to achieve this goal scientifically; a trial-and-error method was used. The development of prosthetic heart valves became the purview of numerous cardiovascular surgeons, who often collaborated with engineers; to distinguish one valve from another, each prosthesis often became identified with the surgeon developer *(6)*.

Lillehei and his colleagues developed four different valves: (1) a nontilting disk valve called the Lillehei-Nakib Toroidal Valve in 1967; (2) two tilting disk valves, the Lillehei-Cruz-Kaster in 1963 and the Lillehei-Kaster in 1970 (produced by Medical Inc. in 1970 and eventually distributed by Medtronic Inc. in 1974); and (3) a bileaflet valve, the Lillehei-Kalke in 1965 (manufactured by Surgitool [now Medical Engineering Corporation, Racine, WI] in 1968 and used clinically by Dr. Lillehei at the New York Cornell Medical Center) (Fig. 12).

The St. Jude bileaflet valve was designed by Chris Posis, an industrial engineer who approached Demetre Nicoloff MD, a cardiovascular surgeon at the University of Minnesota. This valve had floating hinges located near the central axis of the rigid housing as well as an opening to the outer edge of each leaflet, leaving a small central opening (Fig. 13) *(7)*. Nicoloff first implanted this valve in October 1977, and it provided the foundation for the beginning of St. Jude Medical Inc. Dr. Nicoloff was asked to serve as the medical director of the new company; however, he declined because of the demands of his clinical practice. Rather, he suggested that Dr. C.W. Lillehei become the medical director, a post that Lillehei held until his death in 1999 *(6)*.

6. OTHER UNIVERSITY-AFFILIATED MEDICAL DEVICES

Many of the major breakthroughs in cardiac device development at the University of Minnesota occurred in associated collaborations with the Surgery Department. In more recent times, several more cardiovascular medical devices have been invented in departments other than the Department of Surgery, specifically the Departments of Medicine and Radiology. Several areas of cardiovascular devices are described in the following sections.

6.1. Active Compression/Decompression Cardiopulmonary Resuscitation Devices: The CardioPump®

The CardioPump® is an active compression/decompression device for cardiopulmonary resuscitation (CPR). Weighing a mere pound and half, it looks like a modified toilet plunger with a pliable cup that fits onto the patient's chest (Fig. 14). It employs a combination handgrip/pressure gauge instead of a wooden handle. Manual CPR exerts downward pressure on the chest, but the chest has to reexpand naturally; importantly, the CardioPump can apply pressure in both directions. With this action, the heart behaves somewhat like a bellows and allows blood to be pulled back into the heart and air into the lungs.

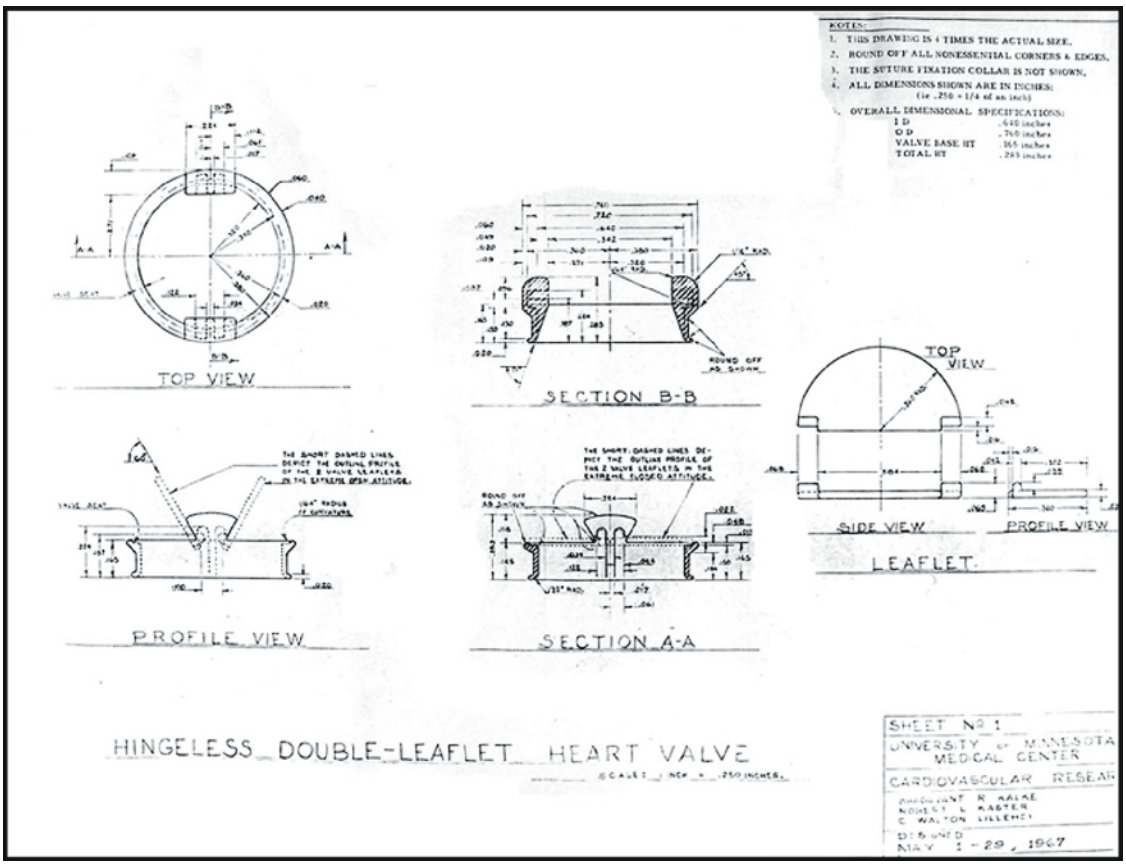

Fig. 12. The Lillehei-Kalke rigid bileaflet prosthesis (1968).

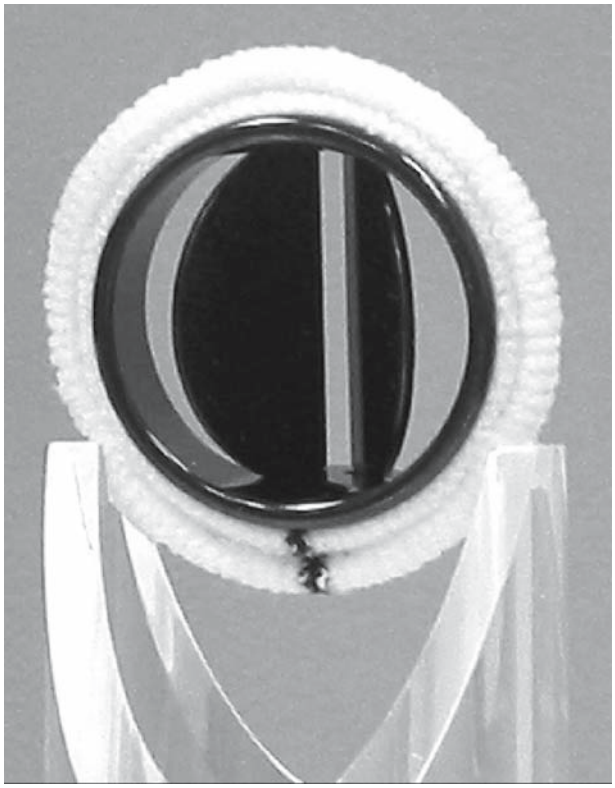

Fig. 13. St. Jude bileaflet prosthesis developed in 1976. Courtesy of St. Jude Medical.

Fig. 14. CardioPump, an active compression/decompression device for cardiopulmonary resuscitation.

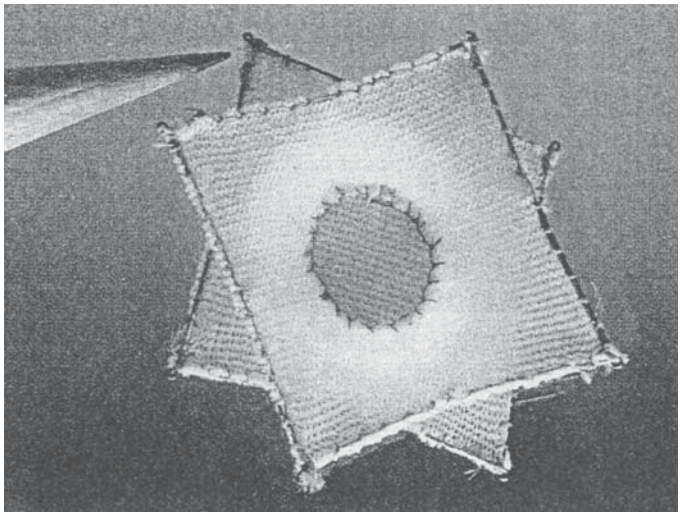

Fig. 15. Self-centering transcatheter device called Angel Wings®. Reprinted from *Heart* 1998;80:517–521. With permission from the BMJ Publishing Group.

Fig. 16. One of the numerous Amplatzer occlusion devices.

Dr. Keith Lurie, from the Department of Medicine (Division of Cardiovascular Medicine), and his colleagues outside the university designed this device and licensed it through a Danish company, Ambu Inc. (Linthicum, MD). It is now considered the first line of therapy for standard CPR and could improve a person's chance of survival and minimize neurological impairment; it has been shown to extend the 1-year survival rate by 10–40%, as indicated in a comparative study of standard CPR and active compression/decompression resuscitation for out-of-hospital cardiac arrest *(8)*.

6.2. Transcatheter Closure Devices for Congenital Heart Defects

Transcatheter closure devices are permanent cardiac implants designed to close defects between chambers of the heart. Such devices are self-expanding, self-centering, umbrella-like devices with a design and shape that varies, as does the exact mode of their deployment. These are implanted in the heart, in a cardiac catheterization laboratory, through catheters inserted into either the artery or vein. Transcatheter closure devices are intended to provide a less-invasive alternative to open heart surgery, which has been the standard of care.

The first reported use of a transcatheter closure device for an atrial septal defect was in 1976 by T.D. King and N.L. Mills (Tulane University Medical School, New Orleans, LA). Despite two decades of research, early models of the device were not approved for clinical use because of persistent residual leakage, high failure rates, wire fractures, or embolization of the device. Nevertheless, several University of Minnesota faculty members used their previous experience with these early devices to devise novel closure models in the early 1990s.

One such enhancement was Angel Wings® (Microvena Corp., White Bear Lake, MN), a transcatheter atrial septal defect closure device designed in 1993 by Gladwin Das MD, an interventional cardiologist in the Department of Medicine (Cardiovascular Division) *(9)*. This device is a self-centering, nitrinol-polyester prosthesis with two square-shape disks and a customized delivery catheter (Fig. 15). The implantation success rate for such closures was 97% for patients with patent foramen ovale and 100% for patients with atrial septal defects in phase II trials, 86% of these patients had zero or 1-mm shunts, and 14% had 1–2-mm shunts. The device was subsequently modified to have two circular disks and to make it retrievable into the delivery catheter and repositionable. The Angel Wings II device is anticipated to enter clinical trials in the near future.

6.3. Amplatzer® Family of Occlusion Devices

Radiologist Kurt Amplatz MD, from the Department of Radiology at the University of Minnesota, has designed a family of occlusion devices. All Amplatzer® occlusion devices (AGA Medical Corp., Golden Valley, MN) are preformed "baskets" of wire that resume their preformed mushroomlike shapes when extruded from the catheter sheaths (Fig. 16). The currently used wire is made from a special alloy of nickel and titanium (Nitinol) that does not break, accepts growth of cardiac endothelial tissue lining, and is absorbed into the heart's septal wall. More recent versions include specialized Dacron fibers, which are contained within the basket component of the device and immediately stop flow. The position of the device is checked by echocardiography and fluoroscopy prior to patient release (*see* Chapter 29).

7. FOOD AND DRUG ADMINISTRATION REGULATES MEDICAL DEVICES

Earl Bakken believed in the "ready, fire, aim" method of device development, which was symbolic of the approach in which devices were actually tested in humans; therefore, the transition from bench to bedside was at an accelerated pace *(5)*. However, dramatic changes in the regulation of medical device

development and use since 1976 have played an important role in the number and types of devices manufactured, as well as the safety of these devices, before clinical use.

In 1976, the Medical Device Amendments to the Federal Food, Drug, and Cosmetic Act established three regulatory classes for medical devices based on the degree of control necessary to ensure the safety and effectiveness of various types of devices. The most regulated class is class III devices, which are designed to support or sustain human life *or* are of substantial importance in preventing impairment of human health *or* present a potential unreasonable risk of illness or injury. All devices placed in class III are subject to premarket approval requirements, including a scientific review, to ensure their safety and effectiveness.

Under Medical Device Reporting in the Food and Drug Administration (FDA), all manufacturers, importers, and user facilities are required to report adverse events and to correct them quickly. Although, since 1984, manufacturers and importers of medical devices have been required to report all device-related deaths, serious injuries, and certain malfunctions to the FDA, numerous reports show underreporting. Therefore, the Safe Medical Devices Act (SMDA) of 1990 was implemented; device user facilities must report device-related deaths to the FDA and the manufacturer. In addition, the SMDA requires that device user facilities submit reports to the FDA on an annual basis (FDA Modernization Act of 1998). In spite of this strict regulatory environment, Minnesota has continued to be a leading state for design, licensing, and manufacture of medical devices.

8. MEDICAL ALLEY

Spurred by the flurry from Minnesota inventors of innovations such as the pacemaker, bubble oxygenator, and artificial heart valve, Medical Alley was founded in 1984 as a nonprofit trade association to support the region's growing health care industry. Medical Alley was considered to denote the rich geographic area of health care-related organizations that extended from Duluth through Minneapolis/St. Paul and further south to Rochester (*see* www.medicalalley.org). More recently, Medical Alley has expanded beyond the Minnesota border into Canada, Wisconsin, Iowa, Illinois, and the Dakotas. This expanded territory is home to over 800 medical device manufacturers and thousands of health care-related organizations, making it one of the highest concentrations of businesses in this industry in the world.

Medical Alley was founded by Earl Bakken, who pioneered the implantable pacemaker business through his company, Medtronic, Inc., in the 1960s. Bakken remains on the Medical Alley board of directors to this day, and Don Gerhardt currently presides as president over the association. Guided by the mission "to promote an environment to enhance innovation in healthcare," Medical Alley is a Minneapolis-based trade association that currently represents a membership of more than 300 health care-related companies and organizations. Its cohorts include a wide cross-section of medical device, equipment, and product manufacturers; health care providers such as hospitals and clinics; health plans and insurance organizations; medical education and research facilities; pharmaceutical and biotechnology companies; and service and consulting organizations.

Medical Alley's primary goals are to: (1) promote greater interest and investment in the region's health care-related research and innovation; (2) focus on legislative issues important to its membership; (3) provide members with educational opportunities that address current issues and trends affecting the health care industry; and (4) assemble leaders from across the industry to solve industrywide problems in health care.

For example, in 2001, Medical Alley announced a structural change that launched two "spin-off organizations"—Alley Institute and Alley Ventures. Alley Institute is a nonprofit organization that was created to impact and grow the business, workforce, and health care activities of the region directly. As a 501(c)(3) organization, Alley Institute can receive local and national foundation grants; it is also a conduit of Small Business Administration (and Small Business Innovation Research) grants for small and emerging medical technology companies. A sample of the projects launched thus far includes

- MAC-CIM (Medical Alley's Consumer-Coverage Interface Model)—Designing and alpha testing of a process to use peoples' personal values to design their health care coverage benefits.
- Minnesota Partnership for End of Life Care—Working together with Blue Cross and Blue Shield of Minnesota, HealthPartners, Allina, and Fairview to manage a grant focused on improving health care at the end of life.
- Class in a Box™—Partnering with WomenVenture to bring innovative tools and materials directly to seventh and eighth graders in their classrooms, a project designed to get kids excited about the wide variety of careers in health care.
- Managing small medical technology companies—Along with the University of St. Thomas, in St. Paul, Minnesota, developing an 11-week mini-MBA course in medical technology management. The faculty includes Medical Alley members who provide real-world experience.

A for-profit organization, Alley Ventures was designed to provide seed and early stage capital funding for small and emerging companies in the areas of medical devices, bioscience, life sciences, and health care. In addition to providing financial support (currently in the range of $50,000–$1,000,000), Alley Ventures also offers assistance in management as well as clinical, engineering, and governing board expertise.

Furthermore, Medical Alley is active in state legislative lobbying, with a government committee and two legislative consultants at the state level. The association also participates in national advocacy and lobbying activities, for example, working with US senators and legislators on the Medical Device User Fee and Modernization Act of 2002.

The host of approx 80 educational seminars annually, Medical Alley promotes interactive learning opportunities at which participants can network and discuss current issues, trends, and regulations affecting the health care industry; such forums are directed primarily to clinical studies, marketing/communications activities, regulatory affairs, reimbursement issues, research and development, and human resources in health care.

In 2004, Medical Alley, in collaboration with the University of Minnesota's Biomedical Engineering Institute, sponsored its

Table 3
Department of Physiology at the University of Minnesota: Chairs/Interim Heads

Physiology department chair/interim head	*Position*	*Years served*
Richard O. Beard	Department chair	1889–1913
Elias P. Lyon	Department chair	1913–1936
Dr. Maurice B. Visscher	Department chair	1936–1968
Eugene Grim	Department chair	1968–1986
Richard E. Poppele	Interim head	1986–1988
Robert F. Miller	Department chair	1988–1998
Joseph DiSalvo	Interim head	1998–2002
Douglas Wangensteen	Interim head	2002–present

third poster session to showcase the ongoing biomedical engineering research. Graduates shared posters, medical device prototypes, and bioengineering innovations on topics ranging from tissue engineering to cellular bioengineering, to medical devices and diagnostic techniques. This interactive forum allowed dialogue and potential collaboration between students and industry professionals.

9. CARDIOVASCULAR PHYSIOLOGY AT THE UNIVERSITY OF MINNESOTA

The Department of Physiology at the University of Minnesota has a rich history of performing basic cardiovascular research and establishing clinical collaborations within the institution. Not only have these individuals published many important basic research papers, but they also have been integrally involved in the training of many generations of cardiac physiologists, surgeons, and biomedical engineers.

One of the more notable chairs of the Department of Physiology was Maurice Visscher, who was present during the Owen Wangensteen and C. Walton Lillehei eras. In 1936, Dr. Visscher returned to the University of Minnesota to succeed Dean Lyon as the head of physiology (Table 3). He first came to Minnesota in 1922 as a graduate student in physiology under the mentorship of Frederick Scott and satisfied the requirements for both PhD and MD degrees in a 4-year period *(10)*.

Interestingly, subsequent to his studies, Visscher served a postdoctoral fellowship in England at the University College, London. While there, he worked under the advisement of the notable cardiac physiologist Ernest Starling, who at that time was near the end of his brilliant career (e.g., Starling's law of the heart). Together in 1927, Starling and Visscher published a classic paper in which, using a heart–lung preparation (introduced by Starling in 1910), they reported that the oxygen consumption of the heart was correlated directly with its volume in diastole without regard to the amount of work the heart was exerting in pumping blood *(11,12)*. After Starling's death in 1927, Visscher continued his research on this topic while serving as the Physiology Department chair in Minnesota; his research was considered to shed valuable light on the mechanisms underlying heart disease caused by coronary occlusion, in general.

It has been described that Owen Wangensteen, recognizing how many such findings were directly applicable to surgery, initiated collaborations with Visscher and the Physiology Department. To this extent, Wangensteen even initiated and conducted a regular "Physiology–Surgery Conference" that was considered "invaluable in acquainting surgical residents with the techniques of experimental physiology" *(12)*. Many also credit Wangensteen's academic philosophies for enabling the pioneering advancements in open heart surgery and subsequent pacemaker technologies at the University of Minnesota.

For example, Earl Bakken asked C. Walton Lillehei in 1997, "How did you have the courage to go ahead with these pioneering-type experiments?" Lillehei replied, "As I think, when I look back, that was part of the Wangensteen training system" *(13)*. He further elaborated:

> *He [Wangensteen] was a unique person in many regards. One [aspect of his] uniqueness was his training system. He had a great faith in research, animal or other types of laboratory research. He felt that the results of his research gave the young investigator the courage to challenge accepted beliefs and go forward, which you would not have had, as I look back, as a young surgical resident. That's why many of the great universities didn't produce much in the way of innovative research, because they were so steeped in tradition. Wangensteen had a wide open mind. If research showed some value then you should pursue it.*

The University of Minnesota has a rich history of basic and applied cardiac research. Noted in Table 4 are several of the physiologists who had full or adjunct appointments in the Physiology Department and worked on topics relevant to the cardiovascular system; these physiologists published numerous papers or served as advisors for numerous theses. Interestingly, the past few years have brought a renewed interest in refocusing the Physiology Department to again be a leader in the cardiovascular field. For example, the department has embarked on creating novel educational outreach programs for the local cardiovascular industry and added Professor Doris Taylor to the faculty as the newly created Medtronic-Bakken Research Chair in Cardiac Repair.

Dr. Lillehei believed that "What mankind can dream, research and technology can achieve." And, with the support of the Lillehei Heart Institute in collaboration with the Biomedical Engineering Institute, the circle has been completed.

REFERENCES

1. Lillehei, C.W. (1994) The birth of open-heart surgery: then the golden years. *Cardiovasc Surg*. 2, 308–317.
2. Lillehei, C.W., Varco, R.L., Cohen, M., Warden, H.E., Patton, C., and Moller, J.H. (1986) The first open-heart repairs of ventricular septal defect, atrioventricular communis, and tetralogy of Fallot using extracorporeal circulation by cross-circulation. *Ann Thorac Surg*. 41, 4–21.
3. Lillehei, C.W. (1982) A personalized history of extracorporeal circulation. *Trans Am Soc Artif Internal Organs*. 28, 5–16.
4. Moore, M. (1992) *The Genesis of Minnesota's Medical Alley*. UMN Medical Foundation Bulletin. Minneapolis Medical Foundation, Minneapolis, MN. Winter 1992.
5. Rhees, D. and Jeffrey, K. (2000) Earl Bakken's little white box: the complex meanings of the first transistorized pacemaker, in *Expos-*

Table 4
Selected Theses From the Department of Physiology at the University of Minnesota: Theses Related to Cardiovascular Physiology

Investigators	*Era*	*Topics*
Maurice Visscher	1920s to 1930s	Coronary blood flow, oxygen delivery rate, and cardiac performance; autoregulation of coronary blood flow; medical research and ethics
Mead Cavert	1970s to 1980s	Clinical cardiology
Marvin Bacaner	1960s to 1990s	Antiarrhythmic, antifibrillatory, and hemodynamic actions of bethanidine sulfate
Irwin J. Fox	1970s to 1980s	Assessment of regional myocardial blood flows; arterial dilution curves in the study of heart disease
Victor Lorber	1950 to 1970s	Cellular junctions in the tunicate heart; regulation of energy liberation in the isolated heart
Michael Hoey	1980s to 2002	Cardiac ablation
Joseph DiSalvo	1990s to present	Chronic atrial–ventricular block; properties and function of phosphatases from vascular smooth muscle
Steven Katz	1990s to present	The renin/angiotensin system and the failing heart
Paul Iaizzo	1990s to present	Intercardiac imaging within large mammalian isolated hearts; cardiac devices; isolated human trabeculae
Robert Bache	2000s to present	Cardiac energetics
John Osborn	1990s to present	Autonomic response and the cardiovascular system; pathophysiology of hypertension
Scott O'Grady	1990s to present	Electrolyte transport in epithelia
Doris Taylor	2003 to present	Cardiac repair and regeneration

ing Electronics (Finn, B., ed.), Harwood, Amsterdam, The Netherlands.
6. DeWall, R. (2000) Evolution of mechanical heart valves. *Ann Thorac Surg*. 69, 1612–1621.
7. Villafana, M. (1989) It will never work! The St. Jude valve. *Ann Thorac Surg*. 48, S53–S54.
8. Plaisance, P., Lurie, K.G., Vicaut, E., et al. (1999) A comparison of standard cardiopulmonary resuscitation and active compression–decompression resuscitation for out-of-hospital cardiac arrest. French Active Compression–Decompression Cardiopulmonary Resuscitation Study Group. *N Engl J Med*. 341, 569–575
9. Das, G.S., Voss, G., Jarvis, G., Wyche, K., Gunther, R., and Wilson, R.F. (1993) Experimental atrial septal defect closure with a new transcatheter, self-centering device. *Circulation*. 88, 1754–1764.
10. Visscher, M.B. (1969) A half century in science and society. *Annu Rev Physiol*. 31, 1–18.
11. Starling, E.H. and Visscher, M.B. (1927) The regulation of the energy output of the heart. *J Physiol Lond*. 62, 243–261.
12. Wilson, L.G. (ed.) (1989) *Medical Revolution in Minnesota: A History of the University of Minnesota Medical School*. Midewiwin Press, St. Paul, MN.
13. Rees, D. (interviewer) (2002) *Pioneers of the Medical Device Industry in Minnesota: An Oral History Project, Earl E. Bakken and Dr. C. Walton Lillehei*. Minnesota Historical Society Oral History Office, St. Paul, MN.

SOURCES

Medical Alley Website: (www.medicalalley.org).
Rigby, M. (1999) The era of transcatheter closure of atrial septal defects. *Heart*. 81, 227–228.
Stephenson, L. (ed.) (1999) *State of the Heart: The Practical Guide to Your Heart and Heart Surgery*. Write Stuff Syndicate, Fort Lauderdale, FL.
US Food and Drug Administration, Center for Devices and Radiological Health. Website: (www.fda.gov/cdrh/pmapage.html).

21 Animal Models for Cardiac Research

ROBERT P. GALLEGOS, MD, ANDREW L. RIVARD, MD, AND RICHARD W. BIANCO

CONTENTS

1. INTRODUCTION

The modern era of cardiac surgery is largely considered to have begun in the animal research laboratories. Today, animal models provide the ultimate preclinical assessment for the study of cardiovascular disease, pharmaceuticals, mechanical devices, and therapeutic procedures. This chapter was designed to provide readers and potential investigators crucial insights into the process of matching an experimental hypothesis to an animal species that will serve as the most appropriate model for specific cardiovascular diseases or for testing a given medical device. A review of the current animal models used in cardiac research is provided and arranged by disease state. Critical factors, including cost, reproducibility, and degree of similarity of the model to human disease are discussed; thus, this chapter can be utilized as a guide in planning research protocols.

2. PROTOCOL DEVELOPMENT

Several scientific governing bodies have developed guidelines in an effort to ensure that animals used in research are ethically and scientifically appropriate. Investigators who plan to utilize animal subjects in their research should first familiarize themselves with *Guide for the Care and Use of Laboratory Animals (1)*. In addition, investigators should use these guidelines in conjunction with accepted scientific methods to develop a standardized protocol for each research project. It is standard procedure that, prior to commencing research, a detailed protocol must undergo review and approval by the local institutional governing body responsible for the safety and ethical use of animals in research. At the University of Minnesota, this is the Institutional Animal Care and Use Committee (*see* www.iacuc.umn.edu).

Both large and small animals have been extensively used in cardiovascular research. Yet, the choice of animal model should be primarily based on: (1) the scientific hypothesis; (2) the lab's capability to employ the model safely in the species chosen (i.e., appropriate animal housing and care, equipment, lab resources); and (3) the degree of the species' similarity to the human anatomy. Many of the best animal models can be expensive to establish and maintain; therefore, funding must be appropriate to complete the required number of animals to satisfy a precalculated statistical power.

From: *Handbook of Cardiac Anatomy, Physiology, and Devices*
Edited by: P. A. Iaizzo © Humana Press Inc., Totowa, NJ

Table 1
Naturally Occurring Animal Models of Cardiovascular Disease

Subaortic stenosis	Dog (Newfoundlands, golden retrievers, rottweilers, boxers, German shepherds, samoyeds); cat; pig; cow
Ventricle septal defect	Dog (English bulldogs, keeshonds [genetic], English springer spaniels, beagles); cat; horse; cow; pig; chicken
Patent ductus arteriosus	Dog (poodles, German shepherds, collies, Pomeranians, Shetlands, Maltese, English springer spaniels, keeshonds, Yorkshire terriers); cat; horse; cow
Tetrology of Fallot	Dog (keeshond, bulldogs, beagles, and samoyeds); cat; horse; cow
Pulmonic stenosis	Dog (English bulldogs, mastiffs, fox terriers, samoyeds, miniature schnauzers, cocker spaniels, West Highland white terriers); cat
Pulmonary valve dysplasia	Dog (beagles: polygenetic transmission; boykin spaniels)
Mitral valve dysplasia	Dog (Great Danes, German shepherds, bull terriers, golden retrievers, Newfoundlands, dalmatians, mastiffs); cat
Tricuspid valve dysplasia	Dog (Old English sheepdogs, German shepherds, weimaraners, Labrador retrievers); cat

Note: Other than the dog, limited literature is available for all other species.

Several obvious technical limitations for the use of small animals exist, for example, in the case of implanting mechanical devices such as heart valves. In such situations, the animal species must be chosen to the fit the device. Nevertheless, great strides have been made in both imaging (ultrasound and magnetic resonance imaging, or MRI) and miniaturized electronic equipment (e.g., Transoma Medical, Arden Hills, MN) that is used for the monitoring of physiological parameters, allowing for more use of smaller animal models.

In choosing the animal species, the researcher should attempt to match the physiological parameter to be investigated in the experimental animal to the corresponding human value to obtain relevant results. Note that tables of known physiological values have been published for many commonly used research animal species, and these should be used to assist in choosing the appropriate model *(2)*.

3. SPONTANEOUSLY OCCURRING ANIMAL MODELS OF CONGENITAL CARDIAC DISEASE

Naturally occurring animal models of cardiac disease arise infrequently and are usually associated with other congenital abnormalities that hinder breeding efforts. Furthermore, genetic manipulation of breeding stock for specific mutations has economical, ethical, and moral issues that preclude the development of such breeding lines. As a result, the commercial availability of animals for such specific research purposes is quite limited, necessitating the development of iatrogenic models in most cases. We have included a brief tabulation of some known cardiac defects, though the use of such models may be impractical because of the lack of availability and uniformity of lesions (Table 1) *(3)*.

4. ALTERNATIVES TO WHOLE ANIMAL MODELS

Isolated cardiac cell lines in culture, segments of myocardium, or isolated hearts may provide an effective alternative to whole animal models in some cases. Isolated preparations have been particularly useful for the study of metabolic pathways because the perfusate can be modified, and the effluent can be easily collected for analysis. In addition, functional measurements can be easily completed in this in vitro environment.

The allure of alternatives to whole animal models is strong, driven by the need both to reduce cost and to limit the number of animals used in research. However, caution must be taken in extrapolating the experimental findings from isolated in vitro models to actual clinical use. For example, studies involving pharmaceutical agents often demonstrate usefulness in vitro, but the concentrations used may be either toxic or not well tolerated by the intact animal. Nevertheless, many researchers have used these alternatives for studies pertaining to myocardial ischemia, transplantation, and pharmaceutical development.

4.1. Isolated Cardiomyocytes

The use of isolated cardiomyocytes has allowed researchers to eliminate confounding interactions with surrounding tissue elements; it has also allowed for measurement of intracellular changes on a single-cell level. Yet, care must be taken to match the culture conditions to those of the intact organ to ensure both the quality and the viability of the cells used *(4,5)*. This simple model does provide an important alternative for the use of whole animals in early phase testing of experimental protocols and is of particular interest for use in the testing of new pharmacological agents or gene therapies.

Cardiac myocyte cultures can be obtained from: (1) freshly isolated tissue; (2) the differentiation of embryonic stem cells or multipotent adult progenitor cells; or (3) available immortalized tumor cell lines such as HL-1 from the At-1 mouse *(6)*. Common functions of cardiac myocytes that can be examined include: (1) contractile (using optical or mechanical detectors); (2) protein/ribonucleic acid (RNA) activity with quantitative polymerase chain reaction (Q-PCR); and (3) membrane integrity (lactate dehydrogenase, creatine phosphokinase, or troponin release) *(5,7–11)*.

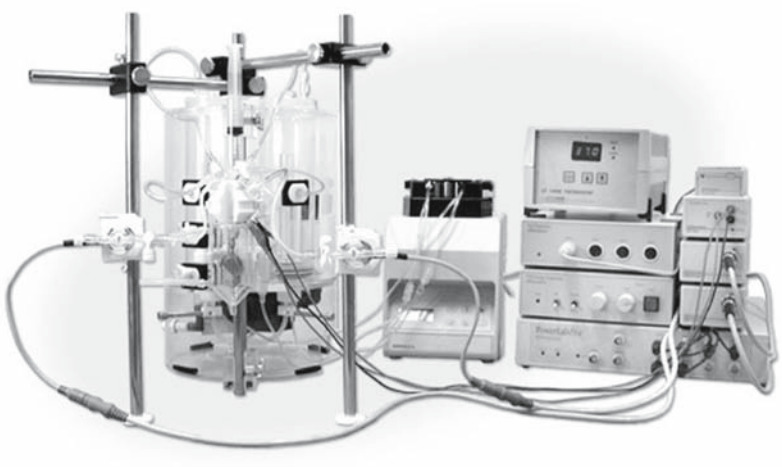

Fig. 1. ADInstruments Langendorff perfusion setup. Reprinted with permission from ADInstruments Inc. (www.adinstruments.com).

4.2. Isolated Perfused Hearts

An isolated heart perfusion setup replicates the physiological conditions outside the body, allowing for easy access for measurement of the perfused effluent. Yet, isolated in vitro perfusion studies have been performed using the entire heart or a portion of the heart (e.g., intraventricular septum, papillary muscle). Commercially available setups for such in vitro studies are available for the mouse, rat, and guinea pig hearts (ADInstruments, Colorado Springs, CO) (Fig. 1). Larger setups have also been described to accommodate canine, porcine, ovine, or human hearts. An excellent example of an application of the isolated heart model is provided on the accompanying Visible Heart® CD (*also see* www.visibleheart.org).

Two different methods of studying the isolated heart are available: Langendorff perfusion or the isolated working heart model *(12,13)*. In the Langendorff method, constant pressure flow through an aortic cannula forces the aortic valve closed, and the perfusate passes through the coronary arteries without flowing through the left ventricle. This perfusion provides the myocardium with energy, allowing the heart to beat without filling the four chambers. This method was named to honor Oscar Langendorff, who in 1895 was the first person to describe an experimental model of an isolated mammalian heart as a technique to assess its contractile activity.

The advantage of the Langendorff perfusion method is that measurement of electrocardiogram changes can be easily assessed, as well as measurement of metabolites that drain from the coronary sinus. Yet, the lack of flow in the ventricle may limit the usefulness of this preparation, for instance, minimal blood entering into the ventricle may promote clot formation, in turn affecting the viability of the preparation. In addition, the lack of flow in the ventricle may result in abnormal 3D conformational changes in the heart, which may cause coronary vascular compression. However, placement of a fluid balloon connected to a pressure transducer may allow control of this phenomenon and may be useful experimentally to assess changes in left ventricular function.

The major disadvantage of the Langendorff preparation is that it does not eject the perfusate from the left ventricle and is therefore a nonwork-producing model. This problem was overcome by Neely, who used an isolated working heart that simulates physiological flow through the heart's four chambers *(14)*. In this model, the perfusate is supplied by a cannula inserted into the left atrium; outflow through the left ventricle is monitored, and left atrial pressure or aortic pressure is controlled. This setup is considered ideal for the study of pressure and flow in the aorta as well as the left and right ventricles.

4.3. Problems With Isolated Perfused Heart Models

Interestingly, both types of isolated heart preparations have problems in common that must be considered when attempting to extrapolate results from the in vivo condition. First, the isolation process used for these models requires global myocardial ischemia (a period of no perfusion). Typically, once the organ is reperfused, baseline data (heart rate, left ventricular pressure, coronary blood flow) must be collected after a stabilization period to ensure viability of the preparation. Clearly, both the ischemic time and stabilization time may influence research outcomes. Therefore, any results obtained must be carefully analyzed with reference to the preparation's baseline state rather than normal in vivo values to avoid falsely attributing changes in cardiac function to the experimental protocol.

The composition of the perfusate can have a great impact on the function and viability of the preparation in both of the aforementioned models. Early studies utilizing isolated heart models have employed the obvious choice of whole blood as a perfusate *(15)*. However, significant problems with clotting and hemolysis may limit the time that the preparation remains viable. Saline compounds, which lack the potential for clotting and hemolysis, are considered useful alternatives to whole blood. However, such buffers have a lower colloid osmotic pressure and, coupled with the lower coronary vascular resistance, will typically result in severe edema; this results in interstitial edema formation and nonuniform perfusion. To extend the usefulness

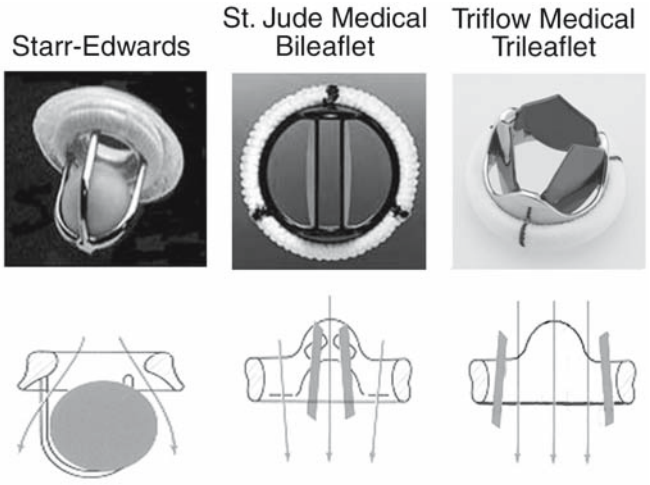

Fig. 2. Comparison of different valves with their flow characteristics. The evolution of the valve from the Starr-Edwards ball, the current standard bileaflet (printed with permission from St. Jude Medical) and a novel trileaflet design (printed with permission from Triflow Medical Inc.) currently in development. Pictured below each valve is a stylized representation of the flow patterns across each valve reflecting the improvement in nonobstructive valve design.

Fig. 3. The Medtronic Mosaic® stented tissue valve. Printed with permission from Medtronic, Inc.

Fig. 4. A typical bileaflet heart valve.

Table 2
Qualities of Ideal Heart Valve Replacement

- Durable
- Does not leak
- Biologically inert
- Nonthrombogenic
- Facilitates laminar flow
- Easily implanted by the surgeon
- Quiet

of the preparation, osmotically active substances can be added to the medium used for bathing and perfusing the preparation in an attempt to limit edema *(16,17)*. Despite the technical difficulties associated with these models, isolated hearts have been used in research ranging from ischemia to transplant studies.

5. ANIMAL MODELS IN VALVE DISEASE

The significant morbidity and mortality associated with heart valve disease has produced a highly lucrative and competitive market for manufactured prosthetic valves. Efforts to develop the ideal replacement heart valve have focused on producing a product that functions like the native valve (Table 2). The dynamics of blood flow through a tube with its specific viscosity is such that the flow is greatest in the center of the tube. Thus, any structure in the center of the valve (i.e., mechanical valve leaflets) will reduce the velocity through that valve. Such basic principles of physics are important in the fundamental design of mechanical valves, as evidenced by the evolution of mechanical design (Fig. 2).

Guidelines for the design and testing of bioartificial and mechanical valves have been established by the Center for Devices and Radiological Health (part of the Food and Drug Administration, or FDA) and the International Organization for Standardization (ISO). More specifically, the FDA has provided industry assistance in the form of guidance documents, advice, reporting, premarket approval, standard formation, and third-party reviews. Typically, prosthetic valve replacements are classified as either tissue (Fig. 3) or mechanical (Figs. 4 and 5); yet, despite their common purpose, specific valve composition and function vary widely. Nevertheless, all valves must undergo performance-based testing to examine hydrodynamic performance (Table 3). For example, accelerated cyclic testing provides wear information, allowing for estimates of structural performance by providing data on fatigue, endurance limits, and damage tolerance of the valve.

Importantly, the FDA requires the demonstration of both efficacy and safety of prototype heart valve replacements prior to final approval for human implantation. This is based on the principle that additional technical and biological information can be gained by observing the valve in actual use. As a result, animal studies remain a crucial component in the overall evaluation of replacement heart valves. All investigational valves undergo a preclinical animal study, with valve implantation in the orthotopic or anatomically normal position (with a required 20-wk minimum duration).

Specifically, the FDA looks for separate data from mechanical and biological valve studies. For example, mechanical

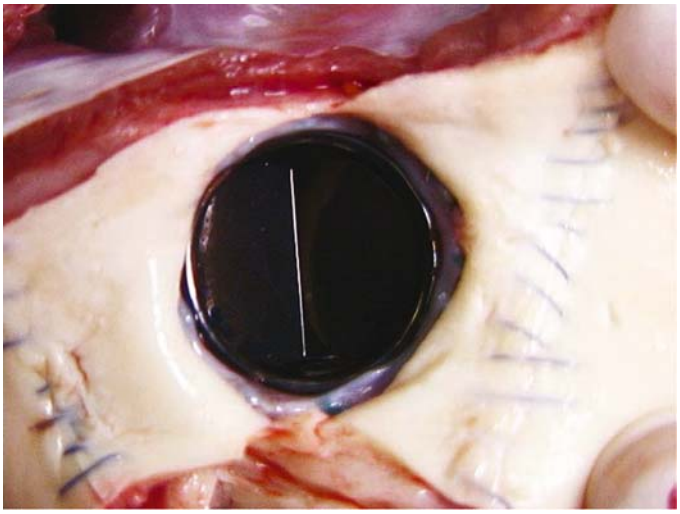

Fig. 5. Normal ovine model of bileaflet valve implantation. Photo courtesy of Richard W. Bianco.

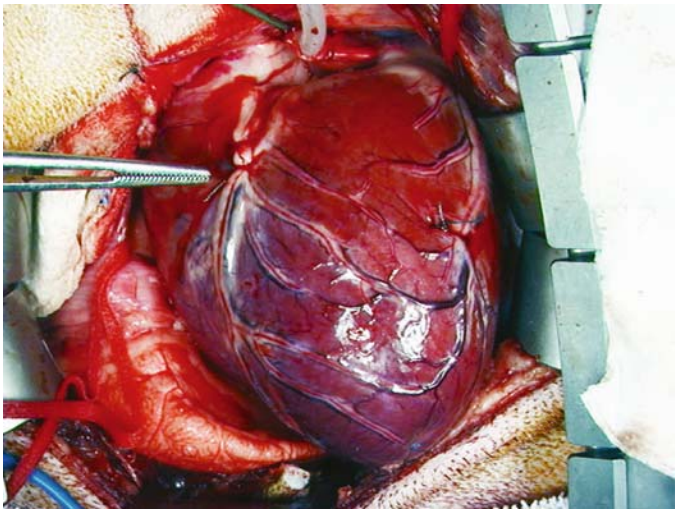

Fig. 6. Ligated left anterior descending coronary artery in an open chest canine model. Photo courtesy of Robert P. Gallegos.

valves generally place extreme shearing forces on the red blood cells and thrombocytes, causing hemolysis and thrombosis that necessitate chronic anticoagulation after valve implantation. On the other hand, biological valves place very low shear forces on the red blood cells and thus do not need anticoagulation; however, they are sensitive to calcification formation, requiring some form of anticalcification treatment before implantation.

The lack of naturally occurring models of valve disease and the need for standardized models for FDA/International Organization for Standardization approval has led to the use of iatrogenic models of valve disease. To date, the ovine model has been used for producing graded stenosis in the aortic and mitral valves by banding the aorta in young animals *(18)*. In contrast, aortic supravalvular stenosis, as well as aortic valvular stenosis, have commonly been induced in the canine model *(19,20)*. In addition, mitral valve regurgitation in the canine is possible by placement of a shunt *(21)* or by incision of the chordae tendinae. Interestingly, experiments have also been performed to induce stenosis or regurgitation in the tricuspid and pulmonic valves *(22)*. However, most valve implantation studies approved for human use are completed in normal animals to strictly examine valve performance (Fig. 6).

A primary advantage of employing the canine model is the large amount of available cardiovascular surgical literature. Historically, the dog was considered the gold standard for acute and chronic models of valve replacement surgery that has been accepted by the FDA. Early success with the canine model in valve replacement identified the need for minimizing the risk of surgical infection at the time of prosthesis implantation. Specifically, the use of preoperative parenteral and postoperative topical antibiotics, strict sterile techniques, minimum numbers of operative arterial and venous lines, and short cardiopulmonary bypass times were noted to minimize the risk of bacterial valve implant seeding *(23)*.

As described in Chapter 5, the anatomy of the porcine heart is similar to humans regarding the conduction system, coronary arteries, blood supply to the conduction system, and great vessels. In addition, the coagulation cascade of the swine is quite similar to that of humans. Despite the advantages, several problems have been identified in using this model for valvular research.

Table 3
Mechanical Valve Fluid Dynamic Testing

- Forward flow testing
- Backflow leakage testing
- Pulsatile flow pressure drop
- Pulsatile flow regurgitation
- Flow visualization
- Cavitation potential
- Verification of the Bernoulli relationship

Source: Replacement Heart Valve Guidelines, 1994, formulated by the US Department of Health and Human Services, Food and Drug Administration, Center for Devices and Radiological Health.

First, the porcine heart is extremely sensitive to anesthesia, and surgical manipulation often results in postsurgical complications, arrhythmias, or death. Second, the growth of young swine is rapid, resulting in heart size and physiological flow that is not constant over the required follow-up periods. Specifically, these alterations often result in fibrous sheathing and obstruction of the valve orifice, thrombus formation, or dehiscence (separation) of the sewing cuff. Finally, significant bleeding complications because of application of anticoagulation therapy and poor survival have limited the use of the pig in studying valve-related thrombosis *(24)*.

The ovine model is now accepted as the gold standard for valve replacement using survival surgeries that meet FDA requirements. Normal cardiovascular physiological parameters of sheep approximate normal human valves in blood pressure, heart rate, cardiac output, and intracardiac pressures *(25)*. In addition, the anatomy of the heart provides a valve orifice diameter that is similar to humans *(26)*. The use of animals of

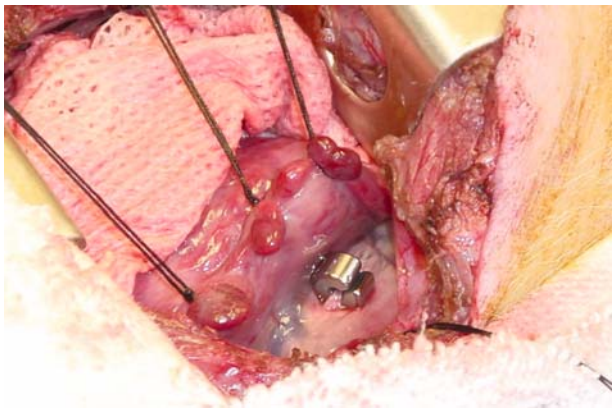

Fig. 7. Ameroid occluder in the canine model. Photo courtesy of Michael Jerosch-Herold and Cory Swingen.

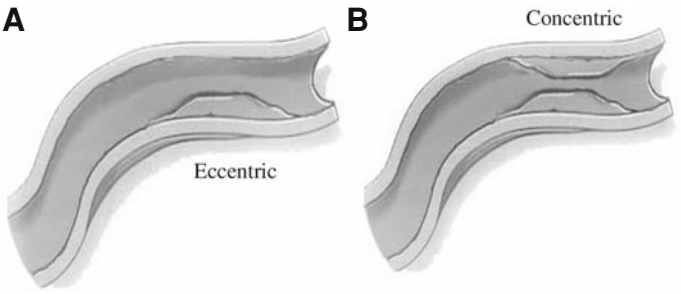

Fig. 8. **(A)** An example of an eccentric vascular constriction as with coronary artery disease. **(B)** A concentric lesion as created by experimental ligation or ameroid occlusion.

similar age and weight (8–12 months, 30–40 kg) allows the testing of replacement valves using a single orifice size for comparison of valve performance to an appropriate standard. Despite the fact that the heart and vessels are small in relation to the animal's weight, the sheep's relatively large left and right atria allow for straightforward surgical approaches to either the mitral or tricuspid valve.

Sheep as experimental animals allow easy handling and long-term husbandry *(24)*. Juvenile sheep grow at a rate that does not cause excessive mitral or aortic stenosis during the postimplantation test periods as compared to the porcine model *(24)*. However, specific attention to gastric decompression, perioperative antibiotics, sterile techniques, and minimally invasive interventions in the postoperative period will increase the success of valve implantation studies in the ovine model *(27)*.

6. ANIMAL MODELS IN MYOCARDIAL ISCHEMIA

Despite tremendous advances in treatment options, atherosclerotic coronary vascular disease remains the leading cause of death worldwide. As a result, this disease continues to be an active area of cardiovascular research. Originally defined by the Greeks as a lack of blood flow, the modern definition of *ischemia* emphasizes both the imbalance between oxygen supply and demand and the inadequate removal of waste products. Impaired oxygen delivery results in a reduction in oxidative phosphorylation, resulting in myocardial dependence on anaerobic glycolysis for the production of high-energy phosphates. This shift in metabolism produces excess lactate, which then accumulates in the myocardium. As impaired adenosine triphosphate production and acidosis prevail, there is a resultant decline in cardiac contractility. Ultimately, if not reversed, myocardial infarction occurs, with permanent cellular loss and impaired cardiac function.

Multiple experimental techniques have been developed for the study of ischemia. Currently, scientists consistently use isolated myocytes to examine single-cell responses; isolated perfused hearts and whole animal models allow a better understanding of the whole organ response. Regardless of the model type, experimental animals remain a crucial tool in the area of research (*see also* Chapter 12).

6.1. Experimental Methods for Creating Ischemia

The ideal model for ischemic investigations would theoretically be in the intact chronically instrumented awake animal because acute surgical trauma and anesthetic agents both depress cardiac function *(2)*. The awake animal model also has the major advantage that it can be used in studies requiring physiological stress (e.g., stress produced by exercise). However, the high cost of the implanted transducers and probes as well as difficulties with measurement techniques often preclude the use of such methodologies.

To date, the majority of studies use anesthetized animal models for the study of ischemia in either closed or open chest models. Closed chest models have the advantage that tissue trauma is minimized, but in such models, direct access to the heart for metabolite measurement is a major limitation. In contrast, the open chest preparation has the advantage that regional function and metabolism can be studied in detail. The open chest models suffer from drawbacks that include a greater susceptibility to temperature variations, and potential for surgical trauma may considerably alter cardiac function (Fig. 7).

Multiple techniques have been used to create models of myocardial ischemia for research purposes, including permanent occlusions, temporary occlusions, or progressive occlusions. Methods to produce complete permanent occlusions include surgical coronary ligation or radiological embolization. Furthermore, permanent or temporary partial coronary occlusions are commonly induced by ligation, balloon occlusion, or clamping. Typically, models of progressive coronary artery occlusions use either balloon/catheter occlusion or ameroid constrictors (Fig. 7).

Regardless of the method chosen, the researcher must be aware that the concentric experimental lesions created differ from those of naturally occurring atherosclerotic coronary vascular disease, which are typically eccentric. Normally, such eccentric stenoses remain vasoactive and are capable of altering coronary blood flow by changing their lumen diameter. It should be noted that no such vasoactivity remains in experimentally created concentric lesions, which prohibits humeral agents from altering regional coronary flow (Fig. 8).

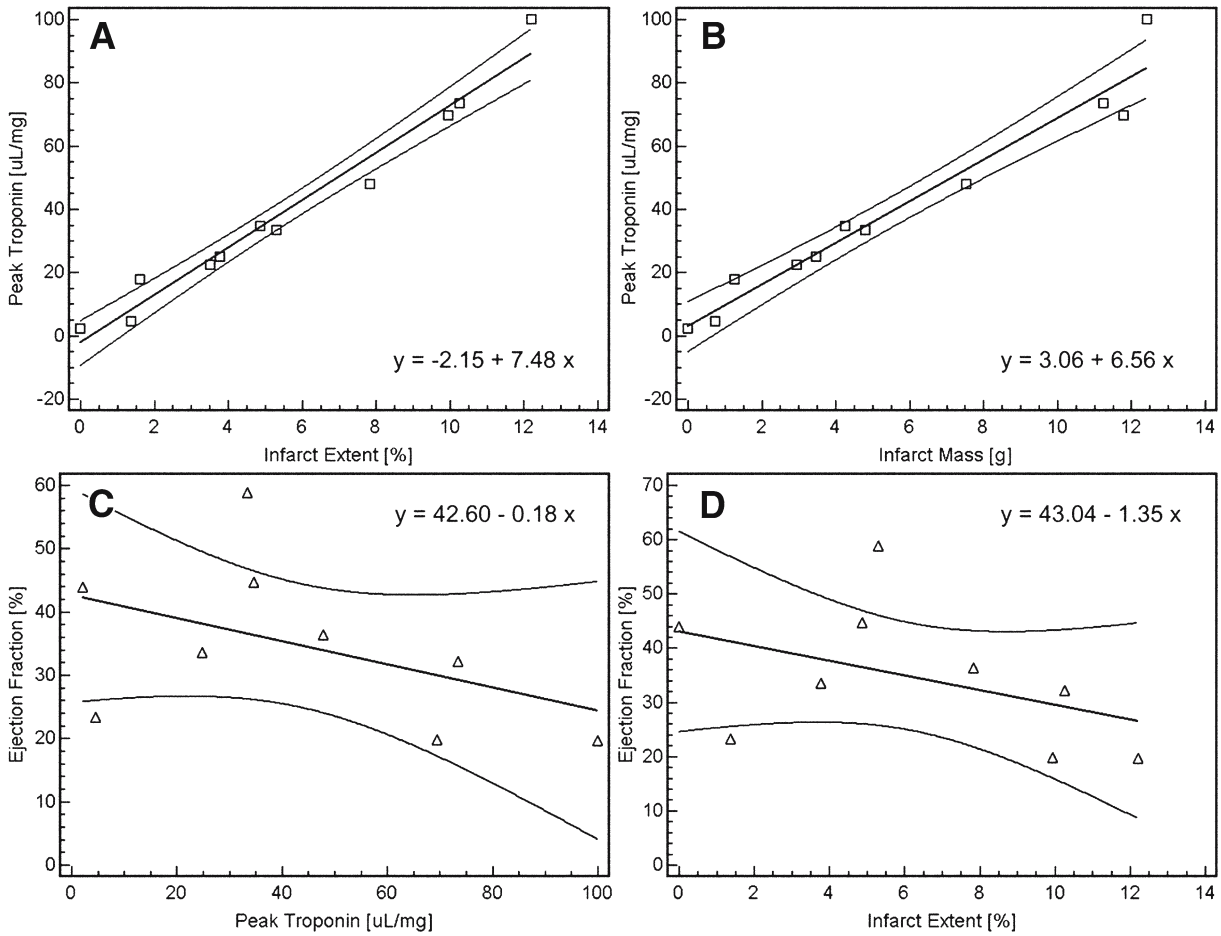

Fig. 9. In a left anterior descending ligation model in the dog, both infarct size as measured by cardiac magnetic resonance imaging (MRI) and peak troponin I are plotted. **(A)** and **(B)** demonstrate good correlation with peak troponin I and both infarct size and mass. In contrast, although a trend between ejection fraction and troponin I and infarct size is evident, correlation is not strong, suggesting that infarct size alone does not determine the effect on cardiac function.

Historical experience has shown that an induced occlusion of the left anterior descending coronary artery is favored over that in the left circumflex coronary artery for the production of regional myocardial ischemia. It is generally accepted that occlusion of the left anterior descending coronary artery results in a larger area of myocardial ischemia and therefore greater impairment of global left ventricular function. However, estimates of infarction size alone have not correlated well with ventricular function (Fig. 9) *(28)*.

In fact, it has been demonstrated that, for the same amount of ischemic myocardium, the compensatory increase by the nonischemic myocardium is different for the left anterior descending coronary artery and the left circumflex coronary arteries *(29)*. Therefore, in an ideal model, both infarct size and its location must be similar to achieve the same degree of impairment in left ventricular global function.

6.2. Localizing and Quantifying Myocardial Ischemia

Blood samples collected from the coronary sinus or from a regional coronary vein are commonly obtained and used for metabolic studies. Yet, such results must be interpreted with the knowledge that these samples include contaminated blood from adjacent noninjured myocardium. However, it should be noted that the use of coronary venous samples for studying metabolism is decreasing because of recent developments in microdialysis, magnetic resonance imaging, nuclear magnetic resonance spectroscopy, and positron emission tomography *(30–32)*.

The size and location of myocardial infarction can be determined by triphenyltetrazolium chloride (TTC) staining, which has been the gold standard for quantifying the extent of myocardial infarction in pathological specimens (Fig. 10) *(33)*. In addition, the assessment of localized tissue blood flow using microspheres (radioactive or colored) remains the gold standard. However, newer noninvasive methods of determining blood flow in the live animal that allow for repeated follow-up determinations of flow are continually under development and improvement, including spectroscopy and MRI.

6.3. Specific Animal Models for Ischemia Investigations

Both large and small animal models have been developed for the study of myocardial ischemia. The advantage of large animal models relates primarily to their similarity in physiology to

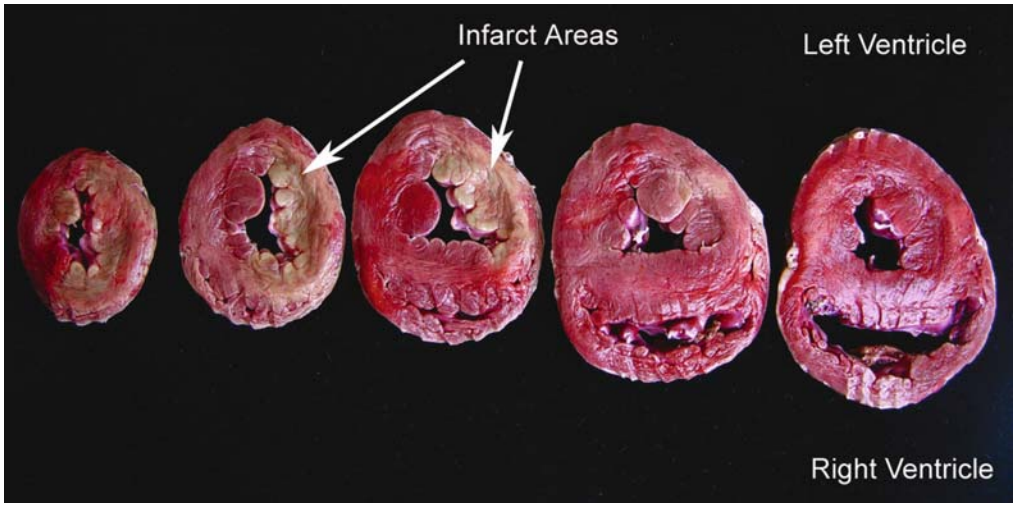

Fig. 10. Triphenyltetrazolium chloride (TTC) staining in canine infarct model showing paleness of myocardium in left anterior coronary artery distribution. Photo courtesy of Robert P. Gallegos.

humans and ease of instrumentation. However, disadvantages include significantly greater care and cost issues, which may make small animal models more attractive, particularly when large numbers of animals are required to achieve significant statistical power.

Traditionally, the dog has been the most frequently utilized animal species for in vivo experimental ischemia studies. The dog is considered a strong model for the condition of chronic ischemia because these animals have a well-developed coronary collateral circulation, similar to humans with chronic ischemia (progressive heart failure). Furthermore, the ease in handling of this species and the lack of significant growth in the adult dog are strengths of this model by allowing long-term follow-up. However, it should be noted that the significant variability in this collateralization may also hamper efforts to create consistent sizes of ischemic regions between animals or may result in a minimized ischemic zone.

The pig heart is more similar to the relatively healthy human heart in that there is limited collateral blood flow; this makes the swine heart ideal for acute ischemia studies. However, long-term follow-up using the swine model generally is considered problematic; if juvenile animals are utilized, significant changes in animal weight will result in both increased difficulties with handling as well as alterations in basic cardiac physiology. More specifically, in consideration of ratios of heart to body weight, in a healthy person the ratio is about 5 g/kg; for pigs weighing between 25 and 30 kg, the ratio is similar to that in humans, but for animals exceeding 100 kg, it is only half that value *(29)*. Importantly, such ratio changes must be considered when interpreting experimental results.

Small animals have also been used as models for investigations of regional myocardial ischemia. Note that it is well established that the collateral circulation of the rat is sparse, and that the rabbit may show intraspecies differences *(34)*. In addition, the guinea pig has such an extensive collateral network that normal perfusion is maintained after a coronary artery occlusion, and infarction does not often develop. Another problem with using these animals is that the small vessel diameters may delay or prevent instantaneous reperfusion following transient vessel occlusions. This is further hampered by the inability to make quantitative assessments of coronary blood flows in these small vessels to verify reperfusion. Nevertheless, the use of small animal models remains quite important for such studies, including recent investigations involving stem cell research and those that require large numbers of animals.

Table 4
Definition of Graft Types

Autograft	Transplant from one site to another in the same individual
Isograft	Transplant from a donor to a genetically identical individual (monozygotic twin)
Syngraft	Transplant from a donor to a recipient with no detectable genetic difference (inbred strain)
Allograft (homograft)	Transplant from a donor to a genetically different individual of the same species
Xenograft (heterograft)	Transplant from a donor to a recipient of another species

7. ANIMAL MODELS IN HEART FAILURE AND TRANSPLANTATION

Dr. Alexis Carrel reported the first heterotopic transplantation (Table 4) of a canine heart connected to the neck vessels of another dog in 1905; the animal succumbed to massive clotting and survived for only 2 hours. Over the next 55 yr, Drs. Richard R. Lower and Norman E. Shumway ultimately perfected an orthotopic transplantation in the canine. In contrast to Carrel's original work, transplants in Shumway's laboratory research were placed orthotopically, and animals survived for up to 21 days before succumbing to rejection. Successful translation of this animal research to clinical practice was first accomplished by Dr. Christiaan N. Barnard in 1967; this required the further

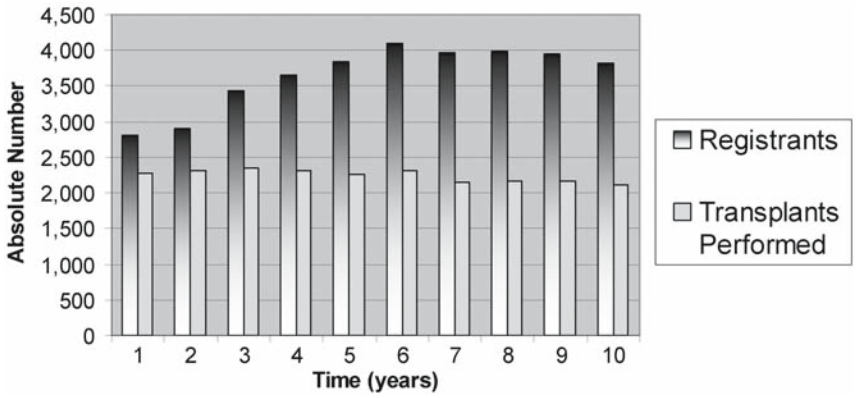

Fig. 11. Total number of United Network for Organ Sharing (UNOS) cardiac transplant waiting list registrants and donor hearts per year. Adapted from the UNOS database.

use of animal models to provide a means to overcome the rejection by the host immune system that plagued previous attempts.

Today, the successful treatment of end-stage cardiac failure is now possible with either organ transplantation or mechanical assist devices (for those who may not initially qualify for transplantation). However, it is clear that too few suitable donor organs are available to meet the current needs (Fig. 11). It is also considered that the undersupply of organs will clearly worsen as the pool of potential donors is reduced further by the projected increased incidences of numerous factors that preclude heart donation, such as diabetes, hypertension, hypercholesterolemia, or infection with human immunodeficiency virus (HIV) or hepatitis B or C. This lack of a reliable and stable source of donor hearts serves as the main impetus for further research into expanding cardiac donor pools, the use of mechanical assist devices, and the potential for cellular-mediated transplantation.

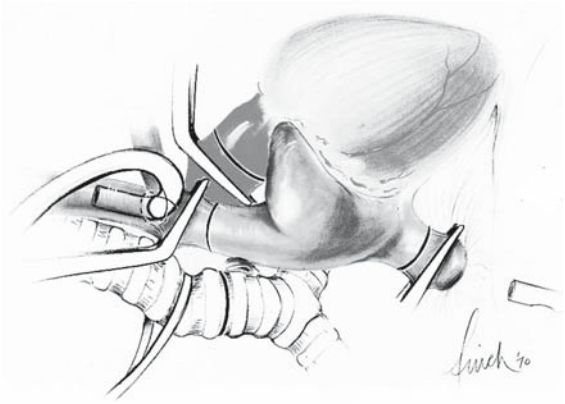

Fig. 12. Orthotopic heart transplant drawing. Original art by Martin E. Finch.

7.1. Methods of Transplantation Research

Large amounts of research have been conducted in the field of cardiac transplantation (heterotopic or orthotopic) (Fig. 12). Orthotopic transplantation (the placement of the donor heart in the anatomically correct position) is considered the gold standard for the study of cardiac transplantation. This method of transplantation requires the use of cardiopulmonary bypass and was possible only after the pioneering efforts of Dr. C. Walton Lillehei (refer to ref. *35* for a complete discussion of the surgical technique)**.** Orthotopic transplantation is technically feasible using available cardiopulmonary bypass circuits in both the canine and porcine animal models. The major disadvantage of orthotopic transplantation is that it requires a high level of surgical knowledge, and supportive technologies are usually found only in sophisticated research facilities (e.g., a university setting).

Furthermore, orthotopic transplantation has traditionally been chosen for the study of organ preservation, graft rejection immunology, immunosuppressive regimens, xenotransplantation, and ischemia/reperfusion injury *(36–38)*. Heterotopic cardiac transplantation places the heart in an anatomical location other than the mediastinum. A heart transplanted into the heterotopic position is connected by matching donor aorta to recipient aorta and donor pulmonary artery to recipient vena cava. As a result, blood flow is typically nonphysiological; normal patterns are limited to the coronary arterial and venous systems. Absence of significant flow in the ventricles, except for drainage of blood from the coronary sinus into its right ventricle, may promote clot formation and has been ultimately associated with failure of the model. An additional disadvantage of the heterotopic transplant model is the increased technical difficulty secondary to the donor/recipient aortic size mismatch, which also depends on the animal's age, weight, and species.

Heterotopic transplantation is generally used for studies of ischemia/reperfusion injury *(39)*, prevention of rejection and immunosuppression *(40)*, or coronary vascular pathology *(41)*. Heterotopic heart transplantations can be performed using small mammal models such as the mouse, rat, hamster, guinea pig, or rabbit; yet, additional skills with microsurgical techniques are then required. A major advantage of this approach is that recipients may retain complete function of their native hearts whether or not the heterotopic donor hearts survive.

7.2. Specific Animal Models for Transplantation Research

The choice of an animal model for cardiac transplantation depends greatly on the area of physiological research. The following is a brief review to introduce the current models that have been used effectively to date in cardiac research laboratories around the world.

7.2.1. The Rodent Transplantation Model

The development of microsurgical techniques has allowed for refinement of heart transplantation in the rodent model. Importantly, the use of rodents in transplantation research can dramatically reduce the costs associated with larger animal models. Typically, Lewis rats have been used for transplantation experiments related to ischemia and reperfusion, prevention of rejection, immunosuppression, and coronary vascular pathology. However, as long as the genetically bred rodent tissue types remain stable, they would also be suitable. Because of the small size of rodents, the technique of heterotopic heart transplantation to the abdominal aorta and inferior vena cava, as described by Ono and Lindsey, has been used extensively *(42)*.

Anatomically, the coronary artery blood flow in rodents differs somewhat from higher order mammals in that the left and right coronary arteries traverse the lateral wall of the right ventricle rather than the atrioventricular sulcus. In addition, the internal mammary arteries supply the atria with blood flow via the cardiomediastinal arteries. Some further disadvantages of the rodent model are that hemodynamic measurement of the transplanted hearts can be difficult, and transplantation uses microvascular surgical techniques requiring a surgical microscope.

Yet, an advantage of this model is its use for xenotransplantation experiments with grafts from mouse to rat, hamster to rat, guinea pig to rat, or hamster to guinea pig. In addition, preservation solutions can be fairly easily evaluated for the end points of survival, histology, and high-energy phosphate analysis. The heterotopic rat transplant model has been extensively used in the pharmaceutical industry to evaluate the effectiveness of antirejection medications. The availability of transgenic or "knockout" rodents will likely dramatically further the use of rodents in this area of research.

7.2.2. The Canine Transplantation Model

The anatomy of the canine heart is similar to that of the human heart (for more details, *see* Chapter 5). As mentioned in Section 6.3, the dog heart has an extensive collateral circulation connecting the left and right coronary circulation. In contrast, nonathletic humans elicit few bridging collaterals. This collateral circulation in the dog is considered theoretically advantageous in heart transplantation experiments because it may protect marginal areas of the heart from ischemia.

From the perspective of an easy-to-employ model, dogs have a minimal amount of adipose tissue, and their skin is loose, allowing tunneling of catheters if vascular access is needed postoperatively. Furthermore, the dog's relatively large thorax and mediastinum allow clear visualization of the heart and great vessels. Thus, the canine model for heart transplantation is generally considered most readily employable for animal studies of organ preservation, reperfusion injury, rejection studies, and posttransplant organ monitoring.

7.2.3. The Swine Transplantation Model

The porcine heart is often considered the most anatomically similar to the human heart (*see* Chapter 5). Specifically, the porcine heart has few collateral vessels, and an end-artery coronary anatomy predominates. Yet, cannulation for cardiopulmonary bypass may be difficult, and the right atrial tissue has typically been described as friable *(2)*. In addition, a surgical cutdown for venous and arterial access may be required secondary to the thick subcutaneous layer of adipose tissue. The pig transplantation model is also prone to postoperative wound infections, necessitating strict sterile techniques during cardiac surgery. Furthermore, juvenile pigs have a tremendous capacity for somatic growth, which can challenge long-term foreign body implantations.

Physiologically, the porcine heart is considered prone to arrhythmia and is sensitive to physical manipulation. Bretylium tosylate can be given to limit such arrhythmias; however, ventricular fibrillation can be a recurrent problem following cardiopulmonary bypass *(43)*. The swine model is considered appropriate for heart transplantation, but is often described as more suited to acute or short-term survival studies *(44)*. Ongoing transgenic breeding projects to create a porcine heart with compatible tissue antigens (to be used as a substitute for the human donor heart) are exciting areas of research that will make the increased use of the swine model more likely.

7.2.4. The Nonhuman Primate Transplantation Model

Researchers in the field of cardiac transplantation have used the nonhuman primate model extensively in developing both the technique of transplantation and the scientific background necessary for the survival of the donor heart *(45,46)*. Numerous programs have successfully used the nonhuman primate in small and large cardiac transplant studies (47–49). Yet, particular problems with the use of primates have been primarily associated with their veterinary care.

Specifically, specialized care is necessary during preoperative and postoperative times, and thus established facilities are required for appropriate holding and colony breeding. Furthermore, nonhuman primates are extremely susceptible to *Mycobacterium tuberculosis*, and appropriate precautions must be taken to minimize the risk of infection. It should be noted that baboons are sensitive to stress and are apt to develop gastroenteritis and bacteremia after surgery; handling of the baboon typically requires sedation (Fig. 13).

Nevertheless, the use of baboons and other nonhuman primates has many advantages as an experimental model in transplant research. First, the size and anatomy of the baboon is very similar to human anatomy. Second, the growth of the baboon can be controlled, and adult weights in the range of 20–30 kg are maintained for 20–30 yr. In addition, cardiac physiological characteristics of the baboon are similar to humans, allowing for the use of standard operative instrumentation.

Yet, cardiac anatomy differs somewhat from humans; the baboon heart has only two aortic arch vessels compared to the three found in humans. From a technical standpoint, the cardiac

tissue of the nonhuman primate is not considered as friable or prone to serious arrhythmias as in the swine.

Adverse immunological responses in the primate are a main concern with xenotransplantation and with antirejection treatments. Interestingly, the human ABO blood-type system is applicable with simian tissue and saliva, but not with simian blood *(50)*. Tissue typing with the major histocompatibility class system using primate tissue is also possible. Hyperacute rejection is inherent to xenotransplantation in this model because of the preexisting antibodies in the recipient; the donor antigens on the surface of the endothelium of the donor's heart that are present to the recipient's intact immune system cause rejection to ensue with subsequent activation of compliment *(51)*. Fortunately, depletion of compliment factors in heterotopic heart transplantation is possible in the primate model, as was performed at the University of Minnesota (Minneapolis, MN) *(52)*.

Heterotopic (nonanatomic and nonfunctional) heart transplantation in the nonhuman primate is an established surgical procedure appropriate for investigation of immunosuppressive drug therapies and study of immune reactions between the donor heart and recipient. Typical locations for hetrotopic implantation of the donor heart include the neck or abdomen of the primate *(53)*.

8. ANIMAL MODELS FOR THE TESTING OF MECHANICAL DEVICES

Maximizing surgical therapies in end-stage heart failure is a growing biomedical field. Devices (i.e., ventricular assist devices) have become increasingly important because of an increased incidence of patients presenting with end-stage heart failure. Interestingly, mechanical ventricular assist devices are filling a niche in which they are both a "bridge to transplant" as well as a "destination therapy" at centers such as the University of Minnesota. Before any such device can be implanted into a human, the procedure requires years of high-level animal testing.

8.1. Animal Model Selection for Device Testing

Animal models are useful for both training and research of mechanical devices, such as the ventricular assist device. The justification for use of a particular animal model is primarily based on past and current successes using a particular animal. From careful selection, the right animal model is based on device size and comparative anatomy. This likely will decrease the difficulty of implanting such devices. Obviously, devices designed for human use will require a comparable size research animal for testing. For example, the sizes of in-line axial flow pump have become relatively compact and have been implanted into the dog, sheep, or calf model *(54,55)*. Larger pumps, based on a moving diaphragm, still require a larger animal, such as the sheep or calf, as would be appropriate for human use *(56)*.

8.2. Federal Guidelines for Device Testing

As an example, ventricular assist device technology is a rapidly advancing field, and the FDA has not published official guidance documents for such devices. However, for these devices the FDA does have specific evaluation criteria that are designed to identify possible hazards prior to clinical usage.

Fig. 13. Sedated baboon. Original art by Martin E. Finch.

Long-term reliability is a current issue of concern with such devices because some patients waiting for a transplant survive longer, and destination therapy may become a reality for numerous device recipients. Consequently, long-term biocompatibility, thrombogenesis (long-term surface-coating antithrombogenic integrity), bacterial infection, battery life, hardware reliability, and software reliability have become important parameters for FDA evaluation of devices. Finally, the ease of patient use related to ventricular assist devices is also of central importance. For more information on animal models, *see* Chapter 5.

9. CELLULAR CARDIOMYOPLASTY

Cellular cardiomyoplasty, the process by which injured myocardium is repaired by cell transplantation, has significant clinical potential *(57,58)*. Much of the excitement about cell-based therapy lies in the premise that repairing the injured heart will overcome the inherent limitations for the broad application of both organ transplantation and mechanical assist devices. A thorough review of the literature for stem cell-mediated cardiac therapy is provided in Chapter 31, and thus the topic is only reviewed briefly in this section.

9.1. The Ideal Cell Population for Cardiomyoplasty

Although recent advances in the field of cardiomyoplasty have been achieved with the advent of stem cell technology, the "ideal" population of cells that is able to engraft damaged myocardium and restore cardiac function effectively without improper differentiation to other contaminating cell types is still an issue of debate. Many cell types with the potential to repair the injured heart have been considered, including differentiated cells (fetal myocytes or satellite muscle cells) and undifferentiated cells (embryonic or adult stem cells).

Although pluripotent embryonic stem cells offer the promise of functional plasticity and the ability to differentiate into any cell type in vitro, extensive experimentation in vivo is still necessary to direct the formation of integrated, functional cardiac tissue properly at the site of injury without improper differentiation to form teratomas or other noncardiac cell types. Multipotent tissue-specific cells that have already committed to a distinct lineage, such as hematopoietic stem cells, mesenchymal stem cells, and endothelial progenitor cells, have also pro-

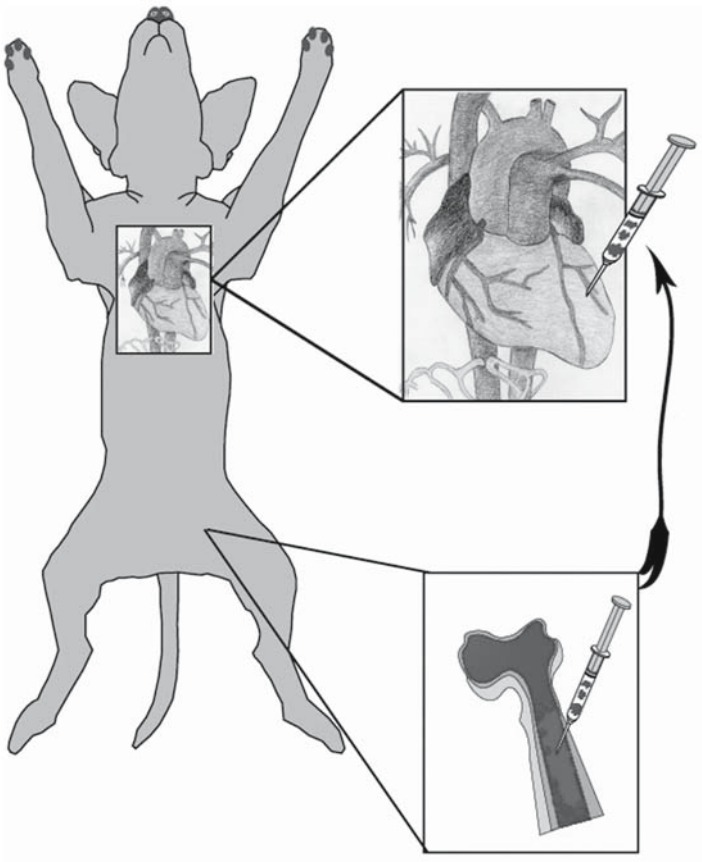

Fig. 14. Canine model for bone marrow-derived multipotent stem cell cardiomyoplasty. Medical art provided by Kathy B. Nichols.

duced encouraging results *(59)*. However, to date, the use of these cells often results in incomplete engraftment and a failure to restore cardiac function over time *(60)*. Regardless of the cell type used in cardiomyoplasty, it is clear that animal models will again play a crucial role in the translational research that will be necessary to advance this theory out of the lab and into clinical practice.

9.2. Animal Models for Stem Cell Research

Although multiple animal species have been used for the study of cellular cardiomyoplasty, most investigators have chosen acute ischemia as their experimental model of choice. However, although effective treatment options for acute ischemia do exist, only limited options are available for chronic myocardial ischemia. This observation strongly suggests that further development of the chronic ischemia models using cardiomyoplasty is warranted. As with most research, the experimental hypothesis will remain fundamental in choosing the correct animal model. However, the availability of appropriate stem cell lines in the desired species will add additional limitations. Fully characterizing cell lines is important and advantageous so that functional changes of the therapy are correctly attributed to the appropriate precursor cell.

The multiple types of stem cells available for the rodent, specifically the rat and mouse, have made small animal models effective for investigations of stem cell engraftments. However, the differences in myocardial perfusion and ventricular thickness may confer differences in nutrient supplies that would support engraftment in small animal models, but may not be translatable to humans.

Ultimately, large animal models that better approximate the diseased human heart will be required to assess fully stem cell engraftment, differentiation, or functional improvement. Large animal models generally are considered better suited for assessment of myocardial function via angiography, echocardiography, or MRI; however, the limited availability of appropriate stem cell lines for use in these models has prevented the widespread use of large animal models.

Nevertheless, stem cell lines are currently under development for the pig, dog, and monkey at the University of Minnesota. More specifically, one laboratory has developed a canine model of cardiomyoplasty for chronic ischemia in which bone marrow-derived stem cells are used (Fig. 14). We have demonstrated successful engraftment (8%) and statistically significant sustained long-term improvement in regional myocardial function by MRI follow-up. Although successful, this first effort has resulted in more questions: How should we deliver cells? When should we deliver the cells? How many cells should be delivered? How often should we deliver cells? Much work has yet to be completed before it can be certain that stem cell therapies can be considered a viable treatment for various forms of myocardial disease.

9.3. Stem Cell Delivery Methods

Multiple methods of stem cell delivery have been investigated, including direct myocardial injection, peripheral transfusion, and stem cell mobilization *(61)*. Direct epicardial myocardial injection can be fairly consistently completed intraoperatively during procedures such as coronary arterial bypass or valve operations. Endocardial injection will likely be completed using commercially available radiographic guided stem cell injection catheters (Fig. 15). Both transfusion and mobilization of resident stem cells offer the least invasive means of stem cell delivery. However, this requires the availability of effective homing signals to direct the correct location for engraftment. This last hurdle could possibly be overcome using guided direct myocardial injections, either surgically or via interventional catheter techniques.

Currently, we believe that multiple stem cell injections may be required to achieve full myocardial regeneration for therapeutic repair. As a result, the use of stem cell injection catheters may become the standard of practice. In addition, advanced imaging techniques such as MRI may allow localization of injured myocardium and direct, in real time, the stem cell injection catheters in the damaged area.

9.4. Stem Cell Engraftment Issues

The ability to track the implanted cell is critical not only to assess the potential of engraftment, but also later to determine differentiation and incorporation into the native tissue. Multiple techniques of cell labeling are currently under investigation, including the use of viral gene transduction (e.g., 4',6-diamidino-2-phenylindole [DAPI], green fluorescent gene, *Lac Z*), incorporation of dyes, and the use of metallic microparticles *(62,63)*.

For example, gene insertion can be fairly easily accomplished (i.e., allowing for fluorescence microscopy or Q-PCR identification of the stem cell). However, the exact insertion site into the deoxyribonucleic acid (DNA) of the cell cannot currently be well controlled, introducing the possibility for nonexpression of the gene or potential disruption of normal cellular transcription and translation processes. The use of dyes incorporated into the cells by pinocytosis has been reported. The primary disadvantage of this technique has been the potential for dye incorporation into native cells in vivo. The use of metallic microparticles has received attention in that such particles may allow real-time identification of cells by MRI imaging and later pathologically by staining. However, information about the potential disruption of cellular function and possible uptake in vivo by native cells has yet to be elucidated fully.

9.5. Functional Assessment of Stem Cell Therapies

Many efforts to demonstrate improvement in cardiac function following cellular cardiomyoplasty have been undertaken. Methods include pressure measurements, ultrasonic microcrystal placement, echocardiography, and MRI. Regardless of the specific method used by the investigators, minimal significant long-term follow-up studies currently exist in the literature. Thus, we conclude that much more research is required before this theory should be applied to humans.

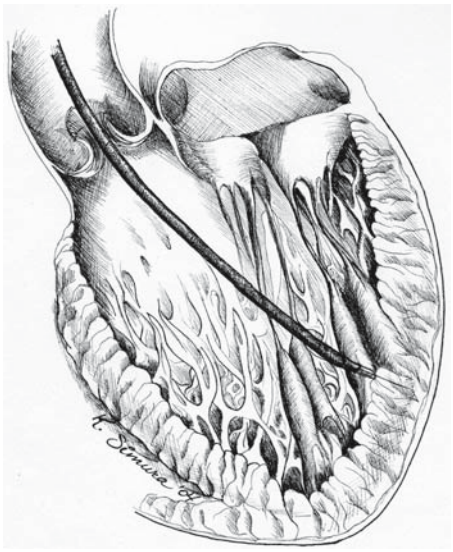

Fig. 15. Catheter-guided stem cell therapy for myocardial infarction. With permission from Katarzyna Simura.

10. SUMMARY

In preparing to embark on a preclinical study of a new cardiovascular device, procedure, drug, or therapy, it is important to select the animal model carefully. This can be done in consultation with your institutional animal care and use committee or by collaboration with a principal investigator. Proper selection of the animal model in the protocol development will allow justification for animal use and maximize the chances for a successful research outcome. New cardiovascular technologies will continue to be introduced in an environment of increasingly tighter regulations for human safety. Correspondingly, the animal model will continue to be important for testing these new therapies before they are applied in clinical studies.

Consultation with experienced centers of experimental research is recommended for additional assistance in preparing research protocols and completing the research necessary in preclinical studies. The Experimental Surgical Services Department at the University of Minnesota provides such a service and is widely used for assessment of techniques and devices in the medical industry.

VISIBLE HEART® CD

Application of the isolated heart model.

REFERENCES

1. Institute of Laboratory Animal Resources, TNRC, and the National Academy of Sciences. (1996, March) *Guide for the Care and Use of Laboratory Animals*. National Academy Press, Wahington, DC.
2. Gross, D.R. (ed.) (1994) *Animal Models in Cardiovascular Research,* 2nd Ed. Kluwer Academic, Dordrecht, The Netherlands, p. 494.
3. Ettinger, S.J. (2000) Congenital heart diseases, in *Textbook of Veterinary Internal Medicine*. Saunders, Philadelphia, PA, pp. 737–787.
4. Haworth, R.A., et al. (1983) Metabolic cost of the stimulated beating of isolated adult rat heart cells in suspension. *Circ Res*. 52, 342–351.

5. Spieckermann, P.G. and Piper, H.M. (1985) Oxygen demand of calcium-tolerant adult cardiac myocytes. *Basic Res Cardiol*. 80, 71–74.
6. Claycomb, W.C., et al. (1998) HL-1 cells: a cardiac muscle cell line that contracts and retains phenotypic characteristics of the adult cardiomyocyte. *Proc Natl Acad Sci USA*. 95, 2979–2984.
7. Niggli, E. (1988) A laser diffraction system with improved sensitivity for long-time measurements of sarcomere dynamics in isolated cardiac myocytes. *Pflugers Arch*. 411, 462–468.
8. Roos, K.P., Brady, A.J., and Tan, S.T. (1982) Direct measurement of sarcomere length from isolated cardiac cells. *Am J Physiol*. 242, H68–H78.
9. Roos, K.P. and Brady, A.J. (1982) Individual sarcomere length determination from isolated cardiac cells using high-resolution optical microscopy and digital image processing. *Biophys J*. 40, 233–244.
10. Murphy, M.P., et al. (1982) Release of enzymes from adult rat heart myocytes. *Circ Res*. 51, 560–568.
11. Tung, L. (1986) An ultrasensitive transducer for measurement of isometric contractile force from single heart cells. *Pflugers Arch*. 407, 109–115.
12. Chinchoy, E., et al. (2000) Isolated four-chamber working swine heart model. *Ann Thorac Surg*. 70, 1607–1614.
13. Hill, A.J., Coles, J.A., Sigg, D.C., Laske, T.G., and Iaizzo, P.A. (2003) Images of the human coronary sinus ostium obtained from isolated working hearts. *Ann Thorac Surg*. 76, 2108.
14. Neely, J.R., Liebermeister, H., and Morgan, H.E. (1967) Effect of pressure development on membrane transport of glucose in isolated rat heart. *Am J Physiol*. 212, 815–822.
15. Wicomb, W.N., Cooper, D.K., and Barnard, C.N. (1982) Twenty-four-hour preservation of the pig heart by a portable hypothermic perfusion system. *Transplantation*. 34, 246–250.
16. Dunphy, G., et al. (1999) The effects of mannitol, albumin, and cardioplegia enhancers on 24-h rat heart preservation. *Am J Physiol*. 276, H1591–H1598.
17. Menasche, P., et al. (1993) Efficacy of lactobionate-enriched cardioplegic solution in preserving compliance of cold-stored heart transplants. *J Heart Lung Transplant*. 12, 1053–1061.
18. Taylor, D.E. and Whamond, J.S. (1975) A method of producing graded stenosis of the aortic and mitral valves in sheep for fluid dynamic studies. *J Physiol*. 244, 16P–17P.
19. Su-Fan, Q., et al. (1984) A new technique for producing pure aortic stenosis in animals. *Am J Physiol*. 246, H296–H301.
20. Rogers, W.A., Bishop, S.P., and Hamlin, R.L. (1971) Experimental production of supravalvular aortic stenosis in the dog. *J Appl Physiol*. 30, 917–920.
21. Spratt, J.A., et al. (1983) Experimental mitral regurgitation. Physiological effects of correction on left ventricular dynamics. *J Thorac Cardiovasc Surg*. 86, 479–489.
22. Swindle, M.M. and Adams, R.J. (eds.) (1988) *Experimental Surgery and Physiology: Induced Animals Models of Human Disease*. Williams and Wilkins, Philadelphia, PA.
23. Bianco, R.W., et al. (1986) Canine model for long-term evaluation of prosthetic mitral valves. *J Surg Res*. 41, 134–140.
24. Grehan, J.F., et al. (2000) Development and evaluation of a swine model to assess the preclinical safety of mechanical heart valves. *J Heart Valve Dis*. 9, 710–719; discussion 719–720.
25. Barnhart, G.R., et al. (1982) Bioprosthetic valvular failure. Clinical and pathological observations in an experimental animal model. *J Thorac Cardiovasc Surg*. 83, 618–631.
26. Sands, M.P., et al. (1969) An anatomical comparison of human pig, calf, and sheep aortic valves. *Ann Thorac Surg*. 8, 407–414.
27. Salerno, C.T., Droel, J., and Bianco, R.W. (1998) Current state of in vivo preclinical heart valve evaluation. *J Heart Valve Dis*. 7, 158–162.
28. Gallegos, R.P., Wang, X., Clarkson, C., Jerosch-Herold, M., and Bolman, R.M. (2003) *Serum Troponin Level Predicts Infarct Size, in American Heart Association*. American Heart Association, San Antonio, TX.
29. Verdouw, P.D., et al. (1998) Animal models in the study of myocardial ischaemia and ischaemic syndromes. *Cardiovasc Res*. 39, 121–135.
30. McFalls, E.O., et al. (1997) Regional glucose uptake within hypoperfused swine myocardium as measured by positron emission tomography. *Am J Physiol*. 272, H343–H349.
31. Headrick, J.P., et al. (1996) Interstitial adenosine and cellular metabolism during beta-adrenergic stimulation of the in situ rabbit heart. *Cardiovasc Res*. 31, 699–710.
32. Massie, B.M., et al. (1994) Myocardial metabolism during increased work states in the porcine left ventricle in vivo. *Circ Res*. 74, 64–73.
33. Lie, J.T., et al. (1971) New histochemical method for morphologic diagnosis of early stages of myocardial ischemia. *Mayo Clin Proc*. 46, 319–327.
34. Winkler, B.S., Binz, K., and Schaper, W. (1984) Myocardial blood flow and infarction in rats, guinea pigs, and rabbits. *J Mol Cell Cardiol*. 16, 48.
35. Kirklin, J.K., Young, J.B., and McGiffin, D. (eds.) (2002) *Heart Transplantation*. Churchill Livingstone, New York, NY, p. 883.
36. Wicomb, W., et al. (1982) Orthotopic transplantation of the baboon heart after 20 to 24 hours' preservation by continuous hypothermic perfusion with an oxygenated hyperosmolar solution. *J Thorac Cardiovasc Surg*. 83, 133–140.
37. Tsutsumi, H., et al. (2001) Cardiac transplantation following a 24-h preservation using a perfusion apparatus. *J Surg Res*. 96, 260–267.
38. Fischel, R.J., et al. (1992) Cardiac xenografting in the pig-to-rhesus monkey model: manipulation of antiendothelial antibody prolongs survival. *J Heart Lung Transplant*. 11, 965–973; discussion 973–974.
39. Langman, L.J., et al. (1997) Pharmacodynamic monitoring of mycophenolic acid in rabbit heterotopic heart transplant model. *Ther Drug Monit*. 19, 146–152.
40. Beschorner, W.E., et al. (2003) Heart xenograft survival with chimeric pig donors and modest immune suppression. *Ann Surg*. 237, 265–272.
41. Perrault, L.P., et al. (2002) Comparison of coronary endothelial dysfunction in the working and nonworking graft in porcine heterotopic heart transplantation. *Transplantation*. 74, 764–772.
42. Ono, K. and Lindsey, E.S. (1969) Improved technique of heart transplantation in rats. *J Thorac Cardiovasc Surg*. 57, 225–229.
43. Swindle, M.M., et al. (1986) Anatomic and anesthetic considerations in experimental cardiopulmonary surgery in swine. *Lab Anim Sci*. 36, 357–361.
44. Kozlowski, T., et al. (1999) Porcine kidney and heart transplantation in baboons undergoing a tolerance induction regimen and antibody adsorption. *Transplantation*. 67, 18–30.
45. Goddard, M.J., et al. (2002) Histopathology of cardiac xenograft rejection in the pig-to-baboon model. *J Heart Lung Transplant*. 21, 474–484.
46. DeBault, L., et al. (1992) Ultrastructural features in hyperacutely rejected baboon cardiac allografts and pig cardiac xenografts. *Transplant Proc*. 24, 612–613.
47. Brenner, P., et al. (2000) Technique of immunoapheresis in heterotopic and orthotopic xenotransplantation of pig hearts into cynomolgus and rhesus monkeys. *Transplant Proc*. 32, 1087–1088.
48. Kurlansky, P.A., et al. (1987) Comparable survival of intra-species and cross-species primate cardiac transplants. *Transplant Proc*. 19, 1067–1071.
49. Lambrigts, D., Sachs, D.H., and Cooper, D.K. (1998) Discordant organ xenotransplantation in primates: world experience and current status. *Transplantation*. 66, 547–561.
50. Wiener, A.S., Socha, W.W., and Moor-Jankowski, J. (1974) Homologous of the human A-B-O blood groups in apes and monkeys. *Haematologia (Budap)*. 8, 195–216.
51. Kroshus, T.J., et al. (1995) Complement inhibition with an anti-C5 monoclonal antibody prevents acute cardiac tissue injury in an ex vivo model of pig-to-human xenotransplantation. *Transplantation*. 60, 1194–1202.
52. Salerno, C.T., et al. (2002) A soluble chimeric inhibitor of C3 and C5 convertases, complement activation blocker-2, prolongs graft survival in pig-to-rhesus monkey heart transplantation. *Xenotransplantation*. 9, 125–134.
53. Cramer, D.V., Podesta, L., and Makowka, L. (1994) *Handbook of Animal Models in Transplantation Research*. CRC Press, Boca Raton, FL, p. 352.

54. Li, X., Bai, J., and He, P. (2002) Simulation study of the Hemopump as a cardiac assist device. *Med Biol Eng Comput*. 40, 344–353.
55. Snyder, T.A., et al. (2002) Platelet activation, aggregation, and life span in calves implanted with axial flow ventricular assist devices. *Ann Thorac Surg*. 73, 1933–1938.
56. Mussivand, T., et al. (1989) In vitro and in vivo performance evaluation of a totally implantable electrohydraulic left ventricular assist system. *ASAIO Trans*. 35, 433–435.
57. Reffelmann, T., et al. (2003) Cardiomyocyte transplantation into the failing heart-new therapeutic approach for heart failure? *Heart Fail Rev*. 8, 201–211.
58. Reffelmann, T. and Kloner, R.A. (2003) Cellular cardiomyoplasty—cardiomyocytes, skeletal myoblasts, or stem cells for regenerating myocardium and treatment of heart failure? *Cardiovasc Res*. 58, 358–368.
59. Reffelmann, T., et al. (2003) Transplantation of neonatal cardiomyocytes after permanent coronary artery occlusion increases regional blood flow of infarcted myocardium. *J Mol Cell Cardiol*. 35, 607–613.
60. Sakai, T., et al. (2002) The use of ex vivo gene transfer based on muscle-derived stem cells for cardiovascular medicine. *Trends Cardiovasc Med*. 12, 115–120.
61. Hill, J.M., et al. (2003) Serial cardiac magnetic resonance imaging of injected mesenchymal stem cells. *Circulation*. 108, 1009–1014.
62. Kraitchman, D.L., et al. (2003) In vivo magnetic resonance imaging of mesenchymal stem cells in myocardial infarction. *Circulation*. 107, 2290–2293.
63. Kraitchman, D.L., et al. (2003) Quantitative ischemia detection during cardiac magnetic resonance stress testing by use of FastHARP. *Circulation*. 107, 2025–2030.

22 Cardiac Arrhythmias and Transcatheter Ablation

FEI LÜ, MD, PhD, SCOTT SAKAGUCHI, MD, AND DAVID G. BENDITT, MD

CONTENTS

1. INTRODUCTION

The normal heartbeat is initiated by specialized cardiac cells (so-called pacemaker cells) located in the right atrium adjacent to its junction with the superior vena cava. These cells make up a specialized, albeit somewhat diffuse, region of the right atrium called the sinus node.

The rate and regularity of activity in the sinus node (the cardiac pacemaker) is determined by both the intrinsic firing rate (automaticity) of the cells within the node and the influence of extrinsic factors on these cells, including autonomic neural tone, electrolytes, and drugs. The usual range of resting sinus rate is 60–100 beats per minute (beats/min), although rates as low as 40 beats/min are common in fit individuals; most average adults have resting rates in the range of 60–70 beats/min. *Bradycardia* (slow heart beat) is a term used to refer to any heart rate less than 60 beats/min, and *tachycardia* (fast heart beat) describes heart rates greater than 100 beats/min.

Bradycardia is usually the result of either "sick sinus syndrome" (otherwise known as sinus node dysfunction) or atrioventricular conduction block (i.e., intermittent or permanent block of impulse transmission from the site of normal pacemaker activity in the atria through the specialized cardiac conduction system to the ventricles). These conditions can be caused by either intrinsic disease of the pacemaker cell region or conduction system tissue or extrinsic factors such as drugs or autonomic system disturbances.

The mechanisms underlying tachycardia are more numerous and complex than those that cause bradycardia. Nevertheless, tachycardias can be classified as caused by abnormally rapid impulse initiation (i.e., abnormal automaticity from the sinus node region or other subsidiary or abnormal pacemaker sites) or abnormal impulse conduction (Table 1).

The term *arrhythmia* is mainly used to refer to disturbances of the normal heart rhythm. An exception to this rule is sinus arrhythmia, which refers to the healthy variation of the sinus rhythm associated with physiological alteration of neural influence on pacemaker automaticity. The most important cause of the sinus rhythm variation is the respiratory cycle, but other factors such as beat-to-beat changes in cardiac output (i.e., ventriculophasic sinus arrhythmia) may also contribute.

Although arrhythmias can occur in clinically normal hearts, they are more commonly associated with structural heart diseases. Myocardial ischemia is the most important of these diseases in the Western world, but other forms of cardiac dysfunction such as cardiomyopathies, valvular heart disease, and certain genetically determined disorders (e.g., long QT syndrome, Brugada syndrome) must also be considered. In certain

From: *Handbook of Cardiac Anatomy, Physiology, and Devices*
Edited by: P. A. Iaizzo © Humana Press Inc., Totowa, NJ

Table 1
Mechanisms of Tachycardias

- ❖ Abnormal impulse initiation
  - Automaticity
    - ♦ Enhanced normal automaticity, as seen in inappropriate sinus tachycardia and some idiopathic ventricular tachycardias
    - ♦ Abnormal automaticity, as presumed to be the case in ectopic atrial tachycardia, accelerated junctional rhythm, and possibly certain idiopathic ventricular tachycardias
  - Triggered activity
    - ♦ Early after-depolarization, as presumed to be the case in torsades de pointes
    - ♦ Delayed after-depolarization, as seen in digitalis-induced arrhythmias or presumed to occur in certain exercise-induced arrhythmias
- ❖ Abnormal impulse conduction
  - Ectopic escape after block, such as junctional escape
  - Unidirectional block and reentry
    - ♦ Orderly reentry (macroreentry and microreentry)
    - ♦ Random reentry, as seen in atrial fibrillation
  - New concepts (reflection, phase 2 reentry, and anisotropic reentry)

regions of the world, infections remain an important cause of heart rhythm disturbance. Most important among these are rheumatic heart disease, common in the Far East, and Chagas disease in South America. In Western countries, myocarditis or pericarditis (most commonly of viral etiology) are occasionally associated with arrhythmias.

The clinical presentation of cardiac arrhythmias ranges from completely asymptomatic or inducing mild symptoms (palpitations and anxiety), to syncope and sudden cardiac death; the impact is largely dependent on arrhythmia-induced hemodynamic changes. The electrophysiological and hemodynamic consequences of a particular arrhythmia are primarily determined by the ventricular rate and duration, the site of origin, and the underlying cardiovascular status (i.e., severity of associated heart and vascular disease).

Many arrhythmias can be readily diagnosed from standard 12-lead electrocardiography (ECG). However, other diagnostic techniques are frequently required for a more precise diagnosis, including prolonged rhythm monitoring (an event monitor, Holter monitor, or implantable recorder) and electrophysiological testing. Exercise stress tests and signal-averaged ECGs may also be used in the assessment regarding the nature of an arrhythmia or susceptibility of the patient to elicit an arrhythmia. Other techniques (such as analysis of heart rate variability, baroreflex sensitivity, assessment of QT dispersion, T-wave alternans, and body surface potential mapping) have provided some useful research information, but their value in daily practice remains to be defined fully at this time.

The clinical goals in the treatment of arrhythmias are twofold: to alleviate symptoms for improved quality of life and to prolong survival. Pharmacological treatment has been the mainstay for the management of cardiac arrhythmias, although in recent years implantable devices and ablation have become increasingly important. Regarding antiarrhythmic drugs, many clinicians find it convenient to categorize them according to the Vaughn-Williams scheme. This classification is simple and has been widely used clinically because it offers a means to keep the principal pharmacological effects of drugs in mind (Table 2). A more comprehensive classification of antiarrhythmic drugs, called the Sicilian Gambit, was introduced in 1991 *(1)* and is based on a more widespread consideration of the cellular basis of drug actions. However, neither classification system offers much help in the treatment of specific arrhythmias. Selection of antiarrhythmic drugs for patients should be individualized based on their specific antiarrhythmic and proarrhythmic actions, the arrhythmia treated, and the nature and severity of any underlying heart diseases.

In patients with ischemia or left ventricular dysfunction of other etiologies, class I agents should be avoided because of their proarrhythmic risk. Class III drugs (i.e., amiodarone, dofetilide), on the other hand, appear to have a neutral effect on survival in these patients. It appears that β-blockers (class II) are the only drugs that have been proven to prolong survival in patients with structural heart disease. Nevertheless, nonpharmacological interventions, such as catheter ablation for supraventricular tachycardias and implantable cardioverter–defibrillators for primary and secondary prevention of sudden cardiac death, are considered the treatments of choice in many clinical settings.

2. TACHYARRHYTHMIAS

2.1. Premature Complexes

Ectopic premature beats may originate from the atria, the atrioventricular junction, and the ventricles. Treatment of premature complexes is usually not necessary. If symptomatic, precipitating factors such as alcohol, tobacco, and caffeine should be identified and then eliminated. Although anxiolytic agents and β-blockers may be used in such cases, they are often problematic in terms of side effects. Other antiarrhythmic drugs may be used depending on the severity of symptoms and underlying cardiac disease, but avoidance of such drugs is the preferred strategy.

Table 2
Vaughn-Williams Classification [a]

- Class I: sodium channel blockers
  - Class Ia: drugs that reduce V_{max} (phase 0 upstroke of action potential) and prolong action potential duration, such as quinidine, procainamide, and disopyramide
  - Class Ib: drugs that do not reduce V_{max} and shorten action potential duration, such as lidocaine, mexiletine, and phenytoin
  - Class Ic: drugs that predominantly slow conduction, moderately reduce V_{max}, and minimally prolong refractoriness, such as flecainide, propafenone, and moricizine
- Class II: β-adrenergic receptor blockers
  - β-blockers may be cardio- or β1-selective drugs such as atenolol, esmolol, and metoprolol or noncardioselective such as carvedilol, pindolol, and propranolol
  - Some (acebutolol, bucindolol, and pindolol) exert intrinsic sympathomimetic activity
  - Some have quinidinelike membrane-stabilizing activity (acebutolol, carvedilol, and propranolol)
  - D-Sotalol has strong class III effects and has been regarded as a class III agent in many conditions
- Class III: potassium channel blockers that prolong refractoriness, such as amiodarone, bretylium, dofetilide, ibutilide, and sotalol; amiodarone has all the four class effects.
- Class IV: calcium channel blockers
  - Dihydropyridine (almodipine and nefedipine)
  - Nondihydropyridine drugs (diltiazem and verapamil)

[a]As discussed in the text, the utility of this classification in terms of selection of therapy is limited, but the groupings permit important toxicity issues to be more readily acknowledged, an important factor in choosing drugs for individual patients.

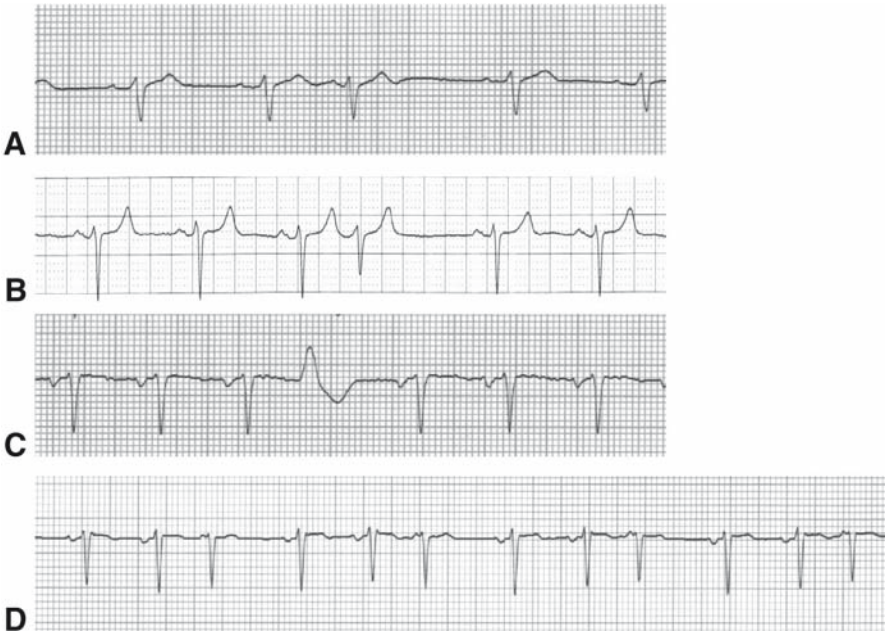

Fig. 1. **(A)** Atrial, **(B)** junctional, **(C)** ventricular premature complexes, and **(D)** multifocal atrial tachycardia.

2.1.1. Atrial Premature Complexes

Atrial premature complexes are recognized during the ECG exam as early P waves, with a P-wave morphology different from that of the sinus P wave (Fig. 1A). The premature P wave is often superposed in the preceding T wave; the T wave preceding a premature beat should be carefully compared to other T waves to see if there may be any buried P waves. Atrial premature complexes can conduct to the ventricles with a normal PR interval when atrioventricular junctions are not refractory or with prolonged PR intervals when atrioventricular junctions are in their relative refractory periods or blocked when atrioventricular junctions are in their effective refractory periods. They almost always enter into the sinus node region and reset the sinus cycle length, resulting in an incomplete compensatory pause (the sum of preatrial and postatrial premature complex intervals is less than that of two normal sinus PP intervals). Atrial premature complexes are frequently found in normal patients and are thus usually asymptomatic. Treatment is usually not necessary.

2.1.2. Multifocal Atrial Tachycardia

Multifocal atrial tachycardia, also called chaotic atrial tachycardia, is characterized by atrial rates between 100 and 130 beats/min, with marked variations in P-wave morphology (arbitrarily defined as at least three P-wave contours). They often manifest as short bursts of tachycardia (Fig. 1D). Treatment is primarily directed toward underlying disorders and is followed by β-blockers if necessary. Verapamil (class IV) or amiodarone may be considered as a second-line therapy. Amiodarone may be predicted as the most effective drug in this setting, but its multiple side effects (particularly pulmonary effects) are of concern because many patients with multifocal atrial tachycardia already have significant underlying pulmonary problems.

2.1.3. Atrioventricular Junctional Premature Complexes

Atrioventricular junctional premature complexes are recognized on the ECG as normal QRS complexes without a preceding P wave (Fig. 1B). Retrograde P waves (inverted in leads II and III and aVF) may be seen after the QRS complexes. Such complexes are less common and often associated with drug intoxication and cardiac diseases. Most junctional beats have an incomplete compensatory pause. Occasionally, a junctional premature beat may fail to conduct to either the atria or the ventricle (concealed junctional beats), but results in usual refractoriness in the atrioventricular junction and blocks subsequent supraventricular beats.

2.1.4. Ventricular Premature Complexes

Ventricular premature complexes are recognized as wide and bizarre QRS complexes not preceded by P waves (Fig. 1C). They often fail to conduct retrogradely to the atria because of poor retrograde (i.e., ventriculoatrial) conduction properties in the diseased hearts of patients who most often manifest such complexes. Thus, ventricular premature complexes do not typically reset the sinus node, and they result in a fully compensatory pause (the sum of pre- and postatrial premature complex intervals equals that of two normal sinus PP intervals). Interpolated ventricular premature complexes do not influence the following sinus beats (i.e., their occurrence is timed so as not to impair the next sinus beat from reaching the ventricles at the expected moment).

They may occur singly, in patterns of bigeminy (sinus beat and ventricular premature complex alternating) and trigeminy (two sinus beats followed by a ventricular premature complex), or couplets or pairs (two consecutive ventricular premature complexes) and nonsustained ventricular tachycardia (arbitrarily defined as three or more consecutive ventricular premature complexes at a rate exceeding 100 beats/min). Their morphology may be monomorphic (uniform) or polymorphic (multiform).

Ventricular premature complexes often bear a fixed coupling interval (between the onset of ventricular premature complex and the onset of its preceding sinus QRS complex). When there is a protected ventricular ectopic focus, the focus is constantly firing without resetting by a sinus beat and thus results in ventricular parasystole. Ventricular parasystole can manifest with varying coupling intervals, whereas the interventricular premature complex intervals remain relatively fixed (i.e., variation <120 ms).

Importantly, the relationship of ventricular premature complexes to sudden cardiac death is poorly defined, but it has been suggested that frequent ventricular premature complexes (>5–10/min) are associated with an increased risk for sudden cardiac death. However, it has been reported that the suppression of ventricular premature complexes using antiarrhythmic drugs does not reduce the risk of sudden cardiac death in patients following myocardial infarction *(2,3)*. At this time, treatment of ventricular premature complexes is primarily aimed at symptomatic alleviation rather than at prolongation of survival.

2.2. Sinus Tachycardias

2.2.1. Physiological Sinus Tachycardia

Physiological sinus tachycardia represents a normal response to a variety of physiological conditions (anxiety and exercise) and pathological stresses (fever, hypotension, thyrotoxicosis, hypoxemia, and congestive heart failure). Sinus tachycardia rarely exceeds 200 beats/min; it should not be treated for itself, but its causes must be explored (e.g., exercise, fever, anemia, hyperthyroidism), and some of these (e.g., fever, anemia, hyperthyroidism) may require therapy.

2.2.2. Inappropriate Sinus Tachycardia

Inappropriate sinus tachycardia is characterized by an increased resting heart rate (>100 beats/min) and an exaggerated heart rate response to minimal stress, usually associated with markedly distressing symptoms (palpitations, fatigue, anxiety, and shortness of breath). The etiologies and underlying mechanisms are unclear. Care must be taken in diagnosing inappropriate sinus tachycardia to exclude secondary sinus tachycardia and to correlate symptoms with tachycardia. Electrophysiological study can be used to exclude atrial tachycardia located close to the sinus node. β-Blockers and calcium channel blockers can be used to treat inappropriate sinus tachycardia, although often with imperfect results. Radiofrequency modification of the sinus node may be considered if drug therapy fails.

2.3. Paroxysmal Supraventricular Tachycardias

Paroxysmal supraventricular tachycardias are a group of supraventricular tachycardias with sudden onset and termination. They are usually recurrent.

2.3.1. Sinus Nodal Reentry Tachycardia

Sinus nodal reentry tachycardia is relatively rare (accounting for approx 3% of all paroxysmal supraventricular tachycardias) and tends to occur mainly in older individuals with other manifestations of sinus node disease. The average rate of sinus nodal reentry tachycardia is 130–140 beats/min. Its P-wave morphology is identical, or very similar, to the sinus P wave. Vagal maneuvers can slow or terminate the tachycardia because it reenters within a region of the heart (i.e., the sinus node) that is heavily influenced by vagal (parasympathetic) nerve endings. Sinus nodal reentry tachycardia should be suspected in anxiety-related sinus tachycardia. β-Blockers and calcium channel blockers (e.g., verapamil, diltiazem) as well as ablation are considered treatment options.

2.3.2. Atrial Tachycardias

Atrial tachycardias, sometimes also called "primary" atrial tachycardias, refer to those tachyarrhythmias that arise in atrial

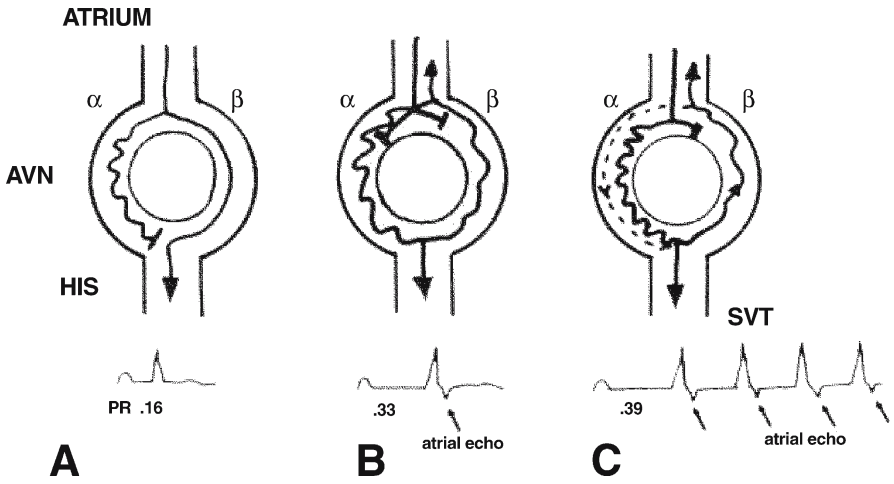

Fig. 2. Schema of the typical atrioventricular nodal (AVN) reentry tachycardia. The atrioventricular node has a slow pathway (α) with short refractoriness and a fast pathway (β) with long refractoriness. **(A)** During sinus rhythm, the impulse conducts the ventricles through the fast pathway, yielding a normal PR interval. The impulse simultaneously goes down the slow pathway, but cannot conduct to the His bundle antegradely or retrogradely to the fast pathway because it is rendered refractory by the prior beat conducted in the fast pathway. **(B)** An atrial premature complex reaches the effective refractory period of the fast pathway and is blocked in the fast pathway. This atrial premature complex is able to conduct slowly down to the slow pathway, yielding a prolonged PR interval. The delay in conduction over the slow pathway gives rise to enough time for the fast pathway to recover and allow the impulse conducted from the slow pathway to continue over the fast pathway retrogradely to the atria, producing an atrial echo beat. At the same time, the returned impulse tries to conduct down over the slow pathway and fails because of unrecovered refractoriness of the slow pathway. **(C)** A sufficiently early atrial premature complex occurs, producing a similar echo beat as in Fig. 2B. However, the returned impulse is able to conduct down over the slow pathway, repeatedly producing another ventricular beat and atrial echo (i.e., supraventricular tachycardia, SVT). Reprinted from ref. *4* with permission. © 1993, Lippincott, Williams, and Wilkins.

tissue because of abnormal automaticity or reentry phenomenon. They are classified separately from sinus node reentry or atrioventricular nodal reentry (*see* Section 2.3.3.) despite the fact that these tachyarrhythmias also arise in the atria. A typical atrial tachycardia has an atrial rate of 150–200 beats/min with a P-wave morphology different from that of sinus P wave. Atrial tachycardia accounts for 5–10% of all paroxysmal supraventricular tachycardias. Atrioventricular block may develop without interrupting the tachycardia. Atrial tachycardia may be caused by automaticity or triggered activity as well as reentry.

Automatic atrial tachycardia has the following features:

1. It cannot be initiated or terminated by atrial stimulation.
2. The first P wave of the tachycardia is the same as the subsequent P waves of the tachycardia.
3. Its rate is often accelerated after initiation until stabilized (at 100–175 beats/min), the so-called warm-up phenomenon.
4. A premature atrial stimulation can reset automatic atrial tachycardia with full or incomplete compensatory pause, usually accompanied by a constant return cycle.
5. Overdrive suppression is a hallmark of automaticity. Both reentrant and automatic atrial tachycardia can be corrected by ablation therapy.

2.3.3. Atrioventricular Nodal Reentry Tachycardia

Atrioventricular nodal reentry tachycardia is the most common of paroxysmal supraventricular tachycardias (elicited in 50–65% of such patients) and usually presents as a narrow QRS complex with regular rates between 120 and 250 beats/min. In the absence of Wolff-Parkinson-White syndrome, atrioventricular nodal reentry tachycardia and atrioventricular reentry tachycardia, using a concealed bypass tract, account for more than 90% of all paroxysmal supraventricular tachycardias.

A schematic representation of a typical atrioventricular nodal reentry circuit is shown in Fig. 2 *(4)*. Retrograde P waves may be absent and buried in the QRS complexes or appear as distortions at the terminal parts of the QRS complex. Atrioventricular nodal reentry tachycardia can be reproducibly initiated and terminated by appropriately timed atrial extrastimuli; this is routinely done as part of the diagnostic electrophysiological catheter evaluation of patients in whom this arrhythmia is suspected. Atrial premature complexes that initiate atrioventricular nodal reentry tachycardia are usually associated with a prolonged PR interval.

In intracardiac recordings, the onset of atrioventricular nodal reentry tachycardia is almost always associated with a prolonged AH interval, which produces sufficient conduction delay in the so-called slow atrioventricular nodal pathway (Fig. 2) to ensure recovery of the fast pathway and permit it to conduct retrogradely back toward the atrium, thereby completing the reentry circuit. A critical balance between conduction delay and recovery of refractoriness is required to sustain the tachycardia. Simultaneous conduction to the ventricles in an antegrade direction and to the atria in a retrograde direction often leads to the buried P wave in the QRS complex. The RP interval is therefore less than 80–100 ms in atrioventricular nodal reentry tachycardia. In contrast, in atrioventricular reentry tachycardia, ventricles and atria are activated sequentially, and the RP interval is expected to be longer than 80 ms on ECGs.

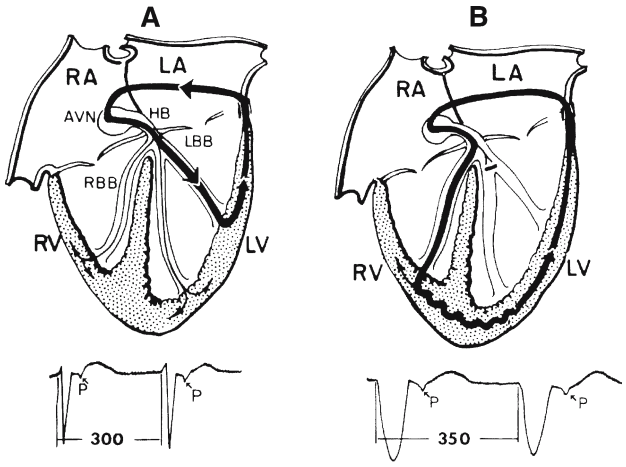

Fig. 3. **(A)** Atrioventricular reentry tachycardia using a left-sided concealed accessory pathway. **(B)** Left bundle branch block prolongs the tachycardia cycle length by 50 ms because of the conduction delay of the tachycardia circuit in the left ventricle. AVN, atrioventricular node; HB, His bundle; LA, left atrium; LBB, left bundle branch; LV, left ventricle; RA, right atrium; RBB, right bundle branch; RV, right ventricle. Reprinted from ref. *4* with permission. © 1993, Lippincott, Williams, and Wilkins.

Acute treatment of atrioventricular nodal reentry tachycardia includes: (1) vagal maneuvers (e.g., carotid sinus massage, Valsalva maneuver); (2) adenosine injection; (3) administration of verapamil, diltiazem, and/or (4) β-blockers; or electrical (direct current) cardio-version. Drugs used for longer term prevention of recurrences of atrioventricular nodal reentry tachycardia include digitalis (currently not often recommended because of low effectiveness), β-blockers, calcium channel blockers, and class Ia and Ic antiarrhythmic drugs. However, the most important advance in the treatment of atrioventricular nodal reentry tachycardia is transcatheter ablation (principally of the "slow"-pathway region). Catheter ablation, in experienced hands, cures atrioventricular nodal reentry tachycardia in almost 100% of cases.

2.3.4. Atrioventricular Reentry Tachycardia Using Concealed Accessory Pathway

Accessory conduction pathways remaining from embryonic development of the heart can create the substrate for reentry paroxysmal supraventricular tachycardia. The most common form of accessory pathway connects the atria to the ventricle (i.e., an accessory atrioventricular connection). This connection is made up of working muscle tissue, but is so small it is usually invisible, even during cardiac surgery. When these connections conduct in the antegrade direction (i.e., from atrium to ventricle), they necessarily modify the QRS configuration, usually by virtue of earlier-than-expected activation of part of the ventricular muscle (i.e., preexcitation). The classic case is the "delta" wave observed at the onset of the QRS in Wolff-Parkinson-White syndrome.

In some cases, accessory connections only conduct in the retrograde direction (i.e., ventricle to atrium). In these cases, there can be no ECG footprint because ventricular preexcitation does not occur (thus the term "concealed" accessory connections). Nevertheless, because retrograde conduction can occur, a reentry tachycardia is possible. This form of accessory pathway most often occurs on the left side of the heart. Atrioventricular reentry tachycardias account for approx 30% of all paroxysmal supraventricular tachycardias.

The impulse circulates antegradely through the atrioventricular node and retrogradely through the concealed accessory pathway (Fig. 3) *(4)*. Both the atria and ventricles are parts of the reentry circuit. Because atrial activation always follows ventricular activation, the P wave usually occurs after the QRS complexes (RP interval > 80 ms). Atrioventricular reentry tachycardia can be initiated and terminated by either atrial or ventricular extrastimuli. Even when the His bundle is refractory, a ventricular premature complex may be able to reset the atria through accessory pathways.

In contrast to the concentric atrial activation sequences in atrioventricular nodal reentry tachycardia, the atrial activation sequences in atrioventricular reentry tachycardia are eccentric when the accessory pathways are located away from atrioventricular node. Medical treatment of atrioventricular reentry tachycardia is similar to that of atrioventricular nodal reentry tachycardia.

Transcatheter ablation is highly effective for eliminating accessory atrioventricular connections. Utilized to correct the problem, mapping and ablation are currently effective in 95–99% of cases.

2.3.5. Wolff–Parkinson–White Syndrome

When there are one or more accessory atrioventricular pathways or connections that conduct in the antegrade direction, the ventricles are preexcited to a varying degree as discussed in Section 2.3.4. The Wolff-Parkinson-White syndrome is applied when tachyarrhythmias occur in the setting of preexcitation. Tachycardias associated with this syndrome include: (1) orthodromic (antegradely through normal atrioventricular conduction system and retrogradely through atrioventricular accessory pathways); (2) antedromic (antegradely through atrioventricular accessory pathways and retrogradely through normal atrioventricular conduction system or another accessory connection); and (3) atrial flutter/fibrillation (activating the ventricles antegradely through both normal atrioventricular conduction system and atrioventricular accessory pathways), as well as other supraventricular tachycardias.

The ECG features of a typical atrioventricular connection (Fig. 4) are: (1) shortened PR intervals less than 120 ms during sinus rhythm, (2) widened QRS durations, and (3) presence of delta waves (a slurred, slowly rising onset of the QRS). The terminal QRS portion is usually normal; sometimes, it is associated with secondary ST-T changes.

In addition to typical atrioventricular pathways, other variants may exist, such as atriohisian, atriofascicular, nodofascicular, and nodoventricular fibers. Lown-Guang-Levine syndrome is applied to recurrent paroxysmal tachycardias (or atrial fibrillation) associated with a short PR interval and a normal QRS complex. Its presumed mechanisms include atriohisian fibers, preferential intranodal pathways or enhanced atrioventricular conduction, and posterior intranodal pathways or an anatomically small atrioventricular node.

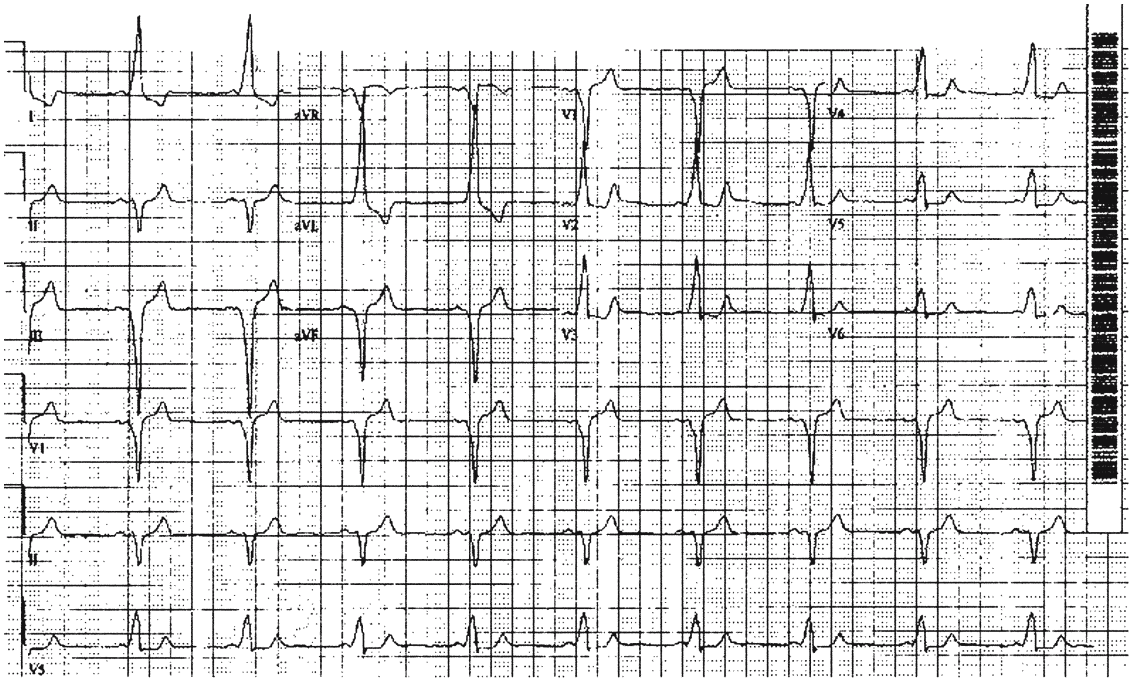

Fig. 4. Wolff-Parkinson-White syndrome with a right posterior septal accessory pathway. *See* text for discussion.

Mahaim fibers were initially recognized as a nodoventricular bypass tract and now include atriofascicular, nodofascicular, nodoventricular, and fasciculoventricular fibers. The majority of these pathways are long right-sided atriofascicular or atrioventricular pathways between the lateral tricuspid and distal right bundle branch in the right ventricular free wall. These fibers almost represent a duplication of the atrioventricular node and are considered capable of only antegrade conduction. Therefore, only "preexcited tachycardia" can result from Mahaim fibers. Often, preexcitation is not initially apparent, but can be exposed by premature right atrial stimulation. The ECG tends to exhibit a left bundle branch block type of morphology with a leftward frontal axis similar to that associated with right ventricular apical pacing.

As a rule, accessory pathways conduct faster than the atrioventricular node, but have a longer refractory period and are therefore prone to conduction block at longer cycle lengths (e.g., a premature beat will tend to block at a longer coupling interval than is the case for the atrioventricular node). Furthermore, accessory pathways do not usually manifest decremental conduction at faster pacing rates. An incessant form of supraventricular tachycardia has been recognized that is usually associated with a slow-conducting posteroseptal accessory pathway as its retrograde limb. The presence of an accessory pathway is not necessarily involved in the mechanism of tachycardia (a bystander). Atrioventricular echoes or atrioventricular reentry tachycardia may be present in 15–20% of patients after successful ablation of accessory pathways.

It is estimated that 10–35% of patients with preexcitation experience atrial fibrillation at some point in their life times. In fact, atrial fibrillation and atrial flutter may be the presenting arrhythmias in up to 20% of patients with accessory atrioventricular pathways. In patients with Wolff-Parkinson-White syndrome, atrial tachyarrhythmias that conduct extremely rapidly (via the accessory pathway) to the ventricles may lead to syncope, ventricular fibrillation, or sudden cardiac death. A grossly irregular RR interval with widened QRS complexes and extremely rapid ventricular rates should immediately suggest the presence of antegrade accessory atrioventricular pathway conduction associated with atrial fibrillation (Fig. 5).

Patients with atrial fibrillation in the presence of an accessory pathway are at increased risk of developing ventricular fibrillation if the shortest preexcited RR interval during atrial fibrillation is less than 250 ms. Intravenous procainamide is the acute treatment of choice for hemodynamically stable preexcited atrial fibrillation. Intravenous atrioventricular nodal blocking agents, such as digoxin and verapamil, are contraindicated in these patients because they may paradoxically enhance antegrade atrioventricular conduction via the accessory pathway conduction, resulting in hypotension or cardiac arrest. Patients who are hemodynamically unstable require immediate direct current cardioversion. As noted, it is likely that most episodes of atrial fibrillation may result from degeneration of orthodromic atrioventricular tachycardia (tachycardia-induced tachycardia). Successful ablation of the accessory atrioventricular pathway eliminates atrial fibrillation in most of these patients.

Radiofrequency ablation of the accessory pathway is the long-term (curative) treatment of choice for symptomatic patients with Wolff-Parkinson-White syndrome; it is safe and effective in more than 95–99% of patients.

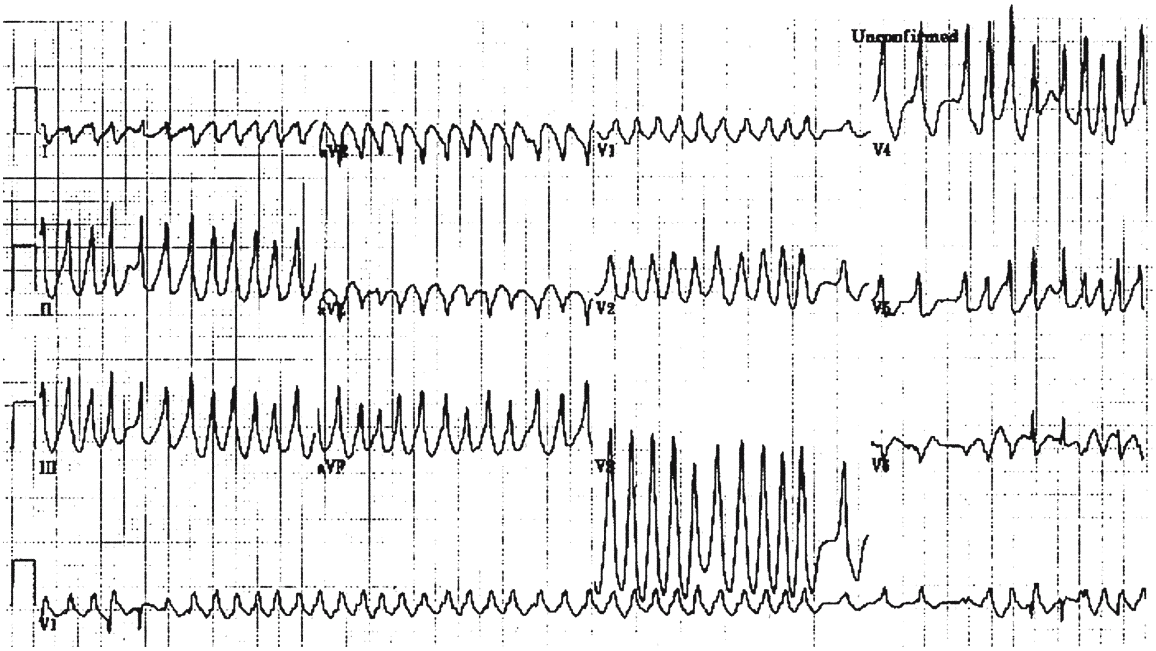

Fig. 5. Preexcited atrial fibrillation. *See* text for discussion.

2.4. Atrial Flutter and Fibrillation

2.4.1. Atrial Flutter

Atrial flutter is characterized by an atrial rate between 250 and 350 beats/min, usually accompanied by 2:1 atrioventricular conduction and resulting in a ventricular rate of approx 150 beats/min. Classical flutter waves (F waves) are regular sawtoothlike atrial activity, most prominent in inferior leads and V1. Atypical F waves may manifest like atrial tachycardia, with a rate between 200 and 300 beats/min in surface ECG, particularly with antiarrhythmic drug therapy. Some atrial flutter may be terminated by rapid atrial pacing (type I atrial flutter) and may not be pace terminable (type II atrial flutter) *(5)*. Although antiarrhythmic drugs may be useful to prevent recurrence of atrial flutter, they are less effective to convert to sinus rhythm. Direct current cardioversion is most effective for treatment of atrial flutter.

Typical atrial flutter is a macroreentrant rhythm confined to the right atrium. The tachycardia circulates around the atrium, but must pass through a relatively narrow isthmus of tissue between the inferior vena cava and the tricuspid valve annulus. Ablation creating conduction block in this isthmus is highly effective; as a result, typical atrial flutter can be easily ablated. Ablation is the treatment of choice in most of these patients. Although systemic embolization is less common in atrial flutter than in atrial fibrillation, anticoagulation in atrial flutter should follow the guidelines for the management of atrial fibrillation *(6)*.

2.4.2. Atrial Fibrillation

Atrial fibrillation is an uncoordinated atrial tachyarrhythmia characterized on ECG by the absence of distinct P-waves before each QRS complex, the presence of rapid atrial oscillations (F-waves), and variable RR intervals (Fig. 6). Paroxysmal atrial fibrillation is arbitrarily defined as lasting more than 2 min and less than 7 d and may be self-terminating in less than 48 h or persistent (lasting longer than 48 h). An episode of atrial fibrillation lasting longer than 7 d is termed *chronic*. If a number of attempts of cardioversion have failed or are not indicated in chronic forms (>1 yr), atrial fibrillation is regarded as permanent. When no history is available, the term *recent or new onset* is often used.

The incidence of atrial fibrillation is strongly age dependent, with a substantial increase of occurrences between the ages of 50 and 60 yr (6.2% in men and 4.8% in women 65 yr or older). In addition to age, other common cardiac precursors include a history of congestive heart failure, valvular heart disease, hypertension, and coronary artery disease. Yet, rheumatic heart disease, together with overt heart failure, is considered as the most powerful predictor for atrial fibrillation. Atrial fibrillation is also common following acute myocardial infarction (10%) or cardiac surgery (~35%), which is usually self-limited. Noncardiac precursors include thyrotoxicosis and pulmonary pathology leading to hypoxemia. Lone atrial fibrillation is said to be present when the tachyarrhythmia occurs in the absence of underlying structural heart disease or transient precipitating factors.

The mechanisms underlying atrial fibrillation include multiple-wavelet reentry and focal-enhanced automaticity. The atrial rate during atrial fibrillation ranges from 350 to 600 beats/min. Because of concealed atrioventricular nodal penetration and subsequent variable degrees of atrioventricular block, the characteristic irregularly irregular ventricular rate is usually between 100 and 160 beats/min in untreated patients with normal atrioventricular conduction properties. Both

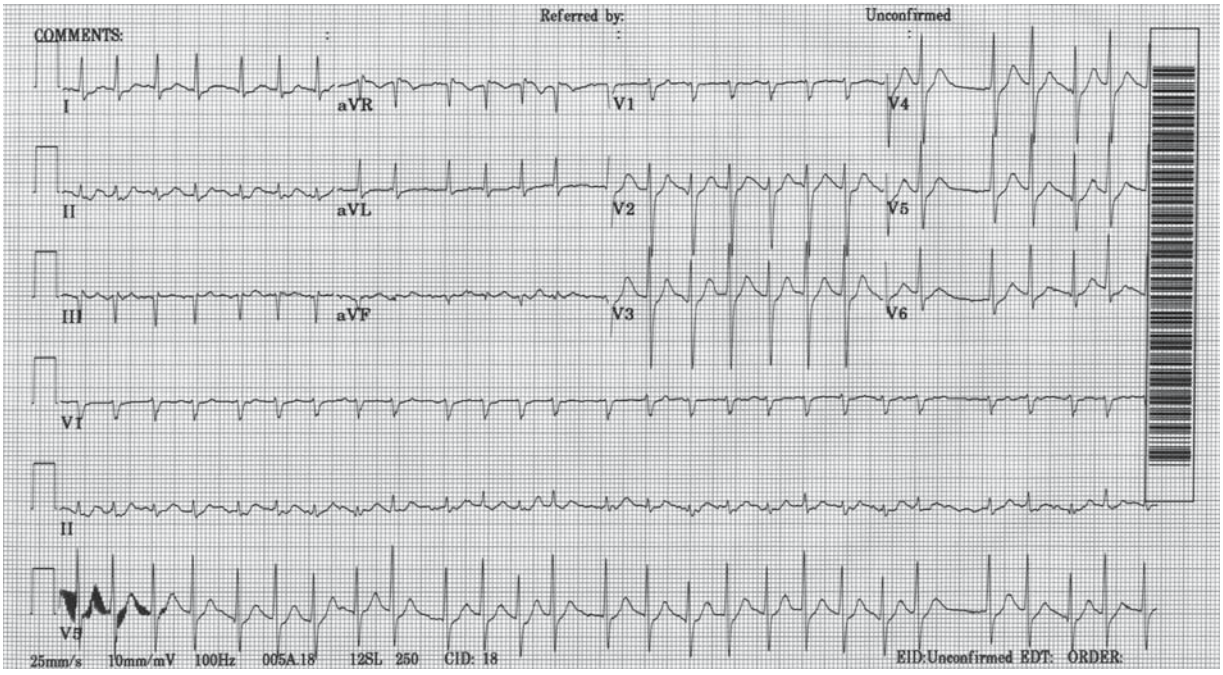

Fig. 6. Atrial fibrillation. *See* text for discussion.

branches of the autonomic nervous system can be involved in the initiation, maintenance, and termination of atrial fibrillation (vagally mediated atrial fibrillation and adrenergically mediated atrial fibrillation). Aberrant conduction may occur when a long ventricular cycle is followed by a short cycle (Ashman phenomenon). Atrial fibrillation itself modifies atrial electrical properties in a way that promotes the occurrence and maintenance of the arrhythmia, a process identified as atrial electrical remodeling.

The major adverse clinical consequences of atrial fibrillation include palpitations, impaired cardiac function, and an increased potential for thromboembolism. Physical findings include an irregularly irregular ventricular rhythm, variations in the intensity of the first heart sound, and the absence of *a* waves in the jugular venous pulse. A peripheral pulse deficit (pulse rate less than heart rate) is often noted during a fast ventricular response. Patients with continuous rapid ventricular rates for a prolonged period are at risk of developing a tachycardia-induced cardiomyopathy.

The ultimate goal of therapies for atrial fibrillation is improvement of symptoms, that is, reduction of atrial fibrillation-associated morbidity and improvement in prognosis. The three basic tenets of therapy for atrial fibrillation are: (1) control of ventricular rate response; (2) restoration and maintenance of sinus rhythm; and (3) prevention of thromboembolism.

A resting ventricular rate under 90 beats/min and ventricular rates between 90 and 115 beats/min during moderate exercise are considered optimal. Commonly used drugs for rate control include β-blockers, calcium channel blockers, and digoxin. In general, sinus rhythm is preferable to atrial fibrillation, as long as it can be achieved and maintained with relative safety.

Approximately 50% of patients with recent onset of atrial fibrillation will convert spontaneously to sinus rhythm within 48 h. Potential precipitating factors should be sought and treated. Sinus rhythm can normally be restored in such cases, either pharmacologically or electrically. Class Ia, Ic, and III antiarrhythmic drugs all have the potential to restore sinus rhythm. Flecainide is a good choice for patients without coronary artery disease or significant left ventricular dysfunction; otherwise, class III agents should be used. Ibutilide and dofetilide have been shown to be effective in the treatment of atrial fibrillation and atrial flutter, particularly in atrial fibrillation following cardiac surgery or for patients in whom direct current cardioversion is not ideal. Approximately 50% of such patients remain in sinus rhythm when treated with various class I and III drugs (6 mo to 3 yr).

Single- or dual-site atrial pacing may also be useful for prevention of recurrence of paroxysmal atrial fibrillation. Implantable atrial defibrillators have been introduced for treatment of recurrent atrial fibrillation. The surgical Maze procedure and catheter ablation may also be considered in refractory patients.

For elective cardioversion of atrial fibrillation lasting longer than 48 h, patients should be anticoagulated for 3–4 weeks before and after cardioversion regardless of their risk of embolization. Transesophageal echocardiography combined with short-term heparin infusion has gained acceptance as an alternative rapid preparation for direct current cardioversion. However, postcardioversion atrial stunning may create a favorable milieu for thrombogenesis, and embolization may occur despite a negative transesophageal echocardiography. Hence, adequate anticoagulation is pivotal in preventing spontaneous embolism in patients with atrial fibrillation.

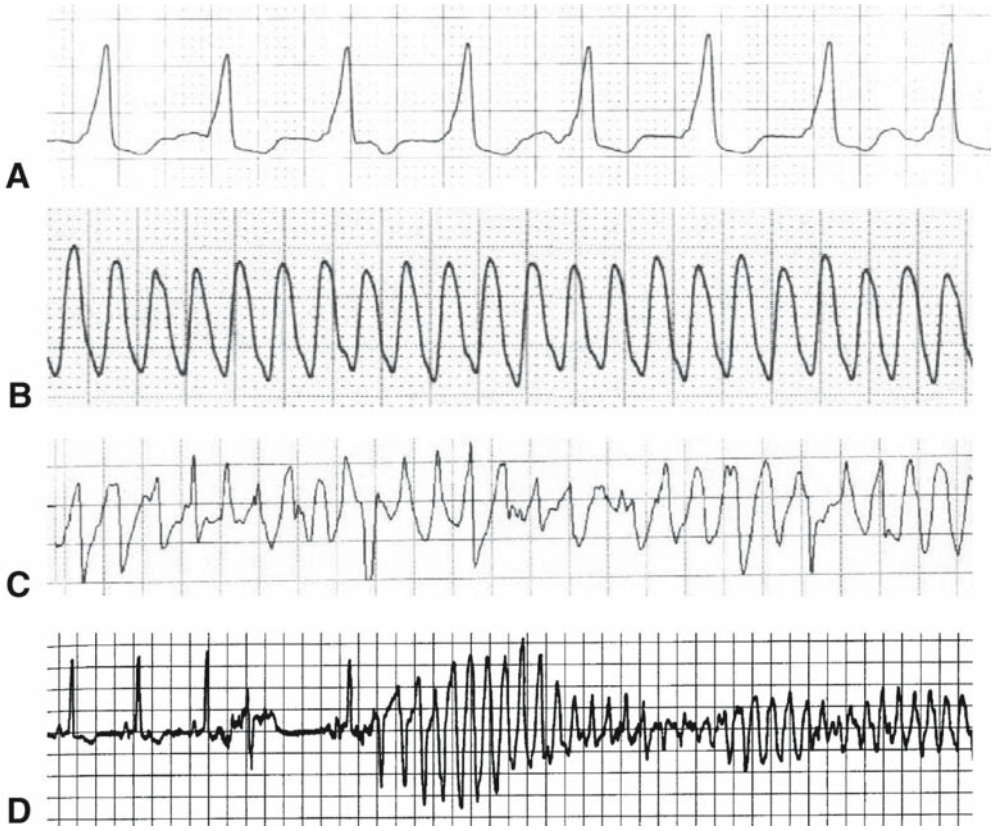

Fig. 7. **(A)** Ventricular tachycardia, **(B)** ventricular flutter, **(C)** ventricular fibrillation, and **(D)** torsades de pointes. *See* text for discussion.

Table 3
Recommendations for Anticoagulation Therapy in Atrial Fibrillation by the American College of Chest Physicians

Age	*No risk factors*	*With any high-risk factors*
< 65 years	Aspirin	Warfarin
65–75 years	Aspirin/warfarin	Warfarin
> 75 years	Warfarin	Warfarin

Source: Modified from ref. *7*.

In addition to rheumatic mitral valve disease and prosthetic valves (mechanical or tissue valves), major risk factors of embolization in nonvalvular atrial fibrillation include: (1) a prior history of ischemic stroke (or transient ischemic attack); (2) congestive heart failure or left ventricular dysfunction (ejection fraction ≤ 35%); (3) advanced age (>65–75 yr old); (4) hypertension; (5) coronary artery disease (particularly myocardial infarction); (6) diabetes; (7) left atrial thrombus; (8) thyrotoxicosis; (9) increased left atrial size (>50 mm); and/or (10) left atrial mechanical dysfunction. Atrial fibrillation patients with any risk factors as listed should be treated with warfarin to achieve an INR (international normalized ratio) of 2.0–3.0 (target INR 2.5) (Table 3) *(7)*. Anticoagulation therapy reduces stroke risk by 68% (4.5 vs 1.4%), yet the major concern with anticoagulation therapy is bleeding, especially in elderly patients (>75 yr old) or when the patient's INR is greater than 4.0. A complete guideline for management of atrial fibrillation was published in October 2001 *(6)*.

2.5. Ventricular Tachyarrhythmias

2.5.1. Ventricular Tachycardias

Although ventricular tachycardias can occur in a clinically normal heart, they generally accompany some form of structural heart disease; this is particularly true for patients with prior myocardial infarction. A fixed substrate, such as an old infarct scar, is most often responsible for episodes of recurrent monomorphic ventricular tachycardia. Yet, acute ischemia may play an even more important role in the pathogenesis of polymorphic ventricular tachycardia or ventricular fibrillation.

Ventricular tachycardia is characterized on an ECG by a wide QRS complex tachycardia at a rate of more than 100 beats/min (Fig. 7). Like ventricular premature complexes, ventricular tachycardias can be monomorphic (Fig. 7A) or polymorphic. *Sustained ventricular tachycardia* is defined as ventricular tachycardia persisting more than 30 s or requiring termination because of hemodynamic compromise. *Nonsustained ventricular tachycardia* refers to ventricular tachycardia lasting longer than 3 consecutive beats but less than 30 s. *Bidirectional ventricular tachycardia* is defined as ventricular tachycardia that shows an alternation in QRS amplitude and axis.

The key marker of ventricular tachycardia on an ECG is ventricular atrial dissociation. Capture and fusion beats also support the diagnosis of ventricular tachycardia; sustained ventricular tachycardia is almost always symptomatic. Nevertheless, the presentation, prognosis, and management of ventricular tachycardia largely depend on the underlying cardiovascular state.

Procainamide and amiodarone are commonly administered for the acute termination of ventricular tachycardia. Yet, an implantable cardioverter–defibrillator, with and without amiodarone, is the most established long-term therapy for ventricular tachycardia. In some cases, ablation provides a cure for normal heart ventricular tachycardia, bundle branch reentry ventricular tachycardia, and selected ischemic ventricular tachycardia. However, as left ventricular function is more severely impaired, it may be prudent to place an implantable cardioverter–defibrillator, even after an apparently successful ablation.

2.5.2. Ventricular Flutter and Ventricular Fibrillation

Electrocardiographically, ventricular flutter (Fig. 7B) usually appears as a "sine wave" with a rate between 150 and 300 beats/min. It is impossible to assign a specific morphology to these oscillations. Ventricular fibrillation (Fig. 7C) is recognized by grossly irregular undulations of varying amplitudes, contours, and rates, which are often preceded by a rapid repetitive sequence of ventricular tachycardia. Spontaneous conversion of ventricular fibrillation to sinus rhythm is rare. Prevention of sudden cardiac death in these patients predominantly depends on implantable cardioverter–defibrillators.

2.5.3. Accelerated Idioventricular Rhythm

Accelerated idioventricular rhythm can be regarded as a type of slow ventricular tachycardia with a rate between 60 and 110 beats/min, usually occurring in acute myocardial infarction, particularly during perfusion. Because the rhythm is usually transient and rarely causes significant hemodynamic compromise, treatment is rarely required.

2.5.4. Torsade de Pointes

When polymorphic ventricular tachycardia occurs in the presence of prolonged QT intervals (congenital or required), it is termed torsade de pointes. It is often preceded by ventricular premature complexes with a long–short sequence (Fig. 7D). Torsade de pointes often has multiple episodes causing recurrent syncope and may generate into ventricular fibrillation, leading to death. Identification of torsades de pointes has important therapeutic implications because its treatment is completely different from that of common polymorphic ventricular tachycardia. Magnesium, pacing, and isoproterenol can be used to treat torsades de pointes if required. Left cervicothoracic sympathectomy has been proposed as a form of therapy for torsades de pointes in patients with congenital long QT syndrome.

2.5.5. Nonparoxysmal Junctional Tachycardia

A nonparoxysmal junctional tachycardia rhythm is recognized by a QRS complex identical to that of sinus rhythm at a rate between 70 and 130 beats/min, usually associated with a warm-up period at its onset. This type of tachycardia frequently results from conditions that produce enhanced automaticity or triggered activity in the atrioventricular junction, such as inferior acute myocardial infarction, digitalis intoxication, and postvalve surgery. Treatment should be directed toward the underlying diseases.

3. BRADYARRHYTHMIAS

Bradycardia may result from either sick sinus syndrome or atrioventricular conduction block. Acute treatment options for symptomatic bradycardia include atropine, isoproterenol, and temporary pacing. When the underlying cause is not reversible, as in the case of drug toxicity (e.g., excess digitalis or β-blocker), then a permanent electronic pacemaker is usually warranted.

3.1. Sinus Node Dysfunction and Sick Sinus Syndrome

Normal sinus node function was briefly discussed in the introductory section. However, it is common for sinus node performance to deteriorate with age or age-related disease states. In that setting, the clinical syndrome of sick sinus syndrome or sinus node dysfunction emerges. In this case, the clinical manifestation may be excessive sinus bradycardia or intermittent periods of bradycardia and atrial tachycardia or atrial fibrillation. In addition, the sinus node may simply become less responsive over time in terms of generating an appropriate heart rate in conjunction with physical exertion; this is a special form of sick sinus syndrome called *chronotropic incompetence*.

Sinus bradycardia is defined as sinus rates of less than 60 beats/min; yet, sinus rates between 50 and 60 beats/min may be not pathological in many subjects. Sinus node dysfunction manifests either significant sinus bradycardia or abrupt and prolonged sinus pauses because of sinus arrest or sinus exit block. Sick sinus syndrome is associated with the following symptoms: fatigue, dizziness, confusion, syncope, and congestive heart failure. In particular, atrial tachyarrhythmias frequently occur in the presence of sick sinus dysfunction (bradycardia–tachycardia syndrome). On surface ECGs, only the second-degree sinoatrial block can be diagnosed, and the first- and the third-degree sinoatrial block cannot be recognized. Currently, Holter monitors and implantable event monitors are useful for making the diagnosis of sick sinus syndrome, particularly when bradycardia is associated with symptoms.

Carotid sinus massage is frequently performed in evaluating sick sinus syndrome. Although carotid sinus syndrome is not the same as sick sinus syndrome, the two often coexist in the same patient. A sinus pause longer than 3 s induced by a 5-s unilateral carotid sinus massage is considered clinically significant.

Because sinus rate can be slowed by vagal tone, assessment of intrinsic heart rate after complete autonomic blockage is often used to determine the integrity of sinus node function. Complete autonomic blockade can be achieved by administration of intravenous propranolol (0.2 mg/kg) and atropine (0.04 mg/kg). A normal intrinsic heart rate (IHR) is estimated using the formula $IHR = 118.1 - (0.57 \times Age)$. An intrinsic heart rate of less than 80 beats/min in elderly patients is usually suggestive of sick sinus syndrome. Sinus node recovery time (normal value < 1500 ms), corrected sinus node recovery time (normal

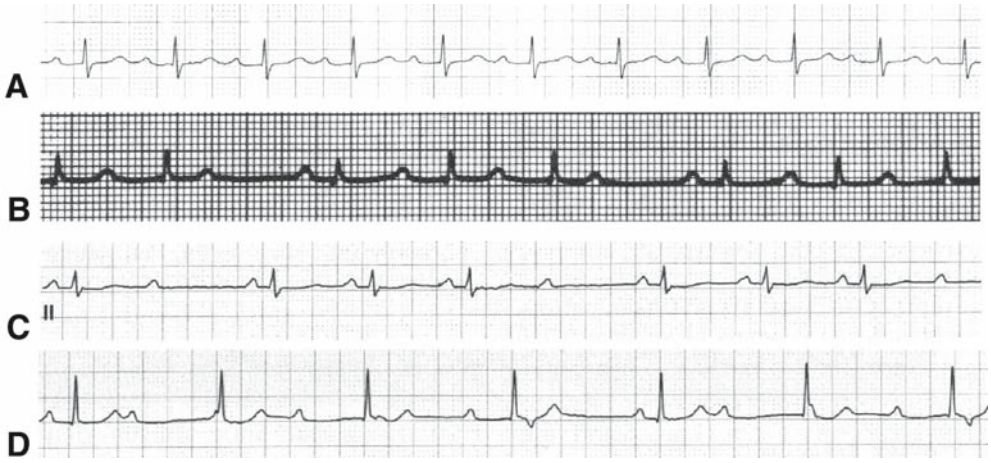

Fig. 8. (**A**) The first-degree, (**B**) Mobitz type I second-degree, (**C**) Mobitz type II second-degree, and (**D**) third-degree atrioventricular block. *See* text for discussion.

value < 550 ms), and less frequently, sinoatrial conduction time (normal value < 125 ms) can be used within the electrophysiology laboratory to evaluate sinus node function when its initial clinical diagnosis is uncertain.

Pacemakers are the mainstay of therapy for sick sinus syndrome. However, it is not uncommon that antiarrhythmic drugs are also needed to suppress a tachycardic component of the condition when it is relevant to the individual patient.

3.2. Atrioventricular Block

The clinical significance of atrioventricular block depends on: (1) the site of block; (2) the risk of progression to complete block; and (3) the subsidiary escape rate. When complete atrioventricular block occurs above the His bundle, escape rhythm is believed to originate from the His bundle or atrioventricular node (40–60 beats/min), which is usually called *junctional escape rhythm with narrow QRS complexes*. When atrioventricular block occurs below the His bundle, the escape is generated in the distal His–Purkinje fibers and is much slower and less reliable (25–45 beats/min), which is usually called *ventricular escape rhythm with wide QRS complexes*.

The *first-degree atrioventricular block* is characterized by a PR interval of more than 0.20 s without drop of QRS complexes following each P wave (Fig. 8A). Conduction delays can occur in the right atrium, at the atrioventricular node, or in the His–Purkinje system. *Second-degree atrioventricular block* is considered present when some atrial impulses fail to conduct to the ventricles.

Mobitz type I second-degree atrioventricular block (Fig. 8B) is characterized by progressive PR interval prolongation until an atrial impulse is blocked (Wenckebach phenomenon). After an incomplete compensatory pause, the Wenckebach cycle starts again with a shorter PR interval compared with the last PR interval prior to block. Mobitz type I block is almost always located at the atrioventricular node, and the risks of development of complete atrioventricular block are low.

In *Mobitz type II* second-degree atrioventricular block (Fig. 8C), atrioventricular conduction fails suddenly without a preceding change in PR interval. It is usually caused by His–Purkinje disease, and when the escape rate is slow and unreliable, it is associated with a high risk of developing complete atrioventricular block. When two or more consecutive atrial impulses fail to conduct, *high-degree atrioventricular block* is considered present, and pacemaker implantation is mandatory.

The *third-degree atrioventricular block* (Fig. 8C) is defined as a complete atrioventricular block, and no atrial impulses can conduct to the ventricles. A permanent pacemaker is normally required in the third-degree atrioventricular block. In this regard, dual-chamber pacing (i.e., pacing both the atrium and the ventricle) has become increasing widely accepted as the approach of choice.

4. ELECTROPHYSIOLOGICAL STUDY AND TRANSCATHETER ABLATION

Electrophysiological study can be useful in evaluating a broad spectrum of cardiac arrhythmias. It can help to: (1) assess the function of the sinus and atrioventricular nodes and the His-Purkinje system; (2) determine the characteristics of reentry tachycardias; (3) assess the efficacy of antiarrhythmic drugs and devices; (4) map the location of arrhythmogenic foci; and (5) identify sites for ablation to treat many forms of tachycardia.

Electrophysiological study is performed in a laboratory similar to a heart catheterization laboratory. The minimum equipment requirement for a comprehensive electrophysiological study includes: (1) a radiographic table; (2) a fluoroscopy unit; (3) a physiological recording and analysis system; (4) a programmable stimulator; (5) a radiofrequency generator; (6) a variety of electrode catheters and introducers; (7) the capability of providing a sterile working environment; and (8) resuscitation equipment.

An electrophysiological study is usually performed on fasting and antiarrhythmic drug-free patients in a sterilized fashion using various degrees of conscious sedation (fentanyl and midazolam), depending on the specific procedure. Vascular accesses are obtained percutaneously through the femoral, subclavian, or internal jugular veins using 1% lidocaine for local

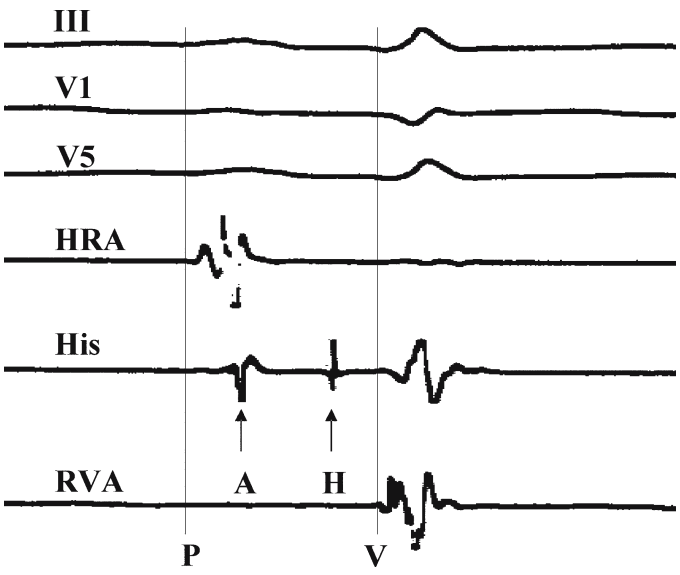

Fig. 9. Measurements in the His bundle electrogram for evaluation of atrioventricular conduction. AH interval, measured from the earliest reproducible rapid deflection of the atrial electrogram in the His recording to the onset of the His deflection, represents conduction time from the low right atrium at the interatrial septum through the atrioventricular node to the His bundle (atrioventricular node function). The HV interval, measured from the beginning of the His deflection to the earliest onset of ventricular activation (surface leads or intracardiac recordings), represents conduction time from the proximal His bundle to the ventricular myocardium (infra-His conduction function). III, surface electrocardiogram (ECG) lead III; V1, surface ECG lead V1; V5, surface ECG lead V5; A, the onset of atrial activation; H, the onset of His activation; His, His bundle; HRA, high right atrium; P, the onset of the P wave; RVA, right ventricular apex; V, the onset of ventricular activation.

anesthesia. Multiple electrode catheters are placed at the key locations of the heart, such as the high right atrium close to the sinus node, the coronary sinus (for recording and stimulating the left atrium), the His bundle region, and the right ventricular apex.

AH and HV intervals are routine baseline measurements of electrophysiological study (Fig. 9). A mapping and ablation catheter is also inserted when ablation is attempted. The ablation catheter usually has a varying deflectable distal segment (1.5–3 in) with a distal electrode of 2.2-mm diameter (7 French) and 4 mm long. Physiological signals are usually digitized at 1000 Hz and filtered between 30 and 500 Hz. Pharmacological provocations, such as isoproterenol, are often required to facilitate induction of tachycardias.

The purpose of ablation is to destroy myocardial tissue by delivering electrical energy over a distal electrode of a catheter placed on the endomyocardium integrally related to the initiation or maintenance of tachycardia. The first successful ablation using direct current shocks in a human was performed in 1982. Such shocks are now replaced by radiofrequency energy at the range of 100 kHz to 1.5 MHz. Lasers, cryothermy, and microwave energy sources have been investigated, and some of these methods continue to be of interest.

Because the radiofrequency portion of the electromagnetic spectrum is conducted through cardiac tissue, it generates resistive heat in the tissue under the tip of the ablation catheter (with the reference patch usually placed on the skin of the patient's thigh). Temperature at the tip of an ablation catheter is controlled between 50 and 70°C to avoid coagulation of blood and desiccation of tissue, which occurs when the temperature reaches 100°C or greater. Irreversible cellular damage and tissue death occur once tissue temperature exceeds 50°C. Application of such radiofrequency energy, for 30–120 s, will normally result in a necrosis lesion with a radius of 4–5 mm and a depth of 2–3 mm. Irrigated-tip catheters can prevent excessive heating of the tip and allow greater power delivery, leading to larger and deeper ablation lesions as required.

Diagnostic electrophysiological study and ablative procedures can normally be accomplished in a single session. Ablation of arrhythmias is usually indicated whenever feasible for the patient's preference or refractoriness of arrhythmias to drug therapy. New technologies such as intracardiac echocardiography, nonfluoroscopic electroanatomical mapping, and noncontact endocardial activation mapping have significantly contributed to advancements in interventional cardiac electrophysiology.

The indications for ablation are summarized in Table 4. Polymorphic ventricular tachycardia and ventricular fibrillation are not indicated for ablation using current ablative techniques. Radiofrequency ablation is now a consistently effective treatment for typical atrial flutter in addition to atrioventricular nodal reentry tachycardia and atrioventricular reentry tachycardia. Atrioventricular junctional ablation plus pacemaker implantation is well accepted in controlling symptoms caused by refractory atrial fibrillation.

Table 4
Indications for Ablation of Arrhythmias

- ❖ Atrial tachycardias
  - Inappropriate sinus tachycardia (often difficult to ablate effectively)
  - Focal atrial tachycardia
  - Typical atrial flutter (type I)
  - Atypical atrial flutter (type II)[a]
- ❖ Atrial fibrillation
  - Atrioventricular nodal modification or complete ablation for rate control
  - Catheter-based Maze procedure[a]
  - Focal atrial fibrillation ablation[a]
  - Pulmonary vein isolation[a]
- ❖ Atrioventricular nodal reentry tachycardia
- ❖ Atrioventricular reentry tachycardia using concealed bypass tracts
- ❖ Wolff-Parkinson-White syndrome
- ❖ Ventricular tachycardia
  - Ischemic ventricular tachycardia (monomorphic, stable)
  - Ischemic ventricular tachycardia (monomorphic, unstable)[a]
  - Nonischemic ventricular tachycardia (stable monomorphic)
  - Idiopathic ventricular tachycardia (including symptomatic ventricular premature complexes)
  - Bundle branch reentry tachycardia

[a]Ablation procedures are under investigation or with clinical indications that are undefined.

Catheter-based radiofrequency ablative approaches, designed to create linear lesions or aimed at focal sources, are exciting new approaches for drug refractory atrial fibrillation patients *(8,9)*. In experienced hands, radiofrequency catheter ablation is able to eliminate spontaneous episodes of ventricular tachycardia in up to two-thirds of patients after myocardial infarction *(10)*. At present, catheter ablation of ventricular tachycardia is largely adjunctive to amiodarone and the implantable cardioverter–defibrillator.

Complications of electrophysiological study and ablation procedures can be related to the catheterization (local vascular complications, vasovagal reactions, and perforation of the heart and vessels, leading to tamponade and internal bleeding); subclavian puncture (pneumothorax, hemothorax, subclavian artery injury, branchial nerve injury, and subclavian arteriovenous fistula); vascular complications (embolization, hypotension, myocardial infarction); and radiofrequency ablation (postablation pain, atrioventricular block, and prolonged radiation exposure). The risk of complications is heavily dependent on the experience and skill of the operator as well as the type of ablation procedure.

Ablation procedures have been shown to be cost-effective in the management of drug-refractory paroxysmal supraventricular tachycardias. The total charges for an outpatient ablation procedure are typically $10,000–12,000. For ablation of Wolff-Parkinson-White syndrome, the cost is $6,600–19,000 per quality-adjusted year of life gained.

4.1. Ablation for Inappropriate Sinus Tachycardia

Ablation procedures on patients with drug-refractory inappropriate sinus tachycardia are frequently performed to eliminate the portions of the sinus nodes that generate the fast heart rates along the superior aspect of the crista terminalis. Because of the anatomical structure of the sinus node, multiple lesions over 3–4 cm along the crista terminalis are often required. Nonfluoroscopic electroanatomical cardiac mapping and intracardiac echocardiography are useful in identification of the earliest activation site and the crista terminalis, respectively. The procedural goal is to achieve approx 30% reduction or more in maximal heart rate during infusion of isoproterenol and atropine. Unfortunately, to date, less than half of such patients elicit sustained improvements of symptoms; many of these patients require an additional ablation session, and some may need complete sinus node ablation and the subsequent implantation of a pacemaker.

4.2. Ablation of Atrial Tachycardia

Right atrial tachycardia, arising along the length of the crista terminalis from the sinus node to the coronary sinus and atrioventricular node (cristal tachycardia), accounts for 83% of all atrial tachycardias. Other sites of atrial tachycardia clustering include the pulmonary vein ostia, coronary sinus ostia, or mitral and tricuspid valve rings. Regardless, appropriate identification at the earliest onset of the P wave is critical for optimal treatment. The "dancing catheter" or "pas de deux," pace mapping, and "destructive mapping" can be used for such atrial tachycardia ablation studies.

In mapping to the midseptum, particularly when the presystolic activity is not significantly early, signals that are not fractionated or multiple sites with similar activation times may suggest an origin of tachycardia in the left atrium, such as within the pulmonary vein ostia. Diagnosis of anteroseptal atrial tachycardia is difficult but possible and in some cases can be ablated without causing atrioventricular block. The average success rate of atrial tachycardia ablation is 91%, with a complication rate of 3% and recurrence rate of 9%. Complications include sinus node dysfunction, atrioventricular block, and phrenic nerve damage.

4.3. Catheter Ablation of Atrial Flutter

4.3.1. Ablation of Typical Atrial Flutter

Endocardial mapping in patients with typical atrial flutter has confirmed that macroreentry can occur in the right atrium. Most of the time, typical atrial flutter rotates in a counterclockwise direction around the tricuspid annulus in the frontal plane, although clockwise rotations have also been observed. On 12-lead ECG, counterclockwise atrial flutter presents a stereotypical "sawtooth" pattern, an upright flutter wave in V1, and inverted flutter waves in the inferior leads and V6. In contrast, during clockwise rotation, flutter waves in V1 are inverted; those in the inferior leads and V6 are upright.

The macroreentrant circuit passes through a critical isthmus bounded by the inferior aspect of the tricuspid annulus, ostium of the inferior vena cava, the coronary sinus ostium, and the eustachian ridge (cavotricuspid isthmus). During endocardial recording, a multielectrode catheter should be placed around the macroreentrant circuit adjacent to the tricuspid valve to evaluate rotation around the tricuspid annulus and through the isthmus. Linear lesions that transect this isthmus cure typical atrial flutter.

Because some atrial flutter circuits may not travel through the isthmus, it is important to confirm that the isthmus is critical to the maintenance of the flutter circuit using pacing maneuvers to demonstrate any potential concealed entrainment. Nonfluoroscopic electroanatomic mapping systems have provided a more precise and effective way to verify the creation of a complete linear ablative lesion. In general, irrigated-tip catheters appear more effective than, and as safe as, conventional catheters for atrial flutter ablation procedures and may also be more useful when conventional 4-mm tipped catheters fail.

Currently, the success rate of the ablation of typical atrial flutter is greater than 90%, with the recurrence rate less than 10%. Confirmation of bidirectional isthmus block significantly reduces recurrence rates *(11)*. Ablation of class Ic atrial flutter (atrial flutter that develops during class Ic antiarrhythmic drug therapy for atrial fibrillation) has been reported as a novel ("hybrid") approach for treating drug-refractory atrial fibrillation *(12)*.

4.3.2. Ablation of Atypical Atrial Flutter

From an ablative viewpoint, the term *atypical atrial flutter* is sometimes used for any macroreentrant atrial tachycardia that does not utilize the cavotricuspid isthmus as a critical component of a tachycardia circuit. Atypical atrial flutter consists of a heterogeneous group of arrhythmias presenting with stable, flutter wavelike morphologies on 12-lead ECG. Techniques for ablation of atypical atrial flutters are evolving, and successful ablation of atypical flutters, with focused sites on the right atrial free wall and the left atrium, has been described.

4.3.3. Ablation of Incisional Atrial Tachycardia

Macroreentrant atrial tachycardia occurs frequently following surgeries for repair of congenital heart disease. The presence of multiple anatomic barriers (surgical incisions, patches, conduits, cavae, the coronary sinus ostium, and the pulmonary venous ostia) as well as atrial tissue damage (hypoxemia, ischemia, surgical scars, and fibrosis) provides rich substrates for reentry. Partially successful Maze surgery and radiofrequency ablative procedures for atrial fibrillation may also leave substrates for intraatrial reentrant tachycardias ("incisional reentry").

The location for subsequent successful ablation varies from patient to patient and can be identified by concealed entrainment. Thus, electroanatomical mapping is useful in identifying the reentrant circuit prior to catheter ablation of incisional reentrant tachycardias. Radiofrequency linear lesions transecting one or more protected isthmuses sustaining macroreentry are associated with acute success rates of 71–93%. However, recurrence rates may be as high as 40–46%.

4.4. Ablation of Atrial Fibrillation

Several catheter-based ablative techniques are currently available that regularly provide symptomatic improvement in patients with drug-refractory atrial fibrillation.

4.4.1. Atrioventricular Nodal Modification or Ablation for Rate Control

Catheter ablation of the atrioventricular junction and insertion of a permanent pacemaker have been shown to be effective in achieving ventricular rate control in patients with drug-refractory atrial fibrillation and are superior to drug therapy for symptomatic relief in selected patients. This approach can also be used for rate control in patients with drug-refractory multifocal atrial tachycardia.

4.4.2. Catheter-Based Maze Procedure

Surgical treatment of atrial fibrillation is ultimately aimed at elimination of the arrhythmia, maintenance of sinus node function, preservation of atrioventricular conduction, and restoration of atrial contractility. Surgical approaches include the modified Cox Maze procedure and the left atrial isolation procedure. The reported overall success rates in eliminating atrial fibrillation are high (over 90%) with low mortality rates (2–3%). Catheter-based Maze procedures have also been introduced.

The technical difficulties in achieving stable linear conduction blocks have been recently improved using new technology, such as intracardiac echocardiography and nonfluoroscopic electroanatomical cardiac mapping systems. In patients with paroxysmal atrial fibrillation, success rates with and without drug therapy at 11-month follow-up were approx 33 and 13% for linear ablations limited to the right atrium and 85 and 60% for biatrial approaches.

4.4.3. Focal Atrial Fibrillation Ablation

One of the most significant recent advancements in transcatheter ablation of cardiac arrhythmias is the routine identification of patients with focal atrial fibrillation *(8,9)*. Focal sources of activity are critical for some patients, with paroxysmal atrial fibrillation serving as either the main abnormality (focal drivers) or the dominant trigger to induce repetitive episodes of atrial fibrillation (focal triggers). A single, rapidly discharging focus can lead to fibrillatory conduction, mimicking the surface ECG features of atrial fibrillation. Clinical experience has demonstrated that the pulmonary veins are the predominant sources of such triggers for atrial fibrillation. The left superior pulmonary vein is the most common focal source,

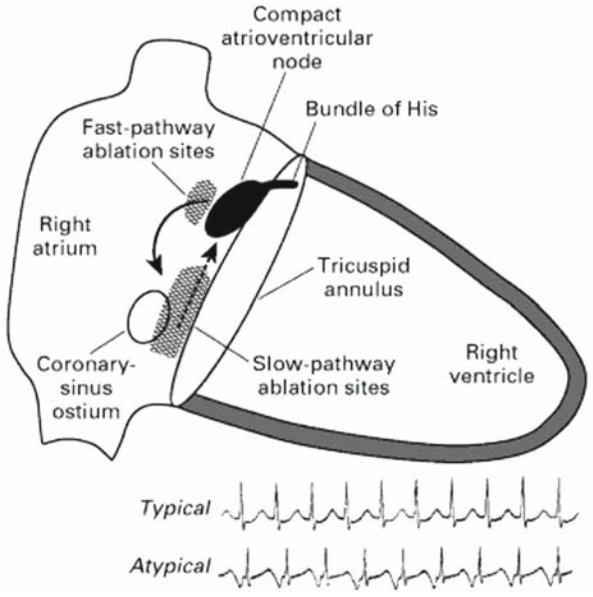

Fig. 10. The slow-pathway (posterior) and fast-pathway (anterior) ablation sites for atrioventricular nodal reentry tachycardia. *See* text for discussion. Reprinted from ref. *14* with permission. © 1999 Massachusetts Medical Society. All rights reserved.

followed by the right superior, left inferior, and right inferior pulmonary veins, respectively.

Electrical isolation of the pulmonary veins from the left atrium results in marked reduction or elimination of atrial fibrillation. This may be accomplished by sequential elimination of earliest breakthroughs at pulmonary venous ostia or by empirically encircling and isolating the ostia with radiofrequency or ultrasound. Saline-irrigated radiofrequency catheters may facilitate success by creating larger lesions; such ablations of focal atrial fibrillation may exceed 70%. Yet, multiple ablation sessions may be required to achieve this degree of drug-free arrhythmia control. It is considered that saline irrigation may reduce charring and perhaps reduce the thromboembolic risk of this procedure. However, long procedure time, high recurrence rates, thromboembolism, and concerns about pulmonary vein stenosis remain problematic.

4.5. Ablation of Atrioventricular Nodal Reentry Tachycardia

Dual pathways are defined as a sudden increase of at least 50 ms in the AH interval with a 10-ms decrease in the coupling interval of an atrial stimulus. A dual-pathway conduction curve can be demonstrated in a majority (85%) of patients with atrioventricular nodal reentry tachycardia. Yet, dual physiology may exist in 25% of patients without supraventricular tachycardias. Most atrioventricular nodal reentry tachycardia conducts antegradely through the slow pathway and conducts retrogradely through the fast pathway (typical). In a small number of patients (4%), tachycardic circuits function in an opposite direction (atypical).

Correction of atrioventricular nodal reentry tachycardia is aimed at ablation of the slow pathway in the posteroinferior area of the Koch's triangle between the coronary sinus ostia and tricuspid annulus (posterior approach) (Fig. 10) *(12)*. The atrial/ventricular signal ratio for slow pathway ablation, measured from a distal electrode pair in sinus rhythmn, is usually less than 1. Ablation of the fast pathway in the anterosuperior area of the Koch's triangle is now rarely performed because of increased risk of damaged normal atrioventricular conduction (anterior approach). The risk of atrioventricular block is 1–2% with a posterior approach, relative to 5.1% with an anterior approach. Yet, in experienced hands, the success rate is almost 100%, with a recurrence rate of less than 3–5% and a risk of complete atrioventricular block less than 1%.

An accelerated junctional rhythm is to be expected with successful ablation of slow-pathway conduction (100% in successful ablation vs 65% in unsuccessful ablation). In addition, putative slow-pathway potentials are often recorded during mapping. Furthermore, residual slow-pathway conduction or atrioventricular nodal echo beats may be present after successful atrioventricular nodal reentry tachycardia ablation and are not necessarily associated with increased recurrence during follow-up.

4.6. Ablation of Accessory Pathways

Most accessory pathways are "left sided." The approximate location of accessory pathways can be determined from surface ECG (Fig. 11) *(13)*. A preablation electrophysiological study is initially performed to determine the precise location of accessory pathways. Yet, accessory pathways can exist at any sites around the tricuspid and mitral annulus: free wall (anterolateral, lateral, and posterolateral) and septum (anteroseptal, midseptal, and posteroseptal). Multiple accessory pathways have been reported in 5–18% of ablation cases.

For treating left-sided accessory pathways, either a "retrograde transaortic approach" or a "transseptal approach" can be used in conjunction with anticoagulation using heparin (target activated clotting time 250–350 s). Ablation can be performed at atrial sites (during orthodromic atrioventricular reentry tachycardia or relatively fast ventricular pacing) or ventricular sites (during sinus rhythm or atrial pacing), targeting at the earliest atrial or ventricular activation, respectively. Accessory pathways often cross the left atrioventricular groove obliquely, with the atrial insertion closer to the coronary ostium. Mechanical mapping (inhibition of accessory conduction by mechanical pressure) and a QS wave analysis of unfiltered unipolar recordings may be helpful.

The optimal ablation site can be found by direct recording of accessory pathway potentials in addition to stable fluoroscopic and electrical characteristics. The success rate of ablation for left free wall accessory pathways is 96%, with a recurrence rate of 3–8% and complication rate of less than 6% (major complications 1.3%: tamponade 1.2%, atrioventricular block 0.5%, systemic embolization 0.08%, and death 0.08%). Ablation of right-sided accessory pathways is associated with a lower success rate (88%) and higher recurrence rates (up to 21% in earlier studies). On the other hand, the annual risk of natural sudden cardiac death in Wolff-Parkinson-White syndrome with symptomatic tachycardia is estimated to be 0.05–0.5%.

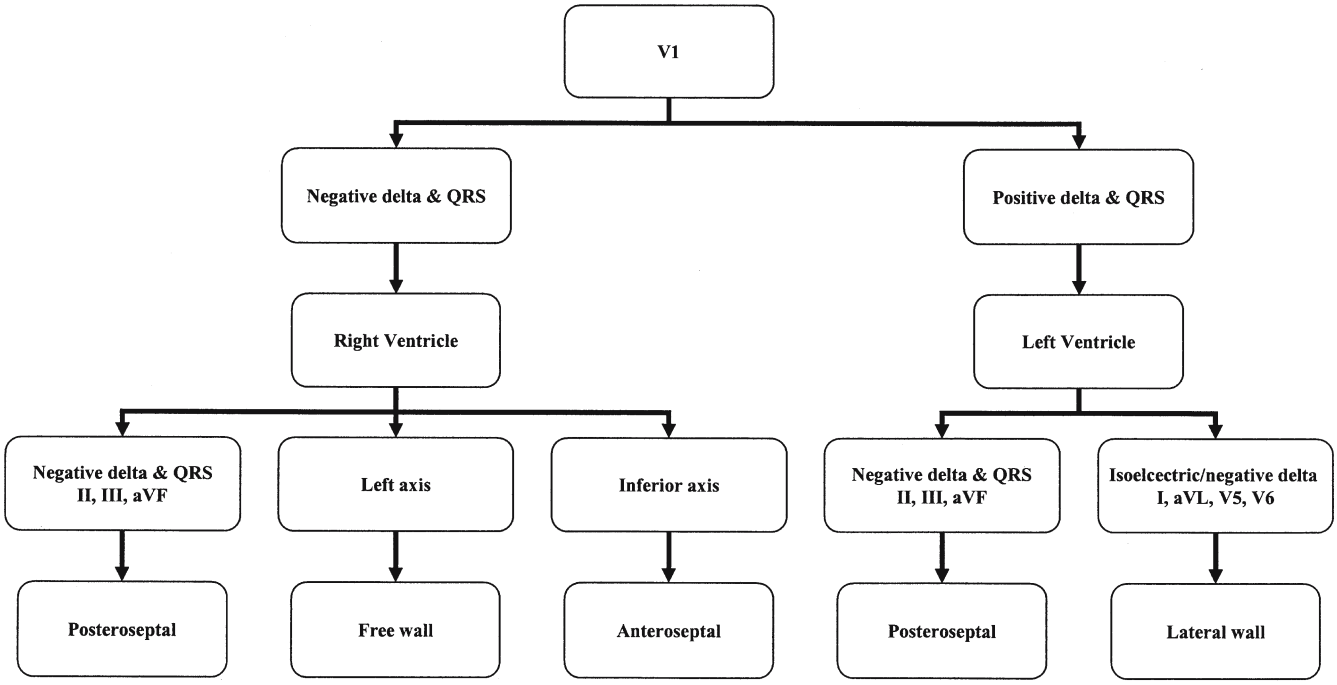

Fig. 11. Determination of the location of accessory pathways based on the delta wave and the QRS complex on surface 12-lead electrocardiogram (ECG). Reprinted from ref. *13* © 1997, with permission from Elsevier.

4.7. Ablation of Ventricular Tachycardia

There are two main substrates for ventricular tachycardia: focal and reentrant. Focal ventricular tachycardias are commonly seen in patients without underlying organic heart disease (*idiopathic ventricular tachycardia*). Idiopathic ventricular tachycardia accounts for 10–15% of all diagnosed sustained ventricular tachycardias. Approximately 70% of idiopathic ventricular tachycardias exhibit a left bundle branch block pattern, suggesting an origin in the right ventricle. These ventricular tachycardias almost uniformly show an inferior frontal plane axis, indicating an origin in the right ventricular outflow tract. Arrhythmogenic right ventricular dysplasia/cardiomyopathy should be suspected when other morphologies exist.

The origin of idiopathic left ventricular tachycardia is usually at the inferior left ventricular midseptum or apex in the region of the posterior fascicle. Radiofrequency ablation of these tachycardias is curative in more than 90% of patients. Frequent isolated ventricular premature complexes or nonsustained ventricular tachycardias in clinically normal hearts can be ablated as well.

Reentrant ventricular tachycardias usually occur in the presence of underlying organic heart disease, particularly in those with prior myocardial infarction. Ablation therapy is limited by their hemodynamic stability. Specifically, at present radiofrequency ablation of ventricular tachycardias is predominantly limited to hemodynamically stable tachyarrhythmias. This only accounts for 5–10% of ischemic ventricular tachycardia *(14)* or 20% of all ventricular tachyarrhythmias requiring clinical assessment *(15)*.

Yet, it has been noted that catheter ablation of ventricular tachycardia after myocardial infarction may eliminate spontaneous episodes of ventricular tachycardia in up to two-thirds of patients in experienced centers *(10)*. If one or two clinically documented ventricular tachycardias are targeted, successful ablation can be achieved in 71–76% of cases *(16)* with few serious complications (<2% of cases) *(14)*.

At present, catheter ablation of ventricular tachycardia in patients following myocardial infarction is used primarily as an adjunctive to amiodarone and implantable cardioverter–defibrillator therapy. More patients with ventricular tachycardia may be eligible for radiofrequency ablation as new technologies such as noncontact endocardial activation mapping and electroanatomical mapping become more common. Experience with ablations of ventricular tachycardia in patients with structural heart diseases other than ischemia is currently limited.

In addition, entrainment is a very useful technique for assessing reentry tachycardia. Entrainment refers to continuous resetting of the reentry tachycardia circuit, by pacing at a slightly faster rate than the tachycardia and resuming the intrinsic rate of tachycardia when pacing is stopped. Each pacing stimulus creates a wavefront that travels in an antegrade direction and resets the tachycardia to the pacing rate. A wavefront propagating retrogradely in the opposite direction collides with the wavefront of the previous beat.

An uncommon form of ventricular tachycardia that can also be corrected by radiofrequency ablation is bundle branch reentry tachycardia. The substrate for this form of reentry is usually

a dilated cardiomyopathy associated with significant conduction system disease. Although cure of bundle branch reentry tachycardia can be easily accomplished by ablating the right bundle branch, long-term survival after radiofrequency ablation is limited by the almost uniform presence of severe left ventricular dysfunction.

5. NEW TECHNOLOGY IN CARDIAC ELECTROPHYSIOLOGY

5.1. Nonfluoroscopic Electroanatomical Cardiac Mapping and Noncontact Endocardiac Activation Mapping

Cardiac mapping is essential for understanding mechanisms of cardiac arrhythmias and for directing curative ablation procedures. Traditional endocardial mapping techniques are time consuming, produce significant X-ray exposure, and are limited by lack of three-dimensional (3D) spatial information. Among the most important new advances in cardiac electrophysiology are 3D mapping systems, such as the nonfluoroscopic electroanatomical cardiac mapping system (CARTO™, Biosense, Tirat Hacarmel, Israel) and the noncontact endocardial activation mapping system (Endocardial Solutions, Inc., St. Paul, MN). These mapping systems will be discussed in detail in other chapters of the book.

5.2. Intracardiac Echocardiography

Several studies have demonstrated that intracardiac echocardiography is a useful tool during radiofrequency ablation procedures *(17)*. Potential benefits of direct endocardial visualization during radiofrequency ablative procedures include: (1) enhanced ability to guide ablative procedures and precise anatomical localization of the ablation catheter tip in relation to important endocardial structures (which cannot be visualized with fluoroscopy); (2) reduction in fluoroscopy time; (3) evaluation of catheter-tip tissue contact; (4) confirmation of lesion formation and identification of lesion size and continuity; (5) immediate identification of complications; and (6) provision of a research tool to help understand the critical role played by specific endocardial structures in arrhythmogenesis. Three-dimensional echocardiography is certainly more useful and probably one of the ideal imaging techniques for cardiac electrophysiology; however, its quality must be improved before it becomes clinically applicable.

5.3. Magnetically Directed Catheter Manipulation

A recent development in the manipulation of intravascular electrode catheters for various electrophysiological study and mapping/ablation purposes has been the development of using magnetic fields to direct malleable catheters. This technique (Stereotaxis Inc., St. Louis, MO) requires catheterization laboratories fitted with large magnets at the bedside and specially designed low-mass catheters capable of direction by the magnetic field.

The principal advantage in terms of mapping is the ability to turn tight corners because the catheters can be relatively supple, and their movement is controlled by magnetic force without manual torque. In addition, the operator can manipulate the catheter with a "joy stick" from outside the laboratory, thereby reducing long-term radiation exposure. Finally, by retaining coordinates in memory, the system can bring the catheter back to a predetermined site with great accuracy. This system is currently in clinical trials.

6. SUMMARY

Cardiac arrhythmias encompass a wide spectrum of abnormalities in electrical generation and conduction at all levels within the heart. They can manifest in either tachycardia or bradycardia. The clinical significance of these cardiac arrhythmias is predominantly related to the hemodynamic consequences and the risk of a life-threatening consequence (e.g., ventricular fibrillation) in addition to associated symptoms. Clinical and basic laboratory research have offered insight into the mechanisms underlying various arrhythmias and provided valuable tools for their treatment.

Historically, pharmacological therapy has been widely used in the management of arrhythmias, and to a large extent, this remains true. Nonpharmacological therapy has begun to play an increasingly important role in curing (ablation) many arrhythmias and preventing life-threatening consequences of others (e.g., greater application of implantable cardioverter–defibrillator therapy for both primary and secondary prevention of sudden cardiac death).

However, current understanding and available technologies are far from ideal for the assessment and treatment of all cardiac arrhythmias. For example, we still strive to achieve more thorough understanding of the underlying mechanisms of many arrhythmias and develop safer antiarrhythmic drugs (i.e., without negative inotropic or proarrhythmic effects). It is expected that the introduction of easier-to-use and more optimal imaging systems for interventional electrophysiology and the clinical application of biological repair of pacemaker cell and conduction abnormalities will substantially improve quality of care in patients with cardiac arrhythmias.

REFERENCES

1. The Sicilian Gambit. A new approach to the classification of antiarrhythmic drugs based on their actions on arrhythmogenic mechanisms. (1991) Task Force of the Working Group on Arrhythmias of the European Society of Cardiology. *Circulation.* 84, 1831–1851.
2. Preliminary report: effect of encainide and flecainide on mortality in a randomized trial of arrhythmia suppression after myocardial infarction. (1989) The Cardiac Arrhythmia Suppression Trial (CAST) Investigators. *N Engl J Med.* 321, 406–412.
3. Effect of the antiarrhythmic agent moricizine on survival after myocardial infarction. (1992) The Cardiac Arrhythmia Suppression Trial II Investigators. *N Engl J Med.* 327, 227–233.
4. Josephson, M.E. (ed.). (1993) *Clinical Cardiac Electrophysiology. Techniques and Interpretations*, 2nd Ed. Lea and Febiger, Malvern, PA.
5. Wells, J.L., Jr., MacLean, W.A., James, T.N., and Waldo, A.L. (1979) Characterization of atrial flutter. Studies in man after open heart surgery using fixed atrial electrodes. *Circulation.* 60, 665–673.
6. Fuster, V., Ryden, L.E., Asinger, R.W., et al. (2001) ACC/AHA/ESC guidelines for the management of patients with atrial fibrillation: executive summary a report of the American College of Cardiology/American Heart Association Task Force on Practice Guidelines and the European Society of Cardiology Committee for Practice Guidelines and Policy Conferences (Committee to Develop Guidelines for the Management of Patients With Atrial Fibrillation)

developed in collaboration with the North American Society of Pacing and Electrophysiology. *Circulation.* 104, 2118–2150.
7. Laupacis, A., Albers, G., Dalen, J., Dunn, M.I., Jacobson, A.K., and Singer, D.E. (1998) Antithrombotic therapy in atrial fibrillation. *Chest.* 114, 579S–589S.
8. Haissaguerre, M., Jais, P., Shah, D.C., et al. (1998) Spontaneous initiation of atrial fibrillation by ectopic beats originating in the pulmonary veins. *N Engl J Med.* 339, 659–666.
9. Chen, S.A., Tai, C.T., Tsai, C.F., Hsieh, M.H., Ding, Y.A. and Chang, M.S. (2000) Radiofrequency catheter ablation of atrial fibrillation initiated by pulmonary vein ectopic beats. *J Cardiovasc Electrophysiol.* 11, 218–227.
10. Stevenson, W.G., Friedman, P.L., Kocovic, D., Sager, P.T., Saxon, L.A., and Pavri, B. (1998) Radiofrequency catheter ablation of ventricular tachycardia after myocardial infarction. *Circulation.* 98, 308–314.
11. Nabar, A., Rodriguez, L.M., Timmermans, C., Smeets, J.L., and Wellens, H.J. (1999) Isoproterenol to evaluate resumption of conduction after right atrial isthmus ablation in type I atrial flutter. *Circulation.* 99, 3286–3291.
12. Nabar, A., Rodriguez, L.M., Timmermans, C., van den Dool, A., Smeets, J.L., and Wellens, H.J. (1999) Effect of right atrial isthmus ablation on the occurrence of atrial fibrillation: observations in four patient groups having type I atrial flutter with or without associated atrial fibrillation. *Circulation.* 99, 1441–1445.
13. Zipes, D.P. (1997). Specific arrhythmias: diagnosis and treatment, in *Heart Disease. A Text Book of Cardiovascular Medicine,* 5th Ed. (Braunwald, E., ed.), Saunders, Philadelphia, PA, pp. 640–704.
14. Morady, F. (1999) Radio-frequency ablation as treatment for cardiac arrhythmias. *N Engl J Med.* 340, 534–544.
15. Cappato, R. and Kuck, K.H. (2000) Catheter ablation in the year 2000. *Curr Opin Cardiol.* 15, 29–40.
16. Stevenson, W.G. and Friedman, P.L. (2000) Catheter ablation of ventricular tachycardia, in *Cardiac Electrophysiology. From Cell to Bedside*, 3rd Ed. (Zipes, D.P. and Jalife, J., eds.), Saunders, Philadelphia, PA, pp. 1049–1056.
17. Kalman, J.M., Olgin, J.E., Karch, M.R., and Lesh, M.D. (1997) Use of intracardiac echocardiography in interventional electrophysiology. *Pacing Clin Electrophysiol.* 20, 2248–2262.

23 Pacing and Defibrillation

TIMOTHY G. LASKE, PhD, ANNA M. LEGREID, PharmD, AND PAUL A. IAIZZO, PhD

CONTENTS

1. INTRODUCTION

Pacing and defibrillation systems monitor and treat inappropriate cardiac rhythms. These rhythms result in cardiac outputs (COs) that are inadequate to meet metabolic demands and are often life threatening. Currently, over 600,000 Americans have pacemakers, and 150,000 have implantable cardioverter–defibrillators (ICDs) *(1)*.

To understand the function of pacing and defibrillation systems best, the underlying physiological situations indicated for their use must also be defined and understood. As with the design of any biomedical device or system, a "first principles" understanding of the appropriate physiological behavior is a prerequisite to the definition of the performance characteristics of the device. The information in this chapter is not totally comprehensive and thus should not be used to make decisions related to patient care. This chapter aims to provide a basic understanding of the physiological conditions that require intervention with pacing or defibrillation systems as well as technical information on these systems to provide a foundation for future research and reading on this topic.

2. CARDIAC RHYTHMS AND ARRHYTHMIAS

2.1. Cardiac Function and Rhythm

CO (liters/minute) is defined as the heart rate (HR, beats per minute) multiplied by the stroke volume (SV, liters), or CO = HR × SV. Normally, the HR is determined by the rate at which the sinoatrial node (the "biological pacemaker") depolarizes. In healthy individuals, the sinoatrial node provides the appropriate HR to meet variable metabolic demands. More specifically, the sinoatrial nodal rate is modulated by (1) sympathetic and parasympathetic innervation; (2) local tissue metabolites and other molecules; (3) neurohormonal factors; or (4) the perfusion of the nodal tissues. SV is the quantity of blood ejected from the heart during each ventricular contraction. The instantaneous stroke volume is governed by a number of factors, including HR, degree of ventricular filling/atrial performance, atrial–ventricular synchrony, and myocardial contractility.

Multiple physiological and pathological conditions exist that may result in an inappropriate CO. These conditions need to be defined to understand the functional requirements of pacing and defibrillation systems and to motivate the logic behind the system features and performance characteristics.

From: *Handbook of Cardiac Anatomy, Physiology, and Devices*
Edited by: P. A. Iaizzo © Humana Press Inc., Totowa, NJ

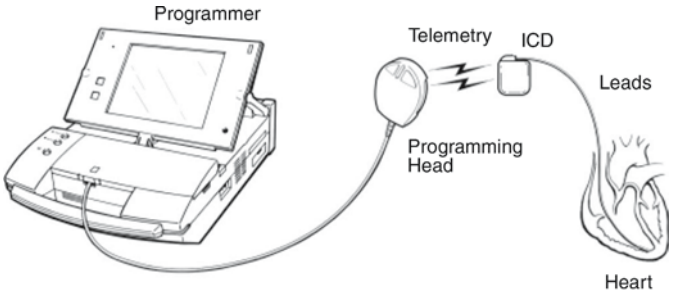

Fig. 1. Schematic of a typical implantable defibrillation system and the associated programmer. ICD, implantable defibrillation device.

2.2. Conditions of the Sinoatrial Node

- Normal sinus rhythm: Sinoatrial nodal rate is appropriate for the current metabolic demand (*see normal.mpg* on the Companion CD).
- Sinus bradycardia: A slow sinoatrial nodal rate, resulting in a slow HR. This may or may not be functionally appropriate. HR↓ → CO↓.
- Sinus tachycardia: A fast sinoatrial nodal rate, resulting in a higher HR. This may or may not be functionally appropriate. HR↑ → CO↑ (for excessive HRs, CO↓ because of reduced filling time).
- Sick sinus syndrome (SSS): Unpredictable sinoatrial nodal rate. The rate is not appropriately coordinated with physiological demand. CO↑ or CO↓
- Chronotropic incompetence: Inappropriate response of the sinoatrial node to exercise. CO is too low for metabolic demands.
- Block: No sinoatrial nodal rhythm. The patient will have either no HR (asystole) or a rate defined by other regions within the heart. A rescue rhythm from the atrioventricular node normally occurs (40–60 beats/min, a so-called junctional rhythm). HR = 0 → CO = 0 or HR↓ → CO↓

2.3. Conditions of the Atrioventricular Node

- First-degree heart block: Defined as an atrioventricular interval longer than 200 ms. (The normal atrioventricular interval is about 120 ms.) SV↓ → CO↓
- Second-degree heart block: Atrial and ventricular activity are not 1:1. Two types of second-degree block are defined:
  - Mobitz type I: "Wenckebach phenomenon." A ventricular beat is dropped after a progressive elongation of the atrioventricular interval. HR↓ (missed beat) → CO↓
  - Mobitz type II: A ventricular beat is dropped without a progressive elongation of the atrioventricular interval. This is often an early indication of progressive disease of the conduction system. HR↓ (missed beat) → CO↓
- Third-degree heart block: No atrioventricular nodal conduction (conduction from the atrium to the ventricles). The atria contract at the sinoatrial nodal rate, and the ventricles are either asystolic or contract at a ventricular rescue rate (25–55 beats/min). HR↓ and SV↓ → CO↓

2.4. Arrhythmias

- Atrial tachycardia/flutter: High atrial rate of nonsinoatrial nodal origin. Not a physiological rate and therefore is decoupled from metabolic demand. HR↑ SV↓ → CO↑ or CO↓ (*see AT.mpg* on the Companion CD).
- Atrial fibrillation: Chaotic depolarization of the atrium. No atrial hemodynamic input to the ventricles, and a nonphysiological rate is conducted through the atrioventricular node to the ventricles. Ventricular output is decoupled from metabolic demand. Stasis of blood in the atria can result in clot formation and stroke. HR↑ SV↓ → CO↑ or CO↓ (*see AF.mpg* on the Companion CD).
- Ventricular tachycardia: High ventricular rate decoupled from sinoatrial nodal and atrial activity. This commonly results from a reentrant conduction loop or an ectopic foci (spontaneously beating region of myocardium). Ventricular rate is nonphysiological and therefore decoupled from metabolic demand. HR↑ SV↓ → CO↑ or CO↓ (*see VT.mpg* on the Companion CD).
- Ventricular fibrillation: Chaotic depolarization of the ventricles. No organized HR. CO = 0 (*see VF.mpg* on the Companion CD).

3. INTRODUCTION TO IMPLANTABLE PACING AND DEFIBRILLATION SYSTEMS

Implantable pacing and defibrillation systems require multiple components, as well as external instruments, for proper function and programming. The implantable portion of the system is composed of the implantable pulse generator (IPG, or pacemaker) or an implantable cardioverter–defibrillator (ICD, or defibrillator) and the pacing and/or defibrillation leads. The IPG and ICD are most commonly implanted in a subcutaneous location in the left pectoral region. Typically, depending on the patient's handedness, the condition of the upper venous system, the presence of other devices, or physician preference, the device may also be placed in the right pectoral region. It may be placed in a submuscular location when the physician is concerned about erosion of either the IPG or ICD through the skin (most common in thin, elderly, or very young patients) or for cosmetic reasons (to reduce the obvious nature of the device). Another variation is to place the device in an abdominal location. This is commonly done in small children to avoid discomfort or interference with the motion of the arm.

In support of the implanted hardware, an external programmer is used to telemeter information to and from the programmable IPG. This allows the physician to set/reset parameters within the device and enables the physician to download information relating to the status of the patient and the device. A complete defibrillation system is shown schematically in Fig. 1 (pacing systems use a similar configuration).

Pacing and defibrillation systems can be implanted using one of several methods. Early systems used leads attached to the epicardial surface of the heart, with the IPG or ICD placed in the abdomen of the patient (because of its large size). Although this technique is still used in certain clinical situations (i.e., for neonates), a transvenous approach for attaching the leads to the heart and a pectoral placement of the IPG or ICD are far more common. Typical procedural techniques for implantable pacing and defibrillation are described to provide a more thorough understanding of the system requirements.

Following anesthesia and sterile preparation of the incision site, one of two techniques is used to access the venous system for the implantation of transvenous leads. Venous access is achieved through either a surgical "cutdown" to the cephalic

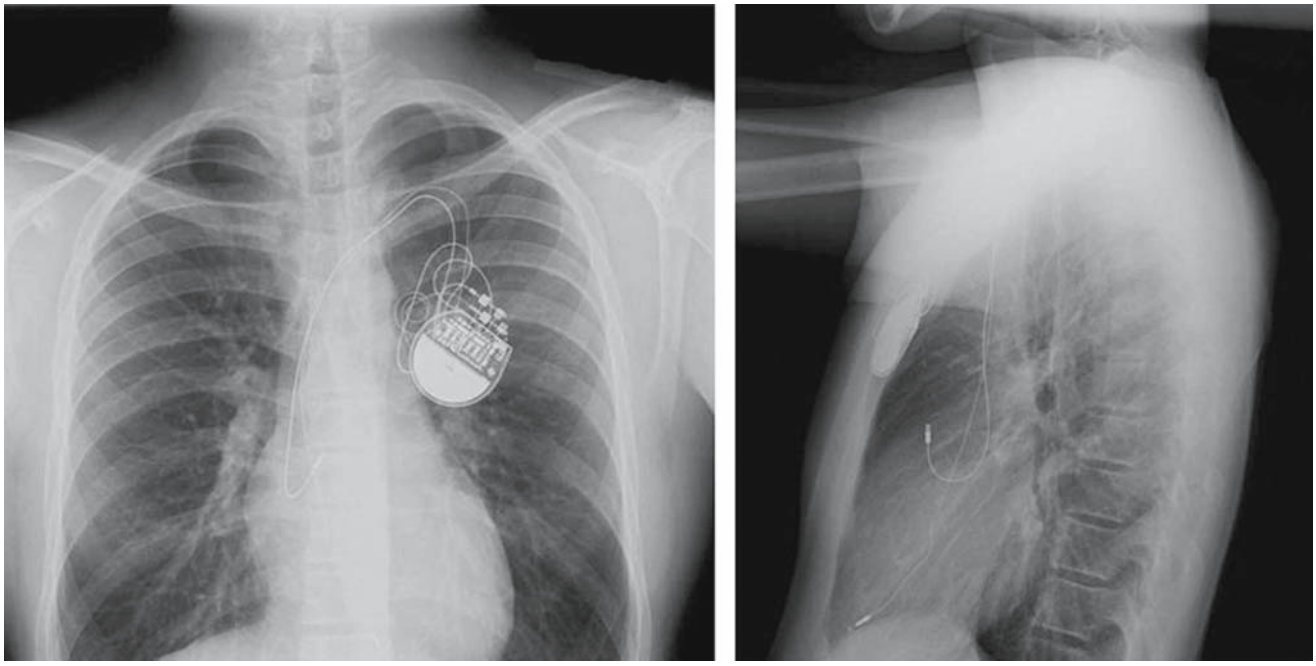

Fig. 2. Chest x-rays of an endocardial, dual-chamber pacing system in a young patient (**left**, anterior view; **right**, lateral view; Sainte-Justine Hospital, Montreal, Quebec, Canada; used with permission). The implantable pulse generator (IPG, pacemaker) is implanted in the left pectoral region. The superior lead is implanted in the right atrial appendage, and the inferior lead is in the right ventricular apex.

vein (the jugular vein is also used, but this is rare) or a transcutaneous needle puncture to the subclavian vein. The cutdown involves a careful surgical dissection to the vessel, placement of a cut through the vessel wall, and direct insertion of the lead into the vessel lumen. The subclavian puncture uses a needle to puncture the vessel, followed by passage of a guidewire through the needle. Subsequently, an introduction catheter (percutaneous lead introducer) with an internal dilator is forced over the wire and into the vein. The dilator is removed, leaving the catheter behind. The lead is then inserted through the catheter. (This technique can be viewed in *styletNew.mpg* on the Companion CD.)

Following insertion into the vein, the leads are advanced through the superior vena cava and into the right atrium for final placement in the right atrium, right ventricle, or coronary sinus/cardiac veins (providing access to the left atrium and ventricle). The leads are secured in the desired location within the heart using either a passive or active means of fixation with electrical performance verified (*see* Section 5.10). Next, an anchoring sleeve is used at the venous entry site to secure each lead to the tissue. This isolates the lead from mechanical forces outside the vein, ensuring adequate lead length remains within the heart to accommodate motion caused by activity, respiration, and heart motion. Following lead implantation, the proximal terminal ends are connected to the IPG or ICD, which is then placed in a subcutaneous or submuscular pocket formed in the tissue. The site is then sutured closed, thus completing the implantation. (Chest x-rays of a dual-chamber endocardial pacing system are shown in Fig. 2. Additional radiographic images of several pacing configurations are found in *xray1.jpg, xray2.jpg, xray3.jpg, xray4.jpg, xray5.jpg,* and *xray6.jpg* on the Companion CD.)

4. CARDIAC PACING

4.1. History

Discoveries relating to the identification of the electrophysiological properties of the heart and the ability to induce cardiac depolarization through artificial electrical stimulation are relatively recent. Gaskell, an electrophysiologist, coined the phrase *heart block* in 1882, and Purkinje first described the ventricular conduction system in 1845. Importantly, Gaskell also related the presence of a slow ventricular rate to disassociation with the atria *(2)*. The discovery of the bundle of His is attributed to its namesake, Wilhelm His Jr. *(3)*. He described the presence in the heart of a conduction pathway from the atrioventricular node through the cardiac skeleton that eventually connected to the ventricles. Tawara later verified the existence of the bundle of His in 1906 *(4)*. He is also credited with being the first to identify clearly the specialized conduction tissues (modified myocytes) that span from the base of the atrial septum to the ventricular apex, including the right and left bundle branches and Purkinje fibers.

The first known instance of electrical resuscitation of the heart was by Lidwell in 1929. Further, Hyman produced the first device for emergency treatment of the heart in 1932. Paul Zoll performed the first clinical transcutaneous pacing in 1952. Importantly for the pacing industry, the first battery-powered pacemaker was developed by Earl Bakken and used in postsurgical pediatric patients by C. Walton Lillehei in 1957 at the University of Minnesota (Fig. 3) *(2,5,6)*.

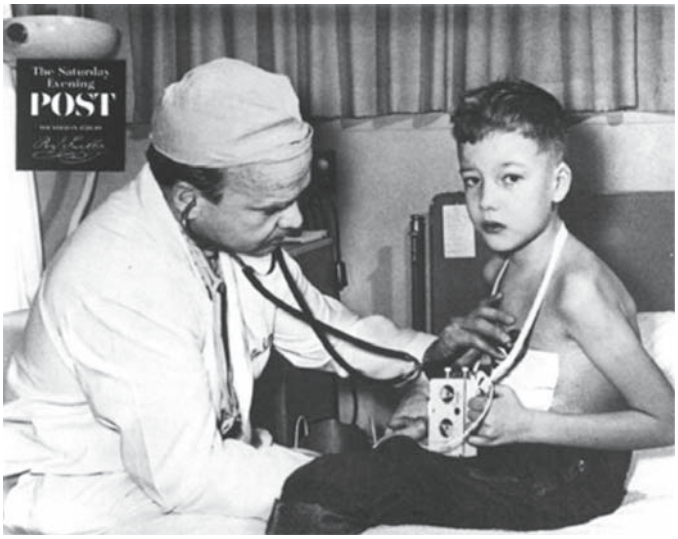

Fig. 3. Dr. C. Walton Lillehei with the first battery-powered, wearable pacemaker.

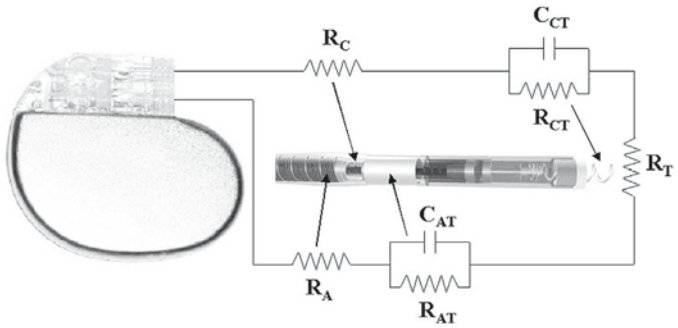

Fig. 4. Bipolar pacing circuit, including an implantable pulse generator and a pacing lead. Resistances: R_C, cathodic lead conductor; R_{CT}, cathode–tissue interface; R_T, tissue; R_{AT}, anode–tissue interface; and R_A, anodic lead conductor. Capacitances: C_{CT}, cathode–tissue interface; and C_{AT}, anode–tissue interface. (Tissue includes myocardium and blood.)

4.2. Artificial Electrical Stimulation

In addition to the spontaneous contraction that occurs within the heart, an artificial electrical stimulus (cardiac pacing) can be used to initiate myocardial contraction. This stimulation, in the form of cardiac pacing, is routinely performed as a means of managing patients with cardiac arrhythmias and conduction abnormalities *(7,8)*. Pacing induces myocardial contraction through the delivery of an electrical pulse to the patient's heart using an IPG (pacemaker) and a cardiac pacing lead. The cardiac pacing lead acts as the electrical conduit for stimulation and sensing, interfacing with the myocardial tissue. The electrical pulse is delivered in either a bipolar mode (involving cathodal and anodal electrodes on the lead) or in a unipolar mode (with a cathode on the lead and the IPG serving as the anode).

To initiate cardiac depolarization, an action potential must be created on a volume of myocardium. As was described in other chapters, a normal myocardial cell has a resting membrane potential of approx –90 mV. The resting membrane potential is dominated by the concentration of potassium. A cellular action potential occurs when the resting membrane potential is shifted toward a more positive value (i.e., less-negative value) to approx –60 to –70 mV. At this threshold potential, the cell's voltage gated sodium channels open and begin a cascade of events. In artificial electrical stimulation (pacing), this shift of the resting potential and subsequent depolarization are produced by the pacing system.

Two theories describe the mechanism by which artificial electrical stimulation initiates myocardial depolarization. The *current density theory* states that a minimum current density (amps/cubic centimeter) is required for stimulation of an excitable tissue. The *electric field theory* requires that a minimum voltage gradient (volts/centimeter) be produced within the myocardium to initiate depolarization *(9)*. These two theories can, in part, be considered related because the passage of current through the tissue (current density theory) will induce a potential difference across the cell membranes because of the limited conductivity of the tissue. Similarly, the creation of a potential within the tissue (electric field theory) will also induce a current. Regardless of the theoretical position taken regarding stimulation, the requirement for artificial stimulation is the shifting of the resting membrane potential from its normal value (typically –90 mV) toward a more positive value until the depolarization threshold is reached.

The impedance (Z) associated with charge transfer from an IPG to the cardiac tissue is composed of resistive (R) and reactive components (X_C, capacitive; X_L, inductive):

$$Z^2 = R^2 + (X_C + X_L)^2$$

The resistive term R includes the direct current (DC) resistance associated with the conductors internal to the lead (R_C, cathodic conductor; R_A, anodic conductor), the cathode–tissue interface R_{CT}, the anode–tissue interface R_{AT}, and the tissue itself R_T:

$$R = R_C + R_{CT} + R_T + R_{AT}$$

The capacitive term X_C is the sum of the capacitance of the cathode–tissue interface C_{CT} and the anode–tissue interface C_{AT}.

$$X_C = C_{CT} + C_{AT}$$

The inductance within the conductors and circuit is extremely small, and this term is typically neglected. Ignoring inductance, the resulting equation for lead impedance is:

$$Z^2 = R^2 + X_C^2$$

Schematic representations of the circuitry for bipolar and unipolar pacing systems are shown in Figs. 4 and 5. In these figures, the electric circuit for the delivery of energy to the myocardium is described as a simple RC circuit in which the IPG acts as the voltage/charge source and the lead conductors, electrodes, and cardiac tissue act as the load. Figure 4 depicts a bipolar pacing circuit in which the cathode and anode both reside on the pacing lead. Figure 5 represents the circuitry associated with a unipolar pacing system. In this case, the circuit is still bipolar, but the anode is the housing of the IPG. The term *unipolar* refers to the polarity of the lead.

Typical pacing circuit impedances range from 400 to 1500 Ω. Approximately 80% of the total impedance is at the tissue interface. (As an example, this will result in a 0.8 V drop at the tissue interface when a 1.0-V pacing pulse amplitude is used.) Using the aforementioned impedances (400 to 1500 Ω), a pacing output of 1.0 V produces currents of 2.5 mA and 0.67 mA.

The most common pacing stimulation waveform used to activate the myocardial tissue electrically is an exponentially decaying square wave. An active recharge is also commonly included at the trailing edge of the stimulation pulse to reduce the postpace polarization on the electrodes by balancing the charge delivered. The stimulating portion of the waveform is characterized by its amplitude (volts) and pulse width (milliseconds). A relationship exists between the required amplitude and pulse width duration for depolarization ("pacing") of the tissue. This relationship, termed a *strength–duration curve*, is most commonly plotted as shown in Fig. 6.

Additional terminology relating to the strength-duration curve includes the rheobase and chronaxie values. *Rheobase* is the threshold voltage at an infinitely long pulse width. *Chronaxie* is the threshold pulse width at two times the rheobase voltage. The output of a clinical IPG is commonly set at twice the voltage threshold corresponding at the chronaxie pulse width to ensure a safety margin *(9)*.

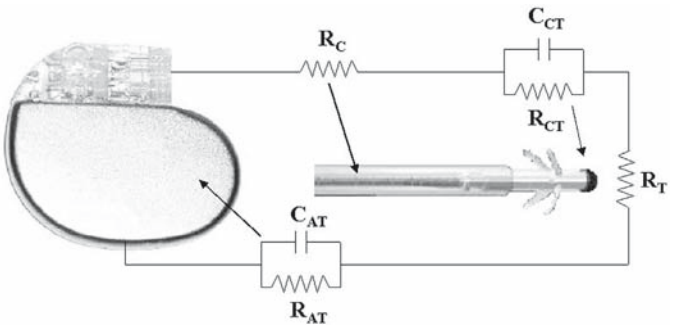

Fig. 5. A pacing circuit (unipolar type) that includes an implantable pulse generator and a pacing lead. Resistances: R_C, cathodic lead conductor; R_{CT}, cathode–tissue interface; R_T, tissue; and R_{AT}, anode–tissue interface. Capacitances: C_{CT}, cathode–tissue interface; and C_{AT}, anode–tissue interface. (Tissue includes myocardium, blood, lungs, etc.)

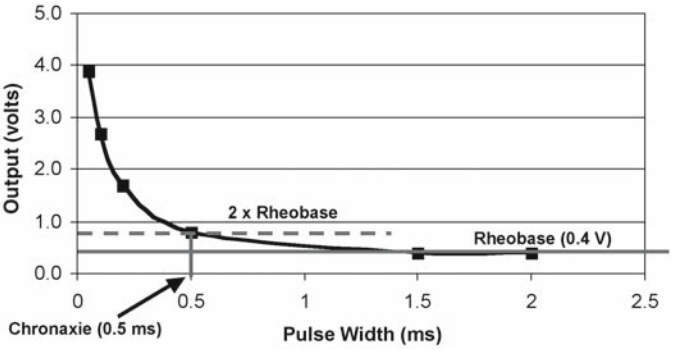

Fig. 6. A typical strength–duration curve for cardiac pacing. This particular curve was obtained using a Medtronic model 5076 bipolar pacing lead positioned in the right ventricular apex of a canine. In this plot, chronaxie and rheobase were 0.5 ms and 0.4 V, respectively.

4.3. Indications for Pacing

Pacing and defibrillation systems are designed to maintain appropriate cardiac rhythms to maximize both the patient's safety and quality of life. With the exception of cases of sudden cardiac death, for which a defibrillator is clearly required, the determination of when to use a pacing or implantable defibrillation system can be complex. This section describes the current classification of indications for pacing and provides a few practical examples of these indications and the decision process associated with choosing the appropriate system for a given patient's condition.

The indications for either pacing or defibrillation therapy are commonly classified in the standard American College of Cardiology/American Heart Association (ACC/AHA) format as follows *(10)*:

- Class I: Conditions for which there is evidence or general agreement that a given procedure or treatment is beneficial, useful, and effective.
- Class II: Conditions for which there is conflicting evidence or a divergence of opinion about the usefulness/efficacy of a procedure or treatment.
- Class IIa: Weight of evidence/opinion is in favor of usefulness/efficacy.
- Class IIb: Usefulness/efficacy is less well established by evidence/opinion.
- Class III: Conditions for which there is evidence or general agreement that a procedure/treatment is not useful/effective and, in some cases, may be harmful.

Cardiac pacing can be used for both temporary and permanent management of heart rhythms and function. Although the permanent pacing systems are the most well known, there are numerous indications for temporary pacing. The most commonly utilized temporary pacing systems are transcutaneous wires stitched directly into the myocardium and connected to an external stimulator. This system can be a small portable unit or a console. Common indications for temporary pacing include postsurgical heart block, heart block following an acute myocardial infarction, pacing for post-/intraoperative cardiac support, and pacing prior to implantation of a permanent pacemaker or during a pulse generator exchange.

The primary indication for the implantation of a permanent pacing system (pacemaker and leads) is to eliminate chronically the symptoms associated with the inadequate CO because of bradyarrhythmias. Typical causes of these bradyarrhythmias are: (1) sinus node dysfunction; (2) acquired permanent or temporary atrioventricular block; (3) chronic bifascicular or trifascicular block; (4) hypersensitive carotid sinus syndrome; (5) neurocardiogenic in origin; or (6) side effect caused by a drug therapy. The type of pacing system employed is dependent on the nature and location of the bradyarrhythmia, the patient's age, previous medical/surgical history, as well as concomitant medical conditions.

For conditions related to dysfunction of the sinoatrial node, an IPG with atrial features is commonly used in combination with a lead placed in/on the atrium. When management of the ventricular rate is required, a device with ventricular functionality and a ventricular lead is used. When management of the

Table 1
Indications for Permanent Pacing in Sinus Node Dysfunction

Class I	1. Sinus node dysfunction with documented symptomatic bradycardia, including frequent sinus pauses that produce symptoms. In some patients, bradycardia is iatrogenic and will occur as a consequence of essential long-term drug therapy of a type and dose for which there are no acceptable alternatives.
	2. Symptomatic chronotropic incompetence.
Class IIa	1. Sinus node dysfunction occurring spontaneously or as a result of necessary drug therapy with heart rate less than 40 beats/min when a clear association between significant symptoms consistent with bradycardia and the actual presence of bradycardia have not been documented.
	2. Syncope of unexplained origin when major abnormalities of sinus node function are discovered or provoked in electrophysiological studies.
Class IIb	1. In minimally symptomatic patients, chronic heart rate less than 40 beats/min while awake.
Class III	1. Sinus node dysfunction in asymptomatic patients, including those in whom substantial sinus bradycardia (heart rate less than 40 beats/min) is a consequence of long-term drug treatment.
	2. Sinus node dysfunction in patients with symptoms suggestive of bradycardia that are clearly documented as not associated with a slow heart rate.
	3. Sinus node dysfunction with symptomatic bradycardia caused by nonessential drug therapy.

Source: Adapted from ref. *11*.

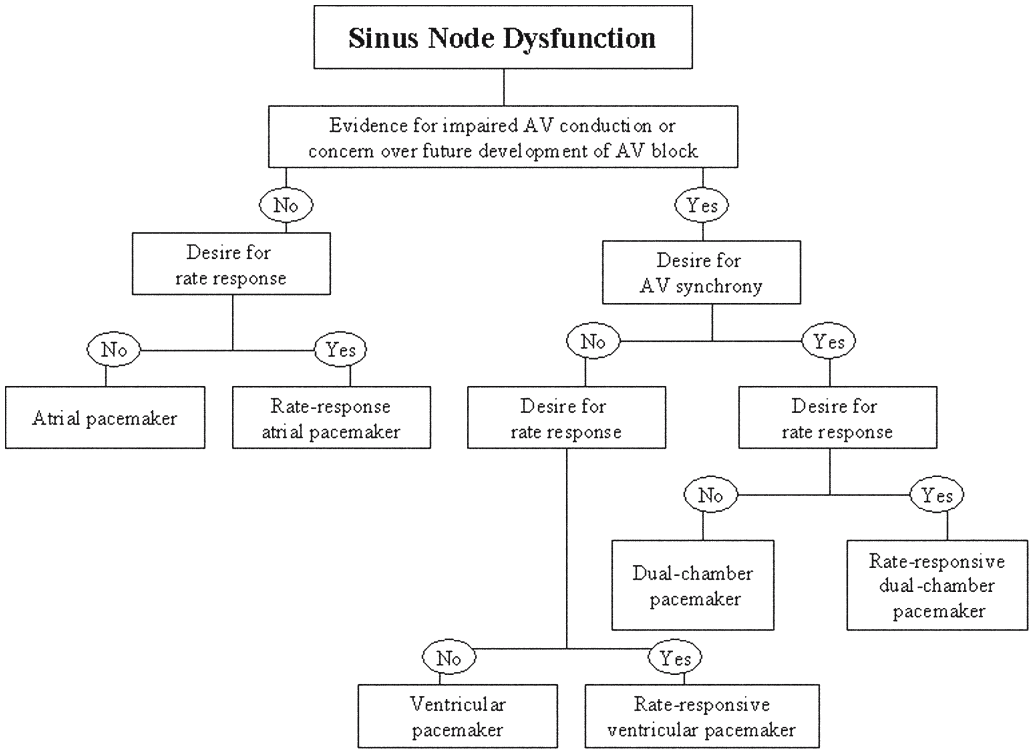

Fig. 7. A typical decision tree employed for determining proper therapy when the implantation of a pacemaker for sinus node dysfunction is considered. Adapted from ref. *11*. AV, atrioventricular.

rhythms of both the upper and lower chambers of the heart is required, a dual-chamber system is implanted.

Two clinical situations are outlined next to illustrate common indications for pacing as well as the decision tree often used to determine the type of pacing system for the particular indication. The indications for pacing in a patient with sinus node dysfunction are found in Table 1, and the decision tree is in Fig. 7 *(11)*. The indications for pacing in an adult with acquired atrioventricular block are found in Table 2, and the decision tree is in Fig. 8 *(11)*.

As an example, a patient with symptomatic chronotropic incompetence would have a class I indication for pacing (Table 1). Because this is related to dysfunction of the sinus node, Fig. 7 would then be used to determine the type of pacing system required. In this situation, rate response (a pacing system that responds to patient activity/exercise) would clearly be desired. If atrioventricular synchrony were also required, a rate-responsive dual-chamber pacemaker would be implanted (most commonly a DDDR system; *see* Section 4.4 to define this system and Table 3).

Table 2
Recommendation for Permanent Pacing in Acquired Atrioventricular Block in Adults

Class I	1. Third-degree and advanced second-degree atrioventricular block at any anatomical level associated with any one of the following conditions: a. Bradycardia with symptoms (including heart failure) presumed to be caused by atrioventricular block. b. Arrhythmias and other medical conditions that require drugs that result in symptomatic bradycardia. c. Documented periods of asystole greater than or equal to 3 s or any escape rate less than 40 beats/min in awake, symptom-free patients. d. After catheter ablation of the atrioventricular junction. There are no trials to assess the outcome without pacing, and pacing is virtually always planned in this situation unless the operative procedure is the atrioventricular junction modification. e. Postoperative atrioventricular block that is not expected to resolve after cardiac surgery. f. Neuromuscular diseases with atrioventricular block such as myotonic muscular dystrophy, Kearn-Sayre syndrome, Erb's dystrophy (limb girdle), and peroneal muscular atrophy, with or without symptoms, because there may be an unpredictable progression of atrioventricular conduction disease. 2. Second-degree atrioventricular block regardless of type or site of block, with associated symptomatic bradycardia.
Class IIa	1. Asymptomatic third-degree atrioventricular block at any anatomical site with average awake ventricular rates of 40 beats/min or faster, especially if cardiomegaly or left ventricular dysfunction is present. 2. Asymptomatic type II second-degree atrioventricular block with a narrow QRS. When type II second-degree atrioventricular block occurs with wide QRS, pacing becomes a class I recommendation. 3. Asymptomatic type I second-degree atrioventricular block with intra- or infra-His levels found at electrophysiological study performed for other indications. 4. First- or second-degree atrioventricular block with symptoms similar to those of pacemaker syndrome.
Class IIb	1. Marked first-degree atrioventricular block (more than 0.30 s) in patients with left ventricular dysfunction and symptoms of congestive heart failure in whom a shorter atrioventricular interval results in hemodynamic improvement, presumably by decreasing left atrial filling pressure. 2. Neuromuscular diseases such as myotonic muscular dystrophy, Kearn-Sayre syndrome, Erb's dystrophy (limb girdle), and peroneal muscular atrophy with any degree of atrioventricular block (including first-degree atrioventricular block), with or without symptoms because there may be unpredictable progression of atrioventricular conduction disease.
Class III	1. Asymptomatic first-degree atrioventricular block. 2. Asymptomatic type I second-degree atrioventricular block at the supra-His (atrioventricular node) level or not known to be intra- or infra-Hissian. 3. Atrioventricular block expected to resolve and unlikely to recur (e.g., drug toxicity, Lyme disease, or during hypoxia in sleep apnea syndrome in absence of symptoms).

Source: Adapted from ref. *11*.

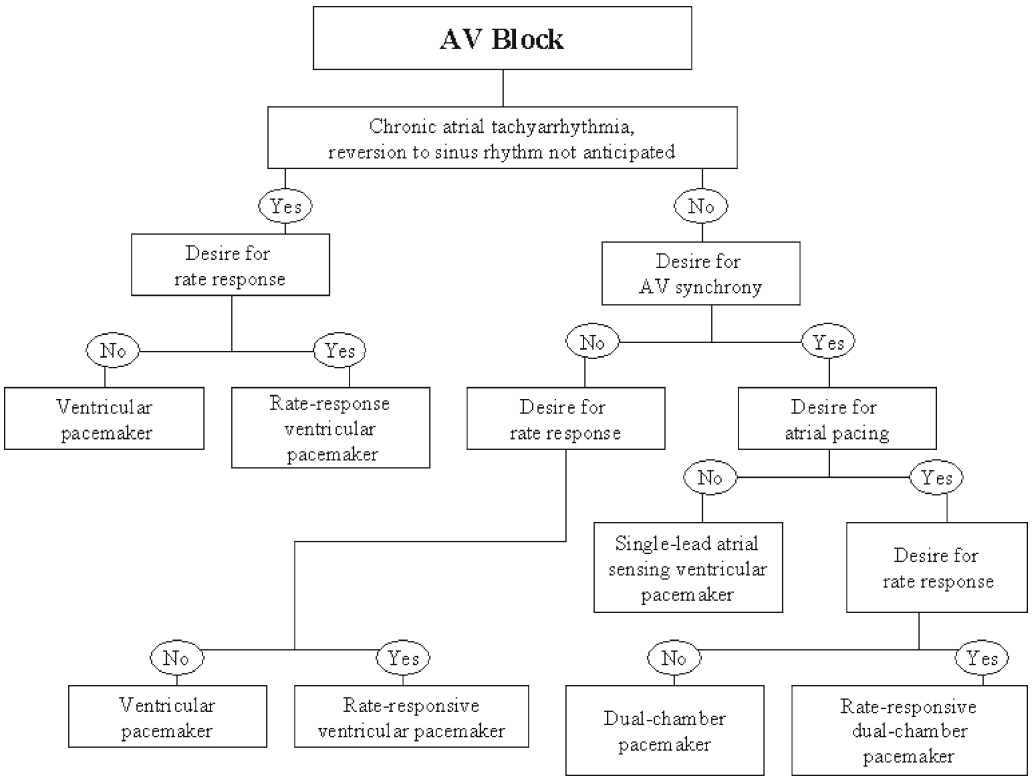

Fig. 8. A typical decision tree employed for determining proper therapy when the implantation of a pacemaker for atrioventricular block is considered. Adapted from ref. *11*. AV, atrioventricular.

Table 3
NASPE/BPEG Classifications for Pacing and Defibrillation Systems

I	*II*	*III*	*IV*
Chamber(s) paced	*Chamber(s) sensed*	*Response to sensing*	*Programmability/rate modulation*
0, none	0, none	0, none	0, none
A, atrium	A, atrium	T, triggered	P, simple programmability
V, ventricle	V, ventricle	I, inhibited	M, multiparameter programmability
D, dual (A + V)	D, dual (A + V)	D, dual (T + I)	C, communication with programmer
			R, rate modulation

Source: Adapted from ref. *12*.
Roman numerals I–IV indicate the position in the coding.
NASPE/BPEG, North American Society of Pacing and Electrophysiology and British Pacing and Electrophysiology Group.

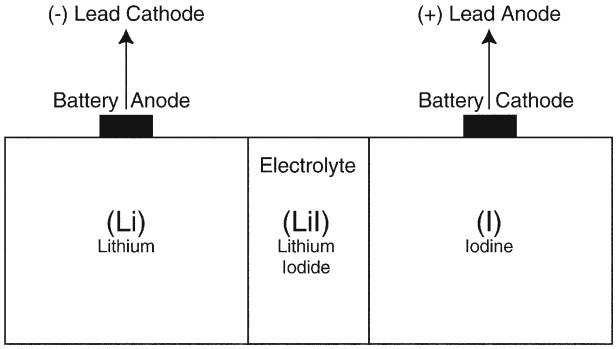

Fig. 9. Schematic of a lithium iodide battery. This is the most common chemistry used in modern pacemakers.

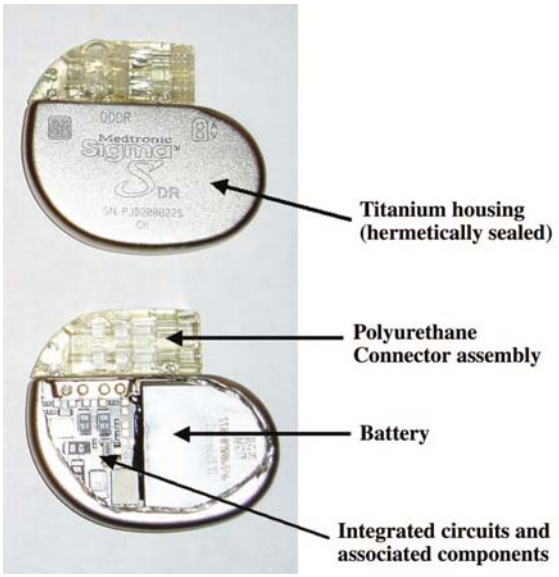

Fig. 10. Cutaway view of an implantable pulse generator (IPG, or pacemaker).

4.4. North American Society of Pacing and Electrophysiology and British Pacing and Electrophysiology Group Codes

To describe the function of a pacing system in a standardized manner, the North American Society of Pacing and Electrophysiology and British Pacing and Electrophysiology Group have developed a standard coding system (NASPE/BPEG code) *(12)*. This code describes the pacing system's functionality using a multiletter designation. The first four letters are typically used, although this practice is evolving as new pacing features and indications are under development. In the four-letter code, the first letter indicates the pacing activity (A, atrial pacing; V, ventricular pacing; D, dual-chamber pacing; O, no pacing); the second indicates sensing (A, atrial sensing; V, ventricular sensing; D, dual-chamber sensing; O, no sensing); the third indicates the reaction to a sensed event (I, inhibit pacing; T, trigger pacing; D, inhibit and trigger; O, no reaction to sensing); and the fourth is used to describe unique device functionality (R, rate responsive, for example). Thus, a VVIR system would pace the ventricles (V—), sense ventricular activity (-V—), inhibit (i.e., withhold pacing) on detection of a sensed event in the ventricle (—I-), and provide rate response to manage chronotropic incompetence (—R). *See* Table 3 for a more complete explanation of the coding system.

4.5. Implantable Pulse Generators

The IPG is an implantable computer with an integral pulse generator and battery. The componentry is typically encased within a hermetically sealed stamped titanium housing with the battery taking up approximately half of the device volume. The most common battery chemistry used in modern pacemakers is lithium iodide. Device longevity is typically 8 to 10 years, but may vary significantly depending on system utilization (Fig. 9).

Electrically insulated feedthroughs connect the internal circuitry to an external connector block, which acts as the interface between the internal circuitry of the IPG and the leads. Typically, the connector block consists of a molded polyurethane superstructure housing metallic contacts. The contacts may be simple machined blocks or "spring-type" metallic beams. The connector block often has set screws to ensure permanent retention of the leads, and these may also enhance electrical contact. A cutaway view of an IPG can be found in Fig. 10, and the

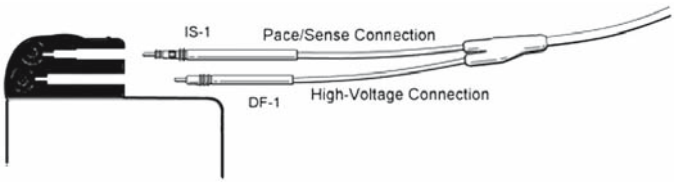

Fig. 11. Schematic of the implantable pulse generator-to-lead interface. The IS-1 connector is the standard configuration for pacing. The DF-1 connector is the standard configuration for high-voltage defibrillation. (*See connectorPlugIn.mpg* on the Companion CD.)

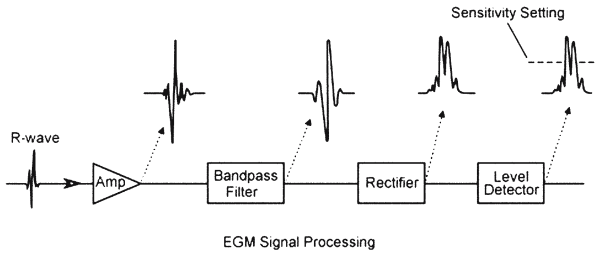

Fig. 12. The electrogram amplification and rectification scheme that is used in most modern implantable pacing and defibrillation systems. EGM, electrogram.

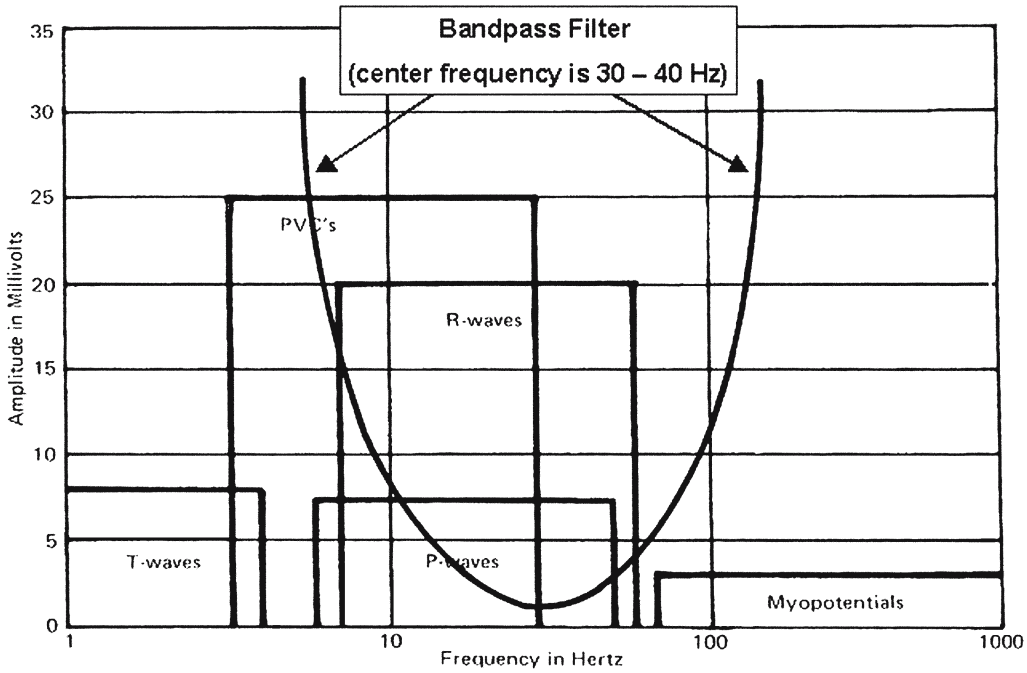

Fig. 13. Plot of electrical signals (amplitude and frequency) frequently encountered by pacing and defibrillation sensing algorithms. A bandpass filter for preferential detection of P waves and R waves is shown (parabolic line). This filter is designed to "reject" myopotentials and T waves.

scheme for connection between the IPG and the leads is shown in Fig. 11.

4.6. Sensing Algorithms

To assess the need for therapeutic intervention, the pacing system must be able to detect and interpret the electrical activity of the heart accurately. The electrical activity of the heart, or electrogram (EGM), is recorded as a differential voltage measured between the bipolar electrode pair on the lead (bipolar lead) or between the cathode on the lead and the housing of the IPG (unipolar lead). This signal is then processed within the IPG and analyzed by the sensing algorithms. Typically, such signals are amplified, filtered, and rectified prior to undergoing analysis by the device (Figs. 12 and 13).

The resulting signal is then passed through a level detector to determine if it exceeds the minimum threshold for detection that was preprogrammed into the device by the clinician. The sensitivity setting, in millivolts, determines what is discarded as noise by the algorithm and which signals will be detected. An ideal sensitivity setting is one that will reliably detect the event of interest (P wave in the atrium, R wave in the ventricle) and ignore physiological and nonphysiological signals.

Most rhythm management decisions are based on the HR detected. The modern IPG continuously measures the time from one sensed event to the next and compares the interval to the rates and intervals programmed by the clinician. For example, if two atrial events occur with a separation of 1500 ms (1.5 s), the HR is 40 beats/min (HR = 60/measured beat-to-beat interval; 60/1.5 = 40 beats/min).

To understand the logic behind sensing algorithms and pacing timing diagrams, specific terminology needs to be introduced. Table 4 includes the most commonly used terms and abbreviations. These terms are freely used in further discussions of the logic behind pacing and defibrillation sensing and therapies without further explanation. This table also provides the reader with the vocabulary required for interpreting and understanding current literature and publications on the topic.

Table 4
Pacing and Timing Abbreviations

AP	Atrial pace
AS	Atrial sense
AR	Atrial refractory event
AEI	Atrial escape interval: longest allowable interval between ventricular and atrial event (also called VA interval)
ARP	Atrial refractory period
AV	Atrioventricular
AV interval	Longest allowable interval between atrial and ventricular event
LR	Lower rate: slowest pacing rate allowed
LR interval	Longest period of time allowed before delivery of a pacing stimulus
MS	Mode switch
PAV	Paced atrioventricular interval: longest allowable interval between paced atrial beat and paced or sensed ventricular beat
PMT	Pacemaker-mediated tachycardia
PVAB	Postventricular atrial blanking period
PVARP	Postventricular atrial refractory period
SAV	Sensed atrioventricular interval: longest allowable interval between sensed atrial beat and paced or sensed ventricular beat
TARP	Total atrial refractory period (AV + PVARP)
UAR	Upper activity rate (also called maximum sensor-indicated rate)
UR	Upper rate: fastest pacing rate allowed
UR interval	Shortest allowable interval between paced beats or a sensed and paced beat
UTR	Upper tracking rate: fastest rate the ventricles may be paced in 1:1 synchrony with the sensed atrial rate (also called maximum tracking rate)
VA interval	Time between ventricular and atrial event
VP	Ventricular pace
VR	Ventricular refractory event
VRP	Ventricular refractory period
VS	Ventricular sense
VSP	Ventricular safety pacing

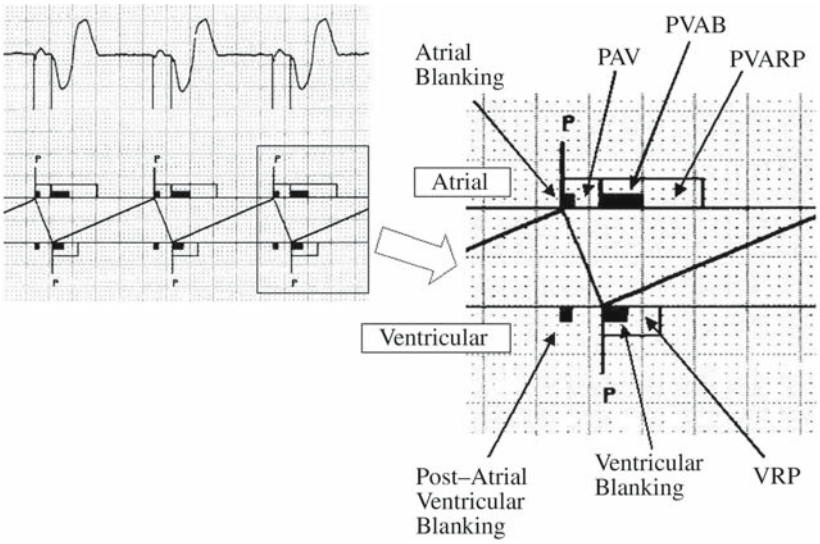

Fig. 14. A typical dual-chamber timing diagram, including subdiagrams for the atrial and ventricular channels. The sequence of events begins with a paced atrial beat P. This paced beat occurs when the maximum allowable interval between sensed atrial events is exceeded. For example, if the minimum rate is programmed to 60 beats/min, an atrial pace will occur when a 1000-ms interval between sensed events is exceeded. Immediately following this pacing pulse, both the atrial and ventricular sensing algorithms are blanked. This means that the threshold detector ignores all sensed activity within that period. The system is blanked to avoid sensing the resultant atrial depolarization on the atrial channel and the atrial pacing spike and the atrial depolarization on the ventricular channel. Concurrently, in the atrium a paced atrioventricular (PAV) interval occurs. This is the longest interval that will be allowed by the device without a paced ventricular beat. The PAV is commonly programmed to 150 ms and is set to optimize filling of the ventricle caused by the atrial contraction. During a cardiac cycle, if the PAV value is reached (meaning an intrinsic ventricular beat does not occur within the programmed interval following the paced atrial beat), a ventricular pacing pulse is then delivered. This pacing pulse is again accompanied by blanking in both channels to avoid oversensing of the pacing pulse and the resultant ventricular depolarization. This interval is referred to as the postventricular atrial blanking (PVAB) period on the atrial channel. Concurrently, the postventricular atrial refractory period (PVARP) occurs on the atrial channel in which the device attempts to avoid sensing of retrograde P waves (i.e., atrial contractions conducted through the atrioventricular node in a retrograde manner), and far-field R waves. The ventricular refractory period (VRP) occurs on the ventricular channel to avoid oversensing of T waves. Following these intervals, the timing is repeated. If the atrial rate stays above the minimum programmed rate (the lower rate) and the SAV is never reached, the device will never pace unless inappropriate sensing occurs.

The decision processes and behaviors of the typical pacing algorithm are usually described using a timing diagram (Fig. 14). An understanding of this diagram will provide the basis for the analysis of the behavior of pacing systems and will communicate the various parameters of concern to the clinician and device manufacturer. The concepts associated with pacemaker timing are shown in Fig. 14; the information is presented in an alternate form in Fig. 15.

The actual behaviors of pacing systems can deviate from the ideal for a number of reasons. For example, the pacing pulse can be of an inadequate energy to pace the chamber, losing capture on one or more beats (Fig. 16). Another situation that commonly arises is oversensing. In this case, the device inappropriately identifies electrical activity as an atrial or ventricular event (Fig. 17). Clinically, this is resolved by reprogramming the device to a lower sensitivity. Conversely, if a system is undersensing, the sensitivity is increased. Assessment of the behavior of the pacing system is vastly simplified through the use of marker channels. These are shown below the electrocardiograms of Figs. 16 and 17. The marker channel reports the behavior of the pacing system to allow a quick assessment of the performance of the algorithms and device output levels.

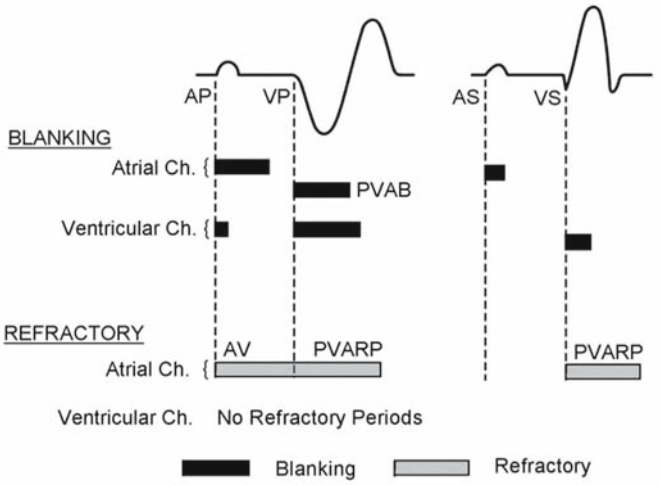

Fig. 15. Blanking and refractory periods. The top trace represents the electrocardiogram. The portion of the diagram on the left is a situation in which both the atrial and ventricular leads are pacing. The portion on the right is a situation in which the system is sensing intrinsic atrial and ventricular activity (i.e., no pacing is occurring). AP, atrial pace; AS, atrial sense; AV, atrioventricular; PVAB, postventricular atrial blanking period; PVARP, postventricular atrial refractory period; VP, ventricular pace; VS, ventricular sense.

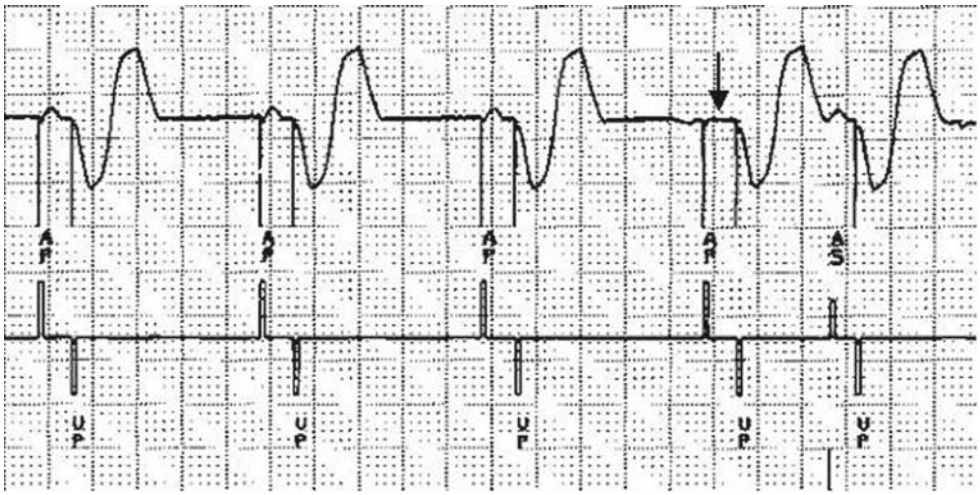

Fig. 16. A surface EKG (above) and pacemaker marker channel (below) printed from a programmer. Note the loss of capture on the atrial channel (indicated by the arrow); notice that no P wave follows the pacing pulse.

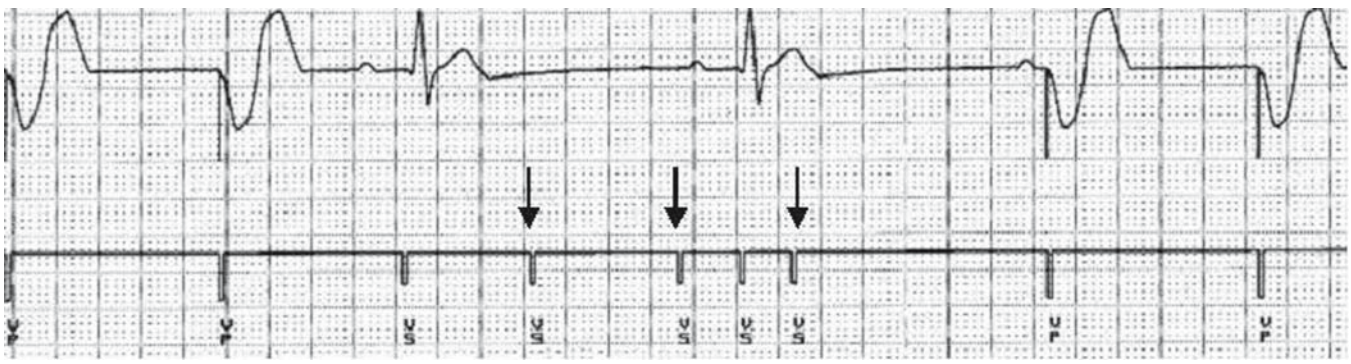

Fig. 17. A surface EKG (above) and pacemaker marker channel (below) printed from a programmer. Note the ventricular oversensing (indicated by the arrows); notice that no QRS complex is associated with the detected event.

Table 5
Effect of Antiarrhythmic Drugs on Pacing Thresholds

Increase at normal drug levels	*Increase at toxic drug levels*	*No increase*
Flecainide	Quinidine	Lidocaine
Propafenone	Procainamide	Mexiletine
Amiodarone	Disopyramide	
Sotalol		

Table 6
Antiarrhythmic Drugs, Action Potential Phases, and Physiological Consequences

Class	*Drug*	*Action potential phase*	*Physiological consequence*
Ia	Quinidine	0	Decreases automaticity of the sodium channel
	Procainamide		Slows conduction velocity
	Disopyramide		Prolongs refractory period
Ib	Lidocaine	0	Decreases automaticity of the sodium channel
	Mexiletine		May or may not slow conduction velocity
	Tocainide		Decreases refractory period
	Phenytoin		
Ic	Flecainide	0	Decreases automaticity of the sodium channel
	Propafenone		Slows conduction velocity
	Encainide		No effect on refractory period
	Moricizine		
II	Propranolol	Sinoatrial node	Decreases automaticity of nodal tissue
	Acebutol		Decreases conduction velocity
	Esmolol		Increases refractory period
III	Bretylium	3	Increases refractory period
	Sotalol [a]		No effect on conduction velocity
	Amiodarone [b]		No effect on automaticity
	Ibutilide		
	Dofetilide		
IV	Verapamil	Sinoatrial node	Decreases automaticity of nodal tissue
	Diltiazem		Decreases conduction velocity
			Increases refractory period

[a] Sotalol exhibits additional beta-blocking activity.
[b] Amiodarone also has Na^+-,beta-, and calcium channel-blocking activity.

4.7. Drug Interactions With Pacing Systems

It is important to note that certain drug therapies have been reported to have an impact on pacing system performance. Although it is rare for antiarrhythmic drugs to affect pacing thresholds significantly, they have been found to alter stimulation thresholds by inducing changes in the lead–myocardial interfacial conductivity and excitability. In addition, they can slow the intrinsic sinus rate, which necessitates pacing for resultant bradycardia. In general, class Ic drugs are most likely to increase pacing thresholds. Class Ia drugs can increase pacing thresholds at toxic dosages, and sotalol and amiodarone can increase pacing thresholds at therapeutic levels, but it is rarely clinically significant. A summary of the more common drugs and their impact on pacing thresholds, action potentials, and the physiological consequences of their action are found in Tables 5 and 6 *(13)*.

4.8. New Indications/Clinical Trials

Today, single- and dual-chamber pacing systems have become the standard method of treating many bradyarrhythmias. Clinical evidence has raised interest in the selection of both the frequency at which patients are paced and the optimal site of stimulation *(14)*. It has long been known that pacing produces a nonphysiological contraction pattern, but recent research has also indicated that potentially detrimental effects may result from long-term pacing *(15–18)*.

Currently, alternate choices in ventricular stimulation sites are of particular interest because of their presumed physiological and hemodynamic benefits. For example, pacing of the bundle of His is thought to produce a more physiological contraction pattern; additional evidence exists that there may also be hemodynamic benefits associated with right ventricular septal and outflow tract pacing *(15,19–24)*.

In patients with heart failure and associated wide QRS complexes, biventricular pacing has been adopted *(25,26)* (*see resync1.mpg* on the Companion CD). Finally, current research in atrial pacing has largely focused on reducing atrial fibrillation, improving methods of pace-terminating atrial tachycardias, and improving ventricular filling and atrial hemodynamics *(27–29)*. Researchers are even investigating the possibility of genetically engineering a biological pacemaker *(30)*.

5. CARDIAC DEFIBRILLATION

Today, sudden cardiac arrest (death) is one of the most common causes of mortality in developed countries; 3 million people experience sudden cardiac arrest worldwide, and the

annual incidence in the United States is 300,000. Sudden cardiac arrest claims more lives in the United States each year than the combination of deaths from acquired immunodeficiency syndrome (AIDS), breast cancer, lung cancer, and stroke *(31)*.

Several studies have identified the primary risk factors for sudden cardiac arrest, including: (1) coronary artery disease; (2) heart failure or decreased left ventricular ejection fraction; (3) previous sudden cardiac arrest events; (4) prior episodes of ventricular tachycardia; (5) hypertrophic cardiomyopathies; and (6) long QT syndrome *(32)*. The combination of any three of these factors increases the risk for sudden cardiac arrest significantly. Of sudden deaths, 90% occur in patients with two or more occlusions in their major coronary arteries *(33)*.

5.1. History

The first documentation of ventricular fibrillation was noted in 1850 *(34)*. A little over a century later, in 1962, the first direct current defibrillator was developed. Ventricular fibrillation began to be recognized as a possible cause of sudden death in the 1970s, and the first transvenous ICD was implanted in the 1990s. Since then, the medical device industry has provided dramatic reductions in ICD size and simultaneously increased safety, efficacy, battery longevity, diagnostics, and memory capabilities. Figure 18 shows the evolution in size of one manufacturer's ICD models.

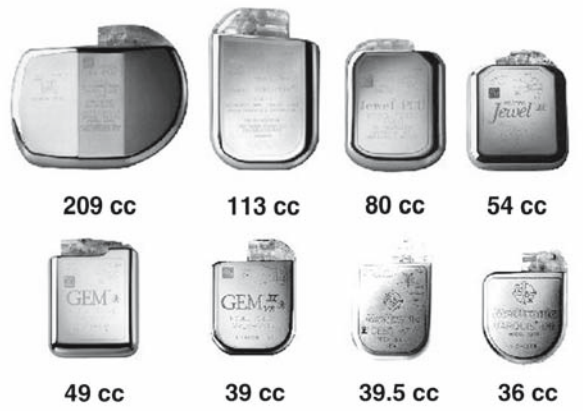

Fig. 18. The evolution of the implantable cardioverter–defibrillator (ICD). Dramatic reductions in size have occurred, with simultaneous improvements in longevity, diagnostics, functionality, and memory.

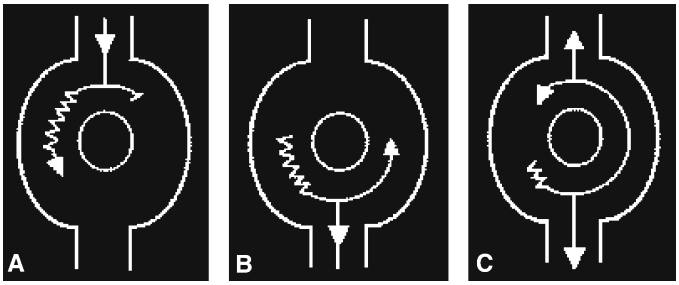

Fig. 19. Reentrant circuits. **(A)** Unidirectional block; **(B)** slow conduction; **(C)** reentry circuit.

5.2. Tachyarrhythmias

The commonly recognized mechanisms that lead to tachyarrhythmias (tachycardias and fibrillation) include reentry circuits, triggered activity, and automaticity. Reentry is considered as the most common tachyarrhythmia mechanism. It can be described as an electrical loop within the myocardium that has a circular, continuous series of depolarizations and repolarizations (Fig. 19).

In general, there are three requirements for reentry to occur: (1) the presence of a substrate, for example, an area of scar tissue; (2) two parallel pathways that encircle the substrate; and (3) one pathway that conducts slowly and one that exhibits unidirectional block. An impulse reaching the substrate is slowed by the unidirectional block and is allowed to conduct slowly down the slow pathway. As the impulse continues to move around the substrate, it conducts in a retrograde manner up the fast pathway, and the impulse continues to conduct in a circular fashion.

Inappropriate atrial tachycardias and ventricular tachycardias can be either hemodynamically stable or unstable. The level of hemodynamic compromise that occurs is typically considered to depend on both the rate and the pathway of the arrhythmia. In general, atrial tachycardias usually result in fast irregular ventricular rates caused by conduction through the atrioventricular node. As atrial rates increase, the rate conducted to the ventricles may or may not be 1:1 because the atrioventricular node has inherent limitations in its ability to conduct depolarizations. If, however, an abnormal pathway exists from the atria to the ventricles, then 1:1 conduction may be possible. Nevertheless, a patient's clinical risks are related to the level of hemodynamic compromise, with the most extreme case being ventricular fibrillation, which if not immediately reversed, most often results in death.

Triggered activity, or hyperautomaticity, is typically not consistently spontaneous and is a less-common mechanism. Early and delayed afterdepolarizations seen in phases 3 and 4 of the action potential are associated with triggered activity. *Automaticity* is defined as the ability of the cell to depolarize spontaneously at regular intervals. In a diseased heart, cells exhibit abnormal automaticity that causes them to depolarize at a rate faster than the intrinsic rate (i.e., phase 4 of the action potential is accelerated).

Common symptoms seen in patients with tachyarrhythmias may include syncopal episodes, palpitations, fatigue, or dyspnea. Both invasive and noninvasive diagnostic tools are available for diagnosing tachyarrhythmias. The common noninvasive procedures include: (1) a thorough patient interview; (2) blood work; (3) a 12-lead electrocardiogram (ECG); (4) tilt table testing; (5) Holter monitoring; (6) exercise stress test; (7) echocardiography; (8) signal average ECG; and/or (9) single-photon emission computed tomography/multiple gated acquisition (SPECT/MuGA). An electrophysiological study using cardiac catheterization and insertable loop recorders is the most commonly used invasive diagnostic procedure.

Therapeutic interventions to manage tachyarrhythmias are aimed at altering the behavior of myocardial cells or the conduction of the electrical impulse in the diseased tissue. They

Table 7
Indications for Implantable Cardioverter–Defibrillator (ICD) Therapy

Class I	1. Cardiac arrest caused by ventricular fibrillation or ventricular tachycardia not because of a transient or reversible cause. 2. Spontaneous sustained ventricular tachycardia in association with structural heart disease. 3. Syncope of undetermined origin with clinically relevant, hemodynamically significant sustained ventricular tachycardia or ventricular fibrillation induced at electrophysiological study when drug therapy is ineffective, not tolerated, or not preferred. 4. Nonsustained ventricular tachycardia in patients with coronary disease, prior myocardial infarction, left ventricular dysfunction, and inducible ventricular fibrillation or sustained ventricular tachycardia at electrophysiological study that is not suppressible by a class I antiarrhythmic drug. 5. Spontaneous sustained ventricular tachycardia in patients without structural heart disease not amenable to other treatments.
Class IIa	1. Patients with left ventricular ejection fraction of less than or equal to 30% at least 1 month postmyocardial infarction and 3 months postcoronary artery revascularization surgery.
Class IIb	1. Cardiac arrest presumed to be caused by ventricular fibrillation when electrophysiological testing is precluded by other medical conditions. 2. Severe symptoms (e.g., syncope) attributable to sustained ventricular tachyarrhythmias while awaiting cardiac transplantation. 3. Familial or inherited conditions with a high risk for life-threatening ventricular tachyarrhythmias, such as long QT syndrome or hypertrophic cardiomyopathy. 4. Nonsustained ventricular tachycardia with coronary artery disease, prior myocardial infarction, left ventricular dysfunction, and inducible sustained ventricular tachycardia or ventricular fibrillation at electrophysiological study. 5. Recurrent syncope of undetermined etiology in the presence of ventricular tachyarrhythmias at electrophysiological study when other causes of syncope have been excluded. 6. Syncope of unexplained origin or family history of unexplained sudden cardiac arrest in association with typical or atypical right bundle branch block and ST segment elevation (Brugada syndrome). 7. Syncope in patients with advanced structural heart disease in whom thorough invasive and noninvasive investigations have failed to define a cause.
Class III	1. Syncope of undetermined cause in a patient without inducible ventricular tachyarrhythmias and without structural heart disease. 2. Incessant ventricular tachycardia or ventricular fibrillation. 3. Ventricular fibrillation or ventricular tachycardia resulting from arrhythmias amenable to surgical or catheter ablation; for example, atrial arrhythmias associated with Wolfe-Parkinson-White syndrome, right ventricular outflow tract ventricular tachycardia, idiopathic left ventricular tachycardia, or fascicular ventricular tachycardia. 4. Ventricular tachyarrhythmias caused by a transient or reversible disorder (e.g., acute myocardial infarction, electrolyte imbalance, drugs, or trauma) when correction of the disorder is considered feasible and likely to reduce the risk or recurrent arrhythmia substantially. 5. Significant psychiatric illnesses that may be aggravated by device implantation or may preclude systematic follow-up. 6. Terminal illnesses with projected life expectancy of less than 6 months. 7. Patients with coronary artery disease with left ventricular dysfunction and prolonged QRS duration in the absence of spontaneous or inducible sustained or nonsustained ventricular tachycardia who are undergoing coronary bypass surgery. 8. New York Heart Association class IV drug-refractory congestive heart failure in patients who are not candidates for cardiac transplantation.

Source: Adapted from ref. *11*.

include attempts to correct the underlying complication, such as coronary reperfusion in the presence of a myocardial infarction/ischemia; antiarrhythmic drugs to restore and maintain normal sinus rhythm; electrical therapies such as antitachycardia pacing, cardioversion, defibrillation; and ablation performed surgically or with the assistance of a catheter. The role of medical devices in the management of these arrhythmias will become clear as device function is described in the remainder of this chapter.

5.3. ICD Indications

As was the case for the pacing indications discussed here, the indications for an ICD are also complex. The current indications by class are shown in Table 7 *(11)*.

5.4. External Cardiac Defibrillators

External defibrillators have become ubiquitous. In addition to traditional use in hospitals and by paramedics, these systems are now commonly found in many schools, public buildings, airports, and homes. As with implantable cardioverter–defibrillators, these systems are used to treat sudden cardiac death. These external systems deliver high-energy shocks (up to 360 J) to the chest of the patient using either patches or paddles. One electrode is typically placed in the right pectoral region and the second in the left axilla for delivery of the energy (Fig. 20).

5.5. Implantable Defibrillators

Similar to a pacemaker, an ICD is a self-contained, implantable computer with an integral pulse generator and battery. In addition to providing pacing therapies for bradyarrhythmias and tachyarrhythmias, ICDs also deliver high-energy discharges. The major components of an ICD include a battery, electronic circuitry and the associated components, high-voltage capacitors, high-voltage transformers, a telemetry antenna, a reed switch triggered on application of a magnetic field, and a connector block.

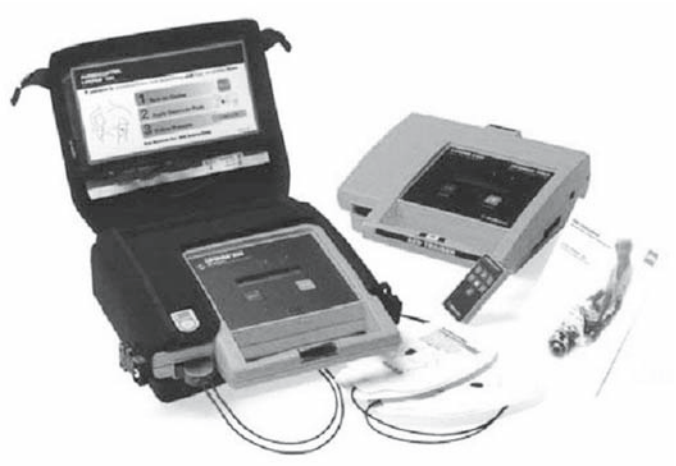

Fig. 20. An external cardiac defibrillator or automatic external defibrillator (LIFEPAK® 500, Medtronic, Inc., Minneapolis, MN).

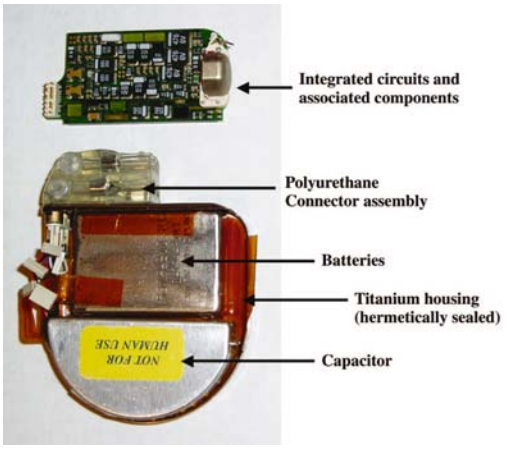

Fig. 21. The inner workings of a modern implantable cardioverter–defibrillator (ICD). A portion of the titanium housing has been removed to expose the typical internal components.

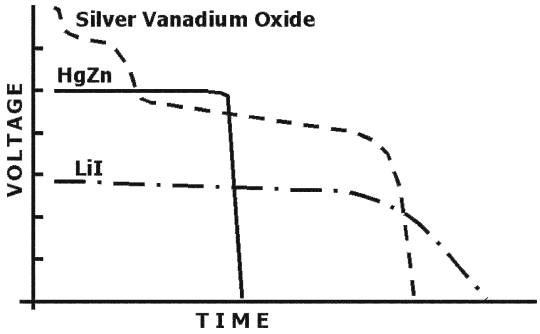

Fig. 22. A typical example of an implantable cardioverter–defibrillator (ICD) depletion curve for a silver vanadium oxide battery. Lithium iodide (LiI) and mercury zinc (HgZn) battery examples are included for comparative purposes.

The componentry is most commonly housed within a hermetically sealed stamped titanium case. Feedthroughs connect the internal circuitry to an external connector block, which acts as the interface between the internal circuitry of the ICD and the leads. The connector block is commonly fabricated from a molded polyurethane superstructure, which houses metallic contacts for interconnection with the leads. The contacts may be simple machined blocks or spring-type metallic beams. The connector block often has set screws to ensure permanent retention of the leads. A cutaway view of an ICD can be found in Fig. 21.

Today, most ICDs will use one or two batteries with silver lithium vanadium oxide chemistry. A typical full charge of this type of battery is 3.2 V. As the ICD battery energy starts to deplete, the voltage will follow the path shown in Fig. 22, in which there are two characteristic plateaus. The voltage is provided to the clinician on device interrogation to determine if the battery is at beginning of life, middle of life, elective replacement indicator, or end of life *(35)*. Each manufacturer and each device from a given manufacturer will have its own elective replacement indicator voltage. This value is representative of the voltage, current drain from the circuitry, and characteristics of the capacitor used. All devices should be replaced before end of life is reached, as this may prolong charge times and postpone needed therapy. The longevity of the device depends on the number of therapies delivered, but is typically 6–8 years.

The primary function of the ICD's capacitor is the accumulation and storage of an adequate amount of energy to shock-terminate a fibrillating heart. As mentioned, a typical voltage of an ICD battery is 3.2 V, whereas the capacitor can store up to 800 V (delivering an energy between 30 and 35 J). Periodic conditioning of each capacitor is required to maintain charge efficiency and therefore guarantee short charge times to allow rapid conversion of the arrhythmia *(36)*. The materials currently used in the capacitors slowly lose efficiency, especially when they are not used for a period of time because of a chemical decay process. This process (termed *deformation*) is mitigated by conditioning the capacitors (termed *reformation*). Reforming of the capacitor should be performed regularly by charging the capacitor to its maximum capacity and leaving the charge on it until it gradually discharges the energy. Fortunately, reformation can be easily programmed at regular intervals in most modern devices (e.g., every 6 months).

5.6. Sensing and Detection

It is desirable for an ICD to be able to sense ventricular rhythms that vary in amplitude, rate, and regularity accurately to distinguish among normal sinus rhythm, ventricular tachycardia, ventricular flutter, ventricular fibrillation, and supraventricular (atrial) arrhythmias (*see* examples in Fig. 23). Current devices adjust their sensitivity on a beat-to-beat basis to sense fine waves of ventricular fibrillation and to avoid oversensing of intrinsic T waves. If an ICD undersenses (misses cardiac activity that it was intended to detect), the device may fail to treat ventricular flutter or may fail to treat a ventricular tachycardia, which subsequently may accelerate into ventricular fibrillation. If an ICD oversenses, overestimating the cardiac rate, it may deliver inappropriate therapy, which will lead to patient discomfort, or more seriously, it may even induce a tachyarrhythmia.

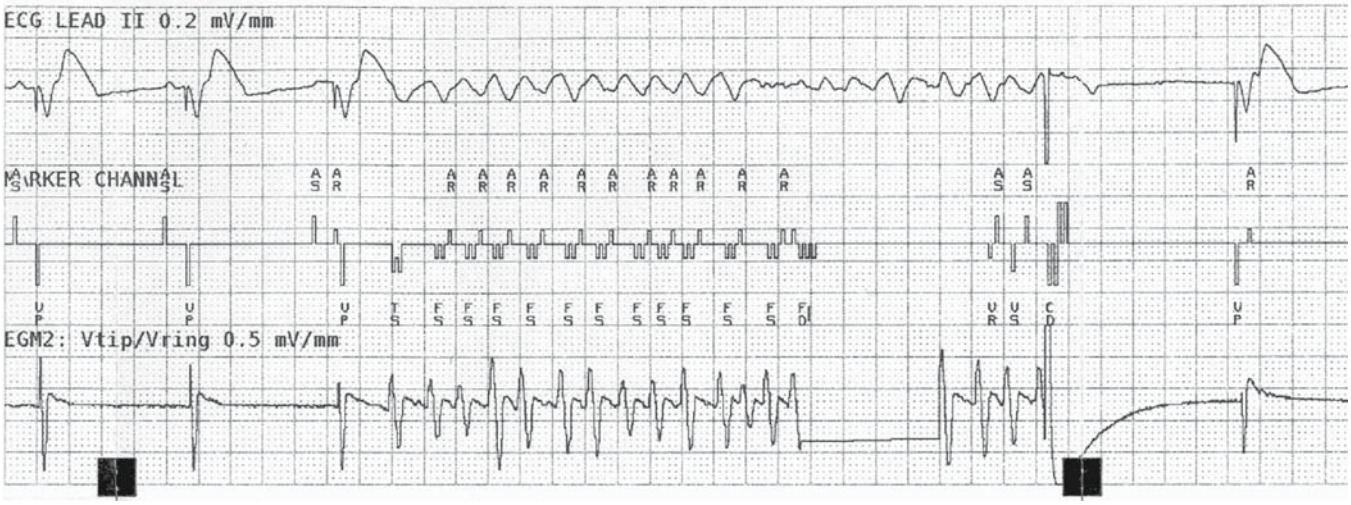

Fig. 23. Ventricular fibrillation and the associated device response (refer to the marker channel).

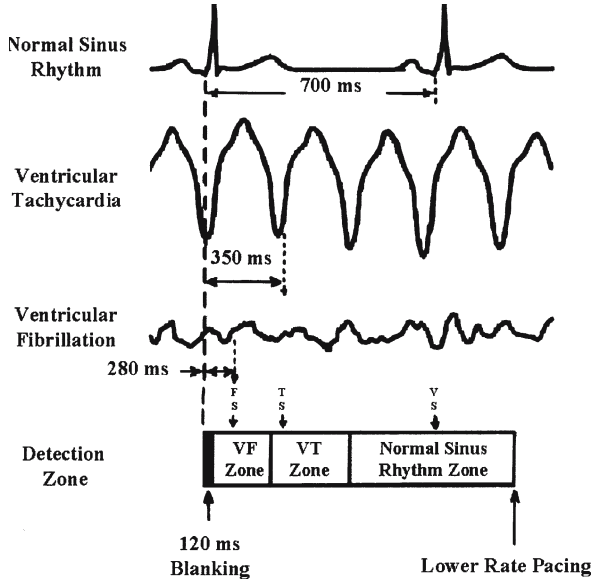

Fig. 24. Tachyarrhythmia detection intervals. The top three traces represent typical electrocardiograms that might be encountered by the device. The detection zones for ventricular fibrillation, ventricular tachycardia, and sinus rhythm are shown at the bottom. Note that an event with a cycle length of 700 ms is categorized as sinus rhythm, 350 ms as ventricular tachycardia (VT), and 280 ms as ventricular fibrillation (VF).

The steps involved in sensing and detection are similar to those discussed previously for the pacemakers. In fact, almost all ICDs on the market today include the pacing algorithms described earlier, with additional functionality/logic for detection and treatment of tachyarrhythmias. Arrhythmia detection typically occurs via the following steps: (1) sense the R wave or P waves; (2) measure the interval or cycle length between consecutive beats; and (3) compare the cycle length to prescribed detection zone intervals to classify the arrhythmia (Fig. 24).

For simplicity sake, this chapter focuses on only two detection zones: the ventricular fibrillation zone and the ventricular tachycardia zone. A fibrillation zone is commonly programmed to detect any interval faster than the interval prescribed by the clinician (e.g., 320 ms = 187.5 beats/min). If a minimum number/percentage of beats is sensed within this interval, the rhythm will be detected as ventricular fibrillation, and the device will treat the rhythm using the high-energy shock amplitudes preprogrammed by the clinician.

During the process of arrhythmia detection, the device counts the number of events in each of the detection zones and compares them to prescribed rules to classify the arrhythmia. Most ICD designs employ two different counters when classifying whether an arrhythmia is ventricular fibrillation or ventricular tachycardia. Typically, the ventricular fibrillation counter uses a probabilistic approach. Because ventricular fibrillation waves are chaotic and vary in amplitude and cycle length, the device will look for a programmed percentage of cycle lengths to fall within the fibrillation detection zone (e.g., 75%; Fig. 25), and if that criterion is met, the device will detect ventricular fibrillation and deliver the appropriate therapy.

Ventricular tachycardias, on the other hand, usually have a regular cycle length. A consecutive event counter is used, which states that a programmed number of cycle lengths (e.g., 18 of 18) needs to be within the tachycardia detection zone to classify the rhythm as ventricular tachycardia. If one cycle length falls out of the ventricular sense zone, the consecutive counter is reset to zero, and the count begins again.

Each ICD has the capability to redetect the same arrhythmia if the initial therapy was not successful. Redetection criteria will often be more aggressive (fewer number of beats sampled) than the initial detection criteria to ensure that subsequent therapies can be delivered quickly. An example of when the redetection criteria may not be as aggressive is when the patient has a long QT interval and is prone to developing torsade de pointes, which may spontaneously terminate.

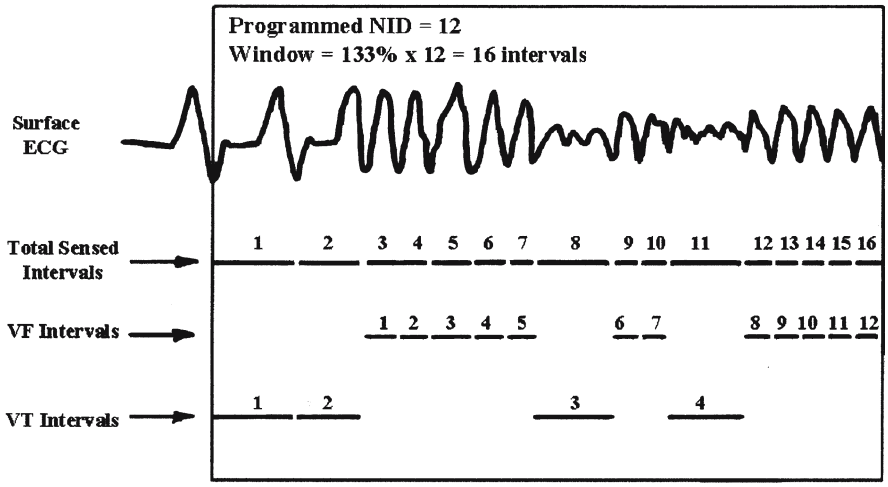

Fig. 25. An example of an implantable cardioverter–defibrillator (ICD) device record including 16 consecutive beats and their classification. Because 12 of 16 events (75%) were within the ventricular fibrillation (VF) detection zone, the arrhythmia would be classified as ventricular fibrillation, and high-voltage shocks would be delivered. ECG, electrocardiogram; VT, ventricular tachycardia.

Devices today have the option of programming an additional detection zone, which is referred to as a *fast ventricular tachycardia* zone. This is a zone that can be programmed for those patients with a fast ventricular tachycardia who may benefit from antitachycardia pacing. Treating a fast ventricular tachycardia with antitachycardia pacing may decrease the number of high-voltage shocks delivered, increasing the patient's quality of life and prolonging device longevity *(37)*.

Evidence of the benefit of this therapeutic approach was seen in the PainFREE Rx trial, which concluded that fast ventricular tachycardias with ventricular cycle lengths less than 320 ms could be terminated by antitachycardia pacing three out of four times with a low incidence of acceleration into ventricular fibrillation and syncopal episodes *(37)*. If a fast ventricular tachycardia zone is programmed, the device will always ensure that the most aggressive therapy is delivered. For example, if a fast ventricular tachycardia has been detected, the device will verify that no ventricular fibrillation intervals fell within that fast ventricular tachycardia zone before delivering antitachycardia pacing.

When targeting treatment of ventricular arrhythmias, it is important to verify that the arrhythmia is of ventricular origin. Each manufacturer will have a unique algorithm for distinguishing a supraventricular (atrial) tachycardia from a ventricular tachycardia. This is very important to avoid inappropriate shocking of a patient with sinus tachycardia caused by exercise or an atrial arrhythmia (atrial fibrillation or atrial flutter).

5.7. ICD Therapies

ICD therapies are programmed to ensure maximum patient safety while attempting to deliver the less aggressive therapies (least painful and least impact on device longevity) that will terminate the arrhythmia. ICD therapies can be tiered, such that the device initially delivers less aggressive therapies that are subsequently increased in aggressiveness until the desired treatment is obtained. A typical delivery order is as follows: antitachycardia pacing (delivering the least amount of energy), followed by cardioversion, and finally by defibrillation. Each of these therapies can be programmed as to the physician's preference.

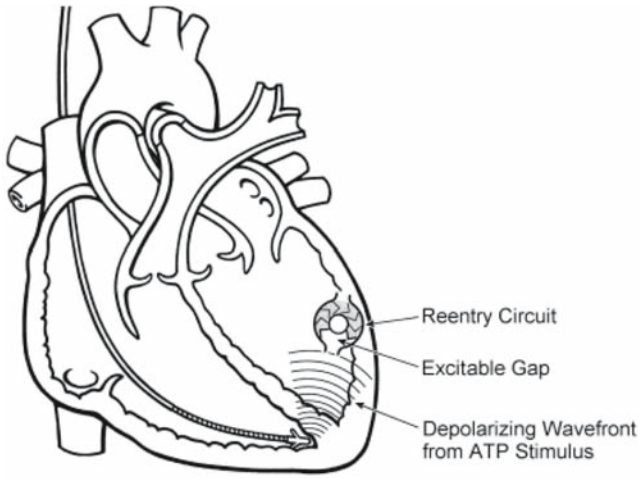

Fig. 26. Antitachycardia pacing therapy. A pacing stimulus is applied to entrain an excitable gap in the reentrant circuit. This disrupts the reentrant circuit and terminates the tachycardia. ATP, antitachycardia pacing.

Antitachycardia pacing is typically used in a clinical situation when one reentrant circuit is repeatedly activating the ventricles and causing a rapid, but regular ventricular tachycardia. The goal of the antitachycardia pacing therapy is to deliver, via a pacing stimulus, a depolarization wave into the area of the excitable gap (an area of repolarized tissue) of the reentry circuit. Recall that a reentrant circuit causes the majority of tachyarrhythmias. Thus, if a pacing pulse reaches the excitable gap before a new wavefront of the reentrant circuit, the reentrant activity is terminated (Fig. 26).

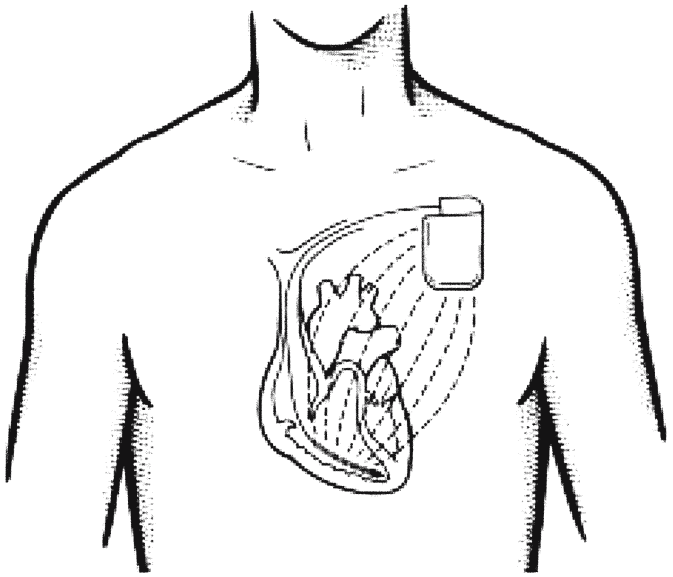

Fig. 27. Electric field between high-voltage electrodes during a shock; note that the implantable cardioverter–defibrillator (ICD) is functioning as one of the electrodes.

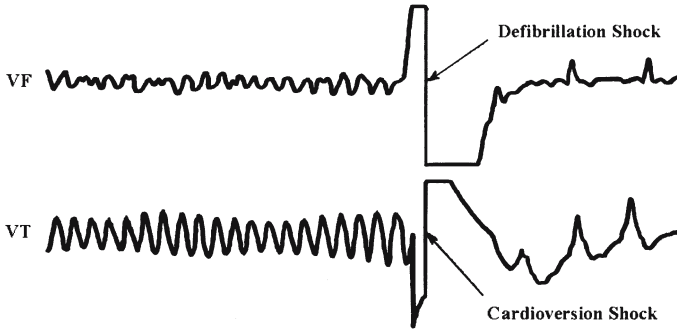

Fig. 28. Examples of successful defibrillation (top electrogram) and cardioversion (lower electrogram) therapies. VF, ventricular fibrillation; VT, ventricular tachycardia.

Cardioversion and defibrillation shocks are high-energy shocks delivered between two or more high-voltage electrodes, one of which is typically the ICD itself (the titanium housing acts as an electrode). The goal of these shocks is to defibrillate a critical mass of the myocardial cells that are depolarizing at a rapid, but irregular rate (Figs. 27 and 28).

Cardioversion can be described as a noncommitted high-voltage shock because the shock needs to be synchronized to a R wave, or the shock will not be delivered. Cardioversion shocks are used to treat ventricular tachycardias or regular fast ventricular tachycardias. Therefore, the shock is delivered on a R-wave that has been detected in the tachycardia detection zone. If the shock would happen to be delivered on a T wave, the underlying arrhythmia could be dangerously accelerated into ventricular fibrillation, which is why a cardioversion shock will be aborted if it is not synchronized to a R wave. The chaotic nature of ventricular fibrillation is treated by delivering a committed asynchronous shock. Both cardioversion and defibrillation gain their energy from the discharge of the ICD's high-voltage capacitor.

Depending on the manufacturer, each device will offer a number of programmable therapies per detection zone, all of which are programmed to physician preferences. The programming of the defibrillation therapy is often based on a specific patient's defibrillation threshold. This threshold is defined as the minimum amount of energy needed to rescue the heart from the fibrillating state (various algorithms exist for determining this energy). The physician typically prefers to set the first defibrillation therapy at an energy output greater than the defibrillation threshold to provide a margin of safety for the patient. A safety margin of at least 10 J greater than the defibrillation threshold is commonly used. For example, if a patient's defibrillation threshold has been determined as 15 J, the device will be programmed to deliver its first therapy at 25 J. Therefore, the maximum output of the device needs to be considered when assessing an appropriate safety margin. If a device has a maximum output of 35 J and the patient's defibrillation threshold is 27 J, there would only be an 8-J safety margin.

The typical shock waveforms delivered by the ICD have evolved over time. Early systems used a monophasic waveform delivered between a dedicated set of electrodes (i.e., delivered with a constant direction of current flow, or polarity). Later, sequential monophasic shocks between selected pairs of electrodes were offered because they were found to produce lower defibrillation thresholds in certain patients. Today, devices typically use a biphasic shock that reverses polarity during the discharge of the capacitors (Fig. 29).

The development of the biphasic waveform was considered a significant improvement in ICD technology, and they have been almost exclusively used since the mid-1990s *(38)*. The percentage of the drop in voltage, prior to termination of the waveform in the current polarity, is known as *tilt*. Tilt is measured from the instant the current starts to flow in one direction (leading edge) to the time that it ends its flow in that same direction (trailing edge). A tilt value can be measured for each direction that the current is flowing: Typical tilts are between 50 and 65% (Fig. 30).

As mentioned, most modern ICDs also include pacemaker functionality. Table 8 provides a final summary of the similarities and differences between IPGs and ICDs.

5.8. Pharmacological Considerations in the Management of Tachyarrhythmias

In contrast to the relatively small effect of antiarrhythmic drugs on pacing thresholds, the defibrillator threshold of an ICD may be changed significantly when used in conjunction with antiarrhythmic drug therapies. There are several positive benefits that have been considered useful in the concomitant use of ICDs and antiarrhythmic drugs. For example, antiarrhythmic drugs may act to decrease the frequency and duration of sustained and nonsustained ventricular tachycardia events that would otherwise require a shock from an ICD. They can also slow the rate of the ventricular tachycardia to increase the efficacy of antitachycardia pacing, decreasing the need for shock therapy. Last, antiarrhythmic agents may lower defibril-

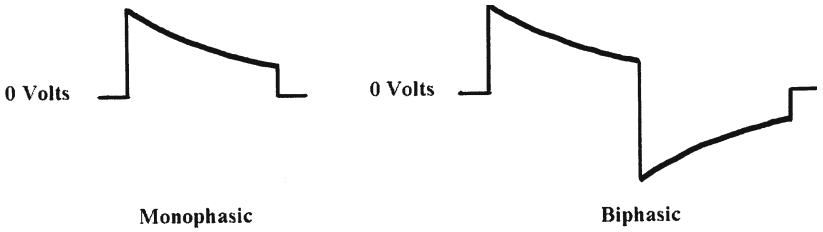

Fig. 29. Monophasic and biphasic shock waveforms.

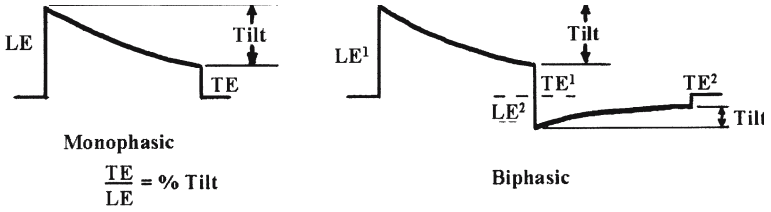

Fig. 30. Determination of the percentage tilt of a defibrillation waveform. LE, leading edge; TE, trailing edge.

Table 8
Comparison of the Principal Differences Between Implantable Pulse Generator (IPG) and Implantable Cardioverter–Defibrillator (ICD)

ICD	*IPG*
• Senses intrinsic rhythms and ventricular tachycardia/ventricular fibrillation and prefers to oversense	• Senses intrinsic rhythms, prefers to undersense
• Paces and shocks when appropriate	• Paces when appropriate
• Saves episode data	• Rejects signals that occur at high rates
• Battery requires high current capability for shocking	• Battery optimized for long-term, low current use

lation thresholds. Therefore, the use of antiarrhythmic drugs with ICDs can decrease the frequency or amplitudes of therapeutic shocks, thereby increasing both patient comfort and prolonging battery longevity *(39)*.

In addition to the benefits, there are also potentially undesired consequences associated with the concurrent use of ICDs and antiarrhythmic drugs *(13)*. Specifically, antiarrhythmic drugs may: (1) alter the detection of the arrhythmia, leading to an increase in the duration of a tachyarrhythmia; (2) increase defibrillation thresholds, making it more difficult to defibrillate the heart successfully; (3) slow the rate of the tachyarrhythmia so much that it no longer falls within the detection zone for both antitachycardia pacing and shock; and/or (4) prolong the width of the QRS complex on the ECG causing double counting and hence inappropriate shocks.

The typical antiarrhythmic drugs that affect defibrillation thresholds are: (1) type I agents, those with sodium channel blocking activities and the membrane stabilization effects; (2) β-blockers and calcium channel antagonists because of their effects on the nodal tissues; and (3) type III agents, which may increase or decrease defibrillation thresholds after long-term therapy (Table 9). Amiodarone has been reported to increase defibrillation thresholds after chronic use.

Table 9
The Impact of Select Antiarrhythmic Drugs on Defibrillation Thresholds

Increase	*Mixed effect*	*Decrease*
Flecainide	Quinidine	Sotalol
Propafenone	Procainamide	Bretylium
Lidocaine	Amiodarone	
Mexiletine		

Antiarrhythmic agents can also be proarrhythmic, which may lead to an increased requirement for ICD therapies. Predisposing factors to proarrhythmias are: (1) electrolyte imbalances such as hypomagnesemia or hypokalemia, (2) underlying ventricular arrhythmias, (3) ischemic heart disease, and (4) poor left ventricular function. One of the most dangerous forms of proarrhythmia is considered torsade de pointes or "twisting of the points." Specifically, torsade is a rapid form of polymorphic ventricular tachycardia associated with delayed ventricular repolarization. It should be noted that both inherited conditions such as long QT syndrome and the exposure to type Ia and III antiarrhythmic drugs that prolong the refractory period on the cardiac action potential put patients at an increased risk of developing torsade de pointes.

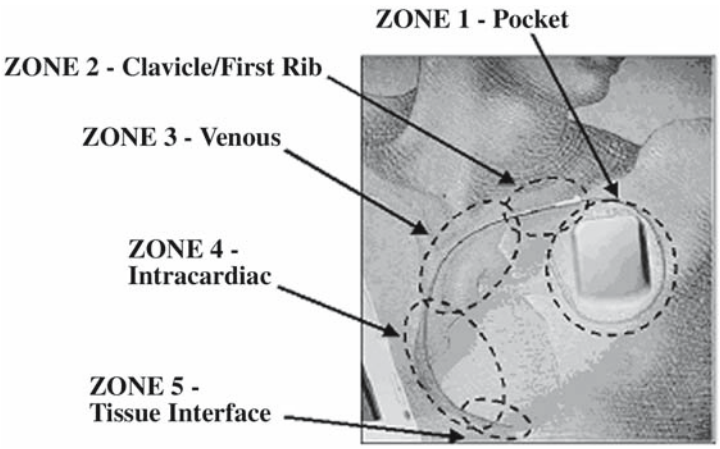

Fig. 31. The anatomical regions commonly spanned by transvenous endocardial pacing leads.

5.9. New Indications/Clinical Trials

This section focuses on some clinical trials that assessed the value of ICD therapy. Clinical trials serve the important role of assessing therapeutic safety and efficacy for: (1) establishing the validity of current clinical indications, (2) determining new indications for use, or (3) driving reimbursement through identification of clinical value. Properly run clinical studies continue to play an important role in continuous improvement of patient outcomes. Yet, an important distinction to make here is that there are major differences between primary and secondary studies.

Specifically, primary studies seek to find morbidity and mortality benefit in those patients who have not experienced an event. These studies identify a patient population considered "at risk" and attempt to identify means to treat such patients before they experience an event such as myocardial infarction or sudden cardiac arrest. In contrast, secondary studies evaluate posttreatment morbidity and mortality benefits to patient populations who have already suffered from an event (e.g., patients postmyocardial infarction or patients who have survived sudden cardiac arrest).

An example of an important clinical trial associated with the identification of the indications for ICD therapy is the Multicenter Automatic Defibrillator Implantation Trial (MADIT). This trial was instrumental in providing clinical evidence for identifying the patients who would benefit from an ICD therapy. The clinical hypothesis stated "in patients with previous myocardial infarction and left ventricular dysfunction, prophylactic therapy with an ICD improves survival versus treatment with conventional medical therapy" *(40)*. The primary end point of the study was a reduction in total mortality, and the secondary end points evaluated mortality associated with arrhythmias as well as cost-effectiveness. There were 196 patients included in the study; there were 39 deaths in the conventional therapy arm and 15 deaths in the ICD arm. The stated conclusions were that, in postmyocardial infarction patients at a high risk for ventricular tachycardia, prophylactic therapy with an ICD reduced overall mortality by 54% and arrhythmic mortality by 75% when compared with conventional therapy.

A follow-up to MADIT was the Multicenter Automatic Defibrillator Implantation Trial II (MADIT-II). The purpose of this study was to investigate the effects of prophylactic implantation of an ICD on the survival of patients postinfarction who presented with significant left ventricular dysfunction (left ventricular ejection fraction $\leq$30%). The primary conclusion of this study was that prophylactic implantation of an ICD in such patients resulted in improved survival and decreased mortality by 28% after 3 years. Importantly, the noted benefits of this study have changed practice in that physicians are now routinely implanting an ICD in postmyocardial infarction patients with left ventricular dysfunction *(41)*.

One last study that needs to be mentioned is the Sudden Cardiac Death in Heart Failure Trial (SCD-HeFT). This study set out to determine if amiodarone or a shock-only ICD reduces all-cause mortality compared to placebo in patients with either ischemic or nonischemic New York Heart Association (NYHA) Class II and III congestive heart failure (CHF) and an injection fraction of equal to or less than 35%. A total of 2521 patients studied at 148 centers in the United States, Canada, and New Zealand. Patients had a minimum follow-up of two and a half years. Results of this study showed that ICDs decreased mortality by 23% and that amiodarone, when used as a primary preventative agent, did not improve survival *(42)*.

5.10. Pacing and Defibrillation Leads

Cardiac pacing and defibrillation leads are the electrical conduit between the IPG or ICD and the heart. Specifically, they transmit therapeutic energies to the cardiac tissue and return sensed information to the IPG or ICD for diagnostic and monitoring purposes. It is noteworthy that such leads must: (1) withstand an extremely harsh environment, (2) permanently span multiple anatomical and physiological environments (Fig. 31), and (3) undergo approx 400 million heartbeat-induced deformations over each 10-year period within the heart (*see fluoro.avi* on the Companion CD).

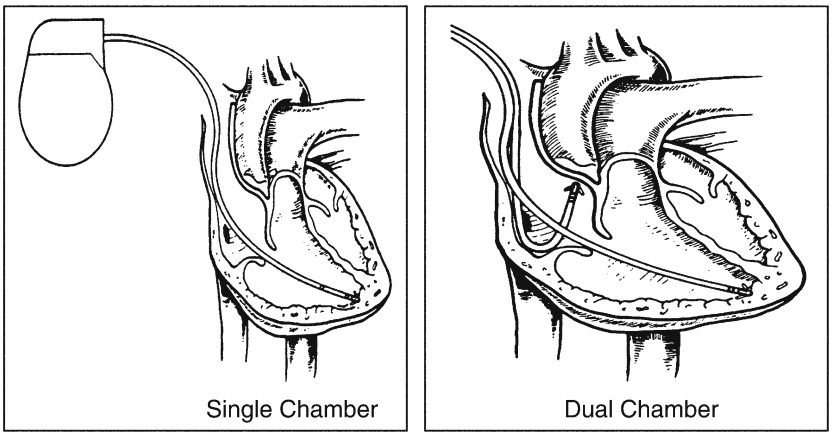

Fig. 32. Examples of single- and dual-chamber endocardial lead configurations.

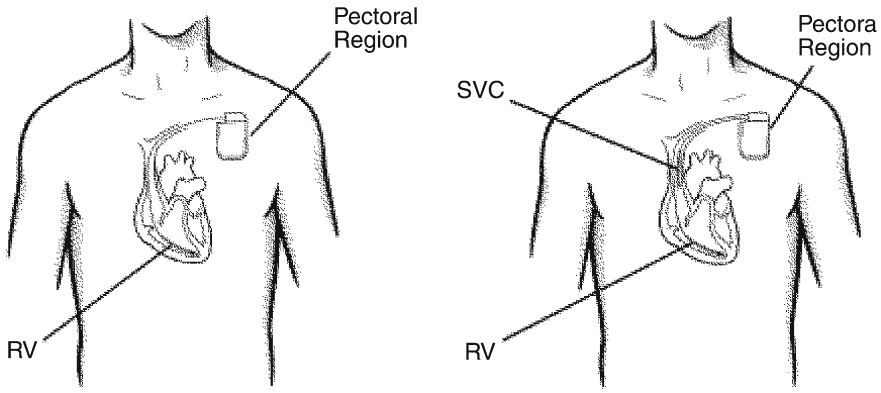

Fig. 33. Implanted configurations for two endocardial defibrillation systems with pectoral implantable cardioverter–defibrillator (ICD) placements. The single-coil system (left) delivers the shock energy from the right ventricular coil to the ICD. The dual-coil system (right) can deliver the energy from the right ventricular coil to a superior vena cava coil and/or the ICD. (*See energyVectorDual.mpg* on the Companion CD.) RV, right ventricle; SVC, superior vena cava.

Leads can be placed either endocardially or epicardially, depending on the patient's indication, physician preference, and/or anatomical considerations. In the case of the endocardial pacing systems (those implanted through the venous system to the endocardial surface of the cardiac chambers), the lead travels from subcutaneous tissue, including muscle and fat, into the bloodstream. These leads then pass through the upper vasculature and are finally permanently placed within the beating heart. Today, the vast majority of pacing systems utilize transvenous endocardial leads. (This lead placement technique can be viewed in *styletNew. mpg* on the Companion CD.)

In contrast, epicardial leads are attached directly to the surface of the heart and are routed through subcutaneous tissue to the ICD or IPG. Epicardial leads are most commonly used in pediatric patients and in adults with compromised venous access to the heart. Typical implanted configurations for endocardial single- and dual-chamber pacing systems are shown in Fig. 32, endocardial defibrillation systems in Fig. 33, and an epicardial defibrillation system with epicardial pacing leads in Fig. 34.

Modern leads are generally constructed of highly biostable and biocompatible polymers and metals. Configurations for the body of the leads (i.e., the portion traveling from the IPG or ICD to the distal electrodes) are chosen based on the number of circuits required, as well as considerations relating to size, handling, and manufacturer preferences (Fig. 35). The electrodes for stimulation and sensing are designed to provide stable electrical performance acutely and chronically.

To provide stability at the cardiac tissue interface, leads often use a mechanism for fixation to cardiac tissue and structures. Passive mechanisms for fixation include polymeric tines designed to entangle in the cardiac trabeculae and shaped segments along the length of the lead. They are termed *passive* because they do not require active deployment by the clinician. Common active means of fixation include helices and hooks or barbs. In addition, some epicardial leads require sutures to maintain a stable position. Finally, some leads have no fixation means whatsoever and count solely on lead stiffness to maintain locational stability (Figs. 36–39).

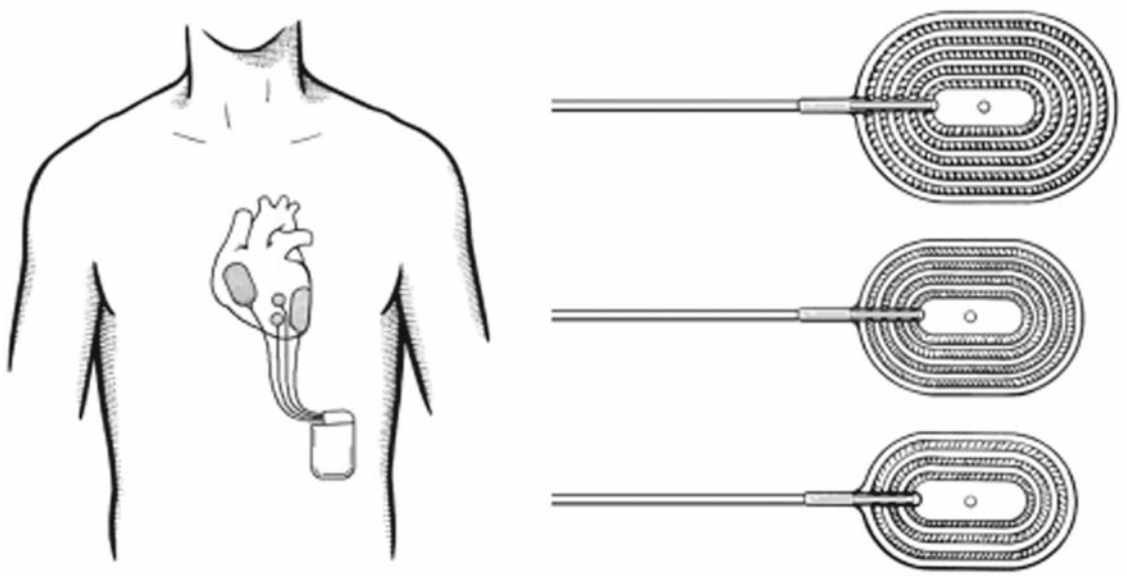

Fig. 34. Implanted configuration of an epicardial defibrillation system with an abdominal implantable cardioverter–defibrillator (ICD) placement. The system shown includes two unipolar epicardial pacing leads for pacing and sensing as well as a pair of epicardial defibrillation patches.

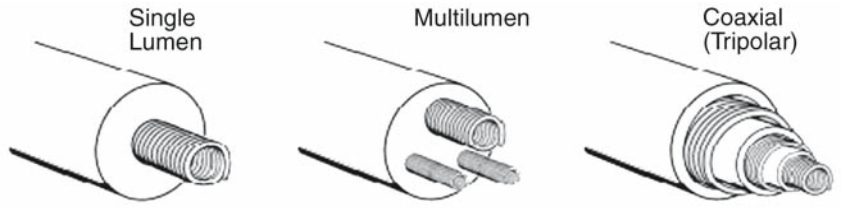

Fig. 35. Typical constructions used for cardiac pacing and defibrillation leads. Left, the single lumen design has a central conductor surrounded by a polymeric insulation; center, the multilumen design uses an extruded polymer to insulate the conductors from one another and from the implanted environment; and right, the coaxial design has conductors embedded within concentric layers of insulation. Today, the most commonly used insulation materials are silicones and polyurethanes, and the conductors are usually coiled or cabled wires. Modern lead body diameters range from approx 4–10 French (1 French = one-third millimeter).

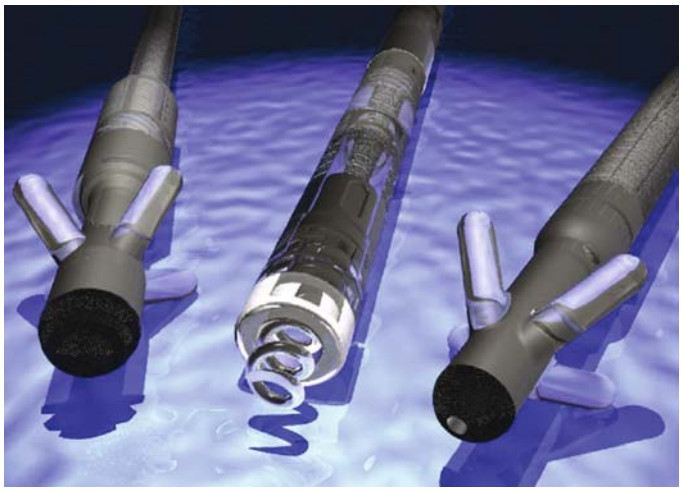

Fig. 36. Endocardial pacing leads: **left** and **right**, passive fixation leads (tined); **center**, an active fixation lead (extendable, retractable helix).

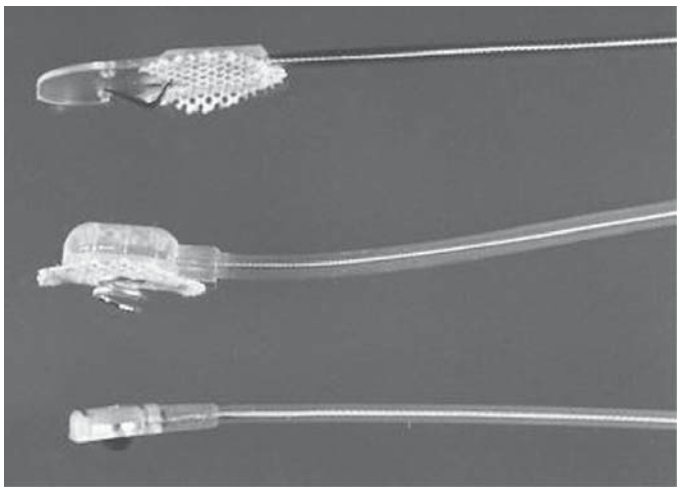

Fig. 37. Epicardial pacing leads: top, stab-in active fixation lead; middle, active fixation lead with helical fixation; and bottom, a hemispherical electrode secured by sutures.

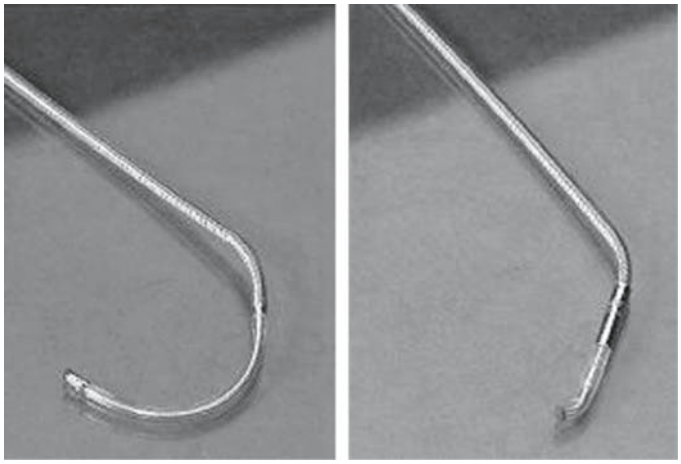

Fig. 38. Pacing leads designed for placement in the cardiac veins; they are shaped to enhance stability. The leads shown are primarily used in biventricular pacing systems for the management of patients with heart failure with the appropriate clinical indications.

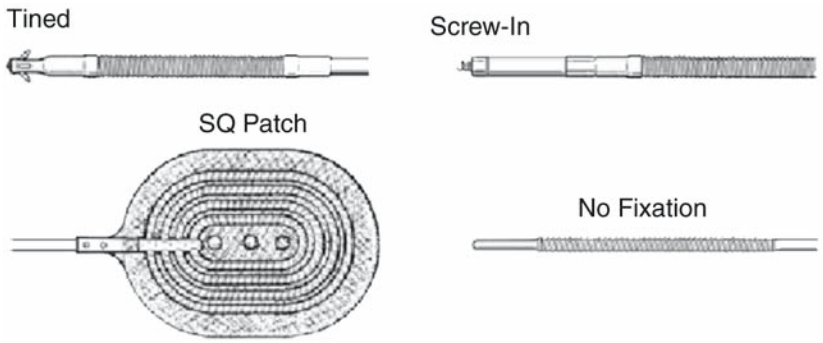

Fig. 39. Cardiac defibrillation leads. Clockwise from upper left: a passive fixation endocardial lead ("integrated bipolar"), an active fixation endocardial lead ("true bipolar"), an endocardial lead with no fixation, and subcutaneous patch. SQ, subcutaneous electrode.

For examples of pacing leads placed within the Visible Heart® preparation, *see* the following movie clips on the Companion CD: *5076huma.mpg* (active fixation pacing lead in human right atrium), *AApendFL.mpg* (active fixation pacing lead in swine right atrium with simultaneous fluoroscopy), *rva4074.mpg* (tined passive fixation lead in swine right ventricle), *5076humv.mpg* (active fixation pacing lead in human right ventricle), and *RV Apex.mpg* (tined passive fixation defibrillation lead in human right ventricle).

Various electrode configurations have been utilized on a variety of commercially available leads. As described, unipolar pacing circuits use a lead with a single cathodal electrode, and the IPG serving as the anode. Bipolar pacing systems use electrodes placed distally on the lead as both the cathode and anode. Pacing leads commonly use a cylindrical electrode placed along the lead body (ring electrode) as the anode; defibrillation leads may use a dedicated ring (the so-called true bipolar leads) or a defibrillation coil as the anode (an "integrated bipolar" lead). Defibrillation leads utilize electrodes with large surface areas, which allow the delivery of high-energy shocks within and around the heart. Defibrillation leads may be unipolar (defibrillation electrode only), or they may have a combination of defibrillation electrodes and pacing electrodes. The most common defibrillation lead configurations used today are shown in Figs. 39–40.

For examples of defibrillation leads placed within the Visible Heart® preparation, *see* the following movie clips on the Companion CD: *6944DEF1.mpg* (defibrillation lead in the right ventricle of a swine heart; ventricular fibrillation is induced with a shock on the T wave and then converted to sinus rhythm with a high-energy shock) and *6932humf.mpg* (defibrillation lead in the right ventricle of a human heart; ventricular fibrillation is converted to sinus rhythm with a high-energy shock).

Typically, the portion of the lead that interfaces with the cardiac tissue has been designed to: (1) minimize inflammatory responses, (2) provide low polarization, (3) provide high capacitance and impedance, and/or (4) act as a fixation mechanism. This distal electrode is most commonly the cathode, but in some cases, a similar electrode is used as the anode on a separate unipolar lead. To suppress inflammation, most modern electrodes incorporate a system for the elution of an anti-inflammatory agent (steroid, e.g., dexamethasone sodium

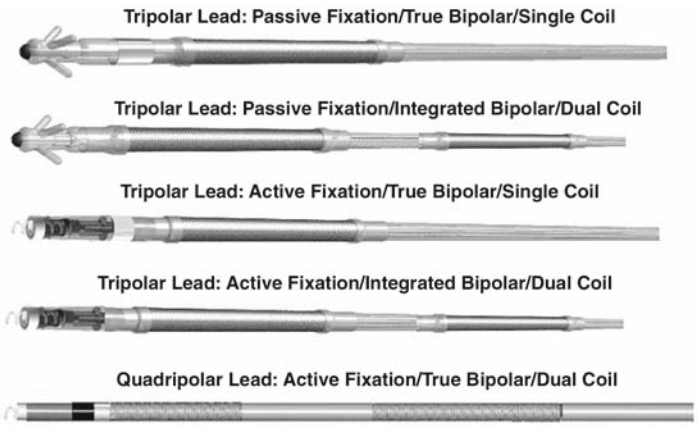

Fig. 40. Endocardial defibrillation leads. Various configurations are shown, including leads with active- and passive-fixation mechanisms, true and integrated bipolar pace/sense circuits, and single- and dual-defibrillation electrodes. The designs shown are typically placed in the right ventricle, with the distal defibrillation coil within the right ventricular chamber and the proximal coil located in the superior vena cava.

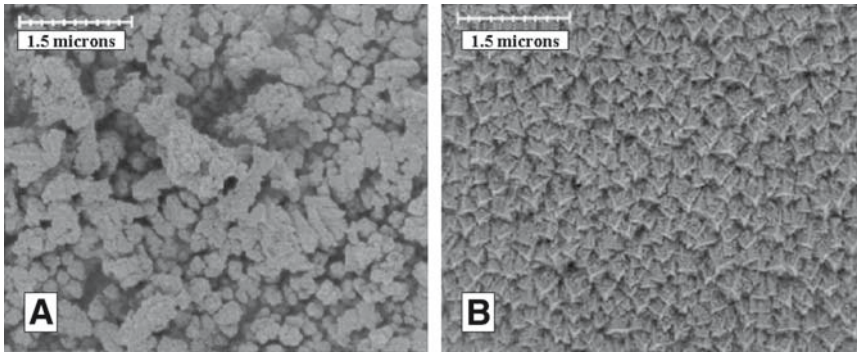

Fig. 41. Common electrode coatings for high capacitance and low polarization. **(A)** A platinized surface at ×20,000; **(B)** a titanium nitride (TiN) surface at ×20,000.

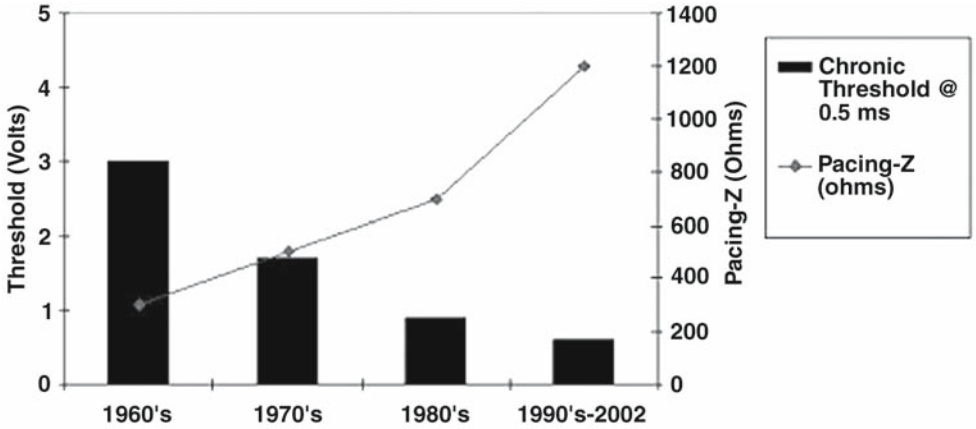

Fig. 42. Evolution of pacing lead impedances and pacing thresholds. From ref. *42*.

phosphate); this helps to manage acute changes in the local tissue, which will then aid in stabilizing pacing and sensing performance.

Coatings are also applied to many pacing electrodes to produce a large surface area that is highly capacitive (to reduce battery drain) and has a low level of polarization following a pacing pulse (to avoid undersensing) (Fig. 41). Interestingly, the size of the pacing cathode has decreased over time to increase the cathode–tissue impedance and increase system efficiencies by reducing current drain (Figs. 42 and 43) *(43)*.

6. SUMMARY

This chapter reviews the basic methodologies and devices employed to provide pacing or defibrillation therapy to the patient with appropriate indications. A brief history is provided on the use of external electricity to deliver lifesaving therapies to the heart. Although significant progress has been made, future developments in materials, electronics, and communication systems will allow ever-increasing utility and patient value.

ACKNOWLEDGMENTS

We would like to acknowledge and thank Mike Leners for the development of procedural animations, Medtronic Training and Education for the use of various graphics, the Visible Heart team for support in capturing the intracardiac footage, Monica Mahre for editorial support, LifeSource, and Drs. Anne Fournier and Suzanne Vobecky of Sainte-Justine Hospital, Montreal, Quebec, Canada, for the radiographic images.

COMPANION CD MATERIAL

Section 2.2. *normall.mpg*
Section 2.4. *AT.mpg*, *AF.mpg*, *VT.mpg*, and *VF.mpg*
Section 3. *styletNew.mpg*, *xray1.jpg, xray2.jpg, xray3.jpg, xray4.jpg, xray5.jpg,* and *xray6.jpg*
Section 4.8. *resync1.mpg*
Section 5.10. *fluoro.avi, styletNew.mpg, 5076huma.mpg*, *AApendFL.mpg, rva4074.mpg, 5076humv.mpg, RV Apex.mpg*, *6944DEF1.mpg,* and *6932humf.mpg*
Figure 11. *connectorPlugIn.mpg*
Figure 33. *energyVectorDual.mpg*

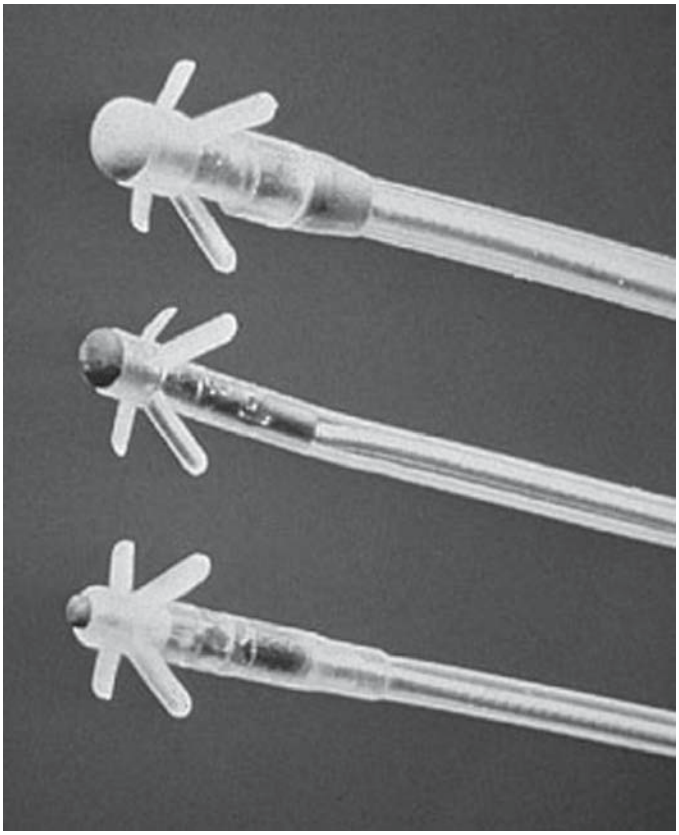

Fig. 43. Passive fixation leads with low (top; ~400–600 Ω), medium (middle; ~600–800 Ω), and high (bottom; ~800–1200 Ω) impedance pacing cathodes.

REFERENCES

1. Maisel, W.H., Sweeney, M.O., Stevenson, W.G., Ellison, K.E., and Epstein, L.M. (2001) Recalls and safety alerts involving pacemakers and implantable cardioverter–defibrillator generators. *JAMA.* 2001.
2. Furman, S. (1995) A Brief History of Cardiac Stimulation and Electrophysiology—The Past 50 Years and the Next Century. NASPE keynote address.
3. His, W., Jr. (1893) Die Tatigkeit des embryonalen Herzens und deren Bedcutung fur die Lehre von der Herzbewegung beim Erwachsenen. *Arb Med Klin Leipzig.* 1, 14–49.
4. Tawara, S. (1906) Das reizleitungssystem des saugetierherzens, in *Anatomisch-histologische studie uber das atrioventrikularbundel und die purkinjeschen faden,* Gustav Fischer, Jena, Germany; pp. 9–70, 114–156.
5. Lillehei, C.W., Gott, V.L., Hodges, P.C., Long, D.M., and Bakken, E.E. (1960) Transistor pacemaker for treatment of complete atrioventricular dissociation. *JAMA.* 172, 2006–2010.
6. Furman, S.C. Walton Lillehei. Available at Website: (http://www.naspe.org/ep-history/notable_figures/walton_lillehei). Accessed November 25, 2003.
7. Winters, S.L., Packer, D.L., Marchlinski, F.E., et al. (2001) Consensus statement on indications, guidelines for use, and recommendations for follow-up of implantable cardioverter defibrillators. *Pacing Clin Electrophysiol.* 24, 262–269.
8. Parsonnet, V., Escher, D.J., Furman, S., et al. (1984) Indications for dual-chamber pacing. *Pacing Clin Electrophysiol.* 7, 318–319.
9. Stokes, K.B. and Kay, G.N. (1995) Artificial electrical stimulation, in *Clinical Cardiac Pacing* (Ellenbogen, K.A., Kay, G.N., and Wilkoff, B.L., eds.), Saunders, Philadelphia, PA, pp. 3–37.
10. Gregoratos, G., Cheitlin, M.D., Conill, A., et al. (1998) ACC/AHA guidelines for the implantations of cardiac pacemakers and antiarrhythmia devices. *J Am Coll Cardil.* 31, 1175–1209.
11. Gregoratos, G., Abrams, J., Epstein, A. E., et al. (2002) ACC/AHA/NASPE guidelines for the implantations of cardiac pacemakers and antiarrhythmia devices. Summary article: a report of the American College of Cardiology/American Heart Association Task Force on Practice Guidelines (ACC/AHA/NASPE Committee to Update the 1998 Pacemaker Guidelines). *J Am Coll Cardiol.* 40, 1703–1719.
12. Bernstein, A.D., Daubert, J.C., Fletcher, R.D., et al. (2002) The revised NAPSE/BPEG generic code for antibradycardia, adaptive-rate, and multisite pacing. *Pacing Clin Electrophysiol.* 25, 260–264.
13. Fogoros, R.N. (1997) *Antiarrhythmic Drugs: A Practical Guide.* Blackwell Science, Cambridge, MA, p. 112.
14. Wilkoff, B.L., Cook, J.R., Epstein, A.E., et al. (2002) Dual-chamber and VVI Implantable Defibrillator Trial Investigators. Dual-chamber pacing or ventricular backup pacing in patients with an implantable defibrillator: the Dual-chamber and VVI Implantable Defibrillator (DAVID) Trial. *JAMA.* 288, 3115–3123.
15. Karpawich, P.P., Rabah, R., and Haas, J.E. (1999) Altered cardiac histology following apical right ventricular pacing in patients with congenital atrioventricular block. *Pacing Clin Electrophysiol.* 22, 1372–1377.
16. Andersen, H.R., Nielsen, J.C., Thomsen, P.E., et al. (1997) Long-term follow-up of patients from a randomised trial of atrial versus

ventricular pacing for sick-sinus syndrome. *Lancet.* 350, 1210–1216.
17. Lamas, G.A., Orav, E.J., Stambler, B.S., et al. (1998) Quality of life and clinical outcomes in elderly patients treated with ventricular pacing as compared with dual-chamber pacing. Pacemaker Selection in the Elderly Investigators. *N Engl J Med.* 338, 1097–1104.
18. Lamas, G.A., Lee, K., Sweeney, M., et al. (2000) The Mode Selection Trial (MOST) in sinus node dysfunction: design, rationale, and baseline characteristics of the first 1000 patients. *Am Heart J.* 140, 541–551.
19. Deshmukh, P., Casavant, D.A., Romanyshyn, M., and Anderson, K. (2000) Permanent direct His bundle pacing: a novel approach to cardiac pacing in patients with normal His–Purkinje activation. *Circulation.* 101, 869–877.
20. Karpawich, P., Gates, J., and Stokes, K. (1992) Septal His–Purkinje ventricular pacing in canines: a new endocardial electrode approach. *Pacing Clin Electrophysiol.* 15, 2011–2015.
21. Karpawich, P.P., Gillette, P.C., Lewis, R.M., Zinner, A., and McNamera, D.G. (1983) Chronic epicardial His bundle recordings in awake nonsedated dogs: a new method. *Am Heart J.* 105, 16–21.
22. Scheinman, M.M. and Saxon, L.A. (2000) Long-term His-bundle pacing and cardiac function. *Circulation.* 101, 836–837.
23. Williams, D.O., Sherlag, B.J., Hope, R.R., El-Sherif, N., Lazzara, R., and Samet, P. (1976) Selective versus non-selective His bundle pacing. *Cardiovasc Res.* 10, 91–100.
24. de Cock, C.C., Giudici, M.C., and Twisk, J.W. (2003) Comparison of the haemodynamic effects of right ventricular outflow-tract pacing with right ventricular apex pacing: a quantitative review. *Europace.* 5, 275–278.
25. Cleland, J.G., Daubert, J.C., Erdmann, E., et al. and CARE-HF Study Steering Committee and Investigators. (2001) The CARE-HF study (Cardiac Resynchronisation in Heart Failure study): rationale, design and end-points. *Eur J Heart Fail.* 3, 481–489.
26. Leclercq, C. and Daubert, J.C. (2003) Cardiac resynchronization therapy is an important advance in the management of congestive heart failure. *J Cardiovasc Electrophysiol.* 14, S27–S29.
27. Saksena, S. (2003) The role of multisite atrial pacing in rhythm control in AF: insights from sub-analyses of the dual-site atrial pacing for prevention of atrial fibrillation study. *Pacing Clin Electrophysiol.* 26, 1565.
28. Leclercq, J.F., De Sisti, A., Fiorello, P., Halimi, F., Manot, S., and Attuel, P. (2000) Is dual-site better than single site atrial pacing in the prevention of atrial fibrillation? *Pacing Clin Electrophysiol.* 23, 2101–2107.
29. Kindermann, M., Schwaab, B., Berg, M., and Frohlig, G. (2000) The influence of right atrial septal pacing on the interatrial contraction sequence. *Pacing Clin Electrophysiol.* 23, 1752–1757.
30. Miake, J., Marban, H., and Nuss, B. (2002) Biological pacemaker created by gene transfer. *Nature.* 419, 132–133.
31. Malineni, K.C. and McCullough, P.A. Sudden cardiac death. Available at Website: (http://www.emedicine.com/med/topic276.htm). Accessed November 25, 2003.
32. Rubart, M. and Zipes, D.P. (1997) Geneis of cardiac arrhythmias: electrophysiological considerations, in *Heart Disease, a Textbook of Cardiovascular Medicine,* 5th Ed., Myerburg, R.J., ed. Saunders, Philadelphia, PA, Chapter 24.
33. Coronary artery disease overview. Available at Website: (http://imaginis.com/heart-disease/cad_ov.asp?mode=1). Accessed November 25, 2003.
34. Electricity and the heart: a historical perspective. Available at Website: (http://www.naspe.org/ep-history/timeline). Accessed November 25, 2003.
35. Lloyd, M.A., Hayes, D.L., and Friedman, P.A. (2000) Troubleshooting, in *Cardiac Pacing and Defibrillation: A Clinical Approach*, Hayes, D.L., Lloyd, M.A., and Friedman, P.A., eds. Blackwell, New York, NY, pp. 347–452.
36. Cummins, R.O. (1989) From concept to standard-of-care? Review of the clinical experience with automated external defibrillators. *Ann Emerg Med.* 18, 1269–1275.
37. Wathen, M.S., Sweeney, M.O., DeGroot, P.J., et al. (2001) Shock reduction using antitachycardia pacing for spontaneous rapid ventricular tachycardia in patients with coronary artery disease. *Circulation.* 104, 796–801.
38. Electricity and the heart: a historical perspective. Available at Website: (http://www.naspe.org/ep-history/timeline/1980s). Accessed November 26, 2003.
39. Carnes, C.A., Mehdirad, A.A., and Nelson, S.D. (1998) Drug and defibrillator interactions. *Pharmacotherapy.* 18, 516–525.
40. Moss, A.J., Hall, W.J., Cannom, D.S., et al. (1996) Improved survival with an implanted defibrillator in patients with coronary disease at high risk for ventricular arrhythmia. Multicenter Automatic Defibrillator Implantation Trial Investigators. *N Engl J Med.* 335, 1933–1940.
41. Kloner, R.A. and Birnbaum, Y. (eds.). (2002) *Cardiovascular Trials Review,* 7th Ed. Le Jacq Communications, Darien, CT, pp. 1065–1066.
42. Bardy, G.H. (2004) *SCD-HeFT: The Sudden Cardiac Death in Heart Failure Trail.* American College of Cardiology Annual Scientific Session. New Orleans, LA, March 7–10, 2004.
43. Brabec, S. and Laske, T.G. (2003) The evolution of bradycardia pacing electrodes. Twelfth World Congress on Cardiac Pacing and Electrophysiology. Hong Kong, February 19–22, 2003.

SOURCES

Ellenbogen, K.A., Kay, G.N., and Wilkoff, B.L. (eds.) (1995) *Clinical Cardiac Pacing.* Saunders, Philadelphia, PA.
Furman, S., Hayes, D.L., and Holmes, D.R. (eds.) (1993) *A Practice of Cardiac Pacing.* Futura, New York, NY, pp. 1–753.

24 Biventricular Pacing for Congestive Heart Failure

FEI LÜ, MD, PhD AND LESLIE W. MILLER, MD

CONTENTS

1. INTRODUCTION

Despite significant advancements in pharmacological therapy, mortality continues to remain high in patients with congestive heart failure *(1)*. Much attention has been paid to optimization of pacing modalities for patients with left ventricular dysfunction when ventricular pacing is required. Patients with congestive heart failure frequently have symptomatic chronotropic incompetence, sinus node dysfunction, or atrioventricular block, all of which are class I indications for cardiac pacing *(2)*. In addition, atrial fibrillation afflicts 10 to 30% of patients with congestive heart failure.

It is well known that atrioventricular nodal ablation plus pacemaker insertion is necessary in patients with refractory atrial fibrillation and uncontrolled ventricular rates. In patients with atrial fibrillation, studies indicated that dual-chamber pacing with a short atrioventricular delay was associated with better cardiac performance. However, this observation was not confirmed in subsequent short- and long-term studies *(3,4)*.

From: *Handbook of Cardiac Anatomy, Physiology, and Devices*
Edited by: P. A. Iaizzo © Humana Press Inc., Totowa, NJ

The ventricular pacing lead of a single- or dual-chamber pacemaker has traditionally been placed without concern for hemodynamic consequences at the right ventricular apex because of ease of placement and superior stability. However, data have indicated that the right ventricular apical pacing may not be optimal. It is currently believed that pacing from the right ventricular apex is associated with deleterious changes, in both animals and humans, in diastolic and systolic function, myocardial perfusion, and neurohumoral status.

For example, Fig. 1 shows the results of one such study that indicated the negative hemodynamic changes during pacing at the right ventricular apex compared with other ventricular sites *(5)*. The detrimental hemodynamic changes associated with right ventricular apical pacing, which are mainly attributed to altered ventricular activation sequences as well as asynchronous contractions, are particularly problematic in patients with the presence of left ventricular dysfunction.

Strong evidence has shown that pacing from the left ventricle (left ventricular pacing alone, biventricular pacing, or multisite left ventricular pacing) was associated with improved hemodynamics in patients with congestive heart failure and

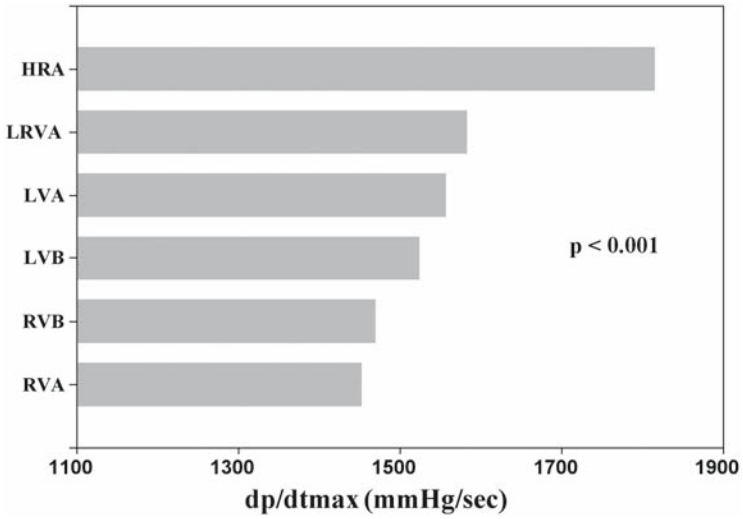

Fig. 1. Ventricular pacing is associated with decreased cardiac function in normal dogs. Right ventricular apical (RVA), left ventricular apical (LVA), and biventricular apical (LRVA) pacing reduced maximal dp/dt by 20, 14, and 13%, respectively, compared with high right atrial (HRA) pacing. LVB, left ventricular basal pacing; RVB, right ventricular basal pacing. *See* ref. *5* for further discussion.

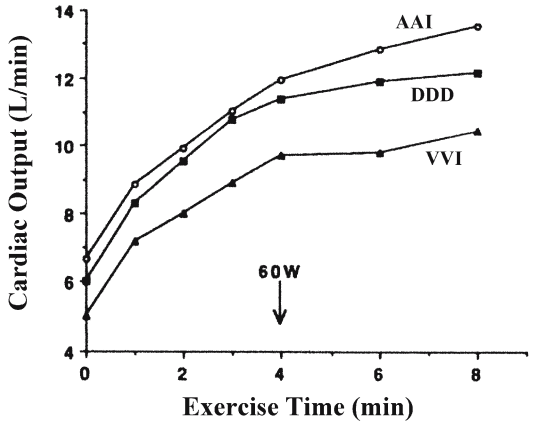

Fig. 2. Effects of pacing configurations on cardiac output during exercise in patients with sinus node dysfunction and normal atrioventricular node function without bundle branch block. Reprinted from ref. *9*, © 1995 with permission from Elsevier.

those with (wide QRS duration) and without (narrow QRS duration) intraventricular conduction delay. Hence, the era of biventricular pacing as a therapeutic intervention for patients with congestive heart failure has ensued. Subsequently, a fifth letter has been introduced to describe multisite pacing as a pacemaker mode within the North American Society of Pacing and Electrophysiology (NASPE)/British Pacing and Electrophysiology Group (BPEG) Generic Pacemaker Code (NBG Code) *(6)*. For example, the fifth letter "V" in DDDRV represents multisite pacing in the ventricles.

2. PHYSIOLOGICAL PACING AND RESYNCHRONIZATION THERAPY

Because of the potential detrimental effects of ventricular pacing on hemodynamics, alternative methods to ensure more physiological pacing are important, particularly in the presence of severe left ventricular dysfunction. Components of such physiological pacing include: (1) appropriate chronotropic response (rate responsive pacing); (2) preservation of atrial function (atrioventricular sequential pacing); (3) maintenance of optimal atrioventricular synchrony (atrioventricular delay); and (4) maintenance of normal ventricular activation sequences (His pacing or biventricular pacing).

Like controlling heart rate as a means to improve cardiac output, modulating atrioventricular synchrony is also important for more normal hemodynamics response. For example, loss of atrial contraction may reduce cardiac output by up to one-third (15 to 30%). Furthermore, the spatiotemporal distribution of contraction is considered to affect ventricular function significantly *(7)*.

The importance of synchronized ventricular activation (and contraction) as manifested by a narrow QRS complex has been demonstrated by Schwaab and colleagues *(8)*. In this acute study in 14 patients with third-degree atrioventricular block, the atrioventricular delay was individually optimized. Right ventricular pacing with decreased QRS duration obtained by alternate pacing sites on the septum was found to be correlated significantly with homogenization of left ventricular contraction and with increased systolic function.

Figure 1 shows the maximal dp/dt during high right atrial, single ventricular, and biventricular pacing in normal dogs *(5)*. In particular, these data indicated that ventricular pacing, particularly right ventricular apical pacing, is associated with reduced maximal dp/dt (an index of cardiac contractility). The importance of maintaining atrioventricular synchrony and normal ventricular activation sequences is further presented in Fig. 2. Figure 2 shows the relative cardiac outputs associated with differant pacing modes during exercise in patients with sinus node dysfunction and normal atrioventricular node function without bundle branch block *(9)*. AAI pacing represents a pacing protocol associated with normal ventricular activation

sequence and atrioventricular conduction. DDD pacing maintains atrioventricular synchrony, but is associated with disturbed ventricular activation sequence. VVI pacing has neither normal ventricular activation sequence nor atrioventricular synchrony. In general, cardiac output was significantly lower during VVI pacing compared with AAI and DDD pacing. Interestingly, at rest and during the initial phase of exercise with a lower workload, there was no significant difference in cardiac output between DDD and AAI pacing. However, AAI pacing was significantly better in maintaining the required performance as the exercise duration increased. Proposed mechanisms for the adverse effects of right ventricular pacing include: (1) paradoxical septal motions; (2) altered ventricular activation sequences; (3) impaired mitral or tricuspid apparatus functions; (4) altered diastolic function; (5) diminished diastolic filling times; and (6) increased serum catecholamine concentrations.

Conduction delays in the atrioventricular node or in the ventricles associated with dilated cardiomyopathy are considered to contribute to left ventricular dysfunction by impairing atrioventricular synchrony, uniformity of ventricular contraction, or relaxation of the left ventricle. It is noteworthy that approx 30% of patients with severe congestive heart failure have intraventricular conduction disturbances, characterized electrically by a widened QRS complex and mechanically by discoordination of ventricular contraction and relaxation patterns *(10)*. A widened QRS duration has been associated with increased mortality in patients with congestive heart failure.

Subsequently, it has been estimated that 10–20% of a generalized heart failure population may be eligible for biventricular pacing *(11,12)*. Again, ventricular dyssynchrony is associated with abnormal motion of the interventricular septum, reduced dp/dt, reduced diastolic filling time, and prolonged mitral regurgitation duration.

The two primary therapeutic mechanisms underlying resynchronization therapy via biventricular pacing are (1) improvement in coordinated contraction and (2) atrioventricular optimization (Table 1). Increased left ventricular filling time, decreased septal dyskinesis, and reduced mitral regurgitation are also considered beneficial in biventricular pacing for the congestive heart failure patient.

Table 1
Mechanisms of Ventricular Synchronization Therapy

- Improved contraction pattern
  - Improves interventricular synchrony
  - Reduces paradoxical septal wall motion
  - Improves left ventricular regional wall motion
  - Lowers end-systolic volumes
  - Improves left ventricular dp/dt
- Atrioventricular interval optimization
  - Reduces mitral regurgitation
  - Increases diastolic filling time
  - Improves left ventricular dp/dt

3. EFFECTS OF BIVENTRICULAR PACING ON CARDIAC FUNCTION

Both animal and human studies have shown that, in the presence of an intrinsic intraventricular conduction delay, pacing from the left ventricle is ultimately associated with a better cardiac function (compared with sinus rhythm and right ventricular apical pacing). Several clinical trials on biventricular pacing for congestive heart failure without traditional indications for pacing, have been described and are summarized in Fig. 3. Such trials include the InSync registry *(13,14)*, the Multisite Stimulation in Cardiomyopathy (MUSTIC) study *(15)*, and the Multicenter InSync Randomized Clinical Evaluation (MIRACLE) study *(16)*.

3.1. InSync Registry

The InSync registry is a prospective observational multicenter European and Canadian study that examined the safety and efficacy of a biventricular pacemaker (with left ventricular pacing leads implanted via cardiac veins) as a supplemental treatment for refractory congestive heart failure *(13,14)*. Between August 1997 and November 1998, there were 103 patients enrolled (with a mean left ventricular ejection fraction of 22% and a mean QRS duration of 178 ms). Over a follow-up period of 12 months, 21 patients died. The 12-month actuarial survival was 78% (confidence interval [CI] 70–87%). Nine surviving patients withdrew from the study for miscellaneous reasons during long-term follow-up.

At each point of follow-up over a 12-month period, a significant shortening of QRS duration was observed, and significant improvements were found in mean New York Heart Association (NYHA) functional class, a 6-min walk test and a quality-of-life score. In the 46 patients with complete echocardiographic data, ejection fractions increased from 21.7 ± 6.4% at baseline to 26.1 ± 9.0% at the last follow-up ($p = 0.006$). In addition, it was shown that the left ventricular end-diastolic dimensions decreased from 72.7 ± 9.2 to 71.6 ± 9.1 mm ($p = 0.233$); interventricular mechanical delays decreased from 27.5 ± 32.1 to 20.3 ± 25.5 ms ($p = 0.243$); mitral regurgitation apical four-chamber areas decreased from 7.66 ± 5.5 to 6.69 ± 5.9 cm^2 ($p = 0.197$); and left ventricular filling times increased from 363 ± 127 to 408 ± 111 ms ($p = 0.002$).

The investigators concluded that long-term cardiac resynchronization could be safely and reliably achieved by transvenous atrial synchronized right and left ventricular pacing. These changes were accompanied by clinically relevant improvements in functional status and quality-of-life scores, as well as a measurable increase in left ventricular performance. Incorporating biventricular pacing in an implantable cardioverter–defibrillator system, when indicated, is feasible and leads to an improvement of heart failure symptoms *(17)*.

3.2. MUSTIC Trial

The MUSTIC trial employed a single-blinded crossover study design *(15)*. In total, 67 patients were enrolled from 15 centers in Europe. All patients had significant heart failure caused by either idiopathic or ischemic left ventricular systolic dysfunction (ejection fraction of less than 35%) and a left ventricular end-diastolic diameter of more than 60 mm. All patients were also in sinus rhythm with a QRS duration of more than 150 ms, and none had a standard indication for pacemaker or defibrillator implantation. Forty-eight patients completed the 6-month randomized crossover study.

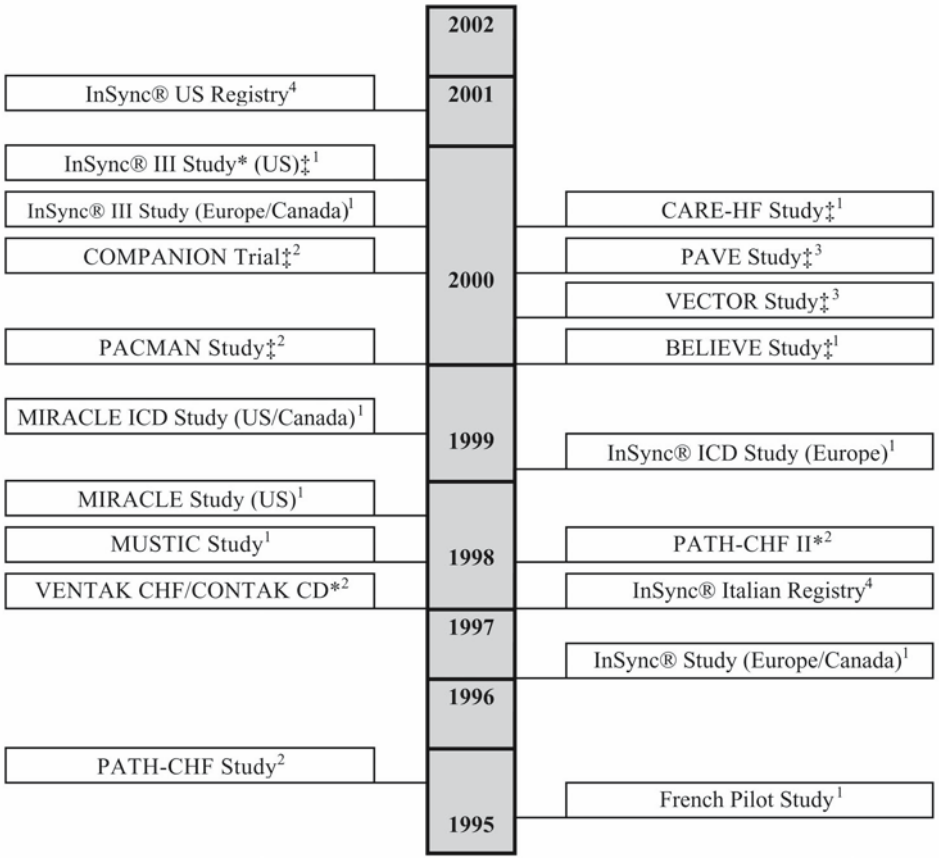

Fig. 3. Clinical trials of cardiac synchronization therapy. *, Investigational device (limited by US federal law to investigational use; ‡, ongoing studies, results not yet published; 1, Medtronic (Minneapolis, MN); 2, Guidant Corp. (Indianapolis, IN); 3, St. Jude Medical (St. Paul, MN); 4, Registry; ICD, implantable cardioverter defibrillator. Visit company websites for details.

Compared with no pacing, biventricular pacing increased patients' 6-min walk distances by 23%, peak oxygen uptakes by 8%, and quality-of-life scores by 32% and decreased hospitalization rates by two-thirds. The authors concluded that atriobiventricular pacing significantly improved exercise tolerance and the quality of life in patients with chronic congestive heart failure and intraventricular conduction delay.

A follow-up study to the MUSTIC trial demonstrated that the benefits of biventricular pacing were sustained at a 12-month follow-up *(18)*. The clinical improvement included a 5% increase in ejection fraction and a 45% reduction in mitral regurgitation. Forty-one patients with persistent atrial fibrillation were included in the follow-up study; these patients had an existing indication for pacemakers because of bradycardia or atrioventricular nodal ablation for rate control. Similar clinical improvements were observed in these patients *(18)*.

3.3. MIRACLE Trial

The MIRACLE study was a randomized, double-blind, controlled trial to assess cardiac resynchronization therapy using a biventricular pacing protocol in patients with congestive heart failure. The MIRACLE trial demonstrated that cardiac resynchronization results in significant clinical improvements in patients who have moderate-to-severe heart failure and an intraventricular conduction delay. All patients studied were on stable medical therapies and had no traditional indications for a pacemaker or implantable cardioverter defibrillator. The indications for the MIRACLE study included: (1) moderate or severe congestive heart failure (NYHA functional class III or IV and 6-min walking distance of 450 m or less); (2) left ventricular ejection fraction of 35% or less; (3) widened QRS duration of 130 ms or more; and (4) enlarged left ventricle (left ventricular end-diastolic diameter 55 mm or larger).

From November 1998 through December 2000, there were 571 patients enrolled from 45 centers in the United States and Canada. Of these, 453 patients (228 patients in the pacing therapy group and 225 patients in the control group without pacing) completed the 6-month follow-up study. The primary end points were the determination of NYHA functional class, assessment of quality of life, and results of the 6-min walk test.

Compared with the control group, patients assigned to cardiac resynchronization therapy elicited improvements in the distance walked in 6 min (+39 vs +10 m; $p = 0.005$), functional class ($p < 0.001$); quality of life scores (−18.0 vs −9.0 points; $p = 0.001$); times on the treadmill during exercise testing (+81 vs +19 s; $p = 0.001$); and ejection fractions (+4.6 vs −0.2%; $p <$

0.001). In addition, fewer patients in the group assigned to cardiac resynchronization therapy required hospitalization (8 vs 15%; $p < 0.05$) or intravenous medications (7 vs 15%; $p < 0.05$) for the treatment of heart failure. There were significant reductions in QRS durations (–20 vs 0 ms; $p < 0.001$), left ventricular end-diastolic dimensions (–3.5 vs 0.0 mm; $p < 0.001$), and mitral regurgitant jets (–.7 vs –0.5 cm^2; $p < 0.001$).

In the intention-to-treat analysis, there were 16 deaths in the control group and 12 deaths in the cardiac resynchronization therapy group. However, this study was not designed to assess whether cardiac resynchronization therapy improved survival in this patient population. Figure 4 shows the Kaplan-Meier estimates of the time to death or hospitalization for worsening heart failure in the control and cardiac resynchronization therapy groups. It was concluded from MIRACLE trial patients in class III and IV systolic heart failure who had intraventricular conduction delays that biventricular pacing (1) was safe and well tolerated; (2) improved quality of life, functional class, and exercise capacity; and (3) improved cardiac structure and function.

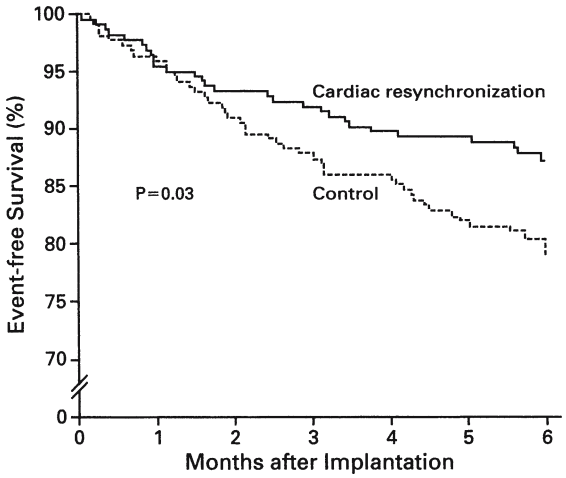

Fig. 4. Kaplan-Meier Estimates of the time to death or hospitalization for worsening heart failure in the control and resynchronization groups. The risk of an event was 40% lower in the resynchronization group (95% confidence interval, 4 to 63%; $p = 0.03$). Reprinted from ref. *16*. © 2002, Massachusetts Medical Society. All rights reserved.

4. EFFECTS OF BIVENTRICULAR PACING ON VENTRICULAR ARRHYTHMIAS

Theoretically, biventricular pacing may alter the substrates responsible for ventricular arrhythmias and, on occasion, may possibly be associated with an increased risk for ventricular arrhythmias. However, currently available data indicate that biventricular pacing reduces the likelihood of ventricular tachyarrhythmias. In addition, there is evidence that biventricular pacing actually inhibits ventricular reentry. Several studies obtained from a small number of patients demonstrated that biventricular pacing may decrease the inducibility of ventricular tachycardia *(19)*, the incidence of spontaneous ventricular arrhythmias (ectopy) *(20)*, and the need for defibrillator therapy *(21)*.

In rare cases, biventricular pacing may suppress refractory ventricular tachycardia in patients in whom it was not controlled by drugs or right ventricular DDD pacing *(22)*. Proposed mechanisms for the protective benefits of biventricular pacing are (1) prevention of ventricular reentry, (2) improvements in cardiac function and myocardial perfusion, (3) reductions in sympathetic activity, or (4) decreases in QT dispersion (Fig. 5) (unpublished data).

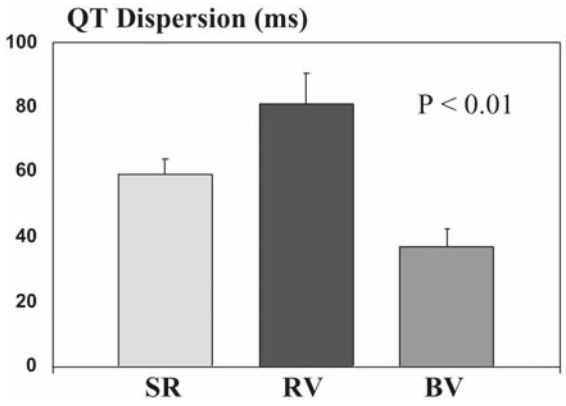

Fig. 5. QT dispersion in 10 patients with congestive heart failure who were treated with biventricular pacing (6 men and 4 women, aged 62 ± 8 years, and left ventricular ejection fraction 19 ± 7%). There was no significant difference in QT intervals between right ventricular (RV) pacing and sinus rhythm (SR; 437 ± 36 ms vs 426 ± 28 ms; $p = 0.26$). QT intervals were significantly shorter during biventricular (BV) pacing (407 ± 30 ms) than during right ventricular pacing (437 ± 36 ms; $p < 0.01$) and during sinus rhythm (426 ± 28 ms; $p < 0.01$). QT dispersion was significantly increased during RV pacing compared with sinus rhythm (81 ± 30 vs 59 ± 16 ms; $p < 0.01$). Biventricular pacing was associated with less QT dispersion (37 ± 17 ms) compared with sinus rhythm (59 ± 16 ms; $p = 0.01$) and right ventricular pacing (81 ± 30 ms, $p < 0.01$). This was also true after correction of QRS durations. It seems that biventricular pacing is associated with less QT dispersion, which may play a role in prevention of sudden cardiac death in patients with congestive heart failure patients with biventricular pacing.

Additional data have indicated that biventricular antitachycardia pacing may be even more effective than right ventricular antitachycardia pacing *(17)*; however, there is controversy regarding this role of biventricular antitachycardia pacing *(23)*. On the other hand, biventricular pacing has been associated with nonphysiological ventricular activation sequences that may augment transmural heterogeneity of repolarization and thus facilitate the genesis of ventricular arrhythmias *(24)*.

To date, there is no evidence that biventricular pacing increases mortality during a 1-year follow-up period. However, it should be noted that such studies were not designed to determine the effects of biventricular pacing on overall survival. Interestingly, it has been suggested that it may be safe to implant a biventricular pacemaker without a backup defibrillator *(23)* because biventricular pacing does not appear to be associated with excess mortality. Two large-scale studies, CArdiac REsynchronisation in Heart Failure (CARE-HF) study in Europe and Comparison of Medical Therapy, Pacing, and Defibrillation in Chronic Heart Failure (Companion) in the United States, are ongoing to examine the long-term effects of biventricular pacing on survival.

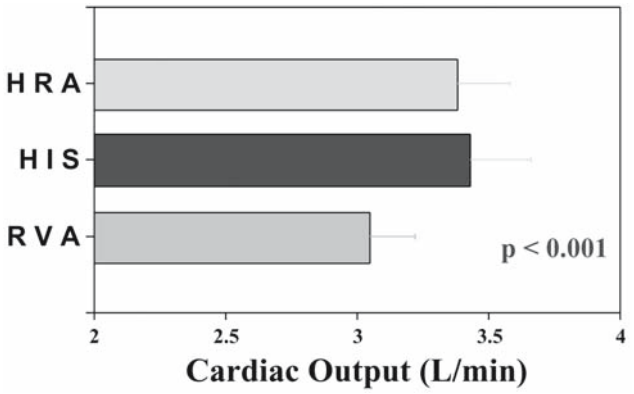

Fig. 6. Cardiac output during atrioventricular sequential pacing in normal hearts. There is a 12% increase in cardiac output during His bundle pacing compared with right ventricular apical (RVA) pacing. HRA, high right atrial pacing. *See* ref. *5* for further discussion.

Sudden cardiac death accounts for up to half of deaths in patients with congestive heart failure. Significant numbers of such patients appear to die suddenly despite noted improvements in their cardiac function under clinical management. Hence, today it is considered that combined biventricular pacing and implantable cardioverter defibrillator therapy may improve prognosis in patients with congestive heart failure *(25, 26)*. In addition, because the use of a transvenous defibrillation lead in the coronary sinus may significantly reduce the defibrillation threshold, the combined use of left ventricular pacing and defibrillation could have enhanced clinical significance *(27)*. Approximately 10% of implantable cardioverter defibrillator patients are indicated for biventricular pacing at the time of implantation *(28)*.

5. EFFECTS OF BIVENTRICULAR PACING ON MECHANICAL REMODELING

Cardiac myocytes are known to adapt to changes in hemodynamic load. Ventricular remodeling refers to changes in left ventricular geometry, mass, or volume in response to myocardial injury or alterations in load (e.g., hypertension). The extent of left ventricular dilation or remodeling in both ischemic and nonischemic cardiomyopathy is a strong predictor of both morbidity and mortality. Angiotensin-converting enzyme inhibitors and β-adrenergic blockers inhibit left ventricular remodeling and improve survival in patients with left ventricular dysfunction. It has been reported that chronic asynchronous electrical activation, such as chronic pacing or left bundle branch block, in the heart induces redistribution of cardiac mass *(29)*.

Further, chronic right ventricular apical pacing may adversely alter cellular growth, especially among the young, on the cellular and subcellular levels, potentially contributing to the diminished function observed clinically *(30)*. It has also been shown that such pacing may increase myocardial perfusion defects and regional wall motion abnormalities, reduce left ventricular ejection fractions, or cause diastolic dysfunction *(31,32)*.

Short-term right ventricular apical pacing has been associated with both impaired left ventricular pump function and relaxation. Long-term right ventricular apical pacing may result in permanent impairment of left ventricular function. In 24 young patients (average age 19 years), Tantengco et al. *(31)* demonstrated that left ventricular function was significantly lower than for age-matched controls after right ventricular apical pacing for 10 years.

In contrast, biventricular pacing resulted in reverse remodeling in patients with congestive heart failure. Lau et al. *(33)* demonstrated that 3 months of biventricular pacing was associated with reduced left ventricular end-systolic and end-diastolic volumes by 33 and 24%, respectively. This was consistent with published data from the MIRACLE study *(16)*. It has also been reported that chronic biventricular pacing may be associated with changes in QRS axis without concomitant changes in QRS duration or lead dislocation *(34)*, suggesting possible electrical remodeling induced by such pacing.

6. OPTIMAL PACING CONFIGURATION

6.1. Optimal Pacing Site

Right ventricular pacing by itself is considered suboptimal today, although several studies have shown that pacing from the high right ventricular septum or right ventricular outflow tract may be associated with better cardiac function compared to pacing within the right ventricular apex *(8,35,36)*. However, this observation was not confirmed by other investigators *(37,38)*. It appears that pacing in a position that results in the greatest reduction in QRS durations may be associated with the most beneficial clinical functional outcome *(39)*. During right ventricular pacing, the posterior or posteroinferior base of the left ventricle is usually the latest activation site.

Although left ventricular pacing is associated with better hemodynamics, the optimal pacing sites are yet to be determined. Yet, the PATH-CHF (Pacing Therapies for Congestive Heart Failure) study showed that the midlateral wall of the left ventricle may be the optimal site for biventricular pacing compared with other sites of the left ventricle *(40,41)*.

Flexibility in the placement of a coronary sinus lead in various locations of the left ventricle is a recent area of vigorous work. Currently, the lateral or posterolateral wall of the left ventricle is targeted for coronary sinus lead placement *(41,42)*. A posterior or lateral branch of the coronary venous system is available on the retrograde coronary sinus venogram in a majority of patients. The clinical utility of pacing on the anterior left ventricular wall remains to be defined fully *(43)*. A multielectrode lead in the coronary sinus may minimize the importance of preselecting an optimal pacing site.

6.2. His Bundle Pacing

One of the main mechanisms considered beneficial in biventricular pacing is the correction of an abnormal ventricular activation sequence. If multisite pacing is truly able to improve cardiac function by resynchronizing the ventricular activation sequence, there might be no better pacing site than His bundle pacing in the absence of intraventricular conduction block. Not surprising, His bundle pacing is considered to be associated with better cardiac function in a normal heart (Fig. 6).

It is interesting to note that His bundle pacing may confer even better hemodynamic changes than those during sinus rhythm; the high output stimuli required for pacing the His bundle likely stimulate the sympathetic nerves across the atrioventricular groove, thus resulting in higher cardiac outputs. The potential benefits of His bundle pacing exist in the presence or absence of atrioventricular synchrony.

6.3. Optimal Interventricular Delay

Interventricular dyssynchrony is considered to contribute directly to impairment of cardiac function. Improved interventricular synchrony provided by biventricular pacing is an important aspect of the overall efficacy of biventricular pacing. Because the location and degree of ventricular dyssynchrony will vary from patient to patient, it is more logical to provide an individualized synchronizing stimulation protocol to patients during cardiac resynchronization therapy. Compared with simultaneous cardiac resynchronization therapy, sequential cardiac resynchronization therapy is considered to improve left ventricular systolic and diastolic performance significantly *(44)*. It has been reported that tissue Doppler imaging, with tissue tracking used to detect these segments with delayed longitudinal contractions, can be used to determine the optimum interventricular delay during cardiac resynchronization therapy *(45)*. The current InSync III trial will examine the safety of sequential right and left ventricular pacing; the results of this study will be released in the near future.

6.4. Optimal Atrioventricular Delay

Consequences of atrioventricular asynchrony include the following: (1) diminished ventricular filling; (2) systolic mitral and tricuspid insufficiency; (3) diastolic mitral regurgitation caused by delayed valve closure; (4) pulmonary venous congestion secondary to atrial contraction against closed mitral valves; and (5) inappropriate decreases in peripheral resistance caused by atrial distension-induced autonomic activation. Therefore, optimizing atrioventricular synchrony is an important parameter that can greatly improve cardiac function, mainly because of enhanced ventricular filling and diminished systolic mitral and tricuspid regurgitation. In many clinical settings, this may contribute more to the observed hemodynamic improvement than correcting an intraventricular conduction defect.

In the MIRACLE trial, all patients underwent atrioventricular optimization for enhanced diastolic filling. This was accomplished using a transmitral Doppler study approach in which atrioventricular delays were adjusted to extend the left ventricular diastolic filling times maximally without truncating the A waves (i.e., atrial kick). This approach emphasized the importance of atrioventricular optimization for ventricular filling, but drew attention away from the improvement of overall cardiac function elicited when employing cardiac resynchronization therapy.

Other approaches used for atrioventricular optimization and programming have included assessment of cardiac outputs, degrees of mitral regurgitation, aortic flows, and pulse pressures. It should be noted that the definition and choice of standardized techniques for adequately assessing atrioventricular optimization remain to be fully investigated.

6.5. Other Pacing Modalities

Animal studies have indicated that nonexcitatory stimulation improves left ventricular function and is superior to biventricular pacing for improving function in an animal model with left bundle branch block without affecting transmitral valve flow and subsequently left ventricular diastolic function *(46, 47)*. Further, the role of paired stimulation based on the post-extrasystolic potentiation effect to augment ventricular function in the failing ventricle is inconclusive *(48,49)*.

7. EFFECTS OF BIVENTRICULAR PACING ON AUTONOMIC NERVOUS ACTIVITY

Sympathetic activity is increased in patients with congestive heart failure, as evidenced by elevated levels of circulating norepinephrine and increases in adrenergic nerve outflow. The initially enhanced sympathetic responses to congestive heart failure are likely to play a compensatory role early during the disease process. However, chronic adrenergic activation is known to be associated with a vicious cycle that promotes progression of disease through multiple effects, including: (1) increased afterload, (2) exertion of direct toxic effects on the failing myocardium, (3) increased myocardial oxygen demands, and (4) triggered ventricular arrhythmias. Elevated plasma norepinephrine levels have been shown to correlate with cardiac mortality rates and are considered to be better prognostic predictors than ejection fractions. To date, β-blocker therapy has been accepted as a standard treatment for moderate congestive heart failure.

In contrast, left ventricular-based pacing has been shown to clinically improve hemodynamics and decrease sympathetic nerve activity compared with right ventricular pacing in patients with more severe left ventricular dysfunctions regardless of their QRS durations *(50)*. Biventricular pacing has been described also to result in a decrease in sympathetic nerve activity associated with improved hemodynamics compared with intrinsic conduction in patients with left ventricular dysfunction and intraventricular conduction delay *(51)*. In addition, chronic biventricular pacing may even decrease serum norepinephrine levels in patients with dilated heart failure, with the greatest sympathetic activation at baseline *(52)*. The evidence of decreased intrinsic heart rates following long-term biventricular pacing may further suggest that biventricular pacing improves contractility without increasing sympathetic activity *(18)*. These combined observations may suggest that chronic biventricular pacing will likely reduce mortality.

8. EFFECTS OF BIVENTRICULAR PACING ON CARDIAC ENERGETICS

There is evidence that ventricular pacing is associated with increased myocardial oxygen consumption in hearts without intraventricular conduction delay *(53)*. If biventricular pacing improves cardiac function at the higher cost of increasing cardiac oxygen consumption, then it follows that there could be a higher mortality rate that would potentially make biventricular pacing less useful. Fortunately, biventricular pacing does not critically increase myocardial oxygen consumption in patients with left bundle branch block *(54,55)*. In contrast, dobutamine to achieve similar systolic changes induced by

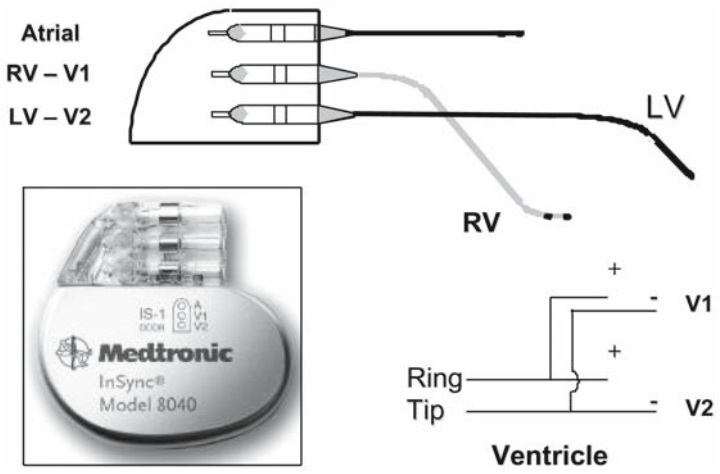

Fig. 7. Medtronic biventricular pacemaker (InSync model 8040) and the Y-adaptor in the header. Most commercially available left ventricular (LV) leads are unipolar with a shared common ring of a bipolar sensing/pacing right ventricular (RV) lead.

biventricular pacing has been shown to increase the energy cost significantly. Hence, biventricular pacing may provide a more efficient way to treat patients with congestive heart failure with intraventricular conduction delay.

9. IMPLANTATION OF BIVENTRICULAR PACEMAKER

9.1. Implantation Considerations

The key procedure for implementation of biventricular pacing is placement of the left ventricular lead. Clinical studies on multisite ventricular pacing in humans have mainly consisted of biventricular pacing modalities with transvenous left ventricular pacing via a coronary venous lead or, less commonly, a left ventricular epicardial lead through thoracotomy. It is usually necessary to target specific sites (posterolateral or lateral walls of the left ventricle) to maximize hemodynamic benefits. However, numerous limitations exist as technical challenges for current transvenous permanent pacing lead systems, such as: (1) patient safety, (2) potential of lead dislodgement, (3) altered pacing thresholds, (4) general lead handling, and (5) ease of use, in addition to variations of coronary vein anatomy *(41)*.

A coronary venogram using two views is usually first obtained to provide a "road map" of the venous anatomy and to guide selection of the appropriate coronary sinus leads. Several delivery systems (including steerable catheters, venogram balloon catheters, and guiding sheaths with different curves) have been developed. An over-the-wire lead system has been described that is able to reduce the implant failure rate and avoid other more invasive means of left ventricular lead implantation *(56)*. Many technical aspects in coronary sinus lead placement remain to be improved, although significant advances continue to be rapid in this field.

It is noteworthy that some investigators have implanted the left ventricular lead through the transseptal approach for left ventricular endocardial pacing *(57)*. This method seems more reasonable to use in patients who require chronic anticoagulation. Another approach reported is the lead placement into the anterior paraseptum, which may be used to pace both ventricles synchronously; this approach has been associated with increased cardiac outputs *(58)*.

9.2. Intraprocedural Testing

Figure 7 shows a device approved by the Food and Drug Administration for biventricular pacing (InSync® model 8040, Medtronic, Minneapolis, MN). This pacemaker has three lead outlets with a Y-adaptor in the header for insertion of both right and left ventricular leads. Most commercially available left ventricular leads are unipolar with a shared common ring of a bipolar sensing/pacing right ventricular lead. During lead positioning, pacing thresholds should be measured in a unipolar manner. Final thresholds should be determined using the intended pacing configuration similar to device connection.

The pacing threshold for left ventricular pacing from the coronary sinus is consistently higher compared to that during endocardial right ventricular pacing. However, it seems that the shape of the strength–duration curve during coronary vein left ventricular pacing is not significantly different from that during endocardial right ventricular pacing (Fig. 8) (unpublished data). The combined lead impedance is less than that of either lead and is typically in the range of 400 Ω. The combined sensing of the two ventricles (which may be separated by 80 to 150 ms) requires additional consideration in device programming to avoid double sensing. This is particularly important during defibrillator implantation.

9.3. Risk and Complication

Of the 528 patients who underwent successful implantation in the MIRACLE study, the median duration of the procedure was 2.7 h (range 0.9–7.3 h). Implantation of the device was unsuccessful in 8% of the patients and was complicated by refractory hypotension, bradycardia, or asystole in 4 patients (2 of whom died) and by perforation of the coronary sinus requiring pericardiocentesis in 2 other patients. Dissection or perforation of the coronary sinus or cardiac vein occurred in about 6% of the patients, and other serious complications (including complete heart block, hemopericardium, and car-

diac arrest) presented in about 1.2% of the patients. Other complications included subsequent lead revision (6%) and explantation because of infection (1.3%).

10. PREDICTION OF EFFICACY OF BIVENTRICULAR PACING

A majority (70–80%) of patients respond well to biventricular pacing. In the MIRACLE trial, biventricular pacing was associated with more patients who elicited improvement (67 vs 39%) and fewer patients who progressively worsened (16 vs 27%) at the end of 6-month follow-up *(16)*. Interestingly, basal demographic, clinical, and functional characteristics have failed to predict the effects of biventricular pacing. Limited data showed that there is increasing benefit for the use of biventricular pacing in patients with a wider QRS duration and severe left ventricular dysfunction *(42,59)*.

However, it must be considered that a significantly enlarged heart may not respond to biventricular pacing, and some of them may not even tolerate the implantation procedure. Unfortunately, early hemodynamic testing does not necessarily predict potential chronic effects of biventricular pacing. Patients who show no improvement are more likely to have had a large myocardial infarction, low cardiac output, and no significant mitral regurgitation as those patients experiencing beneficial results *(60)*.

Reduction in QRS duration induced by biventricular pacing is commonly seen in cardiac resynchronization therapy *(39)*. However, QRS narrowing induced by biventricular pacing does not necessarily correlate with maximal mechanical hemodynamic benefits *(37,59,61)*. For example, one animal study has indicated that improved mechanical synchrony and function do not require electrical synchrony *(62)*. Further, dual-site right ventricular pacing (right ventricular apex and outflow tract) does not improve hemodynamics despite a narrowing QRS duration *(63)*.

Yet, mechanical coordination is considered to play a dominant role in global systolic improvement in left ventricular-based pacing. In patients with complete right bundle branch block and drug-resistant heart failure, only patients with a right bundle branch block associated with a major left intraventricular asynchrony have been shown to respond well to biventricular pacing therapy *(64)*. Importantly, Doppler tissue imaging can be a very useful technique for detecting regional electromechanical delays (defined as the time delay from the onset of the QRS to the onset of the systolic S wave of a given ventricular wall) to guide lead placement to optimize biventricular pacing *(61,64,65)*.

At present, only echocardiographic or other image characteristics associated with left ventricular asynchrony have been reported to predict the effects of biventricular pacing. One of the major challenges in the field of biventricular pacing for congestive heart failure is the predictive clinical identification of patients who will benefit from biventricular pacing.

11. FUTURE PERSPECTIVE

There is growing acceptance for biventricular pacing as a treatment for patients with moderate-to-severe congestive heart failure in the presence of an intraventricular conduction delay. The potential deleterious effects of right ventricular pacing alone in such cases have been established. It seems that left ventricular pacing should be performed when feasible whenever cardiac pacing is required, such as after atrioventricular nodal ablation, to minimize subsequent electrical and mechanical remodeling. Yet, biventricular pacing at present is an imperfect technique for correcting cardiac dyssynchrony. The concept of physiological pacing should always be kept in mind to maximize the benefits of pacing whenever pacing is required, particularly in the presence of left ventricular dysfunction. Nonetheless, the beneficial effects of biventricular pacing will continue to increase clinically if the following important clinical and technical questions can be resolved:

1. What is the impact of cardiac resynchronization therapy on all-cause mortality and sudden cardiac death?
2. Can cardiac resynchronization therapy induce left ventricular reverse remodeling and thus help to prevent, or at least slow, heart failure progression?
3. How can we better select potential responders?
4. What are the optimal pacing sites?
5. How can we best determine the optimal atrioventricular delay?
6. How can we improve the methods for implanting left ventricular leads?

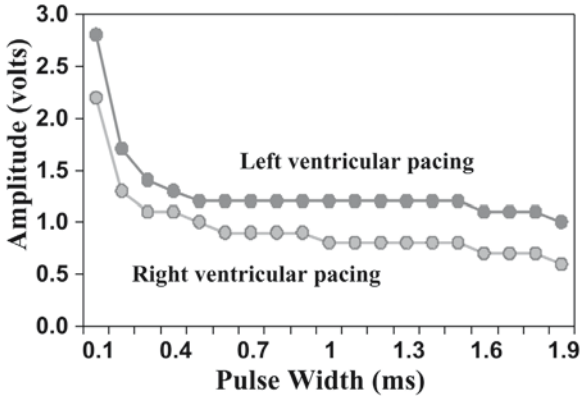

Fig. 8. The strength–duration curves during coronary vein left ventricular pacing in four patients with biventricular pacing with a lead in the right ventricular apex and the lateral wall of the left ventricle using Guidant lead 4512. It appears that there is no substantial difference in the shape of the two curves.

REFERENCES

1. Hunt, S.A., Baker, D.W., Chin, M.H., et al. (2001) ACC/AHA guidelines for the evaluation and management of chronic heart failure in the adult: executive summary. A report of the American College of Cardiology/American Heart Association Task Force on Practice Guidelines (Committee to Revise the 1995 Guidelines for the Evaluation and Management of Heart Failure). *J Am Coll Cardiol*. 38, 2101–2113.
2. Gregoratos, G., Abrams, J., Epstein, A. E., et al. (2002) ACC/AHA/NASPE 2002 guideline update for implantation of cardiac pacemakers and antiarrhythmia devices-summary article. A report of the American College of Cardiology/American Heart Association Task Force on Practice Guidelines (ACC/AHA/NASPE Committee to Update the 1998 Pacemaker Guidelines). *J Am Coll Cardiol*. 40, 1703–1719.

3. Gold, M.R., Feliciano, Z., Gottlieb, S.S., and Fisher, M.L. (1995) Dual-chamber pacing with a short atrioventricular delay in congestive heart failure: a randomized study. *J Am Coll Cardiol.* 26, 967–973.
4. Linde, C., Gadler, F., Edner, M., Nordlander, R., Rosenqvist, M., and Ryden, L. (1995) Results of atrioventricular synchronous pacing with optimized delay in patients with severe congestive heart failure. *Am J Cardiol.* 75, 919–923.
5. Fei, L., Wrobleski, D., Groh, W., Vetter, A., Duffin, E.G., and Zipes, D.P. (1999) Effects of multisite ventricular pacing on cardiac function in normal dogs and dogs with heart failure. *J Cardiovasc Electrophysiol.* 10, 935–946.
6. Bernstein, A.D., Daubert, J.C., Fletcher, R.D., et al. (2002) The revised NASPE/BPEG generic code for antibradycardia, adaptive-rate, and multisite pacing. North American Society of Pacing and Electrophysiology/British Pacing and Electrophysiology Group. *Pacing Clin Electrophysiol.* 25, 260–264.
7. Wyman, B.T., Hunter, W.C., Prinzen, F.W., Faris, O.P., and McVeigh, E.R. (2002) Effects of single- and biventricular pacing on temporal and spatial dynamics of ventricular contraction. *Am J Physiol Heart Circ Physiol.* 282, H372–H379.
8. Schwaab, B., Frohlig, G., Alexander, C., et al. (1999) Influence of right ventricular stimulation site on left ventricular function in atrial synchronous ventricular pacing. *J Am Coll Cardiol.* 33, 317–323.
9. Leclercq, C., Gras, D., Le Helloco, A., Nicol, L., Mabo, P., and Daubert, C. (1995) Hemodynamic importance of preserving the normal sequence of ventricular activation in permanent cardiac pacing. *Am Heart J.* 129, 1133–1141.
10. Stevenson, W.G., Stevenson, L.W., Middlekauff, H.R., et al. (1996) Improving survival for patients with atrial fibrillation and advanced heart failure. *J Am Coll Cardiol.* 28, 1458–1463.
11. Farwell, D., Patel, N.R., Hall, A., Ralph, S., and Sulke, A.N. (2000) How many people with heart failure are appropriate for biventricular resynchronization? *Eur Heart J.* 21, 1246–1250.
12. Shenkman, H.J., Pampati, V., Khandelwal, A.K., et al. (2002) Congestive heart failure and QRS duration: establishing prognosis study. *Chest.* 122, 528–534.
13. Gras, D., Mabo, P., Tang, T., et al. (1998) Multisite pacing as a supplemental treatment of congestive heart failure: preliminary results of the Medtronic Inc. InSync Study. *Pacing Clin Electrophysiol.* 21, 2249–2255.
14. Gras, D., Leclercq, C., Tang, A.S., Bucknall, C., Luttikhuis, H.O., and Kirstein-Pedersen, A. (2002) Cardiac resynchronization therapy in advanced heart failure the multicenter InSync clinical study. *Eur J Heart Fail.* 4, 311–320.
15. Cazeau, S., Leclercq, C., Lavergne, T., et al. (2001) Effects of multisite biventricular pacing in patients with heart failure and intraventricular conduction delay. *N Engl J Med.* 344, 873–880.
16. Abraham, W.T., Fisher, W.G., Smith, A.L., et al. (2002) Cardiac resynchronization in chronic heart failure. *N Engl J Med.* 346, 1845–1853.
17. Kuhlkamp, V. (2002) Initial experience with an implantable cardioverter–defibrillator incorporating cardiac resynchronization therapy. *J Am Coll Cardiol.* 39, 790–797.
18. Linde, C., Leclercq, C., Rex, S., et al. (2002) Long-term benefits of biventricular pacing in congestive heart failure: results from the Multisite Stimulation in Cardiomyopathy (MUSTIC) study. *J Am Coll Cardiol.* 40, 111–118.
19. Zagrodzky, J.D., Ramaswamy, K., Page, R.L., et al. (2001) Biventricular pacing decreases the inducibility of ventricular tachycardia in patients with ischemic cardiomyopathy. *Am J Cardiol.* 87, 1208–1210.
20. Walker, S., Levy, T.M., Rex, S., et al. (2000) Usefulness of suppression of ventricular arrhythmia by biventricular pacing in severe congestive cardiac failure. *Am J Cardiol.* 86, 231–233.
21. Higgins, S.L., Yong, P., Sheck, D., et al. (2000) Biventricular pacing diminishes the need for implantable cardioverter defibrillator therapy. Ventak CHF Investigators. *J Am Coll Cardiol.* 36, 824–827.
22. Garrigue, S., Barold, S.S., Hocini, M., Jais, P., Haissaguerre, M., and Clementy, J. (2000) Treatment of drug refractory ventricular tachycardia by biventricular pacing. *Pacing Clin Electrophysiol.* 23, 1700–1702.
23. Lozano, I., Bocchiardo, M., Achtelik, M., et al. (2000) Impact of biventricular pacing on mortality in a randomized crossover study of patients with heart failure and ventricular arrhythmias. *Pacing Clin Electrophysiol.* 23, 1711–1712.
24. Medina-Ravell, V.A., Lankipalli, R.S., Yan, G.X., et al. (2003) Effect of epicardial or biventricular pacing to prolong QT interval and increase transmural dispersion of repolarization: does resynchronization therapy pose a risk for patients predisposed to long QT or torsade de pointes? *Circulation.* 107, 740–746.
25. Saxon, L.A., Boehmer, J.P., Hummel, J., et al. (1999) Biventricular pacing in patients with congestive heart failure: two prospective randomized trials. The VIGOR CHF and VENTAK CHF Investigators. *Am J Cardiol.* 83, 120D–123D.
26. Bristow, M.R., Feldman, A.M., and Saxon, L.A. (2000) Heart failure management using implantable devices for ventricular resynchronization: Comparison of Medical Therapy, Pacing, and Defibrillation in Chronic Heart Failure (COMPANION) trial. COMPANION Steering Committee and COMPANION Clinical Investigators. *J Card Fail.* 6, 276–285.
27. Butter, C., Meisel, E., Tebbenjohanns, J., et al. (2001) Transvenous biventricular defibrillation halves energy requirements in patients. *Circulation.* 104, 2533–2538.
28. Werling, C., Weisse, U., Siemon, G., et al. (2002) Biventricular pacing in patients with ICD: how many patients are possible candidates? *Thorac Cardiovasc Surg.* 50, 67–70.
29. Prinzen, F.W., Cheriex, E.C., Delhaas, T., et al. (1995) Asymmetric thickness of the left ventricular wall resulting from asynchronous electric activation: a study in dogs with ventricular pacing and in patients with left bundle branch block. *Am Heart J.* 130, 1045–1053.
30. Karpawich, P.P., Rabah, R., and Haas, J.E. (1999) Altered cardiac histology following apical right ventricular pacing in patients with congenital atrioventricular block. *Pacing Clin Electrophysiol.* 22, 1372–1377.
31. Tantengco, M.V., Thomas, R.L., and Karpawich, P.P. (2001) Left ventricular dysfunction after long-term right ventricular apical pacing in the young. *J Am Coll Cardiol.* 37, 2093–2100.
32. Tse, H.F., Yu, C., Wong, K.K., et al. (2002) Functional abnormalities in patients with permanent right ventricular pacing: the effect of sites of electrical stimulation. *J Am Coll Cardiol.* 40, 1451–1458.
33. Lau, C.P., Yu, C.M., Chau, E., et al. (2000) Reversal of left ventricular remodeling by synchronous biventricular pacing in heart failure. *Pacing Clin Electrophysiol.* 23, 1722–1725.
34. Ricci, R., Pignalberi, C., Ansalone, G., et al. (2002) Early and late QRS morphology and width in biventricular pacing: relationship to lead site and electrical remodeling. *J Interv Card Electrophysiol.* 6, 279–285.
35. Takagi, Y., Dumpis, Y., Usui, A., Maseki, T., Watanabe, T., and Yasuura, K. (1999) Effects of proximal ventricular septal pacing on hemodynamics and ventricular activation. *Pacing Clin Electrophysiol.* 22, 1777–1781.
36. Mera, F., DeLurgio, D.B., Patterson, R.E., Merlino, J.D., Wade, M.E., and Leon, A.R. (1999) A comparison of ventricular function during high right ventricular septal and apical pacing after His-bundle ablation for refractory atrial fibrillation. *Pacing Clin Electrophysiol.* 22, 1234–1239.
37. Blanc, J.J., Etienne, Y., Gilard, M., et al. (1997) Evaluation of different ventricular pacing sites in patients with severe heart failure: results of an acute hemodynamic study. *Circulation.* 96, 3273–3277.
38. Butter, C., Auricchio, A., Stellbrink, C., et al. (2000) Should stimulation site be tailored in the individual heart failure patient? *Am J Cardiol.* 86, K144–K151.
39. Alonso, C., Leclercq, C., Victor, F., et al. (1999) Electrocardiographic predictive factors of long-term clinical improvement with multisite biventricular pacing in advanced heart failure. *Am J Cardiol.* 84, 1417–1421.
40. Auricchio, A., Stellbrink, C., Sack, S., et al. (1999) The Pacing Therapies for Congestive Heart Failure (PATH-CHF) study: rationale, design, and endpoints of a prospective randomized multicenter study. *Am J Cardiol.* 83, 130D–135D.

41. Auricchio, A., Klein, H., Tockman, B., et al. (1999) Transvenous biventricular pacing for heart failure: can the obstacles be overcome? *Am J Cardiol.* 83, 136D–142D.
42. Leclercq, C., Cazeau, S., Le Breton, H., et al. (1998) Acute hemodynamic effects of biventricular DDD pacing in patients with end-stage heart failure. *J Am Coll Cardiol.* 32, 1825–1831.
43. Butter, C., Auricchio, A., Stellbrink, C., et al. (2001) Effect of resynchronization therapy stimulation site on the systolic function of heart failure patients. *Circulation.* 104, 3026–3029.
44. O'Cochlain, B., Delurgio, D., Leon, A., and Langberg, J. (2001) The effect of variation in the interval between right and left ventricular activation on paced QRS duration. *Pacing Clin Electrophysiol.* 24, 1780–1782.
45. Sogaard, P., Egeblad, H., Pedersen, A.K., et al. (2002) Sequential versus simultaneous biventricular resynchronization for severe heart failure: evaluation by tissue Doppler imaging. *Circulation.* 106, 2078–2084.
46. Sabbah, H.N., Haddad, W., Mika, Y., et al. (2001) Cardiac contractility modulation with the impulse dynamics signal: studies in dogs with chronic heart failure. *Heart Fail Rev.* 6, 45–53.
47. Marrouche, N.F., Pavia, S.V., Zhuang, S., et al. (2002) Nonexcitatory stimulus delivery improves left ventricular function in hearts with left bundle branch block. *J Cardiovasc Electrophysiol.* 13, 691–695.
48. Frommer, P.L., Robinson, B.F. and Braunwald, E. (1966) Paired electrical stimulation. A comparison of the effects on performance of the failing and nonfailing heart. *Am J Cardiol.* 18, 738–744.
49. Cooper, M.W. (1993) Postextrasystolic potentiation. Do we really know what it means and how to use it? *Circulation.* 88, 2962–2971.
50. Hamdan, M.H., Zagrodzky, J.D., Joglar, J.A., et al. (2000) Biventricular pacing decreases sympathetic activity compared with right ventricular pacing in patients with depressed ejection fraction. C*irculation.* 102, 1027–1032.
51. Hamdan, M.H., Barbera, S., Kowal, R.C., et al. (2002) Effects of resynchronization therapy on sympathetic activity in patients with depressed ejection fraction and intraventricular conduction delay due to ischemic or idiopathic dilated cardiomyopathy. *Am J Cardiol.* 89, 1047–1051.
52. Saxon, L.A., DeMarco, T., Chatterjee, K., and Boehmer, J. (1999) Chronic biventricular pacing decreases serum norepinephrine in dilated heart failure patients with the greatest sympathetic activation at baseline. *Pacing Clin Electrophysiol.* 22(suppl), 830.
53. Baller, D., Wolpers, H.G., Zipfel, J., Hoeft, A., and Hellige, G. (1981) Unfavorable effects of ventricular pacing on myocardial energetics. *Basic Res Cardiol.* 76, 115–123.
54. Nelson, G.S., Berger, R.D., Fetics, B.J., et al. (2000) Left ventricular or biventricular pacing improves cardiac function at diminished energy cost in patients with dilated cardiomyopathy and left bundle-branch block. *Circulation.* 102, 3053–3059.
55. Ukkonen, H., Beanlands, R.S., Burwash, I.G., et al. (2003) Effect of cardiac resynchronization on myocardial efficiency and regional oxidative metabolism. *Circulation.* 107, 28–31.
56. Yu, C.M. and Miu, R. (2002) A new technique for the transvenous implantation of the over-the-wire left ventricular pacing lead in a patient with heart failure. *J Interv Card Electrophysiol.* 7, 189–191.
57. Leclercq, F., Hager, F.X., Macia, J.C., Mariottini, C.J., Pasquie, J.L., and Grolleau, R. (1999) Left ventricular lead insertion using a modified transseptal catheterization technique: a totally endocardial approach for permanent biventricular pacing in end-stage heart failure. *Pacing Clin Electrophysiol.* 22, 1570–1575.
58. Foster, A.H., Gold, M.R., and McLaughlin, J.S. (1995) Acute hemodynamic effects of atrio-biventricular pacing in humans. *Ann Thorac Surg.* 59, 294–300.
59. Kass, D.A., Chen, C.H., Curry, C., et al. (1999) Improved left ventricular mechanics from acute VDD pacing in patients with dilated cardiomyopathy and ventricular conduction delay. *Circulation.* 99, 1567–1573.
60. Reuter, S., Garrigue, S., Barold, S.S., et al. (2002) Comparison of characteristics in responders versus nonresponders with biventricular pacing for drug-resistant congestive heart failure. *Am J Cardiol.* 89, 346–350.
61. Ansalone, G., Giannantoni, P., Ricci, R., et al. (2001) Doppler myocardial imaging in patients with heart failure receiving biventricular pacing treatment. *Am Heart J.* 142, 881–896.
62. Leclercq, C., Faris, O., Tunin, R., et al. (2002) Systolic improvement and mechanical resynchronization does not require electrical synchrony in the dilated failing heart with left bundle-branch block. *Circulation.* 106, 1760–1763.
63. Buckingham, T.A., Candinas, R., Schlapfer, J., et al. (1997) Acute hemodynamic effects of atrioventricular pacing at differing sites in the right ventricle individually and simultaneously. *Pacing Clin Electrophysiol.* 20, 909–915.
64. Garrigue, S., Reuter, S., Labeque, J.N., et al. (2001) Usefulness of biventricular pacing in patients with congestive heart failure and right bundle branch block. *Am J Cardiol.* 88, 1436–1441, A8.
65. Sogaard, P., Kim, W.Y., Jensen, H.K., et al. (2001) Impact of acute biventricular pacing on left ventricular performance and volumes in patients with severe heart failure. A tissue Doppler and three-dimensional echocardiographic study. *Cardiology.* 95, 173–182.

25 Cardiac Mapping Systems

NICHOLAS D. SKADSBERG, PhD, TIMOTHY G. LASKE, PhD, AND PAUL A. IAIZZO, PhD

CONTENTS

1. BACKGROUND

The first electrocardiogram (ECG) recording detailing the structure of atrioventricular conduction was made by Tawara nearly 100 years ago *(1)*. Soon after, Mayer first observed rhythmical pulsations made in ringlike preparations of the muscular tissue of a jellyfish (*Scyphomedusa cassiopeia*) *(2,3)*. In a ringlike preparation of a tortoise heart, Mines was able to initiate circulating excitation using electrical stimulation *(4)*. Shortly thereafter, Lewis and Rothschild described the excitatory process in a canine heart *(5)*, and after a delay because of the events of World War I, Lewis and coworkers reported the first real "mapping" experiment in 1920 *(6)*. These studies were the first attempts to illustrate and document reentry in the intact heart, and their work has had a great influence on subsequent mapping studies. Hence, the field of cardiac electrical mapping was established. Soon after, the idea of mapping arrhythmic activation encompassed an ever-larger number of studies, including those of Barker et al., who performed mapping of the first intact human heart in 1930 *(7)*.

In short, the methodology of cardiac electrical mapping entails registration of the electrical activation sequences of the heart by recording extracellular electrograms. The initial use of cardiac mapping was primarily to understand better the electrical excitation of the normal heart. However, the focus over time has shifted to the study of mechanisms and substrates underlying various arrhythmias. Cardiac mapping has been employed to aid in the guidance of curative surgical and catheter ablation procedures *(8–13)*. More recently, the advent and continued development of highly technical mapping systems have considerably enhanced our understanding of rapid, complex, or transient arrhythmias that cannot be sufficiently characterized with more conventional methodologies. These new systems provide powerful tools in the assessment and subsequent treatment of cardiac patients, particularly with the promise of accurately pinpointing the source of arrhythmias and correcting cardiac function. Despite this increase in knowledge, arrhythmias such as atrial fibrillation to date require more definite treatments in most cases.

From: *Handbook of Cardiac Anatomy, Physiology, and Devices*
Edited by: P. A. Iaizzo © Humana Press Inc., Totowa, NJ

2. CONVENTIONAL METHODOLOGIES

Currently, approx 10 million Americans are afflicted with cardiac arrhythmias (both ventricular and atrial) every year; nonetheless, only a small percentage of patients are expected to have electrophysiological mapping procedures. Yet, cardiac electrical mapping is considered as critical for understanding the pathophysiological mechanisms that underlie arrhythmias as well as the mechanisms of their initiation and sustenance. Further, cardiac mapping is commonly used for evaluating the effect of pharmacological therapies and for directing surgical or catheter ablation procedures; this occurs in the electrophysiology laboratory, as well as for experimental studies on arrhythmias.

More specifically, mapping of the endocardial activation and repolarization processes is critical for the selection of optimal therapeutic procedures. In particular, the mapping of endocardial potential distributions and their evolutions in time are required for precisely determining activation patterns, locating specific arrhythmogenic sites, and identifying areas of abnormal activity or slow conduction pathways.

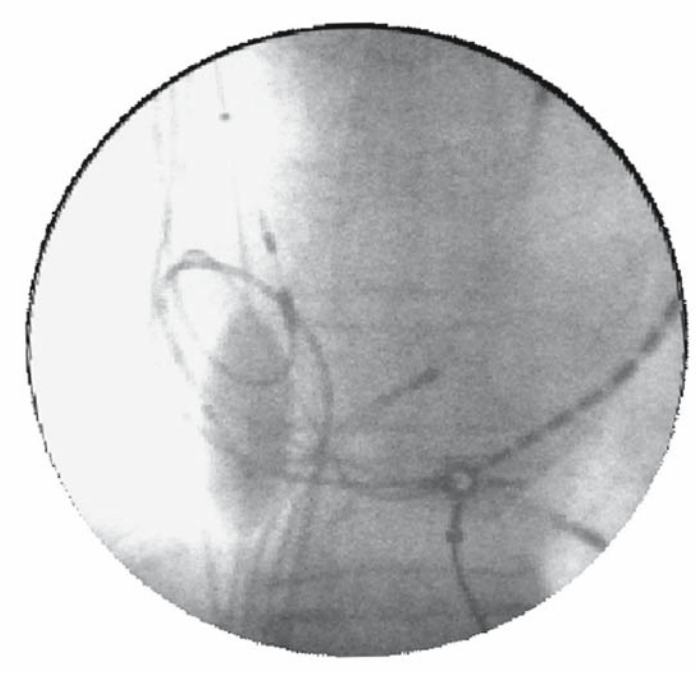

Fig. 1. Image illustrating fluoroscopy's poor soft tissue contrast.

In short, the purpose of cardiac mapping is to characterize and localize the arrhythmogenic structure, and this can be accomplished by a variety of different methods. Cardiac mapping is a broad term that encompasses many applications, such as body surface mapping or epicardial mapping, as well as approaches that include activation maps or isopotential maps. There are fundamental similarities in all of these techniques.

Currently, the gold standard is the clinical electrophysiological study, which is primarily used to determine the source of cardiac arrhythmias and to support the management of treatment through pharmacological means or nonpharmacological interventions such as implantable pacemakers, implantable defibrillators, or radiofrequency ablation therapies. More specifically, this method is used to assess the timing and propagation of cardiac electrical activity involving the 12-lead ECG or recordings of electrical activation sequences termed *extracellular electrograms*, which are obtained using multiple intravascular electrode catheters positioned at various locations within the heart. The technique of catheter-based mapping not only permits better understanding of the underlying mechanisms of various arrhythmias, but also has served as the basis of most of the emerging concepts for treatment. Most important, these methodologies have allowed for widespread applications of ablative techniques in almost all known cardiac arrhythmias. Subsequently, the need for invasive arrhythmia surgery has significantly decreased as a result of these particular catheter-based endocardial mapping and ablation methodologies *(14)*.

Nevertheless, the electrophysiological study is not without limitations. The electrophysiologist can only record electrical activity from the tip of the catheter, which must be in contact with the chamber wall. Such tip areas are relatively small in comparison to the heart's total surface area. Thus, to obtain adequate electrical activity for activation patterns, it often dictates the placement of multiple catheters at numerous locations within the chamber of interest, which in turn requires a considerable amount of time; this also leads to extensive use of fluoroscopy, hence exposing the medical staff and patients to undesirable levels of ionizing radiation *(15)*. Second, and perhaps more important, fluoroscopy does not sufficiently allow for the visualization of the complex 3D cardiac anatomy and/or soft tissue characteristics of the heart's chambers (Fig. 1).

As a direct result, the expedient and reproducible localization of sites of interest is often poor. More specifically, this inability to relate electrophysiological information precisely to a specific spatial location in the heart limits conventional techniques for employing radiofrequency ablation catheters for treatment of complex cardiac arrhythmias. Last, such techniques for mapping electrical potential activity from multiple sites do so sequentially over several cardiac cycles without accounting for likely beat-to-beat variability in activation patterns. Despite these known limitations, electrophysiologists still use these conventional techniques as the gold standard for validation purposes.

3. RECENT DEVELOPMENTS

In an effort to overcome the limitations associated with conventional electrophysiological mapping techniques, considerable advances have been made by a number of companies and such progress is ongoing. More specifically, several highly technical mapping systems have been developed that can function in a complementary role to conventional mapping techniques, or they can be used independently. These techniques can broadly be grouped into two primary technology categories, each possessing their own unique advantages and disadvantages: sequential mapping and continuous mapping.

Three distinct technologies comprise the first category, termed *sequential mapping systems*, and include (1) electroanatomical mapping, commonly called the CARTO™ system using the CARTO™ XP System (Biosense Webster, Diamond Bar, CA); (2) the Real-Time Position Management system (RPM™, Boston Scientific, Natick, MA); and (3) the LocaLisa® system (Medtronic, Inc., Minneapolis, MN). Common to each system is the capability to collect 3D locations as well as their respective electrogram recordings in the target cardiac chamber to create an accurate picture of the heart's electrical sequence.

Continuous mapping systems represent the second primary mapping technology category and consist of basket mapping and noncontact catheter mapping. In this category, the systems allow for the recording of global data so that the rhythm can be characterized in only one to two cardiac beats. Basket catheter mapping necessitates electrode contact with the chamber's walls to obtain sufficiently accurate reconstructed electrograms, whereas noncontact mapping simply needs to be placed in the blood pool of the chamber of interest. Importantly, both methodologies overcome some of the limitations of fluoroscopy by allowing the creation of accurate 3D intracardiac maps, hence providing new and unique insights regarding the specific diagnosis and treatments of complex arrhythmias.

3.1. Sequential Systems

3.1.1. Electroanatomical Mapping Technology

Principally, electroanatomical mapping utilizes ultralow magnetic field technology to reconstruct 3D maps and activation sequences of the chamber of interest *(16–18)*. In short, the CARTO™XP (or 4.2) System uses one reference catheter (REFSTAR™), one mapping catheter (NAVI-STAR™), and a pad that transmits three ultralow magnetic fields (Fig. 2). The CARTO™ XP System utilizes a Windows-based Dell workstation. Further, the amplifiers (or actual CARTO™ units) for both the XP and 4.2 systems are separate pieces of equipment that extract the information from the catheters and the location pad and then send that information to the workstation.

More specifically, three ultralow magnetic fields are generated by coils in the locator pad positioned under the patient's bed. These ultralow fields are detected by the sensors in the distal tips of the mapping catheters, which are then positioned into a heart chamber to be mapped under fluoroscopic guidance. These catheters also have radiofrequency capabilities, including a 4-mm tip and an 8-mm dual-sensor tip. Information within the magnetic fields such as amplitude, frequency, and phase of the field is subsequently used to determine the spatial 3D position (*x*-, *y*-, and *z*-axes) and temporal characteristics (pitch, yaw, and roll) of the catheter's distal tip location within a chamber *(7)*. Catheters are then strategically placed at major anatomical landmarks (i.e., such as the superior and inferior venae cavae, tricuspid valve annulus, coronary sinus ostium, crista terminalis, and His bundle for a right atrium map) to serve as reference points for the electroanatomic map. Recordings of the 3D locations of the catheter tips (via a triangulation calculation) and correlating electrograms from a multitude of points within the chamber are then sequentially recorded and used to reconstruct a 3D representation of the chamber.

After completion of the 3D reconstruction of the chamber's endocardial geometry, the timing of unipolar and bipolar electrogram signals, related to the fiducial point of the reference electrogram, allows collection and display of activation times on the map in relation to the location of the catheter in the heart. To create the activation map, reconstructed locations on the map are color coded, with red and purple representing the regions of earliest and latest electrical activation, respectively, and yellow and green for the intermediate-activated areas. Local activation time is represented on a normal color scale sequence in which red is the earliest signal and purple is the latest recorded signal in reference to the chosen fiducial point. As a result, the sequential recording of different points by dragging the catheter along the endocardial walls of the chamber provides a real-time, color-coded, 3D activation map.

A voltage map displaying the peak-to-peak amplitudes of the electrograms sampled at each site may also be produced and superimposed on the reconstructed chamber. All maps can be shown in single or multiple views concurrently, with the capability to be rotated in virtually any direction. As described, a second catheter equipped with a sensor in its distal tip is also positioned in the chamber of interest and is used to identify small changes in the mapping catheter's relative position that may have been caused by respiration or patient movement. With CARTO™, the reference catheter is positioned on the back of the patient, not within the chamber.

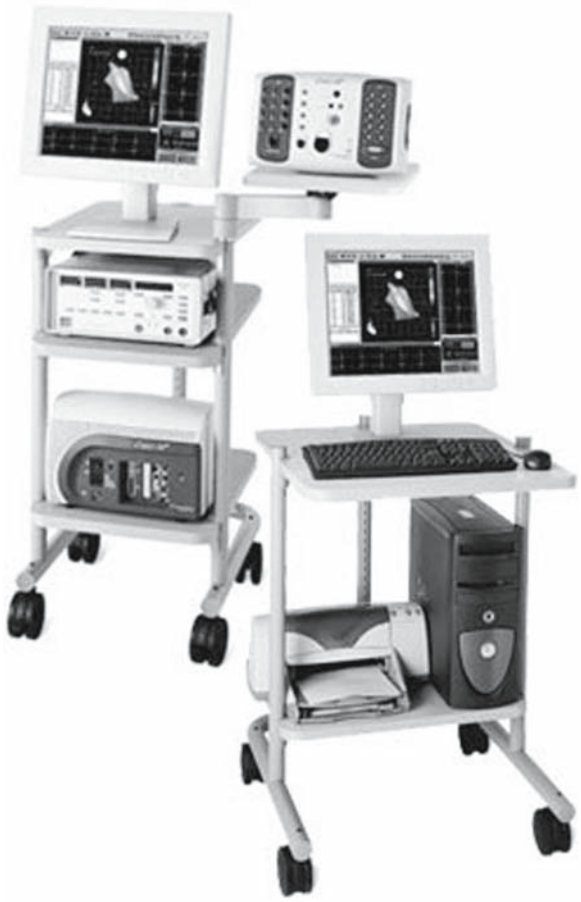

Fig. 2. CARTO™ sequential mapping system. Courtesy of Biosense Webster Inc.

Such electroanatomical mapping has found widespread clinical use and has been used for the study of a variety of cardiac arrhythmias, including atrial fibrillation *(19)*, atrial flutter *(20–23)*, ventricular tachycardia *(24,25)*, and atrial tachycardia *(26,27)*. One of the primary reasons for the success of this method lies in its capability to return to any endocardial location on a previous map of the chamber, without relying on fluoroscopy, with an ablation catheter. The ablation catheter and mapping catheter are typically the same. This enables potential ablation target sites to be analyzed and treated in a single procedure and provides the ability to register the precise location of individual or linear radiofrequency lesions. In addition, the CARTO™XP System allows the construction of 20 different maps simultaneously. Further, the system is considered practical for readily defining mechanisms of arrhythmias and optimal radiofrequency ablation strategies.

The reconstruction process using such a system can be generated in real time; however, because this approach must sequentially acquire points, the process is time consuming *(27,28)* and is governed by the number of points collected. The extent of the time to reconstruct a chamber's geometry relies on the comfort level of the physician manipulating the catheter and

the knowledge of the individual at the workstation. In addition, other limitations associated with electroanatomical mapping include the inability to acquire maps of different heart rhythms simultaneously *(28)* as well as inaccurate mapping because of movement of the patient or catheter. As a direct result, an unstable rhythm proves complicated to delineate and therefore is not a primary indication for this technology.

3.1.2. Real-Time Position Management Technology

Previously, ultrasound ranging has been utilized to represent distance measurements for cardiac chambers and valves accurately. More recently, this technology has been utilized to assess the relative position of catheters within the heart. More important, the RPM system has facilitated radiofrequency catheter ablation procedures because it allows accurate and reproducible tracking of the mapping and ablation catheter. The system consists of an acquisition module and an ultrasound transmitter and receiver unit, both connected to a SPARC 20 computer (Sun Microsystems, Santa Clara, CA). Currently, this system is capable of simultaneously processing 7 position management catheters, 24 bipolar/48 unipolar electrogram signals, a 12-lead ECG, and 2 pressure signals.

A typical procedure utilizing the system places two reference catheters and one mapping/ablation catheter percutaneously into the chamber of interest. In most cases, one of the reference catheters is positioned in the right atrial appendage or coronary sinus and the other in the right ventricular apex. For ablation procedures, a 4-mm tip steerable catheter and radiofrequency ablation system are used. Both the reference and ablation catheters contain ultrasound transducers used to transmit and receive a continuous cycle of ultrasound pulses (558.5 kHz) to and from each other.

This approach derives the velocity of the transmitted signal by calculating the distance between the transmitting transducer and the associated time delay, assuming the speed of sound in blood is 1550 m/s. To create a 3D map, a triangulation algorithm is employed using signals sent back and forth between the catheters to establish a reference frame. A third catheter is then introduced into the same chamber and is tracked with relationship to the reference frame to locate and subsequently record its position. It is through movement of the third catheter in the chamber that the 3D map is consequently created.

Initial benchtop validation studies using this system were performed and reported by de Groot et al. *(29)*. They described the use of the RPM system in a group of patients with various arrhythmias and demonstrated the system's feasibility, safety, and efficacy; the system was then operated without the option of geometry reconstruction.

Schreieck et al. *(30)* evaluated the efficacy of a newly released version of the system, which now includes the option of 3D model reconstruction of the heart chambers for guiding mapping and ablation; they studied 21 patients with different atrial and ventricular arrhythmias. The current version enables geometric reconstruction of all cardiac chambers if desired.

There are a number of advantages associated with the use of the RPM system. One is that it is an independent system capable of displaying a 3D map and recorded electrical activity on a single platform. In addition, the system incorporates cooled radiofrequency ablation methodologies, which have been shown to improve lesion depth and efficacy *(31)*. As well, the system allows for incorporation of activation times to the anatomical model to provide a real-time display of the distal catheter curve; it also stores information regarding the relative catheter positions. The system importantly minimizes the influence of body, cardiac, and respiratory motion on the reference field, and thus there is no need for skin or patch electrodes.

A major disadvantage is that the system is catheter specific (i.e., it is only able to use certain catheter types). Further limitations pointed out by Schreieck et al. *(30)* include: (1) the need for at least three catheters for each electrophysiological study; (2) no real-time display of the ablation catheter; (3) no intracardiac signal at the time of radiofrequency current delivery; (4) dislocation of the reference catheters because of roving catheter manipulation; and (5) an undesired stiffness of the distal part of the mapping/ablation catheter.

3.1.3. LocaLisa® Technology

Another new technique has been developed for real-time, 3D localization of intracardiac catheter electrodes within the chambers of the heart. It works on the principle that when an electrical current is externally applied through the thorax, a voltage drop occurs across the internal organs, including the heart. This particular voltage drop can then be recorded via standard catheter electrodes and subsequently used to determine electrode position within a given 3D space.

Using similar physical properties, the LocaLisa system (Fig. 3) delivers an external electrical field that is detected via standard catheter electrodes. This is achieved by sensing impedance changes between the catheter and reference points. Analogous to the Frank lead system, the electric field is applied in three orthogonal directions (x, y, and z) with different frequencies (~30 Hz) via three applied skin electrode pairs. The system then records the voltage potentials detected by the catheter's electrodes within the three electric fields, allowing for a defined coordinate system to be created.

These voltage potentials are next translated into a measure of distance relative to a fixed reference catheter, giving the user a 3D representation of the catheter location within the heart's chamber. Important catheter locations are subsequently recorded and represented as color-coded spots on a 3D grid, a process that requires a skilled operator's interpretation (Fig. 4). Individual catheter locations can then be saved, annotated, and revisited later in the procedure.

Because the system displays real-time electrode movements, catheter movements caused by the cardiac and respiratory cycles are similar to those observed with fluoroscopy. In initial human validation studies, the LocaLisa system was described to provide clinically feasible and accurate catheter locations within the heart *(32)*. Developers of the system reported successful use in over 250 complex ablation procedures for both ventricular and supraventricular tachyarrhythmias. The capabilities of this system include: (1) ability to use any general catheter to collect data; (2) improvement in visualization of catheters in 3D space; and (3) broad clinical applicability. Such capabilities make this system one of the most powerful tools currently available for ablation procedures. Finally, the approach can be applied with complex catheter designs, such as multielectrode catheters, irrigated electrode catheters, and basket catheters *(33–35)*.

3.2. Continuous Systems

3.2.1. Basket Catheter Mapping Technology

The limited mapping resolution of conventional catheters may be overcome via the use of a multielectrode basket catheter. Basket catheter mapping was developed in the 1990s, and typical catheters contain 32–64 nickel or titanium electrodes *(35,36)* that are 1–2 mm long and 1 mm in diameter (Fig. 5). Depending on the basket catheter shape and radius, the interelectrode distance varies between 3 and 10 mm. Accuracy in the reconstruction of the chamber's geometry and electrical activity created by the basket systems relies on the number of splines on the basket, the number of electrodes on each spline, and the percentage of those that achieve adequate contact with the endocardial surface. Because of specific anatomical features of the chambers that do not allow complete endocardial coverage by the basket catheter electrodes, the quality of contacts of all the electrodes to the endocardium cannot be ensured, and thus it is common that some anatomical regions are not adequately mapped.

The use of basket catheters was reported in a number of animal studies aimed at characterizing both atrial *(35)* and ventricular arrhythmias *(36)*. More specifically, Triedman et al. *(37)* reported studies in which they utilized a Webster-Jenkins catheter (Cordis/Webster), a five-spoke flexible ellipsoid with 25 bipolar electrode pairs, for the mapping of right ventricular activation. Data were obtained of normal sinus rhythm, and during investigations of both acute and chronic pathological sequelae, placements of the catheters in the right atria and ventricles of juvenile sheep were studied. They concluded that employing a basket catheter had the potential to provide rapid, nearly real-time, activation sequence maps, which improved their understanding of the mechanisms of complex reentrant tachyarrhythmias. In addition, this approach should provide assistance with the development of curative ablative therapies targeted for such abnormal rhythms.

Subsequently, Schalij et al. *(38)* reported on the first application of a basket catheter and resultant animation programs in 20 human patients with ventricular tachycardias. The investigators reported that percutaneous endocardial mapping with basket catheters was feasible, of clinical value, and reasonably safe. Since then, basket catheter mapping has been employed in the study of numerous cardiac arrhythmias in various human populations *(39–41)*.

Nevertheless, there are limitations associated with basket catheter mapping that are worth noting. A basket catheter that is too large or small compared with the dimensions of the chamber of interest will result in poor quality electrograms in terms of morphology, stability, and relations with anatomical structures. Another shortcoming cited is that the relative movement between the beating heart and the electrodes is detrimental for the electrical reconstruction process. Furthermore, the use of a basket catheter provides little anatomical information, which may prove somewhat unfavorable for the clinical diagnosis and subsequent successful guidance in ablation procedures. Last, because of product size constraints, the basket catheter approach does not have the ability to map areas of the atrial appendage or pulmonary veins.

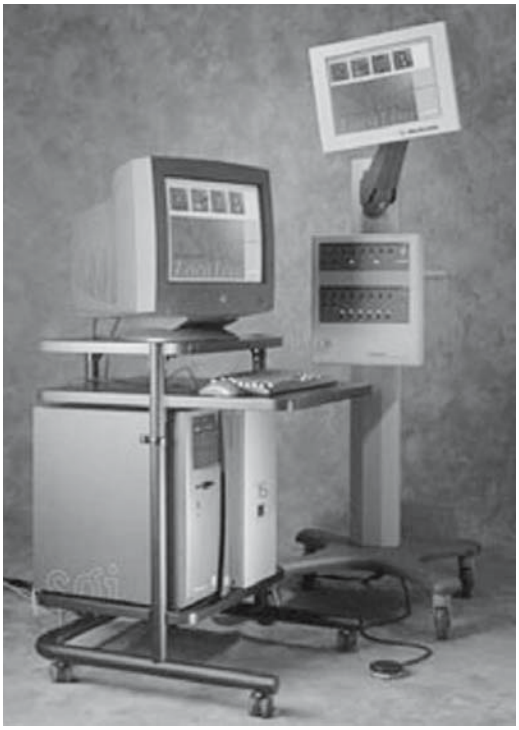

Fig. 3. The LocaLisa® mapping system. Courtesy of Medtronic, Inc.

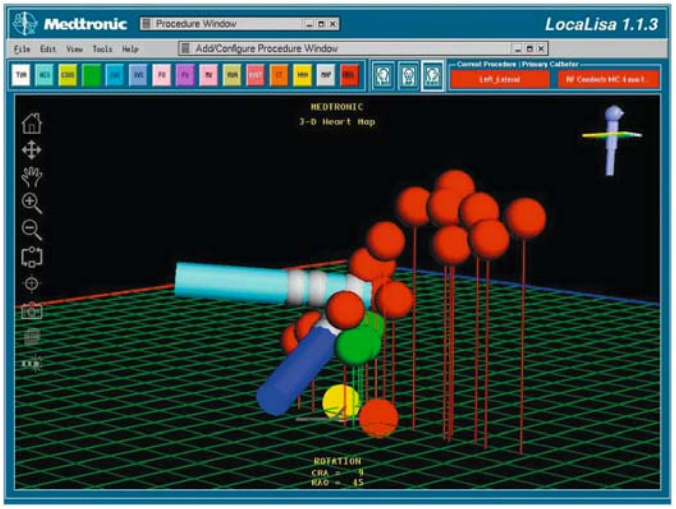

Fig. 4. Screen shot of LocaLisa®'s mapping software. Courtesy of Medtronic, Inc.

Fig. 5. Constellation multielectrode basket catheter. Courtesy of Boston Scientific.

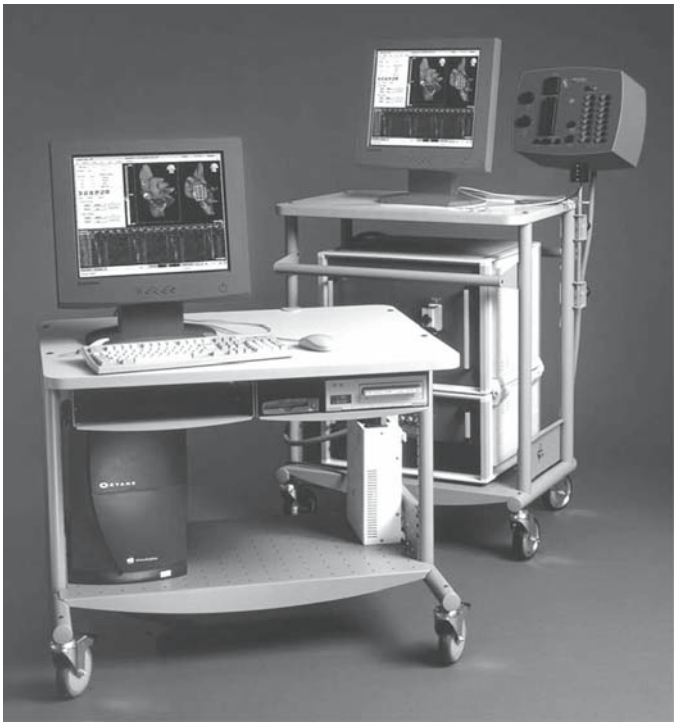

Fig. 6. EnSite® 3000 noncontact mapping system. Courtesy of Endocardial Solutions Inc.

3.2.2. Noncontact Mapping Technology

Most recently, noncontact mapping approaches have had an expanding role in the clinical diagnosis and ablative treatment of complex cardiac arrhythmias, as described by Schilling et al. *(11,42,43)*. One currently available product, the EnSite® 3000 noncontact mapping system (Endocardial Solutions Inc., St. Paul, MN) introduced by Taccardi et al. *(44)*, is comprised of a catheter-mounted, inflatable multielectrode array, a reference patch electrode, amplifiers, and a Silicon Graphics workstation (Fig. 6). To date, this computerized data acquisition system has the capability for 100 analog inputs, which include 64 inputs from the multielectrode array, a 12-lead surface ECG, 16 unipolar or bipolar catheter inputs, and 8 user-defined analog inputs.

Specifically, the 9-French, 110-cm transvenous multielectrode array catheter (Fig. 7) consists of a polyamide insulated wire braid with 64 laser-etched unipolar electrodes, a 7.5-mL inflatable polyurethane balloon, and distal and proximal E1 and E2 ring electrodes, respectively, used by the system's EnGuide® locator technology. Positioned on the proximal end of the catheter is a handle and cable connector that allows the physician to deploy a balloon in the chamber of interest and that provides the electrical connection from the array to the patient interface unit of the system.

The multielectrode array is inserted transvenously into the patient's chamber of interest over a standard 0.032-in guidewire. Once positioned within the chamber, the multielectrode array wire braid is mechanically expanded, and the balloon is typically inflated using a 50/50 contrast-saline solution. Next, a second catheter, termed the *roving* catheter, is introduced into the chamber of interest. Following connection to the breakout box, the system's EnGuide® technology emits a low, 5.68-kHz signal via the tip of the roving catheter; the signal is detected by the E1 and E2 ring electrodes on the multielectrode array catheter.

By determination of the locator signal angles and strengths, the system is able to compute the 3D relationship of the tip of the roving catheter to that of the multielectrode array catheter ring electrodes. To reconstruct the 3D, "virtual" endocardium of the chamber, the roving catheter continues to emit the 5.68-kHz signal as it is moved around the chamber by dragging the tip around the endocardial wall's contour. This approach employs a bicubic spline-smoothing algorithm to create the contour of the chamber's geometry. A convex-hull algorithm is then utilized to omit the previously collected points inferior to the facets created during the collection process, so that the system essentially only stores the most distant points visited by the roving catheter (i.e., those from the endocardial surface during diastole). Further, the roving catheter is used to locate major anatomical locations associated with fluoroscopic imaging. These anatomical landmarks are subsequently labeled on the reconstructed geometry to provide a frame of reference for the physician.

Once the geometry reconstruction is complete, the multielectrode array is used to detect and record the far-field intracavitary electrical potentials from the surrounding myocardium employing an approximation method based on algorithms developed for inverse problems *(45)*. To explain further, the potentials in this field are typically lower in amplitude and frequency than the source potentials of the endocardium itself. Therefore, to improve accuracy and stability in reconstruction, a technique is used based on an inverse solution to the Laplace equation using a boundary element method so that the resulting signals reconstruct and display more than 3,300 "virtual" electrograms.

After the establishment of the chamber's voltage field, cardiac activation can be displayed as computed virtual electrograms or as isopotential maps. Specifically, resulting isopotential maps are dynamic representations of the propagation of the electrical wave front. The electrophysiological information is visually represented by color coding that describes voltage, ranging from red (representing regions of depolarized myocardium) to purple (representing regions electrically neutral) (Fig. 8A). In addition, the system allows the creation of a static representation of the electrical propagations via isochronal maps (Fig. 8B). Consequently, the color-coded electrophysiological information is representative of the time required to activate different regions of the chamber. When ablation is employed, the EnGuide technology aids in navigating the radiofrequency catheter to the appropriate site with an accuracy of ±1 mm.

Most recently, noncontact mapping has been utilized and validated in several clinical settings, such as for the evaluation and treatment of atrial flutter, atrial fibrillation *(46–48)*, and for ventricular tachycardia *(49)*. In such cases, the system has been used to aid in the identification of the critical regions of slow conduction, to identify and then return precisely to areas of interest in the chamber, and subsequently to visualize ablation

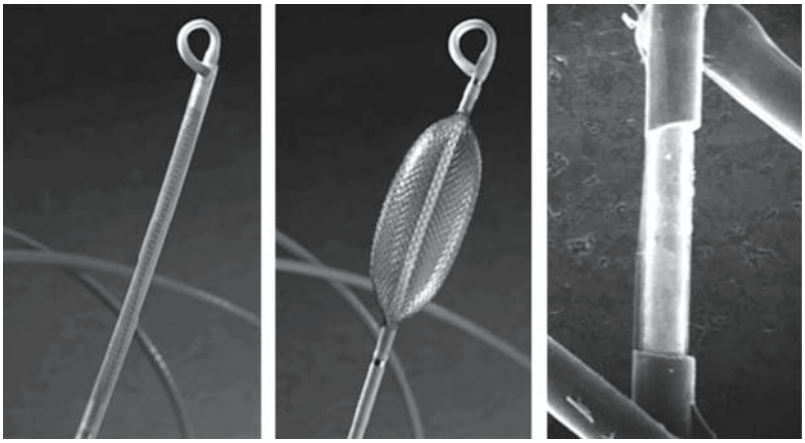

Fig. 7. Multielectrode array catheter. Courtesy of Endocardial Solutions Inc.

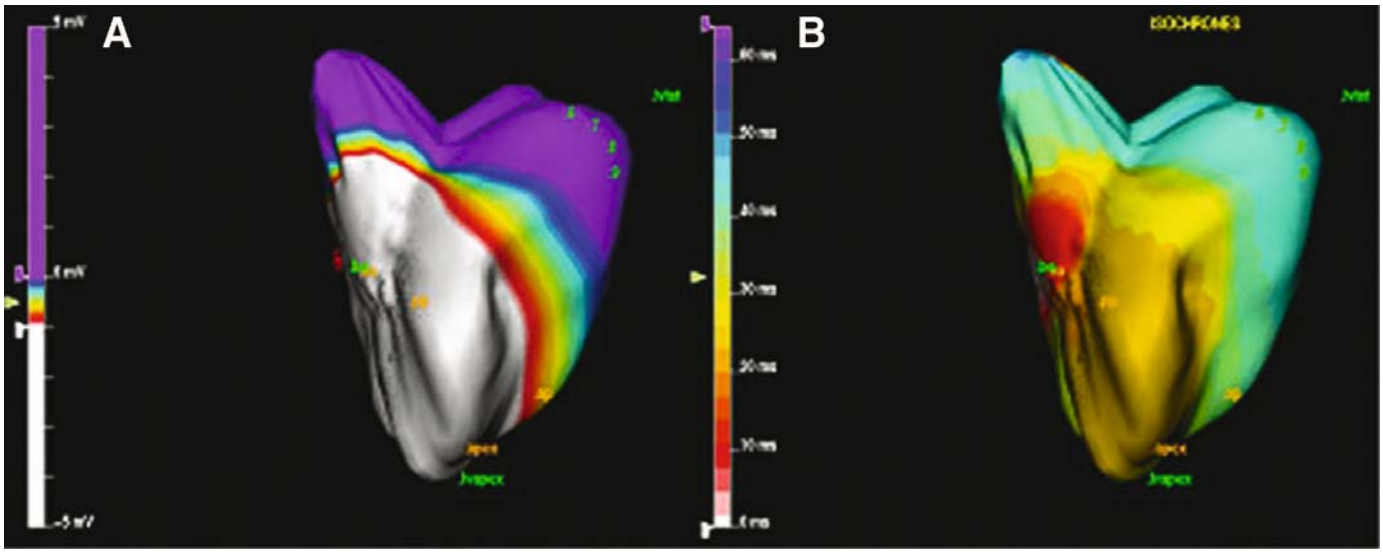

Fig. 8. Swine left ventricular **(A)** isopotential activation map and **(B)** isochronal activation map.

lesion lines that have been created. The EnSite®3000 system permits the detailed reconstruction of global and local cardiac electrical events in the electrophysiological lab. Most important, the system allows a great deal of data to be recorded within a short duration of only one to two heartbeats, thus allowing the physician to adequately evaluate the origination, maintenance, and termination of nonsustained complex cardiac arrhythmias, pathways of reentrant activity, and electrical changes that occur on a beat-to-beat basis.

Despite the vast number of advantages associated with noncontact mapping, there are several current limitations. For example background noise can affect the quality of the recordings and commonly originates from the surrounding environment or from the amplifier circuitry because of electrical fluctuations. To obtain optimally reconstructed electrograms, it has been documented that the distance from the area mapped to the multielectrode array should be less than 40 mm *(42,43,50)*; beyond this distance, there is an overall decrease in the accuracy of the reconstructed electrograms. Noncontact mapping is only able to reconstruct the electrical activity on the endocardial wall of the chamber; thus, it is unable to identify subendocardial activation characteristics that may play a critical role in the successful identification of various arrhythmias and the subsequent therapy employed. The dimensions of the multielectrode array when in full profile are 1.8 × 4.6 cm^2, which can restrict mapping catheter manipulation when placed in particular areas of the heart, such as right and left atrial appendages. Last, despite several software updates, the system is still complex and quite expensive.

4. FUTURE DIRECTIONS

The mapping systems developed and employed to date have revolutionized the clinical electrophysiology laboratory, and their use has led to numerous novel insights into underlying arrhythmia mechanisms. Relative to the multicatheter approach, such technologies have improved resolution, 3D spatial localization, and rapidity of acquisition of the detailed characteristics of cardiac activation in both normal and diseased hearts.

These systems employ novel computational approaches to determine accurately the 3D location of the mapping catheters and anatomic-specific local electrograms. Acquired data of the relative intracardiac catheter position and recorded intracardiac electrograms are commonly used by such systems to reconstruct, in real time, a representation of the 3D geometry of the chamber.

Nevertheless, to date such mapping systems have been very expensive and generally are not required for the diagnosis of more common clinical arrhythmias such as atrioventricular nodal reentry, accessory pathway-mediated tachycardia (Wolff-Parkinson-White syndrome and concealed pathways), or typical atrial flutter. It should be noted that other emerging technologies, such as intracardiac echocardiography *(51)*, are considered useful adjuncts for more precise and rapid positioning and provide reproducible catheter positioning toward specific intracardiac structures that are more difficult to identify during mapping or ablation. The possible contribution of the newer cardiac mapping systems to treat various arrhythmias is likely to be well substantiated. Yet, despite the theoretical clinical advantages highlighted by the discussed technologies, additional prospective studies will ultimately need to be performed to provide further validation of their optimal clinical utilities.

REFERENCES

1. Tawara, S. (1906) Das Reizleitungssystem des Säugetierherzens. Eine Anatomisch-Histologische Studie Über das Atrioventrikularbündel und die Purkinjeschen Fäden.
2. Mayer, A.G. (1906) *Rhythmical Pulsation in Scyphomedusae*. Carnegie Institute of Washington, Washington, DC.
3. Mayer, A.G. (1908) Rhythmical pulsation in scyphomedusae, in II. *Papers from the Marine Biological Laboratory at Tortugas,* Carnegie Institution, Washington, DC, pp. 115–131.
4. Mines, G.R. (1913) On dynamic equilibrium in the heart. *J Physiol (Lond)*. 46, 349–382.
5. Lewis, T. and Rothschild, M.A. (1915) The excitatory process in the dog's heart, II: the ventricles. *Philos Trans R Soc Lond B Biol Sci*. 206, 181–266.
6. Lewis, T., Feil, S., and Stroud, W.D. (1920) Observations upon flutter and fibrillation. II. the nature of auricular flutter. *Heart*. 7, 191–346.
7. Barker, P.S., McLeod, A.G., and Alexander, J. (1930) The excitatory process observed in the exposed human heart. *Am Heart J*. 5, 720–742.
8. Jackman, W.M., Wang, X.Z., Friday, K.J., et al. (1991) Catheter ablation of accessory atrioventricular pathways (Wolff-Parkinson-White syndrome) by radiofrequency current. *N Engl J Med*. 324, 1605–1611.
9. Gasparini, M., Coltorti, F., Mantica, M., Galimberti, P., Ceriotti, C., and Beatty, G. (2000) Noncontact system-guided simplified right atrial linear lesions using radiofrequency transcatheter ablation for treatment of refractory atrial fibrillation. *Pacing Clin Electrophysiol*. 23, 1843–1847.
10. Schmitt, H., Weber, S., Tillmanns, H., and Waldecker B. (2000) Diagnosis and ablation of atrial flutter using a high resolution, noncontact mapping system. *Pacing Clin Electrophysiol*. 23, 2057–2064.
11. Schilling, R.J., Davies, D.W., and Peters, N.S. (1998) Characteristics of sinus rhythm electrograms at sites of ablation of ventricular tachycardia relative to all other sites: a noncontact mapping study of the entire left ventricle. *J Cardiovasc Electrophysiol*. 9, 921–933.
12. Sra, J. and Thomas, J.M. (2001) New techniques for mapping cardiac arrhythmias. *Indian Heart J*. 53, 423–444.
13. Schumacher, B., Jung, W., Lewalter, T., Wolpert, C., and Luderitz, B. (1999) Verification of linear lesions using a noncontact multielectrode array catheter versus conventional contact mapping techniques. *J Cardiovasc Electrophysiol*. 10, 791–798.
14. Calkins, H., Langberg, J., Sousa, J., et al. (1992) Radiofrequency catheter ablation of accessory atrioventricular connections in 250 patients. Abbreviated therapeutic approach to Wolff-Parkinson-White syndrome. *Circulation*. 85, 1337–1346.
15. Wittkampf, F.H., Wever, E.F., Vos, K., et al. (2000) Reduction of radiation exposure in the cardiac electrophysiology laboratory. *Pacing Clin Electrophysiol*. 23, 1638–1644.
16. Ben-Haim, S.A., Osadchy, D., and Schuster, I. (1996) Nonfluoroscopic, in vivo navigation and mapping technology. *Nat Med*. 2, 1393–1395.
17. Gepstein, L., Hayam, G., and Ben-Haim, S.A. (1997) A novel method for nonfluoroscopic catheter-based electroanatomical mapping of the heart. In vitro and in vivo accuracy results. *Circulation*. 95, 1611–1622.
18. Shpun, S., Gepstein, L., Hayam, G., and Ben-Haim, S.A. (1997) Guidance of radiofrequency endocardial ablation with real-time 3D magnetic navigation system. *Circulation*. 96, 2016–2021.
19. Pappone, C., Oreto, G., Lamberti, F., et al. (1999) Catheter ablation of paroxysmal atrial fibrillation using a 3D mapping system. *Circulation*. 100, 1203–1208.
20. Poty, H., Saoudi, N., Abdel Aziz, A., Nair, M., and Letac B. (1995) Radiofrequency catheter ablation of type 1 atrial flutter. Prediction of late success by electrophysiological criteria. *Circulation*. 92, 1389–1392.
21. Sra, J., Bhatia, A., Dhala, A., et al. (2000) Electroanatomic mapping to identify breakthrough sites in recurrent typical human flutter. *Pacing Clin Electrophysiol*. 23, 1479–1492.
22. Willems, S., Weiss, C., Ventura, R., et al. (2000) Catheter ablation of atrial flutter guided by electroanatomic mapping (CARTO): a randomized comparison to the conventional approach. *J Cardiovasc Electrophysiol*. 11, 1223–1230.
23. Shah, D.C., Jais, P., Haissaguerre, M., et al. (1997) Three-dimensional mapping of the common atrial flutter circuit in the right atrium. *Circulation*. 96, 3904–3912.
24. Stevenson, W.G., Delacretaz, E., Friedman, P.L., and Ellison, K.E. (1998) Identification and ablation of macroreentrant ventricular tachycardia with the CARTO electroanatomical mapping system. *Pacing Clin Electrophysiol*. 21, 1448–1456.
25. Tomassoni, G., Stanton, M., Richey, M., Leonelli, F.M., Beheiry, S., and Natale, A. (1999) Epicardial mapping and radiofrequency catheter ablation of ischemic ventricular tachycardia using a three-dimensional nonfluoroscopic mapping system. *J Cardiovasc Electrophysiol*. 10, 1643–1648.
26. Kottkamp, H., Hindricks, G., Breithardt, G., and Borggrefe, M. (1997) Three-dimensional electromagnetic catheter technology: electroanatomic mapping of the right atrium and ablation of ectopic atrial tachycardia. *J Cardiovasc Electrophysiol*. 8, 1332–1337.
27. Marchlinski, F., Callans, D., Gottlieb, C., Rodriguez, E., Coyne, R., and Kleinman, D. (1998) Magnetic electroanatomical mapping for ablation of focal atrial tachycardias. *Pacing Clin Electrophysiol*. 21, 1621–1635.
28. Varanasi, S., Dhala, A., Blanck, Z., Deshpande, S., Akhtar, M., and Sra, J. (1999) Electroanatomic mapping for radiofrequency ablation of cardiac arrhythmias. *J Cardiovasc Electrophysiol*. 10, 538–544.
29. de Groot, N., Bootsma, M., van der Velde, E.T., and Schalij, M.J. (2000) Three-dimensional catheter positioning during radiofrequency ablation in patients: first application of a real-time position management system. *J Cardiovasc Electrophysiol*. 11, 1183–1192.
30. Schreieck, J., Ndrepepa, G., Zrenner, B., et al. (2002) Radiofrequency ablation of cardiac arrhythmias using a three-dimensional real-time position management and mapping system. *Pacing Clin Electrophysiol*. 25, 1699–1707.
31. Soejima, K., Delacretaz, E., Suzuki, M., et al. (2001) Saline-cooled versus standard radiofrequency catheter ablation for infarct-related ventricular tachycardias. *Circulation*. 103, 1858–1862.
32. Wittkampf, F.H., Wever, E.F., Derksen, R., et al. (1999) LocaLisa: new technique for real-time 3-dimensional localization of regular intracardiac electrodes. *Circulation*. 99, 1312–1317.

33. Avitall, B., Helms, R.W., Kotov, A.V., Sieben, W., and Anderson, J. (1996) The use of temperature versus local depolarization amplitude to monitor atrial lesion maturation during the creation of linear lesions in both atria. *Circulation*. 94, I–558.
34. Borggrefe, M., Budde, T., Podczeck, A., and Breithardt, G. (1987) High frequency alternating current ablation of an accessory pathway in humans. *J Am Coll Cardiol*. 10, 576–582.
35. Jenkins, K.J., Walsh, E.P., Colan, S.D., Bergau, D.M., Saul, J.P., and Lock, J.E. (1993) Multipolar endocardial mapping of the right atrium during cardiac catheterization: description of a new technique. *J Am Coll Cardiol*. 22, 1105–1110.
36. Eldar, M., Ohad, D.G., Goldberger, J.J., et al. (1997) Transcutaneous multielectrode basket catheter for endocardial mapping and ablation of ventricular tachycardia in the pig. *Circulation*. 96, 2430–2437.
37. Triedman, J.K., Jenkins, K.J., Colan, S.D., Van Praagh, R., Lock, J.E., and Walsh, E.P. (1997) Multipolar endocardial mapping of the right heart using a basket catheter: acute and chronic animal studies. *Pacing Clin Electrophysiol*. 20, 51–59.
38. Schalij, M.J., van Rugge, F.P., Siezenga, M., and van der Velde, E.T. (1998) Endocardial activation mapping of ventricular tachycardia in patients: first application of a 32-site bipolar mapping catheter electrode. *Circulation*. 98, 2168–2179.
39. Triedman, J.K., Jenkins, K.J., Colan, S.D., Saul, J.P., and Walsh, E.P. (1997) Intra-atrial reentrant tachycardia after palliation of congenital heart disease: characterization of multiple macroreentrant circuits using fluoroscopically based three-dimensional endocardial mapping. *J Cardiovasc Electrophysiol*. 8, 259–270.
40. Greenspon, A.J., Hsu, S.S., and Datorre, S. (1997) Successful radiofrequency catheter ablation of sustained ventricular tachycardia postmyocardial infarction in man guided by a multielectrode "basket" catheter. *J Cardiovasc Electrophysiol*. 8, 565–570.
41. Schmitt, C., Zrenner, B., Schneider, M., et al. (1999) Clinical experience with a novel multielectrode basket catheter in right atrial tachycardias. *Circulation*. 99, 2414–2422.
42. Schilling, R.J., Peters, N.S., and Davies, D.W. (1998) Simultaneous endocardial mapping in the human left ventricle using a noncontact catheter: comparison of contact and reconstructed electrograms during sinus rhythm. *Circulation*. 98, 887–898.
43. Schilling, R.J., Peters, N.S., and Davies, D.W. (1999) Feasibility of a noncontact catheter for endocardial mapping of human ventricular tachycardia. *Circulation*. 99, 2543–2552.
44. Taccardi, B., Arisi, G., Macchi, E., Baruffi, S., and Spaggiari, S. (1987) A new intracavitary probe for detecting the site of origin of ectopic ventricular beats during one cardiac cycle. *Circulation*. 75, 272–281.
45. Khoury, D.S., Taccardi, B., Lux, R.L., Ershler, P.R., and Rudy, Y. (1995) Reconstruction of endocardial potentials and activation sequences from intracavitary probe measurements. Localization of pacing sites and effects of myocardial structure. *Circulation*. 91, 845–863.
46. Schilling, R.J., Kadish, A.H., Peters, N.S., Goldberger, J., and Davies, D.W. (2000) Endocardial mapping of atrial fibrillation in the human right atrium using a noncontact catheter. *Eur Heart J*. 21, 550–564.
47. Schneider, M.A., Ndrepepa, G., Zrenner, B., et al. (2000) Noncontact mapping-guided catheter ablation of atrial fibrillation associated with left atrial ectopy. *J Cardiovasc Electrophysiol*. 11, 475–479.
48. Liu, T.Y., Tai, C.T., and Chen, S.A. (2002) Treatment of atrial fibrillation by catheter ablation of conduction gaps in the crista terminalis and cavotricuspid isthmus of the right atrium. *J Cardiovasc Electrophysiol*. 13, 1044–1046.
49. Strickberger, S.A., Knight, B.P., Michaud, G.F., Pelosi, F., and Morady, F. (2000) Mapping and ablation of ventricular tachycardia guided by virtual electrograms using a noncontact, computerized mapping system. *J Am Coll Cardiol*. 35, 414–421.
50. Kadish, A., Hauck, J., Pederson, B., Beatty, G., and Gornick, C. (1999) Mapping of atrial activation with a noncontact, multielectrode catheter in dogs. *Circulation*. 99, 1906–1913.
51. Lesh, M.D., Kalman, J.M., and Karch, M.R. (1998) Use of intracardiac echocardiography during electrophysiologic evaluation and therapy of atrial arrhythmias. *J Cardiovasc Electrophysiol*. 9, S40–S47.

26 Cardiopulmonary Bypass and Cardioplegia

J. ERNESTO MOLINA, MD, PhD

CONTENTS

1. CARDIOPULMONARY BYPASS

Extracorporeal circulation and *cardiopulmonary bypass* are synonymous terms denoting a method by which the blood that usually returns directly to the heart is temporarily drained from the superior and inferior venae cavae. The blood is diverted into a reservoir, where it is oxygenated and subsequently returned to the patient's arterial circulation. This process effectually excludes the heart from the general circulation and leaves it empty so that it can accommodate surgical intervention (Fig. 1).

The breakthrough technology that first allowed this type of open heart operation was developed by two centers in the United States in the early 1950s. Importantly, Lillehei and Varco *(1)* at the University of Minnesota developed a cross-circulation technique. This technique utilized a human donor, usually the parent of a child undergoing cardiac surgery, who in essence functioned as an extracorporeal pump for the patient's circulatory system. This type of extracorporeal circulation also allowed the blood to be drained from the child's venae cavae so that the surgical procedure could be performed within the empty heart. The subsequent development of the heart–lung machine by Gibbon *(2)* was considered revolutionary in that it eliminated the need for a support donor (a second patient). Gibbon's system has been improved since the mid-1950s and has gradually evolved into the standardized, but very complex and sophisticated, machine it is today.

The basic components of an extracorporeal circuit include: (1) a reservoir into which the patient's blood is diverted, (2) an oxygenator that replaces the function of the lungs, and (3) a pump that propels the oxygenated blood back into the patient's arterial circulation. In this manner, the machine bypasses both the heart and the lungs while maintaining the functions of other organs during surgical intervention within the heart.

1.1. Venous Drainage

The venous blood that is normally delivered to the right atrium is commonly diverted to the heart–lung machine, either by cannulating the veins themselves or by cannulating the right atrial chamber. Surgery performed in or through the right atrial chamber requires that both the right atrium and right ventricle be empty. To do so, cannulas are placed directly into the superior and inferior venae cavae. Constricting tourniquets are then placed around the veins over the cannulas, and blood is diverted into the heart–lung machine (Fig. 1). These procedures constitute total cardiopulmonary bypass.

Venous cannulation is normally performed in one of two ways: (1) by placing a pursestring suture either directly in the superior vena cava or in the right atrium or (2) by advancing the cannula into the superior vena cava. It should be noted that direct cannulation of the superior vena cava generally provides more room for any work that needs to be done inside the right atrium.

A modification of this type of bypass can be used when the cardiac chambers are not surgically entered, such as in coronary bypass operations involving procedures on the surface of the heart. In such cases, a single cannula is placed in the right atrium, or a double-stage cannula is placed with the tip of the cannula in the inferior vena cava and the side drainage holes positioned at the level of the right atrium. Coronary bypass surgery does

From: *Handbook of Cardiac Anatomy, Physiology, and Devices*
Edited by: P. A. Iaizzo © Humana Press Inc., Totowa, NJ

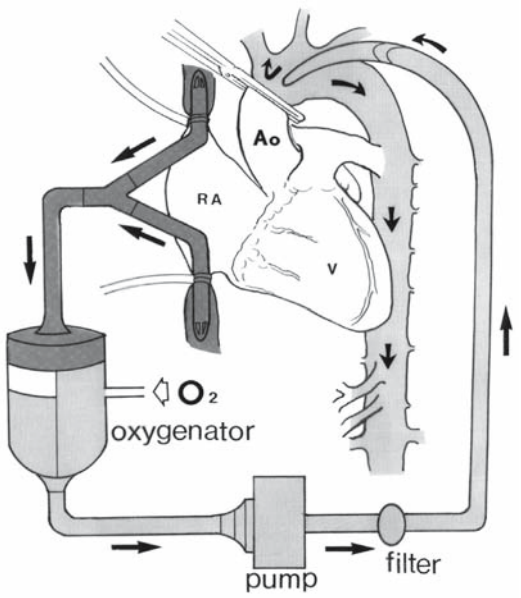

Fig. 1. Total pulmonary bypass showing the venous cannulas in the superior and inferior venae cavae with constrictions around the respective veins. The venous blood is drained into the oxygenator and is propelled by the pump into the distal ascending aorta to maintain perfusion of the entire body. All chambers of the heart therefore are excluded from the perfusion system. Ao, aorta; RA, right atrium; v, ventricle.

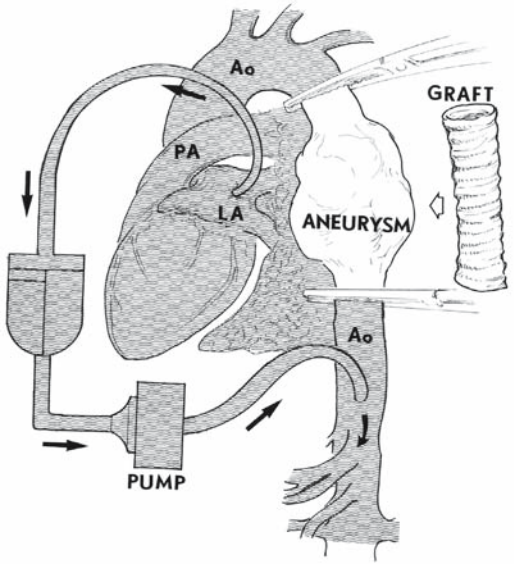

Fig. 2. Left heart bypass showing a cannula inserted in the left atrium, draining approximately half of the cardiac output into the oxygenator, through the pump, and reinfusing in the distal aorta for perfusion of the abdominal organs. The excluded portion is only the descending thoracic aorta (between clamps). The left heart continues to beat and pumps half of the cardiac output to the head and upper organs. The graft is shown in the position in which it will be implanted after the aneurysm is resected. Ao, aorta; LA, left atrium; PA, pulmonary artery.

not involve direct vision of the inside of the cardiac chambers, so there is no need to constrict the superior or inferior venae cavae.

1.2. Arterial Return

Once the blood has been oxygenated in the heart–lung machine, it is returned to the patient's general circulation via cannulas placed directly in the arterial system (Fig. 1). The most common method involves the placement of a cannula in the highest portion of the ascending aorta, below the origin of the innominate artery. Depending on the type of surgery, other sites are also used, including cannulation of the femoral artery in the groin and infusion of the arterial system in a retrograde manner. The ascending aorta is cross-clamped at this point, so no systemic blood enters the coronary artery circulation. The heart is, therefore, totally excluded from circulation. Thus, the heart needs to be protected by using one of a number of methods to infuse cardioplegic solutions (*see* Section 2).

In addition, any blood remaining in the operative field is removed via cardiotomy suction lines, which aspirate it back to the heart–lung machine, where it returns to bypass circulation with the rest of the removed blood.

In some operations involving the descending thoracic aorta, total cardiopulmonary bypass is not necessary. If the portion of the aorta that needs to be isolated lies between the left carotid artery and the diaphragm, only part of the total blood volume needs to be removed, and partial bypass is implemented (Fig. 2). The blood is removed by the heart–lung machine via a cannula inserted in the left atrium or in the left superior pulmonary vein. Then, the blood is infused back into the descending thoracic aorta beyond the level of distal aortic cross-clamping. Doing so allows the heart to continue to beat normally and helps maintain the viability of the proximal organs (head, neck, and arms) while the rest of the lower body is perfused by the pump. This technique is called *left heart bypass* because it involves only the left side of the cardiac chambers.

After a thoracic aorta operation is completed, the bypass is discontinued. The clamps, which were placed to occlude the aorta in the arch and the descending portion, are removed. The normal physiological perfusion of the body (which was interrupted during surgery without ever stopping the heartbeat) is thus reestablished.

In contrast, total cardiopulmonary bypass involves complete stoppage of the heart. After an operation employing total cardiopulmonary bypass and cardiac arrest, the aortic clamp is released, which allows the general circulation to perfuse the coronary arteries and to rewarm the heart. After the air is expelled from the cardiac chambers, the heart usually develops ventricular fibrillation. Such fibrillation normally requires cardioversion with electric shock administered directly to the myocardium, employing paddles that deliver currents that vary from 20 to 30 W/s. The patient is then ventilated using the endotracheal tube connected to the anesthesia machine, which reinflates the lungs. After the normal sinus rhythm of the heart is reestablished, the patient is gradually weaned off the extracorporeal circulation until the heart takes over full function. At this point, the heart–lung machine is stopped, and all cannulas are removed.

In some complex surgical cases involving the aortic arch, a separate and independent perfusion of the arch vessels may require implementation, that is, in addition to the perfusion of the lower part of the body through the cannula inserted in the femoral artery. This situation places a great demand on the perfusionist operating the heart–lung machine. The perfusionist must monitor two separate infusions to regulate pressures and make certain that balanced and sufficient perfusions are achieved in both the upper and lower areas of the patient's body.

Another specialized bypass method that needs description is deep hypothermia and total circulatory arrest. This type of total cardiopulmonary bypass employs decreases in body temperatures to very low levels (15 to 20°C); this is accomplished using heat exchangers installed in the heart–lung machine. Circulation is stopped altogether, and the heart is empty for several minutes, with the entire volume of the patient's blood remaining in the reservoir of the heart–lung machine. Once the target temperature is reached (usually 15°C), the pump is stopped, and arterial perfusion ceases. The venous return, however, is left open to empty the patient's blood volume completely into the reservoir of the heart–lung machine.

This technique is used in special cases to allow repair of very complicated conditions. The period of total circulatory arrest induced during deep hypothermia is usually less than 45 min *(3,4)*. This time restriction ensures that the patient does not suffer neurological deterioration or central nervous system damage during such global ischemia. As soon as the repair is completed, normal cardiopulmonary bypass is reestablished. The patient is gradually rewarmed to a normal core temperature of 37°C prior to removal from extracorporeal circulation.

The use of such deep hypothermia always requires careful evaluation by the surgical team. In such clinical cases, the danger of inducing neurological damage must be weighed against the benefits of correcting the cardiac anomaly.

1.3. Anticoagulation

To prevent the formation of clots during cardiopulmonary bypass procedures, both within the body and in the extracorporeal heart–lung machine, it is necessary to anticoagulate the patient. The most common agent used for such anticoagulation is heparin. It is commonly administered intravenously, before cannulation, at a dose of 300 U/kg of the patient's weight.

There are two types of heparin: (1) the lung-beef type which is extracted from a bovine source, and (2) the porcine mucosal type, which is from a swine source. Since the mid-1980s, the porcine mucosal heparin has been preferred because it is less likely to lead to thrombocytopenia and production of heparin antibodies in the patient *(5)*.

The effectiveness of anticoagulation requires testing, usually by measuring the activated clotting time (ACT) of the patient's blood. The result is expressed in seconds, with normal values ranging between 100 and 120 s. Heparinization is deemed adequate when the ACT runs above 300 s. At any time after such values are achieved, the patient can undergo cannulation and be placed on extracorporeal circulation.

The anticoagulant effects induced during such surgeries must be reversed postoperatively. Protamine, a macromolecule compound, may produce pulmonary vasoconstriction and severe hypotension *(6)*, so it is the drug of choice to neutralize the effects of heparin. Naturally, the amount of protamine necessary to achieve neutralization depends on the amount of heparin used. Initially, a test dose is given; if no reaction occurs, protamine is then administered in the appropriate amount. Its effects are monitored by measuring ACTs until the heparin has been neutralized. Diabetics are generally prone to be more sensitive to protamine. If any reaction or side effect occurs, additional treatments are commonly employed, such as administration of epinephrine, calcium, steroids, or fluids *(7)*.

Occasionally, patients cannot be given heparin because they have developed heparin antibodies from previous exposure. Other anticoagulant agents studied and occasionally used in such cases include hirudin (lepirudin) *(8)*, a potent anticoagulant that is extracted from leeches and lampreys, or heparinoids *(9)* like Orgaran (Org10172, Organon Company, West Orange, NJ), for which a different monitoring protocol is implemented. Unfortunately, to date no drug has been identified that can reverse the effect of Orgaran; thus, it must be metabolized by the human body. For such patients, bleeding is a constant, and often very difficult, postoperative complication.

If the cardiopulmonary bypass takes an extended period of time, coagulopathies are often a complication. In such cases, the body, primarily the liver, is unable to produce the appropriate clotting factors to reverse the anticoagulation status. Other factors that can contribute to coagulopathies include ischemia of the abdominal organs, particularly if necrosis occurs in the liver cells or in the intestine. Bleeding, therefore, can be a very serious and difficult complication to treat; multiple coagulation factors, platelets, and cryoprecipitates may be required.

1.4. Temperatures of Perfusion

Since their inception, cardiopulmonary bypass and extracorporeal circulation have been implemented using some degree of hypothermia. Lowering body temperature decreases the oxygen demands of body tissues, an obviously desirable state of affairs during pulseless circulation as provided by the heart–lung machine.

Several degrees of hypothermia are commonly identifiable relative to extracorporeal circulation interventions. *Normothermia* indicates that core body temperature is between 35.5 and 37°C *(10)*; *mild hypothermia* is between 32 and 35°C; and *moderate hypothermia* is between 24 and 32°C. An important distinction must be made between mild and moderate hypothermia. If the heart is perfused at mild levels (above 31°C), the heart will continue to beat, although at a slower rate. This mild level of hypothermia allows surgical correction of some congenital anomalies without arresting the heart. An additional level of hypothermia used occasionally is *deep* or *profound* hypothermia, that is, below 20°C.

Currently, most open cardiac operations are conducted under conditions somewhere between moderate and mild hypothermia and normothermia. Some centers routinely use moderate hypothermia; others employ normothermia *(11,12)*. One reason to maintain normothermic perfusion is to avoid coagulopathies that may develop when body temperature is lowered to the moderate levels and permit normal function of

the body's enzyme systems. Normothermic temperatures also allow the kidneys to respond better to diuretics.

Several reports have indicated the safety of normothermic perfusion *(10–16)*, but an equal number have suggested complications with this modality *(17,18)*. As a result, spontaneous drifting to mild hypothermic levels is generally preferred. Deep or profound hypothermia is associated with the implementation of total circulatory arrest, as mentioned. With this level of hypothermia, body temperature is usually lowered to between 15 and 18°C. Such operations are thus usually prolonged given the time it takes to cool the body to those levels before surgery and to rewarm it afterward.

1.5. Perfusion Pressures

Under normal physiological conditions, the heart provides a pulsatile pressure and flow. The peak systolic pressure depends on the ventricular function. The diastolic pressure in normal states is primarily regulated by the blood volume and the vascular tonus. During cardiopulmonary bypass, the heart–lung machine facilitates pulseless perfusion; there is no systolic or diastolic pressure, but rather one steady mean pressure throughout the arterial circulatory system. This pressure should be high enough to provide adequate blood oxygen supply to all organs of the body, particularly the brain and kidneys. The patient is typically hypothermic, so oxygen requirements are lowered; the perfusion pressure is usually maintained around 70 mmHg. Occasionally, in patients with severe obstructive carotid disease, a higher perfusion pressure is recommended to ensure proper perfusion of the brain. Yet, this recommendation is somewhat debated because the brain has its own autoregulatory system to maintain low resistance near obstructed areas *(12,14)*.

During cardiopulmonary bypass, if the patient shows decreased vascular tonus (despite adequate volumes of fluid), vasoconstrictors are routinely used; a typical therapy is a bolus or drips of Neo-Synephrine *(10)*. Decreased vascular tonus is common in septic patients with bacterial endocarditis, for whom an emergency operation is necessary to replace the affected valve and reverse the profound heart failure. In general, a mean perfusion pressure of around 70 mmHg during cardiopulmonary bypass should be maintained.

1.6. Hemodilution

Up to a certain level, hemodilution can be a desirable side effect of cardiopulmonary bypass. Lowering the hematocrit prevents coagulation of the red cells, or "sludging," thereby providing better circulation at the capillary level; viscosity of the circulating blood is decreased, on the other hand, to ensure that oxygen is adequately delivered to the body's tissues during cardiopulmonary bypass. Hematocrit levels are monitored and maintained at a minimum between 22 and 26%. Toward the end of the bypass operation, the perfusionist deliberately removes some of the fluid from the patient's circulation to hemoconcentrate the blood toward more normal hematocrit levels *(19,20)*, that is, usually above 30% by the time the patient is removed from cardiopulmonary bypass. Subsequent diuresis or transfusion of red blood cells will further aid in reestablishing the hematocrit to normal levels.

Pulseless perfusion, as provided by the heart–lung machine, and hemodilution invariably lead to a transfer of fluid across the capillary walls into the third space. Therefore, all patients develop, to some degree, peripheral third spacing or edema, which is particularly seen in children and usually requires several days to resolve completely. In an attempt to avoid this condition, plasma expanders (such as albumin, hetastarch, dextran, and mannitol) are usually added to the priming solution of the heart–lung machine.

1.7. Heart–Lung Machine Basics

The basic components of the heart–lung machine include an oxygenator, a reservoir for the perfusion solution, a perfusion pump, line filters, two heat exchangers, and monitoring devices. Although the bubble oxygenator has been used for many years, it has been largely supplanted by the membrane oxygenator. The membrane oxygenator is associated with less trauma to red blood cells and is less likely to produce microbubbles that might pass into the patient's arterial system and form an embolism. In addition, the newer centrifugal pumps (Fig. 3), like the BioMedicus (Medtronic, Inc., Minneapolis, MN), offer a distinct advantage over the older roller-type pumps, such as the standard DeBakey. The older roller pumps use occlusive pressure to propel the blood within the tubing and can cause damage to the red blood cells and dislodge debris from the tubing material. The newer centrifugal pumps minimize trauma to the red blood cells because the motion required to move the blood does not constrict the tubing.

A typical modern heart–lung system uses gravity to divert venous blood from the right atrium or the venae cavae into a large reservoir, which acts as a membrane oxygenator (Fig. 3). To complete the circuit, the cardioplegic solution used to arrest the heart is injected back into the patient's arterial system by two small roller pump heads (Fig. 4).

After the blood is oxygenated in the reservoir, it is passed through heat exchangers that cool or rewarm it as necessary for the current stage of the operation. One heat exchanger provides temperature control for systemic perfusion to the patient's body, whereas the other controls the temperature within the cardioplegia line. The temperature within each circuit is separately controlled by a central regulation unit (Fig. 2). The blood is then filtered, which helps prevent microembolization when it is returned to the patient's arterial system. In addition, two suction lines are employed to aspirate the blood from the operative field into the reservoir, where it is oxygenated before it is pumped back into the patient's arterial system.

The perfusionist monitors the general circulation flow, the electrolyte parameters, the anticoagulation parameters, and the ultrafiltration system (which extracts fluid from the patient's arterial system to avoid overhydration). The perfusionist is also in charge of maintaining the proper pressures within each circuit and monitoring the temperature of the cardioplegic solution. Normally, at 15–20-min intervals, the perfusionist apprises the surgeon of the elapsed time of perfusion and reinfuses the heart as necessary to maintain a temperature within the appropriate range (below 15°C). The perfusionist also remains in direct communication with the anesthesiologist to coordinate administration of any drugs or any other action necessary to

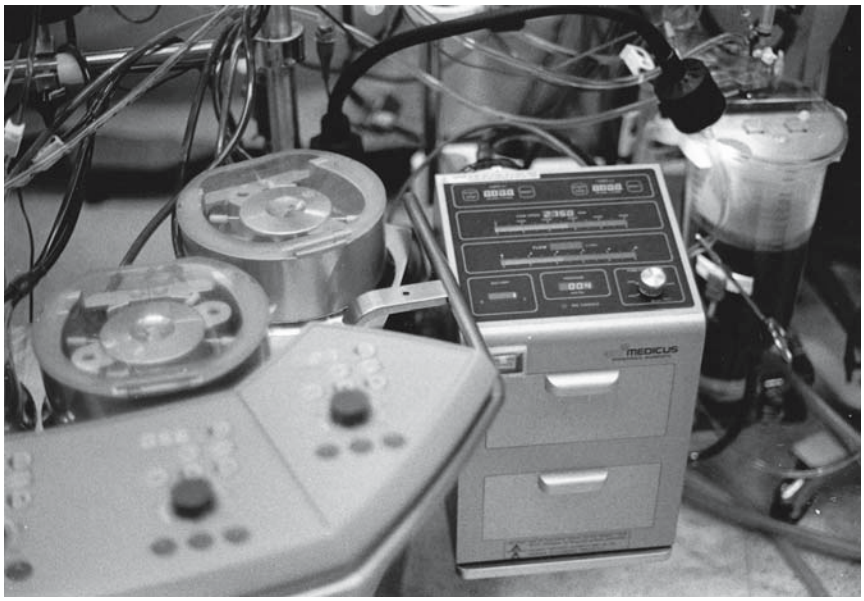

Fig. 3. BioMedicus centrifugal pump. This unit propels the blood back into the arterial system. Two roller pumps (at left) are used for suction. The oxygenator reservoir is shown on the right.

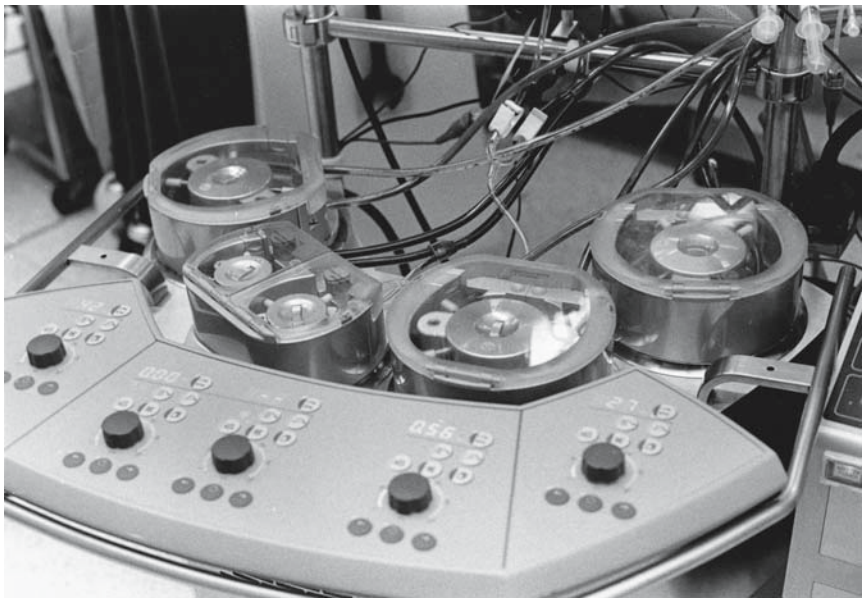

Fig. 4. Typical setup of roller pumps. The three large pumps are used for suction, and the two smaller ones (left of center) are used for the mixing and infusion of cardioplegic solution during cold blood cardioplegia.

maintain the balance of the patient's other organ systems. At the end of cardiopulmonary bypass, the perfusionist administers protamine in the amount sufficient to neutralize the effects of the heparin, thus returning the patient's coagulation system to normal function.

At the conclusion of the surgery, cardiopulmonary bypass is discontinued, and the patient's heart resumes systemic blood circulation. A small volume of blood often remains in the pump and needs to be reinfused into the patient. This remaining blood is sometimes reinfused directly from the reservoir, or it may be concentrated and reinfused later.

1.8. Heart–Lung Machine Priming

Before cardiopulmonary bypass is undertaken, the heart–lung machine needs to be primed. For an adult patient, the priming fluid consists of about 1500 mL of fluid, based on a basic crystalloid solution. In our institution, Plasmalite is the preferred crystalloid solution to which albumin or hetastarch

(about 500 mL for a normal size patient) is added. Doing so helps maintain osmolality and volume in the intravascular space and helps prevent peripheral third spacing and edema. Red cell sludging is prevented within the system by the addition of 10,000 U heparin. For pediatric patients, these amounts are smaller, beginning with a priming of as little as 250 mL of crystalloid solution. The addition of this priming solution effects hemodilution, and the resultant lower blood viscosity allows it to better reach all vital areas of the body (as outlined in Section 1.6). At the end of the perfusion, the blood is hemoconcentrated to normal levels by eliminating the extra fluid from circulation *(19,20)*, and all the air is eliminated. Several areas of the heart–lung machine have an alarm system to prevent any air from entering into the circuitry. Once all the cannulas are in place and the connections are properly made, the surgeon gives the order to begin cardiopulmonary bypass and the operative procedure.

1.9. Hemodynamics

As cardiopulmonary bypass is implemented, the patient's systemic pressure usually drops briefly as the blood is diverted from the heart to the heart–lung machine. This drop is precipitated by the cold (ambient) temperature of the fluid that the heart–lung machine is introducing into the patient's aorta. The drop should last no more than a minute or two before proper pressure and flow is reestablished. In general, it is preferable to maintain a systemic pressure of approx 70 mmHg and flows between 1500 and 2500 mL/m^2 of body surface area throughout the entire operation. If the systemic pressure tends to sag, which can happen because of a variety of factors (e.g., loss of vascular tonus), the anesthesiologist and the perfusionist must coordinate administration of vasoconstrictor agents (such as Neo-Synephrine). If the pressure is too high, vasodilators are administered, or the rate of perfusion is decreased to restore safe pressures.

Venous pressure and oxygen saturations are also monitored very carefully throughout a bypass procedure. An altered venous pressure is one of the most important indicators that a potential obstruction in the venous return has occurred, either at the level of the venous cannula or within the superior or inferior vena cava. Such obstructions can often lead to major procedural complications if they are not monitored and immediately corrected. Typically, the perfusionist reports any concern to the surgeon so the surgeon can check whether any obstruction may exist. During cardiopulmonary bypass, the venous pressure should usually be zero and saturation above 70% because all the blood is completely diverted into the heart–lung machine. Once the pressures are equilibrated, the temperatures must be maintained at the level of hypothermia that the surgeon has chosen.

The records for the cardiopulmonary bypass are normally called *pump records*. They must contain all pertinent information, including: pressures, flows, temperatures, medications, periods of ischemia, and beginning and end times. Precise monitoring during cardiopulmonary bypass is extremely important, especially in patients with compromised renal function (i.e., those who cannot produce urine to remove extra fluid from their own system). In such patients, the most important electrolyte to monitor is potassium, which after any major operation usually rises above the normal level of 4.0 to 4.5 mEq/L or higher. Potassium must be very strictly monitored to prevent severe bradycardia or cardiac arrest. A dialysis system can be used during cardiopulmonary bypass, if necessary, to prevent such serious complications. Even in large medical centers, patients who are normally on dialysis rarely receive potassium during cardiopulmonary bypass.

In general, after weaning from cardiopulmonary bypass, most patients display various degrees of bradycardia, usually because of the persistent effect of the large amount of β-blockers administered preoperatively. Few patients will elicit heart rates greater than 80 beats/min when taken off cardiopulmonary bypass. All patients are commonly provided with a temporary pacemaker system postoperatively. It consists of wires placed on the surface of the heart (external leads) and connected to an external pacemaker unit. Based on many years of research and experience, the optimal postcardiopulmonary bypass heart rate has been determined as 90 beats/min; atrial pacing is set at that rate, with appropriate ventricular sensing. Pacing is usually necessary for only 24 to 48 h. It provides higher cardiac output, significantly improves hemodynamics, and allows the patient to eliminate the extra water that is usually third spaced during the operation.

Ventricular leads are routinely implanted in all patients as a very simple and safe prophylactic lifesaving measure *(21)*. This practice is highly advisable during the postoperative period because serious problems such as complete heart block are completely unpredictable regardless of the patient's age or general health. If serious problems occur, there is no substitute for the ability to pace the ventricle immediately. Once the acute recovery period is over and the patient is stable—typically 5 days after surgery—the temporary pacemaker wires can usually be removed. In rare cases when heart block or severe bradycardia occurs, a permanent pacemaker system may be necessary.

1.10. Summary

In summary, since its first implementation, cardiopulmonary bypass has improved significantly to become a very highly sophisticated, but reliable, procedure. The near future promises even more improvements because research and innovations continue to make cardiac operations safer and more efficient.

2. CARDIOPLEGIA

In the 1950s, the consensus among cardiac surgeons was that the results of the surgical methods at that time were satisfactory *(22)*. Yet, numerous reports described low cardiac output syndrome occurring after surgical correction of congenital anomalies *(23)*. Unfortunately, at that time, no definitive connection was provided between the lack of proper myocardial protection during surgery and the potential for postoperative cardiac dysfunction or high mortality rates.

Not until the advent of coronary bypass in the late 1960s and early 1970s were intraoperative myocardial infarctions or deaths attributed to poor protection of the myocardium *(24,25)*. At that time, several reports also noted that the levels of cardiac enzymes after surgery were significantly elevated, indicating that additional myocardial damage had occurred during the operations *(25)*.

As a result, surgeons of that era showed an increasing interest in attempting to protect the heart during the period of global ischemia (cross-clamping) via infusions of cold perfusates into the coronary circulation. Cold infusion is one of the methods known collectively as *cardioplegia*. Other modes for inducing cessation of cardiac activity employ chemical additions to perfusates or shocking the heart with electrical stimuli. After continued demonstration of its effectiveness, the use of hypothermic cardioplegia became quite widespread.

Yet, today many issues still need to be investigated concerning optimizing cardioplegic methodologies, such as which type of solution to use, how much to inject, how often to reinfuse, how long to extend global ischemia safely using cardioplegia approaches, and how well a specific solution might protect the energy reserves of the myocardium.

Operative settings that require cardioplegia involve aortic cross-clamping and coronary infusion (Fig. 5), usually of cold chemical solutions *(26–30)*. Some surgeons prefer to inject warm *(31,32)* or tepid *(33)* solutions that have been mixed with chemical components (e.g., high-potassium concentrations). Ideally, normal myocardial cells require uninterrupted coronary perfusion. Therefore, the principles of applying cardioplegia are aimed at: (1) conserving energy through the rapid induction of diastolic arrest; (2) slowing the metabolic demands and the degenerative processes that inevitably follow global myocardial ischemia; and (3) preventing unfavorable ischemic changes.

Research over the past 30-plus years has provided several formulations of chemical components that have been used with or without cooling to obtain these three goals. Interestingly, these solutions still vary widely, likely because they have been independently developed at several separate institutions.

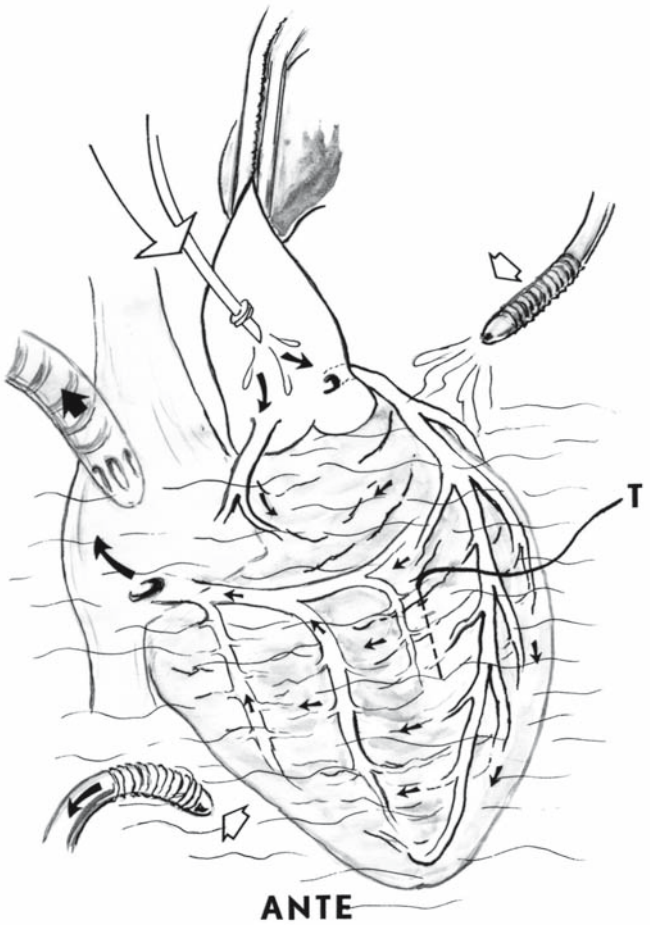

Fig. 5. Antegrade (ANTE) cardioplegia. The ascending aorta is cross-clamped, and cardioplegia is infused into the root of the aorta. The solution runs through the coronary system and leaves the heart via the coronary sinus. At the upper right is an irrigating catheter that provides topical hypothermia. This solution is removed by the suction line at the lower left. T, temperature probe (positioned in the interventricular septum for monitoring purposes).

2.1. Types of Solutions

Crystalloid solutions generally can be divided into two categories based on their formulations: extracellular or intracellular. Extracellular solutions contain calcium and sodium, the primary determinants of transcellular calcium exchange. Cardioplegic cardiac arrest can still be achieved by extracellular solutions containing only moderate amounts of potassium or magnesium. The cold blood cardioplegia solution *(28–34)*, the most common, is considered an extracellular ionic formula. The principal advantage of extracellular-type solutions is that they make it simpler to control equilibration characteristics within the ischemic myocardial tissue. Because no calcium or sodium gradients exist in the extracellular fluid, subsequent replacement is easily achieved without any major reequilibration with the intracellular fluid. The disadvantage of extracellular solutions is that they are more easily washed out by noncoronary flow, but this effect can be counteracted by adding calcium channel blockers or procaine.

Cardioplegia solutions that mimic intracellular ionic concentration usually contain no sodium or calcium. Their advantage, at least in theory, is that the lack of sodium and calcium generates a large osmolar space, which is available for other potentially protective components. This allows the solution to contain a high concentration of glucose, dextrose, mannitol, or histidine without excessive hyperosmolarity. Another advantage of intracellular-type solutions is that their minimal or reduced levels of extracellular calcium will limit contraction or restrict ischemia-induced calcium entry. The disadvantage of such solutions is that the lack of sodium and calcium may, under extreme conditions, predispose the heart to elicit the so-called calcium paradox. Another disadvantage is the potentially complex pattern of subsequent reequilibration then required. As Hearse et al. *(35)* pointed out, low-volume infusion of intracellular solutions offers good protection, but intermediate volumes offer only marginal protection, and high volumes may actually exacerbate injury to the myocardium.

Each of the described crystalloid cardioplegic solutions is considered to contain several components that have been "proven" by these different researchers to provide enhanced protection. For example, in one study published by Hearse and colleagues *(26)*, the effects of changing the composition of a simple cardioplegic solution, when used during a 30-min period of ischemia, were compared. It was shown that, at the end of a

Table 1
Composition of St. Thomas II Solution

Sodium chloride	120	mmol/L
Potassium	16	mmol/L
Sodium bicarbonate	10	mmol/L
Calcium	1.2	mmol/L
Magnesium	16	mmol/L
Procaine	1	mmol/L
Osmolality	280	mosM/Kg H_2O
Oncotic pressure	0.4	
pH	7.8	

Table 2
Composition of Birmingham Solution

Sodium	100	mmol/L
Potassium	30	mmol/L
Calcium	0.7	mmol/L
Glucose	5	g/L
Chloride	84	mmol/L
Albumin	50	g/L
Mannitol	5	g/L
Osmolality	300–335	mosM/L

Table 3
Composition of Bretschneider (Custodiol) Solution

Sodium	15	m*M*
Potassium	9	m*M*
Magnesium	4	m*M*
α-Histidine	180	m*M*
α-Histidine HCl	18	m*M*
Calcium chloride	0.015	m*M*
Mannitol	30	m*M*
Tryptophane	2	m*M*
Ketoglutarate	1	m*M*
pH	7.1–7.2	
Osmolality	295–325	mosM/Kg H_20

period of ischemia when no cardioplegia was used, the percentage of ventricular function recovery was practically nil, only about 3%. However, if potassium was added, the recovery increased to about 30%. Furthermore, if both potassium and magnesium were added, the recovery was even better, up to 68%. And, if potassium, magnesium, and adenosine triphosphate (ATP) were combined, the recovery reached 86%. Finally, if a combination of potassium, magnesium, ATP, creatine phosphate, and procaine was used, the recovery peaked at 93%.

After only crystalloid cardioplegia had been used for several years, it was reconsidered if the use of mixing cold blood with crystalloid solution *(34)* offered even better protection than the crystalloid solution alone; this was considered so if the period of cardiac ischemia was more than 90 min. Although the idea of protecting the heart with blood cardioplegia originated in the early 1950s with Ebert and colleagues *(36)*, it was not until 20 years later when it was reintroduced by Buckberg and associates *(28,32,34,37,38)* that it was popularized to use cold blood cardioplegia among most surgeons in the United States and throughout the world.

Controversy persists regarding the "optimal" formulation to protect and prevent damage to the heart. The following solutions are some of those most commonly used.

2.2. St. Thomas II Solution

The formulation for the St. Thomas II (Plegisol, Abbott Pharmaceutical Products Laboratories, Abbott Park, IL) solution originated with the published research of Hearse, Braimbridge, Stewart, and Jynge *(26,35,39,40)* from the St. Thomas Hospital in London. The basic vehicle was Ringer's solution, to which potassium chloride, procaine, and magnesium were added (Table 1).

St. Thomas II solution is an extracellular-type formulation. It is used extensively as an isolated clear cardioplegic solution and also as a base mix for the cold blood cardioplegia solution proposed by Buckberg and colleagues. It is usually injected into the root of the aorta at temperatures between 4 and 6°C (Fig. 5). Depending on the surgeon's preference, the initial volume is about 1000 mL for a 70-kg adult, followed by 100-mL infusions intermittently every 15 to 20 min—combined with or without topical hypothermia—to maintain the heart's temperature below 15°C.

The size of the catheter and the pressure for injecting the infusion are discussed in Section 2.8.

2.3. Birmingham Solution

Various extracellular solutions were also developed in the United States. Most sought to attain relatively high extracellular concentrations of potassium as an arrest-inducing drug. Birmingham solution was developed by Conti and colleagues *(41)*; its effectiveness was primarily demonstrated by the publications of Kirklin and colleagues *(42)*.

The importance of Birmingham solution is that glucose was included as a substrate for the myocardium (Table 2). The development of this solution gave origin to many other formulations that used the basic additions of glucose, potassium, and insulin.

2.4. Bretschneider Solution (Custodiol)

During the early 1960s and 1970s, Bretschneider in Goettingen, Germany published his studies introducing HTK (histidine-tryptophane-ketoglutarate) also known as Custodiol (Dr. F. Köhler Chemie GmbH, D-6146 Alsbach-Hähnlein, Germany) crystalloid cardioplegic solution *(43,44)* (Table 3). This intracellular-type solution has also been shown to be very effective in protecting the heart during surgery. It has been used extensively in Germany since its introduction. It is used not only as a protective solution for the heart during periods of surgical ischemia, but also as a preservation solution for hearts *(45–47)*, livers, and kidneys *(48)* in the field of transplantation.

According to Preusse et al. *(44)*, the solution must be provided in large amounts, between 3000 and 4000 mL per organ. Therefore, double cannulation of the right atrium is recommended during surgery to open the right atrium and to eliminate the large volume of solution from the general circulation by aspirating it from the coronary sinus orifice (Fig. 6). For Custodiol to be most effective, the period of equilibration is crucial *(43,44)*; that is, it takes about 7 min of infusion to equili-

brate the extracellular and intracellular spaces before the patient's operation can proceed.

This solution has also been used for both antegrade and retrograde (through the coronary sinus) perfusions. One of the considered significant advantages of this solution is its buffering capacity, which even surpasses the buffering properties of blood. Custodiol needs to be stored at a specific temperature (12 to 16°C) to prevent denaturation of the components.

2.5. Glucose–Insulin–Potassium Solutions

Most of the research performed on glucose-insulin-potassium (GIK) solutions was done in the United States. Multiple formulations with these basic components have been widely used for the past 30 years. Studies by Hewitt et al. *(49)* and later by Lolley et al. *(50)* demonstrated that continuous infusion of a solution containing 278 mmol/L of glucose, 20 mmol/L of potassium, and 20 U insulin with 69 mmol/L of mannitol dramatically improved myocardial protection. Those studies illustrated that the combination of glucose, insulin, and potassium improved anaerobic glycolysis and the washout of toxic substances. A slight modification of this basic solution, which included albumin to increase osmolality, was used extensively for many years at the University of Minnesota (Minneapolis, MN) *(51–53)* (Table 4). The only concern with the use of GIK solutions is the inevitable degradation of its constituent insulin over time. Therefore, GIK solutions must be prepared fresh for each use and cannot be stored for prolonged periods.

Many investigators contributed to the formulation of GIK solutions, among them Follete and coworkers *(34)* and Todd and Tyers *(54)*; Roe et al.'s classical solution *(30)* also belongs in this category. The common denominator among these formulations is the use of dextrose as the basic vehicle. Multiple publications have shown protective effects. However, when used alone, GIK solutions often provide insufficient protection during long periods of ischemia (beyond 120 min) or when the left ventricular function is marginal.

Several crystalloid potassium solutions have been formulated without dextrose. The main difference among them is the basic vehicle, which could be formulated with Ringer's or Krebs-Henseleit. Potassium is commonly added at doses between 15 and 125 mmol/L. Some solutions in this group are the University of Wisconsin *(46,55)* and Celsior *(56)* solutions, both used to preserve organs for transplantation. Several agents are considered also available to help increase the osmolality of cardioplegic solutions (Table 5). For example, mannitol has been included in such solutions both to stabilize osmolality and to act as a potential scavenger for oxygen radicals.

2.6. Additional Components

Other components have been added to crystalloid cardioplegic solutions by various investigators based on their own research. These include aspartate *(38)* as a substrate to generate ATP; glutamate *(38)* as a substrate; procaine *(35,40)* as a membrane stabilizer; nifedipine *(57)* to prevent calcium paradox; phosphates *(58–60)* as a base for ATP regeneration; and steroids (methylprednisolone) *(61–63)* as a cellular wall stabilizer. Other elements found to help maintain an alkaline pH include tris hydroxymethyl aminomethane (THAM), as advocated by Buckberg *(28)*, and histidine, as in HTK solution.

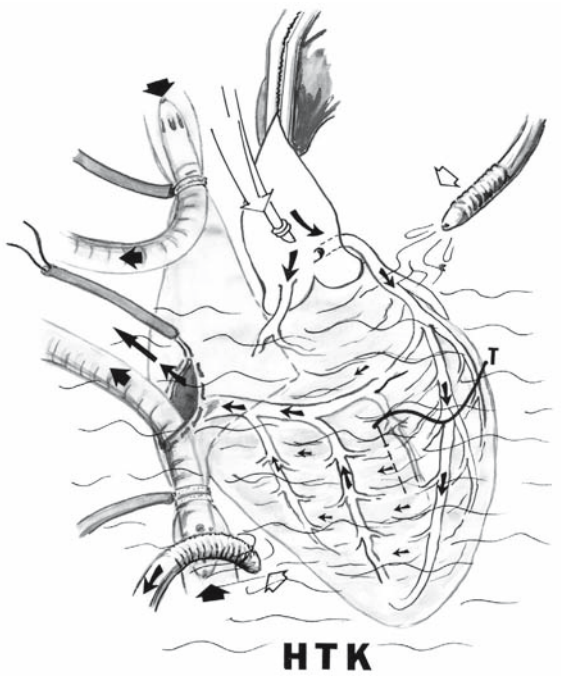

Fig. 6. Antegrade infusion of Bretschneider (HTK, histidine-tryptophane-ketoglutarate) solution. The solution is infused in an antegrade manner into the aortic root while the aorta is cross-clamped. Because this method requires a large volume of solution, the right atrium is opened, and the solution exiting the coronary sinus is aspirated and discarded. The superior and inferior venae cavae are individually cannulated to allow the right atrium to remain empty so that the HTK solution can be evacuated. Topical hypothermia is shown, with the irrigating cannula at the upper right and the suction catheter at the lower left. T, temperature probe.

Table 4
Composition of the Crystalloid Potassium Insulin (University of Minnesota) Solution

Dextrose	50 g/1000	mL
Sodium	3.5	mEq/L
Potassium	30	mEq/L
Chloride	30	mEq/L
Sodium bicarbonate	3.5	mEq/L
Regular insulin	10	U
Mannitol	12.5	g
Albumin	12.5	g
Osmolality	364	mosM/L
pH	7.8	
Oncotic pressure	3	

Table 5
Components Used to Raise Osmolality

Component	*Oncotic pressure (mmHg)*	*Osmolality (mosM)*
Hespan (hetastarch) (6% in 0.9% saline solution)	18.4	311
Mannitol 25% (12.5 g/50 mL)	0.1	—
Albumin 25%	>200	239
Dextran (10% in dextrose)	130.2	319
Plasmanate (5% albumin)	16.86	239
THAM [a]	—	370

[a] THAM, Tris hydroxymethyl aminomethane.

Table 6
Composition of Buckberg's
Cold Blood Cardioplegic Solution

5% dextrose with 1/4 normal saline	422	mL
Potassium chloride	2	mEq/mL
THAM[a]	72	mL
Diluent volume	500	mL
Blood hematocrit	22% = 500	mL
Osmolality	360	mosM/kg
Potassium	22	mEq/L
pH	7.8	
Calcium	0.3	mEq/L
Hematocrit	10%	

[a]THAM, Tris hydroxymethyl aminomethane.

2.7. Cold Blood Cardioplegia

The mixture of blood with crystalloid cardioplegia has become the most favored formulation for cardioplegia among cardiac surgeons, both in the United States and throughout the world. It is considered superior to the use of any other cardioplegic solution alone. The standard proportion of blood to crystalloid solution has remained fairly constant, at 4:1 (4 parts blood to 1 part crystalloid cardioplegia), yet the actual formulation of the crystalloid portion has varied across institutions *(64)*.

Administration of cold blood cardioplegia in the proportions proposed by Buckberg (Table 6) can be easily accomplished using the appropriate equipment available as a kit. The kit contains the necessary caliber of tubing, which is placed into a roller pump that automatically mixes the blood with the clear solution before injection into the root of the aorta (Fig. 7). The kit also includes a heat exchanger, which maintains the temperature of the solution between 4 and 6°C and allows the myocardial temperature to decrease even below 15°C. The significant advantage of cold blood cardioplegia is that it is considered to provide oxygen and nutrients to the ischemic myocardium and offers optimal buffering capacity. This mixture can be injected antegrade (in the root of the aorta) or retrograde (by coronary sinus cannulation using a self-inflating balloon to perfuse the entire heart) *(65)* (Fig. 8).

Cold blood cardioplegia has endured many years of testing, both in its initial form of providing cardioplegia at cold temperatures and in its more recent adaptation to warm cardioplegia as promoted by Lichtenstein et al. *(66)*. The cold blood method is widely used in the pediatric population for correction of all types of congenital anomalies.

2.8. Cardioplegic Administration

Our previous clinical work showed that cardioplegic solutions should be administered at a rapid rate and under moderate pressure *(29,51)*. Doing so shortens the prearrest period, provides better flow distribution, and accelerates the decrease in myocardial temperature. Rapid injection results in a postoperative level of cardiac isoenzymes that is lower than the level in patients who undergo a slower cardioplegic injection *(51)*.

Experimental studies on normal coronary arteries of animals showed that low pressures (less than 30 mmHg) and peak flow rates less than 125 mL/min result in a higher incidence of cellular ischemia, focal necrosis, and uneven flow distribution *(53)*. Consequently, patients with obstructive coronary disease who undergo low-pressure or low-volume cardioplegic injection will inevitably experience an increase in flow distribution problems.

Conversely, pressures higher than 110 mmHg and peak flow rates greater than 1500 mL/min may result in a higher incidence of mechanical and physical trauma to the vascular endothelium *(53)*. These higher levels, however, greatly enhance cellular protection. It should be noted that the use of high pressures in the aortic root of patients with coronary obstructions does not necessarily raise a concern. The rapid administration of cardioplegic solutions causes the temperature of the myocardium to fall rapidly within the protective range below 15°C and induces cardiac arrest.

Cardioplegic solutions are most commonly administered via an injection into the aortic root below the level of the aortic cross-clamp (Fig. 5). This site provides a normal antegrade flow to all areas of the heart. Several aortic valve procedures, however, require the aortic root to remain open for prolonged periods. In such cases, cardioplegic solutions may be administered retrograde, through the coronary sinus, while the valve repair is performed. This option also continuously protects the heart (Fig. 9).

Yet, this approach has several limitations that will be dependent on the degree of hypertrophy the myocardium may have suffered because of a preexisting condition. The pressure in the coronary sinus must be intentionally kept below 50 mmHg to prevent possible injury to the vein, but such reduced pressures may be insufficient to perfuse all areas of the heart. As a result, left ventricular dysfunction is occasionally observed after long periods of retrograde perfusion, even at myocardial temperatures below 15°C. In such cases, decompression of the left ventricular chamber is considered essential to facilitate perfusion of all areas of the heart *(67)*. Therefore, some surgeons still prefer antegrade perfusion through the coronary orifices requiring handheld cannulas, even though this may cause interruptions in the flow of the operation.

Over the past 30 years, the use of cardioplegic solutions should be noted as one of the significant advances in cardiac surgery to increase the safety of such operations. Nevertheless, researchers continue to look for better systems and methods to provide even greater protection of the heart during cardiac surgery.

2.9. Adjunct Topical Hypothermia

The use of cardiac hypothermia has been one of the most important tools for increasing the safety of cardiac operations. The application of topical hypothermia was introduced in the 1960s by Shumway, Lower, and Stofer *(68,69)* and was used exclusively through the 1970s until the introduction of crystalloid cardioplegia.

Topical hypothermia is considered to potentiate the use of all methods of cardioplegic perfusion, keeping the temperature of the heart in a safe range to tolerate global ischemia. The heart can be effectively cooled by a continuous flow of cold (6°C) saline or Ringer's solution over the heart; the remaining solution is removed via wall suction (Figs. 5, 6, 8, and 9). This

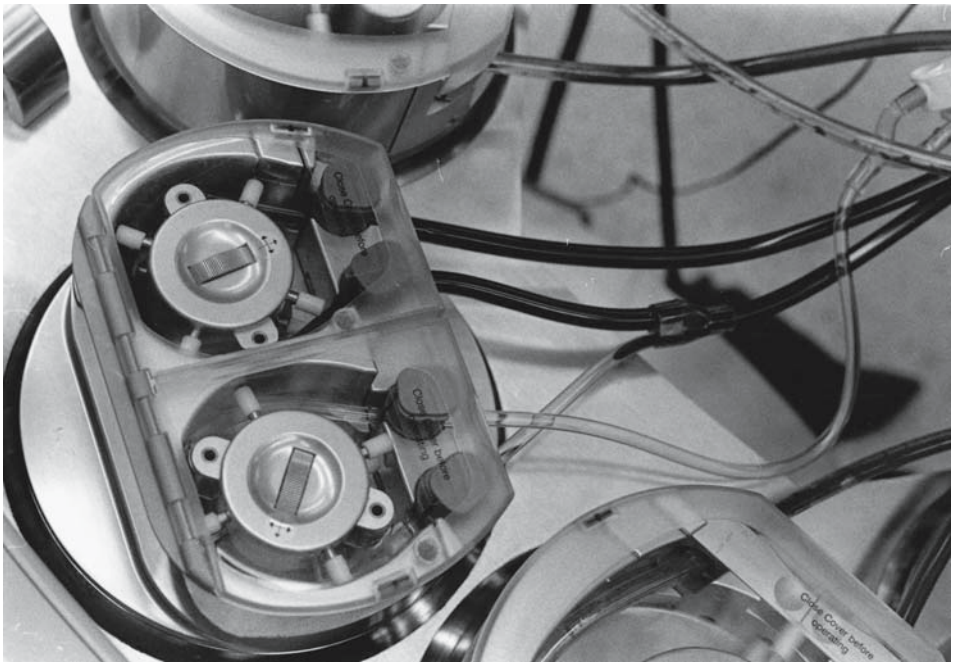

Fig. 7. Roller pumps of cardioplegia infusion system. The upper pump utilizes 1/4-in tubing to move the blood, and the lower pump runs crystalloid cardioplegic solution within 1/16-in tubing. The blood and cardioplegic solution are automatically mixed in a proportion of 4:1 in the outflow line before injection into the ascending aorta.

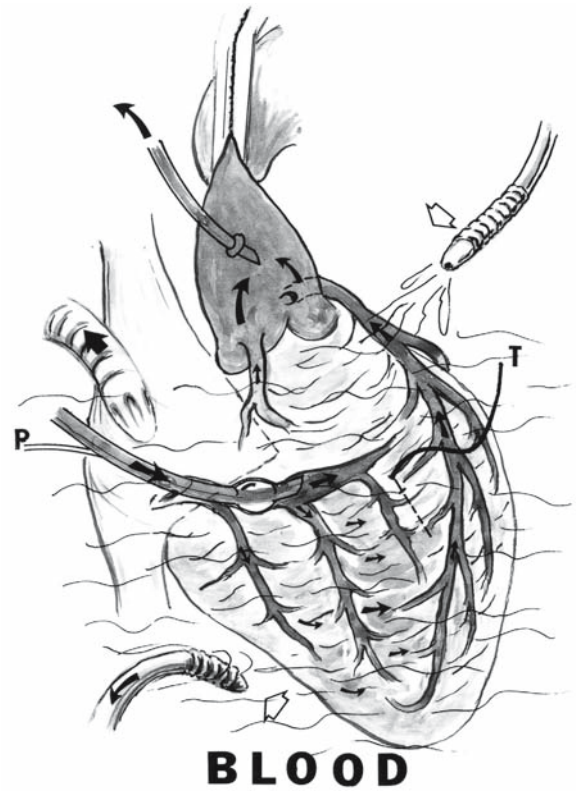

Fig. 8. Cold blood cardioplegia. This may be administered by antegrade infusion into the root of the aorta below the cross-clamp. It may also be accomplished in a retrograde manner through a catheter inserted in the coronary sinus, with the balloon inflated to prevent reflux into the right atrium. Topical hypothermia is used in conjunction with cold blood cardioplegia to potentiate the hypothermic protection of the heart. P, pressure monitoring of the coronary sinus; T, temperature probe.

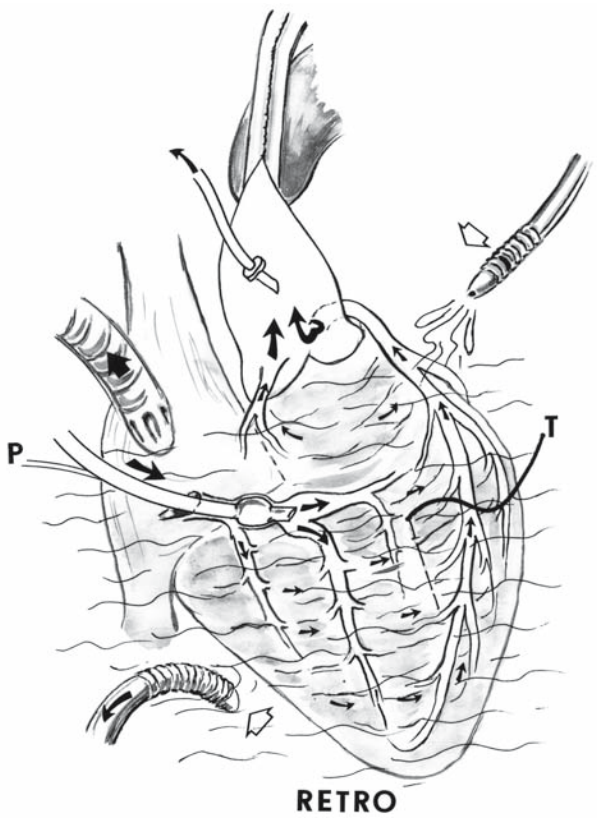

Fig. 9. Retrograde administration of crystalloid cardioplegia. This is accomplished via the coronary sinus, with the balloon inflated, to prevent reflux into the atrium. The solution eventually reaches the aortic root, where it is aspirated. It may also be allowed to drain into the left ventricle, which is vented to the pump. Topical hypothermia is shown using cold saline around the heart. P, pressure line monitoring; T, temperature probe.

technique is now preferred to the older method of applying slush ice over the heart; the latter method was attributed with the induction of frostbite lesions, not only of the heart, but also of the phrenic nerve, which runs along the pericardium. Several types of plastic jackets have also been designed for application around the heart for this purpose. In one case, the jacket is essentially a flat plastic bag through which cold water is continuously recirculated in a closed system by a dedicated perfusion pump.

REFERENCES

1. Lillehei, C.W., Cohen, M., Warden, H.E., and Varco R.L. (1955) The direct-vision intracardiac correction of congenital anomalies by controlled cross circulation. *Surgery.* 38, 11–29.
2. Gibbon, J.H. (1954) Application of a mechanical heart and lung apparatus to cardiac surgery. *Minn Med.* 37(Suppl), 171–180.
3. Bjork, V.O. and Hultquist, G. (1962) Contraindications to profound hypothermia in open-heart surgery. *J Thorac Cardiovasc Surg.* 44, 1–13.
4. Brunberg, J.A., Reilly, E.L., and Doty, D.B. (1974) Central nervous system consequences in infants of cardiac surgery using deep hypothermia and circulatory arrest. *Circulation.* 50(Suppl 2), II60–II68.
5. Bell, W.R. and Royall, R.M. (1980) Heparin-associated thrombocytopenia: a comparison of three heparin preparations. *N Engl J Med.* 303, 902–907.
6. Fadali, M.A., Papacostas, C.A., Duke, J.J., Ledbetter, M., and Osbakken, M. (1976) Cardiovascular depressant effect of protamine sulfate: experimental study and clinical implications. *Thorax.* 31, 320–323.
7. Goldman, B.S., Joison, J., and Austen, W.G. (1969) Cardiovascular effects of protamine sulfate. *Ann Thorac Surg.* 7, 459–471.
8. Greinacher, A., Volpel, H., Janssens, U., et al. (1999) Recombinant hirudin (lepirudin) provides safe and effective anticoagulation in patients with heparin-induced thrombocytopenia: a prospective study. *Circulation.* 99, 73–80.
9. Rowlings, P.A., Mansberg, R., Rozenberg, M.C., Evans, S. and Murray, B. (1991) The use of a low molecular weight heparinoid (Org 10172) for extracorporeal procedures in patients with heparin dependent thrombocytopenia and thrombosis. *Aust N Z J Med.* 21, 52–54.
10. Molina, J.E., Irmiter, R.J., Vogelpohl, D.C., Nielsen, K.L., Callander, D., and Mueller, R. (1995) Normothermic cardiopulmonary bypass for all cardiac operations. *Cor Europ.* 4, 76–79.
11. Singh, A.K., Bert, A.A., Feng, W.C., and Rotenberg, F.A. (1995) Stroke during coronary artery bypass grafting using hypothermic versus normothermic perfusion. *Ann Thorac Surg.* 59, 84–89.
12. Lazenby, W.D., Ko, W., Zelano, J.A., et al. (1992) Effects of temperature and flow rate in regional blood flow and metabolism during cardiopulmonary bypass. *Ann Thorac Surg.* 53, 957–964.
13. Nomoto, S., Shimahara, Y., Kumada, K., Ogino, H., Okamoto, Y., and Ban, T. (1992) Arterial ketone body ratio during and after cardiopulmonary bypass. *J Thorac Cardiovasc Surg.* 103, 1164–1167.
14. Croughwell, N.D., Frasco, P., Blumenthal, J.A., Leone, B.J., White, W.D., and Reves, J.G. (1992) Warming during cardiopulmonary bypass is associated with jugular bulb desaturation. *Ann Thorac Surg.* 53, 827–832.
15. Durandy, Y., Hulin, S., and LeCompte, Y. (2002) Normothermic cardiopulmonary bypass in pediatric surgery. *J Thorac Cardiovasc Surg.* 123, 194.
16. Swaminathan, M., East, C., Phillips-Bute, B., et al. (2001) Report of a sub-study on warm versus cold cardiopulmonary bypass: changes in creatinine clearance. *Ann Thorac Surg.* 72, 1603–1609.
17. Mora, C.T., Henson, M.B., Weintraub, W.S., et al. (1996) The effect of temperature management during cardiopulmonary bypass on neurologic and neuropsychologic outcomes in patients undergoing coronary revascularization. *J Thorac Cardiovasc Surg.* 112, 514–522.
18. Craver, J.M., Bufkin, B.L., Weintraub, W.S., and Guyton, R.A. (1995) Neurologic events after coronary bypass grafting: further observations with warm cardioplegia. *Ann Thorac Surg.* 59, 1429–1433.
19. Naik, S.K., Knight, A., and Elliot, M. (1991) A prospective randomized study of a modified technique of ultrafiltration during pediatric open-heart surgery. *Circulation.* 84(Suppl), III422-III431.
20. Davies, M.J., Nguyen, K., Gaynor, J.W., and Elliott, M.J. (1998) Modified ultrafiltration improves left ventricular systolic function in infants after cardiopulmonary bypass. *J Thorac Cardiovasc Surg.* 115, 361–370.
21. Molina, J.E. (1989) Temporary dual-chamber pacing after open cardiac procedures. *Medtronic News.* 19, 24–28.
22. Melrose, D.G., Dreyer, B., Bentall, H.H., and Baker, J.B. (1955) Elective cardiac arrest. Preliminary communication. *Lancet.* 2, 21–22.
23. Helmsworth, J.A., Kaplan, S., Clark, L.C., Jr., McAdams, A.J., Matthews, E.C., and Edwards, F.K. (1959) Myocardial injury associated with asystole induced with potassium citrate. *Ann Surg.* 149, 200–203.
24. Brewer, D.L., Bilbro, R.H., and Bartel, A.G. (1973) Myocardial infarction as a complication of coronary bypass surgery. *Circulation.* 47, 58–64.
25. Assad-Morell, J.L., Wallace, R.B., Elveback, L.R., et al. (1975) Serum enzyme data in diagnosis of myocardial infarction during or early after aorto-coronary saphenous vein bypass graft operations. *J Thorac Cardiovasc Surg.* 69, 851–857.
26. Hearse, D.J., Stewart, D.A., and Braimbridge, M.V. (1975) Hypothermic arrest and potassium arrest: metabolic and myocardial protection during elective cardiac arrest. *Circ Res.* 36, 481–489.
27. Nelson, R.L., Goldstein, S.M., McConnell, D.H., Maloney, J.V., and Buckberg, G.D. (1976) Improved myocardial performance after aortic cross-clamping by combining pharmacologic arrest with topical hypothermia. *Circulation.* 54(Suppl), III11–III16.
28. Buckberg, G.D., Olinger, G.N., Mulder D.G., and Maloney, J.V. (1975) Depressed postoperative cardiac performance. Prevention by adequate myocardial protection during cardiopulmonary bypass. *J Thorac Cardiovasc Surg.* 70, 974–994.
29. Molina, J.E., Feiber, W., Sisk, A., Polen T., and Collins, B. (1977) Cardioplegia without fibrillation or defibrillation in cardiac surgery. *Surgery.* 81, 619–626.
30. Roe, B.B., Hutchinson, J.C., Fishman, N.H., Ullyot, D.J., and Smith, D.L. (1977) Myocardial protection with cold ischemic potassium-induced cardioplegia. *J Thorac Cardiovasc Surg.* 73, 366–374.
31. Chocron, S., Kaili, D., Yan, Y., et al. (2000) Intermediate lukewarm (20°C) antegrade intermittent blood cardioplegia compared with cold and warm blood cardioplegia. *J Thorac Cardiovasc Surg.* 119, 610–616.
32. Rosenkranz, E.R., Vinten-Johansen, J., Buckberg, G.D., Okamoto, F., Edwards, H., and Bugyi, H. (1982) Benefits of normothermic induction of blood cardioplegia in energy-depleted hearts, with maintenance of arrest by multidose cold blood cardioplegic infusions. *J Thorac Cardiovasc Surg.* 84, 667–677.
33. Hayashida, N., Ikonomidis, J.S., Weisel, R.D., et al. (1994) The optimal cardioplegic temperature. *Ann Thorac Surg.* 58, 961–971.
34. Follette, D.M., Fey, K., Becker, H., et al. (1979) Superiority of blood cardioplegia over asanguineous cardioplegia: an experimental and clinical study. *Chir Forum Exp Klin Forsch.* 279–283.
35. Hearse, D.J., Stewart, D.A., and Braimbridge, M.V. (1976) Cellular protection during myocardial ischemia: the development and characterization of a procedure for the induction of reversible ischemic arrest. *Circulation.* 54, 193–202.
36. Ebert, P.A., Greenfield, L.J., Austen, W.G., and Morrow, A.G. (1962) Experimental comparison of methods for protecting the heart during aortic occlusion. *Ann Surg.* 155, 25–32.
37. Rosenkranz, E.R., Buckberg, G.D., Laks, H., and Mulder, D.G. (1983) Warm induction of cardioplegia with glutamate-enriched blood in coronary patients with cardiogenic shock who are dependent on inotropic drugs and intra-aortic balloon support. *J Thorac Cardiovasc Surg.* 86, 507–518.
38. Beyersdorf, F., Kirsh, M., Buckberg, G. D., and Allen, B.S. (1992) Warm glutamate/aspartate-enriched blood cardioplegic solution for

perioperative sudden death. *J Thorac Cardiovasc Surg*. 104, 1141–1147.
39. Jynge, P., Hearse, D.J., and Braimbridge, M.V. (1977) Myocardial protection during ischemic cardiac arrest. A possible hazard with calcium-free cardioplegic infusates. *J Thorac Cardiovasc Surg*. 73, 848–855.
40. Harlan, B.J., Ross, D., Macmanus, Q., Knight, R., Luber, J., and Starr, A. (1978) Cardioplegic solutions for myocardial preservation: analysis of hypothermic arrest, potassium arrest, and procaine arrest. *Circulation*. 58(suppl I), 114–118.
41. Conti, V.R., Bertranov, E.G., Blackstone, E.H., Kirklin, J.W., and Digerness, S.B. (1978) Cold cardioplegia versus hypothermia for myocardial protection. Randomized clinical study. *J Thorac Cardiovasc Surg*. 76, 577–589.
42. Kirklin, J.W., Conti, V.R., and Blackstone, E.H. (1979) Prevention of myocardial damage during cardiac operations. *N Engl J Med*. 301, 135–141.
43. Bretschneider, J., Hubner, G., Knoll, D., Lohr, B., Nordbeck, H., and Spieckermann, P.G. (1975) Myocardial resistance and tolerance to ischemia: physiological and biochemical basis. *J Cardiovasc Surg*. 16, 241–260.
44. Preusse, C.J., Gebhard, M.M., and Bretschneider, H. J. (1981) Myocardial "equilibration processes" and myocardial energy turnover during initiation of artificial cardiac arrest with cardioplegic solution-reasons for a sufficiently long cardioplegic perfusion. *Thorac Cardiovasc Surg*. 29, 71–76.
45. Preusse, C.J., Schulte, H.D., and Birks, W. (1987) High volume cardioplegia. *Ann Chir Gynaecol*. 76, 39–45.
46. Human, P.A., Holl, J., Vosloo, S., et al. (1993) Extended cardiopulmonary preservation: University of Wisconsin solution versus Bretschneider's cardioplegic solution. *Ann Thorac Surg*. 55, 1123–1130.
47. Reichenspurner, H., Russ, C., Uberfuhr, P., et al. (1992) Myocardial preservation using HTK solution for heart transplantation. A multicenter study. *Eur J Cardiothorac Surg*. 7, 414–419.
48. Groenewoud, A.F. and Thorogood, J. (1992) A preliminary report of the HTK randomized multicenter study comparing kidney graft preservation with HTK and Eurocollins solutions. *Transplant Int*. 5(Suppl I), 429–432.
49. Hewitt, R.L., Lolley, D.M., Adrouny, G.A., and Drapanas, T. (1974) Protective effect of glycogen and glucose on the anoxic arrested heart. *Surgery*. 75, 1–10.
50. Lolley, D.M., Ray, J.F., III, Myers, W.O., Sheldon, G., and Sautter, R.D. (1978) Reduction of intraoperative myocardial infarction by means of exogenous anaerobic substrate enhancement: prospective randomized study. *Ann Thorac Surg*. 26, 515–524.
51. Molina, J.E., Gani, K.S., and Voss, D.M. (1982) How should clear cardioplegia be administered? A method of rapid arrest with high flow and pressure. *J Thorac Cardiovasc Surg*. 84, 762–772.
52. Molina, J.E., Gani, K.S., and Voss, D.M. (1982) Pressurized rapid cardioplegia versus administration of exogenous substrate and topical hypothermia. *Ann Thorac Surg*. 33, 434–444.
53. Molina, J.E., Galliani, C.A., Einzig, S., Bianco, R., Rasmussen, T., and Clack, R. (1989) Physical and mechanical effects of cardioplegic injection on flow distribution and myocardial damage in hearts with normal coronary arteries. *J Thorac Cardiovasc Surg*. 97, 870–877.
54. Todd, G.J. and Tyers, G.F. (1975) Amelioration of the effects of ischemic cardiac arrest by the intracoronary administration of cardioplegic solutions. *Circulation*. 52, 1111–1116.
55. Fremes, S.E., Zhang, J., Furukawa, R.D., Mickle, D.A., and Weisel, R.D. (1995). Cardiac storage with University of Wisconsin solution, calcium, and magnesium. *J Heart Lung Transplant*. 14, 916–925.
56. Ackemann, J., Gross, W., Mory, M., Schaefer, M., and Gebhard, M.M. (2002) Celsior versus Custodiol: early postischemic recovery after cardioplegia and ischemia at 5°C. *Ann Thorac Surg*. 74, 522–529.
57. Nayler, W.G. (1982) Protection of the myocardium against postischemic reperfusion damage. The combined effect of hypothermia and nifedipine. *J Thorac Cardiovasc Surg*. 84, 897–905.
58. Bolling, S.F., Bies, L.E., Gallagher, K.P., and Bove, E.L. (1989) Enhanced myocardial protection with adenosine. *Ann Thorac Surg*. 47, 809–815.
59. Sharov, V.G., Saks, V.A., Kupriyanov, V.V., et al. (1987) Protection of ischemic myocardium by exogenous phosphocreatine. *J Thorac Cardiovasc Surg*. 94, 749–761
60. Foker, J.E., Einzig, S., and Wang, T. (1980) Adenosine metabolism and myocardial preservation. *J Thorac Cardiovasc Surg*. 80, 506–516.
61. Vejlsted, H., Andersen, K., Fischer Hansen B., Hasum, B, and Ambjerg, J. (1983) Myocardial preservation during anoxic arrest. *Scand J Thorac Cardiovasc Surg*. 17, 269–276.
62. Rao, G., King, J., Ford, W., and King, G. (1977) The effects of methylprednisolone on the complications of coronary artery surgery. *Vasc Surg*. 11, 1–7.
63. Kirsh, M.M., Behrendt, D.M., and Jochim, K.E. (1979) Effects of methylprednisolone in cardioplegic solution during coronary bypass grafting. *J Thorac Cardiovasc Surg*. 77, 896–899.
64. The Warm Heart Investigators. (1994) Randomised trial of normothermic versus hypothermic coronary bypass surgery. *Lancet*. 343, 559–563.
65. Menasche, P., Kural, S., Fauchet, M., et al. (1982) Retrograde coronary sinus perfusion: a safe alternative for ensuring cardioplegic delivery in aortic valve surgery. *Ann Thorac Surg*. 34, 647–658.
66. Lichtenstein, S.V., Ashe, K.A., El Dalati, H., Cusimano, R.J., Panos, A., and Slutsky, A.S. (1991). Warm heart surgery. *J Thorac Cardiovasc Surg*. 101, 269–274.
67. Wechsler, A.S. (1982) Deficiencies of cardioplegia—the hypertrophied ventricle, in *A Textbook of Clinical Cardioplegia* (Engelman, R.M. and Levisky, S., eds.), Futura, Mount Kisco, NY, pp. 381–439.
68. Shumway, N.E., Lower, R.R. and Stofer, R.C. (1959) Selective hypothermia of the heart in anoxic cardiac arrest. *Surg Gynecol Obstet*. 109, 750–754.
69. Shumway, N.E. and Lower, R.R. (1959) Topical cardiac hypothermia for extended periods of anoxic arrest. *Surg Forum*. 10, 563–566.

27 Heart Valve Disease

ROBERT P. GALLEGOS, MD
AND R. MORTON BOLMAN III, MD

CONTENTS

1. INTRODUCTION

The function of the heart is to circulate blood in closed circuit to the lungs, where blood is oxygenated, and out to the body, where oxygen provides fuel for cellular metabolism. To accomplish this task, blood is pumped by the right heart system from the body to the lungs. Once oxygenated in the lungs, blood is returned to the left heart, where it is then pumped out to the body. Although described as a biological pump, the heart is actually two biological pumps in series, composed of a right and left heart. Each unit of the heart is composed of an atrial and ventricular chamber; their synchronized contractions result in the forward flow of blood out of the heart. Crucial to the appropriate function of the heart are four valves (the mitral, aortic, tricuspid, and pulmonic) that function in concert to maintain forward flow of blood across the heart. Diseases affecting the heart valves result in either obstruction to forward flow (stenosis) or reversal of flow across an incompetent valve (regurgitation). In either case, significant morbidity and mortality will result if no treatment is offered to the patient.

This chapter was designed to provide a brief overview of the current treatment options for heart valve disease. Major topics of discussion are: (1) development of prosthetic valve replacements, (2) current issues with valve replacement, and (3) major valvular diseases that affect humans in the Western world (Fig. 1).

From: *Handbook of Cardiac Anatomy, Physiology, and Devices*
Edited by: P. A. Iaizzo © Humana Press Inc., Totowa, NJ

2. A NEW FRONTIER: VALVE REPLACEMENT

Before 1950, the ability to operate on the human heart safely and effectively was considered an insurmountable goal. Attempts to operate to correct valvular diseases without stopping the heart resulted in severe, often fatal, complications, including uncontrollable bleeding and the introduction of air emboli *(1)*. The ability to maintain forward flow of blood while stopping the heart to allow the surgeon access to the valve would have to wait first for the development of cross-circulation and later for the perfection of cardiopulmonary bypass by Dr. C. Walton Lillehei, Richard L. Varco, and Dr. F. John Lewis at the University of Minnesota (Minneapolis, MN) *(2)*. With this new approach, a new frontier in surgical options for the treatment of heart valve disease began to emerge (Figs. 2–4).

2.1. Mechanical Prosthetic Valves

By 1961, Dr. Albert Starr and Lowell Edwards had successfully implanted the world's first mechanical valve into a human to replace mitral valves deformed by rheumatic fever *(3)*. Initially, this steel ball-and-cage design was successful in approx 50% of implantations. Major complications were soon recognized, including clot formation, resulting in embolic strokes; significant noise; red blood cell destruction; and healing tissue ingrowth causing valve obstruction.

A complete history of the development of currently used mechanical prostheses is beyond the scope of this text. However, it is important to mention two key aspects of any successful valve design: (1) improved valve hemodynamics and

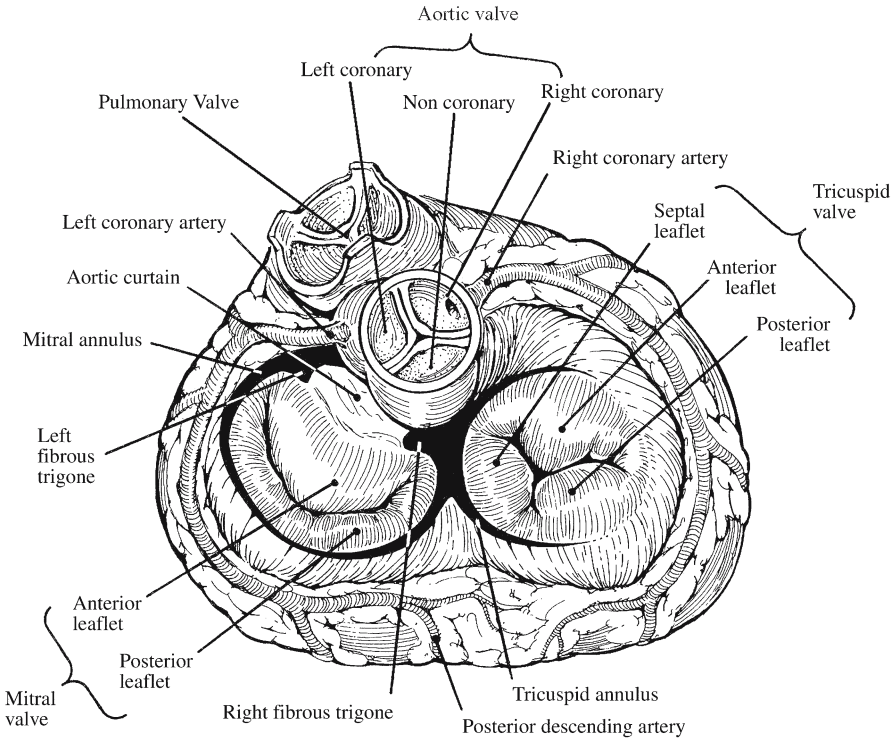

Fig. 1. Apical view of the four heart valves: aortic, mitral, pulmonic, and tricuspid.

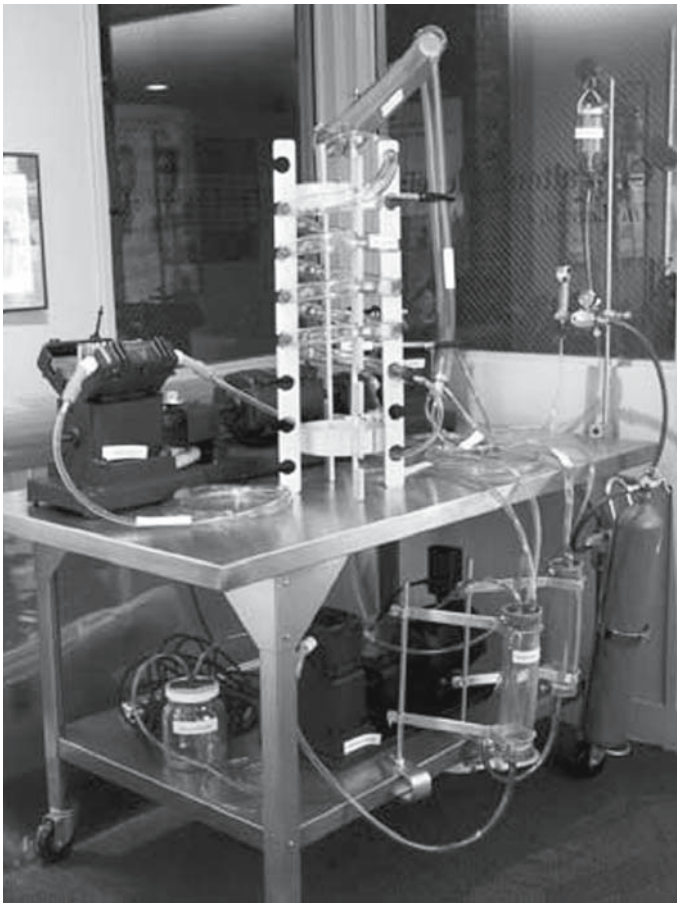

Fig. 2. Heart lung machine developed at the University of Minnesota by Dr. C. Walton Lillehei and Dr. Richard DeWall. Photo courtesy of Dr. Robert Gallegos.

Fig. 3. Dr. C. Walton Lillehei, the father of open heart surgery. Photo courtesy of the Lillehei Heart Institute.

Fig. 4. Drs. Richard Varco and F. John Lewis standing with a cooling device used during open heart surgery. Photo courtesy of the Lillehei Heart Institute.

Table 1
Anticoagulation After Prosthetic Heart Valves

	Warfarin		*Aspirin*
	INR 2–3	*INR 2.5–3.5*	*80–100mg*
Mechanical prosthesis			
• First 3 months postimplantation		+	+
• After initial 3 months			
♦ Aortic valve	+		
♦ Aortic valve + risk factor		+	+
♦ Mitral valve		+	+
♦ Mitral + risk factor		+	+
Biological prosthesis			
• First 3 months postimplantation		+	+
• After initial 3 months			
♦ Aortic valve			+
♦ Aortic valve + risk factor	+		+
♦ Mitral valve			+
♦ Mitral + risk factor	+		+

Source: From ref. *7*. INR, international normalized ratio.

Table 2
Tissue Valve Graft Options: Classification of Bioprosthetic Valves

Bioprosthetic valve	*Description*
Stented porcine valve (xenograft)	A three-leaflet valve supported by three artificial struts or stents to maintain leaflet structure and geometry
Stentless porcine valve (xenograft)	A length of porcine aorta including tissue below (proximal) and above (distal) to the valve, called the *root*
Bovine pericardial valve (xenograft)	A three-leaflet valve created from bovine pericardium attached to a stented frame
Homograft	A human aortic valve and root
Autograft	A pulmonary valve and root excised from and reimplanted in the same patient

(2) reduced thrombogenic (or clot forming) potential. Efforts to optimize valve hemodynamic function date back to the development of the Lillehei/Kaster tilting disk valve, which allowed blood to flow centrally through the valve. At that time, this new type of valve emphasized the requirement to design a valve that would reduce turbulent blood flow, reduce cell destruction, and minimize the transvalvular gradients *(4)*. A transvalvular gradient is defined as the pressure difference across the valve. Despite the advantages of a new steel tilting disk design, careful and strict anticoagulation therapy was still required to reduce the risk of clot formation *(5)*.

The next improvement of heart valves came with the development of the pyrolytic carbon valve leaflets. The nonthrombogenic properties, weight, and strength of pyrolytic carbon were described by Drs. Jack Bokros and Vincent Gott. Subsequently, pyrolytic carbon was used in the creation of a bileaflet valve, inspired by an idea of Dr. Kalke. This valve, manufactured by St. Jude Medical (St. Paul, MN), provides exceptional performance and remains today as the gold standard of valve designs *(6)*.

Yet, since the first implantation, efforts to design the ideal mechanical heart valve prosthesis were affected by the challenges of thrombogenicity, turbulence, and hemolysis. Currently, all patients with mechanical valves still require anticoagulation therapy, typically with oral warfarin; the use of this agent has reduced the risk of thromboembolism to 1–2% per year (Table 1) *(7)*. It should be noted that numerous studies have demonstrated that the risk of thromboembolism is related to the valve implant type, in the descending order of a tricuspid, mitral, and aortic implant. In addition, this risk of emboli appears to be greatest in the early postimplant time period and then reduces, as the valve sewing cuff becomes fully endothelialized.

In general, management of anticoagulation must be individualized to the patient, so to minimize risk of thromboembolism and at the same time prevent bleeding complications. When a patient with a valve prosthesis requires noncardiac surgery, warfarin therapy should be stopped only for procedures with a substantial risk of bleeding. A complete discussion of anticoagulation therapy is beyond the scope of this chapter; however, several excellent reviews are available on this subject *(7)*.

2.2. Biological Prosthetic Valves

Because of the problems related to anticoagulation, much clinical research has focused on developing a tissue valve alternative that avoids the need for anticoagulation. From a historical perspective, Drs. Lower and Shumway performed the first pulmonary valve autotransplant in an animal model *(8)*. In 1967, Dr. Donald Ross completed the first successful replacement of such in a human. The Ross procedure is a well-established method used today; to replace a diseased aortic valve with the patient's own pulmonary valve (Fig. 5). A donor tissue valve or homograft (Table 2) is then used as a prosthetic pulmonary valve.

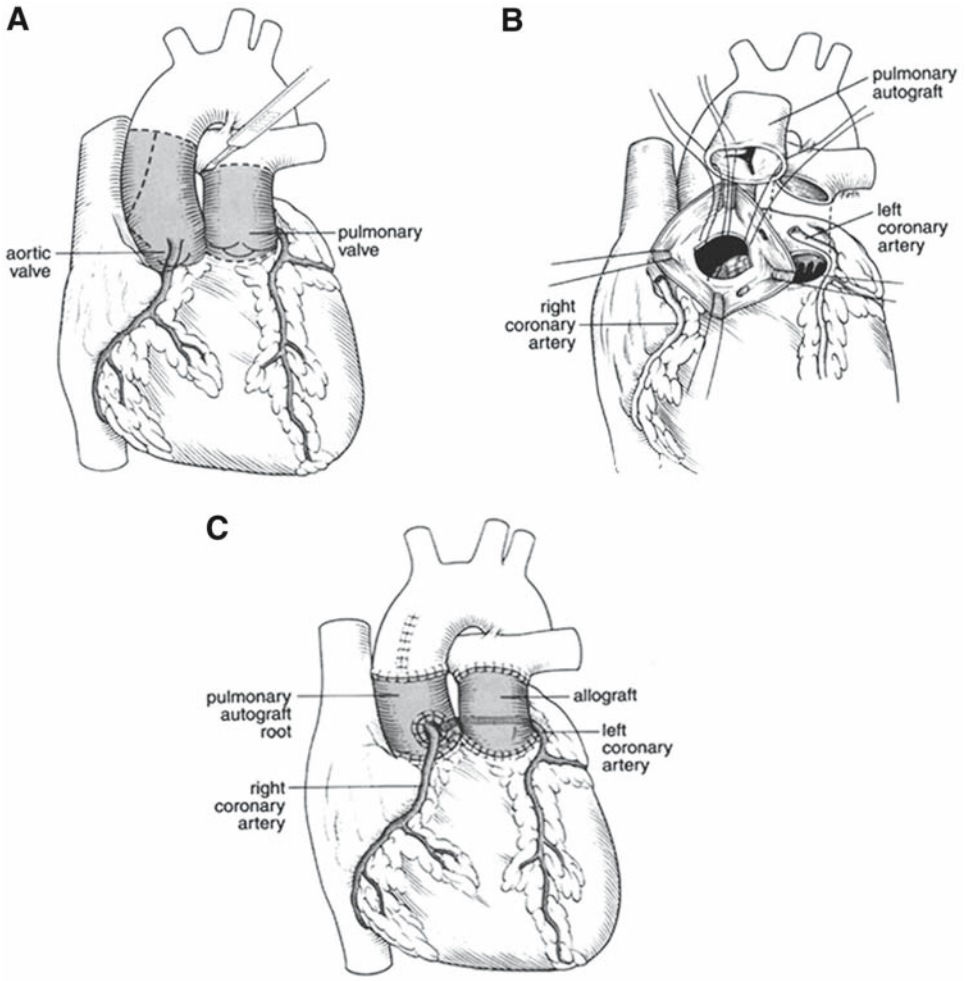

Fig. 5. Schematic drawing of the Ross procedure. **(A)** Resection of the diseased aortic valve. **(B)** Harvesting of native pulmonary valve. **(C)** Implantation of the pulmonic valve in the aortic position and reimplantation of coronary arteries.

In general, tissue valves are significantly more biocompatible than their mechanical counterparts. These valves are naturally less thrombogenic, and thus the patient does not require aggressive anticoagulation. Specifically, a risk of less than 0.7% per year for clinical thromboembolism has been reported in patients with valve replacement eliciting sinus rhythm without warfarin therapy *(7)*. Therefore, this treatment option is advantageous in clinical situations when the use of anticoagulation would significantly increase the patient's morbidity and mortality. Yet, a potential major disadvantage of tissue valves is an early valvular degeneration as a result of leaflet calcification. Methods for tissue preservation to prevent calcification are currently a major focus of research in this field.

2.3. Biological vs Mechanical Valves

The choice of a mechanical or biological valve implant will depend on the patient's disease, the specific native valve involved, and the surgeon's preference and experience. If these factors are not limiting, the choice of valve type should be based on the maximization of benefits over risks for the individual patient. Mechanical valves offer greater durability, but at the cost of requiring lifelong anticoagulation. As such, mechanical valves are well suited for a younger patient who does not desire future reoperations.

Currently, mechanical valve replacement has been standardized and is commonplace, yielding satisfactory valve function that is quite reproducible from patient to patient. The flow gradients with newer bileaflet mechanical valves have dramatically improved from the early ball valve type; currently, a trileaflet valve is in the preclinical stages of development and may eventually not require anticoagulation therapy (*see* Fig. 2 in Chapter 21).

In the interim, bioprosthetic or tissue valves offer a safe alternative for patients in whom the risk of anticoagulation is prohibitively high (e.g., elderly patients older than 70 years of age, women of child-bearing years desiring pregnancy). Yet, the length of durability remains a serious concern for tissue valves, and thus a patient whose life expectancy is greater than that of the prosthesis will encounter the risk of another surgery for a second valve replacement.

Table 3
Reportable Valve Prosthesis Complications

Complication	*Description*
Structural valvular deterioration	Any change in function of an operated valve resulting from an intrinsic abnormality causing stenosis or regurgitation
Nonstructural dysfunction	Any stenosis or regurgitation of the operated valve that is not intrinsic to the valve itself, including inappropriate sizing but excluding thrombosis and infection
Valve thrombosis	Any thrombus, in the absence of infection, attached to or near an operated valve that occludes part of the blood flow path or interferes with function of the valve
Embolism	Any embolic event that occurs in the absence of infection after the immediate perioperative period (new temporary or permanent, focal or global neurological deficit and peripheral embolic event)
Bleeding event (anticoagulant hemorrhage)	Any episode of major internal or external bleeding that causes death, hospitalization, or permanent injury or requires transfusion
Operated valvular endocarditis	Any infection involving an operated valve resulting in valve thrombosis, thrombotic embolus, bleeding event, or paravalvular leak

Source: From ref. *8*.

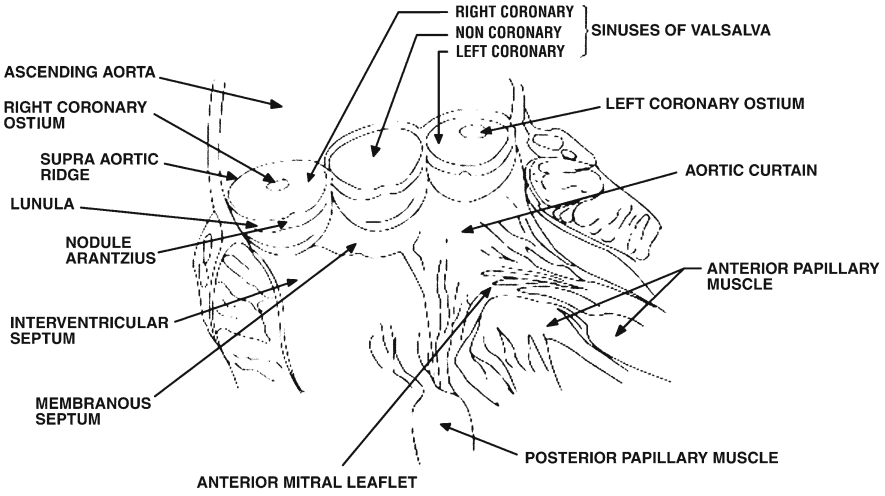

Fig. 6. Anatomy of the aortic valve.

2.4. Prosthetic Heart Valve Endocarditis and Performance Tracking

All patients with prosthetic valves also need appropriate antibiotics for prophylaxis against infective endocarditis. This discussion is beyond the scope of this chapter, but refer to guidelines published by a joint committee from the American Heart Association and American College of Cardiology for the applicable protocols. A registry has been established to track the long-term performance of all clinically approved implanted valve prostheses *(9)*.

Established standards were revised in 1996 and are summarized in Table 3. As alluded to in Chapter 21, investigators seeking approval for all new valves must also report any such complications that occur in the preclinical animal testing phase to the appropriate regulatory authority.

3. SPECIFIC VALVULAR DISEASES: ETIOLOGIES AND TREATMENTS

The remainder of this chapter is devoted to a generalized summary of the most common valvular diseases affecting patients in the Western world. Of the four heart valves, significant clinical disease can primarily affect all but the pulmonary valve. Indications for diagnostic, therapeutic, and follow-up intervention are discussed for each disease. A complete evidenced-based summary of recommendations for intervention and physical activity in individuals with valvular disease is available from several excellent reviews, including those of Bonow et al. *(7)* and Cheitlin et al. *(10)*.

3.1. Aortic Valve Disease

Anatomically, the normal aortic valve is composed of the annulus and the left, right, and noncoronary leaflets (sometimes referred to as "cusps") (Fig. 6). Diseases affecting these structures can be subdivided into aortic stenosis or regurgitation or some combination thereof. Overall, aortic stenosis is considered a surgical disease, with aortic valve replacement considered the standard of care. Treatment of aortic regurgitation is also surgical, although the exact method chosen will vary based on the etiology of the disease.

Table 4
Degree of Aortic Stenosis

	Valve orifice area (cm^2)	*Peak aortic velocity (m/s)*
Mild	>1.5	<3.0
Moderate	>1.0 to 1.5	3.0–4.0
Severe	<1.0	>4.0

Source: From ref. *79*.

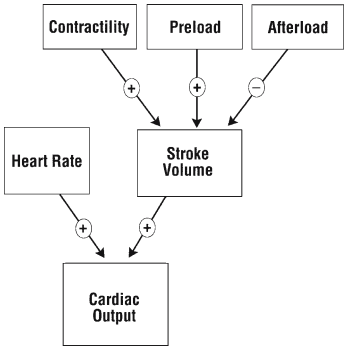

Fig. 7. Determinants of cardiac output include contributions from preload and afterload pressures, contractility, and heart rate. Adapted from L.S. Lilly (ed.), *Pathophysiology of Heart Disease*, © Lea and Febiger, Philadelphia, PA, 1993, p. 149.

3.1.1. Aortic Stenosis

Aortic stenosis causes varying degrees of left ventricular outflow tract obstruction. The various etiologies of aortic stenosis are subdivided into acquired vs congenital. Regardless of the etiology, leaflet calcification is the common feature in aortic stenosis. Among individuals under the age of 70 years, bicuspid aortic valve disease is the most common cause of aortic stenosis. These congenitally abnormal valves typically develop progressive fibrosis and calcification of the leaflets over several decades and can present for surgery at any time, depending on the degree of deformity and rate of progression of the narrowing. Patients over the age of 70 years more typically have so-called senile aortic stenosis; these valves started out as normal valves, but developed thickening, calcification, and stenosis with aging. In a patient with aortic stenosis, careful clinical follow-up is considered mandatory to follow the progression of stenosis, and surgery is indicated at the onset of any symptoms.

Congenital malformations (typically presenting in bicuspid aortic valves) can result in a progressive fibrosis and calcification of the leaflets over several decades. The average rate reduction in valve orifice area has been estimated as about 0.12 cm^2/year, and valve orifice area is typically used to grade the severity of valve stenosis (Table 4) *(11)*. Nevertheless, progression of aortic stenosis does vary significantly, and the appearance of symptoms may not correlate well with the measured valve area. Therefore, careful clinical follow-up is mandatory, as it is difficult to predict an actual individual rate of progression.

Valve stenosis may also be associated with progressive outflow tract obstruction, which can then cause additional increases in left ventricular pressure. Concentric left ventricular hypertrophy is an early response that assists initially in maintaining normal left ventricular systolic wall tension and ejection fraction *(12)*. Once this response becomes inadequate, however, afterload increases and results in a gradual reduction in ejection fraction (Fig. 7). The initial ventricular hypertrophy itself may also be detrimental at this point, producing subendocardial ischemia even in the absence of coronary artery disease *(13,14)*. This results in further systolic and diastolic left ventricular dysfunction and may predispose such patients to both potentially larger degree of myocardial ischemia and higher mortality *(7,13, 15,16)*.

Although aortic stenosis may not produce symptoms early in its course, ultimately symptoms of angina, syncope, heart failure, or even sudden death may develop. Once symptoms are present, average survival is less than 2–3 years without intervention *(17–22)*. Therefore, a high degree of skepticism is necessary to make the diagnosis prior to the onset of symptoms so as to provide the best patient outcome. Aortic stenosis can be detected based on: (1) the presence of a systolic outflow murmur; (2) delayed/diminished carotid upstrokes; (3) sustained left ventricular impulse; (4) reduced intensity of the aortic component of the second heart sound; and/or (5) evidence of left ventricular hypertrophy on exam, chest x-ray, and electrocardiogram (ECG). Typically, echocardiography can be used to confirm the diagnosis of aortic stenosis and provide for the assessment of: (1) the mean transvalvular pressure gradient; (2) derived valve area; (3) left ventricle size (degree of hypertrophy) and function; or (4) the presence of other associated valvular disease. For more details on the clinical use of echocardiography, refer to Chapter 18.

Physicians who follow patients with known aortic stenosis commonly perform an annual history and physical examination and urge the patients to promptly self-report the development of any new symptoms. Although changes in valve area alone are not predictive, annual echocardiography is useful to assess progression of ventricular hypertrophy and alterations in function. In any case, development of any new symptoms (e.g., exertional chest discomfort, shortness of breath, or fainting spells) warrants additional echocardiography assessment given that aortic stenosis can progress rapidly, once such symptoms are present.

In patients considered for aortic valve replacement secondary to aortic stenosis, cardiac catheterization is generally indicated in individuals older than 40 years to assess for significant coronary artery disease. Additional indications include the assessment of the hemodynamic severity of the aortic stenosis when there is a discrepancy between clinical and echocardiographic findings and when there is evidence of pulmonary hypertension or other valvular or congenital disease. Complete evaluation must include: (1) the measurement of transvalvular flow (liters/minute), (2) the determination of the transvalvular pressure gradient (millimeters of mercury), and (3) the calculation of the effective valve area (square centimeters) *(23,24)*.

Medical therapy for aortic stenosis is relegated to the prevention of endocarditis and control of arterial hypertension. As most asymptomatic patients lead a normal life, no intervention

is warranted. Yet, once symptoms develop, prompt intervention should be offered to prevent morbidity and mortality. Interventional radiological therapy using balloon aortic valvotomy effectively reduces the transvalvular pressure gradient. This procedure uses percutaneously inserted catheters advanced into the aortic valve and inflated to fracture calcific deposits and separate fused commissures *(25–27)*. Although successful at providing clinical improvement, the postprocedure valve area rarely exceeds 1.0 cm^2, and aortic regurgitation is often created, increasing the burden on the left ventricle. The rate of significant complications (10%) and symptomatic restenosis (6 to 12 months) unfortunately makes balloon valvotomy an undesirable substitute for aortic valve replacement in most adults with aortic stenosis *(7)*.

Aortic valve replacement is technically possible at any age and is the treatment of choice for aortic stenosis in the majority of adults *(28)*. Yet, the degree of stenosis mandating surgery in asymptomatic patients remains an issue of debate. The degree of improvement following aortic valve replacement is directly related to preoperative left ventricular function; patients with a depressed ejection fraction caused by excessive afterload demonstrate significant improvement in left ventricular function after aortic valve replacement. Conversely, if depressed left ventricular function is caused by myocardial insufficiency, improvement in left ventricular function and resolution of symptoms may not be complete after valve replacement.

In general, survival is improved for patients undergoing aortic valve replacement, with the possible exception of a subset of patients with severe left ventricular dysfunction caused by coronary artery disease *(29,30)*. It is recommended that patients with severe aortic stenosis, with or without symptoms, who are undergoing coronary artery bypass surgery should undergo aortic valve replacement at the time of the revascularization procedure. Similarly, patients with moderate-to-severe aortic stenosis undergoing surgery for the replacement of other heart valves or the aortic root should also undergo aortic valve replacement as part of the surgical procedure. Hence, in the absence of contraindications, aortic valve replacement is indicated in virtually all symptomatic patients with severe aortic stenosis (Table 5).

Table 5
Aortic Valve Replacement in Aortic Stenosis

Symptomatic patients with severe aortic stenosis alone or:
- Undergoing coronary artery bypass surgery
- Undergoing surgery on the aorta or other heart valves

Patients with moderate aortic stenosis and:
- Undergoing coronary artery bypass surgery
- Undergoing surgery on the aorta
- Undergoing surgery on other heart valves

Asymptomatic patients with severe aortic stenosis and left ventricular systolic dysfunction typified by:
- Abnormal response to exercise (e.g., hypotension)
- Ventricular tachycardia
- Marked or excessive left ventricular hypertrophy (>15 mm)
- Valve area <0.6 cm^2
- Prevention of sudden death without the findings listed

Source: From ref. *7*.

Table 6
Etiologies of Aortic Regurgitation
(Subdivided by Presentation Time)

Acute	• Infective endocarditis • Aortic dissection • Trauma
Chronic	• Idiopathic aortic root dilation • Congenital bicuspid valves • Calcific degeneration • Rheumatic disease • Infective endocarditis • Systemic hypertension • Myxomatous proliferation • Ascending aortic dissection • Marfan syndrome • Syphilitic aortitis • Rheumatoid arthritis • Osteogenesis imperfecta • Giant cell aortitis • Ehlers-Danlos syndrome • Reiter's syndrome • Discrete subaortic stenosis • Ventricular septal defects with aortic cusp prolapse

3.1.2. Aortic Regurgitation

Aortic regurgitation results from a structural defect in the aortic valve that allows blood flow to reverse direction across the valve during diastole. The etiologies of aortic regurgitation are best discussed if the disease is divided into acute or chronic aortic regurgitation (Table 6). The majority of such lesions result in chronic aortic regurgitation with insidious dilation of the left ventricle. In contrast, lesions responsible for acute aortic regurgitation may result in sudden catastrophic elevation of left ventricular filling pressure, reduction in cardiac output, and/or sudden death.

3.1.2.1. Chronic Aortic Regurgitation

Valve damage that results in progressively larger retrograde flow across the aortic valve produces the condition of chronic aortic regurgitation. In this situation, aortic regurgitation ultimately results in a combined volume and pressure overloaded left ventricle. Initially, the heart compensates by left ventricular dilation to accommodate a larger volume without changing filling pressures and by ventricular hypertrophy, allowing ejection of a larger total stroke volume *(31)*. The majority of such patients remain asymptomatic for prolonged periods of compensation, during which time they maintain forward stroke volume within the normal ranges. Once the left ventricle can no longer compensate, patients may present with symptoms of dyspnea and exertional angina, reflecting declining systolic function, elevated filling pressures, or diminished coronary flow reserve of the hypertrophied myocardium *(32)*. Several natural history studies have identified age and left ventricular end-systolic pressure (or volume) as predictive factors associated with higher risk of mortality in this clinical population (Table 7) *(7)*.

Table 7
Natural History of Aortic Regurgitation

Asymptomatic patients with normal left ventricular systolic function	• Progression to symptoms and/or left ventricular dysfunction	<6%/year
	• Progression to asymptomatic left ventricular dysfunction	<3.5%/year
	• Sudden death	<0.2%/year
Asymptomatic patients with left ventricular systolic dysfunction	• Progression to cardiac symptoms	>25%/year
Symptomatic patients	• Mortality rate	
	♦ With angina	>10%/year
	♦ With heart failure	>20%/year

Although the progression of asymptomatic aortic regurgitation is slow, approximately one-fourth of patients will develop systolic dysfunction, or even die, before the onset of warning symptoms *(7)*. Therefore, quantitative evaluation of left ventricular function with echocardiography is necessary because a serial history and physical exam alone are insufficient.

The clinical diagnosis of chronic severe aortic regurgitation by a trained physician can be made in the presence of a diastolic murmur (the third heart sound) or a rumble (Austin-Flint sign) on auscultation, combined with a displaced left ventricular impulse and wide pulse pressure *(33,34)*. Similar to aortic stenosis, the chest x-ray and ECG will reflect left ventricular enlargement/hypertrophy and may elicit evidence of conduction disorders. Echocardiography is then indicated to: (1) confirm the diagnosis of aortic regurgitation; (2) assess valve morphology; (3) estimate the severity of regurgitation; (4) assess aortic root size; and (5) assess left ventricular dimension, mass, and systolic function. If the patient has severe aortic regurgitation and is sedentary or has equivocal symptoms, exercise testing is helpful to assess the following: functional capacity, symptomatic responses, and the hemodynamic effects of exercise.

In patients who are symptomatic on initial evaluation, cardiac catheterization and angiography are typically indicated if the echocardiogram is of insufficient quality to assess left ventricular function and to provide additional information as to the severity of aortic regurgitation or for the subsequent evaluation of coronary artery disease for possible revascularization therapy. The ultimate aim of any serial evaluation of the asymptomatic patient with chronic aortic regurgitation is to detect the onset of symptoms and objectively assess changes in left ventricular size and function that may occur in the absence of physical symptoms (Fig. 6)**.** Medical therapy for aortic regurgitation is primarily based on the use of vasodilating agents, which are believed to improve forward stroke volume and reduce regurgitant volume; the use of such agents can often result in regression of left ventricular dilation and hypertrophy.

Initial left ventricular systolic dysfunction in chronic aortic regurgitation is associated with increased afterload pressure and is considered reversible with full recovery of left ventricular size and function following aortic valve replacement *(7)*. However, as the ventricle becomes more hypertrophic and dilation progresses the chamber to a more spherical geometry, depressed myocardial contractility (rather than volume overload) is responsible for the systolic dysfunction. At this stage, neither return of normal left ventricular function nor improved long-term survival have been documented after aortic valve replacement *(7)*. For patients with chronic aortic regurgitation, left ventricular systolic function and end-systolic size have been identified as the most important determinants of postoperative survival and normalization of left ventricular function with aortic valve replacement *(7)*.

In addition, aortic valve replacement and aortic root construction are indicated in patients with proximal aortic disease and aortic regurgitation of any severity when the degree of aortic root dilation reaches or exceeds 50 mm (as commonly assessed by echocardiography) *(35)*. Importantly, the surgical options for treating aortic regurgitation are expanding, with growing experience in aortic homografts, pulmonary autografts, unstented tissue valves, and aortic valve repairs. It is conceivable that the thresholds for recommending operations may even be reduced, should these techniques ultimately demonstrate improved long-term survival or reduce postoperative valve complications.

3.1.2.2. Acute Aortic Regurgitation

When damage to the aortic valve is acute and severe, the subsequent and sudden large regurgitant volumes that return into the left ventricle will decrease the functional forward stroke volume dramatically. In contrast to chronic aortic regurgitation, in such acute cases there is no time for compensatory ventricular hypertrophy and dilation to develop. As a result, the considered typical exam findings of ventricular enlargement and diastolic murmur associated with chronic aortic regurgitation are absent. Instead, the patient with acute aortic regurgitation presents with pronounced tachycardia, pulmonary edema, or potentially life-threatening cardiogenic shock.

Echocardiography, which is considered crucial in the initial workup of acute aortic regurgitation, will likely demonstrate a rapid equilibration of aortic and left ventricular diastolic pressure and may provide some insights regarding the etiology of aortic regurgitation. Echocardiography also allows a rapid assessment of the associated valve apparatus, the aorta, and the degree of pulmonary hypertension (if tricuspid regurgitation is present). Transesophageal echocardiography is indicated when aortic dissection is suspected *(36–38)*. Importantly, acute aortic regurgitation resulting from aortic dissection is a known surgical emergency requiring prompt identification and management. Cardiac catheterization, aortography, and coronary

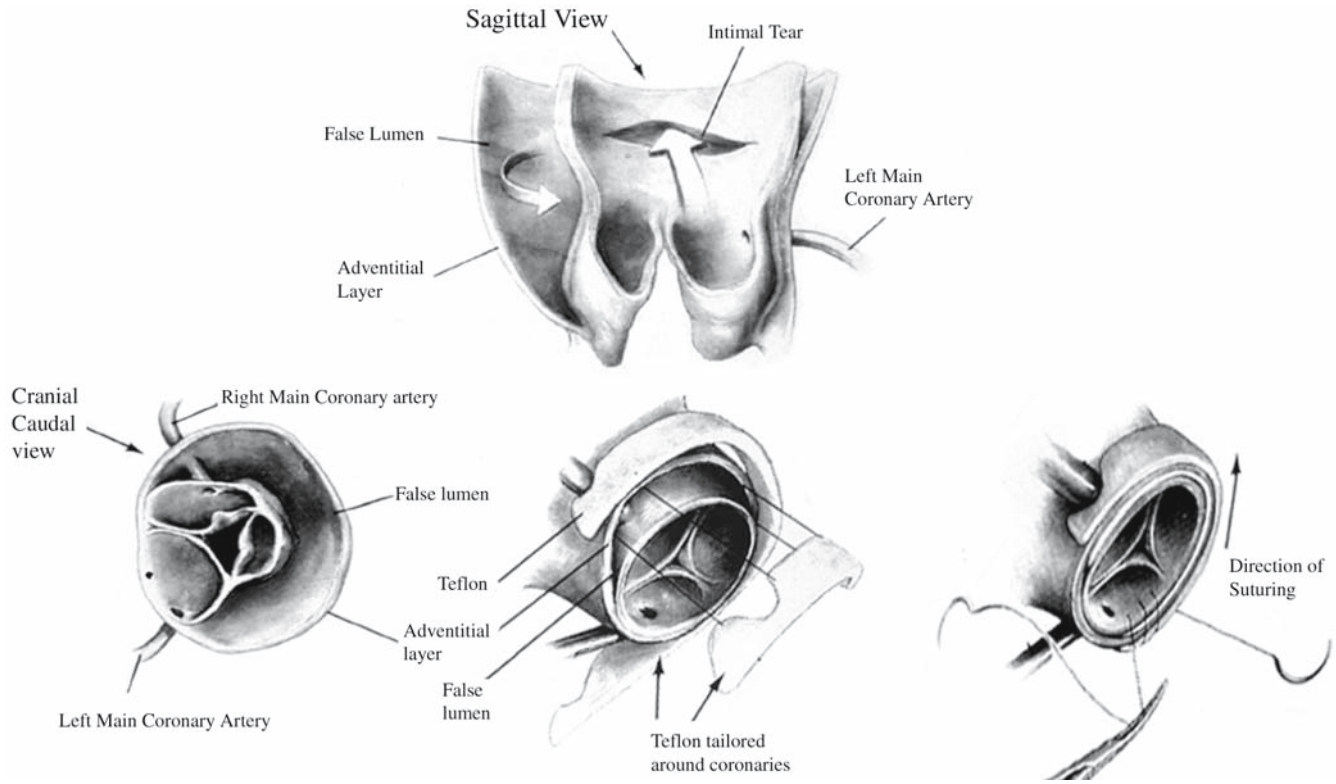

Fig. 8. Aortic aneurysm repair using a Teflon felt reinforcement technique preserving the aortic valve and coronary arteries. From Yun, K.L. and Miller, D.C. Technique of aortic valve preservation in acute Type A aortic dissection, in *Operative Techniques in Cardiac and Thoracic Surgery*, (Cox, J.L. and Sundt III, T.M., eds.), Saunders, Philadelphia, PA, pp. 68–81. © 2003, with permission from Elsevier.

angiography are important components of such an evaluation of aortic dissection with acute aortic regurgitation and thus should be performed if these procedures do not unduly delay the required urgent surgery. Following trauma, computed tomographic imaging is useful in obtaining the appropriate clinical status and underlying diagnosis.

Nevertheless, appropriate treatment of acute aortic regurgitation is dependent on the etiology and severity of the disease. For example, only antibiotic treatment may be required in a hemodynamically stable patient with mild acute aortic regurgitation resulting from infective endocarditis. Conversely, severe acute aortic regurgitation is a surgical emergency, particularly if hypotension, pulmonary edema, or evidence of low output are present. In such cases, temporary preoperative management may include the use of agents such as nitroprusside (to reduce afterload) and inotropic agents such as dopamine or dobutamine (to augment forward flow and reduce left ventricular end-diastolic pressure). Intraaortic balloon counterpulsation is contraindicated in such patients, and β-blockers should be used cautiously because of their potential to reduce output further by blocking the compensatory tachycardia. Mortality associated with acute aortic regurgitation is usually the result of pulmonary edema, ventricular arrhythmias, electromechanical dissociation, or circulatory collapse.

In general, aortic valve replacement is the treatment of choice in aortic regurgitation. In cases of aortic disease resulting in aortic regurgitation, aneurysm repairs (Fig. 8) or aortic root replacements (Figs. 9 and 10) are considered clinically effective. Aortic root replacement with a homograft or autograft should be offered to patients in whom anticoagulation is contraindicated (e.g., elderly with risk, women of childbearing years) as the tissue valve graft does not require anticoagulation. In addition, patients with disease resulting from endocarditis benefit as a homograft appears to have more resistance to infection. Finally, although the use of mechanical valves is effective, the prosthesis may impose a clinically relevant degree of stenosis in certain patients because of unavoidable size mismatch. Homografts and autografts are superior as they can be tailored to provide a larger outflow tract *(39)*. In certain situations, repair of the aorta may involve the use of an artificial conduit using materials such as Dacron (Fig. 10).

Careful postaortic valve replacement follow-up is necessary during the early and long-term postoperative course to evaluate both prosthetic valve and left ventricular function. An excellent predictor of long-term success of aortic valve replacement is a reduction in left ventricular end-diastolic volume within the first 14 days after the operation. It should be emphasized that as much as 80% of the overall reduction in end-diastolic volume that will occur does so in this time period. In addition, the degree of regression in left ventricular dilation correlates well with the magnitude of increase in ejection fraction *(40)*. Nevertheless, long-term follow-up should include an exam at 6 months postaortic valve replacement and then yearly if the clinical course is uncomplicated. Note that serial postoperative

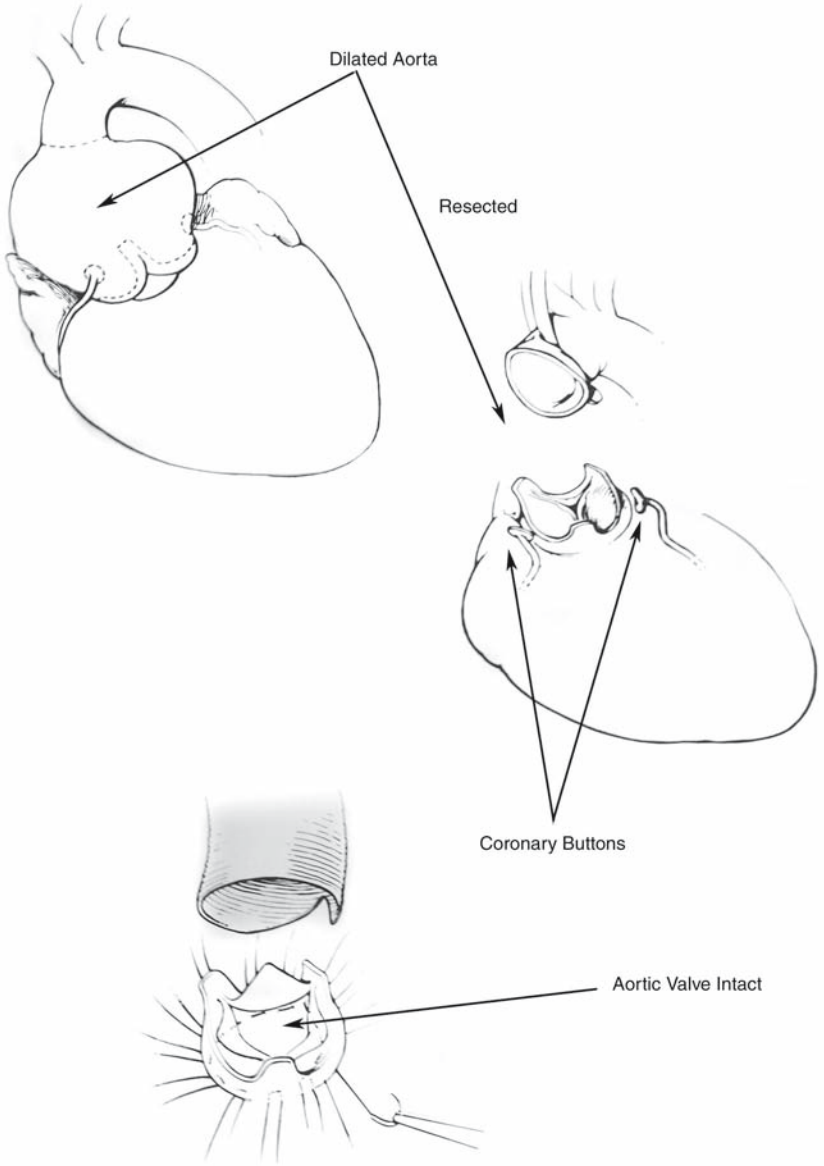

Fig. 9. David procedure for aortic root replacement. The dilated aorta is resected, sparing the aortic valve and coronary buttons. The repair is then completed with insertion of a graft with reimplantation of the coronary arteries. Adapted from Smedira, N. G., (2003) Mitral valve replacement with a calcified anulus, in *Operative Techniques in Cardiac and Thoracic Surgery*, (Cox, J.L. and Sundt III, T.M., eds.), Saunders, Philadelphia, PA, pp. 2–13. © 2003, with permission from Elsevier.

echocardiograms after the initial early postoperative study are usually not indicated. However, repeat echocardiography is warranted at any point when there is: (1) evidence of a new murmur, (2) questions of prosthetic valve integrity, or (3) concerns about adequate left ventricular function.

3.2. Diseases of the Mitral Valve

Diseases of the mitral valve can be subdivided in a similar fashion as those affecting the aortic valve: stenosis and regurgitation. The normal anatomy of the mitral valve consists of a pair of leaflets attached to the left ventricle by chordae tendineae. Normal mitral valve area ranges between 4.0 and 5.0 cm^2. However, in the case of mitral stenosis, symptoms do not typically develop until the functional valve area is reduced to less than 2.5 cm^2 *(41)*. For more details on valve anatomy, refer to Chapter 3 and the Visible Heart® CD.

3.2.1. Mitral Stenosis

Stenosis of the mitral valve orifice typically produces a funnel-shaped mitral apparatus described to resemble a "fish mouth," which then hinders normal diastolic filling of the left ventricle. Roughly 60% of all patients with mitral stenosis present with a history of rheumatic fever *(42,43)*. Three typical pathological processes are observed in such patients: (1) leaflet thickening and calcification; (2) commissural and chordal fusions; or (3) a combination of these processes *(44,45)*. Yet, congenital malformations of the mitral valve are usually responsible for mitral stenosis observed in infants and

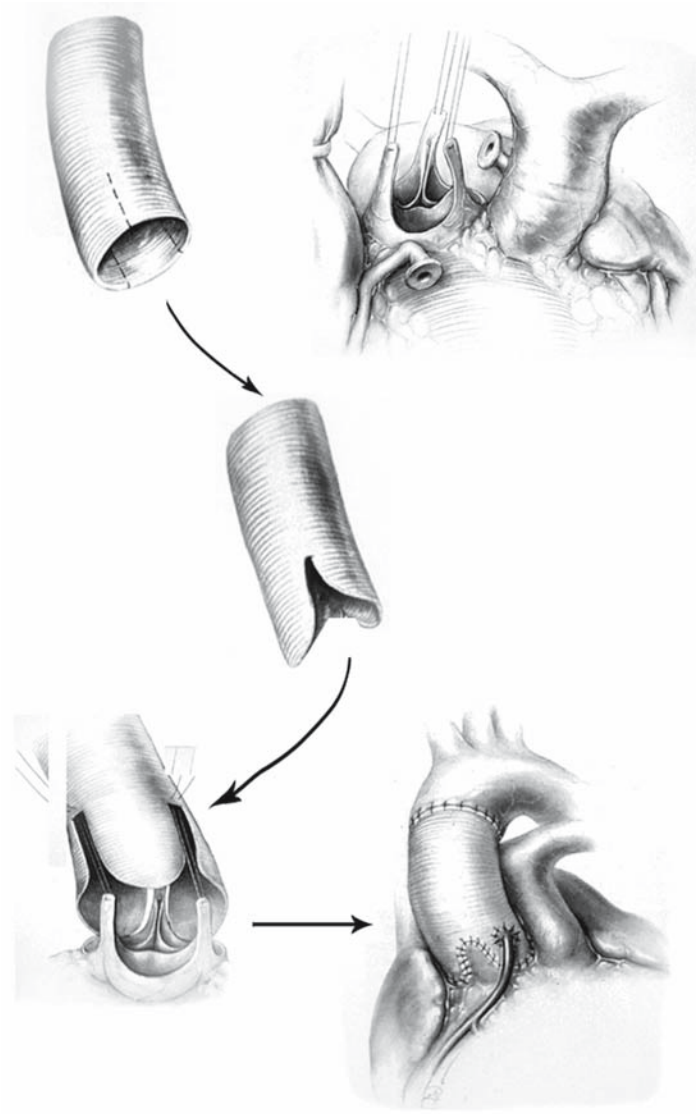

Fig. 10. Aortic root replacement using Dacron graft as the technique used for correct sizing is demonstrated for suturing in place to yield the final graft implantation along with coronary reimplantation. Adapted from M. Yacoub, Valve-conserving operation for aortic root aneurysm or dissection, in *Operative Techniques in Cardiac and Thoracic Surgery*, Vol. 1, No. 1 (Cox, J.L. and Sundt III, T.M., eds.), Saunders, Philadelphia, PA, pp. 57–67. © 2003, with permission from Elsevier.

children *(45)*. Overall, women (at a rate of 2:1) account for the majority of mitral stenosis cases *(42,43,46)*. Other entities can also simulate the clinical features of rheumatic mitral stenosis, such as left atrial myxoma, infective endocarditis, and mitral annulus calcification in the elderly.

Mitral stenosis is a slowly progressive disease with a typical mean age of presentation of symptoms in the fifth to sixth decade of life *(47,48)*. Diagnosis of mitral stenosis may be made solely on the presence of abnormal physical exam findings or may be suggested by symptoms of fatigue, dyspnea, frank pulmonary edema, atrial fibrillation, or embolus *(43)*. In the asymptomatic patient, survival is 80% at 10 years, with 60% of these patients eliciting no progression of symptoms *(7)*. However, once symptoms related to pulmonary hypertension develop, to date there is a dismal 0–15% 10-year survival rate *(7)*. Common causes of death in the untreated patients with mitral stenosis are caused by: (1) progressive heart failure (60–70%); (2) systemic embolism (20–30%); (3) pulmonary embolism (10%); or (4) infection (1–5%) *(45,46)*.

Shortness of breath (dyspnea), precipitated by exercise, emotional stress, infection, pregnancy, or atrial fibrillation, is typically the first symptom to present in patients with mild mitral stenosis *(49)*. Yet, as the obstructions across the mitral valve increase, there will typically be progressive symptoms of dyspnea as the left atrial and pulmonary venous pressures increase *(50)*. Increased pulmonary artery pressures and distension of the pulmonary capillaries can lead to pulmonary edema, which occurs as pulmonary venous pressure exceeds that of plasma

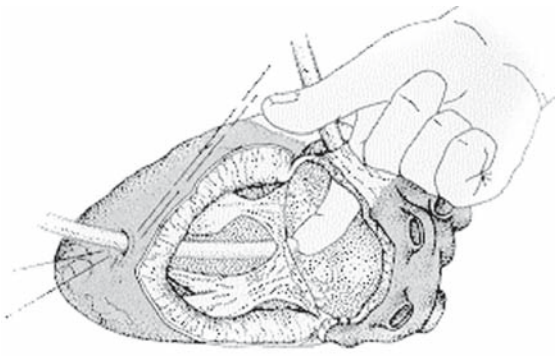

Fig. 11. Treatment of mitral stenosis using the finger fracture closed mitral commissurotomy technique. Adapted from Braunwald (1992), *Heart Disease* (Zipes, D. P., ed.), Saunders, Philadelphia, PA, p. 1016. © 1992, with permission from Elsevier.

oncotic pressure. Subsequently, the pulmonary arterioles will elicit vasoconstriction, intimal hyperplasia, and medial hypertrophy, which then further exacerbates pulmonary arterial hypertension.

Commonly, the diagnosis of mitral stenosis can be made based on patient history, physical examination, chest x-ray, and ECG**.** For example, at the initial examination, a patient may be asymptomatic although abnormal physical findings, including a diastolic murmur, may be present *(47,48)*. At this point, the diagnostic imaging tool of choice is 2D and Doppler transthoracic echocardiography. Transesophageal echocardiography or cardiac catheterization are not required unless questions concerning diagnosis remain *(7)*. Yet, heart catheterization is indicated to: (1) assess the potential for coronary artery disease or aortic valve disease; (2) assess pulmonary artery pressure; (3) perform balloon valvotomy; or (4) evaluate the situation when the clinical status of a symptomatic patient is not consistent with the echocardiography findings.

Typically, echocardiography is capable of providing an assessment of: (1) the morphological appearance of the mitral valve apparatus; (2) ventricular chamber size/function; (3) the mean transmitral gradient *(51,52)*; (4) the relative mitral valve area; and (5) the pulmonary artery pressures *(53)*. If necessary, noninvasive dobutamine or exercise stress testing can be completed with either the patient supine (using a bicycle) or upright (on a treadmill) to assess changes in heart rate and blood pressure in response to their overall exercise tolerance. Patients who are symptomatic with a significant elevation of pulmonary artery pressure (>60 mmHg), mean transmitral gradient (>15 mmHg), or pulmonary artery wedge pressure (>25 mmHg) on exertion have, by definition, a hemodynamically significant mitral stenosis that likely requires further intervention *(7)*.

In mitral stenosis, medical treatment is typically indicated for the prevention of emboli (10–20%)**,** which is primarily associated with the onset of atrial fibrillation *(42,43,54–56)*. Atrial fibrillation ultimately develops in 30–40% of patients with symptomatic mitral stenosis, and importantly, about 65% of all embolic events occur within the first year of the onset of atrial fibrillation *(42,43)*. The etiology behind atrial fibrillation is thought to be disruption of the normal conduction pathways caused by structural changes in the myocardium resulting from a pressure/volume overloaded atrium or, in fewer cases, rheumatic fibrosis of the atrium *(48)*. Development of atrial fibrillation in mitral stenosis occurs more commonly in older patients and has been associated with a decreased 10-year survival rate (25 vs 46%) *(43,46)*.

In addition to the thromboembolic potential, acute onset of atrial fibrillation can herald sudden deterioration in patients with mitral stenosis. This is considered secondary to an acute reduction in left ventricular ejection fraction and elevated pulmonary artery pressures, which thus result from loss of the atrial contribution to left ventricular filling. Urgent treatment of an acute episode of atrial fibrillation with a rapid rate consists of: (1) anticoagulation with heparin; (2) heart rate control (digoxin, calcium channel blockers, β-blockers, or amiodarone); or (3) electrical cardioversion. It should be noted that, in patients with atrial fibrillation for more than 24 to 48 h without anticoagulation, cardioversion is associated with an increased risk of embolism.

In chronic or recurrent atrial fibrillation resistant to prevention or cardioversion, heart rate control (digoxin, calcium channel blockers, β-blockers, or amiodarone) and long-term anticoagulation are considered the mainstays of therapy today *(56,57)*. Yet, use of anticoagulation for patients with mitral stenosis who have not had atrial fibrillation or embolic events is not indicated secondary to the risk of bleeding complications.

The principle for treating symptomatic mitral stenosis rests on the alleviation of the fixed left ventricular inflow obstruction, thereby reducing the transvalvular gradient. Methods of disrupting the fused valve apparatus (open or closed mitral commissurotomy or percutaneous mitral balloon valvotomy) or mitral valve replacement have demonstrated significant postprocedural improvements in both reducing symptoms and increasing survival. The timing of intervention is related to the severity of disease; the method of intervention chosen is based on: (1) morphology of the mitral valve apparatus, (2) presence of other comorbid diseases, and (3) expertise at each specific center. Significant calcification, fibrosis, and subvalvular fusion of the valve apparatus can make either commissurotomy or percutaneous balloon valvotomy less likely to be successful. It should also be noted that the presence of mitral regurgitation is a contraindication for valvotomy/commissurotomy and is considered best treated with mitral valve replacement.

Closed commissurotomy is a surgical technique that uses finger fracture of the calcified valve (Fig. 11). This procedure has the advantage of not requiring cardiopulmonary bypass; however, the operator is not afforded direct visual examination of the valve apparatus. In contrast, open commissurotomy, which uses cardiopulmonary bypass, has gained favor in the United States because it allows inspection of the mitral valve apparatus under direct vision. During this procedure, division of the commissures, splitting of fused chordae tendineae/papillary muscles, debridement of calcium deposits *(7)*, or mitral valve replacement can be completed to attain optimal results. The 5-year reoperation rate following open commissurotomy has been reported to be between 4 and 7%, and the 5-year complication-free survival rate ranges from 80% to 90%.

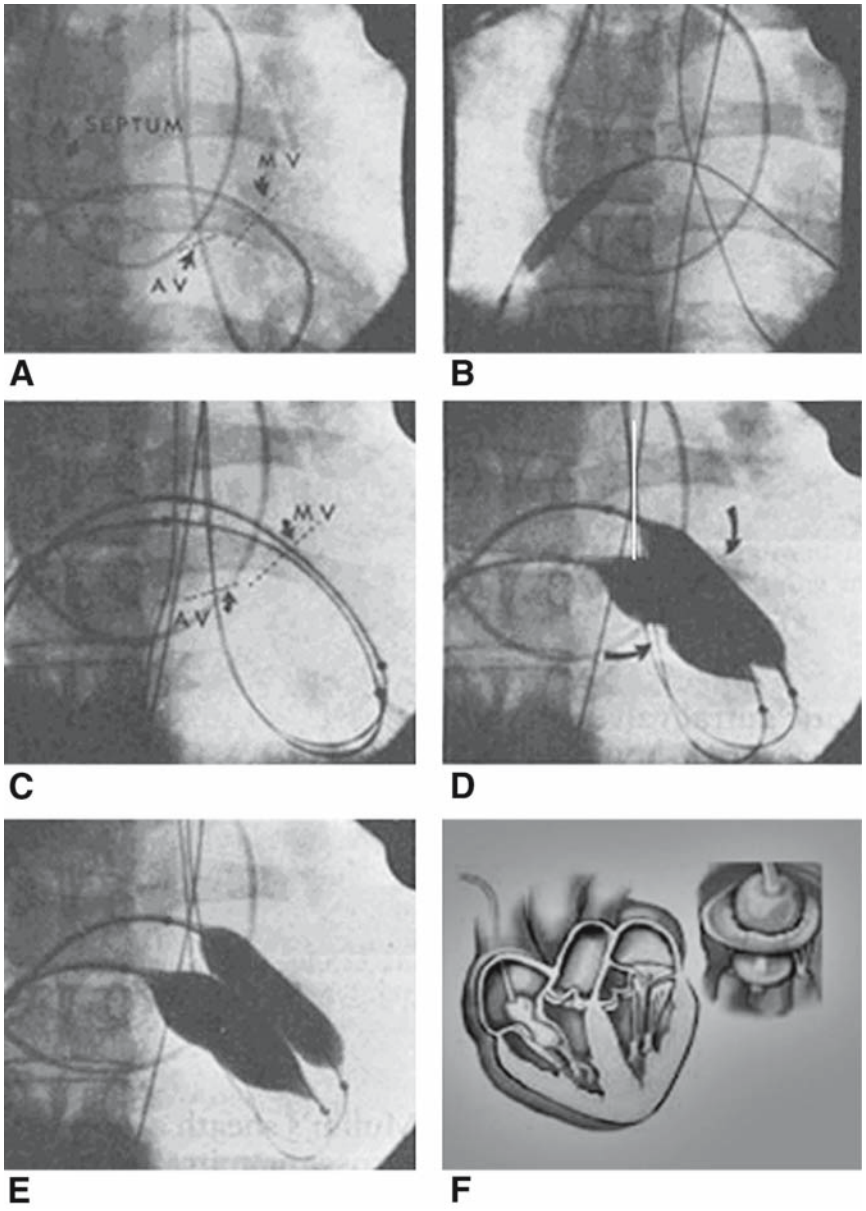

Fig. 12. Treatment of mitral stenosis using balloon valvotomy. Sequence of percutaneous mitral valvotomy: **(A)** Floating balloon catheter in position across the atrial septum through the mitral and aortic valves. The tip is in the ascending aorta. **(B)** An 8-mm dilating balloon catheter enlarging the atrial septal puncture site. **(C)** Two 20-mm dilating balloon catheters advanced into position across the stenotic mitral valve over two separate 0.038-in transfer guidewires. **(D)** Partially inflated dilating balloon catheters across the mitral valve. Note the "waist" produced by the stenotic valve (arrows). **(E)** Fully inflated dilating balloon catheters in position across the mitral valve. **(F)** Illustration of balloon commissurotomy technique. Adapted from Braunwald (1992), *Heart Disease* (Zipes, D.P., ed.) Saunders, Philadelphia, PA. © 2003, with permission from Elsevier.

In centers with highly skilled operators, percutaneous balloon valvotomy is the initial procedure of choice for the symptomatic patient with moderate-to-severe mitral stenosis, those with favorable valve morphology and no significant mitral regurgitation or left atrial thrombus (Fig. 12). Immediate reduction in the transvalvular gradient (50–60%) is associated with gradual regression of pulmonary hypertension over several months *(7)*. If selected appropriately, 80 to 95% of patients undergoing the procedure will achieve a functional mitral valve area larger than 1.5 cm^2 and a resultant decrease in left atrial pressure without complication.

Yet, potential acute complications include mitral regurgitation (10%), an atrial septal defect (5%), left ventricle perforations (0.5–4.0%), emboli formation (0.5–3%), myocardial infarctions (0.3–0.5%), and increased mortality (<1%) *(58)*. Patients with valvular calcification, thickened fibrotic leaflets with decreased mobility, and subvalvular fusions have a higher incidence of acute complications following balloon valvotomy

Table 8
Mitral Valve Replacement for Mitral Stenosis

Moderate-to-severe mitral stenosis (mitral valve area <1.5 cm^2)
- With New York Heart Association functional class III–IV symptoms.
- Who are not considered candidates for percutaneous balloon valvotomy or mitral valve repair.

Patients with severe mitral stenosis (mitral valve area <1 cm^2)
- With severe pulmonary hypertension (pulmonary artery systolic pressure >60 to 80 mmHg).
- With New York Heart Association functional class I–II symptoms who are not considered candidates for percutaneous balloon valvotomy or mitral valve repair.

Source: From ref. *7*.

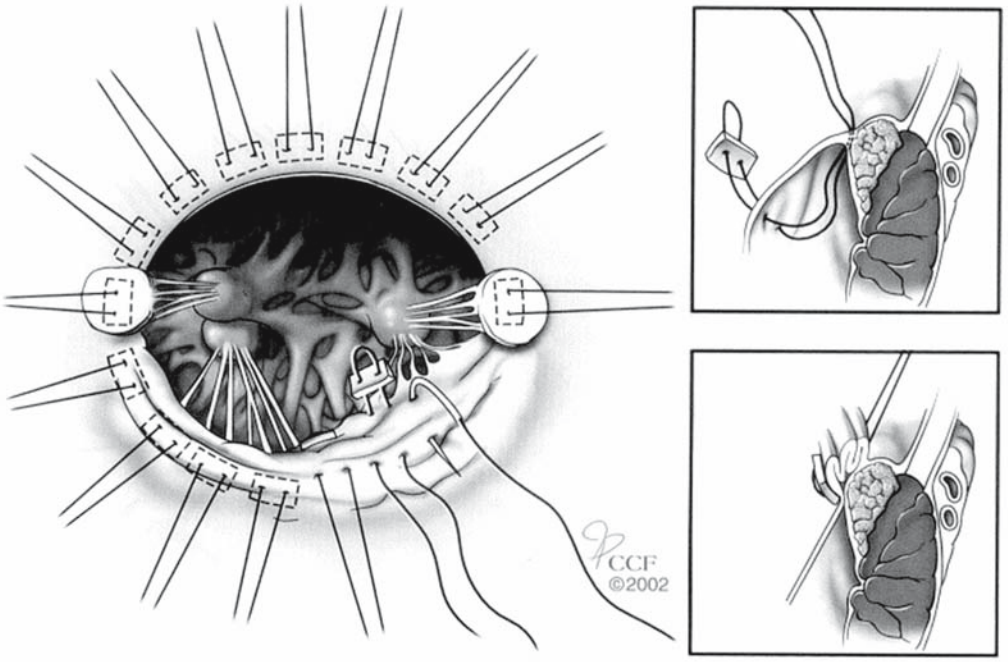

Fig. 13. Placement of circumferential sutures and plication of the anterior leaflet of the mitral valve. Adapted from Smedira, N. G., (2003) Mitral valve replacement with a calcified anulus, in *Operative Techniques in Cardiac and Thoracic Surgery*, Vol. 8, No. 1 (Cox, J.L., ed.), Saunders, Philadelphia, PA, pp. 2–13. © 2003, with permission from Elsevier.

and a higher rate of recurrent stenosis on follow-up. Presence of left atrial thrombus, typically detected by transesophageal echocardiography, is a relative contraindication and, at a minimum, warrants 3 months of oral warfarin anticoagulation in an attempt to resolve the thrombus prior to the procedure. A postprocedure echocardiogram 72 h after the procedure is useful to assess postoperative hemodynamics and exclude significant complications such as mitral regurgitation, left ventricular dysfunction, or an atrial septal defect. However, recurrent symptoms have been reported to occur in as many as 60% of patients 9 years postprocedure *(53,59,60)*; it should be noted that recurrent stenosis accounts for symptoms in less than 20% of such patients *(59)*. In patients with an adequate initial result, progressive mitral regurgitation and development of other valvular or coronary problems are more frequently responsible for recurrent symptoms *(59)*. Thus, in patients presenting with symptoms late after commissurotomy, a comprehensive evaluation is required to look for other causes.

Mitral valve replacement is an accepted surgical procedure for patients with severe mitral stenosis who are not candidates for surgical commissurotomy or percutaneous mitral valvotomy (Table 8, Figs. 13 and 14). In addition, patients with recurrent severe symptoms, severe deformity of the mitral apparatus, severe mitral regurgitation, or a large atrial septal defect should be offered mitral valve replacement.

The risk of mitral valve replacement is also highly dependent on age, left ventricular functional status, cardiac outputs, presence of comorbid medical problems, and concomitant coronary artery disease. More specifically, morbidity and mortality associated with mitral valve replacement are directly correlated with age, with risk in a young healthy person of less than 5%, increasing to as high as 10–20% in the older patient with concomitant medical problems or pulmonary hypertension. Mitral valve replacement is further complicated by: (1) the potential for embolic events, (2) the need for (and risk of) long-term anticoagulation therapy, and/or (3) the potential for valve thrombosis, dehiscence, infection, or malfunction.

3.2.2. Mitral Regurgitation

The common etiologies for mitral regurgitation include mitral valve prolapse secondary to myxomatous degeneration, rheumatic heart disease, coronary artery disease, infective endocarditis, and collagen vascular disease. As with aortic regurgitation, mitral regurgitation has both acute and chronic presentations. In some cases, mitral regurgitation caused by ruptured chordae tendineae or infective endocarditis may present as both acute and severe. Alternatively, mitral regurgitation may worsen gradually over a prolonged period of time. Yet, these very different presentations of mitral regurgitation are both treated with surgical intervention as dictated by the character of the symptoms presented.

3.2.2.1. Acute Severe Mitral Regurgitation

In acute severe mitral regurgitation, a sudden volume overload is imposed on the left ventricle without time for typical compensatory left ventricular hypertrophy. Thus, a sudden drop in forward stroke volume and cardiac output occurs (cardiogenic shock), with simultaneous pulmonary congestion. In severe mitral regurgitation, the hemodynamic overload often cannot be tolerated, and mitral valve repair or replacement must be performed urgently.

The acute nature of this form of mitral regurgitation results in patients who almost always present with symptoms; in a physical exam, it may only be positive for a holosystolic murmur and a third heart sound. Transthoracic echocardiography is typically used to confirm the diagnosis and to assess the general degree of disruption of the mitral valve apparatus. Furthermore, the use of transesophageal echocardiography is the procedure of choice for evaluation of the mitral valve and is warranted if mitral valve morphology and regurgitation are still not clearly elucidated following transthoracic echocardiography. Note that it is the high level of detail provided by transesophageal echocardiography that is also helpful in demonstrating the anatomical cause of mitral regurgitation and, subsequently, directing successful surgical repair. Coronary arteriography is necessary before surgery in all patients older than 40 years. If necessary, myocardial revascularization should be performed during mitral valve surgery in those patients with concomitant coronary artery disease *(61,62)*.

If the patient is not a candidate for surgery or if preoperative stabilization is required, medical therapy can help to diminish the amount of mitral regurgitation, thus increasing forward output and reducing pulmonary congestion; it should be initiated promptly. In normotensive patients, nitroprusside has been used to increase the forward output not only by preferentially increasing aortic flow, but also by partially restoring mitral valve competence as the left ventricular size diminishes *(63,64)*. In hypotensive patients with severe reduction in forward output, aortic balloon counterpulsation can be employed to increase forward outputs and mean arterial pressures while diminishing mitral valve regurgitant volumes and left ventricular filling pressures. If infective endocarditis is the cause of acute mitral regurgitation, identification and treatment of the infectious organism is essential.

3.2.2.2. Chronic Asymptomatic Mitral Regurgitation

As with chronic aortic regurgitation, time for hypertrophy and chamber dilation is typically present in the patient presenting with chronic severe mitral regurgitation *(31,65)*. The dilation, or increase in left ventricular end-diastolic volume, is a compensatory mechanism that permits an increase in total stroke volume and allows for restoration of forward cardiac output *(66)*. At the same time, an increase in left ventricle and left atrial size accommodates the regurgitant volume with a lower filling pressure; consequentially, symptoms of pulmonary congestion abate. Thus, such patients may remain asymptomatic for variable, but significant, time periods; however, the prolonged burden of volume overload may eventually result in left ventricular dysfunction. At this time, contractile dysfunctions impair myocardial ejections, and end-systolic volume increases; there may also be further left ventricular dilations and increased left ventricular filling pressures. Therefore, correction of mitral regurgitation should occur at the diagnosis of severe mitral regurgitation irrespective of the presence or absence of symptoms.

Initial diagnosis of chronic mitral regurgitation is commonly accomplished by physical exam, which may demonstrate findings of left ventricular apical impulse displacement,

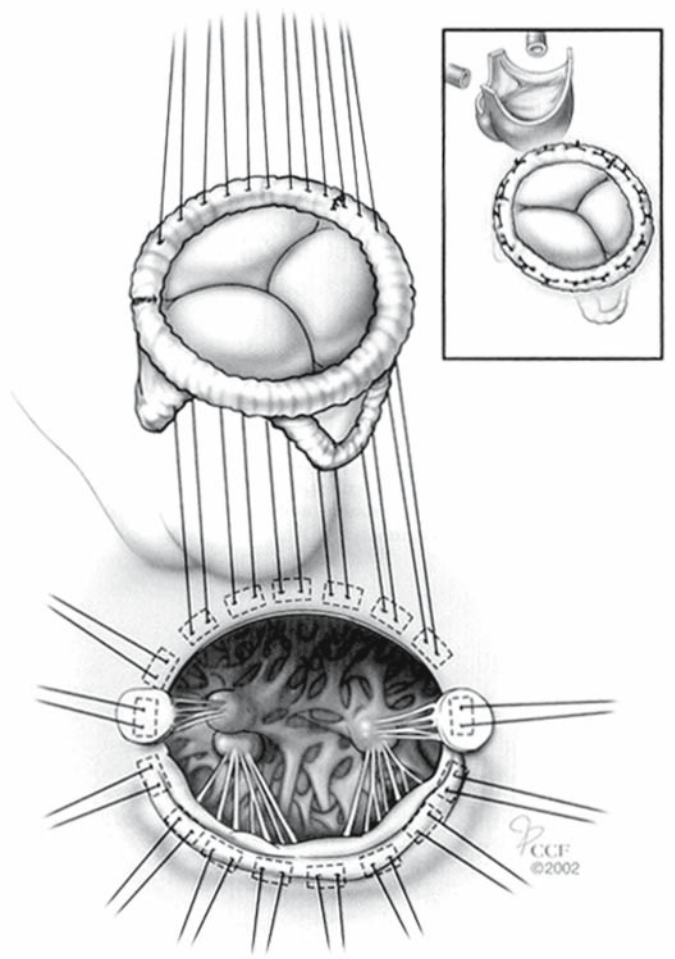

Fig. 14. Mitral valve positioning into the mitral oriface. Adapted from Smedira, N. G., (2003) Mitral valve replacement with a calcified anulus, in *Operative Techniques in Cardiac and Thoracic Surgery*, Vol. 8 No. 1 (Cox, J.L., ed.), Saunders, Philadelphia, PA, pp. 2–13. © 2003, with permission from Elsevier.

indicating that mitral regurgitation is severe and chronic and has likely caused cardiac enlargement. Typically, ECG and chest x-ray can be useful to evaluate rhythm changes and heart sizes, respectively. Nevertheless, an initial echocardiogram, including Doppler interrogation of the mitral valve, is considered indispensable in the management of the patient with mitral regurgitation. Such an echocardiogram typically provides a baseline estimation of left ventricle and left atrial volume, an estimation of left ventricular ejection fraction, and an approximation of the severity of regurgitation. Note that any presence of pulmonary hypertension is worrisome because it likely indicates advanced disease with a worsened prognosis *(67)*.

Serial follow-ups are used to assess changes in symptomatic status, left ventricular functions, and exercise tolerances. Annual echocardiography becomes necessary once patients demonstrate moderate mitral regurgitation. Left ventricular end-systolic dimensions (or volumes) can typically aid in the timing of mitral valve surgery. For example, an end-systolic dimension, which may be less load dependent than ejection fraction, should be less than 45 mm preoperatively to ensure normal postoperative left ventricular function *(66,68)*. In general, if patients become symptomatic, they should undergo mitral valve surgery even if left ventricular function is considered normal. Similar to acute mitral regurgitation, cardiac catheterization is also indicated if: (1) there is discrepancy between clinical and noninvasive findings; (2) there is a need for preoperative coronary assessment for potential revascularization at the time of mitral valve replacement; or (3) an absence of chamber enlargement raises the question of the accuracy of the diagnosis, which should then be assessed with ventriculography at cardiac catheterization.

To date, there is no generally accepted therapy for asymptomatic patients with chronic mitral regurgitation. In such patients who develop symptoms but have preserved left ventricular function, surgery is considered the most appropriate therapy. Atrial fibrillation is commonly associated with mitral regurgitation, and preoperative atrial fibrillation can be an independent predictor of reduced long-term survival after mitral valve surgery for chronic mitral regurgitation *(69)*. Atrial fibrillation should be treated with heart rate control (digitalis, calcium channel blockers, β-blockers, or amiodarone) and anticoagulation to avoid embolism *(70,71)*. Common predictors for the persistence of atrial fibrillation after successful valve surgery include the presence of atrial fibrillation for longer than 1 year or a left atrial size larger than 50 mm *(72)*. Although patients who develop atrial fibrillation also usually manifest other symptomatic or functional changes that would warrant mitral valve repair or replacement, today many clinicians would also consider the onset of episodic or chronic atrial fibrillation an indication, in and of itself, for surgery *(73,74)*.

Three categories of surgical procedures are now in vogue for correction of mitral regurgitation: (1) mitral valve repair, (2) mitral valve replacement with preservation of part or all of the mitral apparatus, and (3) mitral valve replacement with removal of the mitral apparatus. Each procedure has its advantages and disadvantages, as well as separate indications. In general, with the appropriate valve morphology and sufficient surgical expertise, mitral valve repair is the operation of choice. Yet, mitral valve repair may require longer extracorporeal circulation time and may occasionally fail, thus requiring mitral valve replacement. Valve calcification, rheumatic involvement, and anterior leaflet involvement all decrease the likelihood of repair, whereas uncalcified posterior leaflet disease is almost always repairable.

The primary advantage of repair is the avoidance of anticoagulation and prosthetic valve failure. In addition, postoperative left ventricular function and survival are improved with preservation of the mitral apparatus because the mitral apparatus is considered essential for maintenance of normal shape, volume, and function of the left ventricle *(7)*.

Similar advantages are gleaned with the use of mitral valve replacement with preservation of the mitral chordal apparatus, except that it adds both the risks of deterioration inherent in tissue valves and the need for anticoagulation with mechanical valves. Mitral valve replacement, in which the mitral valve apparatus is excised, should be performed only when the native valve and apparatus are so distorted by the preoperative pathology (rheumatic disease, for example), such that the mitral apparatus cannot be spared.

In an asymptomatic patient with normal left ventricular function, repair of a severely regurgitant valve may be offered as a means to: (1) preserve left ventricular size and function and (2) prevent the sequelae of chronic mitral regurgitation (Fig. 15). Similarly, this approach has proven successful in the hemodynamically stable patient with newly acquired severe mitral regurgitation as the result of a ruptured chordae or recent onset of atrial fibrillation. The timing of surgery in asymptomatic patients is indicated by the appearance of echocardiographic indicators of left ventricular dysfunction (i.e., left ventricular ejection fraction less than 60% or left ventricular end-systolic dimension above 45 mm). Mitral valve repair or replacement at this stage will likely prevent further deterioration in left ventricular function and improve survival *(69)*.

Patients with symptoms of congestive heart failure, despite normal left ventricular function as determined by echocardiography (ejection fraction greater than 60%, end-systolic dimension less than 45 mm), will likely require surgery. In both situations, mitral repair is preferred when possible. Mitral valve surgery is recommended for severe symptomatic mitral regurgitation with evidence of left ventricular systolic dysfunction; it is likely both to improve symptoms and to prevent further deterioration of left ventricular function *(75)*.

Ischemic mitral regurgitation is usually caused by left ventricular myocardial infarction, resulting in an associated papillary muscle dysfunction. The prognosis for such a patient with ischemic mitral regurgitation is substantially worse when compared with other etiologies *(62,76)*. Following an acute infarction with the development of severe mitral regurgitation, hypotension and pulmonary edema often occur. Hemodynamic stabilization, usually with insertion of an intraaortic balloon pump, is completed preoperatively, followed by coronary revascularization, which only rarely improves mitral valve function. Unlike the case with nonischemic mitral regurgitation, it is more difficult to demonstrate a benefit of repair over

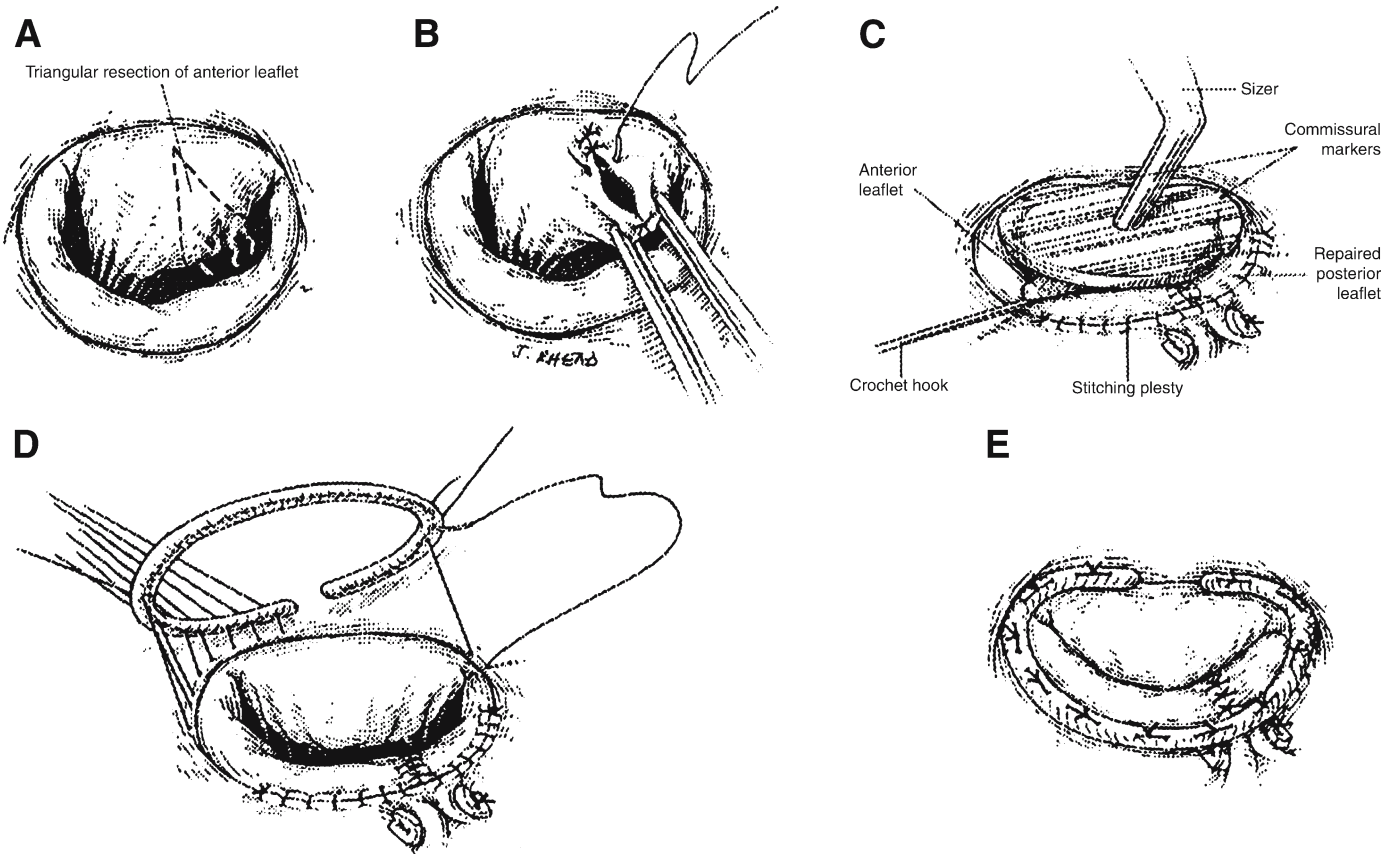

Fig. 15. Operative repair of the mitral valve using a technique developed by Carpentier. **(A)** Triangular resection of anterior leaflet; **(B)** anterior leaflet repair; **(C)** sizing of annulus; **(D)** annuloplasty ring suture technique; and **(E)** completed repair. Adapted from J.W. Kirklin (2003), *Cardiac Surgery*, 3rd Ed., Churchill Livingstone, New York, NY, pp. 673–675.

replacement with ischemic mitral regurgitation. In general, operative mortality increases, and survival is reduced in such patients older than 75 years with coronary artery disease, especially if mitral valve replacement must be performed *(77)*. In these patients, the goal of therapy is typically to first improve the quality of life rather than prolong it, and medical therapy may be utilized to a greater extent to control cardiac symptoms.

3.3. Tricuspid Valve Disease

Tricuspid valve disease can be subclassified as regurgitation, stenosis, or a combination of both; it is most commonly the result of rheumatic fever, with rare cases attributed to infective endocarditis, congenital anomalies, carcinoid causes, Fabry's disease, Whipple's disease, or methysergide therapy *(7)*. Rheumatic tricuspid disease commonly presents as a combination of tricuspid stenosis and tricuspid regurgitation. Furthermore, tricuspid disease commonly presents with concomitant mitral or aortic valve defects, because acute rheumatic fever is also a common etiology for these. It should be noted that right atrial myxomas or any type of large vegetations that produce an outflow tract obstruction will mimic stenosis; however, regurgitation may also result as it often causes associated damage to the leaflet apparatus.

Pure tricuspid regurgitation may result from rheumatic fever, infective endocarditis, carcinoid causes, rheumatoid arthritis, radiation therapy, anorectic drugs, trauma, Marfan's syndrome, tricuspid valve prolapse, papillary muscle dysfunction, or congenital disorders *(7)*. In addition, pressure/volume overload conditions that do not cause direct damage to the leaflets themselves, such as those associated with mitral stenosis and mitral regurgitation, typically cause ventricular enlargement, resultant tricuspid annular dilation, and thus pure tricuspid regurgitation *(7)*.

The clinical features of tricuspid stenosis include auscultation of a tricuspid opening snap and a characteristic murmur. Auscultation may reveal a holosystolic murmur in the lower left parasternal region that may increase on inspiration (Carvallo's sign). In rare instances, severe tricuspid regurgitation may produce systolic propulsion of the eyeballs, pulsatile varicose veins**,** or a venous systolic thrill and detectable murmur in the neck. Echocardiography is commonly used to: (1) assess tricuspid valve structure and function, (2) measure annular size, (3) evaluate right pressures, and (4) rule out other abnormalities influencing tricuspid valve function. Systolic pulmonary artery pressure estimations, combined with information about annular

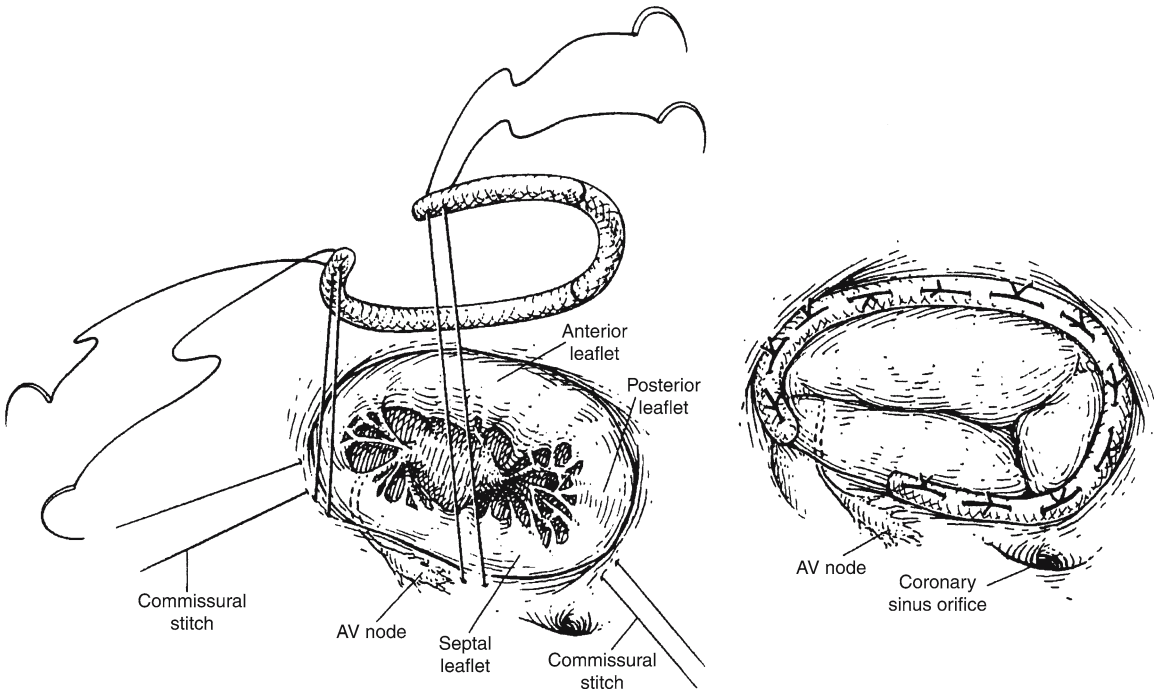

Fig. 16. Tricuspid annuloplasty procedure. AV, atrioventricular.

circumference, further improve the accuracy of clinical assessment *(7)*.

The etiology of tricuspid valve disease and the overall condition of the patient ultimately dictate the therapeutic approach. Tricuspid balloon valvotomy can be used to treat tricuspid stenosis; however, there is the potential for inducing severe tricuspid regurgitation. It has been documented that poor long-term outcome is associated with right ventricular dysfunction or systemic venous congestion associated with severe tricuspid regurgitation *(7)*.

When pulmonary hypertension is the underlying cause of tricuspid annular dilation, medical management alone may result in substantial improvement of tricuspid regurgitation and thus minimize the need for surgical intervention. Surgical options for treating tricuspid regurgitation include annuloplasty or valve replacement (Fig. 16). Tricuspid regurgitation annuloplasty is effective and can be optimized using intraoperative transesophageal echocardiography. Valve replacement with a low-profile mechanical valve or bioprosthesis is often necessary when the valve leaflets themselves are diseased, abnormal, or destroyed *(78)*. In both procedures, care must be taken to avoid causing damage to the conduction system. In such cases, use of biological prostheses is preferred to avoid the high rate of thromboembolic complications known to occur with mechanical prostheses placed in the tricuspid position. Combined tricuspid and mitral valve procedures are often completed in the same interventions, as in the setting of rheumatic disease; however, no long-term data regarding the value of such an approach exists. In patients with associated conduction defects, insertion of a permanent epicardial pacing electrode at the time of valve replacement is also suggested.

4. SUMMARY

The use of cross-circulation followed by the development of the bubble oxygenator for cardiopulmonary bypass was the focal point in the history of cardiac surgery. However, cardiac surgery may be considered still in its infancy, with most of the major developments occurring only in the last 50 years. Tremendous advances in the field of cardiac surgery are certain to result from the numerous ongoing efforts of researchers and clinicians alike.

This chapter was designed to give an introduction to the complex nature of valve disease. Several excellent textbooks have been written that provide greater detail for each valve procedure discussed. Such reference texts are valuable for both the clinician and the engineer interested in understanding the etiology and the current treatment techniques for valve disease. Nevertheless, this basis of understanding, along with the use of further animal and clinical research, will allow the development of the next generation of treatment options for heart valve disease.

ACKNOWLEDGMENT

We graciously thank Andrew L. Rivard MD for his thoughtful insights and diligent assistance with this chapter's preparation and revisions.

VISIBLE HEART® CD

Valve anatomy.

REFERENCES

1. Miller, G.W. (ed.) (2000) *King of Hearts*. Times Books, New York, NY.
2. Bolman, R.M., 3rd and Black, S.M. (2003) Open cardiac repair under direct vision: F. John Lewis and the University of Minnesota. *J Card Surg*. 18, 328–332; discussion 333.
3. Lewis, R.P., et al. (1966) Aortic valve replacement with the Starr-Edwards ball-valve prosthesis. Indications and results. *Am Heart J*. 71, 549–563.
4. Lillehei, C.W., et al. (1974) Heart-valve replacement with Lillehei-Kaster pivoting disk prosthesis. *N Y State J Med*. 74, 1426–1438.
5. Lillehei, C.W., Kaster, R.L., and Bloch, J.H. (1972) New central flow pivoting disk aortic and mitral prosthesis. Clinical experience. *N Y State J Med*. 72, 1738.
6. Emery, R.W., et al. (1978) A new cardiac valve prosthesis: in vitro results. *Trans Am Soc Artif Intern Organs*. 24, 550–556.
7. Bonow, R.O., et al. (1998) ACC/AHA guidelines for the management of patients with valvular heart disease. Executive summary. A report of the American College of Cardiology/American Heart Association Task Force on Practice Guidelines (Committee on Management of Patients With Valvular Heart Disease). *J Heart Valve Dis*. 7, 672–707.
8. Ross, D.N., Turrentine, M.W., Brown, J.W., and Levinson, M.M. (2003) *The Ross Procedure*. Forum Multimedia Publishing, Charlottesville, VA.
9. Edmunds, L.H., Jr., et al. (1996) Guidelines for reporting morbidity and mortality after cardiac valvular operations. Ad Hoc Liaison Committee for Standardizing Definitions of Prosthetic Heart Valve Morbidity of the American Association for Thoracic Surgery and the Society of Thoracic Surgeons. *J Thorac Cardiovasc Surg*. 112, 708–711.
10. Cheitlin, M.D., Douglas, P.S., and Parmley, W.W. (1994) Twenty-Sixth Bethesda conference: recommendations for determining eligibility for competition in athletes with cardiovascular abnormalities. Task Force 2: acquired valvular heart disease. *J Am Coll Cardiol*. 24, 874–880.
11. Otto, C.M., et al. (1992) Physiologic changes with maximal exercise in asymptomatic valvular aortic stenosis assessed by Doppler echocardiography. *J Am Coll Cardiol*. 20, 1160–1167.
12. Krayenbuehl, H.P., et al. (1988) Left ventricular systolic function in aortic stenosis. *Eur Heart J*. 9, E19–E23.
13. Marcus, M.L., et al. (1982) Decreased coronary reserve: a mechanism for angina pectoris in patients with aortic stenosis and normal coronary arteries. *N Engl J Med*. 307, 1362–1366.
14. Bache, R.J., et al. (1981) Regional myocardial blood flow during exercise in dogs with chronic left ventricular hypertrophy. *Circ Res*. 48, 76–87.
15. Koyanagi, S., Eastham, C., and Marcus, M.L. (1982) Effects of chronic hypertension and left ventricular hypertrophy on the incidence of sudden cardiac death after coronary artery occlusion in conscious dogs. *Circulation*. 65, 1192–1197.
16. Gaasch, W.H., et al. (1990) Tolerance of the hypertrophic heart to ischemia. Studies in compensated and failing dog hearts with pressure overload hypertrophy. *Circulation*. 81, 1644–1653.
17. Ross, J., Jr. and Braunwald, E. (1968) Aortic stenosis. *Circulation*. 38, 61–67.
18. Schwarz, F., et al. (1982) The effect of aortic valve replacement on survival. *Circulation*. 66, 1105–1110.
19. Sprigings, D.C. and Forfar, J.C. (1995) How should we manage symptomatic aortic stenosis in the patient who is 80 or older? *Br Heart J*. 74, 481–484.
20. Horstkotte, D. and Loogen, F. (1988) The natural history of aortic valve stenosis. *Eur Heart J*. 9, E57–E64.
21. Iivanainen, A.M., et al. (1996) Natural history of aortic valve stenosis of varying severity in the elderly. *Am J Cardiol*. 78, 97–101.
22. Kelly, T.A., et al. (1988) Comparison of outcome of asymptomatic to symptomatic patients older than 20 years of age with valvular aortic stenosis. *Am J Cardiol*. 61, 123–130.
23. Cheitlin, M.D., et al. (1997) ACC/AHA guidelines for the clinical application of echocardiography. A report of the American College of Cardiology/American Heart Association Task Force on Practice Guidelines (Committee on Clinical Application of Echocardiography). Developed in collaboration with the American Society of Echocardiography. *Circulation*. 95, 1686–1744.
24. Gibbons, R.J., et al. (1997) ACC/AHA guidelines for exercise testing. A report of the American College of Cardiology/American Heart Association Task Force on Practice Guidelines (Committee on Exercise Testing). *J Am Coll Cardiol*. 30, 260–311.
25. McKay, R.G., et al. (1986) Balloon dilatation of calcific aortic stenosis in elderly patients: postmortem, intraoperative, and percutaneous valvuloplasty studies. *Circulation*. 74, 119–125.
26. Safian, R.D., et al. (1987) Postmortem and intraoperative balloon valvuloplasty of calcific aortic stenosis in elderly patients: mechanisms of successful dilation. *J Am Coll Cardiol*. 9, 655–660.
27. Isner, J.M., et al. (1988) Mechanism of aortic balloon valvuloplasty: fracture of valvular calcific deposits. *Ann Intern Med*. 108, 377–380.
28. Tsai, T.P., et al. (1994) Results of coronary artery bypass grafting and/or aortic or mitral valve operation in patients > or = 90 years of age. *Am J Cardiol*. 74, 960–962.
29. Smith, N., McAnulty, J.H., and Rahimtoola, S.H. (1978) Severe aortic stenosis with impaired left ventricular function and clinical heart failure: results of valve replacement. *Circulation*. 58, 255–264.
30. Connolly, H.M., et al. (1997) Aortic valve replacement for aortic stenosis with severe left ventricular dysfunction. Prognostic indicators. *Circulation*. 95, 2395–2400.
31. Grossman, W., Jones, D., and McLaurin, L.P. (1975) Wall stress and patterns of hypertrophy in the human left ventricle. *J Clin Invest*. 56, 56–64.
32. Nitenberg, A., et al. (1988) Coronary flow and resistance reserve in patients with chronic aortic regurgitation, angina pectoris and normal coronary arteries. *J Am Coll Cardiol*. 11, 478–486.
33. Fortuin, N.J. and Craige, E. (1972) On the mechanism of the Austin Flint murmur. *Circulation*. 45, 558–570.
34. Parker, E., Craige, E., and Hood, W.P., Jr. (1971) The Austin Flint murmur and the a wave of the apexcardiogram in aortic regurgitation. *Circulation*. 43, 349–359.
35. Lindsay, J., Jr., Beall, A.C.J., and DeBakey, M.E. (eds.) (1998) *Diagnosis and Treatment of Diseases of the Aorta*. McGraw-Hill, New York, NY, pp. 2461–2482.
36. Smith, M.D., et al. (1995) Transesophageal echocardiography in the diagnosis of traumatic rupture of the aorta. *N Engl J Med*. 332, 356–362.
37. Cigarroa, J.E., et al. (1993) Diagnostic imaging in the evaluation of suspected aortic dissection. Old standards and new directions. *N Engl J Med*. 328, 35–43.
38. Nienaber, C.A., et al. (1993) The diagnosis of thoracic aortic dissection by noninvasive imaging procedures. *N Engl J Med*. 328, 1–9.
39. Schaff, H.V. (1998) Aortic valve replacement with homograft, in *Mastery of Cardiac Surgery* (Kaiser, K., ed.), Lippincott-Raven, Philadelphia, PA, pp. 369–375.
40. Bonow, R.O., et al. (1988) Long-term serial changes in left ventricular function and reversal of ventricular dilatation after valve replacement for chronic aortic regurgitation. *Circulation*. 78, 1108–1120.
41. Gorlin, R. and Gorlin, S. (1951) Hydraulic formula for calculation of the area of stenotic mitral valve, other cardiac values and central circulatory shunts. *Am Heart J*. 41, 1–29.
42. Rowe, J.C., et al. (1960) The course of mitral stenosis without surgery: 10- and 20-year perspectives. *Ann Intern Med*. 52, 741–749.
43. Wood, P. (1954) An appreciation of mitral stenosis. I. Clinical features. *Br Med J*. 4870, 1051–1063.
44. Edwards, J.E., Rusted, I.E., and Scheifley, C.H. (1956) Studies of the mitral valve. II. Certain anatomic features of the mitral valve and associated structures in mitral stenosis. *Circulation*. 14, 398–406.
45. Roberts, W.C. and Perloff, J.K. (1972) Mitral valvular disease. A clinicopathologic survey of the conditions causing the mitral valve to function abnormally. *Ann Intern Med*. 77, 939–975.
46. Olesen, K.H. (1962) The natural history of 271 patients with mitral stenosis under medical treatment. *Br Heart J*. 24, 349–357.

47. Carroll, J.D. and Feldman, T. (1993) Percutaneous mitral balloon valvotomy and the new demographics of mitral stenosis. *JAMA*. 270, 1731–1736.
48. Selzer, A. and Cohn, K.E. (1972) Natural history of mitral stenosis: a review. *Circulation*. 45, 878–890.
49. Hugenholtz, P.G., et al. (1962) The spectrum of pure mitral stenosis. Hemodynamic studies in relation to clinical disability. *Am J Cardiol*. 10, 773–784.
50. Braunwald, E., et al. (1955) The hemodynamics of the left side of the heart as studied by simultaneous left atrial, left ventricular, and aortic pressures; particular reference to mitral stenosis. *Circulation*. 12, 69–81.
51. Holen, J., et al. (1976) Determination of pressure gradient in mitral stenosis with a non-invasive ultrasound Doppler technique. *Acta Med Scand*. 199, 455–460.
52. Hatle, L., et al. (1978) Noninvasive assessment of pressure drop in mitral stenosis by Doppler ultrasound. *Br Heart J*. 40, 131–140.
53. Currie, P.J., et al. (1985) Continuous wave Doppler determination of right ventricular pressure: a simultaneous Doppler-catheterization study in 127 patients. *J Am Coll Cardiol*. 6, 750–756.
54. Coulshed, N., et al. (1970) Systemic embolism in mitral valve disease. *Br Heart J*. 32, 26–34.
55. Daley, R., et al. (1951) Systemic arterial embolism in rheumatic heart disease. *Am Heart J*. 42, 566.
56. Abernathy, W.S. and Willis, P.W., 3rd. (1973) Thromboembolic complications of rheumatic heart disease. *Cardiovasc Clin*. 5, 131–175.
57. Adams, G.F., et al. (1974) Cerebral embolism and mitral stenosis: survival with and without anticoagulants. *J Neurol Neurosurg Psychiatry*. 37, 378–383.
58. Orrange, S.E., et al. (1997) Actuarial outcome after catheter balloon commissurotomy in patients with mitral stenosis. *Circulation*. 95, 382–389.
59. Higgs, L.M., et al. (1970) Mitral restenosis: an uncommon cause of recurrent symptoms following mitral commissurotomy. *Am J Cardiol*. 26, 34–37.
60. Dahl, J.C., Winchell, P., and Borden, C.W. (1967) Mitral stenosis. A long term postoperative follow-up. *Arch Intern Med*. 119, 92–97.
61. Cohn, L.H., et al. (1990) Decreased operative risk of surgical treatment of mitral regurgitation with or without coronary artery disease. *J Am Coll Cardiol*. 16, 1575–1578.
62. Connolly, M.W., et al. (1986) Surgical results for mitral regurgitation from coronary artery disease. *J Thorac Cardiovasc Surg*. 91, 379–388.
63. Chatterjee, K., et al. (1973) Beneficial effects of vasodilator agents in severe mitral regurgitation due to dysfunction of subvalvar apparatus. *Circulation*. 48, 684–690.
64. Yoran, C., et al. (1979) Mechanism of reduction of mitral regurgitation with vasodilator therapy. *Am J Cardiol*. 43, 773–777.
65. Carabello, B.A. (1988) Mitral regurgitation: basic pathophysiologic principles. Part 1. *Mod Concepts Cardiovasc Dis*. 57, 53–58.
66. Zile, M.R., et al. (1984) Chronic mitral regurgitation: predictive value of preoperative echocardiographic indexes of left ventricular function and wall stress. *J Am Coll Cardiol*. 3, 235–242.
67. Crawford, M.H., et al. (1990) Determinants of survival and left ventricular performance after mitral valve replacement. Department of Veterans Affairs Cooperative Study on Valvular Heart Disease. *Circulation*. 81, 1173–1181.
68. Wisenbaugh, T., Skudicky, D., and Sareli, P. (1994) Prediction of outcome after valve replacement for rheumatic mitral regurgitation in the era of chordal preservation. *Circulation*. 89, 191–197.
69. Enriquez-Sarano, M., et al. (1994) Echocardiographic prediction of survival after surgical correction of organic mitral regurgitation. *Circulation*. 90, 830–837.
70. Blackshear, J.L., et al. (1993) Mitral regurgitation associated with reduced thromboembolic events in high-risk patients with nonrheumatic atrial fibrillation. Stroke Prevention in Atrial Fibrillation Investigators. *Am J Cardiol*. 72, 840–843.
71. Beppu, S., et al. (1985) Smoke-like echo in the left atrial cavity in mitral valve disease: its features and significance. *J Am Coll Cardiol*. 6, 744–749.
72. Betriu, A. and Chaitman, B.R. (1982) Preoperative determinants of return to sinus rhythm after valve replacement, in *Cardiac Bioprosthesis* (Cohn L.H. and Gallucci, V., eds.), Yorke Medical Books, New York, NY, pp. 184–191.
73. Chua, Y.L., et al. (1994) Outcome of mitral valve repair in patients with preoperative atrial fibrillation. Should the maze procedure be combined with mitral valvuloplasty? *J Thorac Cardiovasc Surg*. 107, 408–415.
74. Horskotte, D., et al. (1993) The effect of chordal preservation on late outcome after mitral valve replacement: a randomized study. *J Heart Valve Dis*. 2, 150–158.
75. Bonow, R.O., Nikas, D., and Elefteriades, J.A. (1995) Valve replacement for regurgitant lesions of the aortic or mitral valve in advanced left ventricular dysfunction. *Cardiol Clin*. 13, 73–83, 85.
76. Akins, C.W., et al. (1994) Mitral valve reconstruction versus replacement for degenerative or ischemic mitral regurgitation. *Ann Thorac Surg*. 58, 668–675; discussion 675–676.
77. Enriquez-Sarano, M., et al. (1995) Valve repair improves the outcome of surgery for mitral regurgitation. A multivariate analysis. *Circulation*. 91, 1022–1028.
78. Silverman, N. (1998) Tricuspid valve, in *Mastery of Cardiac Surgery* (Kaiser, K., ed.), Lippincott-Raven, Philadelphia, PA, pp. 354–360.
79. Reynolds, T. *The Echocardiographer's Pocket Reference*, 2nd Ed.. Arizona Heart Institute, Phoenix, AZ, p. 464.

28 Less-Invasive Cardiac Surgery

KENNETH K. LIAO, MD

CONTENTS

1. INTRODUCTION

The history of cardiac surgery reflects a constant search by cardiac surgeons for safer and less-invasive ways to treat their patients. Since Dr. F. John Lewis's pioneering operation in 1952, followed by Dr. C. Walton Lillehei's first successful series of intracardiac defect repairs in the mid-1950s, cardiac surgery as a surgical subspecialty has expanded dramatically. Notably, one of the most important technological innovations in cardiac surgery was the development and modification of a cardiopulmonary bypass machine. For years, this machine has been used extensively by cardiac surgeons. Its use has enabled cardiac surgery to become a safe and reproducible daily routine in many hospitals across the country. Now, although most cardiac operations are considered somewhat standardized, continued improvements as well as recognition of the importance of postoperative recovery and quality of life remain significant concerns for patients as well as physicians.

In recent years, there has been a major push to develop and provide "less-invasive cardiac surgery" as standard care. All four of the major steps used in conventional cardiac surgery need to be considered when attempting to develop less-invasive modifications: (1) gaining access to the heart through a full sternotomy or posterolateral thoracotomy; (2) supporting the vital organs through a cardiopulmonary bypass machine; (3) arresting the heart by administering cardioplegia; and/or (4) manipulating the ascending aorta during aortic cannulation, during cross-clamping and side-clamping, and during proximal anastomosis in coronary artery bypass grafting. Unfortunately, any of these steps can impose significant risks or adverse effects. More specifically, a large incision typically corresponds to greater pain, a noticeable scar, more complications, and/or a longer recovery time. Similarly, cardiopulmonary bypass has been known to trigger adverse inflammatory reactions or subsequent multiple organ dysfunction. Finally, manipulating the aorta can lead to strokes (e.g., from plaque dislodgement) or other neurological deficits. Importantly, less-invasive approaches or minimally invasive cardiac surgery can minimize or eliminate complications that may occur relative to each of the four steps commonly used in conventional cardiac surgery. This chapter focuses on less-invasive methodologies commonly employed in adult cardiac surgical procedures.

2. IMPACT OF INCISION SIZE

For years, the physical and emotional impact of a large incision size on the individual patient has been ignored by most cardiac surgeons. Historically, adequate exposure of the target tissues or organs through large skin incisions took priority over concern about incision size; this mindset remained unchallenged until the early 1990s. Subsequently, with novel specially designed instruments, experience with laparoscopic surgery demonstrated that those surgical procedures traditionally performed through large incisions could actually be accomplished with much smaller incisions. The patient benefits of small inci-

From: *Handbook of Cardiac Anatomy, Physiology, and Devices*
Edited by: P. A. Iaizzo © Humana Press Inc., Totowa, NJ

sions have been clearly shown; advantages include less pain, quicker recovery, lower infection rate, shorter hospital stays, and better quality of life *(1,2)*. In some studies, less immune function disturbance has also been reported *(3)*.

Encouraged by positive results from the laparoscopic surgical community, some cardiac surgeons began to modify their approaches to perform less-invasive cardiac surgery. Currently, a variety of approaches have been attempted: (1) thoracoscopies or minithoracotomies to replace thoracotomies and (2) partial sternotomies, partial thoracotomies, or minithoracotomies to replace full sternotomies. Nevertheless, cardiopulmonary bypass support, if required, is established through cannulation in the peripheral vessels such as the femoral arteries, femoral veins, and internal jugular veins. Various studies have reported advantages with smaller incisions or sternum-sparing incisions in terms of pain, time to recovery, infection, and cosmesis *(4,5)*.

However, it must also be considered that smaller incisions have certain drawbacks. To have the same access and visualization as with larger incisions, special instruments and specialized surgical skills are required, and only selected patients are eligible. For surgeons, the initial learning curve to be able to perform such procedures clinically can be very steep. Nevertheless, smaller incisions are certainly very appealing to both patients and referring physicians. To date, more and more surgeons are moving toward smaller incisions and the use of these specialized less-invasive surgical methodologies, even though the conversion process is often considered painfully slow.

3. SIDE EFFECTS OF CARDIOPULMONARY BYPASS

Cardiopulmonary bypass procedures have become commonplace in cardiac surgical suites; however, capabilities to perform the same clinical procedure safely without its use would be desirable, for such bypass procedures are not performed without risks. More specifically, cardiopulmonary bypass has been associated with a complex systemic inflammatory reaction in the host patient. The hallmarks of this reaction are typically increased microvascular permeability in multiple organs, resulting in an increase in interstitial fluid and the activation of humoral amplification systems. The complement system, including the kallikrein-bradykinin cascade, the coagulation cascade, the fibrinolytic cascade, and the arachidonic acid cascade, is activated. Inflammatory mediators, such as cytokines and proteolytic enzymes, are released.

In most classic cardiac cases for which cardiopulmonary bypass is utilized, the heart is stopped to provide a motionless field. Cardiac arrest is initiated with infusion of cardioplegia to the myocardium. Unfortunately, subsequent reperfusion of the heart can cause ischemic reperfusion injury to the myocardium.

Clinical manifestations of this systemic inflammatory reaction and myocardial ischemic reperfusion injury can be subtle, but also serious and even lethal in some patients. The incidence of this systemic reaction has been reported in 5–30% of cardiac surgery patients after cardiopulmonary bypass *(6–11)*. Importantly, this inflammatory response can affect multiple organs. More specifically, examples of this systemic response can vary from: (1) transient subtle cognitive impairment to a permanent stroke; (2) coagulopathy requiring transfusion of blood products to disseminated intravascular coagulation; (3) pulmonary edema to adult respiratory distress syndrome requiring prolonged ventilation support; (4) low cardiac output to acute heart failure requiring inotropic or mechanical circulatory support; or (5) transient kidney insult with increased creatinine to permanent kidney failure requiring hemodialysis. Any of these, or a combination thereof, commonly results in prolonged intensive care unit stays requiring intense monitoring and often increased patient mortality. Importantly, the severity of these reactions tends to be related to cardiopulmonary bypass time, the patient's age, or comorbidities *(9,10)*.

To date, coronary artery disease remains the leading cause of death for individuals living in developed countries. Worldwide, about 800,000 coronary artery bypass grafting (CABG) operations are performed yearly, which represents the majority of all cardiac procedures. Importantly, off-pump beating heart coronary artery bypass grafting (OPCABG) surgery has grown rapidly. For example, OPCABG (a less-invasive surgical approach) currently comprises 20–25% of all CABG procedures performed in the United States. An increasing number of studies, including prospective randomized studies, have demonstrated that when compared to conventional CABG, OPCABG procedures result in: (1) a lower incidence of postoperative neurological deficits; (2) fewer blood transfusions; (3) shorter intubation times; (4) less release of cardiac enzyme; (5) less renal insult; (6) shorter intensive care unit stays; (7) less release of cytokines interleukin 8 (IL-8) and IL-10; or (8) lower mortality *(11–15)*.

It should be noted that the difference in these parameters between OPCABG and CABG procedures mostly ranges from 2 to 10%. In most OPCABG procedures, however, there has been the tendency to bypass fewer vessels; this may result in an incomplete revascularization. Moreover, certain anatomical locations and the nature of target coronary arteries (e.g., arteries located in the posterolateral wall of hypertrophied hearts, intramyocardial arteries, and severely calcified arteries) may preclude safe and reliable anastomoses with OPCABG. Furthermore, with today's available methodologies, OPCABG is more challenging technically for most cardiac surgeons.

It should also be noted that emergency conversion of OPCABG to conventional CABG because of hemodynamic instability carries a significantly higher morbidity and mortality rate than conventional CABG (about six times higher mortality) *(16)*; fortunately the overall conversion is rare, with a rate of only 3.7%. Nevertheless, such concerns have temporarily cooled the initial enthusiasm for OPCABG.

4. EFFECTS OF MANIPULATING THE AORTA

Coronary artery disease is often considered a component of systemic vascular disease. The same risk factors that contribute to coronary artery disease, such as smoking, diabetes, hypertension, and hyperlipidemia, also contribute to carotid artery disease and atherosclerotic changes in the aorta; this is especially true for the ascending aorta. Atheroma in the aorta can present with calcified plaques or with "cheeselike" soft plaques, which can be disrupted (dislodged) during: (1) cannulation of the

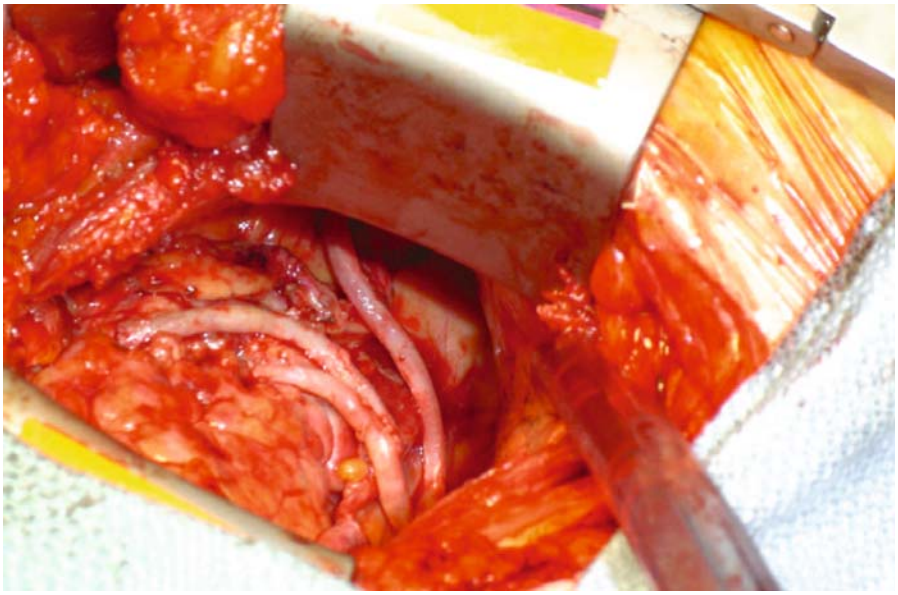

Fig. 1. Totally aortic nontouch technique in off-pump three-vessel coronary artery bypass grafting surgery via left minithoracotomy; the inflow vein grafts come from the distal left subclavian artery in addition to *in situ* left internal mammary artery graft.

ascending aorta for cardiopulmonary bypass, (2) cross-clamping in general, or (3) side-clamping of the ascending aorta for attachment of proximal anastomoses of bypassed grafts.

The mobilized plaques can then cause microembolization or macroembolization of brain vessels, resulting in neurological deficits. Multiple episodes of microembolic events have been documented by transcranial Doppler studies during routine CABG surgery. The number of microembolic signals is reported to be related to the extent that the ascending aorta is manipulated *(17)*. Nevertheless, calcified areas of the aorta (or porcelain aorta) can be identified by palpation and thus avoided during surgery, whereas soft plaques are typically unnoticed until they are disrupted during surgical manipulation. The incidence of plaque formation in the ascending aorta can be as high as 30% *(18)*.

Several methodologies have been described to avoid disrupting plaques when working in the region of the ascending aorta. For example, topical ultrasound devices have been used to identify hidden plaques, especially the soft types. In addition, a single aortic cross-clamp technique has been shown to reduce the risk of plaque disruption during conventional CABG surgery *(19)*. Similarly, aortic cross-clamping or side-clamping can be avoided by using proximal anastomotic devices during OPCABG. Totally aortic "nontouch" techniques have been described that can be applied during OPCABG by using: (1) bilateral *in situ* internal mammary arteries; (2) sequential grafts; (3) *in situ* gastroepiploic arteries; (4) radial artery Y or T grafts from internal mammary arteries; (5) radial artery or vein grafts from innominate, subclavian, axillary arteries; or (6) descending thoracic aorta. Currently, nontouch techniques during OPCABG are gaining popularity, especially in high-risk patients (Fig. 1). Nevertheless, given limited patient numbers and short follow-up times, the long-term graft patency rate for the procedures remains unknown.

5. TECHNOLOGICAL INNOVATIONS

New technologies have played crucial roles in the evolution of less-invasive cardiac surgery. Importantly, they have changed the perceptions of cardiac surgeons regarding how cardiac surgery can or should be performed. With the help of new instruments specifically designed to meet the surgeon's need, less-invasive cardiac surgical procedures once deemed impossible or impractical have now become reality, or even common practice, in some medical centers. These technological innovations have typically involved the aspects of cardiac surgery discussed in this section.

5.1. Sternum-Sparing Surgery, Minithoracotomy, and Thoracoscopy

Major advances in the area of sternum-sparing surgery, minithoracotomy, and thoracoscopy include the development of a cardiopulmonary bypass support system via peripheral access. The application of suction to the venous drainage has made possible aortic valve and mitral valve surgery via partial sternotomy, as well as mitral valve surgery via a minithoracotomy. An earlier breakthrough device in this field was the HeartPort system (Heartport; Redwood City, CA); although its use has proven impractical in most cardiac operations, its potential has significantly changed cardiac surgeons' perception of future technologies. Furthermore, the concept of the HeartPort system led to numerous other technological modifications and innovations in the field of less-invasive cardiac surgery. Such innovations include: (1) transesophageal echocardiography to guide venous cannulation; (2) development of the Chitwood aortic cross-

Fig. 2. An octopus myocardium-stabilizing device was used to steady the coronary artery during direct bypass grafting anastomosis.

clamp; and (3) mitral valve repair or replacement with the assistance of thoracoscopy.

5.2. OPCABG Improvement

New instruments have also been developed to position the heart and to stabilize and improve the visualization of target arteries. For example, an available left ventricle suction device applies –400-mmHg suction to the left ventricular apex and can hold the heart up in different positions. Now widely used in OPCABG surgery, it has less of an effect on the venous return compared with the old "suture retraction" technique. Similarly, a focal myocardial stabilization device has been developed to stabilize segments of target arteries; it has both a suction and a compressing effect on the topical epicardial tissue and thus significantly decreases the motion of target arteries (Fig. 2). An additional noteworthy device is the temporary intracoronary plastic shunt; it can be inserted via arteriotomy to maintain blood flow to the distal myocardium during anastomosis, thus avoiding or minimizing ischemia time. Importantly, the use of such a shunt is considered crucial when the target artery supplies a large territory of myocardium.

5.3. Aortic Nontouch Techniques

Different proximal anastomotic devices are being developed to avoid clamping on the aorta during OPCABG surgery. Two such devices have been approved by the Food and Drug Administration. One is the automated proximal connector from St. Jude Medical (St. Paul, MN), which allows the vein graft to be anastomosed to the aorta without side-clamping and suturing. An early detected drawback of this preliminary model is that the proximal anastomosis must be performed first, making it difficult to assess the length of the vein graft when the distal anastomosis is performed; moreover, a delivery device must be inserted into the lumen of the vein graft, which can denude the endothelium and affect long-term patency. Nevertheless, in time, new innovations will likely correct for these noted compromises. The other device is Heartstring™ Proximal Seal System (Guidant Corporation, Indianapolis, IN), which temporarily occludes aortotomy during direct suture anastomosis of the proximal vein graft to the aortotomy; yet, to date one of the major drawbacks of its use is that the suture can catch the device, which requires that the anastomosis be redone.

5.4. Endoscopic Robotics

Someday soon, will operating rooms be devoid of cardiac surgeons? Perhaps, with the addition of robotics as a forefront technology. For example, Intuitive Surgical's (Sunnyvale, CA) daVinci robotic system has improved significantly and has made operating inside the chest cavity possible. Its 3D visualization, seven degrees of wrist motion, and capability to eliminate human hand tremors facilitate fine cutting and suturing tasks. For those few surgeons who are currently using these sophisticated machines, it has made internal mammary artery takedown and OPCABG surgery via minithoracotomy easier (Fig. 3). Further, it has been described to have been used to repair atrial septal defects and mitral valves without sternotomy or thoracotomy. Currently, the employment of such systems will lead the way in moving toward total endoscopic CABG surgery (Figs. 4 and 5).

Nevertheless, numerous complementary innovations have been required to allow for robotic surgery on the heart. For example, to make OPCABG surgery easier when it is performed via minithoracotomy or total endoscopic robotic approaches, an "endo suction device" and an "endo myocardium stabilizer"

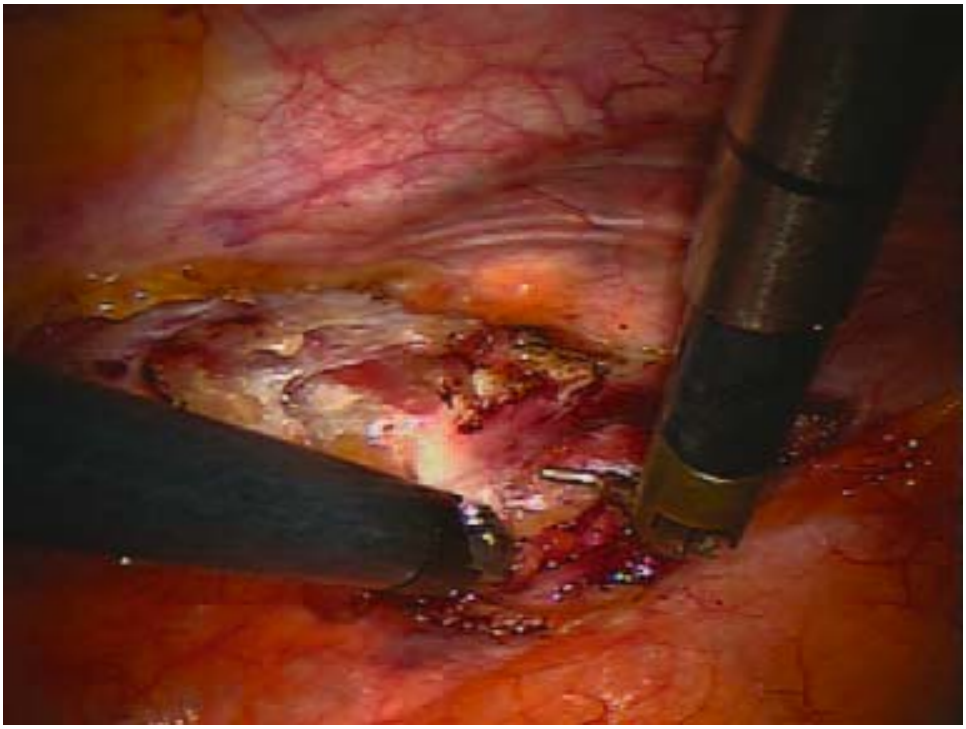

Fig. 3. Robotic arms operate inside the chest cavity to take down left internal mammary artery.

Fig. 4. Robotic arms in the operating room at our Fairview University Hospital. (*See* color version on Companion CD.)

have been developed to position the heart and stabilize the target artery through port accesses. Other devices that are currently being developed include proximal and distal anastomotic devices and endo "U" clips.

6. FUTURE DIRECTIONS

The ultimate goal of less-invasive cardiac surgery is to avoid cardiopulmonary bypass support, sternotomy, and thoracotomy and rather perform surgery through tiny incisions. Various of specially designed instruments have been developed to make such procedures possible, including: (1) automated proximal and distal CABG anastomotic devices; (2) the endo myocardium stabilizer; (3) the endo suture device; and (4) the "endo vascular clamp." The daVinci surgical robotic system has enabled use of such instruments inside the closed chest cavity. It is likely that in the very near future, cardiac surgery will be performed utilizing only three to four key holes in the chest wall (Fig. 6).

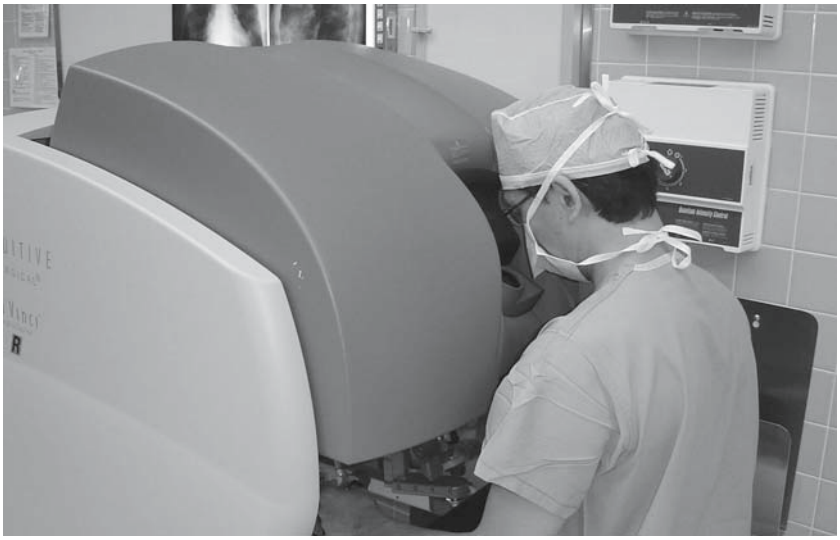

Fig. 5. The surgeon is operating on the robotic console away from the patient. (*See* color version on Companion CD.)

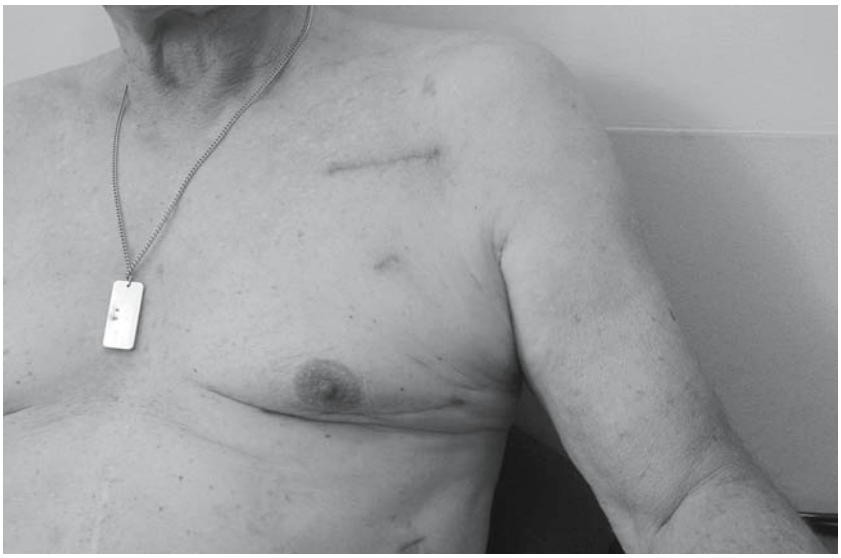

Fig. 6. Small incisions after multivessel off-pump sternum-sparing coronary artery bypass grafting surgery. (*See* color version on Companion CD.)

COMPANION CD MATERIAL

Figures 4, 5, and 6 are shown in color.

REFERENCES

1. Grace, P.A., Quereshi, A., Coleman, J., et al. (1991) Reduced postoperative hospitalization after laparoscopic cholecystectomy. *Br J Surg*. 78, 160–162.
2. Southern Surgeons Club. (1991) A prospective analysis of 1518 laparoscopic cholecystectomies. *N Engl J Med*. 324, 1073–1078.
3. Bruce, D.M., Smith, M., Walker, C.B.J., et al. (1999) Minimal access surgery for cholelithiasis induces an attenuated acute phase response. *Am J Surg*. 178, 232–234.
4. Szwerc, M.F., Benchart, D.H., Wiechmann, R.J., et al. (1999) Partial versus full sternotomy for aortic valve replacement. *Ann Thorac Surg*. 68, 2209–2214.
5. Cosgrove, D.M., Sabik, J.F., and Navia, J.L. (1998) Minimally invasive valve operations. *Ann Thorac Surg*. 65, 1535–1539.
6. Zilla, P., Fasol, R., Groscurth, P., et al. (1989) Blood platelets in cardiopulmonary bypass operations. *J Thorac Cardiovasc Surg*. 97, 379–388.
7. Ko, W., Hawes, A.S., Lazenby, W.D., et al. (1991) Myocardial reperfusion injury. *J Thorac Cardiovasc Surg*. 102, 297–308.
8. Sladen, R.N. and Berkowity, D.E. (1993) Cardiopulmonary bypass and the lung, in *Cardiopulmonary Bypass* (Gravlee, G.P, Davis, R.F., and Utley, J.R., eds.), Williams and Wilkins, Baltimore, MD, p. 468.
9. Tuman, K.J., McCarthy, R.J., Najafi, H., et al. (1992) Differential effects of advanced age on neurologic and cardiac risks of coronary artery operations. *J Thorac Cardiovasc Surg*. 104, 1510–1517.

10. Abel, R.M., Buckley, M.J., Austen, W.G., et al. (1976) Etiology, incidence and prognosis of renal failure following cardiac operations: Results of a prospective analysis of 500 consecutive patients. *J Thorac Cardiovasc Surg*. 71, 323–333.
11. Fernandez-del Castillo, C., Harringer, W., Warshaw, A.L., et al. (1991) Risk factors for pancreatic cellular injury after cardiopulmonary bypass. *N Engl J Med*. 325, 382–387.
12. Cleveland, J.C., Shroyer, A.J., Chen, A.Y., et al. (2001) Off-pump coronary artery bypass grafting decrease risk-adjusted mortality and morbidity. *Ann Thorac Surg*. 72, 1282–1289.
13. Ascione, R., Lloyd, C.T., Underwood, M.J., et al. (2000) Inflammatory response after coronary revascularization with or without cardiopulmonary bypass. *Ann Thorac Surg*. 69, 1198–1204.
14. Diegeler, A., Doll, N., Rauch, T., et al. (2000) Humoral immune response during coronary artery bypass grafting: a comparison of limited approach, "off-pump" technique, and conventional cardiopulmonary bypass. *Circulation*. 102, III95–III100.
15. Reston, J.T., Tregear, S.J., and Turkelson, C.M. (2003) Meta-analysis of short-term and mid-term outcomes following off-pump coronary artery bypass grafting. *Ann Thorac Surg*. 76, 1510–1515.
16. Edgerton, J.R., Dewey, T.M., Magee, M.J., et al. (2003) Conversion in off-pump coronary artery bypass grafting: an analysis of predictors and outcomes. *Ann Thorac Surg*. 76, 1138–1142.
17. Stump, D.A. and Newman, S.P. (1996) Embolic detection during cardiopulmonary bypass, in *Neurosonology* (Tegler, C.H., Babikian, V.L, and Gomez, C.R., eds.), Mosby, St. Louis, MO, pp. 252–255.
18. Goto, T., Baba, T., Matsuyama, K., et al. (2003) Aortic atherosclerosis and postoperative neurological dysfunction in elderly coronary surgical patients. *Ann Thorac Surg*. 75, 1912–1918.
19. Tsang, J.C., Morin, J.F., Tchervenkov, C.I., et al. (2003) Single aortic clamp versus partial occluding clamp technique for cerebral protection during coronary artery bypass: a randomized prospective trial. *J Card Surg*. 18, 158–163.

29 Treatment of Cardiac Septal Defects

The Evolution of the Amplatzer® Family of Devices

JOHN L. BASS, MD

CONTENTS

1. ATRIAL SEPTAL DEFECT

1.1. History

Atrial septal defects are congenital deficiencies in the wall separating systemic and pulmonary venous returns as they enter the heart. This allows blood from the lungs to flow through the defect and increase the volume of blood passing through the pulmonary arteries. In individuals in their 20s, living with such a defect can eventually cause permanent damage to the pulmonary vasculature. To prevent this and other problems associated with these malformations (i.e., cardiac arrhythmias), closure of atrial septal defects is recommended during the first few years of life *(1)*.

The first successful surgical closure of an atrial septal defect was performed on a patient at the University of Minnesota Hospital in 1952 *(2)*. Such an operative approach for correction of a congenital intracardiac defect is considered one of the safest open heart operations performed today, with a mortality rate under 0.5% *(3)*. Nevertheless, such surgical closures are not without potential complications, including: (1) morbidity from the required sternotomy or right thoracotomy, (2) the chance of exposure to blood products, (3) utilization of a chest tube, (4) a 3- to 5-d hospitalization, (5) 4–6 weeks of convalescence, and (6) the possibility of postpericardiotomy syndrome. The opportunity to minimize or eliminate such problems has spurred attempts to develop a method of transcatheter closure.

From: *Handbook of Cardiac Anatomy, Physiology, and Devices*
Edited by: P. A. Iaizzo © Humana Press Inc., Totowa, NJ

Specifically, it is generally considered that secundum atrial septal defects are ideal for transcatheter closure. These defects are typically surrounded by rims of tissue that a device could clasp; they do not have borders formed by valves or the walls of the heart. King and Mills reported the first attempted transcatheter closure of a secundum atrial septal defect in 1976 *(4)*. This was followed by development of the Clamshell/CardioSEAL *(5)*, Sideris Button *(6)*, ASDOS *(7)*, and Angel Wings *(8)* devices (Table 1). These developments were clinically exciting for they provided an alternative to surgical closure.

Initially, their use also presented a number of challenges, including: (1) large devices were required with the central post design; (2) these devices were not self-centering; (3) their center posts could move within the defect; and (4) each device required large delivery systems. Furthermore, in some cases, their use was plagued by embolization (e.g., unbuttoning) *(9)*. Unfortunately, frame fatigue and arm fracture occurred in up to 10% of some early designs, with asymptomatic wire embolization in some patients. In general, each of these designs was considered difficult to use clinically, or it was often impossible to recapture or retrieve after deployment. It was reported that surgical removal was required if they were deployed in an improper position, and residual shunt rates were significant *(10)*.

1.2. Device Design

The ideal septal occluder device would have the following features: (1) easy delivery and implantation; (2) ability to self-

Table 1
History of Transcatheter Closure of Atrial Septal Defects

Device	*Year*
King and Mills	1974
Rashkind	1987
Clamshell[a]	1989
Sideris Button	1990
ASDOS	1991
Angel Wings	1993
CardioSEAL[a]	1996
Amplatzer®	1998
STARFlex[a]	1999
Helex	1999

[a] Clamshell, CardioSEAL, and STARflex devices represent progres-sive modifications of a design.

Table 2
Frequent Complications in Phase II FDA Trial of Amplatzer Septal Occluder

Major complications	*Minor complications*
• Pericardial effusion with tamponade	• Device embolization with percutaneous retrieval
• Repeat surgery	• Cardiac arrhythmia with treatment
• Cardiac arrhythmias requiring permanent pacemaker placement or long-term antiarrhythmic medication	• Pericardial effusion requiring medical management
• Device embolizations requiring immediate surgical removal	• Surgical wound complications

center; (3) ability to pass easily through a small delivery system; (4) recapturability and redeployability; (5) high resiliency without fracturing; and (6) high effectiveness in avoiding significant residual shunts. Furthermore, the materials it is constructed from should be biocompatible and nontoxic. Nevertheless, durability is important when the majority of patients are children, and there is a long "lifetime" after implantation.

All Amplatzer® atrial septal defect devices have been designed to fulfill the aforementioned requirements. For example, the Amplatzer Septal Occluder is a woven mesh of 72 Nitinol (*see* Section 3) wires 0.003- to 0.008-in diameter with shape memory. There are two retention disks with a central waist that sits within the defect (Fig. 1); the left atrial disk is 12–14 mm larger than the waist. The stenting action of the waist and the clasping of the atrial septum by the retention disks hold it in place. Fabric baffles, sewn inside the disks and waist, promote thrombosis and occlusion of the defect. The delivery system is relatively small (6- to 12-French delivery sheaths). Further, the device is recapturable and redeployable with a microscrew/cable attachment. To date, available waist diameters range from 4 to 40 mm, allowing closure of even large defects *(11)*.

As with all implantable devices, animal trials have been performed and have demonstrated the effectiveness of the Amplatzer Septal Occluder approach. In one trial, dilating the foramen ovale in dogs created an atrial septal defect, and a 10-mm device was placed; there was complete occlusion with no residual shunt. Furthermore, the devices were completely covered by a neoendothelium at sacrifice 3 mo after implantation, and no thrombus formed on the device *(12)*. Subsequent patient trials confirmed that no retroaortic rim was required for stable device position and complete closure. Importantly, and even amazingly, patients could be discharged the morning after device placement and remained on low-dose aspirin and endocarditis prophylaxis for 6 mo after closure.

1.3. Food and Drug Administration Testing

A Food and Drug Administration (FDA) clinical trial to determine the effectiveness of the Amplatzer Septal Occluder technology was begun based on the success of animal studies and European trials in humans. Nevertheless, the optimal study design was difficult to determine. Many patients and their families wanted to avoid any such surgery despite the long history of safe surgical closure; in addition, they were concerned about the lack of long-term follow-up of this new device. Thus, randomization was extremely difficult and unsuccessful because many patients and families originally chosen for the surgical group simply opted out of the trial, preferring to wait for final FDA approval. Subsequently, the study design was changed to allow device closure at some institutions with patients recruited to designated surgical centers. Hence, we are left with a trial without true randomization; this illustrates how difficult it is to employ such a study design in the real world.

Importantly, the results of phase II of this FDA trial have shown that an Amplatzer Septal Occluder is more effective and safe compared with the surgical group. At the end of 12 mo, there was complete closure, or a <2-mm residual shunt, in 98.5% of device patients compared to 100% of surgically closed patients. Major and minor complications most frequently observed in either group are listed in Table 2; there was no difference between groups in the incidence of major complications. Minor complications were more common in surgical patients (27/442, 6.1% in the Amplatzer group vs 29/154, 18.8% in the surgery group).

However, recall that these patients were not randomized; there were differences between groups, with the surgical patients younger (18.1 ± 19.3 yr in the Amplatzer group vs 5.9 ± 6.2 yr in the surgery group, $p < 0.001$) and smaller (42.3 ± 27.3 kg in the Amplatzer group vs 20.6 ± 15.2 kg in the surgery group, $p < 0.001$) *(11)*. Nevertheless, based on this positive outcome, the FDA granted premarket approval of the Amplatzer Septal Occluders in December 2001, and to date it remains the only atrial septal defect closure device with FDA approval.

2. THE AMPLATZER® FAMILY OF DEVICES

Amplatzer devices are designed for occlusion of abnormal congenital cardiovascular communications. The devices are based on the model of a self-expanding stent with the ends of the wires bound together forming a closed frame. The shape of the wire frame is tailored to fit the abnormal vascular or intracardiac communication. Retention disks fix the device against vascular or cardiac walls. A central waist further holds the device in place with radial force against the margins of the communication. This provides stable fixation of the device.

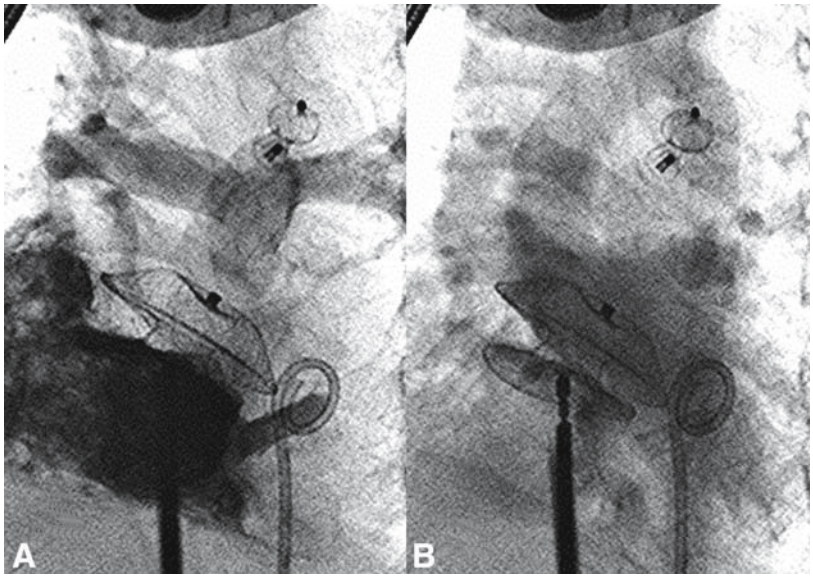

Fig. 1. Amplatzer Septal Occluder device. **(A)** Right atrial angiogram performed after deployment of the device in a secundum atrial septal defect, but before release. The right atrial disk is obscured by contrast with the waist within the atrial septal defect. **(B)** Levophase of the right atrial angiogram opacifying the left atrium. Contrast outlines the left atrial disk completely within the left atrium.

Initially, occlusion occurs through thrombosis within the polyester baffles or the stuffing sutured inside the wire frame. Furthermore, over 3 mo, the device is covered with a protein and cellular layer, reducing the potential for forming a surface thrombus and eliminating the risk of bacterial endocarditis *(12)*.

The development of Amplatzer devices began when thin-wire technology reached a developmental point that allowed the construction of a frame of nontoxic Nitinol wires. Like all stents, the collapsed device is long and narrow to fit through the delivery sheath. It is important to note that Nitinol metal has shape memory. Thus, as it exits the sheath, the device expands and assumes its original shape at body temperature. Each current device also has a microscrew fixed to the proximal end that allows attachment to a delivery cable. This then enables the device to reconnect with the cable after deployment to allow it to be either removed or repositioned. The device is detached by unscrewing once secure, and the effective position is confirmed (e.g., by fluoroscopy).

3. SAFETY

Nickel-containing alloys, such as stainless steel, have been used in human medicine for over 100 yr. Uses include surgical instruments as well as implants such as pacemaker wires, vascular clips, mechanical cardiac valves, orthopedic prostheses, Harrington rods, and inferior vena caval filters. These successful applications have demonstrated the lack of toxicity of nickel-containing metallic implants; no systemic effects were observed or reported. However, a local fibrotic reaction surrounding stainless steel implants was thought to be caused by local passivation of nickel ions into surrounding tissue despite the absence of microscopically visible corrosion. Subsequently, the US Navy developed a new nickel-containing metal, Nitinol, in the 1960s that is an alloy of nickel and titanium and displays superior corrosion resistance. This alloy still carries the name of its heritage: NIckel TItanium–Naval Ordnance Laboratory (Nitinol).

Nitinol has numerous other physical properties besides corrosion resistance that make it attractive to use in biomedical devices, such as superelasticity (pseudoelasticity), thermal shape memory, high resiliency, and fatigue resistance. Originally, thin-wire technology, the development of the "diamond-drawn" wire, provided a shape that could be used in endodontal appliances. The tendency for Nitinol to return to its nominal shape when it is deformed was especially useful in this application. This property has also made Nitinol a valuable material in the production of endoluminal devices; a Nitinol device stretched for introduction through a small delivery catheter would expand to its original shape when deployed. This new alloy has replaced many stainless steel devices, especially self-expanding stents. Fatigue resistance prevents wire fractures and makes Nitinol devices very durable. Its lack of ferromagnetic properties allows magnetic resonance imaging of implanted devices.

To date, Amplatzer devices have proven nontoxic *(13)*. Further, devices that have been immersed in a saline bath while fatigue tested did not corrode. In addition, devices examined after 18 mo of implantation in humans and animals did not reveal surface corrosion. Importantly, nickel levels in patients before and after insertion of an Amplatzer device did not increase. The incidence of nickel allergy is estimated to be around 10% in humans. Nevertheless, with over 60,000 current implants of Amplatzer devices worldwide over the past 8 yr, no case of a reaction has been detected.

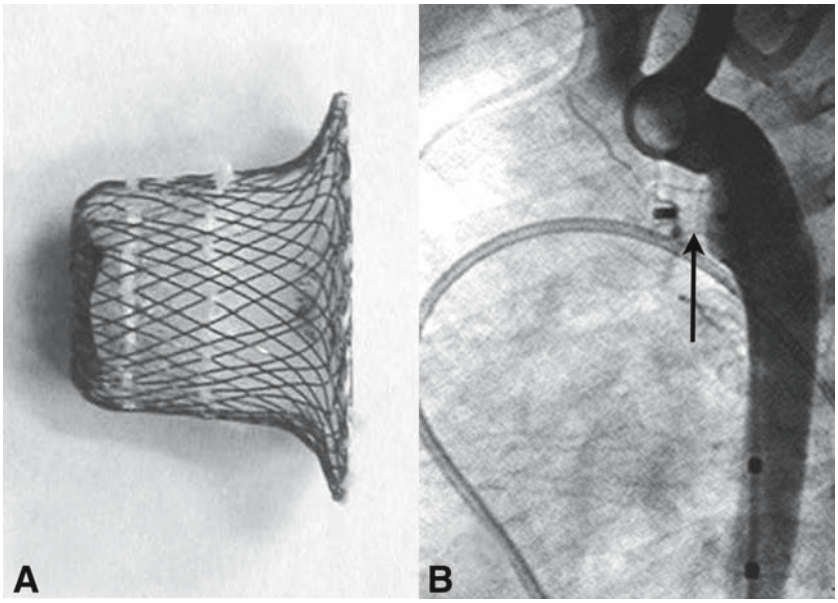

Fig. 2. Amplatzer Ductal Occluder Device. **(A)** Photograph of the device with clearly visible suturing of the baffle and stuffing to the ductal plug. **(B)** Aortogram immediately after device placement. The aortic disk is flat against the aortic wall with the plug within the ductal lumen. There is no flow through the ductus and no obstruction of the aorta or left pulmonary artery.

Thermal shape memory provides great flexibility to devices constructed of Nitinol. The nominal shape is determined by heating a formed wire frame. When cooled, the device retains the memory of its configuration.

4. PATENT DUCTUS ARTERIOSUS AND MUSCULAR VENTRICULAR SEPTAL DEFECT

Patent ductus arteriosus and muscular ventricular septal defects are similar communications to secundum atrial defects in that they are surrounded by normal vessel or muscular ventricular septum. More recent concentric devices, modified from the design of the Amplatzer Septal Occluder device, have now provided the clinical opportunity for transcatheter closure in patients with such defects.

Patent ductus arteriosus is a failure of closure of a vascular channel present before birth; it normally closes in the first 2 d of life. Overcirculation of the lungs results when this vessel remains open, and this can cause damage to the pulmonary vasculature, overwork the heart, or predispose the patient to bacterial endocarditis. Closure is primarily recommended to reduce the workload of the heart, specifically when spontaneous closure is considered no longer likely (beyond 1–2 yr of age) *(14)*. Like operative closure of a secundum atrial septal defect, surgical closure of a patent ductus arteriosus is a low-risk procedure that has been performed for decades *(15)*. Transcatheter closure of such defects is considered to carry a risk at least as low as the major invasive approach.

Successful transcatheter closure of a small patent ductus arteriosus was performed before the design of successful commercially available devices. Specifically, a coil occlusion of a patent ductus arteriosus was first performed at the University of Minnesota in 1972. Filling the aortic ampulla with stainless steel coils and their attached Dacron fibers or "hanging" a coil across the narrowest part of a patent ductus arteriosus produced reliable closure. However, the first embolization coils were not attached to a delivery wire, and the coil sometimes embolized into the pulmonary circulation. This technique was most effective when the narrowest diameter of the patent ductus was <3 mm *(16)*. At that time, a retrievable device that would occlude larger ductus was considered highly desirable.

The Amplatzer Ductal Occluder is shaped and plug sized to the aortic ampulla, with an aortic retention disk designed to prevent embolization through the ductus (Fig. 2). The device is delivered by the venous route; delivery catheters can be small (5–8 French) because of the small collapsed device diameter. This simple modification of a self-expanding stent was extremely successful in producing complete occlusion of even a large patent ductus arteriosus. In the phase II FDA trial, there was over 97% complete closure at 6 and 12 mo. Furthermore, there was only a 2.3% incidence of serious and major adverse events (including one embolization that required surgical removal and one death of a child, not device related, with a chromosomal trisomy) *(17)*. Premarket FDA approval of the Amplatzer Ductal Occluder device was granted in January 2003.

Muscular ventricular septal defects typically occur in the lower, thicker ventricular septum. Procedural closure is recommended for the same indications as both atrial septal defects and patent ductus arteriosus, that is, eliminating overwork of the heart and overcirculation to the lungs. However, unlike the other two defects, it is generally considered that surgery to close muscular ventricular septal defects is not a nontrivial or low-risk option.

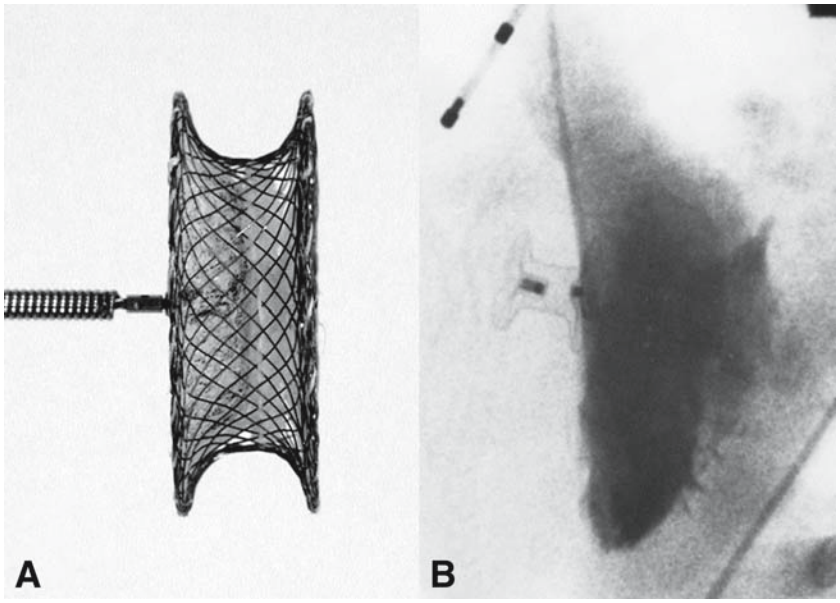

Fig. 3. Amplatzer Muscular Ventricular Septal Occluder. **(A)** Photograph of the device; the waist is wider than that of the Amplatzer Septal Occluder to allow for the thicker muscular ventricular septum. **(B)** Left ventricular angiogram 3 mo after device placement showing complete occlusion of a midmuscular ventricular septal defect.

Surgical closure of muscular ventricular septal defects is often difficult because the right ventricular aspect of the defect can be hidden from the surgeon's eyes by trabeculations within the right ventricular cavity. This results in a high incidence of residual leaks with a right ventricular approach. Directly incising the left ventricle allows clearer visualization of the defect margins, but left ventricular aneurysms or diminished left ventricular function sometimes result *(18)*. The potential for such complications has made transcatheter closure an attractive alternative.

The Amplatzer Muscular Ventricular Septal Occluder is very similar to the Amplatzer Septal Occluder. Fortunately, like a secundum atrial septal defect, muscular ventricular septal defects are separated from cardiac valves by myocardium. Yet, the obvious difference between the two malformations is the thickness of the ventricular myocardium. Hence, these devices were designed with a greater distance between the disks to accommodate such differences in myocardial thicknesses (Fig. 3). In addition, greater stability can be produced by radial force applied against the thicker muscular ventricular septum, and thus the retention disk diameters were decreased to 6–8 mm larger than the waist.

Attempts at transcatheter closure of muscular ventricular septal defects using the Clamshell/CardioSEAL device were reported to produce a 40% incidence of residual leaks *(19)*. It should be noted that these devices have a central post instead of a waist that is the size of the defect. Thus, the "retention" disks designed had to be at least twice the diameter of the defect; residual leaks likely result from migration of the central post within the defect. In contrast, the self-centering Amplatzer Muscular Ventricular Septal Occluder is fixed within the defect by its waist. Another advantage of the Amplatzer device is the smaller maximum device diameter required to close a muscular ventricular septal defect compared with central post devices.

Successful animal trials to close surgically created muscular ventricular septal defects have supported application for human use *(20)*. To date, the Amplatzer Muscular Ventricular Septal Occluder has been deployed in eight patients at the University of Minnesota; it should be noted that three devices were implanted in the operating room directly through the right ventricular wall without cardiopulmonary bypass. Complete defect closure was detected in all eight study subjects, and there were no serious or major adverse events. FDA trials are in progress. This device should significantly improve the care of children who need closure of a muscular ventricular septal defect.

5. ECCENTRIC DEVICE DESIGN

Amplatzer devices designed for closing secundum atrial septal defects, patent ductus arteriosus, and muscular ventricular septal defects are concentrically symmetrical because there are no valves near the edges of the defects they are designed to close. It is noteworthy that perimembranous ventricular septal defects are different in an important way: the aortic and tricuspid valves are close to the defect margins. Previous attempts to close perimembranous ventricular septal defects with the Clamshell and Sideris button devices have been less than optimal. For example, distortion of the aortic valve resulted in aortic insufficiency, and in some cases, the devices embolized *(21)*.

With these challenges in mind, it was considered that the flexibility of shaping the Amplatzer device frame could produce an eccentric, asymmetric device. Subsequently, an Amplatzer Perimembranous Ventricular Septal Occluder (Fig. 4) was designed with a minimal rim of the left ventricular

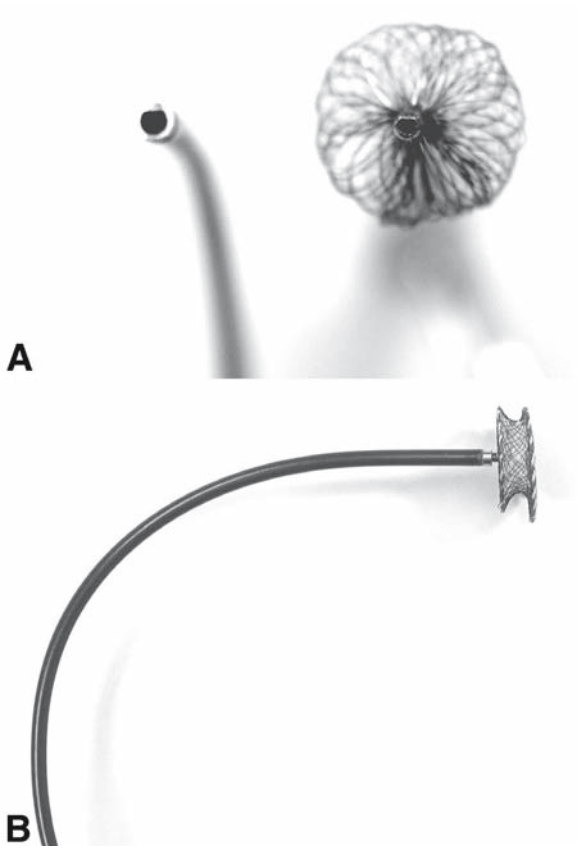

Fig. 4. Amplatzer Perimembranous Ventricular Septal Occluder device. **(A)** Photograph of the perimembranous device showing the delivery cable attached to the right ventricular disk. The asymmetric left ventricular disk is positioned with the minimal rim of the subaortic portion at the top of the device, thus preventing interference with the aortic valve. **(B)** Left ventriculogram after device placement. The asymmetric left ventricular disk avoids distortion of the aortic valve. There is no flow through the device immediately after deployment.

disk (0.5 mm) to sit beneath the aortic valve, whereas a longer (5.5 mm) inferior left ventricular disk with a short waist (1.5 mm) was designed to keep the right ventricular disk away from the tricuspid valve. Recent animal trials have shown that an eccentric design protected the aortic and tricuspid valves, but at the same time allowed closure of perimembranous ventricular septal defects.

It is noteworthy that an initial difficulty in deploying these eccentric devices was in the reliability of delivering the device in the proper (optimal) orientation. For example, advancing a pigtail catheter from the pulmonary artery through a patent ductus often resulted in the curl of the catheter oriented along the lesser curvature of the aorta. Subsequently, a sharply curved delivery sheath was designed to deliver the device to the left ventricular apex, mimicking this property. Yet, simply advancing the asymmetric device through this sheath did not always result in proper device orientation.

Hence, a sharply curved delivery catheter was designed that forced attachment of the device with the longer left ventricular disk along the lesser curvature of the catheter (Fig. 5). When this catheter design was used in combination with the sharply curved delivery sheath positioned in the left ventricular apex, the device was easily advanced to the tip of the delivery sheath to assume proper orientation *(22)*. This was confirmed in human trials; complete closure occurred in 96% of patients, and there were no serious complications, although the numbers were small *(23)*.

The aortic disk of the concentric Amplatzer Ductal Occluder sometimes protrudes into the aortic lumen. This is because the ductus arteriosus forms a 65° angle with the descending aorta, and the concentric device has a 90° angle. An eccentric device was designed to allow the aortic disk to hug the aortic wall (Fig. 6), and a similar combination of a sharply curved delivery catheter and sheath resulted in proper orientation of the device *(24)*.

6. DEVICES WITHOUT FABRIC

The polyester baffles and stuffing of Amplatzer devices sewn within the Nitinol wire frame are considered important for reliably producing thrombosis within the fabric spacing and occlusion of defects. However, sewing the material into the frames is time consuming and costly and limits automation of production. Thus, eliminating fabric could greatly simplify production and might even reduce the size of delivery systems. The initial attempt at a fabric-free device was simply to increase the wire count. Standard Amplatzer devices have a 72-wire Nitinol frame. An angled Ductal Occluder Device was developed with 144 wires. In an animal model, this resulted in complete occlusion of an artificially created patent ductus arteri osus *(25)*. This simple design modification also allowed placement through a 6-French guiding catheter. Yet, human use has revealed the potential for recanalization with this design *(26)*.

Hence, it was considered that a more effective solution would be to place wire mesh inserts within the frame of the device (Fig. 6). Initial experimental trials with the newest design placed in both a patent ductus arteriosus and atrial septal defect suggested that this may again reliably produce occlusion of such defects, but could greatly simplify device production. It remains to be determined how much this will reduce delivery system size.

7. SUMMARY

The Amplatzer family of devices is an interesting case study in the development of minimally invasive cardiac devices. They provide a successful means for transcatheter closures of congenital cardiovascular abnormalities. The simple design of such devices has allowed easy modification for numerous different types of abnormal communications. Unique characteristics of this family of devices include ease of delivery, small delivery systems, retrievability, safety, and effectiveness. To the credit of their inventor (Kurt Amplatz, MD), these devices were initially designed for use in children despite a larger adult market.

Over the past 25 yr, there have been several changes in the therapy of children with congenital heart disease. Noninvasive echocardiographic diagnosis of congenital heart disease was the first significant change to reduce the number of cardiac catheterizations. Balloon dilation of congenital narrowing of valves and arteries was the next big change in management.

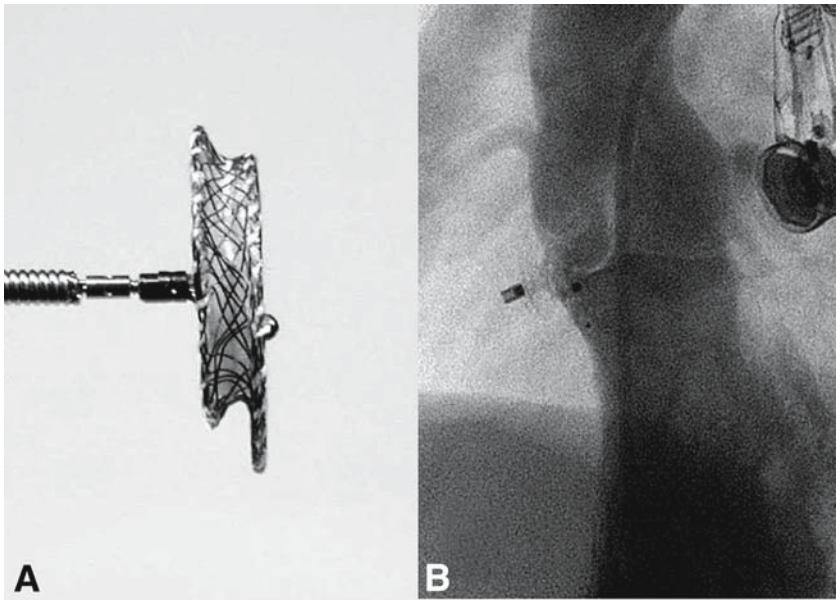

Fig. 5. Delivery system for an asymmetric device. **(A)** Photograph of the slot in the delivery catheter, flat at the upper margin; this matches a flattened area at the upper surface of the microscrew. The microscrew will only fit into the slot in the correct orientation. **(B)** The asymmetric Perimembranous Ventricular Septal Occluder is attached to the curved delivery catheter. The longer rim of the left ventricular disk is oriented along the lesser curvature of the delivery catheter.

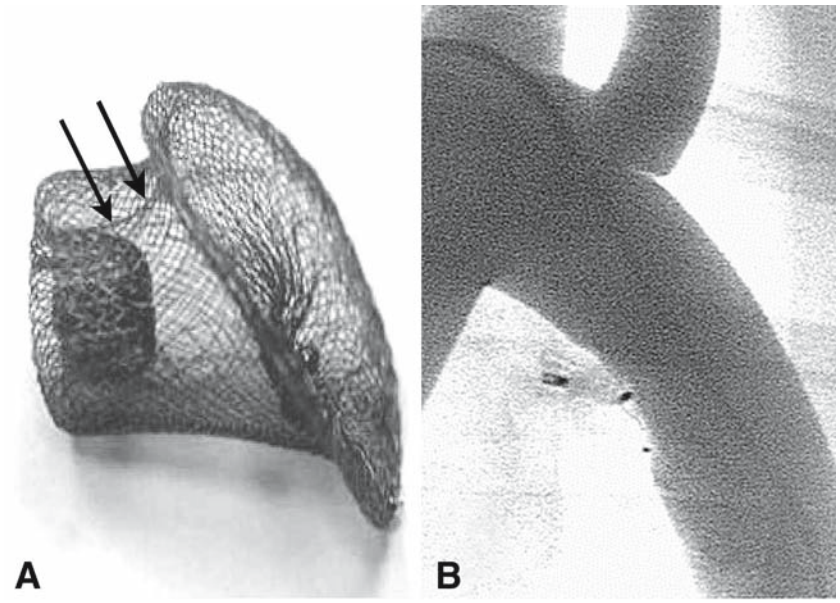

Fig. 6. Angled ductal occluder device without fabric. **(A)** Photograph of the device showing the external frame, which is composed of 144 wires. Arrows indicate a wire insert shaped like the external frame. **(B)** Aortogram performed immediately after device placement in a surgically created "ductus arteriosus" in a canine model. The angled aortic disk lies snuggly along the aortic wall. There is immediate complete occlusion of the ductus.

This caused a return to the cardiac catheterization laboratory for interventional procedures.

The Amplatzer family of devices has further changed the face of treatment of congenital heart disease in children. Yet, transcatheter therapy is not limited to simpler lesions that often precede surgical repair, decreasing the complexity of surgical intervention. Amplatzer devices can also be delivered in the operating room directly through the surface of the heart without cardiopulmonary bypass. This has brought a new era of cooperation between pediatric cardiologists and cardiovascular surgeons.

REFERENCES

1. Latson, L.A. (2000) Atrial septal defect, in *Pediatric Cardiovascular Medicine* (Moller, J.H. and Hoffman, J.I.E., eds.), Churchill Livingstone, New York, NY, pp. 311–321.
2. Lewis, F.J., Varco, R.L., and Taufic, M. (1954) Repair of atrial septal defects in man under direct vision with the aid of hypothermia. *Surgery*. 36, 538–556.
3. Murphy, J.G., Gersh, B.J., McGoon, M.D., et al. (1990) Long-term outcome after surgical repair of isolated atrial septal defect: follow-up at 27–32 yr. *N Engl J Med*. 323, 1645–1650.
4. King, T.D. and Mills, N.L. (1976) Secundum atrial septal defects: nonoperative closure during cardiac catheterization. *JAMA*. 235, 2506–2509.
5. Rome, J.J., Keane, J.F., Perry, S.B., Spevak, P.J., and Lock, J.E. (1990) Double-umbrella closure of atrial septal defects: initial clinical applications. *Circulation*. 82, 751–758.
6. Sideris, E.B., Sideris, S.E., Thanopoulos, B.D., Ehly, R.L., and Fowlkes, J.P. (1990) Transvenous atrial septal defect occlusion by the buttoned device. *Am J Cardiol*. 66, 1524–1526.
7. Hausdorf, G., Schneider, M., Granzbach, B., Kampmann, C., Kargus, K., and Goeldner, B. (1996) Transcatheter closure of secundum atrial septal defects with the atrial septal defect occlusion system: initial experience in children. *Heart*. 75, 83–88.
8. Das, G.S., Voss, G., Jarvis, G., Wyche, K., Gunther, R., and Wilson, R.F. (1993) Experimental atrial septal defect closure with a new, transcatheter, self-centering device. *Circulation*. 88, 1754–1764.
9. Rao, P.S., Berger, F., Rey, C., et al. (2000) Results of transvenous occlusion of secundum atrial septal defects with the fourth generation buttoned device: comparison with first, second and third generation devices. International Buttoned Device Trial Group. *J Am Coll Cardiol*. 36, 583–592.
10. Agarwal, S.K., Ghosh, P.K., and Mittal, P.K. (1996) Failure of devices used for closure of atrial septal defects: mechanisms and management. *J Thorac Cardiovasc Surg*. 112, 21–26.
11. Du, Z.D., Hijazi, Z.M., Kleinman, C.S., Silverman, N.H., Larntz, K., and Amplatzer Investigators. (2002) Comparison between transcatheter and surgical closure of secundum atrial septal defect in children and adults: results of a multicenter nonrandomized trial. *J Am Coll Cardiol*. 39, 1836–1844.
12. Sharafuddin, M.J.A., Gu, X., Titus, J.L., Urness, M.C., Cervera-Ceballos, J.J., and Amplatz, K. (1997) Transvenous closure of secundum atrial septal defects: preliminary results with a new self-expanding Nitinol prosthesis in a swine model. *Circulation*. 95, 2162–2168.
13. Kong, H., Wilkinson, J.L., Coe, J.Y., et al. (2002) Corrosive behavior of Amplatzer devices in experimental and biological environments. *Cardiol Young*. 12, 260–265.
14. Gersony, W.M. and Apfel, H.D. (2000) Patent ductus arteriosus and other aortopulmonary anomalies, In *Pediatric Cardiovascular Medicine* (Moller, J.H. and Hoffman, J.I.E., eds.), Churchill Livingstone, New York, NY, pp. 323–330.
15. Kirklin, J.W. and Barratt-Boyes, B.G. (1993). Patent ductus arteriosus, In *Cardiac Surgery*, 2nd Ed. (Kirklin, J.W. and Barratt-Boyes, B.G., eds.), Churchill Livingstone, New York, NY, p. 854.
16. Nykanen, D.G., Hayes A.M., Benson, L.N., and Freedom, R.M. (1994) Transcatheter patent ductus arteriosus occlusion: application in the small child. *J Am Coll Cardiol*. 23, 1666–1670.
17. Pass, R.H., Hijazi, Z., Hsu, D.T., Lewis, V., and Hellenbrand, W.E. (2004) Multicenter USA Amplatzer PDA occlusion device trial: initial and mid-term results. *J Am Coll Cardiol*. 44:513–5 19..
18. Kirklin, J.K., Castaneda, A.R., Keane, J.F., Fellows, K.E., and Norwood, W.I. (1980) Surgical management of multiple ventricular septal defects. *J Thorac Cardiovasc Surg*. 80, 485–493.
19. Lock, J.E., Block, P.C., Mckay, R.G., Baim, D.S., and Keane, J.F. (1988) Transcatheter closure of ventricular septal defects. *Circulation*. 78, 361–368.
20. Amin, Z., Gu, X., Berry, J.M., et al. (1999) New device for closure of muscular ventricular septal defects in a canine model. *Circulation*. 100, 320–328.
21. Rigby, M.L. and Redington, A.N. (1994) Primary transcatheter closure of perimembranous ventricular septal defect. *Br Heart J*. 72, 368–371.
22. Gu, X., Han, Y.M., Titus, J.L., et al. (2000) Transcatheter closure of membranous ventricular septal defects with a new Nitinol prosthesis in a natural swine model. *Catheter Cardiovasc Interv*. 50, 502–509.
23. Bass, J.L., Kalra, G.S., Arora, R., et al. (2003) Initial human experience with the Amplatzer perimembranous ventricular septal occluder device. *Catheter Cardiovasc Interv*. 53, 238–245.
24. Kong, H., Gu, X., Bass, J.L., et al. (2001) Experimental evaluation of a modified Amplatzer duct occluder. *Catheter Cardiovasc Interv*. 53, 571–576.
25. Bass, J.L., Kong, H., Gu, X., Urness, M., Titus, J., and Hunter, D.W. (2002) Experimental evaluation of a new angled Amplatzer duct occluder. Paper presented at 37th Annual General Meeting of the AEPC, Porto, Portugal, May 15–18.
26. Bass, J.L. (2003) Amplatzer devices without fabric. Sixth International Workshop Catheter Interventions in Congenital Heart Disease, Frankfurt, Germany, June 21.

30 End-Stage Cardiomyopathy

Ventricular Assist Devices

SOON J. PARK, MD

CONTENTS

1. INTRODUCTION

Heart disease is the number one cause of morbidity and mortality in Western society. This problem has become well recognized in the literature over the past few decades, and researchers have mounted intense efforts to remedy the situation. A heart transplant is clearly the most effective therapy for patients with advanced heart failure; it is able to restore them to a near-normal lifestyle, and long-term survival is excellent *(1)*. However, the number of donor hearts available for transplantation is limited to only about 2000 each year, compared to over 10,000 people each year who could benefit from such a therapy.

Successful development of a total artificial heart or advanced ventricular assist devices could help resolve this imbalance. Development efforts to do so were organized under the National Institutes of Health leadership in 1964. The ideal pump was originally thought to be a totally implantable device, with an electrical motor that could completely replace the heart function physiologically as well as anatomically. Yet, despite many decades of research, we still do not have such a device. In the mid-1970s, parallel research on ventricular assist devices took place; the result was a variety of ventricular assist devices described in this chapter.

2. MECHANICS

2.1. Volume Displacement Pumps

The human heart is a volume displacement pump. To create a unidirectional flow with a single pumping chamber, inflow and outflow valves are required. For example, in the left ventricle of the native heart, the mitral valve functions as the inflow valve; the aortic valve functions as the outflow valve. The result is unidirectional blood flow. Similarly, ventricular assist devices designed as volume displacement pumps would require these two types of valves. Some ventricular assist devices have incorporated mechanical prosthetic valves; others have utilized bioprosthetic valves (Fig. 1). Importantly, the choice of valve mandates different types of anticoagulation therapy and thus leads to a different natural history of valve failure.

A major obstacle in designing clinically acceptable ventricular assist devices has been the array of problems associated with the blood contact surfaces. Specifically, any type of stagnant blood flow within the pocket of the pumping chamber can result in thrombus formation. Also, the artificial blood contact surface is quick to promote a clotting cascade, resulting in significant thromboembolism. Yet, initial attempts at making the blood contact surface as smooth as possible have not yielded satisfactory outcomes. One proposed solution for this was the construction of textured blood contact surface to promote early platelet and fibrin deposition, which resulted in formation of stable pseudointima; such a design was applied in the HeartMate® system (Thoratec Corporation; Pleasanton, CA) (Fig. 2) *(2)*.

The mechanism involved in ejecting blood varies from model to model. Some ventricular assist devices either have a compressible blood-filled sac or a flexible diaphragm within a hard shell. In others, compressed air serves as a medium to collapse either the sac or the diaphragm and thereby eject

From: *Handbook of Cardiac Anatomy, Physiology, and Devices*
Edited by: P. A. Iaizzo © Humana Press Inc., Totowa, NJ

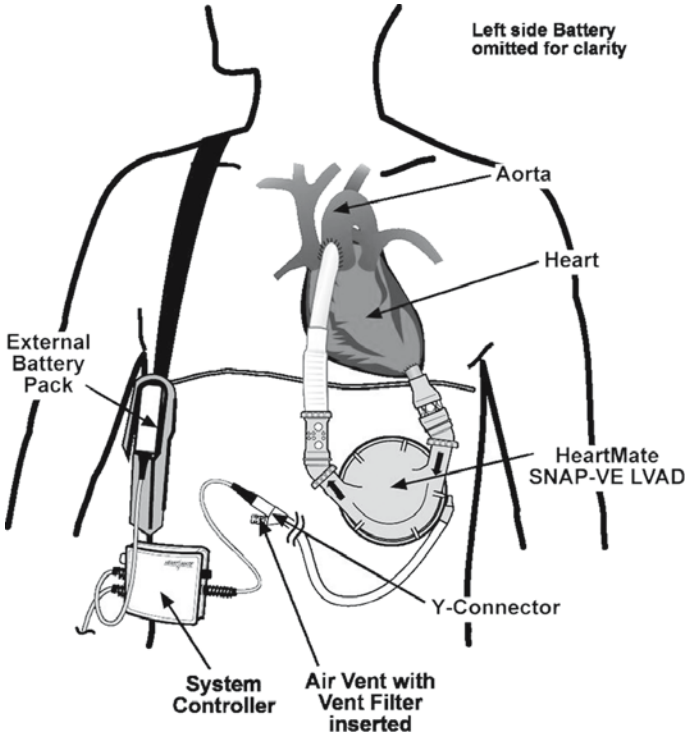

Fig. 1. Schematic of a HeartMate® SNAP-VE ventricular assist device system. One can see the internal connections at the apex of the left ventricle where there is inflow into the device and outflow connected directly to the aorta. This system utilizes an external battery pack and controller system. LVAD, left ventricular assist device.

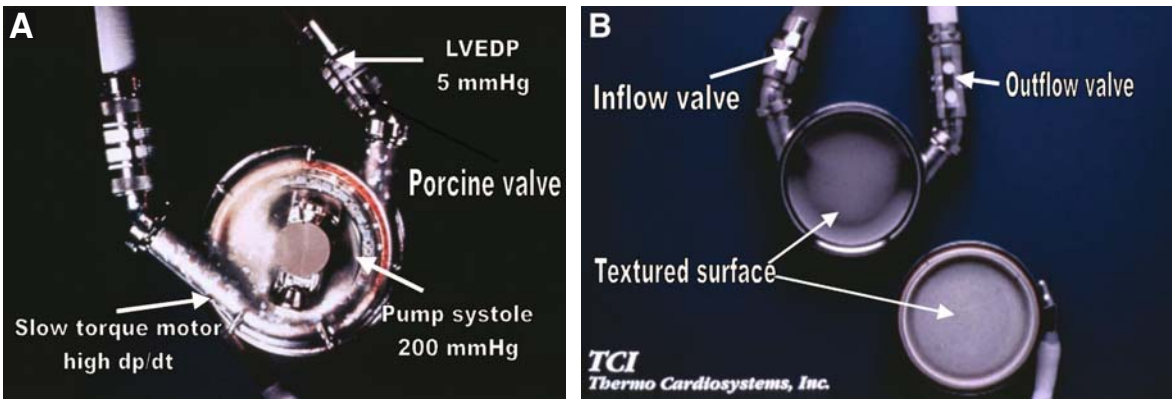

Fig. 2. **(A)** External view of an actual HeartMate®-VE. This pump generates a systolic pressure of 200 mmHg, utilizing a slow torque motor with high dp/dt. **(B)** Shown are the textured blood contact surfaces that promote early platelet and fibrin deposition, resulting in formation of a stable pseudointima. LVEDP, left ventricular end-diastolic pressure. Reprinted with permission from Thoratec Corporation.

blood. Compressed air seems to provide a simple and reliable way of either activating the diaphragm or compressing the sac, with a pressure more comparable to a physiologically acceptable waveform. However, this design requires a bulky driving console, compromising the patient's mobility.

In other ventricular assist devices, the diaphragm is activated by a slow-torque electrical motor that is small enough to be incorporated into the implantable unit. Thus, patient mobility is significantly improved with this type of ventricular assist device compared to the ones driven by a pneumatic console. Because the diaphragm is propulsed by a noncompressible metal, the pressure waveform during ejection is less physiological, with a rather rapid rise in pressure over time (dp/dt); the peak dp/dt could be many times higher than that generated by a normal heart. This could translate into a significant mechanical load on the inflow valve during the ejection phase and subsequent premature inflow valve failure. Furthermore, such an abnormal pulse wave and sudden increase in patient's cardiac output could adversely affect the central nervous system by causing cerebral edema.

A volume displacement pump goes through a natural fluctuation in pressure in the driving chamber, but it either must have an implantable compliance chamber or it must be vented to the outside. Yet, to date ventricular assist devices with a totally implantable compliance chamber are bulkier to implant, and the compliance chamber itself has to be accessed from time to time to compensate for gradual dissipation of gas in the chamber. These features may thus compromise its application in the clinical setting, although its total implantability is attractive. On the other hand, the pumps with external vents still cannot be totally implantable. The driveline exit site can be a significant source of discomfort and infection. Even though patient mobility is significantly improved with an electrical motor-driven system, these systems tend to be bulky and heavy, resulting in pain and abdominal discomfort. Furthermore, this type of system requires replacing the entire system, rather than just switching out the external driving console (as in the air-driven system), when the motor fails.

Some of the volume displacement pumps are designed to be placed outside the body, with inflow and outflow cannulas attaching the system to the ventricle and aorta. This type of system has the benefit of versatility, and even small patients can be supported with these paracorporeal pumps. However, an externally located pump attached to a driving console compromises the patient's quality of life significantly.

Even though volume displacement pumps, with their relatively simple mechanical construction, are effective in replacing cardiac function in the clinical setting, to date they continue to have many shortcomings. Accordingly, different technological platforms are under evaluation for the next generation of ventricular assist devices.

2.2. Axial Flow Pumps

Archimedean pumps have been in use for centuries as a very effective means to transport fluids. A similar type of axial flow pump that featured rapid rotation of an impeller in a blood system was thought to be impractical given concerns about red blood cell destruction (Fig. 3), but that theoretical concern was recently discarded when a Hemopump® was successfully used in a clinical setting without significant hemolysis *(3)*. The Hemopump has thus set the stage for evaluation of other types of axial flow pumps that could be used for blood. Nevertheless, with high-speed axial flow pumps, the heat generated by the motor must be sufficiently less than what the human body is able to dissipate in a physiologically acceptable manner. The amount of heat generated seems to be in an acceptable range, so it has not been a concern in creating clinically acceptable axial flow pumps.

Importantly, an axial flow pump does not require valves to create a unidirectional flow. It does not require an external vent or a compliance chamber, thus making it more likely to utilize this approach to create a totally implantable system (Fig. 4). Furthermore, a motor attached to a turbine to drive the blood could be located even within the heart, and the outflow conduit could be connected to the ascending or descending aorta. Or, a pump could be connected to the apex of the left ventricle with an inflow cannula, and an outflow graft could be connected to the ascending or descending thoracic aorta.

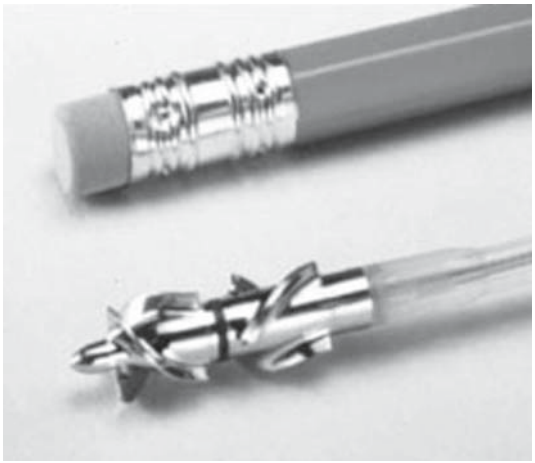

Fig. 3. Relative size of the impeller blade utilized to create flow in the axial pump (compared to a pencil).

Fig. 4. Size of the Jarvik 2000 (Jarvik Heart, Inc. and Texas Heart Institute) axial flow pump, which like other ventricular assist device systems, has an inlet within the left ventricular apex and outflow connected to the aorta. The advantage of this type of system is that it will likely be totally implantable.

Depending on the motor capacity and rotational speed, an axial flow pump could function either as a partial-flow or a full-flow support device. This type of ventricular assist device functions like an open tube in terms of pressure transmission; any pressure generated by the native heart would be transmitted to the distal vascular bed. Therefore, the forward flow generated by an axial flow pump could be augmented by pulsatility from the native heart. The amplitude of pressure waves would depend on the contractual state and preload of the left ventricle.

To date, there is little accumulated clinical experience with axial flow pumps compared with that of volume displacement pumps. However, initial results appeared to be encouraging, with effective circulatory support and durability *(4–6)*. Diminished pulse pressure when utilizing an axial flow pump seemed to be tolerated well in patients, at least for the short term; the

long-term consequences of axial flow pumps have yet to be evaluated. Some axial flow pumps require a suspension of the rotor with a contact point. The concern about potential wear over time needs to be evaluated through in vivo testing, but current in vitro data seem to indicate that the actual wear may be negligible for at least a few years. Hemolysis associated with axial flow pumps has been detectable, but is considered clinically insignificant. These pumps seem to activate platelets because of the physical strain on blood cells; yet, such activation may be an important source of intravascular thrombosis and embolic complications. Currently, intense anticoagulation regimens targeting platelet activation and clotting cascade have been employed to deal with the problems of thromboembolism.

2.3. Centrifugal Pumps

The development of a rare earth-based magnet within the past few decades has provided an additional potential technological platform for designing ventricular assist devices. With this technology, a flow source could be suspended and rotated in a magnetic field, avoiding any need for a contact point and thus eliminating the concern of wear of the rotor over a long period of time. Furthermore, such ventricular assist devices would likely have very little mechanical friction resistance to overcome. Pulsatile flow could also be generated by a rapid variation of rotation speeds. The blood propeller could be designed in either a turbine or centrifugal form, potentially providing a reliable forward flow with pulsatility.

This type of futuristic ventricular assist device could be an open tube system as well, capable of transmitting the native heart's pressure wave. However, if the motor were to fail, the open system could result in significant regurgitant flow, worsening heart failure symptoms. In addition, no reliable backup support mechanism would be readily available unless specifically added (like a hand pump with volume displacement pumps).

3. CLINICAL EXPERIENCE

Before any ventricular assist device is implanted in the clinical setting, it has undergone significant in vitro and in vivo testing, including preclinical animal implant experiments. Nevertheless, even though the efficacy, reliability, and performance of these devices would be well understood, unexpected adverse events could be observed in the clinical setting.

As the various types of ventricular assist devices are introduced in a clinical setting, the initial target population should be individuals who could actually benefit from such a therapy with a minimal risk of adverse events from the device itself. Thus, the most logical place to start is with patients who are at imminent risk of death while waiting for a heart transplant. The risk/benefit ratio seems to favor implantation of such experimental ventricular assist devices as a salvage procedure; that is, the duration of ventricular assist device support would be finite and short term, until a donor heart became available. A prospective trial utilizing such a setting was conducted by Frazier et al. *(7)*, and therapeutic benefit of the ventricular assist device as a bridge to a heart transplant was documented. This trial resulted in approved application of such a device as a bridge therapy to heart transplant.

The number of patients on heart transplant lists can be considered relatively few, compared with the many patients with conditions similar to end-stage heart failure. Nevertheless, because of the limited number of donor hearts available in the United States, many patients are denied a chance at heart replacement therapy. Therefore, the next logical clinical consideration for patients with advanced heart failure is, "Can a ventricular assist device be used to improve longevity and quality of life and not merely as a bridge to a transplant (that is, as a means to an end)?" This question was originally asked in the 1960s when the National Institutes of Health sponsored a research project on the totally artificial heart. Clearly, this question remains at center stage for any development of a circulatory support system.

More specifically, with accumulated experience from the HeartMate-VE system as a bridge to a heart transplant, answers to that question were sought through the Randomized Evaluation of Mechanical Assistance for the Treatment of Congestive Heart Failure (REMATCH) trial under the leadership of Dr. Eric Rose *(8)*. That prospective randomized clinical trial compared the survival outcomes in patients with advanced heart failure who received optimal medical management vs undergoing ventricular assist device implantation.

The trial enrolled 129 patients and demonstrated statistically significant benefits at 1 and 2 yr. Importantly, the ventricular assist device group had about twice the survival rate of the optimal medical management group *(9)*. Nearly all mortality in the optimal medical management group was caused by advanced heart failure. However, infection and device failure accounted for about 60% of the mortality in the ventricular assist device group. Yet, it is considered that both of these complications could be reduced significantly over time.

The REMATCH trial clearly documented efficacy of the ventricular assist device in an evidence-based manner and set the stage for expanded indication of device implantation in the clinical setting. The FDA has now approved the Heartmate-VE as a destination therapy device to treat end-stage heart failure patients "as a means to an end." Such approval should encourage new device development, which in turn should advance the field significantly over time and improve the quality of life and survival rate of patients with advanced heart failure symptoms (Fig. 5).

It should be noted that one of the axial flow pump devices, the DeBakey ventricular assist device by Micromed Technology, Inc. (Houston TX), is currently undergoing a clinical trial to test its efficacy as a bridge to a heart transplant device *(10)*. It is anticipated that many more new and different models of device systems will be evaluated in the near future in similar clinical settings.

4. FUTURE

The future of ventricular assist devices is promising. Currently, we seem to be dealing with early prototypes. Many minor and major advances will take place in the field when we finally have a long-term device that can replace circulatory function. Nevertheless, any device should possess most of the following characteristics:

1. It must be totally implantable to lower the risk of infection significantly and to improve the quality of life for patients.

Fig. 5. One of the author's former patients standing on his tractor, taking a break from plowing his farm fields; he did this while being supported with a ventricular assist device system.

2. It must be effective enough to provide adequate blood flow to meet the variable hemodynamic needs associated with a normal lifestyle (allow for activity and mobility).
3. It must be reliable and durable. The current ventricular assist devices require a major operation to implant, and device failures require additional major surgery to change out the pumps. For FDA approval of the ventricular assist device as a destination therapy, 5–7 yr has been suggested as an acceptable length of time for durability.
4. It must be compatible with human physiology. For example, pressure wave generation over time must be acceptable to the human body, especially to the neurological system. With the axial flow pump design, diminished pulse pressure must be determined to be physiologically acceptable to the human body over the long term. Likewise, with the levitating axial flow pump design and its ability to generate adequate pulse pressures, pressure generation must be acceptable and thus likely to mimic the human physiological pressure waveform.
5. It must be small in size to ensure acceptable quality of life. Currently, the electrical motor-driven ventricular assist device is considered bulky and noisy, with significant motion associated with the slow torque motor. The future ventricular assist device must be even smaller, thus not impinging on other organ space; moreover, it must not cause pain because of motion or heaviness.
6. It must have minimal associated thromboembolic risks. The blood contact surface or physical property of the propulsion mechanism must not trigger intravascular thrombosis. Some of the current ventricular assist devices have associated adverse blood contact properties that are being addressed by aggressive anticoagulation regimens. In the future, the need for anticoagulation must be minimal. An optimal design would minimize the blood contact-related activation of the clotting cascade and thus cause minimal physical deformity of blood cells.

5. SUMMARY

Ventricular assist device development has been an interesting and gratifying clinical area of advancement for the past several decades. Importantly, many patients have been saved from imminent death by appropriate application of ventricular assist devices and subsequent heart transplant. Most of these patients have been able to add years to their lives and enjoy good health. Of clinical interest, some degree of reverse remodeling process has been confirmed in many patients during the unloading period of the left ventricle on the ventricular assist device. Furthermore, a few patients have even demonstrated clinically significant myocardial recovery to the degree at which ventricular assist devices could be explanted safely.

Thus, the exact conditions under which myocardial recovery occurs and ways to enhance incidence of recovery are now under intense investigation. For example, Dr. Jacob Yacoub et al. (Imperial College School of Medicine, Heart Science Centre, Middlesex, UK) have used Clenbutrol, a β-2 agonist, to promote left ventricular hypertrophy and subsequent ventricular assist device removal. This particular drug is under evaluation at other centers as well to validate the initial observation made in England. Such drugs may play an important role in promoting reverse remodeling in failing hearts. The role of the ventricular assist devices as a bridge therapy to myocardial recovery will remain as a very intriguing concept to explore. A combination of new drugs or stem cell infusion and short-term ventricular assist device support may prove to be helpful in successfully repairing failing hearts *(11)*.

REFERENCES

1. Hosenpud, J. D., Bennett, L. E., Keck, B. M., Boucek, M. M., Novick, R. J. (2001) The Registry of the International Society for Heart and Lung Transplantation: Eighteenth Official Report. *J Heart Lung Transplant*. 20, 805–815.
2. Rose, E.A., Levin, H.R., Oz, M.C., et al. (1994) Artificial circulatory support with textured interior surfaces. A counterintuitive approach to minimizing thromboembolism. *Circulation*. 90, II87–II91.
3. Wampler, R.K., Baker, B.A., Wright, W. M. (1994) Circulatory support of cardiac interventional procedures with the Hemopump cardiac assist system. *Cardiology*. 84, 194–201.
4. Westaby, S., Banning, A.P., Jarvik, R., et al. (2000) First permanent implant of the Jarvik 2000 Heart. *Lancet*. 356, 900–903.
5. Noon, G.P., Morley, D., Irwin, S., Benkowski, R. (2000) Development and clinical application of the MicroMed DeBakey VAD. *Curr Opin Cardiol*. 15, 166–171.
6. Wieselthaler, G.M., Schima, H., Hiesmayr, M., et al. (2000) First clinical experience with the DeBakey VAD continuous-axial-flow pump for bridge to transplantation. *Circulation*. 101, 356–359.
7. Frazier, O.H., Rose, E.A., Oz, M. C., et al. (2001) Multicenter clinical evaluation of the HeartMate vented electric left ventricular assist system in patients awaiting heart transplantation. *J Thorac Cardiovasc Surg*. 122, 1186–1195.
8. Rose, E.A., Moskowitz, A.J., Packer, M., et al. (1999) The REMATCH trial: rationale, design, and end points. Randomized Evaluation of Mechanical Assistance for the Treatment of Congestive Heart Failure. *Ann Thorac Surg*. 67, 723–730.
9. Rose, E.A., Gelijns, A.C., Moskowitz, A. J., et al. (2001) Long-term mechanical left ventricular assistance for end-stage heart failure. *N Engl J Med*. 345, 1435–1443.
10. Goldstein, D.J. (2003) Worldwide experience with the MicroMed DeBakey Ventricular Assist Device as a bridge to transplantation. *Circulation*. 108, II272–II277.
11. Suzuki, K., Murtuza, B., Smolenski, R. T., et al. (2001) Cell transplantation for the treatment of acute myocardial infarction using vascular endothelial growth factor-expressing skeletal myoblasts. *Circulation*. 104, I207–I212.

31 Experimental Cell Transplantation for Myocardial Repair

JOSEPH LEE, BS, ATSUSHI ASAKURA, PhD, AND JIANYI ZHANG, MD, PhD

CONTENTS

1. INTRODUCTION

The heart is an organ whose function that hinges critically on its supply of and demand for oxygen. Supply of oxygen to the myocardium is influenced by factors such as blood oxygen content, blood pressure, coronary arterial resistance, and maximal coronary flow reserve. The last is considered the most important factor and is defined as the ratio of maximal achievable myocardial blood flow rate, by pharmacological selective coronary vessel dilation, to basal myocardial blood flow rate. Demand for oxygen by the myocardium is governed by factors such as heart rate, heart wall tension, wall thickness, and contractile state of heart muscle cells (cardiomyocytes).

In the face of stresses that significantly disturb the balance of oxygen supply and demand in the heart, the left ventricle of the heart in particular is known to undergo compensatory structural remodeling. The left ventricle is responsible for pumping blood systemically through the tissue of organs and, as such, is considered key among the four heart chambers. A common clinical complication experienced by the left ventricle is myocardial infarction (more commonly known as a heart attack) in which a segment of the left ventricular myocardium is damaged by a local deficiency in oxygen supply. Subsequently, the damaged chamber cannot generate adequate mechanical forces, a situation that then causes the surrounding myocardia to attempt to compensate with an increase in muscle mass. From a cellular perspective, this increase occurs by expanding the size of existing cardiomyocytes (termed *hypertrophy*) as opposed to generating additional cells (termed *hyperplasia*).

Cardiomyocytes can be damaged or killed by: (1) disrupting their supply of oxygenated blood and (2) overworking them by increasing the demand for work beyond normal limits. Within an area directly affected by myocardial infarction, the dead cardiomyocytes are replaced by fibroblasts, which are incapable of doing cardiac work. In areas outside the infarction, the cardiomyocytes may undergo compensatory hypertrophy. A functionally stable degree of left ventricular hypertrophy is only considered to be temporary, and subsequent compensatory hypertrophy typically overshoots resulting in overgrown cardiomyocytes.

From a clinical perspective, the sequelae of myocardial infarction commonly include progressive myocardial dysfunction and subsequent congestive heart failure. Customarily, congestive heart failure has been considered an end-stage *irreversible* clinical condition for which conventional medical management is primarily intended to relieve symptoms and slow deterioration. Thus, this treatment merely accommodates damaged myocardium instead of effecting direct repair to restore normal structure and function.

The experimental therapy known as *cell transplantation* (or *cellular cardiomyoplasty*) is intended to achieve repair and regeneration of damaged heart muscle. This approach is directed toward transcending the dogma that the heart and its cardiomyocytes are terminally differentiated and incapable of regeneration. Relatively recent studies have shown that the adult

From: *Handbook of Cardiac Anatomy, Physiology, and Devices*
Edited by: P. A. Iaizzo © Humana Press Inc., Totowa, NJ

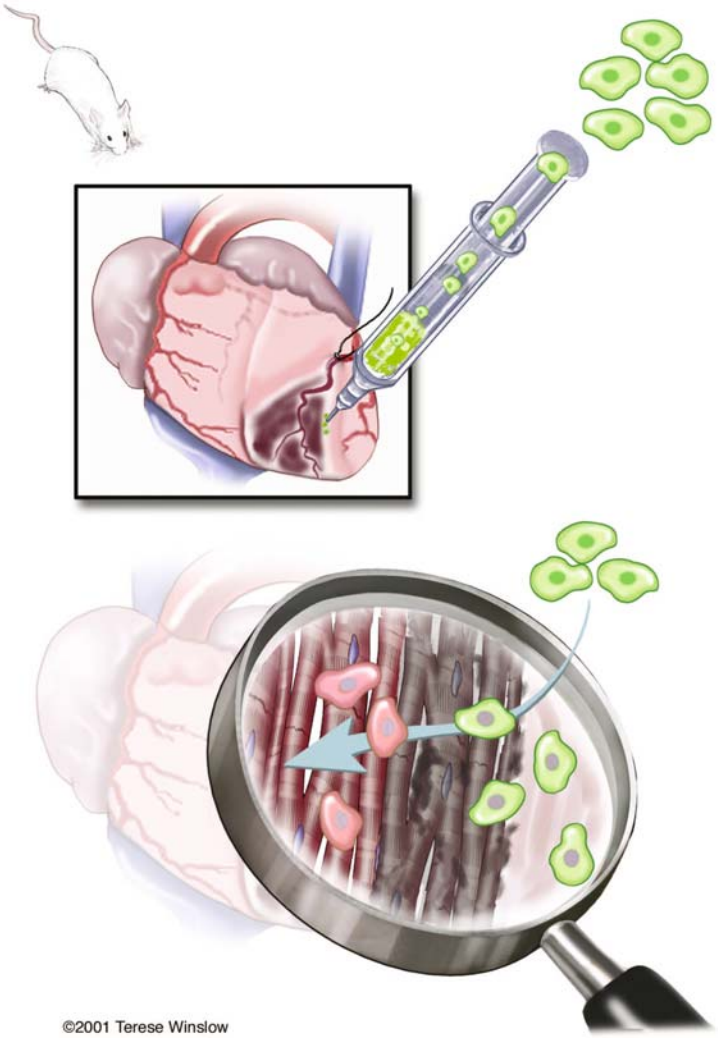

Fig. 1. Schematic of cell transplantation in action. In this example, mouse adult stem cells are delivered to a damaged region of the myocardium by intramyocardial injection to effect tissue repair. The mechanisms of repair are unclear, but could include regeneration of cardiomyocytes, vascular cells, or components of the extracellular matrix. © 2001 Terese Winslow.

human heart is actually capable of cardiomyocyte regeneration by a number of mechanisms.

Some suggest that regeneration occurs by the proliferation (i.e., hyperplasia) of existing cardiomyocytes *(1–4)*. Others have suggested that the presence of extracardiac stem cells, when introduced to the myocardium, spawn both myocytes and vascular cells through a process termed *transdifferentiation* or *plasticity (5–8)*. Others have proposed that intracardiac stem cells exist that might partly function by fusing with existing cardiomyocytes in a process termed *cell fusion (9,10)*.

Nevertheless, in the face of myocardial infarction, the human heart typically elicits little or no regenerative response adequately sufficient for innate cardiac regeneration. Thus, the current major strategy of cell transplantation is to amplify such processes to therapeutic levels.

2. METHODS AND MECHANISMS

In cell transplantation, healthy cells are grafted into the diseased myocardium to elicit repair. Cells can be individual or aggregated and can be delivered either by direct injection into the myocardium or via the blood supply that feeds the myocardium. The potential utility of determined and stem cells for such a therapy have been studied. Cell transplantation studies have been primarily targeted to ischemic and segmental cardiomyopathies, as opposed to treating global, dilated cardiomyopathies. A general protocol for cell transplantation is as follows:

1. Isolate cells of a specific type (e.g., cardiomyocytes, bone marrow stem cells [BMSCs], embryonic stem [ES] cells, etc.) from a source.
2. Purify and perhaps grow larger numbers of the cells in the laboratory; cells can also be genetically manipulated or tagged at this stage.
3. Administer the cells to the patient with the injured myocardium (Fig. 1) *(11)*.
4. Wait and allow the cells to repair injured heart tissue.

The exact mechanism by which implanted cells repair the myocardium remains unclear and probably depends on the

cell type used. In general terms, the new cells could directly replace or stimulate healing in existing host tissue. As potential examples of the first mechanism, new cells would become functional as cardiomyocytes in the myocardium or as endothelial or smooth muscle cells in myocardial blood vessels. As possible examples of the second mechanism, cells might interact with host cells via secreted signals, cell–cell contact, or cellular fusion to initiate events that lead to repair or tissue remodeling.

The result of these interactions could include the recruitment of endogenous repair cells, the stimulation of angiogenesis to increase local blood supply, or the inhibition of programmed cell death in host cardiomyocytes. Transplanted cells might also attenuate the pathological remodeling processes associated with the progressive or neurohormonal remodeling commonly associated with heart failure. The mechanisms of repair are further obfuscated by the variety of cell types studied and, to some degree, by the attempts to engineer specific therapeutic properties into such cells.

Several criteria must be fulfilled for cell transplantation to be deemed a useful therapy *(12)*, including the following: (1) feasibility of transplantation; (2) survival of implanted cells; (3) vasculogenesis and angiogenesis through the cellular graft; (4) proliferative capacity of the therapeutic cells; (5) electromechanical integration of the graft with the host heart; (6) convergence of the phenotype of the implanted cells to that of the host; and (7) contribution of graft to cardiac performance and clinical outcomes. The complexity of this endeavor is illustrated in Fig. 2 *(13)*.

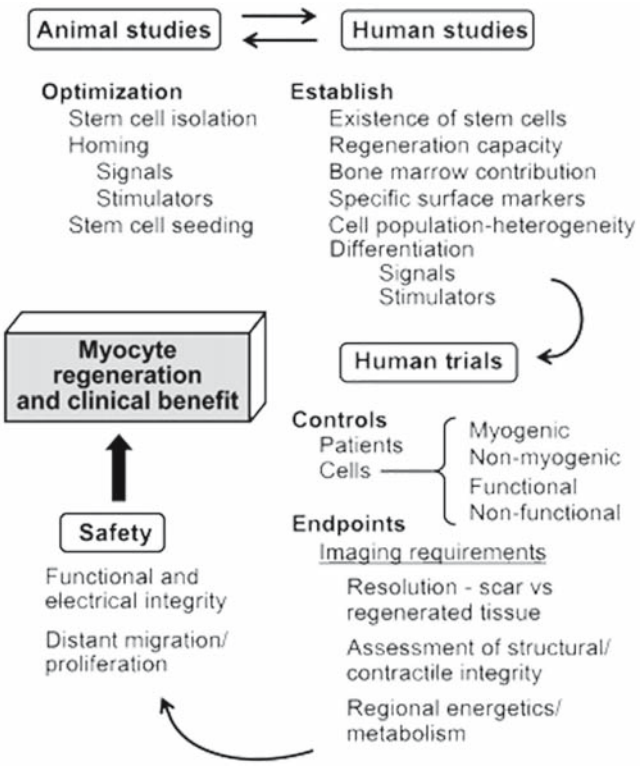

Fig. 2. Interplay among basic, animal, and human studies in cell transplantation. Previous research has established the feasibility and effects of transplantation in animal models. Current research addresses feasibility and efficacy in human trials. Future research must address concerns of safety. (From Caplice NM and Gersh BJ. Stem cells to repair the heart: a clinical perspective. *Circ Res.* 92: 6–8. © 1993 Lippincott, Williams, and Wilkins.)

3. CELLS

A decision of primary importance in cell transplantation is the selection of cell type. Presented in this section is a survey of the major cell types investigated by various laboratories to date.

3.1. Determined Cells

3.1.1. Fetal and Neonatal Heart Muscle Cells

The transplantation of fetal or neonatal cardiomyocytes into myocardial scar tissue is intended for directly restoring contractile function to tissue deficient in its own cardiomyocytes. The motivating hypothesis is that healthy, young cardiomyocytes can replace damaged cardiomyocytes. The feasibility of transplanting these immature cell types into the myocardium was initially demonstrated with rats in 1996. Studies reported transplant survival lasting to 2 mo *(14,15)* and improved cardiac function (increased ventricular wall thickness and attenuated chamber dilatation) after cryoinjury *(16)*. In contrast, adult cardiomyocytes reportedly necrosed 1 day after transplant and were completely dead within 1 wk *(17)*. It is believed that this difference was influenced by the enhanced mitotic potential of fetal/neonatal cardiomyocytes (and the relative mitotic inactivity of adult cardiomyocytes).

Investigators have also observed the growth of new blood vessels into fetal and neonatal cardiomyocyte transplants, suggesting that such transplants would be able to supply blood and oxygen to themselves and perhaps even their injured host tissue *(18,19)*. Importantly, electrical and mechanical coupling (via connexin-43, desmoplakin, and cadherin) within such grafts and between the graft cells and the host have been observed *(20,21)*. Phenotypically, immature cardiomyocytes have been reported either to advance to the adult phenotype *(22)* or to continue to express some fetal protein isoforms *(14,18)*. Furthermore, animals receiving cardiomyocyte transplants elicited attenuated pathologies in the form of decreased infarcts *(19)*, less ventricular enlargement, and reduced pathological remodeling *(18,23)*. In one study, treated animals were reported to display enhanced ventricular function *(24)*.

Nonetheless, long-term graft–host integration has been unsatisfactory so far because competing scar tissue walls off transplants from host tissue and diminishes coupling proteins such as connexin-43 *(23)*. Moreover, fetal/neonatal cardiomyocytes die easily in the face of ischemia and because of the shock of engraftment *(25,26)*; they are not considered ideal for clinical use for additional reasons, including: (1) availability, (2) ethical issues surrounding the use of fetal/neonatal human cell sources, and (3) the immunosuppression required because of the allogeneic sourcing of cells.

3.1.2. Adult Skeletal Myoblasts

In the face of stresses such as trauma and heavy exercise, skeletal muscle is served by satellite cells that assist in repair

and regeneration. Recruited satellite cells spawn skeletal myoblasts that proliferate, fuse into myotubes, and differentiate into functional muscle fibers.

From a cell transplantation perspective, autologous skeletal myoblasts have numerous advantages. They can be easily harvested from the muscles (e.g., thigh) of a patient, and thus their transplantation would not require immunosuppression after administration. Because skeletal myoblasts are proliferative yet fully determined to the myogenic phenotype, they may be expanded in vitro and pose low risk for tumorigenesis in vivo. Myoblasts are somewhat ischemia resistant *(27)*, unlike fetal/neonatal cardiomyocytes. Moreover, reports have suggested that myoblasts may be capable of differentiation into not only myocytes, but also adipocytes and osteocytes in vitro *(28,29)*, suggesting a mesenchymal differentiation potential.

Previous studies on animal models for skeletal myoblast transplantation have demonstrated promising but inconclusive graft structures and functions in vivo. Skeletal myoblasts delivered into cardiac muscle show an affinity for myocardial scar tissue and form into myotubes, but do not form true cardiomyocytes *(30)*. Cardiac proteins (e.g., *N*-cadherin and connexin-43) responsible for electromechanical syncytial cell coupling were produced in vitro, but were absent in vivo *(31)*. Nevertheless, in studies of both small and large animals with infarcts, myocyte transplantation has reportedly enhanced left ventricular function *(30,32–34)*.

Preclinical results have been considered sufficient to warrant human studies. Subsequently, one case study centered on a 73-year-old man experiencing heart failure and with history of a heart attack and high blood pressure. Five months after autologous satellite cell transplantation, this patient exhibited significant improvement, as evidenced by an increased ejection fraction, attenuation of ventricular dilation, improvements in myocardial metabolism, and enhanced myocardial blood flow *(35)*.

Probing further, a phase I clinical trial studied the feasibility and safety of autologous skeletal myoblast transplantation in 10 human patients with severe ischemic cardiomyopathy. The key clinical finding among this group of patients was the restoration of their contractile functions in 63% of the previously akinetic, nonviable scar sites treated with myoblasts *(36)*. All patients lived, with the exception of one 72-year-old man, who died of stroke 17.5 mo after transplantation. Postmortem histological analysis of his treated infarct revealed matured skeletal myotubes with an intact contractile apparatus. These graft cells exhibited upregulation of slow myosin isoform, suggesting that adult skeletal myoblast grafts had converted in vivo to slow-twitch fibers, which would be considered beneficial to cardiac function *(37)*.

A disadvantage of the adult skeletal myoblast approach is that their parent cell, the satellite cell, becomes scarce as patients age (and coincidentally experience greater risk for cardiovascular diseases) and thus might not be available in sufficient amounts when needed. Moreover, studies showed that transplanted myoblasts both fail to transdifferentiate into cardiomyocytes and electromechanically couple in vivo *(30, 31,37)*. Unfortunately, transplanted myoblasts essentially do not behave or function like cardiomyocytes on a cellular level despite improving cardiac performance on a clinical level. Some have addressed this discrepancy by proposing that myoblast transplantation helps not by directly providing contractile work, but instead by beneficial interactions with host cells.

More specifically, grafted cells might secrete molecular signals such as hepatocyte growth factor (HGF) that provide cardioprotective effects or mobilize cardiac stem cells *(38)*. HGF reportedly improves postinfarction cardiac function in vivo *(39)*, and on a cellular level, it has been shown to block apoptosis of cardiomyocytes in vitro *(40)*. Moreover, *in situ* transfection with the HGF gene group reportedly enhanced adult myoblast transplantation in infarcted rat hearts, as evidenced by a reported increase in cardiac performance, neovascularization, and attenuated fibrosis *(41)*. Nonetheless, care must be exercised because the HGF approach has also been implicated in tumorigenesis *(42,43)*.

In summary, adult skeletal myoblast transplantation has promising results in animal and human studies. Yet, further research is required to understand better its mechanism of action. Furthermore, larger randomized clinical trials are necessary to provide sustained evidence regarding its ability to ultimately benefit patients in need.

3.2. Stem Cells

Stem cells are defined by three properties: (1) the capacity for self-renewal; (2) the ability to differentiate into multiple, functional cell types; and (3) the capability to contribute to tissue formation in vivo. Stem cells can be categorized as either adult or embryonic. Currently, it is generally accepted that adult stem cells can differentiate into multiple, but not all, cell types (termed multipotent), whereas ES cells can contribute to nearly all tissues (termed pluripotent).

The ES cell *(44–49)* is considered to have the capacity for unlimited self-renewal and pluripotent differentiation. Yet, adult stem cells have been identified in many tissues, with the best characterization for the hematopoietic stem cell (HSC) *(50)*. Other adult stem cells that have been identified include neural *(51–53)*, gastrointestinal *(54)*, epidermal *(55)*, hepatic *(56)*, mesenchymal *(57–60)*, side population (SP) cells *(61,62)*, circulating endothelial progenitor cells *(63)*, and multipotent adult progenitor cells (MAPCs) *(44)*. The potential benefits of stem cell transplantation are illustrated in Fig. 3 *(64)*.

3.2.1. Embryonic Stem Cell Lines

Human embryonic stem (hES) cell lines have been proposed as a self-renewing and inexhaustible source of nascent cardiomyocytes. Furthermore, their pluripotential poses the possibility of producing specific cardiac cell types, such as cardiac endothelial cells, atrial and ventricular myocytes, and pacemaker cells. In addition to their availability and versatility, hES cell-derived cardiomyocytes would also share the advantages described in Section 3.1.1.

The hES cell lines have been derived from blastocysts and discarded embryos, eliminating the need for repeatedly harvesting cells from human samples *(46,65,66)*. The in vitro differentiation of hES cells into cardiomyocytes has been accomplished by both spontaneous and directed systems. In the former, hES cells were grown in suspension culture to form embryoid bodies that spontaneously spawned pulsatile

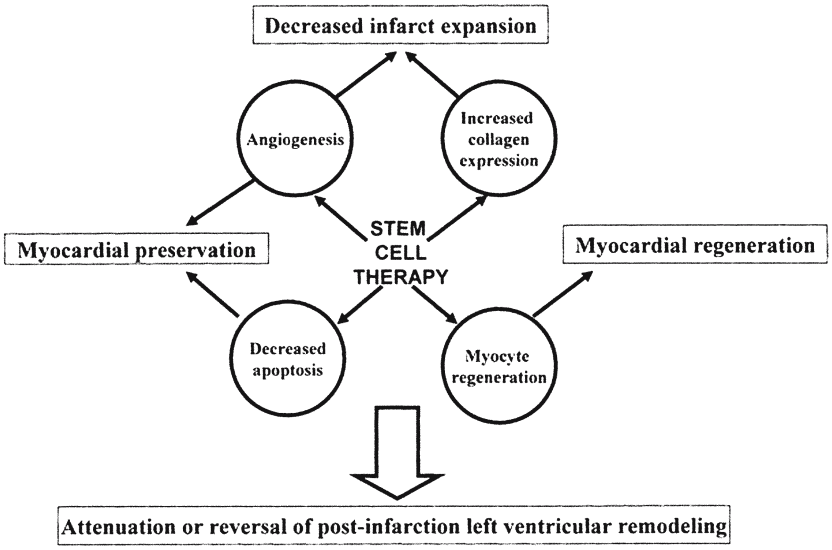

Fig. 3. Interplay among potential mechanisms by which stem cells could effect cardiac repair. These mechanisms include the formation of new vasculature, regeneration of contractile cells, repair of the extracellular matrix, and prevention of programmed cell death as a means to prevent further damage and initiate reparative processes.(From Forrester, J.S., Price, M.J., and Makkar, R.R. Stem cell repair of infarcted myocardium: an overview for clinicians. *Circulation.* 108:1139–1145. © 1993 Lippincott, Williams, and Wilkins.)

cardiomyocytes within days to weeks *(67,68)*. In the latter, hES cells were cocultured with mouse visceral-endoderm (VE)-like cells to induce differentiation *(69)*.

The authenticity of ES cell-derived human cardiomyocytes has been validated by a variety of means, such as reverse transcriptase polymerase chain reaction, immunostaining, electron microscopy, and electrophysiological measurements *(67,68, 70,71)*. Yet, others have argued that these cardiomyocytes resemble those of the embryonic heart tube and not chamber cardiomyocytes *(72)*.

To date, reports on cardiac transplants of ES cell-derived cardiomyocytes are limited. One study demonstrated the feasibility of the method in dystrophic mice and survival of the transplanted cells reaching 7 weeks *(73)*. Additional progress in animal studies as well as in the areas of purity, scale-up (expanding cell numbers), and immunorejection must be made before undertaking clinical trials with hES cell-derived cardiomyocytes. More specifically, purity remains a problem for the differentiation process, which byproduces a variety of noncardiac cell types; cardiac transplantation of such ill-defined and heterogeneous mixtures could be dangerous.

Yet, progress has been made; one group of researchers has produced cultures >99% pure by genetically modifying mouse ES cells with a cardiomyocyte-specific promoter paired with a gene for G418 antibiotic resistance *(73)*. Regarding scale-up, experiments thus far have only been on a relatively small laboratory scale, and mass production methods must be developed to generate adequate numbers of cells to replace the estimated 10^8 cardiomyocytes that die per heart attack in a given patient. Regarding immunosuppression, by current methodologies patients would require lifelong suppression because of the allogeneic nature of cell lines. The banking of designer cell lines with extensive selections of human leukocyte antigen types, attenuation of cell line immunogenicity, and induced graft tolerance are among the methods to be investigated extensively to address these problems with immunorejection *(74)*.

3.2.2. Adult Stem Cells

A sizable body of scientific work has addressed the potential ability of some adult stem cells to transdifferentiate into cardiac cells, giving hope for future means to heal the dying or failing heart. Moreover, studies have shown that tissue-specific stem cells may even have the ability to generate the cells of tissues from unrelated organs. Yet, to date whether this unexpected plasticity constitutes "transdifferentiation" or whether a small population of multipotent stem cells persists in postnatal tissues is not known. However, the finding that stem cells exist in postnatal tissues with previously unknown proliferation and differentiation potentials may implicate the possibility of using allogeneic or autologous stem cells to treat myocardial infarction and perhaps even congestive heart failure.

3.2.2.1. Bone Marrow Stem Cells

Adult BMSCs are considered a heterogeneous population of stem cells that originates from bone marrow and possesses the ability to regenerate various tissues *(5–7)*. This purported multipotential is illustrated in Fig. 4 *(11)*. It is known that the BMSC population is composed of a variety of subpopulations, such as HSCs *(75)*, mesenchymal stem cells (MSCs) *(58,76)*, and SP cells *(77)* (an enriched population of HSCs that gives rise to all hematopoietic lineages following transplantation).

Nonetheless, its precise composition remains unclear, and there has not been a consensus on the exact surface protein markers for all subpopulations. As such, the literature on BMSC transplantation has been plagued by confusion and inconsistencies regarding precisely which subpopulations have been studied, the various names for each respective subpopulation

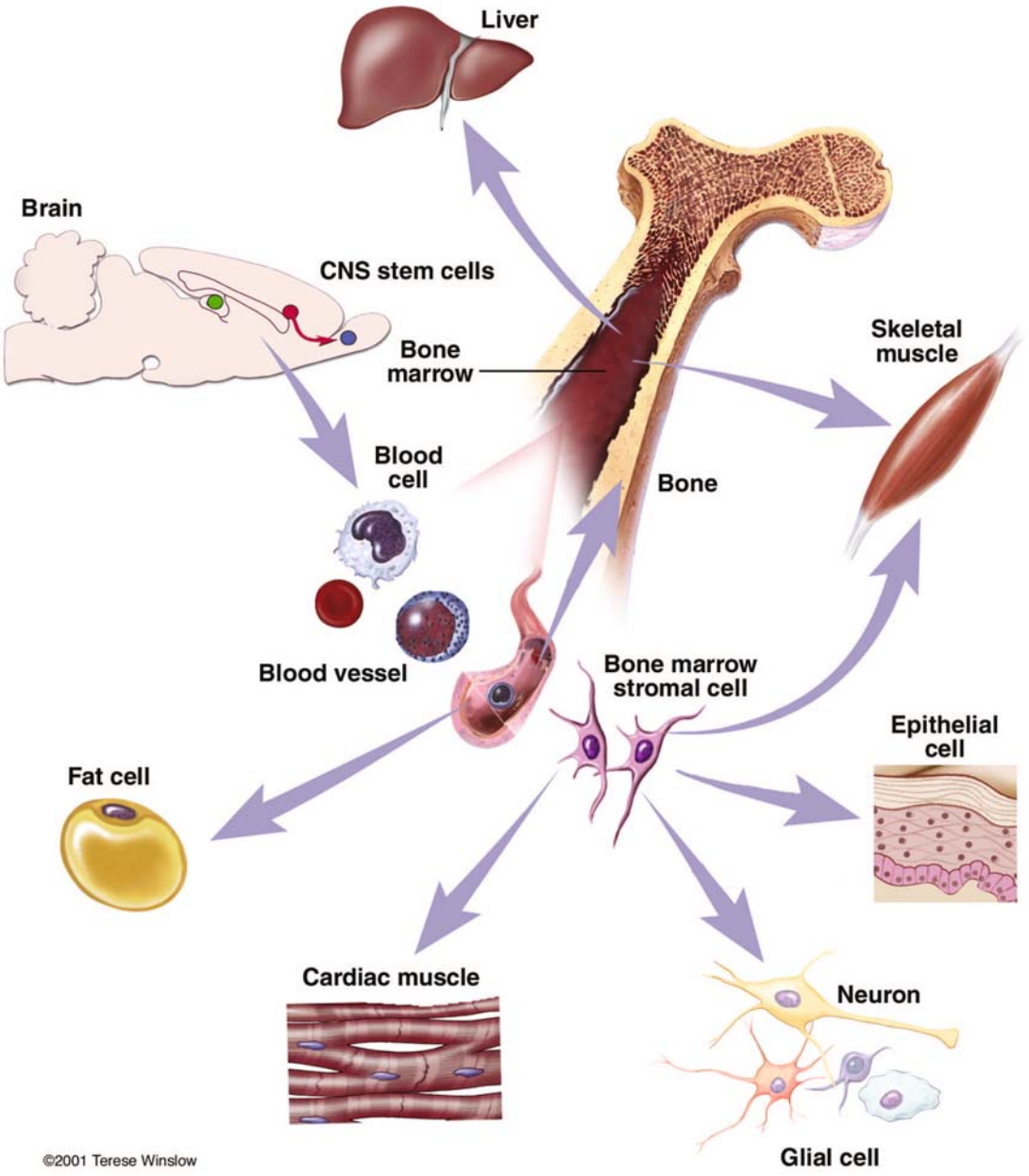

Fig. 4. The purported fates of bone marrow stem cells (BMSCs). Bone marrow stem cells are believed to consist of a heterogeneous population of cells capable of transdifferentiation into a number of respective tissue types. Definitive evidence does not exist for all tissue types illustrated. © 2001 Terese Winslow.

utilized, and what their respective mechanisms of action are. For example, BMSCs have also been called "marrow stromal cells," "stromal stem cells," "marrow mononuclear cells," and "marrow progenitor cells" *(78)*. As shown here, a number of groups have reported that BMSCs can differentiate into a variety of cardiac cell types. Furthermore, some groups proposed specific subpopulations in their studies, whereas others generalized their cells as BMSCs.

Despite such confusion, investigators have reported that BMSCs can differentiate into cardiomyocytes, endothelial cells, and vascular smooth muscle cells following transplantation into the myocardium *(79–83)*. In general, the myocardial microenvironments in vivo are thought to stimulate the multipotential differentiation of BMSCs. More specifically, BMSCs adjacent to cardiomyocytes would transdifferentiate into cardiomyocytes, and similarly, BMSCs adjacent to endothelial or smooth muscle cells would transdifferentiate into vascular cells. In support of this, a recent in vitro study confirmed that direct cell-to-cell contact (and not soluble factors) with cardiomyocytes induced BMSCs to differentiate into cardiomyocytes themselves *(84)*.

From a cell transplantation perspective, autologous BMSCs have several advantages. BMSCs could be easily harvested from a patient by bone marrow aspiration and subsequently grown to

large numbers in the laboratory. Furthermore, on transplantation there would be no need for immunosuppression because of their autologous sourcing. Moreover, there have been reports suggesting that allogeneic BMSCs might even serve as "universal donor cells" and thus obviate the need for immunosuppression *(85,86)*. This would translate into a nonimmunogenic allogeneic cell source, permitting the on-demand delivery of cells to patients and precluding any need for scheduling autologous cell harvesting, laboratory manipulation, and transplantation.

To date, animal studies focusing on BMSCs have been promising. For example, in mice, *Lin⁻ c-kit⁺* (a surface protein marker state of hematopoietic lineage marker negative [*lin⁻*] and stem cell factor receptor positive [*c-kit⁺*]) BMSCs intramyocardially injected into acutely ischemic hearts formed cardiomyocytes and new vessels consisting of BMSC-derived endothelial cells and smooth muscle cells. Nine days after transplant, BMSC-derived myocardium occupied 68% of the infarcted regions *(81)*. In a similar report by the same group, these mice also elicited increases in cardiac performance as evidenced by improvements in several hemodynamic parameters *(87)*.

The MSC, one of the more promising subpopulations of BMSCs, is well characterized *(58,88)* and has shown promise for use in cardiac regeneration both in vitro and in vivo. In rats, MSCs genetically reprogrammed with the Akt1 prosurvival gene reportedly regenerated 80–90% of damaged myocardium, attenuated pathological remodeling, and normalized cardiac performance of the ischemic myocardia *(89)*.

Furthermore, stable graft formation with nascent muscle-specific proteins, reduced contractile dysfunction, and reduced heart wall thinning were all reported in pigs receiving autologous MSC transplants 2 wk after myocardial infarction *(90)*. Unfortunately, all 14 animals in this study progressed to failure at 6–8 wk. Nevertheless, human MSCs transplanted into the healthy hearts of immunodeficient mice hearts appeared to differentiate into cardiomyocytes *(91)*.

Our group has investigated a method for controlling the distribution of transplanted MSCs by entrapping them in a fibrin matrix that can be surgically secured adjacent to areas of infarcted myocardium. To date, initial in vivo findings have indicated a resultant significant left ventricular wall thickening, improved left ventricular contractile performance, minimal myogenic differentiation of MSCs, and significant neovascularization *(92,93)*. This suggests that MSCs may work by increasing blood flow to infarcted areas as opposed to contributing any significant contractile function.

Preclinical results were considered sufficient to warrant human studies. In one human study, six coronary bypass patients receiving intramyocardial injections of autologous AC133+ (a stem cell marker expressed in HSCs and neural stem cells) bone marrow cells exhibited subsequent increases in left ventricular function; five of these patients also elicited increases in myocardial blood flow *(94)*. In another trial, autologous mononuclear bone marrow cells were transplanted into the ischemic hearts of eight patients who, 3 mo later, showed improved clinical symptoms and increased cardiac blood flows and function within the previously infarcted regions *(95)*.

In yet another study, 10 patients receiving intracoronary transplants of autologous BMSCs following standard heart attack therapy showed significant improvements in cardiac function compared to control patients receiving standard therapy alone *(96)*. In the 3-month follow-up studies of the hearts receiving transplants, infarct size had halved on average, infarct wall velocity doubled, and patients exhibited significant increases in their stroke volume index, left ventricular end-systolic volume and contractility, and infarction blood flow in the previously infarcted wall region. The TOPCARE-AMI (Transplantation of Progenitor Cells and Regeneration Enhancement in Acute Myocardial Infarction) study bolstered feasibility and safety by treating 9 patients with autologous BMSCs (and 11 with blood-derived progenitor cells) a few days after their heart attacks. Findings from this trial at 4 mo included significant benefits to the left ventricle, including increases in ejection fraction, improved infarct wall motion, dramatically reduced end-systolic volumes, and enhanced myocardial viability in the infarcted zones *(97)*.

3.2.2.1.1. Side Population Cells

The specific subpopulations of BMSCs responsible for regenerating myocardial tissue remain unclear. Evidence as discussed here showed that MSCs can contribute to myocardial regeneration. Conversely, evidence also suggests that certain subpopulations may not generate similar results, such as certain bone marrow HSCs. For example, lethally irradiated mice, each receiving single green fluorescent protein-labeled HSCs with surface protein markers c-kit⁺ Thy1.1^{lo} Lin⁻ Sca-1⁺, experienced robust reconstitution of their peripheral blood leukocytes, but negligible contributions to brain or liver and no contributions to kidney, gut, lung, skeletal, or cardiac muscle *(98)*.

In contrast, a CD34⁻ subpopulation of HSCs (which are mostly CD34⁺), termed side population (SP) cells, reportedly were able to form cardiomyocytes and endothelial cells in infarcted mouse hearts *(79)*. Bone marrow-derived SP cells typically comprise 0.05% of whole bone marrow and are defined by their ability to exclude Hoechst 33342 dye via multidrug resistance-like proteins *(77)*. Their protein surface markers are CD34$^{-/low}$ c-kit⁺ Sca-1⁺ *(79)*, similar to HSCs. In addition, other similarly Hoechst dye-effluxing SP cells have also been isolated within skeletal muscle, brain, spleen, liver, kidney, lung, small intestine, and the heart itself *(61)*.

There is additional evidence that SP cells can specifically contribute to the regeneration of various tissues, including skeletal muscle *(99)*, vessels *(100)*, and breast *(101)*. Of interest here is that heart-derived SP cells have also demonstrated the ability to form cardiomyocytes in vitro *(102)*. To date, studies of SP cell transplantation into animal models of infarction have yet to surface. Moreover, it remains to be seen whether there exist multiple tissue-specific SP cell types or a single SP cell type that distributes itself hematogenously from a common source such as bone marrow *(103)*. It should be noted that it is possible that a number of the BMSC transplantation studies discussed in this chapter either unknowingly employed or unknowingly excluded SP cells. This will need to be clarified by conducting specific SP-cell-only vs non-SP-cell-only transplantation experiments on animal models of infarction.

3.2.2.1.2. Multipotent Adult Progenitor Cells

MAPCs are cells that are considered to proliferate without senescence and differentiate into mesodermal, neuroectodermal, and endodermal cell types *(45)*. MAPCs are a subpopulation of BMSCs that has been well characterized as "CD34, CD44, CD45, c-KIT and major histocompatibility complex MSC Class I and II negative; expressing low levels of Flk-1, Sca-1 and Thy-1, and higher levels of CD13 and stage-specific antigen 1 (SSEA-1)." MAPCs reportedly also exist in both muscle and brain *(104)*.

Although there are no published studies of MAPC transplantation into injured hearts, there is some evidence that MAPCs can contribute to the myocardium. In one study, MAPCs injected into a mouse blastocyst model and examined 6 through 20 wk later in development were found distributed and functionally integrated in a variety of tissues, including skin, skeletal muscle, liver, small intestine, kidney, spleen, and myocardium *(45)*.

3.2.2.2. Cardiac Stem Cells

Findings have indicated that regenerative stem cells may normally exist within the myocardium. In addition, two populations with differing features have been reported thus far: Sca-1^+ cardiac progenitor cells and Lin^- c-kit^+ cardiac stem cells. The former type is believed to play a role in cell fusion mechanisms, whereas the latter type is not.

3.2.2.2.1. The Sca-1^+ Cardiac Progenitor Cell Population

Adult heart-derived cardiac progenitor cells are stem cells isolated from the myocardium. They are chiefly identified as Sca-1^+ and are considered an SP cell type. Studies employing purported mouse cardiac progenitor cells have shown in vitro differentiation of such cells into cardiomyocytes on 5-azacytidine treatment. Furthermore, in a mouse model of myocardial infarction, transplanted cardiac progenitor cells have been observed to home and engraft into the damaged myocardium and have differentiated into cardiomyocytes with and without cell fusion *(9)*. However, whether they improve cardiac function after injury remains to be seen.

To date, investigators have asserted the uniqueness and legitimacy of cardiac progenitor cells via surface protein markers. Cardiac progenitor cells are identified as Sca-1^+ cells and are largely $CD31^+$ and $CD38^+$. Like bone marrow SP cell types, they efflux Hoechst 33342 dye, but differ by being negative for CD45 and c-kit. They are also negative for "blood cell lineage markers (CD4, CD8, B220, Gr-1, Mac-1, and TER119), c-kit, Flt-1, Flk-1, vascular endothelial-cadherin, von Willebrand factor, and HSC markers CD45 and 34," suggesting a nonhematopoietic and nonendothelial origin *(9)*.

3.2.2.2.2. The Lin^- c-kit^+ Cardiac Stem Cell Population

Spurred by the promising results of Lin^- c-kit^+ bone marrow cells *(87)*, one group of investigators has isolated Lin^- c-kit^+ cells directly from myocardium *(10)*. In vitro, this purported adult cardiac stem cell population was demonstrated to be self-renewing, clonogenic, and multipotent in the production of cardiomyocytes, endothelial cells, and smooth muscle *(10)*. In rat models for myocardial infarction, transplants of such cells were shown to regenerate functional myocardium spanning up to 70% of the left ventricle. The spawning of nascent cardiac cells, as opposed to cell fusion with host cells, has been proposed as the primary mode of action of this cell population. However, it is considered that such nascent cells generated by Lin^- c-kit^+ cardiac stem cell transplantation were too numerous, small, and insufficient in ploidy to have possibly arisen from fusing with the scarce numbers of remaining host cardiomyocytes in infarcted myocardial tissue.

3.2.3. Umbilical Cord Blood Stem Cells

Although no reports have yet surfaced using this cell type for cardiac cell transplantation, some investigators have suggested that the mesenchymal subpopulation of umbilical cord blood stem cells would be capable of multipotential transdifferentiation *(105,106)*. Umbilical cord blood is easily obtainable from its source tissue, normally discarded after childbirth. In addition, cord blood is reported to contain high levels of stem cells and be of low risk for both viral contamination and graft-vs-host disease *(107)*.

3.3. Reprogrammed Cells

The ex vivo genetic engineering of cells for transplantation is intended for circumventing cell shortages or for the introduction of specific therapeutic properties, such as that of pacemaker cells or of promoting angiogenesis.

3.3.1. Engineering New Cell Sources

The clinical application of cellular therapies demands autologous (i.e., patient's own) cells to avoid the immunological rejection that would occur if allogeneic (i.e., someone else's) cells were used. However, obtaining sufficient quantities of an autologous and desired cell type is likely to be difficult in the sick and elderly.

3.3.1.1. In Vitro Cardiomyogenic Differentiation of Mesenchymal Stem Cells

One group of investigators has shown that bone marrow-derived MSCs can multipotentially form cells of bone, cartilage, tendon, fat, skeletal muscle, and heart muscle both in vitro and in vivo *(108)*. Furthermore, fetal sheep systemically administered human MSCs that integrated into multiple tissues during a 13-month period also were shown to differentiate *in situ* into bone marrow stromal cells, thymic stromal cells, chondrocytes, adipocytes, skeletal myocytes, and cardiomyocytes *(86)*. Thus, MSCs appear to maintain their multipotency after transplantation, suggesting their potential usefulness in cell transplantation for myocardial repair *(86)*.

To date, it remains somewhat unclear how adult stem cells may multipotentially differentiate; a definitive mechanism for inducing the cardiomyogenic differentiation of MSCs in vitro has not been reported. Although specific physiological inducers have been shown to drive MSCs to differentiate in vitro into bone, fat, and cartilage *(58)*, the appropriate physiological inducer for cardiomyogenic differentiation of MSCs remains uncertain. Among the candidate promoters is 5-azacytidine, a cytosine analog that has been shown to decrease deoxyribonucleic acid (DNA) methylation in mammalian cells and consequently to promote reprogramming of the cell differentiation fate. Furthermore, in experiments employing the C3H10T1/2 mesenchymal progenitor cell line, 5-azacytidine was shown to

induce differentiation into mesenchymal cell types such as skeletal myocytes, adipocytes, and chondrocytes *(58)*.

More specifically, up to 30% of MSCs treated with 5-azacytidine differentiated into spontaneously beating cells and expressed atrial natriuretic peptide, brain natriuretic peptide, ventricular/atrial myosins, desmin, actinin, and cardiac α-actin, all considered indicative of a fetal ventricular cardiomyogenic phenotype. Interestingly, such cells also expressed several cardiomyocyte-specific transcription factors, such as Nkx2.5/Csx, GATA4, TEF-1, and MEF-2 *(109)*. Such MSC-derived cardiomyocytes have been termed *bone marrow-derived regenerated cardiomyocytes* or *CMG cells (110)*. Further analysis of CMGs also revealed functional adrenergic and muscarinic receptors, which are normally considered to play crucial roles in mediating heart rate, conduction velocity, contractility, and pathological events such as cardiac hypertrophy. Therefore, expression of such features makes CMG cells strong candidates for cell transplantation.

3.3.1.2. Cardiomyogenic Transdifferentiation of Fibroblasts

Fibroblasts are an essentially ubiquitous cell type in the human body that some investigators have proposed as an alternative cell source. Normally, fibroblasts do not afford contractile function, but there have been some groups reporting success in reprogramming fibroblasts into myogenic cells in vitro with the *MyoD* gene and demonstrating the feasibility of transplantation in rat and mice models *(111,112)*. Clinically, such an approach has promise because fibroblasts could be easily harvested because of their natural abundance, grown to large numbers in the laboratory, reprogrammed into cells able to do cardiac work, and finally reintroduced into the same patient as therapy.

3.3.1.3. Somatic Cell Nuclear Transfer

Somatic cell nuclear transfer has also been proposed as an alternate source of cardiomyocytes. This technique involves replacing the nucleus of a host oocyte with the nucleus of a somatic donor. The widely publicized sheep named Dolly was produced by this method *(113)*. Researchers have used this method in a bovine model to produce cardiac cells that were both viable and tolerated following transplantation into the original donor animal *(114)*.

3.3.2. Engineering Therapeutic Properties

3.3.2.1. Vascular Endothelial Growth Factor

Vascular endothelial growth factor (VEGF) is known to encourage the proliferation of new capillaries. Cells modified to express VEGF or related factors may thus have the potential to ameliorate scar formation in injured myocardia. In support of this concept, in scarred rat hearts, researchers have reported angiogenesis and increased regional blood flood caused by the administration of heart cells engineered to produce VEGF at sixfold normal levels *(115)*.

However, it should be noted that conflicting reports have shown that VEGF-enhanced cells may contribute to tumor formation in the hearts of mice and rats *(116,117)*. Moreover, in humans receiving stem cell transplants, VEGF has been implicated in the pathogenesis of hepatic venoocclusive disease *(118)*. Accordingly, attempts are being made to control the expression of VEGF by means such as genetic control elements and polymeric delivery systems *(119)*.

3.3.2.2. Pacemaking

In the future, conventional electronic pacemakers may eventually be replaced by genetically engineered cells with custom-tailored pacemaking abilities. Specifically, investigators have moved toward generating cardiac cells with novel electrophysiological properties intended to correct arrhythmias and other electrical abnormalities in the heart. Both contractile and conductory cells of the heart have been targeted, with specific electrophysiological modifications induced by manipulating the genes of ion channels within those cells *(120–122)*.

3.3.2.3. Defying Apoptosis

Defying or modifying rates of apoptosis (programmed cell death) caused by ischemia is another desirable property under investigation. Investigators have manipulated cytoprotective, heat shock, and inflammatory pathways to prevent cardiac cells from entering apoptosis *(26,123,124)*. Others have employed ex vivo retroviral transduction methodologies to create MSC lines that overexpress the Akt1 prosurvival gene. Interestingly, rats receiving such cells have elicited a reported 80–90% regeneration of damaged myocardium, attenuated pathological remodeling, and normalized cardiac performance in the ischemic myocardia zones. Compared to control cells transduced with the lacZ reporter gene, the Akt1 cells repaired fourfold more myocardial volume *(89)*.

4. SAFETY

One needs to be well aware of the potential risks of any new form of therapy; cell transplantation has the potential for dangerous side effects. Specifically, newly introduced cells could conceivably form cardiac or metastatic tumors, disrupt the electrical rhythm of the heart, produce inappropriate chemical signals that adversely affect normal tissue or normal physiology, or evolve pathological stiffness or fragility, leading to mechanical failure of the heart. Moreover, aberrant cellular behavior or unseen intracellular lesions could unknowingly accumulate during the laboratory production of the therapeutic materials. Although these abnormalities might not be evident ex vivo, they could lead to unforeseen clinical problems in the patient. Therefore, extensive safety measures must be taken as cell transplantation therapies are further developed and more clinical trials are undertaken. Nevertheless, the potential benefits of cell transplantation therapies are exciting and will continue as a major area of intensive research in the near future.

REFERENCES

1. Kajstura, J., Leri, A., Finato, N., Di Loreto, C., Beltrami, C.A., and Anversa, P. (1998) Myocyte proliferation in end-stage cardiac failure in humans. *Proc Natl Acad Sci USA*. 95, 8801–8805.
2. Soonpaa, M.H. and Field, L.J. (1998) Survey of studies examining mammalian cardiomyocyte DNA synthesis. *Circ Res*. 83, 15–26.
3. Beltrami, A.P., Urbanek, K., Kajstura, J., et al. (2001) Evidence that human cardiac myocytes divide after myocardial infarction. *N Engl J Med*. 344, 1750–1757.
4. Urbanek, K., Quaini, F., Tasca, G., et al. (2003) Intense myocyte formation from cardiac stem cells in human cardiac hypertrophy. *Proc Natl Acad Sci USA*. 100, 10,440–10,445.

5. Hirschi, K.K. and Goodell, M.A. (2002) Hematopoietic, vascular and cardiac fates of bone marrow-derived stem cells. *Gene Ther*. 9, 648–652.
6. Jensen, G.S. and Drapeau, C. (2002) The use of *in situ* bone marrow stem cells for the treatment of various degenerative diseases. *Med Hypotheses*. 59, 422–428.
7. Ballas, C.B., Zielske, S.P., and Gerson, S.L. (2002) Adult bone marrow stem cells for cell and gene therapies: implications for greater use. *J Cell Biochem Suppl*. 38, 20–28.
8. Laflamme, M.A., Myerson, D., Saffitz, J.E. and Murry, C.E. (2002) Evidence for cardiomyocyte repopulation by extracardiac progenitors in transplanted human hearts. *Circ Res*. 90, 634–640.
9. Oh, H., Bradfute, S.B., Gallardo, T.D., et al. (2003). Cardiac progenitor cells from adult myocardium: homing, differentiation, and fusion after infarction. *Proc Natl Acad Sci USA*. 100, 12,313–12,318.
10. Beltrami, A.P., Barlucchi, L., Torella, D., et al. (2003) Adult cardiac stem cells are multipotent and support myocardial regeneration. *Cell*. 114, 763–776.
11. US Department of Health and Human Services. (2001) *Stem Cells: Scientific Progress and Future Research Directions*. Available at Website: (http://itpapers.zdnet.com/abstract.aspx?dtid=2&ucid=7&docid=22796). Accessed 15 September 2004.
12. Reffelmann, T., Leor, J., Muller-Ehmsen, J., Kedes, L., and Kloner, R.A. (2003) Cardiomyocyte transplantation into the failing heart-new therapeutic approach for heart failure? *Heart Fail Rev*. 8, 201–211.
13. Caplice, N.M. and Gersh, B.J. (2003) Stem cells to repair the heart: a clinical perspective. *Circ Res*. 92, 6–8.
14. Leor, J., Patterson, M., Quinones, M.J., Kedes, L.H., and Kloner, R.A. (1996) Transplantation of fetal myocardial tissue into the infarcted myocardium of rat. A potential method for repair of infarcted myocardium? *Circulation*. 94, II332–II336.
15. Scorsin, M., Marotte, F., Sabri, A., et al. (1996) Can grafted cardiomyocytes colonize peri-infarct myocardial areas? *Circulation*. 94, II337–II340.
16. Li, R.K., Jia, Z.Q., Weisel, R.D., et al. (1996) Cardiomyocyte transplantation improves heart function. *Ann Thorac Surg*. 62, 654–660; discussion 660–661.
17. Reinecke, H., Zhang, M., Bartosek, T., and Murry, C.E. (1999) Survival, integration, and differentiation of cardiomyocyte grafts: a study in normal and injured rat hearts. *Circulation*. 100, 193–202.
18. Etzion, S., Battler, A., Barbash, I.M., et al. (2001) Influence of embryonic cardiomyocyte transplantation on the progression of heart failure in a rat model of extensive myocardial infarction. *J Mol Cell Cardiol*. 33, 1321–1330.
19. Li, R.K., Mickle, D.A., Weisel, R.D., et al. (1997) Natural history of fetal rat cardiomyocytes transplanted into adult rat myocardial scar tissue. *Circulation*. 96, II179–II186; discussion 186–187.
20. Connold, A.L., Frischknecht, R., Dimitrakos, M., and Vrbova, G. (1997) The survival of embryonic cardiomyocytes transplanted into damaged host rat myocardium. *J Muscle Res Cell Motil*. 18, 63–70.
21. Matsushita, T., Oyamada, M., Kurata, H., et al. (1999) Formation of cell junctions between grafted and host cardiomyocytes at the border zone of rat myocardial infarction. *Circulation*. 100, II262–II268.
22. Soonpaa, M.H., Koh, G.Y., Klug, M.G., and Field, L.J. (1994) Formation of nascent intercalated disks between grafted fetal cardiomyocytes and host myocardium. *Science*. 264, 98–101.
23. Muller-Ehmsen, J., Peterson, K.L., Kedes, L., et al. (2002) Rebuilding a damaged heart: long-term survival of transplanted neonatal rat cardiomyocytes after myocardial infarction and effect on cardiac function. *Circulation*. 105, 1720–1726.
24. Scorsin, M., Hagege, A.A., Marotte, F., et al. (1997) Does transplantation of cardiomyocytes improve function of infarcted myocardium? *Circulation*. 96, II188–II193.
25. Muller-Ehmsen, J., Whittaker, P., Kloner, R.A., et al. (2002) Survival and development of neonatal rat cardiomyocytes transplanted into adult myocardium. *J Mol Cell Cardiol*. 34, 107–116.
26. Zhang, M., Methot, D., Poppa, V., Fujio, Y., Walsh, K., and Murry, C.E. (2001) Cardiomyocyte grafting for cardiac repair: graft cell death and anti-death strategies. *J Mol Cell Cardiol*. 33, 907–921.
27. Jennings, R.B. and Reimer, K.A. (1981) Lethal myocardial ischemic injury. *Am J Pathol*. 102, 241–255.
28. Wada, M.R., Inagawa-Ogashiwa, M., Shimizu, S., Yasumoto, S., and Hashimoto, N. (2002) Generation of different fates from multipotent muscle stem cells. *Development*. 129, 2987–2995.
29. Asakura, A., Komaki, M., and Rudnicki, M. (2001) Muscle satellite cells are multipotential stem cells that exhibit myogenic, osteogenic, and adipogenic differentiation. *Differentiation*. 68, 245–253.
30. Ghostine, S., Carrion, C., Souza, L.C., et al. (2002) Long-term efficacy of myoblast transplantation on regional structure and function after myocardial infarction. *Circulation*. 106, I131–I136.
31. Reinecke, H., MacDonald, G.H., Hauschka, S.D., and Murry, C.E. (2000) Electromechanical coupling between skeletal and cardiac muscle. Implications for infarct repair. *J Cell Biol*. 149, 731–740.
32. Rajnoch, C., Chachques, J.C., Berrebi, A., Bruneval, P., Benoit, M.O., and Carpentier, A. (2001) Cellular therapy reverses myocardial dysfunction. *J Thorac Cardiovasc Surg*. 121, 871–878.
33. Jain, M., DerSimonian, H., Brenner, D.A., et al. (2001) Cell therapy attenuates deleterious ventricular remodeling and improves cardiac performance after myocardial infarction. *Circulation*. 103, 1920–1927.
34. Taylor, D.A., Atkins, B.Z., Hungspreugs, P., et al. (1998) Regenerating functional myocardium: improved performance after skeletal myoblast transplantation. *Nat Med*. 4, 929–933.
35. Zhang, F., Chen, Y., Yang, Z., et al. (2003) Cellular cardiomyoplasty for a patient with heart failure. *Cardiovasc Radiat Med*. 4, 43–46.
36. Menasche, P., Hagege, A.A., Vilquin, J.T., et al. (2003) Autologous skeletal myoblast transplantation for severe postinfarction left ventricular dysfunction. *J Am Coll Cardiol*. 41, 1078–1083.
37. Hagege, A.A., Carrion, C., Menasche, P., et al. (2003) Viability and differentiation of autologous skeletal myoblast grafts in ischaemic cardiomyopathy. *Lancet*. 361, 491–492.
38. Menasche P. (2003) Myoblast-based cell transplantation. *Heart Fail Rev*. 8, 221–227.
39. Jin, H., Yang, R., Li, W., et al. (2003) Early treatment with hepatocyte growth factor improves cardiac function in experimental heart failure induced by myocardial infarction. *J Pharmacol Exp Ther*. 304, 654–660.
40. Kitta, K., Day, R.M., Kim, Y., Torregroza, I., Evans, T., and Suzuki, Y.J. (2003) Hepatocyte growth factor induces GATA-4 phosphorylation and cell survival in cardiac muscle cells. *J Biol Chem*. 278, 4705–4712.
41. Miyagawa, S., Sawa, Y., Taketani, S., et al. (2002) Myocardial regeneration therapy for heart failure: hepatocyte growth factor enhances the effect of cellular cardiomyoplasty. *Circulation*. 105, 2556–2561.
42. Takayama, H., LaRochelle, W.J., Sharp, R., et al. (1997) Diverse tumorigenesis associated with aberrant development in mice overexpressing hepatocyte growth factor/scatter factor. *Proc Natl Acad Sci USA*. 94, 701–706.
43. van der Voort, R., Taher, T.E., Derksen, P.W., Spaargaren, M., van der Neut, R., and Pals, S.T. (2000) The hepatocyte growth factor/Met pathway in development, tumorigenesis, and B-cell differentiation. *Adv Cancer Res*. 79, 39–90.
44. Reyes, M., Lund, T., Lenvik, T., Aguiar, D., Koodie, L. and Verfaillie, C.M. (2001) Purification and ex vivo expansion of postnatal human marrow mesodermal progenitor cells. *Blood*. 98, 2615–2625.
45. Jiang, Y., Jahagirdar, B.N., Reinhardt, R.L., et al. (2002) Pluripotency of mesenchymal stem cells derived from adult marrow. *Nature*. 418, 41–49.
46. Thomson, J.A., Itskovitz-Eldor, J., Shapiro, S.S., et al. (1998) Embryonic stem cell lines derived from human blastocysts. *Science*. 282, 1145–1147.
47. Shamblott, M.J., Axelman, J., Wang, S., et al. (1998) Derivation of pluripotent stem cells from cultured human primordial germ cells. *Proc Natl Acad Sci USA*. 95, 13,726–13,731.
48. Williams, R.L., Hilton, D.J., Pease, S., et al. (1988) Myeloid leukaemia inhibitory factor maintains the developmental potential of embryonic stem cells. *Nature*. 336, 684–687.

49. Orkin, S.H. (1998) Embryonic stem cells and transgenic mice in the study of hematopoiesis. *Int J Dev Biol.* 42, 927–934.
50. Weissman, I.L. (2000) Translating stem and progenitor cell biology to the clinic: barriers and opportunities. S*cience*. 287, 1442–1446.
51. Gage, F.H. (2000) Mammalian neural stem cells. *Science*. 287, 1433–1438.
52. Svendsen, C.N., Caldwell, M.A., and Ostenfeld, T. (1999) Human neural stem cells: isolation, expansion and transplantation. *Brain Pathol*. 9, 499–513.
53. Okabe, S., Forsberg-Nilsson, K., Spiro, A.C., Segal, M. and McKay, R.D. (1996) Development of neuronal precursor cells and functional postmitotic neurons from embryonic stem cells in vitro. *Mech Dev*. 59, 89–102.
54. Potten, C.S. (1998) Stem cells in gastrointestinal epithelium: numbers, characteristics and death. *Philos Trans R Soc Lond B Biol Sci*. 353, 821–830.
55. Watt, F.M. (1998) Epidermal stem cells: markers, patterning and the control of stem cell fate. *Philos Trans R Soc Lond B Biol Sci*. 353, 831–837.
56. Alison, M. and Sarraf, C. (1998) Hepatic stem cells. *J Hepatol*. 29, 676–682.
57. Haynesworth, S.E., Baber, M.A. and Caplan, A.I. (1992) Cell surface antigens on human marrow-derived mesenchymal cells are detected by monoclonal antibodies. *Bone*. 13, 69–80.
58. Pittenger, M.F., Mackay, A.M., Beck, S.C., et al. (1999) Multilineage potential of adult human mesenchymal stem cells. *Science*. 284, 143–147.
59. Gronthos, S., Zannettino, A.C., Graves, S.E., Ohta, S., Hay, S.J. and Simmons, P.J. (1999) Differential cell surface expression of the STRO-1 and alkaline phosphatase antigens on discrete developmental stages in primary cultures of human bone cells. *J Bone Miner Res*. 14, 47–56.
60. Prockop, D.J. (1997) Marrow stromal cells as stem cells for nonhematopoietic tissues. *Science*. 276, 71–74.
61. Asakura, A. and Rudnicki, M.A. (2002) Side population cells from diverse adult tissues are capable of in vitro hematopoietic differentiation. *Exp Hematol*. 30, 1339–1345.
62. Asakura, A., Seale, P., Girgis-Gabardo, A., and Rudnicki, M.A. (2002) Myogenic specification of side population cells in skeletal muscle. *J Cell Biol*. 159, 123–134.
63. Szmitko, P.E., Fedak, P.W., Weisel, R.D., Stewart, D.J., Kutryk, M.J., and Verma, S. (2003) Endothelial progenitor cells: new hope for a broken heart. *Circulation*. 107, 3093–3100.
64. Forrester, J.S., Price, M.J., and Makkar, R.R. (2003) Stem cell repair of infarcted myocardium: an overview for clinicians. *Circulation*. 108, 1139–1145.
65. Reubinoff, B.E., Pera, M.F., Fong, C.Y., Trounson, A., and Bongso, A. (2000) Embryonic stem cell lines from human blastocysts: somatic differentiation in vitro. *Nat Biotechnol*. 18, 399–404.
66. Mitalipova, M., Calhoun, J., Shin, S., et al. (2003) Human embryonic stem cell lines derived from discarded embryos. *Stem Cells*. 21, 521–526.
67. Xu, C., Police, S., Rao, N., and Carpenter, M.K. (2002) Characterization and enrichment of cardiomyocytes derived from human embryonic stem cells. *Circ Res*. 91, 501–508.
68. Kehat, I., Kenyagin-Karsenti, D., Snir, M., et al. (2001) Human embryonic stem cells can differentiate into myocytes with structural and functional properties of cardiomyocytes. *J Clin Invest*. 108, 407–414.
69. Mummery, C., Ward-van Oostwaard, D., Doevendans, P., et al. (2003) Differentiation of human embryonic stem cells to cardiomyocytes: role of coculture with visceral endoderm-like cells. *Circulation*. 107, 2733–2740.
70. Kehat, I., Gepstein, A., Spira, A., Itskovitz-Eldor, J., and Gepstein, L. (2002) High-resolution electrophysiological assessment of human embryonic stem cell-derived cardiomyocytes: a novel in vitro model for the study of conduction. *Circ Res*. 91, 659–661.
71. Vanderlaan, R.D., Oudit, G.Y., and Backx, P.H. (2003) Electrophysiological profiling of cardiomyocytes in embryonic bodies derived from human embryonic stem cells: therapeutic implications. *Circ Res*. 93, 1–3.
72. Fijnvandraat, A.C., van Ginneken, A.C., de Boer, P.A., et al. (2003) Cardiomyocytes derived from embryonic stem cells resemble cardiomyocytes of the embryonic heart tube. *Cardiovasc Res*. 58, 399–409.
73. Klug, M.G., Soonpaa, M.H., Koh, G.Y., and Field, L.J. (1996) Genetically selected cardiomyocytes from differentiating embryonic stem cells form stable intracardiac grafts. *J Clin Invest*. 98, 216–224.
74. Bradley, J.A., Bolton, E.M., and Pedersen, R.A. (2002) Stem cell medicine encounters the immune system. *Nat Rev Immunol*. 2, 859–871.
75. Friedenstein, A.J. (1976) Precursor cells of mechanocytes. *Int Rev Cytol*. 47, 327–359.
76. Caplan, A.I. (1991) Mesenchymal stem cells. *J Orthop Res*. 9, 641–650.
77. Goodell, M.A., Brose, K., Paradis, G., Conner, A.S., and Mulligan, R.C. (1996) Isolation and functional properties of murine hematopoietic stem cells that are replicating in vivo. *J Exp Med*. 183, 1797–1806.
78. Chiu, R.C. (2003) Bone-marrow stem cells as a source for cell therapy. *Heart Fail Rev*. 8, 247–251.
79. Jackson, K.A., Majka, S.M., Wang, H., et al. (2001) Regeneration of ischemic cardiac muscle and vascular endothelium by adult stem cells. *J Clin Invest*. 107, 1395–1402.
80. Tomita, S., Li, R.K., Weisel, R.D., et al. (1999) Autologous transplantation of bone marrow cells improves damaged heart function. *Circulation*. 100, II247–II256.
81. Orlic, D., Kajstura, J., Chimenti, S., et al. (2001) Bone marrow cells regenerate infarcted myocardium. *Nature*. 410, 701–705.
82. Wang, J.S., Shum-Tim, D., Galipeau, J., Chedrawy, E., Eliopoulos, N., and Chiu, R.C. (2000) Marrow stromal cells for cellular cardiomyoplasty: feasibility and potential clinical advantages. *J Thorac Cardiovasc Surg*. 120, 999–1005.
83. Wang, J.S., Shum-Tim, D., Chedrawy, E., and Chiu, R.C. (2001) The coronary delivery of marrow stromal cells for myocardial regeneration: pathophysiologic and therapeutic implications. *J Thorac Cardiovasc Surg*. 122, 699–705.
84. Tomita, S., Nakatani, T., Fukuhara, S., Morisaki, T., Yutani, C., and Kitamura, S. (2002) Bone marrow stromal cells contract synchronously with cardiomyocytes in a coculture system. *Jpn J Thorac Cardiovasc Surg*. 50, 321–324.
85. Saito, T., Kuang, J.Q., Bittira, B., Al-Khaldi, A., and Chiu, R.C. (2002) Xenotransplant cardiac chimera: immune tolerance of adult stem cells. *Ann Thorac Surg*. 74, 19–24.
86. Liechty, K.W., MacKenzie, T.C., Shaaban, A.F., et al. (2000) Human mesenchymal stem cells engraft and demonstrate site-specific differentiation after in utero transplantation in sheep. *Nat Med*. 6, 1282–1286.
87. Orlic, D., Kajstura, J., Chimenti, S., Bodine, D.M., Leri, A., and Anversa, P. (2001) Transplanted adult bone marrow cells repair myocardial infarcts in mice. *Ann N Y Acad Sci*. 938, 221–229; discussion 229–230.
88. Haynesworth, S.E., Goshima, J., Goldberg, V.M., and Caplan, A.I. (1992) Characterization of cells with osteogenic potential from human marrow. *Bone*. 13, 81–88.
89. Mangi, A.A., Noiseux, N., Kong, D., et al. (2003) Mesenchymal stem cells modified with Akt prevent remodeling and restore performance of infarcted hearts. *Nat Med*. 9, 1195–1201.
90. Shake, J.G., Gruber, P.J., Baumgartner, W.A., et al. (2002) Mesenchymal stem cell implantation in a swine myocardial infarct model: engraftment and functional effects. *Ann Thorac Surg*. 73, 1919–1925; discussion 1926.
91. Toma, C., Pittenger, M.F., Cahill, K.S., Byrne, B.J., and Kessler, P.D. (2002) Human mesenchymal stem cells differentiate to a cardiomyocyte phenotype in the adult murine heart. *Circulation*. 105, 93–98.
92. Liu, J., Hu, Q., Mansoor, A., et al. (2003) Autologous mesenchymal stem cell in myocardial infarction. Paper presented at American Heart Association Scientific Sessions 2003, Orlando, FL, November 9–11.
93. Wang, X., Liu, J., Hu, Q., et al. (2003) Relationships between contractile function and increased neovascularization in hearts with patch based autologous stem cell transplantation. Paper presented at

American Heart Association Scientific Sessions 2003, Orlando, FL, November 9–11.
94. Stamm, C., Westphal, B., Kleine, H.D., et al. (2003) Autologous bone-marrow stem-cell transplantation for myocardial regeneration. *Lancet*. 361, 45–46.
95. Tse, H.F., Kwong, Y.L., Chan, J.K., Lo, G., Ho, C.L., and Lau, C.P. (2003) Angiogenesis in ischaemic myocardium by intramyocardial autologous bone marrow mononuclear cell implantation. *Lancet*. 361, 47–49.
96. Strauer, B.E., Brehm, M., Zeus, T., et al. (2002) Repair of infarcted myocardium by autologous intracoronary mononuclear bone marrow cell transplantation in humans. *Circulation*. 106, 1913–1918.
97. Assmus, B., Schachinger, V., Teupe, C., et al. (2002) Transplantation of Progenitor Cells and Regeneration Enhancement in Acute Myocardial Infarction (TOPCARE-AMI). *Circulation*. 106, 3009–3017.
98. Wagers, A.J., Sherwood, R.I., Christensen, J.L., and Weissman, I.L. (2002) Little evidence for developmental plasticity of adult hematopoietic stem cells. *Science*. 297, 2256–2259.
99. Gussoni, E., Soneoka, Y., Strickland, C.D., et al. (1999) Dystrophin expression in the mdx mouse restored by stem cell transplantation. *Nature*. 401, 390–394.
100. Majka, S.M., Jackson, K.A., Kienstra, K.A., Majesky, M.W., Goodell, M.A., and Hirschi, K.K. (2003) Distinct progenitor populations in skeletal muscle are bone marrow derived and exhibit different cell fates during vascular regeneration. *J Clin Invest*. 111, 71–79.
101. Welm, B.E., Tepera, S.B., Venezia, T., Graubert, T.A., Rosen, J.M., and Goodell, M.A. (2002) Sca-1(pos) cells in the mouse mammary gland represent an enriched progenitor cell population. *Dev Biol*. 245, 42–56.
102. Hierlihy, A.M., Seale, P., Lobe, C.G., Rudnicki, M.A., and Megeney, L.A. (2002) The post-natal heart contains a myocardial stem cell population. *FEBS Lett*. 530, 239–243.
103. Asakura, A. (2003) Stem cells in adult skeletal muscle. *Trends Cardiovasc Med*. 13, 123–128.
104. Jiang, Y., Vaessen, B., Lenvik, T., Blackstad, M., Reyes, M., and Verfaillie, C.M. (2002) Multipotent progenitor cells can be isolated from postnatal murine bone marrow, muscle, and brain. *Exp Hematol*. 30, 896–904.
105. Rogers, I. and Casper, R.F. (2003) Stem cells: you can't tell a cell by its cover. *Hum Reprod Update*. 9, 25–33.
106. Erices, A., Conget, P., and Minguell, J.J. (2000) Mesenchymal progenitor cells in human umbilical cord blood. *Br J Haematol*. 109, 235–242.
107. Rocha, V., Wagner, J.E., Jr., Sobocinski, K.A., et al. (2000) Graft-versus-host disease in children who have received a cord-blood or bone marrow transplant from an HLA-identical sibling. Eurocord and International Bone Marrow Transplant Registry Working Committee on Alternative Donor and Stem Cell Sources. *N Engl J Med*. 342, 1846–1854.
108. Fibbe, W.E. and Noort, W.A. (2003) Mesenchymal stem cells and hematopoietic stem cell transplantation. *Ann N Y Acad Sci*. 996, 235–244.
109. Makino, S., Fukuda, K., Miyoshi, S., et al. (1999) Cardiomyocytes can be generated from marrow stromal cells in vitro. *J Clin Invest*. 103, 697–705.
110. Hakuno, D., Fukuda, K., Makino, S., et al. (2002) Bone marrow-derived regenerated cardiomyocytes (CMG cells) express functional adrenergic and muscarinic receptors. *Circulation*. 105, 380–386.
111. Lattanzi, L., Salvatori, G., Coletta, M., et al. (1998) High efficiency myogenic conversion of human fibroblasts by adenoviral vector-mediated MyoD gene transfer. An alternative strategy for ex vivo gene therapy of primary myopathies. *J Clin Invest*. 101, 2119–2128.
112. Etzion, S., Barbash, I.M., Feinberg, M.S., et al. (2002) Cellular cardiomyoplasty of cardiac fibroblasts by adenoviral delivery of MyoD ex vivo: an unlimited source of cells for myocardial repair. *Circulation*. 106, I125–I130.
113. Campbell, K.H., McWhir, J., Ritchie, W.A., and Wilmut, I. (1996) Sheep cloned by nuclear transfer from a cultured cell line. *Nature*. 380, 64–66.
114. Lanza, R.P., Chung, H.Y., Yoo, J.J., et al. (2002) Generation of histocompatible tissues using nuclear transplantation. *Nat Biotechnol*. 20, 689–696.
115. Yau, T.M., Fung, K., Weisel, R.D., Fujii, T., Mickle, D.A., and Li, R.K. (2001) Enhanced myocardial angiogenesis by gene transfer with transplanted cells. *Circulation*. 104, I218–I222.
116. Schwarz, E.R., Speakman, M.T., Patterson, M., et al. (2000) Evaluation of the effects of intramyocardial injection of DNA expressing vascular endothelial growth factor (VEGF) in a myocardial infarction model in the rat—angiogenesis and angioma formation. *J Am Coll Cardiol*. 35, 1323–1330.
117. Lee, R.J., Springer, M.L., Blanco-Bose, W.E., Shaw, R., Ursell, P.C., and Blau, H.M. (2000) VEGF gene delivery to myocardium: deleterious effects of unregulated expression. *Circulation*. 102, 898–901.
118. Iguchi, A., Kobayashi, R., Yoshida, M., et al. (2001) Vascular endothelial growth factor (VEGF) is one of the cytokines causative and predictive of hepatic veno-occlusive disease (VOD) in stem cell transplantation. *Bone Marrow Transplant*. 27, 1173–1180.
119. Lee, M., Rentz, J., Bikram, M., Han, S., Bull, D.A., and Kim, S.W. (2003) Hypoxia-inducible VEGF gene delivery to ischemic myocardium using water-soluble lipopolymer. *Gene Ther*. 10, 1535–1542.
120. Donahue, J.K., Heldman, A.W., Fraser, H., et al. (2000) Focal modification of electrical conduction in the heart by viral gene transfer. *Nat Med*. 6, 1395–1398.
121. Feld, Y., Melamed-Frank, M., Kehat, I., Tal, D., Marom, S., and Gepstein, L. (2002) Electrophysiological modulation of cardiomyocytic tissue by transfected fibroblasts expressing potassium channels: a novel strategy to manipulate excitability. *Circulation*. 105, 522–529.
122. Miake, J., Marban, E., and Nuss, H.B. (2002) Biological pacemaker created by gene transfer. *Nature*. 419, 132–133.
123. Suzuki, K., Murtuza, B., Sammut, I.A., et al. (2002) Heat shock protein 72 enhances manganese superoxide dismutase activity during myocardial ischemia-reperfusion injury, associated with mitochondrial protection and apoptosis reduction. *Circulation*. 106, I270–I276.
124. Suzuki, K., Murtuza, B., Smolenski, R.T., et al. (2001) Overexpression of interleukin-1 receptor antagonist provides cardioprotection against ischemia-reperfusion injury associated with reduction in apoptosis. *Circulation*. 104, I308–I3I3.

32 Genomics-Based Tools and Technology

JENNIFER L. HALL, PhD

CONTENTS

1. INTRODUCTION

Over 16 million people die from cardiovascular disease each year, ranking it as the number one killer of men and women in the United States *(1–7)*. Further, heart disease and stroke kill twice as many women than all forms of cancer combined *(8)*. This chapter introduces genomics tools and technologies that have been instrumental in defining the genetic-based causes of cardiovascular disease, determining the critical genes and signaling pathways governing the transition of the normal heart to failure, and discovering novel drug and device-based therapies to treat cardiovascular disease. The genomics approaches discussed are currently considered "high throughput," but as technology continues to develop and drive this field, it is anticipated that another level of high throughput will be reached that will far surpass current capabilities. Some state-of-the-art technologies and strategies that are on the horizon are also described.

The specific genomics tools described here highlight methods to interrogate the roles of deoxyribonucleic acids (DNAs), ribonucleic acids (RNAs), and proteins in cardiovascular disease. DNA is made up of nucleic acids that form a double helix held together by hydrogen bonds between bases (adenine, guanine, cytosine, thymine) and compose the chromosomes within the nucleus of a cell. A gene is a specific sequence of DNA on the chromosome. It is estimated that the human genome contains 30,000–40,000 genes. DNA is transcribed into RNA, which is made up of the sugar ribose and the four bases—adenine, guanine, cytosine, and uracil (rather than thymidine as in DNA). Messenger RNA (mRNA) carries the code for specific amino acid sequences from the DNA strand to the cytoplasm for protein synthesis. Following an overview of technological approaches, a working example is provided of how our laboratory is utilizing a genomics-based approach to define the critical regulatory genes governing myocardial remodeling and recovery in patients following implantation of a left ventricular assist device.

From: *Handbook of Cardiac Anatomy, Physiology, and Devices*
Edited by: P. A. Iaizzo © Humana Press Inc., Totowa, NJ

2. DEOXYRIBONUCLEIC ACID

Identifying the underlying causes of cardiovascular disease is a critical first step in successful treatment. However, as with cancer, cardiovascular disease is complex and arises from the interaction of many genes as well as environmental factors. The technologies to scan the human genome for gene mutations that may lead to cardiovascular disease are rapidly emerging in the wake of the release of a draft of the human genome sequence in 2001 *(9,10)*. Work to date has identified the following: (1) mutations in genes for ion channels and gap junctions lead to cardiac arrhythmias *(11)*; (2) mutations in genes that encode members of the renin-angiotensin aldosterone system, epithelial sodium channels, adrenoceptors, and G proteins are associated with hypertension *(12–14)*; and (3) mutations in genes that

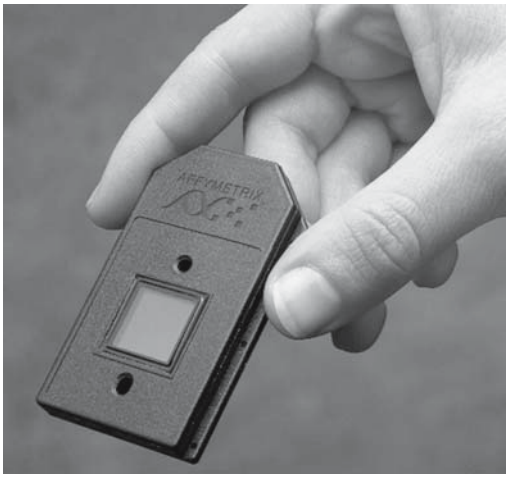

Fig. 1. GeneChip® containing template information for over 22,000 genes. Courtesy of Affymetrix®.

encode sarcomeric proteins lead to hypertrophy or dilated cardiomyopathy *(15)*.

Although these findings have provided insights into the genetic understanding of cardiovascular disease, today this is considered just the tip of the iceberg. The association between gene mutations and cardiomyopathy has been further characterized in multiple transgenic mouse models in which the candidate gene is deleted ("knocked out") and replaced with the mutated form of the gene. These studies have allowed us to test the direct relationship between genotype and phenotype and have been helpful in defining critical regulatory genes in the heart.

Nevertheless, identifying genes and gene interactions associated with a complex disease is a daunting challenge. New advances in technologies to sequence DNA more efficiently and with greater sensitivity have significantly improved chances of defining these associated or linked genes *(8,16–18)*. However, advances in these technologies are not a substitute for clinical studies, the meticulous enrollment of families for linkage studies, and the proper controls that provide the DNA that needs to be sequenced.

Single nucleotide polymorphisms (SNPs or "snips") are the most common mutations in the human genome and occur roughly once every 1000 bases. SNPs are defined as single base substitutions along the genome. Scientists reason that defining susceptibility genes for cardiovascular disease can be aided by identifying the SNPs along the genome and determining whether certain SNPs occur with higher frequency in individuals with cardiovascular disease. Interestingly, the establishment of the SNP consortium by 10 pharmaceutical companies and the Wellcome Trust has to date delivered 2 million mapped SNPs *(19,20)*.

Identifying the SNPs is relatively straightforward, however, what is difficult is determining the association of a particular SNP (or set of SNPs) with a complex disease and defining the genes in these regions in the population. Yet, today's technologies have provided gains in this approach through "multiplexing" strategies that allow amplification of DNA or genotyping of many samples simultaneously *(17)*. Nevertheless, bridging the gap between genetic and epidemiological studies, basic science research, and clinical studies will be required to provide a comprehensive understanding of the critical genes and signaling pathways governing cardiovascular disease.

3. RIBONUCLEIC ACID

The current understanding of the important genes and molecular signaling pathways that regulate myocardial remodeling and the transition to heart failure is based largely on animal models and clinical trials. These studies have confirmed the importance of the neurohormonal systems, including the renin-angiotensin-aldosterone axis, the sympathetic nervous system, and natriuretic peptides in the pathogenesis of the heart failure phenotype *(2,21–26)*. Furthermore, a number of recent failed drug trials have highlighted the potential limitations of animal models in replicating a complex disease such as human heart failure.

Collectively, these findings emphasize the need for resources and tools to utilize tissue from the normal and diseased human heart effectively to increase the basic understanding of the molecular determinants governing the transition to heart failure. The advent of high-throughput, genomics-based strategies has provided a leap forward in the ability to accomplish this and thus to discover novel genes and signaling pathways. For example, the present ability to interrogate nearly the entire genome in a single experiment has allowed scientists to develop unconventional and unbiased approaches to solve problems that may provide a fertile environment for novel drug discovery.

A microarray or gene chip contains oligonucleotides (short strings of bases specific for genes) or complementary DNA (cDNA, individual DNA sequences) for hundreds or thousands of genes on a quartz wafer or glass microscope slide *(27,28)* (Fig. 1). The principle behind this technology is the hybridization potential between nucleic acids. Put simply, this allows a researcher to compare expression of a large number of genes (>22,000) in control and diseased tissues or cells. This is then useful for defining the genes and signaling pathways that may regulate a patient's transition to heart or vascular disease. Furthermore, the identification of these targets can then be used to develop diagnostic tests for early detection and prevention of disease, as well as for novel drug discovery to treat the disease.

Technical use of a microarray depends on the platform employed (oligonucleotide or cDNA). For example, with an oligonucleotide gene chip, the researcher would isolate RNA from the tissue or cells, reverse transcribe the RNA to cDNA, and in vitro transcribe to cRNA with biotin-labeled nucleotides. The biotin-labeled sample is then hybridized to the array, and the arrays are stained with a streptavidin-phycoerythrin conjugate that binds biotin and emits a fluorescent signal. This array is scanned, and the gene expression values are quantitated. For cDNA arrays, RNA from two different tissue or cell populations is isolated and reverse transcribed to cDNA in the presence of nucleotides labeled with two different fluorescent dyes (e.g., Cy3 [green] and Cy5 [red]).

The samples are then simultaneously hybridized to the array, where they "compete" for binding. The slide is scanned, and the

fluorescence is quantitated for each spotted cDNA. Finally, sifting and analyzing the wealth of data from microarray experiments is performed with the help of several different statistical and bioinformatics programs *(29-32)*.

A downfall of the microarray approach is the limitation to study only the sequences represented on the developed chip. Although the sensitivity of this approach has improved, the ability to detect genes with low expression levels reproducibly has been a challenge. Fortunately, the establishment of public databases and resources, including those provided by the National Heart, Lung, and Blood Institute's Programs for Genomics Applications (http://www.nhlbi.nih.gov/resources/pga/) and Cardiac Gene Expression (CaGE) Knowledgebase, has been useful in comparing and analyzing gene expression libraries.

Serial analysis of gene expression (SAGE) is a technique that allows definition of the genes in a given tissue or cell type. This approach was developed by Velculescu et al. *(33)* and is not limited to transcript information printed on a given platform. Briefly, short sequence tags, which carry sufficient information to identify each gene uniquely, are linked together and cloned. Compared to microarrays, SAGE is better able to identify transcripts of low abundance and is thus also perhaps better suited to identify novel genes.

Massively parallel signature sequencing (MPSS) is an emerging technology discovered by the Nobel Prize Laureate Sydney Brenner and colleagues *(34)*. Importantly, this approach is not limited by the sequences spotted on a chip, and its level of sensitivity far outweighs that of the currently used microarray-based platforms. Briefly, MPSS is based on the in vitro cloning of millions of templates on microbeads. Sequencing of the 16–20 base templates on each bead is performed simultaneously using a fluorescence-based signature sequencing approach with repeated cycles of enzymatic cleavage (*see* ref. *34* for an excellent review). This approach is sensitive as well as high throughput in design.

Microarrays, SAGE, and MPSS have the capability to identify critical genes and regulatory signals governing cardiovascular remodeling and disease as well as possibly identify new clinical biomarkers.

4. PROTEIN

Interest in proteomics-based technology and strategies was buoyed, in part, by the somewhat surprising finding that the human genome contained 30,000–40,000 open reading frames, a number much smaller than expected and similar to that of lower organisms. This suggested that the level of diversity and complexity in the human is partly caused by alternative mRNA splicing and posttranslational protein modifications, including such processes as phosphorylation and oxidation/reduction.

Proteomics is defined as the protein component of the human genome. The recent establishment of 10 national proteomics centers funded by the National Heart, Lung, and Blood Institute's Proteomics Initiative will likely provide enormous resources, reagents, and techniques to the scientific community. This program was patterned after the Programs for Genomics Applications; it is considered instrumental in the development of novel and sensitive proteomics-based technologies.

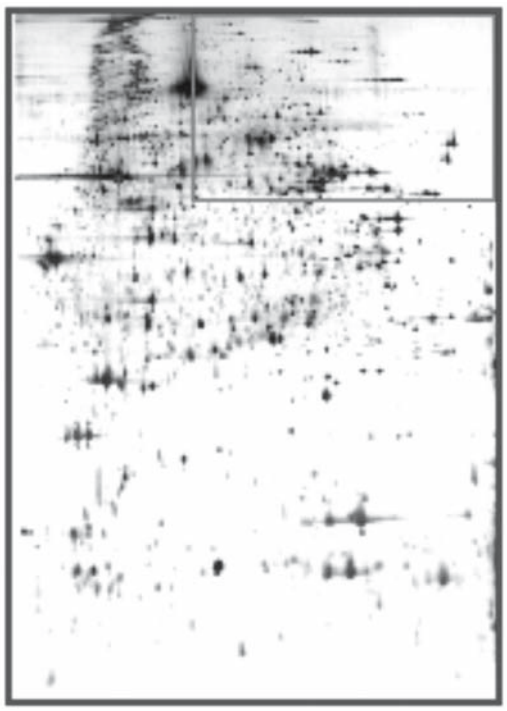

Fig. 2. Two-dimensional gel electrophoresis image; each black spot refers to a protein. From ref. *42*. Used with permission from the Max Delbruck Center for Molecular Medicine.

Many protein databases have been established for the public, including SWISS-PRO/TrEMBL Protein Knowledgebase, the Protein Information Resource, and the Protein Data Bank. The majority of the information in these sites is collated by the National Center for Biotechnology Information's Entrez-Protein database.

Two-dimensional polyacrylamide gel electrophoresis has been routinely used to separate large numbers of proteins (~2000 from a total cardiac protein extract) *(35–38)*. However, the human heart may express more than 10,000 proteins, making sufficient separation difficult. Alternative approaches for identifying these molecules include liquid chromatography and mass spectrometry. Mass spectrometry has become a favored approach for protein identification because of its high sensitivity and high-throughput capacity. In this approach, identifying proteins is done by peptide mass fingerprinting by simply comparing the peptide masses obtained by mass spectrometry of a protein digest with theoretical peptide masses generated *in silico* using protein and nucleotide sequence databases. This works well when the protein of interest has been previously identified, but poorly when trying to make a novel discovery.

The novel identification of amino acid sequences is typically accomplished by employing automated chemical Edman microsequencing or tandem mass spectrometry. The establishment of public protein databases, including HSC-2DPAGE *(39)*, HEART-2DPAGE *(40,41)*, and HP-2DPAGE *(42)* has proven very helpful. A representative illustration of a 2D gel is shown in Fig. 2.

5. DEFINING CRITICAL REGULATORY GENES IN THE REMODELING AND RECOVERY OF THE FAILING HUMAN HEART

To illustrate the use of genomics tools in cardiovascular research, the last section of this chapter introduces a human heart failure project involving the use of a microarray-based approach. The goal of this project is to utilize microarrays to identify candidate genes that are uniquely regulated in the hearts of patients who have recovered from severe end-stage heart failure. The patient cohorts utilized in this study are patients in end-stage heart failure who require a left ventricular assist device to replace the pumping capability of the left ventricle to restore circulation *(43)*.

Tissue samples are harvested from the left ventricle at the time the device is implanted and again at the time the device is explanted. This provides paired patient samples for the design and analysis, which is advantageous for reasons discussed in this section. The majority of these patients (~95%) go on to receive a heart transplant at the time the device is explanted. However, a small percentage of the patients (~5%) establish sufficient recovery of ventricular function to allow explant of the device without a subsequent transplant. Yet, to date the molecular mechanisms governing recovery in this small subset of patients is not known.

Thus, we are employing microarrays as an unbiased and comprehensive screening tool to identify the unique genes differentially regulated in the patients who establish functional recovery. The primary rationale behind this project is to utilize this knowledge as a drug discovery tool to develop novel and efficacious drug therapies for treating patients with heart disease.

A considered strength of this project is the ability to use human heart failure samples. Human heart failure is a complex disease that culminates from the interaction of multiple genetic and environmental factors. Thus, it is also considered that murine, rodent, dog, and pig models of heart failure lack the ability to recapitulate the human disease fully. This is underscored by the fact that multiple drugs that have proved efficacious in animal models have failed in humans *(44–46)*.

The strengths of using human tissue are balanced by the disadvantage of heterogeneity in human studies, including gender, race, age, and the underlying etiology of the disease. It is noteworthy that all of these factors have been shown to influence gene expression *(43,47–60)*. The design of the left ventricular assist device project involves taking two biopsies from the same patient: at the time of device implant and at explant. The paired analysis allows limitation of the effects of these external variables.

Our analysis to date in nonrecovered patients has defined key changes in a host of genes, including significant changes in the PI3Kinase signaling pathway and metallothionein genes *(43)*. Moreover, we found significant changes in genes involved in angiogenesis, including fibroblast growth factor 9 and Sprouty1. Interestingly, a number of genes in both the PI3Kinase and metallothionein pathways, as well as genes regulating angiogenesis, were differentially regulated in early studies from recovered patients. Nevertheless, further studies will be needed to address definitively the differences between the recovered and nonrecovered patients. Yet, these initial studies have highlighted a close coupling between the myocyte and the endothelium in heart recovery, a novel area of research.

We have utilized real-time quantitative polymerase chain reaction as a tool to reconfirm the changes over 40 genes differentially expressed on the microarray in the samples pre- and post-left ventricular assist device *(43)*. Western blots and immunostaining were then used to determine if a significant alteration in mRNA expression leads to a concomitant change in protein expression.

If the gene candidate is pursued as a drug target, medicinal chemists are typically recruited to determine the likelihood of designing a small molecule to block or stimulate the gene or pathway. Studies can then be performed in which the target gene is upregulated or downregulated to mimic changes defined in the human heart and determine the functional effect. Initial studies are routinely completed in cultured cells, and the downstream signaling targets and pathways and alterations in cell size are interrogated. In one approach, the gene of interest can be further tested in vivo by establishing a murine transgenic model harboring heart-specific upregulation.

In our studies to date, we have utilized a human compendium of microarray data to define novel targets involved in cardiovascular disease. With targets in hand, in vitro modeling systems and animal models are used to define the functional role of the gene in cardiovascular remodeling and function.

6. SUMMARY

Heart disease is the number one killer of men and women in the United States. The focus of this chapter was to introduce genomics-based tools and technologies that are used in basic and clinical research to further our understanding of the genetic and molecular basis of cardiovascular disease. Heart disease arises from the interactions of many genes as well as lifestyle and environmental factors. This significantly increases the challenge for the scientist and clinician to define targets for intervention to prevent, slow, or reverse the course of the disease effectively. Today, multiple genomics tools and techniques are available to increase the understanding of the mechanisms leading to cardiovascular disease. Our hope is that these findings will significantly enhance the effective treatment of patients with heart failure, as well as prevent patients with multiple risk factors from developing cardiovascular disease.

REFERENCES

1. Hoeg, J.M. (1997) Evaluating coronary heart disease risk. Tiles in the mosaic. *JAMA*. 277, 1387–1390.
2. Kelly, D.P. and Strauss, A.W. (1994) Inherited cardiomyopathies. *N Engl J Med*. 330, 913–919.
3. Marwick, C. (1997) NHANES III health data relevant for aging nation. *JAMA*. 277, 100–102.
4. Ridker, P.M. and Antman, E.M. (1999) Pathogenesis and pathology of coronary heart disease syndromes. *J Thromb Thrombolysis*. 8, 167–189.
5. Ridker, P.M. (1999) Evaluating novel cardiovascular risk factors: can we better predict heart attacks? *Ann Intern Med*. 130, 933–937.
6. Ridker, P.M. (1999) Inflammation, atherosclerosis, and cardiovascular risk: an epidemiologic view. *Blood Coagul Fibrinolysis*. 10, S9–S12.

7. American Heart Association. (2001) Congestive Heart Failure [abstract]. Available at Website: (www.americanheart.org). Date accessed: Nov. 18, 2004.
8. National Heart, Lung, and Blood Institute. (2003) NHLBI The Heart Truth [abstract]. Available at Website: (http://www.nhlbi.nih.gov/health/hearttruth/). Date accessed: Nov. 18, 2004.
9. Lander, E.S., Linton, L.M., Birren, B., et al. (2001) Initial sequencing and analysis of the human genome. *Nature*. 409, 860–921.
10. Venter, J.C., Adams, M.D., Myers, E.W., et al. (2001) The sequence of the human genome. *Science*. 291, 1304–1351.
11. Cheng, C.F., Kuo, H.C., and Chien, K.R. (2003) Genetic modifiers of cardiac arrhythmias. *Trends Mol Med*. 9, 59–66.
12. Turner, S.T. and Boerwinkle, E. (2000) Genetics of hypertension, target-organ complications, and response to therapy. *Circulation*. 102, IV40–IV45.
13. Turner, S.T., Schwartz, G.L., Chapman, A.B., and Boerwinkle, E. (2001) Use of gene markers to guide antihypertensive therapy. *Curr Hypertens Rep*. 3, 410–415.
14. Turner, S.T., Schwartz, G.L., Chapman, A.B., Hall, W.D., and Boerwinkle, E. (2001) Antihypertensive pharmacogenetics: getting the right drug into the right patient. *J Hypertens*. 19, 1–11.
15. Seidman, C.E. and Seidman, J.G. (1991) Mutations in cardiac myosin heavy chain genes cause familial hypertrophic cardiomyopathy. *Mol Biol Med*. 8, 159–166.
16. Gura, T. (2001) Genetics: SNP-ing drugs to size. *Science*. 293, 595.
17. Gura, T. (2001) Genetics: Can SNPs deliver on susceptibility genes? *Science*. 293, 593–595.
18. Roses, A.D. (2002) SNPs—where's the beef? *Pharmacogenomics J*. 2, 277–283.
19. Mullikin, J.C., Hunt, S.E., Cole, C.G., et al. (2000) An SNP map of human chromosome 22. *Nature*. 407, 516–520.
20. Sachidanandam, R., Weissman, D., Schmidt, S.C., et al. (2001) A map of human genome sequence variation containing 1.42 million single nucleotide polymorphisms. *Nature*. 409, 928–933.
21. Bowles, N.E., Bowles, K.R., and Towbin, J.A. (2000) The "final common pathway" hypothesis and inherited cardiovascular disease. The role of cytoskeletal proteins in dilated cardiomyopathy. *Herz*. 25, 168–175.
22. Francis, G.S., Benedict, C., Johnstone, D.E., et al. (1990) Comparison of neuroendocrine activation in patients with left ventricular dysfunction with and without congestive heart failure. A substudy of the Studies of Left Ventricular Dysfunction (SOLVD). *Circulation*. 82, 1724–1729.
23. Mann, D.L. (1998) Basic mechanisms of disease progression in the failing heart: the role of excessive adrenergic drive. *Prog Cardiovasc Dis*. 41, 1–8.
24. Mann, D.L. (1999) Mechanisms and models in heart failure: a combinatorial approach. *Circulation*. 100, 999–1008.
25. Packer, M. (1992) The neurohormonal hypothesis: a theory to explain the mechanism of disease progression in heart failure. *J Am Coll Cardiol*. 20, 248–254.
26. Packer, M. (1998) Beta-adrenergic blockade in chronic heart failure: principles, progress, and practice. *Prog Cardiovasc Dis*. 41, 39–52.
27. Southern, E., Mir, K., and Shchepinov, M. (1999) Molecular interactions on microarrays. *Nat Genet*. 21, 5–9.
28. Duggan, D.J., Bittner, M., Chen, Y., Meltzer, P., and Trent, J.M. (1999) Expression profiling using cDNA microarrays. *Nat Genet*. 21, 10–14.
29. Dahlquist, K.D., Salomonis, N., Vranizan, K., Lawlor, S.C., and Conklin, B.R. (2002) GenMAPP, a new tool for viewing and analyzing microarray data on biological pathways. *Nat Genet*. 31, 19–20.
30. Doniger, S.W., Salomonis, N., Dahlquist, K.D., Vranizan, K., Lawlor, S.C., and Conklin, B.R. (2003) MAPPFinder: using Gene Ontology and GenMAPP to create a global gene-expression profile from microarray data. *Genome Biol*. 4, R7.
31. Miller, C.J. and Attwood, T.K. (2003) Bioinformatics goes back to the future. *Nat Rev Mol Cell Biol*. 4, 157–162.
32. Quackenbush, J. (2002) Microarray data normalization and transformation. *Nat Genet*. 32, 496–501.
33. Velculescu, V.E., Zhang, L., Vogelstein, B., and Kinzler, K.W. (1995) Serial analysis of gene expression. *Science*. 270, 484–487.
34. Brenner, S., Johnson, M., Bridgham, J., et al. (2000) Gene expression analysis by massively parallel signature sequencing (MPSS) on microbead arrays. *Nat Biotechnol*. 18, 630–634.
35. Frank, R. (2002) High-density synthetic peptide microarrays: emerging tools for functional genomics and proteomics. *Comb Chem High Throughput Screen*. 5, 429–440.
36. Frank, R. and Hargreaves, R. (2003) Clinical biomarkers in drug discovery and development. *Nat Rev Drug Discov*. 2, 566–580.
37. McGregor, E. and Dunn, M.J. (2003) Proteomics of heart disease. *Hum Mol Genet*. 12, R135–R144.
38. Winslow, R.L. and Boguski, M.S. (2003) Genome informatics: current status and future prospects. *Circ Res*. 92, 953–961.
39. Evans, G., Wheeler, C.H., Corbett, J.M., and Dunn, M.J. (1997) Construction of HSC-2DPAGE: a two-dimensional gel electrophoresis database of heart proteins. *Electrophoresis*. 18, 471–479.
40. Pleissner, K.P., Sander, S., Oswald, H., Regitz-Zagrosek, V., and Fleck, E. (1996) The construction of the World Wide Web-accessible myocardial two-dimensional gel electrophoresis protein database "HEART-2DPAGE": a practical approach. *Electrophoresis*.17, 1386–1392.
41. Pleissner, K.P., Soding, P., Sander, S., et al. (1997) Dilated cardiomyopathy-associated proteins and their presentation in a WWW-accessible two-dimensional gel protein database. *Electrophoresis*. 18, 802–808.
42. Muller, E.C., Thiede, B., Zimny-Arndt, U., et al. (1996) High-performance human myocardial two-dimensional electrophoresis database: edition 1996. *Electrophoresis*. 17, 1700–1712.
43. Chen, Y., Park, S., Li, Y., et al. (2003) Alterations of gene expression in failing myocardium following left ventricular assist device support. *Physiol Genomics*. 14, 251–260.
44. Cohn, J.N., Goldstein, S.O., Greenberg, B.H., et al. (1998) A dose-dependent increase in mortality with vesnarinone among patients with severe heart failure. Vesnarinone Trial Investigators. *N Engl J Med*. 339, 1810–1816.
45. Packer, M., Carver, J.R., Rodeheffer, R.J., et al. (1991) Effect of oral milrinone on mortality in severe chronic heart failure. The PROMISE Study Research Group. *N Engl J Med*. 325, 1468–1475.
46. Rouleau, J.L., Pfeffer, M.A., Stewart, D.J., et al. (2000) Comparison of vasopeptidase inhibitor, omapatrilat, and lisinopril on exercise tolerance and morbidity in patients with heart failure: IMPRESS randomised trial. *Lancet*. 356, 615–620.
47. Aronow, B.J., Toyokawa, T., Canning, A., et al. (2001) Divergent transcriptional responses to independent genetic causes of cardiac hypertrophy. *Physiol Genomics*. 6, 19–28.
48. Barrans, J.D., Allen, P.D., Stamatiou, D., Dzau, V.J., and Liew, C.C. (2002) Global gene expression profiling of end-stage dilated cardiomyopathy using a human cardiovascular-based cDNA microarray. *Am J Pathol*. 160, 2035–2043.
49. Blaxall, B.C., Spang, R., Rockman, H.A., and Koch, W.J. (2003) Differential myocardial gene expression in the development and rescue of murine heart failure. *Physiol Genomics*. 15, 105–114.
50. Blaxall, B.C., Tschannen-Moran, B.M., Milano, C.A., and Koch, W.J. (2003) Differential gene expression and genomic patient stratification following left ventricular assist device support. *J Am Coll Cardiol*. 41, 1096–1106.
51. Chen, M.M., Ashley, E.A., Deng, D.X., et al. (2003) Novel role for the potent endogenous inotrope apelin in human cardiac dysfunction. *Circulation*. 108, 1432–1439.
52. Hwang, J.J., Dzau, V.J., and Liew, C.C. (2001) Genomics and the pathophysiology of heart failure. *Curr Cardiol Rep*. 3, 198–207.
53. Hwang, J.J., Allen, P.D., Tseng, G.C., et al. (2002) Microarray gene expression profiles in dilated and hypertrophic cardiomyopathic end-stage heart failure. *Physiol Genomics*. 10, 31–44.
54. Steenbergen, C., Afshari, C.A., Petranka, J.G., et al. (2003) Alterations in apoptotic signaling in human idiopathic cardiomyopathic hearts in failure. *Am J Physiol Heart Circ Physiol*. 284, H268–H276.
55. Tan, F.L., Moravec, C.S., Li, J., et al. (2002) The gene expression fingerprint of human heart failure. *Proc Natl Acad Sci USA*. 99, 11,387–11,392.

56. Towbin, J.A. and Bowles, N.E. (2000) Genetic abnormalities responsible for dilated cardiomyopathy. *Curr Cardiol Rep.* 2, 475–480.
57. Dobson, J.G., Jr., Fray, J., Leonard, J.L., and Pratt, R.E. (2003) Molecular mechanisms of reduced beta-adrenergic signaling in the aged heart as revealed by genomic profiling. *Physiol Genomics.* 15, 142–147.
58. Durier, S., Fassot, C., Laurent, S., et al. (2003) Physiological genomics of human arteries: quantitative relationship between gene expression and arterial stiffness. *Circulation.* 108, 1845–1851.
59. Hsiao, L.L., Dangond, F., Yoshida, T., et al. (2001) A compendium of gene expression in normal human tissues. *Physiol Genomics.* 7, 97–104.
60. Boheler, K.R., Volkova, M., Morrell, C., et al. (2003) Sex- and age-dependent human transcriptome variability: implications for chronic heart failure. *Proc Natl Acad Sci USA.* 100, 2754–2759.

33 Emerging Cardiac Devices and Technologies

PAUL A. IAIZZO, PhD

CONTENTS

1. INTRODUCTION

In previous chapters, authors provided brief histories of cardiac device development and several fairly thorough discussions of currently employed devices or assessment technologies. To gain insight into how rapidly innovations in the area of cardiac disease are progressing, a search of the US Patent and Trademark Office Website (www.uspto.gov) can simply be searched. Such a search produces an impressive number of companies or individuals attempting to secure intellectual property protection in this clinical category. More specifically, the following are the numbers of published patent applications, identified in November 2004, citing the following key words:

- cardiac (18,920 patent applications)
- cardiac surgery (1015 patent applications)
- cardiology (1480 patent applications)
- cardiac electrophysiology (79 patent applications)
- cardiovascular stents (52 patent applications)
- cardiac repair (32 patent applications)

From: *Handbook of Cardiac Anatomy, Physiology, and Devices*
Edited by: P. A. Iaizzo © Humana Press Inc., Totowa, NJ

This does not include all issued patents to date, many of which detail prospective future products. For example, in searching the same database, the key word "cardiac" produces 37,410 issued patents to date since 1976. There are several other places to locate information on up-and-coming cardiac devices, such as the Food and Drug Administration Website (http://www.fda.gov/) or websites listed at the end of this chapter.

It should be mentioned that many novel ideas that eventually lead to new products, therapies, or training first occur through basic cardiac research. For emerging technologies to continue to advance at a rapid rate, it is imperative that laboratories performing basic research in such technological areas continue to receive necessary support. Furthermore, prototype testing and clinical trials are essential to ensure that the best possible technologies are both developed and eventually made available for general use. Yet, it is important to note that many lessons can be learned from trials that employed either misdirected devices or technologies.

The primary goals of this last chapter are to: (1) discuss, in more detail, some of the aforementioned technologies; (2) introduce several additional technological advances associated with

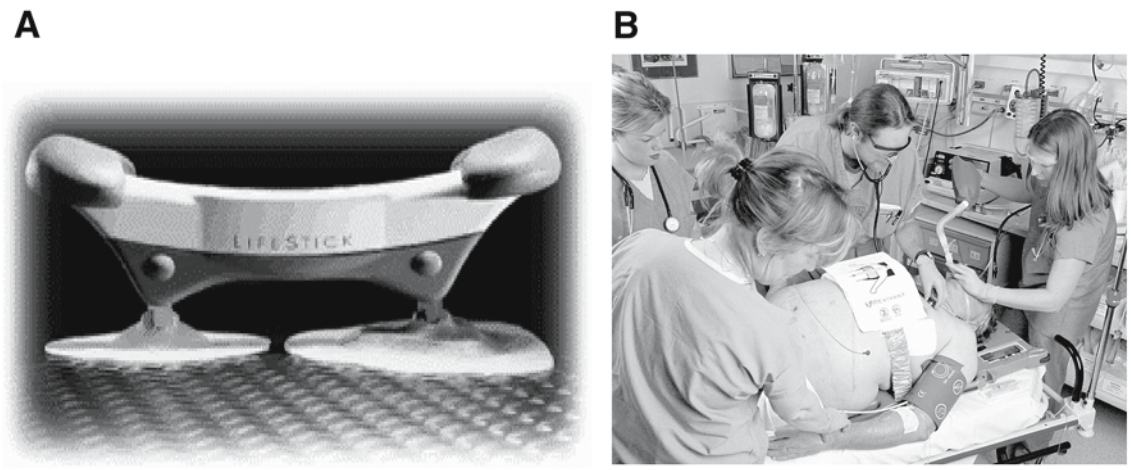

Fig. 1. Various compression–decompression devices. **(A)** The LifeStick™ Resuscitator is an investigational, noninvasive, manually powered cardiopulmonary resuscitation (CPR) device, invented and designed by Datascope Corporation (Montvale, NJ), that is designed to enhance circulatory perfusion by facilitating sequential phased active compression and decompression of the chest and abdomen. **(B)** The AutoPulse Resuscitation System consists of a portable AutoPulse Platform, a single-patient use LifeBand™, rechargeable batteries, battery charger, and carrying case (Revivant Corp., Sunnyvale, CA).

Fig. 2. Shown is the impedance threshold device ResQPod™, distributed by Zoll Medical (Chelmsford, MA). Used with permission from the ZOLL Medical Corporation Website. © 2004.

cardiovascular health care that have been recently introduced or are currently in clinical testing or soon to be released; and (3) discuss future opportunities in the cardiac device arena. It should be noted that other areas of importance in cardiac treatment, such as biological approaches to disease management (e.g., stem cell therapy), genomics (i.e., diagnostics and gene therapy), proteomics, and tissue engineering will also have a major impact on the future of cardiac clinical care; however, detailed discussions of these approaches are beyond the scope of this text. More specifically, this last chapter reviews several innovations in each of the following areas: (1) resuscitation systems and devices; (2) implantable therapies; (3) delivery systems; (4) invasive therapies; (5) procedural improvements; (6) less-invasive surgical approaches; (7) postprocedural follow-ups; and (8) training tools.

2. RESUSCITATION SYSTEMS AND DEVICES

Even before the cardiac patient enters the emergency or operating room, there are many new technologies being developed to aid in the resuscitation of an individual who has suffered from cardiovascular failure. Such devices range from improvements of existing tools (e.g., the automated application of cardiopulmonary resuscitation or CPR) to novel mechanisms that accomplish improved outcomes (e.g., an impedance threshold valve). Furthermore, automated external defibrillators have become commonplace in the United States, with such units purchased for use in schools, health clubs, emergency vehicles, shopping malls, and even homes.

2.1. Active Cardiopulmonary Resuscitation Devices

A number of active compression–decompression devices have been developed (Fig. 1), and numerous clinical trials have suggested improved short-term survival in patients with an out-of-hospital cardiac arrest *(1–7)*. In addition, in one study it was reported that active compression–decompression CPR performed during advanced life support significantly improved long-term survival rates among patients who had cardiac arrest outside the hospital *(6)*. Furthermore, when such active compression–decompression devices were used in combination with inspiratory impedance threshold devices (Fig. 2), there was an even greater positive outcome *(8,9)*. More specifically, it was described that the use of an active compression–decompression device combined with an inspiratory impedance threshold device improved 1-h and 24-h survival in 103 patients who received that form of CPR vs 107 who received standard CPR *(10)*.

The active compression–decompression device used in the previously described study *(10)* was handheld, with a suction cup

Fig. 3. A LIFEPAK 12 internal defibrillator (Medtronic, Inc., Minneapolis, MN) used externally (outside) on an overwintering black bear. In this case, Dr. Tim Laske is using the system to monitor a 12-lead electrocardiogram (ECG) via its connection to surface electrodes.

that attached to the chest and a gauge that helped evaluate the force needed for effective compression and decompression, thus creating a vacuum within the chest (Fig. 1A). It is considered that the vacuum draws more blood back into the heart, which then results in more blood flowing out during the subsequent compression. However, it is also considered that air drawn into the lungs during a decompression can in turn reduce the volume of blood that can be drawn into the heart. Therefore, employing an impedance threshold device can minimize this situation.

The impedance threshold device is a small, 35-mL device that fits on a face mask or an endotracheal tube (Fig. 2). Its pressure-sensitive valves limit the inflow of air during chest decompression, allowing more blood to come into the thorax area *(10)*. Initially, in an animal study, Lurie et al. *(11)* showed an increase in blood flow to vital organs in animals eliciting 6 min of ventricular fibrillation and then 6 min of standard CPR plus the use of an impedance threshold device.

2.2. External Defibrillators

Today, most emergency medicine service units utilize a multitier response system, with emergency medical technicians (EMTs) providing basic life support services, backed up by paramedics if advanced life support is needed. All of these personnel are trained in the use of automated external defibrillators. There are several companies that produce such devices, and their availability is no longer limited to hospital or emergency services settings.

Yet, such units may also have expanded features that not all individuals are sufficiently trained to utilize. For example, the LIFEPAK® 12 defibrillator/monitor series, manufactured by Medtronic, Inc. (Minneapolis, MN), allows the recording of a standard 12-lead ECG even in remote locations (Fig. 3). Nevertheless, with the same equipment, various personnel with different levels of expertise and training can provide lifesaving support, for instance, some units have even incorporated push button turn controls with voice prompts.

To date, devices such as the LIFEPAK 12 defibrillator/monitor series give paramedics access to sophisticated diagnostics and treatment in the field. This single piece of equipment monitors the ECG continuously, measures the level of oxygen in the bloodstream, and if necessary, provides defibrillation or pacing to help maintain the heart's rhythm. Thus, it allows paramedics to perform computerized 12-lead ECGs before the patient reaches the hospital.

Such ECG data can be transmitted by cellular phone to the emergency room physician from the ambulance while en route. With this information in hand, the team of doctors and nurses can be ready and waiting for the patient's arrival; importantly, they can administer treatment in as little as 15 min after the patient enters the emergency room, compared to an hour or more if the ECG is first done at the hospital. It is generally considered that any shortening of the time to treatment can significantly speed recovery and improve a patient's chances of returning to a fully productive life.

Fig. 4. The Bio-Pump was originally developed for cardiopulmonary bypass, but it can be used for short periods of circulatory support (usually 5 or fewer days) beyond the surgical setting (Medtronic, Inc., Minneapolis, MN). The Bio-Pump has been used both in postcardiotomy cardiogenic shock patients (those who have developed heart failure as a result of heart surgery) and as a bridge to transplantation for patients who cannot be weaned from the device. This short-term assist device can be implanted in a broad range of patients, from newborns to adults, and can be used alone or with another Bio-Pump or other type of assist device if biventricular support is needed. The Bio-Pump is an extracorporeal, centrifugal device that can provide support for one or both ventricles. Two disposable models are available: 80-mL model for adults and 48-mL model for children. The transparent pump housing is shaped like a cone. The pump consists of an acrylic pump head with inlet and outlet ports placed at right angles to each other. The impeller, which is a stack of parallel cones, is driven by an external motor and power console. Rotation of this impeller at high speeds creates a vortex, which drives blood flow in relation to rotational speed. Blood enters through an inlet at the top of the cone and exits via an outlet at the base. The adult model pump can rotate up to 5000 rpm and can provide flow rates of up to 10 L/min.

The following scenario has been provided by Medtronic Physio-Control Corporation (Redmond, WA) to demonstrate the significance of such features:

> *By the time a given patient had arrived at the hospital, the symptoms had subsided, and the ECG in the hospital appeared normal, yet the attending doctors compared the ECG done in the ambulance with the one obtained from the patient's physical exam a month prior and then there was no question about the diagnosis, a progressing heart attack. With 12-lead ECGs on board, an ambulance becomes a mobile clinic and paramedics become the doctors' eyes and ears.*

It is likely that more and more computerized data collection (e.g., pressures, flows, etc.) will be performed by paramedics or others prior to a patient entering the hospital setting, which will then be seamlessly integrated with the hospital's electronic database to create a complete picture of a patient's medical condition from initial contact all the way through hospital discharge. Many such developments are currently available, and the challenge for health care providers in the coming years will be to provide the best possible care in the most cost-effective way.

3. IMPLANTABLE THERAPIES

Advances in microtechnologies have now made it possible to create implantable therapies that can be lifesaving, such as implantable defibrillators, which have detected and treated thousands of episodes of sudden cardiac fibrillation. As mentioned, the potential for large numbers of such devices will likely increase at an exponential rate and will be directed specifically to all types of cardiac complications.

3.1. Left Atrial Appendage/Atrial Fibrillation Therapy

There are growing numbers of treatments for the side effects of atrial fibrillation that, in some patients, lead to crippling strokes. The focus of these devices is to modify the role of the left atrial appendage in pathologies associated with atrial fibrillation. More specifically, this tiny alcove of the heart, which has been described to serve as a "starter heart" for the human embryo, can be a site for blood to pool and subsequently form clots that can be expelled into the brain, causing strokes. Today, it is estimated that atrial fibrillation affects 5 million people worldwide and is thought to be responsible for up to 25% of all strokes.

At present, the most common treatment for atrial fibrillation is the administration of a strong anticoagulant drug called coumadin. From a device perspective, suggested approaches to treat this problem include tissue clamps, screens, and other methods to seal off the appendage. More specifically, one start-up company, Atritech Inc. (Plymouth, MN), has promoted a solution to implant a tiny filter into the appendage, letting blood pass through, but trapping clots inside the minichamber; after some time, the body would naturally seals the chamber.

3.2. Cardiac Remodeling

Chronic cardiac remodeling is a well-known response of dilated cardiomyopathy and is thought to play a central role in disease progression *(12–14)*. Associated heart chamber dilation or wall thinning will elevate overall wall stress, which is considered to trigger the local release of neurohormones, which adversely affects myocardial molecular biology and physiology *(15)*. Therapeutic approaches to treat heart failure have been described, primarily as a means to inhibit or even induce reverse remodeling (e.g., β-adrenergic blockade).

Mechanical unloading using left ventricular assist devices (LVADs; *see* Chapter 30) or extracorporeal pumps (Fig. 4) have been employed as alternatives. Such interventions can profoundly unload a heart, leading to reverse remodeling and improved physiological performance *(12)*.

Another approach for accomplishing this benefit is to induce structural remodeling by imposing alteration on or within the heart. For example, the CorCap™ Cardiac Support

Device (Acorn Cardiovascular Inc.™, St. Paul, MN) is a fabric mesh multifilament implant that is surgically positioned around the ventricles of the heart (Fig. 5). This product is designed to reduce ventricular wall stress by supporting the heart muscle. Preclinical studies have shown that supporting the heart in this manner stops deterioration and allows the muscle to heal or remodel *(14)*. More specifically, the deployment of this device is expected to improve the heart's ability to pump blood, provide relief of heart failure symptoms, improve quality of life, and ultimately extend survival for those who suffer from heart failure. Since April 1999, more than 270 implantations of the CorCap™ Cardiac Support Device have been performed worldwide; the devices are currently being evaluated through randomized clinical trials in North America and Europe.

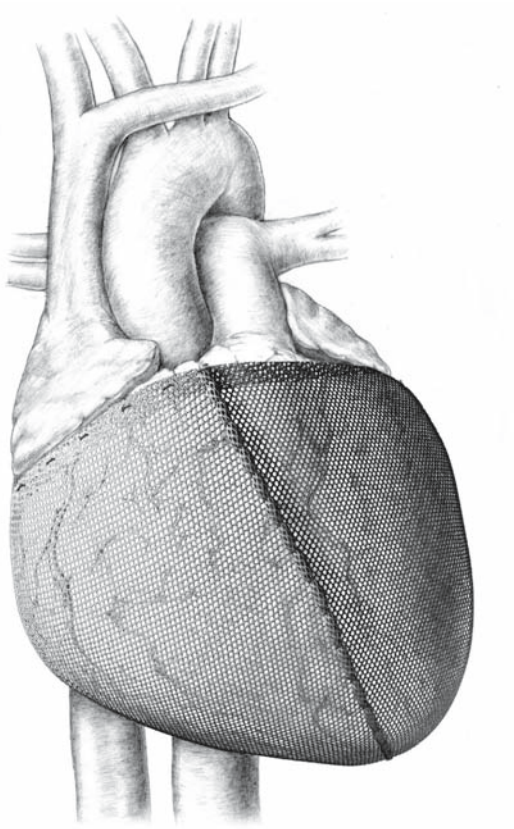

Fig. 5. The CorCap™ Cardiac Support Device (Acorn Cardiovascular Inc.™, St. Paul, MN) is a fabric mesh multifilament implant that is surgically positioned around the ventricles of the heart. Acorn developed a new fabric made from implant-grade polyethylene terepthalate (PET polyester) fabricated into a proprietary mesh design. The CorCap™ Cardiac Support Device fabric is composed of many interlinked filaments, each one-fifth the size of a human hair. The multifilament knit construction provides optimal support with conformability that evenly distributes support over the heart's surface. The proprietary processing of the device produces a highly biocompatible and durable material designed and tested for permanent implantation without adverse effects.

4. CATHETER-DELIVERED DEVICES

The delivery of specialized devices that can be introduced intravascularly or intracardially has been on the rise. Such devices include stents, septal occluder devices, leads, and ablation tools (*see also* Chapters 6, 22, 23, and 29).

4.1. Stents

An intraluminal coronary artery stent is a small, self-expanding, wire mesh tube that is placed within a coronary artery to keep the vessel patent (open). Stents are commonly deployed: (1) during coronary artery bypass graft surgery to keep the grafted vessel open; (2) after balloon angioplasty to prevent reclosure of the blood vessel; or (3) during other heart surgeries. For delivery, a stent is collapsed to quite a small diameter and inserted over a balloon catheter. Typically with the guidance of fluoroscopy, the catheter and stent are moved into the area of the blockage. When the balloon on the delivery catheter is inflated, the stent expands, locking it in place within the vessel, thus forming a scaffold that holds the artery open.

Stents are intended to stay in the vessel permanently, keeping it open to improve blood flow to the myocardium, thereby relieving symptoms (usually angina). Note that a stent may be used instead of angioplasty. The type of stent to be deployed depends on certain features of the artery blockage (i.e., size of the artery and where the blockage is specifically located).

Stents are now considered to reduce the incidence of restenosis, which generally occurs within 4–6 months following an angioplasty procedure. Before stents, the incidence of restenosis was about 35–45%. Restenosis is a renarrowing of the treated coronary artery, which is largely related to the development of neointimal hyperplasia (that which occurs within an artery after it has been treated with a balloon or atherectomy device). In general, restenosis can be considered as scar tissue that forms in response to a previous mechanical insult. Hence, restenosis is somewhat different from atherosclerosis, which is related to calcium, fat, or cholesterol plaque buildup. Some individuals are considered genetically predisposed to develop restenosis.

To date, stents are the only widely employed devices that have been proven to reduce the incidence of restenosis (reduction by approximately one-third). Stents alone are not considered as "cures" for coronary artery disease, but their use will continue to have a major impact on decreasing the need for repeat procedures.

Nevertheless, one of the major goals for improving the outcome of stenting procedures is to minimize further the potential for vessel restenosis. To accomplish this, several new types of stents, called drug-eluting stents, have been employed (Table 1). Such stents are coated with agents that are slowly released, further promoting the vessel from renarrowing and closing.

Yet, it should also be noted that, typically, patients who have had a stent procedure must take one or more blood-thinning agents such as aspirin, ticlopidine, or clopidogrel. Aspirin is typically used indefinitely, and one of the other two drugs is generally prescribed for 2 to 4 weeks. Therefore, goals for future stent technologies will continue to include the development of coatings that will minimize restenosis or the use of anticoagulation therapy (Table 1).

Table 1
Currently Leading Stent Companies

Company	*Stent*	*Stent coatings*
Cook Cardiology	Gianturco-Roubin stents	Pacltaxel (Taxol)
Guidant/ACS	Multilink/Duet/Tetra/Penta Stents	
SCIMED/Boston Scientific	Nir/Wall stents	Paclitaxel
Medtronic/AVE	GFX/S series stents	
Johnson & Johnson/Cordis	Velocity stents	Sirolimus

Company locations: Cook, Bloomington, IN; Guidant, Indianapolis, IN; Boston Scientific, Natick, MA; Medtronic, Minneapolis, MN; Johnson & Johnson, New Brunswick, NJ; AVE, Santa Rosa, CA; Cordis, Warren, NJ.

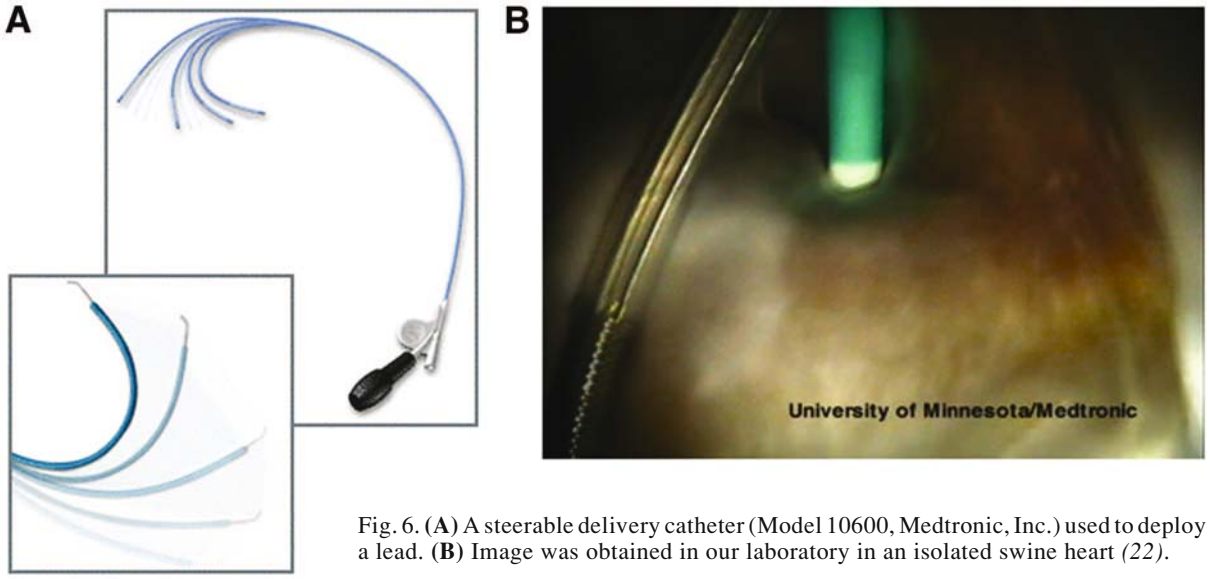

Fig. 6. **(A)** A steerable delivery catheter (Model 10600, Medtronic, Inc.) used to deploy a lead. **(B)** Image was obtained in our laboratory in an isolated swine heart *(22)*.

Table 2
Types of Ablation Energy

- Radiofrequency (RF) energy
- Laser energy
- Microwave energy
- Direct current (DC) shock energy
- Cryoenergy

There are multiple methods of delivering energy during ablation; radiofrequency delivery is the most common.

4.2. Catheter-Delivered Leads

One of the continuing challenges in the area of intracardiac lead development is to downsize lead diameters and at the same time minimize the possibilities for fractures. Similarly, there is rapid development occurring in the placement of leads within the cardiac veins as well as in the development of tools for cannulation of the coronary sinus. For example, the Medtronic Attain™ Deflectable Catheter System features a percutaneous needle and syringe to access the venous insertion site, a guidewire to access the vein, an adjustable hemostasis valve to reduce blood loss during the implant procedure, a deflectable catheter to cannulate the coronary sinus and to deliver the pacing lead, and slitters to remove the deflectable catheter. In addition, the Attain Prevail™, a steerable coronary sinus cannulation tool is available from Medtronic, Inc. (Fig. 6). Such catheters need to be sterile and will likely be single use.

4.3. Endocardial Ablation Devices

Ablation is used to prevent tachyarrhythmias by modifying or destroying abnormal tissue. Clearly identifying the site of origin of the tachyarrhythmia (or tissue that is essential for maintaining reentrant activity) is important to the success of ablation (*see* Chapters 22 and 25); the goal of ablation is to create scar tissue in a critical myocardial area. Because scar tissue is electrically inert, it cannot originate or conduct electrical impulses. Scar tissue is created in the myocardium by either surgical incision or application of energy. Various forms of energy have been employed in the catheter-based approaches of ablation (Table 2). To date, surgical ablation is typically performed during an open chest procedure, but it is likely that with further enhancements of surgical methodologies, it could be performed using less-invasive approaches.

Currently, radiofrequency energy is used for almost all nonoperative ablation procedures (Fig. 7). In the past, DC (direct current) shock energy was used for delivering energy to the endocardium. A standard defibrillator was connected to the ablation catheter to deliver the shock. The DC shock had the following undesirable effects that occurred at the catheter tip during delivery of high energy: (1) excessive tip temperature and (2) irregular-shape lesions that then could be proarrhythmic.

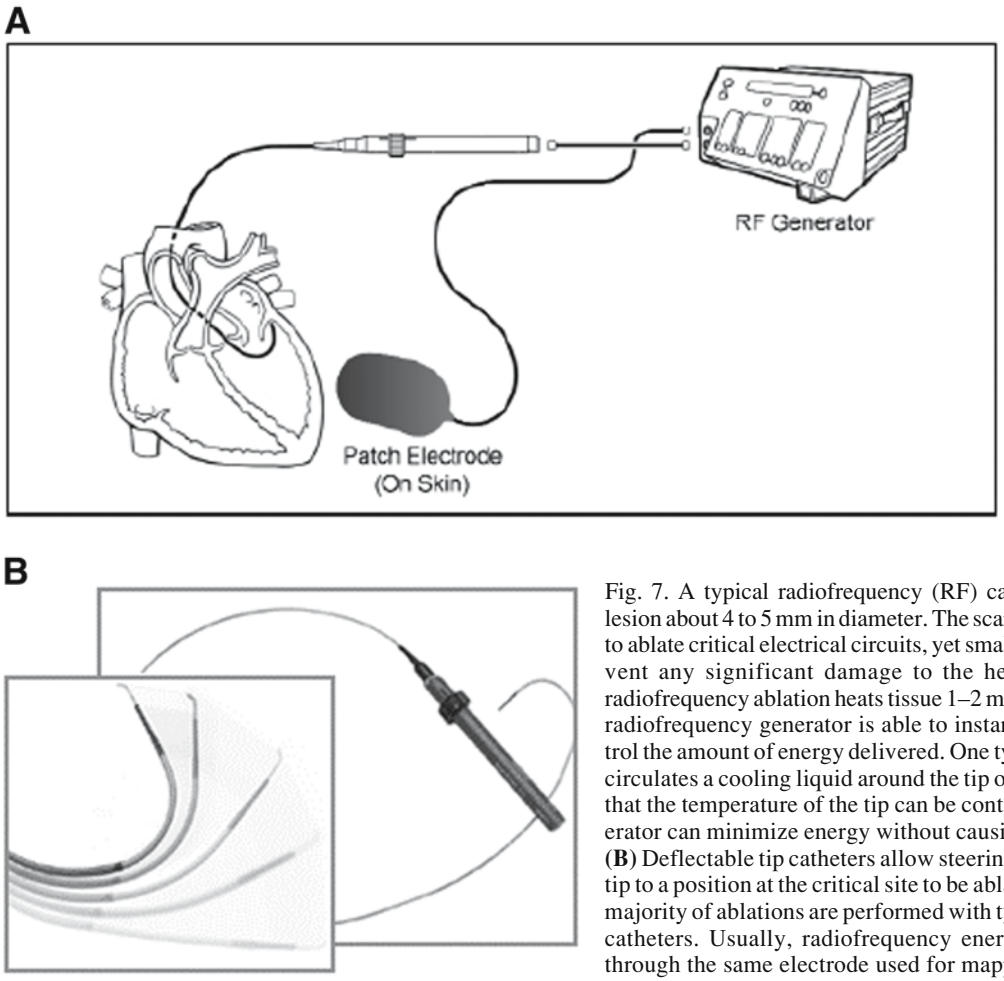

Fig. 7. A typical radiofrequency (RF) catheter creates a lesion about 4 to 5 mm in diameter. The scar is large enough to ablate critical electrical circuits, yet small enough to prevent any significant damage to the heart. Typically, radiofrequency ablation heats tissue 1–2 mm deep. **(A)** The radiofrequency generator is able to instantaneously control the amount of energy delivered. One type of generator circulates a cooling liquid around the tip of the catheter so that the temperature of the tip can be controlled; this generator can minimize energy without causing fluid to boil. **(B)** Deflectable tip catheters allow steering of the catheter tip to a position at the critical site to be ablated. Today, the majority of ablations are performed with typical electrode catheters. Usually, radiofrequency energy is delivered through the same electrode used for mapping.

Radiofrequency ablation catheters use energy similar to electrocautery. Radiofrequency energy heats the catheter tip–tissue interface, with resultant injury to the underlying tissue. Some advantages of radiofrequency ablation are: (1) small amounts of energy are required; (2) output power is easily controlled; (3) it creates small, homogeneous lesions; and/or (4) it does not cause dangerous/unpleasant stimulation or sensory effects. The amount of heating produced during radiofrequency ablation at the electrode tip can result in local blood boiling. To avoid this problem, one type of ablation catheter controls the temperature at the tip by using a cooling fluid.

There are numerous companies working on competing designs of such technologies. Thus, such cardiovascular device companies continue to improve all design aspects of these catheter systems (i.e., improving the ease of positioning of the distal electrode).

Other methods to focally destroy cells endocardially are also emerging: (1) laser energy has been used to destroy arrhythmogenic tissue via a cautery-type process; (2) microwave energy has been investigated as a possible energy source; and (3) cryoablation freezes tissue at the catheter tip to destroy muscle fibers without harming connective tissues (Table 2). Visualization of the exact site where the lesion is to be created remains an area of intense research; advanced echocardiography systems as well as specialized catheters with built-in imaging possibilities are aggressively being pursued *(16–18)*.

5. NOVEL AGENTS TO COAT DEVICES

As described in Section 4.1., drug-coated eluting stents have made a major impact on the field of interventional cardiology. There is little doubt that such combined approaches that incorporate pharmaceutics with implantable devices will continue to expand as a means to improve clinical management of the heart. For example, steroid-eluting pacing leads have been on the market for years to manage acute inflammation associated with lead implantation (*see* Chapter 25).

Steroid-elution technology is considered to reduce inflammation; by eluting a steroid at the lead tip, leads are designed to reduce the typical tissue inflammation. Reduced inflammation allows lower pacing system energy requirements. For example, by reducing tissue inflammation, it has been described that such leads allow the use of lower electrical settings for low, stable, acute, and chronic energy outputs.

6. IMPLANTABLE SENSORS

Device and battery technologies both continue to decrease in size and exhibit improved efficiencies. This in turn creates

increasing possibilities for novel approaches for long-term assessment of various physiological parameters from unique aspects of the cardiovascular system.

One such device, the Medtronic Chronicle®, is intended to sense and continuously collect unique and valuable information (e.g., intracardiac pressures, heart rate, and physical activity) from a sensor placed directly in the heart's chamber. A patient can then periodically download this information to a home-based device that transmits this critical physiological data securely over the Internet to the Medtronic Patient Management Network. Subsequently, physicians can access the network via a controlled Website at any time and review screens that present summaries from the latest downloads, trend information, or detailed records from specified times or problem episodes. The Chronicle Patient Management System is currently undergoing investigational trials in the United States and Europe and is not yet approved for commercial sale.

Other types of implantable sensors that will likely be available in the future include those for blood chemistries (respiratory gases, pH, heparin, polyanions, etc.), flows, cardiac outputs, temperatures, glucose levels, drug levels, or other physiological data.

7. PROCEDURAL IMPROVEMENT

With pressures on the health care system to continually reduce treatment costs and document the outcome benefits of a given therapy, much effort will continue to be placed on procedural improvements for cardiac care.

7.1. Cardiac Imaging

The ability to image internal and external features of the heart continues to improve at a rapid rate and, as indicated in Chapters 18 and 19 on echocardiography and magnetic resonance imaging, respectively, the sophistication of such systems can be quite extreme. Yet, as the cost of computer hardware continues to decrease while capabilities increase, opportunities to develop such technologies for widespread use become feasible.

Intracardiac echocardiography (ICE) has many possible applications, including guidance of radiofrequency ablation procedures and visualization of cardiac anatomy and physiology. Compared to standard 2D imaging, emerging 3D echocardiography may provide additional clinical utility. To assess this, our laboratory compared real-time 3D ICE (RT3D ICE) images to capture real-time video images simultaneously in an isolated four-chamber working swine heart *(19)*. The comparative images obtained in this study verified the ability of RT3D ICE to provide appropriate anatomical identification that could be applied to clinical practice. Stationary anatomical structures (i.e., coronary sinus ostium) are easily visualized with static 3D ICE images (Fig. 8). Moving structures (i.e., valves) were not easily distinguished on RT3D ICE when presented as still images; however, they were more easily identified during acquisition and full-speed playback.

7.2. Specialized Surgical Tools

Cardiovascular device companies typically work closely with clinicians to develop not only new technologies, but also modifications of existing devices or enhanced means to deploy them with better precision. One example of such a collaboration is the recently marketed implant tool for the placement of epicardial leads during a less-invasive surgery. This malleable epicardial lead implant tool features a stainless steel shaft that can be shaped to maneuver and position a lead optimally on the posterior of the heart, either on the right or the left ventricle (Fig. 9).

Another example of an innovative device that has been developed to fit a unique need is the device designed to trap plaque that may dislodge during interventional procedures; such plaque might otherwise migrate to smaller vessels, causing serious endovascular deficits. The SPIDER™ Embolic Protection Device (ev3 Inc., Plymouth, MN) is specially designed for capture and removal of dislodged embolic debris before it can harm the patient (Fig. 10). This device is considered to provide protection while conforming to the requirements of the primary intervention. The SPIDER™ Embolic Protection Device has been recommended to provide distal embolization protection in patients during a general vascular procedure, including peripheral, coronary, and carotid interventions.

7.3. Less-Invasive Surgeries

In Chapter 28, the rapidly advancing field of less-invasive cardiac surgery and some initial uses of robotics to perform epicardial procedures (e.g., bypass grafting and lead implantations) were described. Such approaches are becoming more practical because better tools to perform such procedures are continually refined. For example, the Octopus®3 Tissue Stabilizer (Medtronic, Inc.) is the pioneering and market-leading suction device featuring (1) malleable stabilizer pods that can be formed to the unique contours of the patient's anatomy and (2) a unique tissue-spreading mechanism that enhances stabilization of the anastomotic site and presentation of the coronary (Fig. 11). Similarly, the Starfish™ Heart Positioner (Medtronic, Inc.) has been shown to simplify cardiac positioning and thus minimize associated hemodynamic deterioration *(20)*.

As cardiovascular surgeries employ less-invasive techniques, more and more novel devices and tools will be needed. For example, the HEARTSTRING™ Proximal Seal System (Guidant, Indianapolis, IN) is a unique means to perform bypass procedures that meet the challenge of clampless hemostasis; another example is the Symmetry Bypass System (St. Jude Medical, St. Paul, MN). Both of these devices allow the surgeon to complete coronary artery bypass successfully without cross-clamping or side biting (Fig. 12).

8. TELEMEDICINE

Telecommunication systems and devices, including the utilization of the Internet, have experienced unpredicted growth in the last decade. This explosion in technology has the potential to revolutionize the care of all types of cardiac patients.

8.1. Ambulatory Heart Monitors

Ambulatory heart monitors collect ECGs during daily patient activity. Today, a Holter monitor typically collects up to 48 h of continuous ECG data. The patient wears the monitor and notes

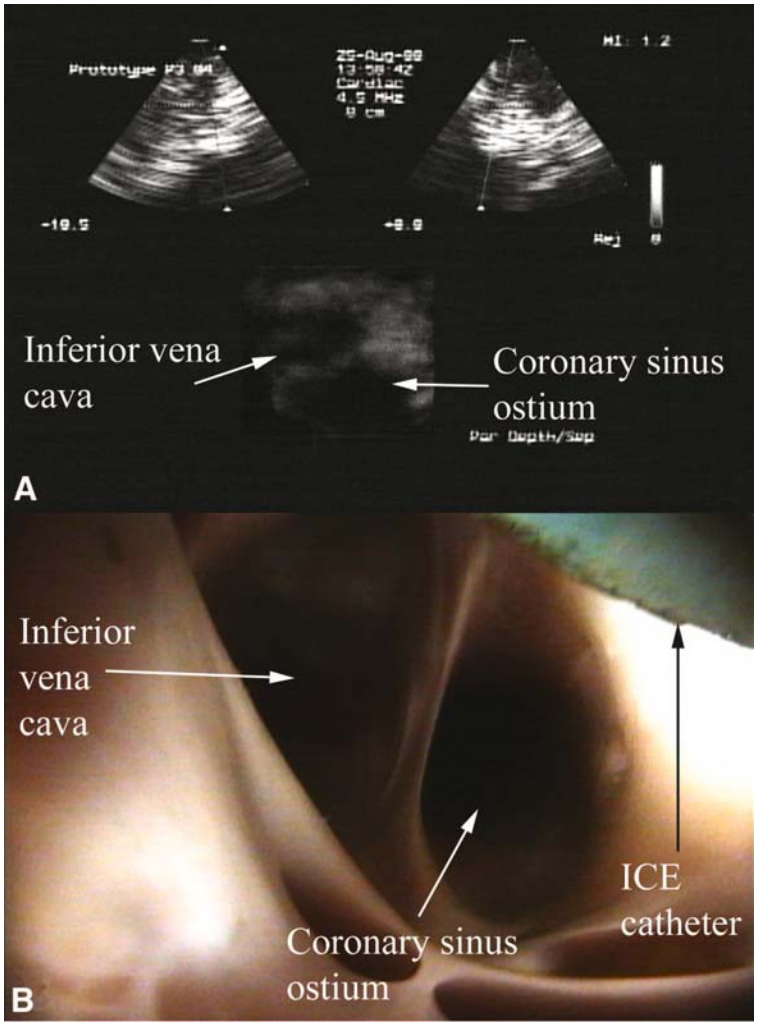

Fig. 8. Utilizing standard cardiac surgery procedures, the heart from a 70-kg swine was explanted to an isolated heart apparatus and reanimated. This preparation utilized a clear, crystalloid perfusate that allowed intracardiac visualization. Following in vitro stabilization, the heart was instrumented with 6-mm videoscopes (Olympus Industrial, Tokyo, Japan) and a 12-French 3D intracardiac echocardiography (ICE) catheter (Duke University, Durham, NC) via access ports in the superior vena cava, left pulmonary vein, aorta, and right atrial appendage. Simultaneous ultrasound (Volumetrics Medical Imaging, Durham, NC) and intracardiac video images of the coronary sinus ostium and the tricuspid, mitral, and aortic valves were recorded to time-synchronized Beta video decks (Sony Beta SP, Tokyo, Japan). **(A)** Real-time 3D ICE (RT3D ICE) image; **(B)** intracardiac visualization. The inferior vena cava and coronary sinus ostium are very distinct in the 3D ICE image *(19)*.

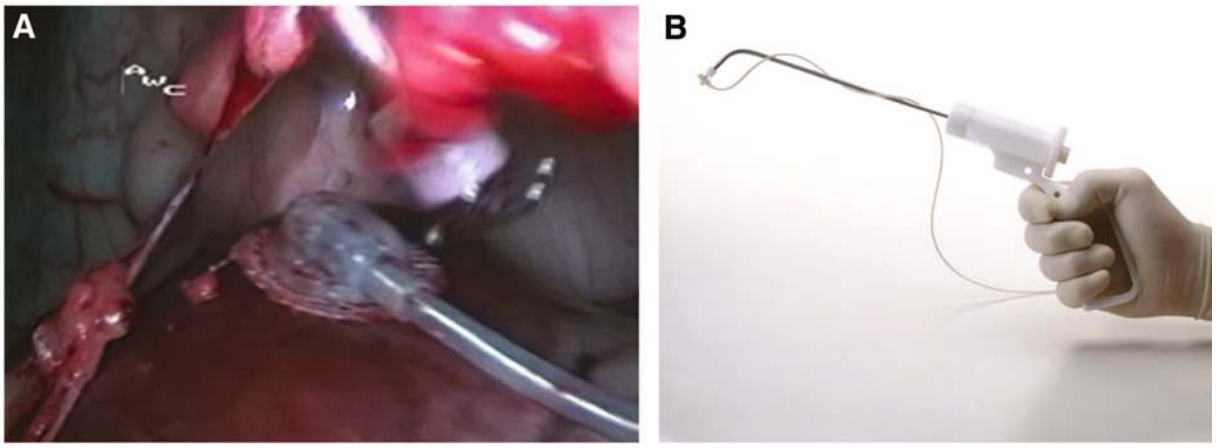

Fig. 9. **(A)** The Model 5071 lead (Medtronic, Inc., Minneapolis, MN) is designed for ventricular pacing and sensing. **(B)** The Model 10626 (Medtronic, Inc.) is a single-use device indicated to facilitate placement of the Model 5071 pacing lead. The lead has application when permanent ventricular dual-chamber pacing systems are indicated. Two leads may be used for bipolar pacing.

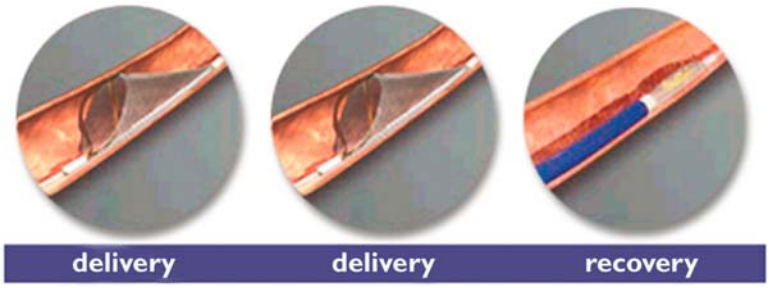

Fig. 10. The SPIDER Embolic Protection Device (ev3 Inc.) provides distal embolization protection in patients during general vascular use, including peripheral, coronary, and carotid interventions. It can be delivered by any guidewire of choice to initially cross the lesion; it has a Nitinol filter design that is HEPROTEC™ coated for patency up to 60 min. The radiopaque gold proximal loop is designed to provide visualization of filter-to-vessel apposition, and there are five filter sizes to match the vessel size appropriately. With permission from ev3 Inc., Plymouth, MN.

Fig. 11. Tools for less-invasive surgery, that is, an open chest procedure in which the heart is not stopped. The Octopus 3 Tissue Stabilizer (Medtronic, Inc., Minneapolis, MN) is a pioneering and market-leading suction device, and the Starfish Heart Positioner (Medtronic, Inc.) has been shown to simplify cardiac positioning; both systems help minimize potential hemodynamic deterioration associated with less-invasive approaches.

the time and type of symptoms experienced, which are then later correlated with the ECG. In contrast, an external event recorder has a memory buffer that can store several weeks of symptom data. Instead of keeping a diary, the patient activates the recorder when symptoms occur; this latter approach is quite convenient for evaluating symptoms that occur infrequently.

A third type of device, an insertable loop recorder, is an implantable ECG recorder with a handheld, patient-controlled activator. The insertable loop recorder continuously records ECGs. When symptoms occur, the patient activates the recorder, and the recorder stores the ECG for a preprogrammed period of time before and after activation. An insertable loop recorder is useful for patients with even more infrequent symptoms and who thus remain undiagnosed after an initial workup. Such an approach is also recommended to the patient for whom an external event recorder is impractical.

More specifically, the Reveal Plus (Medtronic, Inc.) is a second-generation insertable loop recorder; currently, it features autoactivation and is a high-yield, long-term, subcutaneous, leadless ECG monitor that offers continuous 14-month monitoring (Fig. 13). Such systems provide new diagnostic approaches for patients with transient symptoms that may suggest cardiac arrhythmias, including: (1) unexplained syncope, (2) near syncope, (3) episodic dizziness, (4) unexplained recurrent palpitation, and/or (5) seizures and convulsions *(21)* (www.seizuresandfainting.com).

9. TRAINING SYSTEMS

As technologies have become more and more advanced, so has the need to teach students, residents, and physicians how to use them.

9.1. Simulator Mannequins

New products to enhance medical training are rapidly entering the marketplace. The most impressive new systems incorporate computerized mannequins, complex graphics, and sophisticated operator controls in state-of-the-art patient simulators. Students, residents, or physicians learn both medical concepts and manual procedures on life-size, interactive equipment that provides the benefits of anatomical correctness, unlimited repetition, scheduling convenience, and variable "health" conditions. One such system, the Human Patient Simulator, was developed by the University of Florida's College of Medicine to train anesthesiologists in routine and crisis situations. This interactive technology is considered to provide a realistic learning experience adaptable for a wide range of health care practitioners, including medical students, residents, nurses, and biomedical engineers.

The simulator mannequin typically has palpable pulses, heart and lung sounds, simulated muscle twitch responses to nerve

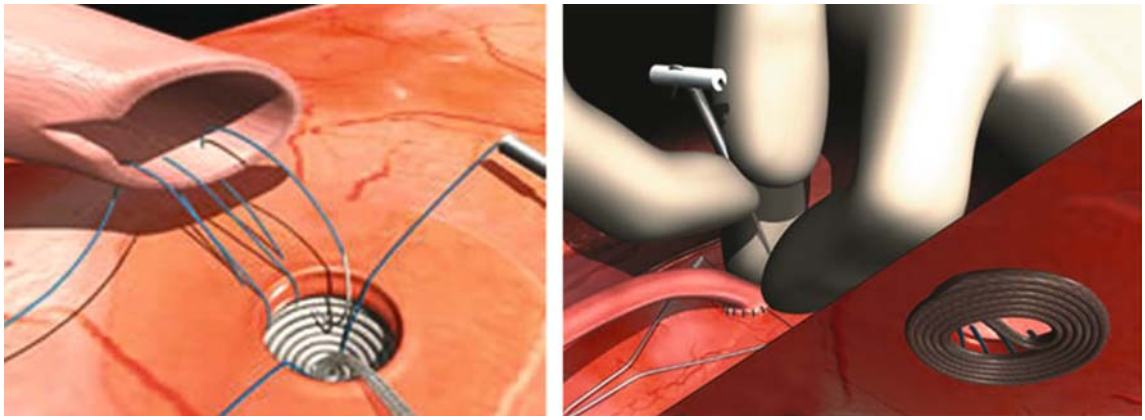

Fig. 12. HEARTSTRING Proximal Seal System (Guidant, Indianapolis, IN) is a surgically intuitive system that meets the challenge of clampless hemostasis with a design that is elegant in its simplicity and profound in its implications for a patient.

stimulation, and a body temperature. Thus, trainees can monitor its heart rate, cardiac rhythms, cardiac output, and blood pressure. Commonly equipped with interface software and an instructor's remote control, the simulator also gives accurate patient responses to over 60 different drugs, mechanical ventilation, and other medical therapies and allows the instructor to introduce new conditions.

Another such device that is currently available is the ultrasound training simulator, which allows students to perform sonographic examinations on a mannequin while viewing real-time sonographic images. The scanning motions and techniques that can be employed by the user realistically simulate the same skills necessary to examine a patient. It is considered that, by allowing trainees to practice on the simulator for as much time as needed to achieve initial competency, users should be able to perform more effectively in a shorter period of time in the actual clinical setting.

9.2. Endovascular Implant Simulators

A new generation of implant simulators that employs both visual and tactile feedback for practicing either right or left heart catheter-based procedures is currently available (e.g., AccuTouch® Endovascular Simulator, Immersion Medical, San Jose, CA, http://www.immersion.com/medical/products/endovascular/). In addition, such devices can be used to simulate the placement of coronary stents (Procedicus VIST™, Mentice AB, Göteborg, Sweden, http://www.mentice.com/). More specifically, the VIST system allows highly realistic simulation-based training of angiography, angioplasty, and coronary stenting using realistic 3D patient anatomies, real nested tools, tactile feedback, as well as different cases/scenarios and complications.

Such systems consist of an interface device, a computer, and one or more displays (e.g., one for the simulated fluoroscopic image and another for the instructional system). The interface device is a virtual patient with an introducer in place; such systems will become more and more realistic in the future. Through this, the different real-life tools and devices can be introduced, and actual tools are used (and reused). All tools are active and can be manipulated at any time in the procedure. In the VIST system, the interface and the tools (catheters, balloons, guidewires, etc.) interact with the simulation through a software package that generates the fluoroscopic display, the forces that are reflected in the tools (for tactile feedback), the

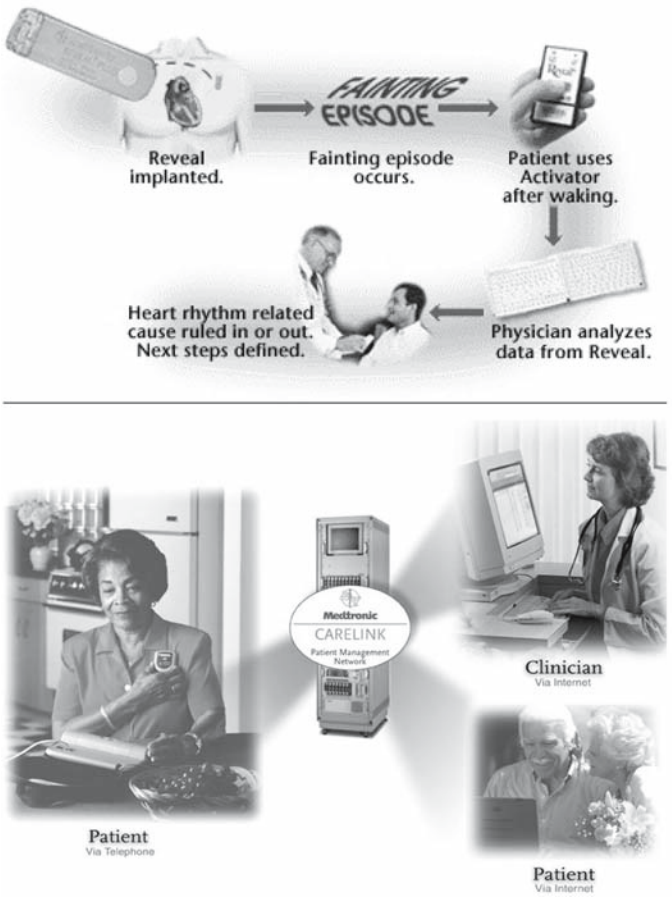

Fig. 13. Reveal Plus is the second-generation Reveal ILR (Medtronic, Inc., Minneapolis, MN). Now with auto-activation, the Reveal Plus ILR is a high-yield, long-term, subcutaneous, and leadless electrocardiogram (ECG) monitor that offers continuous 14-month monitoring. IR, insertable loop recorder.

contrast flow, hemodynamics, and the results of the simulated intervention; a Web-based user interface guides the user through the procedure and facilitates self-learning.

Many training centers around the world, in both academic and corporate settings, have been created, and they utilize various types of simulators; for instance, the Karolinska's training center uses a number of such devices (http://utbildning.ks.se/).

10. SUMMARY

In this book, and more specifically in this chapter, numerous areas of cardiology and cardiac surgery in which the development of innovative technologies continues to mature at a rapid rate have been reviewed. These areas include: (1) resuscitation systems and devices; (2) implantable therapies (e.g., pacemakers, implantable cardioverter defibrillators, stents, septal occluders, valves, annular rings, fibrin patches, etc.); (3) delivery systems/invasive therapies (e.g., angioplasty, ablations, catheters, etc.); (4) procedural improvements (e.g., mapping systems, 3D echocardiography, magnetic resonance imaging, training simulators, etc.); (5) less-invasive surgical approaches (i.e., off-pump, robotics, etc.); (6) postprocedural follow-up/telemedicine (e.g., electrical, functional, adverse events, etc.); and (7) training tools. There is no doubt that continued improvement of all such technologies as well as advances in rehabilitation and other support services (e.g., patient education, training, home monitoring, etc.) will extend or save lives and enhance the overall quality of life for such patients.

Finally, it should be mentioned that much work has been done on the implantable replacement heart, but such prosthetic systems have yet to be used successfully (e.g., the AbioCor™ Implantable Replacement Heart; Abiomed, Danvers, MA). However, when a given patient is at imminent risk of death, the implant of an artificial heart is designed both to extend life and to provide a reasonable quality of life. After implantation, the device does not require any tubes or wires to pass through the skin; power to drive the prosthetic heart is transmitted across the intact skin, avoiding skin penetration that may provide opportunities for infection. Just like the natural heart, the replacement heart consists of two blood-pumping chambers capable of delivering more than 8 L of blood every minute.

In conclusion, it is exciting to think about the technologies that have been employed thus far as well as those that are being developed that will positively affect the overall health care of the cardiac patient. It is an exhilarating time to be working in the field of cardiovascular sciences.

REFERENCES

1. Halperin, H.R., Tsitlik, J.E., Gelfand, M., et al. (1993) A preliminary study of cardiopulmonary resuscitation by circumferential compression of the chest with use of a pneumatic vest. *N Engl J Med*. 329, 762–768.
2. Cohen, T.J., Goldner, B.G., Maccaro, P.C., et al. (1993) A comparison of active compression-decompression cardiopulmonary resuscitation with standard cardiopulmonary resuscitation for cardiac arrests occurring in the hospital. *N Engl J Med*. 329, 1918–1921.
3. Arntz, H.R., Agrawal, R., Richter, H., et al. (2001) Phased chest and abdominal compression-decompression versus conventional cardiopulmonary resuscitation in out-of-hospital cardiac arrest. *Circulation*. 104, 768–772.
4. Tang, W., Weil, M.H., Schock, R.B., et al. (1997) Phased chest and abdominal compression-decompression. A new option for cardiopulmonary resuscitation. *Circulation*. 95, 1335–1340.
5. Kern, K.B., Hilwig, R.W., Berg, R.A., Schock, R.B., and Ewy, G.A. (2002) Optimizing ventilation in conjunction with phased chest and abdominal compression–decompression (Lifestick) resuscitation. *Resuscitation*. 52, 91–100.
6. Plaisance, P., Lurie, K.G., Vicaut, E., et al. (1999) A comparison of standard cardiopulmonary resuscitation and active compression-decompression resuscitation for out-of-hospital cardiac arrest. French Active Compression–Decompression Cardiopulmonary Resuscitation Study Group. *N Engl J Med*. 341, 569–575.
7. Wenzel, V., Lindner, K.H., Prengel, A.W., and Strohmenger, H.U. (2000) Effect of phased chest and abdominal compression–decompression cardiopulmonary resuscitation on myocardial and cerebral blood flow in pigs. *Crit Care Med*. 28, 1107–1112.
8. Voelckel, W.G., Lurie, K.G., Sweeney, M., et al. (2002) Effects of active compression-decompression cardiopulmonary resuscitation with the inspiratory threshold valve in a young porcine model of cardiac arrest. *Pediatr Res*. 51, 523–527.
9. Lurie, K.G., Zielinski, T., McKnite, S., Aufderheide, T., and Voelckel, W. (2002) Use of an inspiratory impedance valve improves neurologically intact survival in a porcine model of ventricular fibrillation. *Circulation*. 105, 124–129.
10. Wolcke, B.B., Mauer, D.K., Schoefmann, M.F., et al. (2003) Comparison of standard cardiopulmonary resuscitation versus the combination of active compression–decompression cardiopulmonary resuscitation and an inspiratory impedance threshold device for out-of-hospital cardiac arrest. *Circulation*. 108, 2201–2205.
11. Lurie, K.G., Voelckel, W.G., Zielinski, T., et al. (2001) Improving standard cardiopulmonary resuscitation with an inspiratory impedance threshold valve in a porcine model of cardiac arrest. *Anesth Analg*. 93, 649–655.
12. Cohn, J.N., Ferrari, R., Sharpe, N., and International Forum on Cardiac Remodelling. (2000) Cardiac remodeling—concepts and clinical implications: a consensus paper from an international forum on cardiac remodeling. *J Am Coll Cardiol*. 35, 569–582.
13. Anversa, P., Olivetti, G., and Capasso, J.M. (1991) Cellular basis of ventricular remodeling after myocardial infarction. *Am J Cardiol*. 68, 7D–16D.
14. Saaverda, W.F., Tunin, R.S., Paolocci, N., et al. (2002) Reverse remodeling and enhanced adrenergic reserve from passive external support in experimental dilated heart failure. *J Am Coll Cardiol*. 39, 2069–2076.
15. Francis, G.S. (2001) Pathophysiology of chronic heart failure. *Am J Med*. 110(Suppl 7A), 37S–46S.
16. Fried, N.M., Tsitlik, A., Rent, K., et al. (2001) Laser ablation of the pulmonary veins using a fiberoptic balloon catheter: implications for treatment of paroxysmal atrial fibrillation. *Lasers Surg Med*. 28, 197–203.
17. Marrouche, N. and Natale, A. (2002) Monitoring pulmonary vein isolation using phased array intracardiac echocardiography in a patient with atrial fibrillation. *Appl Cardiac Imag*. November, 19–22.
18. Haissaguerre, M., Jais, P., Shah, D.C., et al. (1998) Spontaneous initiation of atrial fibrillation by ectopic beats originating in the pulmonary veins. *N Engl J Med*. 339, 659–666.
19. Hill, A.J., McHenry, B.A., Laske, T.G., et al. (2003) Validation of real-time 3D intracardiac echocardiography using Visible Heart™ methodologies. *J Card Fail*. 9, S51.
20. Gründeman, P.F., Verlaan, C. W., van Boven, W.J., and Borst, C. (2004) Ninety-degree anterior cardiac displacement in off-pump coronary bypass grafting: the Starfish cardiac positioner preserves stroke volume and arterial pressure. *Ann Thorac Surg*. 78, 679–684.
21. Zaidi, A., Crampton, S., Clough, P., Scheepers, B., and Fitzpatrick, A. (1999) Misdiagnosis of epilepsy. Many seizure-like episodes have a cardiovascular cause [abstract]. *Pace*. 22(Pt. II), 814.
22. Chinchoy, E., Soule, C.L., Houlton, A.J., et al. (2000) Isolated four-chamber working swine heart model. *Ann Thorac Surg*. 70, 1607–1614.

WEB RESOURCES

http://utbildning.ks.se/simulatorcentrum/sim-eng.php. Accessed 15 September 2004.
http://www.abiomed.com/prodtech/Fabiocor.html. Accessed 15 September 2004.
http://www.acorncv.com/index2.html. Accessed 15 September 2004.
http://www.asme.org/events/nanobio/. Accessed 15 September 2004.
http://www.biotronik.com/content/detail.php?id=1446. Accessed 15 September 2004.
http://www.bostonscientific.com/. Accessed 11 November 2004.
http://www.bris.ac.uk/Depts/BMSC/hps.htm. Accessed 15 September 2004.
http://www.ctsnet.org/. Accessed 11 November 2004.
http://www.ev3.net/index.php?page=spider&Base_Session=706995d371319eb313bc7140ae08e662. Accessed 15 September 2004.
http://www.fda.gov/cdrh/pdf/k013517.pdf. Accessed 15 September 2004.
http://www.fda.gov/. Accessed 11 November 2004.
http://www.guidant.com/. Accessed 15 September 2004.
http://www.ifmbe.org/conferences/Nanotechnology%20and%20Smart%20Materials%20for%20Medical%20Devcies.pdf (Nanotechnology). Accessed 15 September 2004.
http://www.immersion.com/medical/products/endovascular/. Accessed 15 September 2004.
http://www.lifestick.com/. Accessed 15 September 2004.
http://www.medtronic.com/. Accessed 15 September 2004.
http://www.mentice.com/. Accessed 15 September 2004.
http://www.nano.org.uk/med.htm. Accessed 15 September 2004.
http://www.physiocontrol.com/products/lp12.cfm. Accessed 15 September 2004.
http://www.pueblo.gsa.gov/cic_text/health/med-device/mdt.html. Accessed 15 September 2004.
http://www.resqsystems.com/. Accessed 11 November 2004.
http://www.seizuresandfainting.com. Accessed 15 September 2004.
http://www.simulab.com/Human%20Patient%20Simulator.htm. Accessed 15 September 2004.
http://www.sjm.com/index.aspx. Accessed 15 September 2004.
http://www.texasheartinstitute.org/biopump.html. Accessed 15 September 2004.
http://www.tmc.edu/thi/abiocor.html. Accessed 15 September 2004.
http://www.ummc.edu.my/csl/HTML/Ultrasound.html. Accessed 15 September 2004.
http://www.zoll.com/autopulsebyrevivant.htm. Accessed 15 September 2004.
www.uspto.gov. Accessed 15 September 2004.

Index